# The Fate of Contaminants in Urban Soils and Sediments: Novel Assessments and Implications for Risks

---

Dissertation submitted to the Manchester Metropolitan University by

**Raquel B. S. M. Cardoso**

in partial fulfilment of the requirements for the degree of
**Doctor of Philosophy**

**Supervisory team:**
Kevin G. Taylor, University of Manchester
Jianquan Cheng, Manchester Metropolitan University
Neil Breward, British Geological Survey

March 2014

To my beloved parents and brother,
for your love, endless support and dedication,
and without whom none of this would be possible.

*"Temos, todos que vivemos,*
*Uma vida que é vivida*
*E outra vida que é pensada,*
*E a única vida que temos*
*É essa que é dividida*
*Entre a verdadeira e a errada.*
*Qual porém é verdadeira*
*E qual errada, ninguém*
*Nos saberá explicar;*
*E vivemos de maneira*
*Que a vida que a gente tem*
*É a que tem que pensar."*

Fernando Pessoa, Portuguese author (1888 - 1935).

*"In rivers, the water that you touch is the last of what has passed and the first of that which comes; so with present time."*

Leonardo da Vinci, Italian polymath (1452 - 1519).

# Abstract

Soils and road-deposited sediments (RDS) are ubiquitously present in the urban environment and may act as sinks or sources for potentially harmful elements (PHE), namely trace metals, with possible deleterious human health effects. Their proximity to human populations in urban centres evokes the need to fully characterise the occurrence of PHE and their dynamics within and between these media.

This research has provided a detailed characterization of Manchester's soils and RDS in terms of geochemistry, mineralogy and spatial variability by using the quantification and statistical comparison of the presence of PHE in soils and RDS; and by exploring their spatial, geochemical and mineralogical linkages.

Soil and RDS geochemical analysis shows that maximum PHE concentrations are often well above the dataset median values and established guidelines, indicating that contamination is present at many locations especially for Cr (max. soil 1238, RDS 544 mg/kg), Ni (max. soil 148, RDS 82.4 mg/kg), Cu (max. soil 2073, RDS 493 mg/kg), Zn (max. soil 1763, RDS 1325 mg/kg) and Pb (max. soil 2758, RDS 2027 mg/kg). RDS contamination is closely related to the proximity of present-day sources; whereas soil contamination derives mainly from historical sources and the accumulation of trace metals over long periods of time. SEM-EDS analysis of soil and RDS grains reveal the presence of natural and anthropogenic-related grains in different proportions, and the detailed characterization of PHE-bearing grains shows that these, by their morphology of size, are likely to impact human and ecosystem health. In RDS, grain size and speciation analyses provided a further insight on the availability and summer/winter variations of PHE in this media - whereas total extractable concentrations are higher in winter RDS, also due to their generally small grain size, exchangeable and reducible concentrations are higher in summer, when coarse fractions are predominant. Multivariate and spatial statistical analyses reveal that element associations in soils and RDS are diverse and attributed to a plethora of sources (e.g. industry; vehicle-related sources such as automotive electronics, the wear and tear of tyres and car parts, and car servicing and repair businesses; wastewater treatment plants; historical industry and coal-related sources) through the mapping of component scores and the modelling of PHE concentrations by OLS and GWR. These techniques evidence the differences and similarities between element groupings for soils and RDS and are a powerful tool to aid source apportionment.

This research has contributed to a better understanding of the complex controls on PHE dynamics in urban systems, adding vital information to the assessment of risks posed by PHE exposure on human health.

# Acknowledgements

This doctoral thesis would have never been accomplished without the support of my loved ones. Above all, I would like to thank my family - especially my parents, Cirila and Isidro, and my brother Rodolfo for the unconditional support, for which my mere expression of thanks does not suffice. You have been my never empty source of happiness and encouragement.

I would like to thank my principal supervisor, Prof. Kevin G. Taylor from the University of Manchester, for all the good advice and friendship over the last years - thank you for being always available to share your vast knowledge and experience (preferably over a few cups of good coffee!). I also thank my director of studies, Jianquan Cheng; my supervisor from the British Geological Survey, Neil Breward, and former supervisor Fiona Fordyce, for all the knowledge shared which has been of great importance for the outcomes of this work. I also thank the G-BASE field survey and BGS analytical laboratory teams for their valuable contributions.

A special thanks goes to Prof. Maria da Conceição Freitas, my former MSc supervisor, and to Prof. Mário Gonçalves of the Faculty of Sciences, University of Lisbon, for providing access and assistance to the laser diffractometry, sequential extraction and FAAS laboratories at that institution. I also acknowledge all the assistance provided by the laboratory and field work staff who have personally helped me - Dave Groom, Dave McKendry, Vladimir Vishnyakov and Piotr Dobroz, at MMU; and Sandra Moreira, Luís Carita, André Pinto and Vera Lopes at the University of Lisbon. I am deeply thankful for all your advice which has been extremely important to the quality of the data I have obtained. Another special thanks to Dr. Maria de Fátima Araújo from the Portuguese Technological and Nuclear Institute, and Prof. Nuno Leal from the New University of Lisbon, for having introduced me to the world of geochemistry and having made me so enthusiastic about this subject.

Last but not the least, I would like to say a big thank you to all my friends - you know who you are - for always being there for me and for all the good, memorable moments we've always spent, which brought me great joy and will remain forever in my heart. I especially thank Cláudia, Leila, Sandra S., Sandra M. and Sofia for the sharing of our daily lives, even if we were oceans apart... You have been the best friends I could ask for! And of course to my Manchester buddies - Charlotte, Gary, Angela, Noémie, Déborah, Ruggero; as you guys were the sunshine of my Manchester days.

I couldn't finish this without mentioning my true companion - my dog Jameson - who stood by me literally 24/7 through the ups and downs of the thesis writing-up process, was the greatest listener, and provided me with the uttermost unconditional love.

Thank you.

# Contents

# List of Figures

# List of Tables

# Abbreviations

AICc - Corrected Akaike Information Criterion
BGS - British Geological Survey
c. - *Circa,* "approximately"
cf. - *Confer,* "refer to"
EDS - Energy-Dispersive Spectrometry
e.g. - *Exempli Gratia*, “for example”
et al. - *Et Alii*, “and others”
EU - European Union
FAAS - Flame Atomic Absorption Spectroscopy
FCUL - Faculty of Sciences, University of Lisbon
GIS - Geographical Information Systems
GPS - Global Positioning System
GWR - Geographically-Weighted Regression
HCV - Health Criteria Value
HI - Hazard Index
HMSO - Her Majesty's Stationery Office
IC - Inorganic Carbon
IDW - Inverse Distance Weighting
i.e. - *Id Est*, “in other words”
IQR - Interquartile Range
LLD - Lower Limit of Detection
LOI - Loss-on-Ignition
MMU - Manchester Metropolitan University
MO - Met Office UK
OC - Organic Carbon
OLS - Ordinary Least Squares
OM - Organic Matter
OS - Ordnance Survey
PCA - Principal Component Analysis
PHE - Potentially Harmful Element
RDS - Road-Deposited Sediment
REE - Rare Earth Elements
SEM - Scanning Electron Microscope
SGV - Soil Guideline Value
s.l. - *Sensu Lato*, "in general"
SRM - Standard Reference Material
TC - Total Carbon
UN - United Nations
USA - United States of America
UK - United Kingdom
WD - Wavelength-Dispersive
XRF - X-Ray Fluorescence

# Introduction

This PhD Thesis is the result of a three-year project, started in 2009 and developed mostly at the Manchester Metropolitan University, jointly-funded by the British Geological Survey. The main aim of this project is to fully quantify and compare the presence of potentially harmful elements (PHE) in soils and urban sediments of Manchester, UK, exploring the spatial, geochemical and mineralogical linkages within and between these media.

The environmental quality of urban centres is critical to human health: as of 2008, 50% of the world population (3.3 billion people) lived in urban centres, a figure which is set to increase in the next decades. This is due to the generally more favourable socioeconomic conditions in cities, where jobs and income are generated. Therefore, urban populations tend to grow at a very fast rate and so does the importance of PHE characterization and monitoring. This knowledge is a crucial factor for substantiated environmental risk assessments, as precursors of a more sustainable development of urban areas.

Soils and urban sediments, such as road-deposited sediments (RDS), may act as sinks or sources of potentially harmful elements with possible deleterious human health effects. In the urban environment, this risk is enhanced due to the high density of possible contamination sources and the close proximity of these to the receptors. Urban soil quality is of concern under current contaminated land legislation in the UK and most developed countries, in terms of potential impacts and the need for sustainable development. Nevertheless, RDS, the accumulation of particles on urban roads and pavements, remains still a relegated subject in terms of legislation and guidelines although high loadings of contaminant species have been reported in the scientific literature. RDS ubiquitous and sometimes unnoticed presence in the urban environment, as well as its high susceptibility to remobilisation and transport, can turn it into a rather silent threat to human and ecosystem health.

In the urban environment, soils and RDS coexist and may be spatially related. The nature of these media is quite distinct as they often show different physical properties, chemical compositions and temporal variability. However, similar suites of PHE have been reported separately for each media, indicating they may reflect common pollution sources. The spatial, geochemical and mineralogical linkages between soils and RDS have yet to be determined.

The urban environment will form the frontier for environmental research in the future - this study aims to ultimately contribute to a better understanding of PHE dynamics in urban systems, adding vital knowledge on the risks posed to human populations by PHE exposure.

# 1. Background

Throughout most of human history, populations have lived in rural environments. Even as late as 1800 AD only 3% of the population lived in urban areas (Chase-Dunn and Manning, 2002). With the Industrial Revolution and the diminishing of famine and epidemic diseases, human population began to grow exponentially, and this population started to create larger - urban - agglomerations. The definition of urban centres varies between countries, but mainly it is based on factors such as the number of inhabitants, population density, or the provision of public utilities and services. In the UK, population agglomerations are considered urban centres when census output areas forming settlements have populations of over 10,000 (DEFRA, 2009).

According to the "World Urbanization Prospects: The 2007 Revision Population Database" (UN, 2007) approximately 50% of the world population currently lives in urban centres, and this is predicted to increase in the future. According to the same study it is likely that urban populations will represent 69.6% of the total world population by 2050. However, in the United Kingdom this percentage is already greater: in 2005 89.7% of the total UK population resided in urban centres (UN, 2007).

The fast urban growth poses several environmental and health issues, as this profound geographical development has a critical influence on our immediate environment and its quality for human health (Wong et al., 2006). Within the urban environment, where human activities are especially intense, emissions of both metal and organic pollutants are often vastly accelerated, inevitably rendering urban areas particularly susceptible to environmental degradation and contamination (Nriagu and Pacyna, 1988), with consequent impacts on ecosystem and human health.

## 1.1. Trace Elements in the Environment

Metals are a large group of chemical elements which include the elements of the alkali, alkali-earth and transition series, as well as rare-earth metals and metalloids. Metals are characterised by the capacity to lose electrons to form positive ions and the ability to conduct heat and electricity (Chang, 2009). Due to the physico-chemical properties of solid metal materials, namely malleability and ductility, metals became historically important to the technological progress of mankind, firstly by its use in prehistoric tools and artefacts. Metallurgical techniques were soon developed and improved, and metals became a main commodity - intense mining activities started to develop, along with metallurgical facilities (Tylecote, 1987). The process of extracting, concentrating and transforming metals progressively started to leave its impact in the environment - the close link between metals, metal pollution, and human history was formed (Nriagu, 1996). The "boom" of the Industrial

Revolution lead to an exponential increase in the metal emissions into the environment and the legacy of historical metal exploration still remains today, along with continuous present-day inputs.

The toxicity of some metals has been documented throughout history: Greek and Roman physicians diagnosed symptoms of acute lead poisoning long before toxicology became a science. Today, much more is known about the health effects of trace metals. Exposure to trace metals has been linked with developmental retardation, various cancers, lung and respiratory problems, kidney damage, autoimmune diseases, and even death in some instances of exposure to very high concentrations (Silver et al., 1995; Jarup, 2003). These risks are known and widely studied, as human health concerns are usually associated with excessive environmental exposures to metals which cause toxic effects to biological organisms.

In the literature, the metals of environmental concern have often been referred to as "*heavy metals"*, a group name for metals and metalloids that have been associated with contamination and potential toxicity or ecotoxicity (Duffus, 2002). This term is based in metal density and has erroneously been applied, as it assumes that all *heavy metals* and their compounds have highly toxic or ecotoxic properties, which is not true. Hence, the term *trace metal* is preferred and used herein, as it refers to the metals found in low concentration, in mass fractions of parts per million or less, in some specified matrix, e.g., soil, sediment, etc. This is a coherent term which includes the metals of environmental concern focused throughout this text and that has been widely used in most if the cited literature. From a biological perspective, trace metals may include non-essential ones, such as Cd and Pb that can be toxic even at low concentrations, and biologically essential elements, such as Cu and Zn, which might cause toxic effects at elevated concentrations (Wong et al., 2006).

Trace metals may be present in different environmental compartments, such as air, water, soils, sediments, and biota. These compartments are not static or self-contained - they are chemically and physically dynamic, and the interaction between compartments is continuous. Therefore, environmental contamination migrates from one compartment to the other according to physico-chemical conditions of the system, and this issue has been addressed in several studies (Liston and Maher, 1986; Young et al., 2002; Schafer et al., 2009; Taylor and Owens, 2009; Owens et al., 2011; Laidlaw et al., 2012; Qian et al., 2012). Nevertheless, the contaminant toxicity, mobility, concentration, residence time, the proximity to receptors and the existence of a pathway capable of exposing the receptors to the contaminant still remain as the major core-subjects in terms of risk assessments to human health.

The growing awareness towards urban environmental quality led to the development, in the last decades, of a new discipline within environmental geochemistry, as the urban environment is underlined by rather unique geochemical processes. The new discipline of *urban geochemistry* addresses the complex interactions and interrelationships between chemical elements and their

compounds in the urban environment, the influence of past and present human and industrial activities on these and the impacts or effects of geochemical parameters in urban areas on plant, animal and human health (Thornton et al., 2008). In recent years, many studies on urban air quality (e.g. Fenger, 1999; Fang et al., 2005; Zou et al., 2009; Zuurbier et al., 2011) and water, soil and sediment quality (e.g. Carter et al., 2003; Charlesworth et al., 2003; Fordyce et al., 2005; Bretzel and Calderisi, 2006; Taylor and Owens, 2009), have been published, as later discussed.

At present, and more than ever before, urban environmental studies are crucial in terms of risk assessments and the number of publications in this area is rising. Among the studied substances, metals or metalloids make up the top 10 of the list of the most studied environmental chemicals, with copper, lead, zinc, cadmium, iron, nickel, chromium, arsenic, mercury and manganese (Grandjean et al., 2011). These metals remain as the most studied chemicals due to their recognised importance as anthropogenically-derived elements and their known long-term persistency in the environment and/or in living organisms.

## 1.2. Proxies for urban pollution

### *1.2.1. Soils*

Soils can be generally defined as the unconsolidated top layer of the Earth's surface, consisting of mineral particles mixed with organic matter (humus), water and air. Soil is formed by the process of pedogenesis which is a combination of physical, chemical, and biological processes which act upon the parent material or bedrock through a period of time. Therefore, soil forms and evolves through weathering processes driven by geological, biogeochemical, topological, climatic, chronological and, often, anthropogenic influences (Violante et al., 2008). Soils differ from their parent materials in their morphology, physico-chemical, mineralogical properties and biological characteristics; and soil types vary widely from one region to another, mainly depending on the type of bedrock they overlie and the climate and topography in which they form (adapted from Gerrard, 2000; Olson and Daniel, 2005).

Soils are crucial environmental components for many reasons. In the terrestrial environment, they are the substrate which provides support and food for primary producers: soil systems regulate biological activity and molecular exchanges among solid, liquid and gaseous phases, consequently affecting nutrient cycling, plant growth and decomposition of organic materials. Soils also act as filters to protect water quality, influencing water runoff, infiltration, storage or deep drainage. As a non-renewable resource, soil quality is of extreme importance as it is used for our primary food production, and is present ubiquitously in all aspects of our everyday life - the importance of healthy and clean soil for the further development of humanity cannot be overemphasized (Johnson and Demetriades, 2011).

The compositional and morphological characteristics of natural and undisturbed soils are directly related to the breakdown and weathering of their geological parent materials (Olson and Daniel, 2005). However, differences in the geochemical composition of the bedrock and variations in the intensity of soil-forming processes can result in wide ranges of trace element concentrations in natural soils. In contrast, urban soils tend to be highly disturbed due to intense human activities, and may even be exogenous (Wong et al., 2006); for this reason, its geochemical composition may not be related to the local bedrock or superficial deposits. In an urban setting it is common to see vast amounts of excavated soils being moved away from construction sites, or even received from external sources for the construction of made grounds, parks, gardens - or even landfills.

Soils are an important sink for trace metal contaminants in the terrestrial ecosystem - they are the main receptors for PHE contamination in urban environments, from both diffuse and point-sources (Johnson and Demetriades, 2011). In urban areas, soil can be contaminated through a number of anthropogenic processes such as atmospheric deposition of particulates derived mainly from the combustion of fossil fuels and industry, by the discharge and percolation of contaminated waters, and direct dumping of domestic and industrial residues.

Metals are always present in soils at a background level of natural origin, which derives from the parent rock materials and pedogenesis, and often occur as cations which strongly interact with the soil matrix. Even at high concentrations, metals may be present in soils as inert and non-toxic species, but these can become mobilised as a result of changing physical and/or chemical conditions or by saturation beyond the buffering capacity of the soil (Facchinelli et al., 2001). Nevertheless, it is worth mentioning that concentrations of metals in harmful forms may exceed current guidelines in soils not only due to the actions of man, but also by natural geological processes – there may be no distinction between a more toxic man made form and a less toxic natural form for a given metal. To aid in this issue, several methods have been developed and studies on the speciation and bioavailability of trace metals have focused on the interactions between the chemical forms, the behaviour of toxic compounds and their subsequent biological uptake, metabolism and ecological fate (Tessier et al., 1979; Harrison et al., 1981; Scheckel et al., 2009; Wragg et al., 2011).

### *1.2.2. Road-deposited sediments (RDS)*

Road-deposited sediments are the accumulation of particulates on roads and other paved surfaces. RDS is a complex and, to a variable degree, anthropogenically-derived media, mainly composed by mineral and organic material (soil particles and plant and leaf litter), as well as anthropogenic materials such as vehicle tyre, brakes and body wear particles, infrastructure and building materials, road paint, pedestrian debris, and dry/wet atmospheric deposition of particles derived from vehicle exhaust and industrial emissions (Sutherland and Tolosa, 2000; Robertson et al., 2003; Taylor, 2007).

Contrarily to soils, RDS is highly transient in the urban environment and has a short residence time on surfaces (Robertson and Taylor, 2007; Zafra et al., 2011): the amount of RDS on surfaces at a given time is variable, as it is a dynamic balance between the accumulation process and its removal from the surfaces (e.g. urban runoff, atmospheric resuspension, street sweeping). RDS is, therefore, likely to reflect short-term and localised geochemical and contaminant fluctuations, and has been shown to be both spatially and temporally highly variable as it is easily remobilised. RDS has also been documented to carry a high loading of contaminant species, including trace metals (Charlesworth et al., 2003; Robertson and Taylor, 2007; Krčmová et al., 2009; Taylor and Robertson, 2009; Sutherland et al., 2012).

Currently there is a growing awareness of RDS as a potential hazard to human and ecosystem health, but unlike soils there are no guideline values regarding RDS contamination as it is difficult to establish stand-alone threshold values - RDS is extremely prone to remobilisation and transport, affecting human health and other environmental compartments through a large number of connected pathways which depend on local factors and are, therefore, difficult to quantify.

## 1.3. Trace metals: sources, pathways and environmental impacts

In the past few decades, it has been recognised that trace metal enrichments in the environment pose a serious threat to ecosystem health. In general, small amounts of some trace metals are, in fact, essential to support life, as in the case of e.g. Cu and Zn. In contrast, metals may become poisonous to living organisms when present in high concentrations, as they may not be metabolised or excreted and so accumulate in organs and tissues. Other metals, such as Cd and Pb, are not known to be essential to living organisms; therefore, toxicity may occur even at low concentrations. The prolonged presence of trace metals in the urban environment, particularly in urban soils and RDS, and their close proximity to the human population can significantly amplify the exposure of the urban population to metals via inhalation of air particulates, ingestion of food and water, and absorption through the skin by dermal contact (Wong et al., 2006).

Human activities with a noticeable impact on the environment, and consequent contribution to soil and RDS composition in urban settings, typically include traffic-related activities such as fossil fuel combustion, wear and tear of vehicular parts (Chow, 1970; Ornektekin, 1997; Councell et al., 2004; Thorpe and Harrison, 2008; McKenzie et al., 2009; Wik and Dave, 2009); leakage of metal-containing motor oils (Schipper et al., 2007; Sonntag et al., 2012); industry-specific activities (Kelly et al., 1996; Dudka and Adriano, 1997; Govil et al., 2001; Loredo et al., 2003; Krishna and Govil, 2004; Nadal et al., 2004), power generation plants (Mulchi et al., 1990; Pudasainee et al., 2010), the disposal of municipal solid wastes either by incineration or landfill (Lisk, 1988; van der Sloot et al., 1996; Gworek

et al., 2008; Azeez et al., 2011), and the corrosion of construction/building materials (Kayhanian et al., 2009; Engelsen et al., 2012), as summarised in Figure 1 and Table 1:

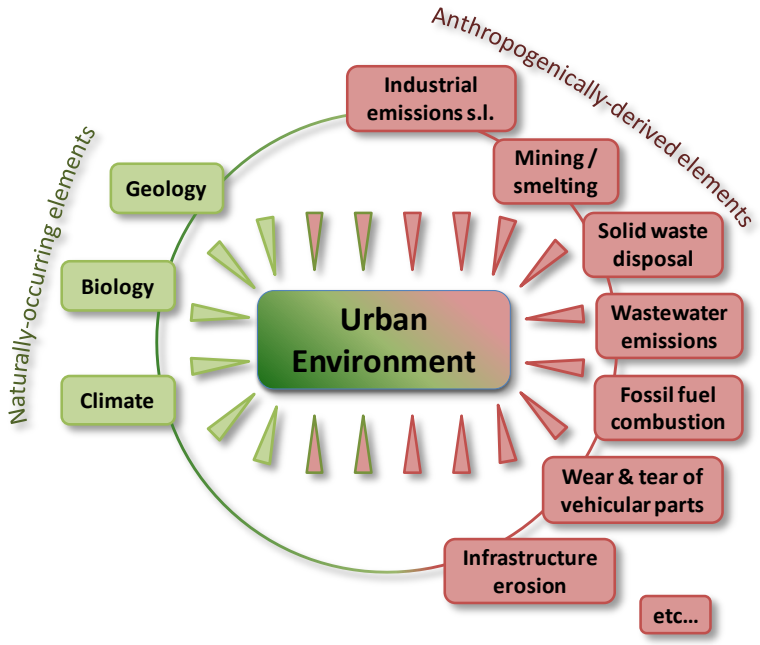


Figure 1: Main influencing factors on soil and sediment composition in the urban environment.

| Activity | Main elements | References |
|---|---|---|
| Fossil fuel combustion *s.l.* | Pb, V, Cd, Cr, Hg, Mn | Nadal et al., 2004 |
| Power generation | Hg, Pb, Cr | Pudasainee et al., 2010; Mulchi et al., 1990 |
| Industry *s.l.* | Pb, Cu, Zn, Cd, As, Ni, Hg | Loredo et al., 2003; Govil et al., 2001; Kelly et al., 1996 |
| Mining / Smelting | Cu, Pb, Zn, As, Cd, Cr | Dudka and Adriano, 1997 |
| Waste disposal (incineration/landfill) | Zn, Cd, Cr, Pb | Azeez et al. 2011; Gworek et al., 2008; van der Sloot et al., 1996; Lisk, 1988 |
| Erosion of construction/building materials | Cr, Cd, Ni, Pb, Zn | Engelsen et al, 2012; Kayhanian et al., 2009 |
| Car exhaust | Pb, Ni | Ornektekin, 1997; Chow, 1970 |
| Brake linings | Cu, Zn | McKenzie et al., 2009; Wik and Dave, 2009; Thorpe and Harrison, 2008 |
| Tyre wear | Zn, Pb, Cu | McKenzie et al., 2009; Thorpe and Harrison, 2008; Councell et al., 2004 |
| Leakage of motor oils | Zn, Cu, Cr | Sonntag et al., 2012; Schipper et al., 2007 |

Table 1: Human activities with potential deleterious impacts on the environment.

Soils and RDS importance as sinks of PHE in urban environments makes them valuable pollution proxies, and environmental risks can be directly inferred from their geochemical analysis as further discussed. However, the resuspension of soil and RDS particles into the atmosphere or their introduction in water systems may affect human populations by different pathways, as atmosphere, soil and water cannot be regarded as independent systems in what concerns human exposure to trace metals (Preciado and Li, 2006; Owens et al., 2011). For instance, a large amount of urban atmospheric particulates is wind-blown dust derived from soil and sediment, together with industrial, residential and vehicular emissions (Young et al., 2002; Thorpe et al., 2007; Johnson and Demetriades, 2011; Laidlaw et al., 2012); and sediment composition in urban river basins has been shown to be heavily influenced by contaminated soil and RDS wash-off (Ball et al., 1998; Carter et al., 2003; Taylor and Owens, 2009). Figure 2 is a summary of these interactions in urban systems.

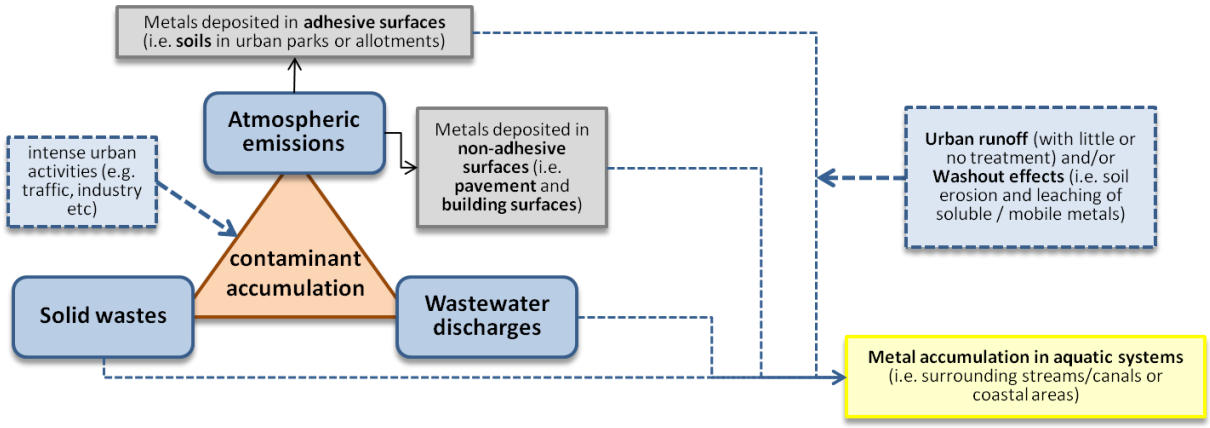


Figure 2: Summary of the possible sources/pathways of metals in urban areas (adapted from Wong et al., 2006).

### *1.3.1. Impacts on air quality*

Direct inhalation of air particulates, especially secondary anthropogenic particles ($PM_{10}$, $PM_{2.5}$), has been proven to impact on human health (Fang et al., 2005; Zuurbier et al., 2011). Motor vehicle exhaust (direct tailpipe emissions from trucks and automobiles) is one of the most important sources of fine particulate matter in the polluted urban environment, as well as industrial emissions which have also been proven to contribute to the total atmospheric particulates in areas where industry is present (e.g. Querol et al., 2001; Ragosta et al., 2002; Razos and Christides, 2010). Large quantities of particles are also reintroduced into the atmosphere by the resuspension of RDS and soil by motor vehicle traffic. As an example, the study performed by Hildermann et al. (1991) addressed the average chemical composition of fine particulate atmospheric emissions from various source types, including tailpipe exhaust emissions from automobiles and heavy-duty diesel trucks, and non exhaust particles such as paved road dust, brake dust, tyre dust and vegetative detritus, among others. Receptor modelling calculations have found that exhaust emissions accounted for approximately 21-49% of the annual average primary fine organic aerosol in the Los Angeles urban area in 1982. These results agree with those later obtained by Schauer et al. (1996) where motor vehicle exhaust accounted for approximately 10 to 36% of the fine particulate mass concentration at the urban sites at Bakersfield and Fresno, USA. Hildermann et al. (1991) also refers that following motor vehicle exhaust, paved road dust was also one of the largest sources of fine particulate matter emissions to the Los Angeles (USA) urban atmosphere, mainly due to the resuspension of RDS by passing traffic and wind turbulence - Lenschow et al. (2001) quantifies the non-exhaust contribution to air particulate matter in Berlin, Germany and concludes that it may account for 45% of the total PM10 concentration. The most significant sources of non-exhaust particulate matter through resuspension are the abrasion of brake and tyre components of vehicles, abrasion of the road surface itself, and soil particles. The latter has been quantified in Bakersfield, California, by Young et al. (2002): 74% of PM10 was composed of soil.

In spite of the ubiquitous presence of minerals with low risk to human and environmental health in atmospheric particulates, which are mainly sourced from the resuspension of soil (and RDS, which in turn contain mineral soil particles), it may also be the source of potentially harmful elements in areas affected by severe historical or present-day soil pollution. Lead has been documented to be sourced mainly from lead-contaminated soils in the atmosphere of Pittsburgh, Detroit, Chicago and Birmingham, USA (Laidlaw et al., 2012). This soil contamination is mainly the result of the past use of lead additives in gasoline, the use of lead in exterior paints, and industrial lead sources. Several other studies have reported the importance of soil particles in the atmosphere, e.g. Lenschow et al. (2001), Fang et al. (2005), and Young et al. (2002), cited above.

While control regulation on atmospheric emissions has led to a substantial reduction in exhaust emissions from road traffic, currently non-exhaust emissions from road vehicles and the resuspension of soil and RDS are unabated (Thorpe and Harrison, 2008). Knowing that trace metals primarily accumulate in the finest fractions of the sediment (Sutherland et al., 2008; Luo et al., 2011; Sutherland et al., 2012), the study of soil and sediment grain size is also of major importance in terms of its potential contribution to respirable air particulates.

### *1.3.2. Impacts on water quality*

The increased transport of particulate-bound metals, or dissolved phase metals, to sewer systems and receiving water bodies during periods of increased rainfall have important impacts upon water quality - materials are mainly supplied via road drains which, in turn, often discharge directly into rivers (Taylor et al., 2008). Soils and RDS in urban systems make a large contribution to the transported metal loading, and these media have been reported to be the main diffuse sources of contaminants in urbanised drainage basins (Sutherland and Tolosa, 2000; Preciado and Li, 2006; McKenzie et al., 2009).

A quantitative assessment of the contribution of RDS to the River Aire (UK) was attempted by Carter et al. (2003), who reported that 19 – 22% of the contaminated sediment flux in the urban river reaches was derived from the road network. Similarly, Yin and Li (2008) found that 60% of the suspended sediments at the outlet of a sewer system in Wuhan City, China was derived from the drainage system (gutter sediments and combined sewer sediments), with about 40% from RDS. As a consequence, the management of urban sediments is a key requirement for sustainable urban development. For example, regular removal of RDS by street sweeping may lead to a significant reduction in both sediment contamination levels and contamination of surface runoff, as shown by Sartor and Gaboury (1984). These authors showed that a maximum of about 30% of the total solids and 40% of the total lead concentrations associated with the street surface contamination could be removed by intensive street cleaning.

The impact of the urban soil contribution to the contamination of waters has been seldom reported, except when jointly described with RDS. Nevertheless, studies of trace metal contamination inputs from soils into waters in agricultural regions are more advanced, as these soils cover extensive areas which affect water quality as precipitation infiltrates and percolates through the soil system, ultimately affecting groundwaters and river systems at a larger scale (He et al., 2005). The impact of soils alone on water quality in the urban systems has therefore been more prominently reported in terms of soil erosion and its presence in RDS, as in the examples of the previous paragraph, rather than in terms of water contamination by soil leaching (e.g. Badin et al., 2009).

During rainfall events, the discharge in urban basins responds more rapidly due to both the impervious nature of urban land surfaces and the engineered nature of urban rivers and waterways. In urban runoff events, finer grain sizes (which carry higher metal concentrations) are more easily mobilised from the road network and exported towards the sewer system and river network (Taylor and Owens, 2009). Grain size characteristics is related to fluid transport theory, as it is well known that sediment grain size is an important factor controlling entrainment and transport thresholds (Bridge, 2003; Sutherland et al., 2012).

Sediment-associated contaminant impact on urban water systems remains as a big issue in terms of contaminant storage in urban river basins: more attention needs to focus on upscaling and connecting urban areas to the rest of the river basin, and sediment management strategies need to be carefully considered within urban systems and river basins (Taylor and Owens, 2009).

### *1.3.3. Impacts on human health*

RDS and soil direct pathways to human exposure include the inhalation of contaminated airborne particulates from indoor and outdoor air, the direct ingestion of contaminated soil, RDS and indoor dusts (specially by children), the ingestion of home-grown or allotment-grown produce, and the absorption of the contaminant through skin contact (Lisiewicz et al., 2000; Hough et al., 2004; Hooker and Nathanail, 2006; Pereira et al., 2007; Laidlaw and Filippelli, 2008).

The impacts of the inhalation of airborne particulates have been widely studied, e.g. (Brunekreef and Forsberg, 2005; Davidson et al., 2005; Delfino et al., 2005) and the contribution of soils and RDS to the mass loading of these airborne particles is unarguable. Air pollution has both acute and chronic effects on human health, affecting a number of different systems and organs. It ranges from minor upper respiratory irritation to chronic respiratory and heart disease, lung cancer, acute respiratory infections in children and chronic bronchitis in adults, aggravating pre-existing heart and lung disease, or asthmatic attacks. In addition, short- and long-term exposures have also been linked with premature mortality and reduced life expectancy (Kampa and Castanas, 2008).

Children are the most affected by direct contact with contaminated soil and RDS: the relationship between atmospheric particulate loading and blood Pb levels in children has been found to have a strong relationship (Laidlaw and Filippelli, 2008), as well as soil Pb and blood Pb levels (Mielke and Reagan, 1998). The latter is mainly due to direct ingestion through hand-to-mouth behaviour, given the close interaction of children with the soil and floor surfaces of the environment, producing an extraordinary exposure response by children (Calabrese et al., 1997; Mielke et al., 2011; Shi et al., 2011). Human exposure to contaminants by ingestion of soil can also happen through the consumption of home-grown or allotment-grown produce or by a traditional subsistence lifestyle (Bacigalupo and Hale, 2012; Doyle et al., 2012). Hough et al. (2004) performed a risk assessment of metal exposure to population subgroups living on, and growing food on, urban sites and calculated hazard indexes (HI) using average daily doses from soil ingestion for the three population subgroups and for five metals (Cd, Cu, Ni, Pb and Zn). In all cases, most of the calculated HI was attributable to dietary exposure (average person 94%, highly exposed person 86%, highly exposed infant 73% of the HI).

Although having a lower relative importance than inhalation and ingestion in terms of adverse human health effects, skin absorption of trace metals may also occur in specific exposure conditions. As an example, the study by Fillon et al. (2009) suggest that is necessary to prevent skin contamination when using toxic substances, as besides absorption through the skin, a small injury to the skin barrier can significantly increase skin absorption to the studied metals, namely Co, Ni and Cr. This kind of exposure can be frequent among e.g. workers of metal refineries, welders and metalworkers (Hinnen and Elsner, 1995; Du Plessis et al., 2010).

The exposure to trace metals, with clear negative consequences on human and ecosystem health, has led to the establishment of a number of regulations in many countries, mainly focusing on water, air and soil pollution, discussed in the following section.

## 1.4. Trace metals in soils

As previously outlined, soils act mainly as sinks for pollution, as the contaminant species tend to remain and increase their concentration in soils through time, and the close proximity to human populations in urban systems enhance the probability of exposure with consequent adverse human health effects. Pollution caused by trace metals in soils is a serious environmental issue because, in comparison with air and water, the soil has a much lower ability to recover from contamination (Violante et al., 2008). In addition, as pollutants can remain in urban soils for long periods, they may also act as sources of further pollution in urban environments (Luo et al., 2011).

It is inarguable that in the last decades, anthropogenic inputs to soils have had a large impact on trace metal concentrations worldwide, from a variety of sources. Nriagu and Pacyna (1988) attempted to quantify these inputs to soils, and the inventory clearly suggested that the principal

sources of trace metals in soils were the disposal of ash residues from coal combustion, the general wastage of commercial products onto land and urban refuse. An interesting finding was that wastes associated with municipal sewage sludge may not be a particularly important source on a global scale, but its trace metal content was often so high on the local scale that it represented one of the most important sources of metal contamination in soils. Values reported therein refer back to 1988 but are yet a good example of how significant is the human influence on the chemical environment.

In soil, trace metals can be involved in many chemical and biological reactions, such as solution and surface complexation, precipitation, sorption-desorption, and oxidation-reduction. In addition, these elements interact strongly with soil components (e.g. minerals, humic substances, microorganisms) depending on the physico-chemical and biological conditions of the soil (Violante et al., 2008). Hence, the risk of metal release from soils into other environmental compartments if physico-chemical conditions are changed needs to be taken into account when assessing the risks posed by elevated trace metal concentrations in soil.

Trace metals are significant natural components of all soils where their presence in the mineral fraction comprises a store of metal species as important components of clays, minerals, iron and manganese oxides, and other organic and inorganic ligands that, in turn, have a significant influence on soil geochemistry (Gadd, 2007). Trace metals are also present in the organic fraction, frequently as bound forms, with some metal recycling occurring as a result of organic matter decomposition. The aqueous phase provides a mobile medium for chemical reactions, metal transfer and circulation through the soil, to organisms, and also to the aquatic environment (Violante et al., 2010).

Trace metal contamination in soils is known since human kind started to extract, concentrate and transform metal ores - historical contamination may date to many centuries ago (Demetriades, 2011). However, it was the Industrial Revolution and the continued industrialization into the 20$^{th}$ century that caused the most severe detrimental effects on soils (Johnson and Demetriades, 2011). Pioneer studies of trace metals in soils of urban areas emerged shortly after it was recognized that the enhancement of metal concentrations in soils could be attributable to general urban air, e.g. fallout from metallurgical industrial activities (Goodman and Roberts, 1971). The awareness of the effects of certain trace metal enrichments on human and ecosystem health dictated that these first studies were mainly focused on Pb, Cd and Hg (Klein, 1972; Linzon et al., 1976; Solomon and Hartford, 1976; Davies, 1978; Carey et al., 1980). This growing awareness also led to the simultaneous development of laws which required county councils in the United Kingdom to submit structure plans containing strategic development proposals for approval. The structure plan provided the framework within which the planning and environmental problems of an area could be examined and related policies developed. A major component of the report on environmental pollution and the condition of land consisted on the assessment of aerial and terrestrial contamination by the

biologically significant metals Pb, Cd, Zn and Cu (Parry et al., 1981). Legislative demands have driven a lot of the soil research since then as soil quality was recognized as fundamental for human and ecosystem health and the sustainable development of urban areas.

### *1.4.1. Preventing the impact of soil pollution on human health: legislative drivers*

The known impacts of trace metal contamination in soils on human health and the recent regeneration of urban areas require that developers, planning authorities and regulators consider more fully the implications and impact on the environment of large-scale development initiatives. This is regulated by legislative frameworks established in the last decades: a review of soil policies can be found in Hannam and Boer (2002). The main purpose of the application of soil laws is to protect the soil while using it sustainably, through the prevention of further degradation, the preservation of soil function and the restoration of degraded soils. Nevertheless, soil legislations are not static and change as the scientific knowledge is improved, and strategies differ from country to country - in order to level the standards in European countries, the European Commission is currently preparing a proposal for a Soil Framework Directive (COM/2012/046) (EU, 2012) following the Thematic Strategy for Soil Protection (COM/2006/231) presented in 2006 (EU, 2006).

In the United Kingdom, where the current study takes place, part 2A of the Environmental Protection Act 1990 outlines an extended statutory regime for the identification and remediation of contaminated land (DEFRA, 2006). As well as acting to prevent new contamination, it also deals with a substantial legacy of land which is already contaminated, for example by past industrial, mining and waste disposal activities. The main objective underlying the introduction of the Part 2A contaminated land regime was to provide an improved system for the identification and remediation of land where contamination is causing unacceptable risks to human health or the wider environment, assessed in the context of the current use and circumstances of the land. This approach recognises that the risks presented vary greatly according to three main factors: 1) the presence of the contaminant in a concentration that may cause significant harm; 2) the proximity of receptors (e.g. humans, ecosystems, groundwater) that could be adversely affected by the contaminant; and 3) the existence of a pathway capable of exposing a receptor to the contaminant (DEFRA, 2006), as schematically represented in Figure 3.


Figure 3: Concept of source, pathway and receptor in the assessment of contaminated land (adapted from Fordyce and Ander, 2003; DEFRA and EA, 2004).

To determine whether land is contaminated, there is a need to establish values or thresholds above which substances may cause harm to receptors. In relation to human health, Health Criteria Values (HCVs) have been derived in a toxicological basis, and these values serve as benchmarks for protecting human health (EA, 2009a). In conjunction with chemical exposure modelling methods, these HCVs enabled the derivation of Soil Guideline Values (SGVs) that may be used in the overall assessment of risks to human health from land contamination. These consider the pathways through which human health can be affected. Both HCV and SGVs are developed and updated by the Contaminated Land Exposure Assessment (CLEA) project of the Environmental Agency, that therefore provides all the technical guidance to regulators and their advisors in support of the statutory regimes addressing land contamination, particularly Part 2A of the Environmental Protection Act.

### *1.4.2. Geochemical survey of the UK: the G-BASE project*

To aid the requirements of environmental legislation and the need to redevelop brownfield sites in urban environments for sustainable planning, geochemical surveys of soil were initiated in many countries, such as the systematic soil survey performed in the UK by the British Geological Survey (BGS) under project G-BASE - Geochemical Baseline Survey of the Environment, which is still a work in progress (Johnson et al., 2005). As of 2011, approximately 88% of the British land territory had been sampled by G-BASE, with over 50000 soil samples collected (Flight and Scheib, 2011). It was acknowledged in 1992 that, as the regional geochemical sampling campaign passed through the country, urban centres should be routinely included, and by 2010 the survey had been completed in 26 UK cities (Flight and Scheib, 2011) including Manchester, data which is part of the present work. Based on the G-BASE soil survey, numerous papers and reports have been published to date and scientific research has been developed in several areas, such as geochemical mapping, medical geology (human and animal health), environmental geochemistry, urban geochemistry, and geological and soil science (Johnson, 2006; BGS, 2012a).

At first, the UK geochemical survey began with a main focus on mineral prospecting, rather than environmental issues. Stream sediment collection was initiated, as these sediments can be used as indicators of the elemental concentrations in the drainage catchment upstream from the sampling site. Soils then started being collected from areas in which stream sediment sampling was not possible, but the importance of soil collection was soon revealed for areas where agriculture is more intensive and population density is greater. G-BASE now routinely collects soils from every second kilometre square of the British National Grid by random selection within each square, as well as stream waters.

Nevertheless, the soil sampling density in urban areas is higher than in rural areas (1 per 0.25 $km^2$), with samples collected as close as possible to the centre of 500 x 500m sub-cells from within each UK

National Grid kilometre square (based on 1:25000 scale Ordnance Survey maps). Common sites for collection include gardens, parks, road verges, open spaces, school yards, sports fields and waste ground (BGS, 2012b).

Following geochemical analyses, the results undergo rigorous quality assurance procedures (Johnson et al., 2005) and geochemical data can then be presented in a number of formats. In addition to presenting results in a series of geochemical atlases, G-BASE rural and urban samples and data are utilized in a wide range of applications and reported in peer-reviewed publications. The project has also made significant contributions to documents prepared by BGS for government bodies in response to legislation and directives in connection with pollution and contamination (Johnson et al., 2005 and references therein). Figure 4 is an example of a geochemical map produced under the G-BASE project, where Pb in surface soils is represented. These maps give a clear image of the distribution of concentrations over the area, allowing the easy recognition of high/low concentration patterns. Regional geochemical datasets like these can be used e.g. to interpret subtle geological changes; to demonstrate the relationships between soils, heavy metal pollution and parent material; in archaeology; and in surface water research (Johnson et al., 2005).

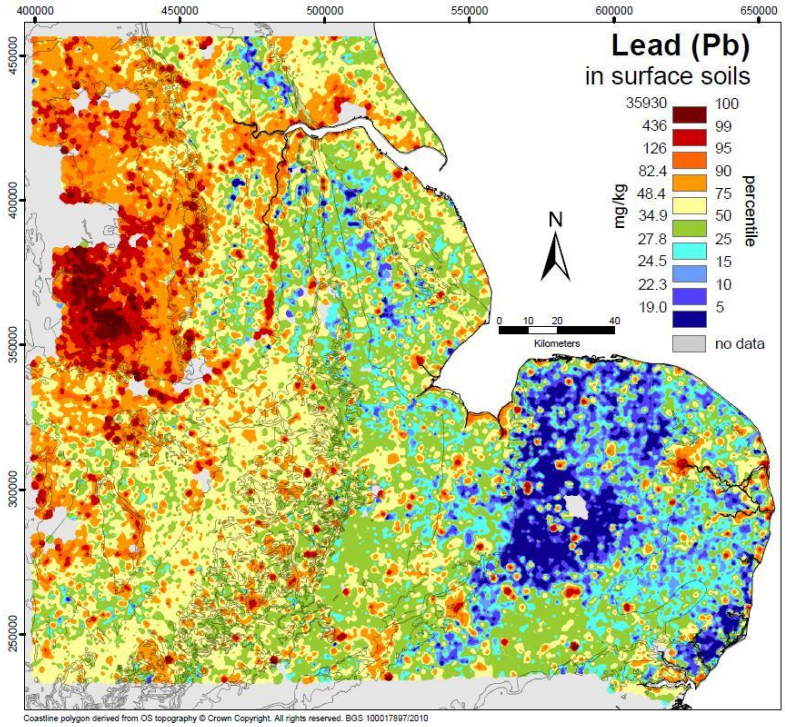


Figure 4: Spatial representation of Pb concentrations in soils of the Northeast England (reproduced with permission from BGS, 2010).

The BGS hosts the UK National Geosciences Data Centre (NGDC) and the G-BASE samples form a part of the national geological sample archive. In addition, urban geochemical datasets for soils have also been published as a series of BGS reports from the G-BASE project (e.g. Brown, 2001a; Fordyce and Ander, 2003; O'Donnell et al., 2004; Fordyce et al., 2012).

The main purpose of systematic urban geochemical mapping under the G-BASE project is to provide an overview of soil quality in the urban environment as a framework to planning and management (Fordyce and Ander, 2003). The data provide a useful insight into the likely controls on element distributions in the urban environment and general relationships with land use, ground types and possible sources of contamination. The overall urban signature is established, so that areas of concern within a city can be highlighted and detailed site investigation and contamination studies can be assessed in terms of the urban geochemical profile in addition to the rural background (Fordyce et al., 2005). The definition of background elemental concentrations in rural environments and enrichment in urban areas is the first step to the further comparison studies between different cities and their spatial and statistical distribution of potentially harmful elements (PHE) (Fordyce et al., 2005). Through the work done by the G-BASE project, it is also possible to identify potential sources of PHE and their distribution for each studied city. Elevated concentrations are typically associated with different ground types and land use – for example, samples collected over made grounds in the Stoke-on-Trent area showed enrichments for the majority of elements, with the exception of $SiO_2$ and MgO, when compared to the rural periphery (Fordyce and Ander, 2003). Different distribution of PHE among different made ground types was also observed – in the same study, specific geochemical signatures were identified for soils developed over colliery waste, domestic or industrial waste, ceramic waste and ironworks slag. As an example, Figure 5 shows urban geochemical maps of Cardiff, Kingston-upon-Hull, Stoke-on-Trent and Glasgow. Pb concentrations are represented as proportional symbol maps, clearly highlighting problematic areas.

The geochemical data obtained by the G-BASE project also have applications to legislative drivers like part 2A of the Environmental Protection Act, which places the responsibility for the identification, assessment, remediation and monitoring of contaminated land with local authorities. The identification of contaminated land relies on the concept of risk assessment, based on a pollutant linkage whereby the presence or source of contamination has the potential to impact on a receptor by means of a pathway, as previously discussed. This approach requires that land be assessed for redevelopment on a site-specific basis – the G-BASE survey highlights potentially contaminated areas, which can be followed up for more detailed investigation. Furthermore, the G-BASE project provides information for all elements (As, Cd, Cr, Pb, Ni and Se) for which SGVs are defined by the Contaminated Land Exposure Assessment of the UK Environment Agency, with the exception of Hg.

The systematic geochemical surveys of the UK carried out by the BGS have evolved throughout time mainly driven by different purposes – from mineral exploration in the past to present day legislative demands – and this has allowed different approaches to be used depending on the media

analysed (e.g. stream sediments and soils) and the techniques used for sampling, chemical analysis and data analysis/interpretation.

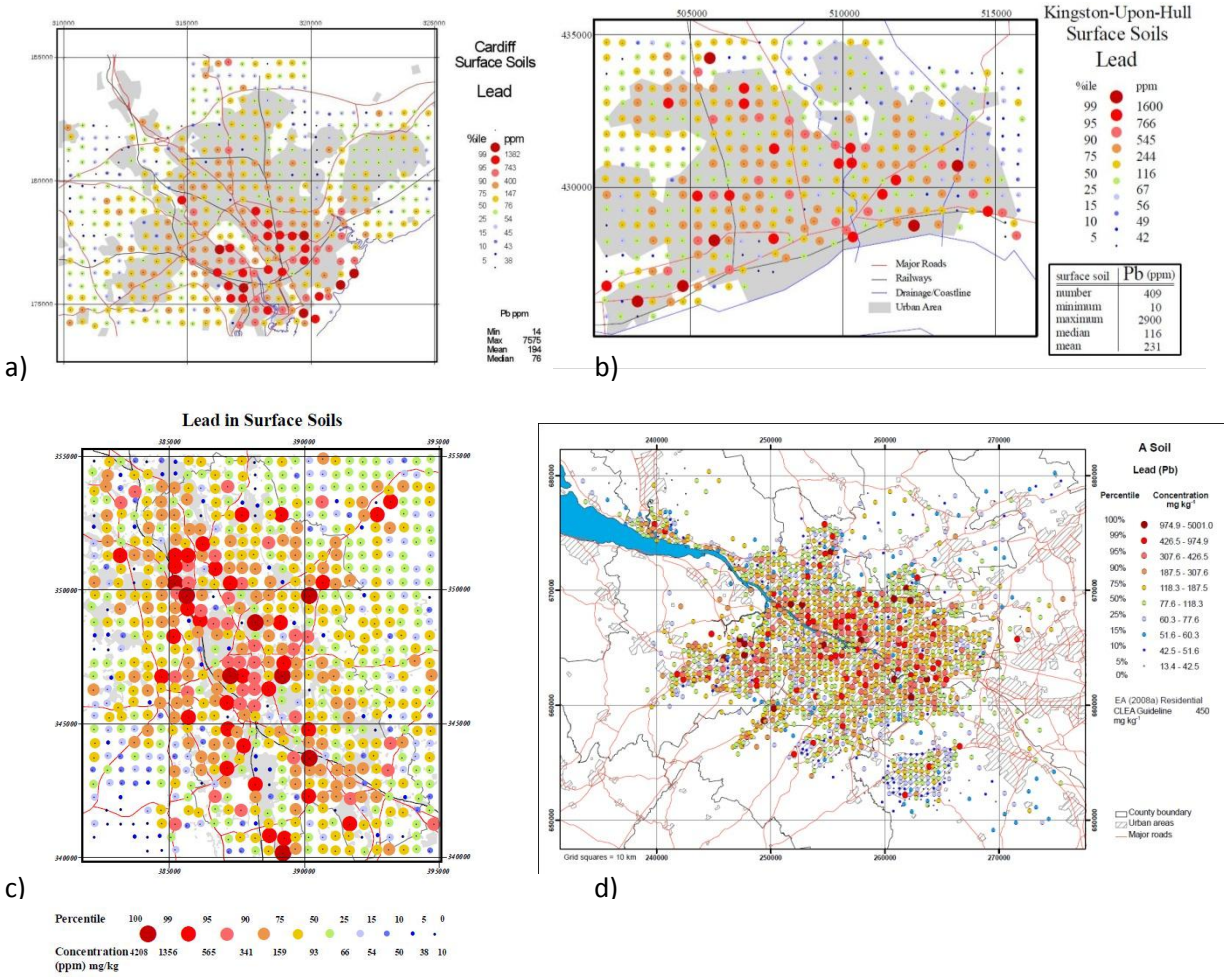


Figure 5: Spatial representation of Pb concentrations in soils of (a) Cardiff (reproduced with permission from Brown, 2001a), (b) Kingston-upon-Hull (reproduced with permission from O'Donnell et al., 2004), (c) Stoke-on-Trent (reproduced with permission from Fordyce and Ander, 2003) and (d) Glasgow (reproduced with permission from Fordyce et al., 2012).

However, the results of these surveys have shown, and continue to show, that the methodology successfully defines the geochemical baseline to a high degree of resolution and produces data with a wide range of applications (Johnson et al., 2005). In addition, quality control procedures have maintained a consistency in the data. Projects such as G-BASE operate on a long-term strategy that meets the needs of a wide variety of applications by producing a systematic and highly controlled database of geochemical results that will be an asset to the nation and in use for many generations (Johnson et al., 2005).

### *1.4.3. Assessing trace metal contamination in soils*

Trace metals are ubiquitously present in natural and undisturbed soils in concentrations that can be considered a natural, geogenic background, which varies depending on the parent materials and the intensity of the pedogenic processes. However, as outlined previously, anthropogenic inputs to

soils add to these baseline trace metal concentrations - soils may become *contaminated* with these elements.

Soil quality may be one of the most contentious topics ever discussed by the soil science community, and several definitions can be taken for soil quality as reported in Karlen et al. (1997), who also suggest that it can be defined as "the capacity of a specific kind of soil to function within natural or managed ecosystem boundaries to sustain plant and animal productivity, maintain or enhance water and air quality, and support human health and habitation". A general assumption regarding soil quality is that a soil can be considered contaminated with potentially harmful elements if their concentration is above established guideline values, and may therefore cause harm to receptors. Soil guideline values differ between countries, as displayed in Table 2.

In the UK, trace metal contamination can be evaluated by comparing elemental concentrations to the established guideline values according to the present or pretended land use, as previously referred in section 1.4.1. These SGVs are derived from health criteria values (HCVs), which are established from a review of the evidence from occupational and environmental epidemiological studies, animal studies, and from scientific understanding of the mechanisms of absorption, transport, metabolism and toxicity of chemicals within the human body.

| Element | Former UK ICRCL soil guideline (1) | Former UK SGV (2) | | | Proposed UK Ecological Guideline (3) | Dutch Soil indicative (target) values 2000 (4) | Dutch Soil Intervention Values 2009 (4, 5) | US-EPA Generic Soil Screening Levels (6) |
|---|---|---|---|---|---|---|---|---|
| | | Residential with plant uptake, or allotment | Residential without plant uptake | Commercial/ industrial | | | | |
| As | 10 | 20 | 20 | 500 | | 29 | 76 | 0,4 |
| Ba | | | | | | 160 | | 5500 |
| Cd | 3 | 1 | 100 | 100 | 1,15 | 0,8 | 13 | 78 |
| Co | | | | | | 9 | 190 | |
| Cr | 600 | 130 | 500 | 2000 | 21,1 | 100 | 180 | 390 |
| Cu | 130 | | | | 88,4 | 36 | 190 | |
| Mo | | | | | | 3 | 190 | |
| Ni | 70 | 50 | 75 | 5000 | 25,1 | 35 | 100 | 1600 |
| Pb | 500 | 450 | 450 | 750 | 167,9 | 85 | 530 | 400 |
| Sb | | | | | | 3 | 22 | 31 |
| Se | 3 | 35 | 260 | 8000 | | 0,7 | 100 | 390 |
| Sn | | | | | | | 900 | |
| Tl | | | | | | 1 | 15 | |
| V | | | | | | 42 | 250 | 550 |
| Zn | 300 | | | | 90,1 | 140 | 720 | 23000 |

Table 2: Soil guideline values: 1 - ICRCL (1987), 2 - EA (2002), 3 - EA (2008), 4 - VROM (2000), 5 - VROM (2009), 6 - US-EPA (1996).

The derivation and application of these values is explained in detail in the Environmental Agency report "Human health toxicological assessment of contaminants in soil" (EA, 2009a). To simplify the assessment of human health risks arising from long-term and on-site exposure to chemical contamination in soil, SGVs have been derived from the HCVs. SGVs are guidelines on the level of long-term human exposure to individual chemicals in soil that, unless stated otherwise, are tolerable

or pose a minimal risk to human health. They represent “trigger values” – indicators to a risk assessor that soil concentrations above this level may pose a possibility of significant harm to human health. Therefore, SGVs can be used as a starting point for evaluating long-term risks to human health from chemicals in soil; and also as an indication of chemical contamination in soil below which the long-term human health risks are considered to be tolerable or minimal (EA, 2009f). Examples of SGVs for As, Ni, Cd and Se are shown in Table 3.

| | As (inorg.) | Ni | Cd | Se |
|---|---|---|---|---|
| Residential | 32 | 130 | 10 | 350 |
| Allotment | 43 | 230 | 1.8 | 120 |
| Commercial | 640 | 1800 | 230 | 13000 |

Table 3: Current UK Soil Guideline Values in mg/kg according to land use. Adapted from Science Reports SC050021, CLEA (EA, 2009b; e; d; c).

If representative soil concentrations of chemicals on a site exceed the SGV, there are three options in terms of determining significant possibility of significant harm under Part 2A of the Environmental Protection Act (EA, 2009f):

- There may be no possibility of significant harm.
- There may be a non-significant possibility of significant harm.
- There may be a significant possibility of significant harm.

These possibilities are assessed taking into account local characteristics such as the proximity of receptors and the probability of a pathway capable of exposing the receptors to the contaminant. Therefore, for an accurate and local soil contamination assessment, SVGs need to be complemented with precise local information about land use before inferring about the possibilities of significant harm to human health (EA, 2009a).

## 1.5. Trace metals in RDS

Road deposited sediments are ubiquitously present in the urban environment and their study remotes to the late 1970’s, early 1980’s (Chow, 1970; Auermann and Bortitz, 1977; Hopke et al., 1980; Harrison et al., 1981), with the growing awareness about the potentially harmful substances contained in these media. Lead was the first element to be studied in detail in RDS, due its relation to leaded fuel combustion and the known hazards to human health (Duggan and Williams, 1977; Thornton et al., 1994; Sutherland, 2002). However, since leaded petrol use was phased out (in the UK this happened in January 2000), it has been documented that Pb concentrations in soils and RDS have dropped significantly. In Manchester, Pb concentrations fell by about 40% from 1975 to (Nageotte and Day, 1998). Nevertheless, nowadays some of the RDS composition is still unquestionably related to the combustion of fossil fuels, as demonstrated by most trace metal studies in RDS - traffic is always a common source.

RDS composition is therefore closely related to traffic and trace metal concentrations are expected to be higher close to major roads, intersections and areas where heavy traffic is frequent. But not only due to fuel combustion - the wear and tear of vehicular parts, brake linings and tyres have been documented to largely contribute to RDS trace metal content as non-exhaust vehicular sources - these are characterised in detail in Thorpe and Harrison (2008). RDS composition is also influenced by other factors, e.g. erosion of infrastructures, namely buildings and roads; atmospheric fallout, lubricating oils and grease, road gritting and inappropriate waste disposal, which may add several components to RDS trace metal composition.

Unlike soils, there are no guideline values derived exclusively for assessing RDS contamination. RDS values can be compared to SGVs, but it must be taken into account that RDS usually has a higher mobility potential and may affect populations through different pathways, more frequently by inhalation and involuntary ingestion of particles which are resuspended by wind or passing traffic. Textural variability is then very important when assessing the risk posed to human populations by contaminated RDS.

### *1.5.1. RDS morphology*

RDS is composed of a wide range of particle sizes, from coarse sands to clays; along with varying proportions of organic matter and anthropogenic materials - RDS texture is highly variable depending largely on local factors. Nevertheless, it is known that metals tend to be more concentrated in the finer fractions of the sediment (clay and silt). Most RDS studies determine trace metal concentrations in the fraction <1 mm or <2 mm, and the <63 µm fraction has been reported as the major host for metals in RDS, dominating almost all fraction loads for a given trace metal (Sutherland, 2002; Irvine et al., 2009; Krčmová et al., 2009; Sutherland et al., 2012). The higher metal concentrations found in the fine fraction can be attributed to the exponential increase in the surface area, charged surface, organic carbon content and sorbtive capacity which has been found to result with decreasing particle size (Robertson and Taylor, 2007).

While the <63 µm fraction is often the most important fraction for many metals, some studies have demonstrated that larger size fractions (>63 µm) may be more important for a few contaminants (e.g. Robertson and Taylor, 2007; Sutherland et al., 2008). In addition, the coarse nature often reported for RDS implies that the coarse grain fractions often contain most of the contaminant loading. Hence, it is important to account for the proportion of each grain size when discussing metal concentrations - an important index of contamination for RDS is the mass loading of a trace element in a given grain size fraction. For example, Robertson and Taylor (2007) reported that, although higher metal concentrations were found in the finer fraction, the dominant loading of all metals was in the coarser fraction due to its mass dominance. Another example is given by Sutherland et al.

(2008), where contaminants such as platinum group elements have been found to have greater concentrations within coarser fractions (>63 μm).

The recognition that contaminant loading and delivery are heterogeneously distributed relative to particle size is important when considering the management and pollution abatement of RDS. Particle size information is required in order to understand the complete environmental implications of RDS within urban environments (Taylor and Owens, 2009; Owens et al., 2011).

### *1.5.2. RDS mineralogy*

RDS mineralogical characteristics are largely dependent on the local sources of minerogenic particles and, like other RDS characteristics, are highly variable. The bulk RDS is frequently composed of significant amounts of quartz grains, followed by and silt and clay minerals, and these mineral materials have been reported to account for about 60% of each RDS sample (Gunawardana et al., 2012) - also Harrison et al. (1981) and Barret et al. (2010), using X-ray diffraction (XRD), showed that quartz is the dominant crystalline phase all in grain-size fractions of RDS. These derive mainly from nearby soils, which in turn can reflect local variations - Gunawardana et al. (2012) observed that RDS samples were predominantly composed of angular particles comprising of Si, Al, Ca and Na which primarily originated from surrounding soil, and that the clay-mineral suites in RDS were different between inland suburbs compared to coastal suburbs. The same occurred for soil samples collected in the same areas as RDS, supporting that the origin of RDS clay minerals is soil. The amount of soil contribution in RDS has also been reported to be of 76% (Hopke et al., 1980), and between 57% and 90% (Hunt et al., 1993), what has clear influences RDS mineralogy.

Few studies have looked into RDS individual grains, but valuable insights have been published by Birch and Scollen (2003), Taylor and Robertson (2009), Barrett et al. (2010), and Gunawardana et al. (2012). These studies focused on detailed, high-resolution, grain-specific mineralogical data.

Birch and Scollen (2003) used scanning-electron microscopy (SEM) techniques and reported that trace metals existed in RDS in three main forms: in the adsorbed phase (in the <63 μm grain size fraction), as particulate metal (in the 63 - 125 μm grain size fraction), and as inclusions in and on inert compounds. These last two forms of occurrence are coherent with the observations by Taylor and Robertson (2009), where samples were analysed by backscatter SEM, electron microprobe and Raman spectroscopy. RDS material was found to be composed of a number of grain types: (i) silicate and alumino-silicate grains derived from a wide range of sources (e.g. soils, building material, building stone, tarmac); (ii) iron oxide grains derived from the corrosion of galvanized steel; (iii) iron-rich glass grains derived as slag material from metal and waste processing activities and (iv) spherical Fe oxide and Fe-rich glass grains derived from high temperature combustion processes; and minor amounts of elemental metallic grains (Fe, Cu, Pb). Contaminant metal concentrations within silicate

and alumino-silicate grains were negligible. Iron oxide grains, on the other hand, contained high concentrations of metals (maximum values of 1.5% Pb, 2.1% Cu, 9.5% Zn, 7.5% Cr and 0.4% Ni), and this supports previous conclusions that the most important carrier for metals in RDS was the reducible fraction (iron oxides). Furthermore, the presence of both haematite and lepidocrocite, as identified by Raman spectroscopy, associated with high levels of Cr and Zn within the Fe oxide grains suggested that these metals originated from the corrosion of galvanized (Zn-plated) Cr-steel from vehicles. Iron oxide grains (haematite or magnetite) were also identified by Barret et al. (2010) in all the grain size fractions analysed. Iron-rich glass grains possessed similar concentrations of Pb, Cu and Ni to Fe oxide grains, but significantly lower concentrations of Zn and Cr (maximum values of 0.7% Cr and 0.4% Ni). These glass grains may have been derived from slag materials produced by metal-smelting or incineration of hazardous waste, which in turn are used in road material and concrete. Spherical Fe oxide particles present were likely to have been be derived from high temperature combustion processes.

Gunawardana et al. (2012) also using SEM imaging of RDS indicated, in addition to soil-derived particles, a high amount of elongated particles with rough surfaces resulting from abrasion, identified as tyre wear particles - elemental analysis indicated that these particles are mainly composed by Fe, Cu, Zn, Ni and Pb. Furthermore, a large amount of spherical particles with smooth surfaces were noted which could be fly ash originating from asphalt and coal combustion. Similarly, these had also been reported by Taylor and Robertson (2009) as iron-rich glass grains and spherical iron oxide particles.

### *1.5.3. RDS temporal variability*

RDS show a transitory, short-term nature within urban systems - Allott et al. (1990), using radiocaesium from the Chernobyl fallout event, has documented the residence time of sediment on street surfaces to be short, in the order of 150 to 250 days. Temporal variation in RDS has also been studied by Robertson and Taylor (2007), who documented that the main variations occurred in terms of metal concentrations, rather than grain-size distribution or organic matter contents. This indicates that these metal variations were the result of variation in sources and accumulation processes – Pb and Zn showed local variability with different temporal patterns at different sites, whereas Fe and Mn displayed consistent variability across sites, suggesting a common, larger-scale control on variability. Copper, expected to be less mobile, was the only metal which did not display any significant temporal variability. Lead and Zn have a common source with traffic, acting as indicators of traffic-related pollution, and this corroborates the fact that levels were lower in summer months when commuter densities dropped. In addition, more mobile metals may be washed away during wetter times due to their greater potential for dissolution, leaving behind more strongly bound

metals such as Cu. This is consistent with the fact that summer months were also the wettest, therefore lower concentrations were found with the exception of Cu. This suggests that metal concentrations in RDS are strongly influenced by weather.

Not only metal concentrations may differ between seasons, but also contaminant loadings. Based on the total road length within the sampled area of the city of Honolulu, Owens et al. (2011) equated an average accumulation of 724 and 198 kg of RDS per km of road, for the summer and fall sampling periods, respectively. This is consistent with the fact that the summer sampling may reflect, in part, material from sand and gravel applied to the roads as part of the winter road maintenance programme.

Nevertheless, it has been observed that larger RDS accumulations generally occur in the driest periods as wash-off events are rare. Coarser sediments may also be more predominant in dry seasons, as fine particles tend to be resuspended increasing the proportion of coarse grained material in the RDS.

## 1.6. The Manchester area and the legacy of an industrial past

The Manchester urban area evolved rapidly in the early 19th century from a series of small towns to a major industrial conurbation with huge material flows and worldwide trade connections (Douglas et al., 2002). A combination of the availability of nearby coalfields, canals, and free trade, which encouraged entrepreneurial enterprise, made Manchester into the 'shock' city of the industrial revolution. The current post-industrial phase in Greater Manchester has to cope with the environmental and social legacies of its industrial past, which have been related in detail by Douglas et al. (2002) - some of Manchester's historical facts extracted from their work are summarised in the text below.

Until the mid-18$^{th}$ century, the settlements of Manchester and Salford had strayed little from their medieval core at the confluence of the rivers Irk and Irwell. The long-established wool and linen textile industry were suddenly transformed by mechanisation in the late 18th century, and the increased volume of production made international trade the new core business of the city - by 1853, the British cotton industry supplied 45% of the total world consumption of cotton cloth (Douglas et al., 2002). The new steam-driven machinery which equipped hundreds of mills was fed by local coal supplied by river. In 1764 the Bridgewater Canal was finished, followed by the first passenger railway to Liverpool in 1830, and the Manchester Ship Canal, in 1894, which boosted even more the local economy. The built-up area also expanded greatly, and population was growing at a very fast rate.

Following the economical prosperity brought by the cotton trade, Manchester started to manufacture machinery of all types including textile machinery, steam engines and locomotives,

armaments, and machine tools. The dominance of cotton in the trade from Manchester fell in the late 19th century as the products of manufacturing and engineering grew in importance.

Manchester was the third port in the country by 1917, with a throughput of 3.84 million tons. The development of the Trafford Park industrial estate alongside the docks led to the creation of over 70000 jobs, in what was and still is the largest industrial estate in England.

All this progress came at a cost for the environment: for 200 years, the rivers of Greater Manchester presented a sorry record of deterioration in quality, as well as the atmosphere. The increasing industrialisation led to many mills, works and factories directly discharging many pollutants, including ashes and cinders, into rivers. Notable cases were the upper reaches of the Irwell where, before 1870, half the capacity of the channel was lost by dumped coal and furnace deposits; and the Manchester Ship Canal, which became polluted virtually as soon as it was completed in 1894, both from the already heavily contaminated River Irwell, the major source of water to the canal, and from the 519 out-falls of sewage and industrial effluent which feed into it. To alleviate this problem, gradual regulation was imposed on what could be discharged into rivers and by 1940, every local authority had its own sewage treatment plant on the banks of a river. Reduction in industrial discharges and the move from steam to diesel and gas power helped lower pollutant loads, but these were countered by an expansion in number of residences and in the per capita use of water and chemicals.

River water quality management has involved major expense since 1974. Much of the 19th century sewage system has been rebuilt, treatment plants have been upgraded, and most small sewage treatment plants have been eliminated. At present, the dock areas cut off from the river flow contain 3–4 m of contaminated sediments, a chemical time bomb from 80 years of environmental neglect. These sediments are heavily contaminated and removal would be both costly and unsafe. The solution is the isolation of the docks from the flowing water in the canal, and treatment of the largely anoxic water by permanent aeration and by bio-manipulation is being carried out.

While water-borne diseases were eased by the sanitary reform measures of 19th century, progress on those related to air pollution, especially bronchitis and other respiratory ailments, was virtually non-existent before 1900. It was not before 1930 that air quality control measures were established - Manchester was a pioneer city in smoke control measures with a campaign for clean air and smokeless zones. After the 2$^{nd}$ world war in 1946, Manchester became the first UK local authority to obtain powers (under Manchester Corporation Act) to establish ‘smokeless zones’. From the early 1960s onwards the reduced levels of smoke and $SO_2$ are clearly reflected in the reduction in deaths from bronchitis.

In the first decade of the 20th century, steelworks, further chemical industries and electric power stations were built in Trafford Park, beginning a period of concentrated point-source emissions which

did not end until the late 1980s and early 1990s. New plants had to install tall chimneys to expel airborne emissions high into the atmosphere, as proposed by the planning authority. Yet these chimneys only shifted the emission problem elsewhere, as pollution was then carried by the prevailing westerly airstream hundreds or thousands of kilometres, causing detrimental impacts further away. The Clean Air Act of 1956 and 1968, repealed and consolidated in 1993, has led to a remarkable decrease in atmospheric emissions through the prohibition of black smoke emissions, introduction of smokeless furnaces and strict control measures for grit and dust emissions.

In the 1960s, high octane petrol was hailed as a revolution in motor car engine efficiency; but a decade later, concern was raised about the impacts of lead emissions on health. As a consequence, lead-free petrol was introduced in 1986, and the technical adoption of catalytic converters was a further step in reducing motor vehicle emissions. The re-introduction of trams to the city centre and their replacement of trains on two suburban rail routes helped to reduce the use of motor vehicles in inner Manchester. Even nowadays, tramways and railways are constantly being updated and expanded.

By the last third of the 20th century, Greater Manchester faced the decaying legacy of the precocious growth of its urban fabric a century earlier. Even though there had been extensive rebuilding of housing around 1900, further slum clearance had to be carried out after 1955. Demolition of some 90 000 dwellings between 1957 and 1976 were carried out in the City of Manchester alone. Even the great infrastructure works on water supply dams, sewers, bridges and hospitals between 1850 and 1900 could not last forever, and Greater Manchester has faced a massive reinvestment in infrastructure renewal since 1975. To date, most of Manchester's Victorian sewers, bridges, dams and hospitals have been renewed, refurbished or replaced.

The rejuvenation of the city centre has seen former warehouses converted to apartments, student residences and office blocks. A good example of urban regeneration is the area of the former Port of Manchester, closed in 1977, which has been redeveloped as a desirable waterside location for modern offices, housing units and leisure pursuits, and is now called "The Quays". More recently, in 2011, the first phase of construction of the MediaCity UK has been finalised. This development's principal tenant is now the BBC, among many other media companies.

Other sites where redevelopment has focused are the over 900 closed landfill sites within Greater Manchester. Initially, these older landfill sites were located at the edge of the cities and towns, but with urban growth many of these sites which were once on the urban fringe became surrounded by settlements. Today, many of them have been converted to other land uses.

The industry has shifted from locations close to canals and former railways to more scattered industrial estates, some on brownfield sites, others in greenfield locations close to motorways and

other major traffic routes. Economic activity close to the core-city has some stability with a broad range of service industries, financial activities and three higher education institutions.

Manchester faced the problems associated with concentrated industry earlier than most places around the world. The British establishment viewed Manchester as a kind of experiment, seeing the city as both an indication of what economic progress really was and as a warning on the environmental and social problems that went with such progress. At present, some of these problems have been mitigated; others are identified for future action. Nevertheless, the legacy of past and present pollution sources still remains in water, air, soils and sediments; and a totally clean urban environment is still beyond realization.

## 1.7. Theoretical framework

As the urban populations grow, so does the importance of urban environmental quality: soils and urban sediments, namely RDS, are crucial media as they may cause direct deleterious human health effects when high trace metal concentrations occur. In dense urban areas, their proximity to receptors enhances the exposure probability through respiration, ingestion or dermal contact. As part of dynamic environmental compartments, soil and RDS contamination is probably linked and is also likely to affect air and water quality.

Manchester was considered the "shock" city of the Industrial Revolution, and has to cope with the environmental and social legacies of its industrial past. Air, water and RDS investigations in the Manchester area have been published, providing useful insights on the environmental conditions of this urban settlement. However, there is still a gap in the published literature in what concerns soil quality in Manchester. Soil contamination assessments have only been performed in a local basis to fulfil the requirements for urban regeneration and redevelopment. This leads to a few preliminary questions:

- ***To what extent have soils in Manchester been affected by anthropogenic contaminants? Is this due to past or present activities?***
- ***Are road-deposited sediments affected in a similar way?***
- ***Which Manchester areas show the highest trace metal concentrations in soils and RDS? Do these high concentration areas exhibit any spatial pattern?***
- ***What are the main sources of soil and RDS trace metal contamination in Manchester?***

These lead to the first step of this research: Sample collection and characterisation.

To assess soil contamination, 75Km$^2$ of urban Manchester, Salford and Trafford have been sampled by the British Geological Survey under project G-BASE (Johnson et al., 2005; Flight and Scheib, 2011), which is described in section 1.4.2. Sampling methodologies used are those developed by the BGS as described by Johnson (2005) and Allen et al. (2011), and summarised in section 2.2. The dense and regular mesh sampling scheme allows for a good representativity of soil geochemistry in an urban, heterogeneous area, as has been pointed out by the work developed by the BGS (Fordyce and Ander, 2003; Fordyce et al., 2005).

Whereas soil sampling methods have been developed and extensively applied since the early 21$^{st}$ century (e.g. Youden and Merlich, 1937; Cline, 1944), RDS is a relatively recent research subject and several sampling methods were reviewed for this study. Throughout the literature there have been reported many different methods for RDS collection. The dustpan-and-brush method for RDS sample collection has been widely used by several authors (Charlesworth and Lees, 1999; Birch and Scollen, 2003; Charlesworth et al., 2003; Barrett et al., 2010; Owens et al., 2011). It consists in using plastic-bristled brushes and plastic collection pans to remove the sediments of urban surfaces. Its simplicity

and low cost makes it a readily available technique which allows sampling of large areas in short periods of time. However, brushing a surface may imply the loss of a part of the fine material which gets resuspended in the atmosphere. Nevertheless, brushing has been revealed as essential to remove sediments which are more strongly bound to the surfaces, noticeably improving recovery rates when used before vacuuming a surface, as described next.

Vacuum systems for sample collection have been used by other authors (e.g. Ball et al., 1998; Bris et al., 1999; Herngren et al., 2006; Poleto et al., 2009), as this method is more efficient in retaining the fine fraction of the sediment, when this fraction is the main object of study. Bris et al. (1999) tested the efficiency of different vacuum cleaner-assisted RDS sampling strategies - dry vacuuming, wet vacuuming and combined brushing plus wet vacuuming. It was concluded that the third method had the best collection efficiency (over 95%), with approximately three times larger surface loads. Nevertheless, this process takes around 20-30 minutes per sample, 4 people to perform sampling, and requires more complex equipment (e.g. power generators) - such sampling obviously implies deviation of the car and pedestrian traffic.

Miguel et al. (1997), as well as Ordoñez et al. (2003) have chosen to sample RDS by brushing small areas of the road surface with a small paintbrush in 16 different locations in a square kilometre, in order to obtain a composite sample for that area. The use of just one composite sample per kilometre square was not appropriate for the present study as the Manchester area is highly heterogeneous, as well as sample characteristics.

In the works by Sutherland (2002; 2003; 2012) and Irvine et al. (2009) a plastic scoop was used to collect RDS. This method prevents the loss of fine grained material by resuspension, but does not allow for all of the sediment on the surface to be recovered, as road surfaces are mostly rough and sediment gets trapped in the meso- and micro-topography rugosities where the scoop does not reach. A sweeping approach practically eliminates this problem.

Every method has its pros and cons, but for the purposes of this work, the use of the dustpan and brush method is favoured. As RDS is temporally highly variable, the study area needed to be sampled as rapidly and effectively as possible so that, for each campaign, samples are collected under similar weather conditions and accumulation times on surfaces. The dustpan and brush method also does not require complex equipment or deviation of traffic, and has been proven to produce reliable results by the previously described studies. The problem of particle resuspension can be overcome by two approaches: when larger RDS accumulations are found, most of it is collected with the aid of plastic scoops before surface brushing. This retains most of the fine material, which tends to sit at the top of the RDS build-ups due to grain size sorting processes. In winter, RDS is generally moistened due to the constant dew/drizzle and low temperatures, even though sampling is carried out after

several days of dry weather. Smaller particles are therefore aggregated and this prevents them from being resuspended during sample collection.

Locations for the RDS collection were selected according to the scheme used for soil collection to test whether spatial variations and patterns in RDS are similar to those recorded for soils. However, as the sample density had to be different due to analysis costs and budget constraints – 1 sample per $km^2$ instead of the 4 per $km^2$ used for soils – RDS sampling locations were selected within each National Grid kilometre square as close as possible to the soil samples which exhibited highest trace metal concentrations. This way, both media may be compared in terms of geochemistry and mineralogy as soil/RDS paired samples, and the winter sampling scheme was first defined. However, some difficulties came up in the field in the end of January 2010, such as the absence of RDS sample in the designated locations due to extensive cleaning after the particularly snowy period of December 2009 – January 2010. Samples were then collected as close as possible to the originally planned locations. In June 2010 these locations were again sampled to account for seasonal changes in mineralogy and/or composition, as it is known that RDS is temporally highly variable. As sequential sampling of the same locations in determined time intervals was not feasible in the scope of the present research, it was chosen to perform sampling under contrasting conditions: over January (cold and wet) and June (warm and dry) (MO, 2010b).

After sample collection, a number of different methods need to be used in order to characterize soils and RDS.

- ***Which techniques can be used to determine soil and RDS composition, and provide a means of easy visualisation and interpretation of these data?***

First of all, both soils and RDS go through the same pre-treatment and bulk geochemical analysis by X-ray fluorescence (XRF) spectrometry at the BGS. XRF has become over the years a method of choice due to the large number of samples to be analysed in this kind of studies, as well as due to the lower limits of detection which are required for many trace elements of geochemical importance (Ingham and Vrebos, 1994). X-ray fluorescence spectrometry technique uses the detection of characteristic radiation, emitted by the atoms of a specific element after these have been excited by bombarding the sample with high-energy X-rays. The emitted radiation has a characteristic energy for each chemical element – its quantification is proportional to the amount of the element present in the sample. With the aid of the equipment software, elemental quantifications are obtained for each sample from the integration of the XRF spectra.

Geochemical data were obtained for both soils and RDS using the same methods of sample preparation and analysis at the BGS laboratories. Nevertheless, as the analysis took place at two different times (2002 and 2010), datasets needed to be checked for slight differences in XRF

calibration in order to make datasets analogous and allow more precise comparisons. The BGS has developed a method of data conditioning and levelling which is described in detail in Lister and Johnson (2005) and in section 2.9.1., which is applied in this work.

After data conditioning and levelling, basic statistics are always fundamental to broadly characterize chemical element distributions, such as the calculation of maximum, minimum, mean, median, standard deviation, variance, skewness and kurtosis for each chemical element / variable. Tests of normality and outlier detection are also routine procedures which are used herein.

As a first step towards answering the preliminary questions posed in the beginning of this section, geochemical data for soils and RDS were mapped using the GIS software ESRI® ArcGIS 10.0 The main objective at this stage was to find a means of easy visualisation which allowed for the delimitation of zones where trace element concentration is higher.

To easily assess spatial distributions of chemical elements and integrate geochemical data in specific areas, image analysis systems were developed from the earliest stages of regional geochemical research. At first, these systems were used for mineral exploration purposes, but soon applications were found concerning the environment and health (Green, 1984). The development of remote sensing systems linked to digital computer systems allowed for greater amounts of data to be handled, and the speed at which data could be processed was then improved. From then on, geochemical mapping became a powerful tool, allowing the development of digital-image data and the integrated study of geochemistry and other disciplines such as solid geology or hydrogeology.

The most common methods of geochemical mapping include the generation of interpolated surfaces, for which inverse distance-weighted and kriging functions can be used with satisfactory results (Yasrebi et al., 2009); as well as proportional symbol/colour maps, which has been extensively used by the BGS as a standard presentation method for urban geochemical data (Brown, 2001a; Fordyce and Ander, 2003; O'Donnell et al., 2004; Fordyce et al., 2005). These methods are applied to provide a spatial overview of soil and RDS geochemistry and highlight areas where high concentrations are found, as described in section 2.9.5.

Interpolated surfaces have the advantage of evidencing any spatial trends that might exist and are a robust presentation method for e.g. rural geochemical data, where element distributions tend to form regional patterns (Johnson et al., 2005). Nevertheless, urban geochemical mapping usually shows steep discontinuities associated with anthropogenic contaminants that are dispersed from point or diffuse sources. Smooth gradients, as those of geophysical maps, are therefore not expected when interpolating urban geochemical data (Reimann et al., 2011b).

Theoretically, kriging methods were shown to be substantially superior to the inverse distance weighting methods when applied to different surface types and sampling patterns (Zimmerman et

al., 1999); and have been used successfully in many studies (Rawlins et al., 2005; Hooker and Nathanail, 2006; Birke et al., 2011). However, Reimann et al. (2011b) suggested that methods not strongly based on statistical assumptions, such as IDW, should be the first choice when interpolating the spatial pattern of geochemical data, and numerous examples of this are available in the recent literature (Fordyce et al., 2005; Flight and Scheib, 2011). Depending on interpolation parameters used, kriging generally generates a smoother surface than IDW - therefore, in an urban environment, IDW might be more suitable to reflect sharp local variations.

As it has been pointed out before, it is necessary to bear in mind that the distribution of urban soils and RDS is highly heterogeneous and it has been proven that elemental concentrations can be significantly variable over short distances (Fordyce and Ander, 2003; Robertson and Taylor, 2007). Interpolation implies an extrapolation of elemental concentrations to areas where these have not been determined, and where surface soils or RDS might not be present. Therefore, in the present work, interpolation methods are not intended to serve as predictive techniques; they are used to provide a better way of evidencing spatial patterns. Alternatively, proportional symbol/colour maps avoid uncertain extrapolations and are also used in the present work.

The visual analysis of geochemical maps allows the definition of areas where elevated concentrations are found. Several hotspots are also evidenced and local variations and transport distances can be inferred. Mapping elemental concentrations is a first step towards identifying sources of contaminants in the urban Manchester area.

The patterns observed when spatially representing elemental concentrations in soils and RDS might often be related, as these concentrations may vary in a similar way across the area. This is due to elemental associations which depend mainly on element sources and/or accumulation processes.

- ***Which elemental associations can be found in soil and RDS?***

To clarify the relationships between different chemical elements, several multivariate statistical methods can be applied, such as factor analysis (FA), or principal component analysis (PCA) which are often confused with each other as both are variable reduction methods that can be used to identify groups of observed variables that tend to hang together empirically. The main difference between these two multivariate statistic types deals with the assumption of an underlying causal structure: factor analysis assumes that the covariation in the observed variables is due to the presence of one or more latent variables (factors) that exert causal influence on these observed variables. On the other hand, PCA makes no assumption about an underlying causal model. Principal component analysis is simply a variable reduction procedure that (typically) results in a relatively small number of components that account for most of the variance in a set of observed variables.

PCA is widely used in the Earth Sciences to reduce the number of variables in a dataset by identifying the pattern of correlations or covariances between them: the new (and fewer) dimensions resulting from the principal component transformations are linear combinations of the observed variables (Reyment and Savazzi, 1999). The reduction to a smaller number of variables allows for a better explanation of the relationships between these, with the identification of chemical element subgroups (Davis, 1974; Field, 2005). When PCA is used for data reduction or exploratory purposes, normality is not a critical assumption (Jolliffe, 2002) and, therefore, there is not a great need to transform the data to approach the normal distribution. Nevertheless, data were subject to standardisation prior to PCA since geochemical data cover a wide range of concentrations (from mg/kg to weight percent).

For each principal component which is calculated, a new variable can be created which contains the component scores for each sample; i.e. its placement on each calculated component.

- ***As principal components represent groups of elements with similar variation, can component scores be mapped, just like the initial geochemical variables? What kind of information can it provide?***

Insights on this question were not easily found throughout the published literature, as component score mapping has been rarely used (Birke et al., 2011; Šajn et al., 2011). This technique is applied in the present work to show how each calculated component is spatially variable and aid in source identification.

As it has been referred, urban geochemical data are not well-behaved statistical data, as those a scientist receives from a well-planned laboratory experiment - data are usually spatially dependent, non-normally distributed, and plagued with many outliers (Reimann et al., 2011a). Most of the classical statistical methods assume statistical independence of individuals and that data are drawn from a single normal distribution, and therefore robust and non-parametric statistical methods should be the first choice when analysing urban geochemical data, which often need to be transformed in order to come near normality.

- ***Which types of data transformations are suitable to make urban geochemical data more "robust" to statistical procedures?***

First of all, some statistical analyses, such as PCA, require that measures are centred and scaled: a typical example in applied geochemistry is the enormous difference in concentration between major and trace elements (often five orders of magnitude). To overcome this, data may be standardised by subtracting the mean or median of the element distribution to each value and dividing by the standard deviation (Davis, 1974).

Most classical statistics, as well as geostatistics, are based on the principle that data are normally distributed - which is rarely the case with geochemical data. There are many transformations which can be applied to make geochemical data approach normality before proceeding to statistical analysis. The most common approach is to log-transform the data, as most of the variables are positively skewed (Miesch and Chapman, 1977) - which is done by simply taking the natural logarithm of each value. This transformation reduces the very high values and spread out the small data values and is thus well suited for right-skewed distributions (Reimann et al., 2011b).

Nevertheless, log-transformation sometimes does not produce satisfactory results, so for these variables another option is to use the Box-Cox transformation (Howarth and Earle, 1979). The algorithm for the Box–Cox transformation estimates the power that is most likely to result in a normal distribution when applied to the given data set. This is an extremely flexible transformation, and as noted above, includes a logarithmic transformation for the special case of the estimated power being zero. In reality, the power may not transform the data to perfect normality; however, the estimate is the power that brings the data closest to normality (Reimann et al., 2011b).

Commonly, the data are first transformed (e.g., to approach a normal distribution), then, if required, centred and then scaled. This way, the interpretation of statistical analyses can be undertaken in a reliable way, as the variable characteristics comply with the assumptions which underlie e each statistical procedure.

In the present research, another issue arises: whereas soil texture does not vary a lot throughout the study area and is mainly associated with the nature of superficial deposits, RDS texture is highly variable - not only spatially, but also temporally.

- ***What implications come from the highly variable texture of RDS? How do grain size distribution and trace element concentration behave, spatially and seasonally?***

It has been reported throughout the literature that trace metal concentrations have a positive correlation to the proportion of fine grained material (Förstner and Wittmann, 1981). Samples collected over a study area may differ in terms of mineralogy and grain size. Therefore, to compensate for the effects of these parameters on trace metal concentrations, a common approach is to normalise the geochemical data using one element as a grain size proxy. This kind of normalisation also allows more consistent comparisons between the geochemistry of different media which are spatially related, after proper investigation on the distribution of the conservative element(s) to be used. Aluminium is frequently used as a normalising element for geochemical data, since it is assumed to have a uniform flux from parent rock material to soils and sediments and shows a strong positive correlation to the fine fraction, mainly constituted by alumino-silicates (Prohic et al., 1995; Covelli and Fontolan, 1997). Furthermore, Al is a major constituent of soils and

sediments. Other elements have been used for geochemical normalisation, e.g. Li (Loring, 1990) or even Cs, Eu, Fe, Rb, Sc, Sm and Th (Ackermann, 1980). Gallium is also used as a normalisation proxy in soil and sediment studies (Wang and Qin, 2007; Alagarsamy and Zhang, 2010). This element is chemically similar to Al and, although it never occurs in a concentrated form, it is not rare and occurs widespread in terrestrial materials. Namely in soils, its distribution is essentially uniform between different horizons and its content varies in the same way as that of clay, making it a good grain-size proxy (Aubert and Pinta, 1977). Gallium is also less prone to anthropogenic input than Al.

In order to compare trace metal concentrations without the bias introduced by the predominance of different grain size fractions, both Al and Ga are tested as grain size proxies, taking into account their relationship with grain size distribution measurements.

Bulk geochemical data are a useful and essential tool to assess soil and RDS contamination - national guidelines are based on such total contents and are currently in use in various countries (EA, 2009f; Flight and Scheib, 2011). Nevertheless, this kind of analysis does not provide direct information on the potential mobility or bioavailability of potentially harmful elements; i.e. the different phases to which these are bound to.

- ***Which metals are more mobile? Which methods can be applied to assess trace metal speciation?***

Sequential extraction techniques have been developed and improved since environmental scientists became aware of the importance of the mobility and bioavailability of trace metals in soils and sediments (Tessier et al., 1979; Ure et al., 1992; Rauret et al., 1999; Rao et al., 2008; Zimmerman and Weindorf, 2010). These techniques are based on the selective extraction of metals bound to different target phases (e.g. exchange sites, organic matter, carbonates, sulphides, etc.), using different reagents (extractants). Undoubtedly, selective extraction methods can assess the amounts of mobile or potentially mobile species (Rao et al., 2008), which in turn may correlate with other environmental variables and land uses.

Although there are several sequential extraction procedures in the literature, the Tessier scheme (Tessier et al., 1979) and the BCR scheme (Rauret et al., 1999; Rauret et al., 2000) are usually the most adopted methods in the majority of published works. For many years, the unofficial benchmark has been the scheme of Tessier et al. (1979), giving rise to many other adapted procedures, some of which are reviewed and compared by Rao et al. (2008) and Filgueiras et al. (2002). The existence of such a diversity of approaches to sequential extraction and the lack of uniformity led the European Community Bureau of Reference (BCR) to develop a standard procedure in the late 1990s, resulting in the BCR Scheme. A series of interlaboratory studies to test the applicability and limitations of the BCR scheme were successfully concluded by the certification of soil and sediment reference

materials (Rauret et al., 2000). BCR has also been successfully applied in other matrices such as different types of soils and sediments.

Unlike the Tessier protocol, where partitioning of the elements is done in five fractions (exchangeable, carbonate-bound, iron/manganese oxide-bound, organic matter-bound, and residual fractions), the BCR protocol extracts elements from three fractions: exchangeable, reducible and oxidisable. The residual fraction generally undergoes digestion using *aqua regia* which, although not dissolving the silicate matrix, gives an estimate of the maximum amounts of elements that are potentially mobile with changing environmental conditions. *Aqua regia* digestion is a well known procedure (ISO, 1995) which does not mobilise trace elements from geological, silicate parent materials but dissolve metal pollutants which largely enter the soil environment in non-silicate bound forms.

The modified 3-step BCR sequential extraction procedure followed by *aqua-regia* digestion (Rauret et al., 2000) are the chosen methods for the present work, which allow the distinction of 4 different fractions (Filgueiras et al., 2002): Exchangeable or acid-extractable, reducible, oxidisable and residual (cf. section 2.6).

Adding to speciation analysis, mineralogical analysis techniques can also be useful to assess metals in different phases, namely microanalysis utilising scanning electron microscopy and energy-dispersive spectroscopy (SEM-EDS) (Adamo et al., 1996; Tanner et al., 2008; Thornton et al., 2008; Taylor and Robertson, 2009; Barrett et al., 2010; Grafe et al., 2011). The SEM allows the observation of individual grain morphology and internal structure, along with detailed, high-resolution geochemical composition of the different features by EDS, as first outlined in section 1.5.2. This adds vital information to the characterisation of contaminant phases and, consequently, SEM-EDS is applied in the present research to aid source apportionment and the assessment of trace metal potential mobility.

In more recent times, geographic information systems (GIS) have become a powerful and readily utilised tool to spatially display and interrogate geochemical data with other environmental information. Not only concentrations can be mapped: urban geochemical data can be integrated with other databases such as population density, traffic networks, buildings, roads, industry and topography, making it an important instrument for environmental planning and monitoring in urban areas. Nowadays, with the addition of spatial and statistical tools within the GIS environment, it has become clear that GIS is an essential tool for studies regarding urban geochemical mapping and modelling, as shown by the GIS-based geochemical studies by Facchinelli et al. (2001), Li et al. (2004), and Thums and Farago (2001).

- ***How can GIS-based spatial statistics tools unveil other influencing factors on urban geochemistry, and aid source apportionment?***

While a great number of studies uses spatial interpolation or multivariate statistical techniques such as cluster and principal component analysis to aid source apportionment, spatial statistical techniques have also been used to model trace metal concentration in environmental media such as air, water, soils and sediments. As mentioned before, GIS allows the storage, analysis and presentation of spatially related data making it well suited for the identification of spatial patterns.

Spatial statistical techniques have been successfully used by several authors to model contamination and other parameters in sediments (Lai et al., 2013), air (Hoek et al., 2008; Madsen et al., 2011; Chen et al., 2012), water (Meeuwig et al., 2000; Varouchakis and Hristopulos, 2013), and soils (Lee et al., 2006; Wu et al., 2010; Terrón et al., 2011; Zhang et al., 2011). Many different models have been applied soils, such as Ordinary Least Squares (OLS) regression (Wu et al., 2010) and Geographically-Weighted Regression (GWR) (Zhang et al., 2009; Zhang et al., 2011). As these are methods of relative simplicity which have provided good results in terms of soil parameter modelling, the applicability of OLS and GWR is explored in this work to model concentrations of Cr, Ni, Cu, Zn, As and Pb in soils and RDS. Nevertheless, and by analysis of the published literature at the time of writing, this kind of spatial statistical analysis had not yet been used regarding contaminant modelling in RDS. The chemical elements to be modelled in this work are selected based on their usually elevated concentrations in Manchester's soils and RDS, for which sources are also pointed out by other techniques used herein.

The selection and creation of suitable sets of environmental variables with potential relationship to soil and RDS contamination in this work is done using the suggestions provided by the basic and multivariate statistics of soil and RDS data, combined with the identification of possible influencing factors through interpretation of concentration maps, which are also presented in this work. Most of the candidate environmental variables used have also been reported in previous works regarding soil and RDS pollution in urban environments, such as those referred in section 1.3 and summarised in Table 1. Therefore, and by the negative impact they may cause in soils and RDS, datasets related to traffic (length of roads and railways within different distance buffers from samples, number of intersections, number of bus stops, average annual daily traffic flow), to human activity concentration (built areas, population density, number of jobs) and to topography (height and slope) have been used to produce new spatial variables. These are then tested and incorporated in OLS and GWR models for soils and sediments, and their applicability is evaluated.

In the present research, soils and RDS are at first characterised individually; however, they show evident similarities - their proximity in the urban environment favours the interchange of trace

elements, organic matter, mineral components, etc; as the same sources and processes affect both media. Therefore, a further attempt is tried to compare soils and RDS in order to assess the extent of their interrelationships.

- ***What are the differences and similarities between soils and RDS? To what extent are these media connected?***

As previously outlined, soils and RDS are fundamental indicators of urban environmental contamination. These media, although having different characteristics, provide valuable geochemical data which support the environmental assessment of urban areas. Both soils and RDS hold similar components, mainly minerals (sand, silt and clay) and organic material of various natures in different proportions. Nevertheless, their textures are different as a reflex of their origin and formation processes - whereas soils are the result of very slow natural processes acting upon bedrock, RDS is formed in a relatively short span of time from the local accumulation of particulates, generated by natural or anthropogenically-derived erosion of soil, buildings and infrastructures, vehicles, among many others.

Still, few studies have attempted to compare soil and RDS texture and composition. Trace metal concentrations in RDS have been observed to be generally higher when compared to their average concentration found in urban soils, as RDS resuspension and deposition may be an important source of these elements in soils. These relative higher concentrations of metal contaminants in RDS have been reported studies regarding both soils and RDS in urban environments (Harrison et al., 1981; Li et al., 2001; Ordoñez et al., 2003; Krčmová et al., 2009). It is also reported that metal concentrations in both media decrease from urban centres to peripheral non-urban areas. The study of 112 RDS samples and 40 soil samples in an industrial city of northern Spain by Ordonez et al. (2003) showed that the mean concentrations of Zn, Cd, Hg, and Pb in soils were appreciably lower than those found in the RDS (approximately, 13, 10, 5, and 3.5 times lower, respectively). Here, anthropogenic heavy metal inputs to both RDS and soils could be appointed to two main sources: the most important was that related to metallurgical activity and transportation of raw materials for local Zn, steel and Al industries. Secondly, exhaust emissions from traffic were an important source in areas with high vehicular density.

A more expanded study by Li et al. (2001), which analysed 505 soil samples from urban parks in Hong Kong area again demonstrated that soils displayed lower metal concentrations when compared to the 45 RDS samples also studied. Nevertheless, these concentrations were higher than those of non-urban parks. Trace metal concentration was also generally proportional to the age of the urban parks, as newly built parks commonly used soils imported from uncontaminated agricultural land.

Another example is the study comprising the analysis of RDS, soils, snow and air particulates from Bratislava, Slovakia (Krčmová et al., 2009). The results showed the highest level of contamination of

RDS in the city centre area. For soils, the spread of increased contamination levels was significantly higher, and together with anthropogenic sources, natural sources of contamination are involved (e.g. naturally increased As levels in soils and rocks); and again, metal concentrations were generally higher in urban soils compared to non-urban areas. High anthropogenic levels of atmospheric contamination were found, reflected in heavy contamination of winter precipitation (snow) mainly due to high contents of As, Fe, Pb, Zn and Cu.

In all of these studies, no spatial-statistical relation was attempted in terms of metal interchange between RDS, soils and other environmental media. The contribution of the joint analysis and quantification of geochemical linkages between soils and RDS still remains a seldom studied subject, which is essential to a better global understanding of contaminant sources and pathways in urban environments, as well as more consistent risk assessments. This relationship between soils and RDS is evident: the atmospheric fallout of RDS particles is likely to increase heavy metal concentration in soils, which in turn can also be a source of natural and anthropogenic elements in road-deposited sediment (Ordoñez et al., 2003).

Nevertheless, the extent to which soil particles contribute to RDS has been addressed only in few studies, which have reported e.g. roadway dusts composed of 76% soil (Hopke et al., 1980), and that soil contributes between 57% and 90% to roadway dusts (Hunt et al., 1993). The contrary, i.e. the quantification of RDS which contributes to soil contamination, hasn't yet been attempted - RDS composition has the contribution of diverse sources which vary significantly at the local scale, therefore a RDS signature in soils is very difficult to achieve. Nevertheless, it is reasonable to say that these mutual contributions can be highly variable and that the interrelationships between these media, both in terms of texture and composition (namely trace metal contamination), remains poorly known.

# 2. Methodologies

## 2.1. Geographical and geological settings

### *2.1.1. Location*

The study area covers 75km$^2$ over the metropolitan boroughs of Manchester, Salford and Trafford (fig. 6), northwest of the United Kingdom. It is located between UK National Grid Reference eastings 375000E to 390000E and northings 395000N to 400000N. The study area was determined by the distribution of the BGS G-BASE soil survey for Manchester. In this area, 300 soil samples and 144 (72 winter + 72 summer) road dust sediment (RDS) samples were collected, according to the scheme illustrated in Figure 6.

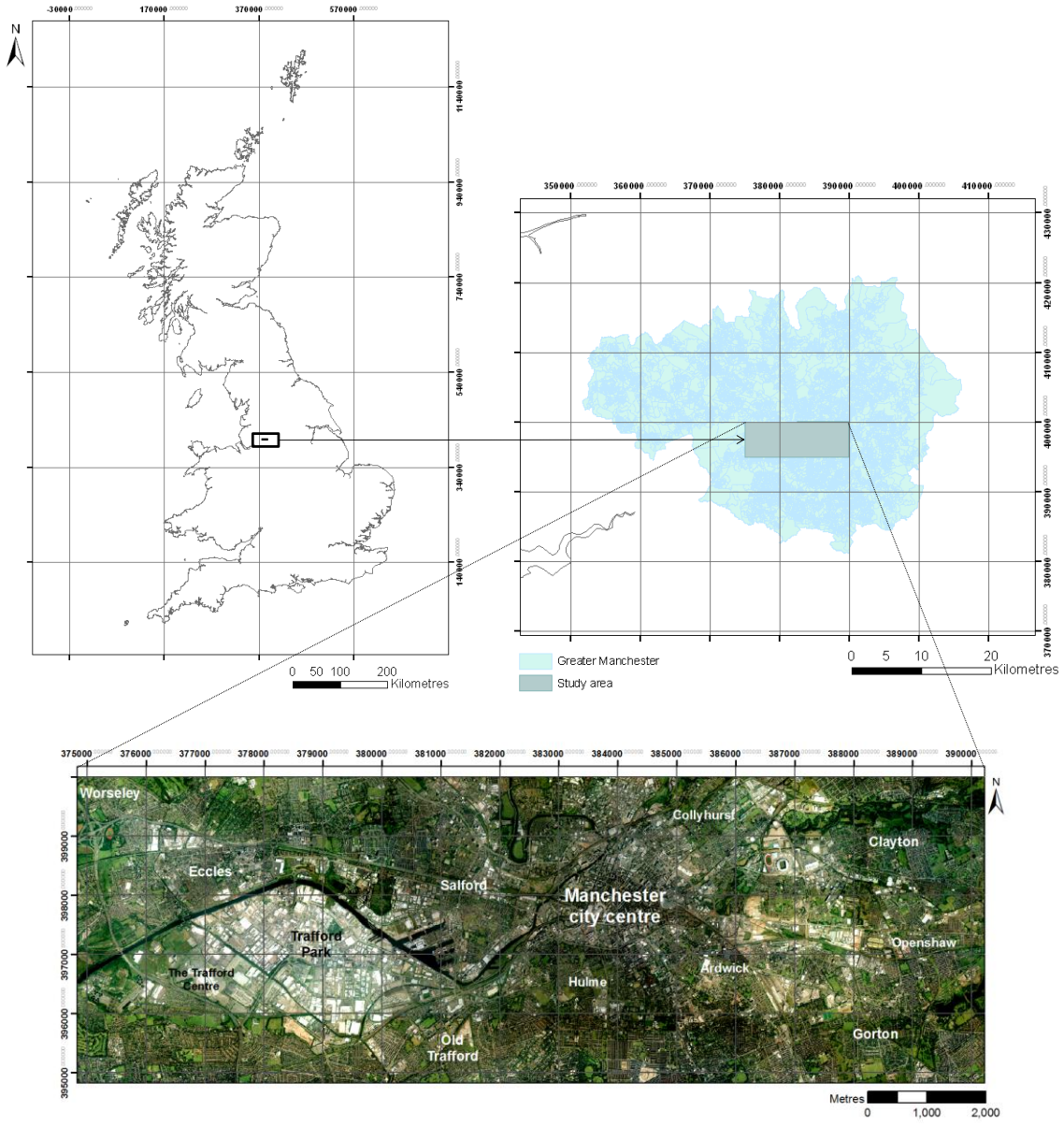


Figure 6: Location of the study area (Manchester, United Kingdom). Aerial image on the bottom shows the 75 km$^2$ covered in this research (©MMU).

## 2.1.2. Bedrock geology

The study area comprises formations of the southern part of the South Lancashire Coalfield and the north-eastern part of the Permo-Triassic Cheshire Basin. Bedrock exposure is poor throughout the area due to an extensive and often thick cover of superficial deposits, described in the next section. The oldest exposed rocks, of Westphalian age, (c. 305 - 298 Ma) are the coal-bearing strata of the South Lancashire Coalfield. The smaller Bradford Coalfield forms a structurally isolated inlier, surrounded by permo-Triassic rocks, and bounded to the east by the Bradford Fault. Nevertheless, the most prominent bedrock exposure is located in the western part of the study area (Patricroft-Eccles), where about 2km$^2$ of Sherwood Sandstone Group rocks are exposed.

The Coal Measures are overlain by a sequence of red beds (Etruria Formation) and grey measures (Halesowen Formation) forming part of the Warwickshire Group. Permo-Triassic rocks (Sherwood and Collyhurst sandstone formations, 298-205 Ma) underlie much of the central, eastern and southern parts of Manchester, where they form the sedimentary fill to the north-eastern part of the Cheshire Basin. This sandstone-dominated sequence, up to 620 m thick, forms the most important groundwater aquifer in north-west England (Tonks et al., 1970; Griffiths et al., 2003).

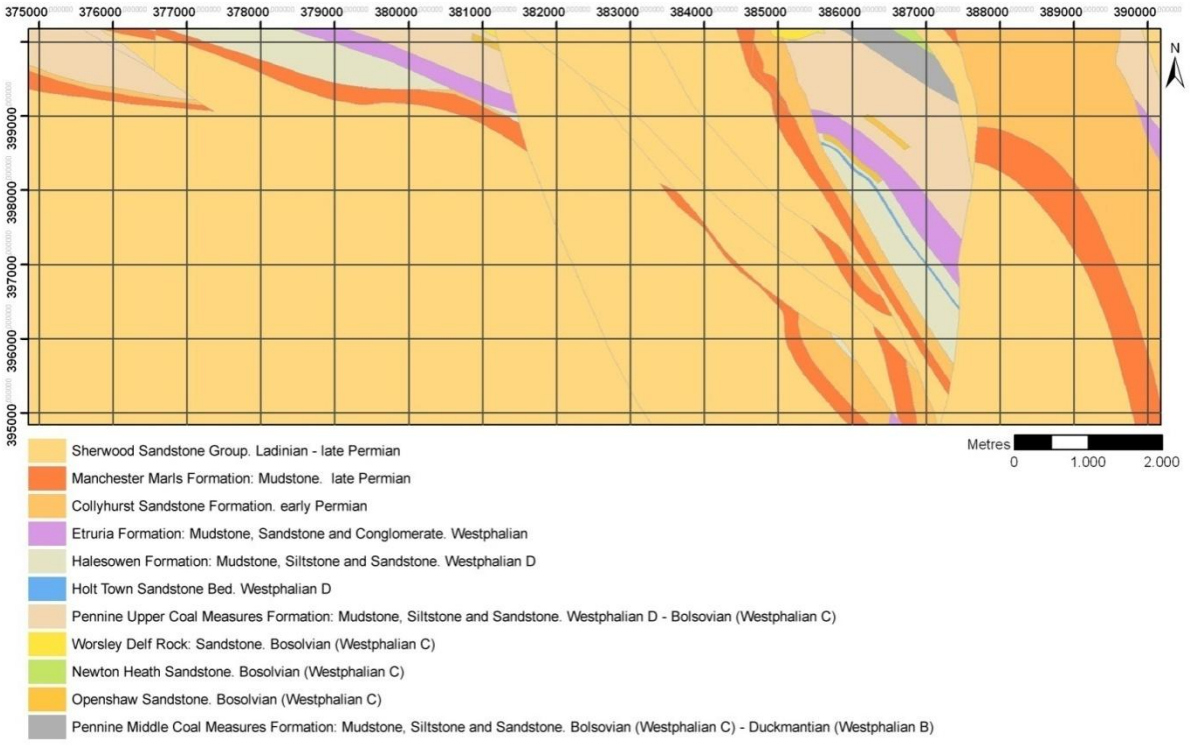


Figure 7: Bedrock formations in the study area (based upon the 1:50.000 scale Digital Geological Map of Great Britain, © British Geological Survey).

## 2.1.3. Superficial geology

Most of the study area is covered by three main types of superficial deposits: glacial deposits, such as till and glacial sand/gravel presumed to be mainly of late-Devensian age (20000 to 14468 BP);

post-glacial deposits of Holocenic age associated with the development of the River Irwell including alluvium and river terrace deposits; and anthropogenic deposits which mark the modification of the surface by men since the Industrial Revolution.

Till and sand/gravel deposits, which are a depositional product of the Devensian glaciation, overlay most of the study area, covering all but the most prominent bedrock features. The tills are accompanied in the lowlands by sequences of outwash sediments forming multi-layered complexes that can reach 40m in thickness. Sand and gravel deposits are the result of the sub- and supraglacially release of large volumes of melt water in the later stages of the glaciation, which caused sediment deposition in ice-contact and proglacial settings. The local formation of transient glacial lakes allowed deposition of silts and laminated clays, although they are not well represented as outcrops in the study area. Permanent snow fields developed after the retreat of the late Devensian ice, providing melt waters which were channelled down the proto-Irwell and its tributaries to deposit a spread of flood gravels across much of the Manchester embayment (Tonks et al., 1970).

Post-glacial Holocene deposits are largely confined to the modern river valleys and include river terrace deposits and tracts of alluvium. A small area of lowland peat is preserved in Trafford Park.

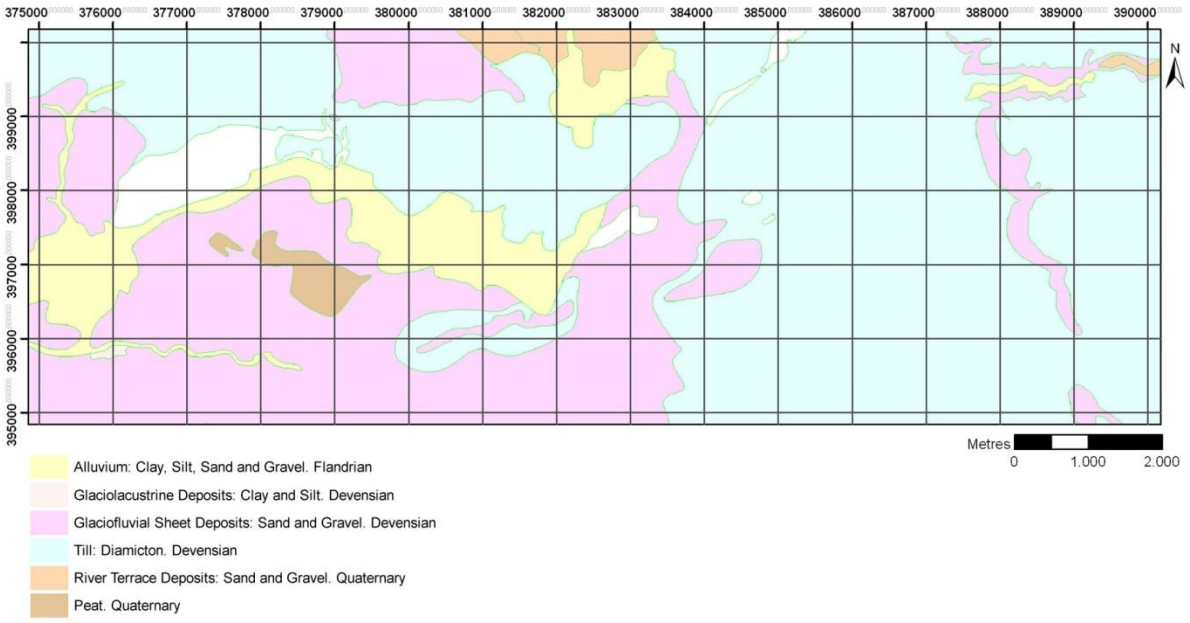


Figure 8: Superficial deposits in the study area (based upon the 1:50.000 scale Digital Geological Map of Great Britain, reproduced with the permission of the British Geological Survey).

## *2.1.4. Climate and natural features*

Temperature shows both a seasonal and a diurnal variation. January is usually the coldest month, with mean daily minimum temperatures of 1.7°C (1981-2010). July is the warmest month, with average maximum temperatures going up to 20.6°C for the same period. An 'air frost' occurs when the temperature at 1.25 metres above the ground falls below 0 °C, and in Manchester this has happened on an average of 41 days per year between 1981 and 2010. The day is shortest in

December and longest in June, which is also the sunniest with an average of 179.7 hours of sunshine. It is worth of notice that, following the Clean Air Act of 1956 and the decline in heavy industry, there has been an increase in sunshine duration over Greater Manchester.

The exposure of NW England to westerly maritime air masses and the presence of areas of high ground mean that the region has some of the wettest places in the UK. The reputedly wet city of Manchester averages 860mm of rain each year, but still, this area benefits from the 'rain shadow' effect of the high ground of N Wales. The driest season is spring whilst there is an autumn/winter maximum, when the Atlantic depressions are at their most vigorous. Snowfall is normally confined to the months from November to April, and the number of days with snow falling is about 20 to 30 per year. The strongest winds are associated with the passage of deep areas of low pressure close to or across the UK. The frequency and strength of these depressions is greatest from December to February, and this is when mean speeds and gusts (short duration peak values) are strongest. There is a prevailing south-westerly wind direction through the year, but a high frequency of north to north-east winds in spring. Topography again plays a part in modifying the climate with channelling of winds between areas of high ground - the Pennines and N Wales give a southerly bias to winds over Greater Manchester (MO, 2010b). Table 4 summarizes the climate averages per year for Manchester Airport weather station (1981-2010).

| Av. Max Temperature | Av. Min Temperature | Days of Air Frost | Hours of Sunshine | mm of Rainfall | Days of Rainfall ≥ 1mm | Wind at 10 m (knots) |
|---|---|---|---|---|---|---|
| 13.5 ºC | 6.6 ºC | 40.8 | 1416.2 | 828.8 | 142.9 | 7.9 |

Table 4: Climate averages for Manchester Airport weather station between 1981 and 2010 (MO, 2010a).

Manchester is located in a bowl-shaped basin, surrounded to the north and east by the Pennine hills. Slopes are progressively lower towards the plain areas of the south and west. The highest part of the study area is therefore located to the east with an average gentle slope towards southwest, and the area lies between 11 and 101 meters above sea level as displayed in Figure 9.

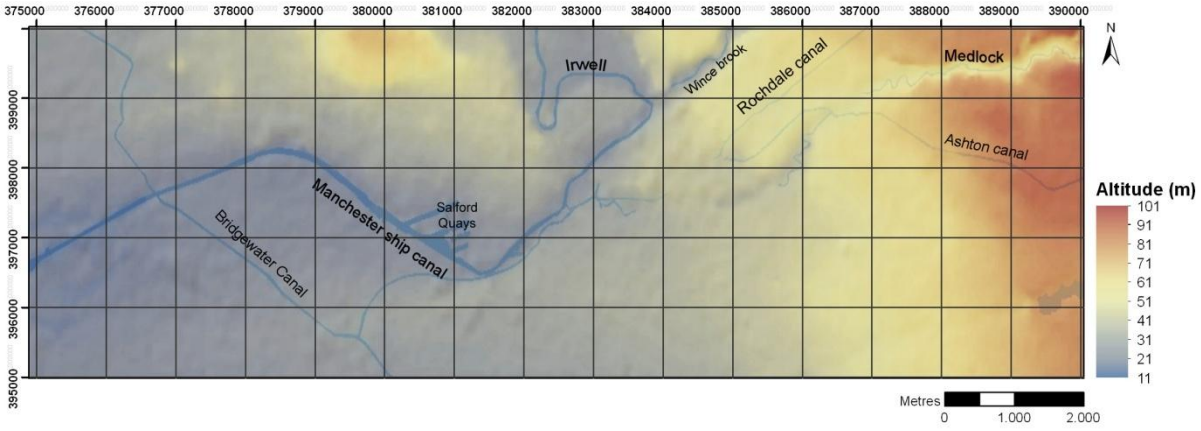


Figure 9: Land topography (adapted from OS MasterMap® Topography Layer)

The confluence of the rivers Irwell, Irk and Medlock is located near the city centre, where some segments are canalised underneath the built-up area. After this point, the Manchester Ship Canal runs for approx. 59 Km outside the study area following the routes of rivers Mersey and Irwell, until it flows into the Mersey estuary by the town of Runcorn.

### *2.1.5. Population*

Manchester is one of the most densely populated areas and the third largest urban settlement in the United Kingdom. Greater Manchester population went from only 77000 people in 1801 to over 2149000 in 1901, in what has been the most abrupt population growth of the city's history, driven by the Industrial Revolution. Since then, population numbers have fluctuated periodically but the growth rates were never as large as those of the 19$^{th}$ century. According to 2011 UK census figures, 2682500 people lived in the 1276 Km$^2$ of Greater Manchester (ONS, 2012). This includes ten local authorities which separately administer their own sections of the Greater Manchester conurbation. The maps in Figure 10 and Figure 11 show the population density and the total population per output area using census data of 2001, as only local authority-level statistics had been published for 2011 by the time of writing.

Nevertheless, Greater Manchester's population grew 5,9% between 2001 and 2011. The largest population densities are found in small output areas which correspond to high volume residential buildings. Areas with higher population densities are mainly located outside the City Centre and Trafford Park cores where commercial and industrial activities, respectively, are the most profuse, as can be observed Figure 12 below. One of the exceptions to this trend of higher population densities in the periphery and higher job densities in the city centre and Trafford Park is the Oxford Road/Wilmslow Road alignment, where there is the highest number of people per output area, as well as a large number of jobs. This is due to the local concentration of universities, local businesses, student residential campuses, hospitals, and the dense residential areas of Rusholme and Moss side.

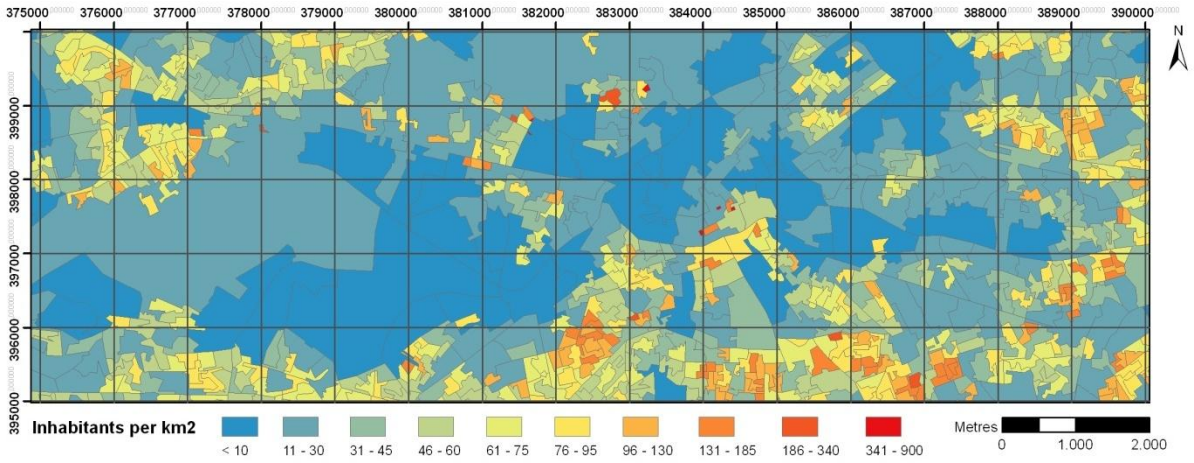


Figure 10: Population density (2001 Census output areas, Crown®, reproduced with permission of the Controller of HMSO)

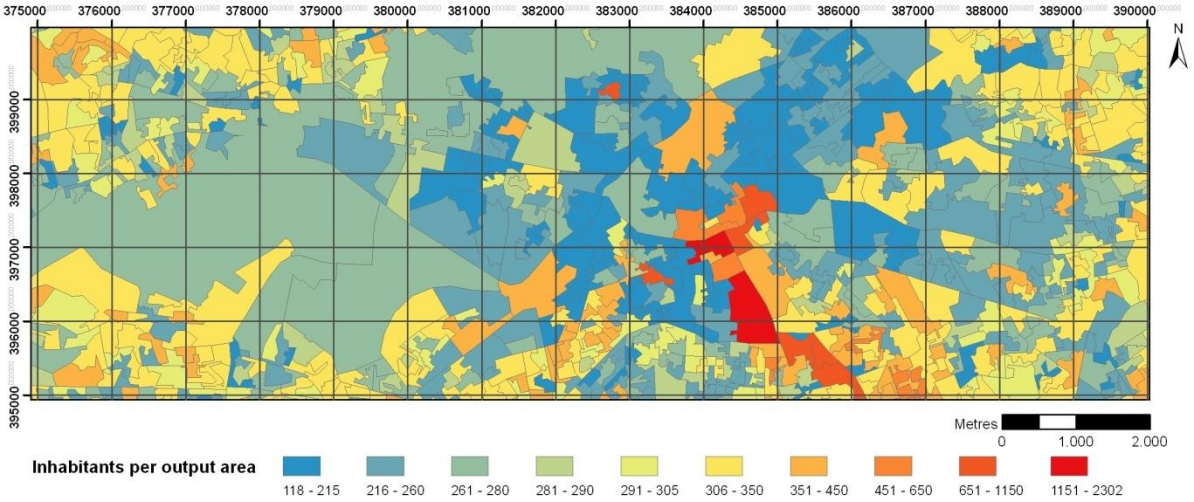


Figure 11: Population per output area (2001 Census output areas, Crown®, reproduced with permission of the Controller of HMSO)

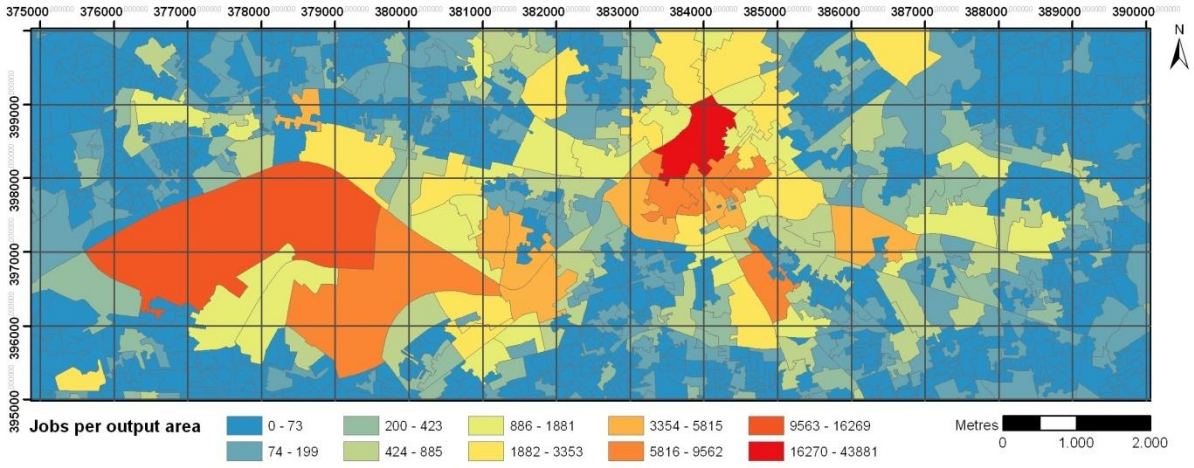


Figure 12: Jobs per output area (2001 Census output areas, Crown®, reproduced with the permission of the Controller of HMSO)

## *2.1.6. Road and rail networks and public amenities*

The region of Manchester is served by dense road infrastructures, with both linear and orbital motorways. Manchester is surrounded by the M60 as the main orbital road, and the Mancunian Way / Trinity Way / A665 together form an inner ring which delimits the Manchester city centre area. Manchester is linked by road to the east (Leeds, Humber ports, M1 and A1) by the M62, which also connects to the west up to Liverpool. The M6 northbound connects Manchester to the Lake District, Carlisle and Scotland; whereas the M6 southbound links to Birmingham, Wales and London. M1 also links Manchester to Sheffield, Nottingham and London. Manchester's city centre is crossed by over 10 train lines, through the main terminals of Manchester Piccadilly, Oxford Road and Victoria. 6 tram lines also connect the city centre to outer city locations.

Within the study area, represented in Figure 13, there are about 253 Km of motorways, A roads and B roads (including slip roads and roundabouts; motorway length is multiplied by the number of dual carriageways); 851 Km of minor roads and local streets; and around 153 Km of pedestrianised

streets, alleys and private roads; as well as 48 Km of railways (tram and train); calculated using GIS tools. The study area is also served by 63 educational facilities, 6 hospitals and 19 leisure or sports centres.


Figure 13: Road and rail networks and public amenities (OS MasterMap® Integrated Transport Network™, Railways and Public Amenities layers).

## 2.1.6.1. Traffic data

The average annual daily traffic flow (AADTF) dataset obtained from the UK Department for Environment, Food and Rural Affairs (DEFRA, 2011) displays the number of vehicles that drive on a stretch of road on an average day of the year. These data were interpolated using the IDW function to produce the maps of Figure 14 and Figure 15, which represent the AADTF for all motor vehicles and the AADTF for heavy goods vehicles, respectively - units represent vehicles per day.

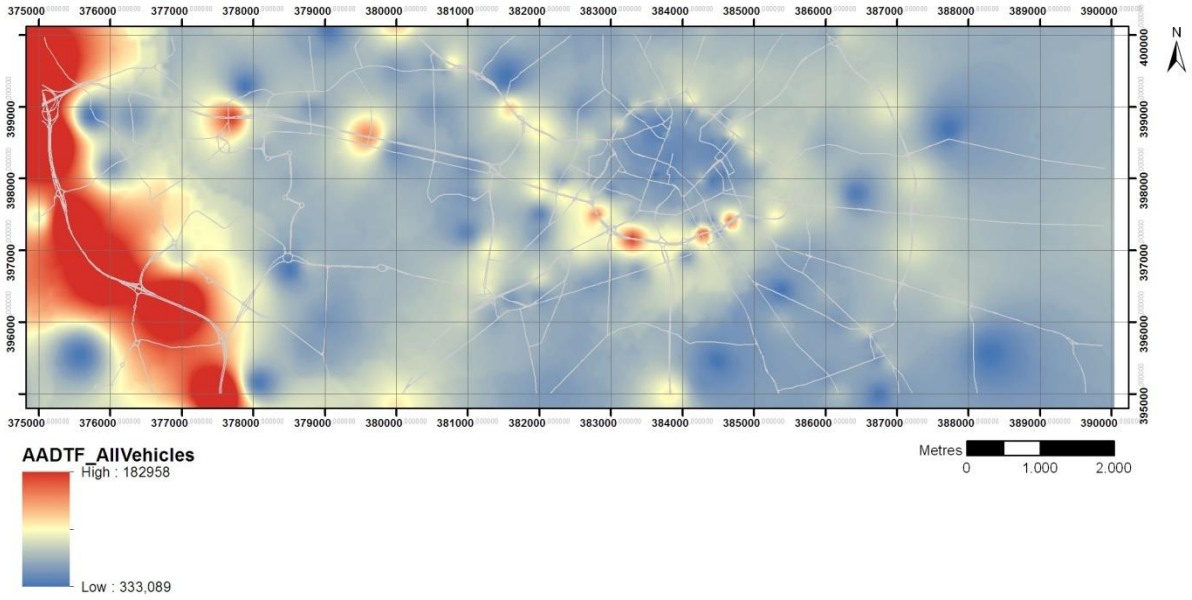


Figure 14: Average annual daily traffic flow for all motor vehicles (DEFRA, 2011) in the study area.

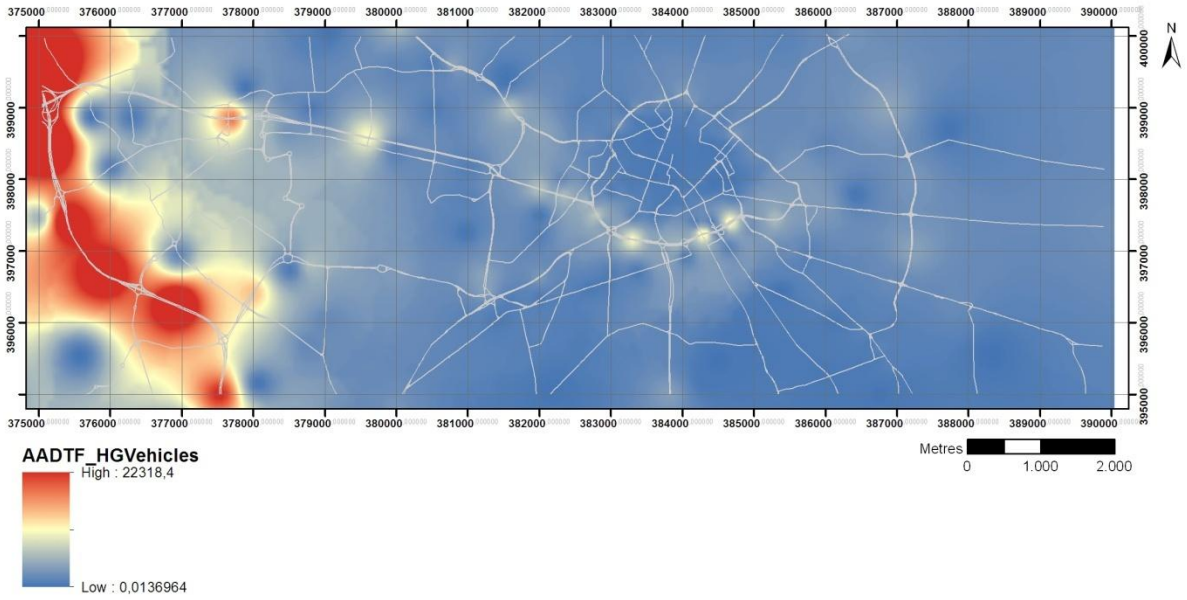


Figure 15: Average annual daily traffic flow for heavy goods vehicles (DEFRA, 2011) in the study area.

It can be observed that the highest traffic volume in the study area occurs at the M60, in the western part of the study area. The M602 (connecting M60 to the ring road through Eccles and Salford), the south segment of the ring road (Mancunian Way), and the A6/Broad Street segment, also display high traffic counts for all motor vehicles. Heavy goods vehicles display largest counts again along the M60, the M602 and the Mancunian Way.

## 2.2. Soil collection

In the Manchester urban area, 300 soil samples were collected by the BGS as part of the G-BASE project in the summer of 2002, as shown in Figure 16. The full field procedures developed and optimised by the G-BASE project are described in detail in Johnson (2005).

Each UK national grid kilometre square on 1:25000 topographic Ordnance Survey maps was divided into four 500m x 500m squares, and sample sites were notionally located at the centre of each square. Sampling was carried out on the least disturbed area of unbuilt ground as close to the centre of each of the 500m sub-cells. This may correspond to domestic gardens, allotments, parks, recreational ground, or road verges.

To ensure sample representativity, each sample is a composite of five sub-samples collected from the corners and centre of a 20m x 20m square in each location, or as close to this dimension as possible depending on the sampling site dimensions, as illustrated in Figure 17. This scheme can also be adjusted e.g. in case of road verges, where samples can be collected from a transect of five sub-sites. Topsoil samples (5 – 20 cm depth) were collected with a handheld Dutch auger. The first 0-5 cm were discarded as these correspond mainly to surface vegetation, surface litter and/or the rootlet zone. The exact coordinates of each central auger hole were recorded using a GPS at the site.

One site in every batch of 100 was designated for collection of a duplicate field sample, collected from an adjacent 20m x 20m square to the original sample. Replicate samples were prepared in the laboratory by taking a sub-sample from the duplicate sample. ANOVA analysis of results helps to determine the within site, between site and laboratory variability (Johnson, 2005).

After collection, samples were taken to the field base and then to the BGS laboratories. Soils were air-dried (<30ºC), freeze dried and dry-sieved through nylon mesh to a <2 mm size fraction. The samples were then homogenised, coned and quartered and sub-samples taken for analyses. A 30 g sub-sample was ground in an agate planetary ball mill until 95% was <53 µm. This pulverised material was further sub-sampled to obtain a 12 g split for element analysis by X-ray fluorescence (XRF) spectrometry (Fordyce et al., 2005; Johnson et al., 2005).

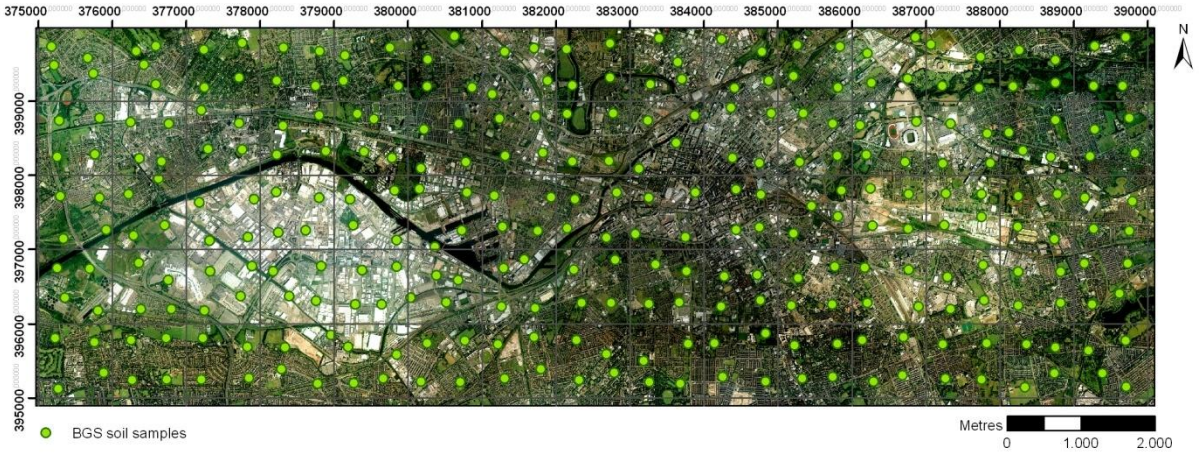


Figure 16: Sampling scheme – BGS soils (aerial image ©MMU).

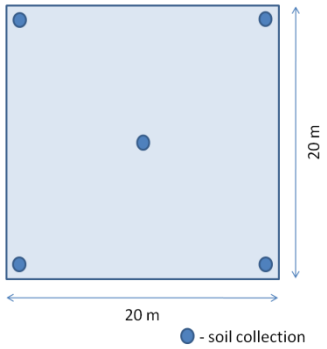


Figure 17: Sub-sampling scheme for soil collection at each site (adapted from Johnson, 2005).

From the 300 samples of the BGS dataset, made available for this work, 150 were sub-sampled by the author from the archives. These were chosen based on the trace metal content and proximity to RDS sample locations. Further analysis was performed on these, such as mineralogical and geochemical characterization of grains by SEM-EDS and organic/inorganic carbon analysis.

## 2.3. RDS collection

RDS sampling was performed seasonally during winter (Jan-Feb 2010) and summer (June-July 2010), at a density of 1 per $km^2$. Sample locations were chosen according to the previously used soil

sampling scheme, but at a lower density - in each kilometre square, one RDS sample was collected as close as possible to the soil sample which displayed higher trace metal concentrations. RDS final sampling locations were recorded by GPS and are shown in Figure 18.

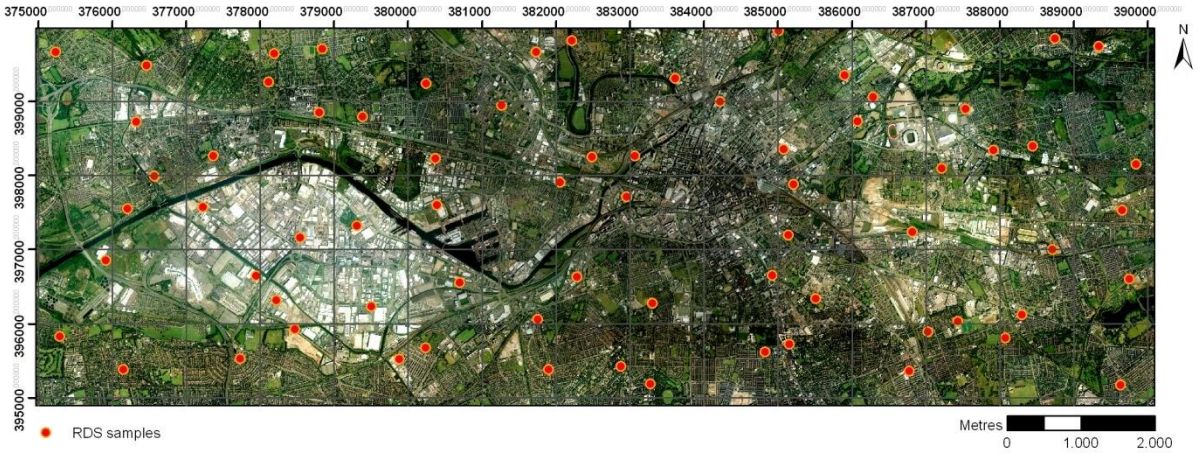


Figure 18: Sampling scheme – road-deposited sediments (aerial image ©MMU).

RDS were collected along the edge of the road kerbs, where maximum accumulation of sediments is observed - most roads are slightly convex and favour sediment accumulations on the kerb sides. This approach also has the objective of making sample collection consistent between sites and between sampling campaigns. In each location, a representative area of approximately 100x50 cm was carefully swept with the aid of clean dustpan and brush kits; plastic scoops were used occasionally prior to sweeping for larger amounts of sediment, to avoid resuspension of fine particles. Utensils were thoroughly cleaned with water and ethanol (to avoid contamination and facilitate drying) after each sample, and then again in the MMU laboratories at the end of each day. This method is quick, prevents cross-contamination, is inexpensive and does not need deviation of the car and pedestrian traffic during sample collection. Variable sample sizes were collected depending on sediment accumulation at each site, but for the majority of locations the collected amounts were greater in summer. Samples were stored in self-sealing plastic bags and taken to the MMU laboratories at the end of each day.

Likewise soils, all RDS samples were air-dried and dry-sieved through a nylon mesh to a <2 mm size fraction. After being homogenised, coned and quartered, the sub-samples were sent to BGS to undergo XRF analysis.

## 2.4. Elemental analysis - XRF

Total element concentrations for 300 soil and 144 RDS samples were determined by X-ray fluorescence (XRF) at the BGS analytical facilities - 48 elements were determined by BGS in soils and 55 in RDS. These elements are in Table 5, along with the correspondent lower limits of detection (LLDs) and the percentage of samples below the LLD for each element. The location of each element in the periodic table is represented in Table 6.

Prior to analysis, samples were prepared and bound into 40 mm pellets. These were analysed using wavelength-dispersive and energy-dispersive X-ray fluorescence equipments (WD-XRF: Philips PANalytical® MagiX-PRO and AxiosMAX® Advanced; ED-XRF: Phillips PANalytical® Epsilon5). Duplicate, replicate, blank, primary (international standards) and secondary (BGS standards) reference materials are included in every batch of samples submitted for analysis.

| | | | | SOIL | RDSS | RDSW |
|---|---|---|---|---|---|---|
| | Element | LLD | units | % under LLD | % under LLD | % under LLD |
| Major elements (wt. %) | $Na_2O$ | 0,3 | wt. % | | | 1,4 |
| | MgO | 0,3 | " | 0,7 | | |
| | $Al_2O_3$ | 0,2 | " | | | |
| | $SiO_2$ | 0,1 | " | | | |
| | $P_2O_5$ | 0,05 | " | | | |
| | $K_2O$ | 0,01 | " | | | |
| | CaO | 0,3 | " | 1,3 | | |
| | $TiO_2$ | 0,02 | " | | | |
| | MnO | 0,005 | " | | | |
| | $Fe_2O_3$ | 0,05 | " | | | |
| | $SO_3$ | 0,5 | " | n.d. | 68,1 | 73,6 |
| Trace elements (mg $kg^{-1}$) | Sc | 3 | mg kg-1 | | 5,6 | 2,8 |
| | V | 3 | " | | | |
| | Cr | 3 | " | | | |
| | Co | 1,5 | " | | | |
| | Ba | 1 | " | | | |
| | Ni | 1,3 | " | | | |
| | Cu | 1,3 | " | | | |
| | Zn | 1,3 | " | | | |
| | Ga | 1 | " | | | |
| | Ge | 0,5 | " | | 4,2 | |
| | As | 0,9 | " | | | |
| | Se | 0,2 | " | 15,7 | 30,6 | 34,7 |
| | Br | 0,8 | " | | 2,8 | |
| | Rb | 1 | " | | | |
| | Sr | 1 | " | | | |
| | Y | 1 | " | | | |
| | Zr | 1 | " | | | |

| | | | | SOIL | RDSS | RDSW |
|---|---|---|---|---|---|---|
| | Element | LLD | units | % under LLD | % under LLD | % under LLD |
| Trace elements (mg $kg^{-1}$) | Nb | 1 | " | | | |
| | Mo | 0,2 | " | 1,0 | | |
| | Hf | 1 | " | | | |
| | Ta | 1 | " | 87,7 | 98,6 | 100 |
| | W | 0,6 | " | | | |
| | Tl | 0,5 | " | 61,3 | 62,5 | 86,1 |
| | Pb | 1,3 | " | | | |
| | Bi | 0,3 | " | 50,3 | 15,3 | 36,1 |
| | Th | 0,7 | " | | | |
| | U | 0,5 | " | 1,7 | 1,4 | 4,2 |
| | Ag | 0,5 | " | 29,0 | 95,8 | 94,4 |
| | Cd | 0,5 | " | 13,7 | 43,1 | 38,9 |
| | Sn | 0,5 | " | | | |
| | Sb | 0,5 | " | 0,3 | | |
| | Te | 1 | " | 95,0 | 100 | 98,6 |
| | I | 0,5 | " | | 19,4 | 16,7 |
| | Cs | 4 | " | 70,7 | 100 | 100 |
| | La | 1 | " | | | |
| | Ce | 1 | " | | | |
| | Nd | 4 | " | | | |
| | Sm | 2 | " | 25,3 | 43,1 | 44,4 |
| | S | 1000 | " | n.d. | 5,6 | 22,2 |
| | Cl | 200 | " | n.d. | 76,4 | 45,8 |
| | Yb | 1,5 | " | n.d. | 65,3 | 63,9 |
| | Hg | 0,6 | " | n.d. | 98,6 | 100 |
| | Pd | 0,5 | " | n.d. | 94,4 | 97,2 |
| | In | 0,5 | " | n.d. | 98,6 | 97,2 |

Table 5: Determined chemical elements and lower limits of detection (LLD = lower limit of detection; n.d. = not determined).

## 2.5. pH, organic matter, total carbon and organic/inorganic carbon analysis

Soil pH was determined by the BGS laboratories by adding 10 g of <2 mm soil sample to 25 ml of 0.01M $CaCl_2.2H_2O$ (calcium chloride). The mixture is shaken to form a slurry prior to analysis by the pH electrode equipment.

Loss on ignition (LOI) of organic matter (OM) has also been determined by the BGS for all 300 soil samples. For the 144 RDS samples, OM was determined at the MMU laboratories following the same procedure. This consists of weighing approximately 2,0000g of <2mm dry sample into appropriate crucibles, which are then heated in a muffle furnace at 450$^{o}$C for a minimum of 4 hours. In this

| | | | | | | | | | | | | | | | | | |
|---|---|---|---|---|---|---|---|---|---|---|---|---|---|---|---|---|---|
| 1 H hydrogen [1.007; 1.009] | | Key: atomic number / Symbol / name / standard atomic weight | | | | | | | | | | | | | | | 2 He helium 4.003 |
| 3 Li lithium [6.938; 6.997] | 4 Be beryllium 9.012 | | | | | | | → element concentration determined by XRF | | | | 5 B boron [10.80; 10.83] | 6 C carbon [12.00; 12.02] | 7 N nitrogen [14.00; 14.01] | 8 O oxygen [15.99; 16.00] | 9 F fluorine 19.00 | 10 Ne neon 20.18 |
| 11 Na sodium 22.99 | 12 Mg magnesium 24.31 | | | | | | | | | | | 13 Al aluminium 26.98 | 14 Si silicon [28.08; 28.09] | 15 P phosphorus 30.97 | 16 S sulfur [32.05; 32.08] | 17 Cl chlorine [35.44; 35.46] | 18 Ar argon 39.95 |
| 19 K potassium 39.10 | 20 Ca calcium 40.08 | 21 Sc scandium 44.96 | 22 Ti titanium 47.87 | 23 V vanadium 50.94 | 24 Cr chromium 52.00 | 25 Mn manganese 54.94 | 26 Fe iron 55.85 | 27 Co cobalt 58.93 | 28 Ni nickel 58.69 | 29 Cu copper 63.55 | 30 Zn zinc 65.38(2) | 31 Ga gallium 69.72 | 32 Ge germanium 72.63 | 33 As arsenic 74.92 | 34 Se selenium 78.96(3) | 35 Br bromine 79.90 | 36 Kr krypton 83.80 |
| 37 Rb rubidium 85.47 | 38 Sr strontium 87.62 | 39 Y yttrium 88.91 | 40 Zr zirconium 91.22 | 41 Nb niobium 92.91 | 42 Mo molybdenum 95.96(2) | 43 Tc technetium | 44 Ru ruthenium 101.1 | 45 Rh rhodium 102.9 | 46 Pd palladium 106.4 | 47 Ag silver 107.9 | 48 Cd cadmium 112.4 | 49 In indium 114.8 | 50 Sn tin 118.7 | 51 Sb antimony 121.8 | 52 Te tellurium 127.6 | 53 I iodine 126.9 | 54 Xe xenon 131.3 |
| 55 Cs caesium 132.9 | 56 Ba barium 137.3 | 57-71 lanthanoids | 72 Hf hafnium 178.5 | 73 Ta tantalum 180.9 | 74 W tungsten 183.8 | 75 Re rhenium 186.2 | 76 Os osmium 190.2 | 77 Ir iridium 192.2 | 78 Pt platinum 195.1 | 79 Au gold 197.0 | 80 Hg mercury 200.6 | 81 Tl thallium [204.3; 204.4] | 82 Pb lead 207.2 | 83 Bi bismuth 209.0 | 84 Po polonium | 85 At astatine | 86 Rn radon |
| 87 Fr francium | 88 Ra radium | 89-103 actinoids | 104 Rf rutherfordium | 105 Db dubnium | 106 Sg seaborgium | 107 Bh bohrium | 108 Hs hassium | 109 Mt meitnerium | 110 Ds darmstadtium | 111 Rg roentgenium | 112 Cn copernicium | | 114 Fl flerovium | | 116 Lv livermorium | | |
| | | 57 La lanthanum 138.9 | 58 Ce cerium 140.1 | 59 Pr praseodymium 140.9 | 60 Nd neodymium 144.2 | 61 Pm promethium | 62 Sm samarium 150.4 | 63 Eu europium 152.0 | 64 Gd gadolinium 157.3 | 65 Tb terbium 158.9 | 66 Dy dysprosium 162.5 | 67 Ho holmium 164.9 | 68 Er erbium 167.3 | 69 Tm thulium 168.9 | 70 Yb ytterbium 173.1 | 71 Lu lutetium 175.0 | |
| 89 Ac actinium | 90 Th thorium 232.0 | 91 Pa protactinium 231.0 | 92 U uranium 238.0 | 93 Np neptunium | 94 Pu plutonium | 95 Am americium | 96 Cm curium | 97 Bk berkelium | 98 Cf californium | 99 Es einsteinium | 100 Fm fermium | 101 Md mendelevium | 102 No nobelium | 103 Lr lawrencium | | | |

Table 6: Periodic Table of the Elements (adapted from IUPAC, 2012).

process, OM is ignited and its content is given by the pondered sample weight difference, given by the formula

$$\text{LOI (\%)} = \frac{m_0 - m_f}{m_0} \times 100$$

where $m_0$ represents the initial weight and $m_f$ the final weight of the sample. Duplicate samples were used to assure reproducibility of the analysis. A general and widely used soil classification according to organic matter content is described in Table 7 below.

| OM content | Classification |
|---|---|
| ≤ 3% | Mineral soil |
| 3 - 15% | Mineral soil with organic matter |
| 15 - 30% | Organic soil |
| > 30% | Peat |

Table 7: Soil classification according to organic matter content (Huang et al., 2009).

Total carbon (TC) contents were determined by dry combustion for 150 soil samples retrieved from the BGS archives. This is done by weighing approximately 0.2000g of ground <2mm sample into tin foil containers, which are rolled into capsules and run in a LECO® TruSpec analyser. This equipment burns each sample in a 950$^{o}$C furnace and the $CO_2$ released is collected and passed through selective infrared (IR) and thermal conductivity detectors to determine carbon content. Blank, soil standard samples (LECO® *SOIL C+N -2*) and duplicates are run as well with each sample batch to calibrate the equipment and ensure the accuracy and precision of the method.

To determine organic carbon (OC), 92 of the 150 soil samples were selected – those with higher TC content. Around 2.00g were weighed and digested in 10ml of 6M HCl, in order to dissociate the carbon bound to carbonates. Samples were then filtered through glass fibre filters using a Buchner vacuum flask device and rinsed thoroughly in deionised water. After drying the fiber glass filters+sample at room temperature, these were folded and encapsulated in tin foil and run in the LECO analyser. Blank filter samples were also prepared and run within each batch of samples, as well as soil standards and duplicates. Inorganic carbon (IC) is given simply by the difference between TC and OC.

## 2.6. Speciation analysis

Extractable trace element contents for Cr, Cu, Zn, Pb and Fe were investigated in 34 RDS samples (17 summer + 17 winter), which were selected due to their high trace metal concentrations determined previously by XRF. Sample extracts were obtained following the modified BCR three step sequential extraction protocol (Rauret et al., 1999); and a fourth step consisted in the digestion of the solid residue by *aqua regia* (ISO, 1995; Larner et al., 2006), to provide a comparison of the sum of the metal concentrations extracted in the four steps with the (total) XRF results for each metal. The procedure is described in Table 8 below. All reagents used were of analytical grade or better; double-

distilled water has also been used for solutions and throughout all procedures. Prior to use, the glass materials have been immersed in 2% concentrated nitric acid (22.54 mol/l) overnight and rinsed with distilled water.

Sample preparation took place in the laboratories of the Geology department of the University of Lisbon, as well as extract analysis by Flame Atomic Absorption Spectroscopy (FAAS) using a Varian SpectrAA FS220 equipment. 25% of the RDS samples were duplicated to evaluate the reproducibility of the analysis and blank samples were also run. When metal concentrations were above the upper limits of detection, extracts were diluted using borosilicate glass volumetric pipettes and double distilled water.

Five calibration solutions were prepared from standard solutions for each metal covering the expected range of concentrations in RDS extracts and considering the limitations of the instrument. The concentrations of the calibration solutions are described in Table 9.

| Step | Fraction | Reagents and procedures |
|---|---|---|
| **1** | **Exchangeable** | Add 20ml of 0.11 mol/l acetic acid ($CH_3COOH$) to 0,5g of RDS sample, shake for 16h at room temperature, then centrifuge at 3000 rpm for 20min. Decant the extract into an analysis tube and store at 4ºC. Add 10ml of double-distilled water, shake for 15min and centrifuge for 20min. at 3000 rpm. Decant and discard the supernatant liquid. |
| **2** | **Reducible** | Add 20mL 0.5 mol/l hydroxylamine hydrochloride ($NH_2OH{\cdot}HCl$) at pH~1.5 to the residue of step 1 and shake for 16 h at room temperature. Centrifuge, decant and store the extract, wash residue, centrifuge, decant and discard the supernatant as in step 1. |
| **3** | **Oxidisable** | Add 5ml of 8.8 mol/l hydrogen peroxide ($H_2O_2$), digest for 1h at room temperature and 1h at a 85ºC water bath. Add another 5ml of $H_2O_2$, digest for 1h at 85ºC with vessels uncovered to reduce volume. Allow to cool, add 25mL of 1 mol/l ammonium acetate ($NH_4COOCH_3$) and shake for 16 h at room temperature. Centrifuge, decant and store the extract, wash residue, centrifuge, decant and discard the supernatant as in step 1. |
| **4** | **Residual** | Add 10ml of aqua regia (3:1 solution of 12 mol/l hydrochloric acid (HCl) and 15.8 mol/l nitric acid ($HNO_3$)) to the residue of the last step and digest for 24h at room temperature. Shake and transfer the mixture to pyrex containers and digest on a hot plate at 130ºC for 15m. Allow to cool, decant and dilute to 25ml with 0.5 mol/l $HNO_3$. |

Table 8: Reagents and procedures employed for the 3-step BCR sequential extraction procedure and *aqua-regia* digestion.

| Element | Concentration of calibration solutions (mg/l) |
|---|---|
| Cr | 0.5; 5.0; 10.0; 15.0; 20.0 |
| Cu | 0.5; 1.0; 3.0; 5.0; 10.0 |
| Zn | 0.1; 0.5; 1.0; 1.5; 2.0 |
| Pb | 0.25; 2.5; 5.0; 12.5; 25.0 |
| Fe | 0.5; 1.0; 5.0; 10.0; 15.0 |

Table 9: Concentrations of the calibration solutions for Cr, Cu, Zn, Pb and Fe.

The phases extracted in each step consist of:

- **Exchangeable, or acid-extractable** - contains the weakly adsorbed metals retained on the solid surface by relatively weak electrostatic interaction, metals that can be released by ion-exchange processes and metals that can be precipitated or co-precipitated with carbonates. The carbonate form is a loosely bound phase and liable to change with

environmental conditions. Changes in the ionic composition, influencing adsorption–desorption reactions or lowering of pH could cause remobilisation of metals from this fraction. Exchangeable or acid-extractable trace metals are the most mobile, i.e. those which are released most readily into the environment.

- **Reducible:** comprises metals bound to Fe and Mn oxides/oxy-hydroxides. These can be present as coatings on mineral surfaces or as fine discrete particles, and can occur by any or a combination of co-precipitation, adsorption, surface complex formation or ion exchange processes. Reduction of Fe(III) and Mn(IV) under anoxic conditions and their subsequent dissolution could release trace metals adsorbed on this fraction into the environment.
- **Oxidisable:** trace metals on this fraction may be associated through complexation or bioaccumulation processes with various forms of organic material such as organic matter, detritus or coatings on mineral particles. Metallic pollutants associated with oxidisable phases are assumed to remain in the soil for longer periods but may be mobilised by decomposition processes. Degradation of organic matter under oxidising conditions can lead to a release of soluble trace metals bound to this component. Amounts of trace metals bound to sulphides might also be extracted during this step.
- **Residual**: contains the metals which remained after the sequential extraction procedure, i.e. those with the lowest mobility. Residual metals that are not released by aqua regia digestion are mostly bound to silicate minerals and are considered unimportant for estimating trace metal mobility.

## 2.7. SEM-EDS

In order to investigate the general grain morphology and internal structure, soil and RDS samples were observed under the scanning-electron microscope (SEM) at Manchester Metropolitan University. Dry samples were sieved to <1 mm and added Buehler® EpoxiCure resin in mounting moulds, pre-coated with release agent. The resin was prepared according to the manufacturer's guidelines and was added Buehler conductive filler in order to eliminate sample charging during SEM observation. Casts were put in a vacuum impregnation chamber under a pressure of approx. 700 mm Hg and then cured at room temperature overnight. After hardening, casts were removed from the moulds and grinded using decreasing grit size abrasive papers, followed by diamond paste-polishing MetaDi® (1 µm) on a micro-cloth, using a grinder/polisher equipment.

Sample mounts were observed under a Zeiss® Supra 40VP SEM system fitted with an EDAX® energy dispersive spectrometry (EDS) device; using a beam of current of 15 kV and a working distance of 15mm. Samples were observed in partial vacuum conditions and using backscattered electron imaging, and chemical composition was determined using the EDS system. A few samples were also

analysed by the Oxford Instruments INCA energy dispersive X-ray spectrometer, also available at MMU.

## 2.8. Grain size analysis

Grain size was investigated in all the RDS samples using a Malvern Instruments® Mastersizer 2000 laser diffractometer in the Geology department of the University of Lisbon. Approximately 1g of sample was weighted in a 100 ml beaker, to which 30ml of deionised water and 5 drops of a deflocculating agent (sodium hexametaphosphate) were added. The mixture was placed in an ultrasound bath for 10 minutes prior to analysis, in order to separate particle aggregates and minimize reading errors. Samples were then washed into the 1000 ml beaker of the sample dispersion unit (Malvern Instruments® Hydro 2000MU), where the sample solution is stirred and pumped/recirculated continuously into the measurement zone. Grain size distribution for each sample was measured 5 times and the final measurement was calculated as the mean value, if standard deviation was less than 5%. Sample duplicates were also run to ensure reproducibility. The system was cleaned by 3 sequential cycles of approx. 800 ml of deionised water between each sample, and deionised water blanks were also run periodically to measure background parameters.

Grain size outputs were grouped in classes according to Friedman and Sanders, 1978 (Friedman and Sanders, 1978) and represented through relative and cumulative frequency graphs.

## 2.9. Data analysis and presentation

### *2.9.1. Data conditioning and levelling*

All soil and RDS samples were analysed for major and trace elements by X-ray fluorescence spectrometry (XRF) in the BGS facilities in Keyworth, Nottingham. In order to make the soil data fit for the purpose for which it is to be used under the G-BASE project, the soil results underwent data conditioning according to the proceedings described in Lister and Johnson (2005).

The data initially goes through a series of error checking and verification procedures, which are essentially a check that the results are reported to an acceptable standard. The quality of the data is then tested by statistical and graphical analysis of the data, element by element, using control samples inserted before submission for analysis. Once the data has been error checked, verified and accepted from the laboratory, further analysis of the data is carried out. These processes include a series of x-y plots of duplicate and replicate samples, more detailed control chart plots, and analysis of variance of the duplicate/replicate pairs to allocate variance in the results to sampling, analytical or between site variability. Analysis of both primary and secondary reference material can quantify analytical accuracy and precision.

The final part of the data conditioning procedure is necessary in order to use the data in context of other previously analysed data sets. This is the process of normalisation and levelling of the data. Normalisation of the secondary reference material results gives levelling factors that are applied to the data to give, ultimately, a single discrete national G-BASE data set. In conjunction with data from the analysis of international reference materials, accepted elemental values for all G-BASE secondary reference materials are determined (Lister and Johnson, 2005). All soil geochemical data have undergone these procedures previously to being used for the purposes of this work.

One of the objectives of the present work is to assess the relationships between RDS and soil - to compare the concentrations of elements in the RDS samples with the original G-BASE soil sample dataset. To allow this, G-BASE Standard Reference Materials (SRM) were included in the analytical runs with the RDS samples, with the purpose of accounting for any slight variations in XRF calibration between the period when the G-BASE Manchester soils were analysed and when the RDS samples were analysed.

The first step for the RDS data levelling involved the deletion of element concentrations determined by procedures not included in the UKAS Accreditation Schedule for the BGS XRF Laboratory, when these elements have also been determined by an accredited procedure (CaO, $SO_3$, $TiO_2$ and $Fe_2O_3$). Elemental results not determined due to spectral interference or low concentration, or those below the lower limit of detection (LLD) were set to 1/2 the detection limit for each element. Following this, a series of x-y regression plots were generated, one for each element, where the mean element concentration in each of the three G-BASE reference materials (S3B, S13 and S15) from the original G-BASE soil analysis is plotted against the results for the same reference materials in the RDS sample runs. In most, cases the graphs generated a near enough 1:1 relationship between the two datasets in which case no data levelling was required. The x-y regression plots (one for each element), with the elemental concentrations in the three reference materials (S3B, S13 and S15) for soil vs RDS batches can be found in Appendix 1, parts A (summer data) and B (winter data).

From the plots it can be observed that for most analytes, the regression line is approximately 1:1 ($Na_2O$, MgO, $Al_2O_3$, $SiO_2$, $K_2O$, CaO, $TiO_2$, $Fe_2O_3$, V, Cr, Co, Ni, Cu, Zn, Ga, Se, Br, Rb, Sr, Y, Zr, Nb, Hf, Th and Sm) and for these no correction factor was applied.

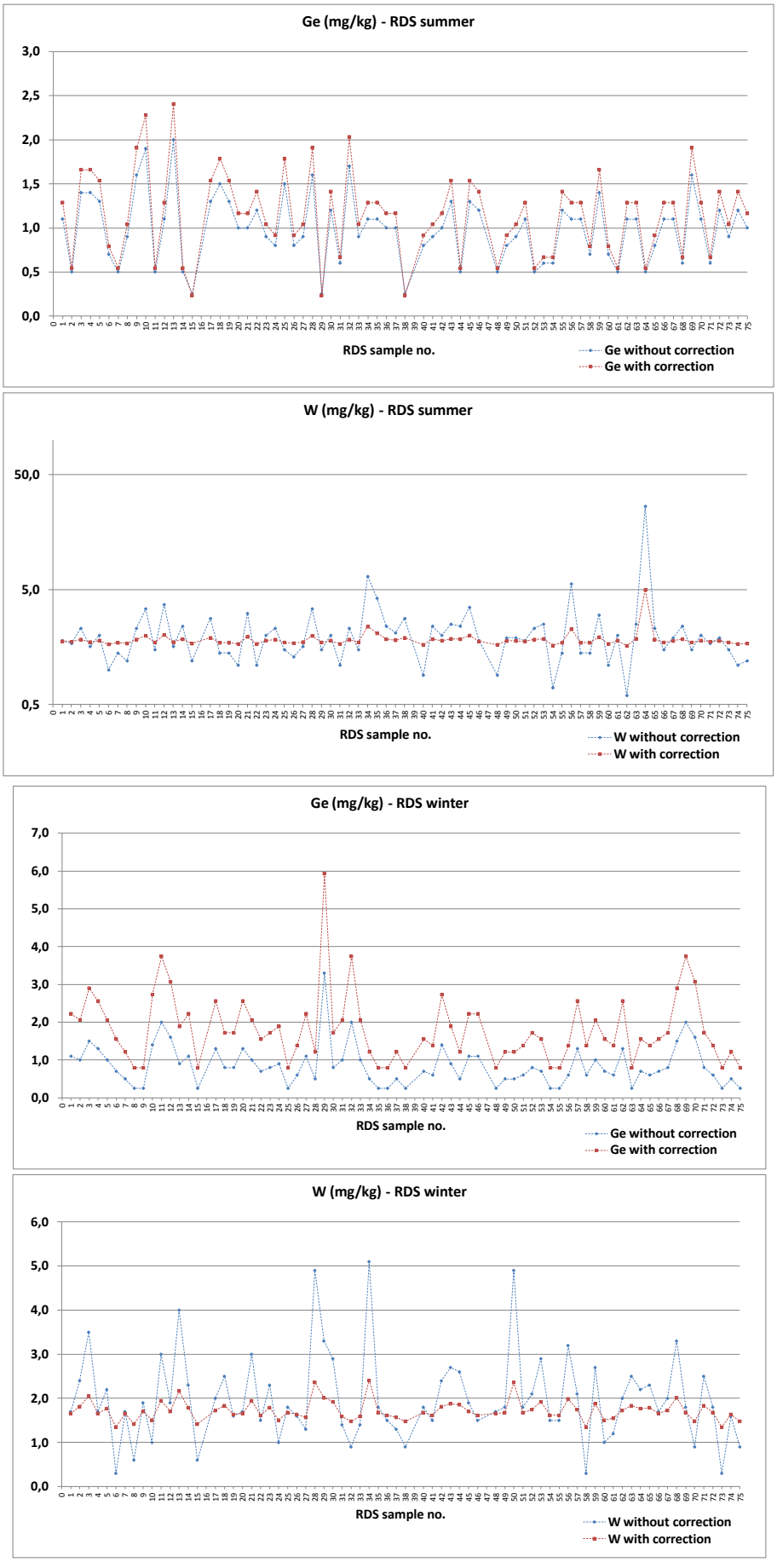


Figure 19: Plots for Ge and W concentrations in RDS samples before and after data levelling.

Other elements such as $P_2O_5$, MnO, Pb, U, I, La, Ce and Nd also show a regression line with $R^2$ of approx. 1, but since this line is generated by only 3 points, the fact that 2 of them are very close together is masking the regression. Nevertheless, the mean values for these elements between soil and RDS batches are very similar - the $R^2$ of approx. 1 is an effect of the high concentrations found in SRM S3B for these elements.

In other cases such as Ba, As, Mo, Ta, Tl, Bi, Ag, Cd, Te and Cs, elemental concentrations can be below the instrumental LLD in the SRMs and therefore x-y regression plots were not produced for these elements. Comparisons of these elements between soil and RDS samples must then be based on the assumption that XRF results are reliable according to the analysis of the primary (international) reference materials; and that analytical conditions for these elements may have changed slightly between the analysis of soil and RDS batches. The concentrations of Sc, Sn and Sb in the SRM S3B did not show any relation between soil and RDS batches and, in addition, S, Cl, Yb, Hg, Pd and In have not been determined in the SRM analysed with the soil batches nor in the soil samples - the same assumption is valid as for the elements cited above.

Two elements which showed differences in the SRMs between soil and RDS-winter batches were Ge and W. When applying the equations to the elemental concentrations determined in RDS for these elements, there was shift in values as observed in Figure 19, where dots are connected to evidence the differences between raw and levelled data - Ge concentrations are moved upwards but with no significant changes in pattern, whereas W shows an equivalent pattern within a smaller range of concentrations.

## *2.9.2. Basic and Multivariate statistics*

In a first approach, after data conditioning and levelling, soil and RDS data were subject to descriptive statistics using IBM® SPSS 19 software. Conventional statistical parameters were calculated for each elemental distribution such as maximum, minimum, arithmetic average (mean), median and standard deviation; as well as skewness and kurtosis. Normality of the distributions was tested using the Kolmogorov-Smirnov test and screened through Q-Q plots; outliers were identified through box-and-whisker plots (Reimann et al., 2005) and their influence on the distribution was measured through the observation of the 5% trimmed mean values.

An introductory method of investigating which relationship exists, if any, between a number of variables is through correlation analysis, which provides a measure of the linear relationship between variables as a precursor to multiple regression and principal component analysis. As geochemical data generally do not follow a normal distribution, the Spearman's rank correlation coefficient has been chosen as it is a non-parametric statistic which can be used when the data have violated parametric assumptions (Field, 2005). This parameter's values (*r*) vary between -1 and 1, and

significant correlations were considered those greater than |0.6| at the 95% confidence level ($p$<0.05). Like in other commonly-used statistics, the $r$ value may be misleading if outliers are present - this must be taken into account when interpreting the results, as outlier values do occur in the geochemical datasets. Outliers are capable of considerably changing the slope of the regression line and, consequently, the value of the correlation coefficient.

Differences between paired samples were evaluated using the paired-samples T-test after data transformation, as this method assumes that data distributions follow a normal distribution (cf. section 2.9.4) - the null hypothesis is that the means of two normally distributed populations are equal. The T-test is used to analyse whether differences between the mean values of condition 1 and condition 2 are statistically meaningful (Field, 2005). A negative T statistic between summer and winter data means that, for the analysed variable, there is a lower mean value in condition A if the statistic is significant at the 95% level ($p$<0.05). A non-parametric equivalent of the dependent samples T-test is the Wilcoxon signed-ranks test - it works in a fairly similar way in that it is based on the differences between scores in the two conditions to compare. Once these differences have been calculated they are ranked, but the sign of the difference (positive or negative) is assigned to the rank. First, the differences between both conditions are calculated and if the difference is 0 (i.e. the scores are the same on both conditions) data is excluded from the ranking. The positive or negative sign of the difference is noted and then the differences are ranked, ignoring whether they are positive or negative. The ranks that come from a positive difference are collected together and added up to get the sum of positive ranks - the same is done for the negative ranks. The test statistic is the smaller of these two values. IBM® SPSS 19 software has been used to calculate Spearman's rank correlation coefficients, T-test statistics and the Wilcoxon signed-ranks test statistics.

To further investigate the relationships between elemental concentrations in soils and RDS, geochemical data were subject to principal component analysis (PCA) using IBM® SPSS 19 software. Prior to PCA, data were subject to standardisation (centring and scaling), as chemical concentrations for major and trace elements were measured in different orders of magnitude - weight percent and milligrams per kilogram, respectively. This was done using the formula

$$x_{ij} = \frac{(x_{ij} - \bar{x_j})}{\sigma_j}$$

where $\bar{x}_j$ and $\sigma_j$ are the median and the standard deviation of the element distribution $j$ (Davis, 1974). Because applied geochemical and environmental data often contain outliers, the median should preferably be used instead of the mean, as the estimate of central location as it is unchanged by extreme values (Reimann et al., 2011b).

The PCA method adequacy to the data was measured through the Kaiser-Meyer-Olkin (KMO) measure of sampling adequacy and Bartlett's test of sphericity. KMO is an index for comparing the

magnitudes of the observed correlation coefficients to the magnitudes of the partial correlation coefficients - large values for the KMO measure indicate that factor analysis of the variables is suitable. KMO varies between 0 and 1, where 0 means that the sum of partial correlations is large relatively to the sum of correlations, indicating diffusion in the pattern of correlations (factor analysis might be inappropriate). Values close to 1 mean that patterns of correlations are relatively compact and so factor analysis should yield distinct and reliable factors (Field, 2005). Bartlett's test of sphericity is used to test the null hypothesis that the variables in the population correlation matrix are uncorrelated, i.e. the correlation matrix is an identity matrix. PCA needs some relationships between variables and an identity matrix means all correlation coefficients would be zero. A significant Bartlett's sphericity test (i.e. the correlation matrix is not an identity matrix) has a significance value less than 0.05 – there are significant relationships between variables.

The KMO values for individual variables are produced on the diagonal of the anti-image correlation matrix, which is also an important part of the SPSS output – as well as checking the overall KMO statistic, the diagonal elements of the anti-image correlation matrix should be above 0.5 for all variables; and the off-diagonal elements should have small values (as they represent the partial correlations between variables).

Data were then subject to the calculation of communalities, principal components and their associated eigenvalues.

Communalities are the proportion of variance of a particular variable that is due to common factors, i.e. the proportion of variance that each variable has in common with other variables. The proportion of variance that is unique to each item is then the respective item's total variance minus the communality (StatSoft, 2011). Using principal component analysis as the extraction method, total variance is used and it is assumed that each variable initial communality is 1, and so the proportions of this due to common factors range between 0 and 1.

To understand what an eigenvalue is, it is necessary to understand the concept of eigenvector. The eigenvectors of a correlation matrix consist in the linear representations that can be identified in a scatterplot graph for the observed variables, i.e. the axis of the ellipsoid produced by the dispersion of the scatterplot points. Eigenvalues are, by its turn, the scaled measure of the ellipsoid eigenvectors – analysing the eigenvalues of a dataset allows for the understanding of how the variances of the correlation matrix are distributed, i.e. the eigenvalues represent how much of the variance is explained by the component (Field, 2005).

In order to decide how many components should be retained, several methods can be used, the most common being the Kaiser criterion and the scree-plot analysis. Kaiser criterion suggests that all components with eigenvalues above 1 should be retained, but this is more accurate when analysing less than 30 variables and when the communalities after extraction are all greater than 0.7 (Field,

2005). Scree plots are graphs of each eigenvalue (Y axis) against the component with which it is associated (X axis). By plotting this graph the relative importance of each component becomes apparent – there is a sharp descent in the curve followed by a tailing off. The cut-off point for selecting components to retain should be at the point of inflexion of this curve (Field, 2005).

After deciding how many components should be retained and entering this parameter in SPSS, the eigenvalues associated with these factors are again calculated (and the percentage of variance explained). The values are the same as the values before extraction, except that the values for the discarded components are ignored. These values are then subject to rotation, which maximizes the loading of each variable on one of the extracted components whilst minimizing the loading on all other components. It works through changing the absolute values of the variables whilst keeping their differential values constant. Orthogonal varimax was the type of rotation chosen for soil geochemical data, as this kind of factor rotation attempts to maximize the dispersion of loadings within factors; i.e. it tries to load a smaller number of variables highly onto each factor resulting in more interpretable clusters of factors, whilst keeping the factors independent (Field, 2005).

Two-dimensional component plots were also generated, representing the loadings of each variable onto each pair of factors. Component scores were stored as new variables, to be used in further analysis and mapping.

### *2.9.3. Geochemical normalisation*

Textural differences such as grain size between different samples have been reported to influence trace metal concentrations, as trace metal sorption is inversely proportional to particle size (Forstner and Salomons, 1980). To make trace metal data more comparable by minimising grain size influence, trace metal normalisation has been attempted, in this case by using Al or Ga as conservative elements. The normalised concentration is the ratio between the trace element concentration and that of the conservative element in the same sample. Values were computed for the whole geochemical dataset using Microsoft® Excel 2007. This is based in the assumption that the conservative elements are correlated to the finer grain size fractions, and have a uniform flux from parent rock materials to soils and sediments (and are therefore not prone to anthropogenic enrichments). This method was used to improve the statistical power in data intercomparison.

### *2.9.4. Data transformations*

The vast majority of variable distributions in the present research were found to be positively skewed, thus deviating from normal distributions. This has been outlined by the basics statistics described in the previous section. Nevertheless, in order to perform certain types of statistics such as ordinary least squares regression and geographically-weighted regression, the assumption of data

normality needs to be achieved. This has been accomplished by means of both outlier exclusion and data transformation through logarithmic (log) and Box-Cox functions.

Log-transformed variables were calculated using Microsoft® Excel 2007 software by using natural logs of each raw variable value (Miesch and Chapman, 1977). Some variables contained zero values, so all values were added a constant (1) prior to applying the log transformation. The transformed variable $Y(s)$ can be defined as

$$Y(s) = \ln(Z(s))$$

where $Z(s)$ is the observed data and $\ln$ is the natural logarithm.

For some variables, the log transformation did not produce satisfactory results, i.e. $Y(s)$ was not closer to a normal distribution than the original distribution. The Box-Cox transformation (Howarth and Earle, 1979) was found more suitable in those cases. The Box-Cox transformation can be defined as

$$Y(s) = (Z(s)^{\lambda} - 1)/\lambda$$

where $\lambda$ is a power to which raw values should be raised. This value varies in order to calibrate the transformation to be maximally effective in moving the variable towards normality. If $\lambda$ = 0, the density distribution reduces to the lognormal form (a special situation). Action®, a Microsoft® Excel plug-in includes an algorithm which was used to determine the optimal $\lambda$ (the value that maximises the function by lowering the skewness and kurtosis parameters of the transformed distribution), and produce the transformed variable using the calculated $\lambda$.

New outlier analysis was performed using the transformed data and extreme values were considered for exclusion in further geostatistical modelling.

### *2.9.5. Geochemical mapping*

To provide a spatial overview on the distribution of elemental concentrations and other environmental parameters, soils and RDS variables were represented as proportional symbol/colour maps as well as interpolated surface maps.

To give a good indication of sampling locations and for straightforward data interpretation, proportional symbol/colour maps were produced for the majority of variables for soils and RDS using GIS software ESRI® ArcGIS 10.0. These maps consist of symbols representing the location of each sample, where the symbol size is proportional to the value at that point. Symbol sizes are classified according to the 5$^{th}$, 10$^{th}$, 15$^{th}$, 25$^{th}$, 50$^{th}$, 75$^{th}$, 90$^{th}$, 95$^{th}$, 99$^{th}$ and 100$^{th}$ percentiles of data, and a different colour is coded for each interval for easy visualisation.

Interpolated surfaces were also produced for variables of environmental concern using inverse distance-weighted (IDW) and kriging functions in ESRI® ArcGIS 10.0 IDW is a simple deterministic

method, which calculates cell values using a linearly weighted combination of a set of sample points, the weight being a function of inverse distance. This is based in the principle that points close to each other have more correlation and similarities than those farther away.

Ordinary kriging was also tested as an interpolation technique. Kriging is a geostatistical interpolation method which is based on statistical models that include autocorrelation; i.e. the statistical relationships among the measured points. Kriging is similar to IDW in that it weights the surrounding measured values to derive a prediction for an unmeasured location. Firstly, semivariograms were computed to determine the spatially dependent variance. Experimental semivariograms were examined for the best models (i.e. stable, exponential, spherical and gaussian) separately and the best fitted model was selected. Nugget variance, range and sill parameters were calculated. Nugget variance is the variance at zero distance, sill is the value at which the semivariograms model attains the range, and the range is the distance at which values of one variable become spatially independent of another. As with IDW interpolation, the measured values closest to the unmeasured locations have the most influence. However, the kriging weights for the surrounding measured points are more sophisticated than those of IDW. IDW uses a simple algorithm based on distance, but kriging weights come from a semivariogram that was developed by looking at the spatial nature of the data. To create a continuous surface of the phenomenon, predictions are made for each location, or cell centers, in the study area based on the semivariogram and the spatial arrangement of measured values that are nearby.

## *2.9.6. Spatial statistical analysis*

### 2.9.6.1. Explanatory variables

In order to model the relationships between trace metals and other explanatory variables which are likely to control their concentrations in soils and RDS, additional variables were created using road, traffic, building, population, jobs and topography datasets in ESRI® ArcGIS 10.0. The calculated explanatory variables are listed in Table 10 and Table 11. These new variables were calculated using as many datasets as possible from those freely available, which are referred to throughout this text and summarised in Table 12. For soils, 26 variables, 10 of which were calculated at 8 different buffer distances, were considered for inclusion in the spatial statistical models, in a total of 96 variables. For RDS, 39 variables were considered, 10 of which at 7 different buffer distances, in a total of 99 variables.

First of all, attributes from the OS MasterMap® Integrated Transport Network (ITN) dataset were directly joined based on spatial location to soil and RDS datasets, in order to obtain distance variables for nearest bus stop, intersection and railway. The same was performed using Landmap Building Heights (UKMap©) dataset for building related data - variables retained were distance to nearest

building, its height, area and volume. Census data (Crown®, HMSO) were only available at the highest spatial resolution (output area) for the year 2001 - Census 2011 data were only available at the local authority level at the time of writing. Population density and number of jobs per output area from the Census 2001 dataset were joined to the soils and RDS datasets based on sample spatial location.

Circular buffer zones were created around each soil and RDS sampling location with varying radii (25, 50, 100, 150, 200, 250, 300 and 350 metres), in order to perform zonal calculations. The number of bus stops and junctions within each buffer distance was counted by spatially joining each buffer layer with the bus and intersections layers. A new count field is created for each buffer distance and added to the soils and RDS datasets.

| Variable | Description | Single value | Distance buffers (m) | | | | | | | |
|---|---|---|---|---|---|---|---|---|---|---|
| | | | 25 | 50 | 100 | 150 | 200 | 250 | 300 | 350 |
| **pH** | Soil pH | x | | | | | | | | |
| **LOI** | Soil LOI organic matter content | x | | | | | | | | |
| **Land_use** | Soil land use (as recorded onsite) | x | | | | | | | | |
| **DistJunct** | Distance to nearest junction | x | | | | | | | | |
| **JunctX** | No. of junctions within X metres distance | | x | x | x | x | x | x | x | x |
| **DistBus** | Distance to nearest bus stop | x | | | | | | | | |
| **BusX** | No. of bus stops within X metres distance | | x | x | x | x | x | x | x | x |
| **RlDist** | Distance to nearest railway | x | | | | | | | | |
| **RailX** | Density of raiways within X metres distance | | x | x | x | x | x | x | x | x |
| **RdGAX** | Density of A-group roads within X metres distance | | x | x | x | x | x | x | x | x |
| **RdGBX** | Density of B-group roads within X metres distance | | x | x | x | x | x | x | x | x |
| **RdGCX** | Density of C-group roads within X metres distance | | x | x | x | x | x | x | x | x |
| **RdAll** | Density of all roads within X metres distance | | x | x | x | x | x | x | x | x |
| **ADTall** | Average anual daily traffic flow - all vehicles | x | | | | | | | | |
| **ADT_HGV** | Average anual daily traffic flow - heavy goods vehicles | x | | | | | | | | |
| **DistBldg** | Distance to nearest building | x | | | | | | | | |
| **BldA0** | Area of nearest building | x | | | | | | | | |
| **BldHt0** | Height of nearest building | x | | | | | | | | |
| **BldV0** | Volume of nearest building | x | | | | | | | | |
| **BldXA** | Area covered by buildings within X metres distance | | x | x | x | x | x | x | x | x |
| **BldXH** | Building average height within X metres distance | | x | x | x | x | x | x | x | x |
| **BldXV** | Building volume within X metres distance | | x | x | x | x | x | x | x | x |
| **Height** | Terrain height | x | | | | | | | | |
| **Slope** | Terrain slope | x | | | | | | | | |
| **PopDens** | Population density per output area | x | | | | | | | | |
| **PopJobs** | Number of jobs per output area | x | | | | | | | | |

Table 10: Explanatory variables for soil spatial statistical analysis.

OS MasterMap® ITN dataset divides roads into 9 different groups, as described in Table 13. For the purposes of this work, the ITN dataset was condensed into three new groups - A, B and C, based on the likelihood of high traffic intensities. Therefore, motorways, A roads and B roads were grouped in Group A to serve as an indicator of heavy traffic. Group B comprises minor roads and local streets, of generally moderate traffic intensity; and group C includes alleys, pedestrianised streets and private roads, as these are the least prone to the impacts of vehicle traffic.

The 3 groups of road data were rasterised with a cell size of 1m, as well as railways from the Strategi® dataset. Zonal statistics were then performed to calculate the length of each road type or railway within each buffer distance, using the zonal statistics as table tool from ArcGIS 10.0 spatial analyst. These values were table-joined to the soils and RDS datasets.

| Variable | Description | Single value | Distance buffers (m) | | | | | | |
|---|---|---|---|---|---|---|---|---|---|
| | | | 25 | 50 | 100 | 150 | 200 | 250 | 300 |
| **LOI** | RDS LOI organic matter content | x | | | | | | | |
| **Land_use** | RDS land use (as recorded onsite) | x | | | | | | | |
| **500_1000** | % grain size fraction between 500 - 1000 µm | x | | | | | | | |
| **250_500** | % grain size fraction between 250 - 500 µm | x | | | | | | | |
| **125_250** | % grain size fraction between 125 - 250 µm | x | | | | | | | |
| **63_125** | % grain size fraction between 63 - 125 µm | x | | | | | | | |
| **32_63** | % grain size fraction between 32 - 63 µm | x | | | | | | | |
| **16_32** | % grain size fraction between 16 - 32 µm | x | | | | | | | |
| **8_16** | % grain size fraction between 8 - 16 µm | x | | | | | | | |
| **4_8** | % grain size fraction between 4 - 8 µm | x | | | | | | | |
| **2_4** | % grain size fraction between 2 - 4 µm | x | | | | | | | |
| **inf_2** | % grain size fraction below 2 µm | x | | | | | | | |
| **1000_63** | % grain size fraction between 1000-63 µm | x | | | | | | | |
| **63_inf2** | % grain size fraction below 63 µm | x | | | | | | | |
| **d0.5** | Median grain size | x | | | | | | | |
| **D** | Volume-weighted mean grain size | x | | | | | | | |
| **DistJunct** | Distance to nearest junction | x | | | | | | | |
| **JunctX** | No. of junctions within X metres distance | | x | x | x | x | x | x | x |
| **DistBus** | Distance to nearest bus stop | x | | | | | | | |
| **BusX** | No. of bus stops within X metres distance | | x | x | x | x | x | x | x |
| **RlDist** | Distance to nearest railway | x | | | | | | | |
| **RailX** | Density of raiways within X metres distance | | x | x | x | x | x | x | x |
| **RdGAX** | Density of A-group roads within X metres distance | | x | x | x | x | x | x | x |
| **RdGBX** | Density of B-group roads within X metres distance | | x | x | x | x | x | x | x |
| **RdGCX** | Density of C-group roads within X metres distance | | x | x | x | x | x | x | x |
| **RdAll** | Density of all roads within X metres distance | | x | x | x | x | x | x | x |
| **ADTall** | Average anual daily traffic flow - all vehicles | x | | | | | | | |
| **ADT_HGV** | Average anual daily traffic flow - heavy goods vehicles | x | | | | | | | |
| **DistBldg** | Distance to nearest building | x | | | | | | | |
| **BldA0** | Area of nearest building | x | | | | | | | |
| **BldHt0** | Height of nearest building | x | | | | | | | |
| **BldV0** | Volume of nearest building | x | | | | | | | |
| **BldXA** | Area covered by buildings within X metres distance | | x | x | x | x | x | x | x |
| **BldXH** | Building average height within X metres distance | | x | x | x | x | x | x | x |
| **BldXV** | Building volume within X metres distance | | x | x | x | x | x | x | x |
| **Height** | Terrain height | x | | | | | | | |
| **Slope** | Terrain slope | x | | | | | | | |
| **PopDens** | Population density per output area | x | | | | | | | |
| **PopJobs** | Number of jobs per output area | x | | | | | | | |

Table 11: Explanatory variables for RDS spatial statistical analysis

| Variable | Source | Web | Year |
|---|---|---|---|
| **DistJunct** | OS MasterMap® Integrated Transport Network Layer™ | ordnancesurvey.co.uk | 2011 |
| **JunctX** | OS MasterMap® Integrated Transport Network Layer™ | ordnancesurvey.co.uk | 2011 |
| **DistBus** | DataGM - © Ordnance Survey | datagm.org.uk | 2010 |
| **BusX** | DataGM - © Ordnance Survey | datagm.org.uk | 2010 |
| **RlDist** | OS MasterMap® Strategi® | ordnancesurvey.co.uk | 2011 |
| **RailX** | OS MasterMap® Strategi® | ordnancesurvey.co.uk | 2011 |
| **RdGAX** | OS MasterMap® Integrated Transport Network Layer™ | ordnancesurvey.co.uk | 2011 |
| **RdGBX** | OS MasterMap® Integrated Transport Network Layer™ | ordnancesurvey.co.uk | 2011 |
| **RdGCX** | OS MasterMap® Integrated Transport Network Layer™ | ordnancesurvey.co.uk | 2011 |
| **RdAll** | OS MasterMap® Integrated Transport Network Layer™ | ordnancesurvey.co.uk | 2011 |
| **ADTall** | © Department for Transport | dft.gov.uk | 2002 and 2010 |
| **ADT_HGV** | © Department for Transport | dft.gov.uk | 2002 and 2010 |
| **DistBldg** | Landmap Building Heights - UKMap© The GeoInformation Group | landmap.ac.uk | 2011 |
| **BldA0** | Landmap Building Heights - UKMap© The GeoInformation Group | landmap.ac.uk | 2011 |
| **BldHt0** | Landmap Building Heights - UKMap© The GeoInformation Group | landmap.ac.uk | 2011 |
| **BldV0** | Landmap Building Heights - UKMap© The GeoInformation Group | landmap.ac.uk | 2011 |
| **BldXA** | Landmap Building Heights - UKMap© The GeoInformation Group | landmap.ac.uk | 2011 |
| **BldXH** | Landmap Building Heights - UKMap© The GeoInformation Group | landmap.ac.uk | 2011 |
| **BldXV** | Landmap Building Heights - UKMap© The GeoInformation Group | landmap.ac.uk | 2011 |
| **Height** | OS MasterMap® Topography Layer™ | ordnancesurvey.co.uk | 2012 |
| **Slope** | OS MasterMap® Topography Layer™ | ordnancesurvey.co.uk | 2012 |
| **PopDens** | Crown®, HMSO - Office for National Statistics | census.ukdataservice.ac.uk | 2001 |
| **PopJobs** | Crown®, HMSO - Office for National Statistics | census.ukdataservice.ac.uk | 2001 |

Table 12: Explanatory variable sources for spatial statistical analysis (under version 2.0 of the Open Government Licence, URL: nationalarchives.gov.uk/doc/open-government-licence/version/2/).

| OS MasterMap® ITN classes | Groups |
|---|---|
| **Motorways** (dual carriageways with a speed limit of max. 70 mph) | **Group A** |
| **A roads** (single or dual carriageways with a speed limit of max. 60 and 70 mph, respectively) | |
| **B roads** (single carriageways with a speed limit of max. 60 mph) | |
| **Minor roads** (max. 30 or 40 mph) | **Group B** |
| **Local streets** (max. 30 mph) | |
| Alleys | **Group C** |
| Pedestrianised streets | |
| Private roads, publicly accessible | |
| Private roads, restricted access | |

Table 13: Classification of roads.

Building data from LandMap® were treated in a similar way: the dataset was rasterised using height as the value field and a cell size of 1m, and zonal statistics was used to calculate the mean building height and the total building area within each distance buffer. These new variables table-joined to the soils and RDS datasets, and building volume variable was also calculated by multiplying building area by the mean height for each distance buffer.

The same work was also done for the average annual daily traffic flow (AADTF) dataset from the UK Department for Transport, for the years of soil and RDS sample collection (2002 for soils and 2010 for RDS). Nevertheless, as this is a point feature dataset, values were first interpolated with a resolution of $1m^2$ and using the IDW method in order to obtain approximate AADTF values at each soil and RDS sample location, prior to zonal statistics.

Terrain slope was derived from the OS MasterMap® Topography layer using the surface slope tool of ArcGIS 10.0 spatial analyst. For each point, altitude and slope values were obtained by performing zonal statistics and joining the obtained tables to the soils and RDS datasets.

### 2.9.6.2. Ordinary least squares regression

Ordinary least squares regression (OLS) was performed using ArcGIS 10.0 OLS tool from the spatial statistics toolset. OLS is the best known of all regression techniques. It is also the proper starting point for all spatial regression analyses, as it provides a global model for the dependent variable (observed metal concentrations), creating a single regression equation to represent it through a number of independent (explanatory) variables (Rawlings et al., 1998). This equation can be described as

$$Y = \beta_0 + \beta_1 X_1 + \beta_2 X_2 + \cdots + \beta_n X_n + \varepsilon$$

where $Y$ is the dependent variable, $X_{1,n}$ are the independent variables, $\beta_{1,n}$ are the regression coefficients, and $\varepsilon$ is the random error term, or residual, representing the unexplained variation of $Y$. In the present work, the dependent variables were Cr, Ni, Cu, Zn, As and Pb; and the independent variables tested were those of Table 10 and Table 11.

Firstly, samples with outlier metal concentrations were censored from the dataset, and log or Box-Cox transformed data were used to ensure distribution normality. For each metal, OLS independent variables were added to the model in a stepwise way, so that the most important predictors were included first. Additionally, variables taken at different distance buffers were tested separately to define which distance maximized the $R^2$ for each variable; and also because these explanatory variables usually show different degrees of global collinearity and produce large variance inflation factors (VIF) if included in the same OLS regression model.

Independent variables which were retained showed a significant *p* value (<0.05) and variance inflation factor (VIF) below 5 (VIF>7.5 indicates variable redundancy), producing models with significant $R^2$, Joint-F (overall model significance) and Joint-Wald statistics (robust overall model significance), and non-significant Koenker (unbiased standard errors) and Jarque-Bera statistics (residuals are normally distributed). A statistical report has been produced for each model, as well as an output feature class with the predicted values, residuals and standardized residuals, which were displayed as a cold-to-hot rendered map. Spatial autocorrelation (Moran's I) tool was used to calculate the degree of spatial dependence present in the OLS residuals - if high/low residuals are clustered, it indicates that the model produces under- and over-predictions in certain areas. This may be the result of key variables being missing from the model, relationships being nonlinear, and/or the presence of influential outliers. If OLS models display statistically significant non-stationarity or

residuals display spatial autocorrelation, geographically-weighted regression is recommended, as explained in the next section.

### 2.9.6.3. Geographically-weighted regression

Geographically weighted regression is a local spatial statistical technique for exploring spatial non-stationarity. Spatial non-stationarity (regional variation) is frequent in environmental modelling, as the processes which underlie the relationship between variables may not be constant throughout the studied area; instead, they change with spatial context. OLS regression models where the residuals show spatial autocorrelation are good candidates for GWR. The OLS regression equation can thus be rewritten reflecting spatial non-stationarity:

$$Y(u,v) = \beta_{0(u,v)} + \beta_{1(u,v)}X_1 + \beta_{2(u,v)}X_2 + \cdots + \beta_{n(u,v)}X_n + \varepsilon(u,v)\ ,$$

where $(u, v)$ are the coordinates of each location.

GWR provides a local model of the predicted variable by fitting a regression equation to every feature in the dataset. GWR fits potentially different coefficient values for each observation as a function of a spatial kernel weighting scheme, the most important characteristic of which is its bandwidth, i.e. the distance within which other areas will have influence (Fotheringham et al., 2002).

In the present work, GWR was performed using the ArcGIS 10.0 GWR tool of the spatial statistics toolset for the same dependent variables (Cr, Ni, Cu, Zn, As and Pb) as for OLS, using an adaptive kernel type, and the kernel extent was defined using the corrected Akaike Information Criterion (AICc) - the bandwidth distance will change according to the spatial density of sampling locations, i.e. the bandwidth becomes a function of the number of nearest neighbours such that each local estimation is based on the same number of features.

The GWR tool produces two kinds of outputs for each analysis: a supplementary table with the summary information about model variables and parameters (number of neighbours, residual squares, effective number, AICc, $R^2$ and adjusted $R^2$), as well as an output feature class containing the local GWR results for each sampling point: condition number (values >30 indicate results are unstable due to local multicollinearity), local $R^2$ (high values indicate the model is predicting well), predicted values, residuals, coefficient standard errors and standardised residuals. This last term is also displayed as a cold-to-hot rendered map, representing the standardised difference between the observed metal concentrations and its predicted value at each sampling point. Spatial autocorrelation (Moran's I) tool was used to to calculate the degree of spatial dependence present in the GWR model residuals. When comparing between different models for the same dependent variable, those with lower lower AICC were chosen - this value measures the information gap between the predicted model and a model representing reality (Fotheringham et al., 2002).

Coefficient raster surfaces were created to assess regional variation in the model explanatory variables and to understand how spatially consistent relationships between metal concentrations and each explanatory variable are across the study area. A map of t-statistics has also been created for each explanatory variable, which shows the statistical significance of the local model at each sampling point - a high absolute t-statistic value indicates the variable contributes significantly to the model. T-statistics are used to represent statistical significance ($p<0.05$ or $p<0.01$) in a positive or negative association, and are calculated at each location as the estimated parameters or coefficients divided by the standardised residuals.

# 3. Urban Soil Geochemistry

## Summary

With the purpose of characterising soil geochemistry in the Manchester urban area, 300 soil samples were collected over 75Km$^2$ of Manchester, Salford and Trafford (UK) by the G-BASE project (Geochemical Baseline Survey of the Environment) of the British Geological Survey. These were chemically analysed for 48 elements by XRF; LOI and pH have also been determined and data were made available for the present work. A subset of samples were further analysed by SEM-EDS for grain morphology and composition at the MMU; at this stage, organic/inorganic carbon have also been determined. Data analysis included element mapping, basic statistics, distribution analysis, correlation analysis and principal component analysis.

In this chapter, the main results are presented and interpreted, areas with the highest concentrations of potentially harmful elements are assessed and probable contaminant sources are targeted.

## 3.1. Exploratory data analysis

### *3.1.1. Preliminary statistics and characterization of variable distributions*

In total, 48 elements were determined in soils at the BGS XRF facilities following the procedure described in section 2.4. However, for the elements Cs, Ta, and Te over 87, 95 and 70% of the samples (respectively) had concentrations below the lower limit of detection (cf. Table 5) and therefore these elements were not considered in further statistical calculations. Cs, Ta and Te concentrations above the LLD are only considered when interpreting geochemical data at the sample scale.

After data conditioning and levelling, as described in section 2.9.1, soil geochemical data for 45 elements and other parameters such as soil pH, organic matter content (LOI), total carbon (TC) and organic/inorganic carbon (OC/IC) data have been subject to exploratory statistics. Maximum, minimum, mean, median, standard deviation, variance, skewness and kurtosis of the data distributions were calculated and are summarised in Table 14.

In a first observation, maximum concentrations are often highly above the median concentrations especially in trace elements, due to the presence of strong outliers. Maximum concentrations for As and Cd are 50 and 89 times higher, respectively, than the median value of the Manchester soil dataset. For Zn, Pb, Cr and Cu, maximum values were between 10 and 24 times higher than the median values. Within the major elements, maximum concentrations for CaO and MnO are the highest above the median - 7.5 and 9.5 times higher, respectively.

| Variable | Units | Minimum | Maximum | Mean | Median | Std. dev. | Variance | Skewness | Kurtosis |
|---|---|---|---|---|---|---|---|---|---|
| Na2O | wt. % | 0,3 | 0,8 | 0,5 | 0,5 | 0,1 | 0,0 | 0,7 | 3,5 |
| MgO | wt. % | 0,2 | 2,7 | 1,0 | 0,9 | 0,4 | 0,1 | 1,7 | 4,0 |
| Al2O3 | wt. % | 5,2 | 23,6 | 10,1 | 9,8 | 2,3 | 5,2 | 1,6 | 5,8 |
| SiO2 | wt. % | 35,5 | 86,2 | 66,2 | 67,0 | 7,0 | 49,6 | -0,8 | 2,1 |
| P2O5 | wt. % | 0,08 | 1,30 | 0,33 | 0,29 | 0,17 | 0,03 | 2,19 | 7,00 |
| K2O | wt. % | 1,11 | 3,60 | 1,67 | 1,62 | 0,34 | 0,11 | 1,87 | 6,85 |
| CaO | wt. % | 0,2 | 8,8 | 1,4 | 1,2 | 1,1 | 1,3 | 2,8 | 12,2 |
| TiO2 | wt. % | 0,12 | 0,93 | 0,46 | 0,44 | 0,11 | 0,01 | 0,68 | 0,90 |
| MnO | wt. % | 0,015 | 0,626 | 0,074 | 0,066 | 0,050 | 0,003 | 7,017 | 68,414 |
| Fe2O3 | wt. % | 1,27 | 20,26 | 4,91 | 4,56 | 1,88 | 3,54 | 2,93 | 16,67 |
| Sc | mg/kg | 3 | 29 | 10 | 10 | 3 | 10 | 1,8 | 6,6 |
| V | mg/kg | 26 | 234 | 87 | 82 | 27 | 720 | 2,0 | 6,2 |
| Cr | mg/kg | 30 | 1238 | 92 | 76 | 92 | 8530 | 8,7 | 91,8 |
| Co | mg/kg | 3,2 | 44,1 | 9,6 | 8,6 | 4,4 | 19,5 | 3,3 | 17,3 |
| Ba | mg/kg | 287 | 5476 | 583 | 511 | 370 | 137126 | 8,4 | 103,0 |
| Ni | mg/kg | 4,5 | 148,3 | 33,5 | 29,4 | 17,8 | 317,4 | 2,9 | 12,4 |
| Cu | mg/kg | 7,2 | 2072,9 | 120,5 | 85,9 | 157,5 | 24803,4 | 7,7 | 83,2 |
| Zn | mg/kg | 25,0 | 1762,9 | 227,2 | 168,8 | 197,1 | 38859,3 | 3,5 | 17,9 |
| Ga | mg/kg | 4,80 | 32,10 | 10,25 | 9,70 | 3,21 | 10,28 | 2,53 | 11,98 |
| Ge | mg/kg | 1,6 | 31,8 | 4,7 | 3,9 | 3,2 | 10,3 | 4,7 | 30,4 |
| As | mg/kg | 2,5 | 1001,0 | 27,9 | 20,1 | 58,4 | 3412,2 | 15,6 | 259,9 |
| Se | mg/kg | 0,1 | 3,2 | 0,5 | 0,4 | 0,4 | 0,2 | 2,1 | 7,1 |
| Br | mg/kg | 1,6 | 38,7 | 15,2 | 14,8 | 5,6 | 31,8 | 0,6 | 1,2 |
| Rb | mg/kg | 36 | 166 | 59 | 57 | 15 | 220 | 2,7 | 14,9 |
| Sr | mg/kg | 43 | 336 | 77 | 70 | 31 | 933 | 3,7 | 22,0 |
| Y | mg/kg | 6 | 44 | 18 | 18 | 5 | 27 | 1,6 | 4,9 |
| Zr | mg/kg | 62 | 500 | 158 | 154 | 40 | 1567 | 2,7 | 19,7 |
| Nb | mg/kg | 2 | 16 | 8 | 8 | 2 | 4 | 0,7 | 1,3 |
| Mo | mg/kg | 0,1 | 21,9 | 3,2 | 2,5 | 2,8 | 7,7 | 3,3 | 15,2 |
| Hf | mg/kg | 1 | 12 | 3 | 3 | 1 | 1 | 2,4 | 16,0 |
| W | mg/kg | 1,0 | 33,2 | 2,9 | 2,3 | 2,8 | 7,8 | 7,1 | 62,4 |
| Tl | mg/kg | 0,25 | 4,1 | 0,5 | 0,3 | 0,4 | 0,2 | 4,0 | 23,9 |
| Pb | mg/kg | 19,5 | 2758,0 | 276,3 | 218,3 | 268,2 | 71942,9 | 5,4 | 40,1 |
| Bi | mg/kg | 0,15 | 34,3 | 0,8 | 0,2 | 2,6 | 6,9 | 9,2 | 102,4 |
| Th | mg/kg | 2,3 | 20,9 | 6,2 | 6,0 | 1,9 | 3,8 | 2,5 | 13,3 |
| U | mg/kg | 0,25 | 4,5 | 2,1 | 2,1 | 0,7 | 0,4 | 0,6 | 2,0 |
| Ag | mg/kg | 0,25 | 7,9 | 0,8 | 0,6 | 0,8 | 0,7 | 4,8 | 32,7 |
| Cd | mg/kg | 0,25 | 80,3 | 1,4 | 0,9 | 4,7 | 22,1 | 16,0 | 269,1 |
| Sn | mg/kg | 3,3 | 365,1 | 29,6 | 18,2 | 36,8 | 1356,7 | 4,7 | 30,8 |
| Sb | mg/kg | 1,9 | 48,7 | 7,6 | 5,4 | 6,6 | 43,5 | 3,2 | 12,9 |
| I | mg/kg | 1,0 | 10,0 | 2,1 | 2,0 | 1,2 | 1,4 | 2,1 | 8,9 |
| La | mg/kg | 6 | 76 | 27 | 26 | 9 | 90 | 1,5 | 4,4 |
| Ce | mg/kg | 14 | 112 | 48 | 46 | 14 | 194 | 1,4 | 3,9 |
| Nd | mg/kg | 8 | 52 | 22 | 21 | 7 | 46 | 1,4 | 3,8 |
| Sm | mg/kg | 1 | 17 | 5 | 4 | 3 | 11 | 0,7 | 0,1 |
| OM (LOI) | wt. % | 2,63 | 21,59 | 8,69 | 8,46 | 2,98 | 8,86 | 0,95 | 1,84 |
| TC (DC) | wt. % | 2,78 | 20,57 | 7,54 | 7,07 | 2,88 | 8,30 | 1,39 | 3,22 |
| OC (DC) | wt. % | 2,53 | 19,18 | 7,49 | 6,83 | 3,10 | 9,60 | 1,08 | 1,78 |
| IC | wt. % | 0,07 | 3,03 | 0,86 | 0,80 | 0,46 | 0,21 | 2,37 | 8,53 |
| pH | - | 3,9 | 7,98 | 6,11 | 6,275 | 0,87 | 0,75 | -0,56 | -0,49 |

Table 14: Summary statistics for Manchester BGS soils.

Most distributions are positively skewed, except for $SiO_2$ and pH - these variables exhibit a slightly negative skewness value. Most distributions are also leptokurtic (kurtosis > 0), as the peaks are more acute around the mean. Sm is close to a mesokurtic distribution (kurtosis=0) and pH shows a negative kurtosis value, as the peak around the distribution mean is lower and wider - pH has a platykurtic distribution. These remarks can be observed as well in the histograms of Figure 98 of Appendix 2.

As is the case for most environmental geochemical data, the Manchester BGS soil dataset often displays outlier values, and distributions are non-normal for all variables. This has been confirmed by the Kolmogorov-Smirnov tests in Table 74 of Appendix 2 - the test is significant (sig. <0.05) for all variables. Only $SiO_2$, Br and TOC show significance values above 0.00 (0.24, 0.46 and 0.08, respectively) - still, distributions are clearly non-normal. The logarithmic transformation brought 13 variables close to normality at the 95% confidence level ($p<0.05$) and the Box-Cox transformation did so for 24 variables out of the 50 variables, as can be observed in Table 75 and Table 76 of Appendix 2.

For easy visualisation of variable distributions, a series of box-and-whisker plots were produced for all variables, displayed in Figure 99 of Appendix 2. The lower edge of the box represents the 1$^{st}$ quartile (Q1) and the upper edge the 3$^{rd}$ (Q3) quartile, and the difference between these values is the interquartile range (IQR). Samples outside this interval are considered outliers and are represented as circles, labelled with the soil sample number.

These are values between 1.5 and 3 times the IQR, measured from the ends of the box. Extreme outliers are those with a value more than 3 times the IQR, measured in the same way, and are represented by an asterisk. The positive skewness of most variables can also be inferred from these plots, as most of them show a large number of upper outliers.

### *3.1.2. Organic matter content, carbon contents and pH*

Manchester soils have undergone the procedures explained in section 2.5. for determination of organic matter contents; total, organic and inorganic carbon contents; and pH. Summary statistics for these parameters are described in Table 14 above. Distribution histograms and box-and-whisker plots can be observed in Figure 98 and Figure 99 of Appendix 2 - distributions are non-normal for all the parameters, as demonstrated by the Kolmogorov-Smirnov tests of Table 74 (Appendix 2).

**pH** values vary between 3.9 and 7.98, displaying a negatively skewed distribution with a median value of 6.28. According to the classification of soils based on pH (US-SCC, 1993), Manchester soils can be classified as displayed in Figure 20. Manchester soils are predominantly neutral to moderately acid, as c. 72% of the total number of samples fall within the 5.6-7.3 pH range. Around 24% of the

samples vary from strongly to extremely acid. At the other end there are slightly to moderately alkaline samples which are much less frequent in the Manchester dataset.

| Classification | pH range | No. of samples |
|---|---|---|
| Ultra acid | < 3.5 | - |
| Extremely acid | 3.5 - 4.4 | 16 |
| Very strongly acid | 4.5 - 5.0 | 25 |
| Strongly acid | 5.1 - 5.5 | 30 |
| Moderately acid | 5.6 - 6.0 | 48 |
| Slightly acid | 6.1 - 6.5 | 63 |
| Neutral | 6.6 - 7.3 | 104 |
| Slightly alkaline | 7.4 - 7.8 | 13 |
| Moderately alkaline | 7.9 - 8.4 | 1 |
| Strongly alkaline | 8.5 - 9.0 | - |
| Very strongly alkaline | > 9.0 | - |

Table 15: Soil pH classes (US-SCC, 1993) and number of Manchester soils in each class.

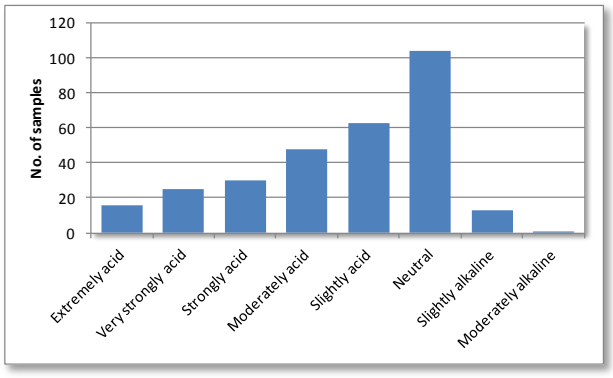


Figure 20: US-SCC (1993) classification of Manchester soils.

Soil pH is an indication of its quality, as it regulates nutrient availability, biogeochemical cycling, contaminant sorption, structural stability and biological activity (EA, 2006). Acidification is a natural soil process, the rate of which can be altered by anthropogenic activity. Sources can be diverse - atmospheric inputs from fossil fuel combustion, liming and fertilization practices, organic waste recycling, etc.

Depending on clay, organic matter and carbonate contents, soils act as a buffer for pH - its value changes little in the addition of an acid or base, and it may be considered that soils behave as weak acids (EA, 2006). Nevertheless, accelerated acidification processes are often associated with extreme events in anthropogenically-impacted areas, and acidification may have dramatic effects upon trace metal availability, leading to potentially toxic concentrations of PHE being released into the soil solution, with deleterious effects upon human and ecosystem health.

Around 61% of Manchester soil samples are below pH 6.5 - Manchester soils are mostly acidic and very low pH values must be carefully investigated for high trace metal contents.

**Organic matter** (OM) contents in Manchester soils determined by LOI have a median value of 8.46%, ranging from 2.63 to 21.59%. According to the soil classification suggested in Huang et al. (2009), most of the Manchester soil samples are classified as mineral soils with organic matter, as 285 soil samples contain between 3 and 15% of OM. 3 samples are essentially mineral soils (below 3% OM), and 12 are organic soils (above 15% OM), as represented in Table 16.

| Classification | OM range | No. of samples | % of samples |
|---|---|---|---|
| Mineral soil | ≤ 3% | 3 | 1 |
| Mineral soil with organic matter | 3 - 15% | 285 | 95 |
| Organic soil | 15 - 30% | 12 | 4 |
| Peat | > 30% | - | - |

Table 16: Manchester soil classifications (Huang et al., 2009), n=300.

Soils with high organic matter content tend to have larger cation exchange capacity - the amount of organic matter may therefore be associated with trace metal concentrations. Soil organic matter also

influences the immobilisation of trace metals (Staunton et al., 2002). Nevertheless, changing conditions or the presence of dissolved organic compounds have been reported to increase the extractability of metals and their bioavailability (Antoniadis and Alloway, 2002). Organic matter plays an essential role in metal cycling in soils, and must be accounted for when interpreting contaminated areas.

**Total carbon** (TC) contents have been determined by dry combustion (DC) for 150 soil samples (cf. section 2.5). This method allows for the quantification of total carbon contributions from both mineral and organic sources at the same time. Furthermore, by eliminating the mineral carbon through acid digestion prior to dry combustion, it is also possible to calculate the relative contributions of organic and inorganic carbon (OC and IC). This last procedure was performed for 91 samples.

Manchester soil samples contain between 2.78 and 20.57% TC with a median of 7.07. Most carbon in the 92 samples consists in OC - its median value is of 6.83% which is very close to the same value for TC; median IC is of only 0.8%. The predominance of OC over IC is seen when values are transformed to 100% total carbon: between 67 and 99% of the total carbon in the samples is OC; whereas IC only accounts for 0.6-32% of the total carbon in soil samples.

Organic carbon is one constituent of the organic matter, and naturally-occurring forms are derived from the decomposition of plants and animals. In soils, a wide variety of organic carbon forms are present and range from freshly deposited litter (e.g., leaves, twigs, branches) to highly decomposed forms such as humus (Schumacher, 2002). Organic carbon can be enriched in soils due to human activities such as sewage sludge application, spill of wastewaters, exploration and/or transformation of hydrocarbons, etc. Inorganic carbon forms are derived from geologic or soil parent material sources and are present in soils typically as carbonates (e.g. calcite, dolomite, siderite). It should be noted that calcite and to some extent, dolomite, may also be present in soils and sediments due to agricultural input (e.g. liming practices) (Schumacher, 2002).

The total carbon contents determined are lower than organic matter contents determined by LOI, as the latter is a mass-based method which accounts for the total mass loss of organic matter, which is composed not only by C, but also have O and N as significant mass constituents. Using values from the 91 samples for which OC contents were calculated, it is observed that OM contents are on average 1.5 times higher than the organic carbon contents determined by DC, mainly due to this difference. Nevertheless, OM and OC contents are highly correlated ($R^2$=0.87, $p<0.01$), as can be observed in Figure 21.

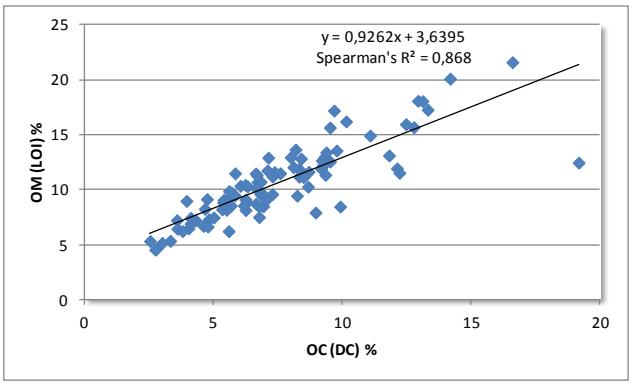


Figure 21: Scatter plot of organic carbon determined by dry combustion vs. organic matter by loss-on-ignition.

The highest differences between OM and OC are observed for the largest values - although samples were coned/quartered to ensure homogeneity, the analysed sample masses were different (OM=2g, OC=0.2g), what might have introduced variability in the results. Samples have been crushed prior to sub-sampling and analysis to minimise this difference, and duplicates were also run to ensure the reproducibility of results.

### *3.1.3. Correlation analysis*

Understanding the basic relationships between chemical composition and other parameters is crucial before any further and more complex data analysis. With the purpose of highlighting some of these relationships, Spearman's rank correlation coefficients ($\rho$) have been calculated for soil variables, according to section 2.9.2. The Spearman's rank correlation matrix is shown in Table 77 (Appendix 2). Correlations within the interval [0.6, 0.7[ are flagged in orange; those above 0.7 are in red and the negative correlations above -0.6 are flagged in blue.

Some expected correlations were found, namely between $Al_2O_3$, $K_2O$, $TiO_2$, Ga, Rb, Y, Nb, Th, La, Ce and Nd ($\rho$>0.7, p<0.01) - these are mainly geogenic elements which are sourced from the soil parent materials. $Fe_2O_3$ is strongly correlated to MnO, Sc, V, Cr, Co, Ba, Ni, Cu, Zn, As, Sr, Y and Mo ($\rho$>0.7, p<0.01). These are expected correlations, as it is known that most of these elements have the tendency to precipitate as oxides or hydroxides of Fe and Mn under the appropriate pH conditions - Fe and Mn oxides have a high sorption capacity and are among the most important compounds in the sorption of trace metallic pollutants, as their cations ($Fe^{2+}$, $Fe^{3+}$, $Mn^{2+}$ and $Mn^{3+}$) exhibit affinities to others with approximately the same physical dimensions, e.g. $Co^{2+}$, $Co^{3+}$, $Ni^{2+}$, $Cu^{2+}$, $Zn^{2+}$, $Cd^{2+}$, $Pb^{4+}$ and $Ag^{+}$ (Kabata-Pendias and Pendias, 2001).

In soils, organic matter (OM) correlates to Br ($\rho$=0.77, p<0.01), what may be an evidence of Br accumulation in soil humus (Yamada, 1968; Maw and Kempton, 1982). Br (in the form of ethylene dibromide) was used as an additive in leaded gasoline, before its use was faded out in the year 2000 - high concentrations of Br in soils may be attributed to this reason, as described in Farmer and Cross (1978). Other elements also related to OM are $P_2O_5$, Ge, Se and Mo (0.6<$\rho$<0.7, p<0.01), and As and

Pb ($0.5<\rho<0.60$, $p<0.01$). Phosphorus, expressed as $P_2O_5$, is a soil macronutrient - phosphate and selenite molecules have similar structures and properties, and both elements are present in fertilisers, along with organic matter (Eich-Greatorex et al., 2010). Moreover, phosphorus has been reported as host for Pb (Cotter-Howells, 1996; Sauvé et al., 1998a) and phosphate as being structurally similar to arsenate (Fendorf et al., 2011) - Pb and As are also correlated to $P_2O_5$ ($\rho$=0.58 and 0.54 respectively, $p<0.01$). Pb and As are also known to widely occur sorbed onto organic matter (Sauvé et al., 1998b; Kabata-Pendias and Pendias, 2001), which could justify the relevant correlation found.

Soil organic and inorganic carbon have been determined in 92 of the Manchester soil samples which were chosen for their elevated trace element contents. For these, OC values correlate significantly to $Fe_2O_3$, Sc, V, Co, Ba, Ni, Ge, As, Se and Mo ($0.7>\rho>0.82$, $p<0.01$) - an indication that these might be associated to the organic fraction of soil in samples of high trace metal content.

Silicon is a major constituent of soil, as quartz ($SiO_2$) is one of the most resistant minerals in soils. $SiO_2$ is therefore related to the coarser fractions of soil, contrarily to $Al_2O_3$ which is used as a proxy for the finer fractions. Therefore, $SiO_2$ shows a negative correlation to $Al_2O_3$ ($\rho$=-0.5, $p<0.01$) and also to elements which are commonly associated to the finer fractions, namely $Fe_2O_3$ and the trace elements Sc, V, Cr, Co, Ni, Cu, Ga, Y, Th, La, Ce and Nd ($-0.8>\rho>-0.6$, $p<0.01$). $SiO_2$ is also negatively correlated to the total carbon content ($\rho$=-0.64, $p<0.01$) and especially organic carbon ($\rho$=-0.78, $p<0.01$); as well as to Sr, an element which is strongly fixed by organic matter (Kabata-Pendias and Pendias, 2001).

Several trace elements of environmental concern are correlated to each other (Cr, Co, Ni, Cu, Zn, As, Pb, Cd, Sn, Sb) - in general, samples are contaminated not only by one element but by a suite of potentially harmful elements - their occurrence in high amounts is often simultaneous. However, these high levels may occur for different suites of elements at different locations, a phenomenon which is not distinguished by the simple correlation analysis presented here. Therefore, the pattern of correlations between these elements needs to be further analysed in order to withdraw more assertive interpretations - specificities of element associations will be pointed out further in this chapter.

## 3.2. Comparison with other soil geochemical studies

During the last decade, the G-BASE project of the BGS has performed a systematic geochemical work all over the UK - by 2010, urban surveys had been completed in 26 UK cities including Manchester (Flight and Scheib, 2011), as referred in section 1.4.2 . Results have gradually been published in peer-reviewed publications and BGS research reports - minimum, maximum and median values for Cr, Ni, Cu, Zn, As, Pb and Cd in 13 UK cities are displayed in Table 17. Accurate comparisons between G-BASE datasets are possible as samples were collected, prepared and analysed using BGS

standard procedures (cf. sections 2.2 and 2.4). Data has also been conditioned and levelled in the same way, as described in section 2.9.1.

By observing this table, Manchester shows the second highest maximum values for As and Cd; nevertheless, the median value for Cd is lower than for more than half of the cities - the maximum value is due to an extreme outlier. Another observation is that maximum Pb and Zn levels in Manchester are lower than in more than half of the other cities; but median values for the same elements are among the highest. In general, Pb and Zn concentrations in Manchester are relatively high, but do not show as strong outliers as in other cities. Maximum, minimum and median values for Ni are amongst the lowest found in this set.

To better rank Manchester median Cr, Ni, Cu, Zn, As, Pb and Cd concentrations against the other 12 cities, column charts were produced and are shown in Figure 22. Cities are ordered by increasing median concentrations. Manchester median concentrations are on the top three for Cu, Zn, As and Pb; and are above 8 of the studied cities for Cr and Ni. Cd displays a lower median value - mainly because only two significant figures are considered for this element and measured values are often very small or even below the LLD, leading to more uniform median values between the UK urban centres. These observations, in spite of being considered only at the city dataset scale, show that the past and present human activities have enriched Manchester soils mainly in Cu, Zn, As and Pb.

Manchester values can also be compared to the National Soil Inventory values, which were first described in McGrath and Loveland (1992) and have recently been improved and republished as *"The advanced soil geochemical atlas of England and Wales"* (Rawlins et al., 2012). This consists in a dataset of 5670 samples analysed for 53 elements - these data have also been conditioned and levelled according to the G-BASE procedures (Lister and Johnson, 2005).

Figure 23 plots Manchester median values for Cr, Ni, Cu, Zn, As, Pb and Cd against the reported median values for England and Wales (Rawlins et al., 2012). It can be observed that median concentrations of the referred elements are never lower in Manchester than in the England and Wales dataset. Nevertheless, Cr, As and Ni median concentrations are very similar between the two datasets - only 1.1 - 1.4 times larger for Manchester data. Zn and Cd are 2.2 and 2.7 times higher in Manchester soils; and the largest differences are observed for Pb and Cu, where Manchester median values are respectively 4.4 and 4.5 times higher than the England and Wales median values.

| City | Count | Cr (mg/kg) | | | Ni (mg/kg) | | | Cu (mg/kg) | | | Zn (mg/kg) | | | As (mg/kg) | | | Pb (mg/kg) | | | Cd (mg/kg) | | |
|---|---|---|---|---|---|---|---|---|---|---|---|---|---|---|---|---|---|---|---|---|---|---|
| | | Min | Max | Med | Min | Max | Med | Min | Max | Med | Min | Max | Med | Min | Max | Med | Min | Max | Med | Min | Max | Med |
| Cardiff (1) | 508 | 1 | 2426 | 72 | 9 | 476 | 26 | 10 | 2046 | 26 | 41 | 23238 | 121 | 6 | 150 | 16 | 14 | 7575 | 76 | 0,50 | 82 | 1 |
| Doncaster (2) | 279 | 21 | 499 | 64 | 5 | 163 | 19 | 8 | 1228 | 31 | 21 | 1463 | 31 | 2 | 74 | 13 | 18 | 1100 | 78 | 0,50 | 7 | 1,0 |
| Glasgow (3) | 1381 | 38 | 4286 | 108 | 6 | 1038 | 47 | 14 | 3680 | 51 | 39 | 1781 | 152 | 1 | 283 | 9 | 13 | 5001 | 127 | 0,25 | 16 | 0,3 |
| Hull (4) | 411 | 22 | 1809 | 83 | 6 | 1123 | 39 | 6 | 1123 | 39 | 20 | 5800 | 132 | 3 | 205 | 20 | 10 | 2900 | 116 | 0,35 | 5 | 0,4 |
| Lincoln (5) | 216 | 19 | 260 | 43 | 2 | 101 | 14 | 4 | 348 | 17 | 7 | 2399 | 61 | 4 | 65 | 11 | 15 | 1400 | 55 | 0,45 | 5 | 0,4 |
| **Manchester** | **300** | **30** | **1238** | **76** | **5** | **148** | **29** | **7** | **2073** | **86** | **25** | **1763** | **169** | **3** | **1001** | **20** | **20** | **2758** | **218** | **0,25** | **80** | **0,9** |
| Mansfield (6) | 257 | 18 | 250 | 54 | 4 | 102 | 16 | 3 | 1731 | 24 | 13 | 1153 | 112 | 3 | 71 | 11 | 1 | 1319 | 76 | 0,35 | 9 | 1,0 |
| Scunthorpe (7) | 196 | 7 | 1108 | 55 | 1 | 202 | 15 | 2 | 433 | 15 | 10 | 10800 | 79 | 3 | 190 | 19 | 9 | 3300 | 45 | 0,45 | 28 | 1,0 |
| Sheffield (8) | 575 | 43 | 1251 | 102 | 8 | 473 | 32 | 12 | 1575 | 51 | 24 | 2678 | 139 | 4 | 239 | 22 | 19 | 4300 | 164 | 0,35 | 8 | 1,0 |
| Stoke-on-Trent (9) | 747 | 22 | 441 | 73 | 5 | 124 | 23 | 7 | 1729 | 33 | 6 | 2589 | 108 | 2 | 136 | 14 | 10 | 4208 | 93 | 0,40 | 43 | 2,0 |
| Swansea (10) | 373 | 20 | 565 | 74 | 8 | 349 | 37 | 7 | 1447 | 115 | 41 | 19047 | 315 | 8 | 2047 | 53 | 20 | 14714 | 225 | 1,00 | 61 | 2,0 |
| Telford (11) | 294 | 25 | 164 | 65 | 7 | 153 | 28 | 8 | 417 | 26 | 46 | 4943 | 264 | 5 | 54 | 10 | 20 | 1236 | 92 | 0,50 | 30 | 1,0 |
| Wolverhampton (12) | 295 | 39 | 1297 | 95 | 12 | 264 | 33 | 10 | 2750 | - | 54 | 6740 | - | 4 | 157 | 17 | 27 | 2853 | 158 | 0,00 | 70 | 1,0 |
| York (13) | 191 | 27 | 639 | 59 | 6 | 84 | 19 | 6 | 277 | 26 | 24 | 898 | 81 | 3 | 93 | 10 | 24 | 2400 | 106 | 0,35 | 9 | 1,0 |
| England & Wales (14) | 5670 | 5,10 | 1141 | 68 | 0,26 | 469 | 21 | 1 | 1321 | 19 | 6 | 3359 | 76 | 0 | 820 | 15 | 13 | 10000 | 49 | 0,14 | 48 | 0,3 |

Table 17: Minimum, maximum and median concentrations for Cr, Ni, Cu, Zn, As, Pb and Cd in UK cities: 1 - Brown (2001b), 2 - O'Donnell (2002), 3 - Fordyce et al. (2012), 4 - O'Donnell et al. (2004), 5 - O'Donnell (2005a), 6 - Freestone (2004), 7 - O'Donnell (2005b), 8 - Freestone et al. (2004), 9 - Fordyce and Ander (2003), 10 - Morley and Ferguson (2001), 11 - Brown (2001c), 12 - Kelly et al. (1996), 13 - O'Donnell (2001), 14 - Rawlins et al. (2012).

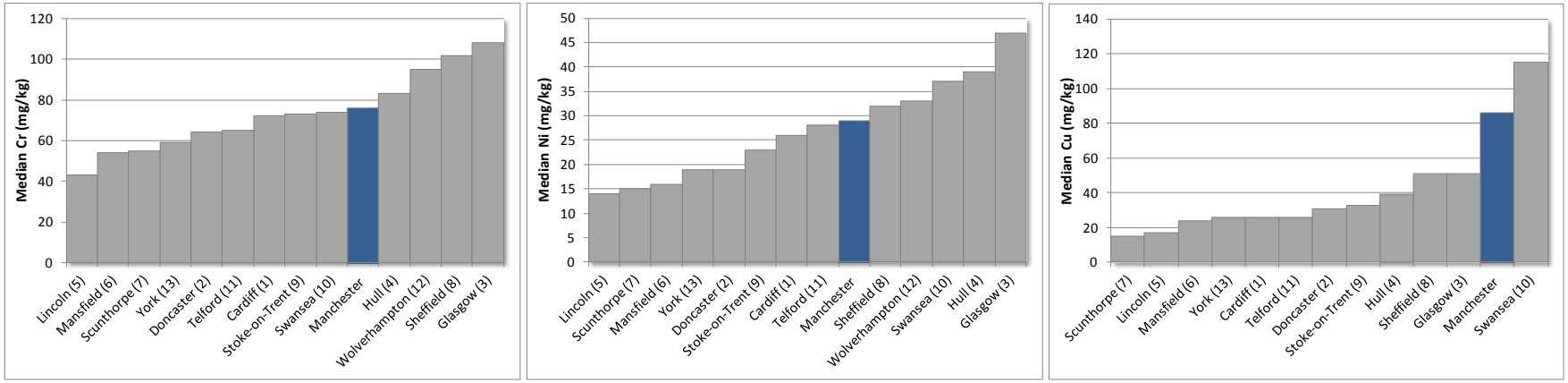


*(cont.)*

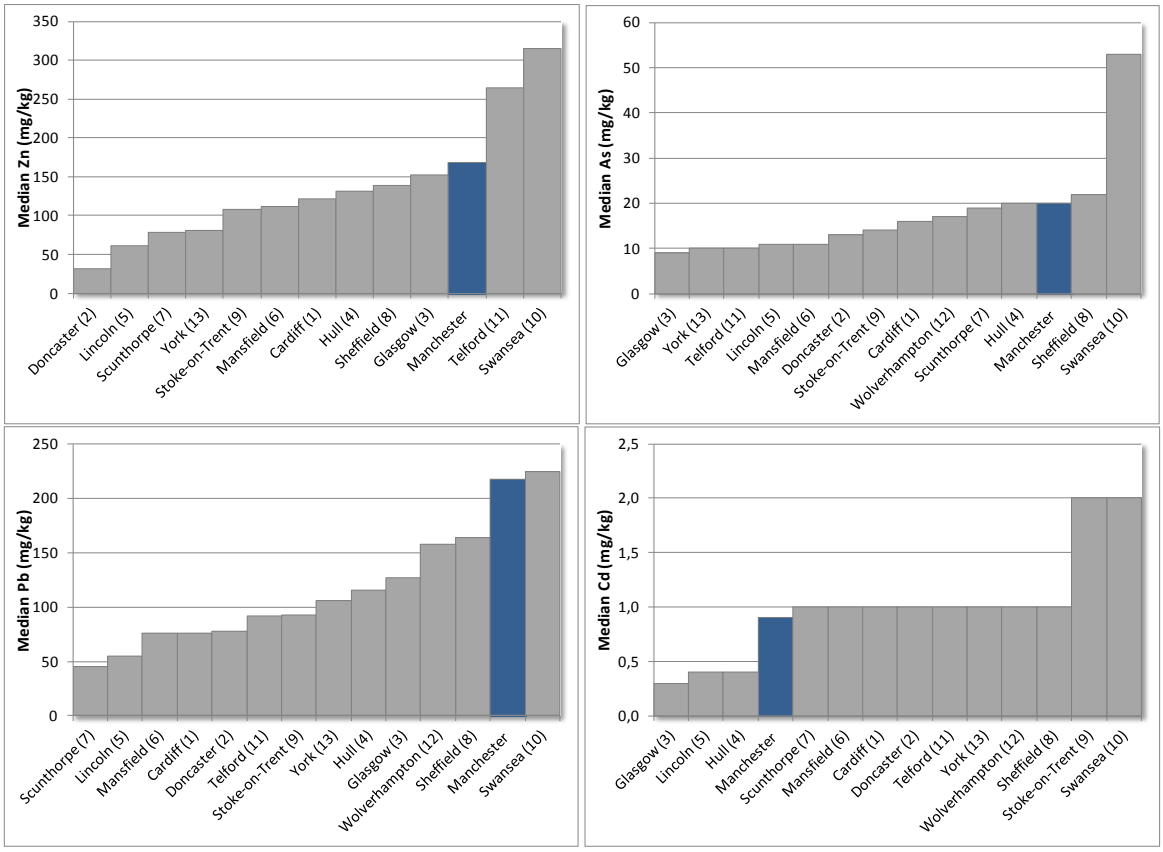


Figure 22: City ranking according to Cr, Ni, Cu, Zn, As, Pb and Cd concentrations (references - cf. Table 17).

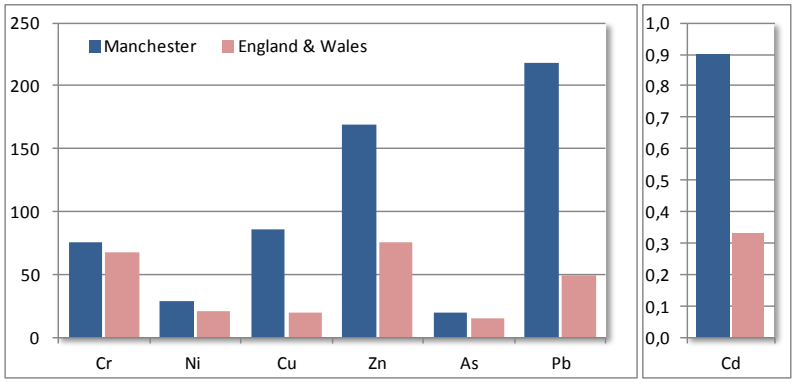


Figure 23: Manchester vs. England and Wales median concentrations (mg/kg).

Although large urban areas were avoided during the National Soil Inventory, the similar values obtained for median Cr, As and Ni between the two datasets indicate that, with the exception of specific locations, their concentrations resemble the national medians. Therefore, it can be assumed that Cu, Zn, Pb and Cd contents in Manchester soils are mostly anthropogenically-derived. The lack of correlations between trace metal contents and local bedrock or superficial geology rules out the hypothesis that these high concentrations in Manchester would be geogenic, as described in the next section.

## 3.3. Relationships with bedrock and superficial geology

The natural pedogenic processes which act upon a parent material or bedrock through a period of time lead to the formation and evolution of soils, as described in section 1.2.1; therefore, the geochemical characteristics of soils are often related to the composition of the parent material in natural, undisturbed soils. Differences between elemental distributions over different bedrocks or superficial deposits are useful to characterise their geogenic elemental concentrations and to determine if elemental concentrations are elevated over certain types of parent material due to natural enrichments.

Using ESRI® ArcGIS 10.0 tools, soil geochemical datasets have been spatially joined to the 1:50.000 scale Digital Geological Map of Great Britain (© British Geological Survey, Figure 7 and Figure 8). Each soil sample was attributed all the corresponding bedrock and superficial deposit variables at each location. The bedrock and superficial deposit groups are summarised in Table 18 and Table 19.

| Code | Description | Age | Rock type(s) | No. of samples |
|---|---|---|---|---|
| **TRIA** | **Triassic rocks (undifferentiated)** | Triassic | Sandstone and conglomerate, interbedded | 214 |
| **PUND** | **Permian rocks (undifferentiated)** | Permian | Sandstone and conglomerate, interbedded / mudstone, siltstone and sandstone | 47 |
| **WAWK** | **Warwickshire group** | Duckmantian (Westphalian B) - Early Permian | Mudstone, siltstone, sandstone, coal, ironstone and ferricrete / Siltstone and sandstone with subordinate mudstone | 17 |
| **PUCM** | **Pennine Upper Coal Measures Formation** | Bosolvian (Westphalian C) - Westphalian D | Mudstone, siltstone, sandstone, coal, ironstone and ferricrete | 20 |
| **PSMCM** | **Pennine Middle Coal Measures Formation** | Duckmantian (Westphalian B) - Bosolvian (Westphalian C) | Mudstone, siltstone, sandstone, coal, ironstone and ferricrete | 2 |

Table 18: Bedrock geology groups in the study area (after the 1:50.000 scale Digital Geological Map of Great Britain © British Geological Survey) and number of soil samples collected over each type.

| Code | Description | Age | Rock type(s) | No. of samples |
|---|---|---|---|---|
| **RTDU-SAG** | **River Terrace Deposits** | Quaternary | Sand and gravel | 85 |
| **ALV-CLSS** | **Alluvium** | Flandrian (Quaternary) | Clay, silt and sand | 27 |
| **TILL-DMT** | **Till** | Devensian (Quaternary) | Diamicton | 180 |
| **GSG-SAGR** | **Glaciofluvial deposits** | Devensian (Quaternary) | Sand and gravel | 8 |

Table 19: Superficial deposit groups in the study area (after the 1:50.000 scale Digital Geological Map of Great Britain © British Geological Survey) and number of soil samples collected over each type.

The data was then exported to IBM® SPSS 19 software where a series of box-and-whisker plots were produced for each element, grouped by bedrock type and superficial deposit type. These are represented from Figure 107 to Figure 110 of Appendix 2. Bar widths are not proportional to the number of samples in each group - please refer to Table 18 and Table 19 above for the number of samples.

It can be observed through Figure 107 that the trace metals of environmental concern - Cr, Ni, Cu, Zn, As, Pb and Cd - tend to show slightly higher median values in soils collected over Permian rocks (PUND) when compared to the other lithologies. Soils located over the Pennine Middle Coal Measures (PSMCM) formation also show higher values for the above elements; nevertheless, it shall

be taken into account that only two soil samples were collected over this bedrock type (each represented by the upper and lower edges of the box-plot, respectively).

Figure 108 shows that concentrations for the above trace metals across different superficial deposits are comparable, as median values are very similar between the different types - superficial deposits do not clearly affect elemental distributions for these trace metals.

In terms of other chemical elements, soils collected over Permian bedrock (PUND) also showed lower median values for $SiO_2$; and higher median values (and higher Q1-Q3 values) for $Al_2O_3$, $TiO_2$, $Fe_2O_3$, Sc, V, Co, Ga and Mo, as represented in Figure 109 of Appendix 2. The reason for this might be that this lithology is mostly overlain by glacial till (43 out of 47 samples), which is consistent with higher Al, Fe, Ga and trace metal concentrations, and lower $SiO_2$ levels, as later described. Concentrations over the other bedrock types are variable, but do not show a natural enrichment pattern for any specific lithology.

Concerning the superficial deposits which are found throughout the area, only the soils collected over glacial till show an enrichment in $Al_2O_3$, $TiO_2$, Ga, Rb, Y, Nb, La, Ce and Nd, as in Figure 110 of Appendix 2. Other superficial deposits do not seem to have a major influence on soil composition, at least by analysing individual element distributions over each deposit type.

It has been pointed out in section 1.2.1 that, unlike natural and undisturbed soils, urban soils may not be related to the bedrock or superficial deposits due to many reasons; e.g. the relocation of excavated land, the use of exogenous soils for landscaping, landfilling, etc. This may affect the conclusions withdrawn from the simple comparison between soil elemental composition and bedrock/superficial deposit type, which assume that the soil is derived from the underlying materials. Nevertheless, the principal component analysis of the geochemical data suggests a more complex relationship between soil geochemistry and the underlying geology. Principal component analysis, a dimension-reduction, non-parametric statistical technique, highlighted groups of elements of geogenic origin, as further discussed in section 3.7.

## 3.4. Relationships with land use and SGVs

Part of the work performed by the BGS sample collectors was the registration of the current land use surrounding each sampling location. Figure 24 is a colour-coded map showing the primary and secondary land uses for the Manchester BGS soil samples. The number of samples collected for each land use is described in Table 20 - the majority of soil samples were collected in urban open spaces, recreational areas and commercial/residential areas, in a total of 268 out of the 300 samples. Inner city locations of Manchester and Salford are dominated by tended but unproductive urban open spaces (light green in Figure 24); whereas in the periphery, recreational areas (orange) and urban open spaces (dark green) are more predominant.

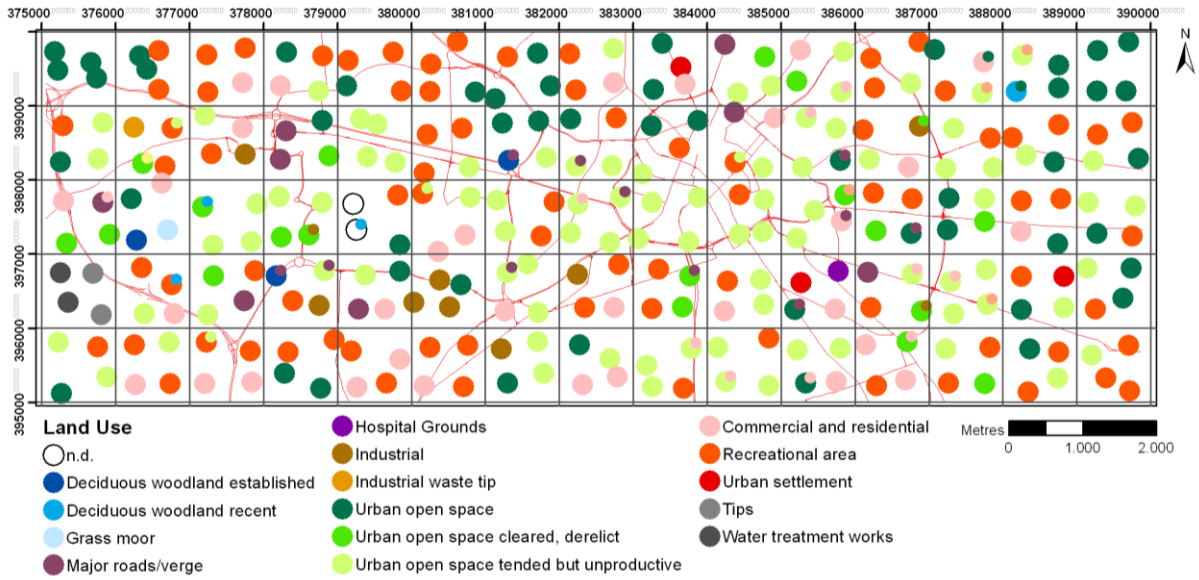


Figure 24: Primary (large symbol) and secondary (small symbol) land uses at soil sampling locations.

| Code | Land Use | no. of samples |
|---|---|---|
| DACA | Urban open space, tended but unproductive | 88 |
| DD00 | Recreational area | 79 |
| DAC0 | Urban open space | 51 |
| DAA0 | Commercial and residential | 32 |
| DACB | Urban open space, cleared/derelict | 18 |
| E000 | Industrial | 8 |
| CB00 | Major roads/verge | 8 |
| AEAB | Deciduous woodland established | 3 |
| DA00 | Urban settlement | 3 |
| 0000 | n.d. | 2 |
| EC00 | Tips | 2 |
| EDA0 | Water treatment works | 2 |
| AEAA | Deciduous woodland, recent | 1 |
| AC00 | Grass moor | 1 |
| DAAB | Hospital Grounds | 1 |
| ECB0 | Industrial waste tip | 1 |

Table 20: Code and number of samples collected for each primary land use category (n.d. = not determined).

The concentration distributions of trace metals of environmental concern, namely Cr, Ni, Cu, Zn, As, Pb and Cd, are displayed from Figure 100 to Figure 106 of Appendix 2, grouped by land use. In these box-and-whisker plots, threshold values for each metal are also displayed as a solid line. Bar widths are not proportional to the number of samples in each class - please refer to Table 20 above for the number of samples. Note that the bottom 9 items of this list (from AEAB - deciduous woodland, established to ECB0 - industrial waste tip) contain too few samples to perform significant statistics - they are present in the box-and-whisker plots to inform about their values but are not compared to the other land uses in this section.

Median concentrations tend to be similar between land uses for the plotted elements. Nevertheless, the industrial land type (E000) shows slightly higher median values for Cr ($\tilde{x}$ =86.5

mg/kg), Cu ($\tilde{x}$ =107 mg/kg), Zn ($\tilde{x}$ =281 mg/kg) and Cd ($\tilde{x}$ =1.1 mg/kg). Values are also rather well-distributed for this land use, with no significant outliers for any of the above metals. On the other hand, urban open spaces (DACA, DAC0, DACB), recreational areas (DD00) and commercial/residential areas (DAA0) show many outliers, also as a consequence of the higher number of samples collected over these land types. The percentage of soil samples above the lowest established or proposed SGVs for each trace metal of environmental concern is shown below in Table 21.

| | Cr (130) | Ni (130) | Cu (88,4) | Zn (90) | As (32) | Pb (450) | Cd (1,8) |
|---|---|---|---|---|---|---|---|
| % samples above lowest SGV | 8,3 | 0,7 | 47,7 | 89,7 | 19,3 | 9,3 | 12,0 |

Table 21: Percentage of soil samples above the lowest established/proposed SGV (in parentheses) for Cr, Ni, Cu, As, Pb and Cd.

**Chromium** concentrations are mostly below the allotment SGV (130 mg/kg), with the exception of outliers and the Industrial land use, for which the 3$^{rd}$ quartile is above this SGV. Only three samples are above the residential SGV (500 mg/kg) - two are located in urban open spaces and one in a recreational area. The sample with the highest Cr content is located in a publicly accessible urban open space next to the Eccles wastewater treatment plant, which is a likely source of this contamination. Conversely, the other two samples effectively collected in the grounds of wastewater treatment plants did not display such a large amount of Cr (161 and 79 mg/kg Cr, respectively).

**Nickel** only displays 2 samples above the residential SGV (130 mg/kg), both in urban open spaces (DACA and DAC0). One of them (140 mg/kg Ni) was collected in the surrounding gardens of a Manchester University's building, off Oxford Road. This sample also displays As and Cd concentrations above the respective SGVs. Median Ni values are well below the lowest SGV for this element.

**Copper** median values are mostly close to the proposed UK ecological guideline of 30 mg/kg, meaning that 50% of the samples are above this level. The industrial land use (E000) is an exception to this and displays the highest median value for Cu ($\tilde{x}$ =107 mg/kg), and c. 75% of the samples are above the 30mg/kg level. The sample with the highest Cu value is the same as for Cr, indicating the wastewater treatment plant as the likely source of contamination.

**Zinc** distributions in all land use types show at least 75% of the values above the proposed UK ecological guideline (90 mg/kg). In the lack of a more recent UK guideline, the 300mg/kg former SGV (ICRCL, 1987) is also used for comparison and is exceeded for samples in all land uses (with n>3). The highest median value is again found for the industrial land type (E000), for which over 50% of samples are above the referred SGV. Nevertheless, samples which display the highest amounts of Zn (>1000 mg/kg) are of commercial/residential land use (in this case a residential garden, 1 sample) and urban open spaces (3 samples).

**Arsenic** median values are higher for recreational areas, although maximum values are reached over urban open spaces (DACA, DAC0, DACB) and woodland (AEAB). Again, the sample showing highest As concentration is located near the Eccles wastewater treatment plant (urban open space), which reaches 1001 mg/kg As. Distributed over the majority of land uses, 58 samples are above the lowest SGV (residential, 32 mg/kg). From these, 24 are above the allotment SGV of 43 mg/kg and the highest As value is clearly above the 640 mg/kg commercial/industrial SGV.

Nevertheless, care should be taken comparing As levels to the SGVs, as this value is calculated for inorganic forms of As – organic/inorganic partitioning of As has not been considered in this work. Organic arsenic compounds are considered to be less toxic to humans than inorganic forms; therefore the SGVs for this element are calculated based on the latter.

**Lead** median values are similar between land uses, although slightly higher in samples collected near major roads/verges (CB00). The industrial land use shows all Pb concentrations below the residential/allotment SGV (450 mg/kg), whereas this SGV is exceeded in other land uses. Maximum Pb values (up to 2758 mg/kg) are observed in recreational areas (DD00), urban open spaces (DACA, DAC0 and DACB) and commercial/residential (DAA0) land uses - 7 samples are in excess of the commercial/industrial SGV of 750 mg/kg.

**Cadmium** displays a greater range of concentrations over urban open spaces (DAC0), for which the highest Cd concentrations are also found. Median values are very similar between land uses and a slightly higher value is observed for the industrial land use ($\tilde{x}$ =1.1 mg/kg). The allotment SGV for Cd (1.8 mg/kg) is exceeded for 40 samples, 2 of which are also above the residential SGV (10 mg/kg). These two most contaminated samples were collected in urban open spaces near the Failsworth wastewater treatment plant, which can be pointed as a possible source.

## 3.5. Mapping

With the objective of spatially displaying element concentrations, soil data have been mapped as a series of proportional symbol/colour maps, generated using ESRI® ArcGIS 10.0, as described in section 2.9.5. These maps provide a spatial overview of soil parameters and highlight areas where high values are found. Proportional symbol/colour maps are shown in Appendix 3 for 22 chemical elements, organic matter, carbon contents and pH.

### *3.5.1. Major element spatial distributions*

Major elements such as $SiO_2$, $Al_2O_3$, $Fe_2O_3$, CaO, MgO and $K_2O$ are the most abundant in soils. From these, $Al_2O_3$ and $SiO_2$ show the highest concentrations, as they are part of alumino-silicate minerals and quartz which are main constituents of soil. The spatial distributions show that city centre soils have highest $SiO_2$ concentrations, conversely to all the other major elements analysed which tend to be more concentrated outside of Manchester city centre (cf. Figure 6 for place names). High $Al_2O_3$

values also tend to coincide with high trace metal contents - as later explained, $Al_2O_3$ is the main constituent of the finer fractions of soil, which in turn act as major hosts for trace metals. $Al_2O_3$ and $SiO_2$ are elements amongst the least prone to anthropogenic inputs - their concentration derives mainly from the natural pedogenic processes which contribute to soil formation and evolution. Despite having a mostly geogenic origin, other major elements may locally be derived from anthropogenic sources; e.g. $Fe_2O_3$ and MnO from smelters or manufacturing industries, CaO from furnace slags and construction materials, $P_2O_5$ from the use of fertilisers, or $Na_2O$ derived from winter road gritting. Nevertheless, their median concentrations (after conversion from oxide percent to element percent) are comparable to those for England and Wales reported in Rawlins et al. (2012), as observed in Table 22.

a)

| %Oxide - Median | |
|---|---|
| Na2O | 0,5 |
| MgO | 0,9 |
| Al2O3 | 9,8 |
| SiO2 | 67,0 |
| P2O5 | 0,29 |
| K2O | 1,62 |
| CaO | 1,2 |
| TiO2 | 0,44 |
| MnO | 0,066 |
| Fe2O3 | 4,56 |

b)

| %Element - Median | | Median EW |
|---|---|---|
| Na | 0,4 | 0,3 |
| Mg | 0,6 | 0,5 |
| Al | 5,2 | 5,8 |
| Si | 31,3 | 29,0 |
| P | 0,12 | 0,09 |
| K | 1,34 | 1,20 |
| Ca | 0,8 | 0,4 |
| Ti | 0,26 | 0,35 |
| Mn | 0,051 | 0,058 |
| Fe | 3,19 | 2,80 |

Table 22: Median concentrations of major elements in Manchester soils and England and Wales soils (grey column). a) oxide percent; b) elemental percent.

## *3.5.2. Trace element spatial distributions*

Observing the spatial distribution of trace element concentrations in the maps of Appendix 3 and, as expected by the preliminary statistical analysis, Manchester soils show localised elevated concentrations of trace elements, namely Sb, Ba, Cd, Cr, Co, Cu, Fe, Pb, Mo, Ni, Sn, V and Zn. To more easily delimit likely contaminated areas, Cr, Ni, Cu, Zn, As, Pb and Cd spatial distributions were investigated in more detail, as these are elements of environmental concern which can reach maximum concentrations several times above their median values in the Manchester area.

The map in Figure 25 represents the areas with concentrations above the 75$^{th}$ percentile for Cr, Ni, Cu, Zn, As, Pb and Cd. Interpolated surfaces were calculated for each of these elements using the inverse distance-weighted (IDW) function with 100 m as the output cell size and a distance radius of 500m, with a minimum selection of 2 nearest neighbour samples (cf. section 2.9.5). Colours corresponding to concentrations below the 75$^{th}$ percentile for each element are hidden, leaving the yellow-orange-red shades of locations with values above this threshold. Seven areas can be delimited by shade overlapping, i.e. where concentrations tend to be systematically high. Each area is described below.

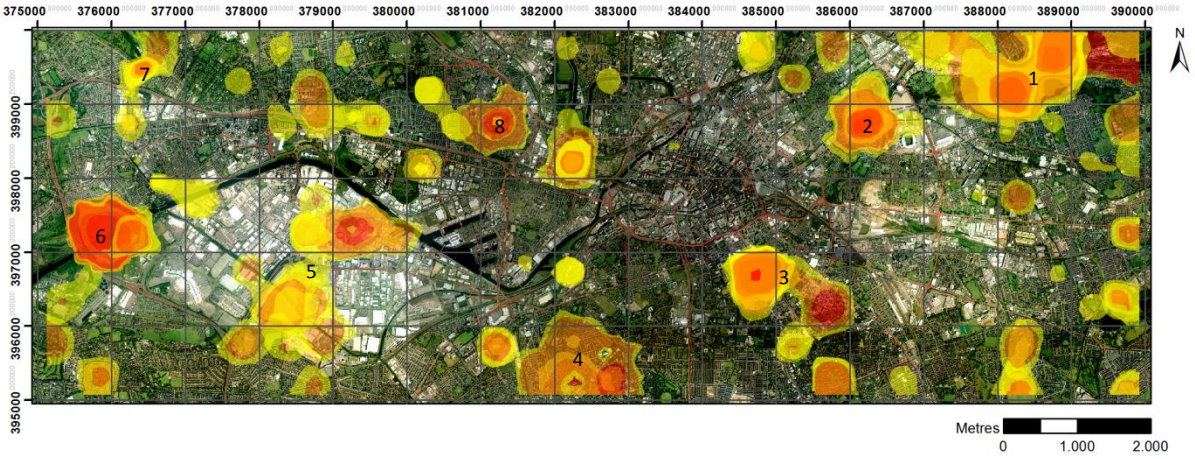


Figure 25: Areas with Cr, Ni, Cu, Zn, As, Pb and Cd concentrations above the 75$^{th}$ percentile in soils. 1-Clayton Vale/Phillips Park; 2-Cambrian St. area ; 3-Oxford Road/Wimslow Road alignment; 4-Old Trafford/Whalley Range; 5-Trafford Park Industrial Estate; 6-Davyhulme Sewage Works; 7-Worsley; 8-Salford.

**1. The Clayton Vale / Phillips Park area.**

This area has a history of intense human activities: mills, chemical and gas works, tanneries, a smallpox hospital, and engineering and textile industries have left their legacy onto this land. Clayton Vale has been redeveloped in the period of 1982-1986 and is now a natural habitat for wildlife. There are no remains of past industrial structures on the Vale, as these were demolished to make way for the site to become a landfill - this site was used as a municipal waste tip and a tip for the ash cinders from Stuart Street Power Station. The site now consists of informal grasslands and wooded slopes. However, there is still evidence of its industrial heritage, such as steep slopes and plateaux created by the landfill and alterations to the river Medlock. In July 2006 it became a local nature reserve. Phillips Park is located adjacent to the Clayton Vale, downstream River Medlock which flows through both these green areas. It opened in 1846 from a previous heavily industrialised area and the site of Bradford Colliery. Much of the area has been cleared and landscaped as a country park (MCC, 2009).

Upstream River Medlock, in the north-eastern corner of the study area there is also the Failsworth wastewater treatment plant, which is still active today. Samples collected nearby show evident signs of Cd contamination.

This whole area shows 10 samples above the 90th percentile (39 mg/kg) for As (max 138 mg/kg), and 7 samples above the 90$^{th}$ percentile (195 mg/kg) for Cu. Concentrations are also amongst the highest found for Ba (between 500-5476 mg/kg), Cd (13-80 mg/kg), Co (11-44mg/kg), and of max. 969 and 974 mg/kg for Pb.

**2. The Cambrian Street area, west of the Manchester City F. C. complex.**

At the present day, this area comprises several car breaking and dismantling businesses, vehicle part traders, welding services, and a tarmac/asphalt company. Chromium, Pb and As are the elements which show a greater enrichment in this area with 713, 2425 and 63 mg/kg, respectively. Here, Pb displays the maximum concentration of the study area.

**3. The Oxford Road / Wilmslow Road alignment.**

This area is characterised by the concentration of Manchester universities, local businesses, student residential campuses, hospitals, and the dense residential areas of Rusholme and Moss side. It has been a dynamic, less industrialised Manchester area since Victorian times, with theatres, cinemas, parks, services, commerce, and the University. Nowadays, Oxford road and Wilmslow road have high daily traffic densities and are part of Manchester's major bus corridor. Here, Pb concentrations range between 594-1153 mg/kg, Cu between 559-663mg/kg, and As concentrations can top 117 mg/kg. Zn is also very high, displaying maximum values of 1763 and 1029 mg/kg.

**4. The Old Trafford residential area, east of Manchester Cricket Ground, and Whalley Range.**

In the 19$^{th}$ century, Old Trafford quickly gained a reputation for being an exclusive suburb in which to reside and to visit for refined leisure activities. The area became the preserve of the professional and the rich who lived in splendid villas overlooking green pastures and farmsteads. As Manchester grew as a city, populations began to move out into the fringe areas and the area began to attract residents with lower incomes and professional status. Old Trafford expanded and became an urban area after the building of the Manchester Ship Canal in the 1890s, and the subsequent development of nearby Trafford Park Industrial Estate - the area of Old Trafford where these high trace metal concentrations are reported is located in the neighbourhood which first housed the Trafford Park industrial workers. By the late 1890s many wealthy Old Traffordians had left the area, and light industry had become established. Over a fifty year period, the appearance of Old Trafford had changed radically (Kay, unpublished). Slum clearances during the 1960s and early 1970s saw some of the old Victorian housing stock demolished, although a few residents preferred renovation to demolition. In contrast, Whalley Range was one of the first wealthy suburban residential estates of Manchester built during the 19$^{th}$ century, which suffered great changes including the demolition of the old large houses and the subsequent redevelopment of their sites (MCC, 2013).

The samples of these areas often show brick and roof tile fragments, and are enriched mainly in Pb, As and Zn with maximum concentrations reaching 2758, 48 and 253 mg/kg, respectively. These are located in residential areas.

**5. The Trafford Park industrial estate area.**

The Trafford Park Industrial Estate was the first planned industrial estate in the world (1896) and remains the largest in Europe. It employed over 31000 people in 1,400 businesses in 2006 - wholesale and retail trade accounted for 37% of total employment, followed by manufacturing with 24% (EKOS, 2008). Present industries comprise food and beverages, chemical products, fabricated metal products, paper, machinery and equipment production, and non-metallic mineral products. Past industries included the Manchester Patent Fuel Company, the Trafford Brick Company, timber

merchants, electrical and engineering manufacturers, a power station, various food industries, and the Ford Motor Company. During the First World War, the park was used for the manufacture of munitions, chemicals and other materiel; as well as during the Second World War, with the fabrication of heavy Avro bombers, all sorts of engines, munitions and gun parts. The area has changed since then and after a period of decline, industry has adapted to the current needs and the area has been redeveloped to include the Trafford Centre, the Old Trafford sports complex, the new Salford Quays, and the recently opened MediaCityUK.

Maximum concentrations in this area are observed for Pb (2425 mg/kg), Cu (5 samples between 265-978 mg/kg) and As, with 13 samples with concentrations above 28 mg/kg.

**6. The surroundings of Davyhulme Sewage Works and Eccles Wastewater Treatment Works.**

The Davyhulme Sewage Works is located in the south bank of the Manchester Ship Canal, upstream Barton Locks. The site is presently operated by United Utilities and provides wastewater treatment for a population of 1.2 million in and around the city of Manchester. Davyhulme was constructed in 1894 and with subsequent development became one of the largest sewage treatment plants in Europe (Dodge and Perkins, 2010). The Eccles Wastewater Treatment Works, also operated by United Utilities, is located on the north bank of Manchester Ship Canal, northeast of the new Salford City Stadium. It is on its grounds that the largest As, Cr and Cu concentrations are found: 84 and 1001 mg/kg for As, 1238 mg/kg for Cr and 743-2073 mg/kg for Cu. Adjacent to the Eccles wastewater treatment works there are the Peel Green allotments, what might be a matter of concern as these are located close to the most contaminated soil samples.

**7. The residential area south of Worsley Golf Club.**

Worsley is nowadays an affluent, predominantly residential area. The Worsley Golf Club was inaugurated in 1894 and occupies a significant area together with the Broadoak Park, adjacent to the Bridgewater Canal. Worsley has a history of mining, farming and handloom weaving. Lime, which was used for agricultural purposes and for making mortar, was quarried nearby - a lime kiln was built at Worsley, of which remains can be seen near Stableford Road (SCC, 2007). The soil samples collected near this place contain about 795 mg/kg of Pb, 1533 mg/kg Ba, 29-41 mg/kg Sb and 19-30 mg/kg Co.

**8. The area between A6 and A57/M602 in Salford.**

This is a mixed residential/commercial area and soil samples were collected in urban open spaces or recreational areas. Salford City grew through industrialisation to become a well-developed cotton town during the Industrial Revolution (SCC, 2012). The rapid population increase was reflected in the vast areas of poor quality housing - some of which have been redeveloped, such as the area sampled and referred here. Pb maximum concentrations in this area go up to 1035 and 1460 mg/kg, and up to

12 for Cd. Zn and Cu are also enriched in some samples, with concentrations ranging between 270-521 and 188-205, respectively.

The areas described above are diverse in terms of present and past land uses and chemical element association types. They are an example of the variety of factors that can influence soil composition at the local scale, and the importance of more detailed, site-specific studies - every site has its own history and is affected by different causes of contamination, which are beyond the scope of this study. Nevertheless, the numerous elements analysed and the dense sampling scheme which was adopted allow for the use of statistical methods which can reveal element associations, their sources and potential threat to human health, as later discussed.

## 3.6. SEM-EDS analysis

To better understand the nature and potential impact of elevated trace metal concentrations in soil, scanning electron microscopy was used to characterize the various morphological and mineralogical forms in which metal is present in soil material. Besides the imaging, which gives information about the actual particle nature, the coupled energy-dispersive spectrometry (EDS) device allows the determination of the detailed chemical composition of each target.

A total of 9 Manchester soil samples have been prepared for observation under the SEM according to the procedure described in section 2.7. These were selected based on their elevated trace metal content, especially in Cr, Cu, Zn, As, Pb and Cd.

In the samples observed under partial vacuum conditions by backscattered secondary electron (BSE) imaging (15kV accelerating voltage, 15mm working distance), bright areas were first identified as these correspond to high concentrations of elements of high atomic number. These areas were subsequently selected for chemical analysis by EDS.

Manchester soils are composed of a wide variety of grains - silicate and alumino-silicate grains and other minerals; spherical grains containing Si, Fe and other metals; Ca-rich grains; fragments of brick, tarmac, concrete and other construction materials; and metal-bearing particles of diverse morphology. General images of soil in polished, resin-cast cross-sections can be observed in Figure 26.

Quartz (Si dominated) grains (a, Figure 26) are the most frequent and vary in shape from angular to sub-rounded. Size is also highly variable depending on the sample - from less than 10µm up to around 450µm. Alumino-silicate/mudstone fragments (b) appear as grains of layered texture and are predominant in sizes <10µm, whereas grains consisting of fragments of rocks show a combination of different components rich in Si, Al and K (c). These are hard to distinguish visually from what is believed to be fragments of tarmac, brick or concrete - nevertheless, these often contain

considerable levels of Ca and grain shape tends to be very angular (Figure 27). The origin of quartz and alumino-silicate grains is closely linked to the pedogenic, soil-forming processes.

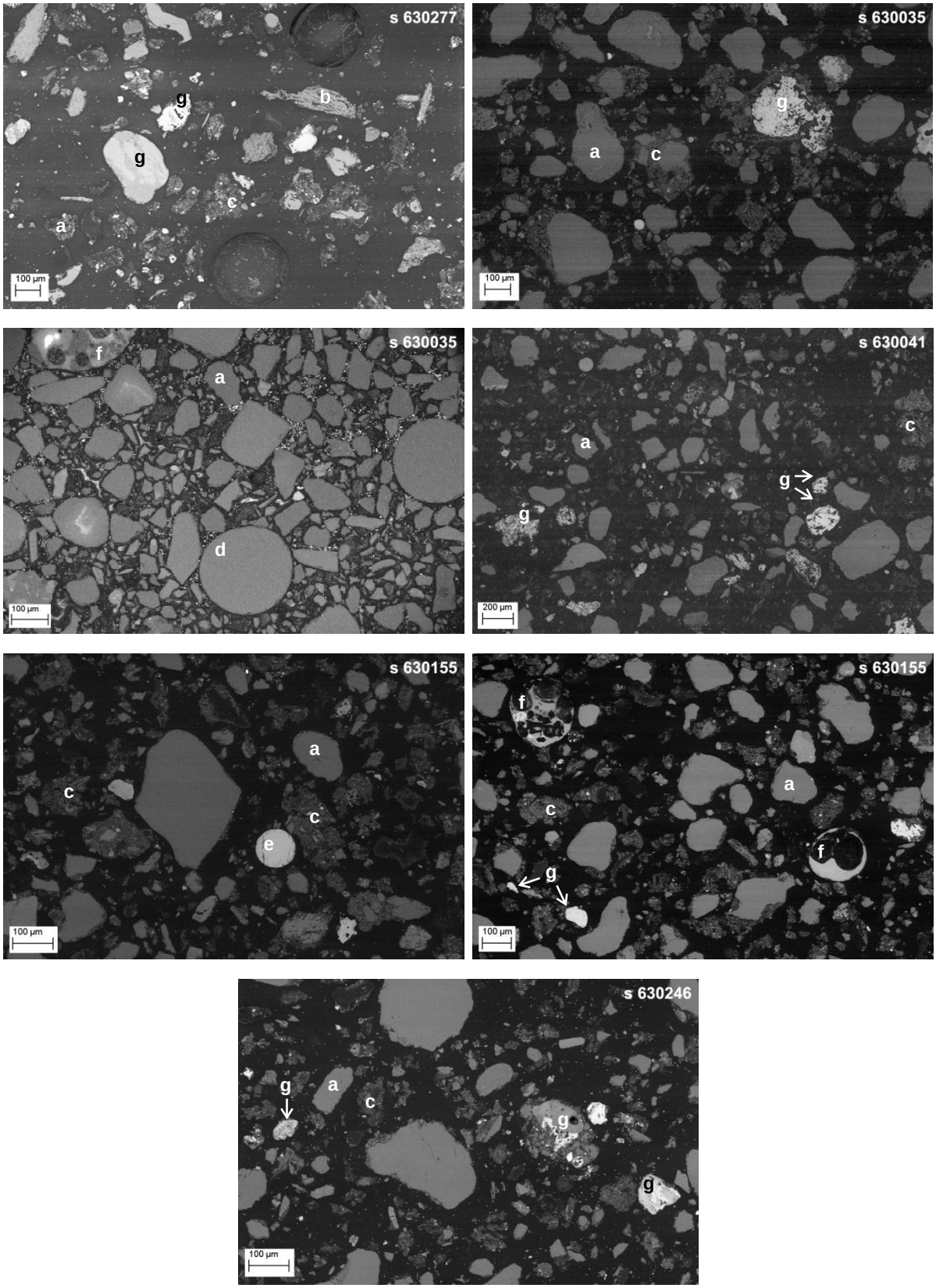


Figure 26: General views of Manchester soils under the SEM (BSE imaging, partial vacuum, 15 kV accelerating voltage) (a - quartz grains, b - alumino-silicate/mudstone fragments; c - tarmac/concrete fragments; d - spherical glass grains; e,f - spherical metal-rich grains; g - iron oxide grains).

In the case of tarmac and brick these come mainly from the erosion or demolition of man-made infrastructures or buildings - this process may also contribute to rock fragment content.

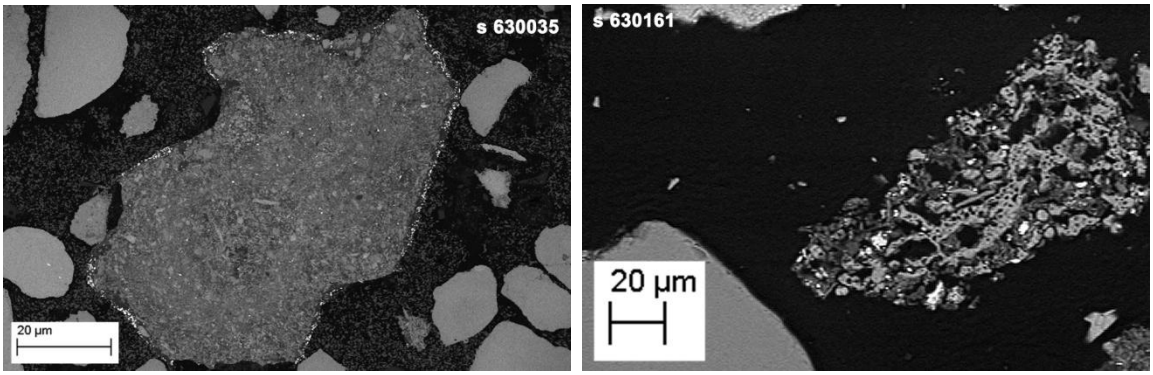


Figure 27: Probable brick/tarmac/concrete fragments of Manchester soils (BSE imaging, partial vacuum, 15 kV accelerating voltage).

Contrastingly, some silicate grains are spherical in shape (d) ranging from <10-200µm in size - these are anthropogenically-derived spherical glass grains. More commonly, a morphologically identical type of grain (e, f) display significant concentrations of Fe and other elements (Al, Ti, Mn, Cr, Mo) in different proportions, as well as internal exsolution structures and air vesicles - these will be discussed further in this text.

Another type of grain which is frequently found in Manchester soils are those composed mostly of iron oxides (g). These often exhibit a porous and/or stratified structure (banding), and are mostly angular in shape. Size is again highly variable (~30-450µm) and these grains may include other metals such as Ti, Mn, Cr, Cu and Co.

Manchester urban soils display other grain types which are generally smaller in size (<50µm) containing significant levels of Ba, Pb, Sn, Ni or REE. Despite being very rare, the amount of metal they contain combined with the morphological aspect and element suites found makes them relevant in the scope of this section.

Figure 28 is a compositional map where brighter areas correspond to higher concentrations of Si, O, Ca, C, Al, Fe and K. The first image is a backscattered electron image similar to those in Figure 26, where brightness is proportional to atomic number. It can be observed that most grains are composed of Si and O, followed by Al and K. Calcium and Fe occur localised in certain grains, whereas C is highlighted only in the matrix area. This is due to the composition of the epoxy resin used for mounting the soil sample.

The focus of soil SEM-EDS analysis is to determine the morphology and composition of metal-bearing grains and for such characterization, several grains from each of the 9 samples were selected, in a total of 71 individual grains. The grain types observed under the SEM are summarised in Table 23 and the elements analysed in Table 24.

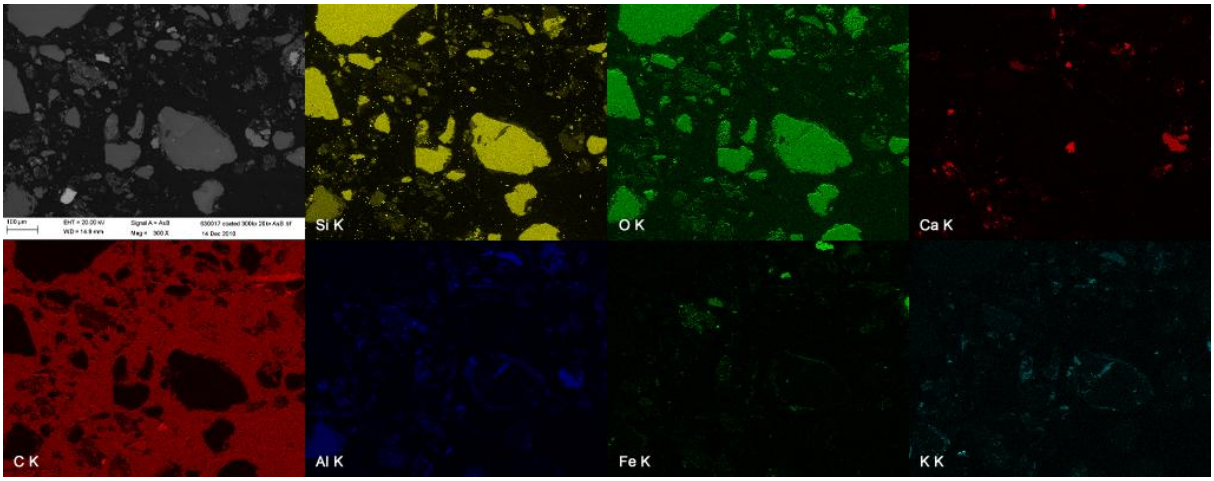


Figure 28: Compositional map of a general view of sample 630017.

| Grain type | N |
|---|---|
| Fe oxide | 24 |
| Fe-rich spherical | 17 |
| Ba-rich | 6 |
| Pb-rich | 4 |
| Brick | 3 |
| Spherical Glass | 3 |
| Zircon | 2 |
| Al/Fe rich | 1 |
| Fe/S-rich | 1 |
| Framboidal Py | 1 |
| S-rich | 1 |
| Ca-rich | 1 |
| Cr-rich | 1 |
| Cu/Sn-rich | 1 |
| Ni-rich | 1 |
| P-rich | 1 |
| REE grain | 1 |
| Feldspar | 1 |
| Sn-rich | 1 |
| Total | 71 |

Table 23: Grain types analysed by SEM-EDS in soil (N=no. of grains).

| | N | Minimum | Maximum | Mean | Std. Dev. |
|---|---|---|---|---|---|
| Si | 70 | 1,25 | 31,43 | 7,71 | 6,06 |
| Al | 69 | 0,35 | 17,04 | 2,83 | 3,27 |
| Fe | 64 | 0,16 | 66,73 | 18,17 | 15,07 |
| Na | 60 | 0,04 | 10,18 | 0,93 | 2,20 |
| Ca | 58 | 0,03 | 13,67 | 1,12 | 2,05 |
| Mg | 54 | 0,02 | 4,97 | 0,56 | 0,97 |
| Cl | 49 | 0,01 | 1,10 | 0,24 | 0,18 |
| K | 48 | 0,02 | 2,44 | 0,31 | 0,39 |
| P | 42 | 0,01 | 9,11 | 0,64 | 1,77 |
| S | 42 | 0,02 | 20,20 | 1,87 | 4,28 |
| Ti | 21 | 0,01 | 2,33 | 0,41 | 0,58 |
| Mn | 7 | 0,14 | 0,71 | 0,34 | 0,20 |
| V | 6 | 0,03 | 3,24 | 0,69 | 1,28 |
| Ba | 6 | 1,68 | 35,85 | 24,87 | 13,07 |
| Cr | 5 | 0,08 | 11,55 | 3,96 | 4,78 |
| Pb | 4 | 0,81 | 52,05 | 31,91 | 21,89 |
| Cu | 3 | 0,15 | 29,30 | 9,90 | 16,80 |
| Mo | 2 | 0,20 | 0,63 | 0,42 | 0,30 |
| Co | 2 | 0,45 | 7,03 | 3,74 | 4,65 |
| Sn | 2 | 24,98 | 34,29 | 29,64 | 6,58 |
| Zr | 2 | 23,27 | 24,32 | 23,80 | 0,74 |
| In | 1 | 1,28 | 1,28 | 1,28 | . |
| Ni | 1 | 4,73 | 4,73 | 4,73 | . |
| Cs | 1 | 0,54 | 0,54 | 0,54 | . |
| La | 1 | 8,97 | 8,97 | 8,97 | . |
| Ce | 1 | 17,28 | 17,28 | 17,28 | . |
| Nd | 1 | 1,33 | 1,33 | 1,33 | . |
| F | 1 | 0,56 | 0,56 | 0,56 | . |

Table 24: Descriptive statistics for elements analysed by SEM-EDS in soil (N=no. of analysis, all values in wt%).

The number of grains in Table 23 is not representative of the overall abundance of the type of grain in soil samples - it represents the number of grains of each kind analysed for the purposes of this work. By general sample analysis and as previously referred, silicate and alumino-silicate grains are the most abundant in soils viewed under the SEM.

Concerning chemical composition (Table 24), concentrations show great variations according to the type of grain analysed: box-and-whisker plots of elemental concentrations grouped by grain type can be observed in Figure 111, Appendix 2.

Similarly to the results of XRF analysis, Si is the most abundant element analysed in the SEM and displays highest concentrations, besides quartz grains, in spherical glass grains and brick fragments. This last type of grain also shows high median concentrations of Al. Aluminium is a common component of the clayey (alumino-silicate) fraction of soil, and appears associated as well to iron - Fe-oxide, Fe-rich spherical and Al/Fe-rich grains display significant Al contents.

Evidently, Fe is largely abundant in Fe oxide and Fe-rich spherical grains; but also in Pb and Cr-rich grains. As the most abundant crustal transition metal (representing 6% of the chemical composition of the Earth's crust), Fe can be leached from rock-forming minerals resulting in pedogenic Fe oxide phases found in nearly all superficial soils and sediments (White, 1995). In addition, a series of anthropogenic sources may also contribute to Fe enrichment in urban soils such as industrial (namely ore-transforming and smelting) and traffic-related sources, and the corrosion of iron and steel construction materials.

Sodium shows similar concentrations across grain types; yet, spherical glass grains display higher concentrations of this element. This might be due to the fact that Na is frequently added as a curing solution compound (sodium monofluorophosphate) in blast-furnace slag cement, to improve the frost salt scaling durability and microstructure of the mortar, as well as its compressive strength (Sisomphon et al., 2011). Calcium also shows significant amounts in this type of grain, although the highest Ca concentration is found for carbonate grains. Magnesium distributions are similar to that of Ca, as these share similar properties as elements of the same periodic table group.

Chlorine highest concentration is obtained for a Pb-rich grain (probably a fragment of lead-paint, $PbCl_2 \cdot Pb(OH)_2$); otherwise, concentrations are also similar between grain types. The highest K concentration is found in feldspar fragments; brick and Pb-rich grains also show slightly higher K median values than the other types.

Phosphorus shows elevated concentrations in Pb-rich grains and brick fragments, but highest concentrations are found in a specifically P-rich grain and in a REE grain.

Sulphur is found in greater concentrations in Fe/S-rich, framboidal pyrite and S-rich grains, which could all be classified as Fe/S-rich grains as they display similar Fe and S content. Nevertheless, they are here separated as their morphology is quite different. Ba-rich grains also have significant S content.

Titanium, Mn, Cr, Cu and Co are more concentrated in Fe oxide and/or Fe-rich spherical grains. Ba, Pb and Zr, as well as Ni, Cs, La, Ce, Nd and F (not plotted in Figure 111 as these elements were only

quantified in one grain) are present in specific grain types which cannot be fitted into the previous categories due to different elemental suites and morphology.

Each soil grain type is described in more detail in the sections to follow.

### *3.6.1. Iron oxide grains*

Iron oxide grains present in Manchester soils are mostly of angular nature, with Fe concentrations that can go up to 67 wt% (sample 630035). Figure 29 below represents different types of iron oxides found in soil samples. These grains can be massive (a, b) or may exhibit internal banding (c, d), villiform (e) and porous structures (f, g), inclusions (h), twinning (i) and/or signs of corrosion (j). A few grains also show an agglomerate structure, where an angular Fe oxide nucleus is coated by silicate and alumino-silicate particles, as represented in Figure 30.

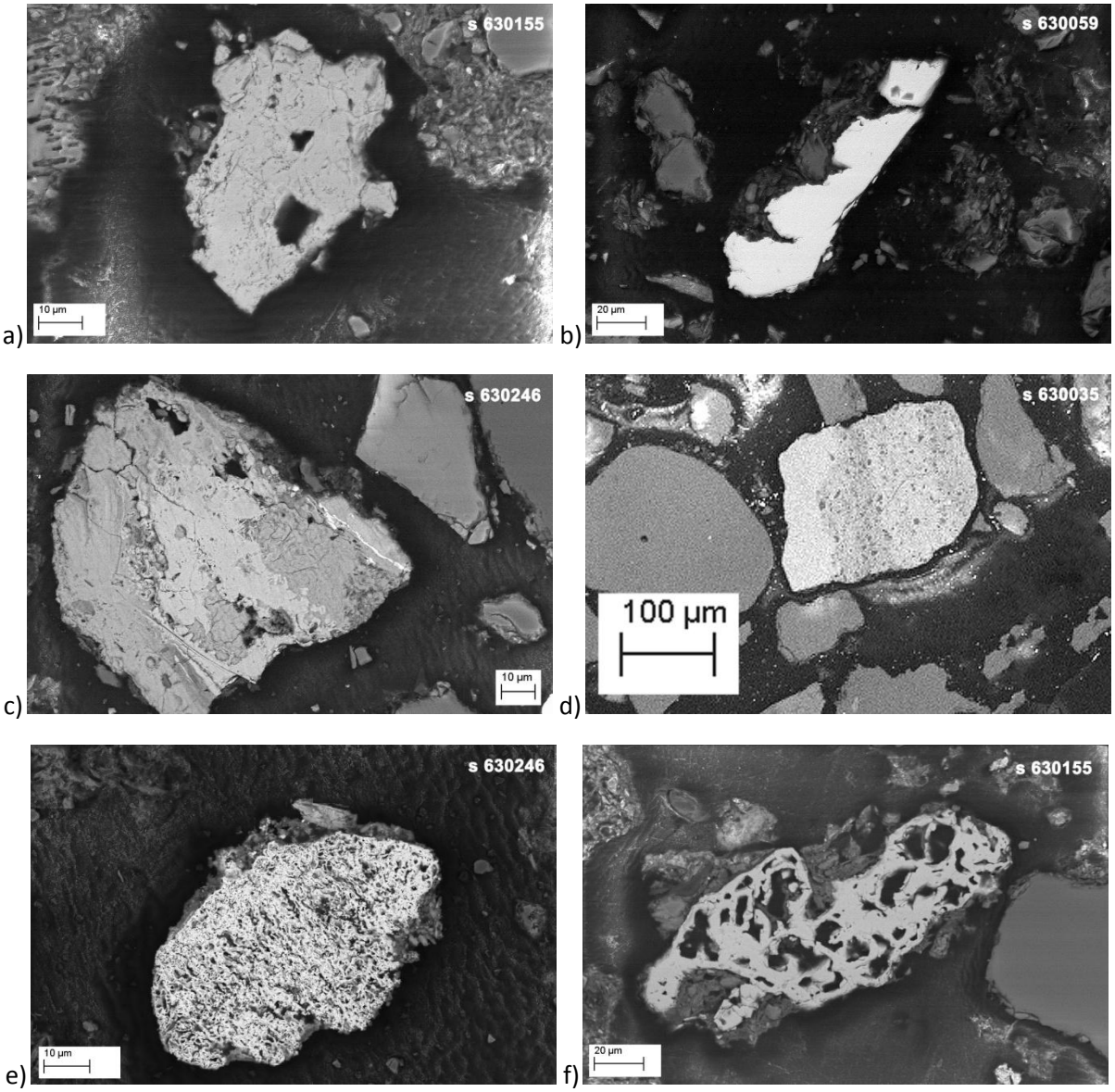


(cont.)

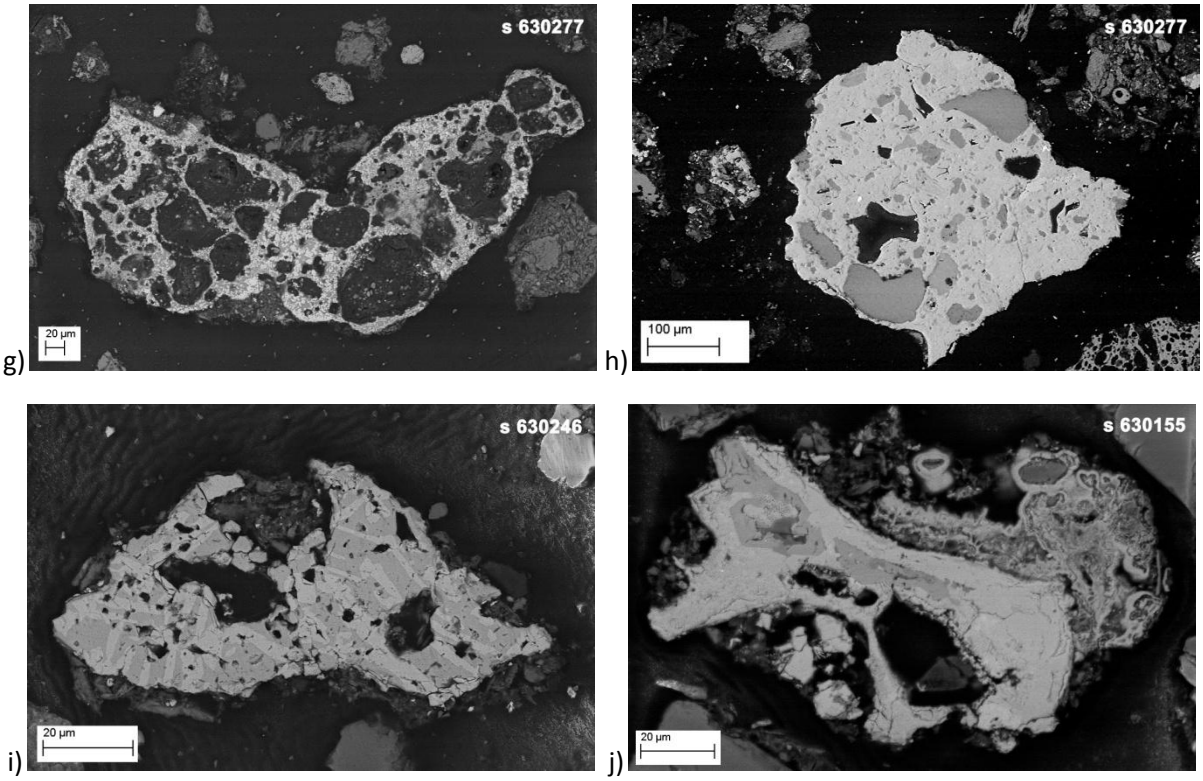


Figure 29: SEM images of Fe-oxide grains in Manchester soils (BSE imaging, partial vacuum, 15 kV accelerating voltage) (a, b - massive; c, d - with internal banding; e - with villiform structures; f, g - porous; h - with inclusions; i - with twinning; j - with signs of corrosion).

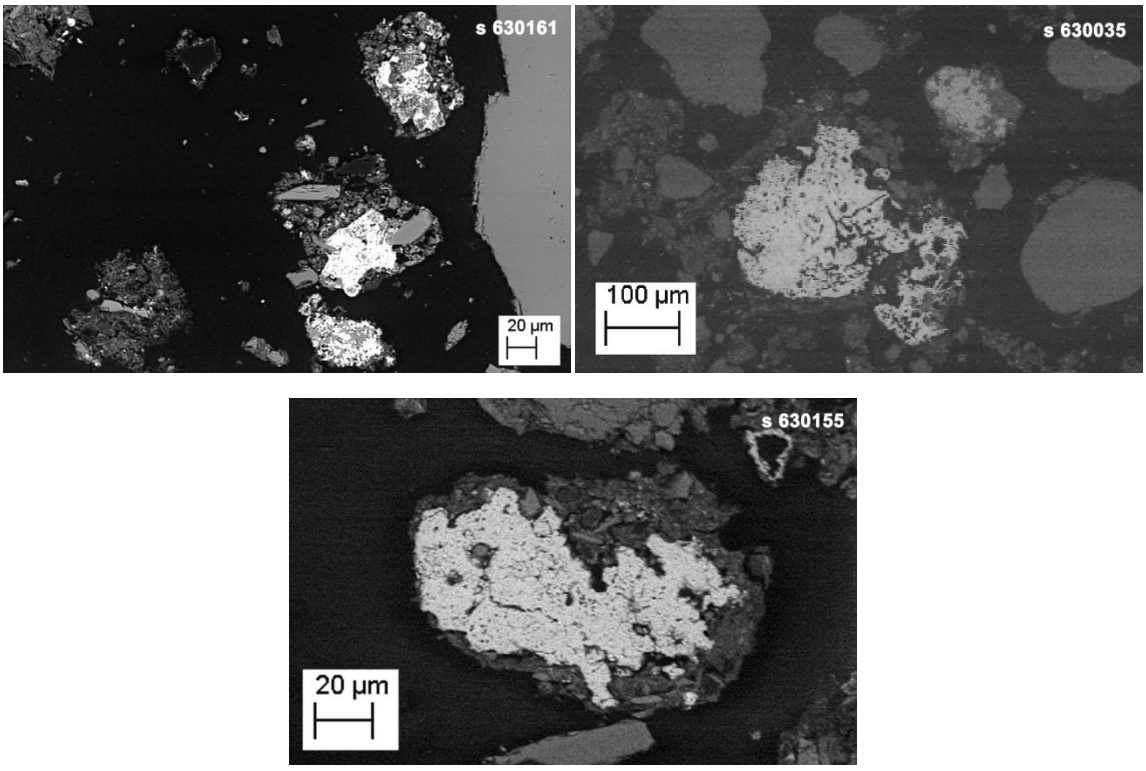


Figure 30: SEM images of Fe-oxide grains with silicate and alumino-silicate coatings in Manchester soils (BSE imaging, partial vacuum, 15 kV accelerating voltage).

The origin of these grains in Manchester soil is complex. As previously referred, Fe is naturally present in soils, provenient from local lithologies or enriched by normal biological processes. Nevertheless, anthropogenic Fe inputs can be very significant as it is a raw-material used with

extensive purposes in the urban environment. These Fe-rich materials may contain different amounts of trace metals of environmental concern such as Cr (Figure 29b: 5.43%, Figure 30a: 1400mg/kg), Co (Figure 29b: 7.03%, Figure 29g: 4500mg/kg), Cu (Figure 29i: 2400mg/kg) and V (Figure 30c, 300mg/kg) - as hosted in Fe-dominated compounds, their potential of mobility and bioavailability increases as soil pH decreases. All five samples containing Cr, Co, Cu and V-bearing Fe-rich grains referred above display pH values below 7.

### *3.6.2. Iron-rich spherical grains*

The majority of the spherical grains found in Manchester soils have significant Fe content, which can go up to 39 wt%. A few examples are shown in Figure 31 below. Besides massive spherical Fe grains (Figure 31 a, b, c-left, o) or Cr-Fe grains (p); exsolution structures rich in Fe (c-right, d, e, h), Cu (f) and Ti-V (g); enclosed minerals of Fe (h, i, k) Ti (j) and air bubbles (b, f, g, h, i, j, k, l, n, o) are also common in this type of grain. Dissolution structures may also occur (d, l, m, n) and might be an indicator of trace metal release into soil, as these particles may be enriched in such metals. Iron, Si, Al and Ca are the most abundant constituents of this kind of grain.

a) 


b) 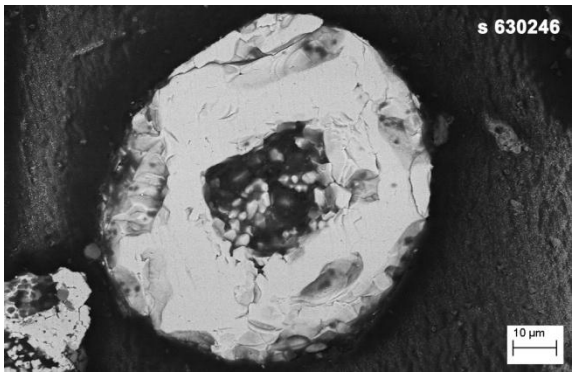


c) 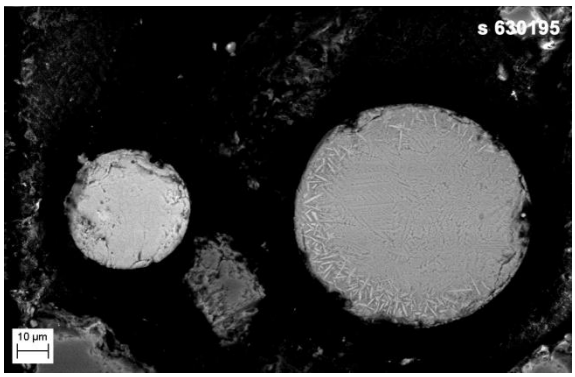


d) 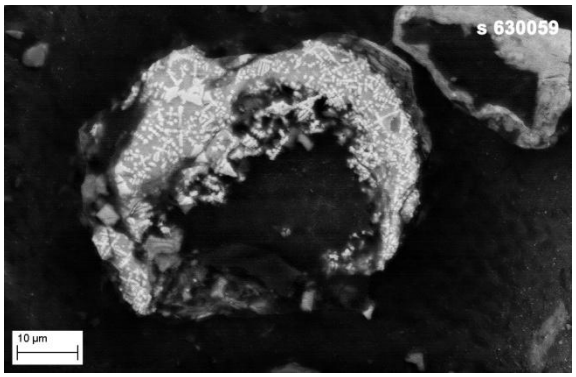


(cont.)

e) 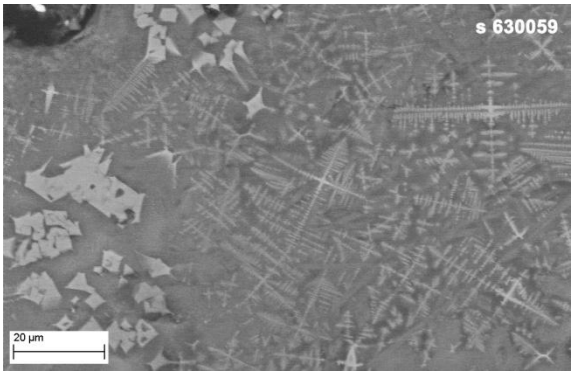


f) 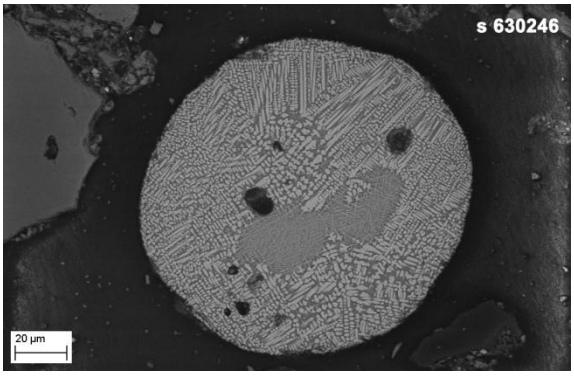


g) 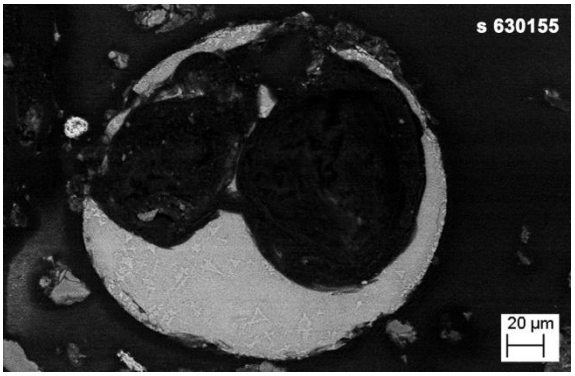


h) 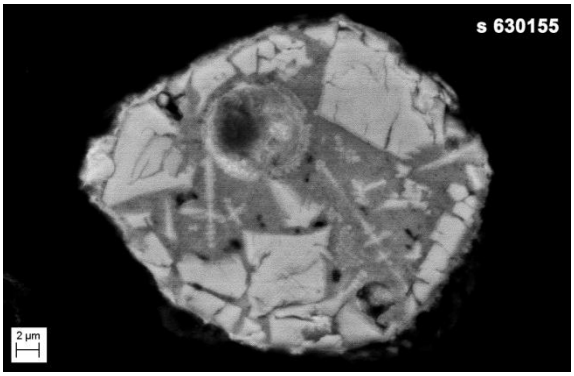


i) 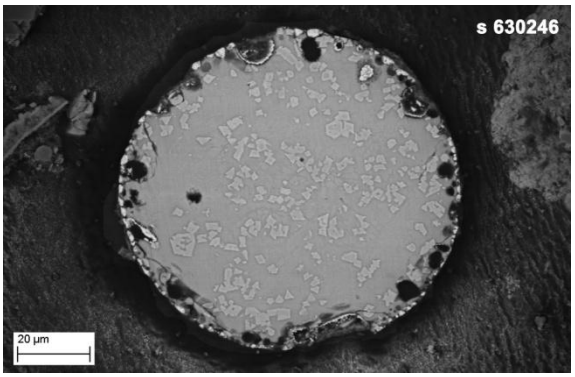


j) 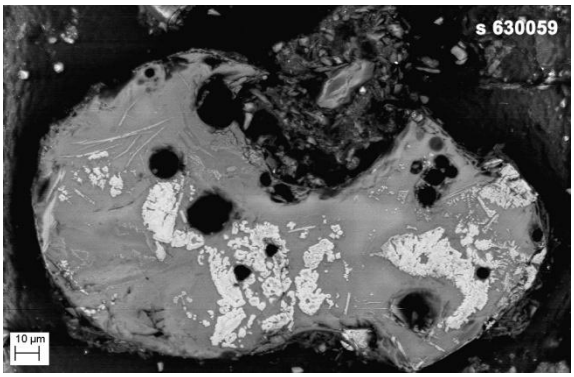


k) 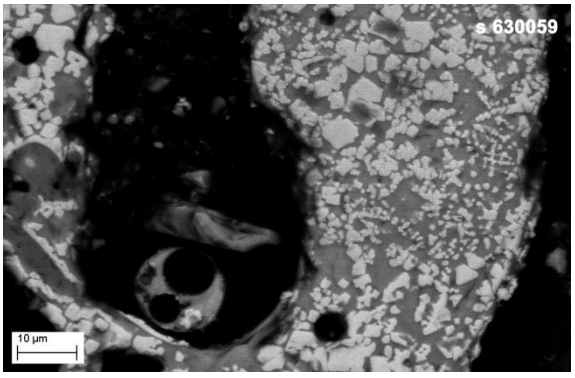


l) 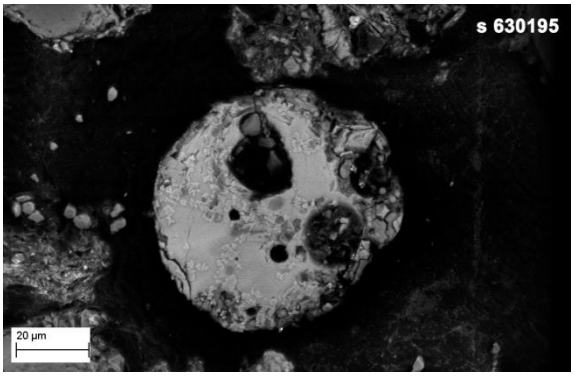


(cont.)

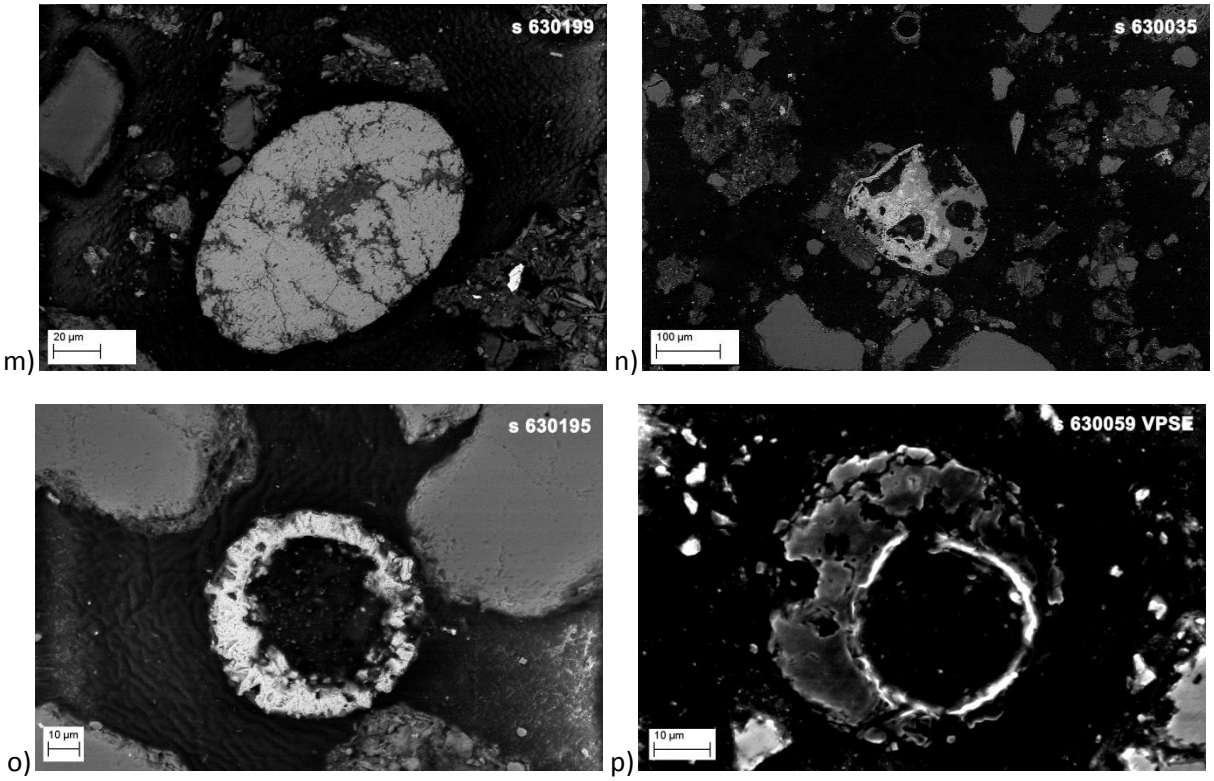


Figure 31: Iron-rich spherical grains in Manchester soils (BSE imaging [except grain p: secondary electron imaging - VPSE], partial vacuum, 15 kV accelerating voltage) (a, b, c [left], o - Fe-dominated; c [right], d, e, h - with Fe-rich exsolution structures, f - with Cu-rich exsolutions; g - with Ti-V-rich exsolutions; h, i, k - with enclosed Fe minerals, j - with enclosed Ti minerals; b, f, g, h, i, j, k, l, n, o - with air bubbles; d, l, m, n - with dissolution structures; p - massive Fe-Cr).

Spherical, metal-rich grains have been reported to result from high temperature combustion processes such as those of blast-furnace smelters (Fredericci et al., 2000; Hleis et al., 2013), or through burning of hazardous or municipal wastes (Liu et al., 2009; Kougemitrou et al., 2011). In addition to the atmospheric emissions of particulates caused by these activities, which are ultimately deposited by atmospheric fallout, the slag products of smelting are commonly used as a component in concrete and other construction materials (Babu and Kumar, 2000; Haiying et al., 2011; Hannesson et al., 2012). The erosion of these materials is likely to release this kind of particle in urban soils, as well as the inadequate disposal of the cinders produced by incineration (Gworek et al., 2008).

Exsolution textures in spherical grains were found in Manchester soils to be composed of Fe, Ti and Cu. They are most likely the result of the cooling of parent material (slag, fly ash) to temperatures at which the component mixture is no longer stable and the different components exsolve (unmix). The formation of crystallites and the inclusion of bubbles in this kind of grain can also be explained by the cooling processes the parent materials undergo. The example of Figure 32 shows perpendicular, dendritic Fe-Mg exsolutions in a Si-K matrix (also represented in Figure 31 d and e). Iron and Mg crystallites are also present, as well as Al lamellae.

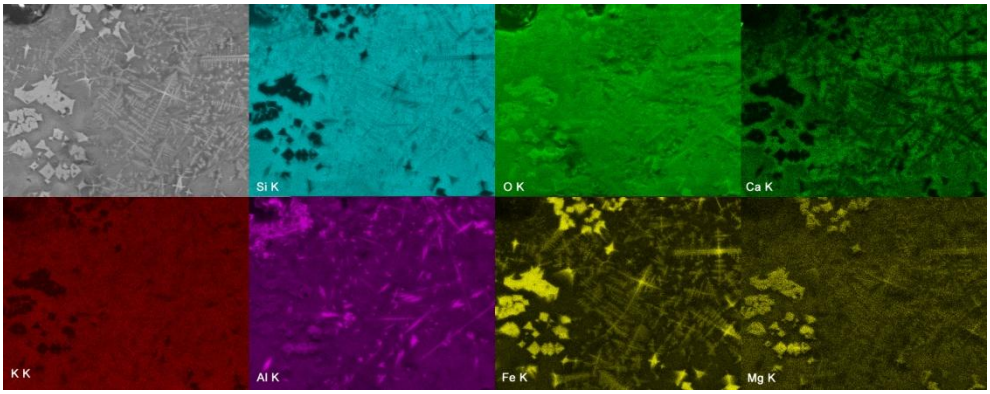


Figure 32: Geochemical map of the exsolution textures and crystallites (sample 630059).

This grain in particular also shows signs of disaggregation, meaning the metal components may have been separated into finer, individual grains or dissolved into the soil solution. Similar grains from the same sample are shown in Figure 31 j and k. This sample (630059) contained visible brick and slag fragments.

The grain of Figure 33 is similar to the previous in composition: it displays Fe inclusions in a Si-Al matrix, with bubbles and signs of disaggregation. The sampling site (630035) is reported to be contaminated with bulk industrial waste.

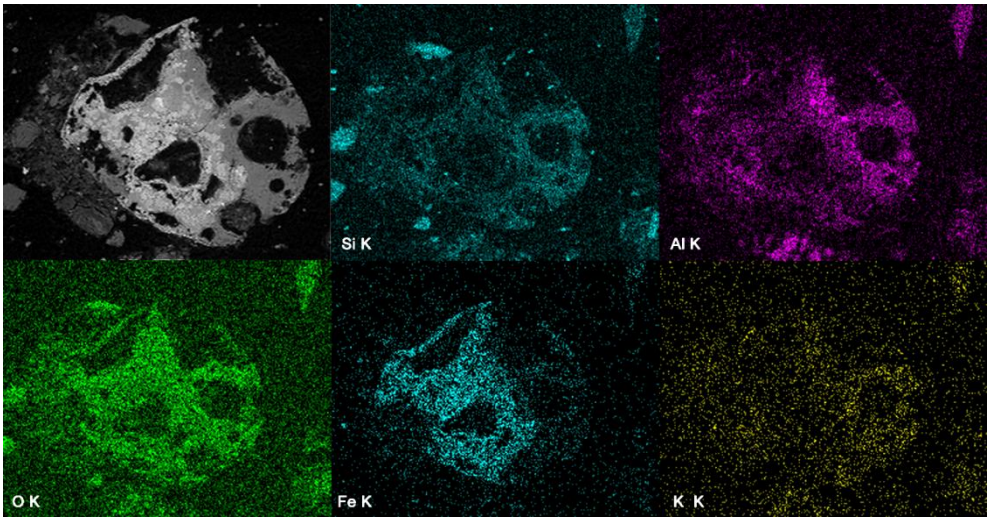


Figure 33: Geochemical map of the exsolution textures and crystallites (sample 630035).

Figure 34 shows a similar type of grain; however, matrix composition is rich in P rather than Si. Crystallite inclusions mostly composed of Fe are better developed, and this grain seems to be coated by a Si-Al material.

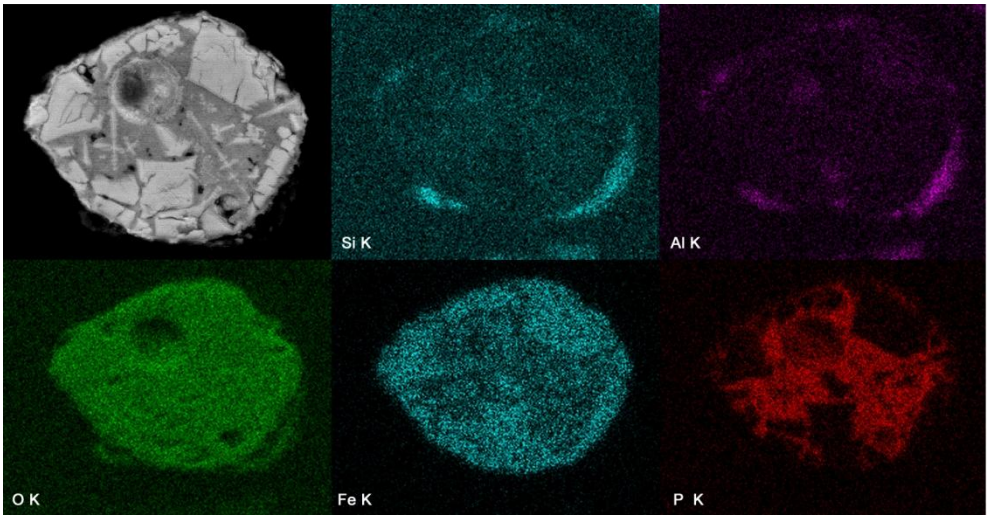


Figure 34: Geochemical map of the exsolution textures and crystallites (sample 630155).

There are also other grains that, although not spherical in shape, resemble the internal structure and composition of the grains described in this section. An example is given in Figure 35, where Fe exsolutions/crystallites are included in a Si-Al-(Ca) matrix. The origin of this type of grain may likely be attributed to high-temperature combustion processes, hence its inclusion in this section.

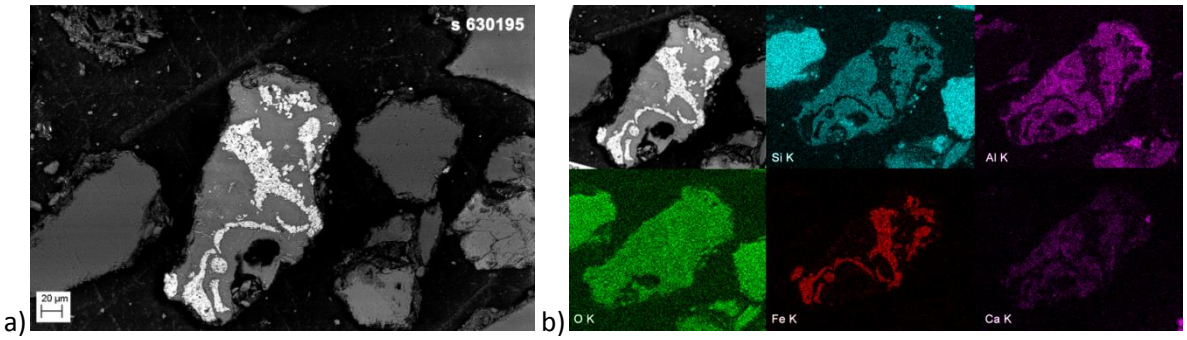


Figure 35: Irregular grain showing Fe-rich crystals in a Si-Al-Ca matrix. a) BSE imaging, partial vacuum, 15 kV accelerating voltage; b) compositional map for the same grain.

As the matrixes of this kind of grain are mostly composed by Si, Al and Ca, the presence of trace metals of environmental concern needs further attention as their potential for mobilization is high. Concentrations can reach 800 mg/kg V and 1500mg/kg Cu (Figure 31f), 11.5% Cr (Figure 31p), and 6300 mg/kg Mo (Figure 33).

### *3.6.3. Lead-rich grains*

Lead is present in soil particles in two main phases: either as massive Pb (Figure 36a: 52% Pb, b: 38.82% Pb, c and d: 36% Pb), which may contain e.g. P (Figure 36b, 2.6% P; c and d: 4000mg/kg P) or V (Figure 36 c and d: 3.24% V), or as small particles in a heterogeneous structure (Figure 36 e and f).

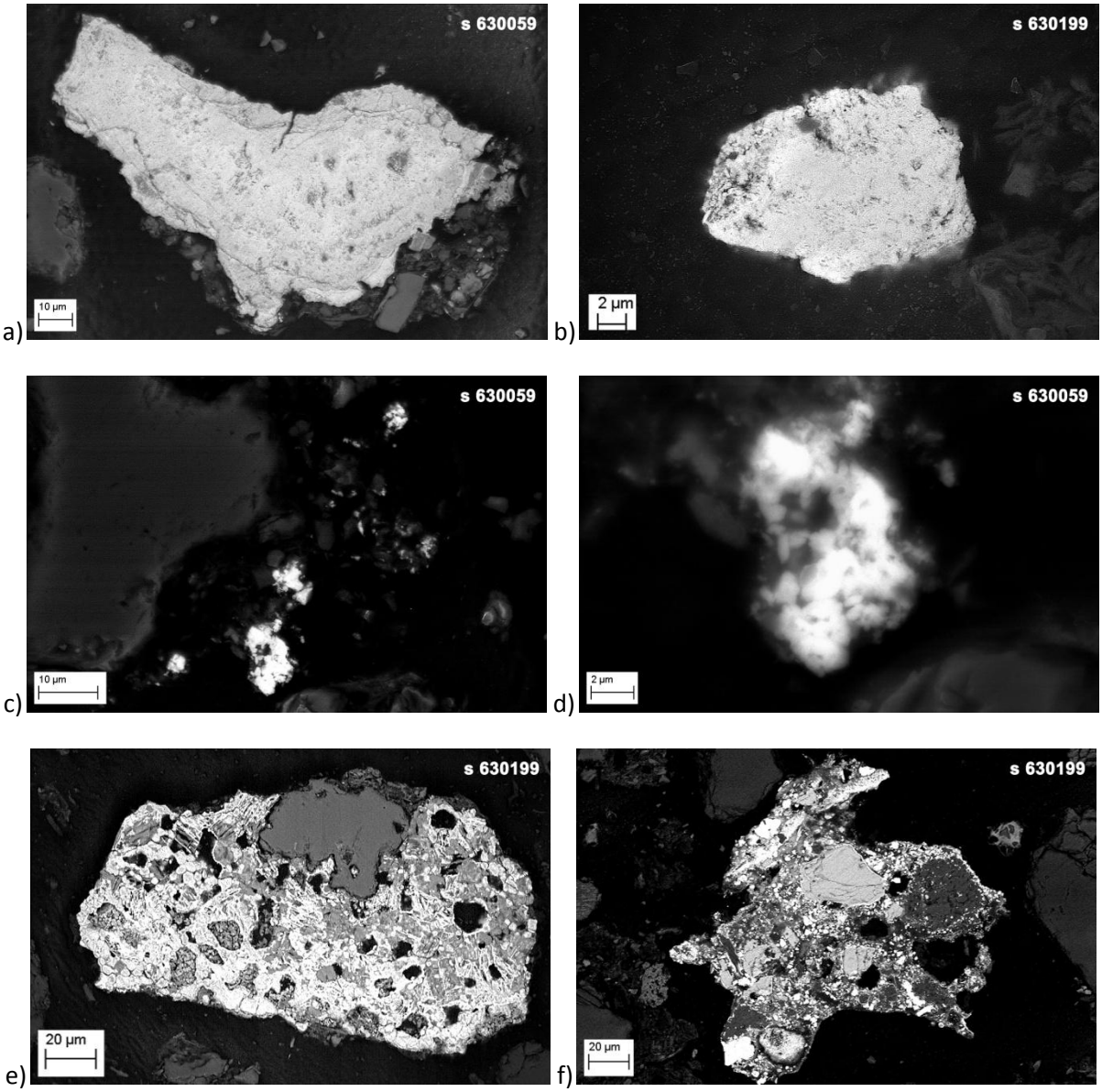


Figure 36: Pb-rich grains in Manchester soils (BSE imaging, partial vacuum, 15 kV accelerating voltage) (a, b, c, d - massive; e, f - heterogeneous structure).

This second sub-type of Pb-rich particle is generally larger in size, and the morphological and compositional heterogeneities are marked. The compositional map of Figure 37a below shows a grain composed of disseminated Pb-P particles, together with more localised Ca-rich and Ba-rich particles. Iron, Si and Al contents within the grain are very small.

Although similar in morphology, the grain represented in Figure 37b shows Pb-S-Mn particles in a Fe-dominated mass, with occasional P-Ca particles and a Si “inclusion”. Lead contents of these two grains are of 7500 and 8100 mg/kg, respectively.

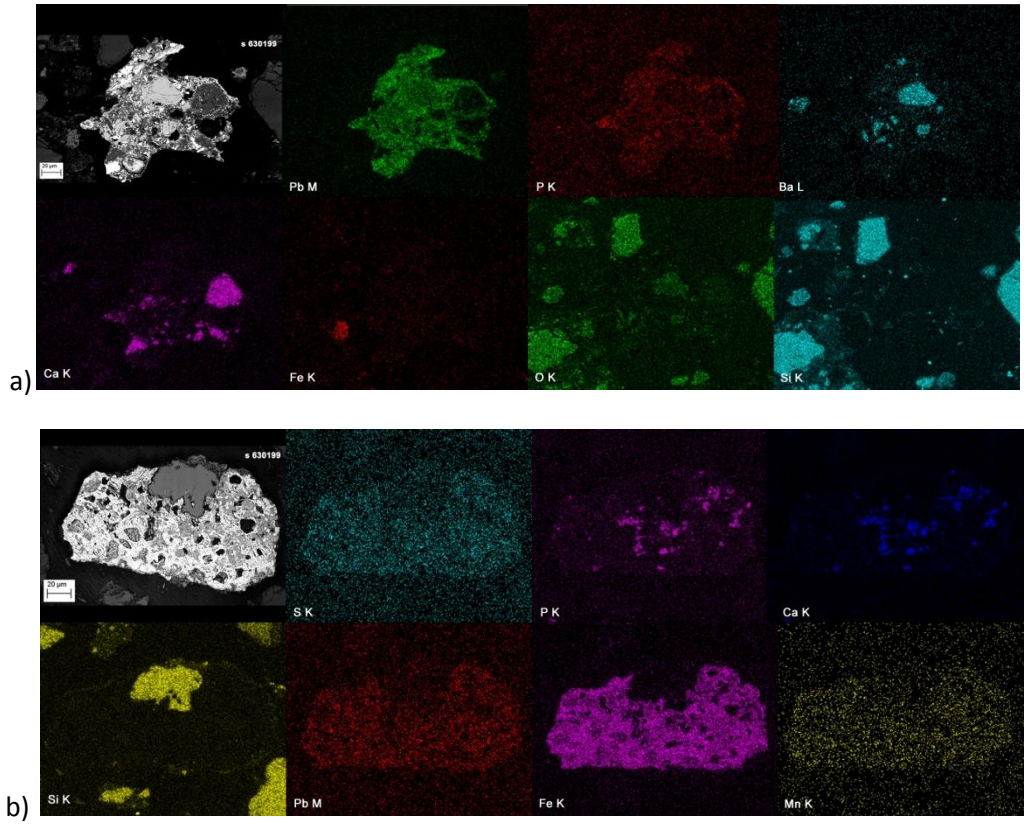


Figure 37: Compositional maps of Pb-rich grains in Manchester soils (sample 630199).

The origin of Pb-rich grains in soils can be attributed mostly to anthropogenic inputs such as the smelting/processing of Pb ore (Dudka and Adriano, 1997), Pb atmospheric deposition from leaded petrol combustion (Izquierdo et al., 2012), coal and oil combustion (Dragovic et al., 2013), production of steel and non-ferrous metals (Lambert et al., 2011), or from leaded paint (Brokbartold et al., 2013).

Sample 630199, which shows the maximum Pb level of the study area (2758 mg/kg), is located in a residential area in Whalley Range with no present-day Pb point source close by. Whalley Range was one of the first suburban residential estates of Manchester, built during the 19$^{th}$ century Industrial Revolution which suffered great changes including the demolition of the old large houses and the subsequent redevelopment of their sites (MCC, 2013). The Pb particles found at this site show similarities both in morphological aspect and composition with those of leaded paint (Hunt et al., 1998), which has likely been used in the buildings which have meanwhile been degraded, converted or demolished in this area.

## *3.6.4. Barium-rich grains*

Barium-rich grains are generally small in size (10-100 µm) and irregular in shape (Figure 38a); they have also been observed together with Si/Ca-rich phases (b), some of which may exhibit weathering signs (c). Barium contents vary between 17.4 and 35.8% and S is also present in significant amounts, between 3.7 and 7.4%.

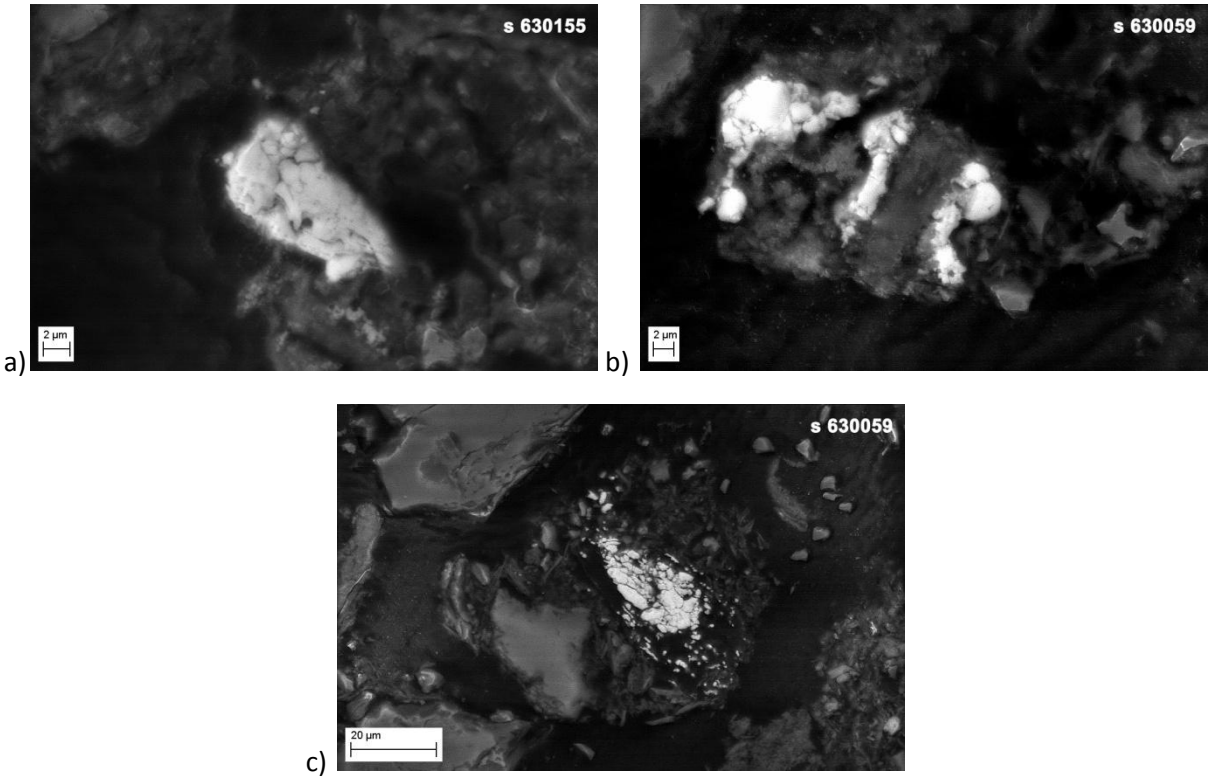


Figure 38: Ba-rich grains in Manchester soils (BSE imaging, partial vacuum, 15 kV accelerating voltage).

This composition is consistent with the presence of barite (barium sulphate), a mineral with vast applications (e.g. drilling muds, chemicals, fillers, glass and ceramics); besides a possible geogenic origin. Barium sulphates have generally low mobility in soils (Kabata-Pendias and Pendias, 2001) - even if released by weathering, Ba readily precipitates as sulfates and carbonates, is strongly adsorbed by clays, and is sorbed onto oxides and hydroxides. The individual grains analysed did not contain other potentially-harmful elements and hence these Ba-rich grains may be considered geogenic.

### *3.6.5. Other types of grains*

As referred previously, the majority of spherical-shaped grains in Manchester soils contain Fe and other metallic elements. Nevertheless, spherical grains composed mostly of Si-Al-Ca are also present, as those represented in Figure 39. The origin of these is also related to high-temperature combustion processes, capable of producing iron-poor slag material (Fredericci et al., 2000).

Accessory resistate minerals such as zircon grains of various sizes are also found in Manchester soils, such as those in Figure 40.

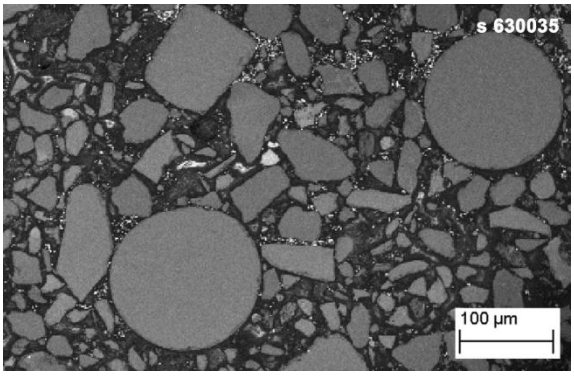


Figure 39: Spherical glass grains (Fe-poor) in Manchester soils (BSE imaging, partial vacuum, 15 kV accelerating voltage).

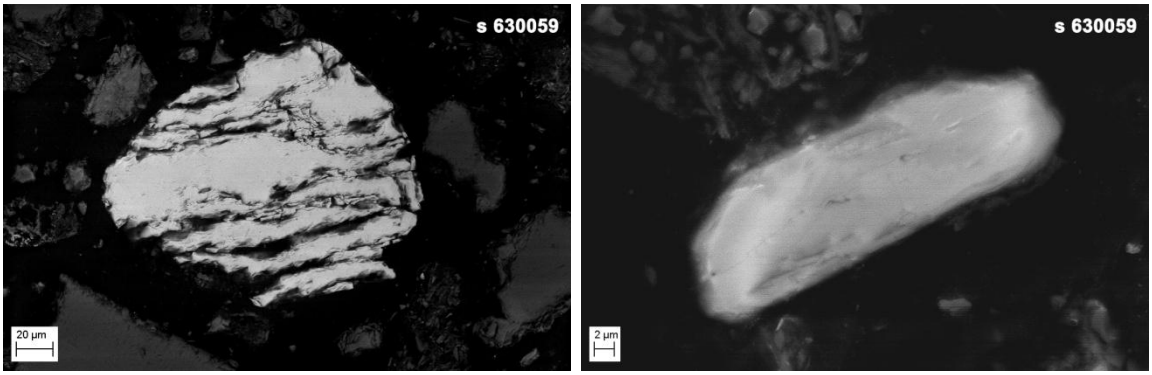


Figure 40: Zircon grains in Manchester soils (BSE imaging, partial vacuum, 15 kV accelerating voltage).

Examples of Fe-S rich grains are represented in Figure 41. These contain between 16-24% Fe and 15-20.2% S. Figure 41a represents a subhedral pyrite grain and Figure 41b is a framboidal pyrite grain, both of which are common in coals (Spears et al., 1994; Ryan and Ledda, 1998) which are present and have been historically explored, processed and burned in the Greater Manchester area.

a) 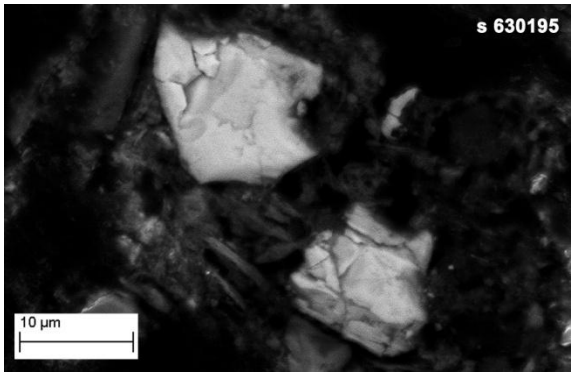

b) 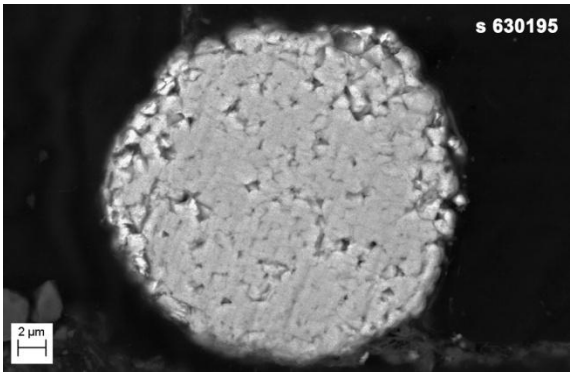


Figure 41: Fe/S-rich grains, a) probable pyrite, b) framboidal pyrite grain.

The presence of odd-shaped metallic fragments, clearly of anthropogenic origin, is also a source of potentially harmful elements in soil, such as chromium-plating fragments (Figure 42a), solder fragments (Figure 42b), and remains of a variety of metallic products. The origins of the majority of this kind of grains are hard to identify, as most can be classified as iron oxide grains.

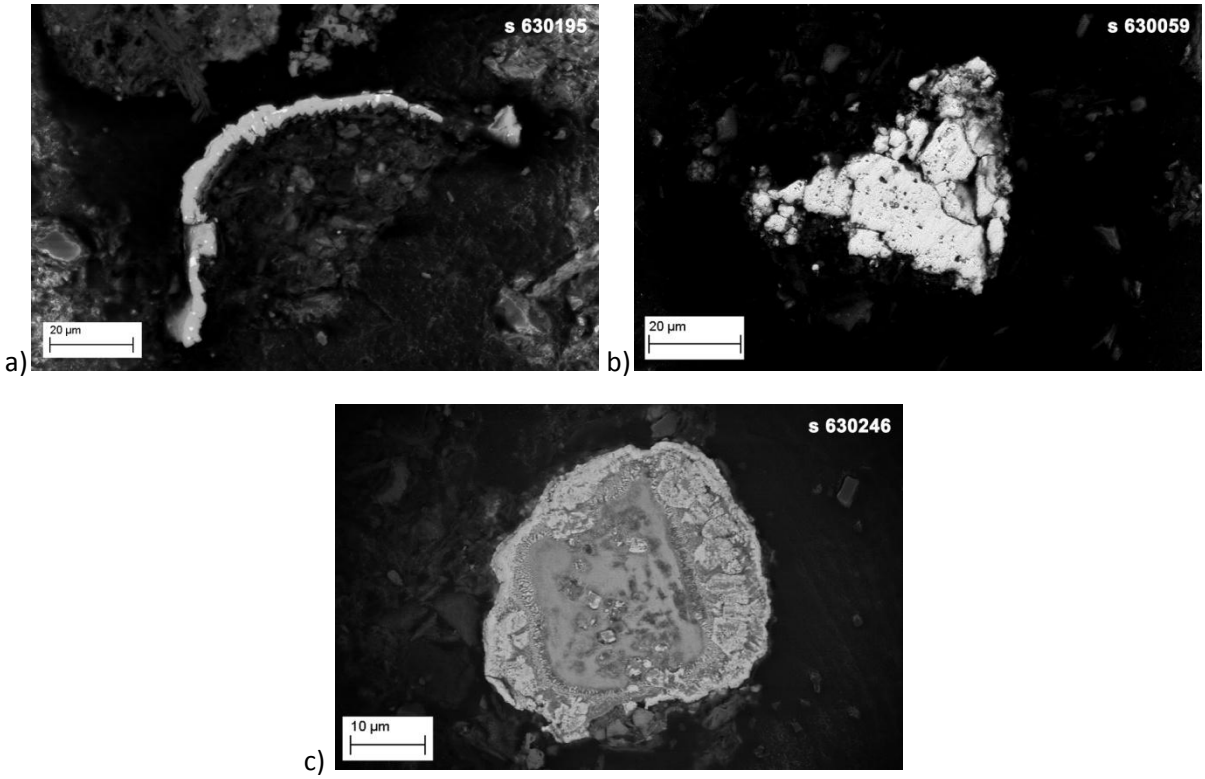


Figure 42: a) Cr-rich fragment (probable chromium-plate); b) Cu/Sn-rich fragment (probable solder fragment) and c) zoned Sn/Fe-rich grain (BSE imaging, partial vacuum, 15 kV accelerating voltage).

## 3.7. Multivariate statistics: Principal component analysis and component score mapping

Principal component analysis (PCA) is widely used in the Earth Sciences to reduce the number of variables in a dataset by identifying the pattern of correlations or covariances between them: the new (and fewer) dimensions resulting from the principal component transformations are linear combinations of the observed variables (Reyment and Savazzi, 1999). The reduction to a smaller number of variables allows for a better explanation of the relationships between these, with the identification of chemical element subgroups. When PCA is used for data reduction or exploratory purposes, normality is not a critical assumption (Jolliffe, 2002) and, therefore, there is not a great need to transform the data to approach the normal distribution. Nevertheless, data were subject to standardisation prior to PCA since geochemical data were measured in different units. Soil geochemical data, organic matter content (LOI) and pH were subject to PCA using IBM® SPSS 19 software. Three sets of PCA analysis were performed: analysis A, using the Kaiser criterion for component selection; analysis B, using the scree plot inflexion point criterion for component selection; and analysis C, using selected geochemical variables.

### *3.7.1. Analysis A*

The first set of PCA (reference #A) was performed using 47 variables and retaining the components with an eigenvalue greater than one, as per the Kaiser criterion (cf. section 2.9.2) in a total of 10

extracted components. KMO and Bartlett's sphericity tests revealed that the Manchester soil dataset of 47 variables is suitable for PCA analysis, as displayed in Table 25 - KMO value is of 0.902, what indicates with a high degree of confidence that PCA analysis is an appropriate method. Bartlett's test is also highly significant, as the Sig. value is less than 0.001.

| KMO and Bartlett's Test | | |
|---|---|---|
| Kaiser-Meyer-Olkin Measure of Sampling Adequacy | | ,902 |
| Bartlett's Test of Sphericity | Approx. Chi-Square | 19840,887 |
| | df | 1081 |
| | Sig. | ,000 |

Table 25: Results for the KMO and Bartlett's tests for BGS soil geochemical data (#A, n=300, 47 variables).

Observing the anti-image correlation matrix for this analysis (Table 79 of Appendix 2), Cd (0.424) was the only element for which the diagonal value was not above 0.5 - but since the removal of this variable did not affect the adequacy statistics, it was considered acceptable. Table 80 of Appendix 2 shows the communalities for soil geochemical data. As an example, we can see that 0.964 (96.4%) of the variance associated with $Al_2O_3$ is common, or shared variance - variables with communalities close to 1 (100%) have none or little specific variance (or random variance). The eigenvalues associated with each linear component before extraction, after extraction and after rotation are listed in Table 81 of Appendix 2. 47 linear components were identified (there are as many eigenvectors as there are variables, consequently as many components as variables). Total eigenvalues are represented in the first column, and in the second column these are expressed in terms of the percentage of variance explained. It is noticeable that the first three factors explain relatively large amounts of variance, whereas subsequent factors explain only smaller amounts. This can also be observed in the scree plot of Figure 43, where the red arrow indicates the inflexion point. The dashed line represents an eigenvalue of 1, and the components above this line (1-10) were chosen to be retained - in this case, the number of components is chosen according to the Kaiser criterion (eigenvalue >1). The eigenvalues associated with these 10 components are again displayed (and the percentage of variance explained) in the columns labelled "extraction sums of squared loadings" (Table 81, Appendix 2). The values in this part of the table are the same as the values before extraction, except for the values of the discarded components which are ignored. The right part of the table labelled "rotation sums of square loadings" refers to the components' eigenvalues and percentage of the total variance after orthogonal Varimax rotation.

Before rotation, factor 1 accounted for considerably more variance than factor 2, whilst after rotation both account for almost the same variance – the relative importance of the two factors is equalised as the factor structure has been optimised by the rotation. Before rotation, factor 1 accounted for 38.04% of the variance which is considerably more than factor 2 (14.42%); but after varimax rotation factors 1 and 2 account for 22.25% and 22.63%, respectively. The 10 retained components in total account for approximately 82% of the total variance.

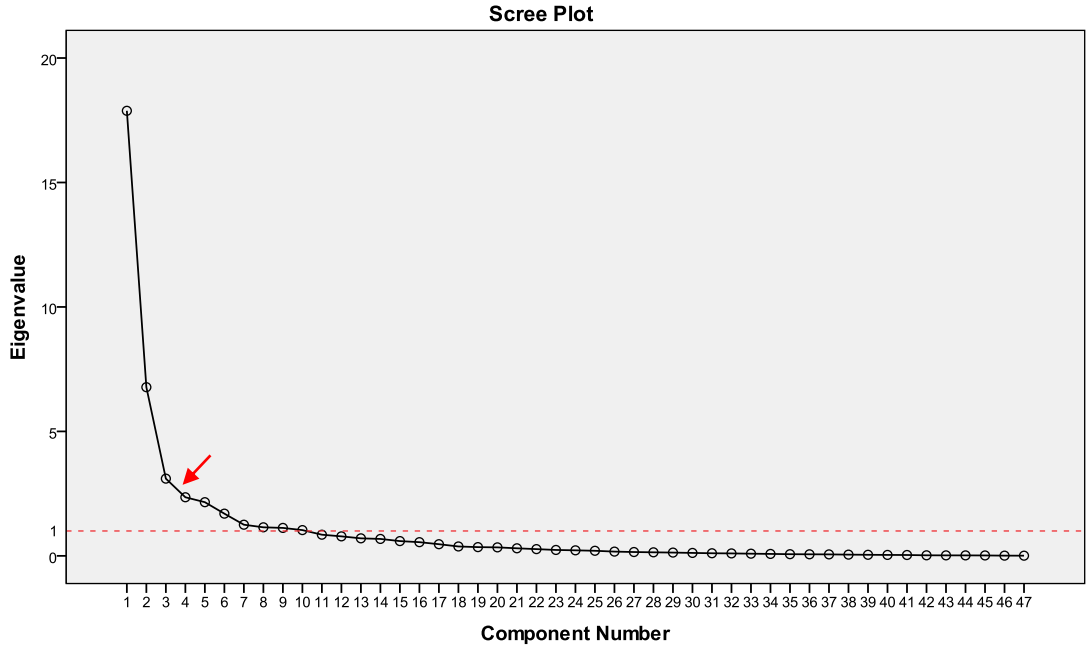


Figure 43: Scree plot - Components vs. eigenvalues for BGS soil geochemical data (PCA #A, n=300, 47 variables).

Table 82 of Appendix 2 shows the rotated component matrix, which is one of the most important PCA outputs - it reveals the groups of variables with highest loadings onto each component, i.e. have a similar variation pattern across the dataset. In geochemical terms, the elements with highest loadings onto each component can be interpreted as those derived from similar sources or enriched through similar processes.

Loadings above 0.7 are shown in red – e.g. it can be observed in the rotated component matrix that $Fe_2O_3$, V, Co, Ni, Ge, Mo and Sn load very highly onto component 1, whereas $Al_2O_3$, $K_2O$, $TiO_2$, Ga, Rb, Nb, Th, La, Ce and Nd load highly onto component 2. Table 26 below summarises the information of Table 82, displaying element loadings onto each of the 10 components, classified by loading magnitude.

| | | Element loading | | |
|---|---|---|---|---|
| | | ]1.0, 0.7] | ]0.7 - 0.6] | ]0.6 - 0.5] |
| component | 1 | $Fe_2O_3$, V, Co, Ni, Ge, Mo, Sn | Sc, Se, Sr, Y | Zn, Sb, La, Ce, Nd, LOI |
| | 2 | $Al_2O_3$, $K_2O$,$TiO_2$, Ga, Rb, Nb, Th, La, Ce, Nd | MgO, Sc, Y, U | V |
| | 3 | Bi, Ag | $P_2O_5$ | Tl, Pb |
| | 4 | Cr, Cu, As | - | - |
| | 5 | CaO, pH | - | - |
| | 6 | Br | I, LOI | - |
| | 7 | $Na_2O$, Zr, Hf | - | - |
| | 8 | MnO | - | Zn |
| | 9 | - | - | Sm |
| | 10 | Cd | - | - |

Table 26: Summary of element loadings onto each calculated component (1 to 10) for BGS soil samples (PCA #A, n=300, 47 variables).

Another way of visualising these results are the component plots in Figure 44 below. Due to the high number of variables, the tri-dimensional plot is difficult to interpret and has been decomposed

into three bi-dimensional plots: Component 1 vs. 2, component 1 vs. 3, and component 2 vs. 3. This way, element groupings can be more easily identified.

Firstly, $SiO_2$ is the only variable which shows a significant negative loading (represented in blue in Table 82 of Appendix 2) onto both factors 1 and 2 – in fact, $SiO_2$ correlates negatively with most elements which show the highest loadings on factors 1 and 2. In spite of being the main constituent of the soil mineral phase, it is inversely proportional to the other main constituent, $Al_2O_3$, and other elements which are related to Al - consequently it shows a negative, although significant, loading value.

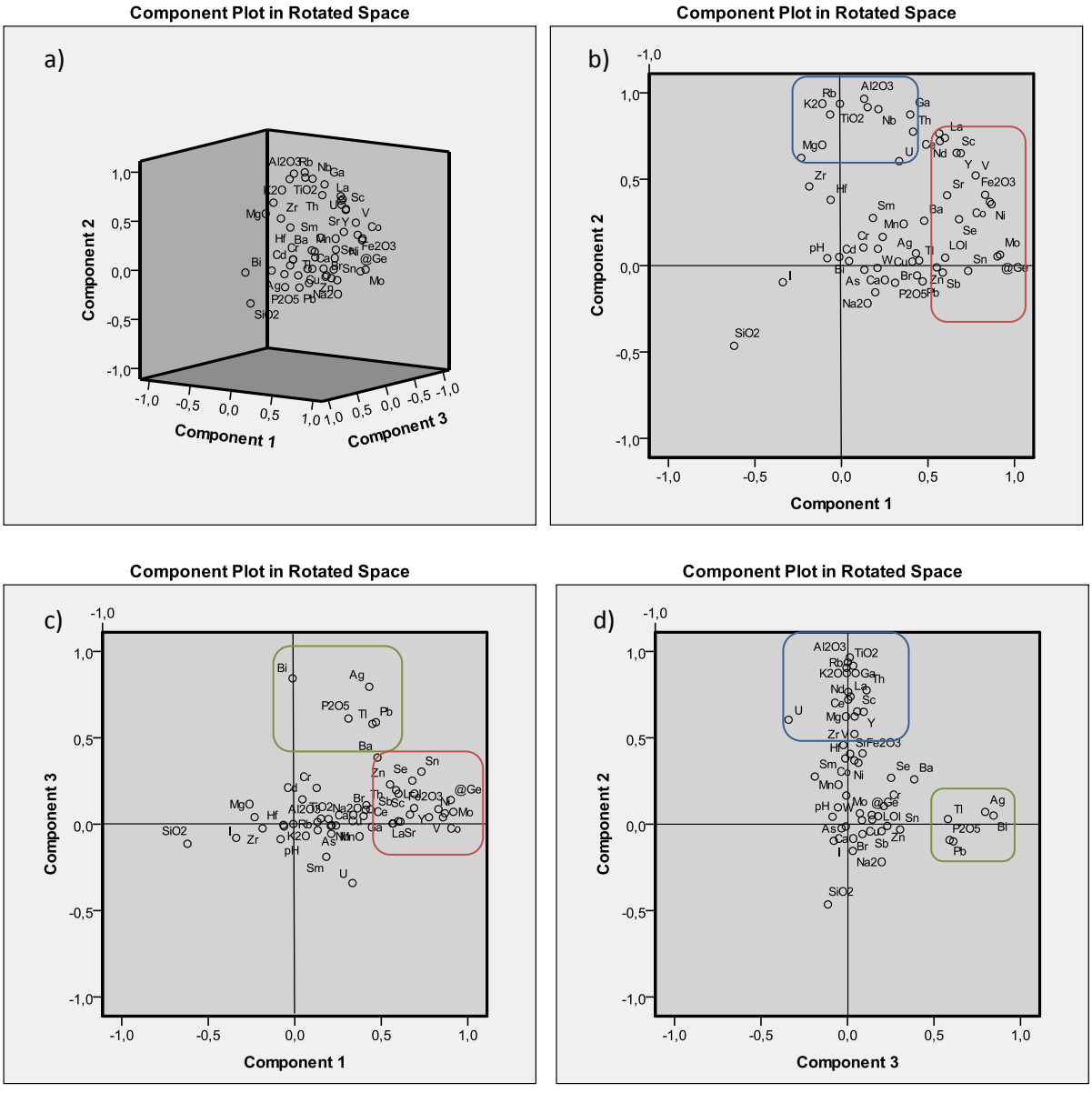


Figure 44: Component plots for components 1, 2 and 3 for BGS soil geochemical data: a) tridimensional plot, b) C1 vs. C2, c) C1 vs. C3 d) C3 vs. C2 (PCA #A, n=300, 47 variables).

•**Component 1**, as already referred, shows high loadings for $Fe_2O_3$, V, Co, Ni, Ge, Mo and Sn; and moderate loadings for Sc, Se, Sr, Y, Zn, Sb, La, Ce, Nd and LOI. These are plotted near the right end of the X axis in Figure 44b, where loadings are above 0.5 for component 1. Elements with the highest

loading values are siderophile or chalcofile, and are likely to be present adsorbed to Fe oxides or in other Fe or S compounds. After rotation, this component accounts for 24.3% of the total variance.

A closer look at Figure 44 also reveals two clusters among the elements with highest loading values for component 1 - Mo and Ge, and $Fe_2O_3$, Co and Ni. Exogenous Mo ores are known in coals, generally associated to organic matter and Ge - coal burning is widely known to produce Mo and Ge-rich ashes (Goldschmidt, 1935). The low loading of Mo and Ge onto component 2 reveals that these are rarely associated to lithophile elements, and that their concentrations may not be the result of natural, geogenic processes (cf. observations for component 2 below) - their higher concentrations are probably a direct result of coal processing/burning activities.

Similarly, Ni, Co and Fe have high chemical affinity, are commonly associated in several minerals (Co-Ni-Fe arsenides and sulphides) and coal. Their high concentrations in the study area are a likely consequence of human activities.

In fact, at the spatial scale, Mo, Co, Ni and Zn enrichments can be very significant at certain locations across the study area and are clearly of anthropogenic origin, namely in areas 1, 3 and 5 (cf. section 3.5.2 and Figure 25). The fact that LOI (organic matter content) also loads onto this factor means that some of these elements might be organic matter-bound to some extent.

Elements with a significant loading onto component 1 are likely enriched in soils by human activities, namely related to coal; nevertheless, some of them have also a geogenic origin, which is indicated by the simultaneous loading onto component 2 (e.g. Sc, Y, V, and REEs).

•**Component 2** shows high loadings for $Al_2O_3$, $K_2O$, $TiO_2$, Ga, Rb, Nb, Th, La, Ce and Nd (upper part of Figure 44b and d); and moderate loadings for MgO, Sc, Y, U and V; which are generally lithophile and strong geogenic elements – i.e. elements which are related to the natural, geologically-derived components of soil. Elements with a high loading onto component 2 can be interpreted as mainly derived from natural processes of soil formation from its parent materials - these elements are rarely influenced by anthropogenic inputs in Manchester soils. Component 2 accounts for 22.6% of the total variance after component rotation.

•**Component 3** displays the highest loading values for Bi and Ag, followed by $P_2O_5$, Pb and Tl, accounting for 6.6% of the total variance (upper part of Figure 44b and right part of Figure 44c). Lead, Bi and Tl are neighbouring elements in period 6 of the periodic table and are chemically similar; furthermore, Bi, Tl and Ag are common by-products of Pb smelting/refining processes and coal combustion (Kabata-Pendias and Pendias, 2001; Shotyk and Krachler, 2004; Jacobson et al., 2005). The presence of $P_2O_5$ with similar loadings, especially for Tl and Pb, might indicate their presence as phosphates; e.g. lead phosphates are expected to form in soils contaminated with Pb if sufficient P is available (Cotter-Howells, 1996), (cf. Figure 36b, c and d). Nevertheless, thallium phosphates have been reported in geological materials, although rarely in soils (Karlsson, 2006; Baturin, 2007).

•**Component 4** accounts for 6.2% of the total variance. The elements with highest loading values for this component are As, Cr and Cu - note that component 4 is not represented graphically in Figure 44. These elements are typical of chromated copper arsenate (CCA), a compound which is used in wood preservation since the mid-1930s. CCA is intended to protect wood against pests such as decay fungi and wood boring insects that can threaten the integrity of wood products (Read, 2003). CCA-treated wooden structures such as wooden decks, bridges, footpaths and utility poles have been often reported to influence As, Cr and Cu contents in nearby soils (Townsend et al., 2003; Gezer et al., 2005; Kim et al., 2007). CCA-treated wood waste is a matter of concern in many countries (Helsen and Van den Bulck, 2005) and recycling or disposal methods need to be carefully implemented; e.g. the burning of CCA-treated wood has been reported to produce ash with high levels of Cu, Cr and As which may contaminate soils by leaching of these metals from burn sites (Harden and Johnson, 2009).

Additionally, As, Cr and Cu are present in effluents and sewage sludge from water treatment plants (Lake et al., 1984; Ščančar et al., 2000; Zhang et al., 2013). Besides point-source contamination near wastewater treatment works, this kind of material has long been added to soils as an amendment (Berrow and Webber, 1972; Sterritt and Lester, 1980; Alloway and Jackson, 1991). The use of sewage sludge in soils may not only increase As, Cr and Cu contents, but also other PHE such as Pb, Cd, Ni and Zn. Nevertheless, the mapping of component 4 (cf. Figure 49 ) highlighted high scores near the Davyhulme Sewage Works and the Eccles Wastewater Treatment Works - a probable source for contamination in As, Cr and Cu is likely related to the WTPs, rather than CCA-related.

•**Component 5**, accounting for 4.8% of the total variance after rotation, shows high loadings for CaO and pH. This is due to the fact that Ca solubility from carbonates increases as pH decreases; therefore, lower pH values cause Ca remobilisation from soils and consequent decrease in concentration. This relationship is reflected on the CaO-pH correlation and shared variance. Soil liming practices (addition of calcium- and magnesium-rich materials to soil) are also used to cause an increase in soil pH. Strontium also shows a moderate loading onto this component (0.434) - Sr and Ca are elements from the same group in the periodic table and share similar chemical properties.

•**Component 6** shows high loadings for Br, I and LOI, and accounts for 4.7% of the total variance after component rotation, similarly to component 5. Bromine and iodine are common in soils and known to be closely related to soil organic matter contents (Maw and Kempton, 1982; Gerzabek et al., 1999), clustering in this component.

•**Component 7**, dominated by Zr, Hf and $Na_2O$, accounts for 4.4% of the total variance. Zirconium and Hf belong to the same periodic table group and are abundant in zircon, a nesosilicate mineral characterised by its high resistance to weathering processes, which is common in several types of rocks, sediments and soils. Sodium is not encountered in natural minerals; however, Na is used in the

process of transforming zircon materials into zirconium oxide (Manhique, 2003; Lubbe et al., 2012), which has a wide range of applications including ceramic manufacturing, motor engine components, high speed cutting tools, heat resistant linings in furnaces, containers for molten metals, and heat shields. Therefore, some of the Zr and Hf (and Na) existent in Manchester soils may be attributed to an anthropogenic origin rather than to a geogenic source - one of the largest manufacturers and suppliers of zirconium chemicals and oxides (MEL Chemicals™) is located in Swinton, approximately 2Km north of the study area.

- **Component 8** accounts for 3.3% of the total variance after rotation and shows a high loading for MnO and Zn. These two elements together are important soil micronutrients (Kabata-Pendias and Pendias, 2001) - Zn is also commonly associated to Mn oxides. Nevertheless, Zn shows a moderate loading value for component 1 as well, which can be the effect of an anthropogenic Zn contribution - Zn can also come from numerous anthropogenic sources, namely the wear and tear of vehicular parts (car body, brake linings and tyres) and industrial applications. In Manchester, Zn is frequently enriched in soils, and therefore anthropogenic sources are the main influence on Zn concentrations.
- **Components 9 and 10** together account for only 5% of the total variance, with high loadings for Sm (mainly geogenic) and Cd (anthropogenic), respectively. As these components account for such little variance, interpretations must be more carefully considered - although Cd is known to have anomalous point concentrations in the study area.

Component scores which were calculated during the PCA analysis were saved as new variables. For each principal component, the new variables contain the component scores for each sample; i.e. the sample placement on each calculated component.

In geochemical terms, principal components represent groups of elements with similar variation within a set of observed variables; therefore, these new variables were exported and mapped using ESRI® ArcGIS™ 10.0 software, similarly to what has been done for the bulk geochemical concentrations. Component scores were interpolated using the IDW method (cf. section 2.9.5 and the Theoretical Framework) - this method has been chosen as it is more suitable to reflect sharp local variations. Interpolation of component scores to uncalculated areas was performed using 100m as the output cell size and a distance radius of 500 m, with a minimum selection of 2 nearest neighbour samples. Areas shaded in red are those where the component score is highest, i.e. the elements represented by the component display the highest concentrations.

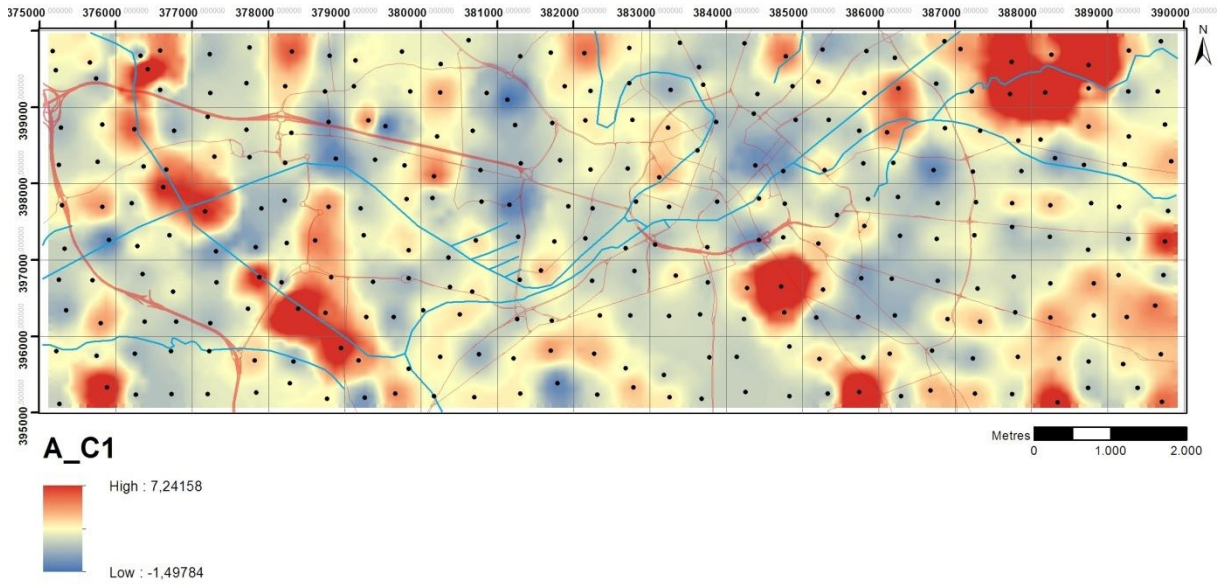


Figure 45: Spatial distribution of component 1 scores for BGS soil geochemical data (PCA #A, n=300, 47 variables) (cf. Table 26 for represented elements).

Component 1 scores (high loadings for $Fe_2O_3$, V, Co, Ni, Ge, Mo and Sn) are represented in Figure 45 and show the highest values in the Clayton Vale - Phillips Park area (around Medlock river and the Ashton canal), in the Oxford Road - Wilmslow Road alignment, and along the Bridgewater Canal (cf. Figure 9 and Figure 25). The highest scores found in Clayton Vale can be explained by the fact that this was a heavily industrialised area in the $18^{th}$-$19^{th}$ centuries, which included collieries and chemical works among many others - industrial infrastructures were demolished and this site was used as a municipal waste tip and a tip for the ash cinders from Stuart Street Power Station. Therefore, elements related to coal extraction and burning are enriched throughout this area. In a similar way, the soil samples collected nearby the Bridgewater canal are likely affected by the transportation of coal from the mines in Worsley, which was the main purpose of the canal in the $18^{th}$ and $19^{th}$ centuries.

Component 2 scores are mapped in Figure 46. This component has the highest loadings for $Al_2O_3$, $K_2O$, $TiO_2$, Ga, Rb, Nb, Th, La, Ce and Nd which are lithophile and generally strong geogenic elements. The spatial pattern roughly resembles that of the superficial deposits most of these soils derive from - highest scores for component 2 are found over the Devensian till/diamicton formation (cf. Figure 8). To determine the component score distribution over each superficial deposit, a grouped box-plot has been produced - the relationship between component 2 scores and each superficial geology type is represented in Figure 47. As pointed out in the map of Figure 8, minimum, median and maximum scores are found over the referred formation (TILL-DMT). The box-and-whisker plots of Figure 110 (Appendix 2) show that samples collected over Devensian till are also individually enriched in these geogenic elements.

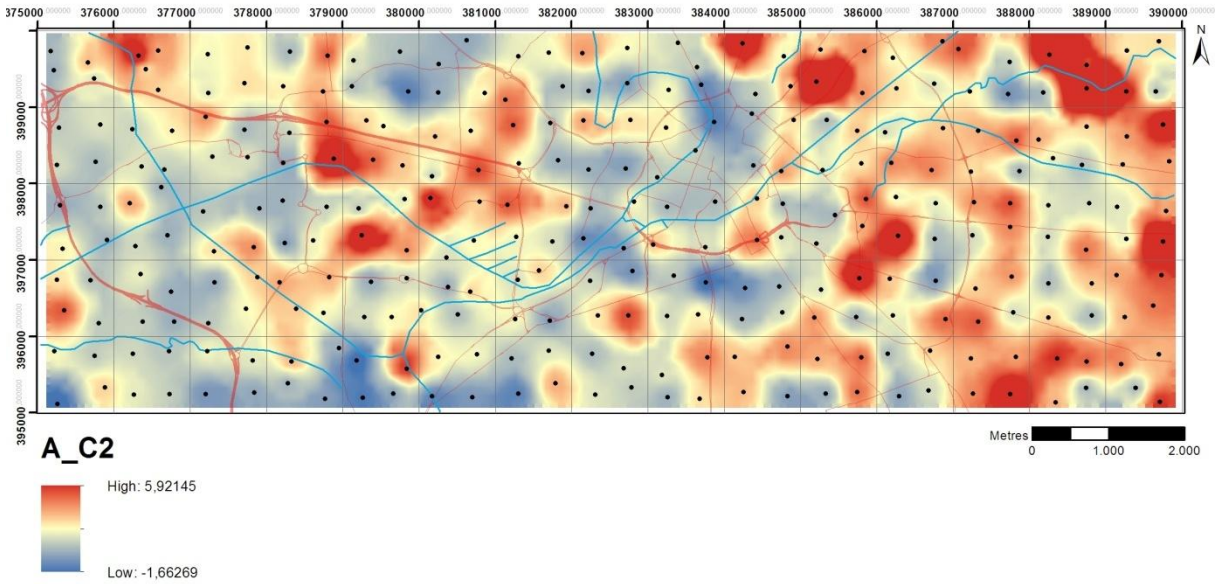


Figure 46: Spatial distribution of component 2 scores for BGS soil geochemical data (PCA #A, n=300, 47 variables) (cf. Table 26 for represented elements).

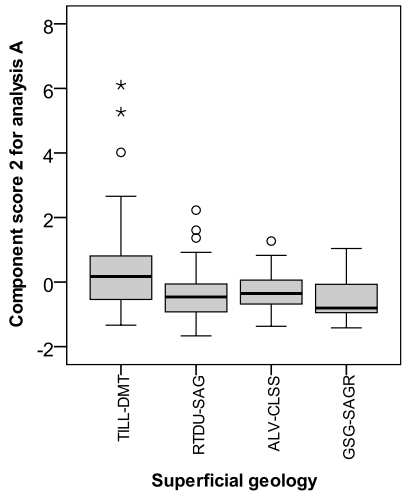


Figure 47: Box-and-whisker plot for component 2, grouped by superficial deposit type (PCA #A, n=300, 47 variables).

Component 3, which represents the common variation of Bi, Ag, $P_2O_5$, Pb and Tl, shows localised hotspots, as displayed in the component map of Figure 48. These are located mainly in the Clayton Vale - Phillips Park area and the Whalley Range - Urmston areas.

As previously noted, the elements represented by component 3 may be historically sourced from the smelting and refining of metallic ores; but also from more recent or present-day point sources: near these contaminated hotspots, namely in Old Trafford, Urmston, Cambrian St., several businesses related to car servicing, breaking and dismantling, or vehicle part traders can be found. The hotspot near Tenax Road is located in the heart of the Trafford Park Industrial Estate, where heavy traffic and industry are present. Also, the Whalley Range area displays the highest Pb concentration found and the absence of present-day or historical sources suggest that the reconversion of the area, namely house demolition and renovation works, may have contributed to the lead content of soils, such as contamination by leaded paint (cf. Figure 36 and section 3.6.3) -

fragments of what appears to be lead paint have been found in the SEM-EDS observation of a sample from this area.

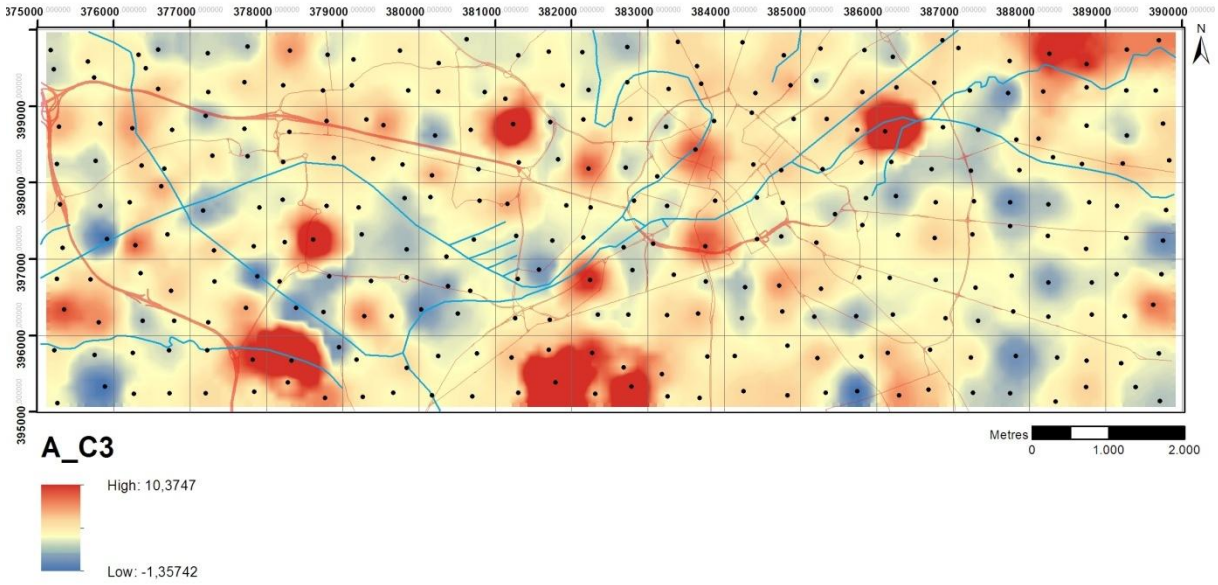


Figure 48: Spatial distribution of component 3 scores for BGS soil geochemical data (PCA #A, n=300, 47 variables) (cf. Table 26 for represented elements).

Component 4 scores (representing As, Cr and Cu) show a clustered spatial pattern around certain points, as observed in Figure 49. One of them is located in the vicinity of the Davyhulme Sewage Works and the Eccles Wastewater Treatment Works, where the highest concentrations for these three elements are found. Another hotspot is found in the grounds of Trafford Ecology Park, just opposite Churchill Point which is an industrial/commercial estate where mainly fragrance and beauty companies are based. At this location, Cr and Cu high concentrations are responsible for this high component 4 score. Another important hotspot is located in the Cambrian Street area, west of the Manchester City stadium, where the scrap metal yards and car breaking businesses are a likely source of metals to the nearby soils.

The maps for components 5 to 10 are represented in Figure 112 of Appendix 2. These components account for a small percentage of the system variance (~23% altogether), as observed in Table 81 of Appendix 2. From these, components 5, 6, 7, 8 and 9 show a dispersed spatial distribution of scores. Nevertheless, the highest scores for component 8 seem to convoy with main roads and junctions, although scattered to a certain extent - a confirmation that these elements might also have a vehicular source. Component 10 accounts mostly for the variation of Cd across the study area - an indication that the variation of this element's concentration is not linked to that of other elements. As described in section 3.5.2. (1), Cd concentrations peak in the Clayton Vale / Phillips Park area.

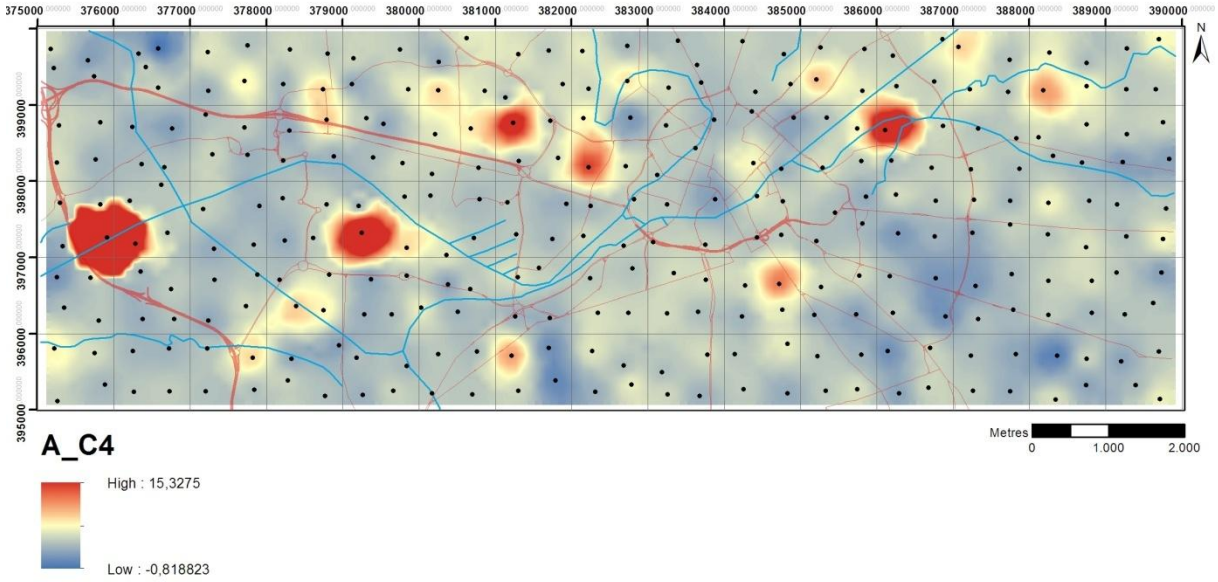


Figure 49: Spatial distribution of component 4 scores for BGS soil geochemical data (PCA #A, n=300, 47 variables) (cf. Table 26 for represented elements).

## *3.7.2. Analysis B*

The previous analysis used the Kaiser criterion (eigenvalue >1) to define how many components to retain in the analysis. Nevertheless, the work of many authors uses the scree plot inflexion point to define how many components should be retained, as components with eigenvalues below this point (even if larger than one) account for much less variance than the first components. Through the scree plot in Figure 43 it is observed that 3 components show eigenvalues above the inflexion point for the soil dataset - calculations were performed again using the same 47 variables to check if there were major differences in the interpretation of results and component score mapping.

As the dataset is the same, the KMO statistic, Bartlett's test and anti-image matrix are the same as for analysis A. Nevertheless, the total variance explained after rotation changes as a smaller number of components have been retained. This is represented in Table 83 of Appendix 2 - in this analysis, the 3 retained components explain 59% of the total variance, after orthogonal Varimax rotation.

Table 84 of Appendix 2 shows the rotated component matrix, where the loading of the chemical elements onto each component can be observed. The elements with highest loadings are summarised in Table 27 below, and represented in the component plots of Figure 50.

| | | Element loading | | |
|---|---|---|---|---|
| | | ]1.0, 0.7] | ]0.7 - 0.6] | ]0.6 - 0.5] |
| component | 1 | $Al_2O_3$, $K_2O$,$TiO_2$, Sc, Ga, Rb, Y, Nb, Th, U, La, Ce, Nd | V | $Fe_2O_3$, Zr |
| | 2 | $Fe_2O_3$, Co, Ni, Ge, Se, Mo, Sn, LOI | $P_2O_5$, V, Zn, Br, Tl, Pb, Ag, Sb | Sc, Y |
| | 3 | CaO | pH | Cr, Cu, As, Sr |

Table 27: Summary of element loadings onto each calculated component (1 to 3) for BGS soil samples (PCA #B, n=300, 47 variables).

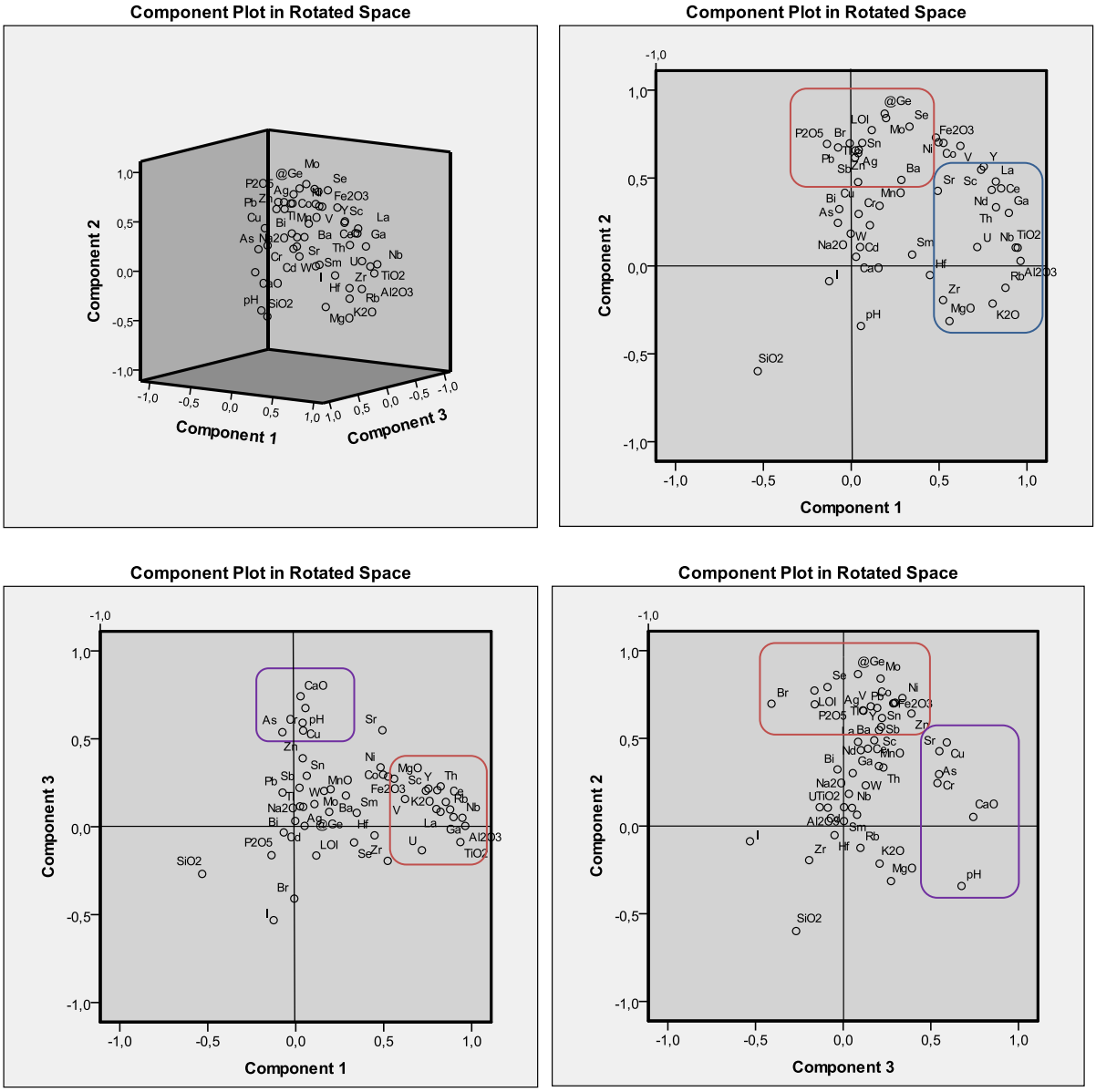


Figure 50: Component plots for components 1, 2 and 3 for BGS soil geochemical data: a) tridimensional plot, b) C1 vs. C2, c) C1 vs. C3 d) C3 vs. C2 (PCA #B, n=300, 47 variables).

Component 1 accounts for 26% of the total variance and shows high loadings for the geogenic elements $Al_2O_3$, $K_2O$, $TiO_2$, Sc, Ga, Rb, Y, Nb, Th, U, La, Ce and Nd (and moderate loadings for V, $Fe_2O_3$ and Zr). These were reported as component 2 in analysis A, plus Zr (component 7, analysis A) and $Fe_2O_3$ (component 1, analysis A) - although the highest loading for this element in the present analysis is onto component 2.

This second component accounts for 24.5% of the total variance and comprises a plethora of mostly anthropogenic elements: $Fe_2O_3$, Co, Ni, Ge, Se, Mo, Sn (and LOI) show the highest loadings, followed by $P_2O_5$, V, Zn, Br, Tl, Pb, Ag, Sb, Sc and Y. These were previously attributed (in analysis A) to components 1, 3, 6 and 8 - in this analysis they are clustered in this single component. This fact has implications on component interpretation, as the elemental sub-groups cannot be easily identified.

Variables with significant loadings onto component 3 are CaO, pH, Cr, Cu, As and Sr, accounting for 8,5% of the total variance. The relationship between CaO and pH is expected, as lower pH values promote Ca remobilisation from soils. Nevertheless, the association of Cr, Cu and As to this component may indicate a strong pH dependence - pH of the soil system is a very important parameter, directly influencing sorption/desorption, precipitation/dissolution, complex formation, and oxidation-reduction reactions. In general, maximum retention of cationic metals, such as Cr, Cu and As, occurs at pH>7 - trace metal hydroxide, oxide, carbonate, and phosphate precipitates form only under alkaline conditions (Lindsay, 2001). At low pH, metals are likely to be remobilised and their soil concentration tends to decrease.

Components 1-3 score maps are represented below from Figure 51 to Figure 53, respectively. The score distribution for component 1 is very similar to that of component 2 of analysis A (Figure 46), representing the score for geogenic elements.

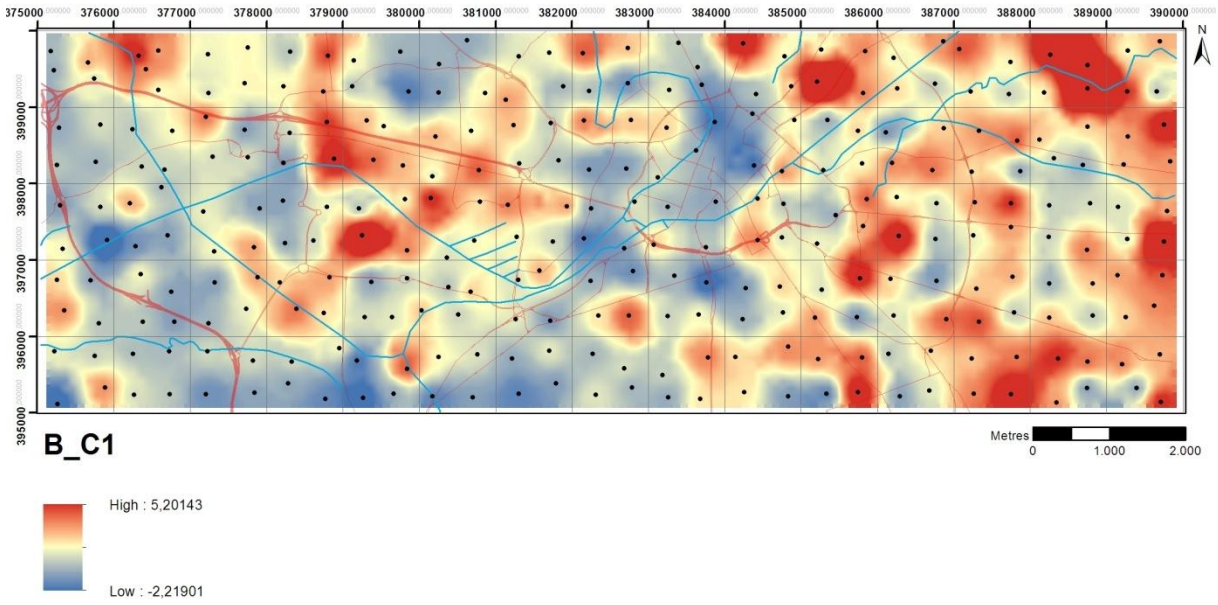


Figure 51: Spatial distribution of component 1 scores for BGS soil geochemical data (PCA #B, n=300, 47 variables) (cf. Table 27 for represented elements).

In this analysis, component 2 represents a series of anthropogenic elements which were previously represented by separate components. Therefore, by looking at Figure 52, the areas previously identified as problematic (section 3.5.2) are also highlighted by the high scores for this component - similarly to components 1 and 3 of analysis A.

It is noticeable that component 3 spatial pattern (Figure 53) shows higher scores (dark red) at locations where soils are neutral to alkaline - locations with soil pH above 7 generally correspond to higher Cr, Cu and As contents, as can be observed in the maps of Appendix 3 (Part A). From the component 3 score map below, it can be interpreted that Cr, Cu and As are likely to be bound as relatively immobile forms in soil where component 3 score is higher - nevertheless, these metals might be released if soil pH conditions change.

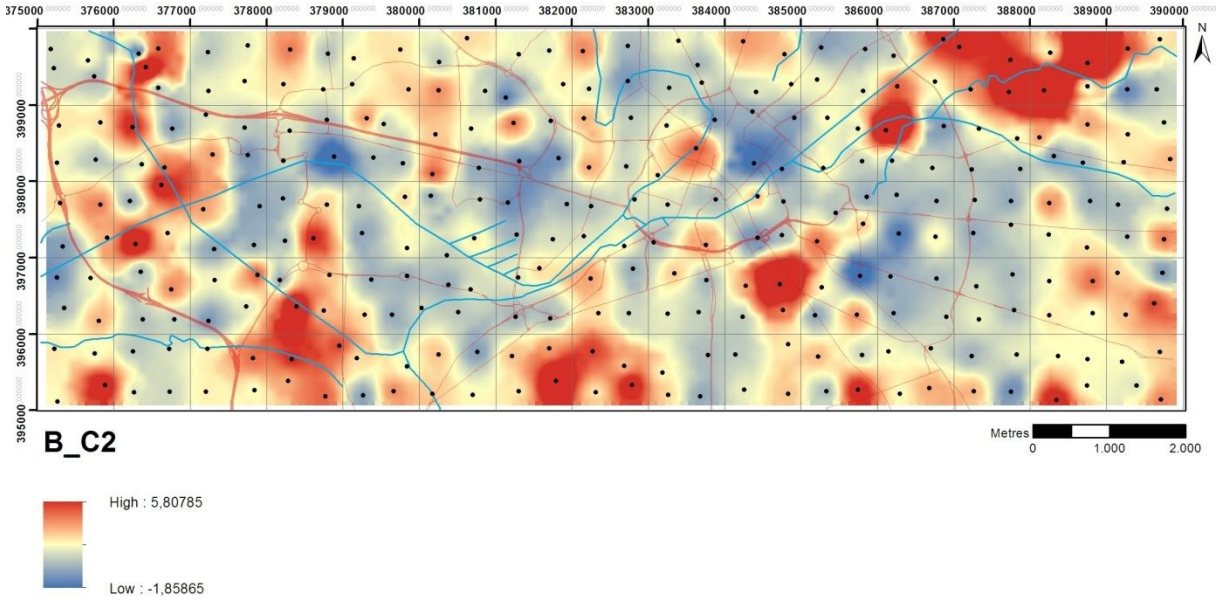


Figure 52: Spatial distribution of component 2 scores for BGS soil geochemical data (PCA #B, n=300, 47 variables) (cf. Table 27 for represented elements).

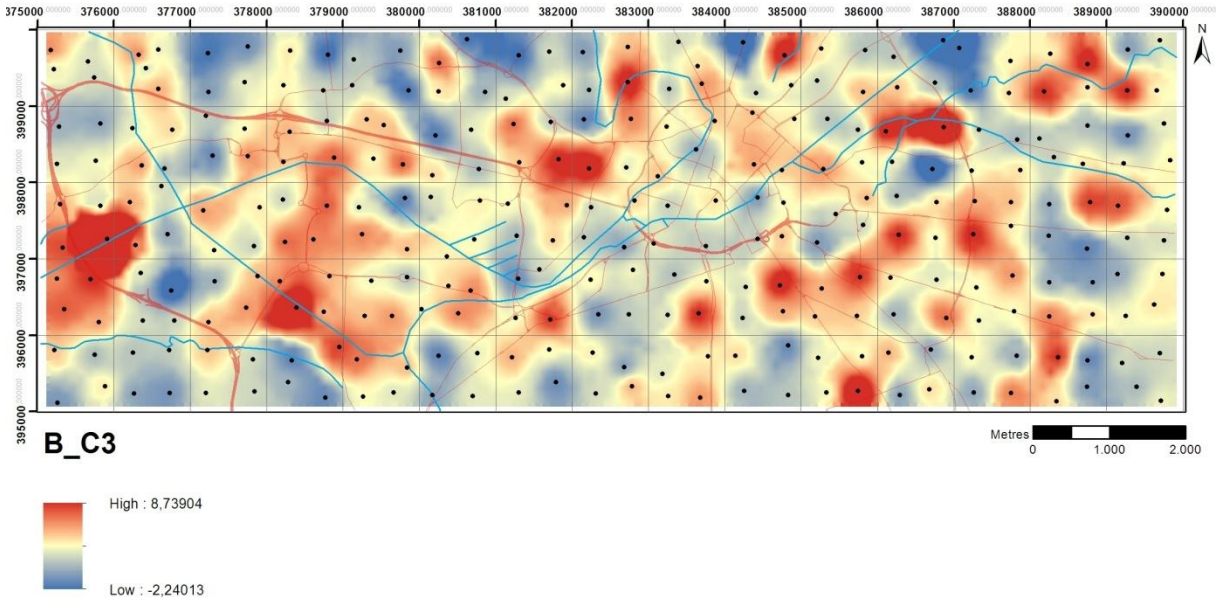


Figure 53: Spatial distribution of component 3 scores for BGS soil geochemical data (PCA #B, n=300, 47 variables) (cf. Table 27 for represented elements).

Enrichments in Cr, Cu and As also occur at other points where pH is lower than 7 (with the consequent increase in metal mobility), and these might pose a greater immediate risk to human health, such as the west end of Phillips park (Phillips park cemetery, samples 630207 and 630290, pH 4.4 and 5.7) and the recreational area and urban open space north of it (samples 630210 and 630278, pH 4.6 and 4.9); the Eccles WTP (630035, pH 4.8), and the soil sample collected near Williamson Building of the University of Manchester (630161, pH 5.3).

Comparing analysis A and B, conclusions regarding the co-occurrence of chemical elements in the soil are very similar - the main difference is that the three components of analysis B condense the information of the 10 components of analysis A. The first analysis favour the identification of areas

where the different groups of anthropogenic elements are enriched, with an easier identification of sources; whereas analysis B favours the grouping of a greater number of variables which, in fact, vary similarly and can be interpreted in a more generalised way.

### *3.7.3. Analysis C*

A third type of PCA analysis was run in order to enhance the correlation patterns between trace metals of environmental concern, discerning the effect of variable exclusion onto the calculated components and the respective factor score mapping. This was done by eliminating variables with non-significant loadings onto any of the previously calculated components (e.g. $Na_2O$, MnO, Bi, Cd) and those for which the sources and correlations found were of more direct interpretation (e.g. Br, LOI, CaO, Sr, Rb, Zr, REEs). From analysis A and B, 17 variables were selected ($Al_2O_3$, $P_2O_5$, $TiO_2$, $Fe_2O_3$, Cr, Co, Ba, Ni, Cu, Zn, Ga, As, Mo, Pb, Ag, Sn and Sb).

KMO and Bartlett's sphericity tests revealed that this reduced, 17-variable soil dataset is suitable for PCA analysis with a KMO value of 0.835, as displayed in Table 28. Bartlett's test is also highly significant, as the Sig. value is less than 0.001.

| KMO and Bartlett's Test | | |
|---|---|---|
| Kaiser-Meyer-Olkin Measure of Sampling Adequacy | | ,836 |
| Bartlett's Test of Sphericity | Approx. Chi-Square | 5591,019 |
| | df | 136 |
| | Sig. | ,000 |

Table 28: Results for the KMO and Bartlett's tests for BGS soil geochemical data (#C, n=300, 17 variables).

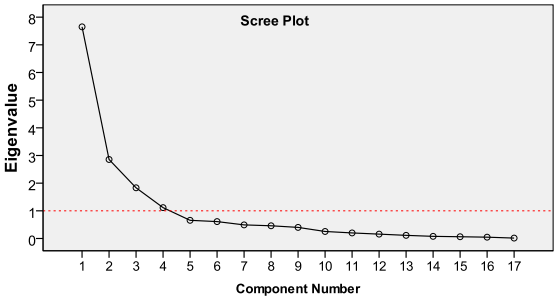


Figure 54: Scree plot - Components vs. eigenvalues for BGS soil geochemical data (PCA #C, n=300, 17 variables).

Concerning component extraction, both the Kaiser criterion (eigenvalue >1) and the scree plot inflexion point criterion are valid, as in Figure 54.

All the elements in the anti-image correlation matrix show diagonal values above 0.58 (Table 85, Appendix 2), which again supports the adequacy of this dataset for PCA variable reduction. As a result of the smaller number of variables in this analysis, communalities are close to 1 for all variables (>0.9) except for Ba and Sb (0.510 and 0.496, respectively, Table 86, Appendix 2). Therefore, the variance for the remaining 15 elements consists mainly of common or shared variance.

Eigenvalues associated with each component are presented in Table 88 (Appendix 2). The first 4 components show eigenvalues greater than 1 and were retained for extraction, explaining 79.14% of the total variance of the dataset. Eigenvalues are also presented in the scree plot of Figure 54 above.

Element loadings onto each calculated component are summarised in Table 29, and presented in more detail in Table 87 (Appendix 2). Loadings can also be graphically visualised in Figure 55.

| | Element loading | | |
|---|---|---|---|
| | ]1.0, 0.7] | ]0.7 - 0.6] | ]0.6 - 0.5] |
| 1 | $Fe_2O_3$, Co, Ni, Mo, Sn | Sb | Zn |
| 2 | $Al_2O_3$, $TiO_2$, Ga | - | - |
| 3 | $P_2O_5$, Pb, Ag | Ba | - |
| 4 | Cr, Cu, As | - | - |

Table 29: Summary of element loadings onto each calculated component (1 to 4) for BGS soil samples (PCA #C, n=300, 17 variables).

The 4 components of this analysis are consistent with the findings of Analysis A (cf. Table 26) - elements in Analysis C which load onto each component (1-4) also do so in Analysis A (1-4), which reinforces the assumption that their occurrence in soils is related to the same sources or processes. Additionally, in Analysis C these components account for a larger percentage of variance, as the number of variables in the system was reduced.

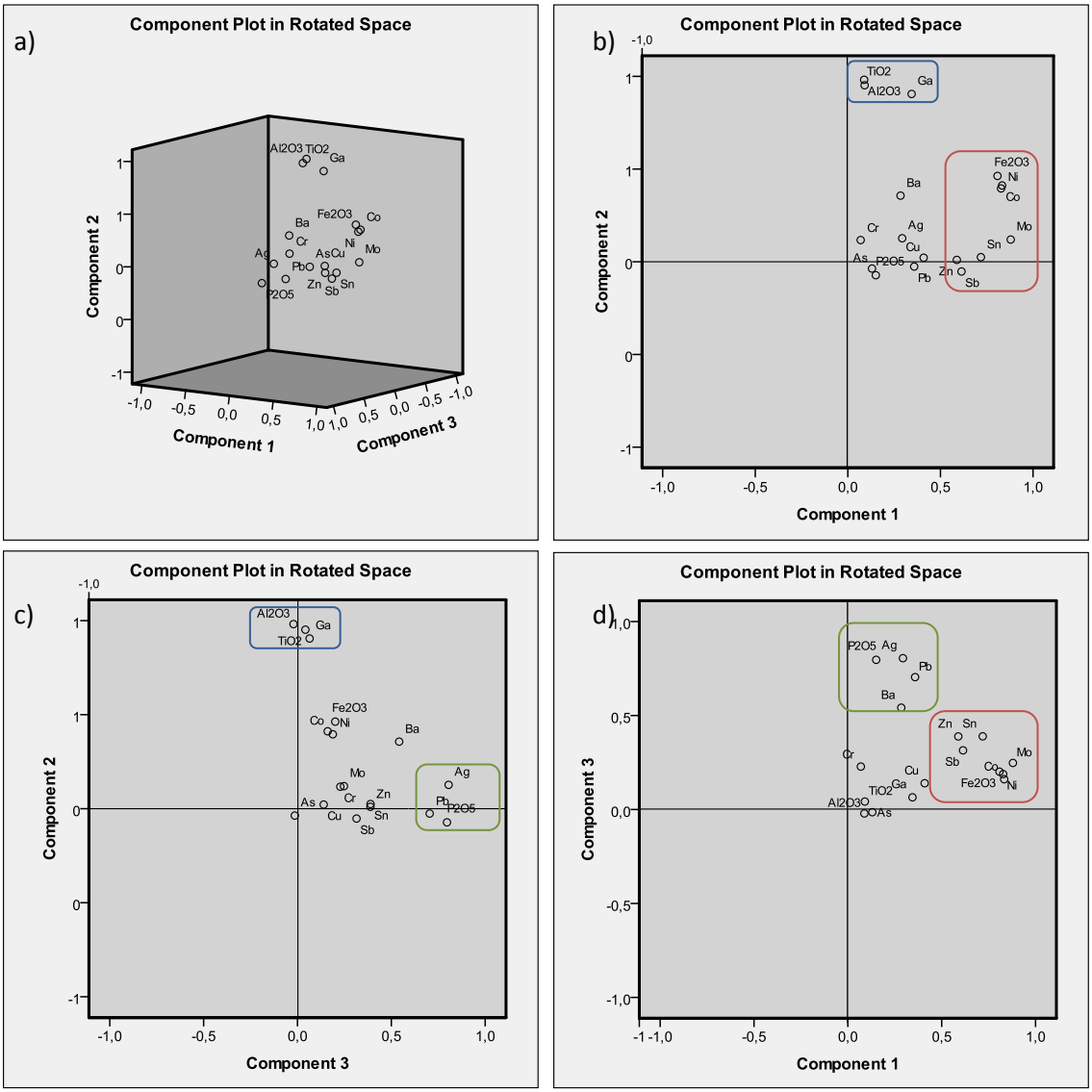


Figure 55: Component plots for components 1, 2 and 3 for BGS soil geochemical data: a) tridimensional plot, b) C1 vs. C2, c) C1 vs. C3 d) C3 vs. C2 (PCA #C, n=300, 17 variables).

The main difference resides in the component score maps of Figure 56 to Figure 59. Component scores were interpolated by the IDW method (cf. section 2.9.5 and the Theoretical Framework), using

the same parameters as for the previous analyses. The reduction in the number of variables enhances hotspot identification (cf. Figure 45 to Figure 49), as areas of high/low scores are more evident as a result of the smaller extent of intermediate score values, hence allowing an easier identification of problematic samples.

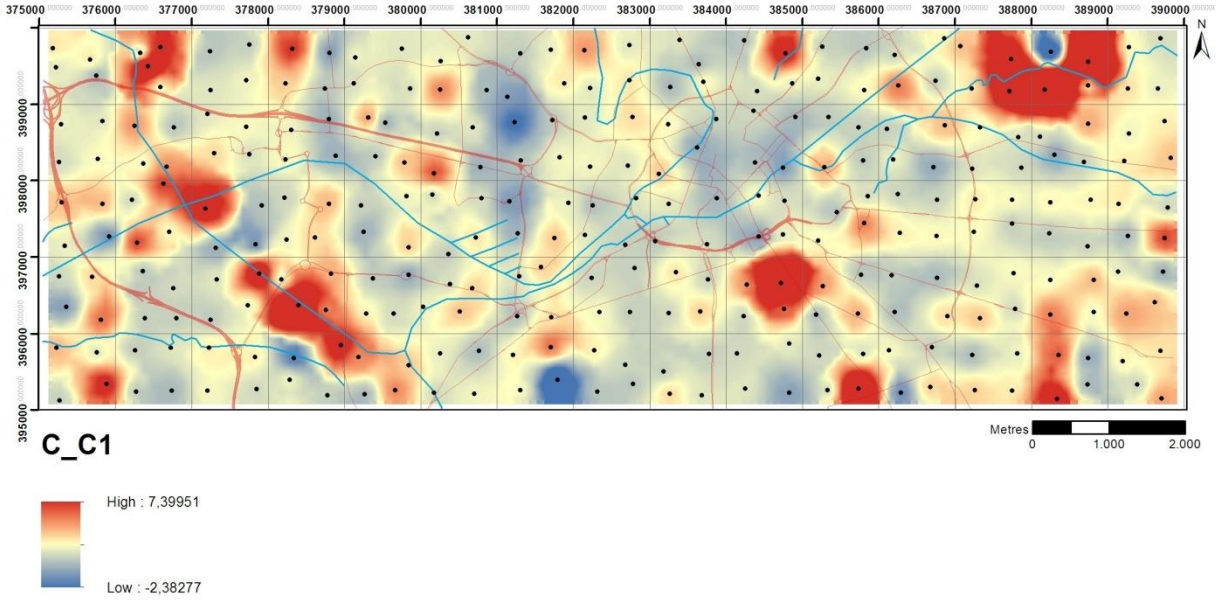


Figure 56: Spatial distribution of component 1 scores for BGS soil geochemical data (PCA #C, n=300, 17 variables) (cf. Table 29 for represented elements).

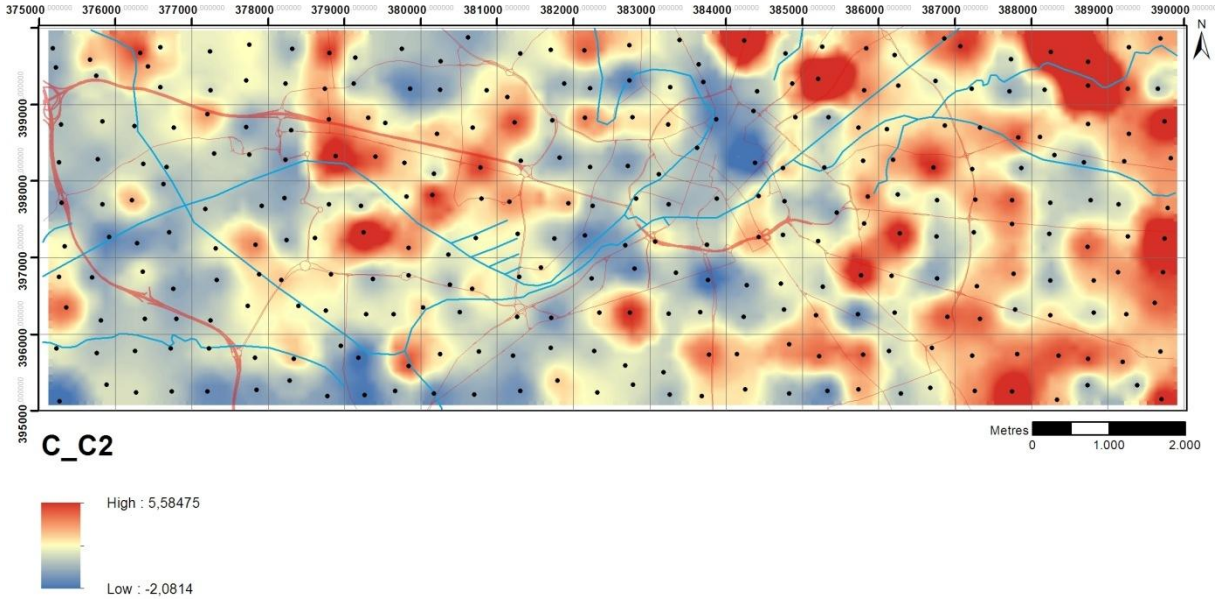


Figure 57: Spatial distribution of component 2 scores for BGS soil geochemical data (PCA #C, n=300, 17 variables) (cf. Table 29 for represented elements).

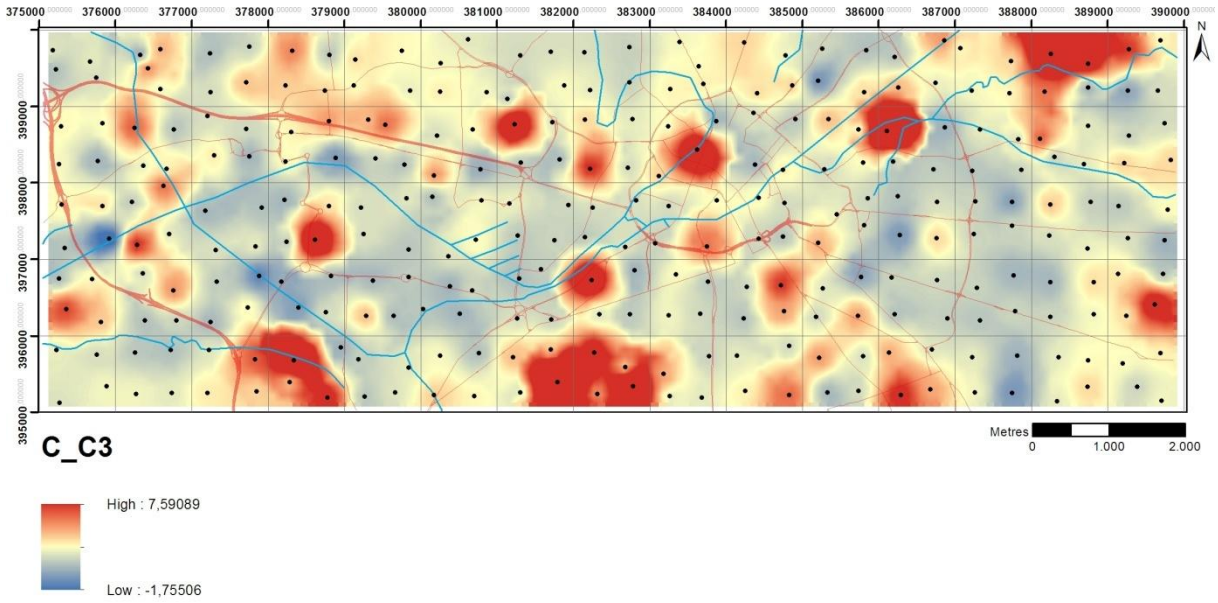


Figure 58: Spatial distribution of component 3 scores for BGS soil geochemical data (PCA #C, n=300, 17 variables) (cf. Table 29 for represented elements).

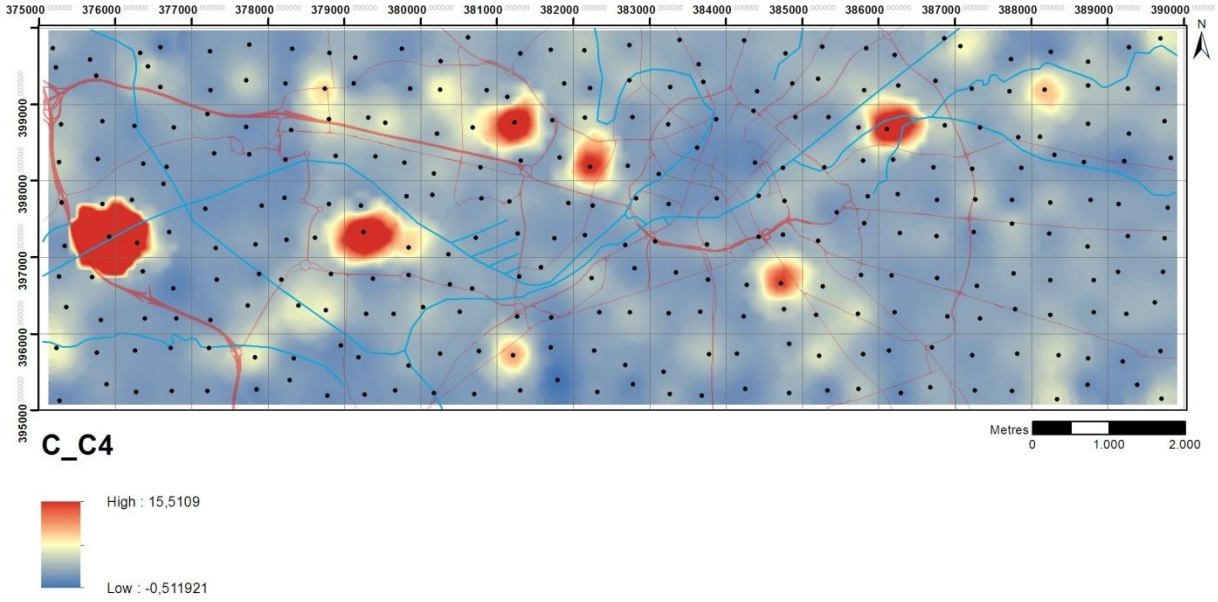


Figure 59: Spatial distribution of component 4 scores for BGS soil geochemical data (PCA #C, n=300, 17 variables) (cf. Table 29 for represented elements).

## 3.8. Main conclusions about Manchester's soil geochemistry

• Manchester topsoils are mainly enriched in Cu, Zn, Pb and Cd, when compared to other UK urban soils and the median values for England and Wales - it can be assumed that Cu, Zn, Pb and Cd contents in Manchester soils are mostly anthropogenically-derived. Manchester soils often display elevated trace metal concentrations which are above the recommended levels, especially for Cr, Cu (ecological guideline), Zn, As, Cd and Pb.

• Mapping of geochemical concentrations defined six main areas where PHE concentrations are systematically above the 75$^{th}$ percentile: the Clayton Vale / Phillips Park area, the Cambrian Street area, the Oxford Road / Wilmslow Road alignment, the Old Trafford residential area, the Trafford Park industrial estate, the surroundings of the Davyhulme and Eccles Wastewater Treatment Works, the residential area south of Worsley Golf Club, and the area between A6 and A57/M602 in Salford. These are areas which are diverse in terms of land uses and chemical element association types - a clear example of the variety of present-day and historical factors which can influence soil composition at the local scale. Present-day sources have a large influence on soils near the Oxford Rd. / Wilmslow road alignment, in the Trafford Park Industrial Estate, and in the Cambrian St. area - at these locations, PHE are likely sourced from heavy traffic, together with diverse industrial activities especially in Trafford Park and around Cambrian St. . Historical contamination, as found in Clayton Vale, Salford and Old Trafford, are likely derived from past industry; whereas in the Worsley area it may be attributed mainly to past mining operations. The water treatment plants of Davyhulme and Eccles may not be actively contributing to soil contamination nowadays, but nearby soils point that these infrastructures might have been important sources of As, Cr and Cu.

• Scanning electron microscope microbeam analysis of soil samples revealed that these are mainly composed, as expected, by silicate and alumino-silicate grains. Fragments of rock, tarmac, brick and other construction materials are also present, as well as iron oxide grains and spherical Fe-rich grains derived from high temperature combustion processes, which may contain varying amounts of PHE. Additionally, Pb, Ba, Zn, Cr and Sn -rich grains are also found, which are of great importance in terms of source apportionment.

• Principal component analysis revealed groups of geochemical variables which show similar variation patterns in Manchester's soils, and their mapping allowed for a more objective interpretation in terms of source apportionment:

- Lithophile and geogenic elements in Manchester soils, i.e. elements related to the natural, geologically-derived components of soil revealed by PCA, include $Al_2O_3$, $K_2O$, MgO, $TiO_2$, Ga, Rb, Nb, Th, U, V, and REEs (Sc, Y La, Ce and Nd). Component score mapping and its comparison to the superficial deposits mapping reveals that the highest concentrations of the referred elements are likely related to the Devensian till-diamicton formation.
- Historical, coal-related contamination highlighted by PCA is mainly represented by $Fe_2O_3$, V, Co, Ni, Ge, Mo, Sn and Zn concentrations - REEs may also show some degree of anthropogenic accumulation in Manchester's soils, as they also load onto this same component. The most affected areas by elevated levels of these elements, pointed out by component score mapping, are located in the Clayton Vale / Phillips Park area, along the Bridgewater Canal, and in the Oxford Road / Wilmslow Road alignment. Clayton Vale was a

heavily industrialised area in the 18th-19th centuries, which included collieries and chemical works, among many other industries - additionally, prior to its redevelopment into a park, the site has been used as a municipal waste tip and a tip for power station ash cinders. The area around the Bridgewater canal is likely affected by the transportation of coal from the mines in Worsley, which was the main purpose of the canal in the 18th and 19th centuries; and by the industries which subsequently were established on its margins due to the easier access for raw materials and goods transport.

- Lead, Pb, Bi, Ag and $P_2O_5$ are likely related to both present day sources, such as the proximity to heavy traffic, vehicle-related businesses and industry; and historical sources, such as lead from pre-2000 gasoline, leaded paint, from coal burning or Pb smelting processes. The mapping of the component score which represents this suite of elements reveals hotspot areas located in the Clayton Vale area, Whalley Range, Urmston, Cambrian St. area and Trafford Park. Whereas in the first three areas these elements seem to be of past origin, the last two clearly reveal the input of present-day industrial activities and traffic.
- Arsenic, Cu and Cr are also related in Manchester's soils and are likely sourced, in the west part of the study area, by the WTPs of Davyhulme and Eccles. Two other important hotspots are located in Trafford Ecology Park and in the Cambrian St. area, where localised inputs may be responsible for the higher levels of these three elements.
- Zn (and Mn) are also clustered in a single component, and highest scores tend to follow the trace of Manchester's busiest roads (M60 and M602, Oxford/Wilmslow road, east part of Mancunian Way, Ashton Old Road). This is a strong indication that vehicles and traffic are a likely source for these elements, as they have long been reported to be sourced from the wear and tear of car bodies, brake linings and tyres. Nevertheless, Zn total concentrations are also high in the Clayton Vale and Worsley areas, where its origin is more likely related to historical mining and industrial activities as previously described.
- Although the Zr and Hf association in soils can be linked to their coexistence in natural zircon, the presence of high Na levels at the same locations revealed by PCA points to an anthropogenic enrichment of these elements, as Na is used in the process of transforming zircon materials into zirconium oxide which is used in numerous applications. One of them is in brick, tile and ceramic manufacturing - a likely source of this association of Zr, Hf and Na in Manchester's soils, which often contain fragments of these materials.

• The use of different parameters in PCA analysis showed that by retaining a greater number of components, there is an easier identification of unapparent element associations which, although accounting for smaller amounts of the total system variance, may as well be interpreted successfully.

Adding to this, mapping has proven very useful for contaminant source targeting, beyond the use of single element spatial distributions. The use of fewer variables, by excluding those of easier interpretation, sharpened the distinction between high and low concentrations in component score mapping; nevertheless, in this case, conclusions were similar regarding the element associations calculated and component scores spatial distribution.

# 4. Urban Sediment Geochemistry

## Summary

Road-deposited sediments (RDS) have been collected over 75km$^2$ of Manchester, Salford and Trafford (UK) in summer and winter, to account for seasonal differences in sediment texture and composition. The 144 RDS samples (72 summer + 72 winter) were chemically analysed by XRF for a total of 55 elements. Grain size distributions and organic matter contents have also been determined for all samples; trace element speciation and SEM-EDS analysis have been performed on smaller sets of samples. All data have been mapped and analysed using basic statistics, correlation analysis, and principal component analysis

This chapter presents and analyses the RDS characteristics in terms of trace element geochemistry, grain size distributions, grain types and trace element speciation - problematic areas are exposed, as well as potential sources of trace elements in RDS.

## 4.1. Exploratory data analysis

### *4.1.1. Preliminary statistics and characterization of variable distributions*

Road-deposited sediments were analysed for a total of 55 elements at the BGS XRF facilities, following the procedure described in section 2.4., which was the same as for soils. The 144 RDS samples were analysed at two different times corresponding to summer and winter samples. A few elements showed concentrations below the lower limits of detection (LLD), which can be observed in Table 5 (section 2.4). Elements with over 70% of samples below the LLD were not considered in further statistical calculations (Cs, Ta, Te, Tl, Ag, Hg, Pd and In). For these, concentrations above the LLD are only considered when interpreting geochemical data at the sample scale.

After data conditioning and levelling, as described in section 2.9.1, RDS geochemical data for 46 elements and organic matter content (LOI) have been subject to exploratory statistics. Maximum, minimum, mean, median, standard deviation, variance, skewness and kurtosis of the data distributions were calculated and are summarised in Table 31 and Table 32.

The presence of strong outliers is common for most of the chemical elements and can be evidenced by the maximum values, which can be several times higher than the median values. This is observed in both seasons for Pb, Bi, Cd and Sb. Table 30 summarises all the elements with maximum concentrations over five times the median concentration for each element. The presence of outliers and its influence in element distributions will be further discussed in this text.

| | RDS summer | RDS winter |
|---|---|---|
| 5*median < max < 10*median | Cr, Cu, Zr, Pb, Cd, Sb, LOI | MgO, Br, Mo, Sb |
| max > 10*median | W, Bi | Pb, Bi, Cd, Cl |

Table 30: Elements with maximum values greater than 5 times the median value for RDS summer and winter.

The majority of the elemental distributions are positively skewed - only $SiO_2$ shows slightly negative skewness values (-1 and -0.7 in summer and winter, respectively). Most distributions are also leptokurtic (kurtosis > 0), as the peaks are more acute around the mean. There are also a few elements for which the distribution is close to a mesokurtic distribution (kurtosis of approx. 0) or slightly platykurtic (negative kurtosis value), as is the case for MgO, Ge, As, Se, Rb, I Sm and S in summer and $SiO_2$, MnO, V, Sm and S in winter. These observations are also shown in the histograms of Figure 113 and Figure 114 of Appendix 4.

Table 89 and Table 90 of Appendix 4 show the Kolmogorov-Smirnov tests for RDS summer and winter data, respectively. This test shows that the distributions of a few elements are close to a normal distribution at the 95% confidence level; namely $Fe_2O_3$, MnO and Rb in both seasons, as the K-S test is not significant ($p>0.05$). MgO, $K_2O$, Ga, Ge and Nd are close to a normal distribution only for summer data, whereas Sc, Cr, U, Ce and Hf distributions only show this property for winter data.

When log-transforming the data, 28 and 32 variables from the summer and winter datasets, respectively, are brought towards normality; whereas the Box-Cox transformation is even more effective for this purpose: 36 and 38 variables are close to normality after transformation, out of the initial 47 variables. The Kolmogorov-Smirnov tables for log- and Box-Cox-transformed datasets can be observed from Table 91 to Table 94 of Appendix 4. Nevertheless, the distributions of 9 variables in the summer dataset ($Na_2O$, Sc, Cr, Se, Hf, U, Cd, I and La) and 7 in the winter dataset (MnO, Ge, Se, Bi, U, Cd, OM) could not be brought to normality using any of the data transformation procedures - further statistics which requires data to be normally distributed need to be carefully interpreted for these elements.

Another way of visualising Manchester RDS data is through the box-and-whisker plots of Figure 115 and Figure 116 of Appendix 4. The lower edge of the box represents the 1$^{st}$ quartile (Q1) and the upper edge the 3$^{rd}$ (Q3) quartile. The difference between these values is the interquartile range (IQR). Samples represented as circles are considered outliers, and are labelled with the RDS sample number. These are values between 1.5 and 3 times the IQR, measured from the ends of the box. Extreme outliers are those with a value more than 3 times the IQR, measured in the same way, and are represented by an asterisk. The positive skewness of most variables can also be inferred from these plots, as most of them show a longer upper whisker and/or upper outliers.

| Variable | Units | Minimum | Maximum | Mean | Median | Std. dev. | Variance | Skewness | Kurtosis |
|---|---|---|---|---|---|---|---|---|---|
| Na2O | wt. % | 0,3 | 3,6 | 0,9 | 0,8 | 0,4 | 0,2 | 3,7 | 21,6 |
| MgO | wt. % | 0,8 | 3,6 | 1,8 | 1,7 | 0,6 | 0,4 | 0,7 | 0,3 |
| Al2O3 | wt. % | 2,7 | 10,9 | 5,5 | 5,2 | 1,5 | 2,4 | 1,0 | 1,7 |
| SiO2 | wt. % | 23,5 | 78,8 | 58,5 | 61,3 | 10,6 | 112,9 | -1,0 | 1,3 |
| P2O5 | wt. % | 0,07 | 0,45 | 0,15 | 0,13 | 0,08 | 0,01 | 1,73 | 2,93 |
| K2O | wt. % | 0,82 | 1,86 | 1,19 | 1,18 | 0,21 | 0,04 | 0,65 | 0,76 |
| CaO | wt. % | 2,6 | 19,8 | 7,7 | 7,3 | 3,2 | 10,5 | 1,7 | 4,1 |
| TiO2 | wt. % | 0,19 | 0,77 | 0,35 | 0,32 | 0,12 | 0,01 | 1,52 | 2,48 |
| MnO | wt. % | 0,033 | 0,145 | 0,066 | 0,062 | 0,020 | 0,000 | 1,232 | 2,453 |
| Fe2O3 | wt. % | 1,94 | 6,15 | 3,38 | 3,32 | 0,87 | 0,76 | 0,67 | 0,61 |
| Sc | mg/kg | 2 | 14 | 6 | 6 | 2 | 6 | 0,4 | 0,9 |
| V | mg/kg | 32 | 110 | 55 | 50 | 17 | 292 | 1,3 | 1,6 |
| Cr | mg/kg | 40 | 544 | 108 | 97 | 67 | 4502 | 4,3 | 25,5 |
| Co | mg/kg | 5,3 | 18,0 | 9,1 | 8,4 | 2,9 | 8,5 | 1,2 | 1,5 |
| Ba | mg/kg | 194 | 1010 | 359 | 345 | 105 | 11063 | 3,7 | 20,5 |
| Ni | mg/kg | 18,4 | 82,4 | 31,2 | 28,5 | 11,9 | 140,7 | 2,1 | 5,2 |
| Cu | mg/kg | 36,4 | 493,2 | 94,4 | 84,3 | 56,9 | 3233,0 | 5,0 | 34,2 |
| Zn | mg/kg | 66,2 | 1325,6 | 325,9 | 301,9 | 174,8 | 30545,3 | 2,9 | 14,4 |
| Ga | mg/kg | 3,40 | 11,10 | 6,28 | 6,00 | 1,69 | 2,85 | 0,81 | 0,39 |
| Ge | mg/kg | 0,3 | 2,0 | 1,0 | 1,0 | 0,4 | 0,1 | 0,2 | -0,1 |
| As | mg/kg | 2,9 | 10,7 | 5,7 | 5,3 | 1,6 | 2,7 | 0,7 | 0,2 |
| Se | mg/kg | 0,1 | 0,5 | 0,2 | 0,2 | 0,1 | 0,0 | 0,6 | -0,2 |
| Br | mg/kg | 0,4 | 17,4 | 4,7 | 3,9 | 3,6 | 13,2 | 1,6 | 2,4 |
| Rb | mg/kg | 24 | 57 | 38 | 38 | 7 | 46 | 0,6 | 0,4 |
| Sr | mg/kg | 63 | 456 | 135 | 129 | 47 | 2211 | 4,6 | 30,5 |
| Y | mg/kg | 8 | 22 | 13 | 13 | 3 | 10 | 1,2 | 1,4 |
| Zr | mg/kg | 74 | 699 | 152 | 131 | 83 | 6873 | 4,5 | 26,7 |
| Nb | mg/kg | 3 | 11 | 5 | 5 | 1 | 2 | 1,3 | 3,0 |
| Mo | mg/kg | 1,7 | 15,4 | 5,2 | 4,7 | 2,7 | 7,1 | 1,9 | 4,7 |
| Hf | mg/kg | 2 | 18 | 4 | 4 | 2 | 5 | 4,5 | 27,5 |
| W | mg/kg | 0,6 | 26,5 | 2,4 | 1,9 | 3,1 | 9,3 | 7,2 | 56,8 |
| Pb | mg/kg | 35,00 | 1184,0 | 159,1 | 142,0 | 141,7 | 20065,1 | 5,5 | 39,0 |
| Bi | mg/kg | 0,2 | 27,3 | 1,2 | 0,6 | 3,2 | 10,6 | 7,6 | 60,9 |
| Th | mg/kg | 1,80 | 10,4 | 3,8 | 3,6 | 1,3 | 1,6 | 2,3 | 9,6 |
| U | mg/kg | 0,3 | 4,3 | 1,5 | 1,5 | 0,5 | 0,3 | 2,3 | 10,2 |
| Cd | mg/kg | 0,25 | 2,6 | 0,5 | 0,5 | 0,4 | 0,2 | 2,7 | 10,3 |
| Sn | mg/kg | 5,10 | 49,3 | 12,8 | 11,2 | 6,5 | 41,7 | 2,9 | 13,6 |
| Sb | mg/kg | 1,40 | 49,7 | 8,1 | 7,0 | 6,4 | 40,5 | 4,2 | 25,5 |
| I | mg/kg | 0,3 | 2,9 | 1,0 | 0,8 | 0,7 | 0,5 | 1,0 | 0,2 |
| La | mg/kg | 5,0 | 29,0 | 13,9 | 13,0 | 3,9 | 15,2 | 1,5 | 3,8 |
| Ce | mg/kg | 11,0 | 54,0 | 26,7 | 26,0 | 8,0 | 63,3 | 1,1 | 2,4 |
| Nd | mg/kg | 8 | 28 | 15 | 14 | 4 | 15 | 1,0 | 1,5 |
| Sm | mg/kg | 0 | 5 | 2 | 2 | 1 | 2 | 0,2 | -1,0 |
| S | mg/kg | 824,0 | 3251,0 | 1667,0 | 1559,0 | 504,4 | 254419,9 | 1,1 | 1,0 |
| Cl | mg/kg | 74 | 385 | 169 | 160 | 62 | 3894 | 1,2 | 2,1 |
| Yb | mg/kg | 0,8 | 2,9 | 1,2 | 0,8 | 0,6 | 0,4 | 1,1 | -0,1 |
| OM (LOI) | wt% | 2,18 | 40,75 | 8,61 | 6,31 | 7,06 | 49,86 | 2,5 | 7,3 |

Table 31: Summary statistics for Manchester RDS - Summer.

| Variable | Units | Minimum | Maximum | Mean | Median | Std. dev. | Variance | Skewness | Kurtosis |
|---|---|---|---|---|---|---|---|---|---|
| Na2O | wt. % | 0,2 | 3,9 | 0,9 | 0,8 | 0,5 | 0,3 | 3,2 | 16,0 |
| MgO | wt. % | 0,6 | 8,7 | 1,9 | 1,7 | 1,1 | 1,2 | 3,6 | 19,8 |
| Al2O3 | wt. % | 2,2 | 10,3 | 5,8 | 5,6 | 1,5 | 2,2 | 0,6 | 1,0 |
| SiO2 | wt. % | 24,4 | 79,3 | 58,1 | 62,0 | 13,7 | 188,5 | -0,7 | -0,5 |
| P2O5 | wt. % | 0,07 | 0,59 | 0,19 | 0,16 | 0,11 | 0,01 | 1,45 | 2,15 |
| K2O | wt. % | 0,56 | 2,03 | 1,14 | 1,12 | 0,22 | 0,05 | 1,05 | 3,63 |
| CaO | wt. % | 2,0 | 27,3 | 7,3 | 6,8 | 4,0 | 15,7 | 2,1 | 8,1 |
| TiO2 | wt. % | 0,14 | 0,76 | 0,36 | 0,33 | 0,12 | 0,01 | 1,20 | 1,94 |
| MnO | wt. % | 0,029 | 0,118 | 0,067 | 0,065 | 0,019 | 0,000 | 0,234 | -0,619 |
| Fe2O3 | wt. % | 1,28 | 6,96 | 3,69 | 3,58 | 1,11 | 1,23 | 0,44 | 0,35 |
| Sc | mg/kg | 2 | 14 | 7 | 7 | 2 | 5 | 0,3 | 0,8 |
| V | mg/kg | 23 | 111 | 56 | 52 | 19 | 370 | 0,7 | -0,1 |
| Cr | mg/kg | 25 | 267 | 94 | 89 | 42 | 1725 | 1,4 | 3,6 |
| Co | mg/kg | 4,3 | 22,7 | 10,3 | 9,4 | 3,6 | 13,0 | 0,9 | 0,9 |
| Ba | mg/kg | 191 | 986 | 359 | 335 | 116 | 13487 | 2,9 | 12,6 |
| Ni | mg/kg | 14,0 | 77,1 | 33,7 | 31,0 | 12,9 | 166,7 | 1,2 | 1,9 |
| Cu | mg/kg | 19,4 | 433,4 | 126,1 | 128,8 | 68,0 | 4628,6 | 1,4 | 4,5 |
| Zn | mg/kg | 100,9 | 1312,3 | 413,9 | 366,3 | 224,9 | 50581,7 | 1,5 | 3,0 |
| Ga | mg/kg | 2,10 | 11,90 | 6,43 | 6,10 | 1,97 | 3,89 | 0,63 | 0,33 |
| Ge | mg/kg | 0,8 | 5,9 | 1,8 | 1,6 | 0,9 | 0,8 | 1,7 | 5,1 |
| As | mg/kg | 2,4 | 25,0 | 6,6 | 5,9 | 3,6 | 12,7 | 3,0 | 12,5 |
| Se | mg/kg | 0,1 | 0,9 | 0,3 | 0,2 | 0,2 | 0,0 | 1,4 | 1,4 |
| Br | mg/kg | 1,2 | 41,9 | 9,3 | 6,3 | 7,3 | 53,8 | 1,6 | 4,1 |
| Rb | mg/kg | 20 | 62 | 38 | 38 | 8 | 57 | 0,6 | 1,0 |
| Sr | mg/kg | 76 | 470 | 133 | 122 | 56 | 3090 | 4,0 | 21,3 |
| Y | mg/kg | 8 | 23 | 13 | 13 | 3 | 12 | 0,7 | 0,0 |
| Zr | mg/kg | 54 | 301 | 138 | 134 | 40 | 1625 | 1,3 | 3,5 |
| Nb | mg/kg | 3 | 10 | 5 | 5 | 2 | 2 | 0,8 | 1,0 |
| Mo | mg/kg | 1,4 | 39,1 | 6,2 | 5,2 | 5,2 | 26,7 | 4,1 | 23,0 |
| Hf | mg/kg | 1 | 8 | 4 | 4 | 1 | 2 | 0,3 | 0,8 |
| W | mg/kg | 1,3 | 2,4 | 1,7 | 1,7 | 0,2 | 0,0 | 1,1 | 1,9 |
| Pb | mg/kg | 28,70 | 2026,9 | 196,5 | 153,5 | 241,2 | 58154,9 | 6,4 | 47,9 |
| Bi | mg/kg | 0,2 | 69,3 | 2,1 | 0,5 | 8,5 | 71,9 | 7,4 | 57,6 |
| Th | mg/kg | 2,20 | 9,5 | 4,4 | 4,3 | 1,2 | 1,4 | 1,3 | 4,0 |
| U | mg/kg | 0,3 | 3,6 | 1,4 | 1,4 | 0,5 | 0,3 | 0,9 | 5,0 |
| Cd | mg/kg | 0,25 | 6,4 | 0,7 | 0,6 | 0,8 | 0,7 | 5,1 | 32,7 |
| Sn | mg/kg | 2,19 | 42,7 | 15,7 | 14,5 | 8,6 | 74,3 | 1,0 | 0,9 |
| Sb | mg/kg | 1,40 | 54,3 | 9,8 | 8,3 | 7,6 | 57,9 | 3,1 | 15,6 |
| I | mg/kg | 0,3 | 7,0 | 1,7 | 1,4 | 1,3 | 1,6 | 1,3 | 2,8 |
| La | mg/kg | 7,2 | 32,2 | 14,0 | 13,3 | 3,9 | 14,9 | 1,6 | 5,8 |
| Ce | mg/kg | 12,3 | 59,6 | 26,6 | 25,5 | 8,1 | 64,8 | 1,1 | 2,8 |
| Nd | mg/kg | 8 | 29 | 15 | 14 | 4 | 19 | 0,9 | 0,7 |
| Sm | mg/kg | 0 | 7 | 2 | 2 | 1 | 2 | 0,7 | 0,1 |
| S | mg/kg | 500,0 | 2935,0 | 1370,8 | 1283,5 | 653,1 | 426491,9 | 0,4 | -0,6 |
| Cl | mg/kg | 100 | 9636 | 728 | 235 | 1571 | 2467176 | 4,2 | 19,7 |
| Yb | mg/kg | 0,8 | 3,8 | 1,2 | 0,8 | 0,7 | 0,5 | 1,4 | 1,5 |
| OM (LOI) | wt% | 2,21 | 37,52 | 11,79 | 8,50 | 8,54 | 72,87 | 1,5 | 1,6 |

Table 32: Summary statistics for Manchester RDS - Winter.

## *4.1.2. Organic matter content and grain size analysis*

Organic matter content and grain size have been determined respectively by loss-on-ignition and by laser diffractometry for the 144 RDS samples, as previously described in sections 2.5 and 2.8.

RDS samples show a large variability in what concerns organic matter contents (OM), within a similar range in both seasons - 2 to 41% in summer and 2 to 38% in winter. Nevertheless, mean and median OM contents are greater in winter samples, and the distribution of OM values is more widespread as can be observed in the box-and-whisker plot of Figure 60 below. Skewness and kurtosis values are larger for the summer distribution (Table 31 and Table 32) - summer OM distribution shows a stronger positive asymmetry with a more acute peak around the mean (OM histograms of Figure 113 and Figure 114, Appendix 4).

For the 72 samples analysed in each batch, 25 duplicates have been analysed in order to ensure the accuracy of the method. Paired-samples T-tests, after log-transforming the organic matter results for the summer dataset, show that the mean difference of the duplicate OM results is not statistically significant at the 95% confidence level ($t_{[summer]}$=0.811, p=0.426; $t_{[winter]}$=0.501, p=0.621; Table 33). Therefore, any differences in the OM content of samples are likely caused by chance and not by manipulation.

| Paired Differences | | | |
|---|---|---|---|
| | | t | Sig. (2-tailed) |
| Pair 1 | LOI_sLOG - LOI2_sLOG | ,811 | ,426 |
| Pair 2 | LOI_w (%) - LOI2_w (%) | ,501 | ,621 |

Table 33: Paired T-tests for RDS organic matter sample duplicates (log-transformed summer data).

As there is no formal classification established of OM contents in RDS, the soil classification (Huang et al., 2009) has been used to compare the levels found in RDS samples, as in Table 34. Most of the RDS samples have OM levels which resemble those of mineral soils with organic matter. As expected by the OM content distribution of the datasets, a greater number of samples with high OM contents is observed in winter, with OM contents in the range of “organic soil” and “peat” categories.

Most samples with the highest OM contents were collected in areas of dense roadside vegetation - by simple visual analysis it was observed that these samples had a significant amount of leaf/plant litter. The generally higher OM content of winter samples may be explained by the build-up of leaf/plant litter during the preceding autumn season, combined with a greater transport/leaching of soil components due to the more frequent rain periods.

Grain sizes were grouped into classes according to Friedman and Sanders (1978): <2µm, 2-4 µm, 4-8 µm, 8-16 µm, 16-32 µm, 32-63 µm, 63-125 µm, 125-250 µm, 2500-500 µm and 500-1000 µm. Results are displayed in detail in Appendix 4, in the graphs of Figure 117, in Table 95 and Table 96.

Grain size data is also summarised in Table 35 below where the 10th, 50th (median) and 90th percentiles, as well as volume-weighted mean particle diameters are displayed. Each sample underwent 5 measurement cycles to ensure method accuracy - differences between measurements for the same sample are negligible in all cases.

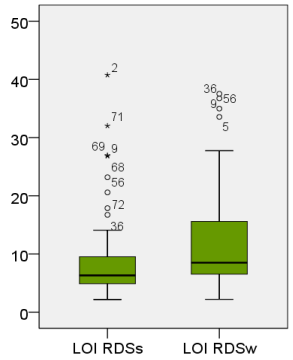


Figure 60: Box-and-whiskers plot for RDS organic matter contents in summer (RDSs) and winter (RDSw).

| Soil OM Classification | Soil OM range | No. of samples RDS summer | No. of samples RDS winter | % of samples RDS summer | % of samples RDS winter |
|---|---|---|---|---|---|
| Mineral soil | ≤ 3% | 6 | 3 | 8,3 | 4,2 |
| Mineral soil with organic matter | 3 - 15% | 58 | 50 | 80,6 | 69,4 |
| Organic soil | 15 - 30% | 6 | 15 | 8,3 | 20,8 |
| Peat | > 30% | 2 | 4 | 2,8 | 5,6 |

Table 34: Comparison of RDS organic matter levels with the soil classification proposed by Huang (2009).

In a preliminary analysis of the grain size distributions obtained for each sample, 31 locations show a coarser grain size in summer, whereas for 24 locations coarse fractions are more predominant in winter samples. Nevertheless, 17 locations show very similar distributions for both winter and summer samples - for these, there are no significant differences in grain size between seasons. Most samples show similar grain size distribution patterns with a shift towards the clay or sand-end between summer and winter; but there are also a few examples where grain size distribution is rather different between the two seasons, with contrasting asymmetry and/or kurtosis. To better interpret these cases, median particle sizes and volume-weighted mean diameters can also be seen in Table 35.

The variations in grain size distribution between summer and winter cannot be easily explained - grain size is dependent of several factors such as weather conditions, nearby sediment sources, pavement characteristics, traffic volume and mean vehicle speed. Nevertheless, most samples tend to be coarser in summer, which may be attributed to the effect of longer dry periods, allowing for both larger sediment accumulations and easier resuspension of the finer particles. The lower mean and median particle sizes in winter may generally be explained by the fact that fine particles tend to aggregate under the constantly wet conditions, and are therefore less prone to resuspension from the pavements.

| | d (0.1) - 10th percentile diameter (µm) | d (0.5) - median (µm) | d (0.9) - 90th percentile diameter (µm) | D - Volume weighted mean diameter (µm) |
|---|---|---|---|---|
| 1S | 7,529 | 138,964 | 429,416 | 185,041 |
| 2S | 18,336 | 381,824 | 767,761 | 383,336 |
| 3S | 7,759 | 125,809 | 453,878 | 184,951 |
| 4S | 3,946 | 114,778 | 567,807 | 204,354 |
| 5S | 4,039 | 123,22 | 605,969 | 216,956 |
| 6S | 7,467 | 131,681 | 490,076 | 196,129 |
| 7S | 7,876 | 142,844 | 456,251 | 194,78 |
| 8S | 6,874 | 171,864 | 493,934 | 216,863 |
| 9S | 2,742 | 44,269 | 282 | 97,435 |
| 10S | 2,656 | 73,13 | 456,528 | 160,365 |
| 11S | 4,877 | 122,377 | 479,975 | 188,65 |
| 12S | 10,916 | 193,598 | 456,972 | 219,892 |
| 13S | 3,351 | 97,646 | 542,855 | 191,934 |
| 14S | 4,589 | 130,548 | 534,63 | 204,035 |
| 15S | 16,168 | 223,605 | 497,795 | 248,867 |
| 17S | 12,771 | 188,812 | 509,189 | 232,905 |
| 18S | 6,768 | 165,447 | 475,733 | 208,286 |
| 19S | 5,021 | 140,217 | 530,82 | 208,561 |
| 20S | 8,693 | 196,915 | 526,412 | 236,215 |
| 21S | 5,48 | 150,122 | 445,495 | 191,607 |
| 22S | 6,095 | 129,982 | 382,524 | 166,073 |
| 23S | 3,97 | 151,998 | 427,226 | 187,38 |
| 24S | 10,114 | 147,842 | 456,506 | 197,582 |
| 25S | 4,456 | 152,891 | 520,455 | 211,406 |
| 26S | 13,78 | 188,698 | 509,578 | 233,115 |
| 27S | 14,36 | 222,108 | 653,039 | 283,397 |
| 28S | 7,389 | 144,551 | 495,549 | 205,925 |
| 29S | 17,044 | 231,178 | 498,068 | 256,39 |
| 30S | 10,465 | 139,338 | 341,398 | 165,269 |
| 31S | 5,976 | 126,057 | 438,838 | 180,119 |
| 32S | 4,906 | 63,121 | 386,586 | 138,372 |
| 33S | 4,134 | 113,145 | 412,903 | 165,454 |
| 34S | 6,55 | 176,667 | 495,61 | 219,161 |
| 35S | 10,527 | 177,247 | 637,256 | 255,779 |
| 36S | 9,78 | 183,419 | 535,497 | 232,959 |
| 37S | 9,665 | 117,669 | 346,938 | 154,875 |
| 38S | 11,408 | 185,629 | 610,13 | 252,677 |
| 40S | 8,458 | 205,09 | 533,306 | 245,287 |
| 41S | 5,173 | 188,278 | 584,325 | 241,873 |
| 42S | 5,728 | 200,12 | 556,297 | 242,226 |
| 43S | 4,981 | 98,699 | 399,494 | 157,425 |
| 44S | 9,403 | 201,046 | 513,665 | 238,081 |
| 45S | 6,594 | 135,027 | 403,649 | 175,975 |
| 46S | 7,582 | 124,11 | 413,761 | 174,942 |
| 48S | 32,05 | 157,008 | 460,496 | 208,442 |
| 49S | 11,461 | 153,685 | 454,555 | 199,74 |
| 50S | 14,191 | 212,313 | 528,163 | 248,359 |
| 51S | 6,859 | 94,111 | 395,755 | 155,146 |
| 52S | 12,114 | 190,175 | 514,847 | 234,328 |
| 53S | 8,564 | 183,23 | 561,697 | 236,458 |
| 54S | 7,536 | 157,992 | 514,448 | 214,758 |
| 55S | 32,113 | 279,085 | 665,488 | 320,222 |
| 56S | 10,519 | 159,501 | 492,74 | 211,332 |
| 57S | 10,711 | 123,139 | 423,473 | 177,04 |
| 58S | 6,635 | 185,643 | 470,057 | 218,189 |
| 59S | 5,3 | 128,705 | 494,022 | 194,964 |
| 60S | 5,53 | 176,838 | 555,121 | 231,783 |
| 61S | 5,129 | 103,594 | 367,211 | 150,06 |
| 62S | 4,481 | 114,42 | 495,786 | 189,81 |
| 63S | 8,777 | 154,909 | 515,631 | 215,016 |
| 64S | 4,431 | 108,355 | 416,144 | 164,761 |
| 65S | 8,015 | 172,517 | 510,818 | 221,127 |
| 66S | 6,869 | 130,8 | 428,205 | 179,583 |
| 67S | 13,437 | 194,357 | 494,077 | 232,353 |
| 68S | 5,244 | 93,371 | 529,849 | 189,983 |
| 69S | 11,6 | 158,879 | 451,982 | 201,305 |
| 70S | 9,724 | 258,552 | 706,812 | 308,252 |
| 71S | 5,286 | 82,938 | 538,654 | 183,037 |
| 72S | 8,852 | 142,329 | 494,103 | 202,737 |
| 73S | 5,699 | 108,899 | 418,916 | 167,232 |
| 74S | 8,066 | 210,075 | 510,72 | 241,307 |
| 75S | 23,976 | 165,017 | 387,849 | 191,935 |

| | d (0.1) - 10th percentile diameter (µm) | d (0.5) - median (µm) | d (0.9) - 90th percentile diameter (µm) | D - Volume weighted mean diameter (µm) |
|---|---|---|---|---|
| 1W | 4,479 | 55,729 | 383,944 | 133,393 |
| 2W | 3,942 | 55,239 | 526,791 | 168,269 |
| 3W | 6,068 | 89,628 | 637,112 | 223,806 |
| 4W | 3,56 | 84,088 | 569,354 | 189,088 |
| 5W | 3,61 | 38,559 | 327,611 | 108,184 |
| 6W | 9,123 | 157,484 | 463,549 | 200,203 |
| 7W | 6,497 | 167,108 | 503,953 | 214,872 |
| 8W | 6,292 | 227,396 | 647,272 | 274,084 |
| 9W | 3,79 | 37,933 | 377,283 | 118,101 |
| 10W | 11,068 | 281,036 | 609,652 | 304,586 |
| 11W | 2,011 | 24,178 | 161,527 | 65,91 |
| 12W | 2,831 | 52,882 | 405,247 | 138,467 |
| 13W | 2,707 | 20,226 | 124,683 | 58,203 |
| 14W | 1,67 | 15,923 | 82,452 | 30,562 |
| 15W | 31,281 | 219,76 | 509,841 | 254,774 |
| 17W | 4,501 | 174,139 | 625,85 | 244,091 |
| 18W | 3,945 | 131,214 | 483,137 | 191,324 |
| 19W | 2,225 | 34,636 | 401,095 | 131,68 |
| 20W | 4,191 | 78,757 | 404,009 | 149,516 |
| 21W | 7,138 | 154,015 | 508,813 | 210,327 |
| 22W | 9,985 | 161,765 | 457,146 | 203,558 |
| 23W | 2,552 | 120,092 | 478,362 | 184,863 |
| 24W | 5,04 | 96,552 | 473,445 | 172,637 |
| 25W | 1,602 | 14,015 | 311,892 | 87,918 |
| 26W | 5,091 | 120,885 | 480,838 | 187,233 |
| 27W | 8,584 | 272,372 | 670,08 | 307,105 |
| 28W | 5,654 | 231,141 | 668,493 | 280,365 |
| 29W | 2,441 | 46,422 | 375,635 | 124,064 |
| 30W | 6,03 | 110,626 | 424,739 | 169,419 |
| 31W | 4,296 | 113,103 | 456,916 | 177,916 |
| 32W | 5,838 | 108,646 | 385,812 | 157,346 |
| 33W | 4,503 | 128,564 | 443,082 | 180,853 |
| 34W | 7,87 | 177,109 | 658,322 | 261,164 |
| 35W | 121,216 | 457,5 | 797,885 | 459,244 |
| 36W | 10,847 | 262,871 | 739,858 | 319,268 |
| 37W | 6,424 | 101,12 | 383,385 | 155,15 |
| 38W | 5,626 | 172,331 | 544,902 | 224,063 |
| 40W | 7,558 | 140,443 | 484,621 | 198,267 |
| 41W | 6,385 | 211,346 | 638,582 | 263,731 |
| 42W | 8,364 | 177,265 | 522,319 | 226,246 |
| 43W | 7,255 | 129,785 | 448,764 | 185,72 |
| 44W | 4,322 | 121,565 | 512,019 | 194,687 |
| 45W | 2,201 | 35,4 | 419,504 | 132,339 |
| 46W | 10,633 | 199,3 | 626,048 | 260,721 |
| 48W | 7,739 | 120,32 | 423,248 | 175,251 |
| 49W | 13,911 | 265,367 | 566,866 | 285,5 |
| 50W | 5,414 | 101,541 | 490,767 | 182,473 |
| 51W | 4,824 | 137,076 | 471,685 | 192,315 |
| 52W | 5,783 | 163,153 | 507,15 | 214,162 |
| 53W | 5,394 | 97,753 | 551,486 | 200,455 |
| 54W | 12,302 | 140,183 | 541,712 | 213,788 |
| 55W | 10,819 | 303,771 | 695,031 | 331,644 |
| 56W | 19,517 | 278,254 | 679,695 | 319,029 |
| 57W | 3,976 | 50,461 | 305,627 | 109,468 |
| 58W | 9,739 | 180,141 | 508,688 | 226,236 |
| 59W | 2,542 | 27,011 | 244,748 | 82,603 |
| 60W | 3,156 | 72,969 | 401,553 | 145,004 |
| 61W | 4,899 | 416,215 | 798,27 | 393,558 |
| 62W | 6,681 | 172,109 | 602,398 | 240,746 |
| 63W | 8,375 | 137,408 | 451,924 | 191,167 |
| 64W | 7,496 | 202,098 | 521,219 | 238,702 |
| 65W | 4,827 | 175,825 | 595,308 | 239,455 |
| 66W | 8,261 | 159,349 | 486,584 | 207,836 |
| 67W | 5,936 | 114,128 | 429,749 | 171,944 |
| 68W | 3,893 | 43,357 | 467,916 | 150,139 |
| 69W | 6,501 | 152,782 | 583,062 | 226,979 |
| 70W | 4,244 | 76,635 | 703,748 | 215,77 |
| 71W | 2,097 | 15,084 | 85,004 | 36,808 |
| 72W | 6,863 | 160,008 | 635,039 | 244,504 |
| 73W | 4,319 | 175,807 | 596,613 | 237,704 |
| 74W | 6,757 | 216,591 | 547,036 | 250,181 |
| 75W | 17,694 | 166,187 | 440,458 | 204,261 |

Table 35: Summary of RDS-summer (left) and winter (right) grain size analysis (144 samples).

However, there is also the wash-off caused by water flow episodes which are more frequent in winter - samples are not only predominantly finer-grained due to wet aggregation, but also total sample weights collected are generally lower in winter due to the more frequent runoff periods.

Some samples which remarkably were amongst those with highest PHE contents (e.g. samples 27, 34, 35 and 55) did not follow this trend - particle diameter was larger in winter samples. In the case of the 4 samples referred, these were in fact collected in main roads or carriageways, suggesting that vehicles travelling at higher mean speeds may be the main factor favouring the accumulation of larger particles (in the magnitude of medium sands), as fine particles are more easily resuspended and removed from the pavement.

The relatively larger mean particle sizes in winter for the referred samples may also be interpreted as an added effect of rainfall - in addition to the prevailing wind resuspension, water runoff preferentially transports the finer particles, enhancing the relative amount of coarse particles on the pavements.

### *4.1.3. Correlation analysis*

The Spearman's rank correlation coefficient has been used to investigate the preliminary relationships between RDS variables, similarly to what has been done for soil data and described in section 2.9.2. The Spearman’s rank correlation matrix for RDS summer and winter are shown in Table 97 and

Table 98 of Appendix 4. Correlations within the interval [0.6, 0.7[ are flagged in orange; those above 0.7 are in red and the negative correlations above -0.6 are flagged in blue.

Aluminium is correlated to MgO, $K_2O$, $TiO_2$, MnO, $Fe_2O_3$, Sc, V, Co, Ga, Y, Nb, Th, La, Ce and Nd, both in summer and winter datasets ($\rho$>0.6, p<0.01). These elements are mainly of geogenic origin in RDS. Iron ($Fe_2O_3$) is strongly correlated to MgO, $TiO_2$, MnO, V, Co, Ni, Ga, Y and Nb in both seasons; as well as to Cr, Ba, Cu, La, Ce and Nd ($\rho$>0.6, p<0.01) only in the winter dataset. Some of these elements, e.g. Co, Ni, Cr, and Cu, are often anthropogenically enriched in RDS samples. Oxides and hydroxides of Fe and Mn are relatively common constituents of soils and can adsorb a variety of trace elements - all the above elements can be associated to these compounds. Rare earth elements (La, Ce and Nd; $\rho$>0.5 in summer and $\rho$>0.6 in winter; p<0.01) and Y ($\rho$>0.7, p<0.01 in both seasons) are also correlated to $Fe_2O_3$.

$P_2O_5$, Br, S, I are strongly correlated to organic matter (OM) ($\rho$>0.7, p<0.01) in both seasons. Selenium is also correlated to this group of elements, but with a greater expression in winter. As pointed out in the previous section, RDS may contain a large amount of OM composed by leaf/plant litter in several degrees of disintegration, which is sourced directly from local vegetation or soil material. These correlations can be interpreted in the same way as for soils (cf. section 3.1.3). In winter, for which the mean LOI values tend to be higher, OM also correlates to the fractions between 8-32µm - OM particulates might be predominant in these fractions.

$K_2O$ and Rb are strongly correlated ($\rho$=0.916 in winter and $\rho$=0.980 in summer, p<0.01) as these are alkali metals with similar properties and part of common minerals. The K and Rb content of RDS may be largely inherited from soils, which have received these elements mainly from parent rocks.

Another suite of elements which are correlated to each other for both summer and winter datasets are Cu, Zn, Mo, Sn and Sb ($\rho$>0.6, p<0.01). These elements are among those with the highest anthropogenic inputs in the area. Cr and Pb also correlate to each other and to the above elements in the winter dataset - two elements which also show significant enrichments. The fact that the concentrations vary in a similar way across the study area for these elements is evidence that contamination sources are responsible for the input of several elements simultaneously; and these also tend to occur in the same form in RDS (e.g. adsorbed in Fe and Mn oxy-hidroxydes or organic matter) - and hence their correlation in both datasets. Nevertheless, this is a simplified analysis and more pertinent observations will be made further in this work.

### *4.1.4. Grain size normalisation*

Road-deposited sediments are texturally and compositionally highly variable, as they are composed of a wide range of particle sizes and different proportions of organic matter, anthropogenic materials and contaminant species (cf. section 1.5). For the present work, RDS were collected in two different

seasons, in order to account for temporal differences in sediment texture and composition - the relative amounts of grain size fractions present in RDS has been shown to vary not only at the spatial scale, but also temporally, as evidenced by the grain size analysis in section 4.1.2. It is also known that trace metals of environmental concern tend to be more concentrated in the finer fractions of the sediment (cf. section 1.7 and references therein).

To compensate for the effects of grain size on trace metal concentrations, a common approach is to normalise the data using one element as a grain size proxy, especially when trace metal content in each grain size fraction is not analytically determined. Many proxy elements for grain size have been reported in the literature, but no references have been found on the normalization of RDS geochemical data. From the elements investigated as grain size proxies for RDS, Al and Ga were chosen to be tested in RDS as they are geogenic elements related to the fine fractions of the sediment, which have successfully been used for soil and sediment normalization (cf. section 1.7).

It has been observed in this work that elevated trace metal concentrations in RDS tend to occur for the same locations both in summer and winter. Therefore, local factors seem to be more important in RDS composition rather than temporal factors. Nevertheless, it is also observed that these concentrations are not the same in summer and winter, and that grain size is also temporally different at each location. Grain size normalization could be a way of minimising the differences in trace metal levels induced by this varying sample grain size, making summer-winter comparisons more robust.

A first step towards choosing a suitable conservative element is to analyse the distributions, descriptive statistics and correlations of Al, Ga, the grain size data and the trace metals of concern. As described in section 4.8, grain size data has first been analysed for 17 selected samples for each season. These have been selected based on their elevated trace element content and the need to study these locations more deeply.

After determination of the grain size distribution, the two (summer and winter) 17-sample datasets were statistically analysed. Due to the small number of samples analysed, which does not allow for multivariate statistics to be performed with reliable results, Spearman's correlation coefficients (ρ) were computed between grain size intervals, $Al_2O_3$ and Ga, which are summarised below in Table 36 (and in Table 109 and Table 110 of Appendix 4).

In both summer and winter datasets, $Al_2O_3$ and Ga showed significant correlations at the 95% or 99% confidence intervals (sig. <0.05 or 0.01, respectively) to the grain size fractions below 63μm, increasing the correlation coefficient and the significance towards the clay size (<2μm); and a negative correlation to fractions between 1000-63μm. Aluminium and Ga concentrations, therefore, varied in the same way as clay-sized fraction contents in these datasets. Furthermore, Ga showed

better correlations to the fine fractions (below 63µm) for both datasets when compared to $Al_2O_3$, suggesting that the former could be a better grain size proxy.

| | | 500-1000_s | 250-500_s | 125-250_s | 63-125_s | 32-63_s | 16-32_s | 8-16_s | 4-8_s | 2-4_s | inf2_s | 1000-63_s | 63-inf2_s | d0.5_s | D_s |
|---|---|---|---|---|---|---|---|---|---|---|---|---|---|---|---|
| Al2O3_s | Correlation Coefficient | -,379 | -,574 | -,049 | ,380 | ,522 | ,469 | ,429 | ,541 | ,651 | **,728** | -,529 | ,529 | -,610 | -,588 |
| | Sig. (2-tailed) | ,134 | ,016 | ,851 | ,132 | ,032 | ,058 | ,086 | ,025 | ,005 | ,001 | ,029 | ,029 | ,009 | ,013 |
| Ga_s | Correlation Coefficient | -,508 | -,651 | -,210 | ,405 | ,622 | ,585 | ,542 | ,668 | **,748** | **,765** | -,661 | ,661 | -,715 | -,685 |
| | Sig. (2-tailed) | ,037 | ,005 | ,419 | ,107 | ,008 | ,014 | ,025 | ,003 | ,001 | ,000 | ,004 | ,004 | ,001 | ,002 |

| | | 500-1000_w | 250-500_w | 125-250_w | 63-125_w | 32-63_w | 16-32_w | 8-16_w | 4-8_w | 2-4_w | inf2_w | 1000-63_w | 63-inf2_w | d0.5 | D |
|---|---|---|---|---|---|---|---|---|---|---|---|---|---|---|---|
| Al2O3_w | Correlation Coefficient | -,567 | -,667 | -,470 | ,205 | ,435 | ,510 | ,491 | ,635 | ,681 | **,754** | -,607 | ,607 | -,600 | -,572 |
| | Sig. (2-tailed) | ,018 | ,003 | ,057 | ,430 | ,081 | ,037 | ,045 | ,006 | ,003 | ,000 | ,010 | ,010 | ,011 | ,016 |
| Ga_w | Correlation Coefficient | -,642 | -,784 | -,618 | ,338 | ,559 | ,640 | ,650 | **,733** | **,745** | **,811** | -,713 | **,713** | -,728 | -,667 |
| | Sig. (2-tailed) | ,005 | ,000 | ,008 | ,184 | ,020 | ,006 | ,005 | ,001 | ,001 | ,000 | ,001 | ,001 | ,001 | ,003 |

Table 36: Spearman's rank correlation coefficients between grain size fraction contents, Al and Ga for RDS data (n=17 samples in each season).

These were very promising results, as they would support Al or Ga as adequate conservative elements to be used in RDS grain size normalisation. Therefore, further grain size analysis took place to include the total number of RDS samples collected in both seasons.

The correlation analysis and further multivariate statistical analysis using the whole datasets (72 samples in each season) revealed that, although correlations between Al, Ga and the <63 µm grain size fractions could still be significant at the 95% confidence level, the correlation coefficients were significantly lower than in the 17-sample datasets - this information can be consulted in Table 97 and

Table 98 of Appendix 4. This is does not support the initial hypothesis that RDS grain size normalisation could be done with the use of a conservative element.

To investigate which other factors could be controlling Al-Ga concentrations and their relationship with grain size, samples were selected not according to their PHE content, but to other characteristics - subsets were created using samples collected on/near roads with heavy traffic, residential areas, near gully pots, or samples with high organic matter content. Statistics performed on the data from these subsets did not highlight any new relationships. This indicates that other methods should be used in the future in order to better investigate the controls on grain size distribution in RDS and the relationship between these and elemental concentrations - RDS grain size variations are the result of very complex and rapid processes, which cannot be easily normalised by the use of grain size proxies, as in soils or other types of sediments. The choice of the sample subset has also been demonstrated to have a major influence on statistical results, and must therefore be carefully and critically interpreted.

Nevertheless, an interesting observation is that, in samples with high PHE contents, these are frequently correlated to the fraction between 63-125μm, which does not agree to the general idea that finer grain size fractions act as a major host for trace metals in soils and sediments. This was an interesting fact which arose during grain size normalisation research, which is further explored in section 4.8.

### *4.1.5. Comparison summer-winter: Wilcoxon signed-ranks test*

As a consequence of the sampling method chosen, for each sampling location two RDS samples were collected: one in winter and other in summer. The main objective of this method is to account for seasonal differences in composition and/or mineralogy, as it is known that RDS is temporally highly variable.

The Wilcoxon signed-ranks test is a non-parametric technique used to evaluate the differences between the paired samples (summer and winter), since data are not normally distributed. The results can be observed in Table 37 and Table 38 - the applied Wilcoxon test gave a non-significant difference ($p<0.05$, Table 38) in concentrations between summer and winter for $Na_2O$, MgO, $SiO_2$, TiO, MnO, V, Cr, Ba, Ga, Se, Rb, Sr, Y, Zr, Nb, Bi, La, Ce, Nd and the volume-weighted mean diameter (D). Table 37 shows the number of samples for which the summer value is higher than the winter value (negative ranks); and vice-versa (positive ranks) - even for those pairs with non-significant difference between summer and winter (grey in Table 38), the season for which concentrations are generally higher may be inferred from this analysis.

| Ranks | | | | |
|---|---|---|---|---|
| | | N | Mean Rank | Sum of Ranks |
| Na2O_w - Na2O_s | Negative Ranks | 24 | 31,29 | 751 |
| | Positive Ranks | 36 | 29,97 | 1079 |
| | Ties | 12 | | |
| MgO_w - MgO_s | Negative Ranks | 31 | 33,82 | 1049 |
| | Positive Ranks | 35 | 33,21 | 1163 |
| | Ties | 6 | | |
| Al2O3_w - Al2O3_s | Negative Ranks | 26 | 32,35 | 841 |
| | Positive Ranks | 44 | 37,36 | 1644 |
| | Ties | 2 | | |
| SiO2_w - SiO2_s | Negative Ranks | 34 | 38,22 | 1300 |
| | Positive Ranks | 38 | 34,96 | 1329 |
| | Ties | 0 | | |
| P2O5_w - P2O5_s | Negative Ranks | 19 | 28,42 | 540 |
| | Positive Ranks | 49 | 36,86 | 1806 |
| | Ties | 4 | | |
| K2O_w - K2O_s | Negative Ranks | 44 | 37,76 | 1662 |
| | Positive Ranks | 26 | 31,67 | 824 |
| | Ties | 2 | | |
| CaO_w - CaO_s | Negative Ranks | 44 | 37,97 | 1671 |
| | Positive Ranks | 28 | 34,20 | 958 |
| | Ties | 0 | | |
| TiO2_w - TiO2_s | Negative Ranks | 32 | 34,69 | 1110 |
| | Positive Ranks | 40 | 37,95 | 1518 |
| | Ties | 0 | | |
| MnO_w - MnO_s | Negative Ranks | 30 | 33,93 | 1018 |
| | Positive Ranks | 37 | 34,05 | 1260 |
| | Ties | 5 | | |
| Fe2O3_w - Fe2O3_s | Negative Ranks | 26 | 30,17 | 785 |
| | Positive Ranks | 46 | 40,08 | 1844 |
| | Ties | 0 | | |
| Sc_w - Sc_s | Negative Ranks | 23 | 32,70 | 752 |
| | Positive Ranks | 45 | 35,42 | 1594 |
| | Ties | 4 | | |
| V_w - V_s | Negative Ranks | 32 | 35,58 | 1139 |
| | Positive Ranks | 40 | 37,24 | 1490 |
| | Ties | 0 | | |
| Cr_w - Cr_s | Negative Ranks | 43 | 37,40 | 1608 |
| | Positive Ranks | 29 | 35,17 | 1020 |
| | Ties | 0 | | |
| Co_w - Co_s | Negative Ranks | 23 | 26,30 | 605 |
| | Positive Ranks | 47 | 40,00 | 1880 |
| | Ties | 2 | | |
| Ba_w - Ba_s | Negative Ranks | 35 | 38,81 | 1359 |
| | Positive Ranks | 37 | 34,31 | 1270 |
| | Ties | 0 | | |
| Ni_w - Ni_s | Negative Ranks | 28 | 32,21 | 902 |
| | Positive Ranks | 44 | 39,23 | 1726 |
| | Ties | 0 | | |
| Cu_w - Cu_s | Negative Ranks | 19 | 30,05 | 571 |
| | Positive Ranks | 53 | 38,81 | 2057 |
| | Ties | 0 | | |

| Ranks | | | | |
|---|---|---|---|---|
| | | N | Mean Rank | Sum of Ranks |
| Zn_w - Zn_s | Negative Ranks | 23 | 26,30 | 605 |
| | Positive Ranks | 49 | 41,29 | 2023 |
| | Ties | 0 | | |
| Ga_w - Ga_s | Negative Ranks | 29 | 38,38 | 1113 |
| | Positive Ranks | 42 | 34,36 | 1443 |
| | Ties | 1 | | |
| Ge_w - Ge_s | Negative Ranks | 11 | 15,36 | 169 |
| | Positive Ranks | 61 | 40,31 | 2459 |
| | Ties | 0 | | |
| As_w - As_s | Negative Ranks | 26 | 32,10 | 835 |
| | Positive Ranks | 44 | 37,51 | 1651 |
| | Ties | 2 | | |
| Se_w - Se_s | Negative Ranks | 24 | 25,96 | 623 |
| | Positive Ranks | 31 | 29,58 | 917 |
| | Ties | 17 | | |
| Br_w - Br_s | Negative Ranks | 15 | 24,83 | 373 |
| | Positive Ranks | 57 | 39,57 | 2256 |
| | Ties | 0 | | |
| Rb_w - Rb_s | Negative Ranks | 34 | 36,04 | 1226 |
| | Positive Ranks | 37 | 35,96 | 1331 |
| | Ties | 1 | | |
| Sr_w - Sr_s | Negative Ranks | 44 | 35,78 | 1575 |
| | Positive Ranks | 28 | 37,63 | 1054 |
| | Ties | 0 | | |
| Y_w - Y_s | Negative Ranks | 34 | 31,62 | 1075 |
| | Positive Ranks | 35 | 38,29 | 1340 |
| | Ties | 3 | | |
| Zr_w - Zr_s | Negative Ranks | 41 | 33,96 | 1393 |
| | Positive Ranks | 31 | 39,85 | 1236 |
| | Ties | 0 | | |
| Nb_w - Nb_s | Negative Ranks | 25 | 35,70 | 893 |
| | Positive Ranks | 42 | 32,99 | 1386 |
| | Ties | 5 | | |
| Mo_w - Mo_s | Negative Ranks | 25 | 31,38 | 785 |
| | Positive Ranks | 45 | 37,79 | 1701 |
| | Ties | 2 | | |
| Hf_w - Hf_s | Negative Ranks | 22 | 34,66 | 763 |
| | Positive Ranks | 48 | 35,89 | 1723 |
| | Ties | 2 | | |
| W_w - W_s | Negative Ranks | 42 | 41,21 | 1731 |
| | Positive Ranks | 30 | 29,90 | 897 |
| | Ties | 0 | | |
| Pb_w - Pb_s | Negative Ranks | 24 | 32,10 | 771 |
| | Positive Ranks | 48 | 38,70 | 1858 |
| | Ties | 0 | | |
| Bi_w - Bi_s | Negative Ranks | 35 | 27,26 | 954 |
| | Positive Ranks | 27 | 37,00 | 999 |
| | Ties | 10 | | |

| Ranks | | | | |
|---|---|---|---|---|
| | | N | Mean Rank | Sum of Ranks |
| Th_w - Th_s | Negative Ranks | 16 | 27,53 | 441 |
| | Positive Ranks | 52 | 36,64 | 1906 |
| | Ties | 4 | | |
| U_w - U_s | Negative Ranks | 40 | 33,03 | 1321 |
| | Positive Ranks | 22 | 28,73 | 632 |
| | Ties | 10 | | |
| Cd_w - Cd_s | Negative Ranks | 23 | 26,28 | 605 |
| | Positive Ranks | 37 | 33,12 | 1226 |
| | Ties | 12 | | |
| Sn_w - Sn_s | Negative Ranks | 25 | 33,36 | 834 |
| | Positive Ranks | 47 | 38,17 | 1794 |
| | Ties | 0 | | |
| Sb_w - Sb_s | Negative Ranks | 23 | 34,17 | 786 |
| | Positive Ranks | 49 | 37,59 | 1842 |
| | Ties | 0 | | |
| I_w - I_s | Negative Ranks | 21 | 22,36 | 470 |
| | Positive Ranks | 48 | 40,53 | 1946 |
| | Ties | 3 | | |
| La_w - La_s | Negative Ranks | 37 | 33,55 | 1242 |
| | Positive Ranks | 35 | 39,61 | 1387 |
| | Ties | 0 | | |
| Ce_w - Ce_s | Negative Ranks | 35 | 37,86 | 1325 |
| | Positive Ranks | 37 | 35,22 | 1303 |
| | Ties | 0 | | |
| Nd_w - Nd_s | Negative Ranks | 38 | 37,74 | 1434 |
| | Positive Ranks | 34 | 35,12 | 1194 |
| | Ties | 0 | | |
| S_w - S_s | Negative Ranks | 46 | 38,25 | 1760 |
| | Positive Ranks | 23 | 28,50 | 656 |
| | Ties | 3 | | |
| Cl_w - Cl_s | Negative Ranks | 2 | 5,50 | 11 |
| | Positive Ranks | 38 | 21,29 | 809 |
| | Ties | 32 | | |
| OM_w - OM_s | Negative Ranks | 20 | 28,40 | 568 |
| | Positive Ranks | 51 | 38,98 | 1988 |
| | Ties | 1 | | |
| 1000-63_w - 1000-63_s | Negative Ranks | 52 | 40,58 | 2110 |
| | Positive Ranks | 20 | 25,90 | 518 |
| | Ties | 0 | | |
| 63-inf2_w - 63-inf2_s | Negative Ranks | 20 | 25,90 | 518 |
| | Positive Ranks | 52 | 40,58 | 2110 |
| | Ties | 0 | | |
| d0.5_w - d0.5_s | Negative Ranks | 43 | 38,67 | 1663 |
| | Positive Ranks | 29 | 33,28 | 965 |
| | Ties | 0 | | |
| D_w - D_s | Negative Ranks | 35 | 41,97 | 1469 |
| | Positive Ranks | 37 | 31,32 | 1159 |
| | Ties | 0 | | |

Table 37: Ranks of the Wilcoxon signed-ranks test for RDS summer and winter datasets.

For the remaining variables there are significant ($p<0.05$ or 0.01) differences between summer and winter. Higher values tend to occur in winter samples for $Al_2O_3$, $P_2O_5$, $Fe_2O_3$, Sc, Co, Ni, Cu, Zn, Ge, As, Br, Mo, Hf, Pb, Th, Cd, Sn, Sb, I, Cl, organic matter (OM), and grain size fraction below 63µm (63-inf2) (pairs labelled "W" in the 4$^{th}$ column, Table 38). Most of these results were expected: it has been previously observed that OM was more abundant in winter samples, and therefore related elements (I, P, Br) were also likely to display higher values in winter. The same occurs for the finer grain size fractions: higher values in winter may also influence the concentrations of related elements (Al, Fe, PHEs). During the winter time, road gritting is a regular procedure throughout Manchester and Cl values in RDS are therefore much higher than in summer.

Conversely, the coarser grain size fractions (1000-63µm), the median diameter (d0.5), CaO, $K_2O$, W, U and S are likely to display larger values in summer (pairs labelled "S" in the 4th column, Table 38).

| Pair | Z | Sig. (2-tailed) | Higher Values |
|---|---|---|---|
| Na2O_w - Na2O_s | -1,217 | 0,224 | W |
| MgO_w - MgO_s | -0,365 | 0,715 | W |
| Al2O3_w - Al2O3_s | -2,351 | 0,019 | W |
| SiO2_w - SiO2_s | -0,081 | 0,935 | W |
| P2O5_w - P2O5_s | -3,872 | 0,000 | W |
| K2O_w - K2O_s | -2,453 | 0,014 | S |
| CaO_w - CaO_s | -2,001 | 0,045 | S |
| TiO2_w - TiO2_s | -1,145 | 0,252 | W |
| MnO_w - MnO_s | -0,756 | 0,450 | W |
| Fe2O3_w - Fe2O3_s | -2,972 | 0,003 | W |
| Sc_w - Sc_s | -2,573 | 0,010 | W |
| V_w - V_s | -0,985 | 0,325 | W |
| Cr_w - Cr_s | -1,650 | 0,099 | S |
| Co_w - Co_s | -3,731 | 0,000 | W |
| Ba_w - Ba_s | -0,250 | 0,803 | S |
| Ni_w - Ni_s | -2,312 | 0,021 | W |
| Cu_w - Cu_s | -4,170 | 0,000 | W |
| Zn_w - Zn_s | -3,979 | 0,000 | W |
| Ga_w - Ga_s | -0,946 | 0,344 | W |
| Ge_w - Ge_s | -6,426 | 0,000 | W |
| As_w - As_s | -2,388 | 0,017 | W |
| Se_w - Se_s | -1,250 | 0,211 | W |
| Br_w - Br_s | -5,284 | 0,000 | W |
| Rb_w - Rb_s | -0,301 | 0,764 | W |
| Sr_w - Sr_s | -1,462 | 0,144 | S |

| Pair | Z | Sig. (2-tailed) | Higher Values |
|---|---|---|---|
| Y_w - Y_s | -0,792 | 0,428 | W |
| Zr_w - Zr_s | -0,441 | 0,660 | S |
| Nb_w - Nb_s | -1,541 | 0,123 | W |
| Mo_w - Mo_s | -2,681 | 0,007 | W |
| Hf_w - Hf_s | -2,810 | 0,005 | W |
| W_w - W_s | -2,340 | 0,019 | S |
| Pb_w - Pb_s | -3,050 | 0,002 | W |
| Bi_w - Bi_s | -0,158 | 0,875 | W |
| Th_w - Th_s | -4,478 | 0,000 | W |
| U_w - U_s | -2,426 | 0,015 | S |
| Cd_w - Cd_s | -2,286 | 0,022 | W |
| Sn_w - Sn_s | -2,694 | 0,007 | W |
| Sb_w - Sb_s | -2,963 | 0,003 | W |
| I_w - I_s | -4,413 | 0,000 | W |
| La_w - La_s | -0,407 | 0,684 | S |
| Ce_w - Ce_s | -0,062 | 0,951 | S |
| Nd_w - Nd_s | -0,673 | 0,501 | S |
| S_w - S_s | -3,300 | 0,001 | S |
| Cl_w - Cl_s | -5,363 | 0,000 | W |
| OM_w - OM_s | -4,068 | 0,000 | W |
| 1000-63_w - 1000-63_s | -4,467 | 0,000 | S |
| 63-inf2_w - 63-inf2_s | -4,467 | 0,000 | W |
| d0.5_w - d0.5_s | -1,958 | 0,050 | S |
| D_w - D_s | -0,870 | 0,384 | S |

Table 38: Wilcoxon signed-ranks test for RDS summer and winter datasets.

These results point that concentrations have a tendency to be higher in winter for each sample pair, with the exception of few variables. Additionally, statistics were non-significant for many elements, meaning the differences for each sample pair were either very small, or the number of sample pairs with positive and negative ranks were similar.

It must be taken into account that summer-winter differences for each sample pair may be very small - this fact is not accounted for in the Wilcoxon signed-ranks test, as original values are ranked (since original distributions generally deviate from normal) and statistics is computed using the calculated ranks. Nevertheless, mean and median concentrations computed for each geochemical variable using the full dataset (Table 31, Table 32 and Table 70) pointed to a very similar summer-winter pattern in concentrations. As discussed further in this work, seasonal effects are less important than the presence of point sources in what concerns average sample composition - summer-winter sample pairs tend to show small differences in composition, compared to the large variations which occur according to location.

## 4.2. Comparison with other RDS geochemical studies

The geochemical study of road-deposited sediments is a relatively recent subject, with the first relevant studies being published in the late 70's (cf. section 1.5). After the phasing-out of leaded gasoline in the year 2000, RDS has become a research subject due to its potential risks to human and environmental health. A few recent studies have been reported below in Table 39, in order to make a preliminary comparison with the PHE levels found. Different analysis methods have been used to determine PHE concentrations in each study, which may introduce data entropy to the comparison; however, the accuracy and precision for each method are reported in the references of Table 39.

In general terms, and despite major differences in sample number and location, RDS collected in this study display similar mean concentrations for Cu and Pb with the other two reported studies for Manchester. However, Zn reported by Robertson et al. (2003) display a rather elevated mean concentration, likely due to high concentrations found in specific outer city samples.

Chromium is the only element for which the highest maximum and mean concentrations are found for the present study. Copper, Ni and Cd values are comparable to other cities - nevertheless, Birmingham shows high Cu levels attributed to silver working and production of brass alloys, Coventry displays high Ni levels which could not be attributed to any particular factor (Charlesworth et al., 2003), whereas Cd concentrations in Avilés are extremely high due to the metalliferous industry present (Ordoñez et al., 2003). Zinc mean levels are also comparable to other cities except Avilés. Arsenic is generally not determined in RDS studies due to method limitations - comparing to Bratislava, mean As levels in Manchester are higher; but lower than those of Avilés.

Although Pb mean values in this study are higher than Birmingham, Coventry or Bratislava, they are comparable to those found previously in Manchester by Robertson et al. (2003) and Carraz et al. (2006). This demonstrates that, although Pb concentrations in RDS have decreased significantly after the phase-out of leaded gasoline in the year 2000 (Nageotte and Day, 1998), there is still a significant anthropogenic sources associated to this element, causing very high levels at some locations. Mean Pb values in Avilés and Oahu are higher than in the present study; however the range of determined concentrations is similar.

The comparison of RDS geochemistry between cities a difficult task due to the existence of specific contamination sources, different for each city; adding to the diverse urban environments (residential, industrial) where RDS samples are collected; and the transient nature of this media. Nevertheless, it can be assumed that RDS is prone to contamination regardless of its location - it only takes traffic and other nearby sources to turn RDS into a mixture of potentially deleterious substances.

| City | Count | Cr (mg/kg) | | | Ni (mg/kg) | | | Cu (mg/kg) | | | Zn (mg/kg) | | | As (mg/kg) | | | Pb (mg/kg) | | | Cd (mg/kg) | | |
|---|---|---|---|---|---|---|---|---|---|---|---|---|---|---|---|---|---|---|---|---|---|---|
| | | Min | Max | Mean | Min | Max | Mean | Min | Max | Mean | Min | Max | Mean | Min | Max | Mean | Min | Max | Mean | Min | Max | Mean |
| **Manchester - summer** | **72** | **40** | **544** | **108** | **18** | **82** | **31** | **36** | **493** | **94** | **66** | **1326** | **326** | **2,9** | **10,7** | **5,7** | **35** | **1184** | **159** | **0,3** | **2,6** | **0,5** |
| **Manchester - winter** | **72** | **25** | **267** | **94** | **14** | **77** | **34** | **19** | **433** | **126** | **101** | **1312** | **414** | **2,4** | **25,0** | **6,6** | **29** | **2027** | **197** | **0,3** | **6,4** | **0,7** |
| Manchester (1) | 18 | - | - | - | - | - | - | 32 | 283 | 113 | 172 | 2183 | 653 | - | - | - | 25 | 645 | 265 | - | - | - |
| Manchester (2) | 100 | - | - | - | - | - | - | 14 | 342 | 88 | 65 | 990 | 268 | - | - | - | 45 | 1461 | 164 | - | - | - |
| Bratislava 2003 (3) | 26 | 5 | 77 | 21 | 0,4 | 30 | 7 | 19 | 353 | 171 | 20 | 390 | 171 | - | - | - | 9 | 427 | 57 | 0,1 | 4,2 | 0,4 |
| Bratislava 2004 (3) | 9 | 46 | 342 | 87 | 17 | 150 | 36 | 89 | 279 | 167 | 203 | 367 | 294 | 2,6 | 3,8 | 3,1 | 26 | 277 | 67 | 0,6 | 1,2 | 0,9 |
| Birmingham, UK (4) | 100 | - | - | - | 0 | 636 | 41 | 16 | 6688 | 467 | 81 | 3165 | 534 | - | - | - | 0 | 146 | 48 | 0,0 | 13,1 | 1,6 |
| Coventry, UK (4) | 49 | - | - | - | 6 | 234 | 130 | 49 | 815 | 226 | 93 | 3038 | 386 | - | - | - | 0 | 199 | 47 | 0,0 | 2,5 | 0,9 |
| Avilés, Spain (5) | 112 | 32 | 54 | 42 | 18 | 50 | 28 | 104 | 374 | 183 | 2422 | 23400 | 4892 | 11,0 | 26,0 | 17,5 | 330 | 964 | 514 | 9,6 | 104,0 | 22,3 |
| Oahu, Hawaii (6) | 20 | - | - | - | - | - | - | 116 | 1147 | 409 | 250 | 3154 | 671 | - | - | - | 59 | 2348 | 537 | - | - | - |

Table 39: Minimum, maximum and median concentrations for Cr, Ni, Cu, Zn, As, Pb and Cd in RDS: 1 - Robertson et al. (2003), 2 - Carraz et al. (2006)3 - Krčmová et al. (2009), 4 - Charlesworth et al. (2003), 5 - Ordoñez et al. (2003), 6 - Sutherland et al. (2012)

## 4.3. Relationships with geology, land use and guidelines

Road-deposited sediment is a complex and often anthropogenically-derived media - its composition results from a wide variety of inputs (cf. section 1.2.2). In order to investigate whether bedrock, superficial geology or land use types have an influence on RDS composition, RDS geochemical datasets have been spatially joined to the 1:50.000 scale Digital Geological Map of Great Britain (© British Geological Survey, Figure 7 and Figure 8) using ESRI® ArcGIS 10.0. Each RDS sample was attributed the corresponding bedrock and superficial deposit variables. Land uses were registered during sample collection, similarly to what has been done for soil samples. The bedrock, superficial deposit and land use groups are summarised in Table 40, Table 41 and Table 42.

| Code | Description | Age | Rock type(s) | No. of samples |
|---|---|---|---|---|
| **TRIA** | **Triassic rocks (undifferentiated)** | Triassic | Sandstone and conglomerate, interbedded | 51 |
| **PUND** | **Permian rocks (undifferentiated)** | Permian | Sandstone and conglomerate, interbedded / mudstone, siltstone and sandstone | 13 |
| **WAWK** | **Warwickshire group** | Duckmantian (Westphalian B) - Early Permian | Mudstone, siltstone, sandstone, coal, ironstone and ferricrete / Siltstone and sandstone with subordinate mudstone | 3 |
| **PUCM** | **Pennine Upper Coal Measures Formation** | Bosolvian (Westphalian C) - Westphalian D | Mudstone, siltstone, sandstone, coal, ironstone and ferricrete | 5 |

Table 40: Bedrock geology groups in the study area (after the 1:50.000 scale Digital Geological Map of Great Britain © British Geological Survey) and number of RDS samples collected over each type.

Most RDS samples were collected in areas of Triassic (TRIA) and Permian (PUND) bedrock types, and Till (TILL-DMT) and River Terrace (RTDU-SAG) superficial deposit types. Out of the 72 pairs of RDS samples, only 3 and 5 were collected, respectively, in locations over Warwickshire Group (WAWK) and Coal Measures formation (PUCM) bedrock types and for that reason the comparison of distributions between these must be carefully interpreted. This is also the case for the glaciofluvial (GSG-SAGR) and alluvionar (ALV-CLSS) superficial deposit types, as only 2 and 3 samples, respectively, were collected over these deposits.

| Code | Description | Age | Rock type(s) | No. of samples |
|---|---|---|---|---|
| **RTDU-SAG** | **River Terrace Deposits** | Quaternary | Sand and gravel | 20 |
| **ALV-CLSS** | **Alluvium** | Flandrian (Quaternary) | Clay, silt and sand | 3 |
| **TILL-DMT** | **Till** | Devensian (Quaternary) | Diamicton | 47 |
| **GSG-SAGR** | **Glaciofluvial deposits** | Devensian (Quaternary) | Sand and gravel | 2 |

Table 41: Superficial deposit groups in the study area (after the 1:50.000 scale Digital Geological Map of Great Britain, © British Geological Survey) and number of RDS samples collected over each type.

The box-and-whisker plots of Figure 125 and Figure 126 (Appendix 4) were produced using IBM® SPSS 19 software, showing elemental distributions of Cr, Ni, Cu, Zn, As, Pb and Cd grouped by bedrock and superficial deposit type (note that bar widths are not proportional to the number of samples in each class - please refer to Table 40 and Table 41 for the number of samples). Nickel is the only trace metal which shows slightly higher median values in RDS collected over Permian rocks (PUND) when compared to TRIA. Furthermore, Ni is also slightly enriched over TILL-DMT in relation

to RTDU-SAGR - it must be taken into account that most PUND is overlain by TILL-DMT in the study area. In soils, Ni again showed a wider distribution with a slightly higher mean value over PUND and TILL_DMT (Figure 107 and Figure 108, Appendix 2), which may suggest a possible Ni input from soils to RDS.

A great part of RDS components are sourced from soil material which is transported and deposited at each location. Some elements such as $Al_2O_3$, $SiO_2$, $TiO_2$, Sc, V, Rb, Co, Ga, Mo, Zr and REEs have been reported in this work to be associated with the geogenic fraction of soil (cf. section 3.3). Therefore, box-and-whisker plots have been produced for these elements in RDS, grouped by bedrock geology and superficial deposit types, represented in Figure 127 and Figure 128.

In terms of superficial geology, $Al_2O_3$, $TiO_2$, Fe2O3, V, Co and Ga show slightly higher median concentrations in samples collected where TILL_DMT is the superficial deposit type (and PUND is the bedrock type, as these formations are superimposed in a large part of the study area). These elements are part of the geogenic component of RDS, as further clarified in section 4.7 (PCA).

In terms of land use types, RDS samples were collected mainly in roads/streets crossing commercial/residential areas and industrial areas with 54 and 12 samples, respectively (Table 42 and Figure 61). Five samples were collected in major roads or verges (dual carriageways and A roads), and 1 in an urban open space (DAC0), which for that reason is not considered for land use intercomparisons. Concentrations of trace metals of environmental concern (Cr, Ni, Cu, Zn, As, Pb and Cd) are represented in the box-and-whisker plots of Figure 118 to Figure 124.

The DAA0 (commercial/residential) and E000 (industrial) land use types display similar median concentrations for the referred PHE, whereas the CB00 (major roads) land use shows the highest mean values of Cr, Cu and As. In the absence of established RDS guidelines, these box-plots also include the soil threshold value where applicable (cf. section 1.4.3). These are used in the RDS plots for qualitative purposes only.

| Code | **Land Use** | **no. of samples** |
|---|---|---|
| CB00 | Major roads/verge | 5 |
| DAA0 | Commercial and residential | 54 |
| DAC0 | Urban open space | 1 |
| E000 | Industrial | 12 |

Table 42: Code and number of samples collected for each primary land use category

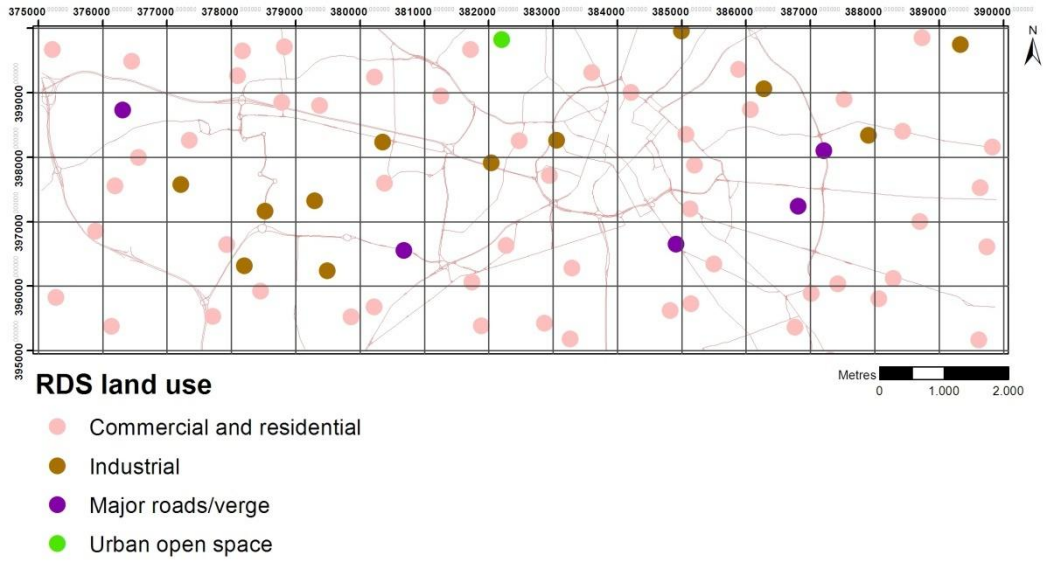


Figure 61: Primary land uses at RDS sampling locations.

As a transient, dynamic media, RDS may not only contribute to soil contamination but also to the increase of contaminated air particulates by resuspension and to water contamination by wash-off from roads and pavements. Nevertheless, the greater proximity of RDS media to soils in this work led to the comparison of RDS geochemical compositions to soil guideline thresholds. For Ni and As, all RDS samples are below the lowest guideline levels (130 and 32 mg/kg, respectively). Median Cr concentrations are also below the lowest SGV, except for major road RDS samples in summer. Copper levels are mostly above the UK ecological guideline, but it must be taken into account that this is a very strict guideline. Lead and Cd concentrations are mostly below the lowest guidelines. Median Zn concentrations are above both the ecological guideline and the ICRCL SGV - from the mentioned elements, Zn shows the highest concentrations.

## 4.4. Mapping

Road-deposited sediment data have been mapped as proportional symbol/colour maps in ESRI® ArcGIS 10.0, as in section 2.9.5. These are presented in Appendix 5, part A for the summer dataset and part B for the winter dataset. A first look at these maps show that chemical concentrations are widely variable across the area, as a consequence of contrasting local settings and consequent sample differences in composition and morphology. The use of proportional symbol/colour maps to display RDS composition is preferred due to the irregular spatial distribution of RDS samples and the heterogeneity of the urban tissue in the study area. Nevertheless, the maps in Figure 62 have been produced to elucidate about the areas where Cr, Ni, Cu, Zn and Pb concentrations are above the 75$^{th}$ percentile. These have been interpolated using the inverse distance-weighted (IDW) function (cf. section 2.9.5) and classes below the 75$^{th}$ percentile value for each element have been hidden.

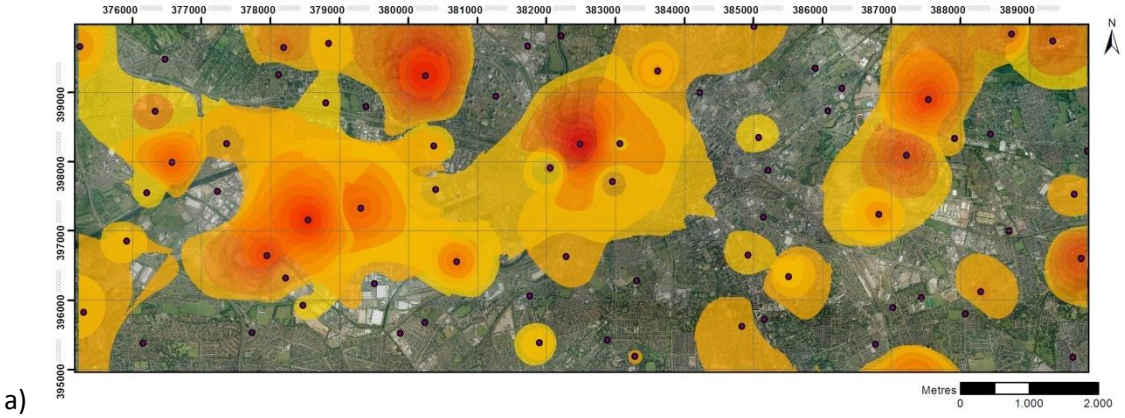


a)

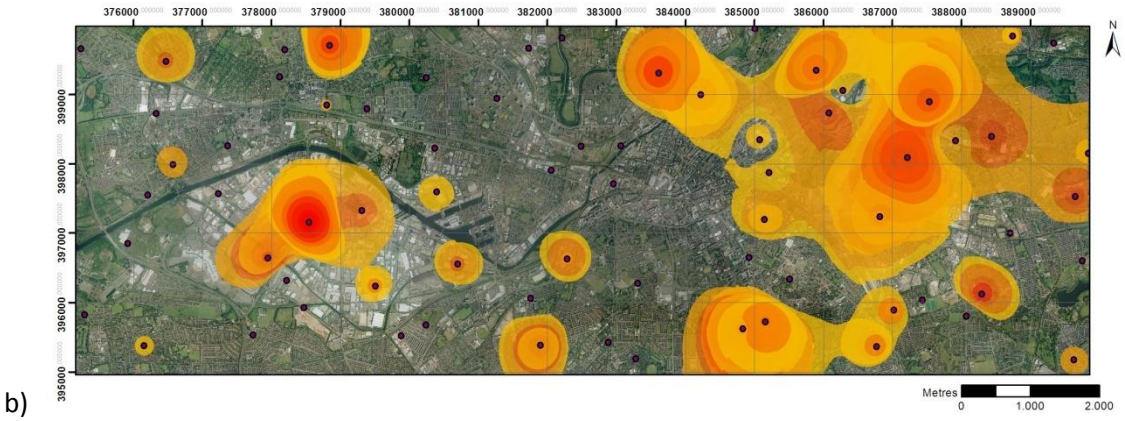


b)

Figure 62: Areas with Cr, Ni, Cu, Zn and Pb concentrations above the 75$^{th}$ percentile in RDS; a) summer, b) winter.

It is noticeable that the dispersion of samples is high and that there are only two locations where the referred trace elements are above the 75$^{th}$ percentile both in summer and winter - the Trafford Park industrial estate area, and the Clayton / Miles Platting area. Other than those, high concentrations are scattered throughout the area, with a predominance of the western area in summer and the eastern area in winter.

A first look at the local settings of samples with high PHE contents, revealed by mapping, does not reveal a specific pattern of contamination sources - samples collected in apparently contrasting local settings may display very similar PHE concentrations.

As previously referred, RDS sampling density has been smaller than that for soils. While PHE spatial distribution in soils allowed the distinction of areas where several samples showed elevated PHE levels, the lower RDS sampling density pointed to specific locations which will be looked at further in detail in the course of this work - critical samples have been chosen to undergo specific analysis, in order to better specify contamination sources and pathways.

## 4.5. Speciation analysis (BCR)

Samples with the highest trace metal contents were subject to speciation analysis through the BCR 3-step sequential extraction procedure, followed by aqua-regia digestion of the solid residue and extract analysis by FAAS for Cr, Cu, Zn, Pb and Fe, as described in section 2.6.

Summary statistics for the BCR results are presented in Table 43 below, and data distributions can be observed in Figure 63. It is noticeable that metal concentrations in the most labile phase - the exchangeable (acid-extractable) phase - are more significant for Zn. Overall, the exchangeable phase metal concentrations also tend to be higher in summer, as further discussed. In the other end, Cr and Fe are metals which tend to be concentrated in the residual phase. Nevertheless, the oxidisable phase also shows significant concentrations of Cr, as well as Cu. Lead is mainly associated to the reducible phase; Zn and Cu also show significant concentrations in this fraction.

| RDS summer | | Min | Max | Median | Mean | StdDev |
|---|---|---|---|---|---|---|
| Fe | Exchangeable | 0,002 | 0,04 | 0,01 | 0,01 | 0,01 |
| | Reducible | 0,12 | 0,48 | 0,21 | 0,24 | 0,11 |
| | Oxidisable | 0,001 | 0,13 | 0,04 | 0,04 | 0,03 |
| | Residual | 0,78 | 2,43 | 1,44 | 1,46 | 0,36 |
| | Total (BCR+AR) | 0,90 | 3,08 | 1,69 | 1,75 | 0,51 |
| | Total (XRF) | 1,44 | 4,30 | 2,34 | 2,53 | 0,72 |
| | Recovery (%) | 62,55 | 71,56 | 72,21 | 69,11 | 70,52 |
| Cr | Exchangeable | n.d. | 19,93 | 5,10 | 5,75 | 6,05 |
| | Reducible | n.d. | 121,39 | 13,48 | 26,05 | 37,73 |
| | Oxidisable | 3,23 | 66,19 | 26,81 | 30,89 | 21,30 |
| | Residual | 6,38 | 89,14 | 31,60 | 37,93 | 28,64 |
| | Total (BCR+AR) | 9,61 | 296,65 | 76,99 | 100,62 | 93,72 |
| | Total (XRF) | 52,70 | 250,70 | 95,40 | 111,73 | 56,65 |
| | Recovery (%) | 18,24 | 118,33 | 80,71 | 90,05 | 165,42 |
| Cu | Exchangeable | n.d. | 87,51 | n.d. | 7,98 | 21,42 |
| | Reducible | n.d. | 208,69 | 30,38 | 40,15 | 48,19 |
| | Oxidisable | n.d. | 99,66 | 23,98 | 29,10 | 27,91 |
| | Residual | n.d. | 39,11 | 2,10 | 5,56 | 9,51 |
| | Total (BCR+AR) | 0 | 434,97 | 56,45 | 82,79 | 107,04 |
| | Total (XRF) | 43,3 | 493,20 | 83,80 | 111,49 | 101,57 |
| | Recovery (%) | 0 | 88,19 | 67,36 | 74,26 | 105,38 |
| Zn | Exchangeable | 81,95 | 1334,32 | 138,14 | 266,70 | 312,98 |
| | Reducible | 20,76 | 585,84 | 128,00 | 176,20 | 164,34 |
| | Oxidisable | 21,31 | 194,55 | 54,60 | 60,98 | 39,91 |
| | Residual | 22,35 | 101,76 | 45,62 | 49,14 | 18,60 |
| | Total (BCR+AR) | 146,37 | 2216,47 | 366,35 | 553,02 | 535,83 |
| | Total (XRF) | 157,10 | 1325,60 | 304,40 | 398,11 | 282,92 |
| | Recovery (%) | 93,17 | 167,21 | 120,35 | 138,91 | 189,39 |
| Pb | Exchangeable | n.d. | 306,78 | 10,39 | 43,95 | 82,60 |
| | Reducible | 30,40 | 463,18 | 121,67 | 164,75 | 113,97 |
| | Oxidisable | n.d. | 275,80 | 18,40 | 53,05 | 74,37 |
| | Residual | n.d. | 109,92 | n.d. | 23,87 | 37,08 |
| | Total (BCR+AR) | 30,40 | 1155,67 | 150,46 | 285,63 | 308,01 |
| | Total (XRF) | 68,20 | 1184,00 | 160,90 | 229,63 | 260,19 |
| | Recovery (%) | 44,58 | 97,61 | 93,51 | 124,39 | 118,38 |

| RDS winter | | Min | Max | Median | Mean | StdDev |
|---|---|---|---|---|---|---|
| Fe | Exchangeable | 0,001 | 0,04 | 0,004 | 0,01 | 0,01 |
| | Reducible | 0,16 | 0,60 | 0,28 | 0,33 | 0,14 |
| | Oxidisable | 0,02 | 0,47 | 0,28 | 0,25 | 0,13 |
| | Residual | 0,74 | 2,60 | 1,22 | 1,35 | 0,48 |
| | Total (BCR+AR) | 0,92 | 3,71 | 1,78 | 1,93 | 0,76 |
| | Total (XRF) | 1,45 | 4,31 | 3,17 | 3,00 | 0,83 |
| | Recovery (%) | 63,23 | 86,23 | 56,21 | 64,37 | 91,75 |
| Cr | Exchangeable | n.d. | 10,59 | n.d. | 1,76 | 3,13 |
| | Reducible | n.d. | 47,69 | 6,54 | 11,94 | 13,73 |
| | Oxidisable | n.d. | 81,29 | 19,85 | 27,21 | 23,30 |
| | Residual | n.d. | 108,51 | 58,44 | 52,19 | 29,82 |
| | Total (BCR+AR) | 0 | 248,09 | 84,82 | 93,11 | 69,98 |
| | Total (XRF) | 42,70 | 198,50 | 117,10 | 120,98 | 43,03 |
| | Recovery (%) | 0 | 124,98 | 72,44 | 76,96 | 162,63 |
| Cu | Exchangeable | n.d. | 59,43 | 7,38 | 10,30 | 14,44 |
| | Reducible | n.d. | 104,58 | 54,75 | 49,18 | 29,88 |
| | Oxidisable | n.d. | 130,73 | 68,44 | 62,08 | 36,82 |
| | Residual | n.d. | 273,51 | 53,02 | 65,18 | 67,18 |
| | Total (BCR+AR) | 0 | 568,25 | 183,58 | 186,75 | 148,31 |
| | Total (XRF) | 39,2 | 433,40 | 182,50 | 186,96 | 86,49 |
| | Recovery (%) | 0 | 131,11 | 100,59 | 99,89 | 171,47 |
| Zn | Exchangeable | 56,86 | 724,74 | 235,45 | 278,61 | 194,32 |
| | Reducible | 155,74 | 657,75 | 466,57 | 442,69 | 148,58 |
| | Oxidisable | 38,97 | 269,12 | 138,31 | 139,26 | 66,55 |
| | Residual | 21,10 | 159,75 | 55,26 | 67,60 | 42,13 |
| | Total (BCR+AR) | 272,68 | 1811,35 | 895,60 | 928,16 | 451,58 |
| | Total (XRF) | 165,60 | 1312,30 | 579,00 | 623,51 | 323,16 |
| | Recovery (%) | 164,66 | 138,03 | 154,68 | 148,86 | 139,74 |
| Pb | Exchangeable | n.d. | 467,76 | n.d. | 32,38 | 112,56 |
| | Reducible | n.d. | 1471,98 | 230,34 | 361,09 | 368,95 |
| | Oxidisable | n.d. | 842,12 | 36,33 | 131,83 | 223,70 |
| | Residual | n.d. | 271,77 | n.d. | 28,24 | 71,76 |
| | Total (BCR+AR) | 0 | 3053,63 | 266,67 | 553,54 | 776,97 |
| | Total (XRF) | 70,20 | 2026,90 | 259,40 | 388,01 | 440,26 |
| | Recovery (%) | 0 | 150,66 | 102,80 | 142,66 | 176,48 |

Table 43: Summary statistics for RDS speciation data (all elements in mg/kg except Fe [%]; n=17 for each season; n.d. - not determined, below instrumental LLD).

Assuming trace element contents obtained by XRF as total concentrations, their comparison to the sum of the 4 phases (pseudo-total concentrations) indicates a mean recovery rate between 74-139% in summer samples and 77-149% in winter samples - these discrepancies may be attributed mostly to the sub-sampling of small amounts of RDS for BCR analysis, taking into account that samples, although disaggregated, may not be homogeneous. Iron was the element with lowest mean recovery rates: ~69% and 64% for summer and winter samples, respectively - this might be due to the presence of geogenic Fe, structurally bound to silicate minerals (especially clays), which are hardly dissociated. Nevertheless, the analysis of duplicate samples (25% of the total) demonstrated that the method produces reproducible results, as the concentration differences between the pairs of samples are non-significant at the 95% confidence level ($p>0.05$, Table 44).

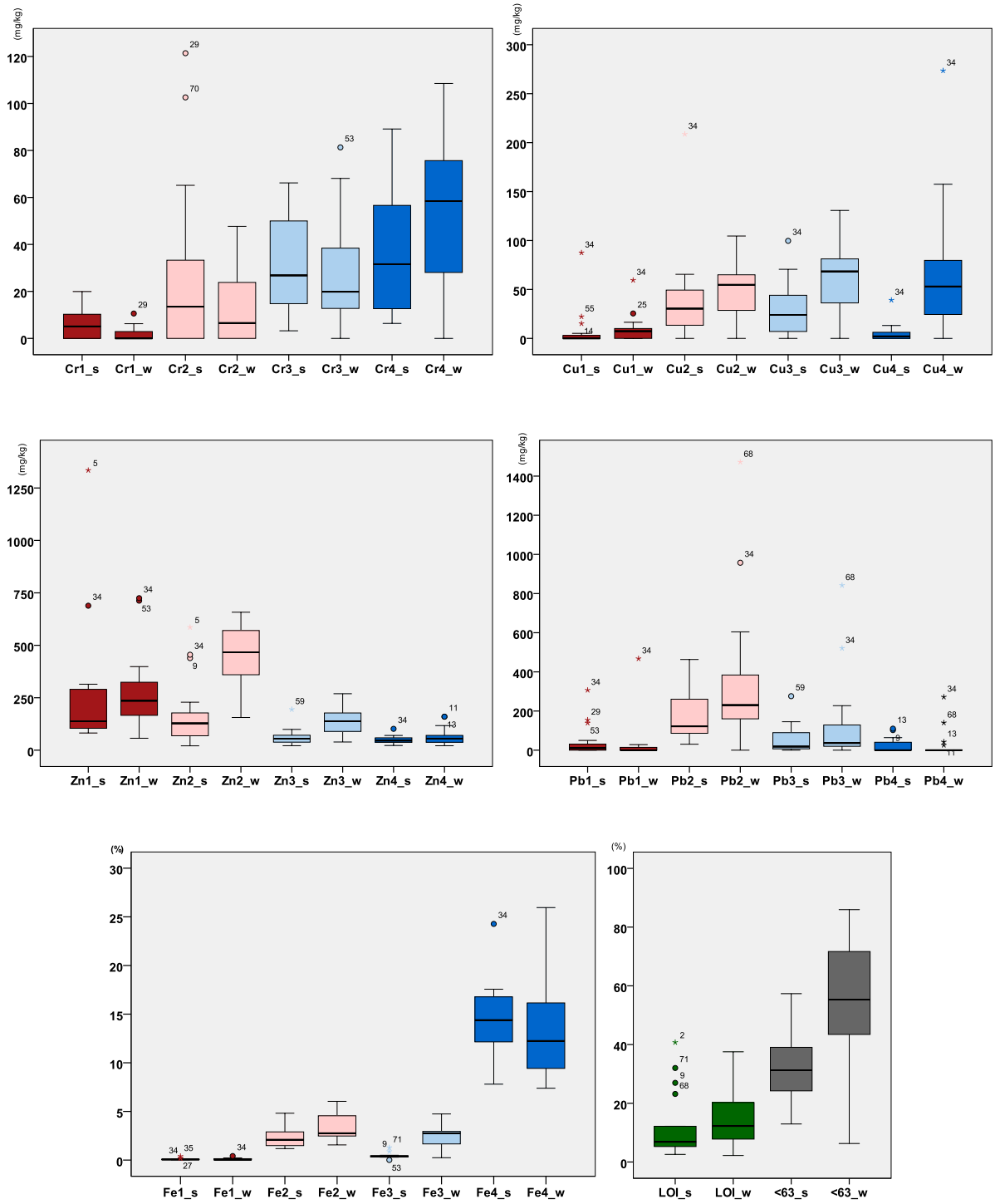


Figure 63: Box-and-whisker plots of RDS speciation data, organic matter (LOI) and grain size fraction below 63µm (n=17 for each bar).

| | Std. Error Mean | t | Sig. (2-tailed) |
|---|---|---|---|
| s5 - s5R | ,1406168 | -1,649 | ,116 |
| s34 - s34R | ,0920567 | 2,029 | ,057 |
| s68 - s68R | ,0727087 | -,329 | ,746 |
| w11 - w11R | ,0515909 | -,246 | ,809 |
| w25 - w25R | ,0951404 | 1,564 | ,134 |
| w35 - w35R | ,0845298 | -,198 | ,845 |
| w55 - w55R | ,1338668 | ,081 | ,937 |
| w70 - w70R | ,0541109 | -,903 | ,378 |

Table 44: Paired T-tests for BCR sequential extraction sample duplicates (data subject to logarithmic transformation).

### *4.5.1. Chromium*

Chromium median concentrations in the exchangeable, reducible and oxidisable phases are higher for summer samples than winter samples, as can be observed in the box-and-whisker plots of Figure 63. The residual phase, however, shows a higher median value in winter - in this season, Cr may show a lower mobility potential in RDS.

Chromium concentrations for all samples are represented in Figure 64. The oxidisable and residual phases contain the majority of the Cr; i.e. Cr is bound to a greater extent to organic matter or sulphides; or in resistant, metallic Cr compounds. This confirms the generally low mobility potential for the studied RDS samples.

However, the reducible phase accounts for a greater proportion of Cr in samples 27s, 29s and 70s (65, 121 and 102mg/kg, respectively). In this case, it is important to note that Cr may exist in 2 valence states - trivalent chromium, Cr (III); or the toxic/carcinogenic hexavalent chromium, Cr (VI). The solid phases of trivalent chromium usually display low solubility, because it precipitates as $Cr(OH)_3$ or as the solid solution $Fe_xCr_{1-x}(OH)_3$; or it is chelated by organic molecules that are adsorbed to mineral surfaces (Wittbrodt and Palmer, 1996). It is therefore more likely to be present in the oxidisable and residual phases. On the other hand, Cr (IV) is a toxic, soluble species which may undergo reduction and precipitation to the more stable Cr (III), depending on the reducing capability of the sediment which in turn is limited to the amount of reductant agents (organic matter, Fe (II), sulphides, etc.) present, and  in the media (Wittbrodt and Palmer, 1996). Cr (IV) is therefore likely to prevail in the reducible phases, which are more expressive under more reducing conditions (summer).

The summer samples 27, 29 and 70 show significant amounts of Cr in the reducible phase, which might indicate that the Cr in these samples may consist of Cr (IV). Nevertheless, investigations on the valence state of Cr are required to confirm this hypothesis. In terms of total Cr (XRF) these samples are well below the max. 251 mg/kg found in sample 34s, where most of the Cr is bound to the residual phase.

The phase ordering for Cr is not easily established, as Cr proportions in different phases are highly variable from sample to sample. Figure 64b shows that the most common phase order may be residual > oxidisable or reducible >> exchangeable, for both summer and winter samples.

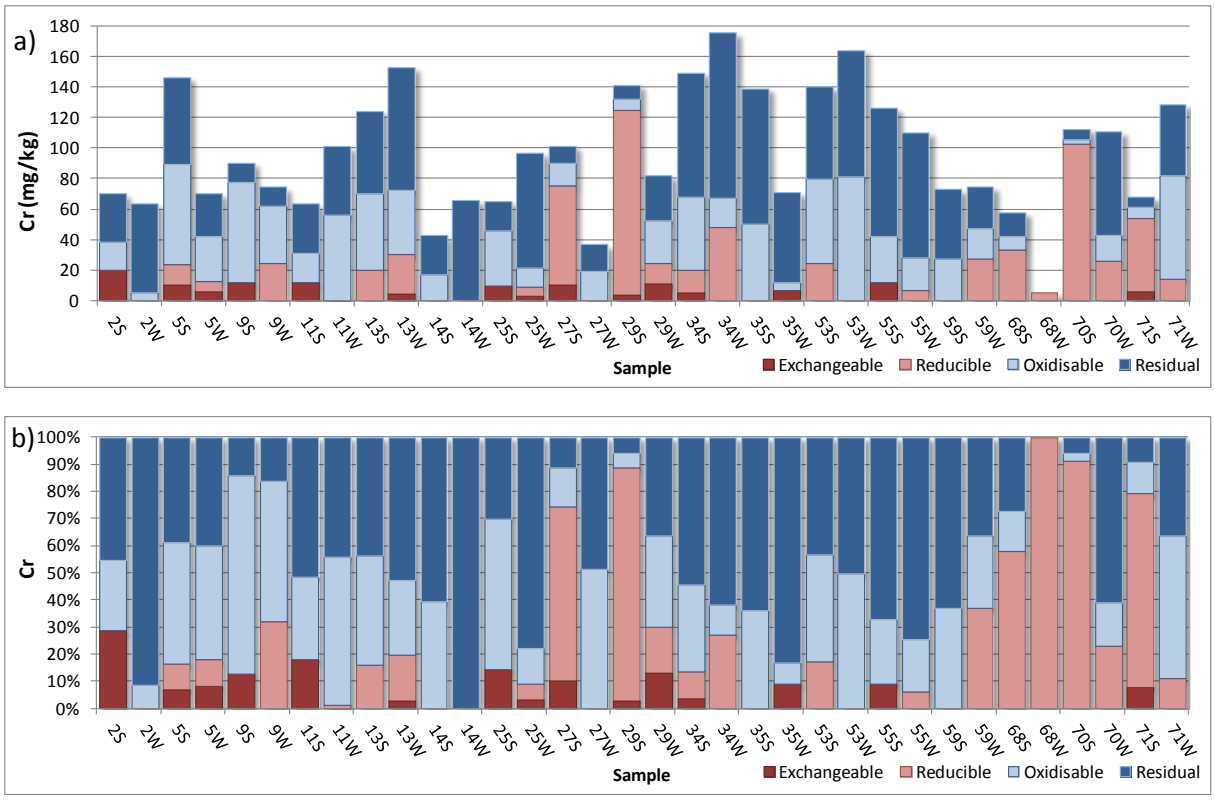


Figure 64: 3-step sequential extraction + *aqua regia* residual digestion results for chromium: a) absolute concentrations, b) relative concentrations: % of the total extracted Cr (s: summer; w: winter).

### *4.5.2. Copper*

Copper median concentrations for each phase tend to be higher for winter samples, as evidenced in Figure 63. In fact, except for sample 35, total (XRF) Cu concentrations are higher in winter - the higher proportion of fine material and especially organic matter (cf. Figure 63) in winter may lead to a greater Cu retention in the RDS. Most Cu is associated to the reducible and oxidisable phases of RDS, followed by the residual and exchangeable phases. The highest proportion of exchangeable Cu is observed for samples 14, 34 and 55 - although total Cu concentrations are higher in winter samples, the amount of Cu in the exchangeable phase, when present, tends to be higher in summer samples (Figure 65b). The maximum exchangeable Cu found in Manchester RDS is of 87.5 mg/kg (~20% of the extractable Cu) - almost three times the proposed UK ecological guideline of 30 mg/kg for total Cu, in soils.

The reducible and oxidisable phases, however, are the major hosts for Cu in the studied RDS samples. Copper adsorbs strongly to clay minerals, iron and manganese oxides, and organic material - hence its greater concentrations in these phases.

Phase ordering for Cu is different between summer and winter: whereas in summer Cu is predominant in the reducible and oxidisable phases, it is predominant in the residual and oxidisable phases in winter (summer: reducible > oxidisable >> residual ~ exchangeable; winter: residual >

oxidisable > reducible > exchangeable). Therefore, Cu is likely to show a greater mobility potential in the summer season in Manchester's RDS.

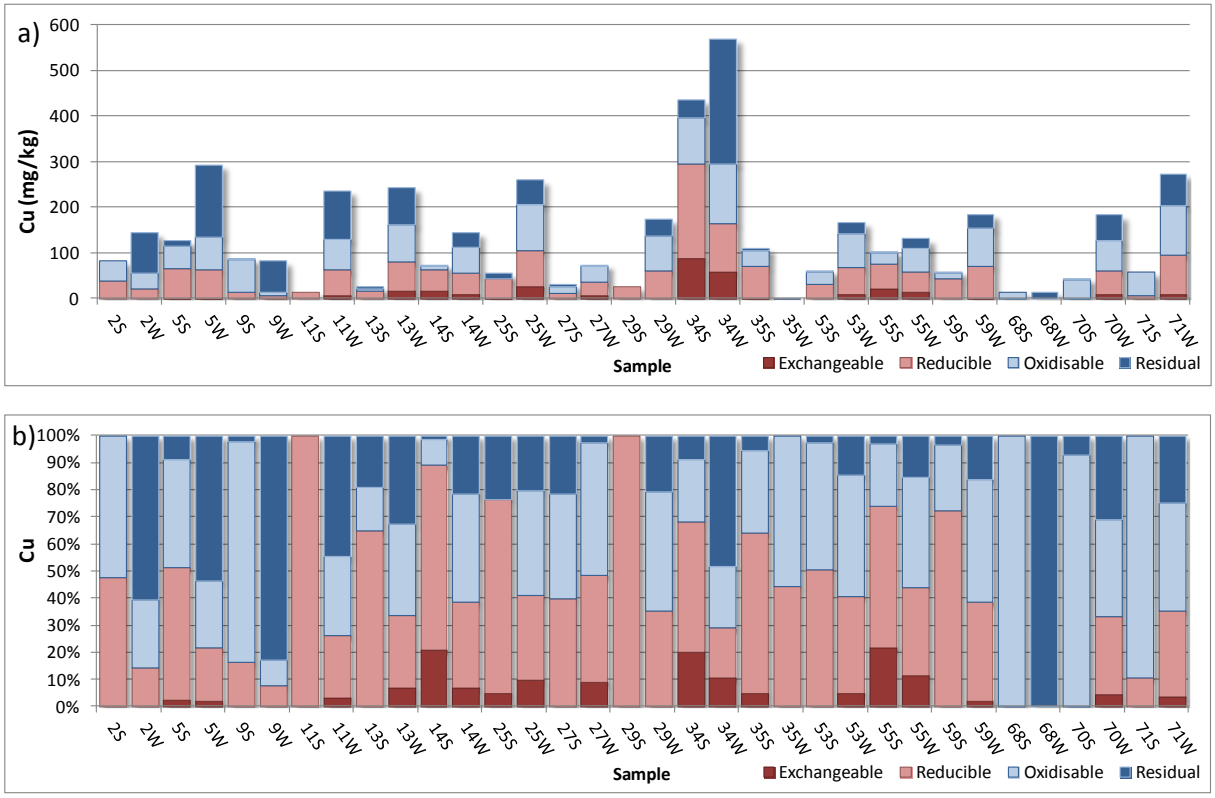


Figure 65: 3-step sequential extraction + *aqua regia* residual digestion results for copper: a) absolute concentrations, b) relative concentrations: % of the total extracted Cu (s: summer; w: winter).

### *4.5.3. Zinc*

From the analysed trace metals, Zinc displays the highest mobility potential - the percentage of Zn in the exchangeable phase varies between 11.7 and 65.0 % of the total extracted Zn. Seasonally, except for sample 5 which is locally affected by car repair / M.O.T businesses, extractable Zn concentrations are higher in winter, as observed in Figure 66a and in the box-plots for each phase in Figure 63. Nevertheless, for each sample pair, the proportion of Zn in the exchangeable phase is higher in summer, generally accompanied by lower Zn concentrations in the reducible phase (Figure 66b) - this last fraction tends to show a larger proportion of Zn in winter.

The oxidisable and residual phases of Zn are of little expression in Manchester RDS - these only account for 6.4 - 38% of the total Zn concentrations. Therefore, phase concentrations of Zn usually display the following order in summer: exchangeable > reducible > oxidisable ~ residual; and in winter: reducible > exchangeable > oxidisable > residual. Note that, although the proportion of exchangeable Zn is larger in summer samples as illustrated in Figure 66b, Zn absolute concentrations in the exchangeable phase are generally higher in winter (Figure 66a and Figure 63).

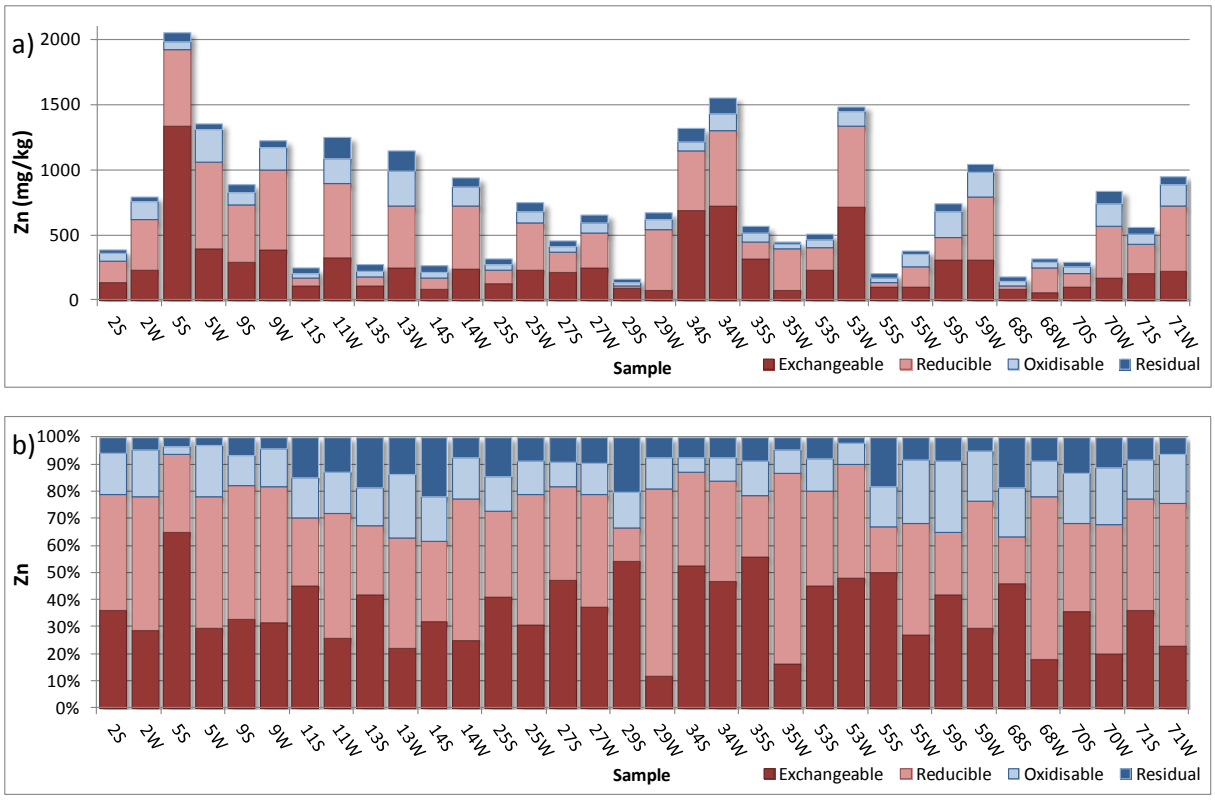


Figure 66: 3-step sequential extraction + *aqua regia* residual digestion results for zinc: a) absolute concentrations, b) relative concentrations: % of the total extracted Zn (s: summer; w: winter).

### *4.5.4. Lead*

Most of the lead present in Manchester RDS is bound to the reducible phase (mainly Fe-Mn oxides), as can be observed in Figure 67 and Figure 63: between 42.1 - 100% of the total extractable Pb is contained in the reducible phase. Statistics show that median concentrations of Pb in this phase are higher in winter samples and, in fact, Figure 67 confirms that this is the case for 11 out of the 14 samples.

When present, Pb in the exchangeable phase always displays a greater proportion in summer samples. The residual Pb also shows a similar behaviour, whereas the oxidisable Pb proportion is generally greater in winter. Therefore, Pb extractable contents typically follow the following phase ordering in summer: reducible >> oxidisable ~ residual or exchangeable; whereas in winter the most typical ranking is reducible >> oxidisable > exchangeable ~ residual.

Samples 34 and 68 display extractable Pb contents which are quite higher than the XRF Pb concentrations determined - in fact, SEM-EDS analysis revealed coarse-sized (40-200µm) Pb-containing grains, which by their heavy mass may significantly alter extractable Pb amounts if unpredictably sub-sampled in the 0.5g of RDS analysed by sequential extraction.

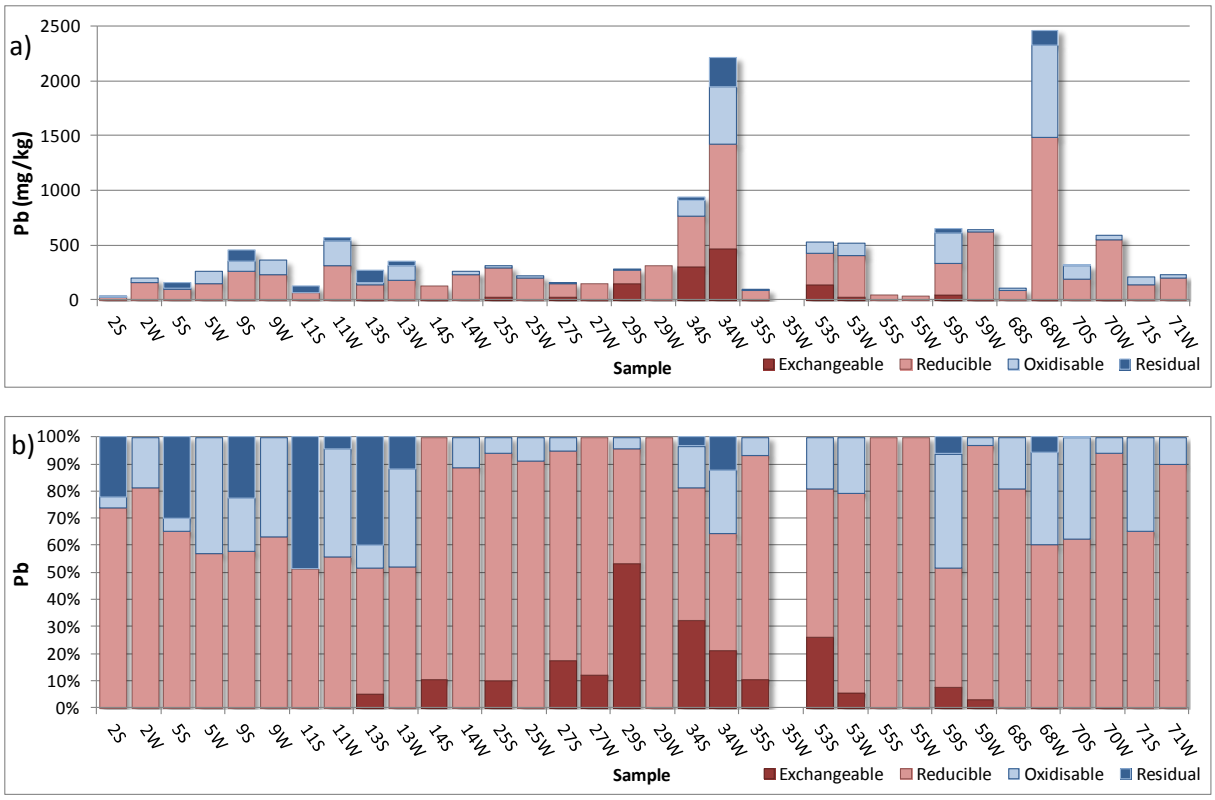


Figure 67: 3-step sequential extraction + *aqua regia* residual digestion results for lead: a) absolute concentrations, b) relative concentrations: % of the total extracted Pb (s: summer; w: winter).

### *4.5.4. Iron*

Iron is a major element in RDS, which may contain up to ~4% Fe. In this media, 50 - 88% of the total extracted iron is largely bound to the residual phase (cf. Figure 63) - resistant, crystalline Fe oxides are abundant in RDS samples, as observed under the SEM and described in the next section.

Figure 68 represent extractable Fe contents for each sample. It can be observed that Fe in the reducible phase displays a nearly constant proportion in RDS samples - regardless of the season or sample, around 10-25% of the Fe is contained in this phase. Iron in the oxidisable phase shows greater concentrations in winter samples, to the detriment of the residual fraction, for which the Fe proportion decreases in winter. Exchangeable (acid-extractable) Fe is negligible in the studied RDS samples, as it has only been detected in three samples with 0.02-0.04% exchangeable Fe. For both seasons, Fe extractable contents typically follow the phase order: residual >> reducible > oxidisable > exchangeable.

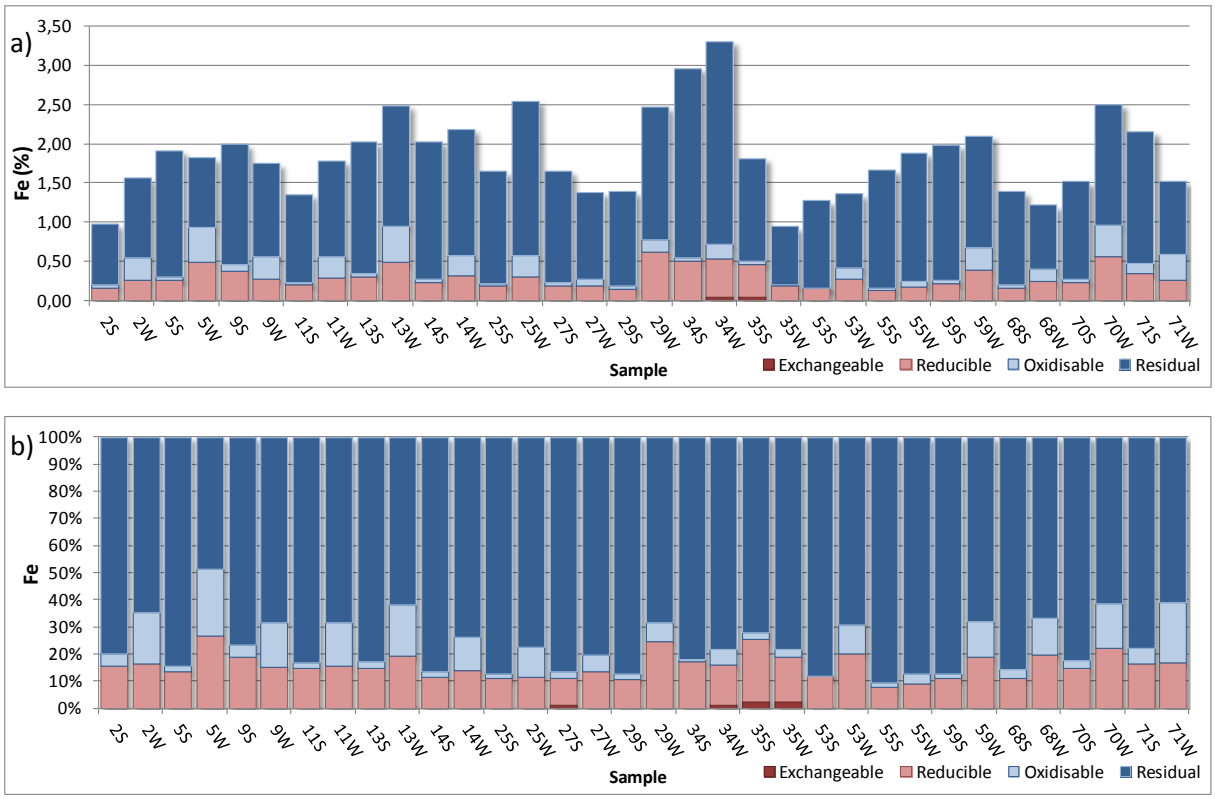


Figure 68: 3-step sequential extraction + *aqua regia* residual digestion results for iron: a) absolute concentrations, b) relative concentrations: % of the total extracted Fe (s: summer; w: winter).

## *Comparative mobility potential in Manchester's RDS*

The speciation analysis revealed that there are differences in the speciation of the analysed metals in Manchester's RDS. Table 45 summarises the phase orderings found for each element - the only phase concentrations which follow an identical order between summer and winter are for Cr and Fe.

| | Summer | Winter |
|---|---|---|
| Cr | Resid>Ox or Red>>Exch | Resid>Ox or Red>>Exch |
| Cu | Red>Ox>>Resid~Exch | Resid>Ox>Red>Exch |
| Zn | Exch>Red>Ox~Resid | Red>>Exch>Ox>Res |
| Pb | Red>>Ox~Resid or Exch | Red>>Ox>Exch~Resid |
| Fe | Resid>>Red>>Ox>Exch | Resid>>Red>Ox>Exch |

Table 45: Phase ordering of extractable metal concentrations in RDS.

In summer, Zn, Cu and Pb are the most prone to remobilization from RDS, as a greater percentage of these elements are mostly bound to the reducible phase, or the exchangeable phase in the case of Zn. Nevertheless, the proportion of exchangeable Zn is larger in summer samples but absolute Zn concentrations in the exchangeable phase are generally higher in winter. The winter season is marked by a remarkable increase of Cu in the residual phase to the detriment of the reducible phase, whereas mean Cu concentrations in the other 2 phases are relatively maintained; and by the increase of Zn in the reducible phase to the detriment of the exchangeable phase, maintaining concentrations in the residual and oxidisable phases. Lead concentrations in the exchangeable phase also drop in the

winter season. The prevalence of Zn, Cu and Pb in the most labile phases is an evidence of the strong anthopogenic contribute to these elements' concentrations in RDS.

In relation to element concentrations for each phase, these reflect the seasonal patterns previously described. The exchangeable fraction is dominated by Zn and Pb in summer and Zn in winter - this is the only element still showing a high proportion of exchangeable concentrations in winter. Lead is the predominant element in the reducible phase, followed by Cu in summer and Zn in winter. The oxidisable phase is dominated by Cr and Cu, whereas Fe is largely contained in the residual fraction. These orderings can also be visually interpreted from Figure 129 and Figure 130 (Appendix 4).

| | Summer | Winter |
|---|---|---|
| Exchangeable | Zn>Pb>Cr>Cu>>Fe | Zn>>Cu>Pb~Cr>>Fe |
| Reducible | Pb>Cu>Zn>Fe>Cr | Pb>Zn>Cu>Cr~Fe |
| Oxidisable | Cr~Cu>Zn~Pb>Fe | Cr~Cu>Pb>Zn>Fe |
| Residual | Fe>Cr>Pb>Zn>Cu | Fe>Cr>Cu>Zn>Pb |

Table 46: Element ordering for each extracted phase in RDS.

Although seasonal differences in Manchester's RDS metal lability are evident, these are not easy to compare to other studies, as to date there is no published material on the phase variations in RDS with time - most speciation studies analyse RDS samples collected at a single point or over short periods of time. Table 47 shows the mean content (% of total extracted) of each element in Manchester's RDS, as well as data from other published studies which employed the same extraction technique. The grain size fraction analysed has always been the <2mm, except in Kartal et al. (2006), where the fraction <74µm was analysed.

Iron is the only element for which the phase ordering and mean contents are similar between all studies. The only prominent difference regards Fe in the oxidisable phase, which is greater in winter - probably due to iron complexation with organic matter, which is very abundant in Manchester's RDS in this season.

Regarding Cr, the main differences are the concentrations in the most labile phase (exchangeable) - studies 2 and 4 (both in Kayseri, Turkey) display larger values then Manchester's RDS. Nevertheless, the sum of the three extracted phases (as a measure of the potential Cr mobility) is the highest for RDS-summer, as the residual and oxidisable phases bear approximately 31 and 25% of the total extracted Cr.

Summer Cu contents are similar to studies 2 (Kayseri, Turkey) and 5 (Hangzou, China), but similarly to Cr, Cu is also depleted in the residual fraction in summer RDS and hence the three potentially labile phases are dominant - more than in any other study. Nevertheless, Cu is less mobile in winter as its concentration in the residual phase increases, and are similar to study 3 (Honolulu, Hawaii).

Zn contents are similar in summer to study 4, and in winter to study 2 - in fact, sampling took place in September in study 4, which corresponds to hot and dry conditions; and in November for study 2

when temperatures fall abruptly and the wet season begins. This suggests that climatic conditions have a strong influence on Zn distribution across the different phases, favouring Zn in the exchangeable phase in summer and in the reducible phase in winter.

Mean Pb contents in RDS from Manchester are similar to studies 1, 2, 3 and 5. Additionally, it is worth noticing that mean Pb in the mobilisable fractions (Exch+Red+Ox) in Manchester's RDS (89.8% in summer and 92.1% in winter) is similar to studies 1 and 3, both from Honolulu, Hawaii. The studies where high levels of Pb are found in the exchangeable fraction (RDS-summer and studies 2, 4 and 5) also show large proportions of Pb in the residual fraction; whereas studies 1, 3 and RDS-winter show the highest content in the sum of the three potentially labile phases.

| | | Exchangeable | Reducible | Oxidisable | Residual | Exch+Red+Ox |
|---|---|---|---|---|---|---|
| **Cr** | **RDS summer (n=17)** | 6,7 | 24,8 | 31,0 | 37,5 | 62,5 |
| | **RDS winter (n=17)** | 2,1 | 16,8 | 27,4 | 53,7 | 46,3 |
| | **1 (n=20)** | n.d. | n.d. | n.d. | n.d. | - |
| | **2 (n=33)** | 10,1 | 19,1 | 11,6 | 59,8 | 40,8 |
| | **3 (n=13)** | n.d. | n.d. | n.d. | n.d. | - |
| | **4 (n=29)** | 30,8 | 2,1 | 25,7 | 41,4 | 58,6 |
| | **5 (n=5)** | 3,6 | 6,3 | 12,7 | 77,4 | 22,6 |
| **Cu** | **RDS summer (n=17)** | 4,4 | 50,0 | 39,3 | 6,3 | 93,7 |
| | **RDS winter (n=17)** | 4,4 | 26,9 | 34,0 | 34,7 | 65,3 |
| | **1 (n=20)** | 7 | 37,2 | 20,5 | 35,3 | 64,7 |
| | **2 (n=33)** | 6 | 43,6 | 25,5 | 24,9 | 75,1 |
| | **3 (n=13)** | 4,9 | 23,6 | 26,2 | 45,4 | 54,7 |
| | **4 (n=29)** | n.d. | n.d. | n.d. | n.d. | - |
| | **5 (n=5)** | 7,3 | 44,6 | 26,8 | 21,3 | 78,7 |
| **Zn** | **RDS summer (n=17)** | 44,5 | 29,6 | 13,6 | 12,2 | 87,8 |
| | **RDS winter (n=17)** | 27,7 | 49,6 | 15,2 | 7,5 | 92,5 |
| | **1 (n=20)** | 27,2 | 42,1 | 9,5 | 21,2 | 78,8 |
| | **2 (n=33)** | 25,1 | 55,1 | 9,6 | 10,2 | 89,8 |
| | **3 (n=13)** | 32,7 | 36,6 | 8,3 | 22,4 | 77,6 |
| | **4 (n=29)** | 33,2 | 29,7 | 20,9 | 16,2 | 83,8 |
| | **5 (n=5)** | 26,7 | 42,5 | 13,2 | 17,6 | 82,4 |
| **Pb** | **RDS summer (n=17)** | 10,2 | 66,2 | 13,4 | 10,2 | 89,8 |
| | **RDS winter (n=17)** | 2,5 | 72,4 | 17,2 | 2,0 | 92,1 |
| | **1 (n=20)** | 1,9 | 78,7 | 11,3 | 8,1 | 91,9 |
| | **2 (n=33)** | 8,9 | 58,3 | 16,4 | 16,4 | 83,6 |
| | **3 (n=13)** | 4,7 | 71 | 15,8 | 8,5 | 91,5 |
| | **4 (n=29)** | 18,3 | 29,2 | 29,8 | 22,7 | 77,3 |
| | **5 (n=5)** | 7,3 | 66,4 | 13,6 | 12,7 | 87,3 |
| **Fe** | **RDS summer (n=17)** | 0,54 | 13,24 | 2,56 | 83,66 | 16,34 |
| | **RDS winter (n=17)** | 0,52 | 16,93 | 12,88 | 69,67 | 30,33 |
| | **1 (n=20)** | n.d. | n.d. | n.d. | n.d. | - |
| | **2 (n=33)** | 0,62 | 15,04 | 1,08 | 83,26 | 16,74 |
| | **3 (n=13)** | n.d. | n.d. | n.d. | n.d. | - |
| | **4 (n=29)** | n.d. | n.d. | n.d. | n.d. | - |
| | **5 (n=5)** | 0,3 | 21,2 | 2,2 | 76,3 | 23,7 |

Table 47: Mean element proportions in each extracted phase, as % of the total extracted content, for this study (RDS summer and winter) and other studies [1-Sutherland et al. (2012), 2-Kartal et al. (2006), 3-Sutherland et al. (2000), 4-Tokalioglu and Kartal (2006), and 5-Zhang and Wang (2009)].

The results of this speciation study confirm that for the analysed samples, Cr, Cu, Zn and Pb are mainly of anthropogenic origin in Manchester's RDS - most of these are concentrated in the mobilisable fractions defined by the BCR procedure. There are also marked differences in terms of potential mobility between the RDS collected in summer and winter, especially for Cu, Zn and Pb - there is a tendency for a larger mobility potential in summer due to the greater trace metal percentages in the most labile phases (exchangeable and reducible). Nevertheless, for each sample pair, total concentrations tend to be greater in winter - the fact that the fate of RDS in winter is mainly to be washed off from the surfaces due to the frequent and more persistent rain events poses a higher contamination risk to the urban river basin, as RDS is transferred between these environmental compartments and redox conditions change.

The summer season is characterised by larger accumulations of RDS on surfaces due to the more sparse rain events: these are mainly coarse sediments, as fine particles easily get not only washed off, but also resuspended in the atmosphere as sediment is dry for longer periods of time. As the proportion of Cu, Zn and Pb is greater in the most labile phases in summer, this poses a more direct risk to human health by inhalation of fine particles. Again, this apparent lower total metal concentration in these 17 summer samples might be due to the dilution effect of the coarser, quartz-dominated fraction, and grain-size normalization of RDS was not performed - individual speciation analysis of each grain size fraction needed to be undertaken to gain a better insight on the risks posed by the larger proportion of trace metals in the exchangeable and reducible fractions.

## 4.6. SEM-EDS analysis

Scanning electron microscopy has been used to investigate metal-bearing grain morphology in RDS, similarly to what has been described for soils in section 3.6. A total of five RDS-winter samples were selected for observation and localised chemical analysis under the SEM by energy-dispersive spectrometry - samples were prepared according to section 2.7. These samples were chosen according to their high total (XRF) contents in trace metals of environmental concern, namely Cr, Cu, Zn, As, Pb and Cd.

A general look at the RDS material revealed that its morphology is similar to that of soils, the main difference being the presence of a larger proportion of odd-shaped grains and grains made of compositionally distinct smaller particles. Besides geogenic grains such as quartz and rock fragments, mostly sourced from soils; fragments of brick, tarmac and construction materials are also abundant, as well as spherical metal-rich particles and anthropogenic metallic grains of diverse shape and size. A general view of Manchester's RDS can be observed below in Figure 69.

A total of 46 individual grains were observed under partial vacuum condition using backscattered secondary electron (BSE) imaging (15kV accelerating voltage, 15mm working distance) and their features were analysed by EDS. These grains of environmental concern were targeted in each sample

due to their distinctive brightness under BSE, as they contain elevated levels of elements of high atomic number. Table 48 summarises the types of RDS grains studied and Table 49 shows the basic statistics for the elements analysed. Note that the results of these tables are not representative of the overall abundance of the grain types and their composition in RDS samples, as the present SEM-EDS analysis is focused on the grain characteristics of those which contain high levels of elements of environmental concern.

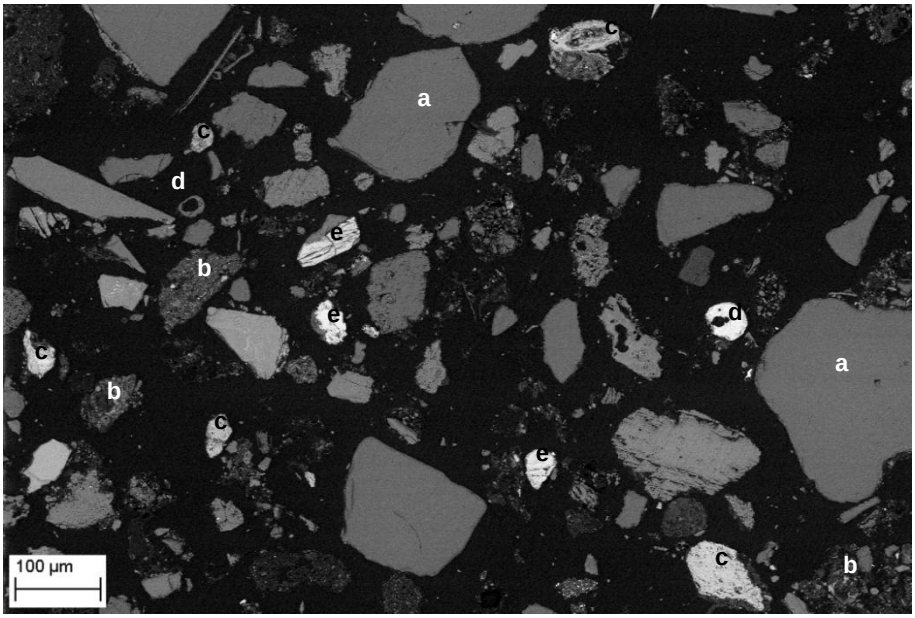


Figure 69: General view of Manchester RDS under the SEM (BSE imaging, partial vacuum, 15 kV accelerating voltage). a) quartz, b) mudstone / brick / agglomerate grains, c) iron oxides, d) spherical grains, e) other metal-rich grains.

| Grain type | N |
|---|---|
| Fe oxide | 8 |
| Pb-rich | 8 |
| Cr-rich | 6 |
| Fe-rich spherical | 6 |
| Zn/Ba-rich | 5 |
| Ti-rich | 5 |
| Rock/brick | 4 |
| Cu-rich | 2 |
| Fe-S | 1 |
| Ni-rich | 1 |
| Total | 46 |

Table 48: Grain types analysed by SEM-EDS in RDS (N=no. of grains).

| | N | Min | Max | Mean | Std Dev |
|---|---|---|---|---|---|
| Si | 46 | 2,34 | 22,00 | 6,84 | 5,08 |
| Al | 45 | 0,18 | 29,40 | 2,55 | 4,70 |
| Ca | 42 | 0,24 | 21,60 | 2,59 | 4,08 |
| Fe | 39 | 0,19 | 61,97 | 19,67 | 16,32 |
| Mg | 33 | 0,06 | 8,63 | 0,85 | 1,56 |
| Na | 33 | 0,02 | 4,11 | 0,75 | 1,07 |
| K | 28 | 0,02 | 3,28 | 0,64 | 0,88 |
| S | 25 | 0,01 | 24,42 | 1,95 | 5,10 |
| Cl | 20 | 0,04 | 0,80 | 0,15 | 0,16 |
| Ti | 15 | 0,08 | 27,47 | 6,70 | 9,43 |
| P | 12 | 0,03 | 0,29 | 0,10 | 0,09 |
| Mn | 10 | 0,14 | 12,63 | 2,41 | 3,99 |
| Pb | 10 | 0,48 | 42,69 | 13,88 | 14,29 |
| Ba | 7 | 0,31 | 35,98 | 16,49 | 15,04 |
| Mo | 6 | 0,29 | 21,02 | 4,29 | 8,28 |
| V | 6 | 0,04 | 0,16 | 0,11 | 0,04 |
| Cr | 6 | 0,03 | 15,57 | 4,62 | 6,95 |
| Zn | 3 | 0,77 | 3,51 | 1,72 | 1,55 |
| Cu | 3 | 0,28 | 36,51 | 14,32 | 19,44 |
| Ni | 2 | 0,70 | 4,99 | 2,85 | 3,03 |
| Co | 2 | 0,31 | 0,44 | 0,38 | 0,09 |
| Sn | 2 | 9,40 | 45,43 | 27,42 | 25,4771 |
| As | 1 | 0,45 | 0,45 | 0,45 | . |
| Zr | 1 | 8,07 | 8,07 | 8,07 | . |

Table 49: Descriptive statistics for elements analysed by SEM-EDS in RDS (N=no. of analysis, all values in wt.%).

The elemental concentrations summarised in Table 49 cover a significant range, as concentrations vary greatly according to the type of grain analysed. Therefore, concentrations were grouped by grain type and are displayed in the box-and-whisker plots of Figure 131, Appendix 4.

Silicon median concentrations are the highest, as expected for the analysed grains, in brick/rock fragments; but Pb-rich, Za/Ba-rich and spherical Fe-rich grains also display significant Si concentrations. Aluminium is also slightly more concentrated in brick/rock fragments and spherical grains; whereas high Ca, Na and K concentrations appear associated to Pb- and Zn/Ba-rich grains, as discussed further in this section. Iron, as expected, is the dominant element in Fe oxides, as well as in spherical Fe-rich grains, Cr-rich and Ti-rich grains. Chlorine is slightly more abundant in some Cr-rich grains found - Cr chloride is used as a pigment in many commercially available dyes, although Cr salts are generally considered toxic. Sulphur only displays significant concentrations in Zn/Ba rich grains and in the Fe-S rich grain (likely an iron sulphide mineral) analysed. Chromium-rich grains are also generally rich in Mg, Mn and V. Zinc and Ba appear to be associated closely in Manchester's RDS, as many grains show high levels of both these elements simultaneously. Each grain type is described more in detail in the following sections.

### *4.6.1. Iron oxide grains*

Manchester's RDS is rich in Fe oxide grains which are mainly of angular nature. Approximate sizes vary between 40 and 260 µm and Fe contents between 17 and 40%. Figure 70 below shows different iron oxide grains which are common in RDS. Grains a) and b) are composed of a Si-Fe matrix with Fe-rich exsolutions. These grains, from distinct sample locations, show a very similar morphology and composition - both also contain 0.56 and 1.39 % Ti. This kind of Fe-Ti oxides exsolutions are common in igneous rocks, which are believed to be the source of these grains in Manchester RDS - probably from the use of such rocks in veneering, cladding and pavements. Grains c) and d) exhibit a more complex internal structure, with banding, inclusions and dissolution textures. These are most likely rusted iron particles from the erosion of iron infrastructures. Massive Fe oxides can also appear joined to silicate material (quartz), such as in Figure 70 e-h.

a) 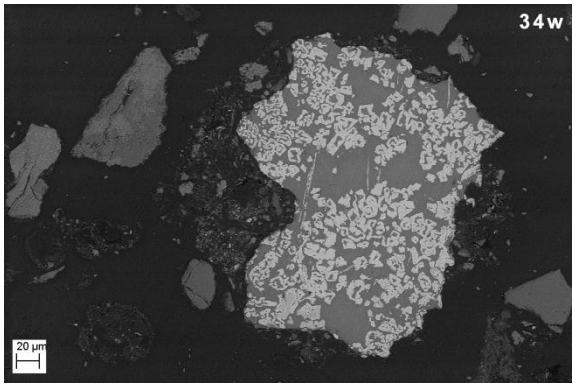

b) 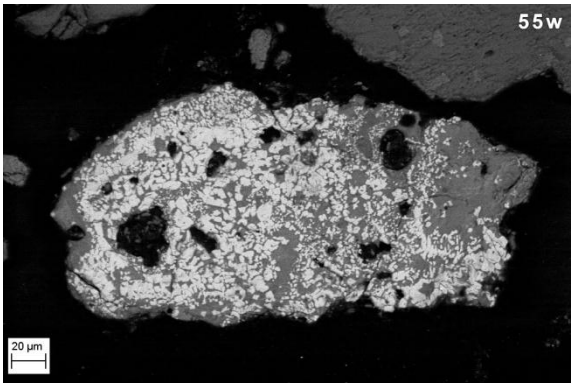

(cont.)

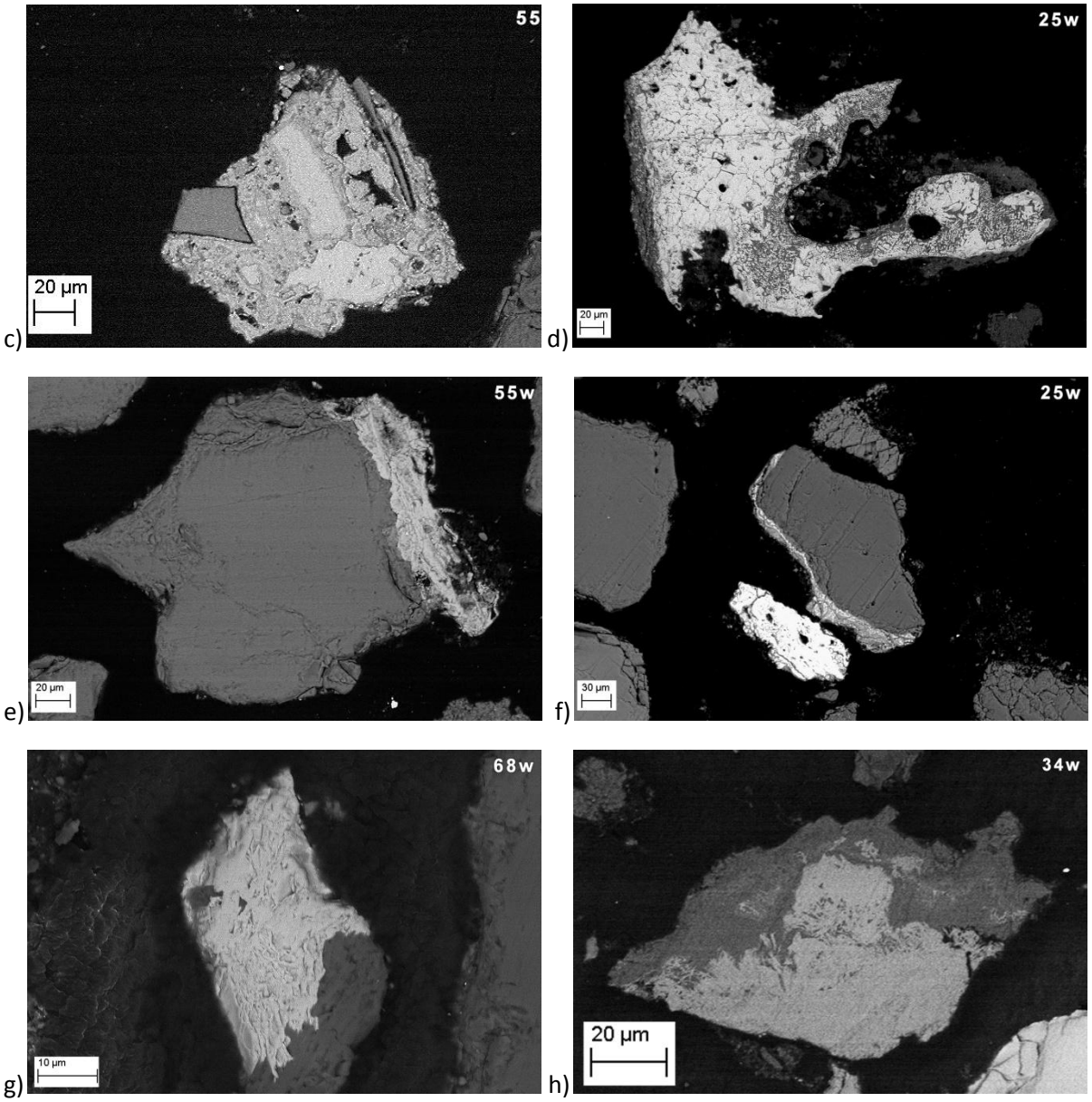


Figure 70: SEM images of Fe-oxide grains in Manchester RDS (BSE imaging, partial vacuum, 15 kV accelerating voltage) (a, b - Si-Fe matrix with Fe-Ti exsolutions; c, d - massive Fe grains with banding, inclusions and corrosion structures; e, f, g, h - massive Fe oxides joined to Si-rich material).

## *4.6.2. Iron-rich spherical grains*

Figure 71 represents different types of spherical Fe-rich grains found in Manchester's RDS. The iron content of these grains varies between 13 and 41.6% and other metals may also be present, such as Ti (c, 1.8%), Pb (d, 4800mg/kg) Co and Cu (e, 4400 and 2800 mg/kg, respectively). These compositions, together with the round shape, size (50-500µm) and the presence of air bubbles and other structures are in agreement to the origin of such grains, as described previously for soils: they result from high temperature combustion processes such as those of blast-furnace smelters (Fredericci et al., 2000; Hleis et al., 2013), or through burning of hazardous or municipal wastes (Liu et al., 2009; Kougemitrou et al., 2011). Besides atmospheric fallout of such particles, furnace slag

materials are also used in cement and other construction materials which are also a likely source of these particles in RDS. An example of this is illustrated in Figure 71f, a fragment of an agglomerate of such spherical particles - note that those containing high atomic number elements appear brighter under BSE conditions.

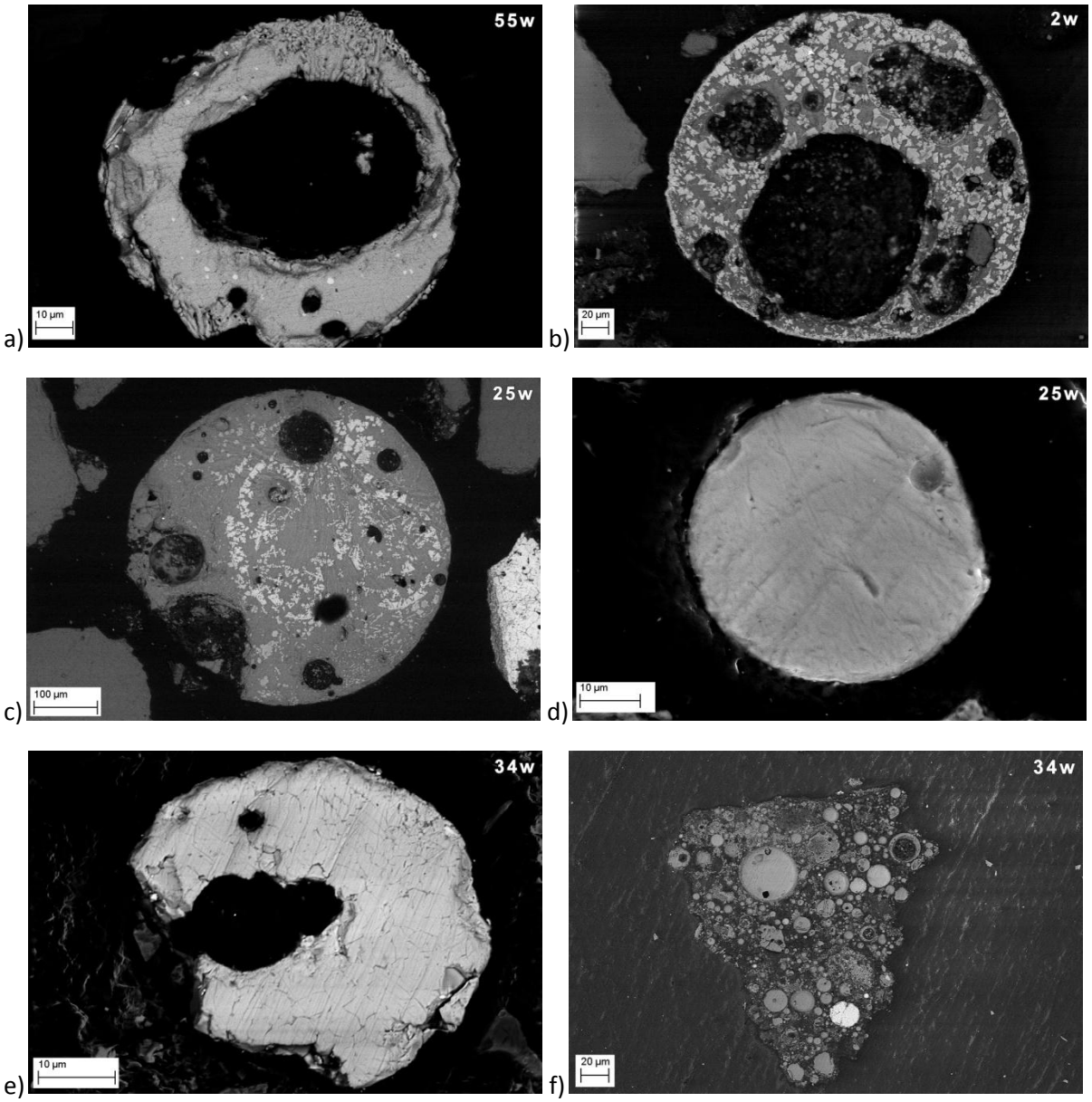


Figure 71: Iron-rich spherical grains in Manchester RDS (BSE imaging, partial vacuum, 15 kV accelerating voltage) (a - massive, with air bubble; b - Fe-rich exsolutions/crystallites in Si-rich matrix; c - Fe-Ti exsolutions; d - massive, Pb-rich; e - Co and Cu-rich; f - spherical particle agglomerate [probable slag fragment]).

It is evident that most of these grains show signs of disaggregation and/or dissolution, and their content in Si and Al is also significant - the potential release of iron and trace metals contained in spherical grains is might be high, according to the varying RDS physicochemical conditions.

### *4.6.3. Lead-rich grains*

The diverse morphologies of Pb-rich grains in Manchester RDS are shown in Figure 72. Massive textures such as grains a), b) and c) contain between 7 and 12 wt% Pb, whereas the agglomerate

texture grain (g-h) and the Fe grain with Pb-rich exsolutions (i, j) are the richest in Pb, containing 42.7 and 34.3 % Pb respectively.

Massive Pb grains of similar size (a-c) also show similar compositions: around 17% Si, 3% Ca and 1-3% Al; and no Fe has been detected.

In more heterogeneous grains, Fe is present and Pb may be also associated to Sn as in grain e) (45.4%Sn), or to a suite of other metals such as in grain f), which has the appearance of a torn metal sheet (~10µm thick) fragment - besides 4.42% Pb, it also contains 6.16% Cu, 3.51 Zn and 3100mg/kg Co. The grain in Figure 72d displays a low Pb content - 0.7% - and the presence of weathering / dissolution structures points to an advanced stage of Pb leaching.

As previously referred, grains g-h and i-j contain the highest Pb levels (42.7 and 34.3%). Grain i-j shows a banded texture rich in Fe (~39%) where lead crystals are incorporated near one edge - Fe content drops to 12% and Pb content goes up to 34.3% in the Pb-rich zone. Disaggregation of this kind of particles can lead to the formation of Pb-rich particles less than 2µm in size, which may be a source or airborne fine particulates in case of resuspension with human health risks associated.

An even larger risk may be posed in case of grain g-h: the close-up reveals that the lead particles (bright) are weakly bonded - not incorporated in a crystalline structure such as in grain i-j - and therefore they are very easily separated. Whereas the whole grain measures ~400 µm on its larger axis, the Pb particles generated by disaggregation can be as small as 0.1µm, or 100nm, which puts it into the ultrafine particle category. These are far smaller than the regulated $PM_{10}$ and $PM_{2.5}$ particle classes and are believed to have several more aggressive health implications than those classes of larger particulates (Heal et al., 2012). Road vehicles are the dominant anthropogenic source of ultrafine particles in urban environments to the atmosphere, contributing as much as 90% of total particle number concentrations (as particles less than 100nm are measured as number concentration per unit volume of air, rather than mass concentration) (Kumar et al., 2010). The spherical grain shapes which can be observed in Figure 73 (a magnified detail of Figure 72h) suggest these were generated by high temperature combustion processes, and then aggregated by Ca-Si-Al material.

a) 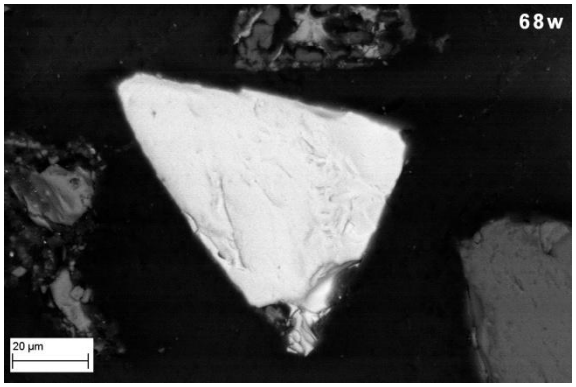


b) 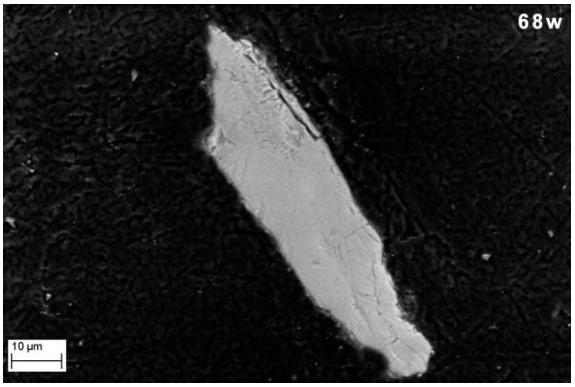


(cont.)

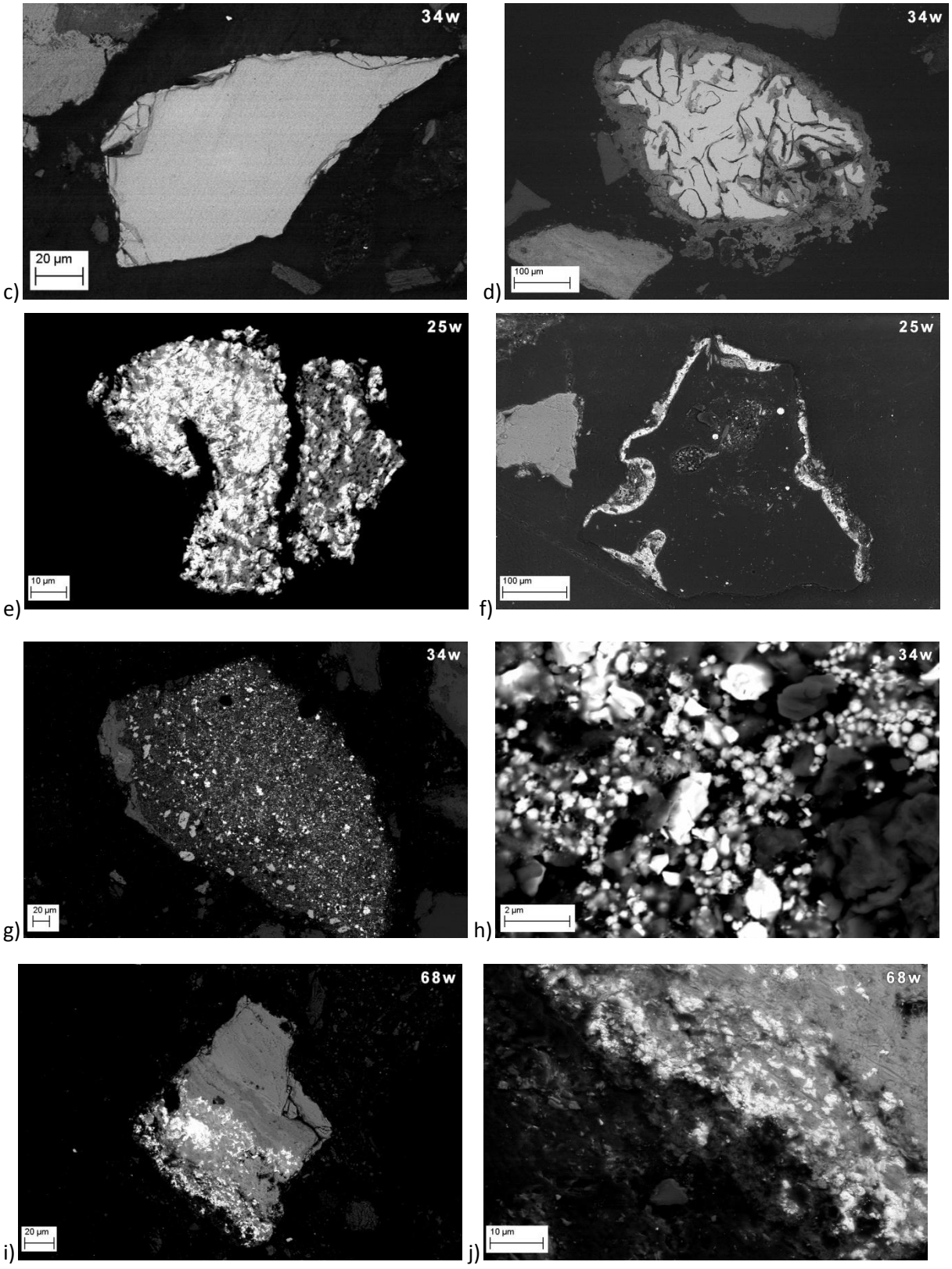


Figure 72: Pb-rich grains in Manchester RDS (BSE imaging, partial vacuum, 15 kV accelerating voltage) (a, b, c - massive; d - low Pb level, dissolution structures; e - Pb-Sn grain; f - probable torn metal sheet; g, h - agglomerate grain; i, j - Pb-rich areas in Fe-rich grain).

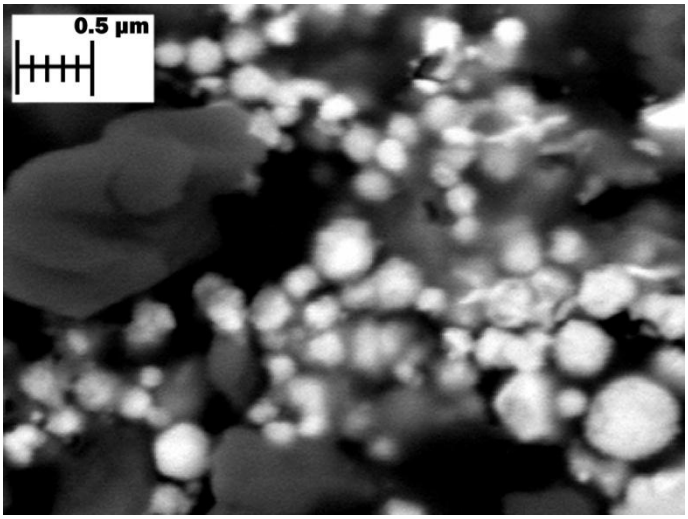


Figure 73: Detail of Pb-rich spherical particles of an agglomerate grain (represented in Figure 72 g-h, sample 34w).

## *4.6.4. Zinc and Barium-rich grains*

Figure 74 represents grains Ba-rich, crystalline silicate grains which are found in Manchester RDS - Si contents are ~11.6% and Ba varies between 5.6 and 23.8 wt%. Nevertheless, Ba appears in close association to Zn in aggregated-texure grains, as shown in Figure 75. Grain a-b is similar to that described previously for Pb: an aggregate-like texture of small, often <100nm Zn (7700 mg/kg) and Ba (34%) particles; bound within Ca-Si material. Grain c-d is larger in size and Zn-Ba rich particles also cover a wider range of sizes - between 0.5 and 30µm. Here, Zn content goes up to 0.9% and Ba up to 36%.

These might be coming from the same source - Ba-Zn additives are widely used as stabilisers in PVC manufacturing to make a range of paste PVC applications (Surgiewicz, 2012). They are the most commonly used stabiliser in flexible foils (e.g.: membranes, stationery and automotive applications), flooring, wall covering, flexible tubing and footwear. Tyre wear is also a known major source of Zn in the environment (Councell et al., 2004) - Zn species in RDS have also been reported to be mostly $Zn(NO_3)_2 \cdot 6H_2O$, $ZnCl_2$ and Zn-sorbed goethite, most likely from the wear and tear of car tyres and brake linings (Barrett et al., 2011).

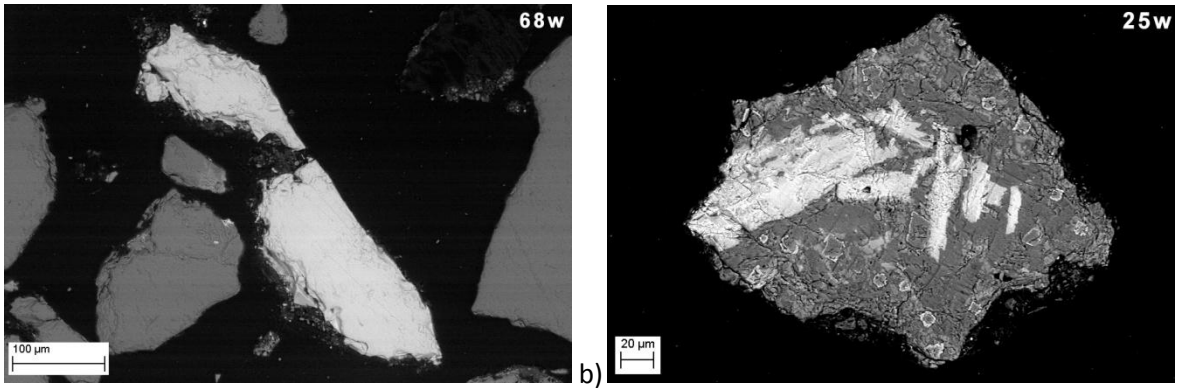


Figure 74: Ba-rich crystalline grains in Manchester RDS (BSE imaging, partial vacuum, 15 kV accelerating voltage).

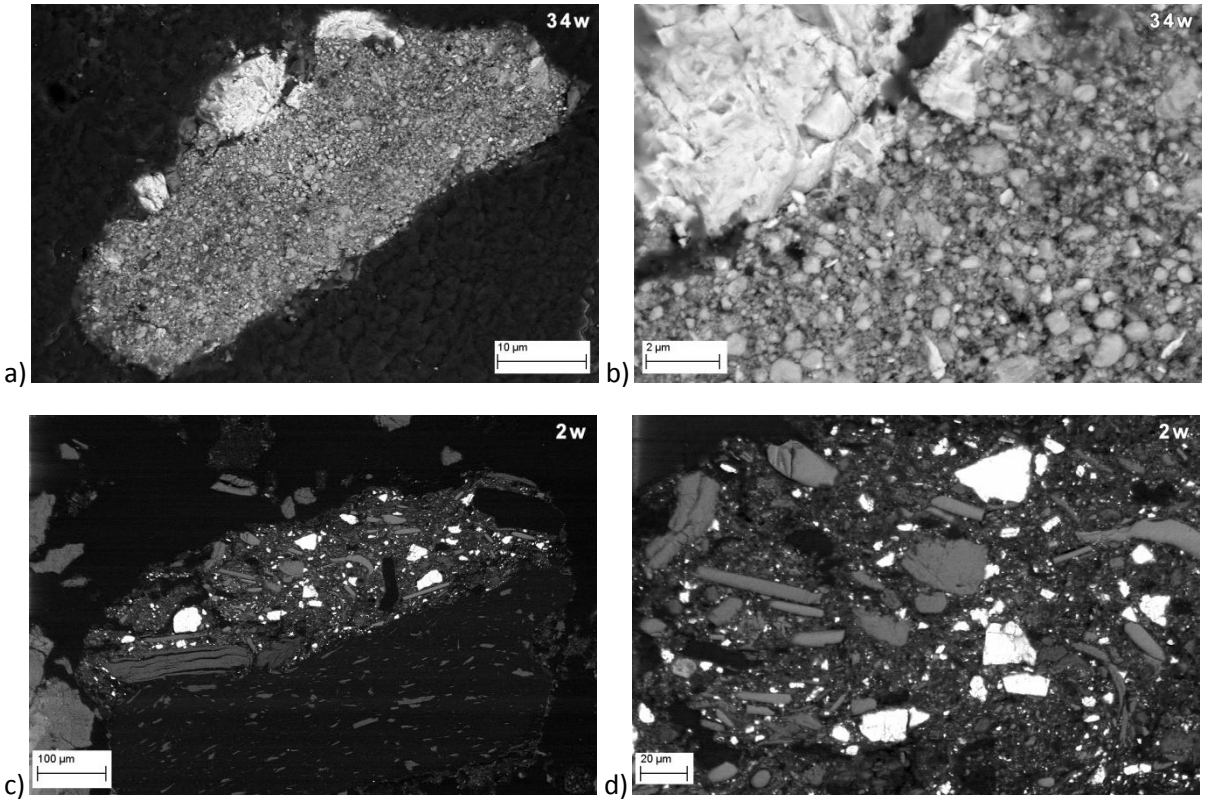


Figure 75: Ba and Zn -rich aggregate grains in Manchester RDS (BSE imaging, partial vacuum, 15 kV accelerating voltage).

These grains may contain low Zn concentrations (less than 1% Zn) compared to other grains rich in e.g. Pb and Cr; nevertheless, these Zn-containing grains are likely very abundant in RDS samples and therefore total Zn concentrations in Manchester RDS are the largest of the trace metals of environmental concern studied for the purposes of this work.

## *4.6.5. Chromium rich grains*

Chromium-containing grains in RDS can either be angular, massive and around 50-150µm size along the major axis (Figure 76a, b and c); or rounded and coarse (410µm) such as grain d), which also shows lenticular pores and signs of weathering. Chromium contents can go up to 15.6 and 11.2 wt% in grain types a- b; but c-d contain 2000 and 4000 mg/kg Cr, respectively.

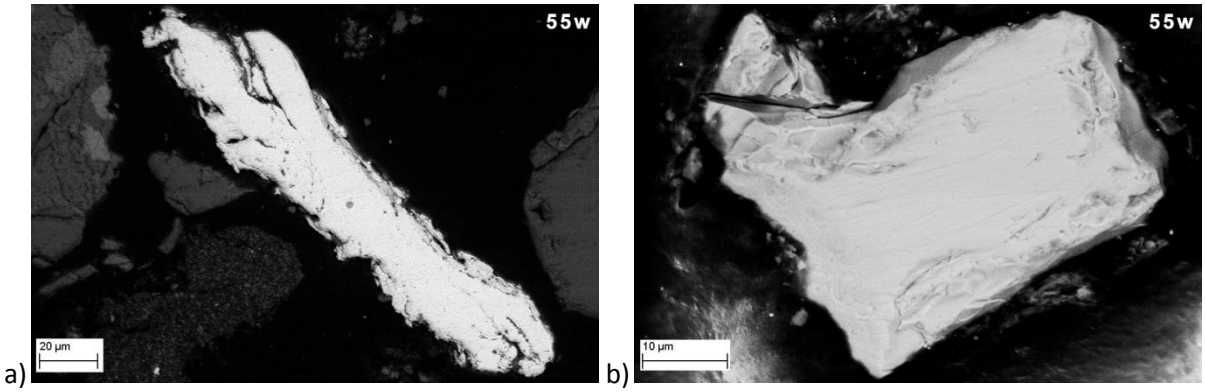


(cont.)

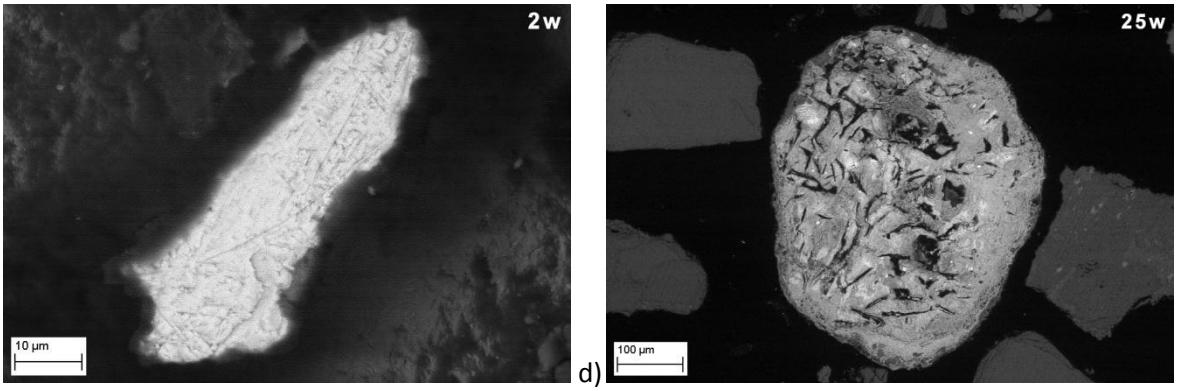


Figure 76: Cr-rich grains in Manchester RDS (BSE imaging, partial vacuum, 15 kV accelerating voltage).

Chromium-rich grains generally contain significant amounts of other metals: for example, grain a) contains ~5% Ni and 43% Fe, which is roughly the composition a Cr-Ni steel alloy. Nonetheless, Cr may come from diverse sources in RDS such as the wear and tear of Cr-plated materials, leakage of motor oils, or high temperature combustion processes such as waste incineration, ore smelting or coal burning (cf. section 1.3) - these sources are not unequivocally distinguished in the present SEM-EDS analysis.

## *4.6.6. Titanium-rich grains*

Titanium-rich grains are abundant in Manchester RDS and can be of various forms: Zn-rich phases can be incorporated in silicate minerals (Figure 77a), in grains made of platy, Ti-rich structures (b), as Ti-Fe alloys (c); or as exsolutions in an Al-Si matrix, these with the smallest Ti content (1.22 wt% max.). The other types of grains contain between 14.8 and 27.5 wt% Ti, together with significant amounts of Fe in grains a) and c) (20-25%); and Al-Si in grain b) (29 and 5.1%, respectively). Titanium is a naturally abundant metal and shows low toxicity, hence, it is widely used in the most diverse applications and the total concentrations found in RDS are unlikely to pose risks to human and ecosystem health.

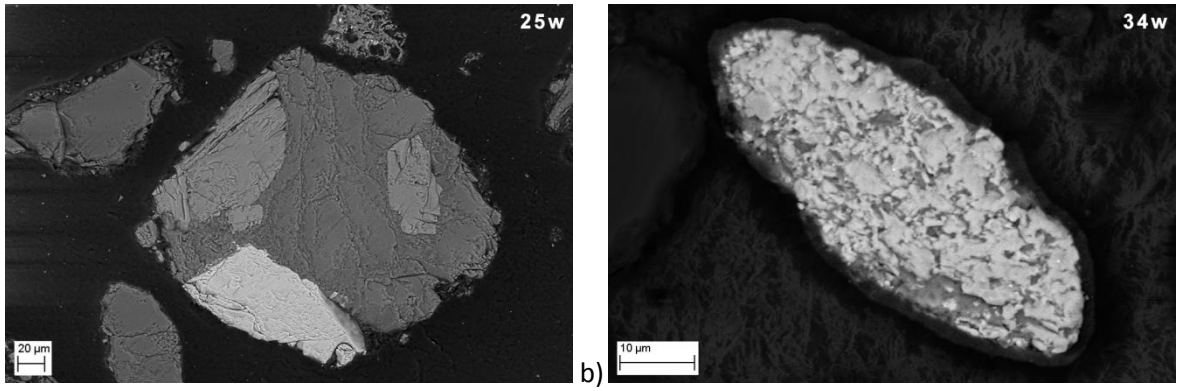


(cont.)

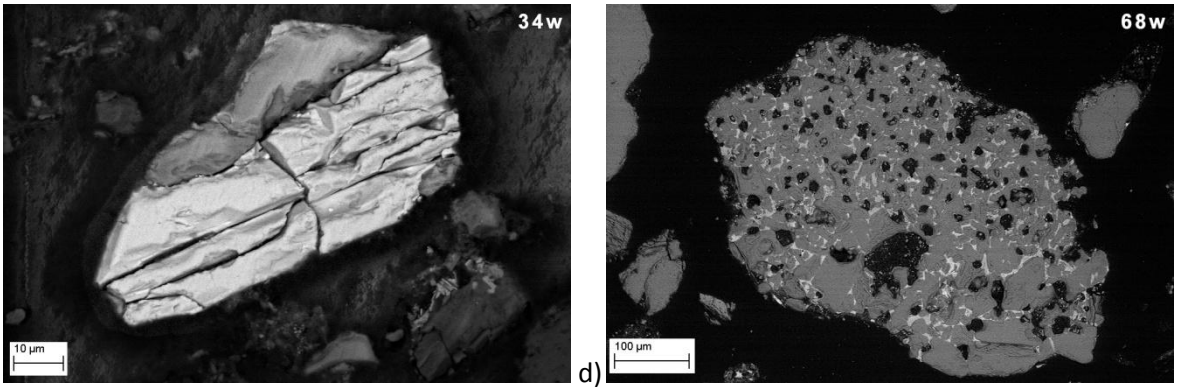


c) d)

Figure 77: Ti-rich grains in Manchester RDS (BSE imaging, partial vacuum, 15 kV accelerating voltage).

### *4.6.7. Molybdenum-rich grains*

A grain of this type is shown in Figure 78. Here, a Ca-rich matrix (21.6 wt%) hosts Mo (21.02%) and Mn (12.6%) spherical structures. The source of these grains and how they originated would require a more profound mineralogical study. Nevertheless, it provides evidence that detailed grain composition is a good insight into the complex issue of RDS contaminant apportionment.

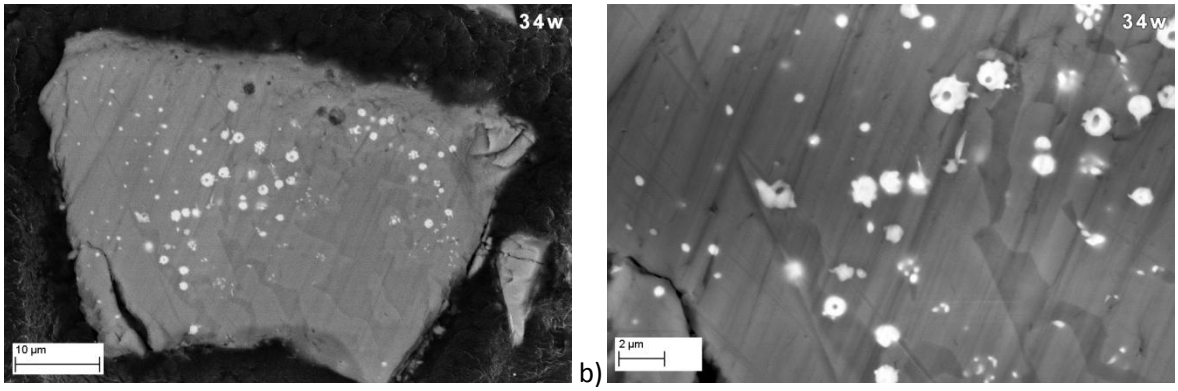


a) b)

Figure 78: Mo-rich grains in Manchester RDS (BSE imaging, partial vacuum, 15 kV accelerating voltage).

## 4.7. Multivariate statistics: Principal component analysis and component score mapping

In order to recognize the pattern of correlations between the analysed elements and other variables, RDS data were subject to principal component analysis (PCA) using IBM® SPSS 19 software, according to the method described in section 2.9.2. This method allows the reduction of the number of variables by identifying the pattern of covariances or correlations among them: the resulting new variables (principal components) are linear combinations of the observed variables. Subgroups of original variables are therefore identified and their interpretation and mapping provide better insight on the element sources and associations. Variables were subject to standardization prior to PCA analysis.

## *4.7.1. Analysis A*

The first set of PCA analysis (reference #A) was performed for summer and winter datasets, using 49 variables (chemical elements, organic matter, volume-weighted mean diameter and percentage of <63µm grain size fraction), and retaining the components with an eigenvalue greater than 1, as per the Kaiser criterion (cf. section 2.9.2). For the RDS-summer (RDSs) dataset 11 components were extracted, whereas 10 were extracted for RDS-winter (RDSw). Table 50 shows the KMO and Bartlett's sphericity tests for RDS summer and winter data. The KMO values of 0.710 and 0.712 found for RDS datasets indicate that there is a good adequacy of the RDS datasets to apply the PCA method - the patterns of correlations are relatively compact and therefore PCA should yield distinct and reliable factors.

a)

| KMO and Bartlett's Test | | |
|---|---|---|
| Kaiser-Meyer-Olkin Measure of Sampling Adequacy | | ,710 |
| Bartlett's Test of Sphericity | Approx. Chi-Square | 4349,645 |
| | df | 1176 |
| | Sig. | ,000 |

b)

| KMO and Bartlett's Test | | |
|---|---|---|
| Kaiser-Meyer-Olkin Measure of Sampling Adequacy. | | ,712 |
| Bartlett's Test of Sphericity | Approx. Chi-Square | 4625,677 |
| | df | 1176 |
| | Sig. | ,000 |

Table 50: Results for the KMO and Bartlett's tests for RDS geochemical data; a) summer and b) winter (#A, n=72, 49 variables).

Communalities for RDS data are displayed in Table 99, Appendix 4. Most of the variance associated with each variable is common, or shared variance - variables with communalities close to 1 (100%) have none or little specific variance (or random variance). The lowest values (which are still satisfactory) are observed for $Na_2O$ and Sm in RDSs; and for W, Sm and Yb in RDSw.

The eigenvalues associated with each linear component before extraction, after extraction and after rotation are listed in Table 100 of Appendix 4. From the 49 linear components identified (there are always as many eigenvectors as initial variables), 11 show eigenvalues above 1 for RDSs and 10 for RDSw. The chosen components explain 83.4% of the total RDSs variance and 83.3% for RDSw. It is also noticed that the first four components explain most of the variance, and subsequent components explain gradually less. This tendency can also be seen in the eigenvalues, represented in the scree plots of Figure 79. The dashed line is the cut-off level for component extraction using the Kaiser criterion in this analysis; the arrow represents the inflection point of the graph for later analysis. For a more in-depth explanation of these tables and their significance, cf. sections 2.9.2 and 3.7.1 .

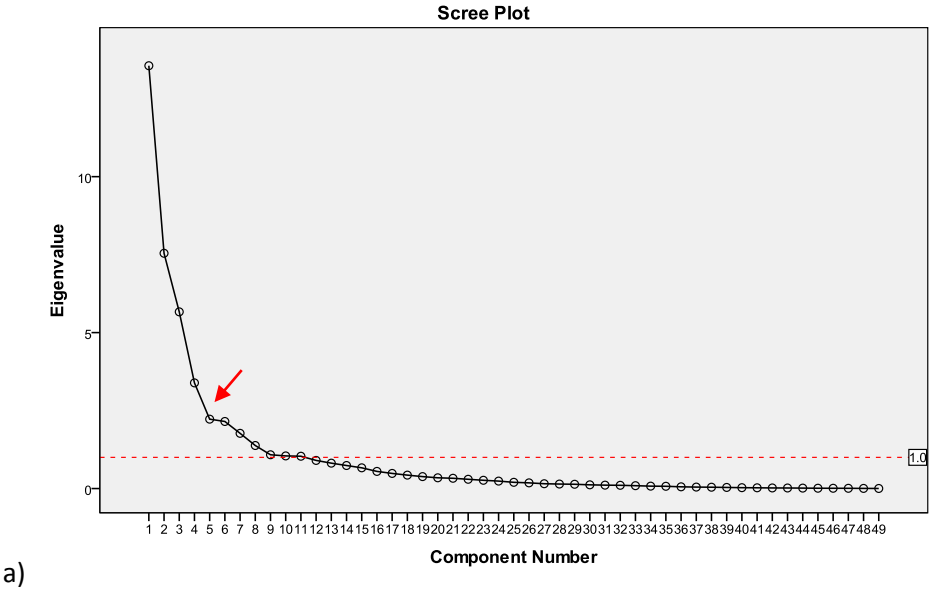


a)

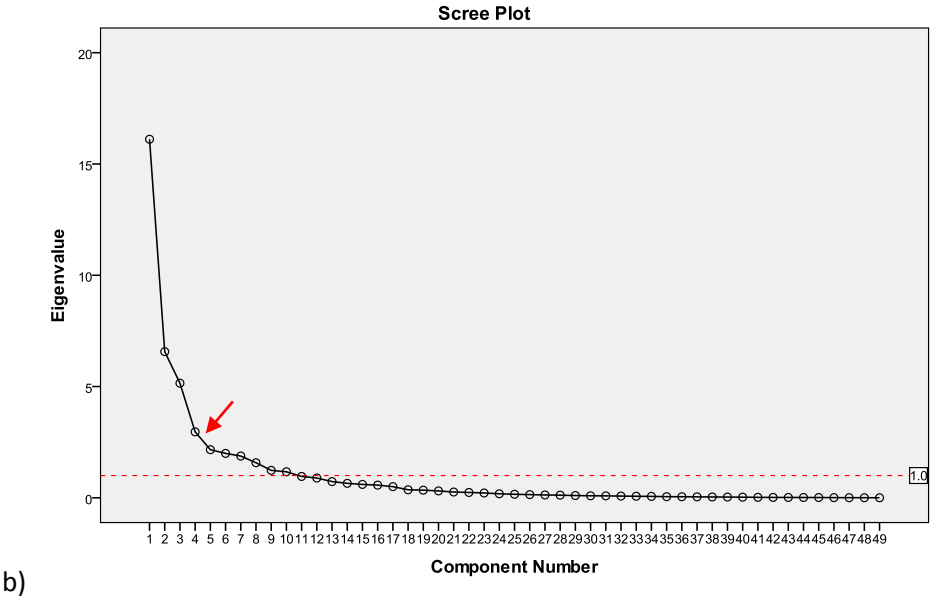


b)

Figure 79: Scree plots - Components vs. eigenvalues for RDS geochemical data: a) summer and b) winter. (PCA #A, n=72, 49 variables).

To maximise variable loadings onto each component, orthogonal Varimax rotation has been chosen. Table 101 of Appendix 4 shows the rotated component matrix, which is one of the most important PCA outputs - it reveals variables with the highest loadings onto each component, i.e. have a similar variation pattern across the dataset. In geochemical terms, the elements with highest loadings onto each component can be interpreted as those derived from similar sources or enriched through similar processes. Loadings above 0.7 are flagged in red and, for an easier visualisation, variables with highest loadings onto each component are summarised below in Table 51 and Table 52, classified by loading magnitude. Colours indicate similar element groupings between RDSs and RDSw.

| | | Element loading - RDSs | | |
|---|---|---|---|---|
| | | ]1.0, 0.7] | ]0.7 - 0.6] | ]0.6 - 0.5] |
| component | 1 | MgO, $Al_2O_3$, $TiO_2$, MnO, $Fe_2O_3$, Sc, V, Co, Ni, Ga, Nb | Y | - |
| | 2 | Ba, Cu, Zn, Pb, Sr, Mo, Sn, Sb | - | |
| | 3 | Th, La, Ce, Nd | Y | $Al_2O_3$, $K_2O$, Rb |
| | 4 | $P_2O_5$, Br, I, S, LOI | - | Se |
| | 5 | Cr, Zr, Hf | - | - |
| | 6 | 63-inf2 | Ge | As |
| | 7 | - | | $K_2O$, Rb |
| | 8 | Bi, Cd | - | - |
| | 9 | | - | Sm |
| | 10 | Yb | - | - |
| | 11 | W | - | - |

Table 51: Summary of element loadings onto each calculated component (1 to 11) for RDS-summer (PCA #A, n=72, 49 variables).

| | | Element loading - RDSw | | |
|---|---|---|---|---|
| | | ]1.0, 0.7] | ]0.7 - 0.6] | ]0.6 - 0.5] |
| component | 1 | MgO, $Al_2O_3$, $TiO_2$, MnO, $Fe_2O_3$, Sc, V, Co, Ni, Ga | Y, Nb | - |
| | 2 | Ba, Cu, Zn, Pb, Sn, Sb | Cr, Sr, Zr | Hf, W |
| | 3 | $K_2O$, Rb, Th, La, Ce | $Al_2O_3$, Nd | Ga, Y, Nb |
| | 4 | $P_2O_5$, Se, Br, I, S, LOI | - | - |
| | 5 | Ge, As | - | - |
| | 6 | CaO | - | - |
| | 7 | Bi, Cd | - | - |
| | 8 | - | 63-inf2 | - |
| | 9 | Cl | $Na_2O$, Mo | - |
| | 10 | U | - | Sm |

Table 52: Summary of element loadings onto each calculated component (1 to 10) for RDS-winter (PCA #A, n=72, 49 variables).

The component plots in Figure 80 and Figure 81 below display the element loadings onto each of the first three components, which were split into bi-dimensional plots: Component 1 vs. 2, component 1 vs. 3, and component 2 vs. 3. The element groupings highlighted in Table 51 and Table 52 can be easily identified.

The first pertinent observation from the principal components calculated is that element groupings (e.g. elements with high loadings onto the same component) are very similar between summer and winter, revealing a consistency in element sources and/or accumulation processes between the two seasons. Therefore, the plots of Figure 80 and Figure 81 (displaying components 1, 2 and 3) are also similar in element distribution - the groups defined by the coloured limits are similar.

Each component is described in more detail as follows.

•**Component 1** accounts for 19.6% of the total variance of RDSs and 17.9% in RDSw, after rotation. It displays high loadings (>0.7) for $Al_2O_3$, MgO, $TiO_2$, MnO, $Fe_2O_3$, Sc, V, Co, Ni, Ga and Nb. While some of these are generally strong geogenic elements – i.e. elements related to mineralogical components such as Al, Ga and Mg (and Ti, Mn and Fe to a lesser extent); Sc, V, Co and Ni are siderophile or chalcofile elements, which may be enriched by anthropogenic activities. These last elements are also grouped in the same component in soils (cf. section 3.7.1), and have been commonly associated in soils to several minerals (Co-Ni-Fe arsenides and sulphides) and coal extraction / burning. Nevertheless, the grouping found in this PCA analysis suggests that all these elements may come

from the same source, namely soils, where Co, Ni, Fe, Sc and V are enriched due to historical coal burning activities. Therefore, in RDS, elements with a high loading onto component 1 may be interpreted as mainly derived from soil material.

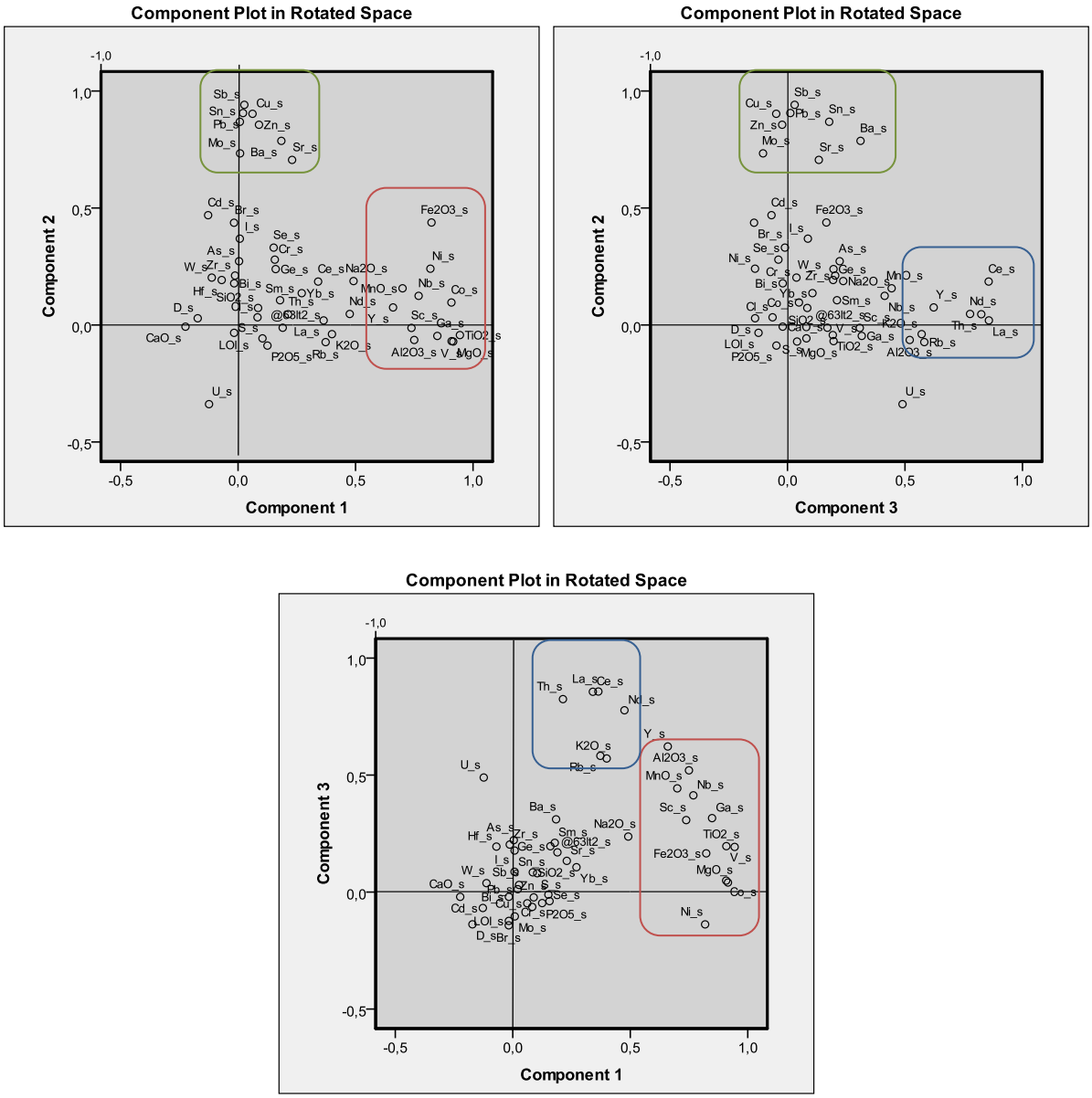


Figure 80: Component plots for components 1 vs. 2, 2 vs. 3 and 1 vs. 3, for RDS summer data (PCA #A, n=72, 49 variables).

•**Component 2** accounts for 14.8% of the total variance for both summer and winter datasets. It comprises high loadings (>0.7) for Ba, Cu, Zn, Pb, Sr, Sn and Sb, which are known anthropogenically-enriched elements in RDS. Sources of these elements in Manchester's RDS seem to be related to industrial activities, as pointed out further in this text. In winter, Cr also shows a high loading (>0.6) onto this component.

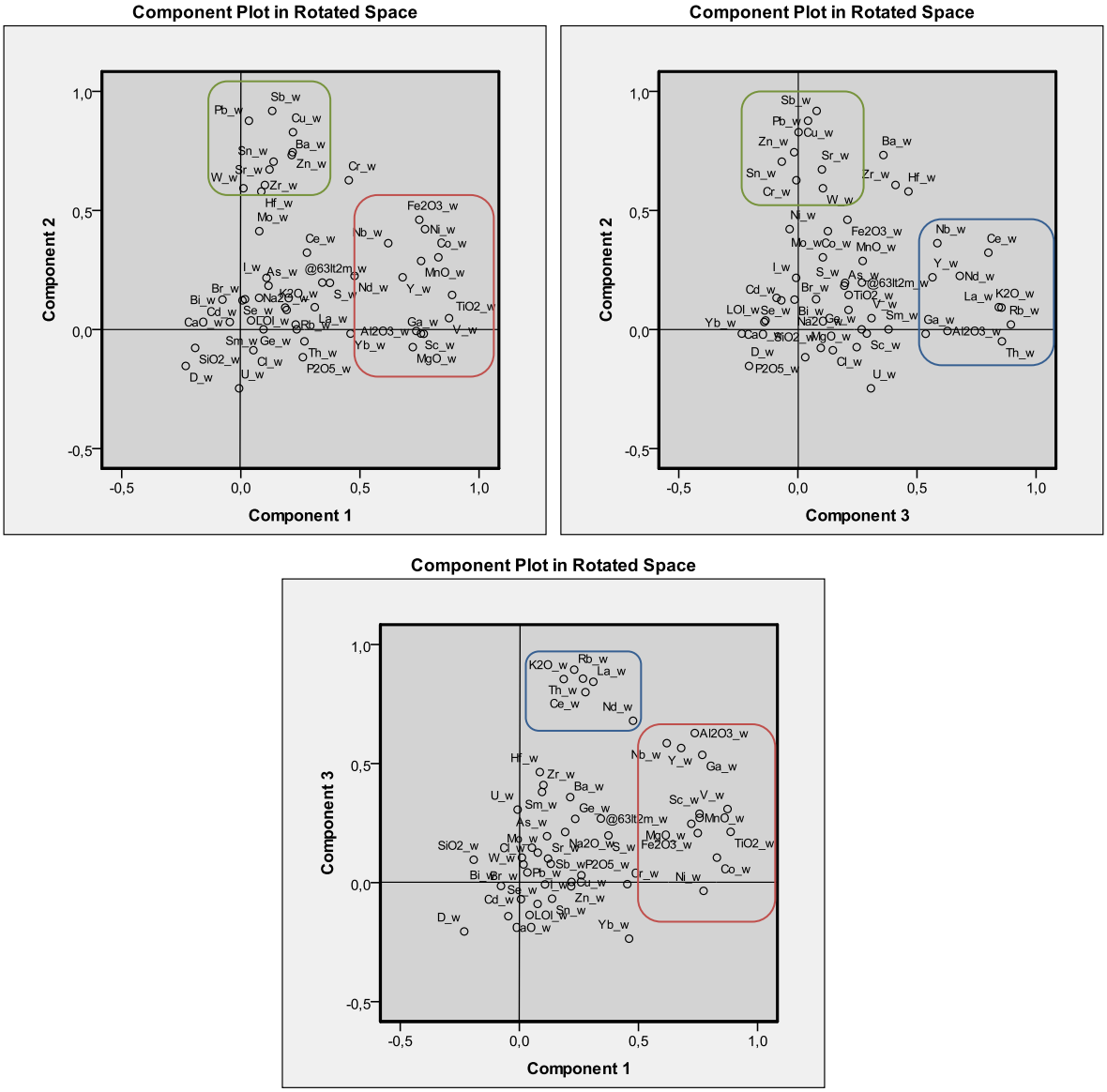


Figure 81: Component plots for components 1 vs. 2, 2 vs. 3 and 1 vs. 3, for RDS winter data (PCA #A, n=72, 49 variables).

•**Component 3**, which accounts for 11.3 and 14.5% of the total variance in RDSs and RDS, respectively, displays the highest loadings for the REE elements La, Ce, Nd, Th and Y; and also for $Al_2O_3$, $K_2O$ and Rb. These are strong geogenic elements, which are present primarily in igneous rocks: $Al_2O_3$, $K_2O$ and Rb are abundant as feldspar, and REE are usually enriched in igneous minerals, and especially in monazite and xenotime. Nevertheless, through weathering processes, these elements become part of sedimentary rocks and REEs tend to be concentrated as they are present in heavy, resistate minerals. The fact that they are clustered in component 3, accounting for a great part of the total variance of the datasets, suggests that these elements may be sourced to RDS by the gritstone and igneous rocks that are used as kerbstones in Manchester's streets, as pavements, or in buildings - most of the raw materials have been reported to come from the Namurian Millstone Grit Group rocks (Johnson and Fletcher, 2011). Nevertheless, modern and more cost-effective kerbstones used

as British standards are made of rock aggregates or concrete, which are also likely sources of these elements to RDS.

•**Component 4** accounts for 10.7 and 11.5% of the total variance in summer and winter, respectively. High loadings (>0.7) are found for organic matter (LOI), Br, I, S, Se and $P_2O_5$, which are elements associated to the organic fraction of RDS which come mainly from nearby soils or from plant and leaf litter which accumulates on surfaces. Bromine and I are closely related to soil organic matter contents (Maw and Kempton, 1982; Gerzabek et al., 1999), as well as S, Se and P (Chesworth, 2008).

•**Components 6 (RDSs)** and **5 (RDSw)** explain 4.9 and 4.4%, respectively, of the total variance of the each dataset. Arsenic and Ge have high loadings onto this component, together with the grain size fraction below 63µm in the summer dataset. Germanium is a Group IV element of the periodic table - it shares properties with C and Si in what concerns valence electrons and therefore is widely used in n-type or p-type semiconductors. Arsenic is added to germanium in the production of semiconductor devices such as transistors and integrated circuits, and also used in laser and light-emitting diodes (LEDs) to convert electricity directly into light. Also, arsenic-germanium chalcogenide glass and glass fibres are used e.g. in highly pure optical glasses (lenses), rewritable CDs and DVDs, optical fibre cables and a number of electronic applications (Bordovskii et al., 2013). The clustering of these two elements onto the same component may be related to this compound and, for RDS collected in summer, it might be more concentrated in the fine fractions of the sediment.

•**Components 8 (RDSs)** and **7 (RDSw)** explain a considerably lower percentage of the total variance: 3.25 and 4.2%, respectively for RDSs and RDSw. Cadmium and Bi display a high loading values on this component, probably related to Sn-Bi-Cd alloys, more commonly known as “Wood’s Metal”, which are used in low-temperature eutectic solders e.g. for the bonding of glass components to metal frames and chassis where high soldering temperatures are not possible; or in light electrical and electronic assemblies (ICdA, 2013). This kind of solder came to replace Pb-containing solders for automotive applications (Lee, 1997).

•**Component 9 in RDS-winter** shows high loadings for Na and Cl and accounts for 4.1% of the total variance: these elements are the main composition of road gritting salts, which are applied to Manchester city streets during winter time to prevent snow and ice accumulation.

• **Components 9, 10 and 11 (RDSs)** and **components 6, 8 and 10 (RDSw)** should not be interpreted as to element sources and associations - either only one variable displays a high loading value, or the component only represents a small percentage of the total variance.

Component scores calculated by PCA analysis were saved as new variables, as they represent each sample placement on the calculated component. Component scores were mapped, similarly to what has been done with total XRF concentrations, after exporting the component data to ESRI® ArcGIS™

10.0 software - in geochemical terms, principal components represent groups of elements with similar variation within a set of observed variables. Scores were interpolated using the IDW method (cf. section 2.9.5 and the Theoretical Framework) - this method has been chosen as it is more suitable to reflect sharp local variations.

Interpolation of component scores to uncalculated areas was performed using 300m as the output cell size and a variable search radius, as samples are unevenly distributed in the study area - 12 nearest input sample points were used to perform interpolation. These maps are used to highlight areas where the component score is the highest: the elements represented by the mapped component show the highest concentrations in the areas shaded in red. Figure 82 below represents component 1 scores for RDS summer (a) and winter (b). This component is dominated by $Al_2O_3$, MgO, $TiO_2$, MnO, $Fe_2O_3$, Sc, V, Co, Ni, Ga and Nb, which are believed to be sourced from soils, as described previously.

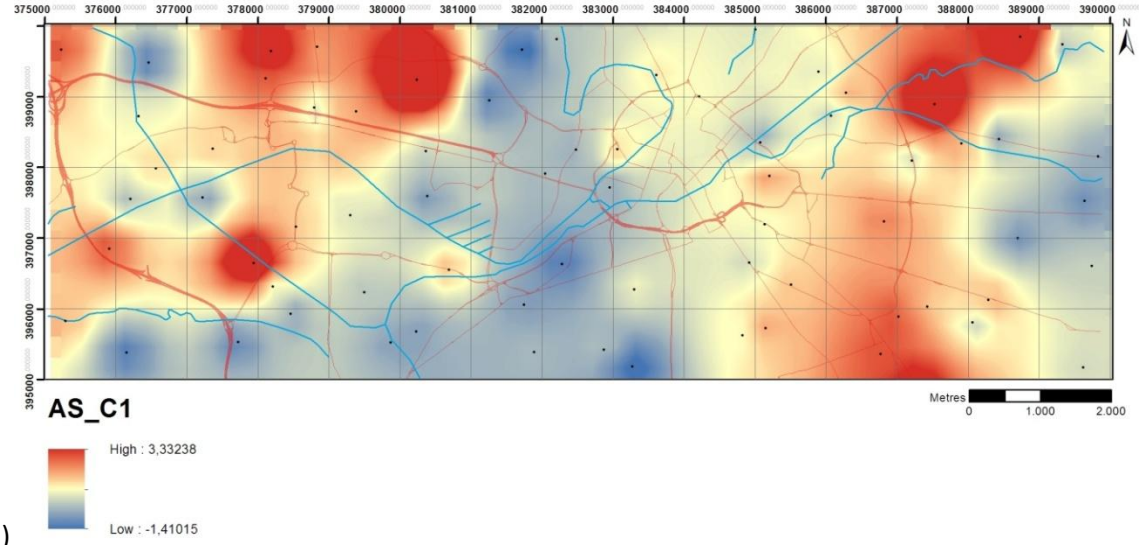


a)

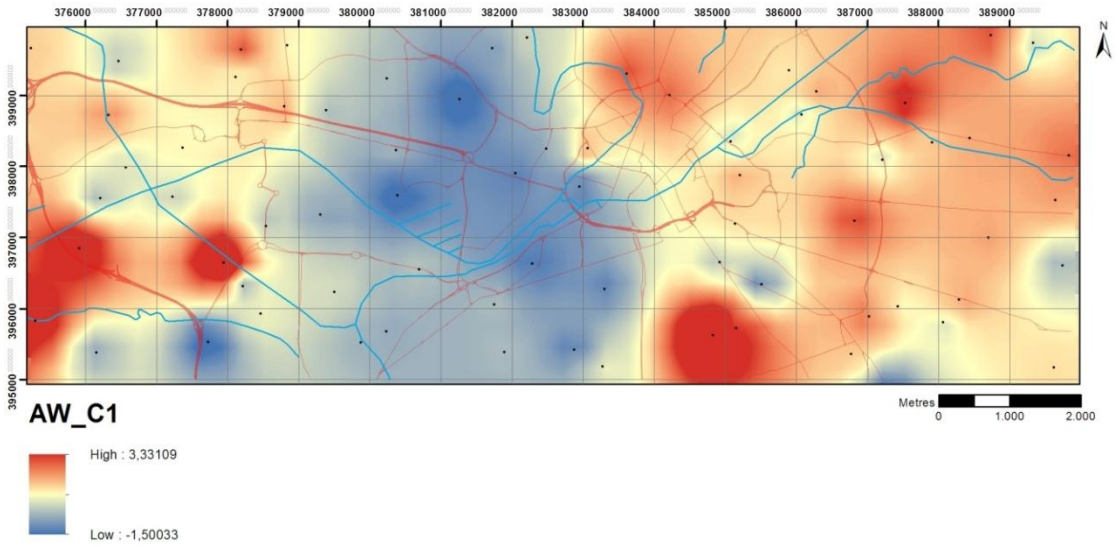


b)

Figure 82: Spatial distribution of component 1 scores for RDS data: a) summer and b) winter (PCA #A, n=72, 49 variables) (cf. Table 51 and Table 52 for represented elements).

This hypothesis is reinforced as 9 out of the 10 samples with the highest scores for component 1 were indeed collected from streets along gardens, parks or vacant land plots - at these locations, RDS samples were generally collected on the street pavements less than 4 meters away from the soil limit.

Component 2 is represented below in Figure 83. This component, which represents Ba, Cu, Zn, Pb, Sr, Sn and Sb, is stronger in the Trafford Park industrial estate between the Manchester ship canal and the Bridgewater canal, where industry is concentrated along with heavy goods transport.

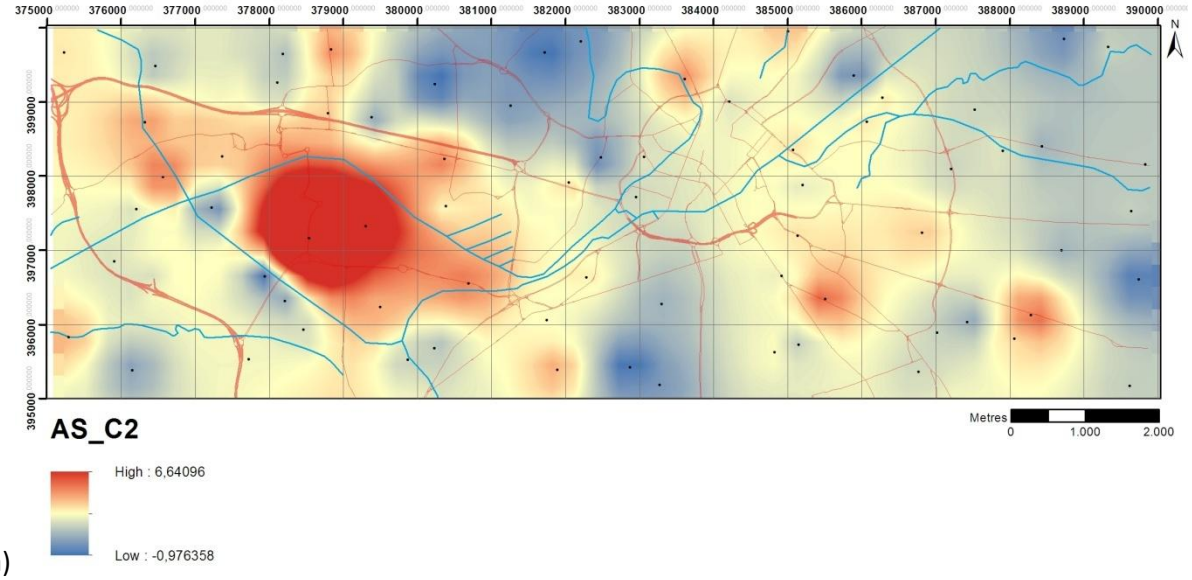


a)

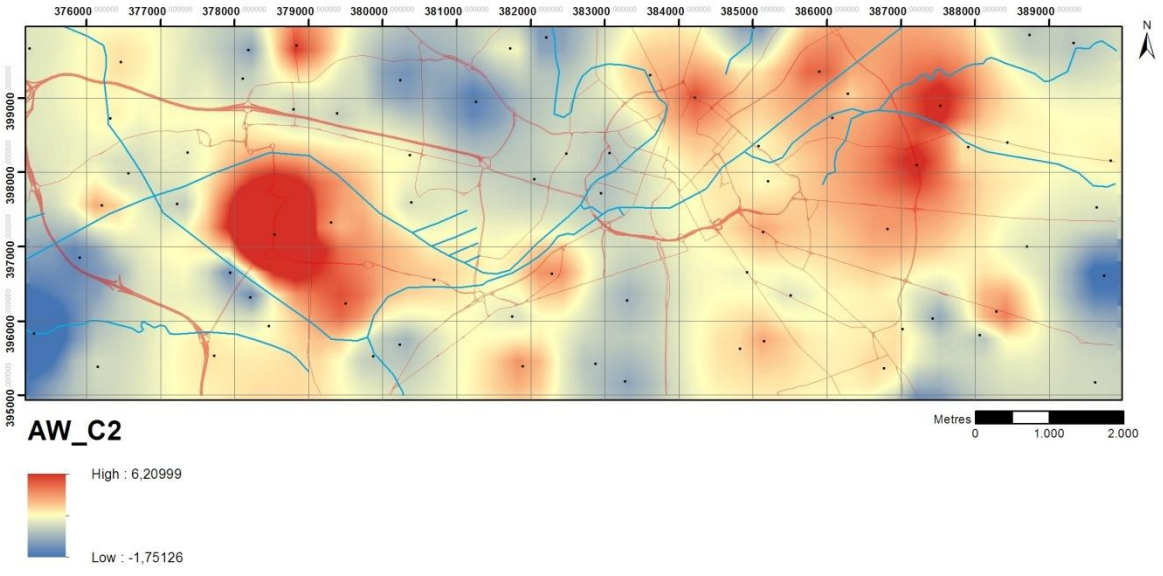


b)

Figure 83: Spatial distribution of component 2 scores for RDS data: a) summer and b) winter (PCA #A, n=72, 49 variables) (cf. Table 51 and Table 52 for represented elements).

In winter (b), component 2 also displays elevated scores in the northeast part of the study area, namely in one sample collected in a dual carriageway. Strong industrial activity seems to be the main source for the elements this component represents.

Component 3, which has the highest loadings for $Al_2O_3$, $K_2O$, Rb and the REE elements La, Ce, Nd, Th and Y, represents mainly geogenic minerals which are thought to be derived from the kerbstones, buildings and pavements made of gritstone, granite (in the commercial sense) and granite aggregates. Seven out of the 9 samples which show the highest loadings for this component are close to kerbs or pavements made from rock aggregates, as can be observed in Figure 85.

Component 4 scores are mapped below in Figure 86. This component represents elements related to the organic fraction of RDS (Br, I, S, Se and $P_2O_5$) - the red shades in Figure 86 represent samples with the highest organic matter content (LOI), always above 20%. The more spread pattern found for winter samples is due to the greatest organic matter contents (and chemical elements associated) in this season.

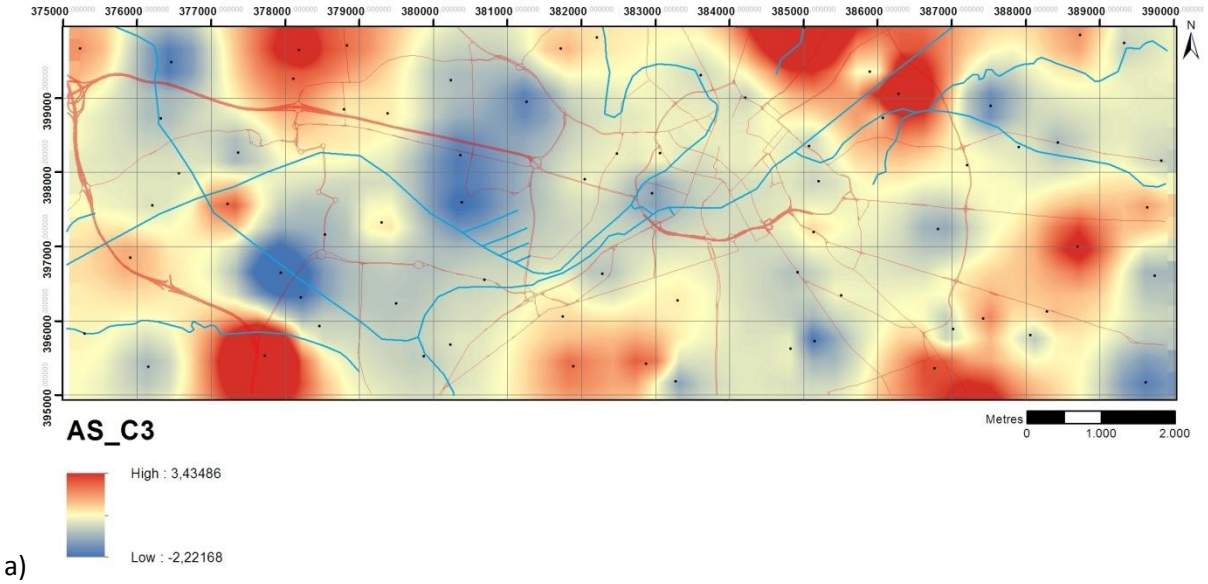


a)

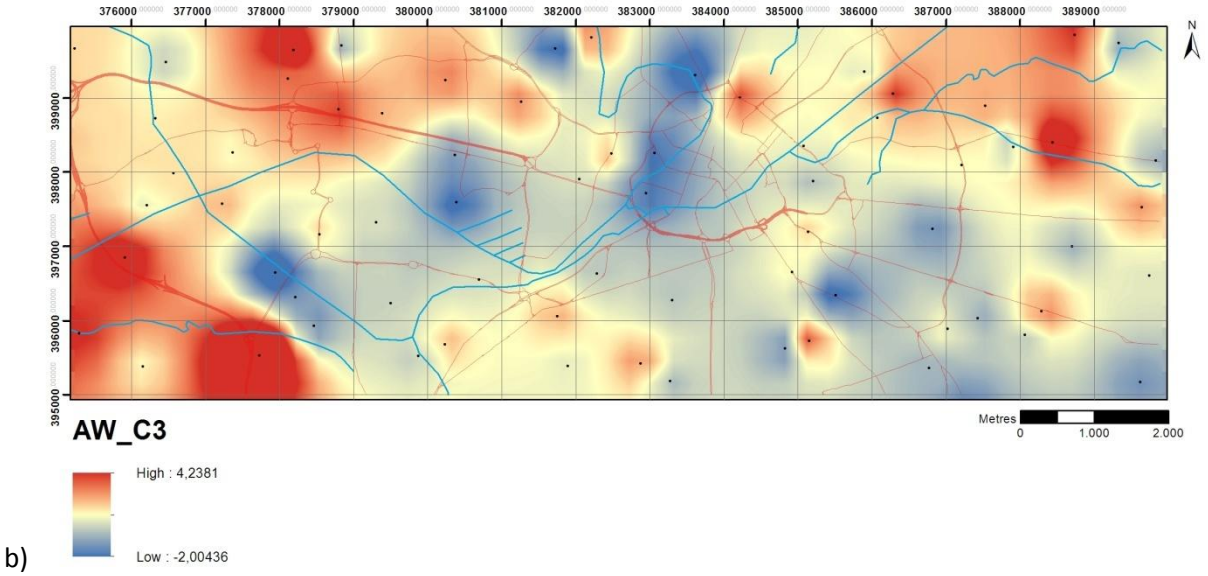


b)

Figure 84: Spatial distribution of component 3 scores for RDS data: a) summer and b) winter (PCA #A, n=72, 49 variables) (cf. Table 51 and Table 52 for represented elements).


Figure 85: Photographs of RDS samples (bags) showing kerbstones and sidewalks made of rock aggregates.

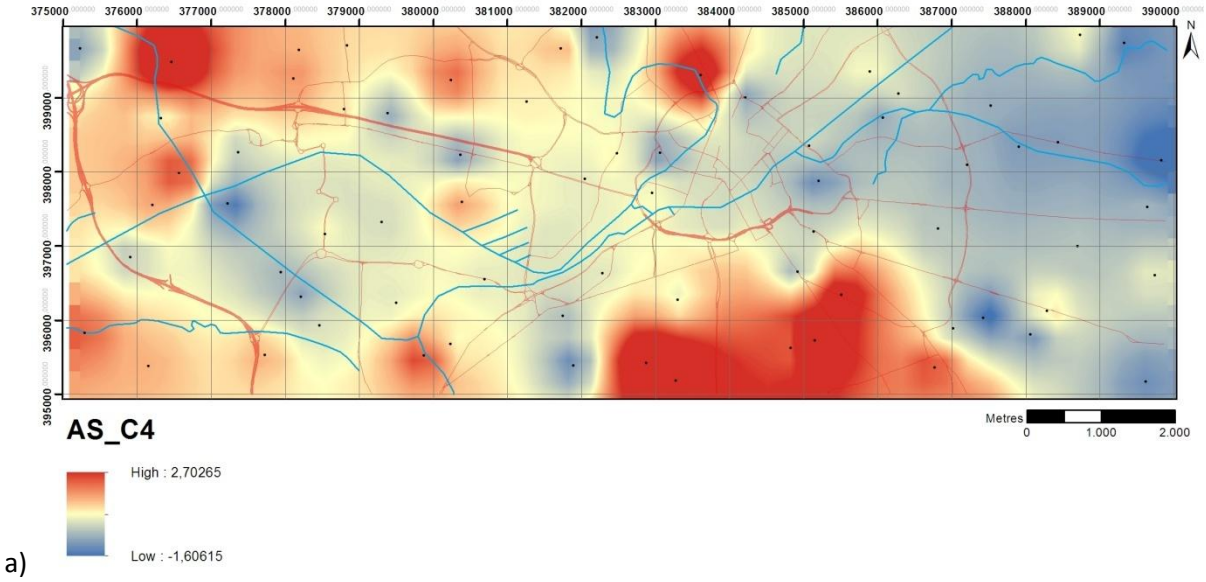


a)

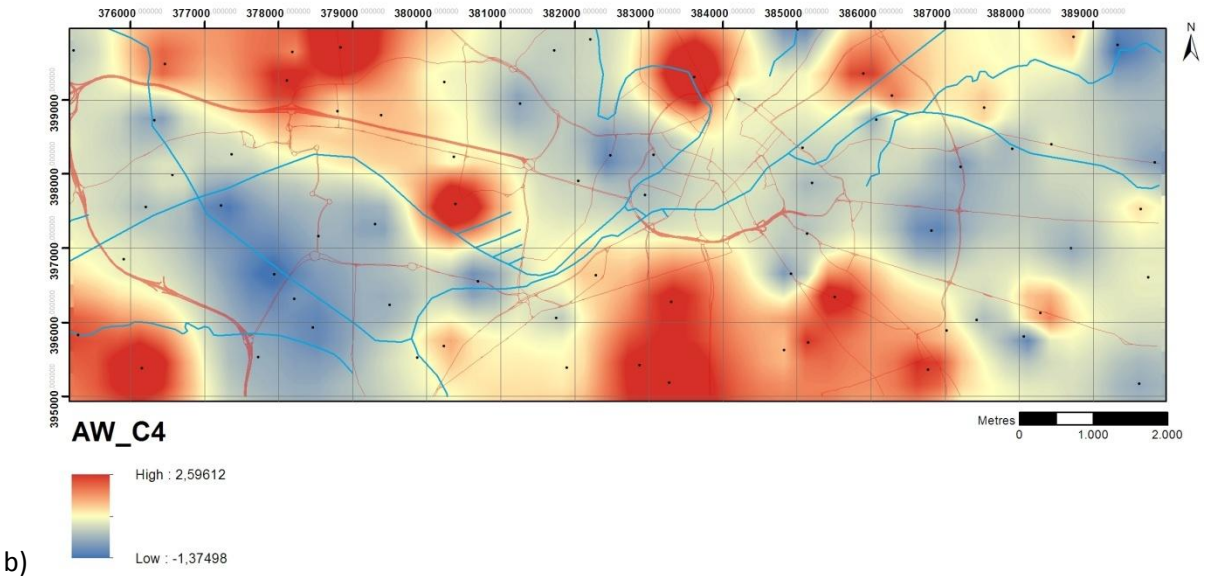


b)

Figure 86: Spatial distribution of component 4 scores for RDS data: a) summer and b) winter (PCA #A, n=72, 49 variables) (cf. Table 51 and Table 52 for represented elements).

Components 6 (RDSs) and 5 (RDSw) represent As and Ge; together with the grain size fraction below 63µm in the summer dataset. The spatial distribution of these components can be observed in

Figure 87. Out of the 7 samples with the highest scores, 3 are located in close proximity to scrapyards/used car parts dealers, two near garage services (an M.O.T. centre and “Redline Automotive”); one next to “Celtech Electronic”, which builds car electronic equipments; and one near “Car Audio Centre Manchester”. This strongly suggests that electronic equipment, more specifically automotive (LEDs, optical fibres, semiconductors, etc) are the dominant source of As and Ge in Manchester’s RDS.

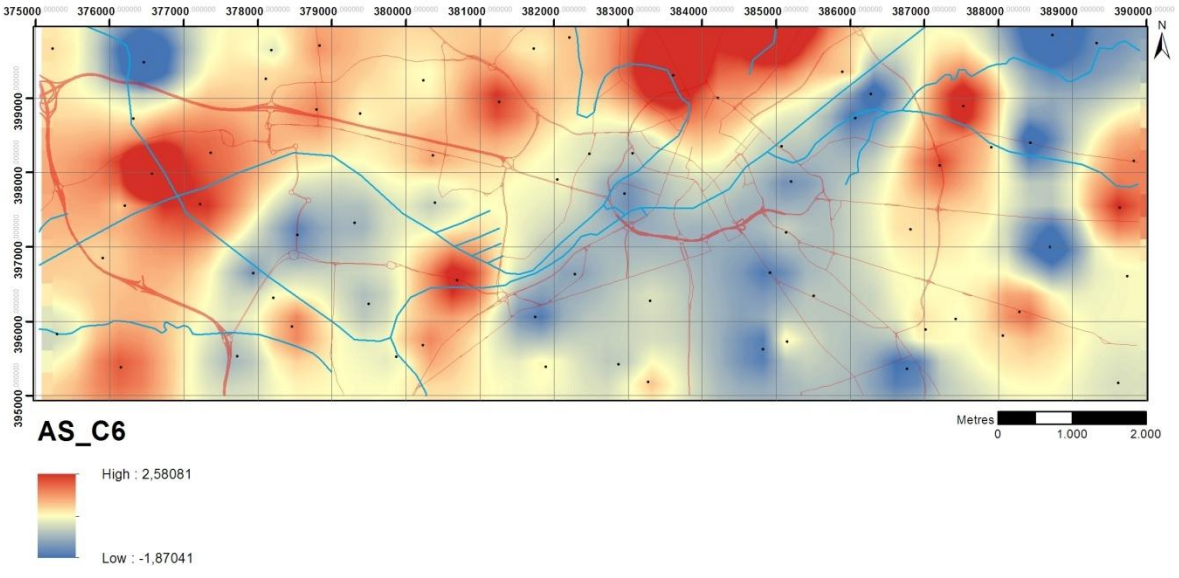


a)

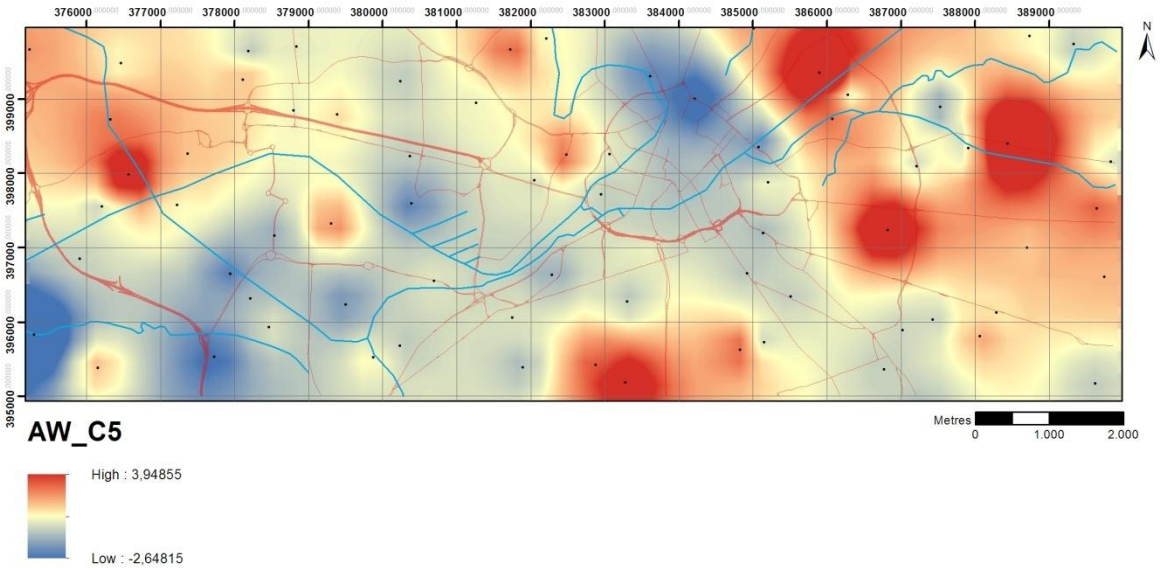


b)

Figure 87: Spatial distribution of component score 6 (RDSs) and 5 (RDSw): a) summer and b) winter (PCA #A, n=72, 49 variables) (cf. Table 51 and Table 52 for represented elements).

Components 8 (RDSs) and 7 (RDSw) score mapping reveals a hotspot west of the Manchester city centre (Figure 88), which is more spread out for RDS winter. This component shows a strong loading for Cd and Bi - the sample with the highest score (responsible for this hotspot) was collected right outside “BBGR Lens Manufacturers” and “Autoglass” - it contains 2.6 and 6.44 mg/kg of cadmium in RDS summer and winter, respectively; and 27.3 and 69.3 mg/kg of bismuth. This proximity points to

RDS contamination by the use of low-temperature alloys to firmly mount glass and precision lenses during grinding and polishing operations - both the above companies perform these operations respectively in the manufacture of prescription lenses, and in the repair of car windshields.

Another evidence for this source of contamination is the total Indium content of this sample: 10.2 (RDSs) and 31.7 mg/kg (RDSw), way above 0.6 mg/kg which is otherwise the maximum concentration found in Manchester's RDS samples. Further investigation on this led to the fact that Indium alloy is used in the production of lenses during the polishing stage and in optics assembly - this alloy is mainly composed by 44-50% Bi, 5.3-10% Cd and 19-51% In (IC, 2013). The use of Indalloy® low temperature alloys (IC, 2013) or similar products by these companies should be further investigated, as it is pointed as a potential source of Cd, Bi and In to the surrounding environment.

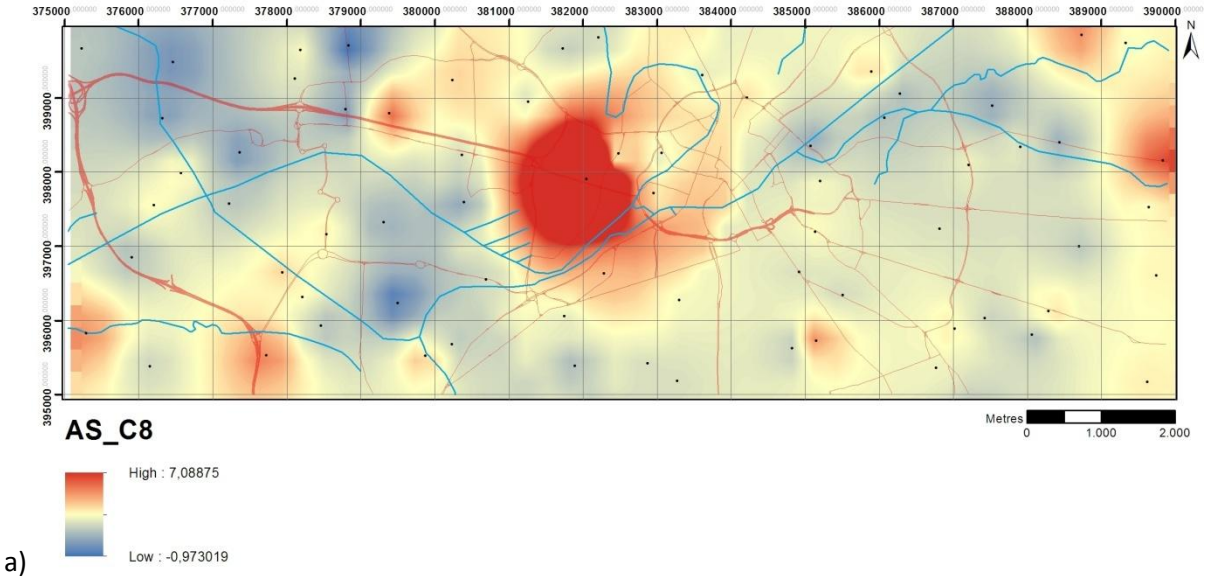


a)

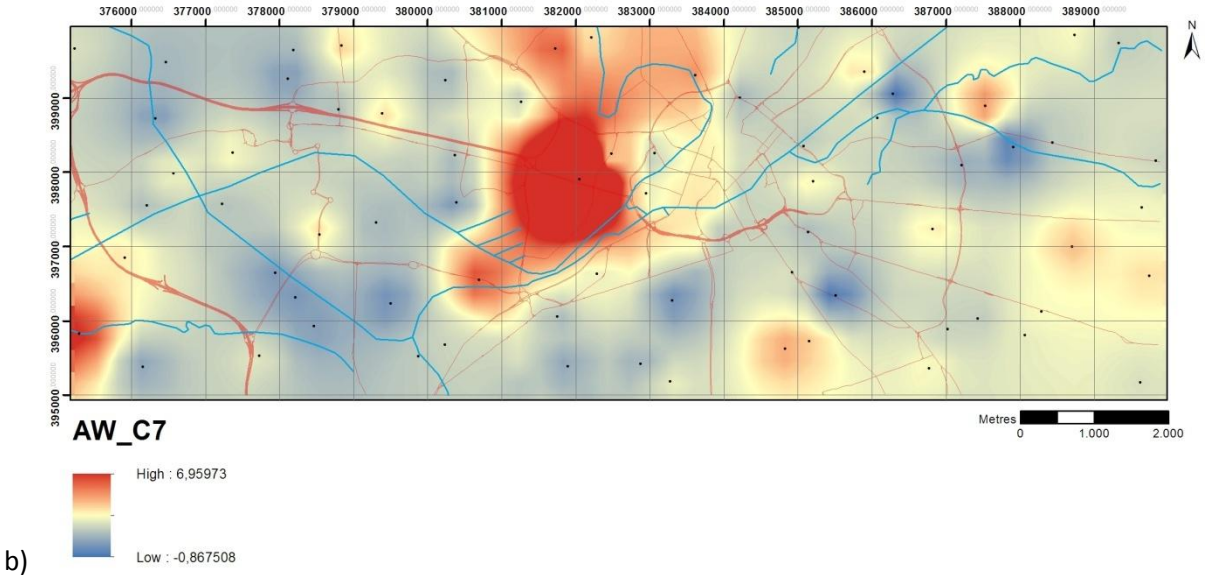


b)

Figure 88: Spatial distribution of component score 8 (RDSs) and 7 (RDSw): a) summer and b) winter (PCA #A, n=72, 49 variables) (cf. Table 51 and Table 52 for represented elements).

Indium is not included in this component as this element was removed from the statistical analysis - 95% of the samples displayed In concentrations below the XRF instrumental LLD for In determination.

Principal components with significant loadings for only one variable, or low loadings for very few variables, should not be interpreted; unless the sample size is 300 or more (Field, 2005). Therefore, components 7, 9, 10 and 11 for RDS-summer and 6, 8, 9 and 10 for RDS-winter have not been interpreted in this analysis.

## *4.7.2. Analysis B*

A second set of analyses were performed on RDS summer and winter data, this time using the inflection point of the scree plot (cf. Figure 79) to investigate whether results yield a significant difference from the previous analysis, where components were retained based on the Kaiser criterion (eigenvalue >1). This way, the first 4 components (those above the inflexion point of the scree plot) were chosen to be retained and calculations were done using the same 49 variables to check if there were major differences in the interpretation of results and component score mapping.

The KMO statistic, Bartlett's test and anti-image matrix are the same as in analysis A, as the datasets are the same. Nevertheless, the total variance explained after rotation changes because a smaller number of components (4, instead of 11 and 10) have been retained. This is represented in Table 102 of Appendix 4 - the 3 retained components in this set of analysis explain 61.5 and 62.8% of the total variance in summer and winter, respectively, after orthogonal Varimax rotation.

The rotated component matrixes are represented in Table 103 of Appendix 4 and summarised below in Table 53 and Table 54. Here, only the elements with the highest loadings for components 1 to 4 are displayed.

| | | Element loading - RDSs | | |
|---|---|---|---|---|
| | | ]1.0, 0.7] | ]0.7 - 0.6] | ]0.6 - 0.5] |
| component | 1 | MgO, $Al_2O_3$, $TiO_2$, MnO, $Fe_2O_3$, Sc, V, Co, Ni, Ga, Y, Nb | Nd | $Na_2O$, $K_2O$, Rb, La, Ce |
| | 2 | Ba, Cu, Zn, Sr, Mo, Pb, Sn, Sb | - | Cd |
| | 3 | $P_2O_5$, Br, I, S, LOI | - | Se, 63-inf2 |
| | 4 | Th | Zr, Hf, La, Ce | $K_2O$, As, Rb, Nd |

Table 53: Summary of element loadings onto each calculated component (1 to 4) for RDS-summer (PCA #B, n=72, 49 variables).

| | | Element loading - RDSw | | |
|---|---|---|---|---|
| | | ]1.0, 0.7] | ]0.7 - 0.6] | ]0.6 - 0.5] |
| component | 1 | MgO, $Al_2O_3$, $TiO_2$, MnO, $Fe_2O_3$, Sc, V, Co, Ni, Ga, Y | Nb | Nd |
| | 2 | Ba, Cu, Zn, Pb, Sn, Sb | Cr, Sr, Zr | Hf, W |
| | 3 | $K_2O$, Rb, Th, La, Ce | Nd | $Al_2O_3$, Ga, Y, Zr, Nb, Hf, U, Sm |
| | 4 | $P_2O_5$, Se, Br, I, S, LOI | - | 63-inf2 |

Table 54: Summary of element loadings onto each calculated component (1 to 4) for RDS-winter (PCA #B, n=72, 49 variables).

The main difference to analysis A is that for the summer dataset, the component dominated by organic matter-related elements explains more variance than the component related to road pavement/kerb material and hence their order is switched relatively to analysis A.

The components found are in all similar to those of analysis A (cf. section 4.7.1, Table 51 and Table 52): equivalent element groupings were found, although the total variance explained by each component is greater in analysis B, as a smaller number of components were retained. A few variables such as the grain size fraction below 63µm, Cd in the summer dataset and Cr in the winter dataset have been included in new components which explain larger percentages of variance. Therefore, the component plots and component score maps of the current analysis are also very similar to analysis A and are omitted in this set of analysis.

### *4.7.3. Analysis C*

The previous PCA analysis A and B revealed that a few elements of environmental concern are clustered in single components - the large number of variables influences the pattern of correlations between variables. To enhance this pattern more specifically for the elements of environmental concern, variables with non-significant loadings onto any of the previously calculated components or in components which explain very small variance percentages (e.g. U, Yb, W, D), and those for which sources and correlations found were of more direct interpretation (e.g. $K_2O$, Rb, Br, I, LOI, $P_2O_5$, CaO, Sr, Rb, Zr, Se, REEs) were eliminated in analysis C. Twenty variables were selected for this analysis: $Al_2O_3$, $TiO_2$, $Fe_2O_3$, Cr, Co, Ba, Ni, Cu, Zn, Pb, Sr, Ga, Mo, As, Ge, Bi, Cd, Sn, Sb, organic matter (LOI) and the grain size fraction <63µm (63-inf2). Organic matter and the fine grain size fraction were kept in this analysis to see if, in the absence of the other elements, these variables would load onto the same component as other trace metals of environmental concern.

KMO and Bartlett's sphericity tests showed that the 20-variable RDS datasets are suitable for PCA analysis, with KMO values of 0.806 and 0.802 respectively for summer and winter datasets as displayed in Table 55 below. Bartlett's test is also highly significant, as the Sig. value is less than 0.001.

a)

| KMO and Bartlett's Test | | |
|---|---|---|
| Kaiser-Meyer-Olkin Measure of Sampling Adequacy | | ,806 |
| Bartlett's Test of Sphericity | Approx. Chi-Square | 1425,534 |
| | df | 210 |
| | Sig. | ,000 |

b)

| KMO and Bartlett's Test | | |
|---|---|---|
| Kaiser-Meyer-Olkin Measure of Sampling Adequacy | | ,802 |
| Bartlett's Test of Sphericity | Approx. Chi-Square | 1482,787 |
| | df | 210 |
| | Sig. | ,000 |

Table 55: Results for the KMO and Bartlett's tests for RDS geochemical data; a) summer and b) winter (#B, n=72, 20 variables).

Both scree plots show two inflection points, as observed in Figure 89: one at the 3rd component and another in the 5th, which also marks the component limit where eigenvalues are greater than one. Therefore, the Kaiser criterion has been used.

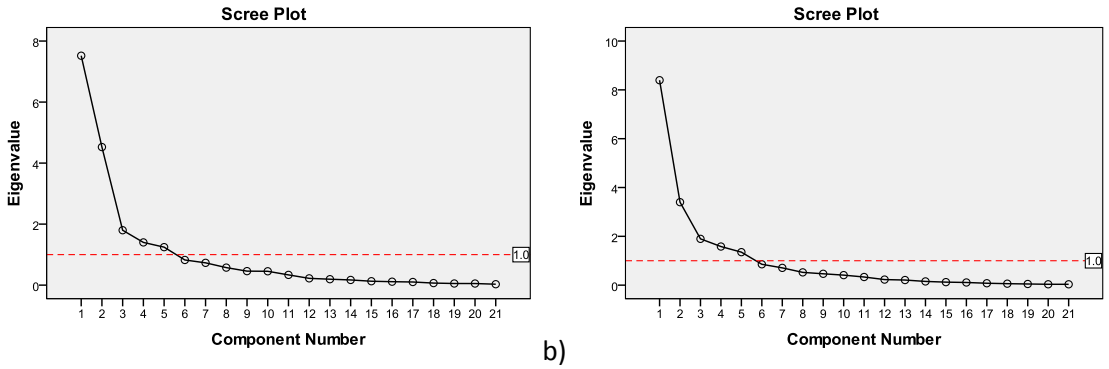


a) b)

Figure 89: Scree plots - Components vs. eigenvalues for RDS geochemical data: a) summer and b) winter. (PCA #B, n=72, 20 variables).

Communalities are close to 1 except for Cr, Ge, Sr, Mo and the grain size fraction <63µm (communalities <0.7, Table 104, Appendix 4). The variance of the remaining 15 elements consists mainly of common, or shared, variance. Eigenvalues associated with each component are presented in

Table 105 of Appendix 4. The first 5 components were retained for extraction, explaining 78.5% of the total dataset variance in summer and 79.1% in winter. Element loadings onto each calculated component are shown in

Table 106 (Appendix 4) and summarised below in Table 56 and the component plots of Figure 98 and Figure 99.

a)

| | | Element loading - RDSs | | |
|---|---|---|---|---|
| | | ]1.0, 0.7] | ]0.7 - 0.6] | ]0.6 - 0.5] |
| component | 1 | Ba, Cu, Zn, Sr, Mo, Pb, Sn, Sb | - | - |
| | 2 | $Al_2O_3$, $TiO_2$, $Fe_2O_3$, Co, Ni, Ga | - | - |
| | 3 | Ge, As | 63-inf2 | - |
| | 4 | Bi, Cd | - | - |
| | 5 | LOI | - | - |

b)

| | | Element loading - RDSw | | |
|---|---|---|---|---|
| | | ]1.0, 0.7] | ]0.7 - 0.6] | ]0.6 - 0.5] |
| component | 1 | Ba, Cu, Zn, Sr, Pb, Sn, Sb | Cr | Mo |
| | 2 | $Al_2O_3$, $TiO_2$, $Fe_2O_3$, Co, Ni, Ga | - | - |
| | 3 | Ge, As | - | - |
| | 4 | Bi, Cd | - | - |
| | 5 | LOI | - | - |

Table 56: Summary of element loadings onto each calculated component (1 to 5) for RDS a) summer and b) winter (PCA #C, n=72, 20 variables).

The interpretation of the obtained components isn't different from that found in analysis A (cf. section 4.7.1): components 1, 2 and 5 of analysis C correspond to components 2, 1 and 4 of analysis A, respectively. Component 3 (Ge, As) corresponds to components 6 (RDSs) and 5 (RDSw) in analysis A, whereas component 4 matches components 8 (RDSs) and 7 (RDSw).

Component 1 explains 30.5 (RDSs) and 28.1% (RDSw) of the total variance of the 20-variable dataset of analysis C, representing Ba, Cu, Zn, Pb Sr, Mo, Sn and Sb. In Figure 92 it is noticeable that high component scores are concentrated in the Trafford Park area, which at the time of writing is Europe's largest industrial estate (EKOS, 2008). The high concentration of different types of industries in this area makes it difficult to apportion the above elements to a specific source. Nonetheless, it is obvious that these elements are sourced to RDS from industrial activity - all the RDS samples with the highest scores in the summer dataset (samples 21, 34, 35, 36, 50 and 51) were

collected in very close proximity to industrial facilities. Additionally to Trafford Park, the winter map (Figure 92b) shows high scores for component 1 in the east Manchester area: these samples (11, 13, 25, 59 and 71) are not in the immediate vicinity of industries, which might indicate that in this season there may be inputs from other sources of these elements to RDS.

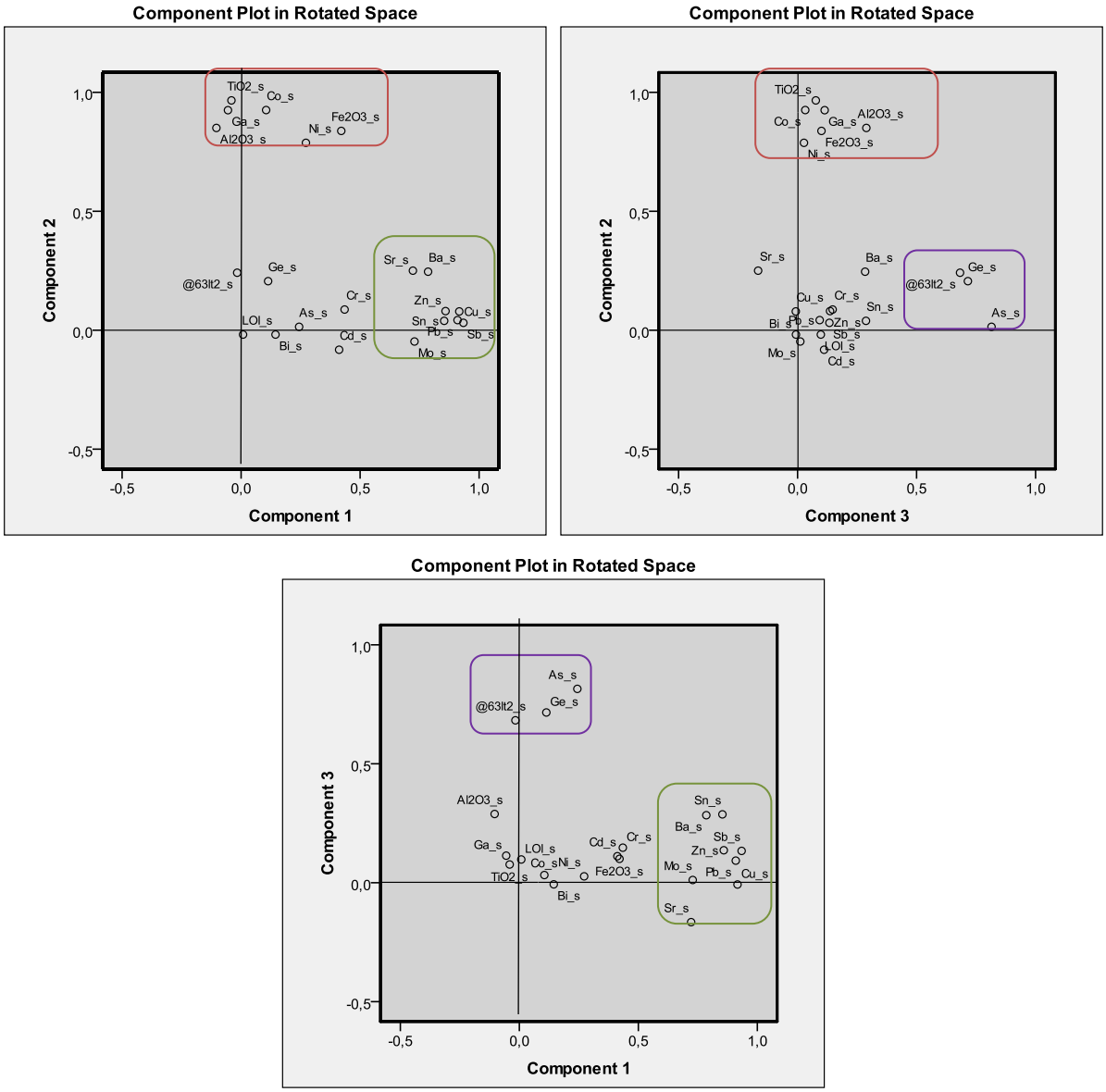


Figure 90: Component plots for components 1 vs. 2, 2 vs. 3 and 1 vs. 3, for RDS summer data (PCA #C, n=72, 20 variables).

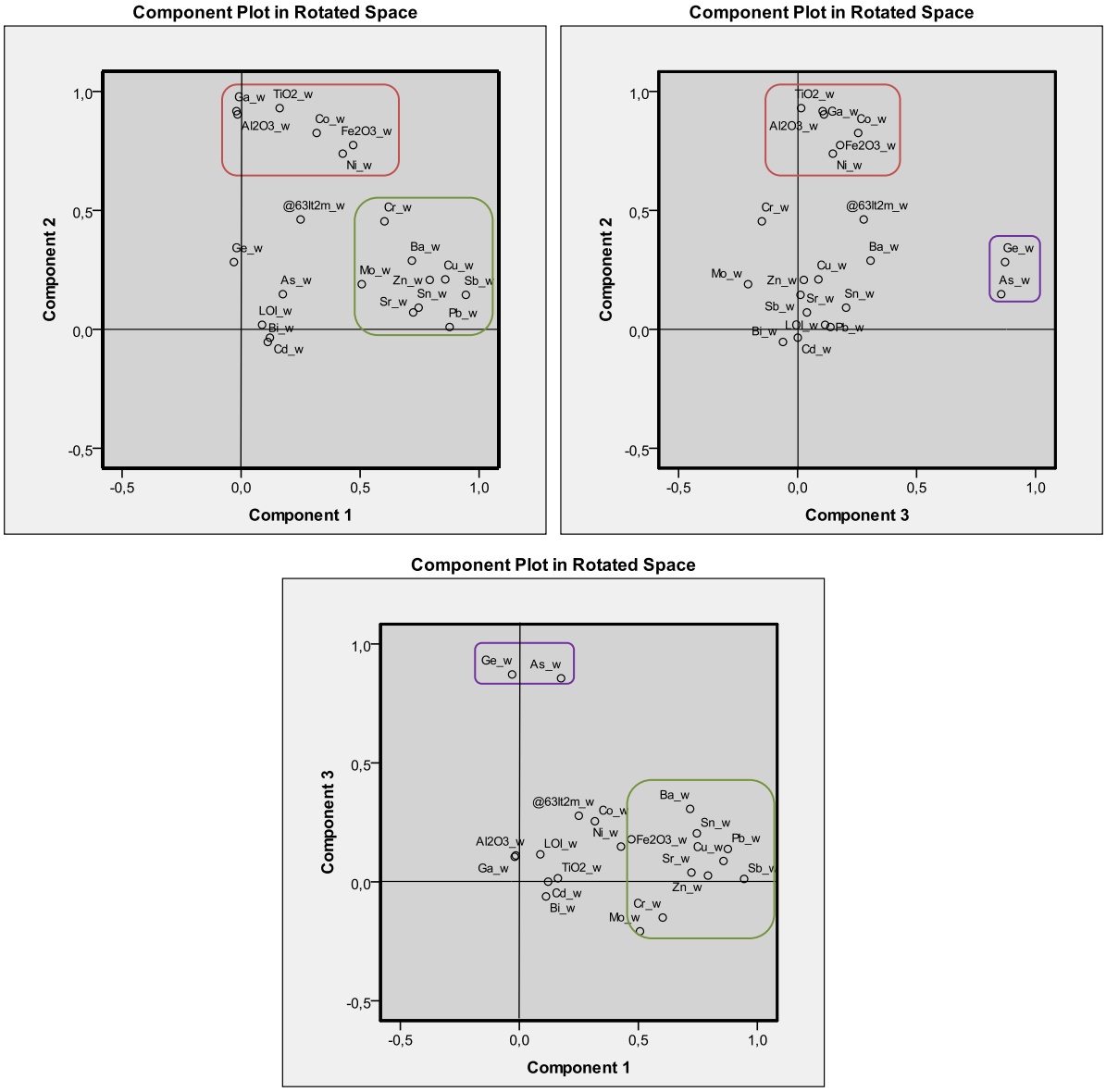


Figure 91: Component plots for components 1 vs. 2, 2 vs. 3 and 1 vs. 3, for RDS summer data (PCA #C, n=72, 20 variables).

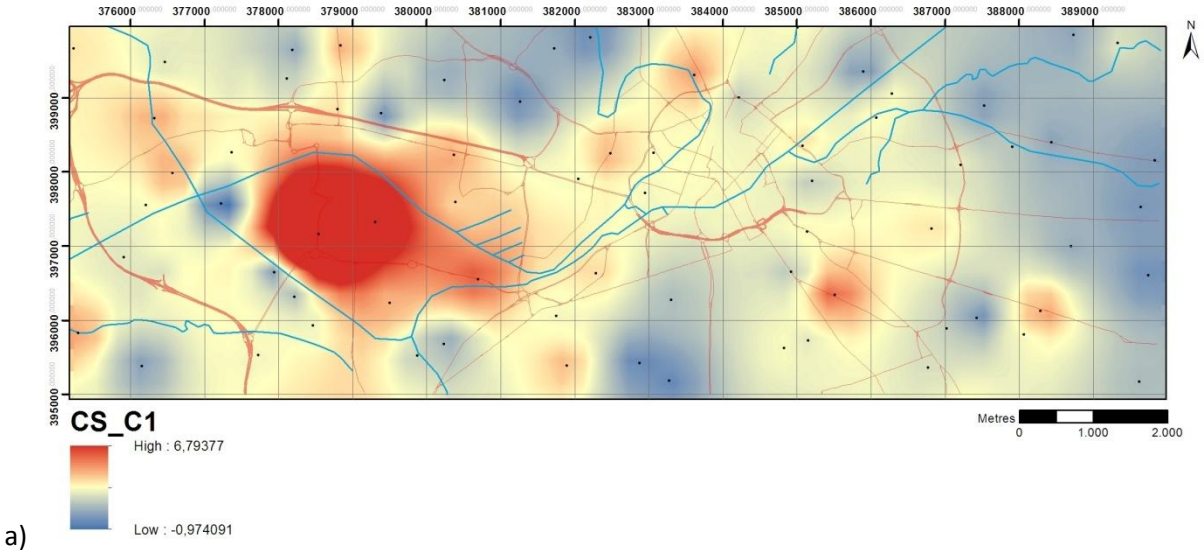


a)

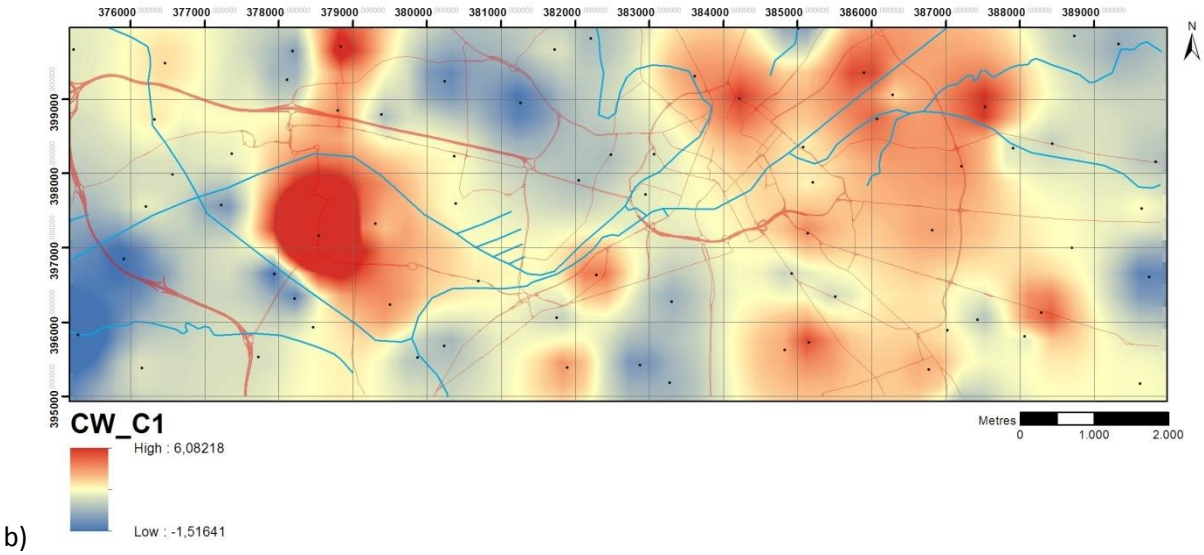


b)

Figure 92: Spatial distribution of component 1 scores for RDS data: a) summer and b) winter (PCA #C, n=72, 20 variables) (cf. Table 56 for represented elements).

Component 2 represents $Al_2O_3$, $TiO_2$, $Fe_2O_3$, Co, Ni and Ga, which account for 23.6 and 24.4% of the total variance, respectively, for summer and winter RDS. These elements are thought to be related to the soil contribution to RDS, as the samples with high scores on this component (4, 6, 13, 14, 46, 48, 70, 71) were collected mainly in residential areas far from other pollution sources referred throughout this chapter. Additionally, all of them were collected a few meters away from residential or urban gardens, and parks.

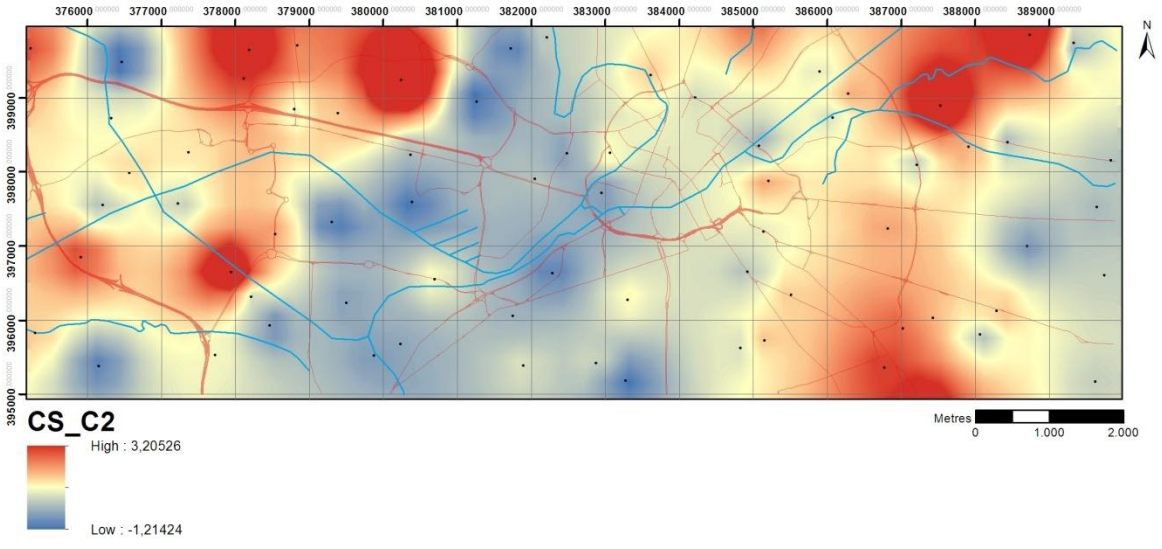


a)

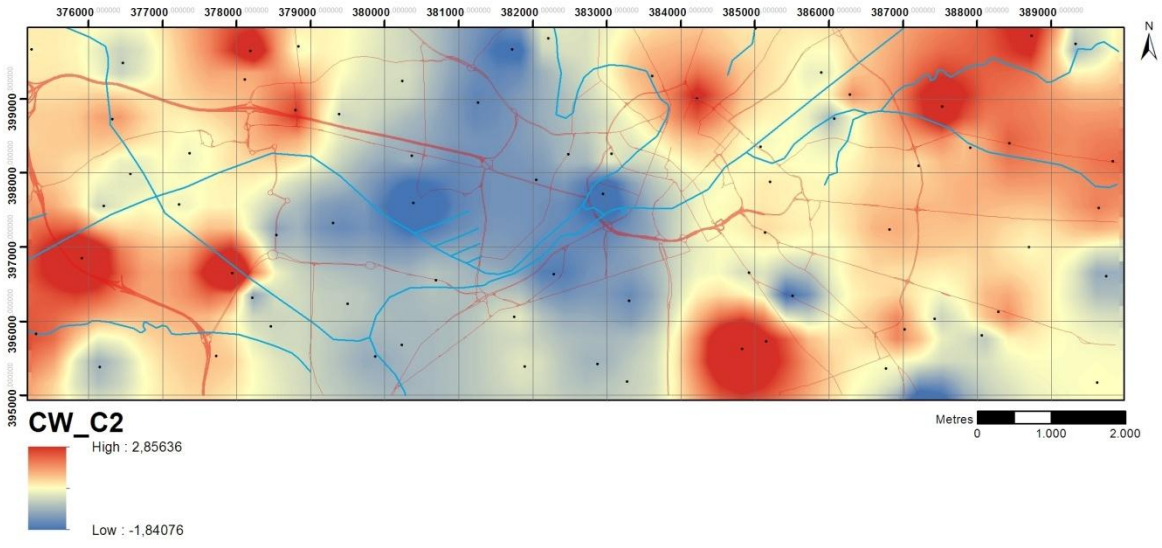


b)

Figure 93: Spatial distribution of component 2 scores for RDS data: a) summer and b) winter (PCA #C, n=72, 20 variables) (cf. Table 56 for represented elements).

Component 3, dominated by As and Ge, explains 9.7 and 9.3% of the total analysis C variance in summer and winter, respectively. When compared to analysis A (components 6 [RDSs] and 5 [RDSw]), the spatial distributions of this component reveal that hotspots are more well defined (Figure 94). These samples (5, 9, 10, 29, 32, 42, 43, 59) are all located near either garage services, M.O.T. centres, scrapyards and car part dealers, car audio repairs or car electronics' manufacturers, pointing vehicle-related materials (especially electronic equipment) as the most potential source of these elements in RDS.

a)

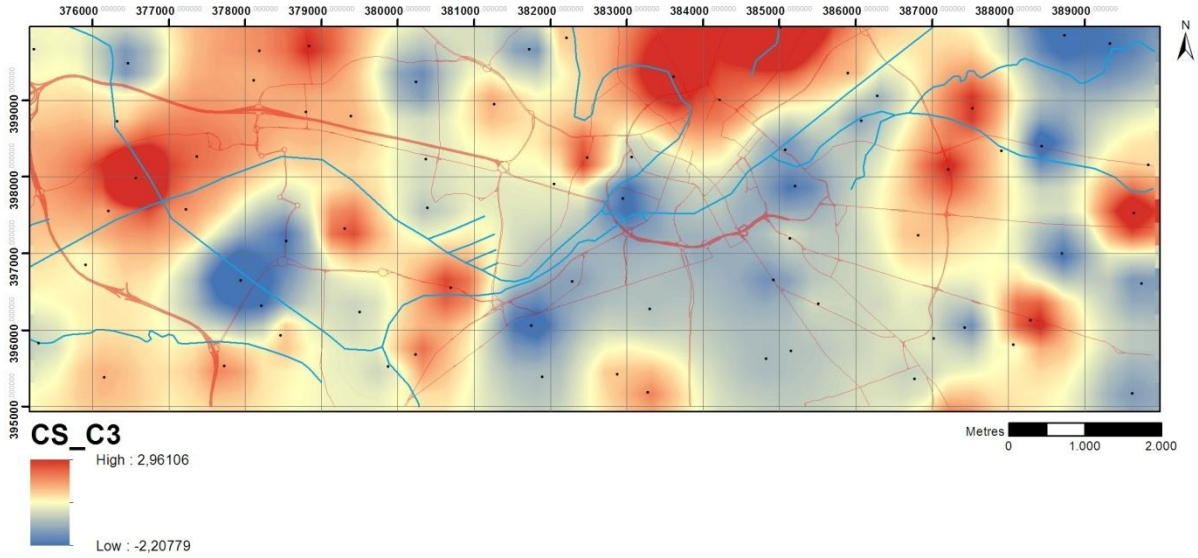


b)

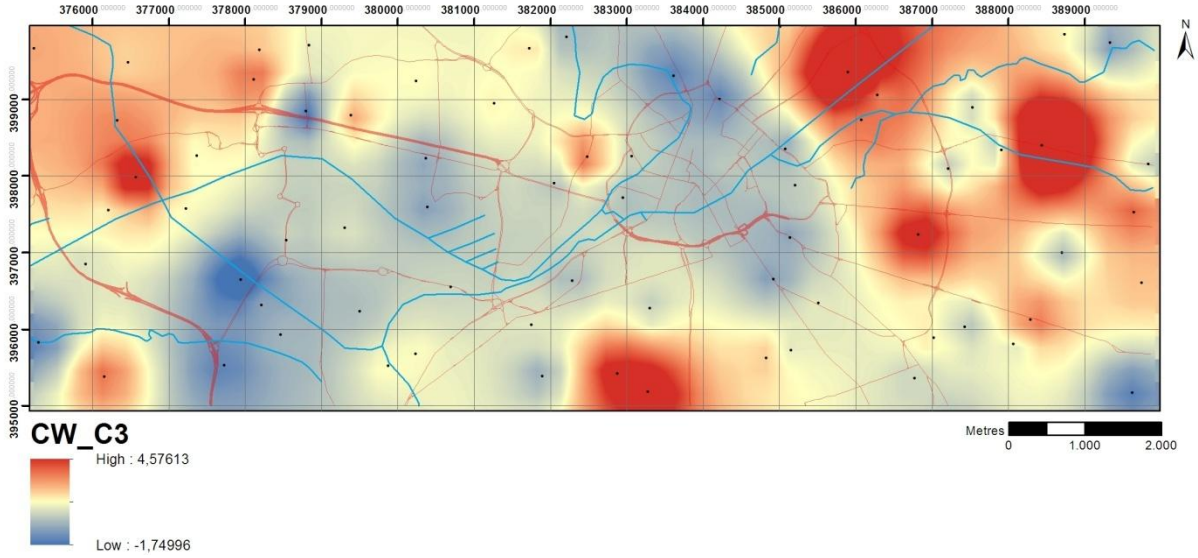


Figure 94: Spatial distribution of component 3 scores for RDS data: a) summer and b) winter (PCA #C, n=72, 20 variables) (cf. Table 56 for represented elements).

Component 4 explains 7.8 and 9.3% of the total variance respectively in summer and winter. Cadmium and Bi spatial distributions, as can be observed in Figure 95, are very similar to that of

analysis A (components 8 [RDSs] and 7 [RDSw], cf. Figure 88), as there is a very likely and specific source for these two elements in RDS: the use of Cd-Bi-In alloy in the lens/glass industry.

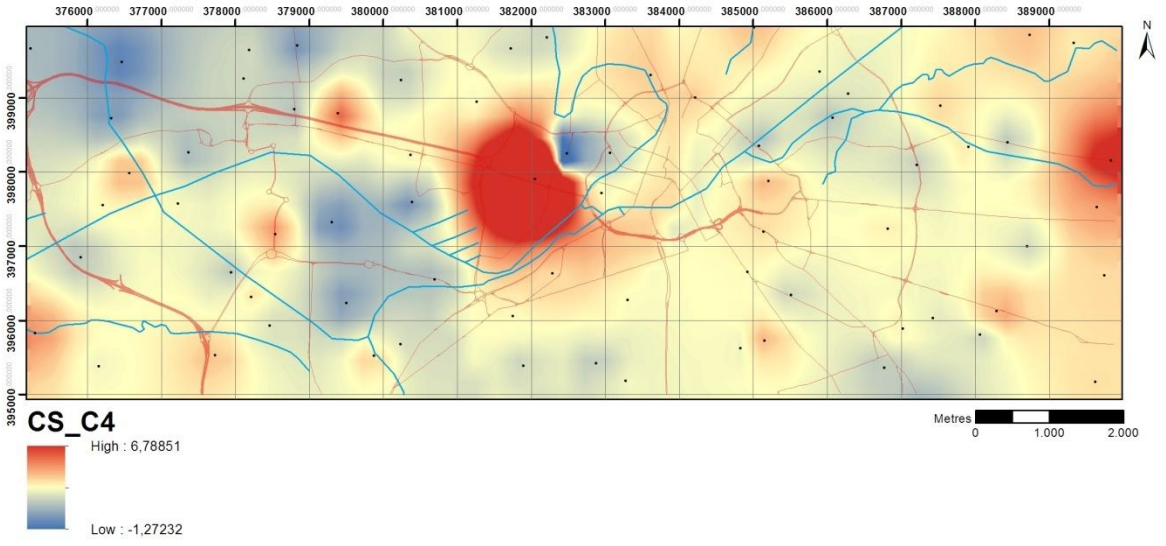


a)

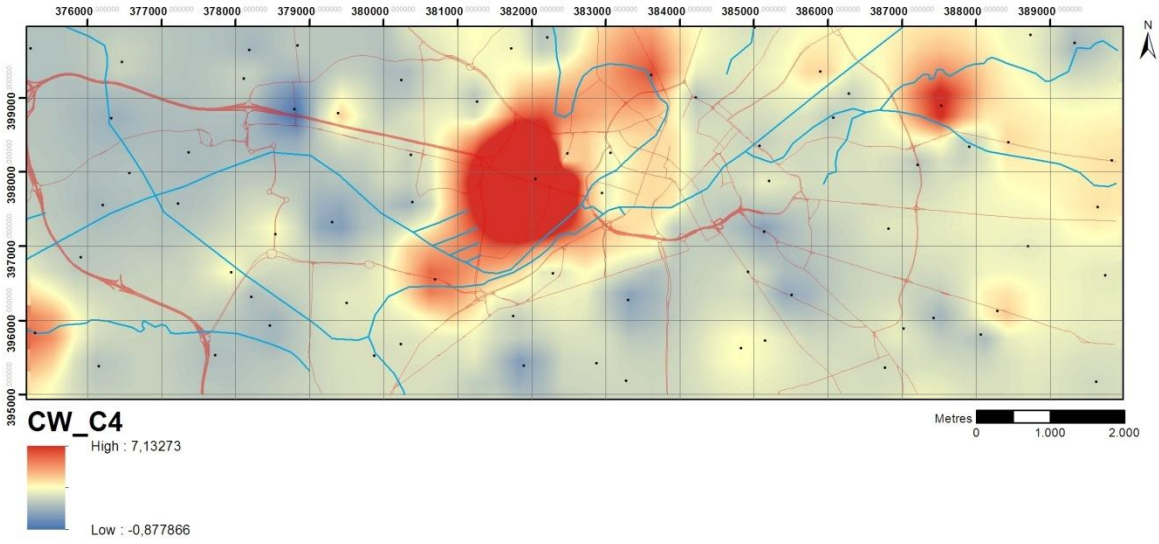


b)

Figure 95: Spatial distribution of component 4 scores for RDS data: a) summer and b) winter (PCA #C, n=72, 20 variables) (cf. Table 56 for represented elements).

Component 5 of analysis C comprises organic matter (LOI) only - this variable is therefore statistically unrelated to the other 19 variables chosen for this analysis. It has been included in case organic matter would have an underlying relationship with the other selected variables, which could have been previously masked in analysis A and B by the other strong associations of organic matter with e.g. I, S, Br or $P_2O_5$. This seems not to be the case, as organic matter does not load on any of the other components in this analysis.

## 4.8. Statistical analysis - critical sample subset

In the course of this research work, a few RDS locations have been reported as systematically showing high concentrations of elements of environmental concern (PHE). Therefore, further analyses have been performed to better characterise these samples, such as speciation analysis (cf.

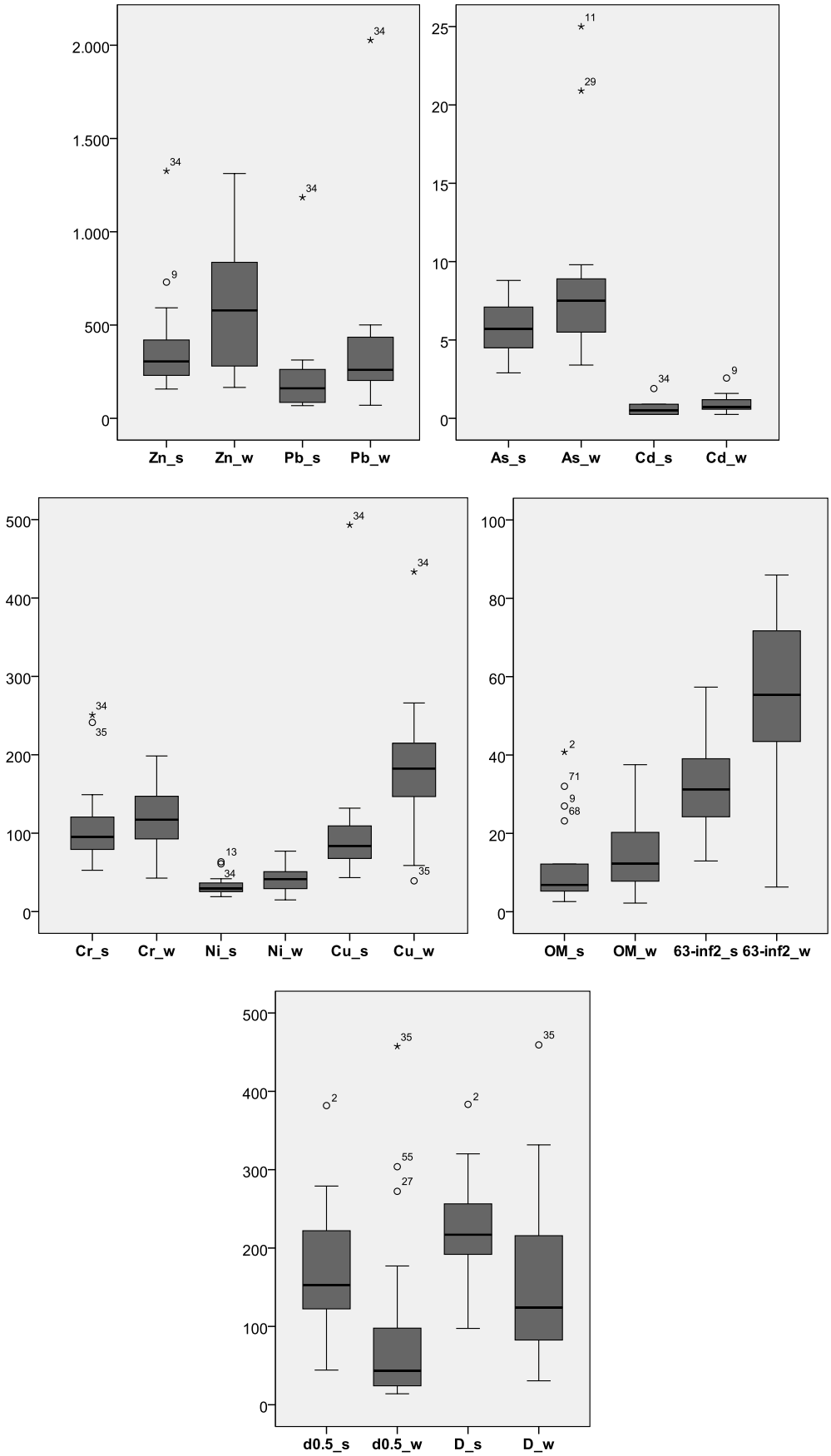


Figure 96: Box-and-whiskers plots of selected variables in RDS samples (RDS-summer N=17; RDS-winter N=17; chemical elements in mg/kg; OM and 63-inf2 in %; d0.5 and D in µm).

Elements only related to the clay-sized fraction (inf2) in winter include $Fe_2O_3$, Ni, reducible Cu (Cu2), oxidisable Cu (Cu3), and residual Zn (Zn4). However, in summer, $Fe_2O_3$, Ni and residual Zn correlate to both the clay sized and the very fine sand-sized (63-125) fractions. These correlations are more evident in the winter dataset probably due to its relatively higher content in clay-sized sediments.

The fact that some metals correlate simultaneously to these two grain size fractions points to a different control in the grain size distribution of metals and their different phases. In the summer dataset, for which grain size distribution tends to be coarser, variables which correlate to both these grain size fractions are total Fe ($Fe_2O_3$) and Ni, and residual Zn (Zn4) as previously observed; as well as reducible and residual Fe (Fe2 and Fe4) phases.

The present analysis suggests that, besides the clay-sized fraction, the 63-125µm grain size fraction may act as a host for PHE, especially in summer. In fact, after the SEM study of RDS samples, most of the iron-bearing grains display sizes within this range (cf. sections 4.6.1 and 4.6.2). However, a subtle explanation for the correlations between metals and both 63-125µm and <2µm grain sizes emerged.

It has been observed that a few metal-bearing grains, measuring around 100µm, are composed of an aggregate-like texture of small, often <100nm particles. This can be observed in Figure 75 a) and b) for Zn and in Figure 72 g) and h) for Pb. Close-ups (Figure 73) reveal that the smaller, metal-rich particles are weakly bonded; i.e. are not incorporated in a crystalline structure and are therefore very easily separated into <2µm and ultrafine particles. This might be a reason for the bimodal correlations which were found - metal-rich grains of the size of very fine sands, which are weathered and split into very fine, clay-sized particles, may cause higher metal concentrations simultaneously in these two grain sizes. The sample which shows the greatest number of this kind of grain is sample 34, for which the largest exchangeable Pb and Zn concentrations were also determined (cf. Figure 66 and Figure 67).

As stated before in section 4.6, these grains may be an important source or airborne fine particulates in case of resuspension, with associated human health risks. Additionally, the finer grains are usually the first to be remobilised by stormwater, with increased implications for water quality. All these risks may increase in case metals are indeed in the exchangeable form - element speciation in specific grains has not been performed in the scope of the present research and may be an appealing subject for future works in the field of human health risk assessments.

## 4.9. Main conclusions about Manchester's urban sediment geochemistry

•The composition of Manchester's RDS has been shown to vary, not only temporally but spatially, influenced by a plethora of natural and anthropogenic factors. Within the natural controls on RDS are the climatic factors such as precipitation, wind and temperature - these are mainly responsible for

RDS sorting, remobilization and transport, events which occur in short periods of time, making RDS a very transient media. The dry or wet conditions also influence the chemistry of RDS constituents, as the elemental oxidation states and mobilization potential are largely influenced by this factor. Anthropogenic factors are, nevertheless, the most important control on RDS composition - the proximity of point sources is highly related to RDS contamination. Seasonal effects are less important in what concerns average sample composition, as summer-winter sample pairs tend to show similar composition regardless of the season. Nevertheless, the drier summer season favours greater RDS accumulations on pavements, which may influence contaminant mass loading; however, when these greater accumulations occur, they tend to be coarser in grain size and hence a great part of the mass loading consists of inert, mineral-dominated material.

•This study also provided evidence that not only the finer fractions of RDS are important PHE carriers, as is the case with natural soils and sediments. In RDS, studies have reported the <63µm grain size fraction as the major host for metals in RDS (Sutherland, 2002; Irvine et al., 2009; Krčmová et al., 2009; Sutherland et al., 2012), but the coarse nature of RDS from other studies has also been reported to be of great influence in metal distribution (e.g. Robertson and Taylor, 2007; Sutherland et al., 2008). In the present work, RDS were collected from different local settings and in two distinct seasons; hence, grain size is highly variable among samples. Nevertheless, in contaminated samples, PHE such as Zn, Pb, Ni and Cu and their different phases can be statistically related to both the <2µm and the 63-125µm grain size fractions, suggesting a different control on the grain size partitioning of these metals. SEM observations pointed to a specific type of grain, which is generally around 100µm and composed of an agglomerate of smaller, <2µm particles, as a possible reason for these correlations.

• Grain size distributions of RDS samples are highly variable - a grain size normalisation attempt has been performed, as trace metals of environmental concern are reported to be preferably concentrated in the finer grain size fractions of the sediment. Through the grain size analysis of a subset of 34 samples (17 summer + 17 winter), Al and Ga emerged as good grain size proxies; but the extension of the analysis to the total, 144-sample dataset disproved this hypothesis. The complex nature of the controls on RDS grain size make traditional grain size normalisation procedures inapplicable to heterogeneous RDS datasets. Therefore, the outcomes of the statistical analysis of specific sample subsets must be carefully interpreted, as it has been demonstrated that results are clearly influenced by the characteristics of the chosen sample subsets.

• Trace metal speciation has been determined for Cr, Cu, Zn, Pb and Fe in selected samples. Extracted phases tend to display larger metal concentrations in winter samples, except Cr where concentrations are lower in winter for the first three extracted phases. Zn is the most available element, with high concentrations in the exchangeable, acid-extractable phase and in the reducible

phase. Lead is preferably bound to the reducible phase, whereas Cu shows higher concentrations in the reducible phase in summer and residual phase in winter. Chromium and Fe display greater proportions in the residual phase.

• Seasonal differences between phase orderings are found for Cu, Zn and Pb; whereas Cr and Fe phases are similar between seasons. Copper tends to be more prone to remobilization in summer, but total extractable concentrations tend to be lower. Zinc also tends to be more available in summer, as a greater percentage of the total extracted Zn is found in the exchangeable phase; nevertheless, Zn displays higher absolute concentrations in the exchangeable phase in winter. Similarly, Pb extractable concentrations are higher in winter but, when present, Pb in the exchangeable phase displays greater proportions in summer.

• The RDS speciation study confirms that, for the analysed samples, Cr, Cu, Zn and Pb are mainly of anthropogenic origin - most of these are concentrated in the mobilisable fractions (exchangeable, reducible and oxidisable) defined by the BCR procedure.

• Scanning electron microscope microbeam analysis showed that RDS is mainly composed by quartz (sand); rock fragments; fragments of brick, concrete, tarmac and other construction materials; spherical metal-rich particles; and anthropogenic metallic grains of diverse shape and size. Grains containing PHE such as Cr, Pb and Zn are common in RDS - these may be very prone to resuspension and transport due to their morphology and recurrent small size.

• The groups of geochemical variables revealed by principal component analysis, which represent elements with a similar variation pattern in Manchester's RDS, makes it possible to define the sources responsible for high concentrations of elements of interest. It is observed that element groupings between summer and winter are very similar, revealing a consistency in element sources and/or accumulation processes between the two seasons. Components identified by PCA are described as follows:

- Elements which are probably related to soil include $Al_2O_3$, MgO, $TiO_2$, MnO, $Fe_2O_3$, Sc, V, Co, Ni, Ga and Nb. Besides geogenic elements, such as Al, Ga and Mg (and Ti, Mn and Fe to a smaller extent); Sc, V, Co and Ni are believed to have been enriched in Manchester's soils due to historical coal extraction and burning activities. This points to soil as a main source of these elements in Manchester's RDS - analysing the component score mapping, samples with high scores for this component (9 out of 10) were in fact collected from streets along gardens, parks or vacant land plots and RDS samples were generally collected less than 4 meters away from the soil limit.
- Rare earth elements such as La, Ce, Nd, and Y; Th, and $Al_2O_3$, $K_2O$ and Rb are also related in Manchester's RDS. These are geogenic elements, which are present mainly in igneous rocks - these elements may be sourced to RDS by the igneous rocks and gritstones that are used

as kerbstones in Manchester's streets, as pavements, or in buildings; or from rock aggregates which are commonly used in Manchester's street pavements, kerbstones and sidewalks. Seven out of the 9 samples which show the highest loadings for this component were collected on or close to pavements or kerbs made from rock aggregates.

- The organic matter-related component of RDS is also represented by high concentrations of Br, I, S Se and $P_2O_5$ - elements which come mainly from nearby soils, or from plant and leaf litter which accumulates directly on surfaces.
- Barium, Cu, Zn, Pb, Sr, Sn and Sb are anthropogenic elements enriched in Manchester's RDS in areas close to industrial activites, with especially high component scores in the Trafford Park Industrial Estate, where industry is concentrated along with heavy goods transport.
- The association of As and Ge in RDS is likely related to their use in electronic equipment - component score mapping strongly suggests that automotive electronic equipment (LEDs, optical fibres, semiconductors, etc) are the dominant source of As and Ge in Manchester's RDS, due to the proximity of high score samples to scrapyards, car part dealers, garage services, an automotive electronic equipment manufacturer and a car audio centre.
- Cadmium and Bi are also related in RDS - a probable source is their use in Sn-Bi-Cd alloys, which are commonly used in low-temperature soldering of heat sensitive materials such as glass, and light electronic assemblies. Component score mapping revealed a hotspot in the immediate vicinity of a lens manufacturer and an Autoglass centre, strongly suggesting that these elements are related to the use of low-temperature alloys to firmly mount glass and precision lenses during grinding and polishing operations. Another evidence which points to this source of contamination is the high Indium content of RDS - Indium alloy (approx. 44-50% Bi, 5.3-10% Cd and 19-51% In) is generally used in the production of lenses during the polishing stage, and in optics assembly.

• The retention of fewer components in PCA analysis #B produced element associations which were less specific - a criterion which favours the retention of a larger number of components (eigenvalue >1) should be preferably used, as a means to more accurate source identifications. The use of a smaller number of variables in analysis #C revealed that critical element groupings were very similar to those found in the previous rounds of analysis, although component mapping showed sharper variations - the pattern of correlations between the critical variables was unaffected by the exclusion of variables of easier interpretation.

• Seventeen locations which revealed high PHE levels in summer and winter datasets were selected for further analysis, in a total of 34 samples. The statistical analysis of these data subsets again suggest that, besides the clay-sized fraction, the 63-125µm grain size fraction may act as a host for

PHE, especially in summer. This might be related to the existence metal-rich grains of the size of very fine sands, which are weathered and split into clay-sized particles, which may cause higher metal concentrations simultaneously in the two grain sizes. The combination of SEM observations with XRF, sequential extraction and grain size analysis results provided a more realistic picture of the actual forms of trace metals in RDS, and a better insight on the grain size fractions which are more likely to act as hosts for contaminants; adding to the element associations and sources distinguished by principal component analysis.

# 5. Spatial statistical analysis

Soils and road-deposited sediments were collected for the present research across 75km$^2$ of the Manchester and Salford urban areas, which display marked heterogeneities in terms of land uses and geographical characteristics. In the previous chapters, soil and RDS contaminations have been attributed to several sources, which have been found to locally influence the geochemical composition of these media. In a generalised way, potentially-harmful element (PHE) concentrations at any location are likely to depend on the environmental characteristics of the surrounding area, particularly those related to the presence of contamination sources and the efficiency of contaminant dispersion.

As a first step towards investigating which present-day variables may have a greater influence on soil and RDS PHE concentrations, a series of environmental datasets were produced as described in section 2.9.6.1. These explanatory variables were chosen according to their potential influence on present-day soil and RDS geochemical composition, including road, traffic, junctions, bus stops, railways, building, population, jobs, and topography parameters, as shown in Table 10 and Table 11 - in total, 96 variables were tested for soils and 99 for RDS. The dependent variables modelled were Cr, Ni, Cu, Zn, As and Pb.

Land-use regression modelling is a way of evaluating the influence of the environmental variables on the geochemical composition of soils and RDS (cf. section 1.7). It is done by constructing regression equations describing the relationship between measured concentrations and relevant environmental variables. The resulting equations may then be used to better understand the contributing factors and predict concentrations at unmeasured locations on the basis of these explanatory variables. These regression equations can be obtained by several methods - in the present research, this has been done using ordinary least squares (OLS) and geographically-weighted regression (GWR) methods (cf. section 1.7 - theoretical framework and 2.9.6 - methodological framework).

## 5.1. Ordinary Least Squares

Ordinary least squares (OLS) regression analysis has been performed in a stepwise approach using ArcGIS® 10.0 OLS tool, as described in detail in section 2.9.6.2. Geochemical variables (Cr, Ni, Cu, Zn, As and Pb) have been transformed using the Box-Cox transformation, so that distributions would approach the normal distribution (cf. section 2.9.4). Geographical data were also transformed when needed using the logarithmic (variables with the suffix _LOG or _LG) or the Box-Cox transformation (variables with the suffix _BC).

Each of the trace metals of concern were selected as the dependent variable. Prior to modelling the dependent variable, outlier values for each metal were removed from the dataset - by doing so,

model performance is generally enhanced. Censored samples are referred below in Table 57. Explanatory variables were added to the model in decreasing order of importance - those which were most likely to influence trace metal concentrations were added first. Explanatory variables which were not statistically significant were removed and other variables were subsequently added, until all explanatory variables have been tested. Additionally, variables which are correlated to each other (and therefore display a degree of redundancy, which is the case for parameters measured at different distance buffers) were tested separately before inclusion in the OLS models - if included simultaneously, the variance inflation factor (VIF) calculated for each variable would display values above 7.5. In such case, redundant explanatory variables were removed (one by one) from the model before further calculations. For each model, 96 explanatory variables were tested for each soil dependent variable; and 99 for each RDS dependent variable.

| | Soils | RDSs | RDSw |
|---|---|---|---|
| **Cr** | 630017, 630246, 630187, 630195, 630161, 630059 | 23, 69, 62, 33, 22 | 73 |
| **Ni** | 630277, 630161, 630293 | - | - |
| **Cu** | 630017, 630059, 630293 | 34 | 34 |
| **Zn** | 630286, 630277, 630293 | 34, 60 | - |
| **As** | 630017, 630293 | - | 11, 29, 49, 73 |
| **Pb** | 630199, 630246, 630161, 630027, 630293 | 34 | 34, 49, 61 |

Table 57: Outlier samples omitted from the spatial statistical analysis.

The calculated models have been evaluated through the outputs of the OLS tool in ArcGIS® 10.0 - the report of statistical results and the output feature class of model residuals. The statistical report contains relevant information for assessing variable and model performance, such as (ESRI, 2012):

• **Multiple and Adjusted R-Squared of the model**: $R^2$ values are measures of model performance. The adjusted $R^2$ value reflects model complexity (the number of variables) and is consequently a more accurate measure of model performance. Possible values range from 0.0 to 1.0 - higher $R^2$ values indicate a better adequacy of the model; e.g. a greater percentage of the variation in the dependent variable is explained by the explanatory variables of the model.

• **Coefficients, p-value, robust p-value,** and **variance inflation factor (VIF) of each explanatory variable:** *Coefficients* ($\beta_{1,n}$ in the regression equation) represent the strength, type and sign of relationship the explanatory variable has to the dependent variable. For strong relationships, the coefficient is relatively large. Weak relationships are associated with coefficients near zero; and $\beta_0$ (represented in the OLS statistical report as "*intercept*") represents the expected value for the dependent variable if all the explanatory variables were zero. *P-value* and *robust p-value* are the probabilities calculated for the coefficients associated with each independent variable - the null hypothesis for this statistical test states that a coefficient is not significantly different from zero. Small p-values reflect small probabilities and suggest that the coefficient is, indeed, important to the model with a value that is significantly different from zero - the associated variable is an effective

predictor. When the Koenker (BP) statistics (explained below) is significant, the robust values must be used. The *VIF* measures the redundancy among explanatory variables, as previously referred - those associated with *VIF* values larger than about 7.5 should be removed (one by one) from the regression model.

- **Joint F-statistic and Joint Wald statistic:** Both are measures of overall model statistical significance. The null hypothesis for these tests is that the explanatory variables in the model are not effective. Therefore, a very small p-value (probability) indicates a significant model. The Joint F-Statistic is trustworthy only when the Koenker (BP) statistic (explained below) is not statistically significant. If the Koenker (BP) statistic is significant, the Joint Wald Statistic should be consulted to determine overall model significance.

- **Koenker (BP) statistic:** Determines whether the explanatory variables in the model have a consistent relationship to the dependent variable both in geographic space and in data space. When the model is consistent in geographic space, the spatial processes represented by the explanatory variables behave the same everywhere in the study area (the processes are stationary). When the model is consistent in data space, the variation in the relationship between predicted values and each explanatory variable does not change with changes in explanatory variable magnitudes (there is no heteroscedasticity in the model; i.e. there is a homogeneity of variable variances). The null hypothesis for this test is that the model is stationary; therefore, a very small p-value for this statistic indicates that the model displays statistically significant heteroscedasticity and/or non-stationarity. When results from this test are statistically significant, the robust coefficient p-values must be consulted to assess the effectiveness of each explanatory variable. Regression models with statistically significant non-stationarity are generally good candidates for geographically weighted regression (GWR) analysis.

- **Jarque-Bera statistic:** indicates whether or not the residuals (the difference between the observed dependent variable values and the predicted/estimated values) are normally distributed. The null hypothesis for this test is that the residuals are normally distributed - a small p-value for this test means that the residuals are not normally distributed, indicating that the model is biased. In this case, the bias is likely a result of model misspecification.

After analysing these parameters of the statistical report, the residual spatial autocorrelation also needs to be assessed. This is performed by running the Spatial Autocorrelation (Moran's I) tool on the regression residuals, which are represented in the output feature class of the OLS analysis. This needs to be performed to ensure residuals are spatially random - the clustering of high/low residuals indicates the model produces under- and over-predictions in certain areas. In case residuals are spatially autocorrelated, this may indicate that key variables are missing from the model, relationships are nonlinear, and/or influential outliers are present. A very small p-value of the z-score

calculated by the global Moran's I tool indicates that the spatial distribution of high/low values is more spatially clustered than would be expected if underlying spatial processes were random. Conversely, a non-significant p-value indicates that the spatial distribution of residual values is likely random - this is the optimal situation for a reliable OLS model.

The results below display the best models calculated for Manchester's soils and RDS. Analysis set #A comprise the best model results using the calculated environmental explanatory variables; whereas analysis set #B include the calculated explanatory variables and the concentrations of the other chemical elements as explanatory variables in the model.

### *5.1.1. Soils*

**Analysis #A**

The OLS models calculated for Manchester's soils in analysis set #A were not satisfactory, as $R^2$ values were very low for all dependent variables. Additionally, explanatory variable coefficients frequently displayed unexpected values for the models with the best $R^2$ - this may indicate problems with the models, such as the lack of key explanatory variables or spatially varying relationships. Removing these variables not only decreased the $R^2$, but also modified the significance and/or sign of other explanatory variables, previously relevant for the model - the subsequent removal of these other variables left the models with too few variables to be interpreted. This reveals that the independent variables tested (Table 10) cannot explicitly explain the variation of Cr, Ni, Cu, Zn, As or Pb in Manchester's soils through OLS with a good degree of confidence, unlike in RDS, as discussed in the next section.

As previously stated in the course of this work, Manchester's soils are influenced by a plethora of factors, mainly related to historical contamination - the most affected areas are located away from present-day sources, with the exception of Trafford Park Industrial Estate which is likely receiving recurrent contamination inputs. This part of the geostatistical work aims more particularly at relating the geographical variables which are more likely to affect PHE concentrations in the present-day or recent past: with the exception of terrain variables, LOI and pH, all other variables are related to human activities and infrastructures which are likely to impact soil and RDS quality.

Therefore, performing OLS regression in soil data using only the environmental variables calculated as predictors has not shown satisfactory results. This is a likely result of the historical contamination of Manchester's soils, which has been previously reported in Chapter 3 (cf. sections 3.5.2 and 3.7) - variables which could express the presence and nature of past human occupation and activities at each location are absent from the freely available datasets. In addition, relationships between environmental variables and the elements to be modelled may be spatially variable, and need to be further explored through GWR, as detailed in section 6.2.1.

**Analysis #B**

Stepwise OLS has been performed again using the calculated environmental variables, plus the elemental concentrations for other elements which are likely related to the dependent variable. These relationships have been reported and interpreted previously in this work by correlation and PCA, and not surprisingly the dependent variables can be modelled with reasonable $R^2$ values. The models and explanatory variables of analysis #B are shown in Table 58 for each dependent variable.

| Dependent variable | Model $R^2$ (Adjusted) | Independent variables | Coefficient | Coefficient robust *p* | Joint F-Statistic Probability | Joint Wald Statistic Probability | Koenker (BP) Statistic Probability | Jarque-Bera Statistic Probability | AICc |
|---|---|---|---|---|---|---|---|---|---|
| Cr | 0,702758 | (constant) | 0,88831 | 0,00000 | 0,000000 | 0,000000 | 0,010882 | 0,000000 | -2741,5 |
| | | MGO_BC | 0,00226 | 0,00000 | | | | | |
| | | V_BC | 0,03630 | 0,00000 | | | | | |
| | | ZN_BC | 0,00565 | 0,00110 | | | | | |
| | | ZR_BC | 0,00360 | 0,00000 | | | | | |
| | | W_BC | 0,00299 | 0,00037 | | | | | |
| | | BI_BC | 0,00019 | 0,03625 | | | | | |
| | | CD_BC | 0,00077 | 0,00055 | | | | | |
| Ni | 0,920178 | (constant) | -46,52580 | 0,00000 | 0,000000 | 0,000000 | 0,020012 | 0,000011 | -501,7 |
| | | FE2O3_BC | 0,39932 | 0,00008 | | | | | |
| | | V_BC | 2,78082 | 0,00000 | | | | | |
| | | CO_BC | 0,95752 | 0,00000 | | | | | |
| | | ZN_BC | 0,34773 | 0,00000 | | | | | |
| | | SR_BC | 51,42165 | 0,00000 | | | | | |
| | | W_BC | 0,09288 | 0,00835 | | | | | |
| Cu | 0,837993 | (constant) | -2,44446 | 0,00000 | 0,000000 | 0,000000 | 0,000014 | 0,000000 | -32,9 |
| | | NI_BC | 0,34044 | 0,00000 | | | | | |
| | | ZN_BC | 1,14222 | 0,00000 | | | | | |
| | | AS_BC | 0,36088 | 0,02901 | | | | | |
| | | W_BC | 0,25007 | 0,00159 | | | | | |
| | | SN_BC | 0,77386 | 0,00000 | | | | | |
| | | BL300A_LOG | 0,02127 | 0,01209 | | | | | |
| Zn | 0,832646 | (constant) | -80,49013 | 0,00171 | 0,000000 | 0,000000 | 0,005809 | 0,000000 | -866,0 |
| | | BA_BC | 93,93110 | 0,00132 | | | | | |
| | | CU_BC | 0,07575 | 0,00000 | | | | | |
| | | PB_BC | 0,03140 | 0,00057 | | | | | |
| | | CD_BC | 0,04108 | 0,00000 | | | | | |
| | | SB_BC | 0,03861 | 0,00009 | | | | | |
| | | PH_BC | 0,00123 | 0,00001 | | | | | |
| As | 0,786567 | (constant) | -5,311584 | 0,007803 | 0,000000 | 0,000000 | 0,000161 | 0,000000 | -736,2 |
| | | FE2O3_BC | 0,14608 | 0,004203 | | | | | |
| | | CR_BC | 6,526261 | 0,001441 | | | | | |
| | | GE_BC | 0,505194 | 0,000000 | | | | | |
| | | BR_BC | 0,008957 | 0,003796 | | | | | |
| Pb | 0,755978 | (constant) | -585,9412 | 0,000003 | 0,000000 | 0,000000 | 0,126488 | 0,039271 | 100,3 |
| | | NA2O_BC | 0,681342 | 0,000726 | | | | | |
| | | SIO2_BC | 0,000039 | 0,000000 | | | | | |
| | | P2O5_BC | 0,104576 | 0,018954 | | | | | |
| | | CAO_BC | 0,149852 | 0,000003 | | | | | |
| | | BA_BC | 670,2059 | 0,000002 | | | | | |
| | | BR_BC | 0,045179 | 0,000806 | | | | | |
| | | MO_BC | 0,136892 | 0,000650 | | | | | |
| | | SN_BC | 0,676257 | 0,000000 | | | | | |
| | | SB_BC | 0,109343 | 0,002790 | | | | | |

Table 58: Best-fit OLS models for Cr, Ni, Cu, Zn, As and Pb in Manchester's soils (analysis set #B).

R-squared values are quite satisfactory and vary between 0.70 (Cr) and 0.92 (Ni) - the calculated models explain between 70 and 92% of the variation of the dependent element. A first observation is

that none of the calculated explanatory environmental variables were fit for inclusion in the models, when used along with geochemical concentrations as explanatory variables. Only Cu seems to have a weak relationship to the built-up area within 300m of soil sampling locations (BL300A_LOG, $\beta$=0.02127, p=0.01209). Otherwise, Cr, Ni, Cu, Zn, As and Pb concentrations can be modelled using the concentrations of related elements. This is possible as each of these elements' sources may be similar across the study area - as described in chapter 3, more specifically in sections 3.5.2 and 3.7, past or present contaminant inputs may contribute to soil enrichment not only in a single trace element, but several elements concomitantly.

For all these models, the Joint F-statistic and Joint Wald statistic are significant ($p<0.01$), meaning that the independent variables effectively explain the dependent element variation - the models are, overall, significant. The Koenker (BP) statistic is significant ($p<0.05$ or 0.01) for all models except Pb, revealing that these display statistically significant heteroscedasticity and/or non-stationarity. The Jarque-Bera statistic indicates that the residuals of all models are not normally distributed as should be ideal - the statistic value is significant ($p<0.05$) for all models.

The residual maps for the above models are displayed in section A.1 of Appendix 6. These maps highlight the locations with the largest differences between the measured dependent variable values and those estimated by the model, represented by the blue (< -2.5 standard deviations) and red (> 2.5 standard deviations) extremes; locations where model performance is best are shaded in yellow. However, these maps should be interpreted with caution, as the values are not normally distributed (the Jarque-Bera statistic is significant for all models) and models may also display statistically significant heteroscedasticity and/or non-stationarity. For Cr, the largest residual deviations are found in the area between A6 and A57/M602 in Salford, along the Mancunian Way, and in the Oxford Road and Davyhulme areas. The calculated model tends to overestimate Ni values for samples near the Mancunian Way and Ashton New Road, whereas in the south-western part of the study area Ni modelled values are generally lower than the observed values. The Zn model is less stable in the north-western part, from Worsley through north Salford, showing a greater number of samples with significant differences between observed and estimated values. Over- and underestimations for Cu, As and Pb display a more scattered pattern throughout the study area - . Residuals are not spatially autocorrelated, as revealed by the Moran's I statistic which is not significant ($p>0.05$) and, therefore, the spatial distribution of residual values is likely random for all models.

The fact that residuals are not normally distributed with a mean of zero (as pointed out by the Jarque-Bera statistic) indicates that key variables may be missing from the models, namely related to historical industry. Another reason why these models need to be interpreted with caution is that they display statistically significant non-stationarity; i.e. the relationships between the explanatory

and dependent variables vary regionally in the study area, and/or the residual variance is inconsistent. This is the case for all models with the exception of Pb, as the Koenker (BP) statistic is significant. Geographically weighted regression has also been performed, as further discussed, in an attempt to improve model significance - this type of spatial statistical modelling incorporates regional variation into the regression model.

## *5.1.2. RDS*

### *Analysis #A*

The OLS models calculated for Cr, Ni, Cu, Zn, As and Pb in Manchester's RDS display $R^2$ values ranging between 0.12 (Ni) and 0.38 (Zn) for the summer dataset, and between 0.14 (Cr) and 0.53 (Zn) for the winter dataset, using the calculated environmental variables (analysis #A). Parameters of the calculated models can be observed below in Table 59 and Table 60, and variable nomenclature in Table 11 (section 2.9.6.1). For all models, the Joint F-statistic and Joint Wald statistic are significant ($p<0.01$ or 0.05) - the independent variables effectively explain the dependent element variation, making models overall significant. The Koenker (BP) statistic is not significant in most models. Nevertheless, this statistic is significant for Cu (summer, p= 0.018), and As (winter, p=0.031), and therefore these models may display statistically significant heteroscedasticity and/or non-stationarity. The Jarque-Bera statistic is not significant ($p>0.05$) for all models except for As (winter, p= 0.04), indicating residuals are normally distributed except for this last element. The Moran's I statistic revealed that the spatial distribution of residual values is likely random for all models except again for As (winter, z= 1.957263, p=0.050317) - the Moran's I statistic is not significant ($p>0.05$) for all the remaining models.

| Dependent variable | Model $R^2$ (Adjusted) | Independent variables | Coefficient | Coefficient robust *p* | Joint F-Statistic Probability | Joint Wald Statistic Probability | Koenker (BP) Statistic Probability | Jarque-Bera Statistic Probability | AICc |
|---|---|---|---|---|---|---|---|---|---|
| Cr summer #A | 0,259583 | Intercept | 1,84690 | 0,00000 | 0,000064 | 0,000008 | 0,532637 | 0,808126 | -235,0 |
| | | RDGC50_LOG | -0,00790 | 0,00277 | | | | | |
| | | RDALL300_L | 0,02424 | 0,04679 | | | | | |
| Ni summer #A | 0,116397 | Intercept | 0,76352 | 0,00000 | 0,002096 | 0,000425 | 0,848233 | 0,914475 | -578,4 |
| | | 63INF2_LG | 0,02158 | 0,00076 | | | | | |
| Cu summer #A | 0,198275 | RDGA100_LG | 0,01188 | 0,00031 | 0,000468 | 0,000001 | 0,017945 | 0,730802 | -156,5 |
| | | BLD50V_LOG | 0,01303 | 0,02990 | | | | | |
| Zn summer #A | 0,375503 | Intercept | 4,57499 | 0,00000 | 0,000000 | 0,000000 | 0,053525 | 0,141098 | 37,4 |
| | | LOI_BC | 0,72602 | 0,00000 | | | | | |
| | | RDGA100_LG | 0,03042 | 0,01953 | | | | | |
| As summer #A | 0,271791 | Intercept | -1,29902 | 0,01654 | 0,000018 | 0,000000 | 0,406439 | 0,273911 | 4,8 |
| | | BUS50_LOG | 0,17561 | 0,02330 | | | | | |
| | | SLOPE_LOG | 0,13551 | 0,01180 | | | | | |
| | | 63INF2_LG | 1,96746 | 0,00000 | | | | | |
| Pb summer #A | 0,246190 | Intercept | 3,61288 | 0,00000 | 0,000064 | 0,000043 | 0,073489 | 0,710717 | 90,5 |
| | | LOI_BC | 0,48412 | 0,00361 | | | | | |
| | | RDGB25_LOG | 0,10317 | 0,00590 | | | | | |
| | | RDGA150_LG | 0,05810 | 0,00387 | | | | | |

Table 59: Best-fit OLS models for Cr, Ni, Cu, Zn, As and Pb in Manchester's RDS - summer (analysis set #A).

Considering the explanatory variables which show robust probabilities and interpretable coefficients, it is noticeable that the amount of grain size fraction <63µm (63inf2_LG) is an important predictor for all the winter models - and the only explanatory variable of this set for the summer and winter models of Ni. Organic matter content (LOI_BC) is also a good predictor in Zn models and the Pb (summer) model.

| Dependent variable | Model $R^2$ (Adjusted) | Independent variables | Coefficient | Coefficient robust *p* | Joint F-Statistic Probability | Joint Wald Statistic Probability | Koenker (BP) Statistic Probability | Jarque-Bera Statistic Probability | AICc |
|---|---|---|---|---|---|---|---|---|---|
| Cr winter #A | 0,136396 | Intercept | 2,40477 | 0,00015 | 0,002551 | 0,000327 | 0,154826 | 0,563989 | 67,2 |
| | | BLDGV0_LOG | 0,09850 | 0,00855 | | | | | |
| | | 63INF2W_LG | 0,58724 | 0,04814 | | | | | |
| Ni winter #A | 0,295781 | Intercept | 1,36842 | 0,00000 | 0,000001 | 0,000000 | 0,955799 | 0,101303 | 32,5 |
| | | 63INF2W_LG | 1,02540 | 0,00000 | | | | | |
| Cu winter #A | 0,345434 | Intercept | -6,26350 | 0,05618 | 0,000004 | 0,000000 | 0,458865 | 0,226072 | 338,9 |
| | | POPDENS_LG | 0,98206 | 0,04062 | | | | | |
| | | POPJOBS_LG | 0,82380 | 0,00854 | | | | | |
| | | RDGA25_LOG | 0,46700 | 0,00089 | | | | | |
| | | BUS100_LOG | 1,18821 | 0,01973 | | | | | |
| | | 63INF2W_LG | 5,20038 | 0,00017 | | | | | |
| Zn winter #A | 0,528691 | Intercept | 2,65925 | 0,00000 | 0,000000 | 0,000000 | 0,545553 | 0,154992 | 62,7 |
| | | LOI_BC_W | 0,32716 | 0,00001 | | | | | |
| | | POPJOBS_LG | 0,09739 | 0,00002 | | | | | |
| | | BUS100_LOG | 0,15449 | 0,04074 | | | | | |
| | | RDGA100_LG | 0,03779 | 0,01529 | | | | | |
| | | 63INF2W_LG | 0,85356 | 0,00042 | | | | | |
| As winter #A | 0,162438 | Intercept | 0,44479 | 0,27338 | 0,000824 | 0,011031 | 0,031032 | 0,044253 | -29,7 |
| | | RDGA25_LOG | 0,02648 | 0,00816 | | | | | |
| | | 63INF2W_LG | 0,39156 | 0,04554 | | | | | |
| Pb winter #A | 0,364681 | Intercept | -2,43421 | 0,02188 | 0,000001 | 0,000000 | 0,341132 | 0,679547 | 90,2 |
| | | POPDENS_LG | 0,22447 | 0,00450 | | | | | |
| | | POPJOBS_LG | 0,19062 | 0,00025 | | | | | |
| | | RDGB300_LG | 0,45843 | 0,00008 | | | | | |
| | | 63INF2W_LG | 0,97588 | 0,01094 | | | | | |

Table 60: Best-fit OLS models for Cr, Ni, Cu, Zn, As and Pb in Manchester's RDS - winter (analysis set #A).

Unlike soils, some of the calculated environmental variables showed reasonable relationships to the trace metals modelled. These variables include road density, building volume, number of bus stops, all at different distance buffers; as well as terrain slope, population density and number of jobs per census output area (cf. variable nomenclature in Table 11). These are all positively correlated to the presence of the studied trace metals in RDS - except for C roads, for which the coefficient is negative (RDGC50_LOG in Cr summer model). This road subtype only includes low traffic paths: alleys, pedestrianised streets and private roads. Therefore, a higher density of this road type implies very low traffic, which may explain the negative relationship to Cr concentrations assuming traffic volume as a possible Cr source to RDS. From these models, road density variables are the most frequent explanatory variables, followed by bus stop density (at 50 and 100m radiuses), population density, jobs per output area, and building data.

Residual maps for all models are shown in section A.2 and A.3 of Appendix 6. For the summer dataset, Cu, Zn and Pb residuals reveal that the model performs well across the study area; whereas

the Cr model tends to display over- and underestimates outside the Manchester city centre, and Ni within the Trafford park area. Arsenic residual values in the southwest part of the study area also tend to display over- and underestimates. Concerning winter data, residuals are more homogeneously distributed for Cr, Zn and Pb, indicating these models perform well in predicting these elements' concentrations. Nickel still displays frequent extreme residuals (<-2.5 or >2.5 standard deviations); and Cu seems to be underestimated in the eastern part of the study area and the inverse in the western part. The arsenic model residuals are not normally distributed, indicating a key variable may be missing from this model and therefore the obtained residual map is likely biased.

Although trace metal concentrations may be explained by this set of variables with reasonable statistical confidence, $R^2$ values for all models are still low and Cu (summer), and As (winter), display statistically significant heteroscedasticity and/or non-stationarity. Therefore, geochemical concentrations have been added as explanatory variables for analysis set #B, as it is known that the dependent variables chosen have statistical relationships with other chemical elements and are likely to enhance the model performance.

### *Analysis #B*

The inclusion of geochemical concentrations as further explanatory variables to model Cr, Ni, Cu, Zn, As and Pb increased the model performance - $R^2$ values range between 0.44 to 0.71 in summer models and between 0.51 and 0.88 in winter models. These show overall significance, as the Joint F-statistic and Joint Wald statistic are highly significant ($p<0.01$) - the independent variables effectively explain the dependent element variation. The Koenker (BP) statistic is not significant for all models, indicating these are likely stationary in both geographic and data space. Model residuals are normally distributed except for Ni, Cu and As in the summer dataset and Cr and Cu in the winter dataset, as the Jarque-Bera statistic is significant ($p<0.01$) for these elements. The spatial distribution of residuals is random except for Ni (summer), which displays a significant Moran's I value ($z= 3.142162$, $p=0.001677$). Regression parameters are shown in Table 61 and Table 62.

In addition to the chemical elements used as explanatory variables, which display significant coefficients due to their chemical and/or source affinities to the dependent variables, environmental variables are also part of the calculated models - only Ni and Cu (summer) models do not include at least one environmental explanatory variable. Road density within 25 metres distance (RDGA25_LOG [road group A], RDGB25_LOG [road group B]) and within 100 m distance (RDALL100_L, all roads) are included in the calculated models for Cr (summer), Cr, Ni, Cu and As (winter). The number of bus stops is also an explanatory variable for summer As and Pb; building area for Zn (summer) and Pb (winter); and the average annual daily traffic flow of heavy goods vehicles for winter Zn. Some of the chemical elements which are explanatory variables in the above models have previously been related to the dependent variables, namely in the components calculated by PCA (cf. section 4.7) - Cr to Zr,

Ba and Sb; Ni to V, Fe2O3 and Co; Cu to Zn, Sn and Sb; Zn to Cu and Sb; As to Ge; and Pb to Ba, Sn and Sb. Possible explanations for these element associations are covered in section 4.7.1.

| Dependent variable | Model $R^2$ (Adjusted) | Independent variables | Coefficient | Coefficient robust *p* | Joint F-Statistic Probability | Joint Wald Statistic Probability | Koenker (BP) Statistic Probability | Jarque-Bera Statistic Probability | AICc |
|---|---|---|---|---|---|---|---|---|---|
| Cr summer #B | 0,603123 | Intercept | -8,68277 | 0,00007 | 0,000000 | 0,000000 | 0,812347 | 0,059906 | -273,2 |
| | | NI_BC | 5,96332 | 0,00000 | | | | | |
| | | ZR_BC | 6,01660 | 0,00109 | | | | | |
| | | MO_BC | 0,03288 | 0,00448 | | | | | |
| | | POPJOBS_LG | 0,00592 | 0,00029 | | | | | |
| | | RDGA25_LOG | 0,00772 | 0,03590 | | | | | |
| | | RDGB25_LOG | 0,00909 | 0,01485 | | | | | |
| | | 63INF2_LG | -0,16810 | 0,00319 | | | | | |
| Ni summer #B | 0,693983 | Intercept | 0,28117 | 0,00000 | 0,000000 | 0,000000 | 0,580869 | 0,000002 | -651,8 |
| | | V_BC | 0,45396 | 0,00000 | | | | | |
| | | CR_BC | 0,02073 | 0,00096 | | | | | |
| | | CD_BC | 0,00079 | 0,01360 | | | | | |
| Cu summer #B | 0,568989 | Intercept | 1,39036 | 0,00000 | 0,000000 | 0,000000 | 0,116804 | 0,000228 | -200,6 |
| | | FE2O3_BC | 0,06998 | 0,00480 | | | | | |
| | | ZN_BC | 0,06719 | 0,00969 | | | | | |
| | | SN_BC | 0,33265 | 0,00001 | | | | | |
| Zn summer #B | 0,708410 | Intercept | 1,77734 | 0,02736 | 0,000000 | 0,000000 | 0,570668 | 0,289433 | -14,0 |
| | | CU_BC | 0,94795 | 0,01169 | | | | | |
| | | SB_BC | 0,38152 | 0,00000 | | | | | |
| | | LOI_BC | 0,45444 | 0,00000 | | | | | |
| | | BLD100A_LG | 0,03852 | 0,02099 | | | | | |
| As summer #B | 0,440313 | Intercept | -145,98810 | 0,00018 | 0,000000 | 0,000000 | 0,151097 | 0,000103 | -12,3 |
| | | BA_BC | 144,03397 | 0,00018 | | | | | |
| | | SE_BC | 0,13097 | 0,00806 | | | | | |
| | | BUS50_LOG | 0,17686 | 0,01843 | | | | | |
| | | SLOPE_LOG | 0,11513 | 0,00875 | | | | | |
| | | 63INF2_LG | 1,37116 | 0,00052 | | | | | |
| Pb summer #B | 0,624066 | Intercept | -140,03716 | 0,04257 | 0,000000 | 0,000000 | 0,340429 | 0,438417 | 0,6 |
| | | BA_BC | 142,46116 | 0,03717 | | | | | |
| | | SE_BC | 0,26953 | 0,00115 | | | | | |
| | | W_BC | 0,37226 | 0,01057 | | | | | |
| | | SB_BC | 0,40198 | 0,00003 | | | | | |
| | | BUS200_LG | 0,12659 | 0,01347 | | | | | |

Table 61: Best-fit OLS models for Cr, Ni, Cu, Zn, As and Pb in Manchester's RDS - summer (analysis set #B).

The residual maps of section A.4 and A.5 of Appendix 6 show that residual distribution has improved when compared to the maps of analysis set #A. The only element which displays a greater number of under- and overestimates is Ni - furthermore, the model tends to underestimate Ni values in the Trafford Park industrial estate region. This has already been pointed out by the Moran's I statistic, which revealed that Ni values are likely clustered. Nevertheless, all models revealed stationarity and consistent residual variance (the Koenker (BP) statistic is not significant), which is an improvement from the models calculated in analysis set #A.

| Dependent variable | Model $R^2$ (Adjusted) | Independent variables | Coefficient | Coefficient robust *p* | Joint F-Statistic Probability | Joint Wald Statistic Probability | Koenker (BP) Statistic Probability | Jarque-Bera Statistic Probability | AICc |
|---|---|---|---|---|---|---|---|---|---|
| Cr winter #B | 0,696435 | Intercept | 77,99917 | 0,00016 | 0,000000 | 0,000000 | 0,547160 | 0,000000 | -3,3 |
| | | FE2O3_BC_W | 0,29341 | 0,01859 | | | | | |
| | | CO_BC_W | 0,30656 | 0,02747 | | | | | |
| | | BA_BC_W | -59,60521 | 0,00026 | | | | | |
| | | SB_BC_W | 0,43703 | 0,00000 | | | | | |
| | | LOI_BC_W | -0,21822 | 0,00006 | | | | | |
| | | RDGB25_LOG | 0,04289 | 0,00118 | | | | | |
| Ni winter #B | 0,879153 | Intercept | 1,08301 | 0,00006 | 0,000000 | 0,000000 | 0,031700 | 0,084244 | -86,0 |
| | | FE2O3_BC_W | 0,34593 | 0,00000 | | | | | |
| | | CO_BC_W | 0,38705 | 0,00032 | | | | | |
| | | SE_BC_W | 0,04446 | 0,01268 | | | | | |
| | | RDALL100_L | 0,11421 | 0,00019 | | | | | |
| | | RAILDST0_L | 0,03352 | 0,00765 | | | | | |
| Cu winter #B | 0,795171 | Intercept | 2,90351 | 0,00001 | 0,000000 | 0,000000 | 0,928272 | 0,000006 | 255,5 |
| | | FE2O3_BC_W | 1,29885 | 0,00045 | | | | | |
| | | SN_BC_W | 0,84350 | 0,00815 | | | | | |
| | | SB_BC_W | 1,96585 | 0,00232 | | | | | |
| | | RDGA25_LOG | 0,25098 | 0,00197 | | | | | |
| Zn winter #B | 0,856647 | Intercept | 3,17628 | 0,00000 | 0,000000 | 0,000000 | 0,416465 | 0,052112 | -23,0 |
| | | V_BC_W | 0,17934 | 0,01467 | | | | | |
| | | CD_BC_W | 0,09710 | 0,00043 | | | | | |
| | | SB_BC_W | 0,59447 | 0,00000 | | | | | |
| | | LOI_BC_W | 0,17537 | 0,00004 | | | | | |
| | | HGVEH_LOG | 0,06893 | 0,00057 | | | | | |
| As winter #B | 0,514049 | Intercept | -27,83446 | 0,00132 | 0,000000 | 0,000000 | 0,182127 | 0,624046 | -89,2 |
| | | BA_BC_W | 23,05724 | 0,00083 | | | | | |
| | | GE_BC_W | 0,10924 | 0,02163 | | | | | |
| | | SE_BC_W | 0,06464 | 0,00010 | | | | | |
| | | U_BC_W | 0,06997 | 0,01789 | | | | | |
| | | RDGA25_LOG | 0,02668 | 0,00014 | | | | | |
| Pb winter #B | 0,715799 | Intercept | 3,20781 | 0,00000 | 0,000000 | 0,000000 | 0,666521 | 0,425998 | 35,6 |
| | | SE_BC_W | 0,17386 | 0,00001 | | | | | |
| | | TH_BC_W | 0,37554 | 0,00436 | | | | | |
| | | SN_BC_W | 0,08542 | 0,03101 | | | | | |
| | | SB_BC_W | 0,40590 | 0,00000 | | | | | |
| | | BLD50A_LOG | 0,06246 | 0,00307 | | | | | |

Table 62: Best-fit OLS models for Cr, Ni, Cu, Zn, As and Pb in Manchester's RDS - winter (analysis set #B).

## 5.2. Geographically-weighted regression

While OLS regression is a global spatial statistical model, geographically-weighted regression (GWR) is a local form of linear regression used to model spatially varying relationships; i.e. it is a local modelling technique for exploring spatial non-stationarity. Therefore, this method is useful if OLS models are non-stationary or for which the residuals display spatial autocorrelation. Similarly to OLS, GWR has been performed using ArcGIS® 10.0 GWR tool, as described in detail in section 2.9.6.3.

The inputs of the GWR tool in ArcGIS® 10.0 include the dependent variable to be modelled (Cr, Ni, Cu, Zn, Pb, As and Fe); the explanatory variables, previously tested by OLS; the adaptive kernel type used with the corrected Akaike Information Criterion (AICc), which defines the extent of the adaptive kernel - bandwidth distance will change according to the spatial density of sampling locations. Similarly to OLS, outlier samples (cf. Table 57) were censored from the dataset.

The GWR tool provides several outputs - the overall report of statistical results and an output feature class of model residual, which includes fields for observed and predicted dependent variable values, condition number, local $R^2$, explanatory variable coefficients, and standard errors. Maps of GWR estimations and t-statistics at the sampled locations have also been produced.

The statistical report contains relevant information for assessing model performance, such as (ESRI, 2012):

• **Number of neighbours** (or bandwidth, when choosing the "fixed" kernel option): by using the AICc criterion and the adaptive kernel, the ArcGIS tool will compute the optimal adaptive number of neighbours - bandwidth distance will change according to the spatial density of sampling points; i.e. Instead of a specific distance, the number of neighbours used for the analysis is reported.

• **Residual squares:** the sum of the squared residuals in the model - the residual being the difference between an observed dependent variable value and its estimated value returned by the GWR model. The smaller this measure, the closer the fit of the GWR model to the observed data.

• **Effective number:** reflects a trade-off between the variance of the fitted values and the bias in the coefficient estimates, and is related to the choice of bandwidth. As the bandwidth approaches infinity, the geographic weights for every observation approach 1, and the coefficient estimates will be very close to those for a global OLS model. Therefore, for very large bandwidths, the effective number of coefficients approaches the actual number - local coefficient estimates will have a small variance but will be quite biased. For extremely small bandwidths, the effective number of coefficients is the number of observations - local coefficient estimates will have a large variance but a low bias.

• **Sigma:** the estimated standard deviation for the residuals. Smaller values of this statistic are preferable, as this value is the square root of the normalized residual sum of squares (the residual sum of squares divided by the effective degrees of freedom of the residual).

• **AICc:** the corrected Akaike Information Criterion. is a measure of model performance and is helpful for comparing different regression models. Taking into account model complexity, the model with the lower AICc value provides a better fit to the observed data. Comparing the GWR AICc value to the OLS AICc value is one way to assess the benefits of moving from a global model (OLS) to a local regression model (GWR).

• **$R^2$:** a measure of goodness of fit, varying from 0.0 to 1.0. It represents the proportion of the dependent variable variance accounted for by the regression model.

• **$R^2$ adjusted:** a normalized computation of the $R^2$ - it includes the degrees of freedom of the numerator and denominator of the $R^2$ calculations; the denominator being the sum of squared dependent variable values. This has the effect of compensating for the number of variables in a

model and, consequently, the adjusted $R^2$ value is commonly smaller than the R2 value. However, in making this adjustment, the interpretation of the value as a proportion of the variance explained is lost and the use of the AICc to compare models is therefore preferred.

The output feature class of model residuals is displayed as a classified colour map of the standardised residuals at each location. As for OLS, high/low residuals (indicating over- and under-predictions) should be randomly distributed - this is assessed by running the Spatial Autocorrelation (Moran's i) tool on the regression residuals. The residuals feature class includes the following fields for each sample location, accessible from the attribute table (ESRI, 2012):

- **Condition number:** Results associated with condition numbers larger than 30 may be unreliable - this diagnostic evaluates local multicollinearity. A model with no multicollinearity would show condition numbers close to 1.
- **Local $R^2$:** indicates how well the local regression model fits the observed dependent variable values. This parameter can be mapped in order to observe where the GWR model predicts well and where it predicts poorly.
- **Predicted:** the estimated dependent variable values at each location, calculated by the GWR model.
- **Residual and Standardised Residuals:** the difference between estimated values and observed values. Standardised residuals are rendered in the output feature class map.
- **Coefficients (C1, C2, etc):** Local estimated $\beta$ values for each explanatory variable in the model.
- **Coefficient standard error:** a measure of the reliability of each coefficient estimate. This parameter shall display a small value relatively to the actual coefficient values, in order to obtain a higher degree of confidence in the estimated coefficients.

If the coefficient raster option is selected, the GWR tool creates coefficient raster surfaces for the model intercept and each explanatory variable. This is useful to assess how spatially consistent (stationary) the relationships between the dependent variable and each explanatory variable are. A map containing the GWR predictions at the sampled locations can also be displayed - GWR calibrates the regression equation using known dependent variable values from the input feature class, and then creates a new output feature class with dependent variable estimates at sample locations.

The results in the following sections refer the models calculated for Cr, Ni, Cu, Zn, As and Pb through GWR for Manchester's soils and RDS. Similarly to OLS, GWR has been computed as sets #A and #B: analysis set #A comprise the best model results using the calculated environmental explanatory variables, and analysis set #B include the concentrations of the other chemical elements as explanatory variables in the model, in addition to the calculated environmental variables. GWR models have not been computed for all dependent variables tested - model design problems were

encountered, mainly due to multicollinearity between explanatory variables and/or very low $R^2$ values. Calculated models are summarised in Table 63.

| | Soil | | RDS | | | |
|---|---|---|---|---|---|---|
| | A | B | A-summer | A-winter | B-summer | B-winter |
| Cr | √ | × | × | × | × | × |
| Ni | × | × | × | √ | × | × |
| Cu | √ | × | √ | √ | × | √ |
| Zn | √ | × | √ | × | × | × |
| As | √ | × | × | √ | × | × |
| Pb | √ | √ | √ | × | √ | √ |

Table 63: GWR models for Manchester's soils and RDS for analysis sets #A and #B (√: calculated model).

T-statistics and parameter estimate maps have also been produced in order to visualise the areas of statistically significant positive or negative relationships between the explanatory variables and the modelled metals. These are displayed in Appendix 6, part B.

## *5.2.1. Soils*

### *Analysis #A*

Geographically-weighted regression models for soils have been calculated for Cr, Cu, Zn and Pb using environmental explanatory variables (analysis set #A). Although OLS regression did not produce consistent results for soils using environmental explanatory variables as pointed out in section 6.1.1., GWR models were successfully computed - an indication that the relationships between the modelled elements and the environmental variables are likely non-stationary.

Model results for Cr, Cu, Zn, As and Pb are summarised in Table 64 below. R-squared values are small, ranging between 0.033 (Cu) and 0.063 (Zn). Road-related variables and building-related variables were more often associated to the modelled elements. Condition numbers (CN) for Cr and Cu are relatively high, with maximum CN of 28 and 25, respectively. Still, these CN are below the threshold of 30, which would indicate problems with multicollinearity. Bandwidth values approach the number of samples used to calculate each model, after outlier removal, which may indicate poorly fitted GWR models. Parameter estimate minimum, mean and maximum values for each explanatory variable are also reported in Table 64, as well as the t-statistics produced for each model. The t-statistic values within the 95% confidence interval (]-2.5, -1.96] or ]1.96, 2.5]) and the 99% confidence level (<-2.5 or >2.5) are also reported. Variables contribute significantly to the model where t-statistics values are high - explanatory variables with t-statistic values below -1.96 have a statistically significant negative association to the modelled variable; whereas values >1.96 indicate a statistically significant positive association.

| Soil Cr A | min | mean | max | % of t-statistic values between: | | | | |
|---|---|---|---|---|---|---|---|---|
| | | | | <-2.5 | ]-2.5, -1.96] | ]-1.96, 1.96] | ]1.96, 2.5] | >2.5 |
| Intercept | 0,992 | 0,995 | 0,998 | | | | | |
| rdGC250_lg | -1,25E-04 | 8,18E-05 | 2,08E-04 | 0 | 0 | 100 | 0 | 0 |
| Height_lg | 3,92E-04 | 1,45E-03 | 2,45E-03 | 0 | 0 | 50 | 3 | 47 |
| Condition Number | 22,590 | 25,317 | 28,312 | | | | | |
| Adjusted $R^2$ | 0,042 | | | | | | | |
| AICc | -2402 | | | | | | | |
| Bandwidth size | 292 | | | | | | | |

| Soil Cu A | min | mean | max | % of t-statistic values between: | | | | |
|---|---|---|---|---|---|---|---|---|
| | | | | <-2.5 | ]-2.5, -1.96] | ]-1.96, 1.96] | ]1.96, 2.5] | >2.5 |
| Intercept | 4,474 | 4,667 | 4,838 | | | | | |
| rdGA300_lg | -0,035 | -0,031 | -0,026 | 47 | 48 | 5 | 0 | 0 |
| bl100H_lg | -0,182 | -0,147 | -0,113 | 0 | 0 | 100 | 0 | 0 |
| bl250H_lg | 0,076 | 0,120 | 0,154 | 0 | 46 | 54 | 0 | 0 |
| Condition Number | 17,706 | 21,650 | 25,274 | | | | | |
| Adjusted $R^2$ | 0,0334 | | | | | | | |
| AICc | 488 | | | | | | | |
| Bandwidth size | 291 | | | | | | | |

| Soil Zn A | min | mean | max | % of t-statistic values between: | | | | |
|---|---|---|---|---|---|---|---|---|
| | | | | <-2.5 | ]-2.5, -1.96] | ]-1.96, 1.96] | ]1.96, 2.5] | >2.5 |
| Intercept | 2,829 | 2,877 | 2,932 | | | | | |
| rdGA300_lg | -0,009 | -0,007 | -0,005 | 50 | 22 | 29 | 0 | 0 |
| bl350H_lg | -0,063 | -0,038 | -0,017 | 35 | 9 | 56 | 0 | 0 |
| Condition Number | 14,086 | 17,924 | 21,237 | | | | | |
| Adjusted $R^2$ | 0,063 | | | | | | | |
| AICc | -349 | | | | | | | |
| Bandwidth size | 298 | | | | | | | |

| Soil As A | min | mean | max | % of t-statistic values between: | | | | |
|---|---|---|---|---|---|---|---|---|
| | | | | <-2.5 | ]-2.5, -1.96] | ]-1.96, 1.96] | ]1.96, 2.5] | >2.5 |
| Intercept | 2,009 | 2,055 | 2,104 | | | | | |
| rdGC150_lg | 0,007 | 0,009 | 0,011 | 0 | 0 | 15 | 24 | 61 |
| rdGA350_lg | -0,014 | -0,011 | -0,010 | 100 | 0 | 0 | 0 | 0 |
| bl100H_lg | -0,057 | -0,041 | -0,028 | 50 | 48 | 2 | 0 | 0 |
| Condition Number | 10,646 | 11,397 | 13,055 | | | | | |
| Adjusted $R^2$ | 0,117 | | | | | | | |
| AICc | -306 | | | | | | | |
| Bandwidth size | 295 | | | | | | | |

| Soil Pb A | min | mean | max | % of t-statistic values between: | | | | |
|---|---|---|---|---|---|---|---|---|
| | | | | <-2.5 | ]-2.5, -1.96] | ]-1.96, 1.96] | ]1.96, 2.5] | >2.5 |
| Intercept | 5,281 | 5,378 | 5,454 | | | | | |
| rdGC250_lg | 0,023 | 0,026 | 0,029 | 0 | 0 | 100 | 0 | 0 |
| rdGA350_lg | -0,037 | -0,028 | -0,018 | 40 | 18 | 42 | 0 | 0 |
| Condition Number | 5,736 | 5,895 | 6,200 | | | | | |
| Adjusted $R^2$ | 0,035 | | | | | | | |
| AICc | 505 | | | | | | | |
| Bandwidth size | 293 | | | | | | | |

Table 64: GWR model summaries for Cr, Cu, Zn, As and Pb in soils (analysis set #A).

T-statistics and parameter estimate maps for Manchester soils are displayed in Appendix 6, part B.1.

In the Cr model, HEIGHT has a high proportion of significantly positive relationships ($t>1.96$, $p<0.05$) with 50% of samples. The remaining 50% of samples do not show significant relationships with HEIGHT in the model - t-statistic values range between -1.96 and 1.96. The same happens for 100% of the samples for rdGC250. In fact, rdGC250 coefficients are very small for all samples - there is very little spatial difference in this variable, suggesting an element of homogeneity. Figure 132 displays the t-statistic values and parameter estimates for HEIGHT and rdGC250 and it can be observed that the strongest positive relationships for HEIGHT are located in the eastern part of the study area (red points) - these represent a statistically significant positive influence on Cr soil concentrations at the $t>2.5$ ($p<0.01$) confidence level. Parameter estimates are also higher for samples of this area. The eastern part of the study area has the highest altitudes, as shown in Figure 9, suggesting that this fact favours the accumulation of Cr in soils. Nevertheless, and as expected, rdGC250 t-statistic values and parameter estimates do not show a great variation across the study area.

The Cu model displays significantly negative relationships ($t<-1.96$) for 95% of the samples for rdGA300, and 46% of the samples for bl250H - considering these samples, these variables are negatively associated with Pb concentrations. This is also shown in Figure 133, where t-statistic values are below -1.96 at most sample locations for rdGA300 and at 46% of the sample locations for bl100H (blue points). Statistically significant negative relationships are preferably located in the western part of the study area. In this region, more specifically in the northeast section for rdGA300 and the southeast section for bl250H, parameter estimates are more strongly negative. This suggests that both the length of A roads within a 300m buffer and the average building height within a 250m buffer around each sample point are negatively related to Cu concentrations, and this relationship is more statistically significant in the eastern part of the study area. The variable bl250H does not show significant relationships with any samples in the model - 100% of the samples are within the -1.96 - 1.96 t-statistics interval (yellow points in the t-statistics map). Although relationships are not statistically significant, parameter estimates are larger in the western part of the study area.

In the Zn model, 72% of the samples are significantly negatively related to rdGA300 ($t<-1.96$). These samples are located in the eastern two-thirds of the study area, as shown in Figure 134 (blue points). Parameter estimates are more strongly negative in the northeast section, although parameter estimates vary within a short range of values. Similarly to Cu, the length of A roads within a 300m buffer seems to have a negative influence on Zn concentrations, and this relationship is more statistically significant in the eastern part of the study area. A statistically significant negative relationship is also found between bl350H and 44% of the samples. Nevertheless, Figure 134 shows that these are located in the western part of the study area (blue points), where parameter estimates are also more strongly negative - average building height within 350 meters of the

sampling point shows a negative relationship to Zn content in soils, more pronouncedly in the western area.

The As model reveals statistically significant positive relationships (t>1.96) between rdGC150 and 85% of soil samples, and this positive relationship is stronger in the western two-thirds of the study area, as mapped in Figure 135 (orange and red points). Parameter estimates are higher in the Old Trafford - Trafford Park area: in this region, the length of C roads within 150m of each sample seems to be more positively related to As concentrations in soils. All samples display a statistically significant negative relationship (t<-2.5, p<0.01) to rdGA350, as represented by the blue points in Figure 135. Parameter estimates for this explanatory variable display a very short value range and are more negative north of the Manchester city centre. Another variable with statistically significant negative relationships to As concentrations is bl100H, with 98% of the samples displaying t-statistic values below -1.96. These are preferably located in the east of the study area, where parameter estimates are also more strongly negative.

In the Pb model, 58% of the samples are significantly negatively related to rdGA350 (t<-1.96), whereas rdGC250 does not show significant relationships with any samples in the model (1.96<t<1.96). In the maps of Figure 136, the significantly negative relationships are observed for rdGA350 in the northeast sector of the study area, where the strongest negative parameter estimates are also found. This may indicate that road length within a 350m distance buffer is negatively related to soil Pb concentrations, especially in the north-eastern sector.

### *Analysis #B*

Lead has also been modelled using other chemical elements as explanatory variables (analysis set #B). Parameter estimates for each explanatory variable and t-statistic values within the 95% confidence interval (]-2.5, -1.96] or ]1.96, 2.5]) and the 99% confidence level (<-2.5 or >2.5) are reported in Table 64. This model explains a greater percentage of the system variance when compared to analysis #A models, with an $R^2$ of 0.63. Also, parameter estimates display higher minimum and maximum values, as well as a wider range of values. Bandwidth size is close to the number of samples used for the model.

| **Soil Pb B** | min | mean | max | % of t-statistic values between: | | | | |
|---|---|---|---|---|---|---|---|---|
| | | | | <-2.5 | ]-2.5, -1.96] | ]-1.96, 1.96] | ]1.96, 2.5] | >2.5 |
| Intercept | 2,843 | 3,024 | 3,333 | | | | | |
| Na2O_BC | 0,681 | 0,801 | 0,933 | 0 | 0 | 0 | 9 | 91 |
| Sn_BC | 1,298 | 1,403 | 1,462 | 0 | 0 | 0 | 0 | 100 |
| Condition Number | 21,453 | 21,913 | 22,348 | | | | | |

| | |
|---|---|
| Adjusted $R^2$ | 0,633 |
| AICc | 221 |
| Bandwidth size | 293 |

Table 65: GWR model summary for Pb in soils (analysis set #B).

This model displays significantly positive relationships for both explanatory variables considered, $Na_2O$ and Sn, with all samples displaying t-statistic values above 1.96. This is also observed in the maps of Figure 137 - the highest t-statistic values for $Na_2O$ are observed in the eastern sector of the study area; whereas the opposite trend is observed for Sn, with the western part displaying the highest values (dark red points). Parameter estimates also follow this trend for each explanatory variable. $Na_2O$ and Sn have been related to Pb in soils previously in this work - spearman's rank coefficients between Pb and these elements in soils are of 0.28 and 0.77 ($p<0.01$), respectively (cf. Table 77). Sodium has been associated through SEM analysis to Pb in spherical glass grains derived from high temperature combustion processes; whereas Sn-Pb alloys have been used as solders for many years - coincidently, high Pb concentrations in soils are found, near businesses related to car servicing, breaking and dismantling (cf. Figure 48), apart from historical contamination.

## *5.2.2. RDS*

### *Analysis #A, summer*

GWR models for Cu, Zn and Pb in RDS-summer are summarised in Table 66. R-squared values are substantially better than those found for soils in analysis set #A, varying between 0.217 (Pb) and 0.531 (Zn). Condition numbers are also improved in RDS, confirming that multicollinearity is not an issue. Nevertheless, bandwidth sizes approach the number of samples used in the model for Cu and Pb. T-statistics and parameter estimate maps for Manchester soils are displayed in Appendix 6, part B.2.

The Cu model displays rdGA100 and bld50V as explanatory variables. rdGA100 is significantly positively associated to all samples, with t-statistic values above 2.5. The mapping of t-statistics of Figure 138 shows that the highest values are obtained in the central part of the study area, covering the west of Manchester city centre, the Oxford Road area, Old Trafford and Salford (dark red points). Parameter estimates are also the highest in this region, although value range is small (0.011 - 0.015). Parameter estimates for bld50V displays higher values in the eastern part of the study area. Nevertheless, this explanatory variable does not show significant relationships with any samples in the model, with 100% of the samples in the t-statistics range between -1.96 and 1.96 - this is also evident in the t-statistic map of Figure 138 (yellow points). Copper has been related to brake lining and tyre wear particles, as well as with the leakage of motor oils (Table 1) and therefore the positive relationship with the length of A roads within 100m of each sample is easily explained.

The Zn model displays statistically significant positive relationships to LOI and rdGA100, with 91% and 49% of the samples, respectively, displaying t-statistics above 1.96. This is displayed in Figure 139, where the highest t-values are found in the northeast sector of the study area for LOI, and just west of Manchester city centre for rdGA100 (red points). Parameter estimates follow the same trend,

being higher in the same regions as the t-statistic values. Organic matter content (LOI) has been positively related to RDS summer Zn - these display a spearman's rank correlation coefficient of 0.549 ($p<0.01$), as in Table 97. Similarly to Cu, traffic-related sources also contribute to Zn in RDS, as has been extensively reported (cf. Table 1), explaining the relationship between this element and rdGA100 evidenced by GWR.

| **RDSsummer Cu A** | min | mean | max | % of t-statistic values between: | | | | |
|---|---|---|---|---|---|---|---|---|
| | | | | <-2.5 | ]-2.5, -1.96] | ]-1.96, 1.96] | ]1.96, 2.5] | >2.5 |
| Intercept | 2,182 | 2,204 | 2,228 | | | | | |
| rdGA100_lg | 0,011 | 0,013 | 0,015 | 0 | 0 | 0 | 0 | 100 |
| Bld50V_lg | 0,008 | 0,010 | 0,012 | 0 | 0 | 100 | 0 | 0 |
| Condition Number | 8,990 | 11,758 | 15,378 | | | | | |

| | |
|---|---|
| Adjusted $R^2$ | 0,227 |
| AICc | -149 |
| Bandwidth size | 71 |

| **RDSsummer Zn A** | min | mean | max | % of t-statistic values between: | | | | |
|---|---|---|---|---|---|---|---|---|
| | | | | <-2.5 | ]-2.5, -1.96] | ]-1.96, 1.96] | ]1.96, 2.5] | >2.5 |
| Intercept | 3,993 | 4,574 | 5,305 | | | | | |
| LOI_BC | 0,252 | 0,725 | 1,067 | 0 | 0 | 8 | 4 | 87 |
| rdGA100_lg | 0,008 | 0,036 | 0,066 | 0 | 0 | 51 | 34 | 15 |
| Condition Number | 8,963 | 11,280 | 15,044 | | | | | |

| | |
|---|---|
| Adjusted $R^2$ | 0,531 |
| AICc | 51 |
| Bandwidth size | 45 |

| **RDSsummer Pb A** | min | mean | max | % of t-statistic values between: | | | | |
|---|---|---|---|---|---|---|---|---|
| | | | | <-2.5 | ]-2.5, -1.96] | ]-1.96, 1.96] | ]1.96, 2.5] | >2.5 |
| Intercept | 3,624 | 3,847 | 4,042 | | | | | |
| LOI_BC | 0,287 | 0,443 | 0,611 | 0 | 0 | 54 | 17 | 29 |
| rdGB25_lg | 0,046 | 0,055 | 0,066 | 0 | 0 | 100 | 0 | 0 |
| rdGA150_lg | 0,056 | 0,068 | 0,079 | 0 | 0 | 0 | 25 | 75 |
| Condition Number | 11,186 | 12,482 | 13,826 | | | | | |

| | |
|---|---|
| Adjusted $R^2$ | 0,217 |
| AICc | 123 |
| Bandwidth size | 72 |

Table 66: GWR model summaries for Cu, Zn and Pb in RDS summer (analysis set #A).

In the Pb model, and similarly to Zn, LOI and rdGA150 are explanatory variables with a high proportion of samples with statistically significant positive relationships - 46% and 100% of samples, respectively, display t-statistic values above 1.96. The length of B roads within 25m of each sample point (rdGB25) displays positive parameter estimates; however, t-statistic values between -1.96 and 1.96 reveal that this explanatory variable does not show statistically significant relationships with any samples in the model. It can be observed in Figure 140 that the strongest positive relationships are found in the eastern sector for LOI and in the western sector for rdGA150 (red points), whereas relationships are non-significant for rdGB25 across the study area (yellow points). Similarly to rdgA100 in the Zn model, rdGA150 in the Pb model also displays the highest parameter estimates

just west of Manchester city centre; and LOI parameter estimates are also the highest in the eastern sector. Again, organic matter content displays a statistically significant ($p<0.01$) spearman's rank correlation coefficient of 0.309 with Pb in RDS-summer (cf. Table 97), and traffic - and hence the A-road density - has been a long known source of Pb to RDS.

### *Analysis #A, winter*

GWR models for RDS-winter data have been calculated for Ni, Cu and As. R-squared values of 0.40 have been obtained for Ni and Cu and 0.226 for As. The proportion of grain size fraction below 63µm (63inf2W) is an explanatory variable common to all models. Table 67 shows a summary of parameter estimates and the percentage of samples within the t-statistic significance intervals for each variable in the GWR models.

The only explanatory variable included in the Ni model is 63inf2W. As observed in Figure 142, this variable's performance is best in the east part of the study area and also along the M602; nevertheless, all other samples are also significantly positively related ($t>1.96$) to this variable. Parameter estimates are the highest just west of Manchester city centre, in the Oxford Road area, Hulme and north Salford.

The Cu model evidences bus100 and 63inf2W as explanatory variables, which are significantly positively related to 31 and 68% of RDS winter samples, respectively ($t>1.96$). The maps of Figure 143 show that these relationships are stronger in the southwest corner of the study area for bus100 and in the western half for 63inf2W (orange and red points). Highest parameter estimates coincide with the southwest corner for bus100, but 63inf2W displays the highest coefficients in the north-western sector.

The As model includes rdGA25 as an explanatory variable, for which 33% of the samples show statistically significant positive relationships. 63inf2W displays positive relationships for 49% of RDS winter samples. In terms of their spatial distribution, represented in Figure 144, rdGA25 shows significant positive relationships to samples in the west third of the study area (orange points), along with higher parameter estimates; whereas 63inf2W performs better in the eastern half, where parameter estimates are also higher.

It has been reported throughout the literature that trace metal concentrations usually have a positive correlation to the proportion of fine grained material (cf. section 1.7 and 4.1.4) - the inclusion of this variable in the model is not unanticipated, especially in winter samples, where fine-grained material is often predominant as well as higher trace metal concentrations. Spearman's rank correlation coefficients between 63inf2W and Ni, Cu and As were of 0.530, 0.390 and 0.419 ($p<0.01$), respectively.

| RDSwinter Ni A | min | mean | max | % of t-statistic values between: <-2.5 | ]-2.5, -1.96] | ]-1.96, 1.96] | ]1.96, 2.5] | >2.5 |
|---|---|---|---|---|---|---|---|---|
| Intercept | 0,622 | 1,379 | 1,788 | | | | | |
| 63inf2W_lg | 0,768 | 1,009 | 1,299 | 0 | 0 | 0 | 3 | 97 |
| Condition Number | 18,740 | 21,657 | 26,083 | | | | | |

| | |
|---|---|
| Adjusted $R^2$ | 0,402 |
| AICc | 41 |
| Bandwidth size | 42 |

| RDSwinter Cu A | min | mean | max | % of t-statistic values between: <-2.5 | ]-2.5, -1.96] | ]-1.96, 1.96] | ]1.96, 2.5] | >2.5 |
|---|---|---|---|---|---|---|---|---|
| Intercept | -8,169 | -0,179 | 7,970 | | | | | |
| bus100_lg | 0,533 | 1,178 | 2,077 | 0 | 0 | 69 | 30 | 1 |
| 63inf2W_lg | 2,733 | 6,181 | 9,871 | 0 | 0 | 32 | 10 | 58 |
| Condition Number | 24,192 | 25,937 | 29,174 | | | | | |

| | |
|---|---|
| Adjusted $R^2$ | 0,404 |
| AICc | 347 |
| Bandwidth size | 49 |

| RDSwinter As A | min | mean | max | % of t-statistic values between: <-2.5 | ]-2.5, -1.96] | ]-1.96, 1.96] | ]1.96, 2.5] | >2.5 |
|---|---|---|---|---|---|---|---|---|
| Intercept | 0,318 | 0,597 | 0,824 | | | | | |
| rdGA25_lg | 0,018 | 0,024 | 0,031 | 0 | 0 | 67 | 33 | 0 |
| 63inf2W_lg | 0,201 | 0,316 | 0,460 | 0 | 0 | 51 | 6 | 43 |
| Condition Number | 22,792 | 24,091 | 25,512 | | | | | |

| | |
|---|---|
| Adjusted $R^2$ | 0,226 |
| AICc | -25 |
| Bandwidth size | 72 |

Table 67: GWR model summaries for Ni, Cu and As in RDS winter (analysis set #A).

### *Analysis #B, summer*

Only Pb produced a consistent GWR model for RDS summer, including other chemical elements as explanatory variables. The summary of parameter estimates and the percentage of samples within the t-statistic significance intervals are shown below in Table 68. The r2 value of 0.727 is the highest found so far for a GWR model, confirming that the inclusion of geochemical variables substantially improves model performance.

The statistically significant positive relationships (t>1.96) observed in all samples in the model for Se and Sb, and for 84% of samples for W, had been previously pointed out by the calculation of spearman's rank correlation coefficients: Pb showed $\rho$ values of 0.419, 0.694 and 0.605 with Se, Sb and W, respectively (cf. Table 97). Bus200 is the other explanatory variable considered in the model - nevertheless, this variable is not significantly related with any samples in the model as 100% of the samples show t-statistic values between -1.96 and 1.96.

| RDSsummer Pb B | min | mean | max | % of t-statistic values between: | | | | |
|---|---|---|---|---|---|---|---|---|
| | | | | <-2.5 | ]-2.5, -1.96] | ]-1.96, 1.96] | ]1.96, 2.5] | >2.5 |
| Intercept | 3,775 | 3,877 | 4,000 | | | | | |
| Se_BC | 0,194 | 0,256 | 0,322 | 0 | 0 | 0 | 15 | 85 |
| W_BC | 0,244 | 0,424 | 0,587 | 0 | 0 | 17 | 21 | 63 |
| Sb_BC | 0,465 | 0,552 | 0,645 | 0 | 0 | 0 | 0 | 100 |
| bus200_lg | 0,069 | 0,090 | 0,108 | 0 | 0 | 100 | 0 | 0 |
| Condition Number | 13,906 | 14,557 | 15,179 | | | | | |

| | |
|---|---|
| Adjusted $R^2$ | 0,727 |
| AICc | 52 |
| Bandwidth size | 72 |

Table 68: GWR model summary for Pb in RDS summer (analysis set #B).

Figure 141 shows that the explanatory variables are better predictors in different sectors of the study area: the highest statistically significant positive relationships are found outside Manchester city centre for Se, in the eastern sector for W and in the western sector for Sb (red points). Parameter estimates follow approximately the same trend. Bus200 coefficients are higher in the southeast sector of the study area, although relationships between this variable and RDS samples are not statistically significant. Lead has previously been reported as globally correlated to Se, W and Sb, with spearman's rank correlation coefficients of 0.419, 0.605 and 0.694, respectively.

### *Analysis #B, winter*

Copper and Pb were successfully modelled for RDS winter using chemical concentrations of other elements as explanatory variables. Table 69 shows the percentage of samples within the t-statistic significance intervals and a summary of parameter estimates. R-squared values were, again, improved with the addition of geochemical variables: 0.838 for Cu and 0.787 for Pb.

All explanatory variables used to model Cu concentrations have been found to be significantly positively related to 100% of RDS winter samples (t>2.5 for $Fe_2O_3$, Sn and Sb; t>1.96 for rdGA25). T-statistic values (Figure 145) display an east to west trend for Sn and Sb; while the opposite occurs for $Fe_2O_3$ for which the highest values are found in the eastern half of the study area (dark red points). Parameter estimates follow the same trends as the T-statistic values. rdGA25 strongest positive relationships are found for samples in the southeast quadrant, along with the highest parameter estimates for this variable. Iron, Sn and Sb have been previously related to Cu, with spearman's rank coefficients of 0.633, 0.767 and 0.794, respectively (cf. Table 98) - these are known anthropogenically-enriched elements in Manchester's RDS, especially in areas of strong industrial activities (cf. section 4.7.1). Traffic related sources may also be influential to Cu concentrations in RDS, as this element can be derived mainly from the wear and tear of brake linings (cf. Table 1).

| RDSwinter Cu B | min | mean | max | % of t-statistic values between: | | | | |
|---|---|---|---|---|---|---|---|---|
| | | | | <-2.5 | ]-2.5, -1.96] | ]-1.96, 1.96] | ]1.96, 2.5] | >2.5 |
| Intercept | 2,227 | 2,849 | 3,726 | | | | | |
| Fe2O3_BC | 0,998 | 1,498 | 1,866 | 0 | 0 | 0 | 0 | 100 |
| Sn_BC | 0,716 | 0,783 | 0,848 | 0 | 0 | 0 | 0 | 100 |
| Sb_BC | 1,446 | 1,938 | 2,378 | 0 | 0 | 0 | 0 | 100 |
| rdGA25_lg | 0,220 | 0,271 | 0,343 | 0 | 0 | 0 | 28 | 72 |
| Condition Number | 12,950 | 14,022 | 14,995 | | | | | |

| | |
|---|---|
| Adjusted $R^2$ | 0,838 |
| AICc | 255 |
| Bandwidth size | 71 |

| RDSwinter Pb B | min | mean | max | % of t-statistic values between: | | | | |
|---|---|---|---|---|---|---|---|---|
| | | | | <-2.5 | ]-2.5, -1.96] | ]-1.96, 1.96] | ]1.96, 2.5] | >2.5 |
| Intercept | 2,802 | 3,354 | 3,698 | | | | | |
| Se_BC | 0,115 | 0,166 | 0,200 | 0 | 0 | 0 | 10 | 90 |
| Th_BC | 0,072 | 0,174 | 0,274 | 0 | 0 | 100 | 0 | 0 |
| Sn_BC | 0,082 | 0,101 | 0,116 | 0 | 0 | 85 | 15 | 0 |
| Sb_BC | 0,446 | 0,545 | 0,649 | 0 | 0 | 0 | 0 | 100 |
| Bld50A_lg | 0,017 | 0,032 | 0,053 | 0 | 0 | 100 | 0 | 0 |
| Condition Number | 0,072 | 0,174 | 0,274 | | | | | |

| | |
|---|---|
| Adjusted $R^2$ | 0,787 |
| AICc | 65 |
| Bandwidth size | 72 |

Table 69: GWR model summaries for Cu and Pb in RDS winter (analysis set #B).

The Pb model includes Se, Th, Sn, Sb and bld50A as explanatory variables. From these, Th and bld50A are not significantly related with any samples in the model as 100% of samples show t-statistic values between -1.96 and 1.96. For Se and Sb, all samples display statistically significant positive associations; nevertheless, only 15% of samples are significantly positively related to Sn in the Pb model. In Figure 146 it is observed that the distribution of t-statistic values and parameter estimates is quite different for each explanatory variable: Se shows a west to east trend; Sb trends inversely, from east to west; Sn significant relationships are only found in the southwest corner of the study area; all with similar trends concerning parameter estimates. Th and bld50A only display non-significant relationships, but parameter estimates are higher in the east sector for Th and in the west sector for bld50A. Pb had shown a global statistically significant relationship to Se, Sn and Sb, with ρ values of 0.569, 0.721 and 0.711, respectively (cf. Table 98) and, therefore, the use of these elements to model Pb is not unexpected. Lead, Sn and Sb are also clustered in the same component in PCA analysis, as discussed in section 4.7.1.

## 5.3. Discussion

The regression models obtained for the potentially harmful elements (PHE) Cr, Ni, Cu, Zn, As and Pb revealed that most of the calculated environmental variables (Table 10 and Table 11) were unrelated to trace metal concentrations in soils and RDS - from these, road, building, bus, population and terrain variables were those which more frequently displayed statistically significant relationships in

OLS and GWR models. Organic matter content and the amount of grain size fraction <63µm also showed significant relationships in the models. However, the addition of other chemical elements as explanatory variables (analysis sets #B) significantly increased model performances, as $R^2$ values were larger than those obtained using only the environmental variables (analysis sets #A). Better model performances were also obtained for RDS rather than soils - it was expected that soils would produce more robust regression models due to the more regular and dense sampling scheme across the study area, but the lack of variables which would explain historical contamination likely caused soil models to underperform. On the other hand, RDS are more prone to present-day contamination inputs which can be explained by the calculated environmental variables, and therefore model performances were higher than for soils.

Ordinary least squares regression models in soils did not produce the desired results using environmental variables, displaying very low $R^2$ values and non-significant coefficients. This is a likely result of the reasons mentioned above - the historical contamination of Manchester's soils, previously reported throughout Chapter 3, is not explained by the calculated environmental variables. OLS only produced results for the target PHE in soils in analysis set #B, where chemical concentrations of other elements were used as explanatory variables. Due to RDS being more closely related to present-day contamination inputs, OLS models could be calculated using both environmental variables and geochemical variables as predictors - OLS model performances are better using both at the same time.

Comparisons between OLS and GWR model performances for soils cannot be made except for Pb - OLS analysis #A did not produce results to compare to GWR analysis #A; and GWR analysis #B was only computed for Pb, whereas it has been computed for all variables in analysis #A. The soil Pb model obtained through OLS (analysis #B) displayed an $R^2$ of 0.76 and included 9 geochemical variables; whereas the model obtained through GWR displayed an $R^2$ of 0.63 and only 2 variables were considered, both with significantly positive associations to all soil samples. Although the AICc value is higher for the GWR Pb model (221 vs. 100 for OLS), the higher adjusted $R^2$ and the inclusion of a greater number of variables make the OLS model preferable.

Nevertheless, in RDS, GWR results were superior to those obtained by OLS. Again, the only PHE with models to be compared between OLS and GWR are Cu, Zn, Pb (analysis #A, summer); Ni, Cu, As (analysis #A, winter); Pb (analysis #B, summer); and Cu and Pb (analysis #B, winter). The GWR models displayed the highest $R^2$ and AICc values for these elements except for Pb (analysis #A, summer): for this element, OLS $R^2$ is of 0.25 vs. the 0.22 in GWR; but the AICc value is higher in GWR (123 vs. 91 on OLS). Overall, it can be affirmed that GWR outperforms OLS for modelling trace metal concentrations in RDS.

One fact that undermined the interpretation of GWR soil models is the surprisingly negative relationship obtained between variables which, by common sense, would display a positive relationship to PHE concentrations, such as the influence of road variables on Pb or Zn concentrations. Statistically significant negative relationships were found across the study area, indicating that low PHE concentrations are related to the presence of high traffic rates, which is contrary to what has been reported throughout the literature and this work itself. This fact suggests that there may be issues of missing variables, which compromise the overall interpretability of the GWR soil models. In addition to weak $R^2$ and unexpected variable relationships, parameter coefficients were also low and varied within a short range of values, suggesting very small spatial variation for the variables included in each model. An explanation for the unexpected coefficients and poorly fitted GWR models in soils may be that road and building data, when taken at different distance buffers from soil samples, may not include any roads or buildings if buffer size is small - a great percentage of soil samples recorded zero occurrences for roads and buildings at small distance buffers. Nevertheless, even variables taken at large distance buffers (up to max. 350m) produced unexpected coefficient signs in the models, such as rdGA300 (negatively related to Cu and Zn) and rdGA350 (negatively related to Pb and As). This may be due to the long distances separating some soil samples, often contaminated, from the closest roads: these samples, such as those located in the Clayton Vale / Phillips Park area, are historically contaminated (cf. sections 3.5.2 and 3.7) in which are now public open spaces, far from roads and buildings. Contrarily, C roads - rdGC150 and rdGC250 - displayed significantly positive relationships in the As and Pb models, respectively. This road group consists of low traffic paths: alleys, pedestrianised streets and private roads, which can be found in the areas mentioned above, of pronounced soil contamination. Another reason for the negative relationships between modelled PHE and building data may be that large industrial buildings are generally more sparsely distributed and soil PHE concentrations in these areas are likely high; whereas commercial/residential areas are more densely covered by buildings and infrastructures, with generally lower soil contamination levels.

This is not the case for RDS - as samples were actually collected on roads or kerbs, road lengths (and buildings, in most cases) are always present, enabling even small buffers to record results. Furthermore, rdGA variables (road group which includes motorways, A roads and B roads) were those with the strongest positive relationships with Cu, Zn, and Pb.

As previously referred, GWR models for RDS performed well for most elements, as the calculated environmental variables were able to explain significant amounts of the overall variance, with $R^2$ values ranging between 0.22 and 0.53 for analysis #A. Performances were higher using other chemical elements as explanatory variables, with $R^2$ values going up to 0.84 for analysis #B. Statistically significant positive relationships for the great majority of variables extended all across

the study area or in a west-east trend for RDS summer. RDS winter also displayed statistically significant positive relationships in the whole area; however, a few variables displayed an east-west trend. This inverse trending between summer and winter may be caused by the prevalent higher concentrations of the modelled trace metals in the western area in winter; whereas in summer, higher concentrations occur more frequently in the eastern area. This trending may be inferred by comparing the maps of Appendix 5 or, more easily, from the maps of section 4.7: these represent the spatial distribution of component scores obtained by PCA, which represent groups of elements with common variance. It is observed that higher component scores are more spread in the western area in winter for components which include Cu, Zn, Pb, Sn, Sb, Se, As, and organic matter content (components 2, 4, 6 (summer) and 5 (winter) of PCA #A).

The developed models, due to their characteristics and the several difficulties encountered especially for soils, may not perform as it would be desired for predictive purposes. The main reason for this fact might be that datasets which could be important for the present research were unavailable due to budget constraints or complete unavailability; e.g. detailed small scale surveys of different types of present-day industry (especially metallurgical), of automotive-related businesses, of the presence and nature of historical industry, etc.. There is a plethora of known sources of contaminants which cannot be simply expressed by the datasets available for this research. Models could also benefit if more complex mathematical procedures would have been explored; however, this would be beyond the scope of this research work. Producing the environmental datasets and performing the stepwise testing of environmental variables are very time-consuming processes - the availability of time and the collection of a greater amount of spatial variables would certainly allow a greater improvement in model performance.

## 5.4. Main conclusions about Manchester's soils and RDS spatial statistics

• The application of ordinary least squares regression (OLS) and geographically-weighted regression (GWR) to Manchester soil and RDS data has been able to inform about the relationships between selected potentially harmful elements (Cr, Ni, Cu, Zn, As and Pb) and environmental/geochemical variables. It has been observed that the spatially and temporally heterogeneous nature of Manchester's soil and RDS data made it hard to obtain stable models, especially for soils.

• The calculated environmental variables revealed not suitable to model PHE concentrations in soil through OLS - the stepwise testing of the variables showed that these could not explain soil PHE concentrations with a reasonable degree of confidence (analysis set #A); and consequently the addition of geochemical variables was performed as an attempt to improve model performance, which was confirmed. In spite of the high $R^2$ found for soil OLS models when including other

geochemical elements as explanatory variables (analysis set #B), which range between 0.70 (Cr) and 0.92 (Ni), all models display statistically significant non-stationarity and heteroscedasticity and, furthermore, residuals are not normally distributed.

• Conversely, RDS OLS models showed significant relationships with some of the environmental variables calculated for the purposes of this work, such as road densities, built-up areas, density of bus stops, terrain slope, population density and number of jobs per census output area (analysis set #A). Nevertheless, highest model adequacies were again obtained for RDS analyses when using concentrations of other chemical elements as explanatory variables (analysis set #B). Analysis set #A $R^2$ values range between 0.12 (Ni) and 0.38 (Zn) in summer, and between 0.14 (Cr) and 0.53 (Zn) in winter; whereas analysis set #B $R^2$ values range between 0.44 (As) and 0.71 (Zn) in summer, and between 0.51 (As) and 0.88 (Ni) in winter models: it is clear that the inclusion of chemical elements as explanatory variables increase OLS model performance in RDS. Another observation is that some of the explanatory geochemical variables included in the models had previously been related to the dependent variables, namely in the components calculated by PCA (cf. section 4.7) - Cr to Zr, Ba and Sb; Ni to V, Fe2O3 and Co; Cu to Zn, Sn and Sb; Zn to Cu and Sb; As to Ge; and Pb to Ba, Sn and Sb. This spatial statistics shows that RDS contaminants are not only related to other chemical elements in terms of sources (as previously discussed in section 4.7), but also related spatially - PHE may be modelled using those same elements and environmental parameters as explanatory variables.

• GWR models for soils were computed for Cr, Cu, Zn and Pb using environmental explanatory variables (analysis set #A), and for Pb using other chemical elements as explanatory variables (analysis set #B). Road- and building-related variables were more often associated to the modelled elements. Nevertheless, model performances were low, with $R^2$ values ranging between 0.033 (Cu) and 0.063 (Zn) for analysis set #A, and an $R^2$ value of 0.633 for Pb in analysis set #B. The t-statistics and parameter estimate maps for Manchester soils showed unexpected relationships between environmental variables and soil PHE concentrations - for example, statistically significant negative relationships were found between road variables and road-related elements such as Pb and Zn, indicating that low PHE concentrations are related to the presence of high traffic rates. This fact suggests that there may be issues of missing variables, which compromise the overall interpretability of the models. Parameter coefficients generally varied within very short ranges of values, suggesting very weak spatiality in the variables. Statistically significant relationships were mostly concentrated in the east part of the study area, where models tend to perform better. Nevertheless, a few variables displayed significant relationships in the whole area, such as rdGA350 (negative), bl100H (negative) and rdGC150 (positive) for As; and $Na_2O$ (positive) and Sn (positive) for Pb.

• GWR models for RDS summer were successfully computed for Cu, Zn and Pb (#A) and for Pb (#B). For RDS winter, Ni, Cu and As were modelled (#A), as well as Cu and Pb (#B). Analysis set #A $R^2$ values

range between 0.22 (Pb) and 0.53 (Zn) in summer, and between 0.23 (As) and 0.40 (Ni and Cu) in winter; whereas analysis set #B $R^2$ values are of 0.73 for Pb (summer), 0.79 for Pb (winter) and 0.84 for Cu (winter). For these elements there was a clear improvement in overall model performance between analysis sets #A and #B. Contrarily to soils, and as expected, road variables display positive relationships to PHE concentrations; and also with building variables, organic matter (LOI) and fine fraction contents (63inf2). Some of the chemical elements used as explanatory variables, LOI and 63inf2, which revealed statistically significant relationships to PHE in GWR models, had previously been related to this same PHE by other statistical methods such as PCA and spearman's rank correlation - the coexistence of elements due to chemical affinities and similar sources are likely responsible for these relationships. The positive relationships between Cu, Zn and Pb and road variables is easily explained, as road traffic has long been recognised as a source of these elements to RDS. In terms of statistically significant relationships between each explanatory variable and RDS samples, these were mostly positive. In general, for RDS summer, statistically significant positive relationships extended all across the study area or in a west-east trend. RDS winter also displayed statistically significant positive relationships in the whole area; however, a few variables displayed an east-west trend, or performed better in the southwest corner of the study area.

- OLS and GWR regression modelling of trace metals in soils and sediments would certainly benefit if a wider variety of environmental datasets would be available for use, such as detailed, small scale surveys of the different types of present-day and historical industry. In addition, a denser sampling scheme for RDS could also bring improvements to model performance.

# 6. Comparison RDS-Soil

The study of soils and urban sediments from Manchester, described in chapters 3 and 4, has pointed out clear similarities between these two media, which are spatially connected. This has been possible as RDS samples were collected close to previously sampled soils - RDS sampling locations were selected according to those of soils with high PHE content, as sample density was smaller (cf. sections 2.2 and 2.3 for more information on the sampling strategy). Figure 97 represents selected soil (green) and RDS sampling locations.

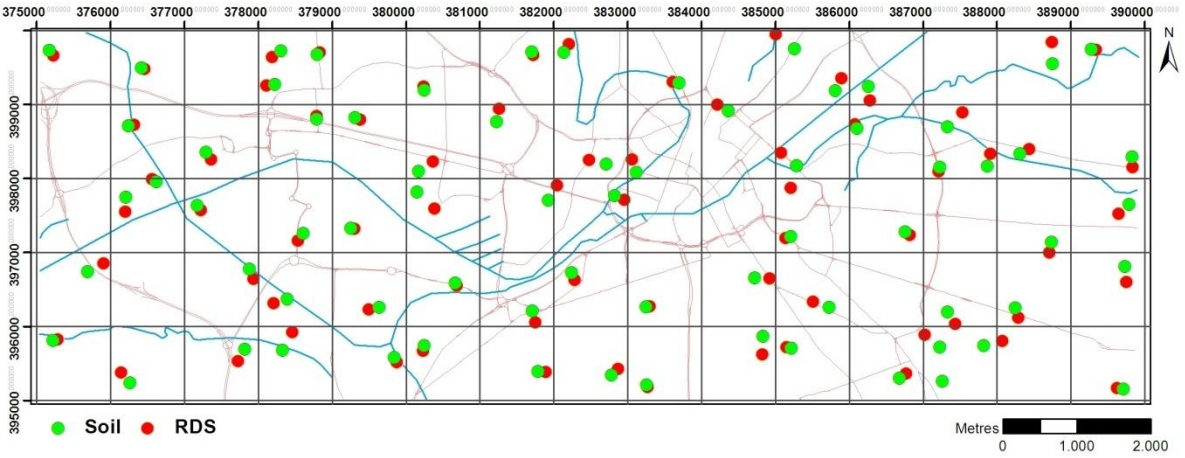


Figure 97: RDS and soil sampling locations.

As previously stated, both soils and RDS hold similar components, mainly minerals (sand, silt and clay) and organic material of various natures in different proportions. Nevertheless, their textures are different as a response to different origin and formation processes - whereas soils are the result of very slow natural processes acting upon bedrock, RDS is formed in a relatively short span of time from the local accumulation of particulates, generated by natural or anthropogenically-derived erosion of soil, buildings, infrastructures, vehicles; inputs from traffic and industry; etc.

Some studies have reported that RDS display higher PHE contents than soils, suggesting that RDS may be a source of contaminant elements to soils (Harrison et al., 1981; Li et al., 2001; Ordoñez et al., 2003; Krčmová et al., 2009). Nevertheless, the median PHE concentrations in Manchester's RDS tend to be lower than the same elements in soils, with a few exceptions.

Table 70 displays the median concentrations for the 72-sample soil subset, RDS summer, and RDS winter. A simple analysis shows that most elements display higher median concentrations in soils (Table 70a), with the exception of Na, Mg, Ca, Cu, Cr, Zn, Sr, Mo, Bi, Hf, Sb and I (Table 70b) - the highest median concentrations for these elements are found in RDS. Nevertheless, Cu, Sb, I and Hf show higher median concentrations only in the RDS winter dataset. Chromium, Cu and Zn are common vehicle-related elements - Cr in chrome plating and alloys; Cu in wiring, car brakes and several other components; and Zn in tyres and galvanized steel coatings. Nevertheless, it is noticed

through the maximum and minimum values represented in Table 71 that Cr, Cu and Zn display higher maximum concentrations in soils, although the median values are higher in RDS. That is, with the exception of soil outlier samples, these three metals tend to be higher in RDS and may be contributing to soil enrichment.

a)

| Variable | Median - soil n=72 | Median - RDSs n=72 | Median - RDSw n=72 |
|---|---|---|---|
| $Al_2O_3$ | 10,4 | 5,2 | 5,6 |
| $SiO_2$ | 65,0 | 61,3 | 62,0 |
| $P_2O_5$ | 0,33 | 0,13 | 0,16 |
| $K_2O$ | 1,65 | 1,18 | 1,12 |
| $TiO_2$ | 0,47 | 0,32 | 0,33 |
| MnO | 0,075 | 0,062 | 0,065 |
| $Fe_2O_3$ | 5,24 | 3,32 | 3,58 |
| Sc | 11 | 6 | 7 |
| V | 92 | 50 | 52 |
| Co | 10,1 | 8,4 | 9,4 |
| Ba | 602 | 345 | 335 |
| Ni | 36,1 | 28,5 | 31,0 |
| Ga | 10,65 | 6,00 | 6,10 |
| Ge | 4,8 | 1,0 | 1,6 |
| As | 26,3 | 5,3 | 5,9 |
| Se | 0,6 | 0,2 | 0,2 |
| Br | 16,4 | 3,9 | 6,3 |
| Rb | 59 | 38 | 38 |
| Y | 20 | 13 | 13 |
| Zr | 154 | 131 | 134 |
| Nb | 8 | 5 | 5 |
| W | 2,6 | 1,9 | 1,7 |
| Tl | 0,5 | - | - |
| Pb | 333,1 | 142,0 | 153,5 |
| Th | 6,6 | 3,6 | 4,3 |
| U | 2,1 | 1,5 | 1,4 |
| Ag | 0,8 | - | - |
| Cd | 1,1 | 0,5 | 0,6 |
| Sn | 25,4 | 11,2 | 14,5 |
| La | 29 | 13 | 13 |
| Ce | 51 | 26 | 25 |
| Nd | 23 | 14 | 14 |
| Sm | 4 | 2 | 2 |
| OM (LOI) | 9,55 | 6,31 | 8,50 |

b)

| Variable | Median - soil n=72 | Median - RDSs n=72 | Median - RDSw n=72 |
|---|---|---|---|
| $Na_2O$ | 0,5 | 0,8 | 0,8 |
| MgO | 0,9 | 1,7 | 1,7 |
| CaO | 1,5 | 7,3 | 6,8 |
| Cr | 86 | 97 | 89 |
| Zn | 254,1 | 301,9 | 366,3 |
| Sr | 80 | 129 | 122 |
| Mo | 3,3 | 4,7 | 5,2 |
| Bi | 0,3 | 0,6 | 0,5 |
| Cu | 115,9 | 84,3 | 128,8 |
| Hf | 3,5 | 3,5 | 4,2 |
| Sb | 7,5 | 7,0 | 8,3 |
| I | 1,0 | 0,8 | 1,4 |

Table 70: Median element concentrations and organic matter contents for soils and RDS. a) higher median value in soils; b) higher median value in RDS. All elements in mg/kg, except oxides and OM (wt.%).

High Ca concentrations in RDS occur mainly due to the erosion of concrete construction materials, which provide a constant Ca input to RDS - in a similar way, Sr (which replaces Ca in crystalline structures) is also enriched in RDS. Sodium and Mg (and Cl, which has not been determined in soils) are likely added to the roads by salt gritting, enhancing these elements' concentrations in RDS - nevertheless, Na and Mg are also present in concrete and other materials used in pavements, which

are also a likely source due to the small difference noted in median and maximum concentrations between summer and winter RDS samples.

In recent years, Sb has also been associated with traffic - it is used as constituent of brake linings; as a flame retardant in vulcanization of tyre rubber; and in a number of alloys for motor bearings (Fujiwara et al., 2011). Molybdenum is used as well on vehicles, namely in light Mo-steel and brake linings. Bismuth is also probably sourced from automotive applications such as the low temperature alloys used in the bonding of glass components to metal frames or in electronic assemblies. In addition to Cr, Cu and Zn, RDS may contribute to higher levels of Na, Mg, Cl, Ca, Sr, Sb, Mo and Bi in soils.

a)

| Variable | Range - soil, n=72 | Range - RDSs, n=72 | Range - RDSw, n=72 |
|---|---|---|---|
| $Al_2O_3$ | 5,2 - 23,6 | 2,7 - 10,9 | 2,2 - 10,3 |
| $SiO_2$ | 35,5 - 86,2 | 23,5 - 78,8 | 24,4 - 79,3 |
| $P_2O_5$ | 0,08 - 1,30 | 0,07 - 0,45 | 0,07 - 0,59 |
| $K_2O$ | 1,11 - 3,60 | 0,82 - 1,86 | 0,56 - 2,03 |
| $TiO_2$ | 0,12 - 0,93 | 0,19 - 0,77 | 0,14 - 0,76 |
| MnO | 0,015 - 0,626 | 0,033 - 0,145 | 0,029 - 0,118 |
| $Fe_2O_3$ | 1,27 - 20,26 | 1,94 - 6,15 | 1,28 - 6,96 |
| Sc | 3 - 29 | 2 - 14 | 2 - 14 |
| V | 26 - 234 | 32 - 110 | 23 - 111 |
| Cr | 30 - 1238 | 40 - 544 | 25 - 267 |
| Co | 3,2 - 44,1 | 5,3 - 18,0 | 4,3 - 22,7 |
| Ba | 287 - 5476 | 194 - 1010 | 191 - 986 |
| Ni | 4,5 - 148,3 | 18,4 - 82,4 | 14,0 - 77,1 |
| Cu | 7,2 - 2072,9 | 36,4 - 493,2 | 19,4 - 433,4 |
| Zn | 25,0 - 1762,9 | 66,2 - 1325,6 | 100,9 - 1312,3 |
| Ga | 4,80 - 32,10 | 3,40 - 11,10 | 2,10 - 11,90 |
| Ge | 1,6 - 31,8 | 0,3 - 2,0 | 0,8 - 5,9 |
| As | 2,5 - 1001,0 | 2,9 - 10,7 | 2,4 - 25,0 |
| Se | 0,1 - 3,2 | 0,1 - 0,5 | 0,1 - 0,9 |
| Rb | 36 - 166 | 24 - 57 | 20 - 62 |
| Y | 6 - 44 | 8 - 22 | 8 - 23 |
| Nb | 2 - 16 | 3 - 11 | 3 - 10 |
| W | 1,0 - 33,2 | 0,6 - 26,5 | 1,3 - 2,4 |
| Tl | 0,25 - 4,1 | | |
| Pb | 19,5 - 2758,0 | 35,0 - 1184,0 | 28,7 - 2026,9 |
| Th | 2,3 - 20,9 | 1,8 - 10,4 | 2,2 - 9,5 |
| U | 0,25 - 4,5 | 0,25 - 4,3 | 0,25 - 3,6 |
| Ag | 0,25 - 7,9 | | |
| Cd | 0,25 - 80,3 | 0,25 - 2,6 | 0,25 - 6,4 |
| Sn | 3,3 - 365,1 | 5,1 - 49,3 | 2,2 - 42,7 |
| I | 1,0 - 10,0 | 0,3 - 2,9 | 0,3 - 7,0 |
| La | 6 - 76 | 5 - 29 | 7 - 32 |
| Ce | 14 - 112 | 11 - 54 | 12 - 60 |
| Nd | 8 - 52 | 8 - 28 | 8 - 29 |
| Sm | 1 - 17 | 0 - 5 | 0 - 7 |

b)

| Variable | Range - soil, n=72 | Range - RDSs, n=72 | Range - RDSw, n=72 |
|---|---|---|---|
| $Na_2O$ | 0,3 - 0,8 | 0,3 - 3,6 | 0,2 - 3,9 |
| MgO | 0,2 - 2,7 | 0,8 - 3,6 | 0,6 - 8,7 |
| CaO | 0,2 - 8,8 | 2,6 - 19,8 | 2,0 - 27,3 |
| Sr | 43 - 336 | 63 - 456 | 76 - 470 |
| Sb | 1,9 - 48,7 | 1,4 - 49,7 | 1,4 - 54,3 |
| Br | 1,6 - 38,7 | 0,4 - 17,4 | 1,2 - 41,9 |
| Bi | 0,15 - 34,3 | 0,15 - 27,3 | 0,15 - 69,3 |
| Mo | 0,1 - 21,9 | 1,7 - 15,4 | 1,4 - 39,1 |
| Hf | 1 - 12 | 2 - 18 | 1 - 8 |
| Zr | 62 - 500 | 74 - 699 | 54 - 301 |
| OM (LOI) | 2,63 - 21,59 | 2,18 - 40,75 | 2,21 - 37,52 |

Table 71: Maximum and minimum element concentrations and organic matter contents for soils and RDS. a) higher maximum value in soils; b) higher maximum value in RDS. All elements in mg/kg, except oxides and OM (wt.%).

Soils are the major sink for metal contaminants released into the terrestrial environment by anthropogenic activities (Kirpichtchikova et al., 2006) - these tend to accumulate through time as metals cannot be destroyed by biogeochemical processes and may be strongly bound to other compounds, e.g. Fe and Mn oxy-hydroxides, clay minerals or organic matter. The generally higher

median and maximum PHE concentrations in Manchester's soils (e.g. Ni, As, Pb, Cd, Sn, Co) can be explained by the intense industrial activity which has historically affected this area, combined with high volumes of vehicle traffic, which has become more environmental-friendly only in recent years. The higher Cr, Cu and Zn median concentrations in RDS can be explained by their continuous input from the ubiquitous vehicle sources - these PHE, together with Na, Mg, Cl, Ca, Sr, Sb, Mo and Bi, may be those of higher concern regarding a possible transfer from RDS to soils and the consequent accumulation in this media.

Scatter plots (element in soil vs. element in RDS) and Spearman's rank correlation coefficient analysis did not reveal direct relationships between soil and RDS variables.

## 6.1. Wilcoxon signed-rank test

The Wilcoxon signed-rank test is used to ascertain if there are statistically significant differences in elemental concentrations between soil and RDS paired samples. This test was used in detriment of the T-test since distributions deviate from normal for most soil and RDS variables - the Wilcoxon test statistic is calculated onto the ranked difference values instead of the untransformed values (cf. section 2.9.2).

Since there are two values for RDS variables at each location (one for summer and one for winter) and these tend to be similar between seasons, an arithmetic average (mean) value has been calculated at each RDS location, for each variable. This mean RDS value (RDSm) is then paired to the correspondent soil sample, prior to the statistical analysis. Calculations have been performed as well between soil-RDS summer pairs and soil-RDS winter pairs, but results were in all cases similar to those calculated using Soil-RDS mean pairs.

The number of samples with negative ranks (RDS>soil), positive ranks (soil>RDS), the mean and sum of ranks are represented in Table 72. The Z statistic, as well as the significance and the media in which higher values are found are shown in Table 73. This statistic has been computed only for the variables of interest in terms of soil-RDS transfers.

As concentration values display pronounced differences between soils and RDS, the Wilcoxon signed-ranks test statistics has been in most cases significant at the 99 or 95% confidence level ($p<0.01$ or 0.05, Table 73). This was not the case when comparing RDS summer and RDS winter in section 4.5.1 - statistics were non-significant for a greater number of variables, as summer and winter elemental concentrations tended to be very similar.

In this analysis, $Na_2O$, MgO, CaO, Zn, Sr, Mo and Bi display significantly higher concentrations in RDS when compared to the correspondent soil pairs, as previously indicated by the mean and maximum values of Table 70 and Table 71. Reasons for this are also explained in the previous section. The remaining variables tend to show higher values in soils.

This analysis substantiates the previous conclusion that RDS is likely to contribute with $Na_2O$, MgO, CaO, Zn, Sr, Mo and Bi to soils. On a local scale, RDS accumulations on pavements may be resuspended in the atmosphere by passing traffic and particle fallout may occur over nearby soils. In a similar way, RDS particles together with water runoff may get sprayed into the atmosphere by car tyres in fast traffic, or may be projected onto nearby soils if the water on the surface displays considerable depth as traffic moves.

**Ranks**

| | | N | Mean Rank | Sum of Ranks |
|---|---|---|---|---|
| Na2O_BGS - Na2O_m | Negative Ranks | 62 | 36,10 | 2238 |
| | Positive Ranks | 5 | 8,00 | 40 |
| | Ties | 5 | | |
| MgO_BGS - MgO_m | Negative Ranks | 68 | 37,23 | 2532 |
| | Positive Ranks | 4 | 24,13 | 97 |
| | Ties | 0 | | |
| Al2O3_BGS - Al2O3_m | Negative Ranks | 2 | 1,50 | 3 |
| | Positive Ranks | 70 | 37,50 | 2625 |
| | Ties | 0 | | |
| CaO_BGS - CaO_m | Negative Ranks | 71 | 36,99 | 2626 |
| | Positive Ranks | 1 | 2,00 | 2 |
| | Ties | 0 | | |
| MnO_BGS - MnO_m | Negative Ranks | 26 | 31,37 | 816 |
| | Positive Ranks | 46 | 39,40 | 1813 |
| | Ties | 0 | | |
| Fe2O3_BGS - Fe2O3_m | Negative Ranks | 8 | 13,25 | 106 |
| | Positive Ranks | 64 | 39,41 | 2522 |
| | Ties | 0 | | |
| V_BGS - V_m | Negative Ranks | 5 | 6,80 | 34 |
| | Positive Ranks | 67 | 38,72 | 2594 |
| | Ties | 0 | | |
| Cr_BGS - Cr_m | Negative Ranks | 39 | 34,32 | 1339 |
| | Positive Ranks | 33 | 39,08 | 1290 |
| | Ties | 0 | | |
| Co_BGS - Co_m | Negative Ranks | 28 | 34,64 | 970 |
| | Positive Ranks | 44 | 37,68 | 1658 |
| | Ties | 0 | | |
| Ba_BGS - Ba_m | Negative Ranks | 2 | 10,50 | 21 |
| | Positive Ranks | 70 | 37,24 | 2607 |
| | Ties | 0 | | |
| Ni_BGS - Ni_m | Negative Ranks | 24 | 31,83 | 764 |
| | Positive Ranks | 48 | 38,83 | 1864 |
| | Ties | 0 | | |

**Ranks**

| | | N | Mean Rank | Sum of Ranks |
|---|---|---|---|---|
| Cu_BGS - Cu_m | Negative Ranks | 29 | 31,93 | 926 |
| | Positive Ranks | 43 | 39,58 | 1702 |
| | Ties | 0 | | |
| Zn_BGS - Zn_m | Negative Ranks | 49 | 36,27 | 1777 |
| | Positive Ranks | 23 | 37,00 | 851 |
| | Ties | 0 | | |
| As_BGS - As_m | Negative Ranks | 1 | 1,00 | 1 |
| | Positive Ranks | 71 | 37,00 | 2627 |
| | Ties | 0 | | |
| Sr_BGS - Sr_m | Negative Ranks | 65 | 37,52 | 2439 |
| | Positive Ranks | 7 | 27,07 | 190 |
| | Ties | 0 | | |
| Mo_BGS - Mo_m | Negative Ranks | 50 | 37,74 | 1887 |
| | Positive Ranks | 22 | 33,68 | 741 |
| | Ties | 0 | | |
| Pb_BGS - Pb_m | Negative Ranks | 12 | 18,63 | 224 |
| | Positive Ranks | 60 | 40,08 | 2405 |
| | Ties | 0 | | |
| Bi_BGS - Bi_m | Negative Ranks | 48 | 33,90 | 1627 |
| | Positive Ranks | 23 | 40,39 | 929 |
| | Ties | 1 | | |
| Cd_BGS - Cd_m | Negative Ranks | 11 | 21,18 | 233 |
| | Positive Ranks | 61 | 39,26 | 2395 |
| | Ties | 0 | | |
| Sn_BGS - Sn_m | Negative Ranks | 14 | 13,86 | 194 |
| | Positive Ranks | 58 | 41,97 | 2434 |
| | Ties | 0 | | |
| Sb_BGS - Sb_m | Negative Ranks | 37 | 36,00 | 1332 |
| | Positive Ranks | 35 | 37,03 | 1296 |
| | Ties | 0 | | |

Table 72: Ranks of the Wilcoxon signed-ranks test for soil (BGS) and RDS-mean (m) datasets.

Soils may also be affected by RDS, on a distal scale, if irrigated or flooded with water from an RDS-affected water body - storm drains carry urban runoff from the street surfaces (as well as other impervious surfaces) to receiving water bodies (i.e. rivers, canals or docks). In addition to this surface water runoff, the urban drainage system also has to deal with industrial and domestic wastewaters and sewage - in a combined sewer system, effluents are ultimately transferred to water treatment

plants but, during storm events, water is discharged directly (including sewage) through a combined sewage overflow outlet into receiving water bodies, causing water quality deterioration (Taylor and Owens, 2009).

| Pair | Z | Sig. (2-tailed) | Higher Values |
|---|---|---|---|
| Na2O_BGS - Na2O_m | -6,870 | 0,000 | RDS |
| MgO_BGS - MgO_m | -6,832 | 0,000 | RDS |
| Al2O3_BGS - Al2O3_m | -7,357 | 0,000 | Soil |
| CaO_BGS - CaO_m | -7,363 | 0,000 | RDS |
| MnO_BGS - MnO_m | -2,798 | 0,005 | Soil |
| Fe2O3_BGS - Fe2O3_m | -6,779 | 0,000 | Soil |
| V_BGS - V_m | -7,183 | 0,000 | Soil |
| Cr_BGS - Cr_m | -0,137 | 0,891 | RDS |
| Co_BGS - Co_m | -1,930 | 0,054 | Soil |
| Ba_BGS - Ba_m | -7,256 | 0,000 | Soil |
| Ni_BGS - Ni_m | -3,086 | 0,002 | Soil |
| Cu_BGS - Cu_m | -2,177 | 0,029 | Soil |
| Zn_BGS - Zn_m | -2,598 | 0,009 | RDS |
| As_BGS - As_m | -7,368 | 0,000 | Soil |
| Sr_BGS - Sr_m | -6,310 | 0,000 | RDS |
| Mo_BGS - Mo_m | -3,216 | 0,001 | RDS |
| Pb_BGS - Pb_m | -6,120 | 0,000 | Soil |
| Bi_BGS - Bi_m | -2,000 | 0,046 | RDS |
| Cd_BGS - Cd_m | -6,066 | 0,000 | Soil |
| Sn_BGS - Sn_m | -6,285 | 0,000 | Soil |
| Sb_BGS - Sb_m | -0,101 | 0,920 | RDS |

Table 73: Wilcoxon signed-ranks test for soil and RDS-mean datasets.

Soils, as previously referred, act as a sink for contaminants and therefore concentrations for many elements, including PHE, is higher in this media than in RDS. The soil contribution to RDS composition may be effective in locations where soils are being constantly eroded, e.g. in the immediate vicinity of public or private gardens, parks and land plots.

Despite the referred mechanisms of contaminant transfer between RDS and soils, the identified present-day sources are likely to affect both media simultaneously at the local scale and this has been observed in samples collected in the area of highest traffic and industrial density; e.g. samples collected in/near the Trafford Park Industrial Estate. Soil sample 630020, which is located nearby RDS sample 34 on Tenax Road (a dual carriageway in the Trafford Park Industrial Estate), displays CaO, Zn, Pb and Sb concentrations which are approximately 3 times the soil median. Cu and Cd are also very high with 4 times the median soil dataset value; Sn is 10 times and Bi peaks at 42 times the median value. RDS sample 34 also displays the highest levels of the dataset for Zn, Pb, Cu, Sn, Sb, Ba, Br and Sr.

## 6.2. SEM analysis

Soil and RDS samples observed under the SEM display several similarities in what concerns general composition, grain types and grain morphologies. Figure 26 and Figure 69 are general views of Manchester's soil and RDS, respectively; and these images reveal this close resemblance.

Nevertheless, whereas in soils there is a greater density of silicate grains (quartz) at the same optical scale, RDS displays a greater proportion of other grain types. Additionally, RDS grains tent to be more angular or irregular in shape than soil grains, as a likely consequence of particle transport mechanisms on road surfaces. RDS also displays a larger proportion of brick, concrete and/or tarmac fragments.

Iron oxide grains of similar morphology and composition are found across both soils and RDS. The same is valid for iron-rich spherical grains, which are of clear anthropogenic origin, resulting from high temperature combustion processes - these may also contain varying amounts of PHEs in both media. However, signs of disaggregation/dissolution of this type of grain are more pronounced in soils, and therefore the potential remobilization of PHE from these grains may be larger in this media.

In addition to massive Pb grains, present in both media, lead-rich particles likely from leaded paint are found only in soils. RDS, however, showed lead-rich grains with an agglomerate structure, not observed in soils - these may pose increased human health risks, as these grains are likely to be dissociated into respirable, ultrafine, Pb-rich particles.

Zinc-rich grains are very rare in Manchester's soils. In RDS, Zn-rich grains are more abundant and usually contain significant amounts of Ba - this element is used with Zn in the manufacture of PVC products, which are widely used e.g. in automotive applications. Additionally, Zn may also be sourced in RDS from car tyre and break lining wear and tear, and hence its relative abundance in RDS. Chromium-rich grains are found both in soils and RDS, although with different morphologies.

As expected, the similarities between soils and RDS are more common than the differences - the predominant grain types are the same (quartz and other mineral grains, rock fragments and iron oxides). Nevertheless, PHE-rich grains may be different in size, shape and relative abundance: it is remarkable that Ba-Zn and agglomerate grains have not been observed in soil material. A hypothesis might be that these anthropogenic grains are those sourced mainly from vehicle traffic and therefore are more concentrated on street pavements or in very close vicinity to high-traffic roads. Additionally, these grains might be highly prone to breakdown and remobilization from RDS by water runoff and therefore are less likely to affect soils by resuspension and atmospheric fallout.

## 6.3. PCA analysis

The variable reduction technique of principal component analysis produced distinct results in terms of element groupings in soils and RDS. In soils, the two first components explain 46.9% of the total dataset variance (analysis #A) - component 1 includes anthropogenic elements related to historical coal mining and burning, as well as heavy industry ($Fe_2O_3$, V, Co, Ni, Ge, Mo and Sn); whereas component 2 represents the variation of geogenic elements ($Al_2O_3$, $K_2O$, $TiO_2$, Ga, Rb and REEs), derived from natural soil forming processes. In RDS, the first two components account for 34.4 and

32.7% of the total variance for summer and winter data, respectively. Component 1 includes geogenic elements such as $Al_2O_3$, MgO, $TiO_2$, MnO, $Fe_2O_3$, Sc, and Ga - also grouped in soils in component 2. Nevertheless, component 1 in RDS also includes Co, Ni , V and Y, which were grouped in component 1 in soils as strong anthropogenic elements. The grouping of $Al_2O_3$, MgO, $TiO_2$, MnO, $Fe_2O_3$, Sc, V, Co, Ni, Ga and Nb in RDS suggests that these elements are likely derived from nearby soils, where Co, Ni, Fe, Sc and V are enriched due to historical anthropogenic activities. In fact, RDS samples with the highest scores for component 1 were collected on pavements in the close vicinity of gardens, parks or land plots (RDS samples 4, 6, 13, 14, 42, 46, 48, 61 and 71), pointing to these nearby soils as the source of component 1 elements.

RDS component 2 represents Ba, Cu, Zn, Pb, Sr, Sn and Sb (and Cr in winter), which are identified as strong anthropogenic elements related to present-day industry and heavy traffic. In soils, these elements do not group in a single component - Cr and Cu (and As) cluster in component 4, related to wastewater treatment plants and local industry; Zn, Sn and Sb are included in component 1, as elements derived from past contaminant sources; and Pb is closely related to P, Bi and Ag in component 3, pointing more specifically to by-products of Pb smelting/refining, coal combustion, processes, leaded gasoline, and leaded paints as Pb sources. Therefore, the source of these elements in RDS may not be as related to soils, as was the case for the elements of RDS component 1 - instead, they appear to derive mainly from present-day anthropogenic inputs.

Another difference pointed out by PCA are the different origins for As and Cd in soils and RDS. Arsenic in RDS is very likely connected to its use, together with Ge, in automotive electronic applications (LEDs, glass fibres, integrated circuits, etc) - in soils, As highest concentrations are related to wastewater treatment plants, or to historically contaminated sites such as Clayton Vale. Cadmium (and Bi) in RDS seem to be related to the use of Cd-Bi-Sn alloys, which are used as low-temperature solders in substitution of Pb solders for automotive uses. On the other hand, Cd in soils is likely derived from similar sources as arsenic - the WTPs are a Cd hotspot, as well as past industrial sites such as the Clayton Vale area, where maximum Cd concentrations are found. Additionally, Cd in soils near the Salford Royal NHS Foundation Trust and locations with present-day industry could indicate that these might be contributing to Cd contents in soils. Nevertheless, RDS collected near these soil Cd hotspots did not reveal very significant enrichments, as would be expected in the close proximity of present-day sources.

## 6.4. Spatial statistics

The application of OLS and GWR in soils and RDS data, as discussed in section 5.3., revealed that both media behave very differently concerning trace metal modelling using environmental variables. Therefore, it is difficult to find similarities in contaminant sources or element/environmental variable relationships between both media. While OLS performed well for RDS and not for soils using only

environmental variables, they performed reasonably for both media using other chemical elements as explanatory variables, with $R^2$ values going up to 0.92. Using GWR as the regression method; i.e. taking into account the weights of sample contribution proportional to distance (Fotheringham et al., 2002), the spatial variability that is characteristic of anthropogenic processes has been taken into account. This method performed better for RDS, and allowed the distinction of a west-east trend of significant explanatory variable/trace metal relationship in RDS summer and east-west trend in winter, trend which cannot be easily explained. While greatest traffic densities are felt in the east of the study area, in the Manchester district; most of the heavy industrial activity is located in the Trafford and Salford districts. Prevailing wind direction data was not able as well to explain these patterns, as wind directions are predominantly from south to north in January and from east to west in June, the months when RDS collection took place. Consequently, neither OLS nor GWR provided common solid correspondences in terms of source apportionment between soils and sediments. However, this analysis revealed very important in revealing the influence, especially of road traffic indicators, in RDS trace metal concentrations through GWR and, additionally, the use of the local t-statistics maps allowed the critical analysis of the findings which may also suggest areas for further model improvement.

# 7. Global conclusions

With the objective of fully characterising the presence and nature of potentially harmful elements in soils and urban sediments over 75 $km^2$ of Manchester, UK, these have been sampled and analysed through a plethora of methods to explore the geochemical, mineralogical and spatial linkages within and between these environmental media. The preliminary characterization of soils and RDS morphology and geochemistry provided a basis for the development of this study, followed by detailed further chemical and mineralogical analysis and statistical investigations on the data obtained. The following sections summarise the main findings and conclusions of this research; and the last section deals with the key implications and recommendations for future work.

## 7.1. Soils

Geochemical characterization of Manchester's soils (chapter 3), in a total of 300 samples (4 per $km^2$, section 2.2) started with the analysis of 48 chemical elements by XRF, from which three elements (Cs, Ta and Te) were removed from the dataset prior to statistical calculations due to the large number of samples below the lower limits of detection. After data conditioning and levelling (section 2.9.1), basic statistics showed that maximum concentrations were often highly above the median concentrations especially in trace elements, indicating strong local enrichments. Therefore, most distributions were positively skewed and distributions were non-normal for all chemical elements. Two additional datasets were created using logarithmic and Box-Cox transformed values, so that data could be used in statistical analysis which required data normality. Basic correlation statistics pointed out the main elemental relationships, which were confirmed and further explored in section 3.7 by principal component analysis.

Soil pH varied from neutral to extremely acid, with around 24% of samples below pH 5.5 (section 3.1). Organic matter contents in soil are varied, with a median of 8.5% and a maximum value of 21.6%. Most of the carbon in soil samples was organic carbon (median of 6.8%), whereas inorganic carbon only contributed to a median of 0.8% in the analysed samples.

Manchester soils are mainly enriched in Cu, Zn, Pb and Cd, when compared to other 12 UK cities and the median values for England and Wales (section 3.2). Manchester is on the top three cities for median concentrations of Cu, Zn, As and Pb; and above 8 cities for Cr and Ni. The lack of correlations between trace metal contents and local bedrock or superficial geology does not support that these high PHE concentrations in Manchester would be geogenic (section 3.3) - differences between elemental distributions over different bedrocks or superficial deposits are useful to characterise their geogenic elemental concentrations and to determine if PHE concentrations are elevated over certain types of parent material due to natural enrichments. When grouping PHE by land use type (section 3.4), median concentrations tended to be similar between land uses. Nevertheless, the industrial

land type (E000) showed slightly higher median values for Cr, Cu, Zn and Cd. On the other hand, urban open spaces (DACA, DAC0, DACB), recreational areas (DD00) and commercial/residential areas (DAA0) showed many upper outliers for these PHE.

Mapping of geochemical concentrations (section 3.5) defined six main areas where PHE concentrations are systematically above the 75$^{th}$ percentile: the Clayton Vale / Phillips Park area, the Cambrian Street area, the Oxford Road / Wilmslow Road alignment, the Old Trafford residential area, the Trafford Park industrial estate, the surroundings of the Davyhulme and Eccles Wastewater Treatment Works, the residential area south of Worsley Golf Club, and the area between A6 and A57/M602 in Salford. These are areas which are diverse in terms of land uses and chemical element association types - a clear example of the variety of present-day and historical factors which can influence soil composition at the local scale. Present-day sources have a large influence on soils near the Oxford Rd. / Wilmslow road alignment, in the Trafford Park Industrial Estate, and in the Cambrian St. area - at these locations, PHE are likely sourced from heavy traffic, together with diverse industrial activities especially in Trafford Park and around Cambrian St.. Historical contamination, as found in Clayton Vale, Salford and Old Trafford, are likely derived from past industry; whereas in the Worsley area it may be attributed mainly to past mining operations. The water treatment plants of Davyhulme and Eccles may not be actively contributing to soil contamination nowadays, but nearby soils point that these infrastructures might have been important sources of As, Cr and Cu.

Scanning electron microscope microbeam analysis of soil samples (section 3.6) revealed that these are mainly composed, as expected, by silicate and alumino-silicate grains from various sizes (<10 - 450µm). Fragments of rock, tarmac, brick and other construction materials are also present. Iron oxide grains (up to 67% Fe, section 3.6.1) often exhibit a porous and/or stratified structure (banding), and are mostly angular in shape. Their size is again highly variable (~30-450µm) and these grains may include other metals such as Ti, Mn, Cr, Cu and Co. Spherical iron-rich grains (section 3.6.2), which likely result from high temperature combustion processes such as those of blast-furnace smelters or burning of wastes, can display a variety of PHE in their composition. The presence of these PHE needs further attention as their potential for mobilization is high, with most grains displaying dissolution/corrosion structures. Concentrations can reach 800 mg/kg V, 1500mg/kg Cu, 11.5% Cr, and 6300 mg/kg Mo in this type of grain. Lead-rich grains (up to 52% Pb, section 3.6.3) are either massive, or display an agglomerate-like structure - the Pb present in the most Pb-contaminated sample is likely from leaded paint, as this location was one of the first suburban residential estates in Manchester, now redeveloped. Accessory grain types are generally smaller in size (<50µm) and may contain significant levels of Ba - , Pb, Sn, Ni or REE. The fact that all soil samples analysed under the SEM display pH values between 4.85 - 7 indicates that the trace metals identified may be subject to

leaching - low pH soils exhibit low cation exchange capacity and PHE may be released into the soil solution, which directly affects PHE availability to organisms.

Principal component analysis (section 3.7) revealed groups of geochemical variables which show similar variation patterns in Manchester's soils, and their mapping allowed for a more objective interpretation in terms of source apportionment. Main conclusions from the three sets of PCA analysis performed on soil data were as follows:

• Lithophile and geogenic element groupings in Manchester's soils included $Al_2O_3$, $K_2O$, MgO, $TiO_2$, Ga, Rb, Nb, Th, U, V, and REEs (Sc, Y La, Ce and Nd). Component score mapping and its comparison to superficial deposits mapping revealed that the highest concentrations of the referred elements are likely related to the Devensian till-diamicton formation.

• Historical, coal-related contamination highlighted by PCA is mainly represented by $Fe_2O_3$, V, Co, Ni, Ge, Mo, Sn and Zn. The most affected areas by elevated levels of these elements, pointed out by component score mapping, were located in the Clayton Vale / Phillips Park area, along the Bridgewater Canal, and in the Oxford Road / Wilmslow Road alignment. Clayton Vale was a heavily industrialised area in the $18^{th}$-$19^{th}$ centuries, which included collieries and chemical works, among many other industries - additionally, prior to its redevelopment into a park, the site has been used as a municipal waste tip and a tip for power station ash cinders. The area around the Bridgewater canal was likely affected by the transportation of coal from the mines in Worsley, which was the main purpose of the canal in the $18^{th}$ and $19^{th}$ centuries; and by the industries which subsequently were established on its margins due to the easier access for raw materials and goods transport.

• Lead, Pb, Bi, Ag and $P_2O_5$ were likely related to both present day sources, such as the proximity to heavy traffic, vehicle-related businesses and industry; and historical sources, such as lead from pre-2000 gasoline, leaded paint, from coal burning or Pb smelting processes (Kabata-Pendias and Pendias, 2001; Shotyk and Krachler, 2004; Jacobson et al., 2005; Cotter-Howells, 1996). The mapping of the component score which represents this suite of elements revealed hotspot areas located in the Clayton Vale area, Whalley Range, Urmston, Cambrian St. area and Trafford Park. Whereas in the first three areas these elements seem to be of past origin, the last two clearly reveal the input of present-day industrial activities and traffic. Fragments of leaded paint in soils of the Whalley Range area, observed through the SEM, confirmed their historical source.

• Arsenic, Cu and Cr were also related in Manchester's soils and are likely sourced, in the west part of the study area, by the WTPs of Davyhulme and Eccles - these elements usually display high levels in WTP effluents and sewage sludge (Lake et al., 1984; Ščančar et al., 2000; Zhang et al., 2013). Two other important hotspots were located in Trafford Ecology Park and in the Cambrian St. area, where localised inputs from nearby industry may be responsible for the higher levels of these three elements. This set of elements in soils has also been reported to be sourced from CCA-treated wood

(Townsend et al., 2003; Gezer et al., 2005; Kim et al., 2007); nevertheless, further investigation would be needed to assess if this was also the case in Manchester's soils.

• Zn (and Mn) were also clustered in a single component, and highest scores tended to follow the trace of Manchester's busiest roads (M60 and M602, Oxford/Wilmslow road, east part of Mancunian Way, Ashton Old Road). This is a strong indication that vehicles and traffic are a likely source for these elements, as they have long been reported to be sourced from the wear and tear of car bodies, brake linings and tyres. Nevertheless, Zn total concentrations were also high in the Clayton Vale and Worsley areas, where its origin is more likely related to historical mining and industrial activities as previously described.

• Although the Zr and Hf association in soils can be linked to their coexistence in natural zircon, the presence of high Na levels at the same locations revealed by PCA pointed to an anthropogenic enrichment of these elements, as Na is used in the process of transforming zircon materials into zirconium oxide which is used in numerous applications (Manhique, 2003; Lubbe et al., 2012). One of them is in brick, tile and ceramic manufacturing - a likely source of this association of Zr, Hf and Na in Manchester's soils, which often contain fragments of these materials. Additionally, one of the largest manufacturers and suppliers of zirconium chemicals and oxides (MEL Chemicals™) is located in Swinton, approximately 2Km north of the study area.

The use of different parameters in PCA analysis showed that by retaining a greater number of components, there is an easier identification of unapparent element associations which, although accounting for smaller amounts of the total system variance, may as well be interpreted successfully in terms of source apportionment. Adding to this, mapping has proven very useful for contaminant source targeting, beyond the use of single element spatial distributions. The use of fewer variables, by excluding those of easier interpretation, sharpened the distinction between high and low concentrations in component score mapping; nevertheless, in this case, conclusions were similar regarding the element associations calculated and component scores spatial distribution.

Spatial statistics using Manchester soil data aimed at spatially relating concentrations of Cr, Ni, Cu, Zn, As and Pb to environmental variables which are likely to affect soil quality, directly or indirectly, such as road, traffic, building, population, jobs and topography data. 26 variables, 10 of which were calculated at 8 different buffer distances, were considered for inclusion in the spatial statistical models, in a total of 96 variables. The calculated environmental variables revealed not suitable to model PHE concentrations in soil through ordinary least squares (OLS) regression (section 5.1.1) - the stepwise testing of the variables showed that these could not explain soil PHE concentrations with a reasonable degree of confidence (analysis set #A); and consequently the addition of geochemical variables was performed as an attempt to improve model performance, which was confirmed. In spite of the high $R^2$ found for soil OLS models when including other geochemical elements as

explanatory variables (analysis set #B), which range between 0.70 (Cr) and 0.92 (Ni), all models display statistically significant non-stationarity and heteroscedasticity and, furthermore, residuals are not normally distributed. Geographically-weighted regression (GWR) models for soils were computed for Cr, Cu, Zn and Pb using environmental explanatory variables (analysis set #A), and for Pb using other chemical elements as explanatory variables (analysis set #B). Road- and building-related variables were more often associated to the modelled elements. Nevertheless, model performances were low, with adjusted $R^2$ values ranging between 0.033 (Cu) and 0.063 (Zn) for analysis set #A, and an $R^2$ value of 0.633 for Pb in analysis set #B. Parameter coefficients generally varied within very short ranges of values, suggesting heterogeneity in the variables. Statistically significant relationships were mostly concentrated in the east part of the study area, where models tend to perform better. Nevertheless, a few variables displayed significant relationships in the whole area, such as A-road length within a 350m buffer (rdGA350, negative), average building height within a 100m buffer (bl100H, negative) and C-road length within a 150m buffer (rdGC150 positive) for As; and $Na_2O$ (positive) and Sn (positive) for Pb. However, the t-statistics and parameter estimate maps for Manchester soils showed unexpected relationships between environmental variables and soil PHE concentrations - for example, statistically significant negative relationships were found between road variables and known road-related elements such as Pb and Zn, indicating that low PHE concentrations were related to the presence of high traffic rates, which is contrary to common sense. This fact suggests that there may be issues of missing variables, which compromise the overall model interpretability - it has been reported throughout this work that Manchester's soils are heavily influenced by past human activities (chapter 3), which cannot be unequivocally explained by the calculated environmental variables.

Another explanation for the unexpected coefficients and poorly fitted GWR models in soils may be that road and building data, when taken at different distance buffers from soil samples, may not include any roads or buildings if buffer size is small - a great percentage of soil samples recorded zero occurrences for roads and buildings at small distance buffers. Nevertheless, even variables taken at large distance buffers (up to max. 350m) produced unexpected coefficient signs in the models, such as rdGA300 (negatively related to Cu and Zn) and rdGA350 (negatively related to Pb and As). This may also be due to the long distances separating some soil samples, often contaminated, from the closest roads: these samples, such as those located in the Clayton Vale / Phillips Park area, are historically contaminated (cf. sections 3.5.2 and 3.7) in which are now public open spaces, far from roads and buildings. Contrarily, C roads - rdGC150 and rdGC250 - displayed significantly positive relationships in the As and Pb models, respectively. This road group consists of low traffic paths: alleys, pedestrianised streets and private roads, which can be found in the areas mentioned above, of pronounced soil contamination. Another reason for the negative relationships between modelled PHE and building data may be that present-day large industrial buildings are generally more sparsely

distributed and soil PHE concentrations in these areas are likely high; whereas commercial/residential areas are more densely covered by buildings and infrastructures, with generally lower soil contamination levels.

## 7.2. RDS

Urban road-deposited sediments characterisation started with their collection in two seasons: 72 RDS samples were collected in summer and 72 in winter, to account for seasonal differences in sediment texture and composition (section 2.3). Locations for the RDS collection were selected according to the scheme used for soil collection to test whether spatial variations and patterns in RDS are similar to those recorded for soils. However, as the sample density had to be lower - 1 sample per $km^2$ instead of the 4 per $km^2$ used for soils - RDS sampling locations were selected within each National Grid kilometre square as close as possible to the soil samples which exhibited highest trace metal concentrations. RDS samples were analysed for 55 chemical elements by XRF and, after data conditioning and levelling (section 2.9.1), 8 elements were removed from the dataset (Cs, Ta, Te, Tl, Ag, Hg, Pd and In) as over 70% of the samples were above the lower limits of detection. For these, concentrations above the LLD are only considered when interpreting geochemical data at the sample scale. Basic statistics (section 4.1.1) showed that the majority of the elemental distributions were positively skewed and displayed frequent upper outliers, indicating strong enrichments at certain locations. To achieve data normality, required in certain statistical methods, logarithmic and Box-Cox transformations were applied, creating four new datasets (two for summer data and two for winter data). Basic correlation statistics (section 4.1.3) revealed the main elemental relationships, which were confirmed and further explored in section 4.7 by principal component analysis.

RDS samples show a large variability in what concerns organic matter contents (OM) (section 4.1.2), within a similar range in both seasons - between 2 and 41% in summer, and 2 and 38% in winter. Nevertheless, mean and median OM contents are greater in winter samples - a consequence of the greater leaf/plant litter accumulation in fall/winter. Grain size data were obtained for RDS by laser diffractometry, and 31 locations showed a coarser grain size in summer, whereas for 24 locations coarse fractions were more predominant in winter samples. 17 locations showed very similar distributions for both winter and summer. The variations in grain size distribution between summer and winter cannot be easily explained - grain size is dependent of several factors such as weather conditions, nearby sediment sources, pavement characteristics, traffic volume and mean vehicle speed. Nevertheless, a greater number of samples tended to be coarser in summer, which may be attributed to the effect of longer dry periods, allowing for both larger sediment accumulations and easier resuspension of the finer particles. The lower mean and median particle sizes in winter may generally be explained by the fact that fine particles tend to aggregate under the constantly wet conditions, and are therefore less prone to resuspension from the pavements.

However, there is also the wash-off caused by water flow episodes which are more frequent in winter - samples are not only predominantly finer-grained due to wet aggregation, but also total sample weights collected are generally lower in winter due to the more frequent runoff periods. Some samples which remarkably were amongst those with highest PHE contents did not follow this trend - particle diameter was larger in winter samples. These samples were in fact collected in main roads or carriageways, suggesting that vehicles travelling at higher mean speeds may be the main factor favouring the accumulation of larger particles (in the magnitude of medium sands), as fine particles are more easily resuspended and removed from the pavement. The relatively larger mean particle sizes in winter for the referred samples may also be interpreted as an added effect of rainfall - in addition to the prevailing wind resuspension, water runoff preferentially transports the finer particles, enhancing the relative amount of coarse particles on the pavements.

Grain size distributions of RDS samples are highly variable - a grain size normalisation attempt has been performed, as trace metals of environmental concern are reported to be preferably concentrated in the finer grain size fractions of the sediment. Through the grain size analysis of a subset of 34 samples (17 summer + 17 winter), Al and Ga emerged as good grain size proxies; but the extension of the analysis to the total, 144-sample dataset disproved this hypothesis. The complex nature of the controls on RDS grain size make traditional grain size normalisation procedures not appropriate to heterogeneous RDS datasets. Therefore, the statistical analysis of specific sample subsets is discouraged, as it has been demonstrated that results are clearly influenced by the characteristics of the chosen sample subsets.

Comparisons between RDS trace metal concentrations and geological parameters such as bedrock and superficial deposits type revealed that only Ni might be related to these parameters (section 4.3). Nickel showed slightly higher median values in RDS collected over Permian bedrock. Furthermore, Ni is also slightly enriched over till superficial deposits - it must be taken into account that most Permian bedrock is overlain by till superficial deposits in the study area. In soils, Ni had also shown a slightly higher mean value over Permian bedrock and till superficial deposits, which may suggest a Ni input from soils to RDS. From the different land uses where RDS were sampled, the commercial/residential (DAA0) and industrial (E000) land use types displayed similar median concentrations for the Cr, Ni, Cu, Zn, As, Pb and Cd, whereas major roads (CB00) showed the highest mean values of Cr, Cu and As.

A first look at the spatial distribution of element concentrations in Manchester's RDS (section 4.4) showed that these are widely variable across the area, as a consequence of contrasting local settings and the heterogeneity of the urban tissue in the study area. There were two locations - the Trafford Park industrial estate area, and the Clayton / Miles Platting area - where the PHE concentrations were systematically above the 75$^{th}$ percentile both in summer and winter. Other than those, high

concentrations of PHE were scattered throughout the area, with predominance in the western area in summer and in the eastern area in winter.

Extractable trace element contents for Cr, Cu, Zn, Pb and Fe were investigated in 34 RDS samples (17 summer + 17 winter), which were selected due to their high trace metal concentrations determined previously by XRF (section 4.5). Sample extracts were obtained following the modified BCR three step sequential extraction protocol (Rauret et al., 1999); and a fourth step consisted in the digestion of the solid residue by *aqua regia* (ISO, 1995; Larner et al., 2006), to provide a comparison of the sum of the metal concentrations extracted in the four steps with the (total) XRF results for each metal. Extract analysis was undertaken by FAAS. Extracted phases tended to display larger metal concentrations in winter samples, except Cr where concentrations were lower in winter for the first three extracted phases. Zinc was the most available element, with high concentrations in the exchangeable, acid-extractable phase and in the reducible phase. Lead was preferably bound to the reducible phase, whereas Cu showed higher concentrations in the reducible phase in summer and residual phase in winter. Chromium and Fe displayed greater proportions in the residual phase. Seasonal differences between phase orderings were found for Cu, Zn and Pb; whereas Cr and Fe phases are similar between seasons. Copper tended to be more prone to remobilization in summer, but total extractable concentrations tended to be lower. Zinc also tended to be more available in summer, as a greater percentage of the total extracted Zn is found in the exchangeable phase; nevertheless, Zn displayed higher absolute concentrations in the exchangeable phase in winter. Similarly, Pb extractable concentrations were higher in winter but, when present, Pb in the exchangeable phase displayed greater proportions in summer.

The RDS speciation study confirmed that, for the analysed samples, Cr, Cu, Zn and Pb were mainly of anthropogenic origin - most of these are concentrated in the mobilisable fractions (exchangeable, reducible and oxidisable) defined by the BCR procedure. There were also marked differences in terms of potential mobility between the RDS collected in summer and winter, especially for Cu, Zn and Pb - there is a tendency for a larger mobility potential in summer due to the greater trace metal percentages in the most labile phases (exchangeable and reducible). Nevertheless, for each sample pair, total concentrations tended to be greater in winter - the fact that the fate of RDS in winter is mainly to be washed off from the surfaces due to the frequent and more persistent rain events poses a higher contamination risk to the urban river basin, as RDS is transferred between these environmental compartments and redox conditions change. Nonetheless, the summer season was characterised by larger accumulations of RDS on surfaces due to the more sparse rain events: these were mainly coarse sediments, as fine particles easily get not only washed off, but also resuspended in the atmosphere as sediment is dry for longer periods of time. As the proportion of Cu, Zn and Pb was greater in the most labile phases in summer, this poses a more direct risk to human health by

inhalation of fine particles. Again, this apparent lower total metal concentration in these 17 summer samples might be due to the dilution effect of the coarser, quartz-dominated fraction, and grain-size normalization of RDS was not performed - individual speciation analysis of each grain size fraction needed to be undertaken to gain a better insight on the risks posed by the larger proportion of trace metals in the exchangeable and reducible fractions.

Scanning electron microscope microbeam analysis (section 4.6) showed that RDS is mainly composed by quartz (sand); rock fragments; fragments of brick, concrete, tarmac and other construction materials; spherical metal-rich particles; and anthropogenic metallic grains of diverse shape and size. In total, 46 individual trace metal-bearing grains were observed under partial vacuum condition using backscattered secondary electron (BSE) imaging. Grains containing PHE such as Cr, Pb and Zn are common in RDS - these may be very prone to resuspension and transport due to their morphology and recurrent small size. Iron oxide grains (up to 40% Fe, section 4.6.1) in RDS may display Fe-Ti exsolution structures, typical of igneous rock minerals ehich are likely sourced to RDS by the use of such rocks in veneering, cladding and pavements. Other iron oxide grains displayed more complex internal structures, with banding, inclusions and dissolution textures. These were most likely rusted iron particles from the erosion of iron infrastructures. Spherical Fe-rich grains (section 4.6.2), which likely result from high temperature combustion processes, contained a wide range of other metals such as Ti (1.8%), Pb (4800mg/kg) Co (4400mg/kg) and Cu (2800 mg/kg). Besides atmospheric fallout of such particles, furnace slag materials are also used in cement and other construction materials which are also a likely source of these particles in RDS. Lead-rich grains (up to 43% Pb, section 4.6.3) displayed massive or agglomerate-like structures and also contained smaller amounts of other metals such as Cu, Zn, Co and Sn. Close up views on Pb-rich agglomerate grains revealed that lead particles were weakly bonded - not incorporated in a crystalline structure - and therefore could be very easily separated. Whereas the whole grain measured ~400 μm, the Pb particles generated by disaggregation were as small as 0.1μm, or 100nm, which puts it into the ultrafine particle category. These are far smaller than the regulated $PM_{10}$ and $PM_{2.5}$ particle classes and are believed to have several more aggressive health implications than those classes of larger particulates (Heal et al., 2012). The spherical grain shapes observed suggest these were generated by high temperature combustion processes, and then aggregated by Ca-Si-Al material. Zinc and Barium-rich grains (section 4.4) were also common in Manchester's RDS, and may be sourced from Ba-Zn additives which are widely used as stabilisers in PVC manufacturing to make a range of paste PVC applications and tyre wear.

Principal component analysis (section 4.7) supported the definition of possible contaminant sources, responsible for high concentrations of elements of interest. It is observed that element groupings between summer and winter are very similar, revealing a consistency in element sources

and/or accumulation processes between the two seasons. Components identified by PCA can be described as follows:

• Elements which were probably related to soil include $Al_2O_3$, MgO, $TiO_2$, MnO, $Fe_2O_3$, Sc, V, Co, Ni, Ga and Nb. Besides geogenic elements, such as Al, Ga and Mg (and Ti, Mn and Fe to a smaller extent); Sc, V, Co and Ni are believed to have been enriched in Manchester's soils due to historical coal extraction and burning activities. This points to soil as a main source of these elements in Manchester's RDS - analysing the component score mapping, samples with high scores for this component (9 out of 10) were in fact collected from streets along gardens, parks or vacant land plots and RDS samples were generally collected less than 4 meters away from the soil limit.

• Rare earth elements such as La, Ce, Nd, and Y; Th, and $Al_2O_3$, $K_2O$ and Rb were also related in Manchester's RDS. These are geogenic elements, which are present mainly in igneous rocks - these elements may be sourced to RDS by the igneous rocks and gritstones that are used as kerbs in Manchester's streets, as pavements, or in buildings; or from rock aggregates which are commonly used in Manchester's street pavements, kerbstones and sidewalks. Seven out of the 9 samples which showed the highest loadings for this component were collected on or close to pavements or kerbs made from rock aggregates.

• The organic matter-related component of RDS was also represented by high concentrations of Br, I, S Se and $P_2O_5$ - elements which come mainly from nearby soils, or from plant and leaf litter which accumulates directly on surfaces.

• Barium, Cu, Zn, Pb, Sr, Sn and Sb were anthropogenic elements enriched in Manchester's RDS in areas close to industrial activites, with especially high component scores in the Trafford Park Industrial Estate, where industry is concentrated along with heavy goods transport.

• The association of As and Ge in RDS is likely related to their use in electronic equipment - component score mapping strongly suggested that automotive electronic equipment (LEDs, optical fibres, semiconductors, etc) are the dominant source of As and Ge in Manchester's RDS, due to the proximity of high score samples to scrapyards, car part dealers, garage services, an automotive electronic equipment manufacturer and a car audio centre.

• Cadmium and Bi were also related in RDS - a probable source is their use in Sn-Bi-Cd alloys, which are commonly used in low-temperature soldering of heat-sensitive materials such as glass, and light electronic assemblies. Component score mapping revealed a hotspot in the immediate vicinity of a lens manufacturer and an Autoglass centre, strongly suggesting that these elements are related to the use of low-temperature alloys to firmly mount glass and precision lenses during grinding and polishing operations. Another evidence which pointed to this source of contamination was the high Indium content of RDS - Indium alloy (approx. 44-50% Bi, 5.3-10% Cd and 19-51% In) is generally used in the production of lenses during the polishing stage, and in optics assembly.

The retention of fewer components in PCA analysis #B produced element associations which were less specific - a criterion which favours the retention of a larger number of components (eigenvalue >1) should be preferably used, as a means to more accurate source identifications. The use of a smaller number of variables in analysis #C revealed that critical element groupings were very similar to those found in the previous rounds of analysis, although component mapping showed sharper variations - the pattern of correlations between the critical variables was unaffected by the exclusion of variables of easier interpretation.

Seventeen locations which revealed high PHE levels in summer and winter datasets were selected for further analysis, in a total of 34 samples. The statistical analysis of these data subsets again suggest that, besides the clay-sized fraction, the 63-125µm grain size fraction may act as a host for PHE, especially in summer. This might be related to the existence metal-rich grains of the size of very fine sands, which are weathered and split into clay-sized particles, which may cause higher metal concentrations simultaneously in the two grain sizes. The combination of SEM observations with XRF, sequential extraction and grain size analysis results provided a more realistic picture of the actual forms of trace metals in RDS, and a better insight on the grain size fractions which are more likely to act as hosts for contaminants; adding to the element associations and sources distinguished by principal component analysis.

Spatial statistics using Manchester RDS summer and winter data consisted in applying ordinary least squares (OLS) regression and geographically weighted regression (GWR) in order to inform about the relationships between selected potentially harmful elements (Cr, Ni, Cu, Zn, As and Pb) and environmental/geochemical variables which are likely to affect RDS quality, directly or indirectly, such as road, traffic, building, population, jobs and topography data. In total, 99 environmental variables were tested for each trace metal. RDS OLS models (section 5.1.2) showed significant relationships between PHE and some of the environmental variables calculated for the purposes of this work, such as road densities, built-up areas, density of bus stops, terrain slope, population density and number of jobs per census output area (analysis set #A). Nevertheless, the highest model performances were obtained for RDS analyses when using concentrations of other chemical elements as explanatory variables (analysis set #B). Analysis set #A adjusted $R^2$ values ranged between 0.12 (Ni) and 0.38 (Zn) in summer, and between 0.14 (Cr) and 0.53 (Zn) in winter; whereas analysis set #B $R^2$ values ranged between 0.44 (As) and 0.71 (Zn) in summer, and between 0.51 (As) and 0.88 (Ni) in winter models: it is clear that the inclusion of chemical elements as explanatory variables increase OLS model performance in RDS. Another observation was that some of the explanatory geochemical variables included in the models had previously been related to the dependent variables, namely in the components calculated by PCA (cf. section 4.7) - Cr to Zr, Ba and Sb; Ni to V, Fe2O3 and Co; Cu to Zn, Sn and Sb; Zn to Cu and Sb; As to Ge; and Pb to Ba, Sn and Sb.

This spatial statistic model shows that RDS contaminants are not only related to other chemical elements in terms of sources (as previously discussed in section 4.7), but also related spatially - PHE may be modelled using those same elements and environmental parameters as explanatory variables.

GWR models for RDS summer were successfully computed for Cu, Zn and Pb (#A) and for Pb (#B). For RDS winter, Ni, Cu and As were modelled (#A), as well as Cu and Pb (#B). Analysis set #A global $R^2$ values range between 0.22 (Pb) and 0.53 (Zn) in summer, and between 0.23 (As) and 0.40 (Ni and Cu) in winter; whereas analysis set #B global $R^2$ values are of 0.73 for Pb (summer), 0.79 for Pb (winter) and 0.84 for Cu (winter). For these elements there was a clear improvement in overall model performance between analysis sets #A and #B. Contrarily to soils, and as expected, road variables display positive relationships to PHE concentrations; and also with building variables, organic matter (LOI) and fine fraction contents (63inf2). Some of the chemical elements used as explanatory variables, LOI and 63inf2, which revealed statistically significant relationships to PHE in GWR models, had previously been related to this same PHE by other statistical methods such as PCA and spearman's rank correlation - the coexistence of elements due to chemical affinities and similar sources are likely responsible for these relationships. The positive relationships between Cu, Zn and Pb and road variables can be easily explained, as road traffic has long been recognised as a source of these elements to RDS. In terms of statistically significant relationships between each explanatory variable and RDS samples, these were mostly positive. In general, for RDS summer, statistically significant positive relationships extended all across the study area or in a west-east trend. RDS winter also displayed statistically significant positive relationships in the whole area; however, a few variables displayed an east-west trend, or performed better in the southwest corner of the study area.

## 7.3. Soil-RDS relationship

One of the goals of the present research work was to identify the relationships between soil and RDS. These two media present marked differences in terms of texture and composition - chapter 6 has shown that, for the majority of the chemical elements analysed, concentrations are higher in soils, as this media usually acts as a sink for trace metal contaminants. Higher median concentrations in RDS were obtained for $Na_2O$, MgO, CaO, Cu, Cr, Zn, Sr, Mo, Bi, Hf, and Sb - many of these are most commonly traffic-related (Cr, Cu, Zn, Mo, Sb and Bi), others mainly related to cement-based construction materials such as Ca, Mg and Na (and Sr).

The Wilcoxon signed-rank statistic tested whether there are statistically significant differences in elemental concentrations between soil and RDS paired samples. This test revealed that $Na_2O$, MgO, CaO, Zn, Sr, Mo and Bi display significantly higher concentrations in RDS when compared to the

correspondent soil pairs - this had been previously indicated by the mean and maximum concentration values calculated for the whole datasets.

The observation of cross sections of resin-cast samples under the SEM showed that similar grain types and morphologies can be found between soils and RDS. Nevertheless, whereas soils have a large proportion of quartz grains, RDS samples show a greater amount of brick/tarmac/concrete fragments and grains tend to be more angular and less corroded than in soils. Iron oxide grains and iron-rich spherical grains are also common in both media. Regarding Pb-bearing grains, leaded paint fragments are mostly found in soils whereas RDS display Pb grains consisting of agglomerates of ultrafine Pb-rich particles, which pose a greater human health risk as these particles are in the respirable fraction range - and RDS can be easily resuspended. Some of the Zn grains found also display this type of morphology. Zn-Ba grains are also very common in RDS, and remarkably have not been observed in soils.

Elements which may derive from soil contribution to RDS are $Al_2O_3$, MgO, $TiO_2$, MnO, $Fe_2O_3$, Sc, V, Co, Ni, Ga and Nb - principal component analysis revealed that, in RDS, these elements are grouped in a single component and spatially related to locations where RDS has been collected in very close proximity to soils. Whereas $Al_2O_3$, MgO, $TiO_2$ and Ga - and MnO, $Fe_2O_3$ and Sc to a lesser extent - are mainly geogenic elements; V, Co and Ni are enriched in soils mainly due to past contamination sources, especially industry (mills, smelters, chemical works, etc) and coal burning activities. The grouping of these elements in one single component in RDS pointed to soil as their common source.

In soils, high levels of Cr and Cu are related to local industry and WTPs; Zn, Sb and Sb are likely derived from past industrial sources; and Pb (and P, Bi and Ag) are a probable consequence of Pb smelting/refining, coal combustion, leaded gasoline and leaded paint. In RDS, however, the sources of these elements were more diffuse, but clearly related to heavy traffic and industrial areas.

The locations where both RDS and soil contamination is more pronounced were in, or in the vicinities of, the Trafford Park Industrial Estate. Otherwise, the hypothesis that RDS with high PHE concentrations are located near soils with a similar type of contamination, or vice-versa, cannot be unequivocally met. It must also be taken into account that RDS sampling points may sometimes not be as close to soil samples as it would be the ideal and, for that reason, soil and RDS paired samples may show a less perceptible relationship. It has been demonstrated in chapter 4 that RDS contamination is closely related to the proximity of present-day sources; whereas soil may be contaminated in the absence of these, mainly due to historical sources and the accumulation of trace metals over long periods of time.

## 7.4. Key repercussions and recommendations for future work

Soils and road-deposited sediments have been shown to contain varying amounts of potentially harmful elements. These media are ubiquitously present in the urban environment and, although having distinct characteristics, their composition is often controlled by anthropogenic factors. Trace metals are the most studied chemicals in terms of human and ecosystem health risk assessments due to their recognised importance as anthropogenically-derived elements, and their known long-term persistency in the environment and/or in living organisms.

This work has shown that Manchester soils and RDS display high concentrations of elements such as Cr, Ni, Cu, Zn, As, Pb and Cd, which are frequently in excess of the established guidelines. These media are spatially related in the urban environment, and their composition is likely to influence other environmental compartments such as air and water through particle resuspension or wash off. In a similar way, air particulates may influence soil and RDS quality through the fallout of particulate matter from e.g. motor vehicle exhaust and industrial emissions. This brings serious implications in terms of human exposure - direct pathways include the inhalation of contaminated airborne particulates from indoor and outdoor air, the direct ingestion of contaminated soil, RDS and indoor dusts (specially by children), the ingestion of home-grown or allotment-grown produce, and the absorption of the contaminant through skin contact. The impacts of soil and RDS contamination on human and ecosystem health, and associated contaminant pathways, are thoroughly described in section 1.3.

Soils act mainly as sinks for pollution in the terrestrial ecosystem, as the contaminant species tend to remain and increase their concentration in soils through time - they are the main receptors for PHE contamination in urban environments, from both diffuse and point-sources (Johnson and Demetriades, 2011). In urban areas, soil can be contaminated through a number of anthropogenic processes such as atmospheric deposition of particulates derived mainly from the combustion of fossil fuels and industry, by the discharge and percolation of contaminated waters, and direct dumping of domestic and industrial residues. This also makes soils a likely source of contamination to other environmental compartments, ultimately affecting human health.

Soils have been reported to act as a source of contaminated airborne particles, such as Pb sourced mainly from lead-contaminated soils in the atmosphere of Pittsburgh, Detroit, Chicago and Birmingham, USA (Laidlaw et al., 2012); furthermore, 74% of Bakersfield's $PM_{10}$ (California) is reported to be composed of soil particulates, according to Young et al. (2002). Direct particle resuspension from soils is less likely to happen if soils are vegetated and soil moisture is high. This is the case at many locations throughout the Manchester urban area, due to the usually persistent wet weather conditions - soil particles are stabilised by plant cover and wet conditions favour particle

bonding. Nevertheless, soil excavation and transport happens frequently throughout the area - at the time of sampling several locations were being redeveloped for industrial, commercial and residential uses; and soil movements cause the emergence of large quantities of dust into the atmosphere. These may act as occasional or temporary point sources of contaminated soil particles into the atmosphere - Ketchman and Bilec (2013) have reported that the majority of regional $PM_{10-2.5}$ (89%) and $PM_{2.5}$ (90%) emissions were a direct result of soil-hauling activities in Pittsburgh, Pennsylvania (USA). Personal exposure of construction workers may also be an issue of concern, as heavy equipment operators have been reported to receive average gross personal exposures up to 0.694 $mg/m^3$ at waste disposal sites (Pannell and Grogin, 2000), where the permissible exposure limit for dusts containing silica was established at 0.182 $mg/m^3$ in accordance with the US Occupational Safety and Health Administration (OSHA, 1970).

- In Manchester, in sites where soil contamination is present such as those described in section 3.5.2 and 3.7.1, further preventive measures are recommended to minimise dust emissions (e.g. wind fencing, quick stabilization of excavation surfaces, watering/graveling, and other engineering controls and containment methods) and prevent human exposure in site (e.g. use of respiratory protections, appropriate protective clothes and PM monitoring devices), whenever major works involving soil excavation take place. Nevertheless, site-specific investigations should be undertaken at specific sites to more accurately inform about the risks to local workers and populations.

The transfer of contaminants from soils to groundwater is important in terms of contaminated soil management and groundwater conservation. Contaminants can be transported either in dissolved form or associated with particles and, in both cases, soil structure can significantly modify contaminant transfer because it determines flow velocity, that is to say the way soil solution and bulk soil are in contact (Badin et al., 2009). Nevertheless, water from public provision in the UK is unlikely to pose a risk to human health, due to the current high standard of public water quality and the minimal use of private wells in city areas (Fordyce et al., 2012); however, the protection of water resources is a major ecological issue in the urban environment, as soils are known to be a filter for percolating waters which eventually reach the urban river basin and groundwaters.

- Further interpretation and use of the Manchester soil data should be carried out in the future to investigate the risk to groundwater resources from surface contaminants, as topsoil maximum concentrations for As and Cd are 50 and 89 times higher, respectively, than the median value of the Manchester soil dataset; and for Zn, Pb, Cr and Cu, maximum values were between 10 and 24 times higher than the median values.

In terms of potential direct human exposure to urban soils, comparisons with the current UK contaminated land soil guideline values (SGV) have shown that the trace metals of environmental

concern which more frequently display concentrations in excess of the lowest established or proposed SGV are Cd, As, Cu and Zn, with 12, 19, 48 and 90% of the sites surveyed, respectively, above the reference values. Nevertheless, Cu and Zn reference values used correspond to the proposed UK ecological guideline (EA, 2008), values which are lower than all the previous guidelines. Therefore, the high proportion of Manchester soils that exceed these guidelines is a consequence of the low concentrations at which these guidelines are set.

- It is recommended that further studies are carried out with the objective of determining whether source-pathway-receptor linkages are likely at these sites as a further step to risk assessment.

Contrastingly to soils, RDS displays a transient and unconsolidated nature. This kind of urban material is highly prone to resuspension from road surfaces by wind and traffic-induced turbulence. RDS have been reported to be the second largest source (after motor vehicle exhaust) of fine particulate matter emissions to the Los Angeles urban atmosphere (Hildermann et al., 1991), mainly due to the resuspension of RDS by passing traffic and wind turbulence. Lenschow et al. (2001) quantified the non-exhaust contribution to air particulate matter (PM) in Berlin, Germany and concluded that it may account for 45% of the total $PM_{10}$ concentration.

As RDS is a great contributor to air PM, inhalation is likely the pathway which offers the most significant exposure route for the potentially harmful elements in Manchester's RDS, rather than ingestion or dermal absorption. The long-term exposure of populations and daily commuters to trace metal contaminants in PM may incur in deleterious health effects - epidemiological studies have proven that high PM concentrations enhances cardiovascular and pulmonary problems in urban populations, and mortality has shown to correlate with the mass of fine particles ($PM_{2.5}$) in ambient air (e.g. Dockery and Pope, 1994; Pope et al., 2002). Furthermore, human health effects due to the inhalation of trace metal contaminants such as Cr, Pb, Cu, Zn, As are numerous and include oxidative stress (and associated tissue inflammation and cell damage), pulmonary, cardiovascular and neurological diseases, and several types of cancer (Lee and Fraumeni, 1969; Hayes, 1988; Anttila et al., 1995; Prieditis and Adamson, 2002; Laidlaw and Filippelli, 2008; Karlsson et al., 2009). The speciation of these trace metals in RDS, and consequently in PM, influences the speed and extension of the adverse health effects and, therefore, future work may need to consider the physicochemical properties of individual trace metal species in relation to their toxicological potency.

The speciation analysis developed in this work identified Zn, Cu and Pb as the most soluble (and hence likely bioaccessible) PHE in Manchester's RDS, especially in summer when concentrations of these metals are higher in the exchangeable and reducible phases; nevertheless, total concentrations have been found to be higher in winter RDS, when sediment grain size also tends to be smaller. The generally coarser grain size of RDS in summer samples can be attributed to the higher resuspension

rates of RDS in this season due to sediment dryness, combined with longer residency times on surfaces due to less frequent rain events. Therefore, and despite total PHE concentrations being generally higher in winter, the higher resuspension potential in summer combined with the higher mass loading and higher metal concentrations on the exchangeable and reducible phases leads to a likely greater risk of adverse human health effects by inhalation in this season.

- Further studies regarding different PHE species in RDS and ambient PM are necessary to clarify the relative contribution of RDS species to PM, and to quantify the effects of short- and long-term human exposure to both these media in the urban environment. It is recommended that these studies are performed seasonally due to the differences found in PHE speciation between wet and dry seasons.

Nevertheless, even more insoluble phases (which can be related to low bioaccessibility) may be damaging if the inhaled particles are very small in size - PHE-bearing nanoparticles have shown increased toxicity when compared to micrometer particles, as these particles produce enhanced inflammatory responses when compared to larger particles of the same chemical composition (Donaldson and Tran, 2002; Duffin et al., 2007). Therefore, even if PHE are present in insoluble phases, SEM-EDS analysis has shown that PHE-bearing (namely Pb and Zn) particles in Manchester's RDS can be smaller than 100nm in size, which can be classified as nanoparticles. The extent to which resuspended RDS contributes to the nanoparticle-sized components of PM has yet to be determined and, therefore, the study of nanoparticle-sized PHE-bearing grains in RDS can further improve the assessment of risks posed by RDS resuspension and inhalation.

Although fine-grained particles are more easily resuspended into the atmosphere and more likely to cause adverse human health effects, this study also provided evidence that not only the finer fractions of RDS are important PHE carriers, as is the case with natural soils and sediments. In RDS, several studies have reported the <63µm grain size fraction as the major host for metals in RDS (Sutherland, 2002; Irvine et al., 2009; Krčmová et al., 2009; Sutherland et al., 2012), but the coarse nature of RDS from other studies has also been reported to be of great influence in metal distribution (e.g. Robertson and Taylor, 2007; Sutherland et al., 2008). In the present work, RDS were collected from different local settings and in two distinct seasons; hence, grain size is highly variable among samples. Nevertheless, in contaminated samples, PHE such as Zn, Pb, Ni and Cu and their different phases can be statistically related to both the <2µm and the 63-125µm grain size fractions, suggesting a different control on the grain size partitioning of these metals. SEM observations pointed to a specific type of grain, which is generally around 100µm and composed of an agglomerate of smaller, <2µm particles, as a possible reason for these correlations. This type of agglomerate grain also generates the nanoparticle-sized grains referred in the previous paragraph.

- Agglomerate-structured PHE-containing grains in RDS should be further studied in terms of composition, occurrence and sources; as their disaggregation into ultrafine particles is likely and these have a higher associated risk to human health.

The brushing method chosen for RDS sampling used in this work allowed a quick and cost-effective way of sample collection, under similar weather conditions and accumulation times on surfaces, which are important factors to account for when comparing chemical and sedimentological features between seasons or between soils and RDS. However, this sampling method does not favour the retention of ultrafine material and, furthermore, some of this material may also be lost during sample preparation for observation and analysis by SEM-EDS. Therefore, only a small number of grains <2um are observed in Manchester's RDS - the aforementioned agglomerate grains are more frequently observed.

- More effective sample collection and handling methods must be investigated for a detailed analysis of nanoparticle-sized grains in RDS, involving e.g. wet/dry vacuuming and filtering.

Locations where Manchester's RDS have displayed trace metal concentrations in excess of the 75$^{th}$ percentile for summer and winter samples were mostly located within or near industrial areas, in dual carriageways, or roads where high traffic rates are frequent, such as the samples referred in Table 107. These are locations where further investigations on the quantity, grain size and composition of resuspended particles would better inform about the risks posed by population and pedestrian exposure.

Not only ambient air is influenced by RDS composition. Water quality is also of great concern, as RDS is washed off frequently from road surfaces, entering sewer systems or water bodies - materials are mainly supplied via road drains which, in turn, often discharge directly into rivers (Taylor et al., 2008). Soils and RDS in urban systems make a large contribution to the transported metal loading, and these media have been reported to be the main diffuse sources of contaminants in urbanised drainage basins (Sutherland and Tolosa, 2000; Preciado and Li, 2006; McKenzie et al., 2009). Carter et al. (2003) reported that 19 - 22% of the contaminated sediment flux in the River Aire (UK) reaches was derived from RDS. Similarly, Yin and Li (2008) found that 60% of the suspended sediments at the outlet of a sewer system in Wuhan City, China was derived from the drainage system (gutter sediments and combined sewer sediments), with about 40% from RDS. In urban runoff events, finer grain sizes (which carry higher metal concentrations) are more easily mobilised from the road network and exported towards the sewer system and river network (Taylor and Owens, 2009). RDS is, therefore, a significant source of trace metal contaminants to urban water systems - sediment management strategies need to be carefully considered within urban systems and river basins. This work has revealed that

- Further work should include more detailed investigations on the RDS contribution to surface runoff suspended loading and the impact of the trace metal content of RDS on stormwater quality, which is linked to the phase changes that occur in response to the different physicochemical conditions these metals are subject to through the process of RDS transport and deposition.

The composition of Manchester's RDS has been shown to vary, not only temporally but spatially, influenced by a plethora of natural and anthropogenic factors. Within the natural controls on RDS are the climatic factors such as precipitation, wind and temperature - these are mainly responsible for RDS sorting, remobilization and transport, events which occur in short periods of time, making RDS a very transient media. The dry or wet conditions also influence the chemistry of RDS constituents, as the elemental oxidation states and mobilization potential are largely influenced by this factor. Anthropogenic factors are, nevertheless, the most important control on RDS composition - the proximity of point sources is highly related to RDS contamination. In the beginning of this research it was hypothesised that season would play an important role in trace metal concentrations in RDS, but in fact the proximity of sources displayed a greater influence on RDS chemical composition, regardless of the season - local factors are stronger controls on composition than temporal factors, as summer-winter sample pairs tend to show small differences in composition, compared to the large variations which occur according to location. Apart from composition, which tends to remain similar between seasons, the drier summer season favours greater RDS accumulations on pavements, which influences contaminant mass loading. However, when these greater accumulations occur, they tend to be coarser in grain size and hence a great part of the mass loading consists of inert, mineral-dominated material. As stated before, there may be the hypothesis that a significant amount of finer grain size fractions is resuspended into the atmosphere especially in summer, contributing to the relative predominance of coarse grain size fractions in RDS. Combined with the greater amounts of exchangeable/reducible PHE in this season, the quantification of the RDS contribution to PM is suggested for future works regarding urban environmental quality.

The definition of contaminant sources is essential for a better understanding of contaminant dynamics in the urban system. This has been attained in the present work by the use of several techniques including the detailed mapping of chemical concentrations and other parameters, of geographical features, of statistical parameters, and spatial statistics. All of these evidenced spatial patterns which have been interpreted with the objective of fully assess parameter variability within the study area and ultimately identify sources which explain the variations observed. From these methods, component score mapping has been demonstrated to be of great aid in source identification. This method has been rarely used in soil studies (e.g. Birke et al., 2011; Šajn et al., 2011) and consists in the mapping of component scores obtained by principal component analysis,

allowing the identification of sources through the patterns generated for each chemical element/variable group - in geochemical terms, principal components represent groups of elements or variables with similar variation within a set of observed variables. This method has allowed the identification of sources which are responsible for the simultaneous input of several suites of chemical elements to Manchester's soils and RDS, and the application of this method is recommended in future works. Further work regarding method applicability to different kinds of datasets and/or environmental media should be performed.

Nevertheless, spatial statistical techniques have also been employed in the present research work. These techniques have been successfully used by several authors to model contamination and other parameters in sediments (Lai et al., 2013), air (Hoek et al., 2008; Madsen et al., 2011; Chen et al., 2012), water (Meeuwig et al., 2000; Varouchakis and Hristopulos, 2013), and soils (Lee et al., 2006; Wu et al., 2010; Terrón et al., 2011; Zhang et al., 2011). Ordinary Least Squares (OLS) regression and Geographically-Weighted Regression (GWR) were explored in the present work. However, this kind of spatial statistics had not yet been used regarding contaminant modelling in RDS, by the analysis of the existing literature, and produced good results in this work. The advantage of spatial statistical methods is that they allow exploring spatial non-stationarity and modelling the relationships between selected PHE and a plethora of explanatory variables. In soils and RDS, however, PHE numerical modelling has been important only to determine how strong the relationships are between PHE and other variables, through global and local $R^2$, as source apportionment cannot be clearly discerned from OLS and GWR outputs. Chemical elements used as independent variables to model PHE concentrations were often similar to the element groupings found by PCA - the co-occurrence of chemical elements in soils and RDS, and their similar variations across the area, likely caused this behaviour. Further improvement of spatial statistical models should include an investigation on the use of component scores as variables for OLS and GWR, in order to model PHE not only using individual trace metal concentrations, but also parameters (scores) which explain the variation of a suite of related elements. OLS and GWR regression modelling of trace metals in soils and RDS would also certainly benefit if a wider variety of environmental datasets would be available for use, such as detailed, small scale surveys of the different types of present-day and historical industry. In addition, a denser sampling scheme for RDS could also bring improvements to model performance.

The dynamic nature of soils and RDS and their constant interaction with other environmental compartments makes it difficult to clearly assess and quantify their relative contribution as sinks or sources of contamination in the urban environment. Nevertheless, one of the objectives of the present work has been to find linkages between soil and RDS chemical composition, morphology and contamination sources. The extent to which soil particles contribute to RDS has been addressed in

very few studies, which have reported e.g. roadway dusts composed of 76% soil (Hopke et al., 1980), and that soil contributes between 57% and 90% to roadway dusts (Hunt et al., 1993). In the present work, soils have been found to contribute to RDS composition: besides geogenic components such as $SiO_2$, $Al_2O_3$, MgO, $TiO_2$ and Ga; and MnO, $Fe_2O_3$ and Sc to a lesser extent, Manchester's soils are likely contributors of V, Co and Ni to RDS (section 6.3). These last elements are enriched in soils mainly from past anthropogenic activities and their presence in RDS collected in close proximity of contaminated soil samples corroborates this source. Furthermore, geogenic components of RDS observed under the SEM revealed clear similarities with soil particles - namely quartz, silt and clay contents; and iron oxides and spherical Fe-rich grains are also common in both media.

Higher trace metal concentrations in RDS, when compared to soils, have been reported by Harrison et al., 1981; Li et al., 2001; Ordoñez et al., 2003; and Krčmová et al., 2009. However, this study reveals that in Manchester, from the selected PHE, only Zn displays significantly higher concentrations in RDS, when comparing soil-RDS paired samples - this element is closely related to tyre wear, brake linings, and wear and tear of vehicular parts. Nickel, Cu, As, Pb and Cd concentrations, on the other hand, are enhanced in soils. The generally higher median and maximum concentrations of these elements in soils can be explained by the intense industrial activity which has historically affected this area, combined with high volumes of vehicle traffic, which has become more environmental-friendly only in recent years with the removal of Pb from fuel and the use of catalysers and alternative sources of energy. Furthermore, industry emissions are now regulated and tend to decrease - the drive for greener energy sources and the drastic reduction of emissions to comply with legislation has diminished contamination inputs to the environment. This results in less contaminated RDS, which represent present-day inputs; while soils still carry the legacy of contamination from Manchester's industrial past. Nevertheless, the identified present-day sources are likely to affect both media simultaneously at the local scale and this has been observed in samples collected in areas of high traffic and industrial density; e.g. samples collected in/near the Trafford Park Industrial Estate.

The conclusions reached in the present research work contribute to a global understanding of soil and RDS geochemistry in urban environments, based on samples collected over 75 $Km^2$ of Manchester at varying sample densities. Up-scaling of these results to other urban centres displaying different characteristics in terms of climate, contaminant sources and soil/RDS dynamics using different approaches regarding sample collection and analysis, should be done with caution.

This research has provided a comprehensive interpretation of the geochemistry, mineralogy and spatial variability of Manchester's soils and RDS, ultimately linking contamination to its sources through spatial and statistical methods. A key observation is the importance of distinguishing local

sources and land uses in the urban environment if contaminant species are to be modelled and understood.

# References


ACKERMANN, F. (1980). A procedure for correcting the grain size effect in heavy metal analyses of estuarine and coastal sediments. *Environmental Technology Letters,* 1**,** 518 - 527.

ADAMO, P., DUDKA, S., WILSON, M. J. & MCHARDY, W. J. (1996). Chemical and mineralogical forms of Cu and Ni in contaminated soils from the Sudbury mining and smelting region, Canada. *Environmental Pollution,* 91**,** 11-19.

ALAGARSAMY, R. & ZHANG, J. (2010). Geochemical characterisation of major and trace elements in the coastal sediments of India. *Environmental Monitoring and Assessment,* 161**,** 161-176.

ALLEN, M. A., CAVE, M. R., CHENERY, S. R. N., GOWING, C. J. B. & REEDER, S. (2011). Sample Preparation and Inorganic Analysis for Urban Geochemical Survey Soil and Sediment Samples. *Mapping the Chemical Environment of Urban Areas*, 28-46. John Wiley & Sons, Ltd.

ALLOTT, R. W., HEWITT, C. N. & KELLY, M. R. (1990). The environmental half-lives and mean residence times of contaminants in dust for an urban environment: Barrow-in-Furness. *Science of The Total Environment,* 93**,** 403-410.

ALLOWAY, B. J. & JACKSON, A. P. (1991). The behaviour of heavy metals in sewage sludge-amended soils. *Science of the Total Environment,* 100**,** 151-176.

ANTONIADIS, V. & ALLOWAY, B. J. (2002). The role of dissolved organic carbon in the mobility of Cd, Ni and Zn in sewage sludge-amended soils. *Environmental Pollution,* 117**,** 515-521.

ANTTILA, A., HEIKKILA, P., PUKKALA, E., NYKYRI, E., KAUPPINEN, T., HERNBERG, S. & HEMMINKI, K. (1995). Excess lung cancer among workers exposed to lead. *Scand J Work Environ Health,* 21**,** 460-9.

AUBERT, H. & PINTA, M. (1977). *Trace elements in soils,* Amsterdam, Elsevier, pp.

AUERMANN, E. & BORTITZ, S. (1977). Contamination of vegetable foods by lead-containing road dust. *Nahrung-Food,* 21**,** 793-797.

AZEEZ, J. O., HASSAN, O. A. & EGUNJOBI, P. O. (2011). Soil Contamination at Dumpsites: Implication of Soil Heavy Metals Distribution in Municipal Solid Waste Disposal System. *Soil & Sediment Contamination,* 20**,** 370-386.

BABU, K. G. & KUMAR, V. S. R. (2000). Efficiency of GGBS in concrete. *Cement and Concrete Research,* 30**,** 1031-1036.

BACIGALUPO, C. & HALE, B. (2012). Human health risks of Pb and As exposure via consumption of home garden vegetables and incidental soil and dust ingestion: A probabilistic screening tool. *Science of the Total Environment,* 423**,** 27-38.

BADIN, A. L., BEDELL, J. P. & DELOLME, C. (2009). Effect of water content on aggregation and contaminant leaching: the study of an urban Technosol. *Journal of Soils and Sediments,* 9**,** 653-663.

BALL, J. E., JENKS, R. & AUBOURG, D. (1998). An assessment of the availability of pollutant constituents on road surfaces. *The Science of The Total Environment,* 209**,** 243-254.

BARRETT, J. E. S., TAYLOR, K. G., HUDSON-EDWARDS, K. A. & CHARNOCK, J. M. (2010). Solid-phase speciation of Pb in urban road dust sediment: A XANES and EXAFS study. *Environmental Science & Technology,* 44**,** 2940-2946.

BARRETT, J. E. S., TAYLOR, K. G., HUDSON-EDWARDS, K. A. & CHARNOCK, J. M. (2011). Solid-phase speciation of Zn in road dust sediment. *Mineralogical Magazine,* 75**,** 2611-2629.

BATURIN, G. N. (2007). Tellurium and thallium in ferromanganese crusts and phosphates on oceanic seamounts. *Doklady Earth Sciences,* 413**,** 331-335.

BERROW, M. L. & WEBBER, J. (1972). Trace elements in sewage sludges. *Journal of the Science of Food and Agriculture,* 23**,** 93-100.

BGS (2010). Lead (Pb) in surface soils: Central and Eastern England. *British Geological Survey G-BASE geochemical map, Keyworth, Nottingham, UK.*

BGS (2012a). *G-BASE Research Activities.* British Geological Survey, URL: bgs.ac.uk/gbase/research.html, accessed on August 17, 2012.

BGS (2012b). *Geochemical Baseline Survey of the Environment (G-BASE) web page.* British Geological Survey, URL: bgs.ac.uk/gbase/home.html?src=sfb, accessed on July 19, 2012.

BIRCH, G. F. & SCOLLEN, A. (2003). Heavy metals in road dust, gully pots and parkland soils in a highly urbanised sub-catchment of Port Jackson, Australia. *Australian Journal of Soil Research,* 41**,** 1329-1342.

BIRKE, M., RAUCH, U. & STUMMEYER, J. (2011). Urban Geochemistry of Berlin, Germany. *Mapping the Chemical Environment of Urban Areas*, 245-268*.* John Wiley & Sons, Ltd.

BORDOVSKII, G. A., MARCHENKO, A. V., KOZHOKAR, M. Y., NASREDINOV, F. S. & SEREGIN, P. P. (2013). Composition determination of multicomponent chalcogenide glassy semiconductors with X-ray fluorescence analysis. *Glass Physics and Chemistry,* 39**,** 377-381.

BRETZEL, F. & CALDERISI, M. (2006). Metal Contamination in Urban Soils of Coastal Tuscany (Italy). *Environmental Monitoring and Assessment,* 118**,** 319-335.

BRIDGE, J. S. (2003). *Rivers and Floodplains: Forms, Processes and Sedimentary Record,* Oxford, UK, Blackwell Science Ltd., 504 pp.

BRIS, F.-J., GARNAUD, S., APPERRY, N., GONZALEZ, A., MOUCHEL, J.-M., CHEBBO, G. & THÉVENOT, D. R. (1999). A street deposit sampling method for metal and hydrocarbon contamination assessment. *The Science of The Total Environment,* 235**,** 211-220.

BROKBARTOLD, M., TEMMINGHOFF, E. J. M., WENG, L. P. & MARSCHNER, B. (2013). Unique Characteristics of Pb in Soil Contaminated by Red Lead Anti-Corrosion Paint. *Soil & Sediment Contamination,* 22**,** 839-855.

BROWN, S. E. (2001a). Geochemical baseline data for the urban area of Cardiff. *British Geological Survey Research Report IR/01/102*.

BROWN, S. E. (2001b). Geochemical baseline data for the urban area of Cardiff. *British Geological Survey Research Report IR/01/102, 59pp*.

BROWN, S. E. (2001c). Geochemical baseline data for the urban area of Telford. *British Geological Survey Research Report IR/01/086, 59pp.*

BRUNEKREEF, B. & FORSBERG, B. (2005). Epidemiological evidence of effects of coarse airborne particles on health. *European Respiratory Journal,* 26**,** 309-318.

CALABRESE, E. J., STANEK, E. J., JAMES, R. C. & ROBERTS, S. M. (1997). Soil ingestion: A concern for acute toxicity in children. *Environmental Health Perspectives,* 105**,** 1354-1358.

CAREY, A. E., GOWEN, J. A., FOREHAND, T. J., TAI, H. & WIERSMA, G. B. (1980). Heavy-metal concentrations in soils of 5 United States cities. *Pesticides Monitoring Journal,* 13**,** 150-154.

CARRAZ, F., TAYLOR, K. G., STAINSBY, S. & ROBERTSON, D. J. (2006). Contaminated urban road deposited sediment (RDS), Greater Manchester, UK: a spatial assessment of potential surface water impacts. *North West Geography,* 6**,** 10-19.

CARTER, J., OWENS, P. N., WALLING, D. E. & LEEKS, G. J. L. (2003). Fingerprinting suspended sediment sources in a large urban river system. *The Science of The Total Environment,* 314-316**,** 513-534.

CHANG, R. (2009). *Chemistry,* 9th edition*.* McGraw-Hill, 1085 pp.

CHARLESWORTH, S., EVERETT, M., MCCARTHY, R., ORDONEZ, A. & DE MIGUEL, E. (2003). A comparative study of heavy metal concentration and distribution in deposited street dusts in a large and a small urban area: Birmingham and Coventry, West Midlands, UK. *Environment International,* 29**,** 563-573.

CHARLESWORTH, S. M. & LEES, J. A. (1999). The distribution of heavy metals in deposited urban dusts and sediments, Coventry, England. *Environmental Geochemistry and Health,* 21**,** 97-115.

CHASE-DUNN, C. & MANNING, E. S. (2002). City systems and world systems: Four millennia of city growth and decline. *Cross-Cultural Research,* 36**,** 379-398.

CHEN, L., WANG, Y. M., LI, P. W., JI, Y. Q., KONG, S. F., LI, Z. Y. & BAI, Z. P. (2012). A land use regression model incorporating data on industrial point source pollution. *Journal of Environmental Sciences-China,* 24**,** 1251-1258.

CHESWORTH, W. (2008). *Encyclopedia of Soil Science*, Springer, 902 pp.

CHOW, T. J. (1970). Lead accumulation in roadside soil and grass. *Nature,* 225**,** 295-&.

CLINE, M. G. (1944). Principles of Soil Sampling. *Soil Science,* 58**,** 275-288.

COTTER-HOWELLS, J. (1996). Lead phosphate formation in soils. *Environmental Pollution,* 93**,** 9-16.

COUNCELL, T. B., DUCKENFIELD, K. U., LANDA, E. R. & CALLENDER, E. (2004). Tire-wear particles as a source of zinc to the environment. *Environmental Science & Technology,* 38**,** 4206-4214.

COVELLI, S. & FONTOLAN, G. (1997). Application of a normalization procedure in determining regional geochemical baselines. *Environmental Geology,* 30**,** 34-45.

DAVIDSON, C. I., PHALEN, R. F. & SOLOMON, P. A. (2005). Airborne particulate matter and human health: A review. *Aerosol Science and Technology,* 39**,** 737-749.

DAVIES, B. E. (1978). Plant-available lead and other metals in British garden soils. *Science of the Total Environment,* 9**,** 243-262.

DAVIS, J. C. (1974). *Statistics and Data Analysis in Geology,* 3rd. New York, John Wiley & Sons, 656 pp.

DEFRA (2006). Environmental Protection Act 1990: Part 2A - Contaminated Land. *Department for Environment, Food and Rural Affairs, London*.

DEFRA (2009). Defra Classification of Local Authorities in England - Updated technical guide. *Department for Environment, Food and Rural Affairs, London*.

DEFRA (2011). *Department of Transport data web page.* UK Department for Environment, Food and Rural Affairs, URL: dft.gov.uk/traffic-counts/download.php, accessed on July 19, 2011.

DEFRA & EA (2004). Model procedures for the management of land contamination - Contaminated Land Report 11. *Department for Environment, Food and Rural Affairs, London; and Environment Agency, Bristol*.

DELFINO, R. J., SIOUTAS, C. & MALIK, S. (2005). Potential role of ultrafine particles in associations between airborne particle mass and cardiovascular health. *Environmental Health Perspectives,* 113**,** 934-946.

DEMETRIADES, A. (2011). The Lavrion Urban Geochemistry Study, Hellas. *Mapping the Chemical Environment of Urban Areas*, 424-456. John Wiley & Sons, Ltd.

DOCKERY, D. W. & POPE, C. A. (1994). Acute Respiratory Effects of Particulate Air Pollution. *Annual Review of Public Health,* 15**,** 107-132.

DODGE, M. & PERKINS, C. (2010). Maps, Memories and Manchester: The Cartographic Imagination of the Hidden Networks of the Hydraulic City. *Paper for Mapping, Memory and the City: An International Interdisciplinary Conference. University of Liverpool, 25-26th February 2010.*

DONALDSON, K. & TRAN, C. L. (2002). Inflammation caused by particles and fibers. *Inhalation Toxicology,* 14**,** 5-27.

DOUGLAS, I., HODGSON, R. & LAWSON, N. (2002). Industry, environment and health through 200 years in Manchester. *Ecological Economics,* 41**,** 235-255.

DOYLE, J. R., BLAIS, J. M., HOLMES, R. D. & WHITE, P. A. (2012). A soil ingestion pilot study of a population following a traditional lifestyle typical of rural or wilderness areas. *Science of the Total Environment,* 424**,** 110-120.

DRAGOVIC, S., CUJIC, M., SLAVKOVIC-BESKOSKI, L., GAJIC, B., BAJAT, B., KILIBARDA, M. & ONJIA, A. (2013). Trace element distribution in surface soils from a coal burning power production area: A case study from the largest power plant site in Serbia. *CATENA,* 104**,** 288-296.

DU PLESSIS, J. L., ELOFF, F. C., BADENHORST, C. J., OLIVIER, J., LAUBSCHER, P. J., VAN AARDE, M. N. & FRANKEN, A. (2010). Assessment of Dermal Exposure and Skin Condition of Workers Exposed to Nickel at a South African Base Metal Refinery. *Annals of Occupational Hygiene,* 54**,** 23-30.

DUDKA, S. & ADRIANO, D. C. (1997). Environmental impacts of metal ore mining and processing: A review. *Journal of Environmental Quality,* 26**,** 590-602.

DUFFIN, R., TRAN, L., BROWN, D., STONE, V. & DONALDSON, K. (2007). Proinflammogenic Effects of Low-Toxicity and Metal Nanoparticles In Vivo and In Vitro: Highlighting the Role of Particle Surface Area and Surface Reactivity. *Inhalation Toxicology,* 19**,** 849-856.

DUFFUS, J. H. (2002). "Heavy metals" - A meaningless term? (IUPAC technical report). *Pure and Applied Chemistry,* 74**,** 793-807.

DUGGAN, M. J. & WILLIAMS, S. (1977). Lead-in-dust in city streets. *Science of The Total Environment,* 7**,** 91-97.

EA (2002). Contaminated Land Exposure Assessment (CLEA) soil guideline values. *Environment Agency, Bristol*.

EA (2006). The development and use of soil quality indicators for assessing the role of soil in environmental interactions. Science report - SC030265. *Environment Agency, Bristol*.

EA (2008). Guidance on the use of soil screening values in ecological risk assessment. Science report - SC070009/SR2b. *Environment Agency, Bristol*.

EA (2009a). Human health toxicological assessment of contaminants in soil. Science report - final SC050021/SR2. *Environment Agency, Bristol*.

EA (2009b). Soil Guideline Values for cadmium in soil. Science report SC050021 / Cadmium SGV. *Environment Agency, Bristol*.

EA (2009c). Soil Guideline Values for inorganic arsenic in soil. Science report SC050021 / Arsenic SGV. *Environment Agency, Bristol*.

EA (2009d). Soil Guideline Values for nickel in soil. Science report SC050021 / Nickel SGV. *Environment Agency, Bristol*.

EA (2009e). Soil Guideline Values for selenium in soil. Science report SC050021 / Selenium SGV. *Environment Agency, Bristol*.

EA (2009f). Using soil guideline values. Science report - SC050021/SGV introduction. *Environment Agency, Bristol*.

EICH-GREATOREX, S., KROGSTAD, T. & SOGN, T. A. (2010). Effect of phosphorus status of the soil on selenium availability. *Journal of Plant Nutrition and Soil Science,* 173**,** 337-344.

EKOS (2008). *Trafford Park Masterplan - vision and implementation report.* EKOS Consulting Ltd., URL: trafford.gov.uk/cme/live/dynamic/DocMan2Document.asp?document_id=DD1FBEE9-38F4-4024-B10C-C0515C48C2C4, accessed on Nov 27, 2012.

ENGELSEN, C. J., WIBETOE, G., VAN DER SLOOT, H. A., LUND, W. & PETKOVIC, G. (2012). Field site leaching from recycled concrete aggregates applied as sub-base material in road construction. *Science of the Total Environment,* 427**,** 86-97.

ESRI (2012). *ArcGIS 10.0 Resources.* ESRI, URL: resources.arcgis.com/en/help/main/10/, accessed on Nov 29, 2012.

EU (2006). Thematic Strategy for Soil Protection - Commission document number 231 of 2006. European Comission.

EU (2012). The implementation of the Soil Thematic Strategy and ongoing activities - Commission document number 046 of 2012. European Comission.

FACCHINELLI, A., SACCHI, E. & MALLEN, L. (2001). Multivariate statistical and GIS-based approach to identify heavy metal sources in soils. *Environmental Pollution,* 114**,** 313-324.

FANG, G. C., WU, Y. S., HUANG, S. H. & RAU, J. Y. (2005). Review of atmospheric metallic elements in Asia during 2000-2004. *Atmospheric Environment,* 39**,** 3003-3013.

FARMER, J. G. & CROSS, J. D. (1978). Bromine in soil — An indicator of automobile exhaust lead pollution? *Water, Air, & Soil Pollution,* 9**,** 193-198.

FENDORF, S., NICO, P. S., KOCAR, B. D., MASUE, Y. & TUFANO, K. J. (2011). Arsenic Chemistry in Soils and Sediments. *ChemInform,* 42.

FENGER, J. (1999). Urban air quality. *Atmospheric Environment,* 33**,** 4877-4900.

FIELD, A. P. (2005). *Discovering statistics using SPSS,* 2. London, Sage, 822 pp.

FILGUEIRAS, A. V., LAVILLA, I. & BENDICHO, C. (2002). Chemical sequential extraction for metal partitioning in environmental solid samples. *Journal of Environmental Monitoring,* 4**,** 823-857.

FILON, F. L., D'AGOSTIN, F., CROSERA, M., ADAMI, G., BOVENZI, M. & MAINA, G. (2009). In vitro absorption of metal powders through intact and damaged human skin. *Toxicology in Vitro,* 23**,** 574-579.

FLIGHT, D. M. A. & SCHEIB, A. J. (2011). Soil Geochemical Baselines in UK Urban Centres: The G-BASE Project. *Mapping the Chemical Environment of Urban Areas*, 186-206. John Wiley & Sons, Ltd.

FORDYCE, F. M. & ANDER, E. L. (2003). Urban Soils Geochemistry and GIS-aided Interpretation – A Case Study from Stoke-on-Trent. *British Geological Survey Research Report IR/01/35R*.

FORDYCE, F. M., BROWN, S. E., ANDER, E. L., RAWLINS, B. G., O'DONNELL, K. E., LISTER, T. R., BREWARD, N. & JOHNSON, C. C. (2005). GSUE: urban geochemical mapping in Great Britain. *Geochemistry: Exploration, Environment, Analysis,* 5**,** 325-336.

FORDYCE, F. M., NICE, S. E., LISTER, T. R., O DOCHARTAIGH, B. E., COOPER, R., ALLEN, M., INGHAM, M., GOWING, C., VICKERS, B. P. & SCHEIB, A. (2012). Urban soil geochemistry of Glasgow. Edinburgh, UK. *British Geological Survey Research Report OR/08/002*.

FORSTNER, U. & SALOMONS, W. (1980). Trace metal analysis of polluted sediments, part 1 - assessment of sources and intensities. *Environmental Technology Letters,* 1**,** 494-505.

FÖRSTNER, U. & WITTMANN, G. T. W. (1981). *Metal Pollution in the Aquatic Environment,* 2. Berlin, Springer-Verlag, 486 pp.

FOTHERINGHAM, A. S., BRUNSDON, C. & CHARLTON, M. (2002). *Geographically Weighted Regression: The Analysis of Spatially Varying Relationships*, Wiley, 284 pp.

FREDERICCI, C., ZANOTTO, E. D. & ZIEMATH, E. C. (2000). Crystallization mechanism and properties of a blast furnace slag glass. *Journal of Non-Crystalline Solids,* 273**,** 64-75.

FREESTONE, S. E., O'DONNELL, K. E. & BROWN, S. E. (2004). Geochemical baseline data for the urban area of Sheffield. *British Geological Survey Research Report IR/02/084, 72pp.*

FREESTONE, S. E. O. D., K.E.; BROWN, S.E.. . NOTTINGHAM, UK, (2004). Geochemical baseline data for the urban area of Mansfield. *British Geological Survey Research Report IR/02/082, 74pp.*

FRIEDMAN, G. M. & SANDERS, F. E. (1978). *Principles of sedimentology,* New York, Wiley, 798 pp.

FUJIWARA, F., REBAGLIATI, R. J., MARRERO, J., GÓMEZ, D. & SMICHOWSKI, P. (2011). Antimony as a traffic-related element in size-fractionated road dust samples collected in Buenos Aires. *Microchemical Journal,* 97**,** 62-67.

GADD, G. M. (2007). Transformation and Mobilization of Metals, Metalloids, and Radionuclides by Microorganisms. *Biophysico-Chemical Processes of Heavy Metals and Metalloids in Soil Environments*, 53-96. John Wiley & Sons, Inc.

GERRARD, J. (2000). *Fundamentals of Soils*, Taylor & Francis, 264 pp.

GERZABEK, M. H., MURAMATSU, Y., STREBL, F. & YOSHIDA, S. (1999). Iodine and bromine contents of some Austrian soils and relations to soil characteristics. *Journal of Plant Nutrition and Soil Science-Zeitschrift Fur Pflanzenernahrung Und Bodenkunde,* 162**,** 415-419.

GEZER, E. D., YILDIZ, U. C., TEMIZ, A., YILDIZ, S. & DIZMAN, E. (2005). Cu, Cr and As distribution in soils adjacent to CCA-treated utility poles in Eastern Blacksea Region of Turkey. *Building and Environment,* 40**,** 1684-1688.

GOLDSCHMIDT, V. M. (1935). Rare Elements in Coal Ashes. *Industrial & Engineering Chemistry,* 27**,** 1100-1102.

GOODMAN, G. T. & ROBERTS, T. M. (1971). Plants and soils as indicators of metals in the air. *Nature,* 231**,** 287-&.

GOVIL, P. K., REDDY, G. L. N. & KRISHNA, A. K. (2001). Contamination of soil due to heavy metals in the Patancheru industrial development area, Andhra Pradesh, India. *Environmental Geology,* 41**,** 461-469.

GRAFE, M., LANDERS, M., TAPPERO, R., AUSTIN, P., GAN, B., GRABSCH, A. & KLAUBER, C. (2011). Combined Application of QEM-SEM and Hard X-ray Microscopy to Determine Mineralogical Associations and Chemical Speciation of Trace Metals. *Journal of Environmental Quality,* 40**,** 767-783.

GRANDJEAN, P., ERIKSEN, M. L., ELLEGAARD, O. & WALLIN, J. A. (2011). The Matthew effect in environmental science publication: A bibliometric analysis of chemical substances in journal articles. *Environmental Health,* 10.

GREEN, P. (1984). Digital image-processing of integrated geochemical and geological information. *Journal of the Geological Society,* 141**,** 941-949.

GRIFFITHS, K. J., SHAND, P. & INGRAM, J. (2003). Baseline Report Series, 8: The Permo-Triassic Sandstones of Manchester and East Cheshire. *Groundwater Systems and Water Quality Commissioned Report CR/03/265N; Science Group: Air, Land & Water Technical Report NC/99/74/8, 51pp*.

GUNAWARDANA, C., GOONETILLEKE, A., EGODAWATTA, P., DAWES, L. & KOKOT, S. (2012). Source characterisation of road dust based on chemical and mineralogical composition. *Chemosphere,* 87**,** 163-170.

GWOREK, B., DMUCHOWSKI, W. & CHMIELEWSKI, W. (2008). *The influence of the waste disposal on heavy metals in soil and plants,* London, Taylor & Francis Ltd, 125-131 pp.

HAIYING, Z., YOUCAI, Z. & JINGYU, Q. (2011). Utilization of municipal solid waste incineration (MSWI) fly ash in ceramic brick: product characterization and environmental toxicity. *Waste management (New York, N.Y.),* 31**,** 331-41.

HANNAM, I. & BOER, B. (2002). *Legal and Institutional Frameworks for Sustainable Soils: A Preliminary Report,* Gland, Switzerland and Cambridge, UK, International Union for Conservation of Nature and Natural Resources, 88 pp.

HANNESSON, G. M., KUDER, K., SHOGREN, R. & LEHMAN, D. (2012). The influence of high volume of fly ash and slag on the compressive strength of self-consolidating concrete. *Construction and Building Materials,* 30**,** 161-168.

HARDEN, J. D. & JOHNSON, P. D. (2009). The Application of Soil Amendments to the Retardance of Rainwater-Leached Metals from CCA-Treated Wood Ash in Soil. *Soil & Sediment Contamination,* 18**,** 412-428.

HARRISON, R. M., LAXEN, D. P. H. & WILSON, S. J. (1981). Chemical associations of lead, cadmium, copper and zinc in street dusts and roadside soils. *Environmental Science & Technology,* 15**,** 1378-1383.

HAYES, R. B. (1988). Review of occupational epidemiology of chromium chemicals and respiratory cancer. *Science of the Total Environment,* 71**,** 331-339.

HE, Z. L., YANG, X. E. & STOFFELLA, P. J. (2005). Trace elements in agroecosystems and impacts on the environment. *Journal of Trace Elements in Medicine and Biology,* 19**,** 125-140.

HEAL, M. R., KUMAR, P. & HARRISON, R. M. (2012). Particles, air quality, policy and health. *Chemical Society Reviews,* 41**,** 6606-6630.

HELSEN, L. & VAN DEN BULCK, E. (2005). Review of disposal technologies for chromated copper arsenate (CCA) treated wood waste, with detailed analyses of thermochemical conversion processes. *Environmental Pollution,* 134**,** 301-314.

HERNGREN, L., GOONETILLEKE, A. & AYOKO, G. A. (2006). Analysis of heavy metals in road-deposited sediments. *Analytica Chimica Acta,* 571**,** 270-278.

HILDEMANN, L. M., MARKOWSKI, G. R. & CASS, G. R. (1991). Chemical composition of emissions from urban sources of fine organic aerosol. *Environmental Science & Technology,* 25**,** 744-759.

HINNEN, U. & ELSNER, P. (1995). Irritancy exposure assessment in metal workers. in SURBER, C., ELSNER, P. & BIRCHER, A. J. (Eds.) *Current Problems in Dermatology*, 67-71. New York, USA, S. Karger AG.

HLEIS, D., FERNANDEZ-OLMO, I., LEDOUX, F., KFOURY, A., COURCOT, L., DESMONTS, T. & COURCOT, D. (2013). Chemical profile identification of fugitive and confined particle emissions from an integrated iron and steelmaking plant. *Journal of Hazardous Materials,* 250-251**,** 246-255.

HOEK, G., BEELEN, R., DE HOOGH, K., VIENNEAU, D., GULLIVER, J., FISCHER, P. & BRIGGS, D. (2008). A review of land-use regression models to assess spatial variation of outdoor air pollution. *Atmospheric Environment,* 42**,** 7561-7578.

HOOKER, P. J. & NATHANAIL, C. P. (2006). Risk-based characterisation of lead in urban soils. *Chemical Geology,* 226**,** 340-351.

HOPKE, P. K., LAMB, R. E. & NATUSCH, D. F. S. (1980). Multielemental characterization of urban roadway dust. *Environmental Science & Technology,* 14**,** 164-172.

HOUGH, R. L., BREWARD, N., YOUNG, S. D., CROUT, N. M. J., TYE, A. M. & THORNTON, I. (2004). Assessing potential risk of heavy metal exposure from consumption of home-produced vegetables by urban populations. *Environmental Health Perspectives,* 112**,** 215-221.

HOWARTH, R. & EARLE, S. (1979). Application of a generalized power transformation to geochemical data. *Mathematical Geology,* 11**,** 45-62.

HUANG, P., PATEL, M., SANTAGATA, M. C. & BOBET, A. (2009). *Classification of Organic Soils*, Indiana Department of Transportation and Purdue University, Indiana, USA, 170 pp.

HUNT, A., HAWKINS, J., GILLIGAN, E. & BHATIA, S. (1998). A Comparison of the Lead Particle Content of Indoor Dust before and after a Lead Paint Abatement: A New Source of Lead Recontamination. *Indoor and Built Environment,* 7**,** 32-46.

HUNT, A., JOHNSON, D. L., THORNTON, I. & WATT, J. M. (1993). Apportioning the sources of lead in-house dusts in the london borough of Richmond, England. *Science of the Total Environment,* 138**,** 183-206.

IC (2013). *Indalloy® low temperature alloys for lens blocking.* Indium Corporation technical sheet, URL: documents.indium.com/qdynamo/download.php?docid=363, accessed on October 04, 2013.

ICDA (2013). *Cadmium in alloys.* International Cadmium Association web page, URL: cadmium.org/pg_n.php?id_menu=10, accessed on September 09, 2013.

ICRCL (1987). Guidance on the Assessment and Redevelopment of Contaminated Land, note no. 59/83 (2nd Edition). *Interdepartmental Committee for the Redevelopment of Contaminated Land Guidance, London*.

INGHAM, M. N. & VREBOS, B. A. R. (1994). High productivity geochemical XRF analysis. in GILFRICH, J. V., GOLDSMITH, C. C., HUANG, T. C., JENKINS, R., NOYAN, I. V., SMITH, D. K. & PREDECKI, P. K. (Eds.) *Advances in X-Ray Analysis, Vol 37*, 717-724. New York, Plenum Press.

IRVINE, K., PERRELLI, M., NGOEN-KLAN, R. & DROPPO, I. (2009). Metal levels in street sediment from an industrial city: spatial trends, chemical fractionation, and management implications. *Journal of Soils and Sediments,* 9**,** 328-341.

ISO (1995). Soil quality, extraction of trace elements soluble in aqua regia, ISO 11466.3. *International Organization for Standardization, Switzerland - Subcommittee SC 3: Chemical methods and soil characteristics*.

IUPAC (2012). *Periodic Table of the Elements.* International Union of Pure and Applied Chemistry, URL: iupac.org/reports/periodic_table/, accessed on June 14, 2012.

IZQUIERDO, M., TYE, A. M. & CHENERY, S. R. (2012). Sources, lability and solubility of Pb in alluvial soils of the River Trent catchment, UK. *Science of the Total Environment,* 433**,** 110-122.

JACOBSON, A., KLITZKE, S., MCBRIDE, M., BAVEYE, P. & STEENHUIS, T. (2005). The desorption of silver and thallium from soils in the presence of a chelating resin with thiol functional groups. *Water, Air, and Soil Pollution,* 160**,** 41-54.

JOHNSON, C. (2005). G-BASE Field Procedures Manual. *British Geological Survey Internal Report, IR/05/097*.

JOHNSON, C. (2006). *G-BASE bibliography, version 1.1 (March 2006)*, British Geological Survey, 28 pp.

JOHNSON, C., BREWARD, N., ANDER, E. L. & AULT, L. (2005). G-BASE: baseline geochemical mapping of Great Britain and Northern Ireland. *Geochemistry: Exploration, Environment, Analysis,* 5**,** 347-357.

JOHNSON, C. & FLETCHER, M. (2011). *Strategic Stone Study: A Building Stone Atlas of Greater Manchester*, English Heritage Publications, 17 pp.

JOHNSON, C. C. & DEMETRIADES, A. (2011). Urban Geochemical Mapping: A Review of Case Studies. *Mapping the Chemical Environment of Urban Areas*, 7-27. John Wiley & Sons, Ltd.

JOLLIFFE, I. T. (2002). *Principal Component Analysis*, Springer, 487 pp.

KABATA-PENDIAS, A. & PENDIAS, H. (2001). *Trace elements in soils and plants,* Boca Raton, Florida, CRC press, 293 pp.

KAMPA, M. & CASTANAS, E. (2008). Human health effects of air pollution. *Environmental Pollution,* 151**,** 362-367.

KARLEN, D. L., MAUSBACH, M. J., DORAN, J. W., CLINE, R. G., HARRIS, R. F. & SCHUMAN, G. E. (1997). Soil quality: A concept, definition, and framework for evaluation. *Soil Science Society of America Journal,* 61**,** 4-10.

KARLSSON, H. L., GUSTAFSSON, J., CRONHOLM, P. & MÖLLER, L. (2009). Size-dependent toxicity of metal oxide particles - A comparison between nano- and micrometer size. *Toxicology Letters,* 188**,** 112-118.

KARLSSON, U. (2006). Environmental levels of thallium: influence of redox properties and anthropogenic sources. *Ph. D. Thesis,* Örebro University, Department of Natural Sciences, 44pp.

KARTAL, S., AYDIN, Z. & TOKALIOGLU, S. (2006). Fractionation of metals in street sediment samples by using the BCR sequential extraction procedure and multivariate statistical elucidation of the data. *Journal of Hazardous Materials,* 132**,** 80-89.

KAY, A. (unpublished). *Old Trafford - the evolution of a Victorian suburb.* Copsewood Editorial, URL: editorial.copsewood.net/files/OT_book.pdf, accessed on Nov. 26, 2012.

KAYHANIAN, M., VICHARE, A., GREEN, P. G. & HARVEY, J. (2009). Leachability of dissolved chromium in asphalt and concrete surfacing materials. *Journal of Environmental Management,* 90**,** 3574-3580.

KELLY, J., THORNTON, I. & SIMPSON, P. R. (1996). Urban Geochemistry: A study of the influence of anthropogenic activity on the heavy metal content of soils in traditionally industrial and non-industrial areas of Britain. *Applied Geochemistry,* 11**,** 363-370.

KETCHMAN, K. & BILEC, M. (2013). Quantification of Particulate Matter from Commercial Building Excavation Activities Using Life-Cycle Approach. *Journal of Construction Engineering and Management,* 139**,** 10.

KIM, H., KIM, D.-J., KOO, J.-H., PARK, J.-G. & JANG, Y.-C. (2007). Distribution and mobility of chromium, copper, and arsenic in soils collected near CCA-treated wood structures in Korea. *Science of the Total Environment,* 374**,** 273-281.

KIRPICHTCHIKOVA, T. A., MANCEAU, A., SPADINI, L., PANFILI, F., MARCUS, M. A. & JACQUET, T. (2006). Speciation and solubility of heavy metals in contaminated soil using X-ray

microfluorescence, EXAFS spectroscopy, chemical extraction, and thermodynamic modeling. *Geochimica et Cosmochimica Acta,* 70**,** 2163-2190.

KLEIN, D. H. (1972). Mercury and other metals in urban soils. *Environmental Science & Technology,* 6**,** 560-&.

KOUGEMITROU, I., GODELITSAS, A., TSABARIS, C., STATHOPOULOS, V., PAPANDREOU, A., GAMALETSOS, P., ECONOMOU, G. & PAPADOPOULOS, D. (2011). Characterisation and management of ash produced in the hospital waste incinerator of Athens, Greece. *Journal of Hazardous Materials,* 187**,** 421-432.

KRČMOVÁ, K., ROBERTSON, D., CVEČKOVÁ, V. & RAPANT, S. (2009). Road-deposited sediment (RDS), soil and precipitation in Bratislava, Slovakia: compositional and spatial assessment of contamination. *Journal of Soils and Sediments,* 9**,** 304-316.

KRISHNA, A. K. & GOVIL, P. K. (2004). Heavy metal contamination of soil around Pali industrial area, Rajasthan, India. *Environmental Geology,* 47**,** 38-44.

KUMAR, P., ROBINS, A., VARDOULAKIS, S. & BRITTER, R. (2010). A review of the characteristics of nanoparticles in the urban atmosphere and the prospects for developing regulatory controls. *Atmospheric Environment,* 44**,** 5035-5052.

LAI, T. M., LEE, W., HUR, J., KIM, Y., HUH, I. A., SHIN, H. S., KIM, C. K. & LEE, J. H. (2013). Influence of Sediment Grain Size and Land Use on the Distributions of Heavy Metals in Sediments of the Han River Basin in Korea and the Assessment of Anthropogenic Pollution. *Water Air and Soil Pollution,* 224**,** 12.

LAIDLAW, M. A. S. & FILIPPELLI, G. M. (2008). Resuspension of urban soils as a persistent source of lead poisoning in children: A review and new directions. *Applied Geochemistry,* 23**,** 2021-2039.

LAIDLAW, M. A. S., ZAHRAN, S., MIELKE, H. W., TAYLOR, M. P. & FILIPPELLI, G. M. (2012). Resuspension of lead contaminated urban soil as a dominant source of atmospheric lead in Birmingham, Chicago, Detroit and Pittsburgh, USA. *Atmospheric Environment,* 49**,** 302-310.

LAKE, D. L., KIRK, P. W. W. & LESTER, J. N. (1984). Fractionation, Characterization, and Speciation of Heavy Metals in Sewage Sludge and Sludge-Amended Soils: A Review. *Journal of Environmental Quality,* 13**,** 175-183.

LAMBERT, T. W., BOEHMER, J., FELTHAM, J., GUYN, L. & SHAHID, R. (2011). Spatial Mapping of Lead, Arsenic, Iron, and Polycyclic Aromatic Hydrocarbon Soil Contamination in Sydney, Nova Scotia: Community Impact From the Coke Ovens and Steel Plant. *Archives of Environmental & Occupational Health,* 66**,** 128-145.

LARNER, B. L., SEEN, A. J. & TOWNSEND, A. T. (2006). Comparative study of optimised BCR sequential extraction scheme and acid leaching of elements in the certified reference material NIST 2711. *Analytica Chimica Acta,* 556**,** 444-449.

LEE, A. M. & FRAUMENI, J. F. (1969). Arsenic and Respiratory Cancer in Man: An Occupational Study. *Journal of the National Cancer Institute,* 42**,** 1045-1052.

LEE, C. S.-L., LI, X., SHI, W., CHEUNG, S. C.-N. & THORNTON, I. (2006). Metal contamination in urban, suburban, and country park soils of Hong Kong: A study based on GIS and multivariate statistics. *Science of the Total Environment,* 356**,** 45-61.

LEE, N.-C. (1997). Getting Ready For Lead-Free Solders. *Soldering & Surface Mount Technology,* 9**,** 65-69.

LENSCHOW, P., ABRAHAM, H. J., KUTZNER, K., LUTZ, M., PREUSS, J. D. & REICHENBACHER, W. (2001). Some ideas about the sources of PM10. *Atmospheric Environment,* 35**,** S23-S33.

LI, X., LEE, S.-L., WONG, S.-C., SHI, W. & THORNTON, I. (2004). The study of metal contamination in urban soils of Hong Kong using a GIS-based approach. *Environmental Pollution,* 129**,** 113-124.

LI, X., POON, C. S. & LIU, P. S. (2001). Heavy metal contamination of urban soils and street dusts in Hong Kong. *Applied Geochemistry,* 16**,** 1361-1368.

LINDSAY, W. L. (2001). *Chemical Equilibria in Soils*, Blackburn Press, 449 pp.

LINZON, S. N., CHAI, B. L., TEMPLE, P. J., PEARSON, R. G. & SMITH, M. L. (1976). Lead contamination of urban soils and vegetation by emissions from secondary lead industries. *Journal of the Air Pollution Control Association,* 26**,** 650-654.

LISIEWICZ, M., HEIMBURGER, R. & GOLIMOWSKI, J. (2000). Granulometry and the content of toxic and potentially toxic elements in vacuum-cleaner collected, indoor dusts of the city of Warsaw. *The Science of The Total Environment,* 263**,** 69-78.

LISK, D. J. (1988). Environmental implications of incineration of municipal solid waste and ash disposal. *Science of the Total Environment,* 74**,** 39-66.

LISTER, T. R. & JOHNSON, C. C. (2005). G-BASE data conditioning procedures for stream sediment and soil chemical analyses. *British Geological Survey Internal Report IR/05/150*.

LISTON, P. & MAHER, W. (1986). Trace-metal export in urban runoff and its biological significance. *Bulletin of Environmental Contamination and Toxicology,* 36**,** 900-905.

LIU, Y. S., ZHENG, L. T., LI, X. D. & XIE, S. D. (2009). SEM/EDS and XRD characterization of raw and washed MSWI fly ash sintered at different temperatures. *Journal of Hazardous Materials,* 162**,** 161-173.

LOREDO, J., ORDONEZ, A., CHARLESWORTH, S. & DE MIGUEL, E. (2003). Influence of industry on the geochemical urban environment of Mieres (Spain) and associated health risk. *Environmental Geochemistry and Health,* 25**,** 307-323.

LORING, D. H. (1990). Lithium -- a new approach for the granulometric normalization of trace metal data. *Marine Chemistry,* 29**,** 155-168.

LUBBE, S., MUNSAMI, R. & FOURIE, D. (2012). Beneficiation of zircon sand in South Africa. *Journal of the Southern African Institute of Mining and Metallurgy,* 112**,** 583-588.

LUO, X. S., YU, S. & LI, X. (2011). Distribution, availability, and sources of trace metals in different particle size fractions of urban soils in Hong Kong: Implications for assessing the risk to human health. *Environmental Pollution,* 159**,** 1317-1326.

MADSEN, C., GEHRING, U., HABERG, S. E., NAFSTAD, P., MELIEFSTE, K., NYSTAD, W., LODRUP CARLSEN, K. C. & BRUNEKREEF, B. (2011). Comparison of land-use regression models for predicting spatial NOx contrasts over a three year period in Oslo, Norway. *Atmospheric Environment,* 45**,** 3576-3583.

MANHIQUE, A. (2003). Optimisation of alkali-fusion process for zircon sands : a kinetic study of the process. *MSc dissertation,* University of Pretoria, Pretoria, 86pp.

MAW, G. A. & KEMPTON, R. J. (1982). Bromine in soils and peats. *Plant and Soil,* 65**,** 103-109.

MCC (2009). *The Medlock Valley.* Manchester City Council, URL: philipspark.org.uk/MedlockValley/, accessed on Oct 26, 2012.

MCC (2013). *History of the Whalley Range Conservation Area.* Manchester City Council, URL: manchester.gov.uk/info/511/conservation_areas/1226/whalley_range_conservation_area/2, accessed on July 13, 2013.

MCGRATH, S. P. & LOVELAND, P. J. (1992). Soil Geochemical Atlas of England and Wales. *Blackie Academic and Professional, Glasgow*.

MCKENZIE, E. R., MONEY, J. E., GREEN, P. G. & YOUNG, T. M. (2009). Metals associated with stormwater-relevant brake and tire samples. *Science of the Total Environment,* 407**,** 5855-5860.

MEEUWIG, J. J., KAUPPILA, P. & PITKANEN, H. (2000). Predicting coastal eutrophication in the Baltic: a limnological approach. *Canadian Journal of Fisheries and Aquatic Sciences,* 57**,** 844-855.

MIELKE, H. W., ALEXANDER, J., LANGEDAL, M. & OTTESEN, R. T. (2011). Children, Soils, and Health: How Do Polluted Soils Influence Children's Health? *Mapping the Chemical Environment of Urban Areas*, 134-150. John Wiley & Sons, Ltd.

MIELKE, H. W. & REAGAN, P. L. (1998). Soil Is an Important Pathway of Human Lead Exposure. *Environmental Health Perspectives,* 106.

MIESCH, A. & CHAPMAN, R. (1977). Log transformations in geochemistry. *Mathematical Geology,* 9**,** 191-198.

MIGUEL, E. D., LLAMAS, J. F., CHACÓN, E., BERG, T., LARSSEN, S., ROYSET, O. & VADSET, M. (1997). Origin and patterns of distribution of trace elements in street dust: Unleaded petrol and urban lead. *Atmospheric Environment,* 31**,** 2733-2740.

MO (2010a). *Manchester Airport weather station 1981–2010 averages.* Met Office UK, URL: metoffice.gov.uk/climate/uk/averages/19812010/sites/manchester_airport.html, accessed on Sept 19, 2012.

MO (2010b). *North West England & Isle of Man: climate.* Met Office UK, URL: metoffice.gov.uk/climate/uk/nw/, accessed on Sept 19, 2012.

MORLEY, S. E. & FERGUSON, A. J. (2001). Geochemical baseline data for the urban area of Swansea. *British Geological Survey Research Report IR/01/036, 53pp.*

MULCHI, C. L., MASTRADONE, P. J. & ARMBRUSTER, J. A. (1990). Investigation of trace metal concentrations in crops and soils near a fossil-fuel power plant in Maryland, USA. *Journal of the Air and Waste Management Association,* 40**,** 185-193.

NADAL, M., SCHUHMACHER, M. & DOMINGO, J. L. (2004). Metal pollution of soils and vegetation in an area with petrochemical industry. *Science of The Total Environment,* 321**,** 59-69.

NAGEOTTE, S. M. & DAY, J. P. (1998). Lead concentrations and isotope ratios in street dust determined by electrothermal atomic absorption spectrometry and inductively coupled plasma mass spectrometry. *Analyst* 123**,** 59-62.

NRIAGU, J. O. (1996). A history of global metal pollution. *Science,* 272**,** 223-224.

NRIAGU, J. O. & PACYNA, J. M. (1988). Quantitative assessment of worldwide contamination of air, water and soils by trace metals. *Nature,* 333**,** 134-139.

O'DONNELL, K. E. (2001). Geochemical baseline data for the urban area of York. *British Geological Survey Research Report IR/02/085, 59pp.*

O'DONNELL, K. E. (2002). Geochemical baseline data for the urban area of Doncaster. *British Geological Survey Research Report IR/02/079, 71pp.*

O'DONNELL, K. E. (2005a). Geochemical baseline data for the urban area of Lincoln. *British Geological Survey research report IR/02/081, 79pp.*

O'DONNELL, K. E. (2005b). Geochemical baseline data for the urban area of Scunthorpe. *British Geological Survey Research Report IR/02/083, 83pp.*

O'DONNELL, K. E., FREESTONE, S. E. & BROWN, S. E. (2004). Geochemical baseline data for the urban area of Kingston-upon-Hull. *British Geological Survey Research Report IR/02/080, 61pp.*

OLSON, K. R. & DANIEL, H. (2005). Factors of Soil Formation. *Encyclopaedia of Soils in the Environment*, 532-535. Oxford, Elsevier.

ONS (2012). *Census for England and Wales, 2011.* Office for National Statistics, United Kingdom, URL: ons.gov.uk/ons/guide-method/census/2011/index.html, accessed on Aug 02, 2012.

ORDOÑEZ, A., LOREDO, J., DE MIGUEL, E. & CHARLESWORTH, S. (2003). Distribution of heavy metals in the street dusts and soils of an industrial city in Northern Spain. *Archives of Environmental Contamination and Toxicology,* 44**,** 160-170.

ORNEKTEKIN, S. (1997). A study of heavy metal pollution from motor vehicle emissions and its effect on soil in Iskenderum, North-east Mediterranean. *Turkish Journal of Engineering and Environmental Sciences,* 21**,** 45-49.

OSHA (1970). Toxic and Hazardous Substances. *Occupational Safety and Health Administration, 29 CER 1910.1000.,* Washington D.C. Government Printing Office**,** Table Z-3.

OWENS, P. N., CALEY, K. A., CAMPBELL, S., KOITER, A. J., DROPPO, I. G. & TAYLOR, K. G. (2011). Total and size-fractionated mass of road-deposited sediment in the city of Prince George, British

Columbia, Canada: implications for air and water quality in an urban environment. *Journal of Soils and Sediments,* 11**,** 1040-1051.

PANNELL, M. A. & GROGIN, P. W. (2000). Quantifying the exposure of heavy-equipment operators to respirable crystalline silica dust. *Journal of Environmental Health,* 63**,** 13-17.

PARRY, G. D. R., JOHNSON, M. S. & BELL, R. M. (1981). Trace metal surveys of soil as a component of strategic and local planning policy development. *Environmental Pollution Series B, Chemical and Physical,* 2**,** 97-107.

PEREIRA, P., LOPES, W. A., CARVALHO, L. S., DA ROCHA, G. O., BAHIA, N. D. C., LOYOLA, J., QUITERIO, S. L., ESCALEIRA, V., ARBILLA, G. & DE ANDRADE, J. B. (2007). Atmospheric concentrations and dry deposition fluxes of particulate trace metals in Salvador, Bahia, Brazil. *Atmospheric Environment,* 41**,** 7837-7850.

POLETO, C., BORTOLUZZI, E., CHARLESWORTH, S. & MERTEN, G. (2009). Urban sediment particle size and pollutants in Southern Brazil. *Journal of Soils and Sediments,* 9**,** 317-327.

POPE, I. C., BURNETT, R. T., THUN, M. J. & ET AL. (2002). Lung cancer, cardiopulmonary mortality, and long-term exposure to fine particulate air pollution. *Journal of the American Medical Association,* 287**,** 1132-1141.

PRECIADO, H. F. & LI, L. Y. (2006). Evaluation of metal loadings and bioavailability in air, water and soil along two highways of British Columbia, Canada. *Water Air and Soil Pollution,* 172**,** 81-108.

PRIEDITIS, H. & ADAMSON, I. Y. R. (2002). Comparative pulmonary toxicity of various soluble metals found in urban particulate dusts. *Experimental Lung Research,* 28**,** 563-576.

PROHIC, E., MIKO, S. & PEH, Z. (1995). Normalization and Trace Element Contamination of Soils in a Karstic Polje - An Example from the Sinjsko Polje, Croatia. *Geologia Croatica,* 48**,** 67-86.

PUDASAINEE, D., KIM, J. H., LEE, S. H., PARK, J. M., JANG, H. N., SONG, G. J. & SEO, Y. C. (2010). Hazardous air pollutants emission from coal and oil-fired power plants. *Asia-Pacific Journal of Chemical Engineering,* 5**,** 299-303.

QIAN, Y., GALLAGHER, F. J., FENG, H. & WU, M. Y. (2012). A geochemical study of toxic metal translocation in an urban brownfield wetland. *Environmental Pollution,* 166**,** 23-30.

QUEROL, X., ALASTUEY, A., RODRIGUEZ, S., PLANA, F., MANTILLA, E. & RUIZ, C. R. (2001). Monitoring of PM10 and PM2.5 around primary particulate anthropogenic emission sources. *Atmospheric Environment,* 35**,** 845-858.

RAGOSTA, M., CAGGIANO, R., D'EMILIO, M. & MACCHIATO, M. (2002). Source origin and parameters influencing levels of heavy metals in TSP, in an industrial background area of Southern Italy. *Atmospheric Environment* 36**,** 3071 - 3087.

RAO, C., SAHUQUILLO, A. & LOPEZ SANCHEZ, J. (2008). A Review of the Different Methods Applied in Environmental Geochemistry For Single and Sequential Extraction of Trace Elements in Soils and Related Materials. *Water, Air, & Soil Pollution,* 189**,** 291-333.

RAURET, G., F. LOPEZ-SANCHEZ, J., SAHUQUILLO, A., RUBIO, R., DAVIDSON, C., URE, A. & QUEVAUVILLER, P. (1999). Improvement of the BCR three step sequential extraction procedure prior to the certification of new sediment and soil reference materials. *Journal of Environmental Monitoring,* 1**,** 57-61.

RAURET, G., LOPEZ-SANCHEZ, J. F., SAHUQUILLO, A., BARAHONA, E., LACHICA, M., URE, A. M., DAVIDSON, C. M., GOMEZ, A., LUCK, D., BACON, J., YLI-HALLA, M., MUNTAU, H. & QUEVAUVILLER, P. (2000). Application of a modified BCR sequential extraction (three-step) procedure for the determination of extractable trace metal contents in a sewage sludge amended soil reference material (CRM 483), complemented by a three-year stability study of acetic acid and EDTA extractable metal content. *Journal of Environmental Monitoring,* 2**,** 228-233.

RAWLINGS, J. O., PANTULA, S. G. & DICKEY, D. A. (1998). *Applied Regression Analysis: A Research Tool*, Springer, 657 pp.

RAWLINS, B. G., LARK, R. M., O'DONNELL, K. E., TYE, A. M. & LISTER, T. R. (2005). The assessment of point and diffuse metal pollution of soils from an urban geochemical survey of Sheffield, England. *Soil Use and Management,* 21**,** 353-362.

RAWLINS, B. G., MCGRATH, S. P., SCHEIB, A. J., BREWARD, N., CAVE, M., LISTER, T. R., INGHAM, M., GOWING, C. & CARTER, S. (2012). *The advanced soil geochemical atlas of England and Wales.* British Geological Survey, URL: bgs.ac.uk/gbase/advsoilatlasEW.html, accessed on Nov. 15, 2012.

RAZOS, P. & CHRISTIDES, A. (2010). An Investigation on Heavy Metals in an Industrial Area in Greece. *International Journal of Environmental Research,* 4**,** 785-794.

READ, D. (2003). Report on Copper, Chromium and Arsenic (CCA) Treated Timber. *Environmental Risk Management Authority of New Zealand* Technical Report, 68pp.

REIMANN, C., BIRKE, M. & FILZMOSER, P. (2011a). Data Analysis for Urban Geochemical Data. *Mapping the Chemical Environment of Urban Areas*, 99-115. John Wiley & Sons, Ltd.

REIMANN, C., FILZMOSER, P., GARRETT, R. & DUTTER, R. (2011b). *Statistical Data Analysis Explained: Applied Environmental Statistics with R*, John Wiley & Sons, 362 pp.

REIMANN, C., FILZMOSER, P. & GARRETT, R. G. (2005). Background and threshold: critical comparison of methods of determination. *Science of the Total Environment,* 346**,** 1-16.

REYMENT, R. A. & SAVAZZI, E. (1999). *Aspects of multivariate statistical analysis in geology,* Amsterdam, Elsevier, 285 pp.

ROBERTSON, D. & TAYLOR, K. (2007). Temporal Variability of Metal Contamination in Urban Road-deposited Sediment in Manchester, UK: Implications for Urban Pollution Monitoring. *Water, Air, & Soil Pollution,* 186**,** 209-220.

ROBERTSON, D. J., TAYLOR, K. G. & HOON, S. R. (2003). Geochemical and mineral magnetic characterisation of urban sediment particulates, Manchester, UK. *Applied Geochemistry,* 18**,** 269-282.

RYAN, B. & LEDDA, A. (1998). A review of sulphur in coal. *British Columbia Geological Survey,* paper 1998-l**,** 1-22.

ŠAJN, R., GOSAR, M., BIDOVEC, M., PIRC, S. & ALIJAGIĆ, J. (2011). Geochemical Mapping of Ljubljana Urban and Suburban Area, Slovenia. *Mapping the Chemical Environment of Urban Areas*, 375-392. John Wiley & Sons, Ltd.

SARTOR, J. D. & GABOURY, D. R. (1984). Street sweeping as a water pollution control measure: Lessons learned over the past ten years. *Science of The Total Environment,* 33**,** 171-183.

SAUVÉ, S., MCBRIDE, M. & HENDERSHOT, W. (1998a). Lead Phosphate Solubility in Water and Soil Suspensions. *Environmental Science & Technology,* 32**,** 388-393.

SAUVÉ, S., MCBRIDE, M. & HENDERSHOT, W. (1998b). Soil Solution Speciation of Lead (II): Effects of Organic Matter and pH. *Soil Science Society of America Journal,* 62**,** 618-621.

ŠČANČAR, J., RADMILA MILAČIČA, C., STRAŽAR, M. & BURICA, O. (2000). Total metal concentrations and partitioning of Cd, Cr, Cu, Fe, Ni and Zn in sewage sludge. *Science of the Total Environment,* 250**,** 9-19.

SCC (2007). *Worsley Village - Conservation Area Appraisal.* Salford City Council, URL: salford.gov.uk/d/worsley-conservation-area-formal-adoption-web-.pdf, accessed on Nov. 26, 2012.

SCC (2012). *Salford local history.* Salford City Council, URL: salford.gov.uk/localhistory-salford.htm, accessed on Nov. 26, 2012.

SCHAFER, J., NORRA, S., KLEIN, D. & BLANC, G. (2009). Mobility of trace metals associated with urban particles exposed to natural waters of various salinities from the Gironde Estuary, France. *Journal of Soils and Sediments,* 9**,** 374-392.

SCHAUER, J. J., ROGGE, W. F., HILDEMANN, L. M., MAZUREK, M. A., CASS, G. R. & SIMONEIT, B. R. T. (1996). Source apportionment of airborne particulate matter using organic compounds as tracers. *Atmospheric Environment,* 30**,** 3837-3855.

SCHECKEL, K. G., CHANEY, R. L., BASTA, N. T. & RYAN, J. A. (2009). Advances in assessing bioavailability of metal(loid)s in contaminated soils. in SPARKS, D. L. (Ed.) *Advances in Agronomy, Volume 104*, 1-52. San Diego, Elsevier Academic Press Inc.

SCHIPPER, P. N. M., COMANS, R. N. J., DIJKSTRA, J. J. & VERGOUWEN, L. (2007). Runoff and windblown vehicle spray from road surfaces, risks and measures for soil and water. *Water Science and Technology,* 55**,** 87-96.

SCHUMACHER, B. A. (2002). *Methods for the determination of total organic carbon in soils and sediments*, United States Environmental Protection Agency, Environmental Sciences Division, 23 pp.

SHI, G., CHEN, Z., BI, C., WANG, L., TENG, J., LI, Y. & XU, S. (2011). A comparative study of health risk of potentially toxic metals in urban and suburban road dust in the most populated city of China. *Atmospheric Environment,* 45**,** 764-771.

SHOTYK, W. & KRACHLER, M. (2004). Atmospheric deposition of silver and thallium since 12 370 14C years BP recorded by a Swiss peat bog profile, and comparison with lead and cadmium. *Journal of Environmental Monitoring,* 6**,** 427-433.

SISOMPHON, K., COPUROGLU, O. & FRAAIJ, A. L. A. (2011). Durability of blast-furnace slag mortars subjected to sodium monofluorophosphate application. *Construction and Building Materials,* 25**,** 823-828.

SOLOMON, R. L. & HARTFORD, J. W. (1976). Lead and cadmium in dusts and soils in a small urban community. *Environmental Science & Technology,* 10**,** 773-777.

SONNTAG, D. B., BAILEY, C. R., FULPER, C. R. & BALDAUF, R. W. (2012). Contribution of Lubricating Oil to Particulate Matter Emissions from Light-Duty Gasoline Vehicles in Kansas City. *Environmental Science & Technology,* 46**,** 4191-4199.

SPEARS, D. A., MARTINEZ TARAZONA, M. R. & LEE, S. (1994). Pyrite in UK coals: its environmental significance. *Fuel,* 73**,** 1051-1055.

STATSOFT (2011). *Electronic Statistics Textbook.* StatSoft, URL: statsoft.com/textbook/, accessed on Nov 11, 2012.

STAUNTON, S., A. VIOLANTE, P. M. H. J. M. B. & GIANFREDA, L. (2002). Direct and indirect effects of organic matter on metal immobilisation in soil. *Developments in Soil Science*, 79-97. Elsevier.

STERRITT, R. M. & LESTER, J. N. (1980). The value of sewage sludge to agriculture and effects of the agricultural use of sludges contaminated with toxic elements: A review. *Science of the Total Environment,* 16**,** 55-90.

SURGIEWICZ, J. (2012). Assessment of hazards posed by metallo-organic compounds in industrial production and processing of polyvinyl chloride. *Medycyna Pracy,* 63**,** 419-429.

SUTHERLAND, R. A. (2002). Lead in grain size fractions of road-deposited sediment. *Environmental Pollution,* 121**,** 229-237.

SUTHERLAND, R. A. (2003). A First Look at Platinum in Road-Deposited Sediments and Roadside Soils, Honolulu, Oahu, Hawaii. *Archives of Environmental Contamination and Toxicology,* 44**,** 0430-0436.

SUTHERLAND, R. A., GRAHAM PEARSON, D. & OTTLEY, C. J. (2008). Grain size partitioning of platinum-group elements in road-deposited sediments: Implications for anthropogenic flux estimates from autocatalysts. *Environmental Pollution,* 151**,** 503-515.

SUTHERLAND, R. A., TACK, F. M. G., TOLOSA, C. A. & VERLOO, M. G. (2000). Operationally defined metal fractions in road deposited sediment, Honolulu, Hawaii. *Journal of Environmental Quality,* 29**,** 1431-1439.

SUTHERLAND, R. A., TACK, F. M. G. & ZIEGLER, A. D. (2012). Road-deposited sediments in an urban environment: A first look at sequentially extracted element loads in grain size fractions. *Journal of Hazardous Materials,* 225-226**,** 54-62.

SUTHERLAND, R. A. & TOLOSA, C. A. (2000). Multi-element analysis of road-deposited sediment in an urban drainage basin, Honolulu, Hawaii. *Environmental Pollution,* 110**,** 483-495.

TANNER, P. A., MA, H.-L. & YU, P. K. N. (2008). Fingerprinting Metals in Urban Street Dust of Beijing, Shanghai, and Hong Kong. *Environmental Science & Technology,* 42**,** 7111-7117.

TAYLOR, K. G. (2007). Urban environments. in PERRY, C. T. & TAYLOR, K. G. (Eds.) *Environmental sedimentology*, 191-222. Oxford, Blackwell.

TAYLOR, K. G. & OWENS, P. N. (2009). Sediments in urban river basins: a review of sediment-contaminant dynamics in an environmental system conditioned by human activities. *Journal of Soils and Sediments,* 9**,** 281-303.

TAYLOR, K. G., OWENS, P. N., BATALLA, R. J. & GARCIA, C. (2008). Sediment and contaminant sources and transfers in river basins. *Sustainable Management of Sediment Resources, volume 4*, 83-135. Elsevier.

TAYLOR, K. G. & ROBERTSON, D. J. (2009). Electron microbeam analysis of urban road-deposited sediment, Manchester, UK: Improved source discrimination and metal speciation assessment. *Applied Geochemistry,* 24**,** 1261-1269.

TERRÓN, J., MARQUES DA SILVA, J., MORAL, F. & GARCÍA-FERRER, A. (2011). Soil apparent electrical conductivity and geographically weighted regression for mapping soil. *Precision Agriculture,* 12**,** 750-761.

TESSIER, A., CAMPBELL, P. G. C. & BISSON, M. (1979). Sequential extraction procedure for the speciation of particulate trace metals. *Analytical Chemistry,* 51**,** 844-851.

THORNTON, I., FARAGO, M., THUMS, C., PARRISH, R., MCGILL, R., BREWARD, N., FORTEY, N., SIMPSON, P., YOUNG, S., TYE, A., CROUT, N., HOUGH, R. & WATT, J. (2008). Urban geochemistry: research strategies to assist risk assessment and remediation of brownfield sites in urban areas. *Environmental Geochemistry and Health,* 30**,** 565-576.

THORNTON, I., WATT, J. M., DAVIES, D. J. A., HUNT, A., COTTER-HOWELLS, J. & JOHNSON, D. L. (1994). Lead contamination of UK dusts and soils and implications for childhood exposure: An overview of the work of the Environmental Geochemistry Research Group, Imperial College, London, England 1981–1992. *Environmental Geochemistry and Health,* 16**,** 113-122.

THORPE, A. & HARRISON, R. M. (2008). Sources and properties of non-exhaust particulate matter from road traffic: A review. *Science of The Total Environment,* 400**,** 270-282.

THORPE, A. J., HARRISON, R. M., BOULTER, P. G. & MCCRAE, I. S. (2007). Estimation of particle resuspension source strength on a major London Road. *Atmospheric Environment,* 41**,** 8007-8020.

THUMS, C. & FARAGO, M. (2001). Investigating urban geochemistry using Geographical Information Systems. *Science Progress,* 84**,** 183-204.

TOKALIOGLU, S. & KARTAL, S. (2006). Multivariate analysis of the data and speciation of heavy metals in street dust samples from the Organized Industrial District in Kayseri (Turkey). *Atmospheric Environment,* 40**,** 2797-2805.

TONKS, L. H., JONES, R. C. B., LLOYD, W. & SHERLOCK, R. L. (1970). *The geology of Manchester and the south-east Lancashire coalfield: explanation of sheet 85,* London, Cedric Chivers, 240 pp.

TOWNSEND, T., SOLO-GABRIELE, H., TOLAYMAT, T., STOOK, K. & HOSEIN, N. (2003). Chromium, copper, and arsenic concentrations in soil underneath CCA-treated wood structures. *Soil & Sediment Contamination,* 12**,** 779-798.

TYLECOTE, R. F. (1987). *The early history of metallurgy in Europe*, Longman, 391 pp.

UN (2007). *World Urbanization Prospects: The 2007 Revision Population Database*, United Nations, New York, pp.

URE, A. M., QUEVAUVILLER, P., MUNTAU, H. & GRIEPINK, B. (1992). Speciation of heavy metals in soils and sediments An account of the improvement and harmonization of extraction techniques undertaken under the auspices of the BCR of the Commission of the European Communities. *Workshop on the Sequential Extraction of Trace Metals in Soil and Sediments.* Sitges, Spain, Gordon Breach Science Publishing Ltd.

US-EPA (1996). Soil Screening Guidance: Technical Background Document EPA/540/R-95/128. *United States Environmental Protection Agency, Washington DC*.

US-SCC (1993). *Soil survey manual, Chapter 3 - selected chemical properties.* Department of Agriculture Handbook no. 18, United States Soil Conservation Service, URL: soils.usda.gov/technical/manual/contents/chapter3.html, accessed on Nov 26, 2012.

VAN DER SLOOT, H. A., COMANS, R. N. J. & HJELMAR, O. (1996). Similarities in the leaching behaviour of trace contaminants from waste, stabilized waste, construction materials and soils. *Science of The Total Environment,* 178**,** 111-126.

VAROUCHAKIS, E. A. & HRISTOPULOS, D. T. (2013). Improvement of groundwater level prediction in sparsely gauged basins using physical laws and local geographic features as auxiliary variables. *Advances in Water Resources,* 52**,** 34-49.

VIOLANTE, A., COZZOLINO, V., PERELOMOV, L., CAPORALE, A. G. & PIGNA, M. (2010). Mobility and bioavailability of heavy metals and metalloids in soil environments. *Journal of Soil Science and Plant Nutrition,* 10**,** 268-292.

VIOLANTE, A., HUANG, P. M. & GADD, G. M. (2008). *Biophysico-Chemical Processes of Heavy Metals and Metalloids in Soil Environments*, John Wiley & Sons, 658 pp.

VROM (2000). Circular on target values and intervention values for soil remediation. *Ministerie van Volkshuisvesting, Ruimtelijke Ordening en Milieubeheer, Amsterdam*.

VROM (2009). Soil Remediation Circular. *Ministerie van Volkshuisvesting, Ruimtelijke Ordening en Milieubeheer, Amsterdam*.

WANG, X.-S. & QIN, Y. (2007). Some characteristics of the distribution of heavy metals in urban topsoil of Xuzhou, China. *Environmental Geochemistry and Health,* 29**,** 11-19.

WHITE, A. F. (1995). Chemical weathering rates of silicate minerals in soils. in WHITE, A. F. & BRANTLEY, S. L. (Eds.) *Chemical Weathering Rates of Silicate Minerals*, 407-461.

WIK, A. & DAVE, G. (2009). Occurrence and effects of tire wear particles in the environment - A critical review and an initial risk assessment. *Environmental Pollution,* 157**,** 1-11.

WITTBRODT, P. R. & PALMER, C. D. (1996). Effect of temperature, ionic strength, background electrolytes, and Fe(III) on the reduction of hexavalent chromium by soil humic substances. *Environmental Science & Technology,* 30**,** 2470-2477.

WONG, C. S. C., LI, X. & THORNTON, I. (2006). Urban environmental geochemistry of trace metals. *Environmental Pollution,* 142**,** 1-16.

WRAGG, J., CAVE, M., BASTA, N., BRANDON, E., CASTEEL, S., DENYS, S., GRON, C., OOMEN, A., REIMER, K., TACK, K. & VAN DE WIELE, T. (2011). An inter-laboratory trial of the unified BARGE bioaccessibility method for arsenic, cadmium and lead in soil. *Science of the Total Environment,* 409**,** 4016-4030.

WU, J., EDWARDS, R., HE, X. Q., LIU, Z. & KLEINMAN, M. (2010). Spatial analysis of bioavailable soil lead concentrations in Los Angeles, California. *Environmental Research,* 110**,** 309-317.

YAMADA, Y. (1968). Occurrence of bromine in plants and soil. *Talanta,* 15**,** 1135-1141.

YASREBI, J., SAFFARI, M., FATHI, H., KARIMIAN, N., MOAZALLAHI, M. & GAZNI, R. (2009). Evaluation and comparison of ordinary kriging and inverse distance weighting methods for prediction of spatial variability of some soil chemical parameters. *Research Journal of Biological Sciences,* 4**,** 93-102.

YIN, C. Q. & LI, L. Q. (2008). An investigation on suspended solids sources in urban stormwater runoff using Be-7 and Pb-210 as tracers. *Water Science and Technology,* 57**,** 1945-1950.

YOUDEN, W. J. & MERLICH, A. (1937). Selection of efficient methods for soil sampling. *Contributions from Boyce Thompson Institute,* 9**,** 59-70.

YOUNG, T. M., HEERAMAN, D. A., SIRIN, G. & ASHBAUGH, L. L. (2002). Resuspension of soil as a source of airborne lead near industrial facilities and highways. *Environmental Science & Technology,* 36**,** 2484-2490.

ZAFRA, C. A., TEMPRANO, J. & TEJERO, I. (2011). Distribution of the concentration of heavy metals associated with the sediment particles accumulated on road surfaces. *Environmental Technology,* 32**,** 997-1008.

ZHANG, C., CHEN, H., YU, Y.-X., WANG, L.-J., HAN, J.-B. & TAO, P. (2013). Pollution Characteristics of Heavy Metals in Sludge from Wastewater Treatment Plants and Sludge Disposal in Chinese Coastal Areas. *Huanjing Kexue,* 34**,** 1345-1350.

ZHANG, C., TANG, Y., XU, X. & KIELY, G. (2011). Towards spatial geochemical modelling: Use of geographically weighted regression for mapping soil organic carbon contents in Ireland. *Applied Geochemistry,* 26**,** 1239-1248.

ZHANG, C. S., TANG, Y., LUO, L. & XU, W. L. (2009). Outlier identification and visualization for Pb concentrations in urban soils and its implications for identification of potential contaminated land. *Environmental Pollution,* 157**,** 3083-3090.

ZHANG, M. K. & WANG, H. (2009). Concentrations and chemical forms of potentially toxic metals in road-deposited sediments from different zones of Hangzhou, China. *Journal of Environmental Sciences-China,* 21**,** 625-631.

ZIMMERMAN, A. J. & WEINDORF, D. C. (2010). Heavy metal and trace metal analysis in soil by sequential extraction: a review of procedures. *International journal of analytical chemistry,* Volume 2010**,** ID: 387803.

ZIMMERMAN, D., PAVLIK, C., RUGGLES, A. & ARMSTRONG, M. (1999). An Experimental Comparison of Ordinary and Universal Kriging and Inverse Distance Weighting. *Mathematical Geology,* 31**,** 375-390.

ZOU, B., WILSON, J. G., ZHAN, F. B. & ZENG, Y. (2009). Spatially differentiated and source-specific population exposure to ambient urban air pollution. *Atmospheric Environment,* 43**,** 3981-3988.

ZUURBIER, M., HOEK, G., OLDENWENING, M., MELIEFSTE, K., VAN DEN HAZEL, P. & BRUNEKREEF, B. (2011). Respiratory Effects of Commuters' Exposure to Air Pollution in Traffic. *Epidemiology,* 22, 219-227.

# The Fate of Contaminants in Urban Soils and Sediments: Novel Assessments and Implications for Risks

# APPENDICES

## *1. Data conditioning and levelling*

### Part A: RDS summer Standard Reference Material (SRM) plots

X = SRM average elemental concentration analysed with the RDS summer batches

Y = SRM average elemental concentration analysed with the soil batches

Units: Oxides expressed in weight %, other elements in mg/kg.

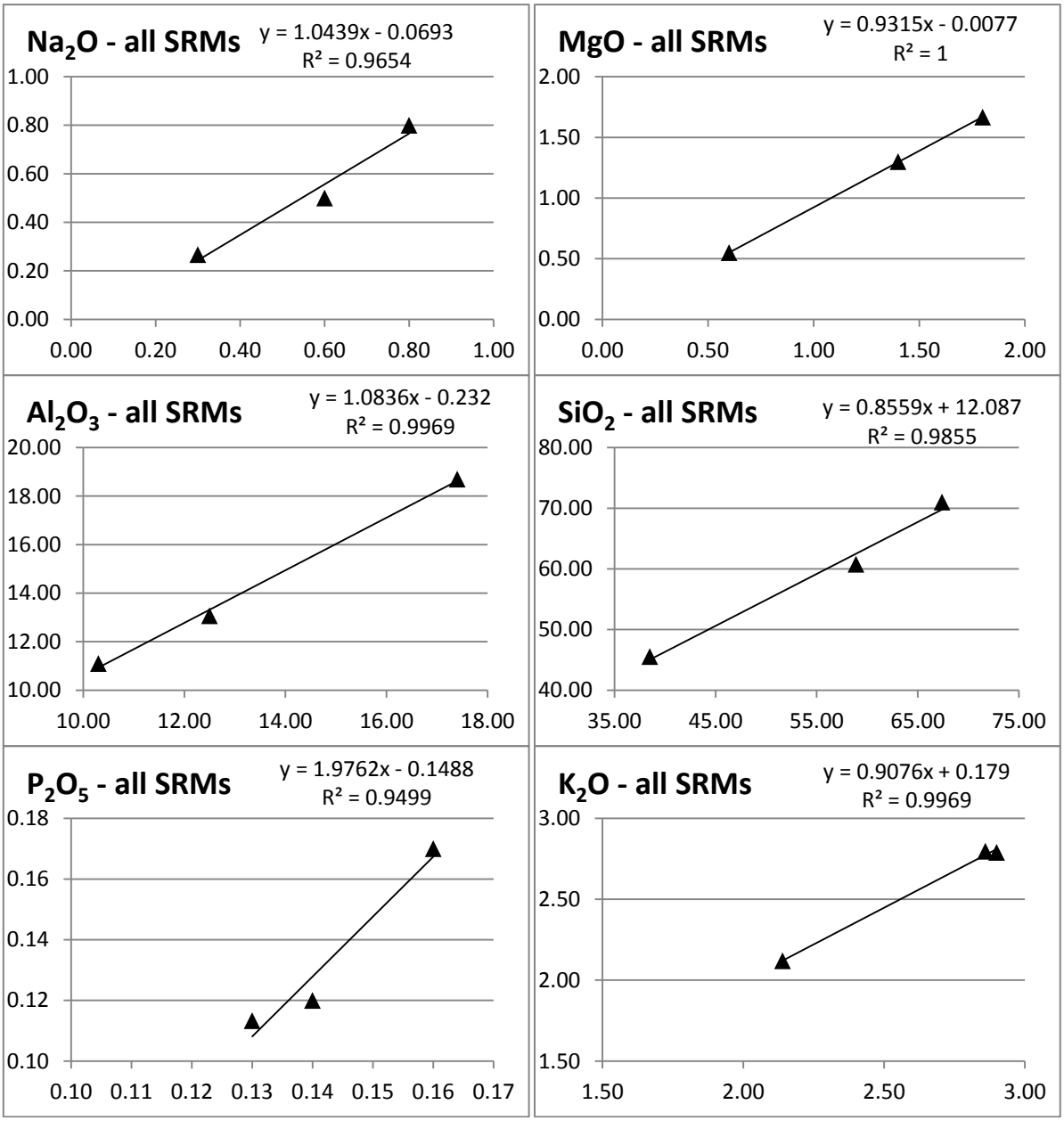

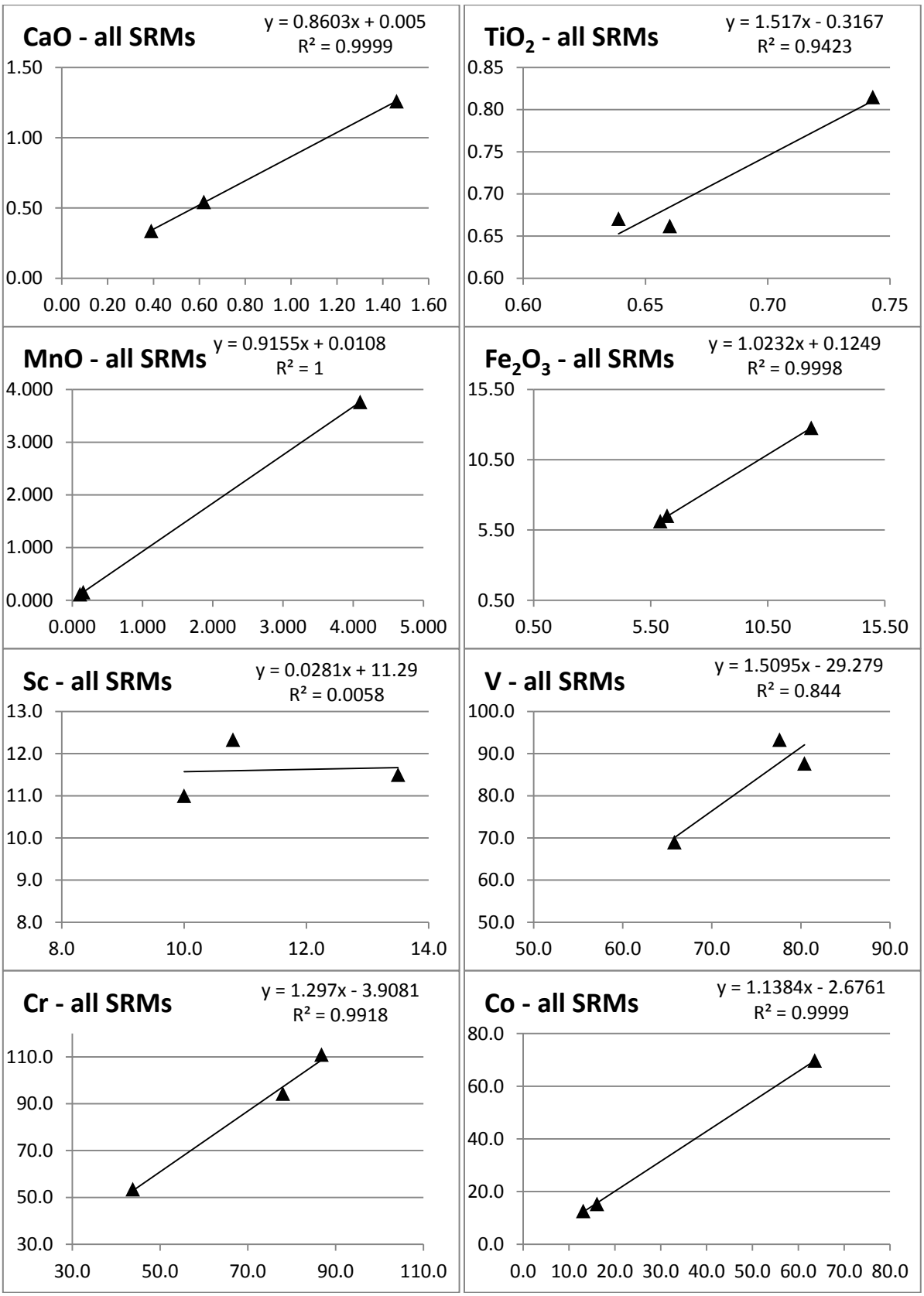
CaO - all SRMs
y = 0.8603x + 0.005
R² = 0.9999
1.50
1.00
0.50
0.00
0.00 0.20 0.40 0.60 0.80 1.00 1.20 1.40 1.60
TiO2 - all SRMs
y = 1.517x - 0.3167
R² = 0.9423
0.85
0.80
0.75
0.70
0.65
0.60
0.60 0.65 0.70 0.75
MnO - all SRMs
y = 0.9155x + 0.0108
R² = 1
4.000
3.000
2.000
1.000
0.000
0.000 1.000 2.000 3.000 4.000 5.000
Fe2O3 - all SRMs
y = 1.0232x + 0.1249
R² = 0.9998
15.50
10.50
5.50
0.50
0.50 5.50 10.50 15.50
Sc - all SRMs
y = 0.0281x + 11.29
R² = 0.0058
13.0
12.0
11.0
10.0
9.0
8.0
8.0 10.0 12.0 14.0
V - all SRMs
y = 1.5095x - 29.279
R² = 0.844
100.0
90.0
80.0
70.0
60.0
50.0
50.0 60.0 70.0 80.0 90.0
Cr - all SRMs
y = 1.297x - 3.9081
R² = 0.9918
110.0
90.0
70.0
50.0
30.0
30.0 50.0 70.0 90.0 110.0
Co - all SRMs
y = 1.1384x - 2.6761
R² = 0.9999
80.0
60.0
40.0
20.0
0.0
0.0 10.0 20.0 30.0 40.0 50.0 60.0 70.0 80.0

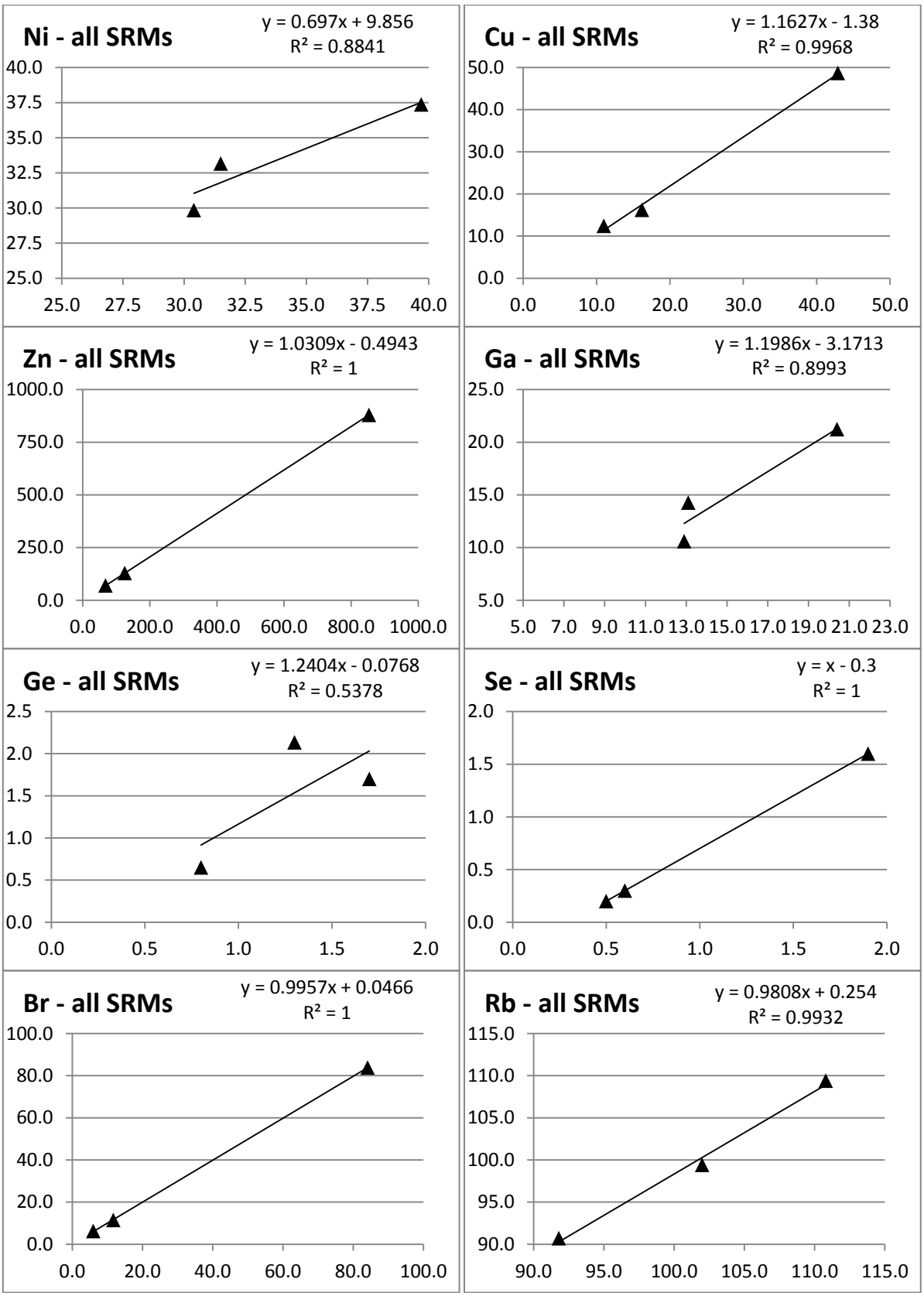
Ni - all SRMs
y = 0.697x + 9.856
R² = 0.8841
40.0
37.5
35.0
32.5
30.0
27.5
25.0
25.0 27.5 30.0 32.5 35.0 37.5 40.0
Cu - all SRMs
y = 1.1627x - 1.38
R² = 0.9968
50.0
40.0
30.0
20.0
10.0
0.0
0.0 10.0 20.0 30.0 40.0 50.0
Zn - all SRMs
y = 1.0309x - 0.4943
R² = 1
1000.0
750.0
500.0
250.0
0.0
0.0 200.0 400.0 600.0 800.0 1000.0
Ga - all SRMs
y = 1.1986x - 3.1713
R² = 0.8993
25.0
20.0
15.0
10.0
5.0
5.0 7.0 9.0 11.0 13.0 15.0 17.0 19.0 21.0 23.0
Ge - all SRMs
y = 1.2404x - 0.0768
R² = 0.5378
2.5
2.0
1.5
1.0
0.5
0.0
0.0 0.5 1.0 1.5 2.0
Se - all SRMs
y = x - 0.3
R² = 1
2.0
1.5
1.0
0.5
0.0
0.0 0.5 1.0 1.5 2.0
Br - all SRMs
y = 0.9957x + 0.0466
R² = 1
100.0
80.0
60.0
40.0
20.0
0.0
0.0 20.0 40.0 60.0 80.0 100.0
Rb - all SRMs
y = 0.9808x + 0.254
R² = 0.9932
115.0
110.0
105.0
100.0
95.0
90.0
90.0 95.0 100.0 105.0 110.0 115.0

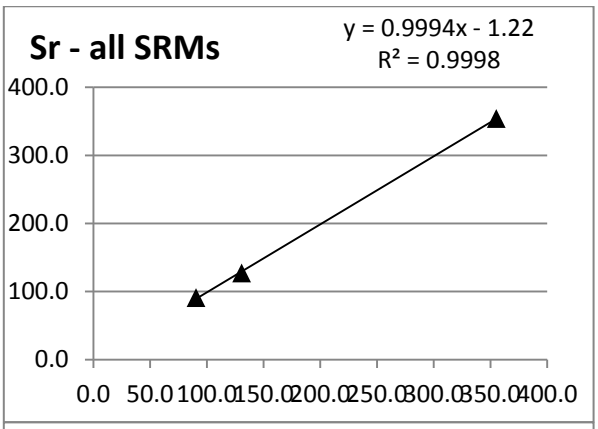
Sr - all SRMs
y = 0.9994x - 1.22
R² = 0.9998
400.0
300.0
200.0
100.0
0.0
0.0 50.0 100.0 150.0 200.0 250.0 300.0 350.0 400.0

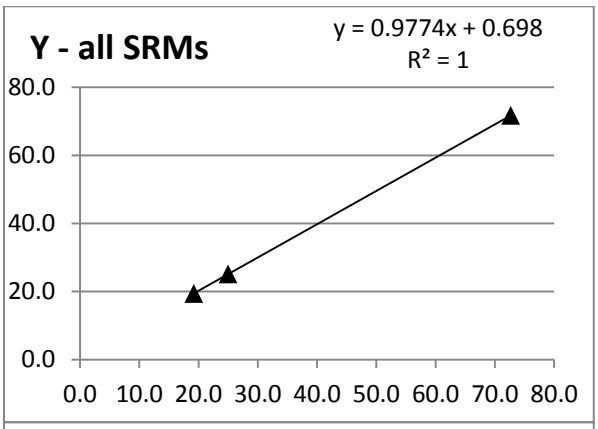
Y - all SRMs
y = 0.9774x + 0.698
R² = 1
80.0
60.0
40.0
20.0
0.0
0.0 10.0 20.0 30.0 40.0 50.0 60.0 70.0 80.0

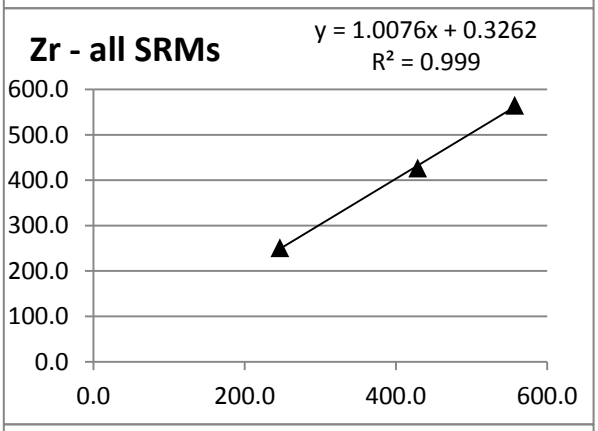
Zr - all SRMs
y = 1.0076x + 0.3262
R² = 0.999
600.0
500.0
400.0
300.0
200.0
100.0
0.0
0.0 200.0 400.0 600.0

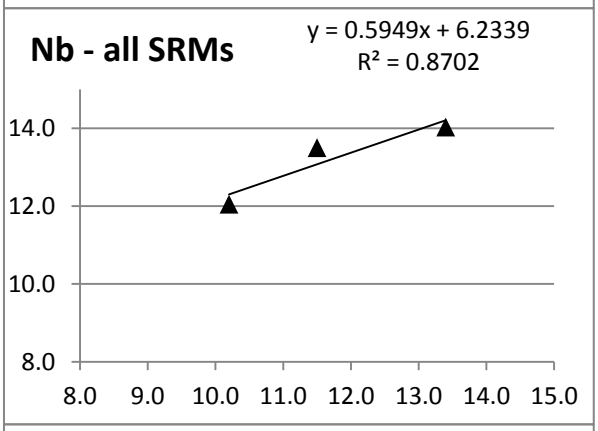
Nb - all SRMs
y = 0.5949x + 6.2339
R² = 0.8702
14.0
12.0
10.0
8.0
8.0 9.0 10.0 11.0 12.0 13.0 14.0 15.0

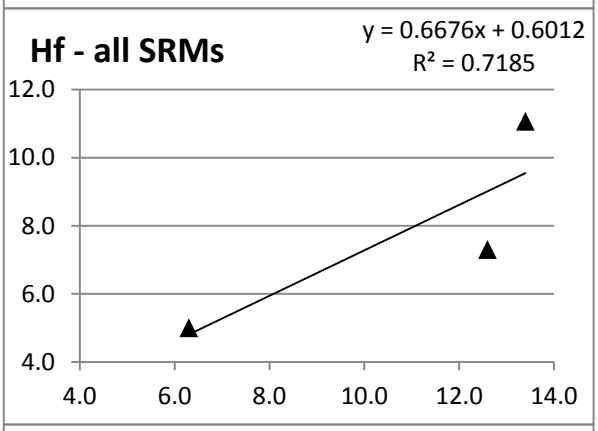
Hf - all SRMs
y = 0.6676x + 0.6012
R² = 0.7185
12.0
10.0
8.0
6.0
4.0
4.0 6.0 8.0 10.0 12.0 14.0

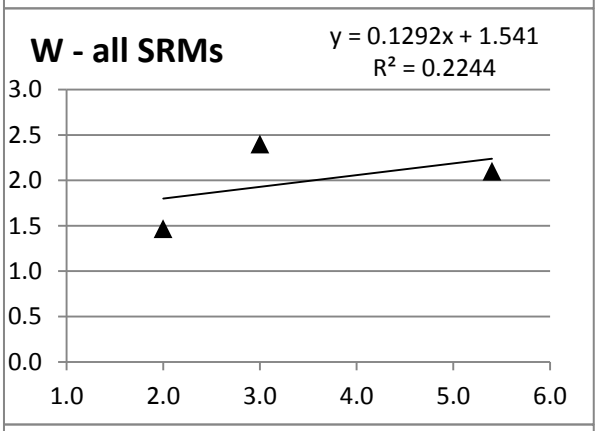
W - all SRMs
y = 0.1292x + 1.541
R² = 0.2244
3.0
2.5
2.0
1.5
1.0
0.5
0.0
1.0 2.0 3.0 4.0 5.0 6.0

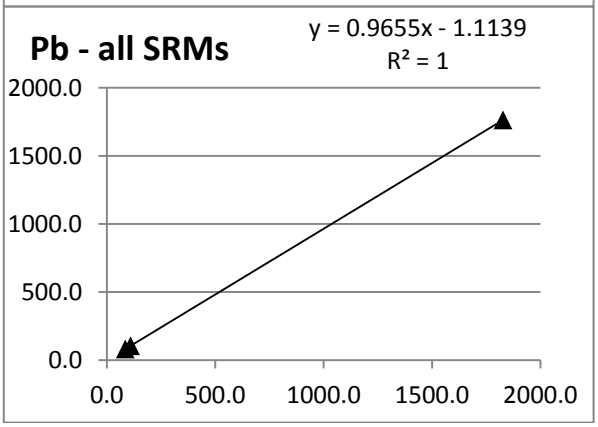
Pb - all SRMs
y = 0.9655x - 1.1139
R² = 1
2000.0
1500.0
1000.0
500.0
0.0
0.0 500.0 1000.0 1500.0 2000.0

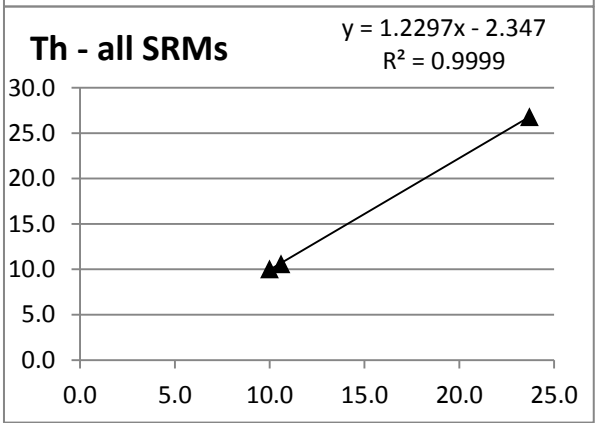
Th - all SRMs
y = 1.2297x - 2.347
R² = 0.9999
30.0
25.0
20.0
15.0
10.0
5.0
0.0
0.0 5.0 10.0 15.0 20.0 25.0

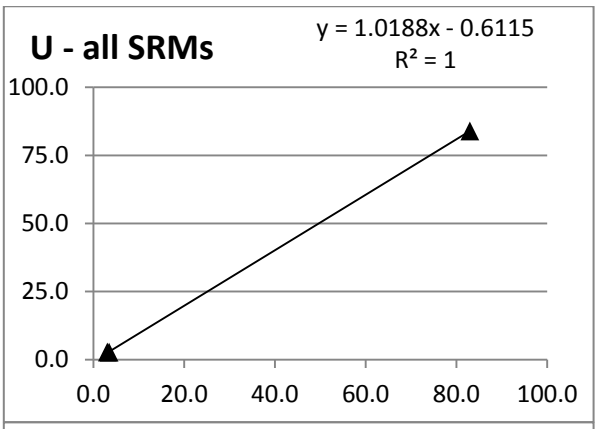
U - all SRMs
y = 1.0188x - 0.6115
R² = 1
100.0
75.0
50.0
25.0
0.0
0.0
20.0
40.0
60.0
80.0
100.0

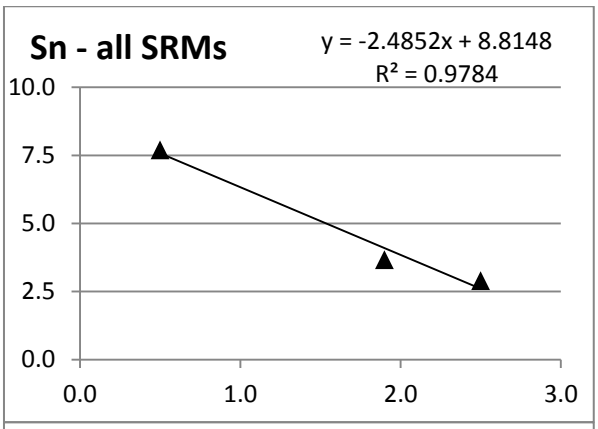
Sn - all SRMs
y = -2.4852x + 8.8148
R² = 0.9784
10.0
7.5
5.0
2.5
0.0
0.0
1.0
2.0
3.0

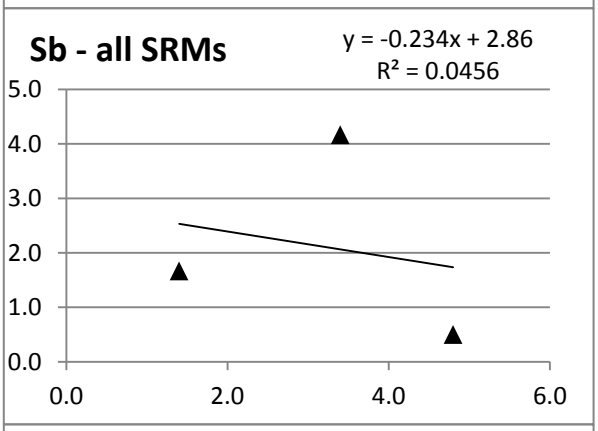
Sb - all SRMs
y = -0.234x + 2.86
R² = 0.0456
5.0
4.0
3.0
2.0
1.0
0.0
0.0
2.0
4.0
6.0

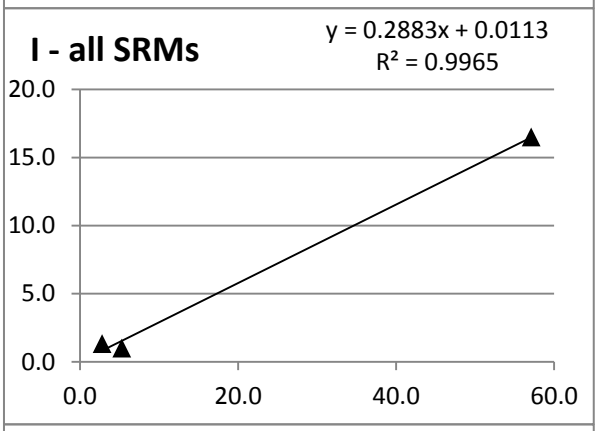
I - all SRMs
y = 0.2883x + 0.0113
R² = 0.9965
20.0
15.0
10.0
5.0
0.0
0.0
20.0
40.0
60.0

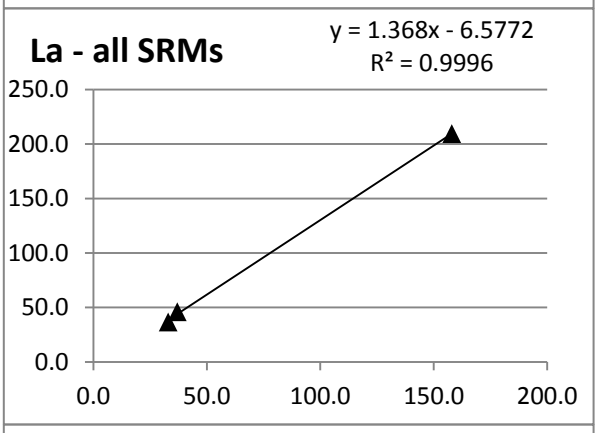
La - all SRMs
y = 1.368x - 6.5772
R² = 0.9996
250.0
200.0
150.0
100.0
50.0
0.0
0.0
50.0
100.0
150.0
200.0

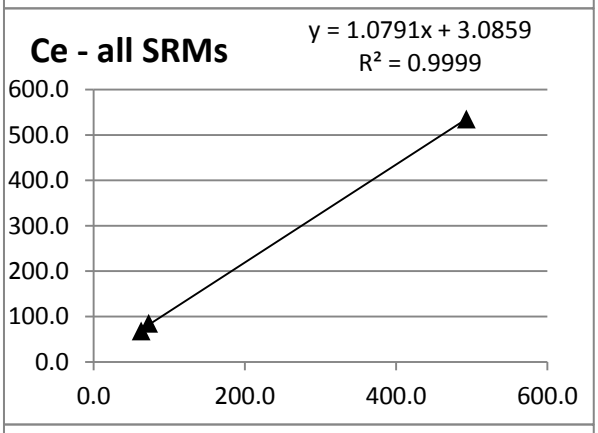
Ce - all SRMs
y = 1.0791x + 3.0859
R² = 0.9999
600.0
500.0
400.0
300.0
200.0
100.0
0.0
0.0
200.0
400.0
600.0

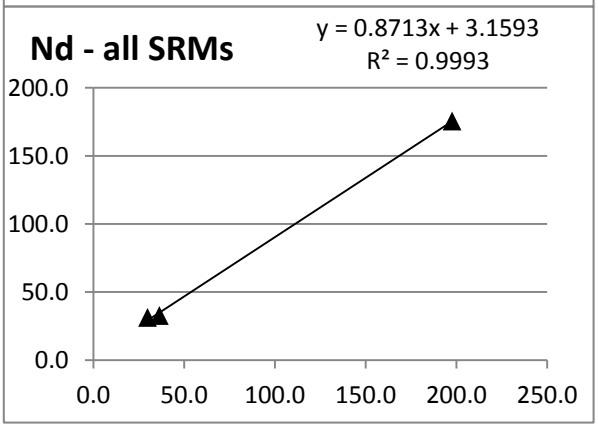
Nd - all SRMs
y = 0.8713x + 3.1593
R² = 0.9993
200.0
150.0
100.0
50.0
0.0
0.0
50.0
100.0
150.0
200.0
250.0

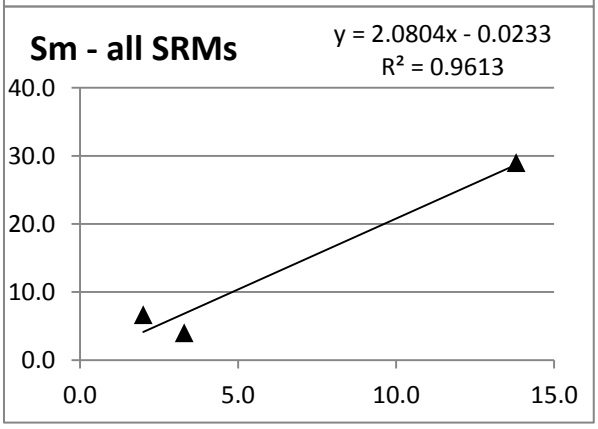
Sm - all SRMs
y = 2.0804x - 0.0233
R² = 0.9613
40.0
30.0
20.0
10.0
0.0
0.0
5.0
10.0
15.0

## Part B: RDS winter Standard Reference Material (SRM) plots

X = SRM average elemental concentration analysed with the RDS winter batches

Y = SRM average elemental concentration analysed with the soil batches

Units: Oxides expressed in weight %, other elements in mg/kg.

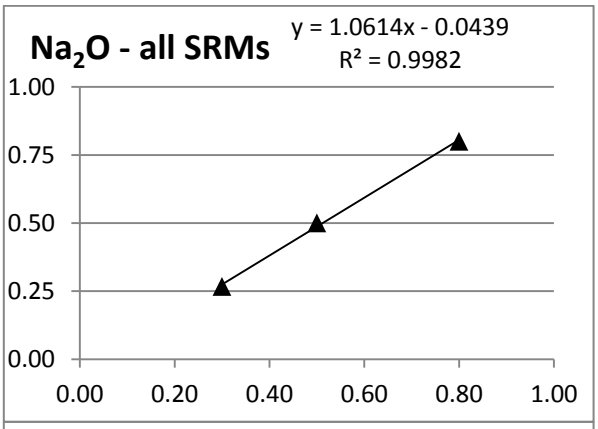


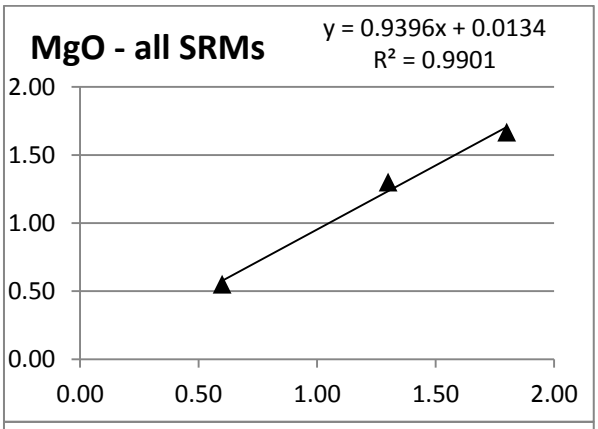


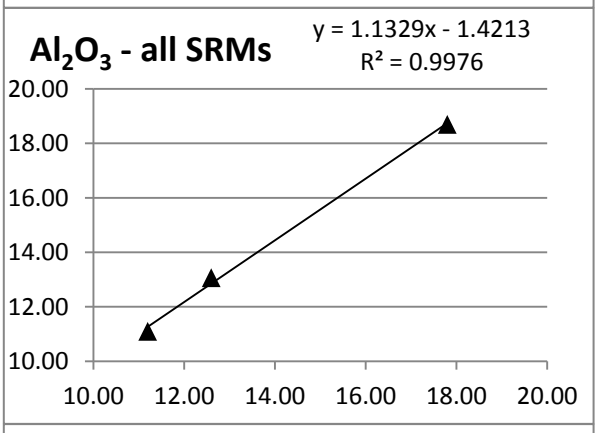


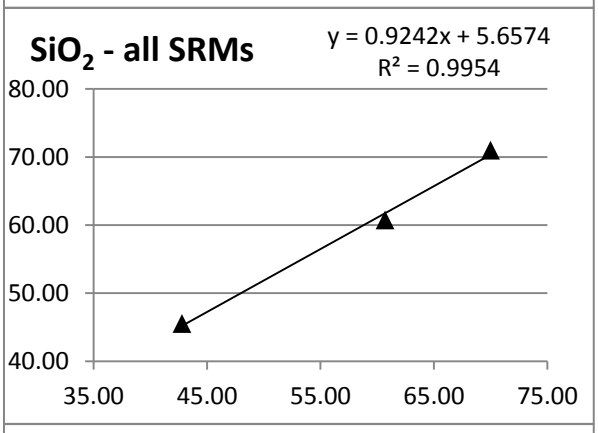


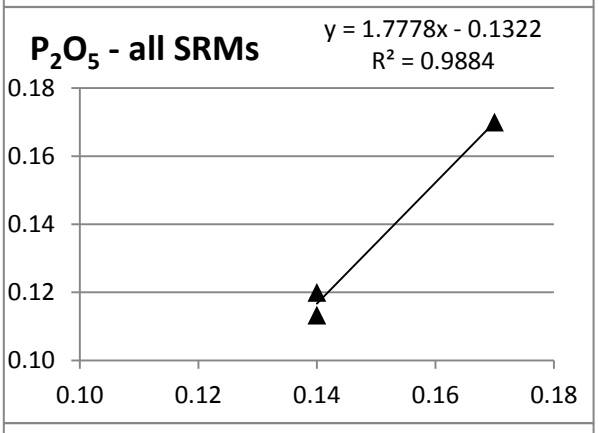


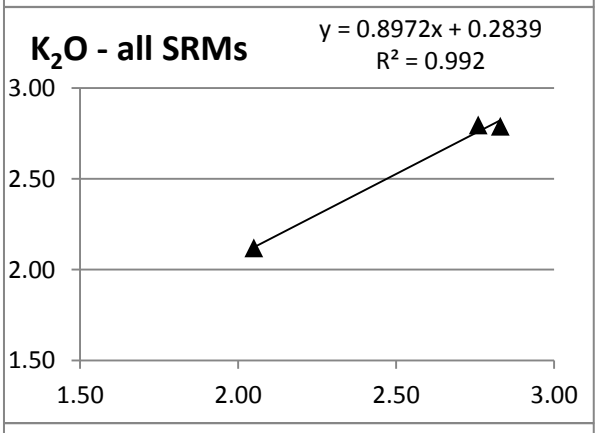


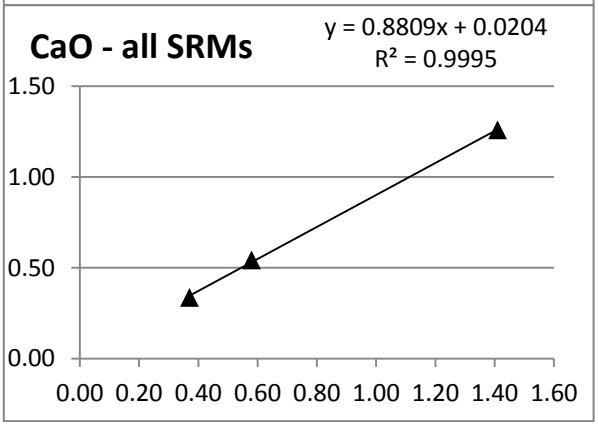


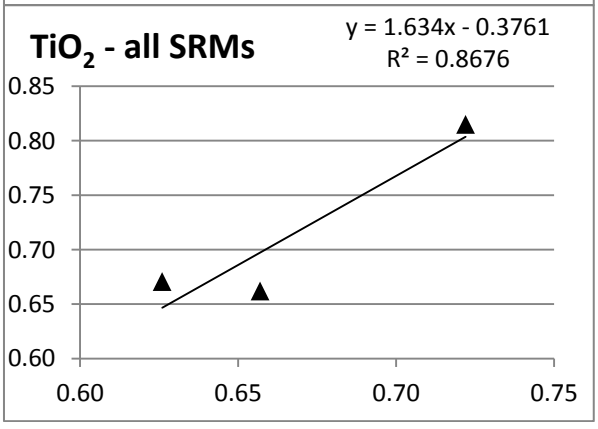

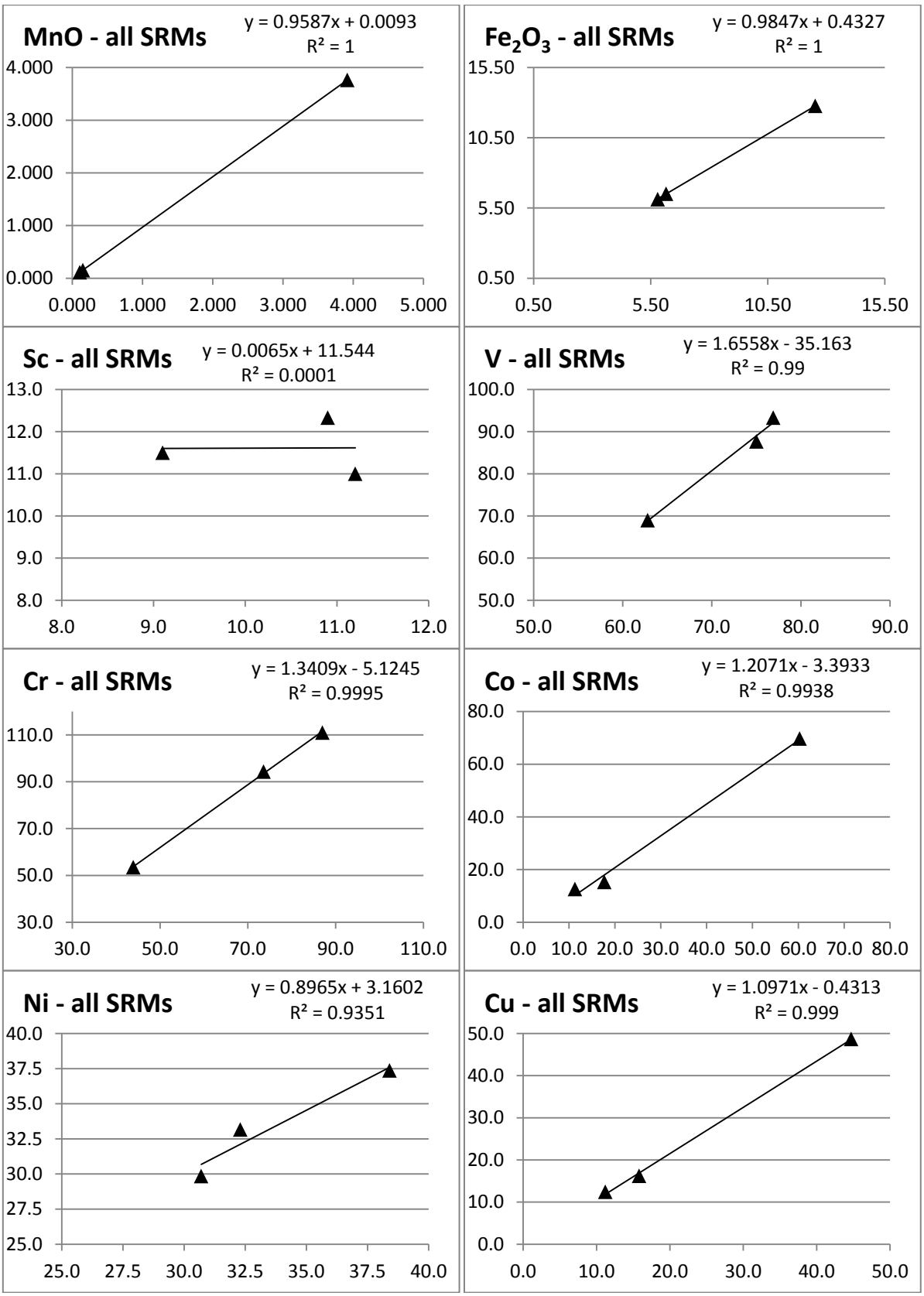
MnO - all SRMs
y = 0.9587x + 0.0093
R² = 1
4.000
3.000
2.000
1.000
0.000
0.000 1.000 2.000 3.000 4.000 5.000
Fe2O3 - all SRMs
y = 0.9847x + 0.4327
R² = 1
15.50
10.50
5.50
0.50
0.50 5.50 10.50 15.50
Sc - all SRMs
y = 0.0065x + 11.544
R² = 0.0001
13.0
12.0
11.0
10.0
9.0
8.0
8.0 9.0 10.0 11.0 12.0
V - all SRMs
y = 1.6558x - 35.163
R² = 0.99
100.0
90.0
80.0
70.0
60.0
50.0
50.0 60.0 70.0 80.0 90.0
Cr - all SRMs
y = 1.3409x - 5.1245
R² = 0.9995
110.0
90.0
70.0
50.0
30.0
30.0 50.0 70.0 90.0 110.0
Co - all SRMs
y = 1.2071x - 3.3933
R² = 0.9938
80.0
60.0
40.0
20.0
0.0
0.0 10.0 20.0 30.0 40.0 50.0 60.0 70.0 80.0
Ni - all SRMs
y = 0.8965x + 3.1602
R² = 0.9351
40.0
37.5
35.0
32.5
30.0
27.5
25.0
25.0 27.5 30.0 32.5 35.0 37.5 40.0
Cu - all SRMs
y = 1.0971x - 0.4313
R² = 0.999
50.0
40.0
30.0
20.0
10.0
0.0
0.0 10.0 20.0 30.0 40.0 50.0

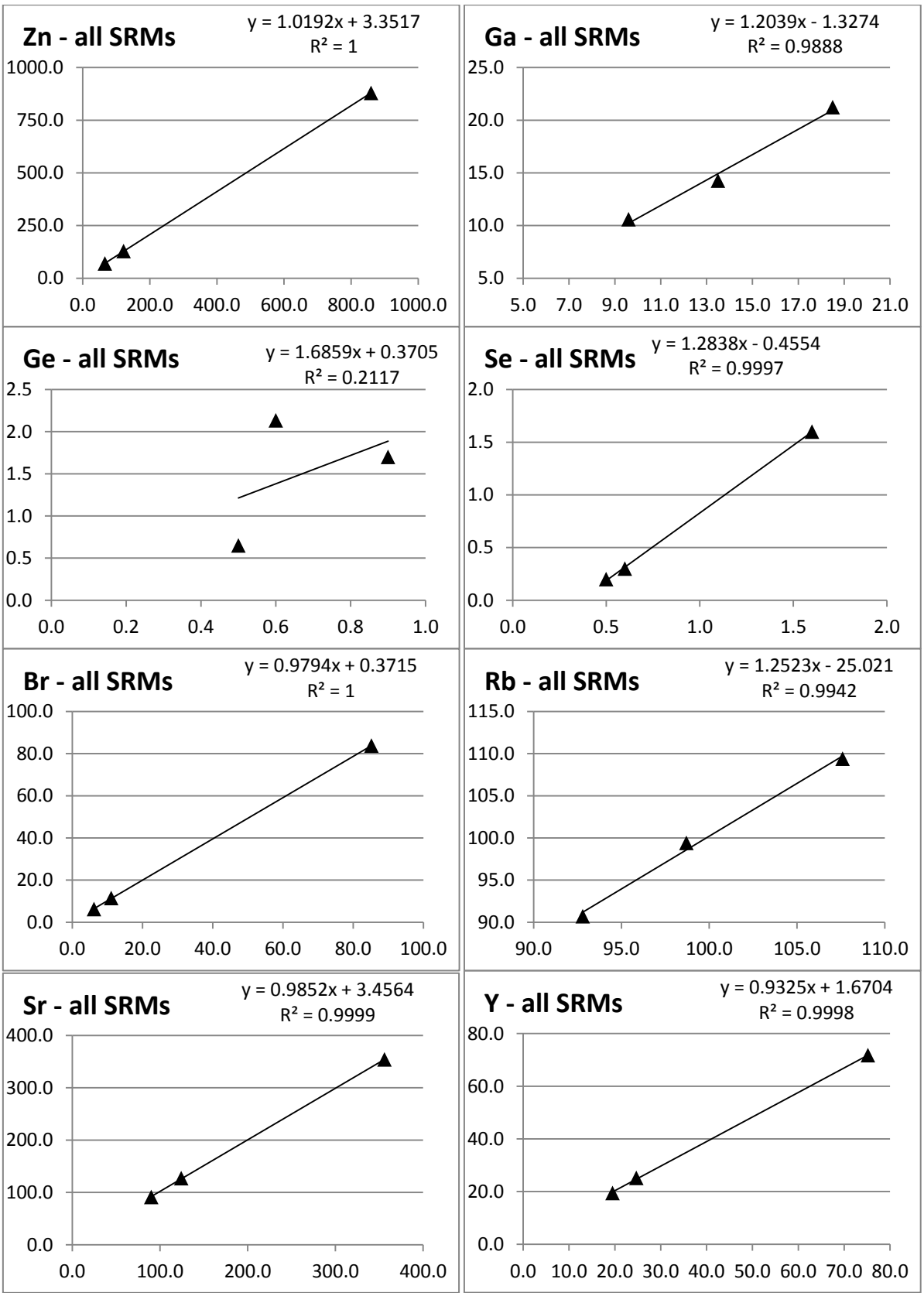
Zn - all SRMs
y = 1.0192x + 3.3517
R² = 1
1000.0
750.0
500.0
250.0
0.0
0.0 200.0 400.0 600.0 800.0 1000.0
Ga - all SRMs
y = 1.2039x - 1.3274
R² = 0.9888
25.0
20.0
15.0
10.0
5.0
5.0 7.0 9.0 11.0 13.0 15.0 17.0 19.0 21.0
Ge - all SRMs
y = 1.6859x + 0.3705
R² = 0.2117
2.5
2.0
1.5
1.0
0.5
0.0
0.0 0.2 0.4 0.6 0.8 1.0
Se - all SRMs
y = 1.2838x - 0.4554
R² = 0.9997
2.0
1.5
1.0
0.5
0.0
0.0 0.5 1.0 1.5 2.0
Br - all SRMs
y = 0.9794x + 0.3715
R² = 1
100.0
80.0
60.0
40.0
20.0
0.0
0.0 20.0 40.0 60.0 80.0 100.0
Rb - all SRMs
y = 1.2523x - 25.021
R² = 0.9942
115.0
110.0
105.0
100.0
95.0
90.0
90.0 95.0 100.0 105.0 110.0
Sr - all SRMs
y = 0.9852x + 3.4564
R² = 0.9999
400.0
300.0
200.0
100.0
0.0
0.0 100.0 200.0 300.0 400.0
Y - all SRMs
y = 0.9325x + 1.6704
R² = 0.9998
80.0
60.0
40.0
20.0
0.0
0.0 10.0 20.0 30.0 40.0 50.0 60.0 70.0 80.0

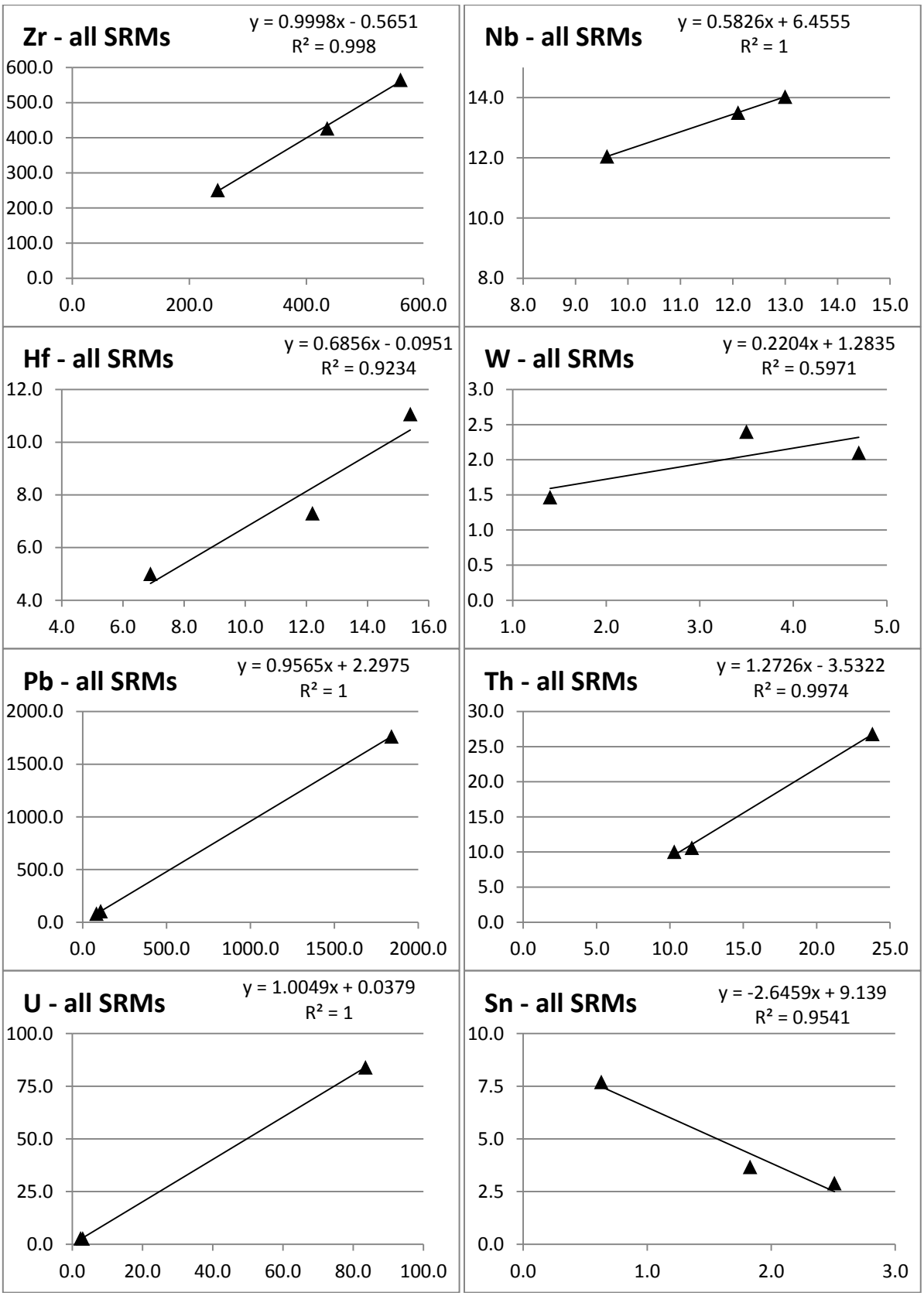
Zr - all SRMs
y = 0.9998x - 0.5651
R² = 0.998
600.0
500.0
400.0
300.0
200.0
100.0
0.0
0.0
200.0
400.0
600.0
Nb - all SRMs
y = 0.5826x + 6.4555
R² = 1
14.0
12.0
10.0
8.0
8.0
9.0
10.0
11.0
12.0
13.0
14.0
15.0
Hf - all SRMs
y = 0.6856x - 0.0951
R² = 0.9234
12.0
10.0
8.0
6.0
4.0
4.0
6.0
8.0
10.0
12.0
14.0
16.0
W - all SRMs
y = 0.2204x + 1.2835
R² = 0.5971
3.0
2.5
2.0
1.5
1.0
0.5
0.0
1.0
2.0
3.0
4.0
5.0
Pb - all SRMs
y = 0.9565x + 2.2975
R² = 1
2000.0
1500.0
1000.0
500.0
0.0
0.0
500.0
1000.0
1500.0
2000.0
Th - all SRMs
y = 1.2726x - 3.5322
R² = 0.9974
30.0
25.0
20.0
15.0
10.0
5.0
0.0
0.0
5.0
10.0
15.0
20.0
25.0
U - all SRMs
y = 1.0049x + 0.0379
R² = 1
100.0
75.0
50.0
25.0
0.0
0.0
20.0
40.0
60.0
80.0
100.0
Sn - all SRMs
y = -2.6459x + 9.139
R² = 0.9541
10.0
7.5
5.0
2.5
0.0
0.0
1.0
2.0
3.0

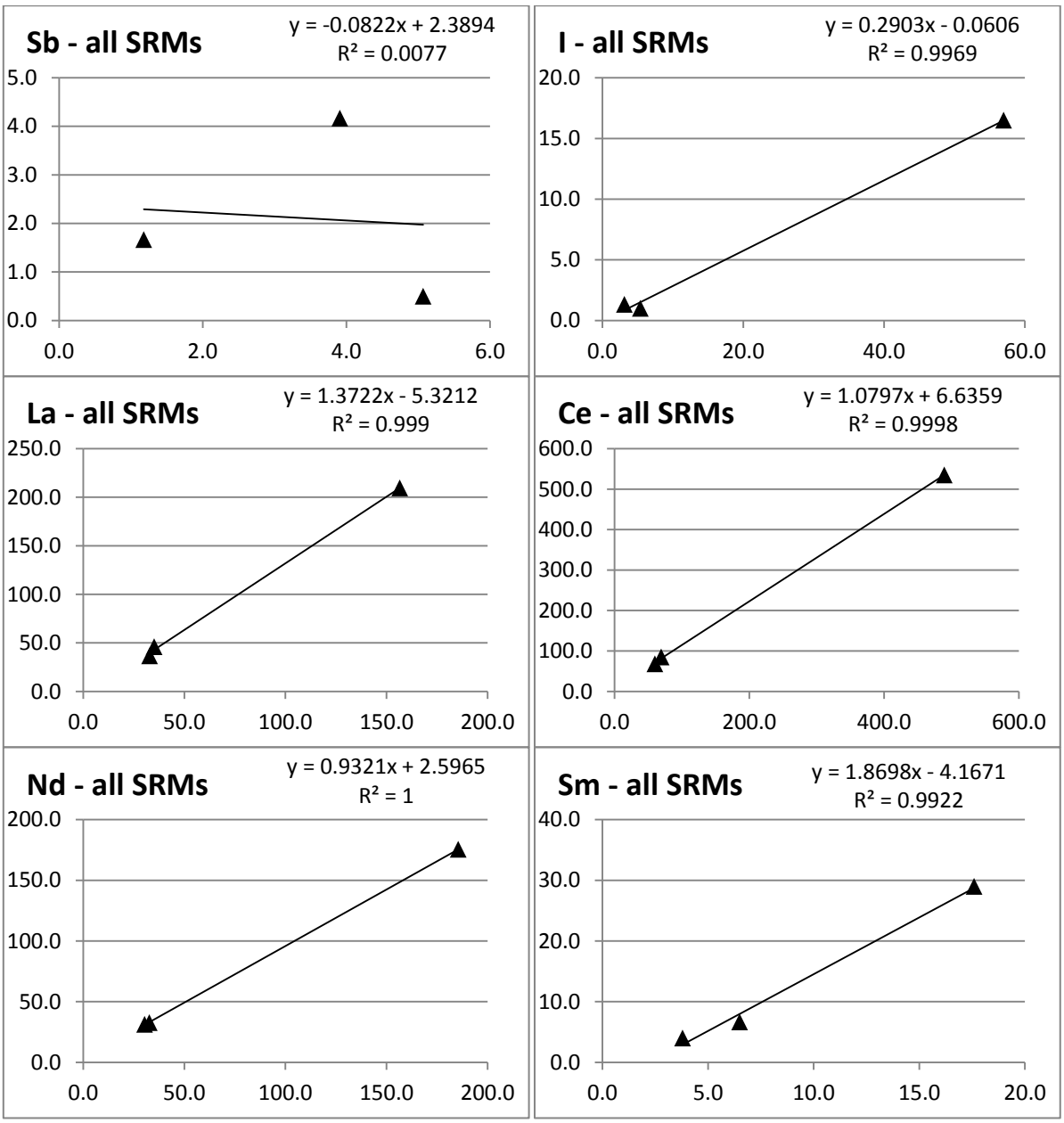
Sb - all SRMs
y = -0.0822x + 2.3894
R² = 0.0077
I - all SRMs
y = 0.2903x - 0.0606
R² = 0.9969
La - all SRMs
y = 1.3722x - 5.3212
R² = 0.999
Ce - all SRMs
y = 1.0797x + 6.6359
R² = 0.9998
Nd - all SRMs
y = 0.9321x + 2.5965
R² = 1
Sm - all SRMs
y = 1.8698x - 4.1671
R² = 0.9922

## 2. Soil Statistics

Figure 98: Histogram plots for soil variables (oxides, LOI, TC, OC and IC concentrations are expressed in wt. %; other chemical elements in mg/kg).

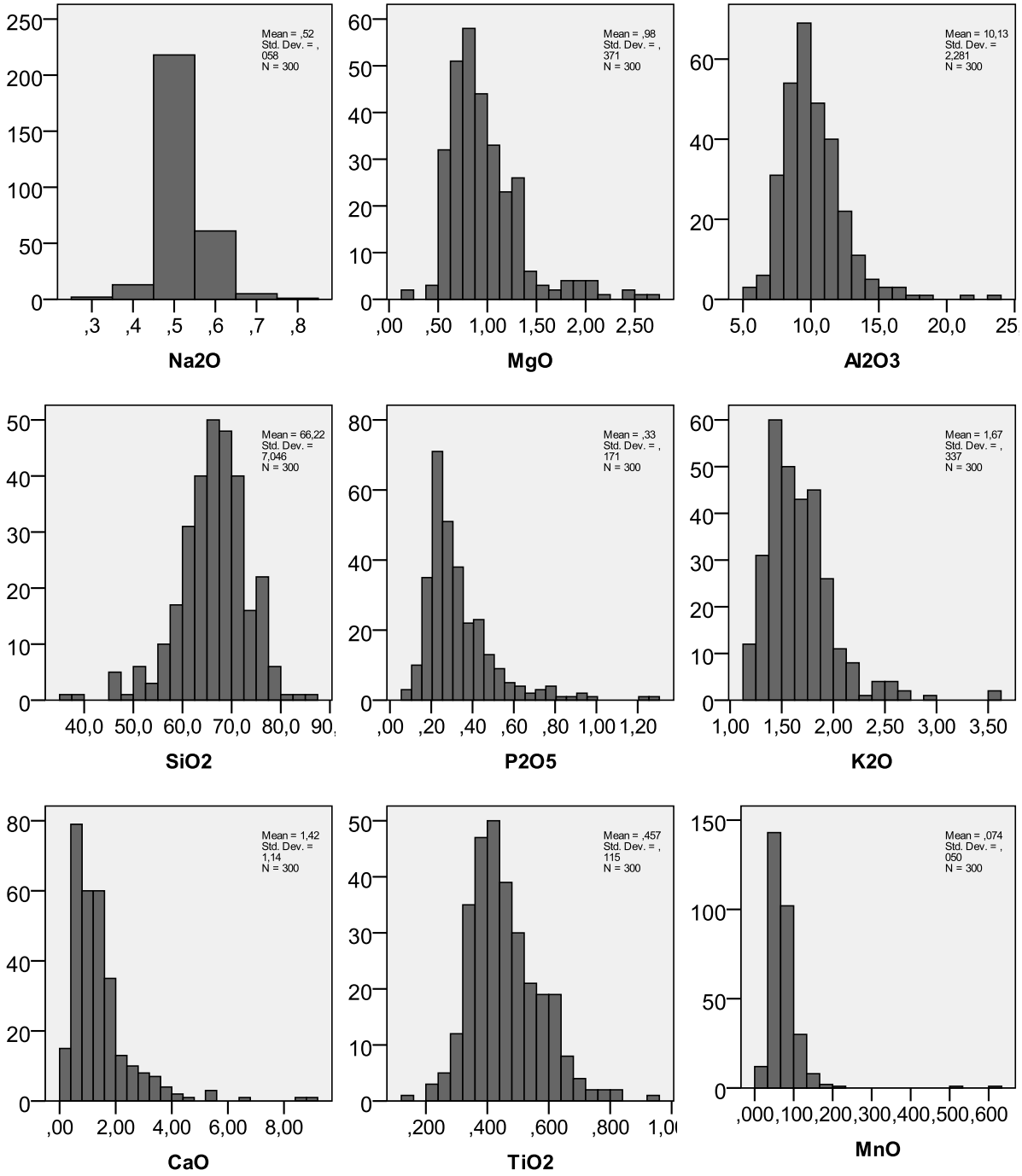

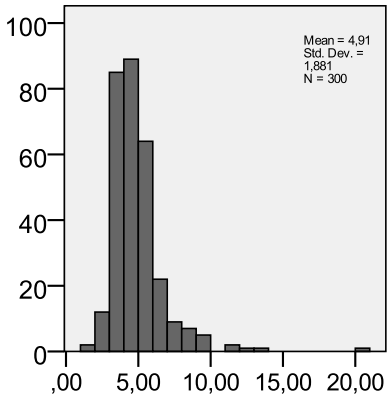
Mean = 4,91
Std. Dev. = 1,881
N = 300
Fe2O3

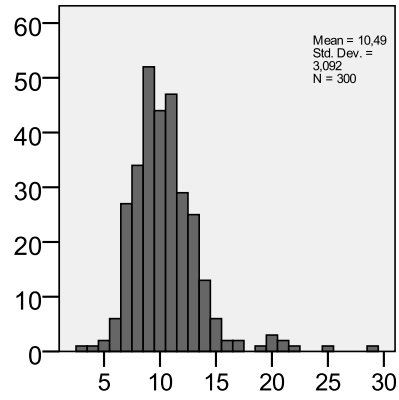
Mean = 10,49
Std. Dev. = 3,092
N = 300
Sc

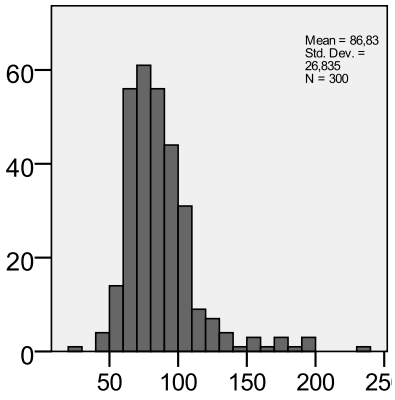
Mean = 86,83
Std. Dev. = 26,835
N = 300
V

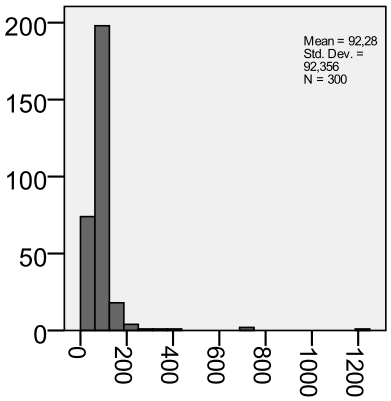
Mean = 92,28
Std. Dev. = 92,356
N = 300
Cr

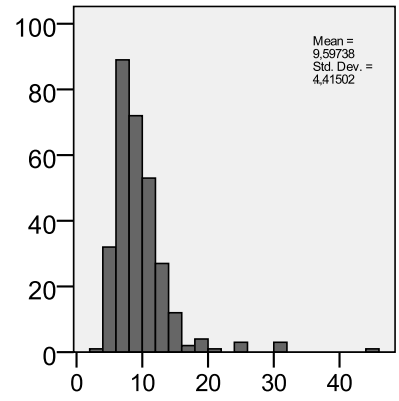
Mean = 9,59738
Std. Dev. = 4,41502
Co

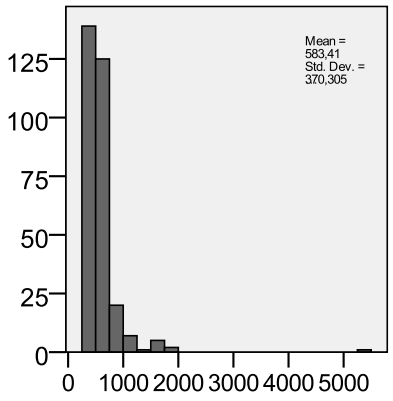
Mean = 583,41
Std. Dev. = 370,305
Ba

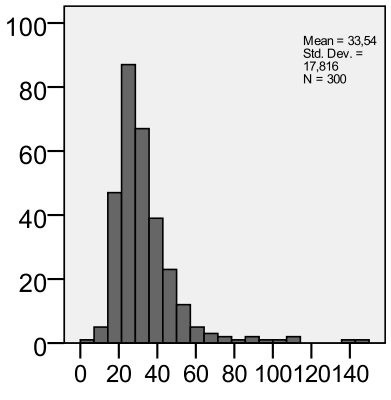
Mean = 33,54
Std. Dev. = 17,816
N = 300
Ni

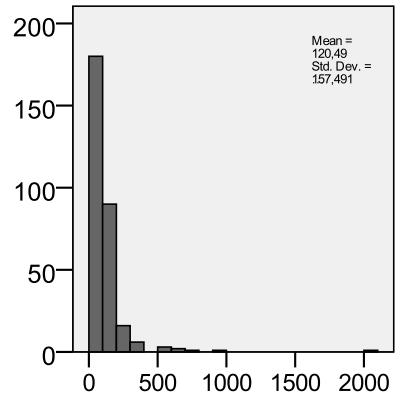
Mean = 120,49
Std. Dev. = 157,491
Cu

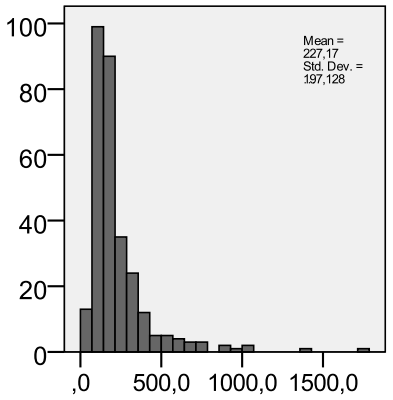
Mean = 227,17
Std. Dev. = 197,128
Zn

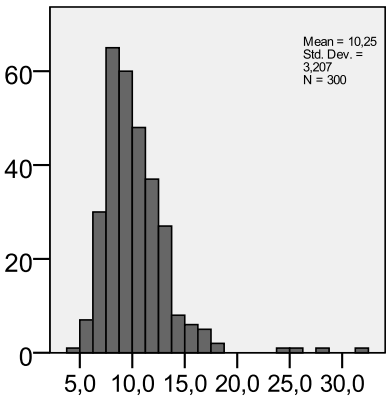
Mean = 10,25
Std. Dev. = 3,207
N = 300
Ga

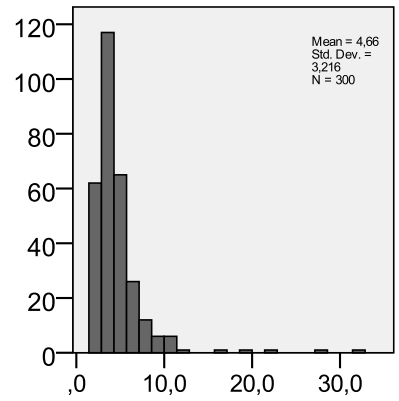
Mean = 4,66
Std. Dev. = 3,216
N = 300
Ge

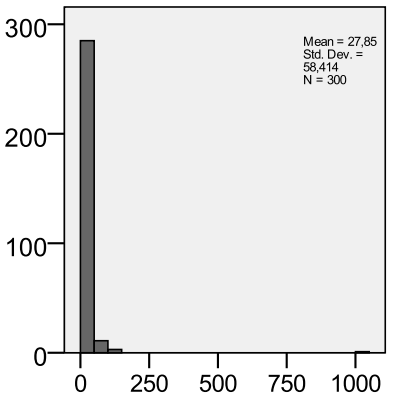
Mean = 27,85
Std. Dev. = 58,414
N = 300
As

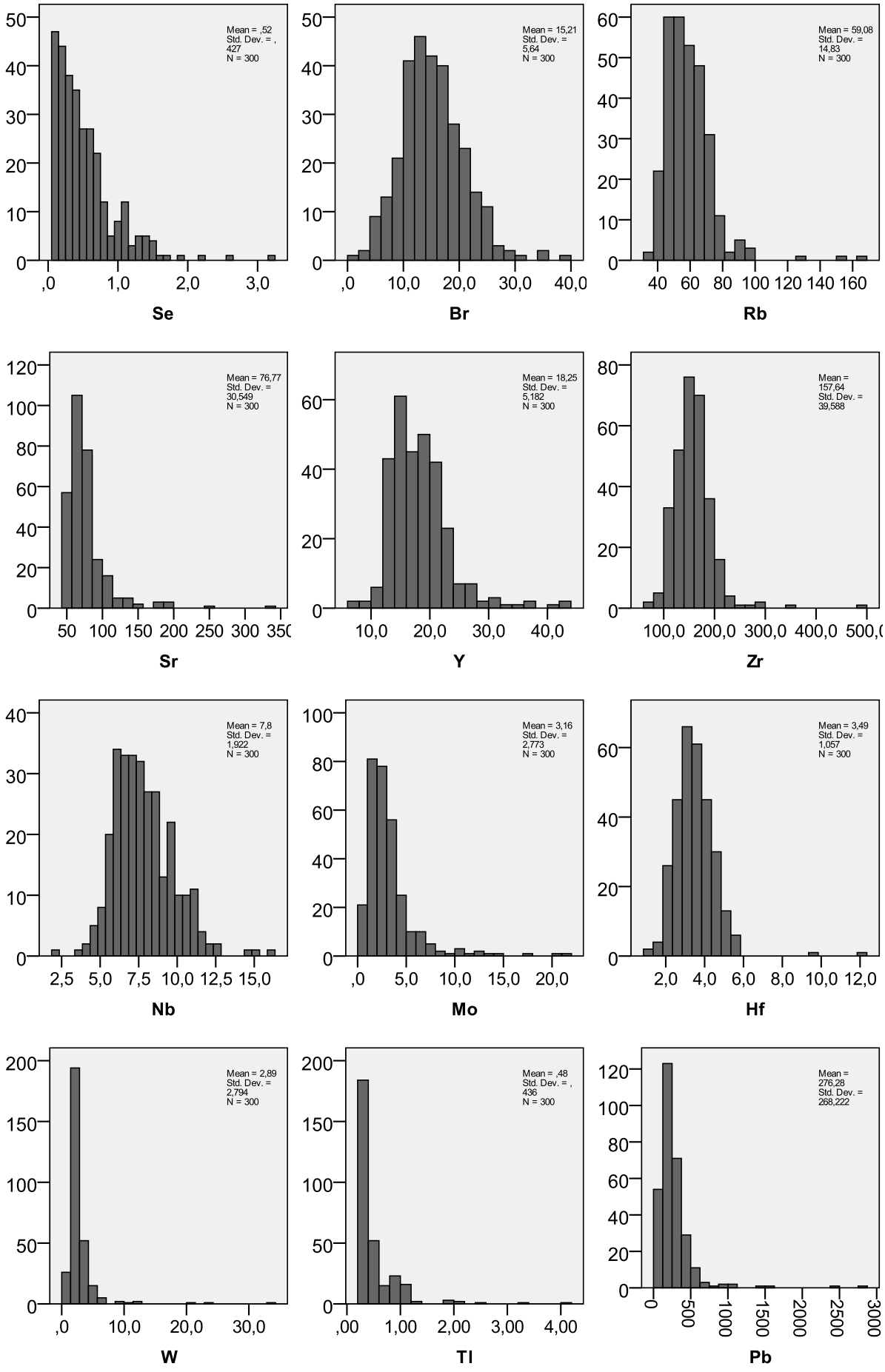
Mean = ,52
Std. Dev. = ,427
N = 300
Se
Mean = 15,21
Std. Dev. = 5,64
N = 300
Br
Mean = 59,08
Std. Dev. = 14,83
N = 300
Rb
Mean = 76,77
Std. Dev. = 30,549
N = 300
Sr
Mean = 18,25
Std. Dev. = 5,182
N = 300
Y
Mean = 157,64
Std. Dev. = 39,588
Zr
Mean = 7,8
Std. Dev. = 1,922
N = 300
Nb
Mean = 3,16
Std. Dev. = 2,773
N = 300
Mo
Mean = 3,49
Std. Dev. = 1,057
N = 300
Hf
Mean = 2,89
Std. Dev. = 2,794
N = 300
W
Mean = ,48
Std. Dev. = ,436
N = 300
Tl
Mean = 276,28
Std. Dev. = 268,222
Pb

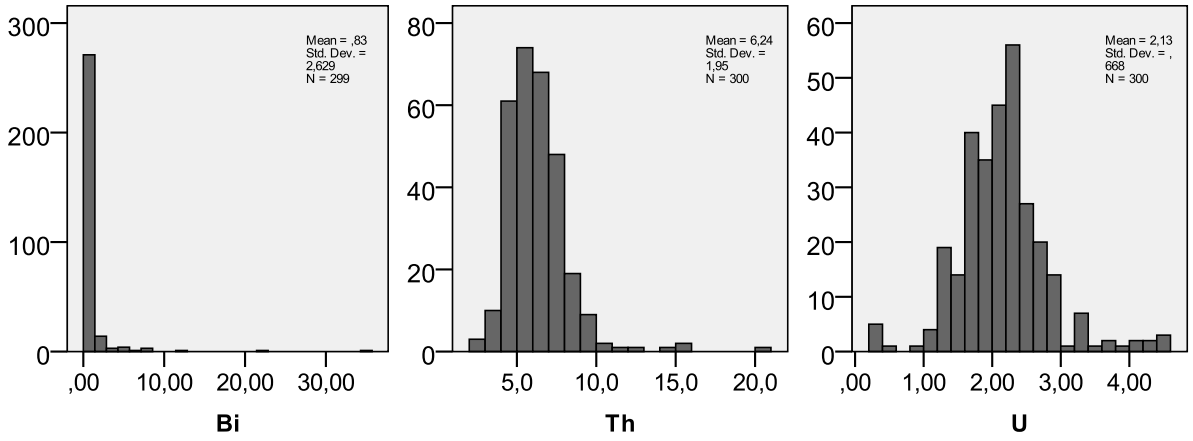
Mean = ,83
Std. Dev. = 2,629
N = 299
Bi
Mean = 6,24
Std. Dev. = 1,95
N = 300
Th
Mean = 2,13
Std. Dev. = ,668
N = 300
U

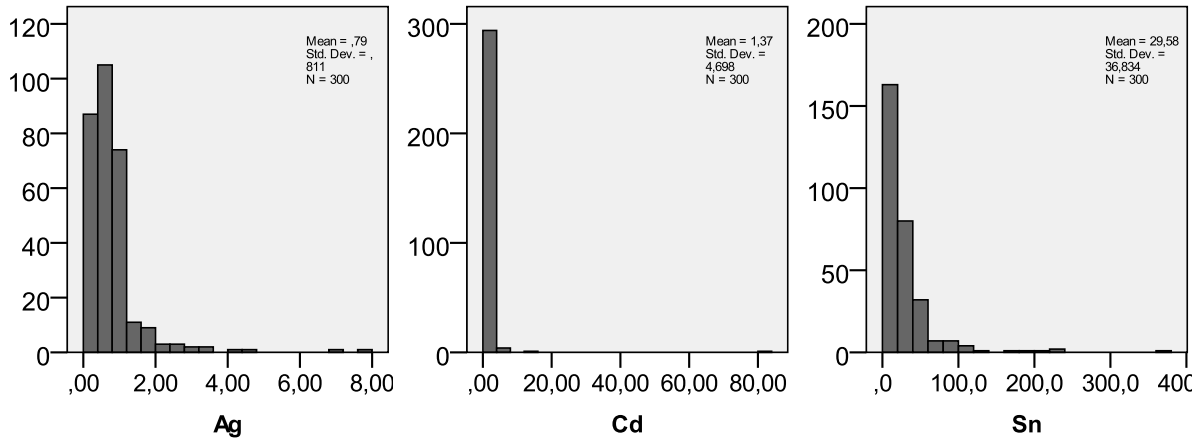
Mean = ,79
Std. Dev. = ,811
N = 300
Ag
Mean = 1,37
Std. Dev. = 4,698
N = 300
Cd
Mean = 29,58
Std. Dev. = 36,834
N = 300
Sn

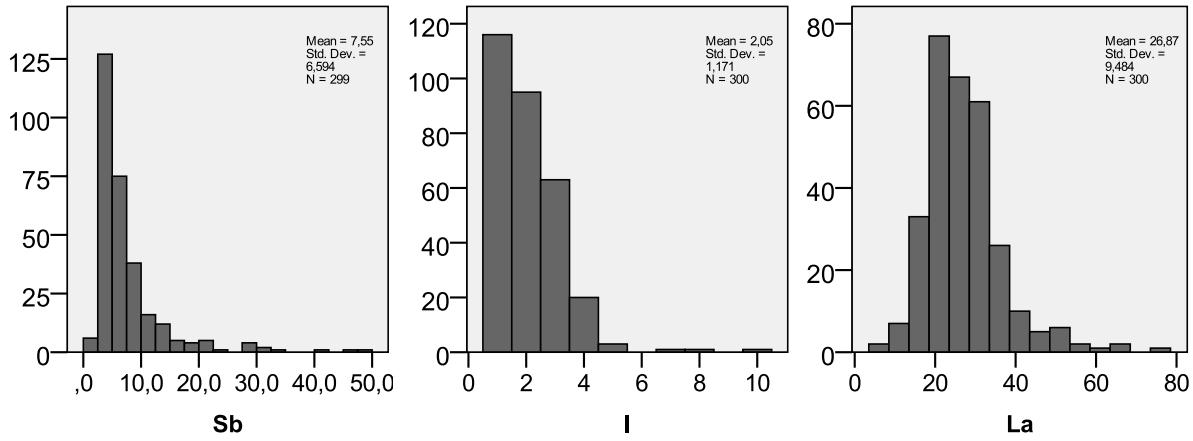
Mean = 7,55
Std. Dev. = 6,594
N = 299
Sb
Mean = 2,05
Std. Dev. = 1,171
N = 300
I
Mean = 26,87
Std. Dev. = 9,484
N = 300
La

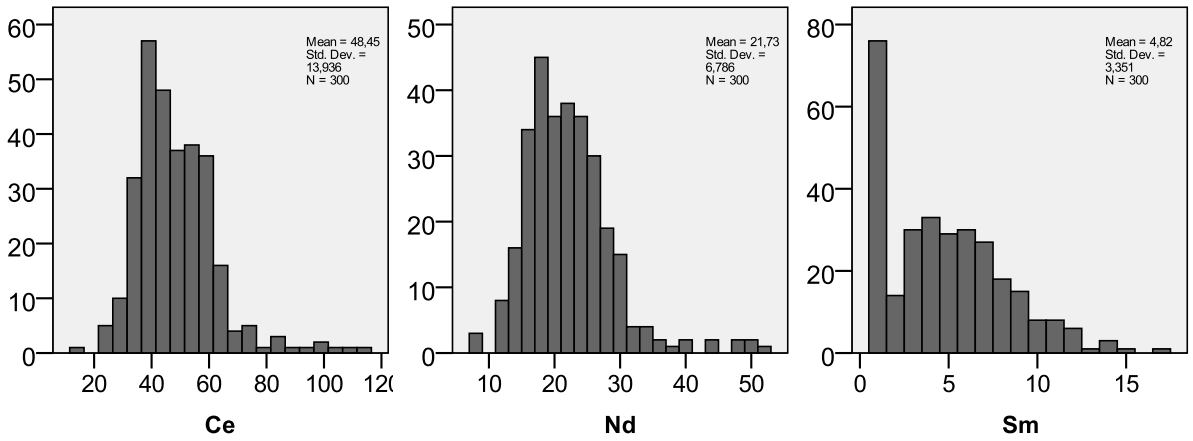
Mean = 48,45
Std. Dev. = 13,936
N = 300
Ce
Mean = 21,73
Std. Dev. = 6,786
N = 300
Nd
Mean = 4,82
Std. Dev. = 3,351
N = 300
Sm

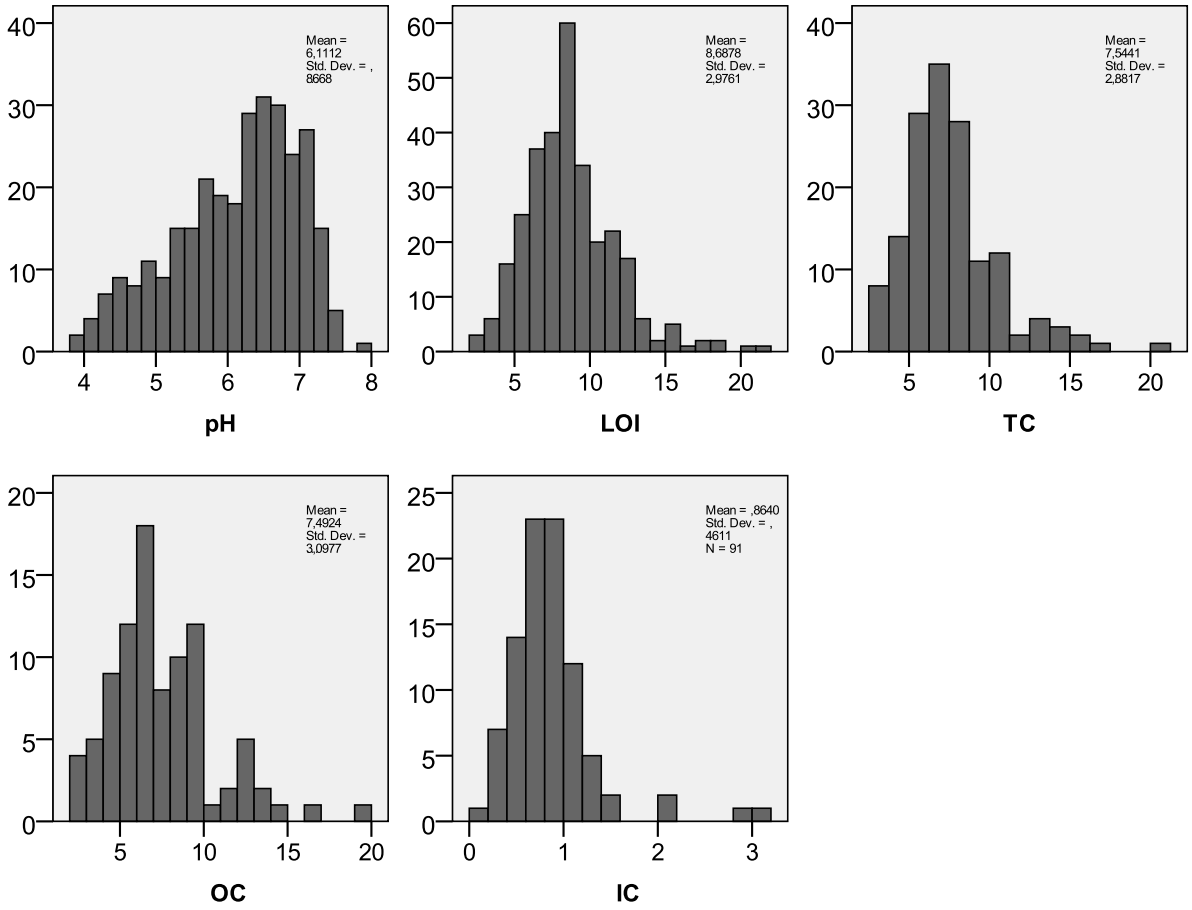
Mean = 6,1112
Std. Dev. = ,8668
pH
Mean = 8,6878
Std. Dev. = 2,9761
LOI
Mean = 7,5441
Std. Dev. = 2,8817
TC
Mean = 7,4924
Std. Dev. = 3,0977
OC
Mean = ,8640
Std. Dev. = ,4611
N = 91
IC

Figure 99: Box-and-whisker plots for soil variables (oxides, LOI, TC, OC and IC concentrations are expressed in wt. %; other chemical elements in mg/kg).

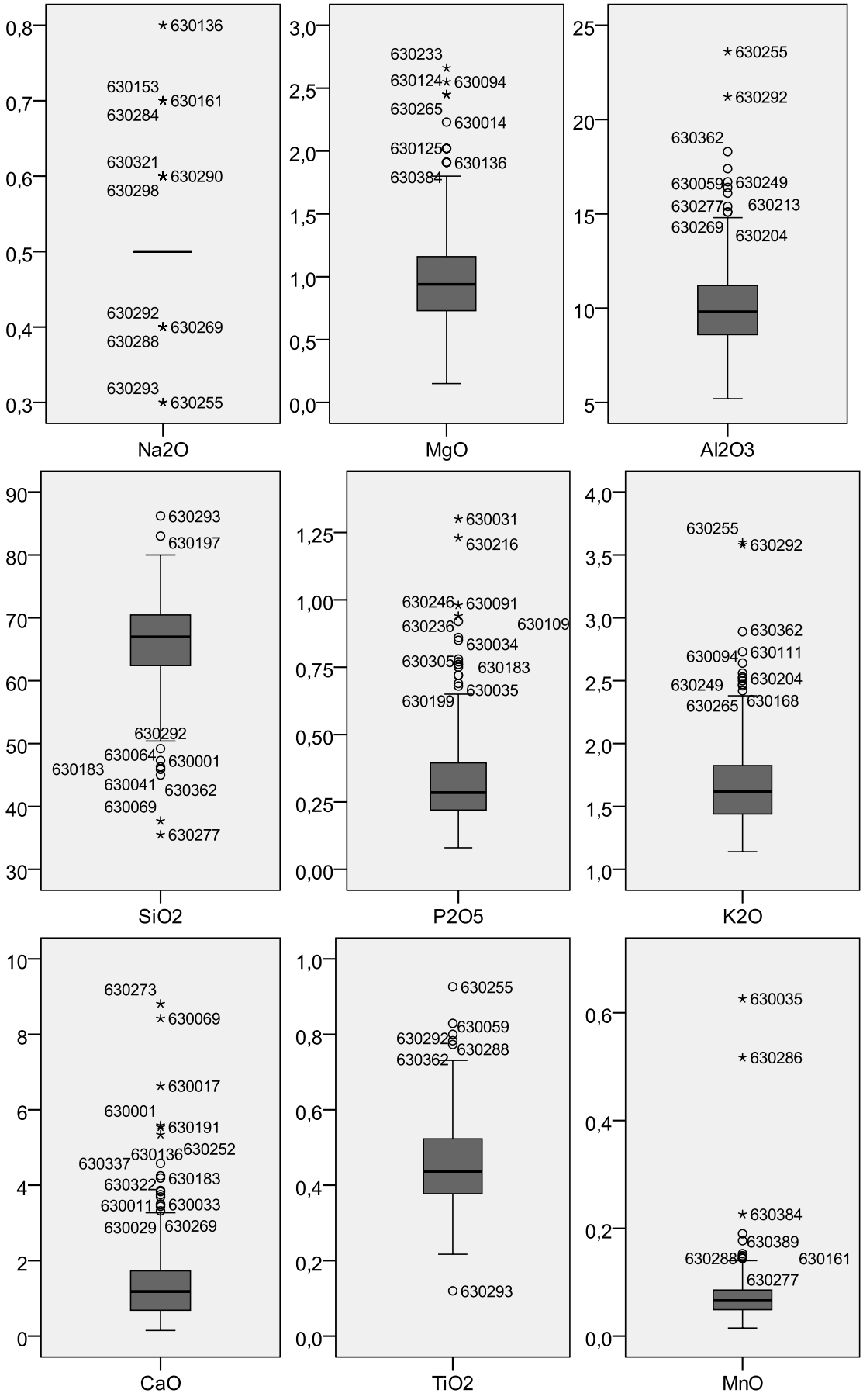

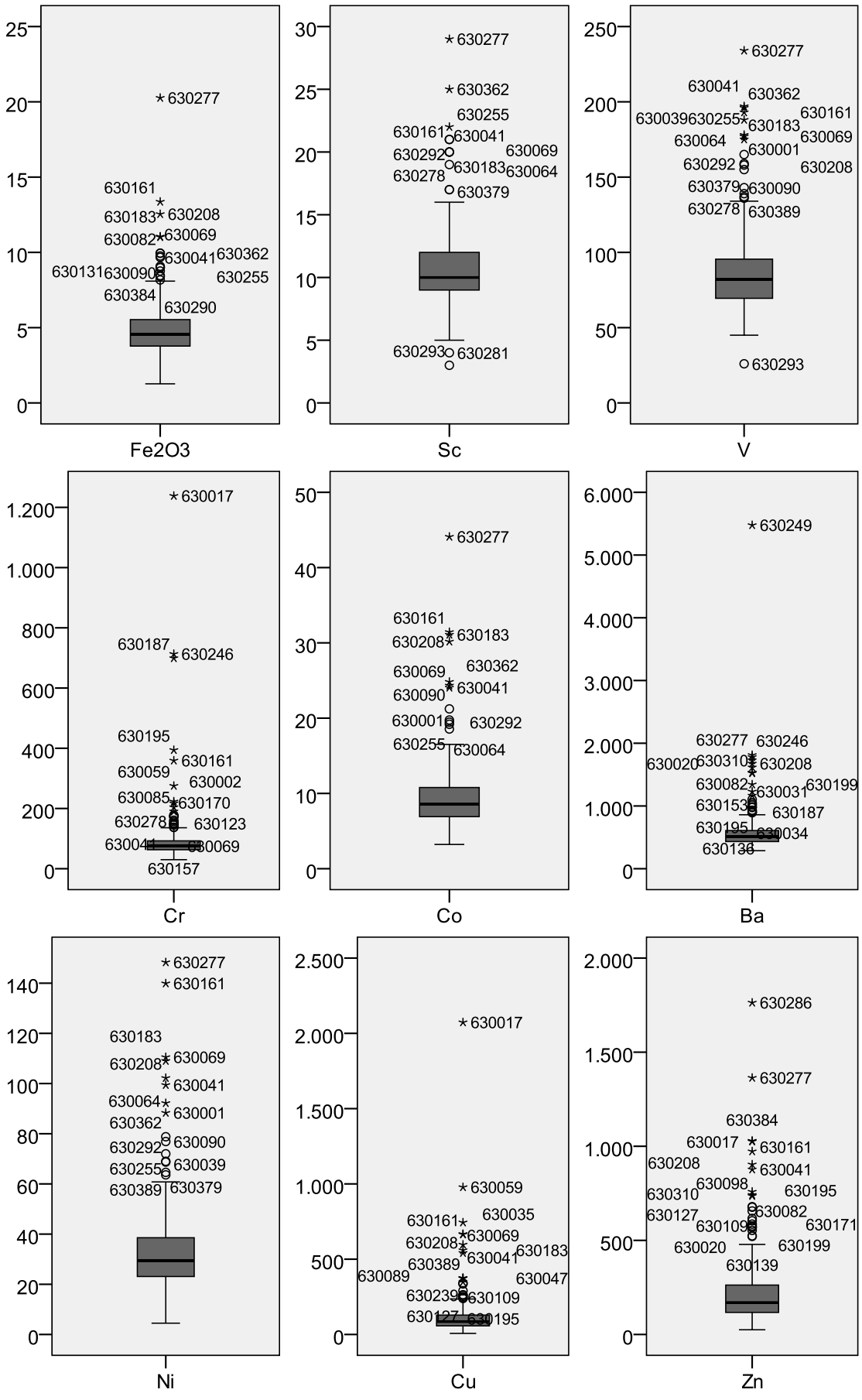
Fe2O3
Sc
V
Cr
Co
Ba
Ni
Cu
Zn

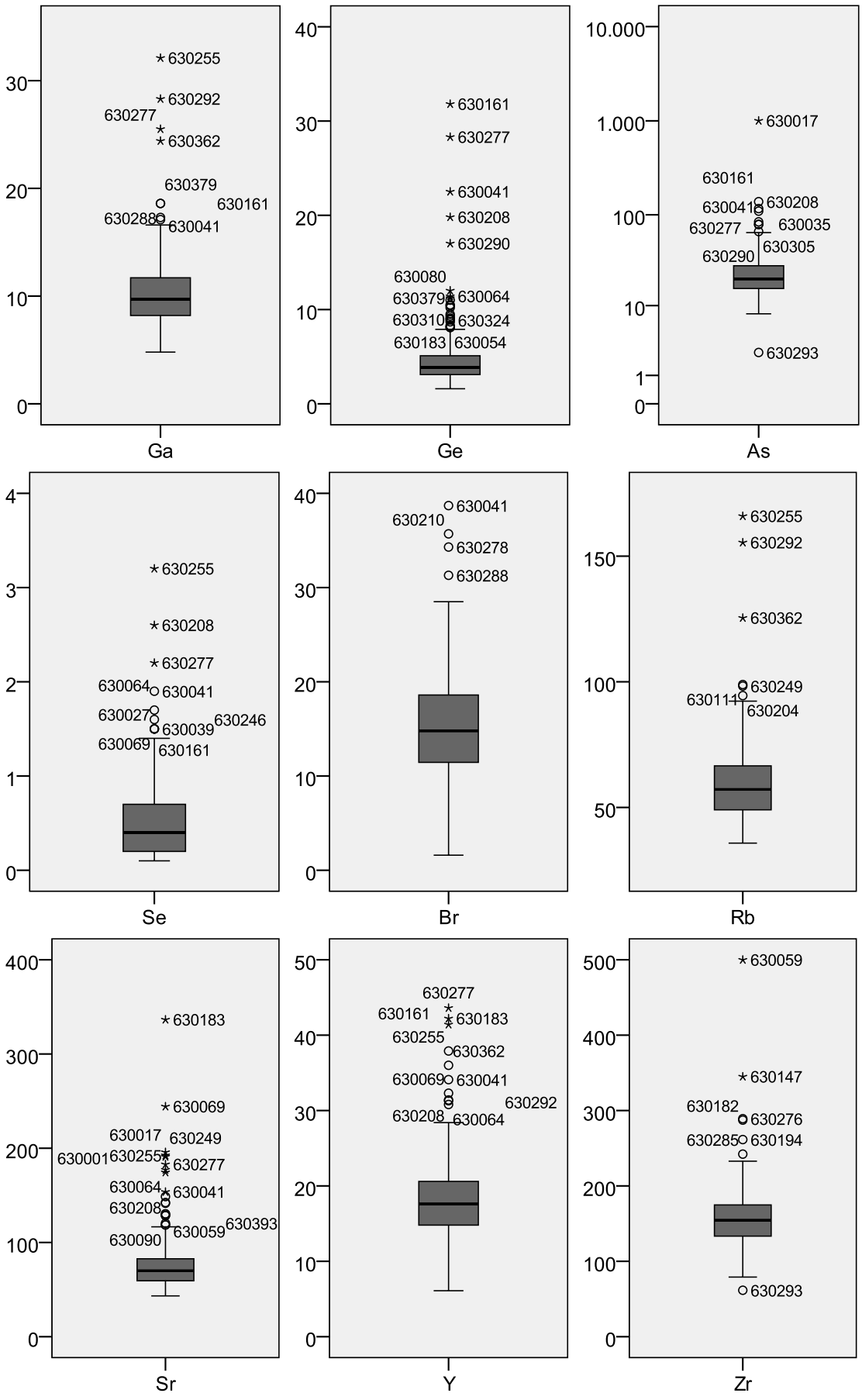
Ga
630255
630292
630277
630362
630379
630161
630288
630041
Ge
630161
630277
630041
630208
630290
630080
630379
630064
630310
630324
630183
630054
As
630017
630161
630041
630208
630277
630035
630305
630290
630293
Se
630255
630208
630277
630064
630041
630027
630039
630246
630069
630161
Br
630041
630210
630278
630288
Rb
630255
630292
630362
630249
630114
630204
Sr
630183
630069
630017
630249
630001
630255
630277
630064
630041
630208
630059
630393
630090
Y
630277
630161
630183
630255
630362
630069
630041
630292
630208
630064
Zr
630059
630147
630182
630276
630285
630194
630293

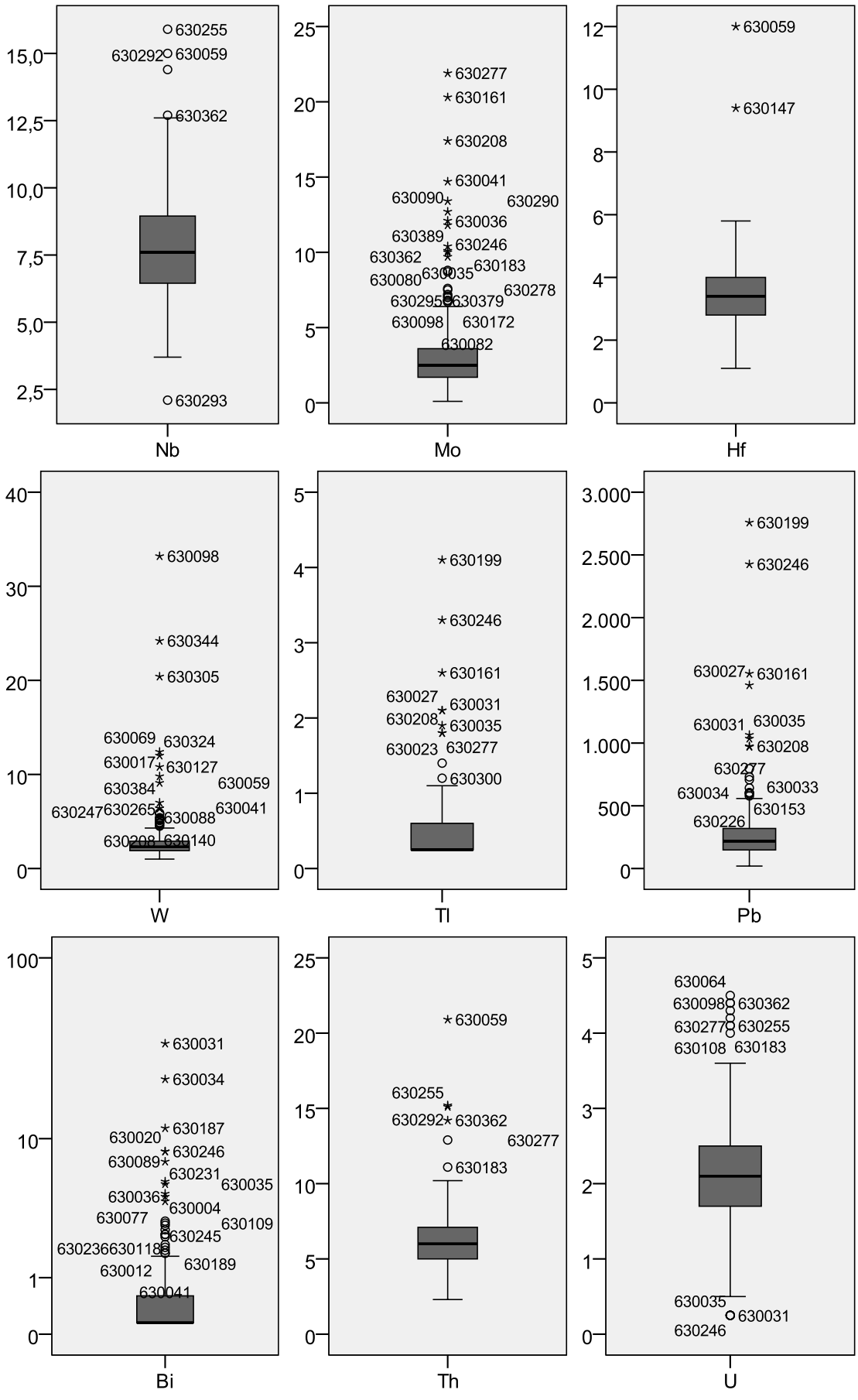
Nb
Mo
Hf
W
Tl
Pb
Bi
Th
U

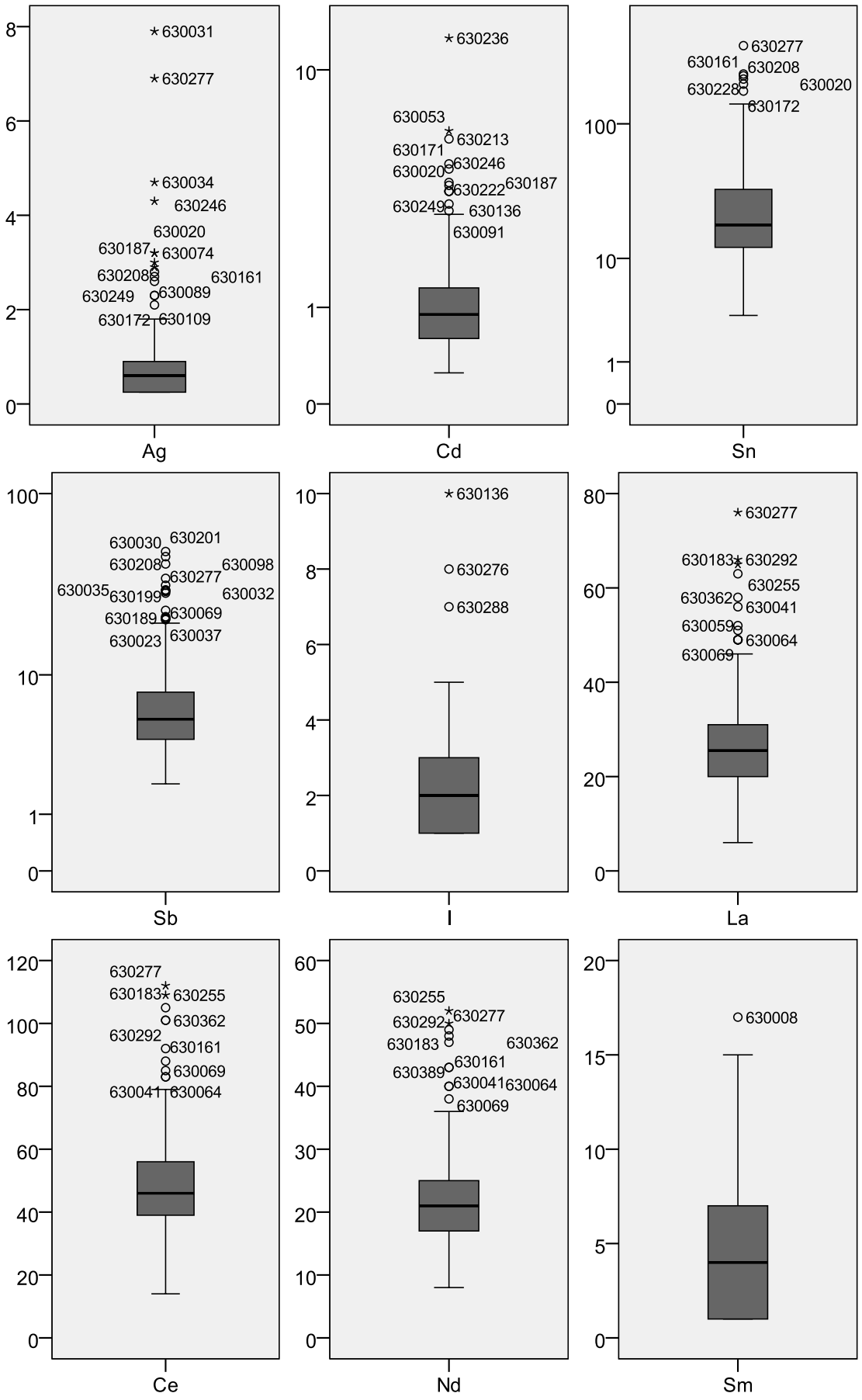
Ag
630031
630277
630034
630246
630020
630187
630074
630208
630161
630249
630089
630172
630109
Cd
630236
630053
630213
630171
630246
630020
630187
630222
630249
630136
630091
Sn
630277
630161
630208
630228
630020
630172
Sb
630030
630201
630208
630098
630277
630035
630199
630032
630189
630069
630023
630037
I
630136
630276
630288
La
630277
630183
630292
630255
630362
630041
630059
630064
630069
Ce
630277
630183
630255
630362
630292
630161
630069
630041
630064
Nd
630255
630292
630277
630183
630362
630389
630161
630041
630064
630069
Sm
630008

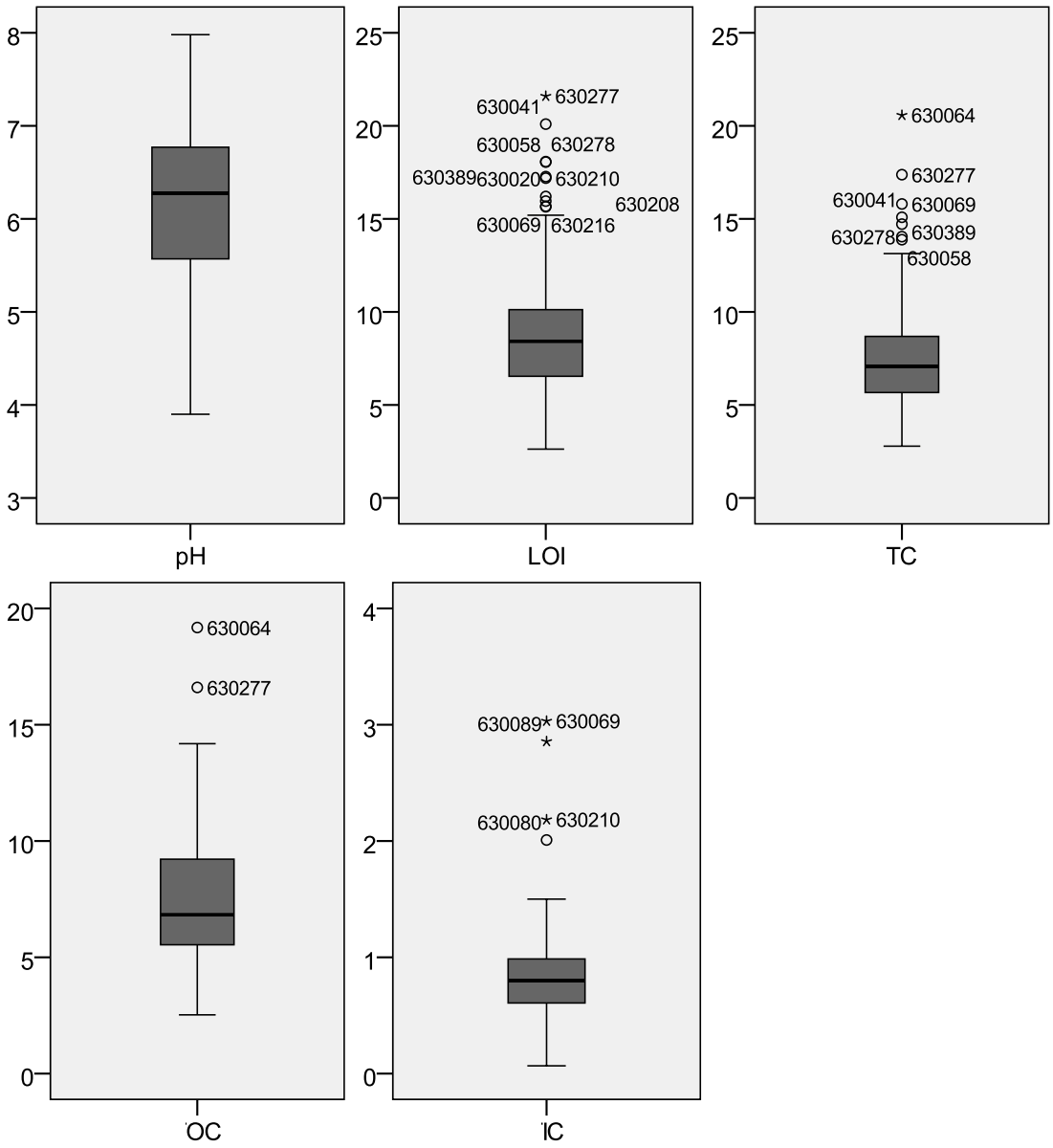
8
7
6
5
4
3
pH
25
20
15
10
5
0
630041
630277
630058
630278
630389
630020
630210
630208
630069
630216
LOI
25
20
15
10
5
0
630064
630277
630041
630069
630278
630389
630058
TC
20
15
10
5
0
630064
630277
OC
4
3
2
1
0
630089
630069
630080
630210
IC

Table 74: Kolmogorov-Smirnov test for soil data distributions.

| Element | Kolmogorov-Smirnov | | | Element | Kolmogorov-Smirnov | | |
|---|---|---|---|---|---|---|---|
| | Statistic | df | Sig. | | Statistic | df | Sig. |
| Na2O | ,405 | 300 | ,000 | Y | ,088 | 300 | ,000 |
| MgO | ,178 | 300 | ,000 | Zr | ,094 | 300 | ,000 |
| Al2O3 | ,087 | 300 | ,000 | Nb | ,086 | 300 | ,000 |
| SiO2 | ,056 | 300 | ,024 | Mo | ,200 | 300 | ,000 |
| P2O5 | ,155 | 300 | ,000 | Hf | ,085 | 300 | ,000 |
| K2O | ,104 | 300 | ,000 | W | ,291 | 300 | ,000 |
| CaO | ,158 | 300 | ,000 | Tl | ,312 | 300 | ,000 |
| TiO2 | ,087 | 300 | ,000 | Pb | ,198 | 300 | ,000 |
| MnO | ,189 | 300 | ,000 | Bi | ,397 | 299 | ,000 |
| Fe2O3 | ,132 | 300 | ,000 | Th | ,104 | 300 | ,000 |
| Sc | ,148 | 300 | ,000 | U | ,094 | 300 | ,000 |
| V | ,130 | 300 | ,000 | Ag | ,254 | 300 | ,000 |
| Cr | ,292 | 300 | ,000 | Cd | ,406 | 300 | ,000 |
| Co | ,149 | 300 | ,000 | Sn | ,245 | 300 | ,000 |
| Ba | ,245 | 300 | ,000 | Sb | ,232 | 299 | ,000 |
| Ni | ,157 | 300 | ,000 | I | ,220 | 300 | ,000 |
| Cu | ,268 | 300 | ,000 | La | ,118 | 300 | ,000 |
| Zn | ,215 | 300 | ,000 | Ce | ,088 | 300 | ,000 |
| Ga | ,107 | 300 | ,000 | Nd | ,096 | 300 | ,000 |
| Ge | ,207 | 300 | ,000 | Sm | ,127 | 300 | ,000 |
| As | ,373 | 300 | ,000 | OM (LOI) | ,093 | 300 | ,000 |
| Se | ,163 | 300 | ,000 | TC (DC) | ,111 | 150 | ,000 |
| Br | ,053 | 300 | ,043 | OC (DC) | ,110 | 91 | ,008 |
| Rb | ,094 | 300 | ,000 | IC | ,161 | 91 | ,000 |
| Sr | ,190 | 300 | ,000 | pH | ,091 | 300 | ,000 |

Table 75: Kolmogorov-Smirnov test for log-transformed soil data distributions.

| Element | Kolmogorov-Smirnov | | | Element | Kolmogorov-Smirnov | | |
|---|---|---|---|---|---|---|---|
| | Statistic | df | Sig. | | Statistic | df | Sig. |
| Na2O_LOG | ,387 | 300 | ,000 | Y_LOG | ,045 | 300 | ,200 |
| MgO_LOG | ,135 | 300 | ,000 | Zr_LOG | ,046 | 300 | ,200 |
| Al2O3_LOG | ,049 | 300 | ,075 | Nb_LOG | ,039 | 300 | ,200 |
| SiO2_LOG | ,081 | 300 | ,000 | Mo_LOG | ,077 | 300 | ,000 |
| P2O5_LOG | ,067 | 300 | ,002 | Hf_LOG | ,065 | 300 | ,004 |
| K2O_LOG | ,067 | 300 | ,002 | W_LOG | ,146 | 300 | ,000 |
| CaO_LOG | ,034 | 300 | ,200 | Tl_LOG | ,375 | 300 | ,000 |
| TiO2_LOG | ,043 | 300 | ,200 | Pb_LOG | ,047 | 300 | ,200 |
| MnO_LOG | ,059 | 300 | ,014 | Bi_LOG | ,286 | 300 | ,000 |
| Fe2O3_LOG | ,058 | 300 | ,017 | Th_LOG | ,042 | 300 | ,200 |
| Sc_LOG | ,101 | 300 | ,000 | U_LOG | ,136 | 300 | ,000 |
| V_LOG | ,068 | 300 | ,002 | Ag_LOG | ,186 | 300 | ,000 |
| Cr_LOG | ,135 | 300 | ,000 | Cd_LOG | ,100 | 300 | ,000 |
| Co_LOG | ,056 | 300 | ,024 | Sn_LOG | ,073 | 300 | ,001 |
| Ba_LOG | ,123 | 300 | ,000 | Sb_LOG | ,087 | 300 | ,000 |
| Ni_LOG | ,056 | 300 | ,022 | I_LOG | ,255 | 300 | ,000 |
| Cu_LOG | ,061 | 300 | ,010 | La_LOG | ,074 | 300 | ,000 |
| Zn_LOG | ,083 | 300 | ,000 | Ce_LOG | ,044 | 300 | ,200 |
| Ga_LOG | ,047 | 300 | ,200 | Nd_LOG | ,056 | 300 | ,026 |
| Ge_LOG | ,081 | 300 | ,000 | Sm_LOG | ,185 | 300 | ,000 |
| As_LOG | ,079 | 300 | ,000 | OM_LOG | ,057 | 300 | ,019 |
| Se_LOG | ,107 | 300 | ,000 | TC_LOG | ,062 | 150 | ,200 |
| Br_LOG | ,072 | 300 | ,001 | TOC_LOG | ,055 | 91 | ,200 |
| Rb_LOG | ,051 | 300 | ,056 | TIC_LOG | ,103 | 91 | ,018 |
| Sr_LOG | ,100 | 300 | ,000 | pH_LOG | ,116 | 300 | ,000 |

Table 76: Kolmogorov-Smirnov test for Box-Cox-transformed soil data distributions.

| Element | Kolmogorov-Smirnov | | | Element | Kolmogorov-Smirnov | | |
|---|---|---|---|---|---|---|---|
| | Statistic | df | Sig. | | Statistic | df | Sig. |
| Na2O_BC | ,393 | 300 | ,000 | Y_BC | ,045 | 300 | ,200 |
| MgO_BC | ,135 | 300 | ,000 | Zr_BC | ,046 | 300 | ,200 |
| Al2O3_BC | ,034 | 300 | ,200 | Nb_BC | ,054 | 300 | ,037 |
| SiO2_BC | ,036 | 300 | ,200 | Mo_BC | ,077 | 300 | ,000 |
| P2O5_BC | ,054 | 300 | ,032 | Hf_BC | ,065 | 300 | ,004 |
| K2O_BC | ,036 | 300 | ,200 | W_BC | ,082 | 300 | ,000 |
| CaO_BC | ,034 | 300 | ,200 | Tl_BC | ,396 | 300 | ,000 |
| TiO2_BC | ,054 | 300 | ,037 | Pb_BC | ,047 | 300 | ,200 |
| MnO_BC | ,038 | 300 | ,200 | Bi_BC | ,327 | 300 | ,000 |
| Fe2O3_BC | ,050 | 300 | ,066 | Th_BC | ,042 | 300 | ,200 |
| Sc_BC | ,101 | 300 | ,000 | U_BC | ,085 | 300 | ,000 |
| V_BC | ,055 | 300 | ,029 | Ag_BC | ,186 | 300 | ,000 |
| Cr_BC | ,046 | 300 | ,200 | Cd_BC | ,100 | 300 | ,000 |
| Co_BC | ,038 | 300 | ,200 | Sn_BC | ,033 | 300 | ,200 |
| Ba_BC | ,044 | 300 | ,200 | Sb_BC | ,087 | 300 | ,000 |
| Ni_BC | ,056 | 300 | ,022 | I_BC | ,262 | 300 | ,000 |
| Cu_BC | ,061 | 300 | ,010 | La_BC | ,074 | 300 | ,000 |
| Zn_BC | ,050 | 300 | ,066 | Ce_BC | ,044 | 300 | ,200 |
| Ga_BC | ,030 | 300 | ,200 | Nd_BC | ,056 | 300 | ,026 |
| Ge_BC | ,031 | 300 | ,200 | Sm_BC | ,171 | 300 | ,000 |
| As_BC | ,050 | 300 | ,071 | OM_BC | ,046 | 300 | ,200 |
| Se_BC | ,107 | 300 | ,000 | TC_BC | ,336 | 300 | ,000 |
| Br_BC | ,033 | 300 | ,200 | TOC_BC | ,437 | 300 | ,000 |
| Rb_BC | ,038 | 300 | ,200 | TIC_BC | ,424 | 300 | ,000 |
| Sr_BC | ,048 | 300 | ,099 | pH_BC | ,051 | 300 | ,055 |

Table 77: Spearman's rank correlation coefficients for BGS soil data (n=300, n=92 for OC and IC).

| | | Na2O | MgO | Al2O3 | SiO2 | P2O5 | K2O | CaO | TiO2 | MnO | Fe2O3 | Sc | V | Cr | Co | Ba | Ni | Cu | Zn | Ga | @Ge | As | Se | Br | Rb |
|---|---|---|---|---|---|---|---|---|---|---|---|---|---|---|---|---|---|---|---|---|---|---|---|---|---|
| Na2O | CC (ρ) | | ,011 | ,073 | -,132 | ,161 | -,033 | ,175 | ,129 | ,164 | ,126 | ,154 | ,099 | ,168 | ,137 | ,186 | ,139 | ,171 | ,221 | ,102 | ,128 | ,139 | ,124 | ,081 | -,012 |
| | Sig. (2-tailed) | | ,854 | ,206 | ,022 | ,005 | ,575 | ,002 | ,026 | ,004 | ,030 | ,008 | ,086 | ,003 | ,018 | ,001 | ,016 | ,003 | ,000 | ,077 | ,026 | ,016 | ,032 | ,163 | ,836 |
| MgO | CC (ρ) | | | ,628 | -,278 | -,216 | ,692 | ,257 | ,586 | ,256 | ,263 | ,426 | ,304 | ,367 | ,257 | ,157 | ,278 | -,018 | -,007 | ,523 | -,120 | -,071 | -,126 | -,258 | ,632 |
| | Sig. (2-tailed) | | | ,000 | ,000 | ,000 | ,000 | ,000 | ,000 | ,000 | ,000 | ,000 | ,000 | ,000 | ,000 | ,006 | ,000 | ,754 | ,901 | ,000 | ,039 | ,223 | ,029 | ,000 | ,000 |
| Al2O3 | CC (ρ) | | | | -,503 | -,045 | **,787** | ,060 | **,966** | ,454 | ,611 | **,717** | ,660 | ,580 | ,520 | ,445 | ,547 | ,199 | ,182 | **,930** | ,204 | ,258 | ,260 | -,034 | **,880** |
| | Sig. (2-tailed) | | | | ,000 | ,433 | ,000 | ,301 | ,000 | ,000 | ,000 | ,000 | ,000 | ,000 | ,000 | ,000 | ,000 | ,001 | ,002 | ,000 | ,000 | ,000 | ,000 | ,000 | ,563 | ,000 |
| SiO2 | CC (ρ) | | | | | -,349 | -,341 | -,405 | -,544 | -,605 | -,766 | -,778 | -,776 | -,726 | -,696 | -,703 | -,789 | -,607 | -,572 | -,630 | -,534 | -,589 | -,525 | -,321 | -,359 |
| | Sig. (2-tailed) | | | | | ,000 | ,000 | ,000 | ,000 | ,000 | ,000 | ,000 | ,000 | ,000 | ,000 | ,000 | ,000 | ,000 | ,000 | ,000 | ,000 | ,000 | ,000 | ,000 | ,000 |
| P2O5 | CC (ρ) | | | | | | -,239 | -,018 | ,042 | ,257 | ,316 | ,218 | ,325 | ,304 | ,307 | ,395 | ,323 | ,473 | ,484 | ,103 | ,596 | ,583 | ,610 | ,644 | -,153 |
| | Sig. (2-tailed) | | | | | | ,000 | ,753 | ,469 | ,000 | ,000 | ,000 | ,000 | ,000 | ,000 | ,000 | ,000 | ,000 | ,000 | ,076 | ,000 | ,000 | ,000 | ,000 | ,008 |
| K2O | CC (ρ) | | | | | | | ,182 | **,731** | ,344 | ,400 | ,506 | ,412 | ,435 | ,340 | ,355 | ,376 | ,063 | ,081 | ,692 | -,029 | ,052 | -,014 | -,256 | **,944** |
| | Sig. (2-tailed) | | | | | | | ,002 | ,000 | ,000 | ,000 | ,000 | ,000 | ,000 | ,000 | ,000 | ,000 | ,275 | ,163 | ,000 | ,617 | ,368 | ,808 | ,000 | ,000 |
| CaO | CC (ρ) | | | | | | | | ,043 | ,337 | ,281 | ,358 | ,202 | ,308 | ,306 | ,345 | ,373 | ,319 | ,377 | ,128 | ,061 | ,072 | -,007 | -,147 | ,082 |
| | Sig. (2-tailed) | | | | | | | | ,458 | ,000 | ,000 | ,000 | ,000 | ,000 | ,000 | ,000 | ,000 | ,000 | ,000 | ,026 | ,294 | ,214 | ,897 | ,011 | ,159 |
| TiO2 | CC (ρ) | | | | | | | | | ,441 | ,616 | **,729** | ,684 | ,586 | ,524 | ,475 | ,555 | ,229 | ,204 | **,920** | ,266 | ,299 | ,333 | ,080 | **,837** |
| | Sig. (2-tailed) | | | | | | | | | ,000 | ,000 | ,000 | ,000 | ,000 | ,000 | ,000 | ,000 | ,000 | ,000 | ,000 | ,000 | ,000 | ,000 | ,166 | ,000 |
| MnO | CC (ρ) | | | | | | | | | | **,742** | ,618 | ,662 | ,665 | ,678 | ,581 | **,711** | ,539 | ,535 | ,548 | ,448 | ,511 | ,406 | ,183 | ,394 |
| | Sig. (2-tailed) | | | | | | | | | | ,000 | ,000 | ,000 | ,000 | ,000 | ,000 | ,000 | ,000 | ,000 | ,000 | ,000 | ,000 | ,000 | ,001 | ,000 |
| Fe2O3 | CC (ρ) | | | | | | | | | | | **,840** | **,888** | **,732** | **,869** | **,777** | **,911** | ,697 | ,605 | **,776** | ,691 | **,743** | ,646 | ,294 | ,494 |
| | Sig. (2-tailed) | | | | | | | | | | | ,000 | ,000 | ,000 | ,000 | ,000 | ,000 | ,000 | ,000 | ,000 | ,000 | ,000 | ,000 | ,000 | ,000 |
| Sc | CC (ρ) | | | | | | | | | | | | **,870** | ,691 | **,798** | **,703** | **,850** | ,537 | ,482 | **,831** | ,595 | ,592 | ,563 | ,240 | ,576 |
| | Sig. (2-tailed) | | | | | | | | | | | | ,000 | ,000 | ,000 | ,000 | ,000 | ,000 | ,000 | ,000 | ,000 | ,000 | ,000 | ,000 | ,000 |
| V | CC (ρ) | | | | | | | | | | | | | **,753** | **,829** | **,767** | **,896** | ,645 | ,566 | **,812** | **,718** | **,723** | ,683 | ,409 | ,515 |
| | Sig. (2-tailed) | | | | | | | | | | | | | ,000 | ,000 | ,000 | ,000 | ,000 | ,000 | ,000 | ,000 | ,000 | ,000 | ,000 | ,000 |
| Cr | CC (ρ) | | | | | | | | | | | | | | ,674 | **,722** | **,775** | ,624 | ,613 | ,667 | ,443 | ,594 | ,469 | ,215 | ,474 |
| | Sig. (2-tailed) | | | | | | | | | | | | | | ,000 | ,000 | ,000 | ,000 | ,000 | ,000 | ,000 | ,000 | ,000 | ,000 | ,000 |
| Co | CC (ρ) | | | | | | | | | | | | | | | **,742** | **,890** | ,676 | ,602 | ,673 | ,690 | ,694 | ,607 | ,290 | ,412 |
| | Sig. (2-tailed) | | | | | | | | | | | | | | | ,000 | ,000 | ,000 | ,000 | ,000 | ,000 | ,000 | ,000 | ,000 | ,000 |
| Ba | CC (ρ) | | | | | | | | | | | | | | | | **,838** | **,783** | **,782** | ,604 | ,661 | **,721** | ,646 | ,342 | ,386 |
| | Sig. (2-tailed) | | | | | | | | | | | | | | | | ,000 | ,000 | ,000 | ,000 | ,000 | ,000 | ,000 | ,000 | ,000 |
| Ni | CC (ρ) | | | | | | | | | | | | | | | | | **,761** | ,695 | **,710** | **,706** | **,724** | ,627 | ,323 | ,432 |
| | Sig. (2-tailed) | | | | | | | | | | | | | | | | | ,000 | ,000 | ,000 | ,000 | ,000 | ,000 | ,000 | ,000 |
| Cu | CC (ρ) | | | | | | | | | | | | | | | | | | **,852** | ,367 | ,697 | **,760** | ,643 | ,425 | ,103 |
| | Sig. (2-tailed) | | | | | | | | | | | | | | | | | | ,000 | ,000 | ,000 | ,000 | ,000 | ,000 | ,075 |
| Zn | CC (ρ) | | | | | | | | | | | | | | | | | | | ,327 | ,602 | ,682 | ,540 | ,361 | ,109 |
| | Sig. (2-tailed) | | | | | | | | | | | | | | | | | | | ,000 | ,000 | ,000 | ,000 | ,000 | ,059 |
| Ga | CC (ρ) | | | | | | | | | | | | | | | | | | | | ,426 | ,463 | ,462 | ,144 | **,804** |
| | Sig. (2-tailed) | | | | | | | | | | | | | | | | | | | | ,000 | ,000 | ,000 | ,012 | ,000 |
| @Ge | CC (ρ) | | | | | | | | | | | | | | | | | | | | | **,848** | **,837** | ,671 | ,079 |
| | Sig. (2-tailed) | | | | | | | | | | | | | | | | | | | | | ,000 | ,000 | ,000 | ,175 |
| As | CC (ρ) | | | | | | | | | | | | | | | | | | | | | | **,827** | ,600 | ,136 |
| | Sig. (2-tailed) | | | | | | | | | | | | | | | | | | | | | | ,000 | ,000 | ,018 |
| Se | CC (ρ) | | | | | | | | | | | | | | | | | | | | | | | ,687 | ,115 |
| | Sig. (2-tailed) | | | | | | | | | | | | | | | | | | | | | | | ,000 | ,047 |
| Br | CC (ρ) | | | | | | | | | | | | | | | | | | | | | | | | -,171 |
| | Sig. (2-tailed) | | | | | | | | | | | | | | | | | | | | | | | | ,003 |
| Rb | CC (ρ) | | | | | | | | | | | | | | | | | | | | | | | | |
| | Sig. (2-tailed) | | | | | | | | | | | | | | | | | | | | | | | | |

| | | Sr | Y | Zr | Nb | Mo | Hf | W | Tl | Pb | Bi | Th | U | Ag | Cd | Sn | Sb | I | La | Ce | Nd | Sm | OM (LOI) | TC | TOC | TIC | pH |
|---|---|---|---|---|---|---|---|---|---|---|---|---|---|---|---|---|---|---|---|---|---|---|---|---|---|---|---|
| Na2O | CC (ρ) | ,160 | ,201 | ,252 | ,146 | ,098 | ,228 | ,099 | ,115 | ,280 | ,102 | ,168 | ,043 | ,183 | ,173 | ,206 | ,167 | -,055 | ,098 | ,151 | ,107 | ,100 | ,047 | ,021 | ,073 | -,015 | ,079 |
| | Sig. (2-tailed) | ,005 | ,000 | ,000 | ,011 | ,090 | ,000 | ,086 | ,047 | ,000 | ,077 | ,003 | ,457 | ,001 | ,003 | ,000 | ,004 | ,340 | ,091 | ,009 | ,064 | ,084 | ,413 | ,796 | ,489 | ,889 | ,172 |
| MgO | CC (ρ) | ,362 | ,419 | ,309 | ,576 | -,139 | ,263 | ,129 | -,002 | -,107 | -,013 | ,490 | ,257 | -,015 | ,020 | -,090 | -,117 | -,191 | ,411 | ,431 | ,398 | ,173 | -,093 | -,208 | -,101 | -,122 | ,319 |
| | Sig. (2-tailed) | ,000 | ,000 | ,000 | ,000 | ,016 | ,000 | ,026 | ,976 | ,064 | ,828 | ,000 | ,000 | ,799 | ,728 | ,121 | ,043 | ,001 | ,000 | ,000 | ,000 | ,003 | ,108 | ,011 | ,342 | ,247 | ,000 |
| Al2O3 | CC (ρ) | ,540 | **,792** | ,607 | **,941** | ,192 | ,463 | ,244 | ,123 | ,083 | ,100 | **,846** | ,629 | ,139 | ,190 | ,101 | ,120 | -,201 | **,807** | **,842** | **,770** | ,253 | ,145 | ,031 | ,114 | ,106 | ,049 |
| | Sig. (2-tailed) | ,000 | ,000 | ,000 | ,000 | ,001 | ,000 | ,000 | ,034 | ,151 | ,085 | ,000 | ,000 | ,016 | ,001 | ,081 | ,037 | ,000 | ,000 | ,000 | ,000 | ,000 | ,012 | ,709 | ,281 | ,317 | ,402 |
| SiO2 | CC (ρ) | -,690 | -,715 | -,063 | -,528 | -,584 | -,207 | -,367 | -,368 | -,452 | -,231 | -,663 | -,314 | -,435 | -,490 | -,461 | -,504 | ,317 | -,679 | -,701 | -,644 | -,203 | -,557 | -,642 | -,777 | -,451 | -,069 |
| | Sig. (2-tailed) | ,000 | ,000 | ,277 | ,000 | ,000 | ,000 | ,000 | ,000 | ,000 | ,000 | ,000 | ,000 | ,000 | ,000 | ,000 | ,000 | ,000 | ,000 | ,000 | ,000 | ,000 | ,000 | ,000 | ,000 | ,000 | ,232 |
| P2O5 | CC (ρ) | ,096 | ,201 | -,120 | -,011 | ,483 | ,025 | ,224 | ,341 | ,535 | ,347 | ,133 | ,024 | ,538 | ,511 | ,488 | ,481 | ,140 | ,201 | ,140 | ,139 | -,018 | ,633 | ,542 | ,477 | ,395 | -,377 |
| | Sig. (2-tailed) | ,096 | ,000 | ,038 | ,847 | ,000 | ,670 | ,000 | ,000 | ,000 | ,000 | ,021 | ,679 | ,000 | ,000 | ,000 | ,000 | ,015 | ,000 | ,015 | ,016 | ,753 | ,000 | ,000 | ,000 | ,000 | ,000 |
| K2O | CC (ρ) | ,532 | ,574 | ,435 | **,733** | -,005 | ,325 | ,165 | ,021 | -,039 | ,007 | ,650 | ,435 | ,037 | ,079 | -,035 | ,009 | -,264 | ,544 | ,578 | ,530 | ,158 | -,092 | -,142 | ,026 | -,125 | ,274 |
| | Sig. (2-tailed) | ,000 | ,000 | ,000 | ,000 | ,934 | ,000 | ,004 | ,722 | ,496 | ,900 | ,000 | ,000 | ,528 | ,174 | ,546 | ,879 | ,000 | ,000 | ,000 | ,000 | ,006 | ,113 | ,082 | ,808 | ,238 | ,000 |
| CaO | CC (ρ) | ,620 | ,243 | -,138 | ,120 | ,153 | -,018 | ,083 | ,106 | ,307 | ,066 | ,226 | -,001 | ,246 | ,227 | ,236 | ,243 | -,364 | ,110 | ,167 | ,163 | ,064 | ,089 | ,129 | ,336 | ,006 | **,796** |
| | Sig. (2-tailed) | ,000 | ,000 | ,017 | ,038 | ,008 | ,751 | ,150 | ,068 | ,000 | ,254 | ,000 | ,991 | ,000 | ,000 | ,000 | ,000 | ,000 | ,056 | ,004 | ,005 | ,269 | ,124 | ,116 | ,001 | ,954 | ,000 |
| TiO2 | CC (ρ) | ,526 | **,807** | ,647 | **,959** | ,233 | ,503 | ,283 | ,167 | ,126 | ,125 | **,850** | ,655 | ,186 | ,229 | ,126 | ,142 | -,116 | **,822** | **,855** | **,779** | ,244 | ,254 | ,122 | ,174 | ,169 | -,024 |
| | Sig. (2-tailed) | ,000 | ,000 | ,000 | ,000 | ,000 | ,000 | ,000 | ,004 | ,029 | ,031 | ,000 | ,000 | ,001 | ,000 | ,030 | ,014 | ,045 | ,000 | ,000 | ,000 | ,000 | ,000 | ,137 | ,099 | ,109 | ,675 |
| MnO | CC (ρ) | ,601 | ,611 | ,134 | ,480 | ,534 | ,191 | ,307 | ,236 | ,388 | ,225 | ,574 | ,296 | ,394 | ,409 | ,413 | ,441 | -,308 | ,544 | ,571 | ,541 | ,221 | ,296 | ,350 | ,526 | ,103 | ,126 |
| | Sig. (2-tailed) | ,000 | ,000 | ,020 | ,000 | ,000 | ,001 | ,000 | ,000 | ,000 | ,000 | ,000 | ,000 | ,000 | ,000 | ,000 | ,000 | ,000 | ,000 | ,000 | ,000 | ,000 | ,000 | ,000 | ,000 | ,330 | ,029 |
| Fe2O3 | CC (ρ) | **,761** | **,875** | ,169 | ,655 | **,741** | ,250 | ,283 | ,406 | ,551 | ,259 | **,801** | ,428 | ,529 | ,525 | ,570 | ,579 | -,473 | **,793** | **,815** | **,752** | ,279 | ,460 | ,672 | **,764** | ,297 | ,027 |
| | Sig. (2-tailed) | ,000 | ,000 | ,003 | ,000 | ,000 | ,000 | ,000 | ,000 | ,000 | ,000 | ,000 | ,000 | ,000 | ,000 | ,000 | ,000 | ,000 | ,000 | ,000 | ,000 | ,000 | ,000 | ,000 | ,000 | ,004 | ,642 |
| Sc | CC (ρ) | **,795** | **,900** | ,246 | **,755** | ,585 | ,315 | ,322 | ,341 | ,432 | ,195 | **,834** | ,519 | ,446 | ,439 | ,405 | ,455 | -,346 | **,844** | **,867** | **,804** | ,307 | ,446 | ,563 | **,718** | ,336 | ,105 |
| | Sig. (2-tailed) | ,000 | ,000 | ,000 | ,000 | ,000 | ,000 | ,000 | ,000 | ,000 | ,001 | ,000 | ,000 | ,000 | ,000 | ,000 | ,000 | ,000 | ,000 | ,000 | ,000 | ,000 | ,000 | ,000 | ,000 | ,001 | ,070 |
| V | CC (ρ) | **,736** | **,887** | ,165 | **,710** | **,717** | ,277 | ,434 | ,433 | ,501 | ,193 | **,819** | ,489 | ,450 | ,470 | ,488 | ,579 | -,358 | **,849** | **,854** | **,781** | ,261 | ,536 | ,682 | **,778** | ,339 | -,078 |
| | Sig. (2-tailed) | ,000 | ,000 | ,004 | ,000 | ,000 | ,000 | ,000 | ,000 | ,000 | ,001 | ,000 | ,000 | ,000 | ,000 | ,000 | ,000 | ,000 | ,000 | ,000 | ,000 | ,000 | ,000 | ,000 | ,000 | ,001 | ,177 |
| Cr | CC (ρ) | ,689 | **,716** | ,217 | ,611 | ,514 | ,310 | ,479 | ,325 | ,443 | ,322 | **,716** | ,347 | ,494 | ,566 | ,443 | ,515 | -,357 | ,658 | ,691 | ,615 | ,179 | ,386 | ,378 | ,575 | ,230 | ,088 |
| | Sig. (2-tailed) | ,000 | ,000 | ,000 | ,000 | ,000 | ,000 | ,000 | ,000 | ,000 | ,000 | ,000 | ,000 | ,000 | ,000 | ,000 | ,000 | ,000 | ,000 | ,000 | ,000 | ,002 | ,000 | ,000 | ,000 | ,028 | ,128 |
| Co | CC (ρ) | **,756** | **,810** | ,080 | ,571 | **,713** | ,194 | ,346 | ,397 | ,544 | ,250 | **,724** | ,368 | ,506 | ,508 | ,522 | ,566 | -,438 | **,722** | **,744** | **,712** | ,262 | ,432 | ,648 | **,778** | ,276 | ,041 |
| | Sig. (2-tailed) | ,000 | ,000 | ,167 | ,000 | ,000 | ,001 | ,000 | ,000 | ,000 | ,000 | ,000 | ,000 | ,000 | ,000 | ,000 | ,000 | ,000 | ,000 | ,000 | ,000 | ,000 | ,000 | ,000 | ,000 | ,008 | ,479 |
| Ba | CC (ρ) | **,781** | **,758** | ,081 | ,509 | ,667 | ,222 | ,369 | ,511 | ,688 | ,363 | ,670 | ,294 | ,633 | ,674 | ,643 | ,697 | -,438 | ,637 | ,662 | ,607 | ,201 | ,504 | ,611 | **,701** | ,300 | ,046 |
| | Sig. (2-tailed) | ,000 | ,000 | ,162 | ,000 | ,000 | ,000 | ,000 | ,000 | ,000 | ,000 | ,000 | ,000 | ,000 | ,000 | ,000 | ,000 | ,000 | ,000 | ,000 | ,000 | ,000 | ,000 | ,000 | ,000 | ,004 | ,425 |
| Ni | CC (ρ) | **,841** | **,853** | ,064 | ,600 | **,748** | ,233 | ,419 | ,433 | ,598 | ,282 | **,772** | ,372 | ,554 | ,582 | ,592 | ,626 | -,509 | **,771** | **,786** | **,718** | ,242 | ,494 | ,693 | **,820** | ,272 | ,087 |
| | Sig. (2-tailed) | ,000 | ,000 | ,267 | ,000 | ,000 | ,000 | ,000 | ,000 | ,000 | ,000 | ,000 | ,000 | ,000 | ,000 | ,000 | ,000 | ,000 | ,000 | ,000 | ,000 | ,000 | ,000 | ,000 | ,000 | ,009 | ,132 |
| Cu | CC (ρ) | ,621 | ,568 | -,097 | ,267 | **,734** | ,117 | ,406 | ,431 | **,743** | ,361 | ,473 | ,149 | ,645 | **,712** | **,836** | **,746** | -,411 | ,457 | ,479 | ,405 | ,148 | ,545 | ,586 | ,661 | ,283 | ,002 |
| | Sig. (2-tailed) | ,000 | ,000 | ,092 | ,000 | ,000 | ,042 | ,000 | ,000 | ,000 | ,000 | ,000 | ,010 | ,000 | ,000 | ,000 | ,000 | ,000 | ,000 | ,000 | ,000 | ,010 | ,000 | ,000 | ,000 | ,007 | ,969 |
| Zn | CC (ρ) | ,600 | ,496 | -,079 | ,236 | ,638 | ,127 | ,334 | ,406 | **,757** | ,386 | ,427 | ,077 | ,640 | **,772** | **,779** | **,763** | -,361 | ,399 | ,411 | ,329 | ,093 | ,497 | ,402 | ,502 | ,086 | ,075 |
| | Sig. (2-tailed) | ,000 | ,000 | ,171 | ,000 | ,000 | ,028 | ,000 | ,000 | ,000 | ,000 | ,000 | ,185 | ,000 | ,000 | ,000 | ,000 | ,000 | ,000 | ,000 | ,000 | ,109 | ,000 | ,000 | ,000 | ,418 | ,195 |
| Ga | CC (ρ) | ,660 | **,898** | ,481 | **,917** | ,408 | ,412 | ,301 | ,257 | ,271 | ,173 | **,904** | ,627 | ,291 | ,312 | ,253 | ,297 | -,261 | **,886** | **,919** | **,837** | ,299 | ,315 | ,303 | ,414 | ,217 | ,000 |
| | Sig. (2-tailed) | ,000 | ,000 | ,000 | ,000 | ,000 | ,000 | ,000 | ,000 | ,000 | ,003 | ,000 | ,000 | ,000 | ,000 | ,000 | ,000 | ,000 | ,000 | ,000 | ,000 | ,000 | ,000 | ,000 | ,000 | ,039 | ,995 |
| Ge | CC (ρ) | ,456 | ,598 | -,103 | ,286 | **,829** | ,058 | ,270 | ,510 | ,671 | ,293 | ,451 | ,262 | ,550 | ,533 | ,632 | ,691 | -,215 | ,535 | ,505 | ,462 | ,171 | ,660 | **,777** | **,824** | ,385 | -,310 |
| | Sig. (2-tailed) | ,000 | ,000 | ,074 | ,000 | ,000 | ,320 | ,000 | ,000 | ,000 | ,000 | ,000 | ,000 | ,000 | ,000 | ,000 | ,000 | ,000 | ,000 | ,000 | ,000 | ,003 | ,000 | ,000 | ,000 | ,000 | ,000 |
| As | CC (ρ) | ,511 | ,632 | -,014 | ,323 | **,804** | ,133 | ,293 | ,500 | ,649 | ,344 | ,514 | ,259 | ,590 | ,630 | ,681 | **,707** | -,247 | ,528 | ,535 | ,447 | ,182 | ,596 | ,679 | **,783** | ,370 | -,276 |
| | Sig. (2-tailed) | ,000 | ,000 | ,812 | ,000 | ,000 | ,022 | ,000 | ,000 | ,000 | ,000 | ,000 | ,000 | ,000 | ,000 | ,000 | ,000 | ,000 | ,000 | ,000 | ,000 | ,002 | ,000 | ,000 | ,000 | ,000 | ,000 |
| Se | CC (ρ) | ,416 | ,589 | ,023 | ,328 | **,732** | ,127 | ,230 | ,540 | ,609 | ,390 | ,456 | ,317 | ,572 | ,579 | ,540 | ,619 | -,086 | ,514 | ,519 | ,454 | ,175 | ,670 | **,712** | **,768** | ,527 | -,369 |
| | Sig. (2-tailed) | ,000 | ,000 | ,695 | ,000 | ,000 | ,028 | ,000 | ,000 | ,000 | ,000 | ,000 | ,000 | ,000 | ,000 | ,000 | ,000 | ,137 | ,000 | ,000 | ,000 | ,002 | ,000 | ,000 | ,000 | ,000 | ,000 |
| Br | CC (ρ) | ,051 | ,237 | -,108 | ,043 | ,534 | ,036 | ,268 | ,421 | ,481 | ,248 | ,133 | ,141 | ,348 | ,390 | ,395 | ,415 | ,263 | ,232 | ,216 | ,178 | ,035 | **,765** | ,652 | ,695 | ,464 | -,538 |
| | Sig. (2-tailed) | ,374 | ,000 | ,062 | ,460 | ,000 | ,540 | ,000 | ,000 | ,000 | ,000 | ,022 | ,015 | ,000 | ,000 | ,000 | ,000 | ,000 | ,000 | ,000 | ,002 | ,545 | ,000 | ,000 | ,000 | ,000 | ,000 |
| Rb | CC (ρ) | ,536 | ,663 | ,528 | **,835** | ,084 | ,377 | ,180 | ,058 | ,025 | ,047 | **,746** | ,527 | ,077 | ,110 | ,003 | ,059 | -,211 | ,654 | ,681 | ,621 | ,184 | -,035 | -,106 | ,005 | -,045 | ,155 |
| | Sig. (2-tailed) | ,000 | ,000 | ,000 | ,000 | ,146 | ,000 | ,002 | ,315 | ,672 | ,422 | ,000 | ,000 | ,183 | ,057 | ,958 | ,306 | ,000 | ,000 | ,000 | ,000 | ,001 | ,546 | ,198 | ,964 | ,669 | ,007 |

| | | Sr | Y | Zr | Nb | Mo | Hf | W | Tl | Pb | Bi | Th | U | Ag | Cd | Sn | Sb | I | La | Ce | Nd | Sm | OM (LOI) | TC | TOC | TIC | pH |
|---|---|---|---|---|---|---|---|---|---|---|---|---|---|---|---|---|---|---|---|---|---|---|---|---|---|---|---|
| Sr | CC (ρ) | | **,803** | ,122 | ,613 | ,552 | ,251 | ,311 | ,350 | ,483 | ,190 | **,748** | ,372 | ,488 | ,484 | ,443 | ,527 | -,563 | ,675 | **,712** | ,640 | ,227 | ,257 | ,454 | ,688 | ,213 | ,395 |
| | Sig. (2-tailed) | | ,000 | ,035 | ,000 | ,000 | ,000 | ,000 | ,000 | ,000 | ,001 | ,000 | ,000 | ,000 | ,000 | ,000 | ,000 | ,000 | ,000 | ,000 | ,000 | ,000 | ,000 | ,000 | ,000 | ,042 | ,000 |
| Y | CC (ρ) | | | ,382 | **,843** | ,582 | ,383 | ,314 | ,383 | ,440 | ,224 | **,924** | ,564 | ,450 | ,450 | ,416 | ,459 | -,384 | **,894** | **,930** | **,846** | ,318 | ,409 | ,541 | ,654 | ,309 | ,033 |
| | Sig. (2-tailed) | | | ,000 | ,000 | ,000 | ,000 | ,000 | ,000 | ,000 | ,000 | ,000 | ,000 | ,000 | ,000 | ,000 | ,000 | ,000 | ,000 | ,000 | ,000 | ,000 | ,000 | ,000 | ,000 | ,003 | ,566 |
| Zr | CC (ρ) | | | | ,629 | -,121 | ,591 | -,001 | -,082 | -,101 | ,029 | ,449 | ,449 | -,033 | -,014 | -,133 | -,146 | ,129 | ,366 | ,427 | ,356 | ,160 | -,085 | -,290 | -,355 | ,006 | -,041 |
| | Sig. (2-tailed) | | | | ,000 | ,036 | ,000 | ,988 | ,155 | ,081 | ,619 | ,000 | ,000 | ,573 | ,815 | ,021 | ,011 | ,025 | ,000 | ,000 | ,000 | ,006 | ,144 | ,000 | ,001 | ,958 | ,482 |
| Nb | CC (ρ) | | | | | ,275 | ,505 | ,278 | ,162 | ,142 | ,118 | **,882** | ,652 | ,209 | ,238 | ,141 | ,183 | -,204 | **,828** | **,870** | **,785** | ,278 | ,200 | ,153 | ,252 | ,150 | ,046 |
| | Sig. (2-tailed) | | | | | ,000 | ,000 | ,000 | ,005 | ,014 | ,042 | ,000 | ,000 | ,000 | ,000 | ,014 | ,002 | ,000 | ,000 | ,000 | ,000 | ,000 | ,000 | ,061 | ,016 | ,156 | ,430 |
| Mo | CC (ρ) | | | | | | ,076 | ,343 | ,472 | ,632 | ,240 | ,461 | ,255 | ,559 | ,546 | ,629 | ,682 | -,302 | ,531 | ,502 | ,454 | ,161 | ,609 | **,772** | **,821** | ,357 | -,190 |
| | Sig. (2-tailed) | | | | | | ,191 | ,000 | ,000 | ,000 | ,000 | ,000 | ,000 | ,000 | ,000 | ,000 | ,000 | ,000 | ,000 | ,000 | ,000 | ,005 | ,000 | ,000 | ,000 | ,001 | ,001 |
| Hf | CC (ρ) | | | | | | | ,119 | -,018 | ,030 | -,005 | ,423 | ,313 | ,128 | ,158 | ,092 | ,077 | ,008 | ,370 | ,398 | ,310 | ,103 | ,131 | -,030 | -,061 | -,048 | -,062 |
| | Sig. (2-tailed) | | | | | | | ,039 | ,751 | ,599 | ,926 | ,000 | ,000 | ,026 | ,006 | ,111 | ,185 | ,891 | ,000 | ,000 | ,000 | ,074 | ,023 | ,716 | ,565 | ,650 | ,283 |
| W | CC (ρ) | | | | | | | | ,210 | ,262 | ,092 | ,335 | ,249 | ,251 | ,263 | ,273 | ,318 | -,099 | ,337 | ,321 | ,314 | ,046 | ,353 | ,278 | ,374 | ,161 | -,099 |
| | Sig. (2-tailed) | | | | | | | | ,000 | ,000 | ,112 | ,000 | ,000 | ,000 | ,000 | ,000 | ,000 | ,086 | ,000 | ,000 | ,000 | ,424 | ,000 | ,001 | ,000 | ,127 | ,088 |
| Tl | CC (ρ) | | | | | | | | | ,548 | ,301 | ,300 | ,031 | ,404 | ,420 | ,402 | ,440 | -,196 | ,299 | ,302 | ,242 | ,075 | ,388 | ,425 | ,460 | ,323 | -,146 |
| | Sig. (2-tailed) | | | | | | | | | ,000 | ,000 | ,000 | ,595 | ,000 | ,000 | ,000 | ,000 | ,001 | ,000 | ,000 | ,000 | ,195 | ,000 | ,000 | ,000 | ,002 | ,011 |
| Pb | CC (ρ) | | | | | | | | | | ,367 | ,362 | -,003 | ,609 | ,647 | **,768** | **,728** | -,277 | ,316 | ,330 | ,260 | ,074 | ,523 | ,438 | ,484 | ,135 | -,008 |
| | Sig. (2-tailed) | | | | | | | | | | ,000 | ,000 | ,952 | ,000 | ,000 | ,000 | ,000 | ,000 | ,000 | ,000 | ,000 | ,202 | ,000 | ,000 | ,000 | ,202 | ,889 |
| Bi | CC (ρ) | | | | | | | | | | | ,163 | -,011 | ,477 | ,491 | ,348 | ,345 | -,098 | ,156 | ,178 | ,187 | ,037 | ,217 | ,155 | ,239 | ,322 | -,100 |
| | Sig. (2-tailed) | | | | | | | | | | | ,005 | ,851 | ,000 | ,000 | ,000 | ,000 | ,091 | ,007 | ,002 | ,001 | ,525 | ,000 | ,060 | ,022 | ,002 | ,086 |
| Th | CC (ρ) | | | | | | | | | | | | ,571 | ,373 | ,379 | ,337 | ,371 | -,368 | **,867** | **,914** | **,819** | ,291 | ,312 | ,359 | ,440 | ,212 | ,072 |
| | Sig. (2-tailed) | | | | | | | | | | | | ,000 | ,000 | ,000 | ,000 | ,000 | ,000 | ,000 | ,000 | ,000 | ,000 | ,000 | ,000 | ,000 | ,044 | ,212 |
| U | CC (ρ) | | | | | | | | | | | | | ,121 | ,125 | ,047 | ,092 | ,011 | ,604 | ,589 | ,562 | ,204 | ,268 | ,338 | ,373 | ,388 | -,129 |
| | Sig. (2-tailed) | | | | | | | | | | | | | ,037 | ,031 | ,415 | ,112 | ,851 | ,000 | ,000 | ,000 | ,000 | ,000 | ,000 | ,000 | ,000 | ,026 |
| Ag | CC (ρ) | | | | | | | | | | | | | | **,716** | ,611 | ,613 | -,229 | ,337 | ,364 | ,342 | ,099 | ,451 | ,491 | ,550 | ,385 | -,046 |
| | Sig. (2-tailed) | | | | | | | | | | | | | | ,000 | ,000 | ,000 | ,000 | ,000 | ,000 | ,000 | ,087 | ,000 | ,000 | ,000 | ,000 | ,432 |
| Cd | CC (ρ) | | | | | | | | | | | | | | | ,669 | ,603 | -,229 | ,377 | ,379 | ,329 | ,050 | ,490 | ,394 | ,550 | ,251 | -,056 |
| | Sig. (2-tailed) | | | | | | | | | | | | | | | ,000 | ,000 | ,000 | ,000 | ,000 | ,000 | ,389 | ,000 | ,000 | ,000 | ,016 | ,337 |
| Sn | CC (ρ) | | | | | | | | | | | | | | | | **,719** | -,354 | ,322 | ,346 | ,286 | ,106 | ,497 | ,479 | ,554 | ,319 | -,059 |
| | Sig. (2-tailed) | | | | | | | | | | | | | | | | ,000 | ,000 | ,000 | ,000 | ,000 | ,068 | ,000 | ,000 | ,000 | ,002 | ,309 |
| Sb | CC (ρ) | | | | | | | | | | | | | | | | | -,331 | ,364 | ,364 | ,305 | ,051 | ,502 | ,543 | ,631 | ,302 | -,082 |
| | Sig. (2-tailed) | | | | | | | | | | | | | | | | | ,000 | ,000 | ,000 | ,000 | ,382 | ,000 | ,000 | ,000 | ,004 | ,158 |
| I | CC (ρ) | | | | | | | | | | | | | | | | | | -,283 | -,307 | -,284 | -,145 | ,121 | -,134 | -,260 | ,089 | -,364 |
| | Sig. (2-tailed) | | | | | | | | | | | | | | | | | | ,000 | ,000 | ,000 | ,012 | ,036 | ,102 | ,013 | ,399 | ,000 |
| La | CC (ρ) | | | | | | | | | | | | | | | | | | | **,912** | **,832** | ,309 | ,411 | ,474 | ,571 | ,307 | -,066 |
| | Sig. (2-tailed) | | | | | | | | | | | | | | | | | | | ,000 | ,000 | ,000 | ,000 | ,000 | ,000 | ,003 | ,256 |
| Ce | CC (ρ) | | | | | | | | | | | | | | | | | | | | **,854** | ,439 | ,394 | ,430 | ,556 | ,354 | -,009 |
| | Sig. (2-tailed) | | | | | | | | | | | | | | | | | | | | ,000 | ,000 | ,000 | ,000 | ,000 | ,001 | ,877 |
| Nd | CC (ρ) | | | | | | | | | | | | | | | | | | | | | ,300 | ,361 | ,479 | ,609 | ,404 | ,001 |
| | Sig. (2-tailed) | | | | | | | | | | | | | | | | | | | | | ,000 | ,000 | ,000 | ,000 | ,000 | ,989 |
| Sm | CC (ρ) | | | | | | | | | | | | | | | | | | | | | | ,035 | ,044 | ,141 | ,106 | ,020 |
| | Sig. (2-tailed) | | | | | | | | | | | | | | | | | | | | | | ,547 | ,595 | ,182 | ,315 | ,729 |
| OM (LOI) | CC (ρ) | | | | | | | | | | | | | | | | | | | | | | | **,898** | **,868** | ,589 | -,346 |
| | Sig. (2-tailed) | | | | | | | | | | | | | | | | | | | | | | | ,000 | ,000 | ,000 | ,000 |
| TC | CC (ρ) | | | | | | | | | | | | | | | | | | | | | | | | **,986** | ,520 | -,276 |
| | Sig. (2-tailed) | | | | | | | | | | | | | | | | | | | | | | | | ,000 | ,000 | ,001 |
| TOC | CC (ρ) | | | | | | | | | | | | | | | | | | | | | | | | | ,414 | -,165 |
| | Sig. (2-tailed) | | | | | | | | | | | | | | | | | | | | | | | | | ,000 | ,119 |
| TIC | CC (ρ) | | | | | | | | | | | | | | | | | | | | | | | | | | -,346 |
| | Sig. (2-tailed) | | | | | | | | | | | | | | | | | | | | | | | | | | ,001 |
| pH | CC (ρ) | | | | | | | | | | | | | | | | | | | | | | | | | | |
| | Sig. (2-tailed) | | | | | | | | | | | | | | | | | | | | | | | | | | |

Figure 100: Cr concentrations in soil according to land use, black line: residential SGV; red line: Allotment SGV (EA, 2002).

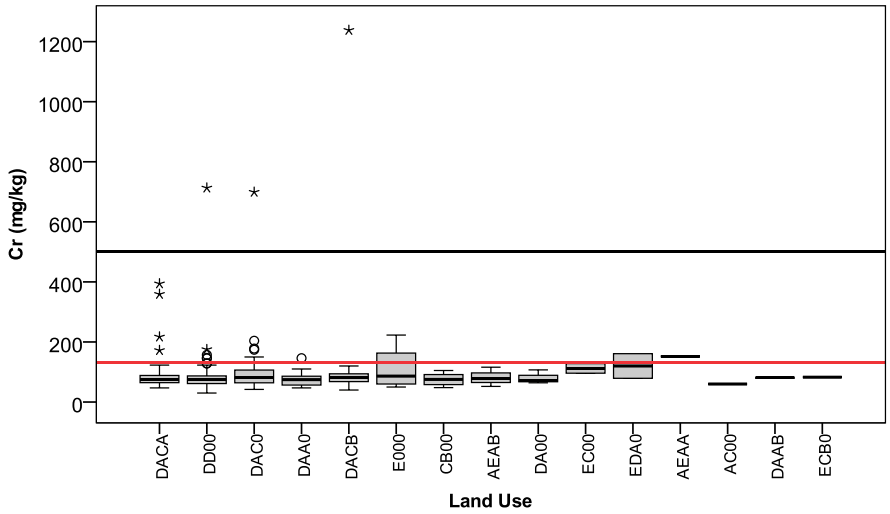


Figure 101: Ni concentrations in soil according to land use, black line: residential SGV (EA, 2009d).

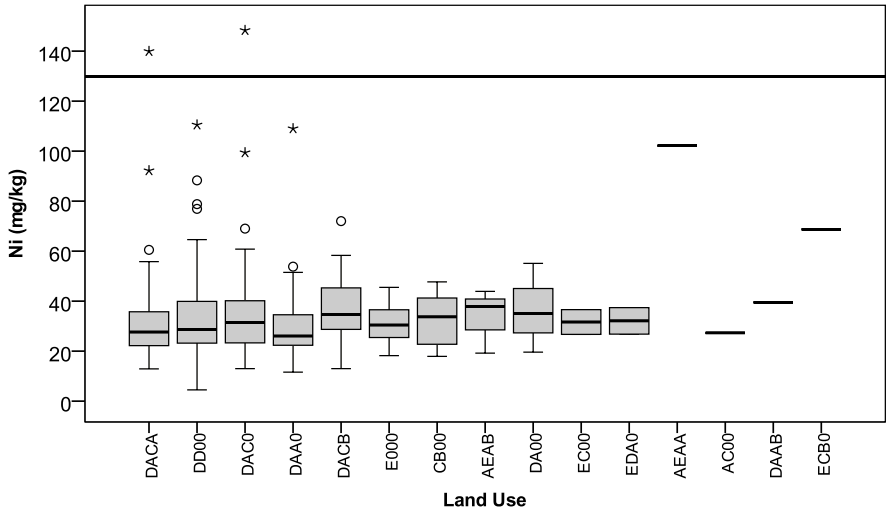


Figure 102: Cu concentrations in soil according to land use, green line: proposed UK ecological guideline (EA, 2008).

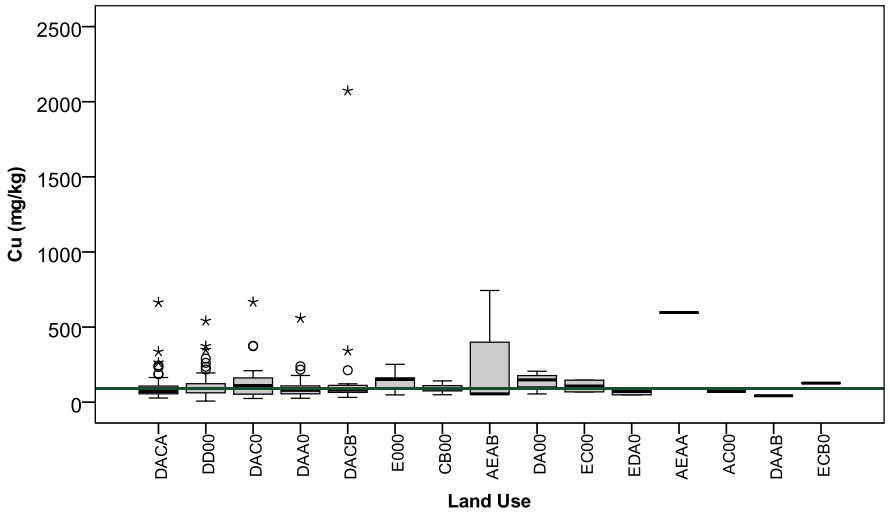


Figure 103: Zn concentrations in soil according to land use, green line: proposed UK ecological guideline (EA, 2008); purple line: former UK ICRCL SGV (ICRCL, 1987).

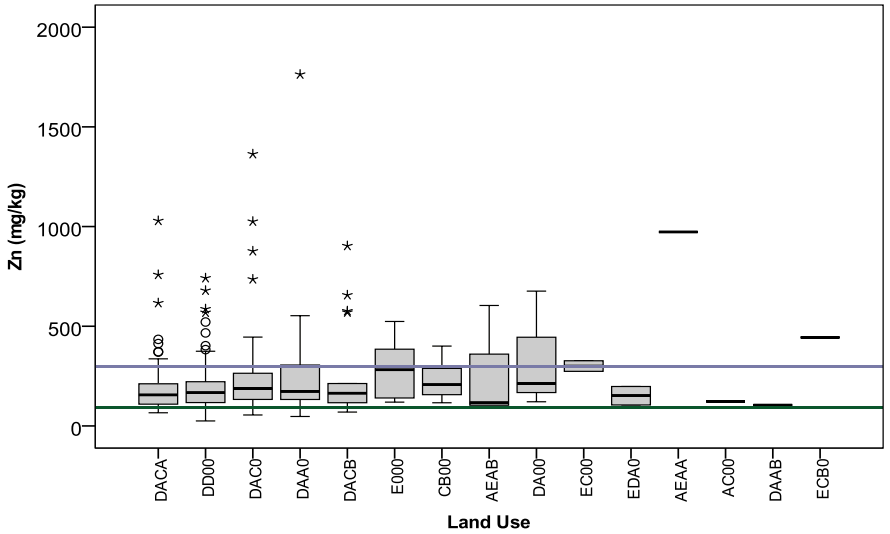

Figure 104: As concentrations in soil according to land use, black line: residential SGV; red line: allotment SGV; brown line: commercial/industrial SGV (EA, 2009c). (Note: logarithmic scale).

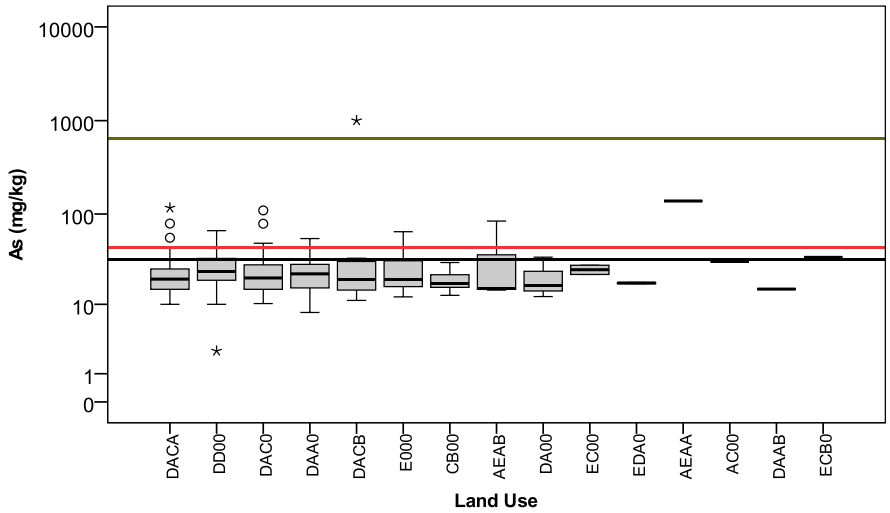


Figure 105: Pb concentrations in soil according to land use, black line: residential and allotment SGV; brown line: commercial/industrial SGV (EA, 2002).

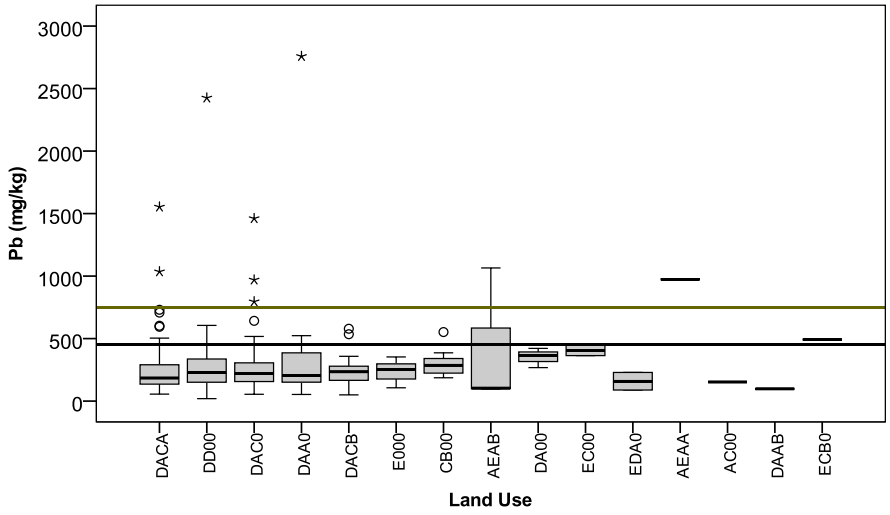


Figure 106: Cd concentrations in soil according to land use, black line: residential SGV; red: allotment SGV (EA, 2009b). (Note: logarithmic scale).

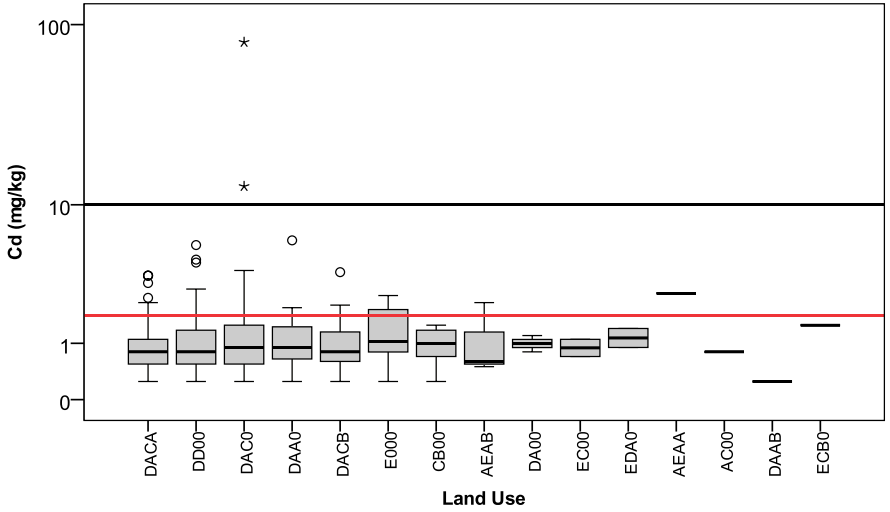


Table 78: Land use code key

| Code | Land Use |
|---|---|
| DACA | Urban open space, tended but unproductive |
| DD00 | Recreational area |
| DAC0 | Urban open space |
| DAA0 | Commercial and residential |
| DACB | Urban open space, cleared/derelict |
| E000 | Industrial |
| CB00 | Major roads/verge |
| AEAB | Deciduous woodland established |
| DA00 | Urban settlement |
| 0000 | n.d. |
| EC00 | Tips |
| EDA0 | Water treatment works |
| AEAA | Deciduous woodland, recent |
| AC00 | Grass moor |
| DAAB | Hospital Grounds |
| ECB0 | Industrial waste tip |

Figure 107: Box-and-whisker plots for soil elemental concentrations, grouped by bedrock geology type (As and Cd in logarithmic scale).

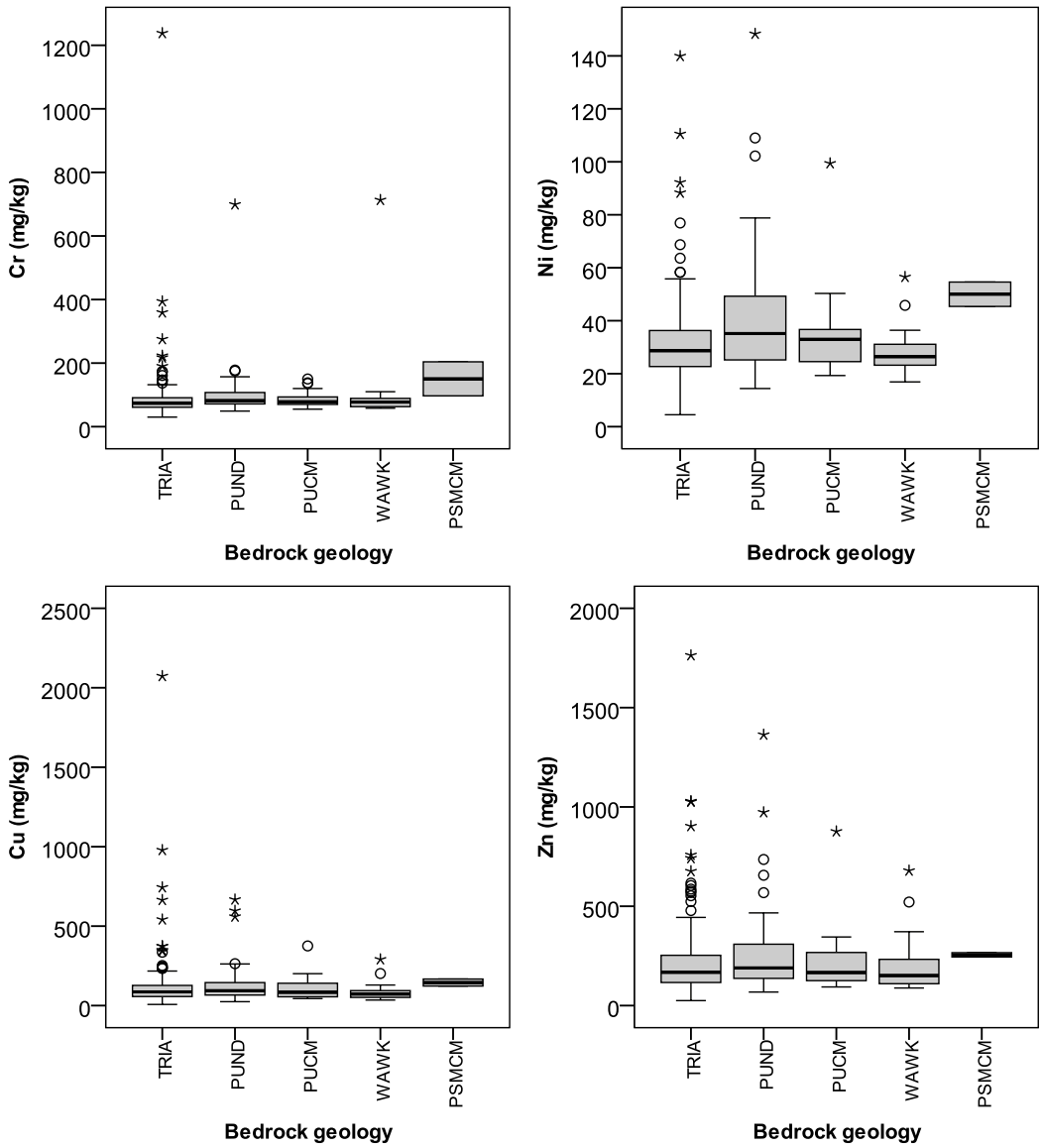

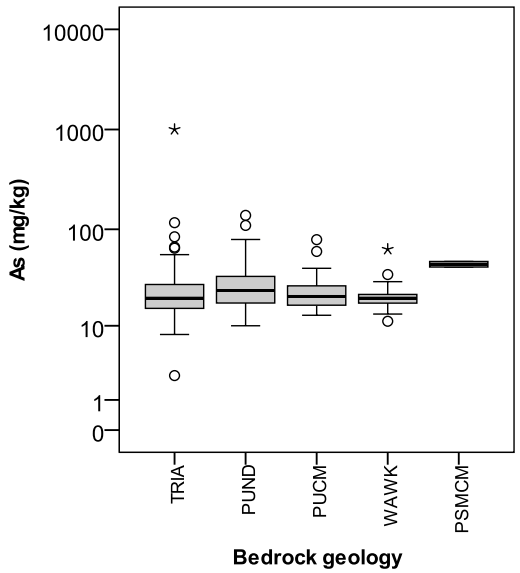
As (mg/kg)
10000
1000
100
10
1
0
TRIA
PUND
PUCM
WAWK
PSMCM
Bedrock geology

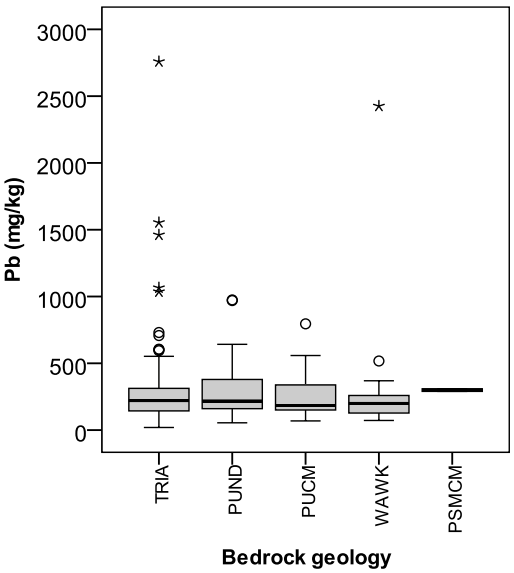
Pb (mg/kg)
3000
2500
2000
1500
1000
500
0
TRIA
PUND
PUCM
WAWK
PSMCM
Bedrock geology

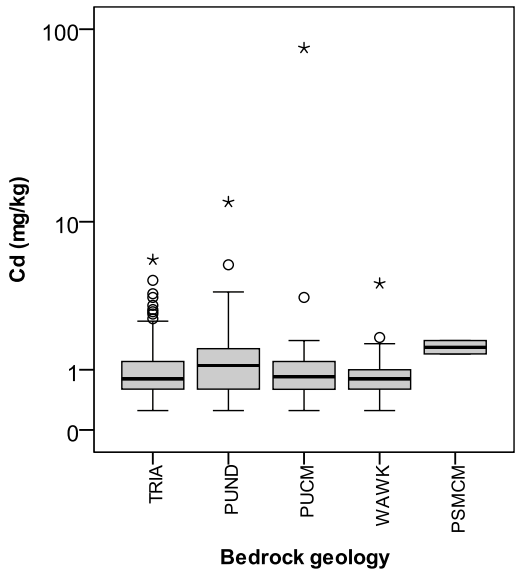
Cd (mg/kg)
100
10
1
0
TRIA
PUND
PUCM
WAWK
PSMCM
Bedrock geology

Figure 108: Box-and-whisker plots for soil elemental concentrations, grouped by superficial deposit type (As and Cd in logarithmic scale).

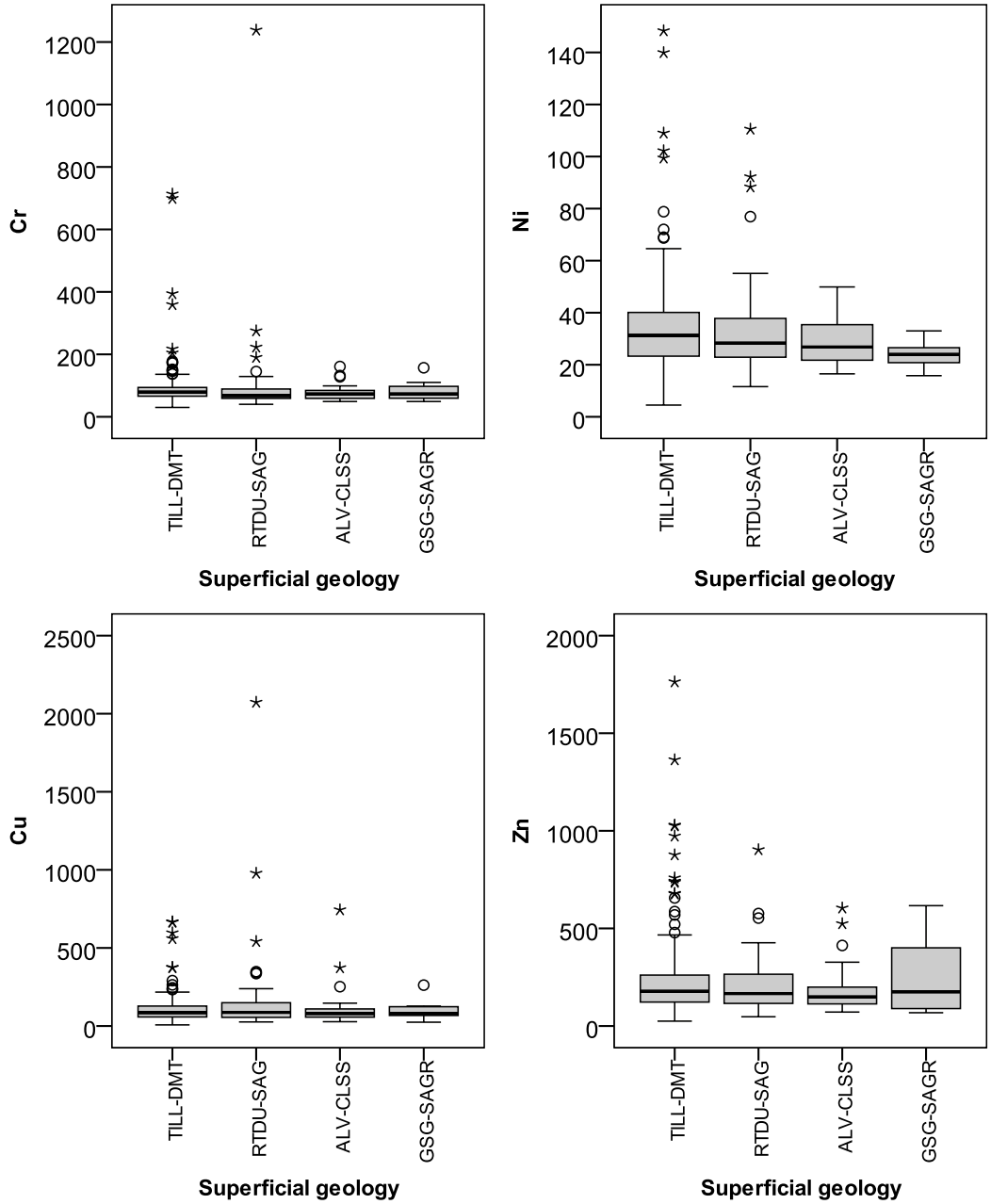

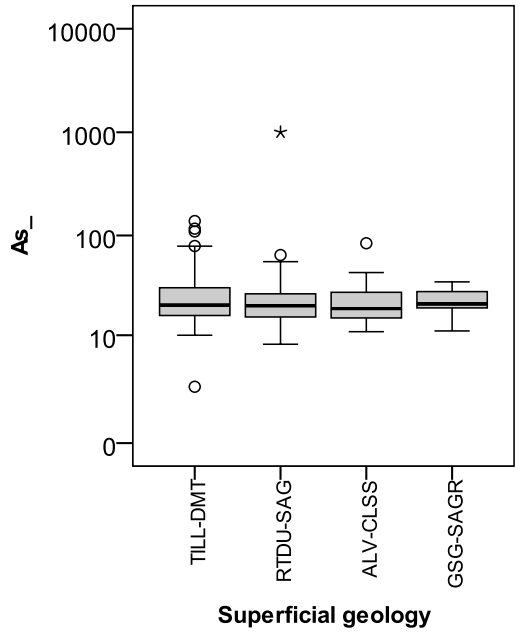
As_
10000
1000
100
10
0
TILL-DMT
RTDU-SAG
ALV-CLSS
GSG-SAGR
Superficial geology

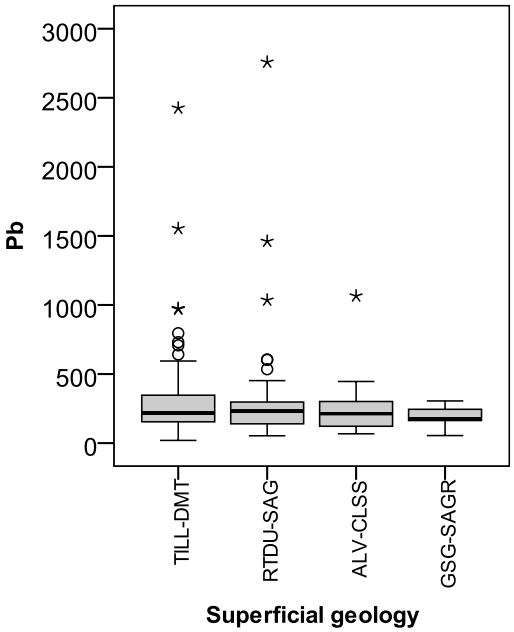
Pb
3000
2500
2000
1500
1000
500
0
TILL-DMT
RTDU-SAG
ALV-CLSS
GSG-SAGR
Superficial geology

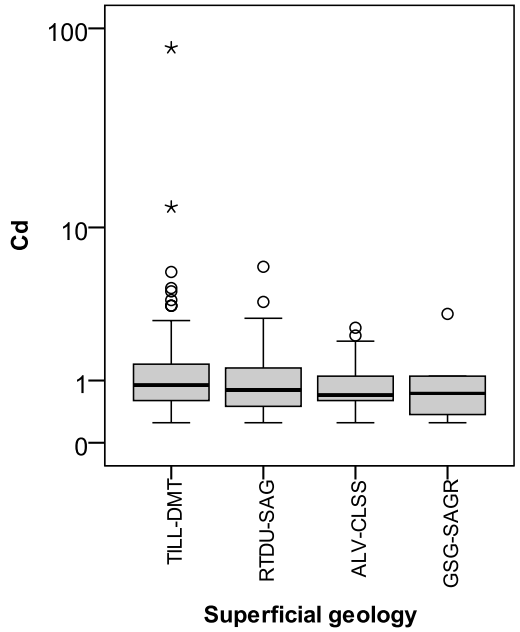
Cd
100
10
1
0
TILL-DMT
RTDU-SAG
ALV-CLSS
GSG-SAGR
Superficial geology

Figure 109: Box-and-whisker plots for soil concentrations in $Al_2O_3$, $SiO_2$, $TiO_2$, $Fe_2O_3$, Sc, V, Co, Ga and Mo, grouped by bedrock geology type.

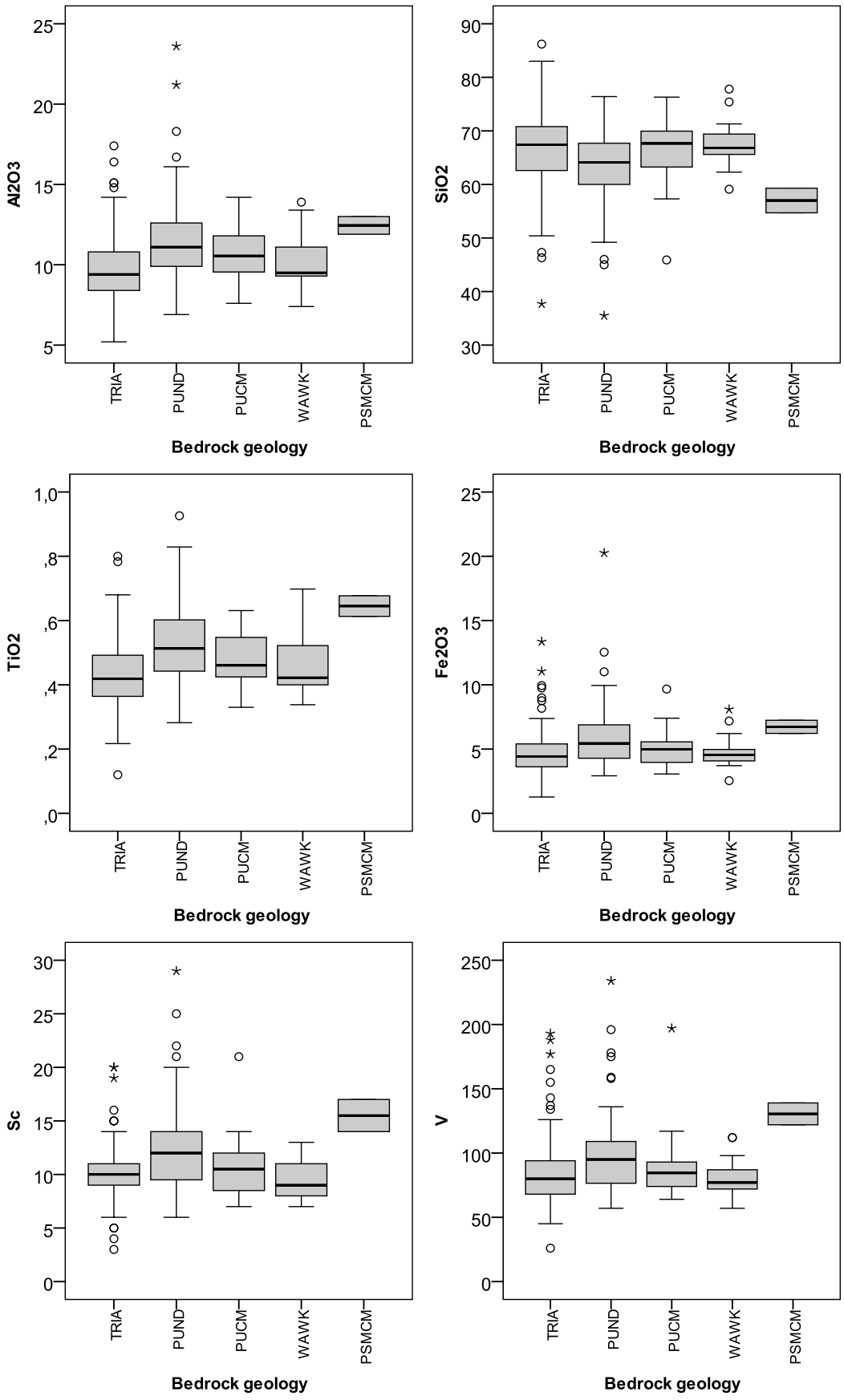

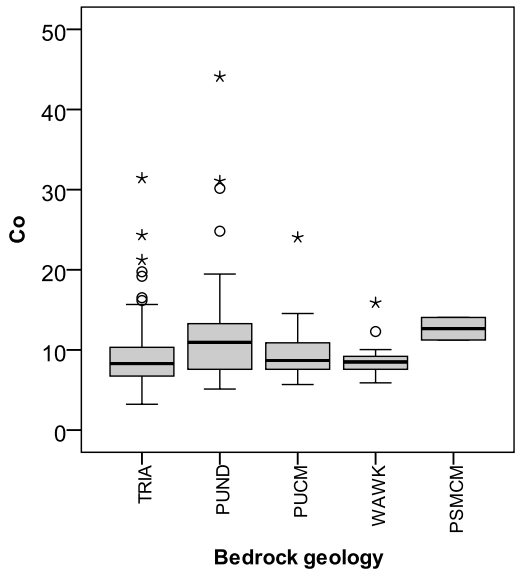
Co
50
40
30
20
10
0
TRIA
PUND
PUCM
WAWK
PSMCM
Bedrock geology

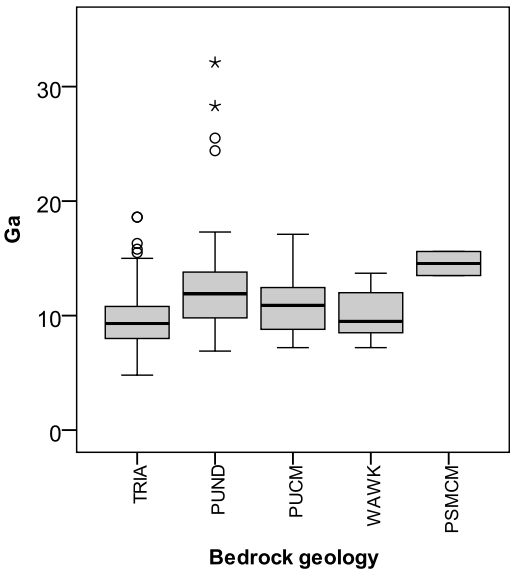
Ga
30
20
10
0
TRIA
PUND
PUCM
WAWK
PSMCM
Bedrock geology

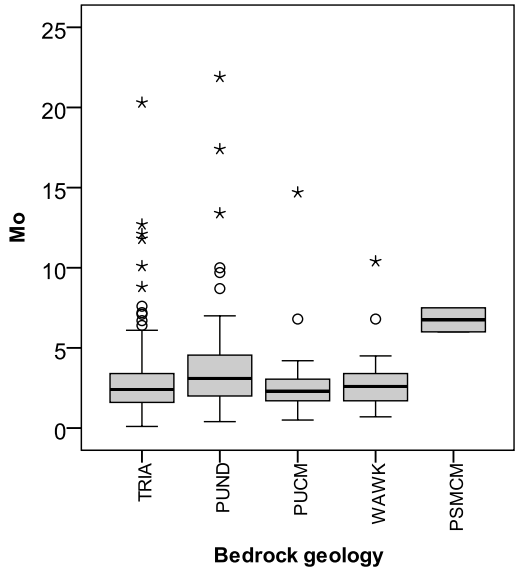
Mo
25
20
15
10
5
0
TRIA
PUND
PUCM
WAWK
PSMCM
Bedrock geology

Figure 110: Box-and-whisker plots for soil concentrations in $Al_2O_3$, $TiO_2$, Ga, Rb, Y, Nb, La, Ce and Nd, grouped by superficial deposit type.

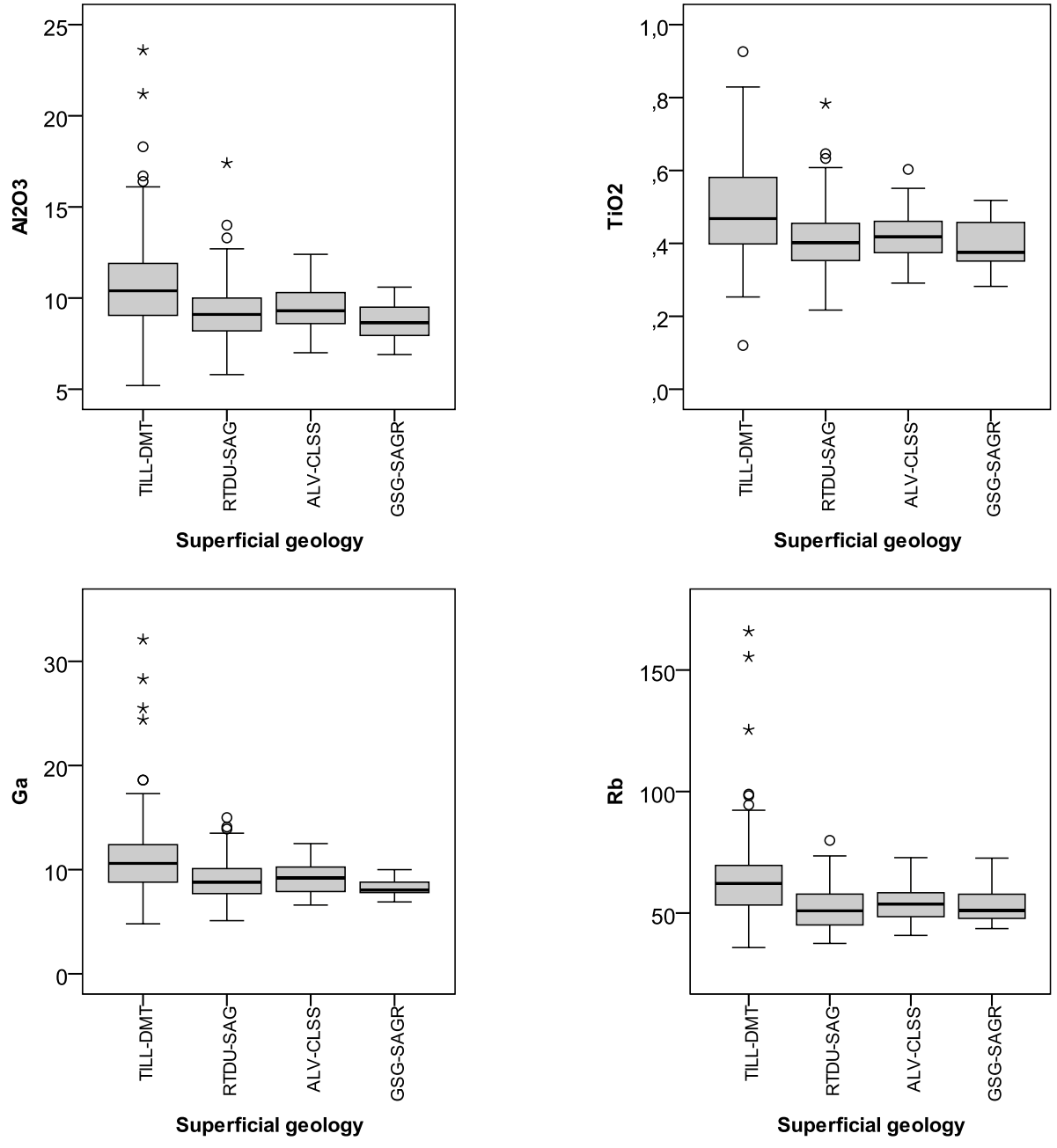

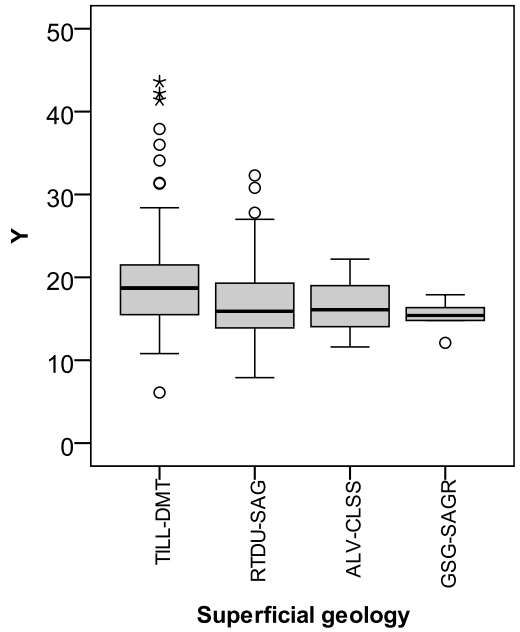
Y
50
40
30
20
10
0
TILL-DMT
RTDU-SAG
ALV-CLSS
GSG-SAGR
Superficial geology

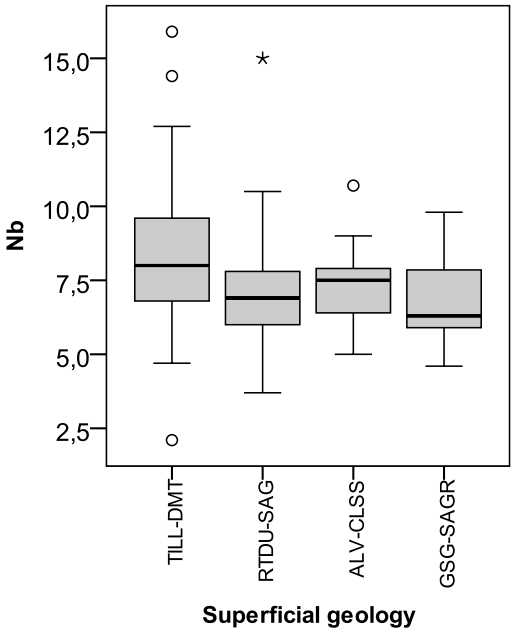
Nb
15,0
12,5
10,0
7,5
5,0
2,5
TILL-DMT
RTDU-SAG
ALV-CLSS
GSG-SAGR
Superficial geology

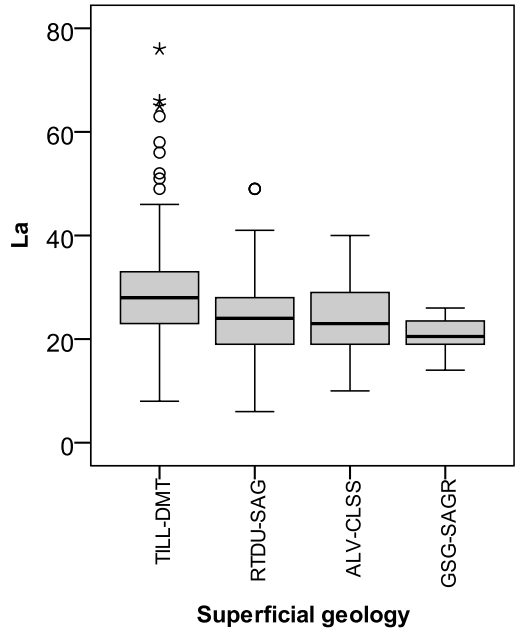
La
80
60
40
20
0
TILL-DMT
RTDU-SAG
ALV-CLSS
GSG-SAGR
Superficial geology

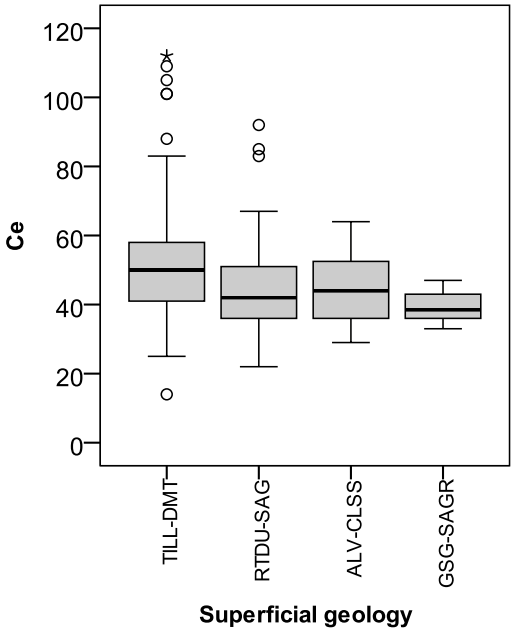
Ce
120
100
80
60
40
20
0
TILL-DMT
RTDU-SAG
ALV-CLSS
GSG-SAGR
Superficial geology

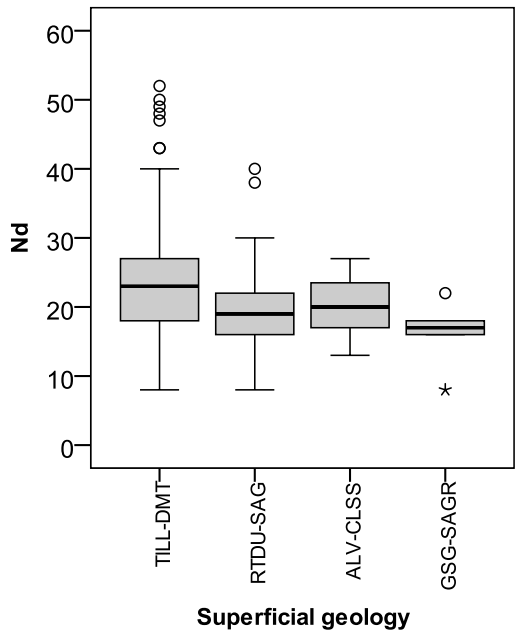
60
50
40
30
20
10
0
Nd
TILL-DMT
RTDU-SAG
ALV-CLSS
GSG-SAGR
Superficial geology

Figure 111: Box-and-whisker plots for soil SEM data, grouped by grain type (all concentrations in wt%).

NOTE: 1 sample analysed for Al/Fe rich, Fe/S-rich, Framboidal Py, S-rich, Ca-rich, Cr-rich, Cu/Sn-rich, Ni-rich, P-rich, REE grain, Feldspar and Sn-rich grain types.

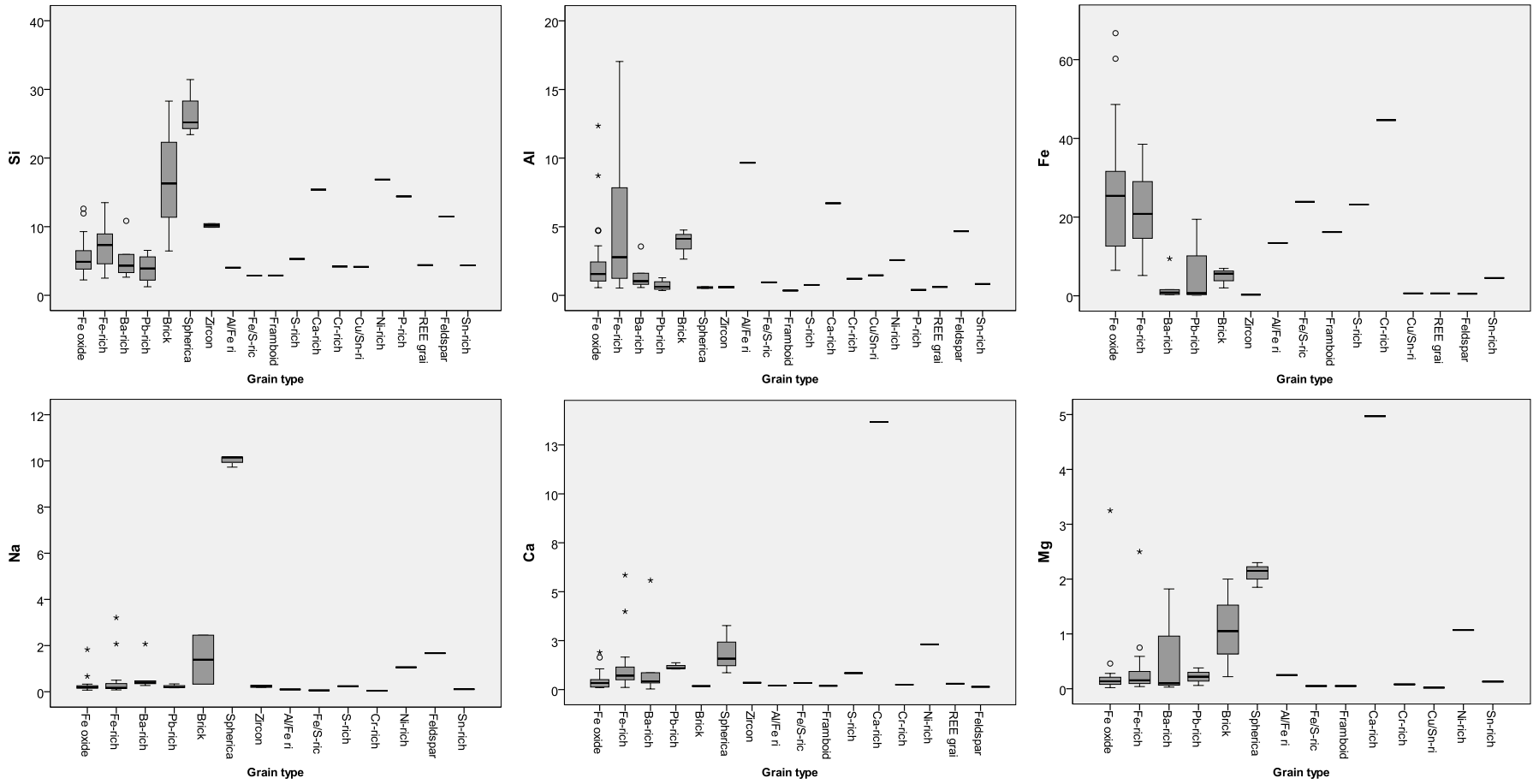

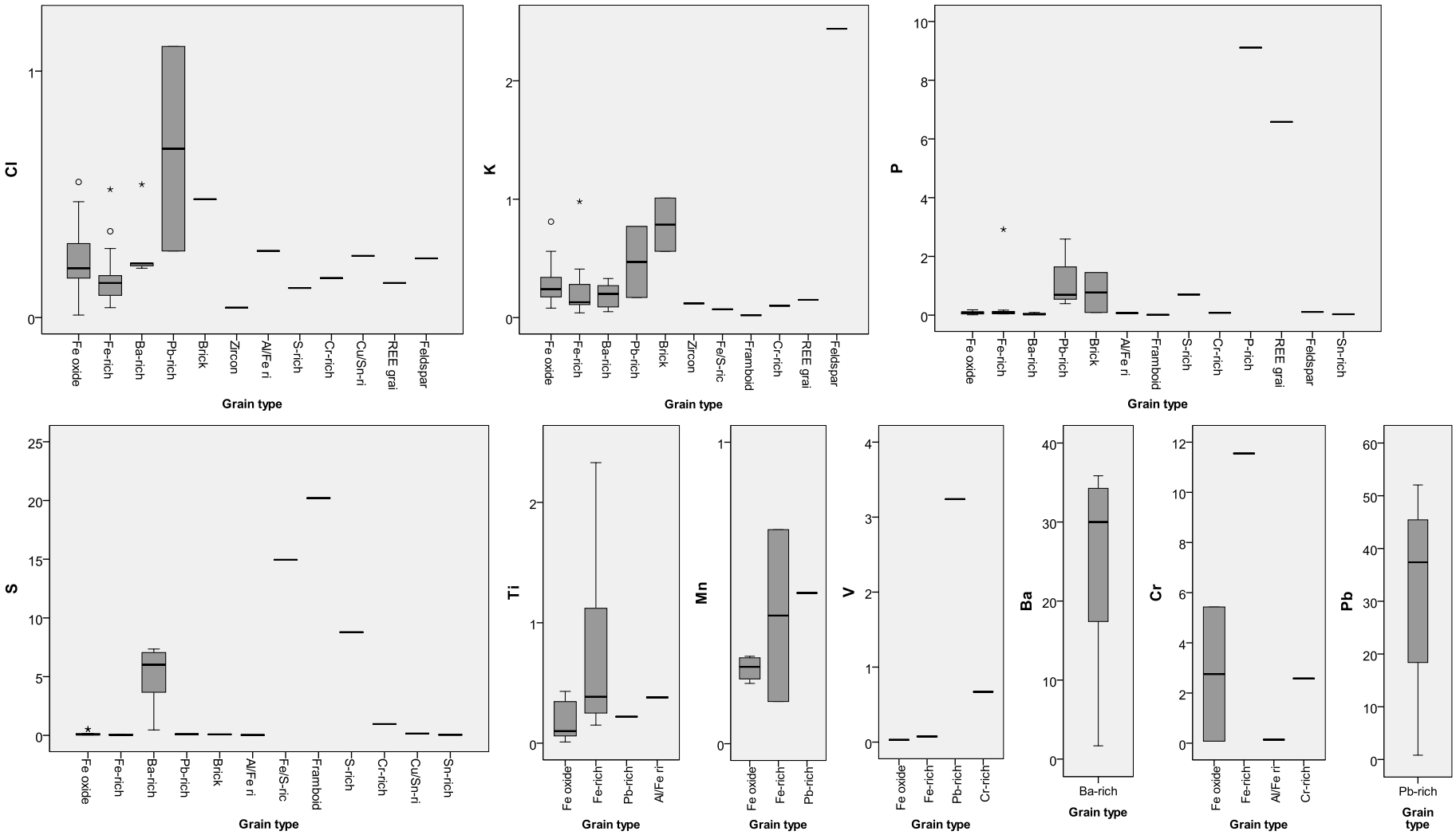
Cl
Fe oxide
Fe-rich
Ba-rich
Pb-rich
Brick
Zircon
Al/Fe ri
S-rich
Cr-rich
Cu/Sn-ri
REE grai
Feldspar
Grain type
K
Fe oxide
Fe-rich
Ba-rich
Pb-rich
Brick
Zircon
Fe/S-ric
Framboid
Cr-rich
REE grai
Feldspar
Grain type
P
Fe oxide
Fe-rich
Ba-rich
Pb-rich
Brick
Al/Fe ri
Framboid
S-rich
Cr-rich
P-rich
REE grai
Feldspar
Sn-rich
Grain type
S
Fe oxide
Fe-rich
Ba-rich
Pb-rich
Brick
Al/Fe ri
Fe/S-ric
Framboid
S-rich
Cr-rich
Cu/Sn-ri
Sn-rich
Grain type
Ti
Fe oxide
Fe-rich
Pb-rich
Al/Fe ri
Grain type
Mn
Fe oxide
Fe-rich
Pb-rich
Grain type
V
Fe oxide
Fe-rich
Pb-rich
Cr-rich
Grain type
Ba
Ba-rich
Grain type
Cr
Fe oxide
Fe-rich
Al/Fe ri
Cr-rich
Grain type
Pb
Pb-rich
Grain type

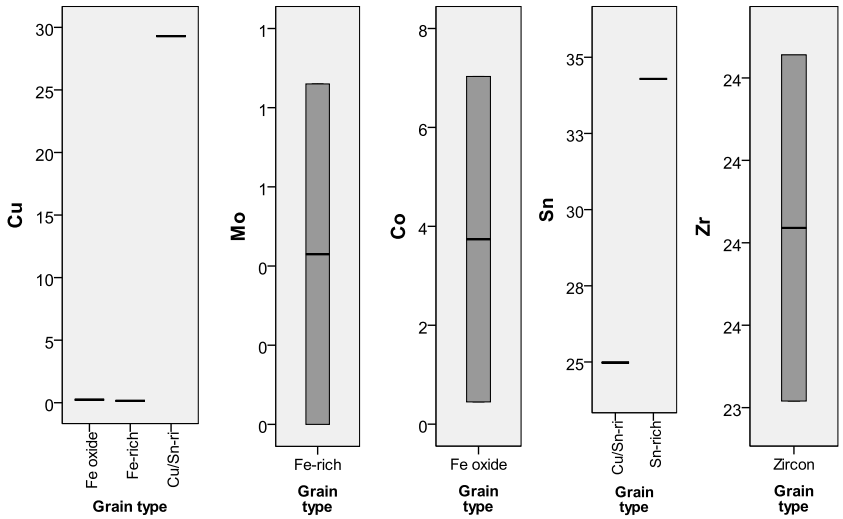
Cu
30
25
20
15
10
5
0
Fe oxide
Fe-rich
Cu/Sn-ri
Grain type
Mo
1
1
1
0
0
0
Fe-rich
Grain type
Co
8
6
4
2
0
Fe oxide
Grain type
Sn
35
33
30
28
25
Cu/Sn-ri
Sn-rich
Grain type
Zr
24
24
24
24
23
Zircon
Grain type

Table 79: Anti-image correlation matrix for BGS soil geochemical data (PCA #A, n=300, 47 variables).

| | Na2O | MgO | Al2O3 | SiO2 | P2O5 | K2O | CaO | TiO2 | MnO | Fe2O3 | Sc | V | Cr | Co | Ba | Ni | Cu | Zn | Ga | Ge | As | Se | Br | Rb | Sr | Y | Zr | Nb | Mo | Hf | W | Tl | Pb | Bi | Th | U | Ag | Cd | Sn | Sb | I | La | Ce | Nd | Sm | LOI | pH |
|---|---|---|---|---|---|---|---|---|---|---|---|---|---|---|---|---|---|---|---|---|---|---|---|---|---|---|---|---|---|---|---|---|---|---|---|---|---|---|---|---|---|---|---|---|---|---|
| Na2O | 0,646 | -,055 | ,190 | -,171 | ,006 | -,037 | ,063 | -,189 | -,040 | ,060 | -,009 | ,071 | ,066 | -,020 | ,045 | -,061 | ,182 | -,185 | -,071 | -,060 | -,071 | ,066 | -,106 | ,108 | -,094 | -,101 | -,169 | -,009 | ,055 | -,061 | ,000 | ,029 | -,020 | ,027 | -,125 | ,041 | ,005 | -,031 | -,092 | -,024 | -,033 | ,118 | ,111 | ,017 | -,095 | ,213 | -,002 |
| MgO | -,055 | 0,772 | -,025 | -,142 | -,186 | -,511 | -,236 | -,154 | -,069 | -,049 | -,052 | -,045 | -,124 | ,032 | -,030 | -,103 | ,021 | ,081 | -,075 | ,124 | ,064 | ,188 | -,057 | ,430 | ,134 | -,027 | ,248 | -,107 | ,027 | -,067 | ,043 | -,113 | ,086 | ,008 | -,117 | ,125 | ,056 | -,041 | -,001 | ,022 | -,151 | ,000 | ,075 | -,002 | -,116 | ,196 | ,051 |
| Al2O3 | ,190 | -,025 | 0,911 | ,068 | ,070 | ,001 | ,016 | -,535 | -,055 | ,117 | -,030 | -,010 | -,069 | -,054 | -,215 | ,053 | -,066 | -,036 | -,564 | ,160 | ,195 | ,131 | ,001 | -,042 | ,058 | -,040 | -,001 | ,100 | ,138 | -,011 | ,094 | ,071 | ,080 | -,056 | -,179 | ,025 | ,041 | -,085 | -,020 | -,037 | ,067 | -,046 | -,190 | ,039 | ,165 | ,258 | ,014 |
| SiO2 | ,171 | -,142 | ,068 | 0,925 | ,194 | ,217 | ,460 | ,191 | -,004 | ,280 | ,117 | ,170 | ,071 | -,144 | ,130 | ,141 | -,004 | -,053 | -,094 | -,185 | -,027 | -,005 | ,041 | -,195 | -,160 | -,066 | -,141 | -,231 | ,028 | -,021 | ,063 | ,082 | -,170 | ,052 | ,189 | -,179 | -,089 | -,059 | -,088 | ,075 | ,105 | ,046 | ,142 | ,088 | ,021 | ,119 | -,105 |
| P2O5 | ,006 | -,186 | ,070 | ,194 | 0,858 | ,192 | ,177 | -,046 | -,126 | ,028 | -,094 | ,059 | -,050 | ,020 | ,163 | ,147 | ,047 | -,036 | ,107 | -,187 | ,004 | -,259 | ,016 | -,180 | -,202 | -,023 | -,025 | ,059 | ,135 | ,043 | -,166 | ,122 | -,170 | -,107 | ,016 | ,021 | -,244 | -,021 | ,018 | ,056 | -,063 | -,109 | ,101 | -,017 | ,055 | -,141 | ,037 |
| K2O | -,037 | -,511 | ,001 | ,217 | ,192 | 0,792 | ,132 | ,137 | ,043 | ,075 | ,046 | ,094 | ,061 | -,002 | ,022 | -,026 | -,031 | -,072 | ,232 | -,228 | -,034 | ,017 | ,174 | -,910 | -,027 | -,157 | -,145 | ,029 | ,103 | ,028 | -,038 | ,045 | ,093 | ,049 | ,220 | ,033 | -,156 | ,110 | ,025 | ,038 | ,220 | ,070 | -,036 | ,097 | ,041 | -,349 | -,144 |
| CaO | ,063 | -,236 | ,016 | ,460 | ,177 | ,132 | 0,598 | ,120 | -,067 | ,139 | -,257 | ,148 | ,089 | -,058 | ,287 | ,068 | ,049 | ,000 | -,154 | -,101 | -,118 | -,073 | ,111 | -,031 | -,540 | ,139 | -,213 | -,184 | -,005 | ,033 | -,076 | ,001 | -,108 | -,123 | ,118 | -,028 | ,036 | -,007 | -,131 | ,065 | ,086 | ,097 | ,263 | ,118 | -,110 | -,110 | -,406 |
| TiO2 | -,189 | -,154 | -,535 | ,191 | -,046 | ,137 | ,120 | 0,902 | ,076 | ,020 | ,009 | -,019 | ,099 | -,005 | ,039 | ,067 | -,009 | -,015 | ,167 | ,026 | -,131 | -,041 | ,070 | -,132 | ,142 | -,058 | -,150 | -,576 | ,010 | ,072 | -,089 | ,007 | -,105 | ,039 | ,296 | -,093 | -,052 | ,048 | -,042 | ,027 | -,078 | ,002 | -,055 | -,029 | ,053 | -,336 | -,027 |
| MnO | -,040 | -,069 | -,055 | -,004 | -,126 | ,043 | -,067 | ,076 | 0,807 | -,083 | -,035 | -,119 | ,135 | ,025 | -,019 | ,026 | -,322 | -,471 | ,039 | ,183 | ,170 | ,014 | -,065 | -,077 | ,171 | -,093 | -,045 | ,057 | -,066 | ,058 | ,019 | -,076 | ,029 | ,011 | ,192 | -,017 | ,059 | -,002 | ,227 | -,035 | -,019 | ,012 | -,064 | -,112 | -,014 | ,080 | ,010 |
| Fe2O3 | ,060 | -,049 | ,117 | ,280 | ,028 | ,075 | ,139 | ,020 | -,083 | 0,947 | -,040 | -,005 | ,094 | -,367 | -,064 | -,097 | -,003 | ,029 | -,223 | ,181 | -,122 | ,003 | ,104 | -,050 | ,100 | -,156 | -,132 | -,090 | -,263 | ,068 | ,143 | ,177 | -,135 | ,094 | ,116 | -,052 | -,087 | -,036 | -,311 | -,040 | ,127 | -,008 | ,097 | ,097 | -,060 | -,003 | -,040 |
| Sc | -,009 | -,052 | -,030 | ,117 | -,094 | ,046 | -,257 | ,009 | -,035 | -,040 | 0,979 | -,145 | -,065 | -,045 | ,021 | ,028 | ,136 | ,002 | -,030 | -,110 | -,022 | ,002 | ,015 | -,047 | ,074 | -,156 | ,128 | ,034 | ,020 | -,035 | ,095 | ,083 | ,040 | ,137 | -,097 | -,045 | -,143 | -,012 | ,083 | -,012 | ,033 | -,020 | -,151 | -,020 | ,053 | -,073 | ,003 |
| V | ,071 | -,045 | -,010 | ,170 | ,059 | ,094 | ,148 | -,019 | -,119 | -,005 | -,145 | 0,967 | ,005 | -,008 | -,019 | -,411 | ,145 | ,049 | ,007 | -,117 | -,085 | -,133 | -,134 | -,061 | -,093 | ,085 | ,053 | -,136 | -,044 | ,022 | -,026 | -,091 | ,130 | ,012 | -,066 | ,021 | -,015 | ,149 | ,136 | -,119 | ,127 | ,047 | ,015 | ,011 | ,023 | -,059 | -,005 |
| Cr | ,066 | -,124 | -,069 | ,071 | -,050 | ,061 | ,089 | ,099 | ,135 | ,094 | -,065 | ,005 | 0,864 | -,017 | -,002 | -,107 | -,030 | -,133 | -,032 | ,080 | -,491 | -,009 | ,097 | -,047 | -,003 | -,048 | -,191 | -,008 | -,019 | ,023 | -,082 | ,069 | -,163 | -,079 | ,040 | ,005 | -,012 | -,025 | ,066 | ,081 | ,028 | ,081 | ,060 | ,105 | -,047 | -,129 | -,066 |
| Co | -,020 | ,032 | -,054 | -,144 | ,020 | -,002 | -,058 | -,005 | ,025 | -,367 | -,045 | -,008 | -,017 | 0,965 | ,183 | -,265 | ,049 | -,066 | ,059 | -,089 | ,035 | -,077 | ,128 | ,022 | -,104 | -,071 | ,104 | ,098 | -,023 | -,014 | -,041 | -,032 | ,078 | ,162 | -,076 | ,131 | -,131 | ,047 | ,070 | ,013 | -,147 | ,001 | -,060 | -,140 | ,057 | -,007 | ,114 |
| Ba | ,045 | -,030 | -,215 | ,130 | ,163 | ,022 | ,287 | ,039 | -,019 | -,064 | ,021 | -,019 | -,002 | ,183 | 0,831 | ,165 | ,141 | -,142 | ,035 | -,324 | -,011 | -,053 | ,099 | ,019 | -,619 | ,237 | -,067 | -,071 | -,052 | ,003 | -,021 | ,036 | -,140 | ,132 | -,005 | ,112 | -,290 | -,068 | ,025 | ,020 | ,146 | ,042 | ,210 | -,070 | -,137 | -,184 | ,080 |
| Ni | -,061 | -,103 | ,053 | ,141 | ,147 | -,026 | ,068 | ,067 | ,026 | -,097 | ,028 | -,411 | -,107 | -,265 | ,165 | 0,946 | -,180 | -,091 | -,050 | -,296 | ,259 | ,051 | -,069 | ,022 | -,277 | -,010 | ,065 | -,015 | ,004 | -,065 | -,148 | ,029 | -,046 | -,059 | ,090 | -,015 | -,011 | -,243 | -,014 | ,123 | ,101 | -,090 | -,055 | -,040 | ,097 | ,039 | -,105 |
| Cu | ,182 | ,021 | -,066 | -,004 | ,047 | -,031 | ,049 | -,009 | -,322 | -,003 | ,136 | ,145 | -,030 | ,049 | ,141 | -,180 | 0,81 | -,018 | ,128 | -,094 | -,701 | -,086 | ,058 | ,113 | -,212 | ,147 | -,068 | -,056 | -,024 | -,003 | -,035 | ,049 | ,066 | -,032 | -,493 | ,207 | ,006 | ,046 | -,339 | -,103 | ,014 | ,034 | ,016 | ,047 | -,023 | -,109 | ,031 |
| Zn | -,185 | ,081 | -,036 | -,053 | -,036 | -,072 | ,000 | -,015 | -,471 | ,029 | ,002 | ,049 | -,133 | -,066 | -,142 | -,091 | -,018 | 0,932 | ,053 | -,046 | -,040 | -,033 | ,069 | ,049 | ,076 | ,030 | ,124 | -,049 | -,020 | -,073 | -,050 | ,060 | -,081 | ,033 | -,033 | ,008 | -,031 | -,025 | -,154 | -,110 | -,110 | -,063 | ,030 | ,110 | ,012 | -,050 | -,111 |
| Ga | -,071 | -,075 | -,564 | -,094 | ,107 | ,232 | -,154 | ,167 | ,039 | -,223 | -,030 | ,007 | -,032 | ,059 | ,035 | -,050 | ,128 | ,053 | 0,929 | -,312 | -,170 | -,215 | -,040 | -,374 | ,181 | ,039 | ,135 | -,011 | -,027 | -,003 | -,055 | -,063 | ,038 | ,043 | ,000 | ,016 | -,084 | ,156 | ,009 | ,025 | -,121 | -,033 | -,099 | -,049 | ,013 | -,134 | -,084 |
| Ge | -,060 | ,124 | ,160 | -,185 | -,187 | -,228 | -,101 | ,026 | ,183 | ,181 | -,110 | -,117 | ,080 | -,089 | -,324 | -,296 | -,094 | -,046 | -,312 | 0,903 | -,033 | ,028 | -,097 | ,260 | ,402 | -,207 | -,040 | ,032 | -,287 | ,077 | ,196 | -,045 | -,040 | ,039 | ,029 | -,111 | ,098 | -,014 | -,181 | -,100 | -,129 | -,014 | -,016 | -,023 | -,009 | ,169 | ,109 |
| As | -,071 | ,064 | ,195 | -,027 | ,004 | -,034 | -,118 | -,131 | ,170 | -,122 | -,022 | -,085 | -,491 | ,035 | -,011 | ,259 | -,701 | -,040 | -,170 | -,033 | 0,657 | ,108 | -,127 | -,026 | ,011 | -,034 | ,191 | ,056 | ,005 | -,050 | ,040 | -,071 | ,098 | ,085 | ,205 | -,039 | -,012 | -,058 | ,247 | ,041 | ,005 | -,016 | -,065 | -,077 | ,058 | ,164 | ,103 |
| Se | ,066 | ,188 | ,131 | -,005 | -,259 | ,017 | -,073 | -,041 | ,014 | ,003 | ,002 | -,133 | -,009 | -,077 | -,053 | ,051 | -,086 | -,033 | -,215 | ,028 | ,108 | 0,945 | -,356 | -,034 | ,009 | -,065 | -,025 | ,039 | -,033 | -,007 | ,211 | -,206 | ,093 | -,025 | -,025 | -,092 | ,010 | -,233 | ,009 | -,036 | ,085 | ,026 | ,038 | ,052 | -,124 | ,132 | ,080 |
| Br | -,106 | -,057 | ,001 | ,041 | ,016 | ,174 | ,111 | ,070 | -,065 | ,104 | ,015 | -,134 | ,097 | ,128 | ,099 | -,069 | ,058 | ,069 | -,040 | -,097 | -,127 | -,356 | 0,839 | -,124 | -,079 | -,011 | -,071 | -,036 | ,105 | ,041 | -,082 | ,105 | -,072 | ,020 | ,028 | ,167 | ,079 | ,153 | -,011 | ,036 | -,158 | ,076 | ,021 | ,044 | ,002 | -,534 | ,193 |
| Rb | ,108 | ,430 | -,042 | -,195 | -,180 | -,910 | -,031 | -,132 | -,077 | -,050 | -,047 | -,061 | -,047 | ,022 | ,019 | ,022 | ,113 | ,049 | -,374 | ,260 | -,026 | -,034 | -,124 | 0,818 | -,091 | ,129 | ,171 | -,060 | -,093 | -,030 | ,012 | -,053 | -,064 | -,049 | -,280 | -,010 | ,159 | -,132 | -,068 | -,043 | -,198 | -,039 | ,148 | -,084 | -,102 | ,352 | ,121 |
| Sr | -,094 | ,134 | ,058 | -,160 | -,202 | -,027 | -,540 | ,142 | ,171 | ,100 | ,074 | -,093 | -,003 | -,104 | -,619 | -,277 | -,212 | ,076 | ,181 | ,402 | ,011 | ,009 | -,079 | -,091 | 0,856 | -,390 | ,217 | -,034 | ,046 | -,009 | ,095 | ,002 | ,076 | ,048 | ,043 | -,193 | ,056 | ,094 | ,021 | -,080 | -,232 | -,024 | -,330 | ,007 | ,170 | ,186 | -,009 |
| Y | -,101 | -,027 | -,040 | -,066 | -,023 | -,157 | ,139 | -,058 | -,093 | -,156 | -,156 | ,085 | -,048 | -,071 | ,237 | -,010 | ,147 | ,030 | ,039 | -,207 | -,034 | -,065 | -,011 | ,129 | -,390 | 0,955 | -,041 | -,200 | -,187 | -,069 | ,142 | -,041 | -,239 | -,128 | -,030 | -,074 | ,083 | ,019 | ,080 | -,064 | ,157 | -,122 | -,095 | -,225 | ,015 | ,041 | ,017 |
| Zr | -,169 | ,248 | -,001 | -,141 | -,025 | -,145 | -,213 | -,150 | -,045 | -,132 | ,128 | ,053 | -,191 | ,104 | -,067 | ,065 | -,068 | ,124 | ,135 | -,040 | ,191 | -,025 | -,071 | ,171 | ,217 | -,041 | 0,741 | -,158 | -,038 | -,475 | ,077 | -,013 | ,010 | ,004 | -,234 | -,147 | -,010 | -,026 | ,053 | -,019 | -,266 | ,018 | -,150 | -,039 | ,060 | ,274 | -,009 |
| Nb | -,009 | -,107 | ,100 | -,231 | ,059 | ,029 | -,184 | -,576 | ,057 | -,090 | ,034 | -,136 | -,008 | ,098 | -,071 | -,015 | -,056 | -,049 | -,011 | ,032 | ,056 | ,039 | -,036 | -,060 | -,034 | -,200 | -,158 | 0,948 | ,108 | -,047 | -,040 | ,011 | ,046 | ,004 | -,102 | ,001 | ,052 | -,022 | ,035 | ,027 | ,056 | -,049 | -,044 | -,004 | ,041 | ,097 | ,065 |
| Mo | ,055 | ,027 | ,138 | ,028 | ,135 | ,103 | -,005 | ,010 | -,066 | -,263 | ,020 | -,044 | -,019 | -,023 | -,052 | ,004 | -,024 | -,020 | -,027 | -,287 | ,005 | -,033 | ,105 | -,093 | ,046 | -,187 | -,038 | ,108 | 0,966 | ,040 | -,222 | ,059 | ,004 | ,041 | -,025 | ,024 | -,027 | ,074 | -,014 | ,037 | -,011 | -,052 | -,023 | ,038 | ,062 | -,118 | ,060 |
| Hf | -,061 | -,067 | -,011 | -,021 | ,043 | ,028 | ,033 | ,072 | ,058 | ,068 | -,035 | ,022 | ,023 | -,014 | ,003 | -,065 | -,003 | -,073 | -,003 | ,077 | -,050 | -,007 | ,041 | -,030 | -,009 | -,069 | -,475 | -,047 | ,040 | 0,849 | -,020 | ,058 | ,102 | ,081 | -,113 | ,166 | -,063 | ,015 | -,018 | -,090 | ,029 | -,026 | ,067 | ,121 | -,026 | -,221 | ,091 |
| W | ,000 | ,043 | ,094 | ,063 | -,166 | -,038 | -,076 | -,089 | ,019 | ,143 | ,095 | -,026 | -,082 | -,041 | -,021 | -,148 | -,035 | -,050 | -,055 | ,196 | ,040 | ,211 | -,082 | ,012 | ,095 | ,142 | ,077 | -,040 | -,222 | -,020 | 0,718 | ,035 | -,101 | ,012 | -,068 | -,258 | ,058 | -,009 | -,092 | -,251 | -,006 | ,037 | -,012 | -,112 | -,027 | ,154 | ,140 |
| Tl | ,029 | -,113 | ,071 | ,082 | ,122 | ,045 | ,001 | ,007 | -,076 | ,177 | ,083 | -,091 | ,069 | -,032 | ,036 | ,029 | ,049 | ,060 | -,063 | -,045 | -,071 | -,206 | ,105 | -,053 | ,002 | -,041 | -,013 | ,011 | ,059 | ,058 | ,035 | 0,893 | -,650 | -,043 | -,023 | ,025 | -,050 | ,062 | -,061 | -,071 | -,012 | -,041 | -,014 | ,033 | ,057 | -,017 | ,095 |
| Pb | -,020 | ,086 | ,080 | -,170 | -,170 | ,093 | -,108 | -,105 | ,029 | -,135 | ,040 | ,130 | -,163 | ,078 | -,140 | -,046 | ,066 | -,081 | ,038 | -,040 | ,098 | ,093 | -,072 | -,064 | ,076 | -,239 | ,010 | ,046 | ,004 | ,102 | -,101 | -,650 | 0,836 | ,119 | -,250 | ,380 | -,071 | ,004 | ,031 | -,054 | ,044 | ,144 | -,027 | ,109 | -,079 | -,099 | -,104 |
| Bi | ,027 | ,008 | -,056 | ,052 | -,107 | ,049 | -,123 | ,039 | ,011 | ,094 | ,137 | ,012 | -,079 | ,162 | ,132 | -,059 | -,032 | ,033 | ,043 | ,039 | ,085 | -,025 | ,020 | -,049 | ,048 | -,128 | ,004 | ,004 | ,041 | ,081 | ,012 | -,043 | ,119 | 0,651 | -,021 | ,168 | -,702 | -,125 | ,103 | -,024 | ,117 | ,000 | ,007 | -,141 | ,001 | -,046 | ,176 |
| Th | -,125 | -,117 | -,179 | ,189 | ,016 | ,220 | ,118 | ,296 | ,192 | ,116 | -,097 | -,066 | ,040 | -,076 | -,005 | ,090 | -,493 | -,033 | ,000 | ,029 | ,205 | -,025 | ,028 | -,280 | ,043 | -,030 | -,234 | -,102 | -,025 | -,113 | -,068 | -,023 | -,250 | -,021 | 0,924 | -,256 | -,047 | ,042 | ,189 | ,105 | ,193 | -,064 | -,165 | -,006 | ,151 | -,027 | -,141 |
| U | ,041 | ,125 | ,025 | -,179 | ,021 | ,033 | -,028 | -,093 | -,017 | -,052 | -,045 | ,021 | ,005 | ,131 | ,112 | -,015 | ,207 | ,008 | ,016 | -,111 | -,039 | -,092 | ,167 | -,010 | -,193 | -,074 | -,147 | ,001 | ,024 | ,166 | -,258 | ,025 | ,380 | ,168 | -,256 | 0,9 | -,075 | ,020 | -,021 | -,007 | -,027 | -,004 | ,063 | ,014 | -,066 | -,297 | ,089 |
| Ag | ,005 | ,056 | ,041 | -,089 | -,244 | -,156 | ,036 | -,052 | ,059 | -,087 | -,143 | -,015 | -,012 | -,131 | -,290 | -,011 | ,006 | -,031 | -,084 | ,098 | -,012 | ,010 | ,079 | ,159 | ,056 | ,083 | -,010 | ,052 | -,027 | -,063 | ,058 | -,050 | -,071 | -,702 | -,047 | -,075 | 0,858 | ,102 | -,283 | ,012 | -,132 | ,019 | -,015 | ,065 | ,049 | ,067 | -,039 |
| Cd | -,031 | -,041 | -,085 | -,059 | -,021 | ,110 | -,007 | ,048 | -,002 | -,036 | -,012 | ,149 | -,025 | ,047 | -,068 | -,243 | ,046 | -,025 | ,156 | -,014 | -,058 | -,233 | ,153 | -,132 | ,094 | ,019 | -,026 | -,022 | ,074 | ,015 | -,009 | ,062 | ,004 | -,125 | ,042 | ,020 | ,102 | **,424** | -,015 | ,031 | ,008 | ,146 | -,101 | -,015 | ,033 | -,152 | ,017 |
| Sn | -,092 | -,001 | -,020 | -,088 | ,018 | ,025 | -,131 | -,042 | ,227 | -,311 | ,083 | ,136 | ,066 | ,070 | ,025 | -,014 | -,339 | -,154 | ,009 | -,181 | ,247 | ,009 | -,011 | -,068 | ,021 | ,080 | ,053 | ,035 | -,014 | -,018 | -,092 | -,061 | ,031 | ,103 | ,189 | -,021 | -,283 | -,015 | 0,916 | -,037 | ,107 | -,026 | -,088 | -,014 | ,038 | -,067 | -,003 |
| Sb | -,024 | ,022 | -,037 | ,075 | ,056 | ,038 | ,065 | ,027 | -,035 | -,040 | -,012 | -,119 | ,081 | ,013 | ,020 | ,123 | -,103 | -,110 | ,025 | -,100 | ,041 | -,036 | ,036 | -,043 | -,080 | -,064 | -,019 | ,027 | ,037 | -,090 | -,251 | -,071 | -,054 | -,024 | ,105 | -,007 | ,012 | ,031 | -,037 | 0,957 | ,061 | -,008 | ,077 | ,022 | ,045 | -,050 | -,060 |
| I | -,033 | -,151 | ,067 | ,105 | -,063 | ,220 | ,086 | -,078 | -,019 | ,127 | ,033 | ,127 | ,028 | -,147 | ,146 | ,101 | ,014 | -,110 | -,121 | -,129 | ,005 | ,085 | -,158 | -,198 | -,232 | ,157 | -,266 | ,056 | -,011 | ,029 | -,006 | -,012 | ,044 | ,117 | ,193 | -,027 | -,132 | ,008 | ,107 | ,061 | 0,762 | ,010 | -,006 | ,030 | ,040 | -,137 | ,022 |
| La | ,118 | ,000 | -,046 | ,046 | -,109 | ,070 | ,097 | ,002 | ,012 | -,008 | -,020 | ,047 | ,081 | ,001 | ,042 | -,090 | ,034 | -,063 | -,033 | -,014 | -,016 | ,026 | ,076 | -,039 | -,024 | -,122 | ,018 | -,049 | -,052 | -,026 | ,037 | -,041 | ,144 | ,000 | -,064 | -,004 | ,019 | ,146 | -,026 | -,008 | ,010 | 0,985 | ,230 | -,030 | ,062 | -,117 | ,022 |
| Ce | ,111 | ,075 | -,190 | ,142 | ,101 | -,036 | ,263 | -,055 | -,064 | ,097 | -,151 | ,015 | ,060 | -,060 | ,210 | -,055 | ,016 | ,030 | -,099 | -,016 | -,065 | ,038 | ,021 | ,148 | -,330 | -,095 | -,150 | -,044 | -,023 | ,067 | -,012 | -,014 | -,027 | ,007 | -,165 | ,063 | -,015 | -,101 | -,088 | ,077 | -,006 | -,230 | 0,941 | -,082 | -,610 | -,081 | ,035 |
| Nd | ,017 | -,002 | ,039 | ,088 | -,017 | ,097 | ,118 | -,029 | -,112 | ,097 | -,020 | ,011 | ,105 | -,140 | -,070 | -,040 | ,047 | ,110 | -,049 | -,023 | -,077 | ,052 | ,044 | -,084 | ,007 | -,225 | -,039 | -,004 | ,038 | ,121 | -,112 | ,033 | ,109 | -,141 | -,006 | ,014 | ,065 | -,015 | -,014 | ,022 | ,030 | -,030 | -,082 | 0,979 | ,023 | -,080 | -,128 |
| Sm | -,095 | -,116 | ,165 | ,021 | ,055 | ,041 | -,110 | ,053 | -,014 | -,060 | ,053 | ,023 | -,047 | ,057 | -,137 | ,097 | -,023 | ,012 | ,013 | -,009 | ,058 | -,124 | ,002 | -,102 | ,170 | ,015 | ,060 | ,041 | ,062 | -,026 | -,027 | ,057 | -,079 | ,001 | ,151 | -,066 | ,049 | ,033 | ,038 | ,045 | ,040 | ,062 | -,610 | ,023 | 0,744 | ,099 | -,015 |
| LOI | ,213 | ,196 | ,258 | ,119 | -,141 | -,349 | -,110 | -,336 | ,080 | -,003 | -,073 | -,059 | -,129 | -,007 | -,184 | ,039 | -,109 | -,050 | -,134 | ,169 | ,164 | ,132 | -,534 | ,352 | ,186 | ,041 | ,274 | ,097 | -,118 | -,221 | ,154 | -,017 | -,099 | -,046 | -,027 | -,297 | ,067 | -,152 | -,067 | -,050 | -,137 | -,117 | -,081 | -,080 | ,099 | 0,824 | -,062 |
| pH | -,002 | ,051 | ,014 | -,105 | ,037 | -,144 | -,406 | -,027 | ,010 | -,040 | ,003 | -,005 | -,066 | ,114 | ,080 | -,105 | ,031 | -,111 | -,084 | ,109 | ,103 | ,080 | ,193 | ,121 | -,009 | ,017 | -,009 | ,065 | ,060 | ,091 | ,140 | ,095 | -,104 | ,176 | -,141 | ,089 | -,039 | ,017 | -,003 | -,060 | ,022 | ,022 | ,035 | -,128 | -,015 | -,062 | 0,741 |

Table 80: Communalities for BGS soil geochemical data (Extraction method: Principal component. PCA #A, n=300, 47 variables).

**Communalities**

| | Initial | Extraction | | Initial | Extraction |
|---|---|---|---|---|---|
| Na2O | 1,000 | ,705 | Sr | 1,000 | ,808 |
| MgO | 1,000 | ,682 | Y | 1,000 | ,953 |
| Al2O3 | 1,000 | ,964 | Zr | 1,000 | ,880 |
| SiO2 | 1,000 | ,838 | Nb | 1,000 | ,947 |
| P2O5 | 1,000 | ,759 | Mo | 1,000 | ,890 |
| K2O | 1,000 | ,868 | Hf | 1,000 | ,756 |
| CaO | 1,000 | ,859 | W | 1,000 | ,544 |
| TiO2 | 1,000 | ,939 | Tl | 1,000 | ,815 |
| MnO | 1,000 | ,755 | Pb | 1,000 | ,853 |
| Fe2O3 | 1,000 | ,895 | Bi | 1,000 | ,784 |
| Sc | 1,000 | ,928 | Th | 1,000 | ,902 |
| V | 1,000 | ,926 | U | 1,000 | ,777 |
| Cr | 1,000 | ,829 | Ag | 1,000 | ,853 |
| Co | 1,000 | ,904 | Cd | 1,000 | ,840 |
| Ba | 1,000 | ,473 | Sn | 1,000 | ,701 |
| Ni | 1,000 | ,944 | Sb | 1,000 | ,595 |
| Cu | 1,000 | ,897 | I | 1,000 | ,633 |
| Zn | 1,000 | ,750 | La | 1,000 | ,923 |
| Ga | 1,000 | ,938 | Ce | 1,000 | ,954 |
| Ge | 1,000 | ,881 | Nd | 1,000 | ,859 |
| As | 1,000 | ,900 | Sm | 1,000 | ,500 |
| Se | 1,000 | ,810 | LOI | 1,000 | ,784 |
| Br | 1,000 | ,845 | pH | 1,000 | ,761 |
| Rb | 1,000 | ,919 | | | |

Table 81: Eigenvalues associated to each calculated component for BGS soil geochemical data (Extraction method: Principal component. PCA #A, n=300, 47 variables).

| Total Variance Explained | | | | | | | | | |
|---|---|---|---|---|---|---|---|---|---|
| | Initial Eigenvalues | | | Extraction Sums of Squared Loadings | | | Rotation Sums of Squared Loadings | | |
| Component | Total | % of Variance | Cumulative % | Total | % of Variance | Cumulative % | Total | % of Variance | Cumulative % |
| 1 | 17,880 | 38,043 | 38,043 | 17,880 | 38,043 | 38,043 | 11,398 | 24,252 | 24,252 |
| 2 | 6,777 | 14,418 | 52,461 | 6,777 | 14,418 | 52,461 | 10,637 | 22,631 | 46,883 |
| 3 | 3,102 | 6,601 | 59,062 | 3,102 | 6,601 | 59,062 | 3,166 | 6,736 | 53,618 |
| 4 | 2,354 | 5,009 | 64,071 | 2,354 | 5,009 | 64,071 | 2,897 | 6,163 | 59,782 |
| 5 | 2,156 | 4,588 | 68,659 | 2,156 | 4,588 | 68,659 | 2,236 | 4,757 | 64,539 |
| 6 | 1,696 | 3,608 | 72,268 | 1,696 | 3,608 | 72,268 | 2,213 | 4,708 | 69,247 |
| 7 | 1,252 | 2,663 | 74,931 | 1,252 | 2,663 | 74,931 | 2,065 | 4,393 | 73,640 |
| 8 | 1,147 | 2,441 | 77,372 | 1,147 | 2,441 | 77,372 | 1,550 | 3,298 | 76,938 |
| 9 | 1,123 | 2,389 | 79,761 | 1,123 | 2,389 | 79,761 | 1,287 | 2,738 | 79,676 |
| 10 | 1,035 | 2,203 | 81,964 | 1,035 | 2,203 | 81,964 | 1,075 | 2,288 | 81,964 |
| 11 | ,850 | 1,809 | 83,773 | | | | | | |
| 12 | ,784 | 1,667 | 85,440 | | | | | | |
| 13 | ,704 | 1,498 | 86,938 | | | | | | |
| 14 | ,680 | 1,447 | 88,385 | | | | | | |
| 15 | ,594 | 1,263 | 89,648 | | | | | | |
| 16 | ,550 | 1,170 | 90,819 | | | | | | |
| 17 | ,468 | ,996 | 91,815 | | | | | | |
| 18 | ,378 | ,803 | 92,618 | | | | | | |
| 19 | ,351 | ,747 | 93,366 | | | | | | |
| 20 | ,341 | ,726 | 94,092 | | | | | | |
| 21 | ,304 | ,647 | 94,739 | | | | | | |
| 22 | ,271 | ,577 | 95,315 | | | | | | |
| 23 | ,238 | ,505 | 95,820 | | | | | | |
| 24 | ,222 | ,473 | 96,294 | | | | | | |
| 25 | ,204 | ,435 | 96,729 | | | | | | |
| 26 | ,171 | ,364 | 97,093 | | | | | | |
| 27 | ,154 | ,328 | 97,421 | | | | | | |
| 28 | ,143 | ,303 | 97,724 | | | | | | |
| 29 | ,132 | ,281 | 98,005 | | | | | | |
| 30 | ,118 | ,251 | 98,257 | | | | | | |
| 31 | ,105 | ,223 | 98,480 | | | | | | |
| 32 | ,099 | ,210 | 98,689 | | | | | | |
| 33 | ,088 | ,187 | 98,876 | | | | | | |
| 34 | ,078 | ,166 | 99,042 | | | | | | |
| 35 | ,067 | ,143 | 99,185 | | | | | | |
| 36 | ,063 | ,134 | 99,320 | | | | | | |
| 37 | ,059 | ,126 | 99,446 | | | | | | |
| 38 | ,050 | ,106 | 99,551 | | | | | | |
| 39 | ,043 | ,092 | 99,643 | | | | | | |
| 40 | ,038 | ,080 | 99,723 | | | | | | |
| 41 | ,035 | ,074 | 99,797 | | | | | | |
| 42 | ,023 | ,048 | 99,845 | | | | | | |
| 43 | ,020 | ,042 | 99,888 | | | | | | |
| 44 | ,019 | ,041 | 99,929 | | | | | | |
| 45 | ,017 | ,036 | 99,964 | | | | | | |
| 46 | ,009 | ,020 | 99,984 | | | | | | |
| 47 | ,007 | ,016 | 100,000 | | | | | | |

Table 82: Rotated component matrix (Varimax rotation with Kaiser normalisation) for BGS soil geochemical data (PCA #A, n=300, 47 variables).

| Rotated Component Matrix | | | | | | | | | | |
|---|---|---|---|---|---|---|---|---|---|---|
| | Component | | | | | | | | | |
| | 1 | 2 | 3 | 4 | 5 | 6 | 7 | 8 | 9 | 10 |
| Na2O | ,195 | -,155 | ,031 | -,163 | ,233 | ,090 | ,700 | ,230 | ,099 | -,007 |
| MgO | -,232 | ,624 | ,041 | -,081 | ,430 | -,108 | ,015 | ,177 | ,048 | -,024 |
| Al2O3 | ,131 | ,966 | ,013 | -,011 | -,041 | -,033 | ,103 | ,004 | ,013 | ,016 |
| SiO2 | -,620 | -,465 | -,113 | -,141 | -,309 | -,307 | ,017 | -,109 | ,039 | -,044 |
| P2O5 | ,310 | -,099 | ,612 | ,060 | -,063 | ,489 | -,037 | ,149 | -,057 | ,067 |
| K2O | -,066 | ,874 | -,004 | ,000 | ,121 | -,241 | -,154 | ,051 | ,009 | -,015 |
| CaO | ,208 | -,013 | -,010 | ,239 | ,871 | -,021 | -,005 | -,010 | ,000 | -,010 |
| TiO2 | ,151 | ,917 | ,033 | -,024 | -,060 | ,110 | ,238 | ,025 | -,020 | ,014 |
| MnO | ,238 | ,166 | -,007 | ,099 | ,029 | ,078 | -,025 | ,803 | -,025 | ,093 |
| Fe2O3 | ,830 | ,410 | ,087 | ,112 | ,056 | -,020 | -,002 | ,109 | ,012 | ,038 |
| Sc | ,666 | ,652 | ,056 | ,049 | ,166 | ,142 | -,007 | ,045 | ,060 | ,030 |
| V | ,776 | ,522 | ,040 | ,077 | ,049 | ,178 | -,055 | ,083 | ,030 | ,001 |
| Cr | ,127 | ,105 | ,210 | ,858 | ,124 | ,022 | ,047 | ,059 | ,007 | ,019 |
| Co | ,857 | ,369 | ,040 | ,089 | ,116 | ,022 | -,031 | ,086 | ,029 | ,033 |
| Ba | ,478 | ,260 | ,386 | ,102 | -,005 | -,099 | ,013 | -,084 | ,014 | -,034 |
| Ni | ,868 | ,355 | ,063 | ,128 | ,170 | ,053 | -,022 | ,093 | ,014 | ,064 |
| Cu | ,410 | ,023 | ,083 | ,819 | ,083 | -,040 | ,110 | ,121 | -,115 | ,039 |
| Zn | ,551 | -,010 | ,230 | ,288 | ,082 | -,024 | ,141 | ,514 | -,132 | ,041 |
| Ga | ,397 | ,874 | ,047 | ,036 | -,065 | ,022 | -,021 | ,038 | ,068 | -,021 |
| Ge | ,902 | ,053 | ,140 | ,059 | -,122 | ,112 | -,001 | ,078 | ,093 | -,022 |
| As | ,133 | -,024 | -,035 | ,931 | ,045 | ,039 | -,079 | ,046 | -,039 | -,004 |
| Se | ,679 | ,268 | ,252 | ,099 | -,206 | ,315 | -,072 | ,063 | ,217 | ,066 |
| Br | ,437 | -,057 | ,087 | ,071 | -,292 | ,733 | -,024 | ,066 | ,084 | -,063 |
| Rb | -,009 | ,937 | ,002 | ,016 | -,009 | -,163 | -,108 | ,036 | ,037 | -,015 |
| Sr | ,611 | ,407 | ,015 | ,277 | ,434 | -,020 | -,008 | -,061 | ,010 | ,022 |
| Y | ,690 | ,650 | ,094 | ,077 | ,086 | ,029 | ,129 | ,065 | ,101 | ,010 |
| Zr | -,186 | ,458 | -,024 | ,026 | -,143 | -,005 | ,777 | -,094 | -,016 | ,026 |
| Nb | ,213 | ,906 | -,006 | ,037 | ,023 | ,012 | ,281 | ,007 | ,008 | ,013 |
| Mo | ,916 | ,063 | ,071 | ,144 | -,048 | ,064 | -,034 | ,110 | -,016 | -,012 |
| Hf | -,062 | ,381 | -,013 | ,206 | -,078 | ,040 | ,732 | -,087 | -,116 | ,025 |
| W | ,211 | ,097 | -,055 | ,170 | -,035 | ,055 | ,078 | ,286 | -,604 | -,035 |
| Tl | ,449 | ,030 | ,580 | ,100 | -,085 | ,001 | ,047 | ,250 | ,359 | -,255 |
| Pb | ,469 | -,091 | ,590 | ,143 | -,023 | -,038 | ,159 | ,271 | ,327 | -,219 |
| Bi | -,013 | ,050 | ,844 | ,036 | -,014 | ,057 | -,057 | -,068 | -,107 | ,212 |
| Th | ,414 | ,775 | ,110 | ,237 | ,024 | -,051 | ,239 | ,018 | ,036 | -,010 |
| U | ,334 | ,605 | -,341 | -,092 | -,039 | ,179 | ,141 | -,214 | -,250 | ,119 |
| Ag | ,430 | ,071 | ,796 | ,084 | -,003 | ,006 | ,024 | -,035 | -,125 | ,074 |
| Cd | ,044 | ,027 | ,144 | ,042 | -,054 | -,045 | ,032 | ,078 | ,100 | ,891 |
| Sn | ,732 | -,031 | ,304 | ,130 | ,013 | -,139 | ,064 | ,055 | -,162 | ,044 |
| Sb | ,586 | -,040 | ,197 | ,115 | -,027 | -,036 | ,089 | ,318 | -,246 | -,165 |
| I | -,339 | -,096 | -,079 | -,089 | -,135 | ,658 | ,170 | -,010 | -,103 | -,060 |
| La | ,598 | ,739 | ,018 | ,049 | -,012 | ,101 | ,073 | ,015 | ,005 | ,023 |
| Ce | ,565 | ,765 | ,004 | ,102 | ,026 | ,071 | ,131 | ,032 | ,104 | ,060 |
| Nd | ,569 | ,721 | ,004 | -,011 | ,046 | ,084 | ,011 | ,031 | ,005 | ,077 |
| Sm | ,182 | ,276 | -,189 | -,001 | ,030 | -,037 | ,050 | ,134 | ,562 | ,127 |
| LOI | ,599 | ,046 | ,177 | ,085 | -,056 | ,608 | -,005 | ,022 | -,098 | ,032 |
| pH | -,082 | ,043 | -,087 | ,002 | ,775 | -,371 | ,011 | ,040 | ,045 | -,057 |

Figure 112: Spatial distribution of component scores for BGS soil geochemical data, components C4 to C10 (PCA #A, n=300, 47 variables).

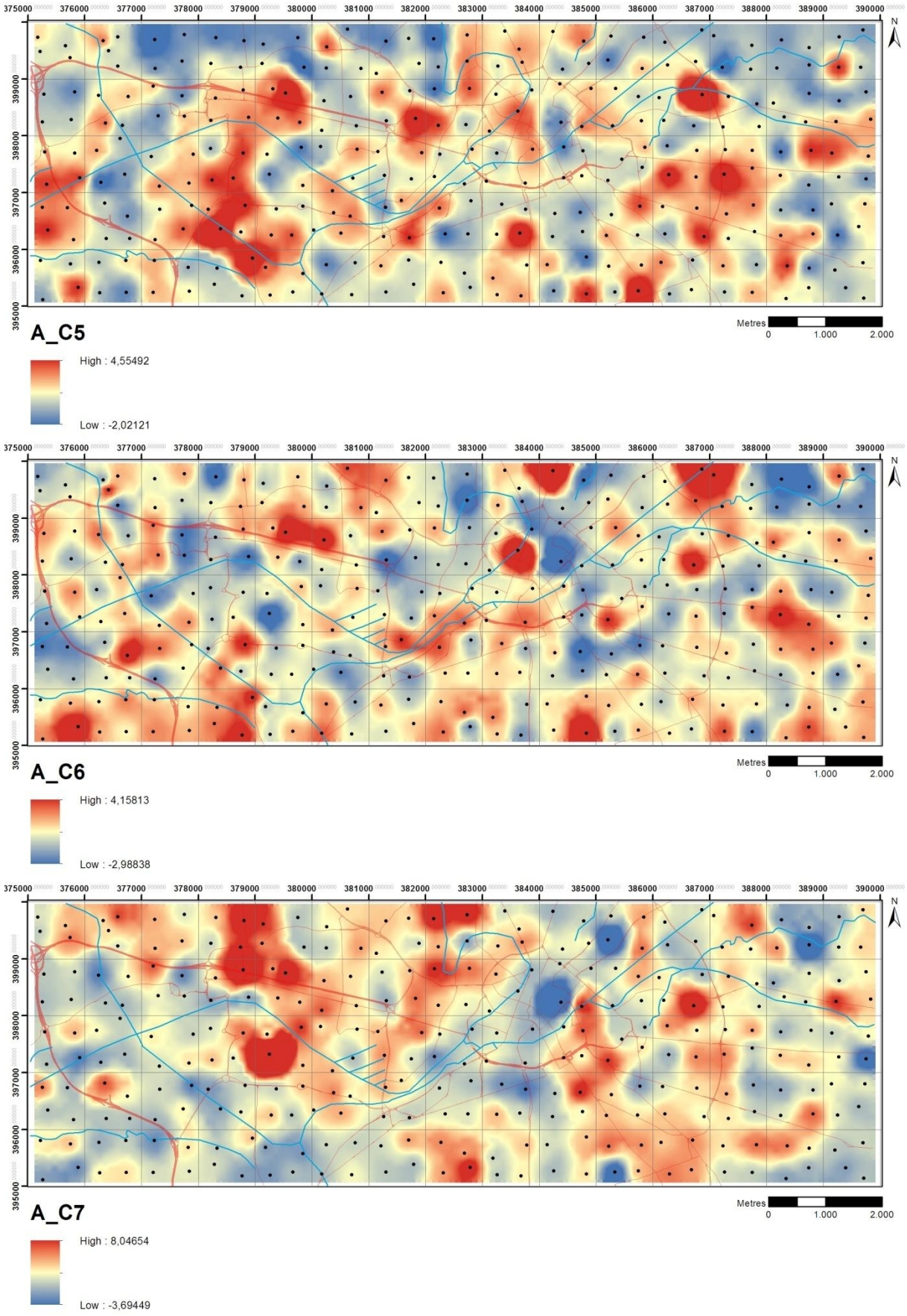

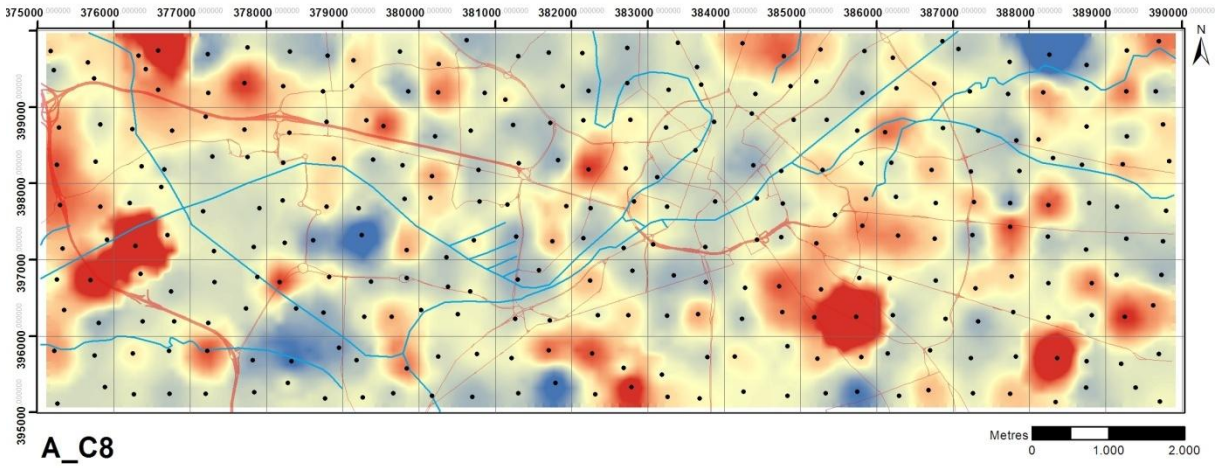


**A_C8**

High : 8,46312

Low : -3,40902

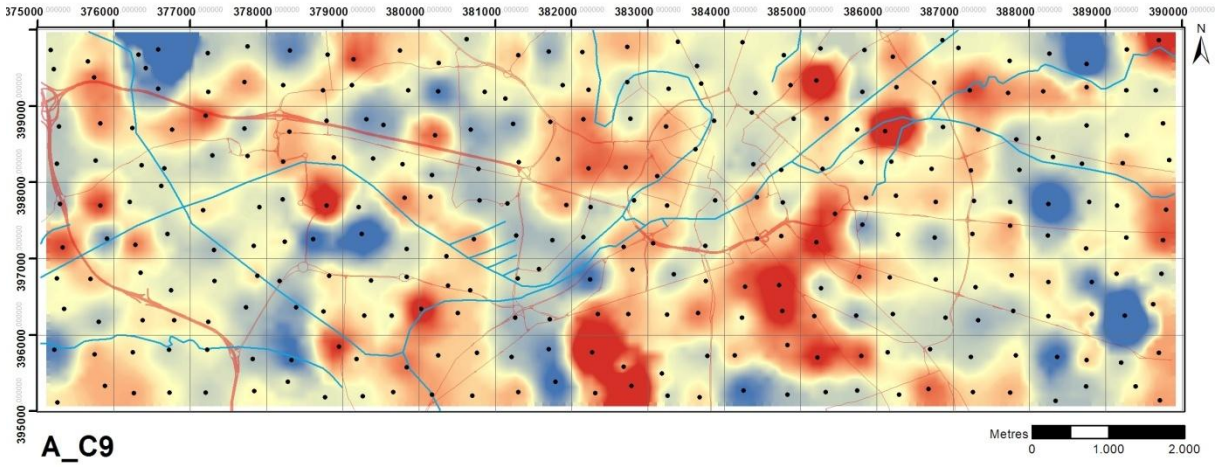


**A_C9**

High : 4,9378

Low : -7,42469

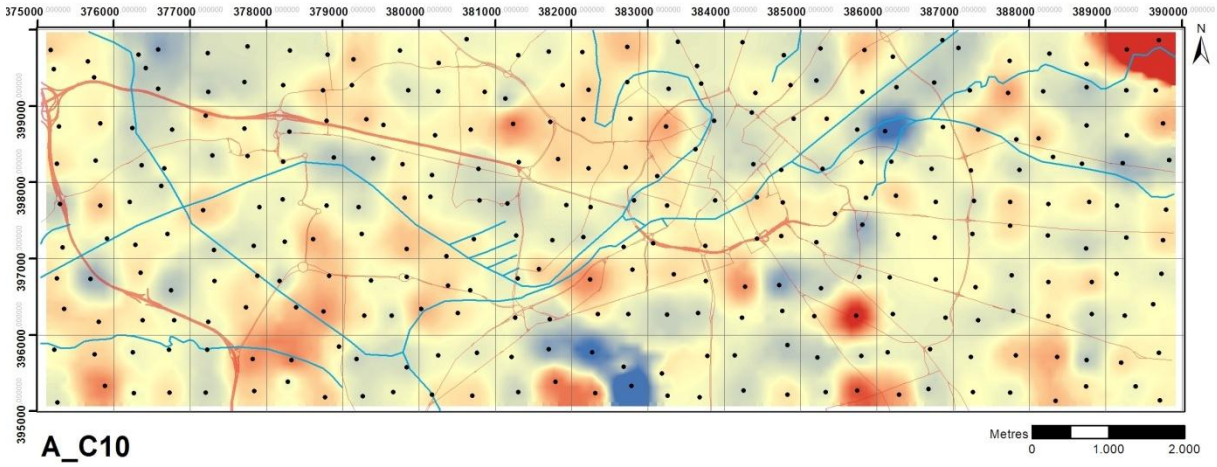


**A_C10**

High : 15,0472

Low : -4,08132

Table 83: Eigenvalues associated to each calculated component for BGS soil geochemical data (Extraction method: Principal component. PCA #B, n=300, 47 variables).

| Total Variance Explained | | | | | | | | | |
|---|---|---|---|---|---|---|---|---|---|
| | Initial Eigenvalues | | | Extraction Sums of Squared Loadings | | | Rotation Sums of Squared Loadings | | |
| Component | Total | % of Variance | Cumulative % | Total | % of Variance | Cumulative % | Total | % of Variance | Cumulative % |
| 1 | 17,880 | 38,043 | 38,043 | 17,880 | 38,043 | 38,043 | 12,233 | 26,028 | 26,028 |
| 2 | 6,777 | 14,418 | 52,461 | 6,777 | 14,418 | 52,461 | 11,512 | 24,494 | 50,522 |
| 3 | 3,102 | 6,601 | 59,062 | 3,102 | 6,601 | 59,062 | 4,014 | 8,539 | 59,062 |
| 4 | 2,354 | 5,009 | 64,071 | | | | | | |
| 5 | 2,156 | 4,588 | 68,659 | | | | | | |
| 6 | 1,696 | 3,608 | 72,268 | | | | | | |
| 7 | 1,252 | 2,663 | 74,931 | | | | | | |
| 8 | 1,147 | 2,441 | 77,372 | | | | | | |
| 9 | 1,123 | 2,389 | 79,761 | | | | | | |
| 10 | 1,035 | 2,203 | 81,964 | | | | | | |
| 11 | ,850 | 1,809 | 83,773 | | | | | | |
| 12 | ,784 | 1,667 | 85,440 | | | | | | |
| 13 | ,704 | 1,498 | 86,938 | | | | | | |
| 14 | ,680 | 1,447 | 88,385 | | | | | | |
| 15 | ,594 | 1,263 | 89,648 | | | | | | |
| 16 | ,550 | 1,170 | 90,819 | | | | | | |
| 17 | ,468 | ,996 | 91,815 | | | | | | |
| 18 | ,378 | ,803 | 92,618 | | | | | | |
| 19 | ,351 | ,747 | 93,366 | | | | | | |
| 20 | ,341 | ,726 | 94,092 | | | | | | |
| 21 | ,304 | ,647 | 94,739 | | | | | | |
| 22 | ,271 | ,577 | 95,315 | | | | | | |
| 23 | ,238 | ,505 | 95,820 | | | | | | |
| 24 | ,222 | ,473 | 96,294 | | | | | | |
| 25 | ,204 | ,435 | 96,729 | | | | | | |
| 26 | ,171 | ,364 | 97,093 | | | | | | |
| 27 | ,154 | ,328 | 97,421 | | | | | | |
| 28 | ,143 | ,303 | 97,724 | | | | | | |
| 29 | ,132 | ,281 | 98,005 | | | | | | |
| 30 | ,118 | ,251 | 98,257 | | | | | | |
| 31 | ,105 | ,223 | 98,480 | | | | | | |
| 32 | ,099 | ,210 | 98,689 | | | | | | |
| 33 | ,088 | ,187 | 98,876 | | | | | | |
| 34 | ,078 | ,166 | 99,042 | | | | | | |
| 35 | ,067 | ,143 | 99,185 | | | | | | |
| 36 | ,063 | ,134 | 99,320 | | | | | | |
| 37 | ,059 | ,126 | 99,446 | | | | | | |
| 38 | ,050 | ,106 | 99,551 | | | | | | |
| 39 | ,043 | ,092 | 99,643 | | | | | | |
| 40 | ,038 | ,080 | 99,723 | | | | | | |
| 41 | ,035 | ,074 | 99,797 | | | | | | |
| 42 | ,023 | ,048 | 99,845 | | | | | | |
| 43 | ,020 | ,042 | 99,888 | | | | | | |
| 44 | ,019 | ,041 | 99,929 | | | | | | |
| 45 | ,017 | ,036 | 99,964 | | | | | | |
| 46 | ,009 | ,020 | 99,984 | | | | | | |
| 47 | ,007 | ,016 | 100,000 | | | | | | |

Table 84: Rotated component matrix (Varimax rotation with Kaiser normalisation) for BGS soil geochemical data (PCA #A, n=300, 47 variables).

| Rotated Component Matrix | | | | | | | |
|---|---|---|---|---|---|---|---|
| | Component | | | | Component | | |
| | 1 | 2 | 3 | | 1 | 2 | 3 |
| Na2O | -,003 | ,184 | ,033 | Sr | ,493 | ,427 | ,549 |
| MgO | ,559 | -,314 | ,273 | Y | ,754 | ,565 | ,217 |
| Al2O3 | ,964 | ,028 | ,005 | Zr | ,523 | -,194 | -,194 |
| SiO2 | -,532 | -,599 | -,268 | Nb | ,947 | ,104 | ,051 |
| P2O5 | -,138 | ,694 | -,162 | Mo | ,198 | ,841 | ,213 |
| K2O | ,805 | -,214 | ,208 | Hf | ,448 | -,052 | -,049 |
| CaO | ,027 | ,052 | ,742 | W | ,106 | ,232 | ,129 |
| TiO2 | ,936 | ,105 | -,087 | Tl | ,024 | ,657 | ,116 |
| MnO | ,161 | ,342 | ,204 | Pb | -,075 | ,674 | ,194 |
| Fe2O3 | ,525 | ,700 | ,285 | Bi | -,068 | ,323 | -,032 |
| Sc | ,739 | ,547 | ,204 | Th | ,824 | ,334 | ,230 |
| V | ,621 | ,683 | ,158 | U | ,717 | ,107 | -,134 |
| Cr | ,042 | ,296 | ,547 | Ag | ,043 | ,660 | ,113 |
| Co | ,497 | ,703 | ,296 | Cd | ,050 | ,108 | ,005 |
| Ba | ,285 | ,489 | ,177 | Sn | ,063 | ,700 | ,290 |
| Ni | ,482 | ,730 | ,338 | Sb | ,021 | ,616 | ,222 |
| Cu | ,039 | ,477 | ,591 | I | -,126 | -,087 | -,532 |
| Zn | ,040 | ,642 | ,389 | La | ,823 | ,480 | ,085 |
| Ga | ,897 | ,302 | ,055 | Ce | ,853 | ,441 | ,141 |
| Ge | ,190 | ,866 | ,085 | Nd | ,799 | ,432 | ,101 |
| As | -,076 | ,245 | ,538 | Sm | ,347 | ,064 | ,079 |
| Se | ,332 | ,793 | -,089 | LOI | ,117 | ,773 | -,164 |
| Br | -,008 | ,697 | -,409 | pH | ,055 | -,342 | ,675 |
| Rb | ,878 | -,124 | ,098 | | | | |

Table 85: Anti-image correlation matrix for BGS soil geochemical data (PCA #C, n=300, 17 variables).

| | Al2O3 | P2O5 | TiO2 | Fe2O3 | Cr | Co | Ba | Ni | Cu | Zn | Ga | As | Mo | Pb | Ag | Sn | Sb |
|---|---|---|---|---|---|---|---|---|---|---|---|---|---|---|---|---|---|
| Al2O3 | 0,589 | ,289 | -,763 | ,023 | -,117 | -,107 | -,198 | ,108 | -,334 | ,009 | -,796 | ,339 | ,369 | ,197 | -,093 | ,182 | ,037 |
| P2O5 | ,289 | 0,766 | -,306 | ,098 | -,024 | -,024 | ,036 | -,042 | ,005 | -,058 | -,142 | ,016 | -,024 | -,139 | -,475 | ,150 | -,049 |
| TiO2 | -,763 | -,306 | 0,741 | -,114 | ,045 | ,136 | ,130 | -,047 | ,114 | -,046 | ,296 | -,098 | -,134 | -,085 | ,112 | -,073 | -,031 |
| Fe2O3 | ,023 | ,098 | -,114 | 0,937 | ,028 | -,359 | ,013 | -,098 | ,063 | -,039 | -,124 | -,086 | -,303 | -,030 | -,058 | -,291 | -,016 |
| Cr | -,117 | -,024 | ,045 | ,028 | 0,832 | ,073 | ,035 | -,125 | -,049 | -,107 | ,085 | -,508 | ,035 | -,258 | -,139 | ,080 | ,088 |
| Co | -,107 | -,024 | ,136 | -,359 | ,073 | 0,897 | ,122 | -,617 | ,046 | -,031 | ,026 | -,037 | -,137 | -,001 | -,049 | ,080 | ,018 |
| Ba | -,198 | ,036 | ,130 | ,013 | ,035 | ,122 | 0,907 | -,160 | ,098 | -,083 | ,111 | -,091 | -,104 | -,163 | -,259 | -,008 | -,060 |
| Ni | ,108 | -,042 | -,047 | -,098 | -,125 | -,617 | -,160 | 0,893 | -,267 | -,025 | -,155 | ,249 | -,139 | ,072 | ,097 | ,049 | -,039 |
| Cu | -,334 | ,005 | ,114 | ,063 | -,049 | ,046 | ,098 | -,267 | 0,758 | -,119 | ,410 | -,715 | -,105 | -,118 | -,032 | -,290 | -,101 |
| Zn | ,009 | -,058 | -,046 | -,039 | -,107 | -,031 | -,083 | -,025 | -,119 | 0,968 | ,059 | ,038 | -,030 | -,118 | ,023 | -,151 | -,169 |
| Ga | -,796 | -,142 | ,296 | -,124 | ,085 | ,026 | ,111 | -,155 | ,410 | ,059 | 0,746 | -,392 | -,296 | -,184 | ,032 | -,134 | -,013 |
| As | ,339 | ,016 | -,098 | -,086 | -,508 | -,037 | -,091 | ,249 | -,715 | ,038 | -,392 | 0,584 | ,053 | ,260 | ,105 | ,185 | ,023 |
| Mo | ,369 | -,024 | -,134 | -,303 | ,035 | -,137 | -,104 | -,139 | -,105 | -,030 | -,296 | ,053 | 0,921 | -,025 | ,053 | -,045 | -,069 |
| Pb | ,197 | -,139 | -,085 | -,030 | -,258 | -,001 | -,163 | ,072 | -,118 | -,118 | -,184 | ,260 | -,025 | 0,884 | -,133 | ,033 | -,140 |
| Ag | -,093 | -,475 | ,112 | -,058 | -,139 | -,049 | -,259 | ,097 | -,032 | ,023 | ,032 | ,105 | ,053 | -,133 | 0,849 | -,362 | ,039 |
| Sn | ,182 | ,150 | -,073 | -,291 | ,080 | ,080 | -,008 | ,049 | -,290 | -,151 | -,134 | ,185 | -,045 | ,033 | -,362 | 0,892 | -,046 |
| Sb | ,037 | -,049 | -,031 | -,016 | ,088 | ,018 | -,060 | -,039 | -,101 | -,169 | -,013 | ,023 | -,069 | -,140 | ,039 | -,046 | 0,966 |

Table 86: Communalities for BGS soil geochemical data (Extraction method: Principal component. PCA #C, n=300, 17 variables).

| Communalities | | |
|---|---|---|
| | Initial | Extraction |
| Al2O3 | 1,000 | ,972 |
| P2O5 | 1,000 | ,666 |
| TiO2 | 1,000 | ,916 |
| Fe2O3 | 1,000 | ,926 |
| Cr | 1,000 | ,853 |
| Co | 1,000 | ,901 |
| Ba | 1,000 | ,510 |
| Ni | 1,000 | ,900 |
| Cu | 1,000 | ,877 |
| Zn | 1,000 | ,619 |
| Ga | 1,000 | ,944 |
| As | 1,000 | ,908 |
| Mo | 1,000 | ,871 |
| Pb | 1,000 | ,642 |
| Ag | 1,000 | ,761 |
| Sn | 1,000 | ,691 |
| Sb | 1,000 | ,496 |

Table 87: Rotated component matrix (Varimax rotation with Kaiser normalisation) for BGS soil geochemical data (PCA #C, n=300, 17 variables).

| Rotated Component Matrix | | | | |
|---|---|---|---|---|
| | Component | | | |
| | 1 | 2 | 3 | 4 |
| Al2O3 | ,088 | ,982 | -,021 | ,009 |
| P2O5 | ,151 | -,073 | ,797 | ,062 |
| TiO2 | ,091 | ,952 | ,042 | ,008 |
| Fe2O3 | ,808 | ,463 | ,201 | ,135 |
| Cr | ,069 | ,117 | ,228 | ,885 |
| Co | ,833 | ,412 | ,161 | ,110 |
| Ba | ,285 | ,357 | ,542 | ,091 |
| Ni | ,827 | ,396 | ,188 | ,155 |
| Cu | ,409 | ,022 | ,140 | ,830 |
| Zn | ,588 | ,010 | ,389 | ,349 |
| Ga | ,344 | ,905 | ,065 | ,049 |
| As | ,130 | -,037 | -,014 | ,943 |
| Mo | ,879 | ,120 | ,248 | ,146 |
| Pb | ,358 | -,026 | ,704 | ,129 |
| Ag | ,293 | ,127 | ,805 | ,103 |
| Sn | ,719 | ,025 | ,389 | ,150 |
| Sb | ,614 | -,052 | ,315 | ,131 |

Table 88: Eigenvalues associated to each calculated component for BGS soil geochemical data (Extraction method: Principal component. PCA #C, n=300, 17 variables).

| Total Variance Explained | | | | | | | | | |
|---|---|---|---|---|---|---|---|---|---|
| | Initial Eigenvalues | | | Extraction Sums of Squared Loadings | | | Rotation Sums of Squared Loadings | | |
| Component | Total | % of Variance | Cumulative % | Total | % of Variance | Cumulative % | Total | % of Variance | Cumulative % |
| 1 | 7,650 | 44,998 | 44,998 | 7,650 | 44,998 | 44,998 | 4,686 | 27,564 | 27,564 |
| 2 | 2,856 | 16,797 | 61,795 | 2,856 | 16,797 | 61,795 | 3,411 | 20,067 | 47,631 |
| 3 | 1,833 | 10,779 | 72,575 | 1,833 | 10,779 | 72,575 | 2,716 | 15,974 | 63,606 |
| 4 | 1,115 | 6,561 | 79,136 | 1,115 | 6,561 | 79,136 | 2,640 | 15,530 | 79,136 |
| 5 | ,657 | 3,864 | 83,000 | | | | | | |
| 6 | ,611 | 3,592 | 86,592 | | | | | | |
| 7 | ,491 | 2,890 | 89,483 | | | | | | |
| 8 | ,459 | 2,702 | 92,185 | | | | | | |
| 9 | ,401 | 2,358 | 94,543 | | | | | | |
| 10 | ,253 | 1,490 | 96,033 | | | | | | |
| 11 | ,201 | 1,181 | 97,214 | | | | | | |
| 12 | ,158 | ,927 | 98,141 | | | | | | |
| 13 | ,113 | ,668 | 98,809 | | | | | | |
| 14 | ,077 | ,454 | 99,263 | | | | | | |
| 15 | ,063 | ,371 | 99,634 | | | | | | |
| 16 | ,048 | ,279 | 99,914 | | | | | | |
| 17 | ,015 | ,086 | 100,000 | | | | | | |

## *3. Soil Mapping*

### Proportional symbol/colour maps for Manchester soil

Chemical elements in alphabetical order followed by LOI, TC, TOC, TIC and pH.

# Aluminium

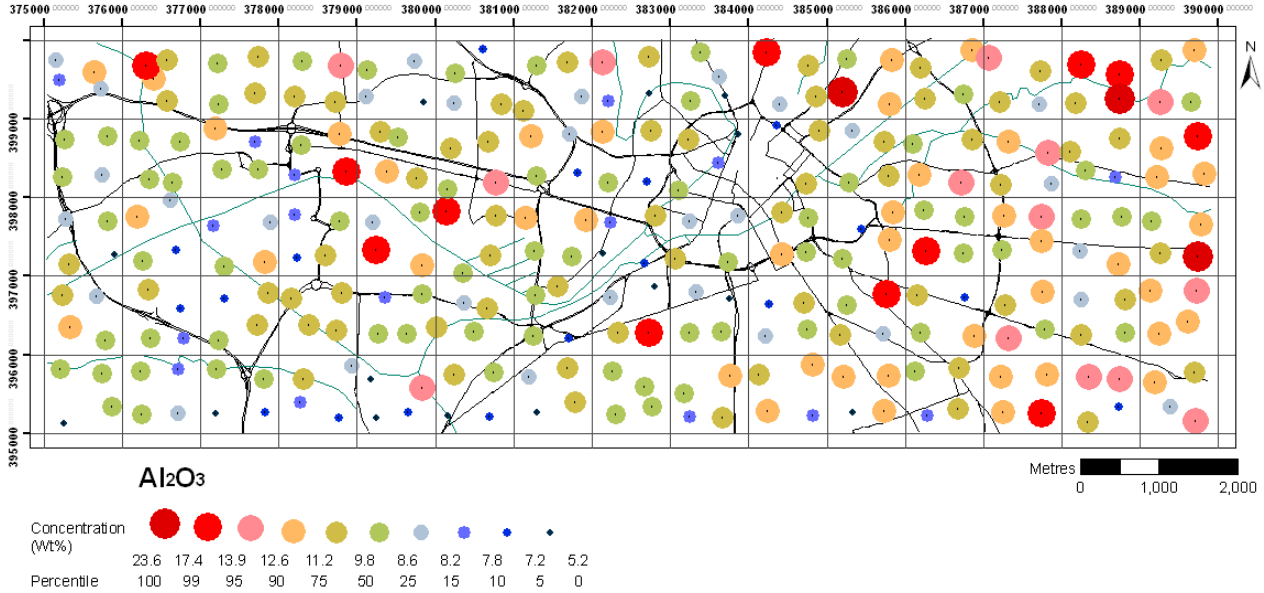


# Antimony

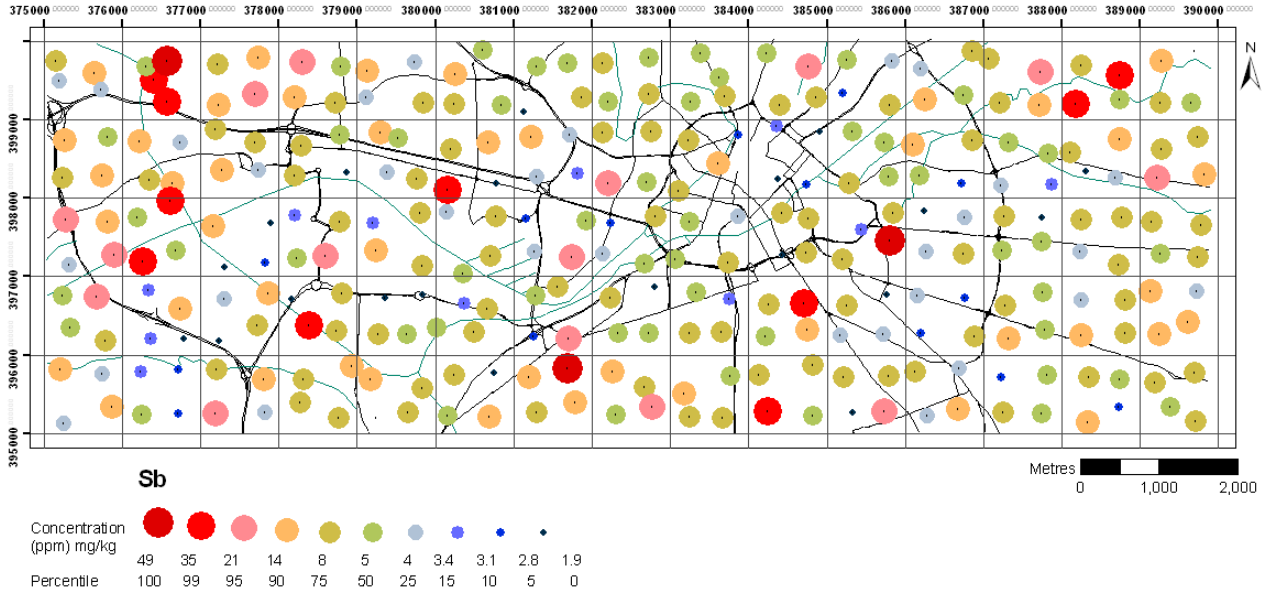

# Arsenic

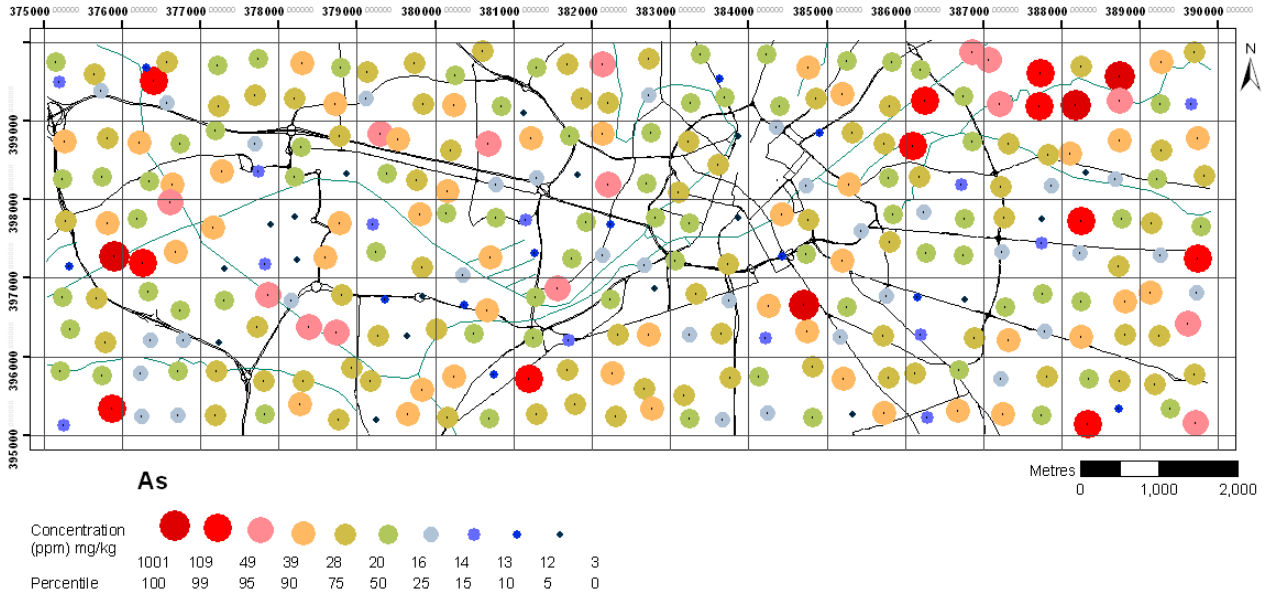


# Barium

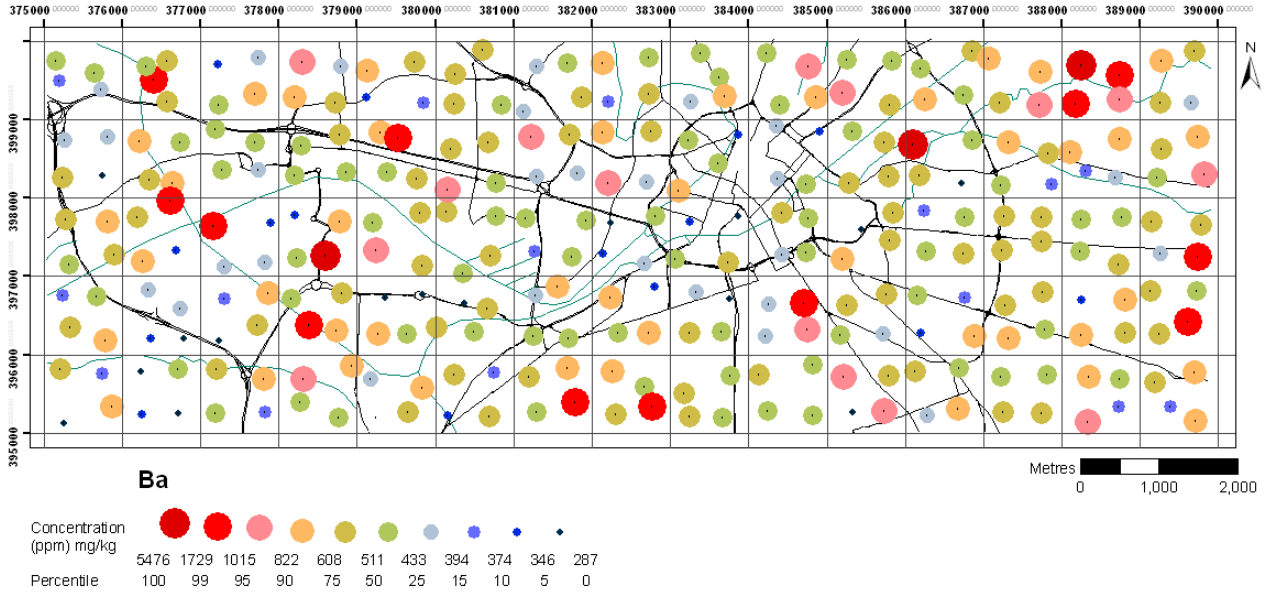

# Cadmium

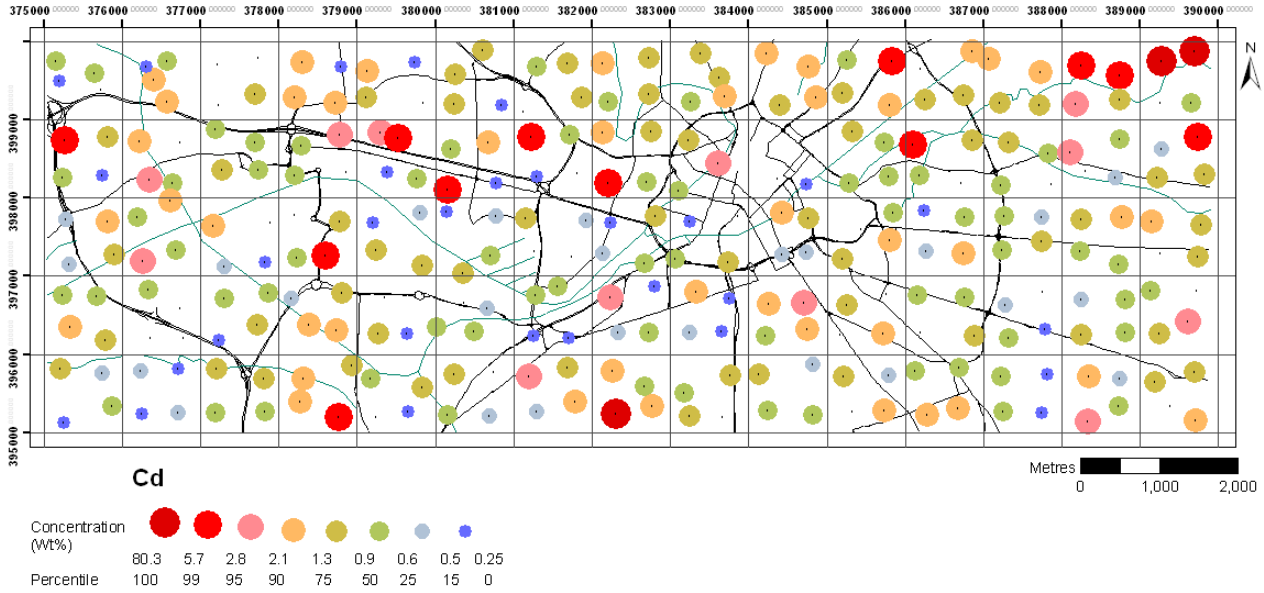


# Calcium

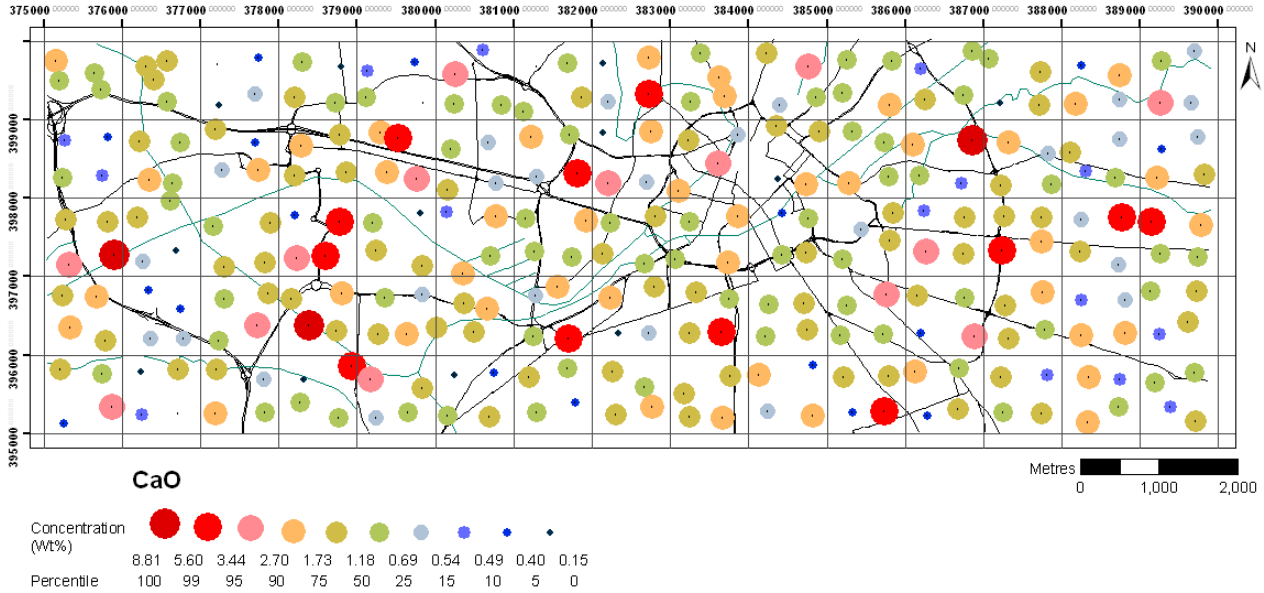

# Chromium

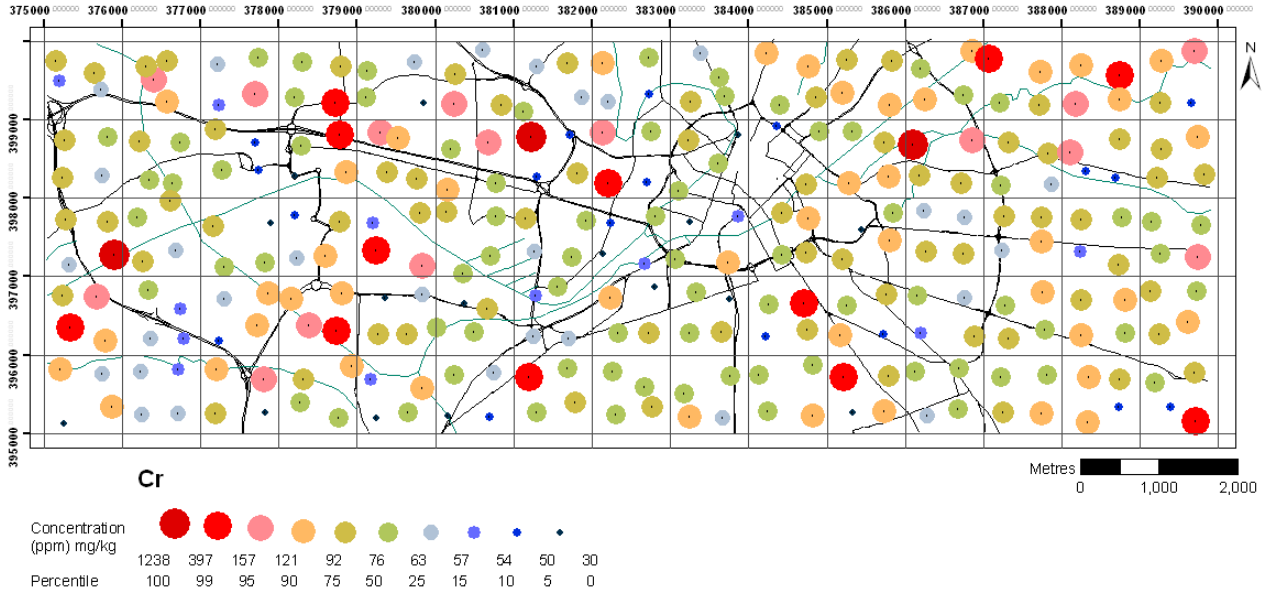


# Cobalt

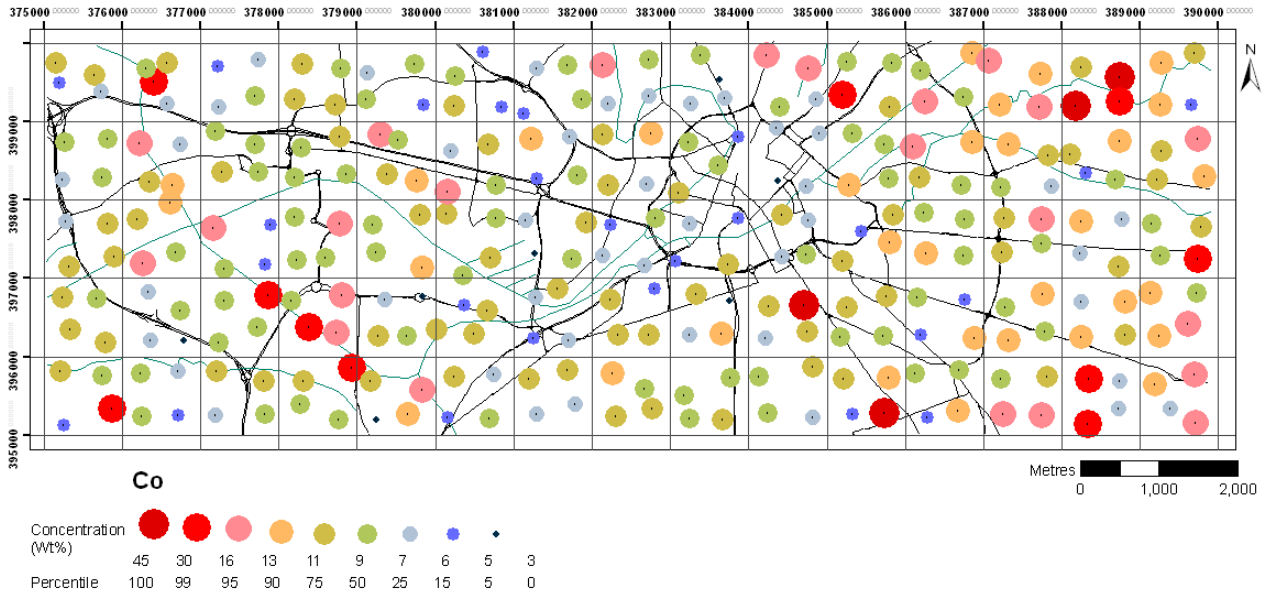

# Copper

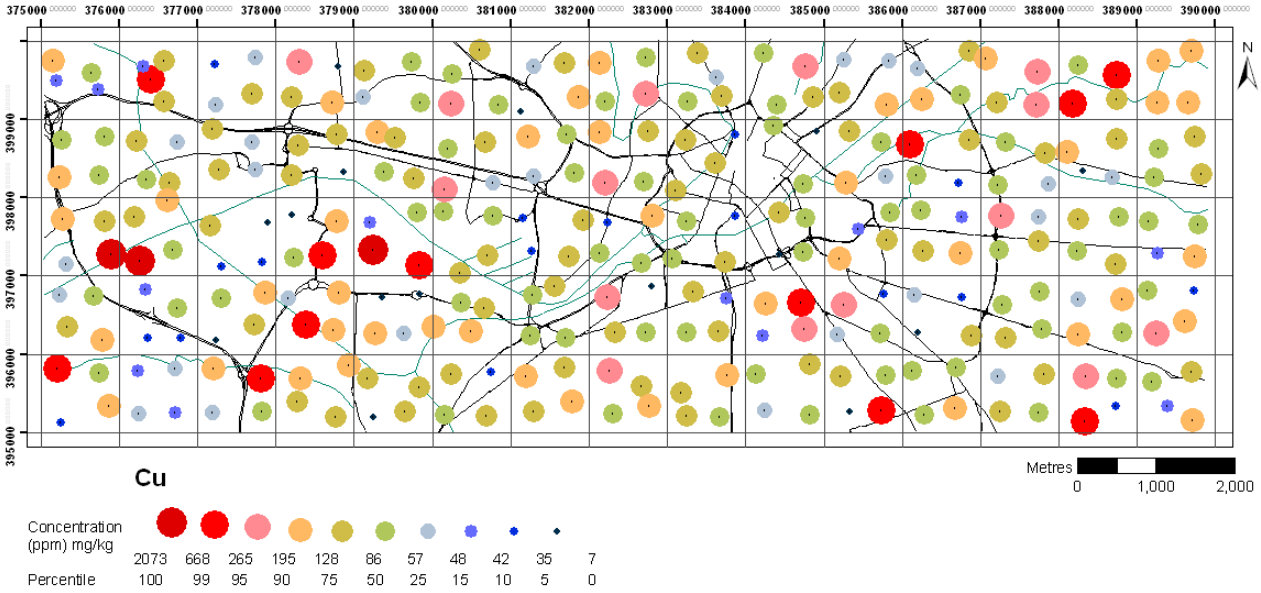
375000 376000 377000 378000 379000 380000 381000 382000 383000 384000 385000 386000 387000 388000 389000 390000
399000 398000 397000 396000 395000
N
Cu
Metres
0 1,000 2,000
Concentration (ppm) mg/kg
2073 668 265 195 128 86 57 48 42 35 7
Percentile
100 99 95 90 75 50 25 15 10 5 0

# Iron

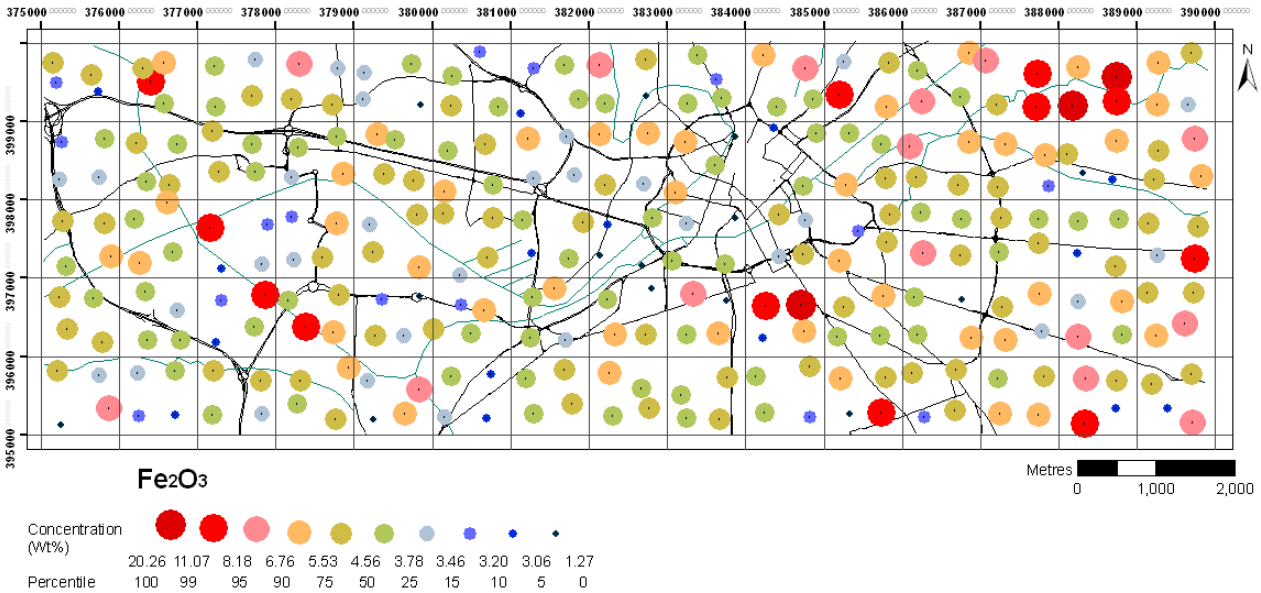
375000 376000 377000 378000 379000 380000 381000 382000 383000 384000 385000 386000 387000 388000 389000 390000
399000 398000 397000 396000 395000
N
Fe2O3
Metres
0 1,000 2,000
Concentration (Wt%)
20.26 11.07 8.18 6.76 5.53 4.56 3.78 3.46 3.20 3.06 1.27
Percentile
100 99 95 90 75 50 25 15 10 5 0

# Lead

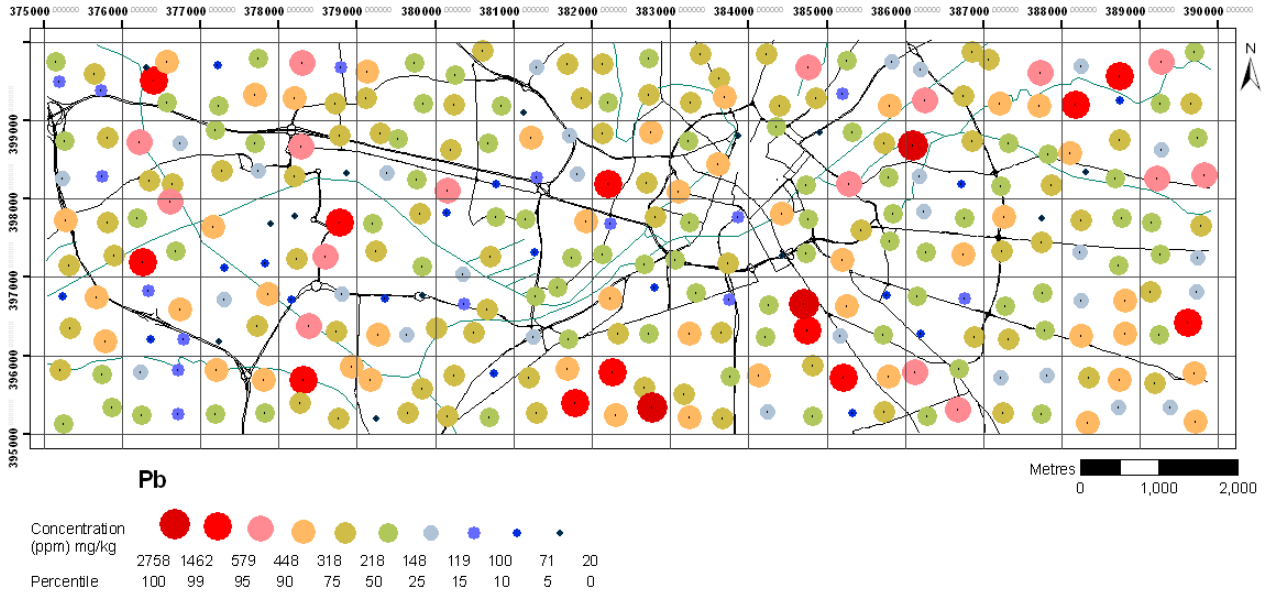


# Magnesium

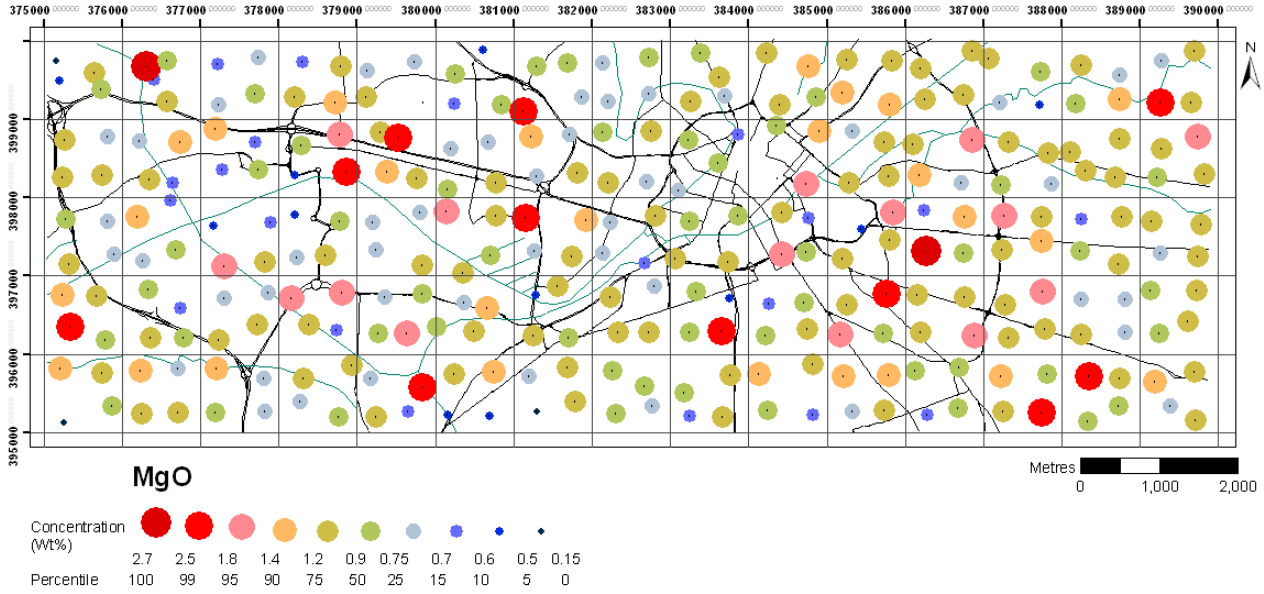

# Manganese

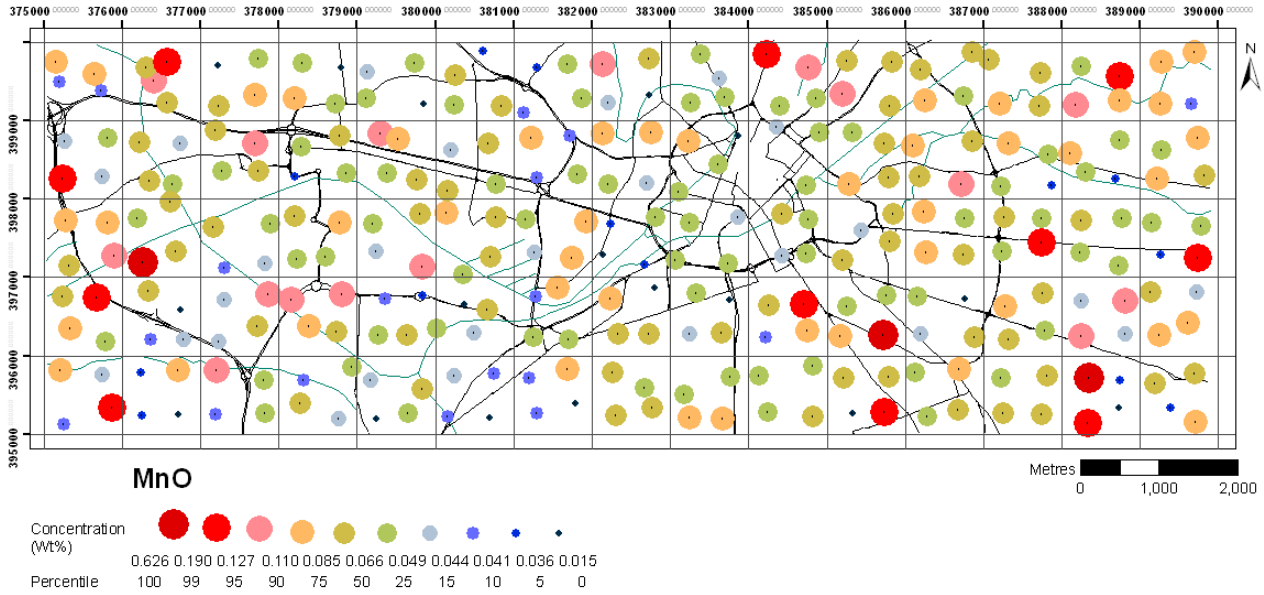


# Molybdenum

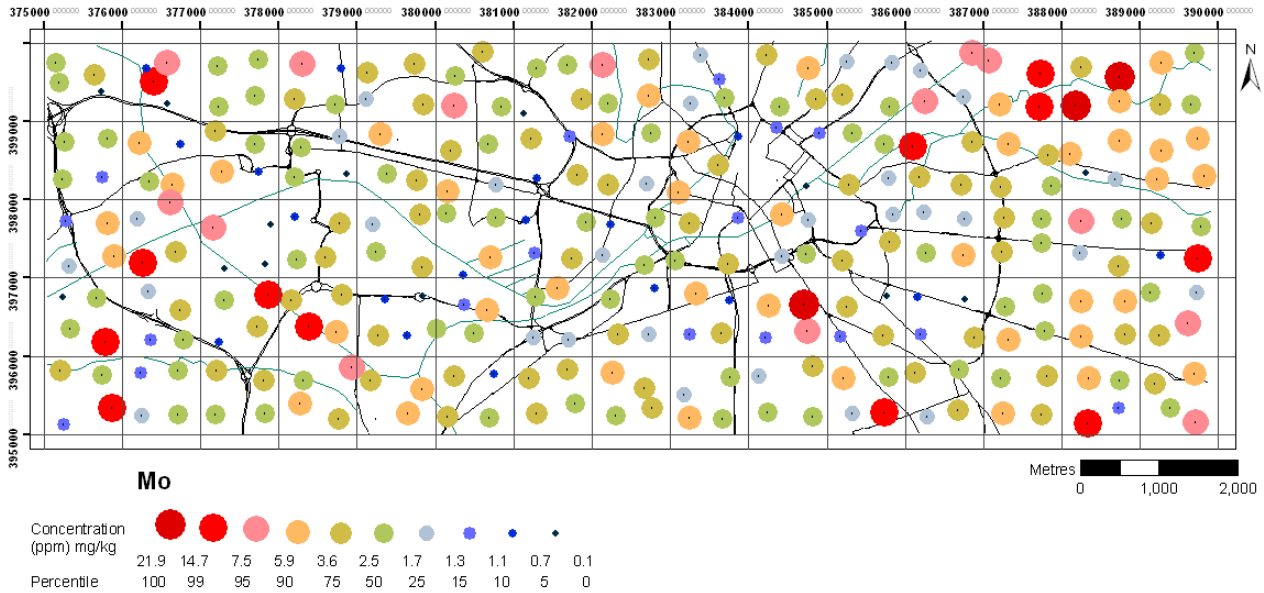

# Nickel

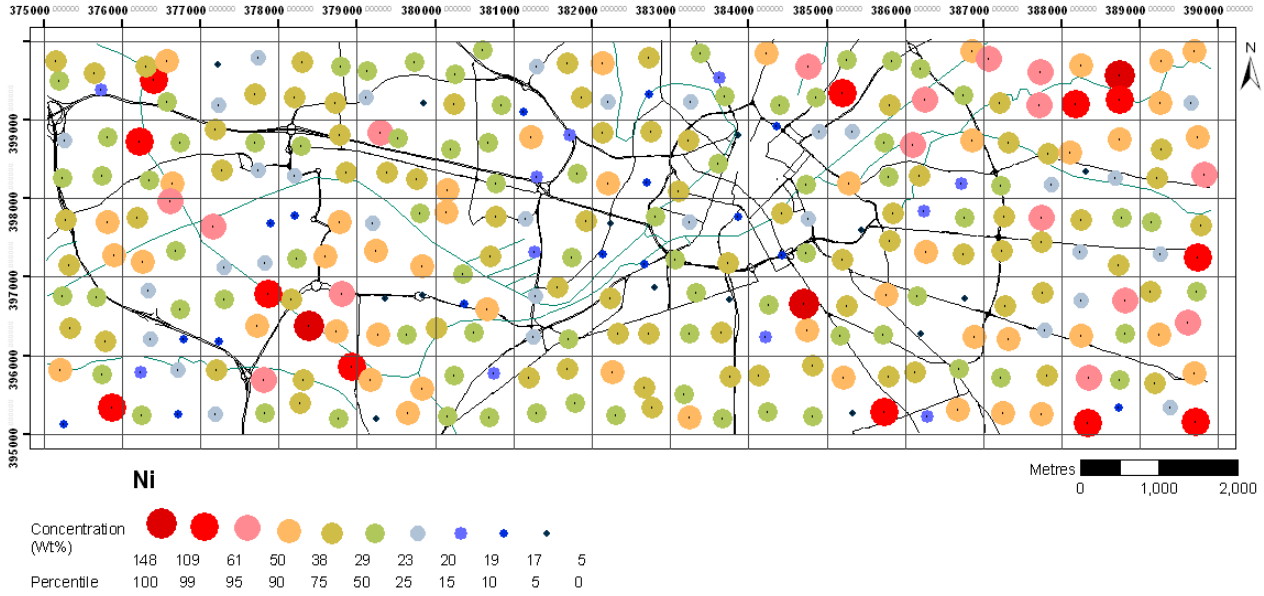


# Phosphorus

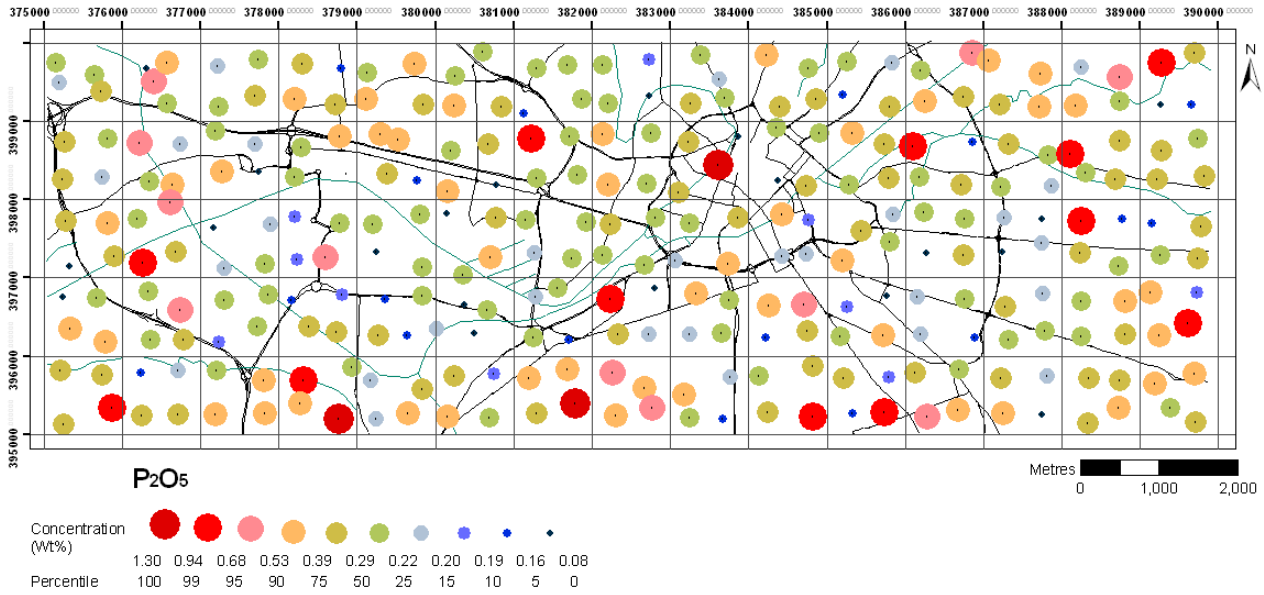

# Potassium

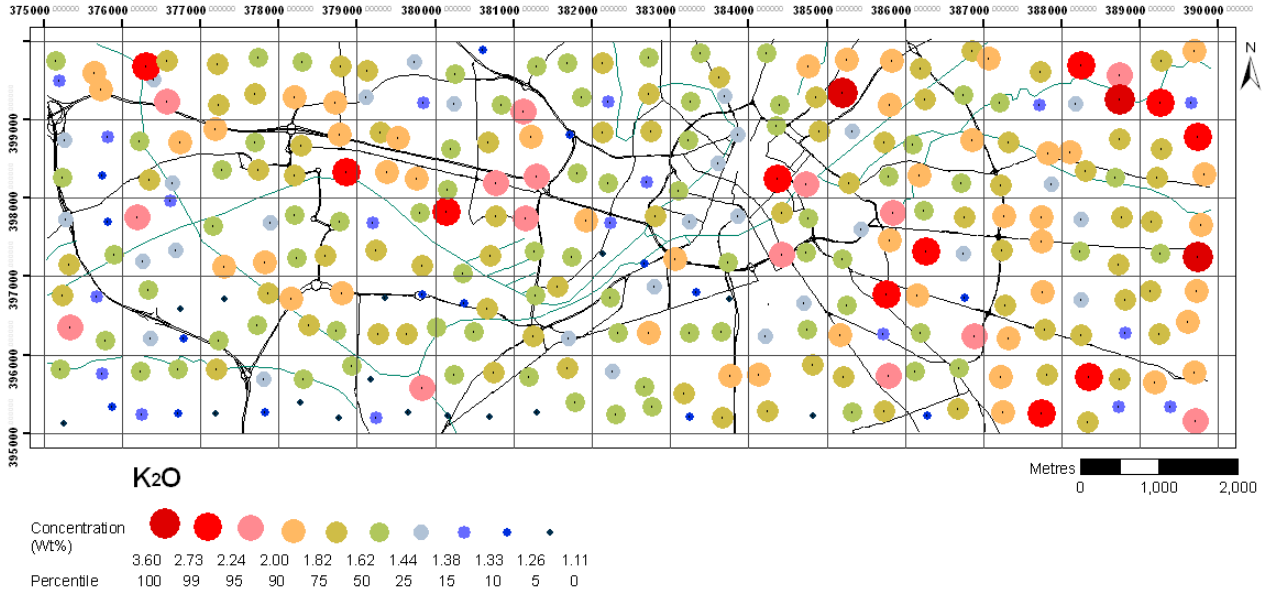


# Silicon

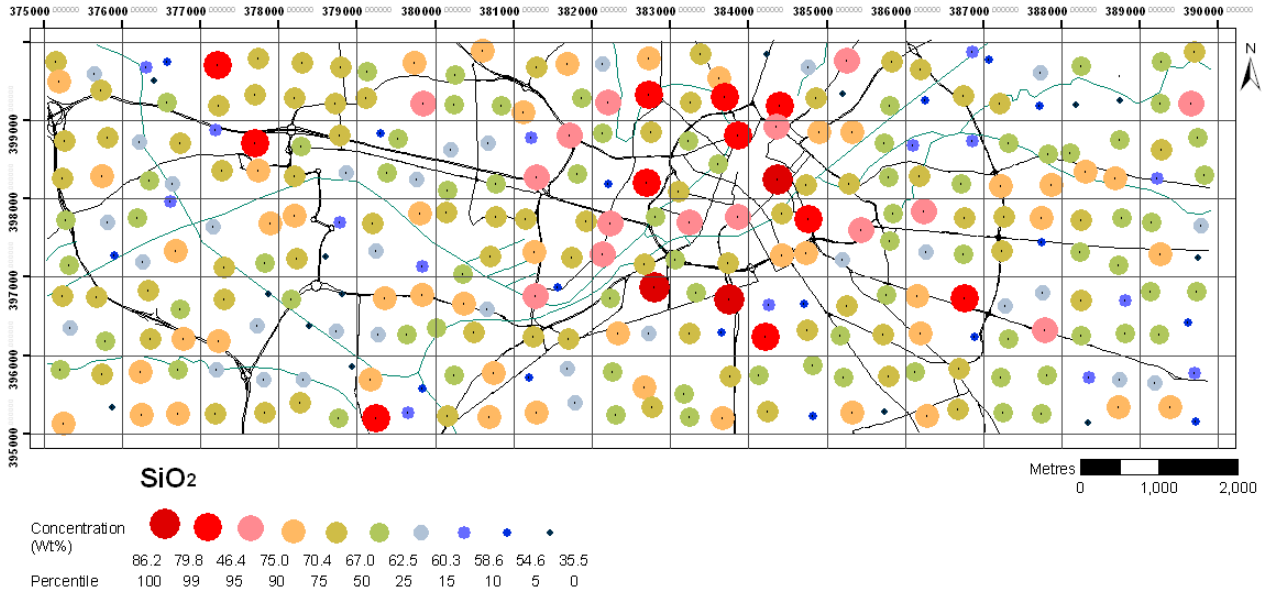

# Tin

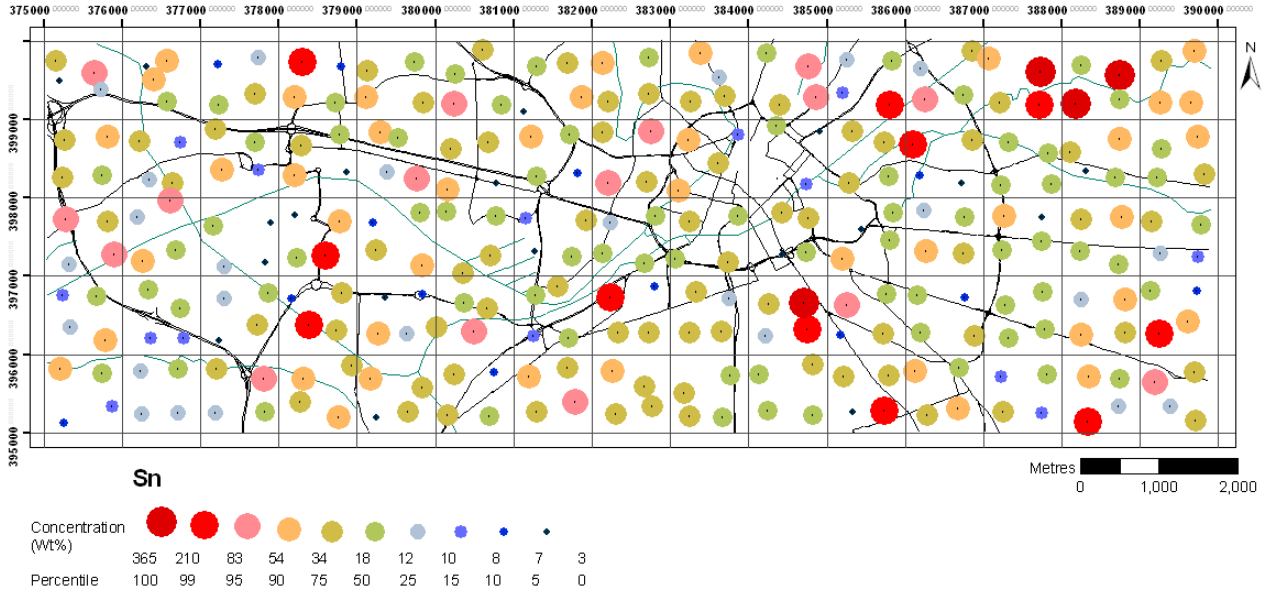


# Titanium

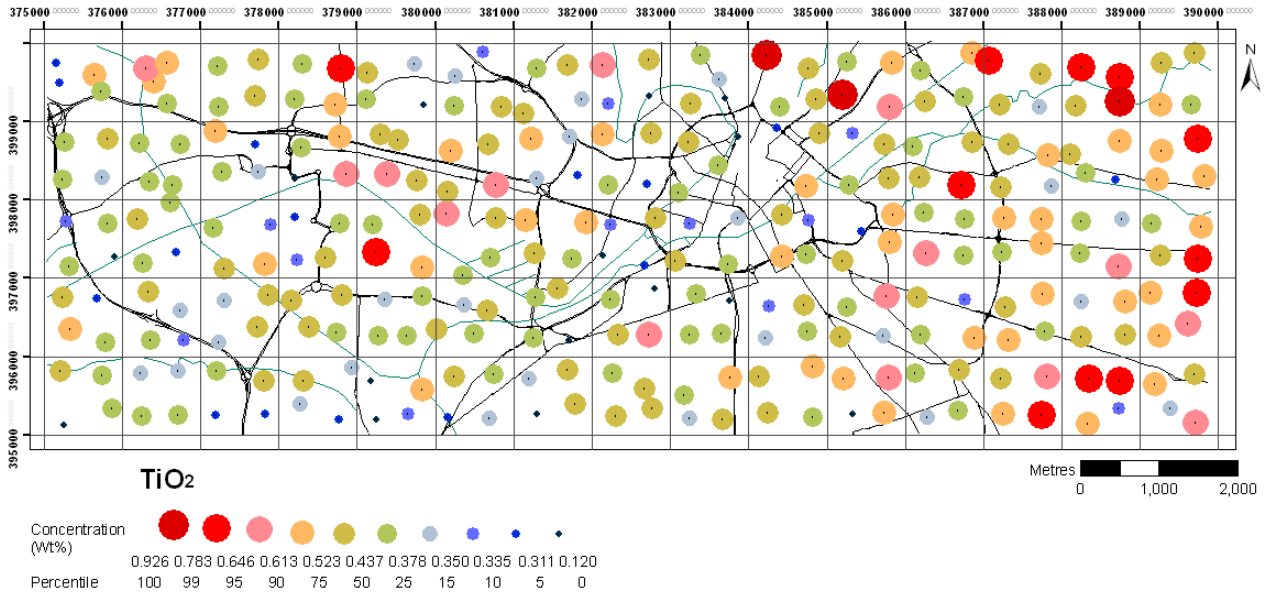

# Uranium

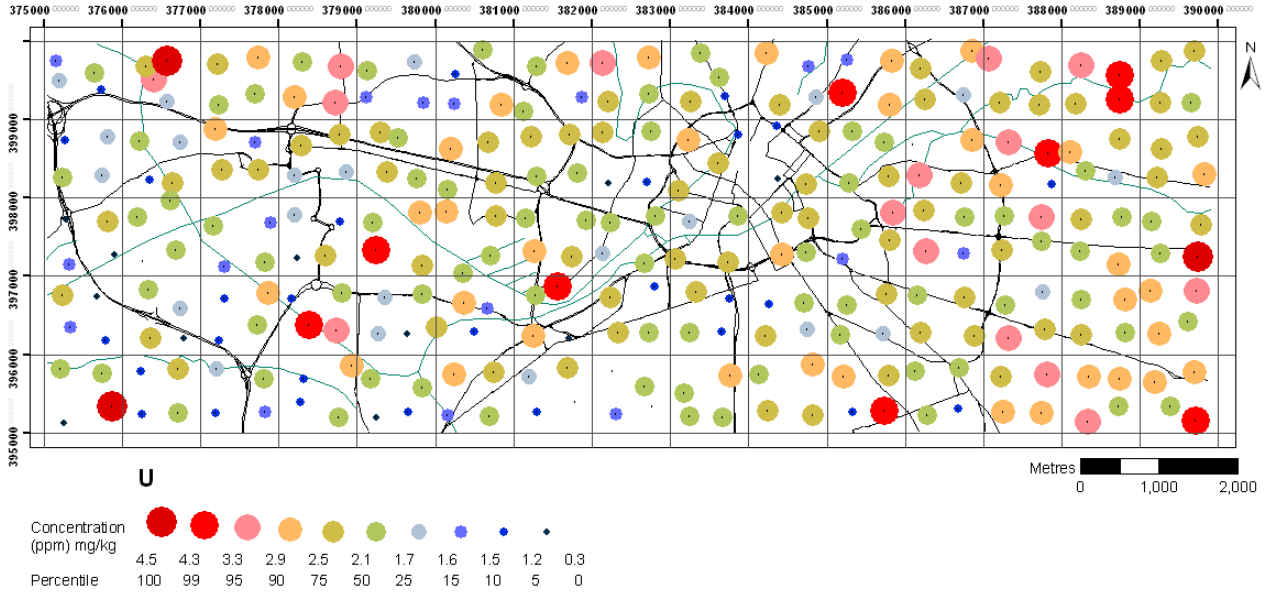


# Vanadium

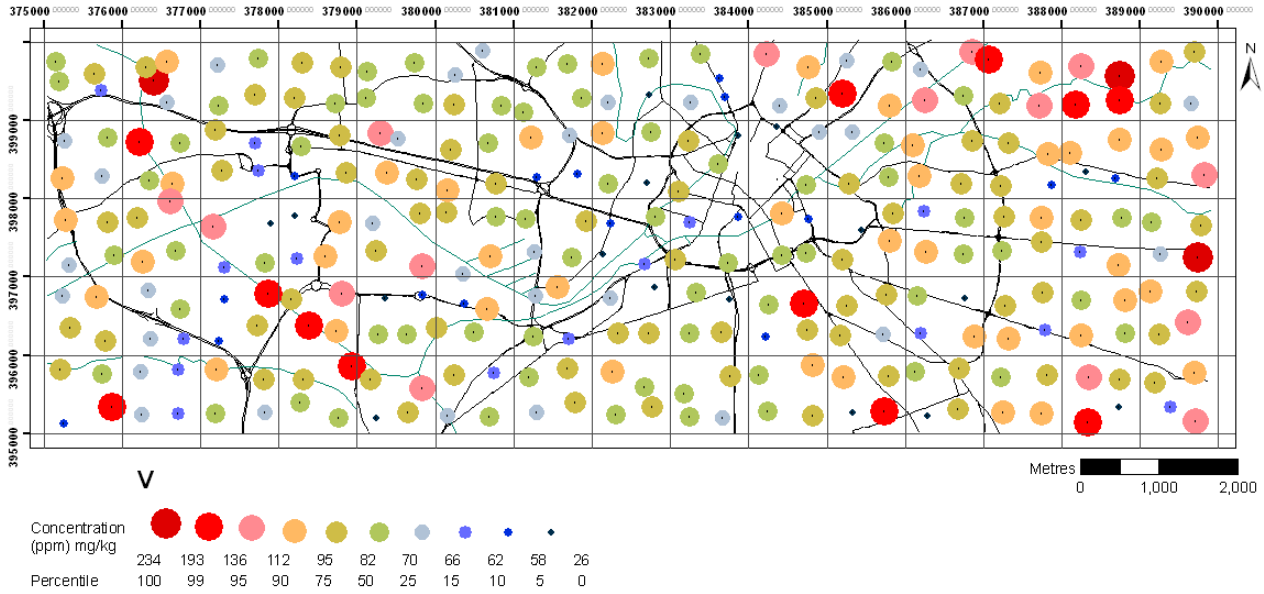

# Zinc

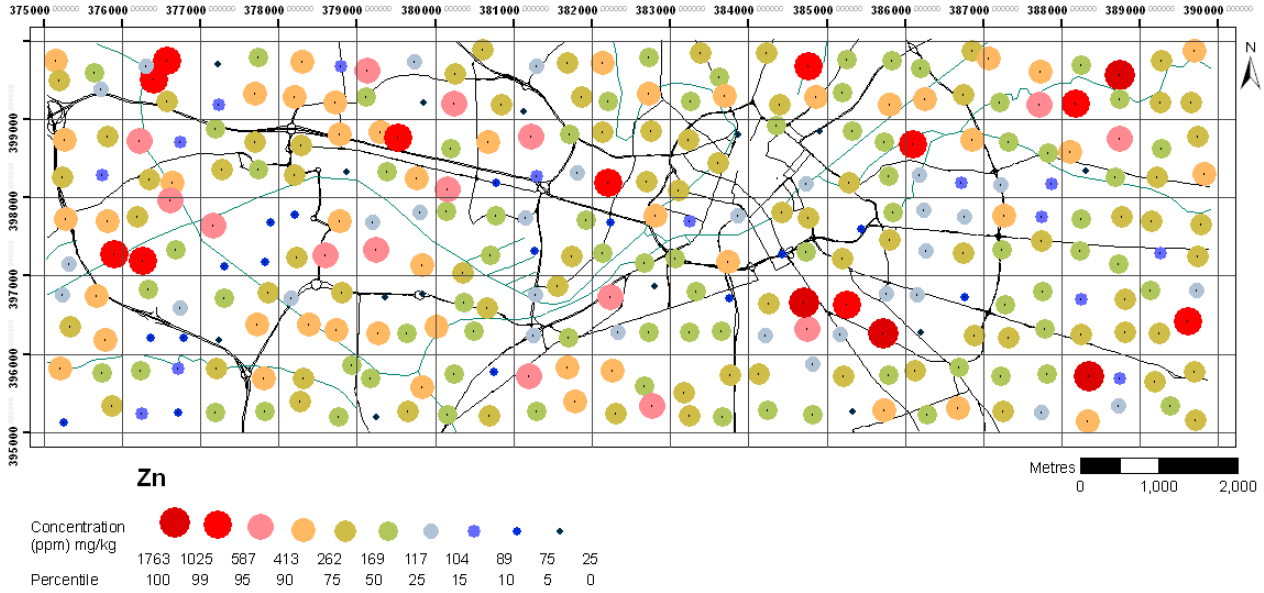


# Organic matter

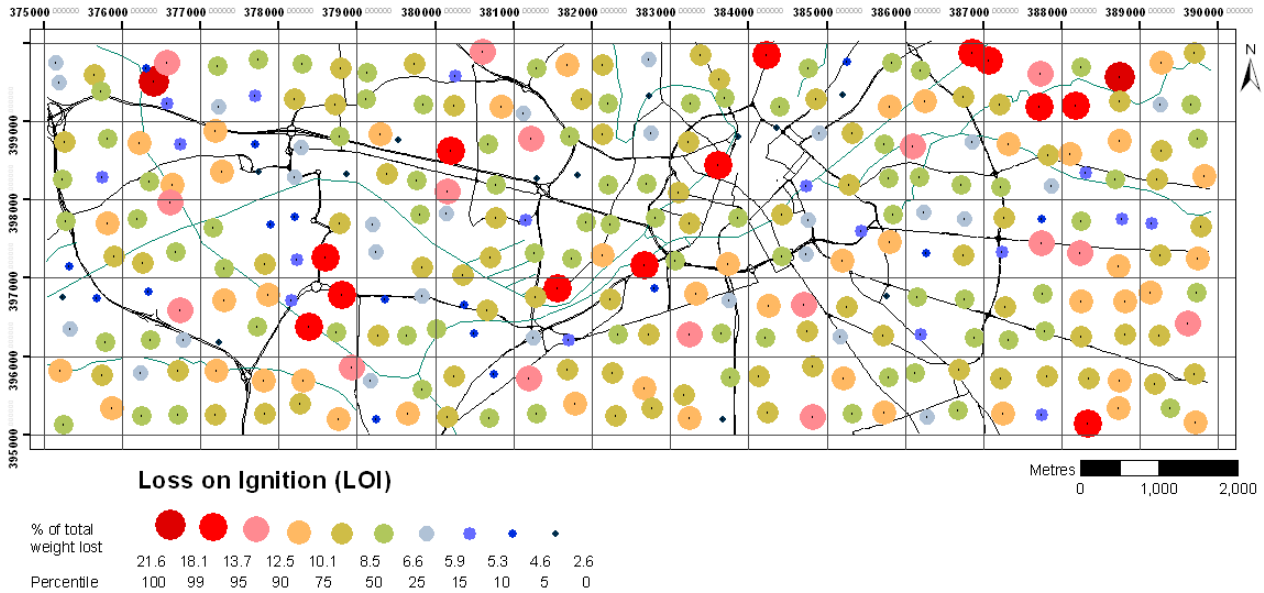

# Total Carbon

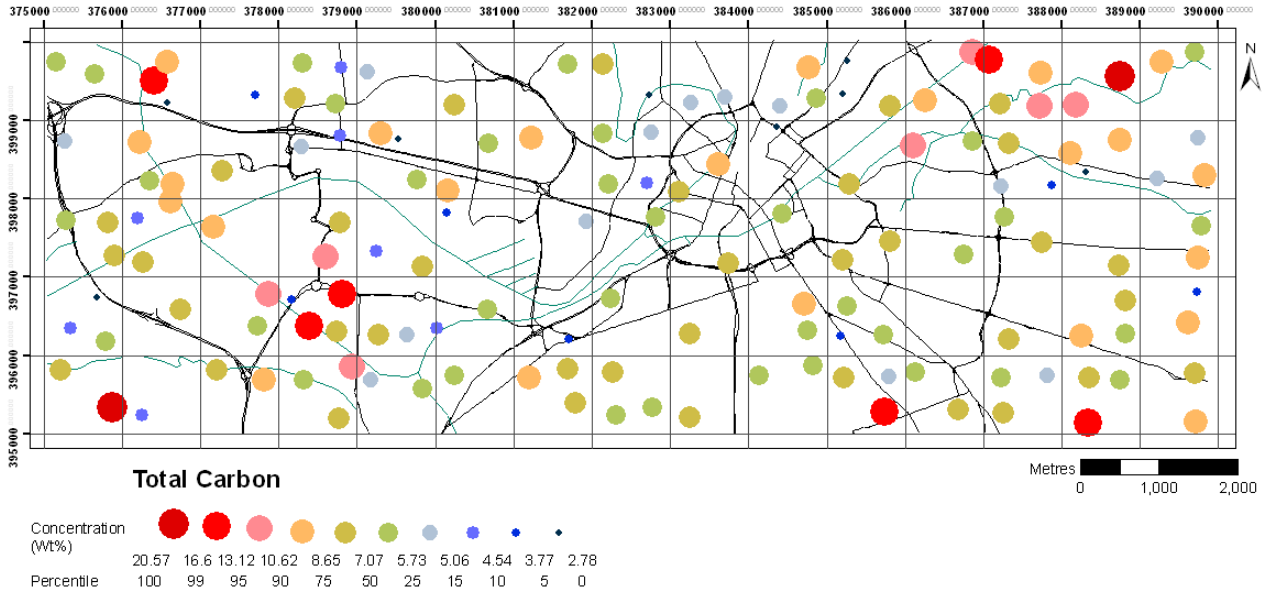


# Total Organic Carbon

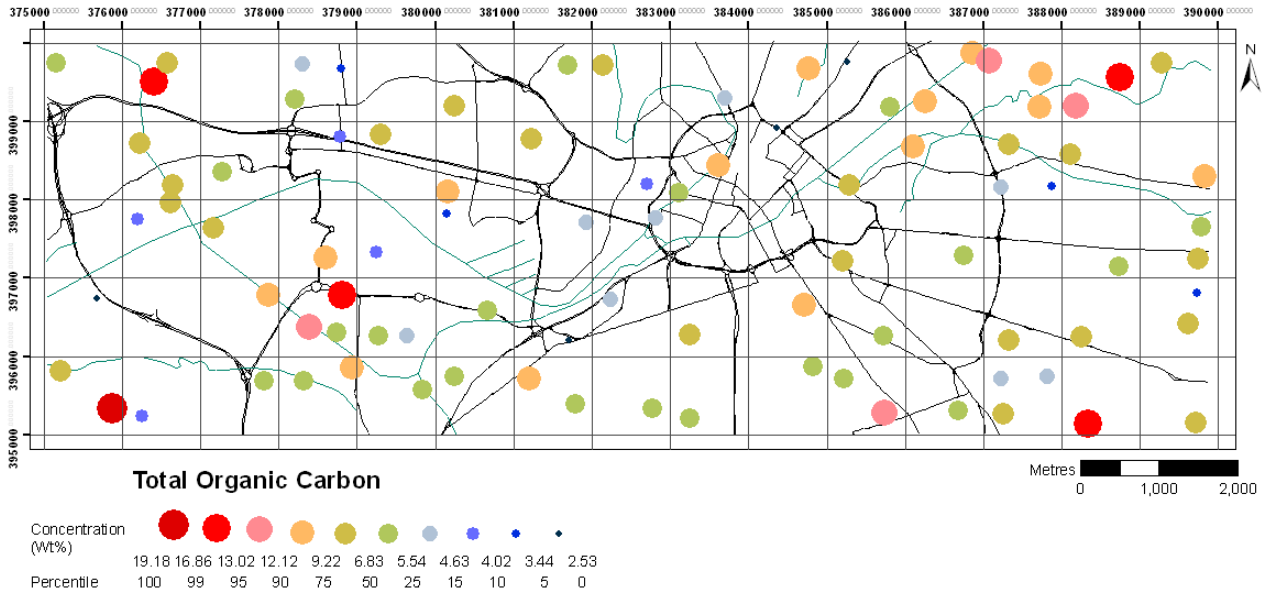

# Proportion Organic/Inorganic Carbon

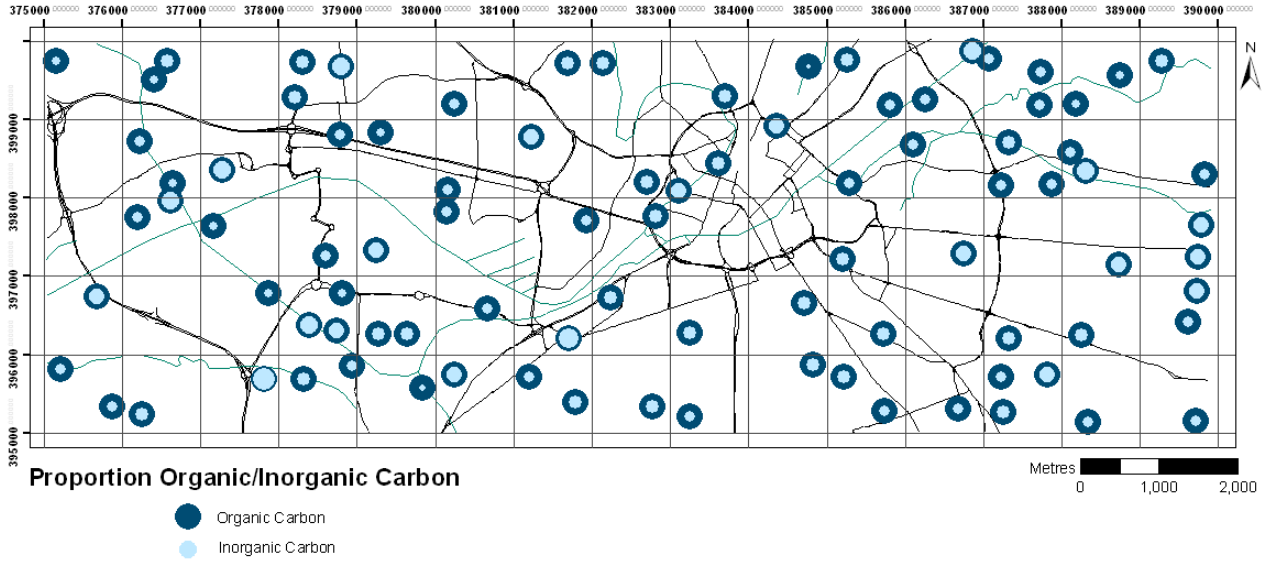


# pH

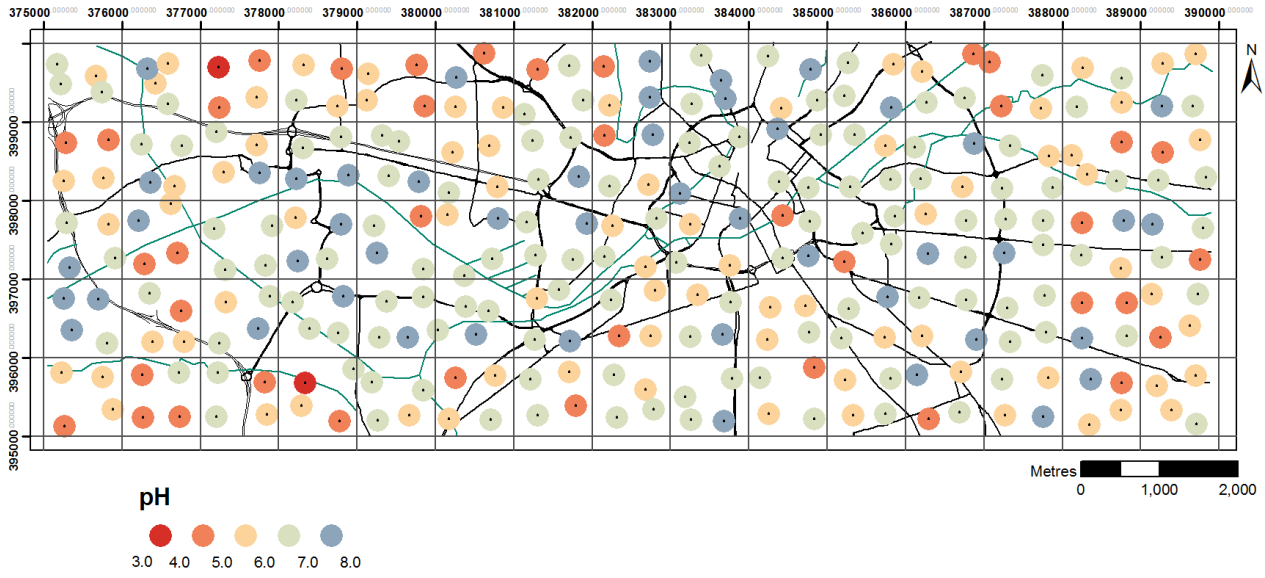

## 4. RDS Statistics

Figure 113: Histogram plots for RDS summer variables (oxides and LOI are expressed in wt. %; other chemical elements in mg/kg).

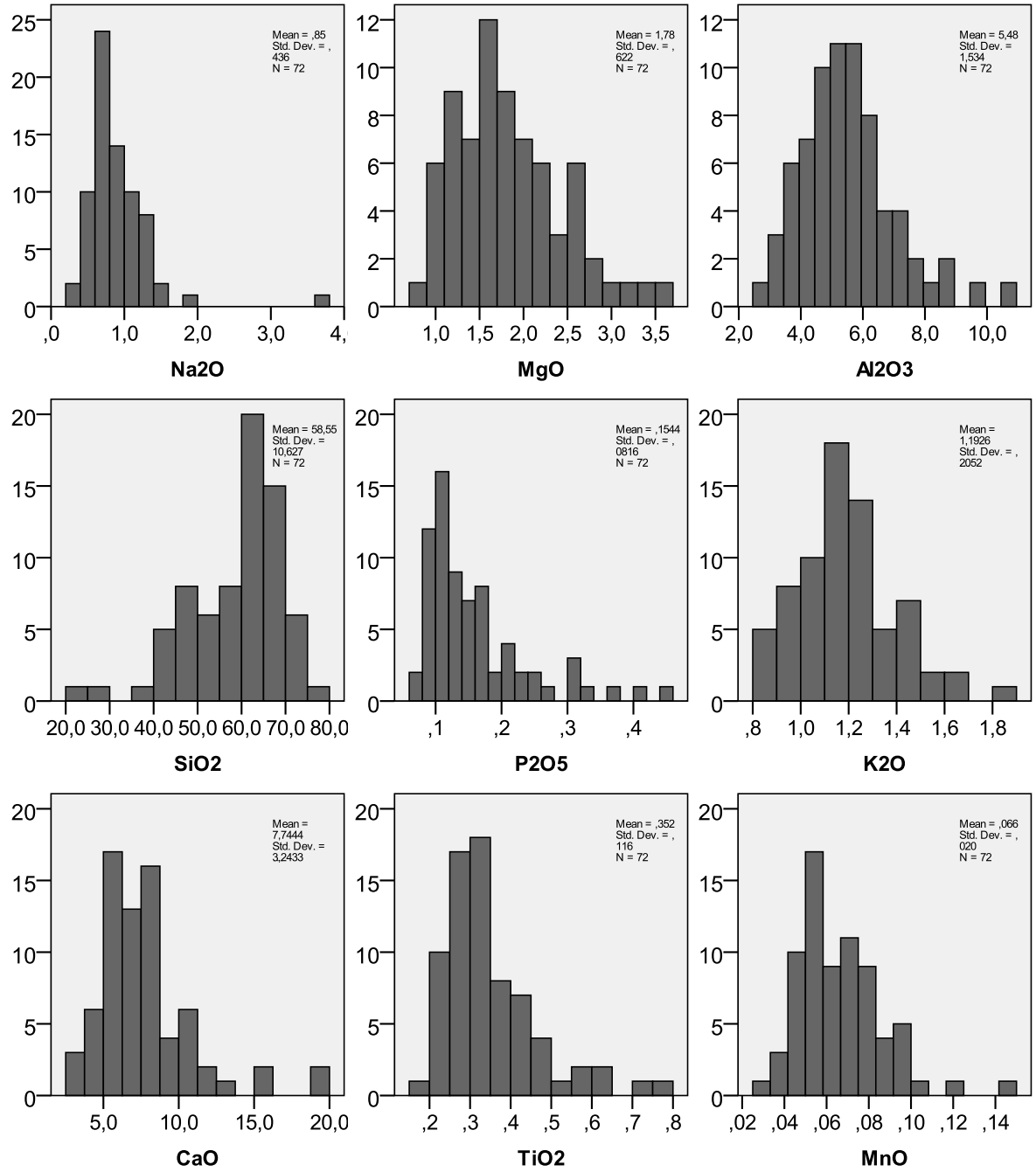

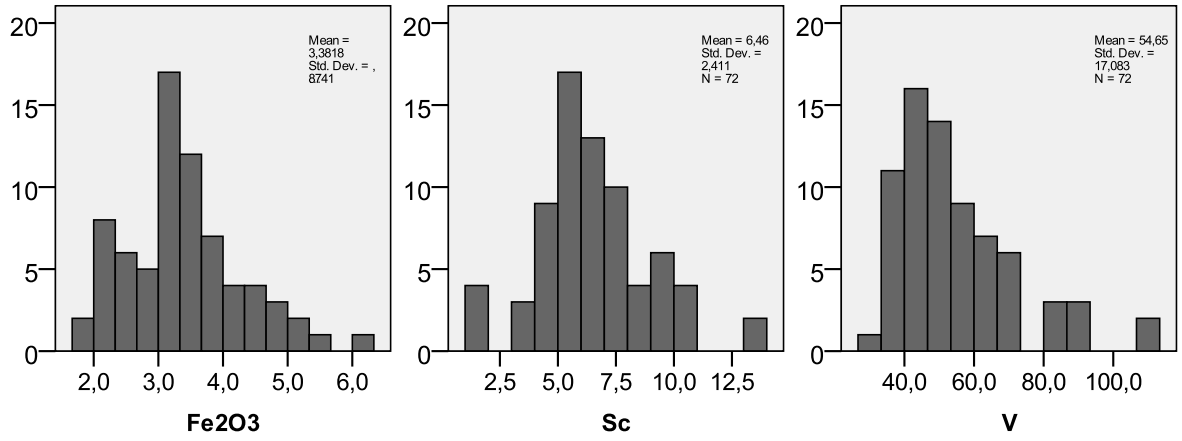
Mean = 3,3818
Std. Dev. = ,8741
Fe2O3
Mean = 6,46
Std. Dev. = 2,411
N = 72
Sc
Mean = 54,65
Std. Dev. = 17,083
N = 72
V

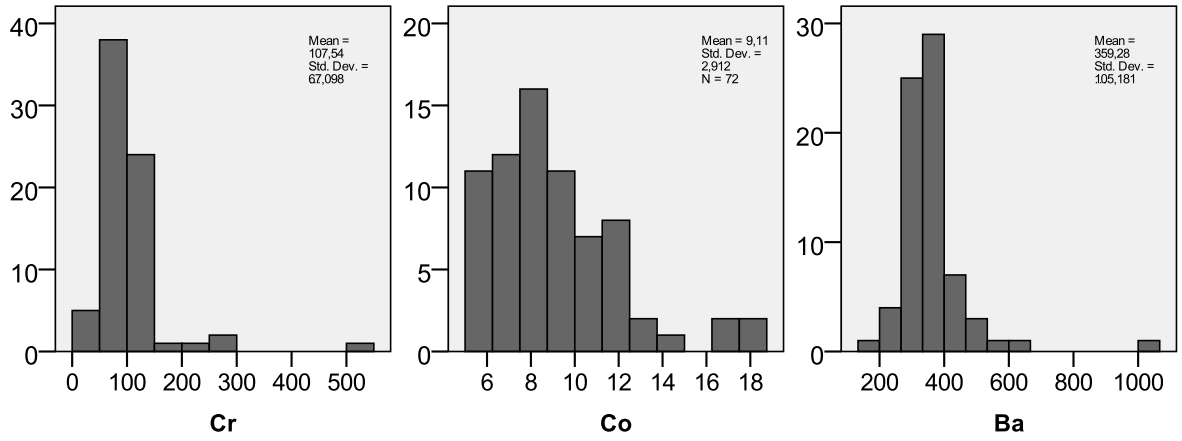
Mean = 107,54
Std. Dev. = 67,098
Cr
Mean = 9,11
Std. Dev. = 2,912
N = 72
Co
Mean = 359,28
Std. Dev. = 105,181
Ba

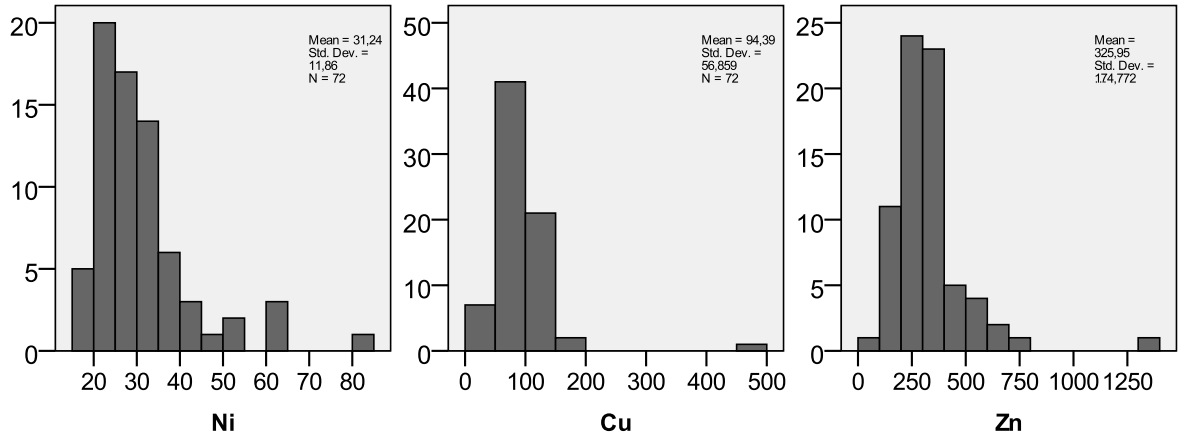
Mean = 31,24
Std. Dev. = 11,86
N = 72
Ni
Mean = 94,39
Std. Dev. = 56,859
N = 72
Cu
Mean = 325,95
Std. Dev. = 174,772
Zn

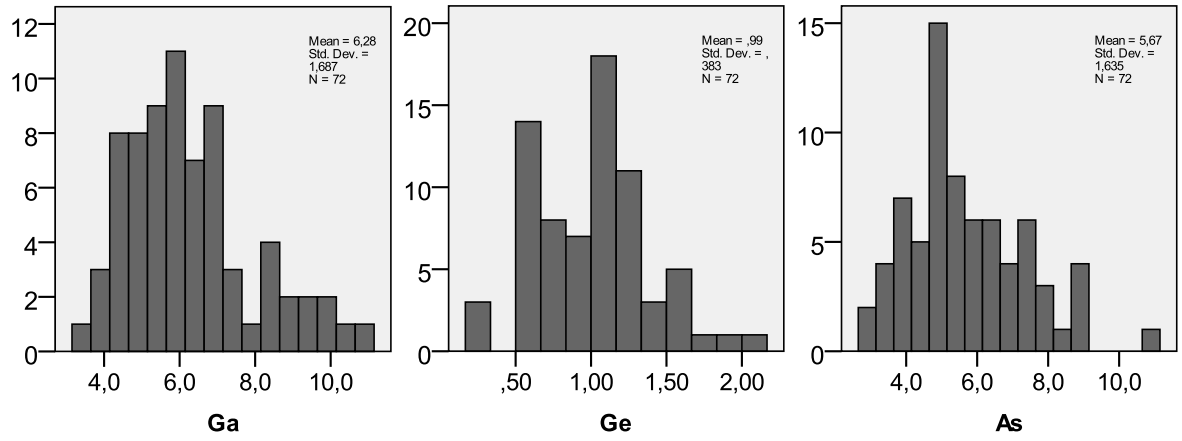
Mean = 6,28
Std. Dev. = 1,687
N = 72
Ga
Mean = ,99
Std. Dev. = ,383
N = 72
Ge
Mean = 5,67
Std. Dev. = 1,635
N = 72
As

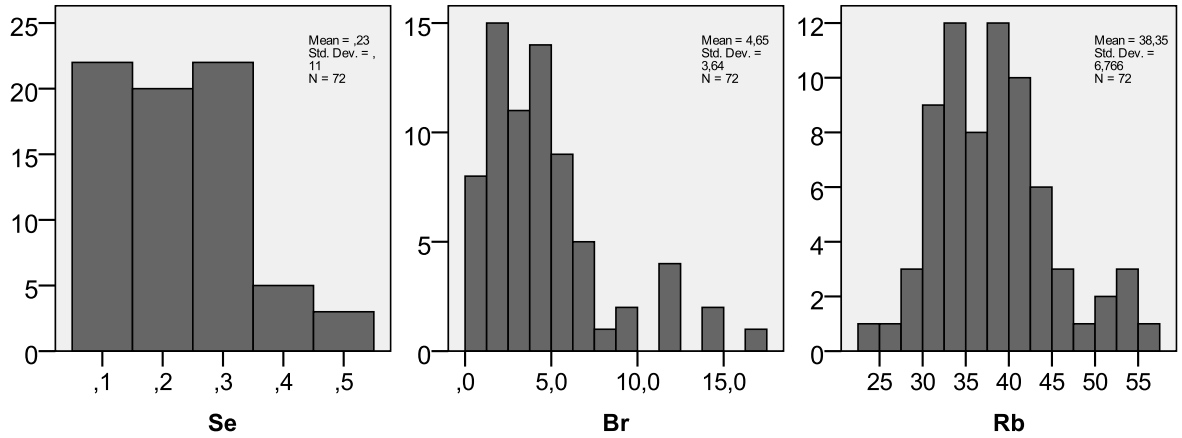
Mean = ,23
Std. Dev. = ,11
N = 72
Se
Mean = 4,65
Std. Dev. = 3,64
N = 72
Br
Mean = 38,35
Std. Dev. = 6,766
N = 72
Rb

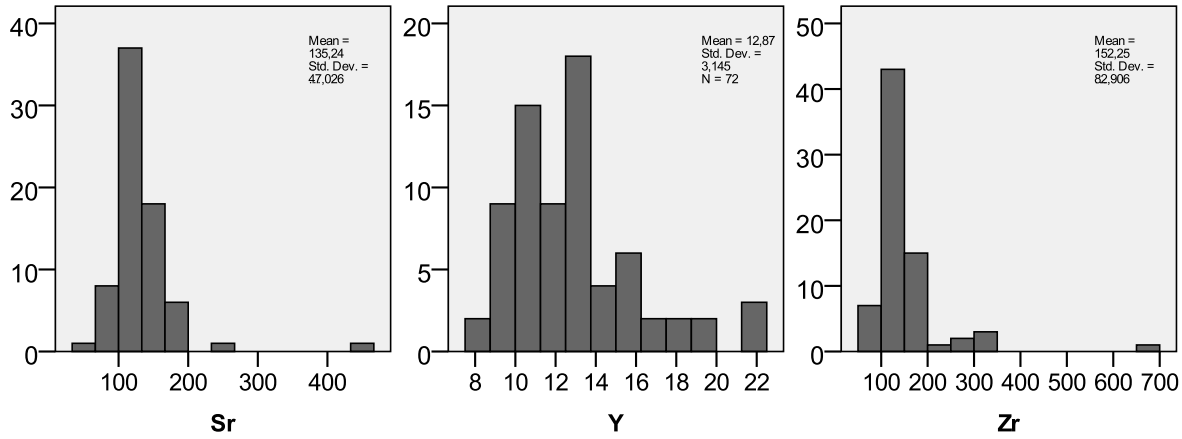
Mean = 135,24
Std. Dev. = 47,026
Sr
Mean = 12,87
Std. Dev. = 3,145
N = 72
Y
Mean = 152,25
Std. Dev. = 82,906
Zr

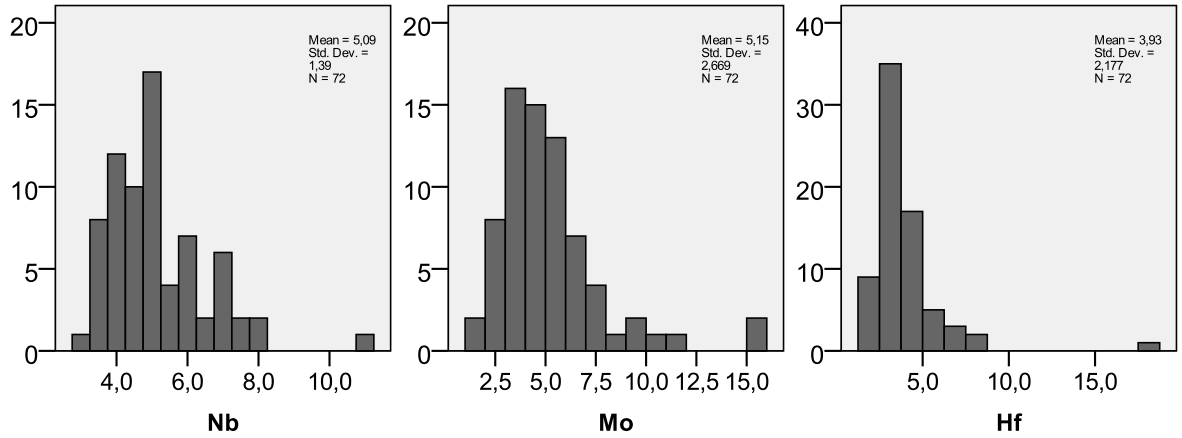
Mean = 5,09
Std. Dev. = 1,39
N = 72
Nb
Mean = 5,15
Std. Dev. = 2,669
N = 72
Mo
Mean = 3,93
Std. Dev. = 2,177
N = 72
Hf

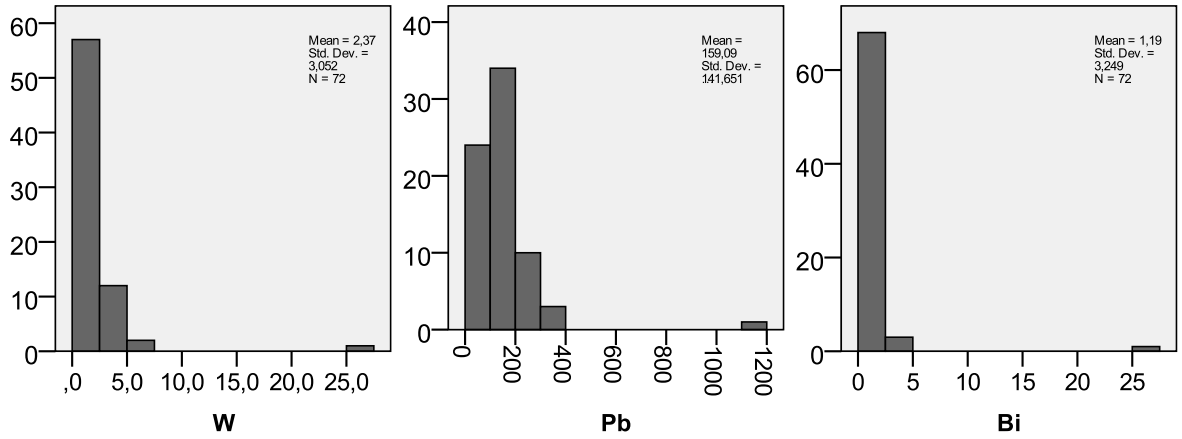
Mean = 2,37
Std. Dev. = 3,052
N = 72
W
Mean = 159,09
Std. Dev. = 141,651
Pb
Mean = 1,19
Std. Dev. = 3,249
N = 72
Bi

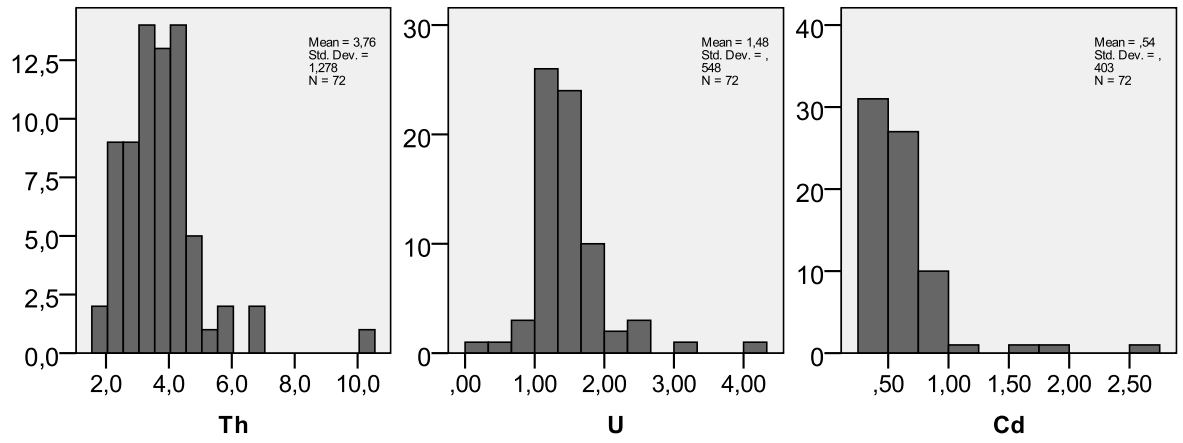
Mean = 3,76
Std. Dev. = 1,278
N = 72
Th
Mean = 1,48
Std. Dev. = ,548
N = 72
U
Mean = ,54
Std. Dev. = ,403
N = 72
Cd

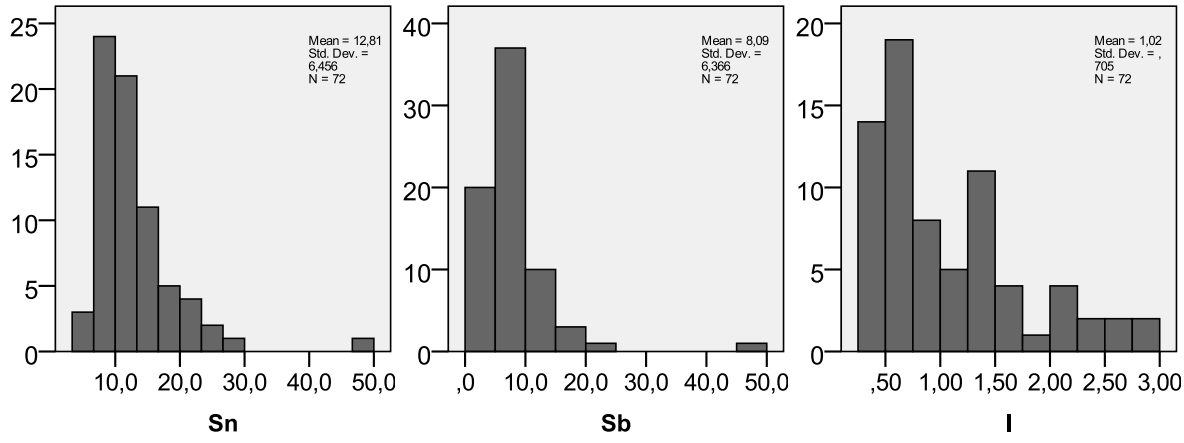
Mean = 12,81
Std. Dev. = 6,456
N = 72
Sn
Mean = 8,09
Std. Dev. = 6,366
N = 72
Sb
Mean = 1,02
Std. Dev. = ,705
N = 72
I

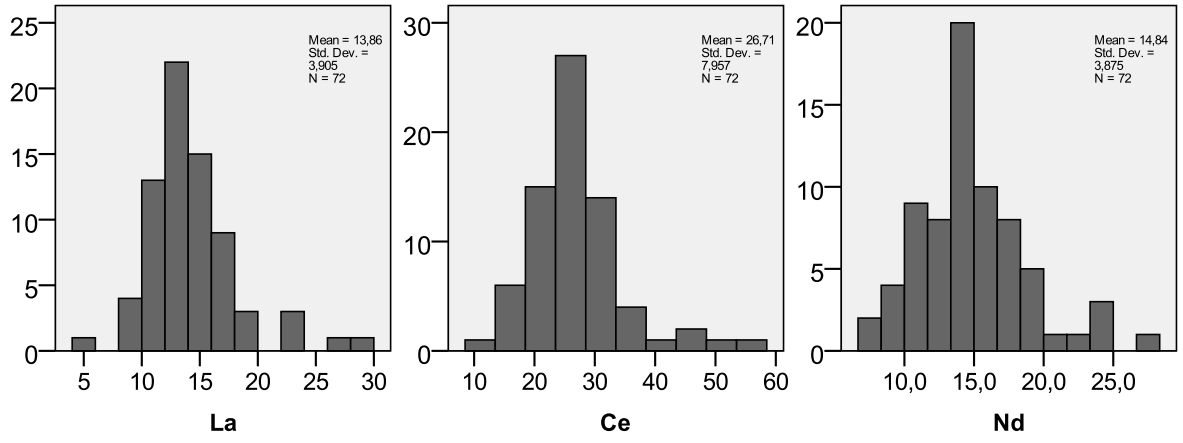
Mean = 13,86
Std. Dev. = 3,905
N = 72
La
Mean = 26,71
Std. Dev. = 7,957
N = 72
Ce
Mean = 14,84
Std. Dev. = 3,875
N = 72
Nd

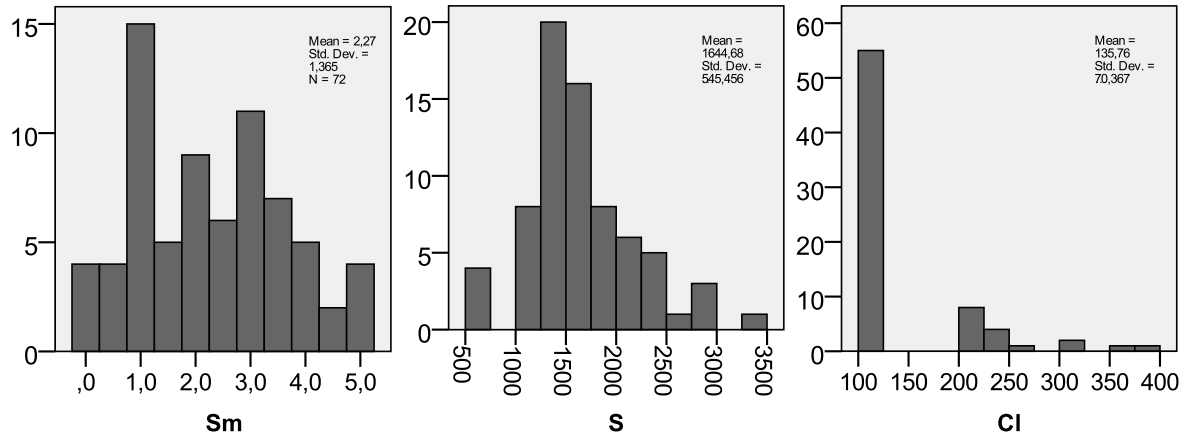
Mean = 2,27
Std. Dev. = 1,365
N = 72
Sm
Mean = 1644,68
Std. Dev. = 545,456
S
Mean = 135,76
Std. Dev. = 70,367
Cl

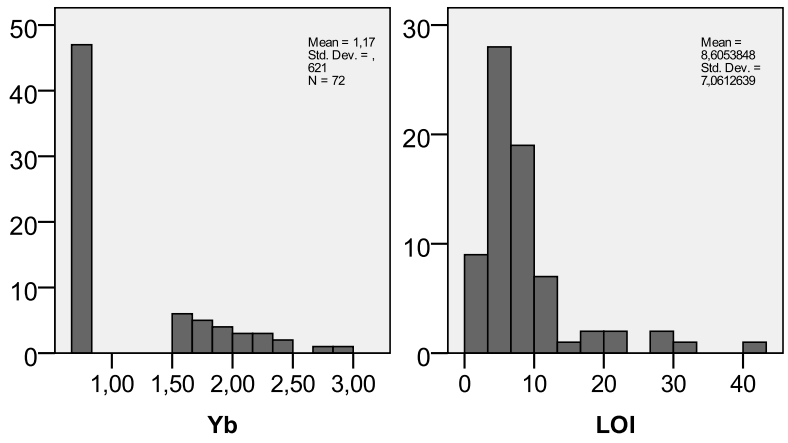


Figure 114: Histogram plots for RDS winter variables (oxides and LOI are expressed in wt. %; other chemical elements in mg/kg).

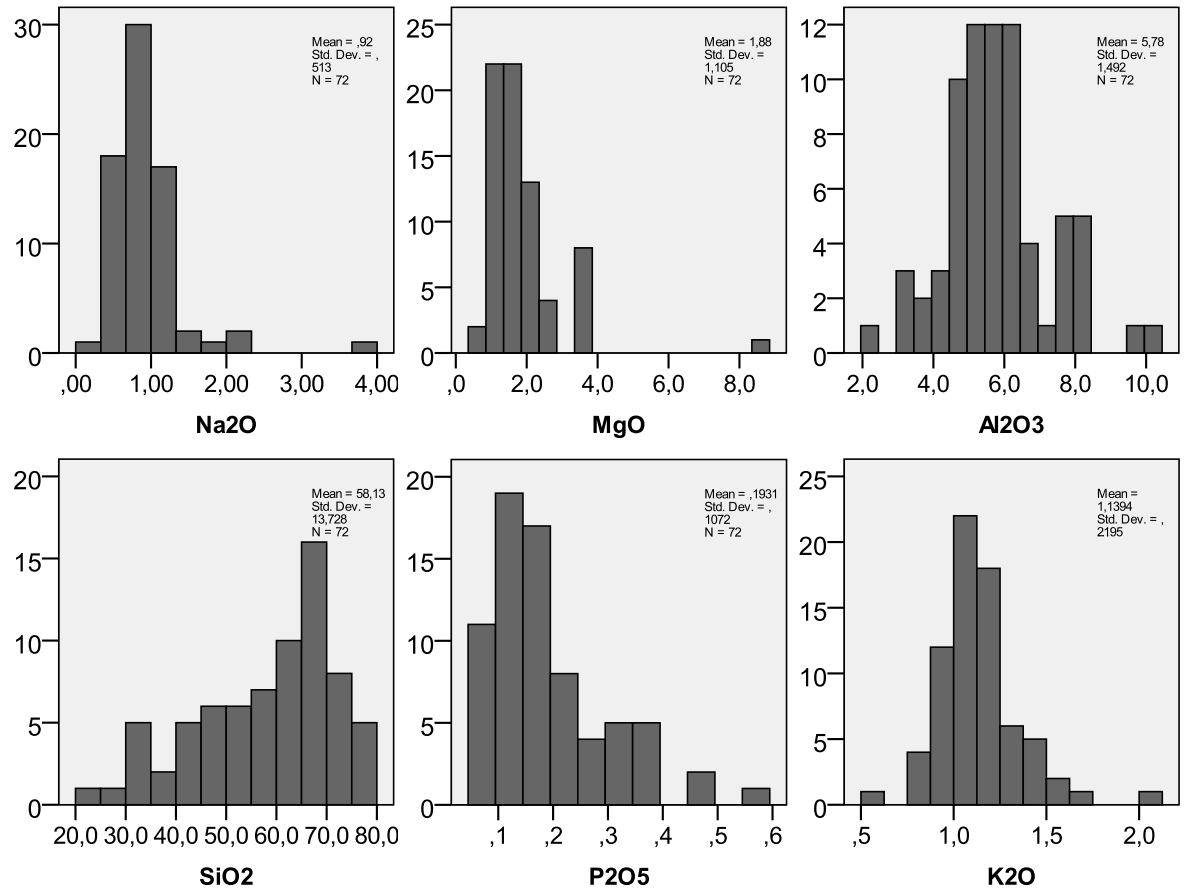

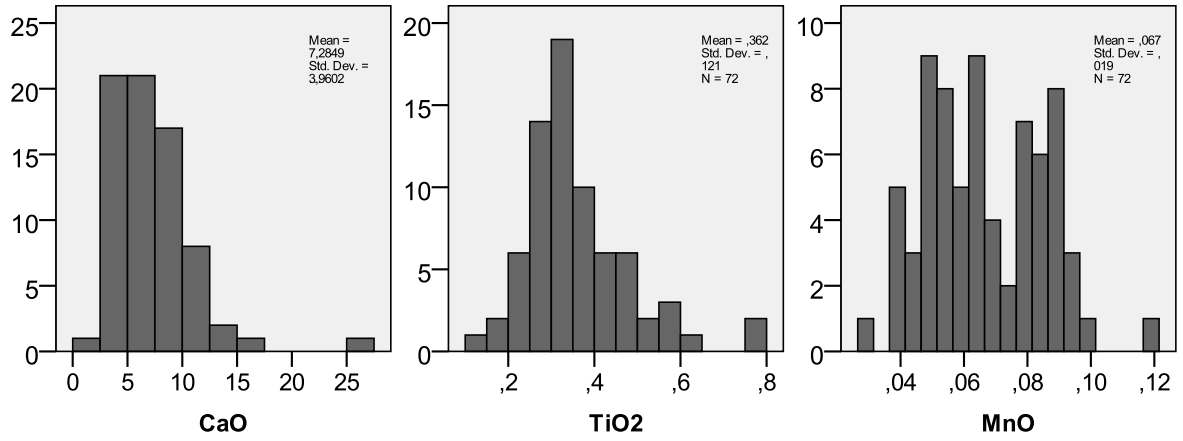
Mean = 7,2849
Std. Dev. = 3,9602
CaO
Mean = ,362
Std. Dev. = ,121
N = 72
TiO2
Mean = ,067
Std. Dev. = ,019
N = 72
MnO

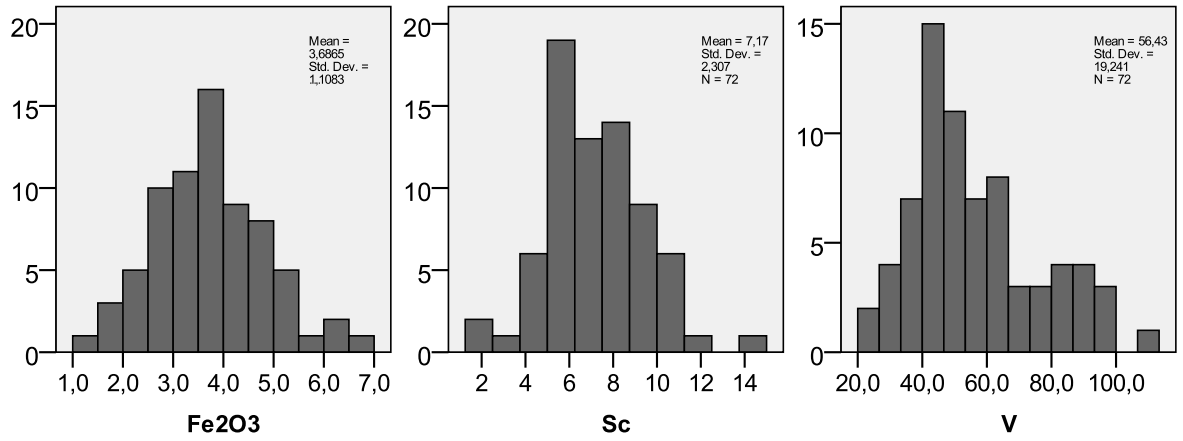
Mean = 3,6865
Std. Dev. = 1,1083
Fe2O3
Mean = 7,17
Std. Dev. = 2,307
N = 72
Sc
Mean = 56,43
Std. Dev. = 19,241
N = 72
V

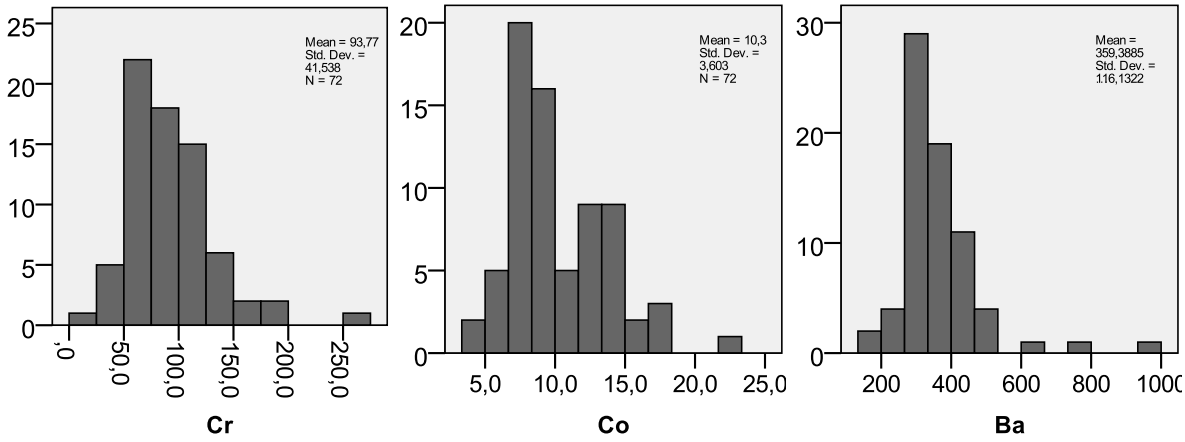
Mean = 93,77
Std. Dev. = 41,538
N = 72
Cr
Mean = 10,3
Std. Dev. = 3,603
N = 72
Co
Mean = 359,3885
Std. Dev. = 116,1322
Ba

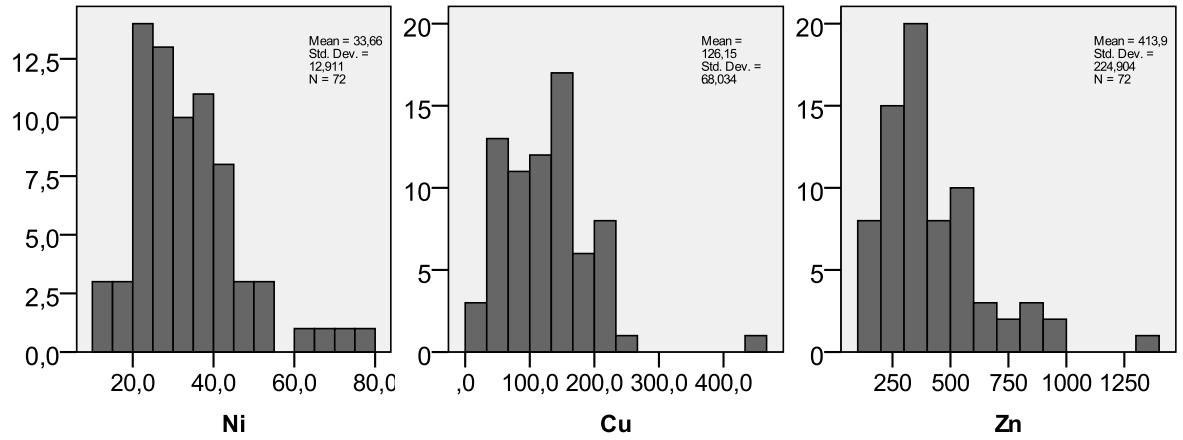
Mean = 33,66
Std. Dev. = 12,911
N = 72
Ni
Mean = 126,15
Std. Dev. = 68,034
Cu
Mean = 413,9
Std. Dev. = 224,904
N = 72
Zn

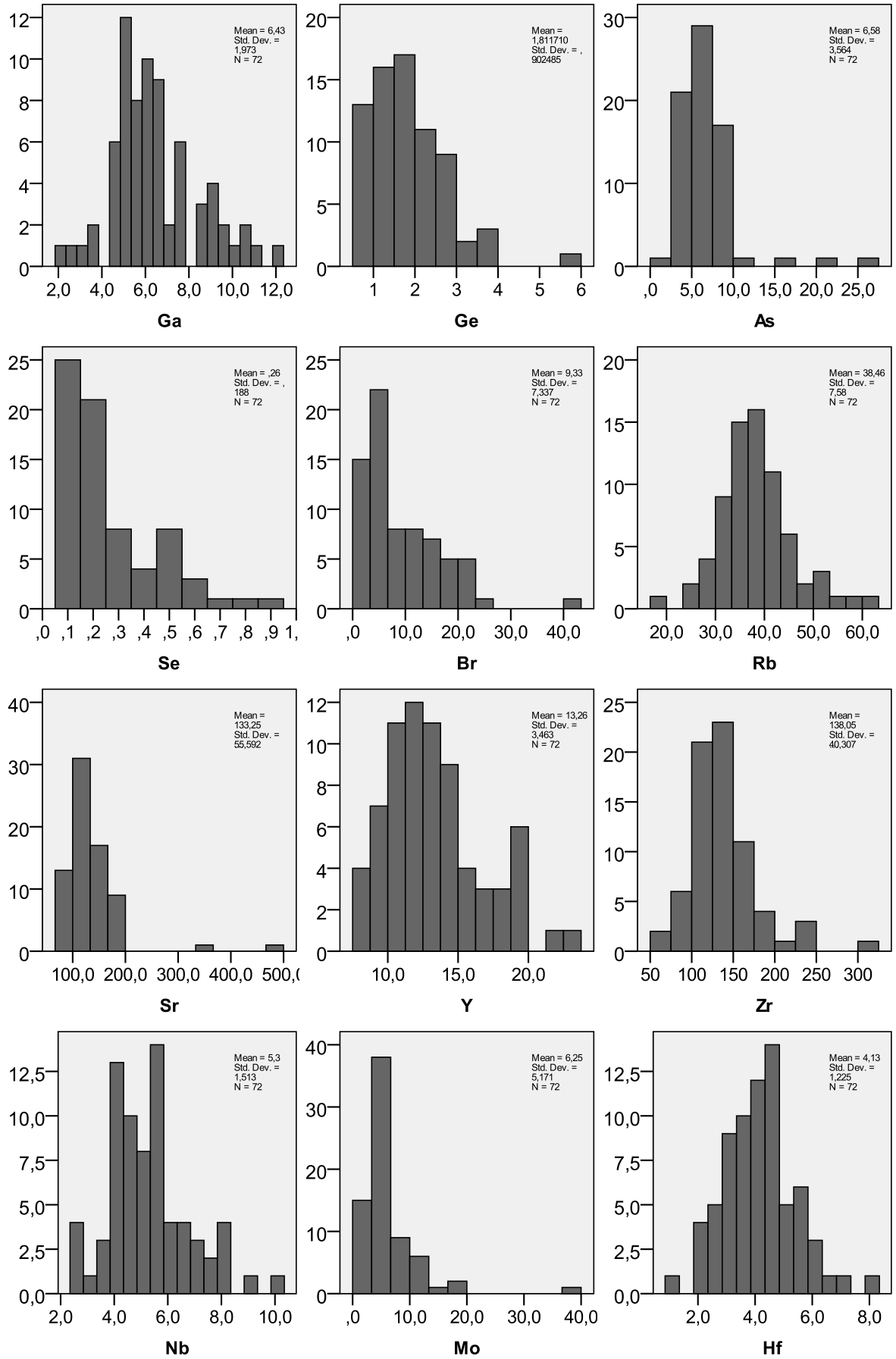
Mean = 6,43
Std. Dev. = 1,973
N = 72
Ga
Mean = 1,811710
Std. Dev. = ,902485
Ge
Mean = 6,58
Std. Dev. = 3,564
N = 72
As
Mean = ,26
Std. Dev. = ,188
N = 72
Se
Mean = 9,33
Std. Dev. = 7,337
N = 72
Br
Mean = 38,46
Std. Dev. = 7,58
N = 72
Rb
Mean = 133,25
Std. Dev. = 55,592
Sr
Mean = 13,26
Std. Dev. = 3,463
N = 72
Y
Mean = 138,05
Std. Dev. = 40,307
Zr
Mean = 5,3
Std. Dev. = 1,513
N = 72
Nb
Mean = 6,25
Std. Dev. = 5,171
N = 72
Mo
Mean = 4,13
Std. Dev. = 1,225
N = 72
Hf

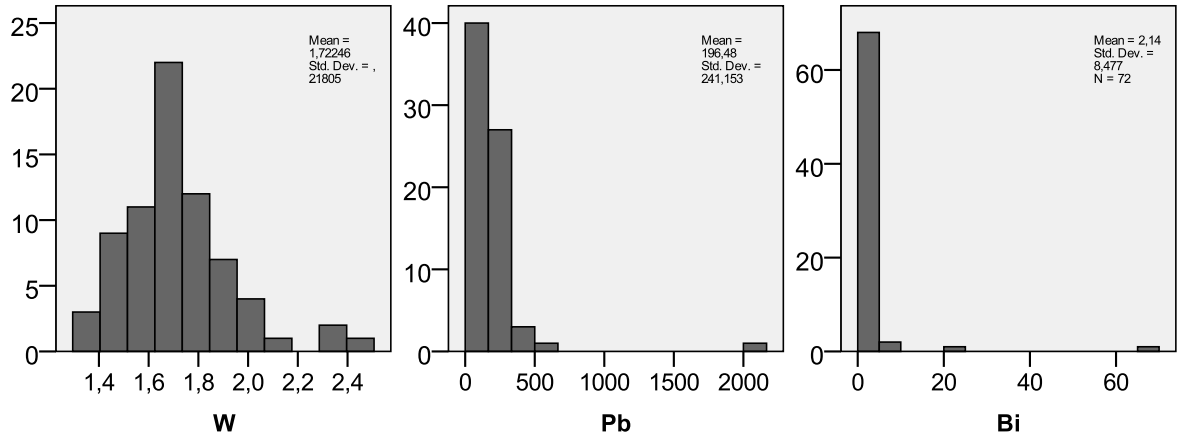
Mean = 1,72246
Std. Dev. = , 21805
W
Mean = 196,48
Std. Dev. = 241,153
Pb
Mean = 2,14
Std. Dev. = 8,477
N = 72
Bi

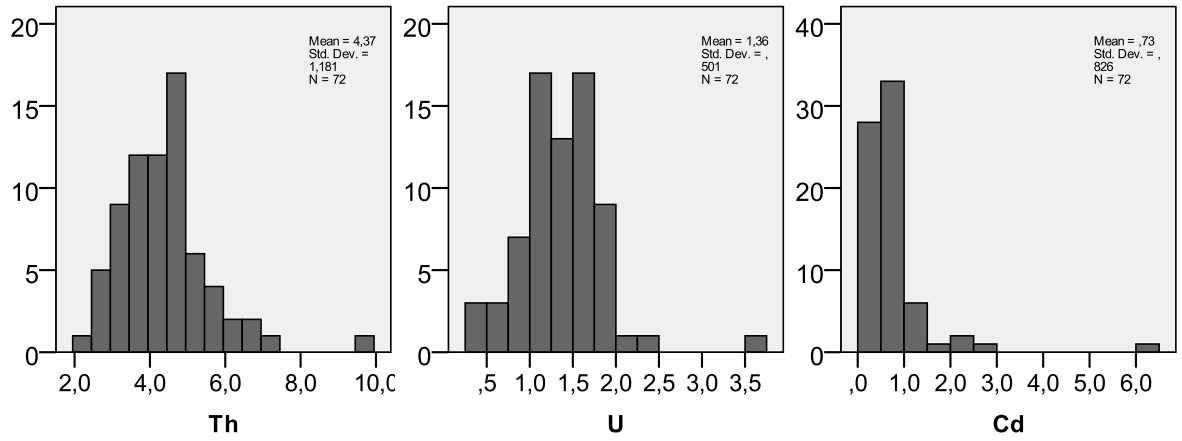
Mean = 4,37
Std. Dev. = 1,181
N = 72
Th
Mean = 1,36
Std. Dev. = , 501
N = 72
U
Mean = ,73
Std. Dev. = , 826
N = 72
Cd

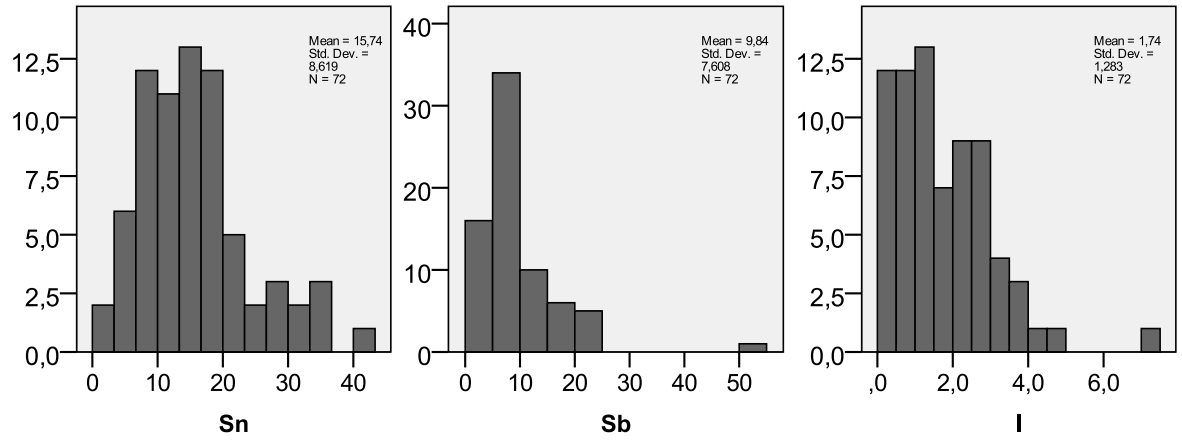
Mean = 15,74
Std. Dev. = 8,619
N = 72
Sn
Mean = 9,84
Std. Dev. = 7,608
N = 72
Sb
Mean = 1,74
Std. Dev. = 1,283
N = 72
I

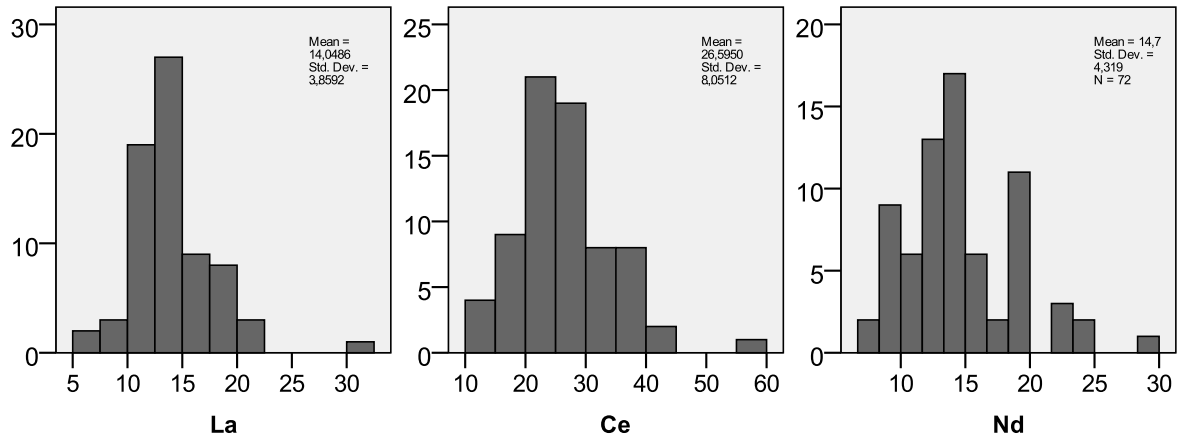
Mean = 14,0486
Std. Dev. = 3,8592
La
Mean = 26,5950
Std. Dev. = 8,0512
Ce
Mean = 14,7
Std. Dev. = 4,319
N = 72
Nd

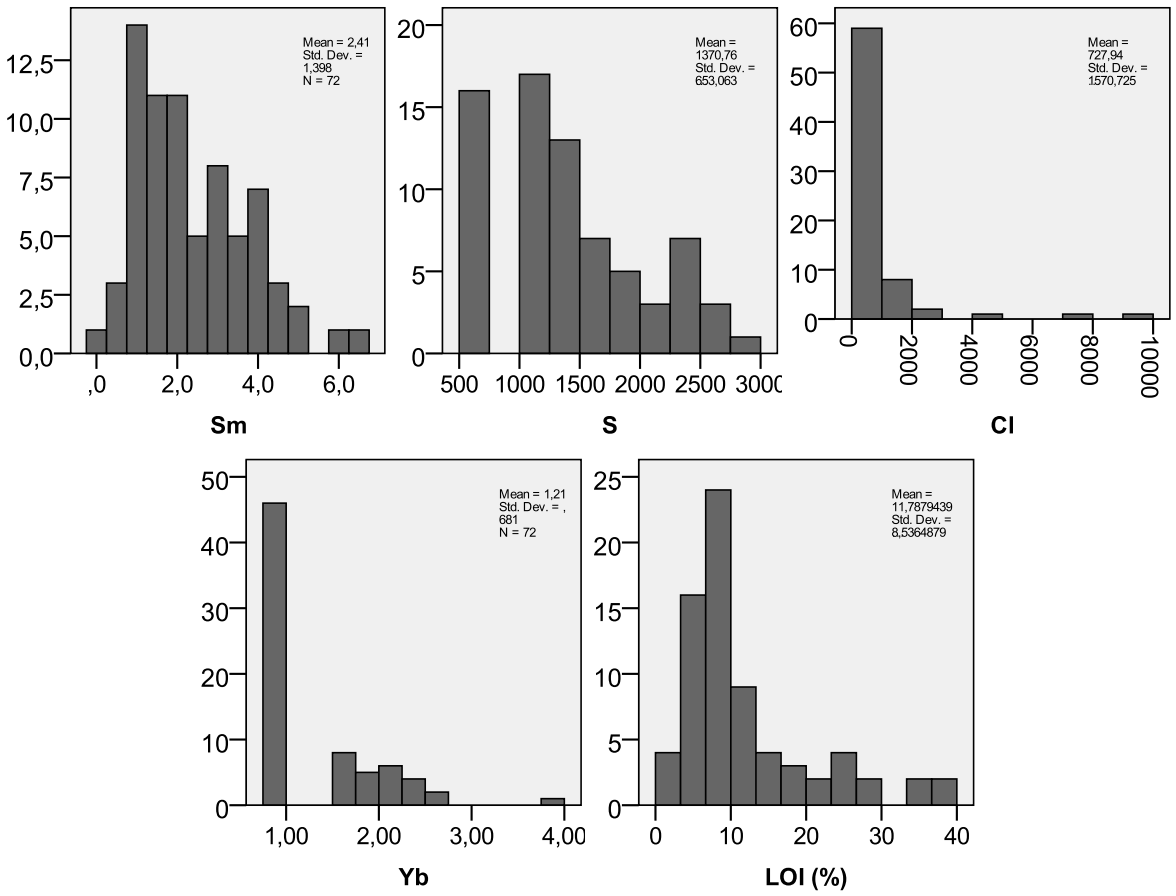
Mean = 2,41
Std. Dev. = 1,398
N = 72
Sm
Mean = 1370,76
Std. Dev. = 653,063
S
Mean = 727,94
Std. Dev. = 1570,725
Cl
Mean = 1,21
Std. Dev. = ,681
N = 72
Yb
Mean = 11,7879439
Std. Dev. = 8,5364879
LOI (%)

Figure 115: Box-and-whisker plots for RDS summer variables (oxides and LOI are expressed in wt. %; other chemical elements in mg/kg).

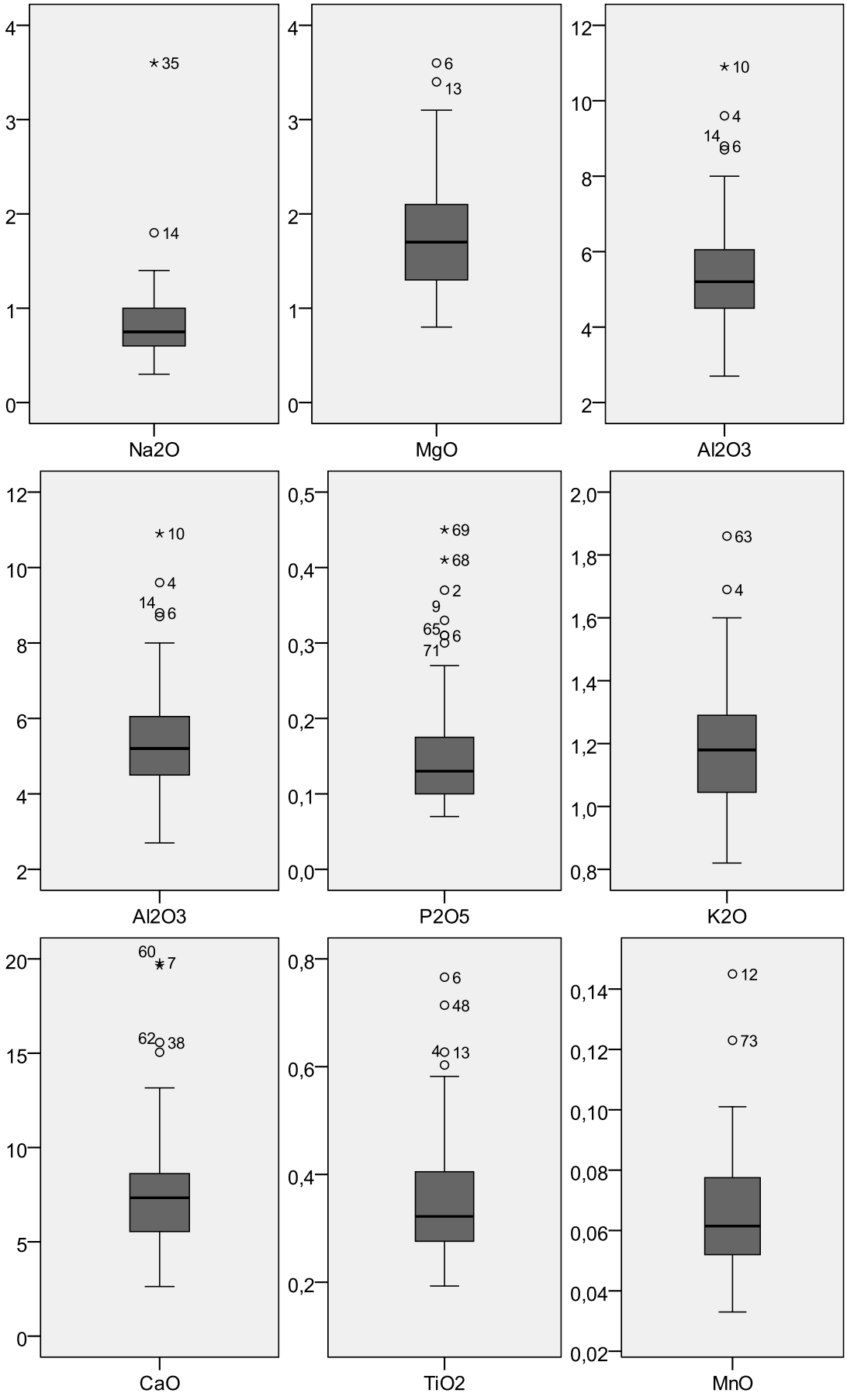

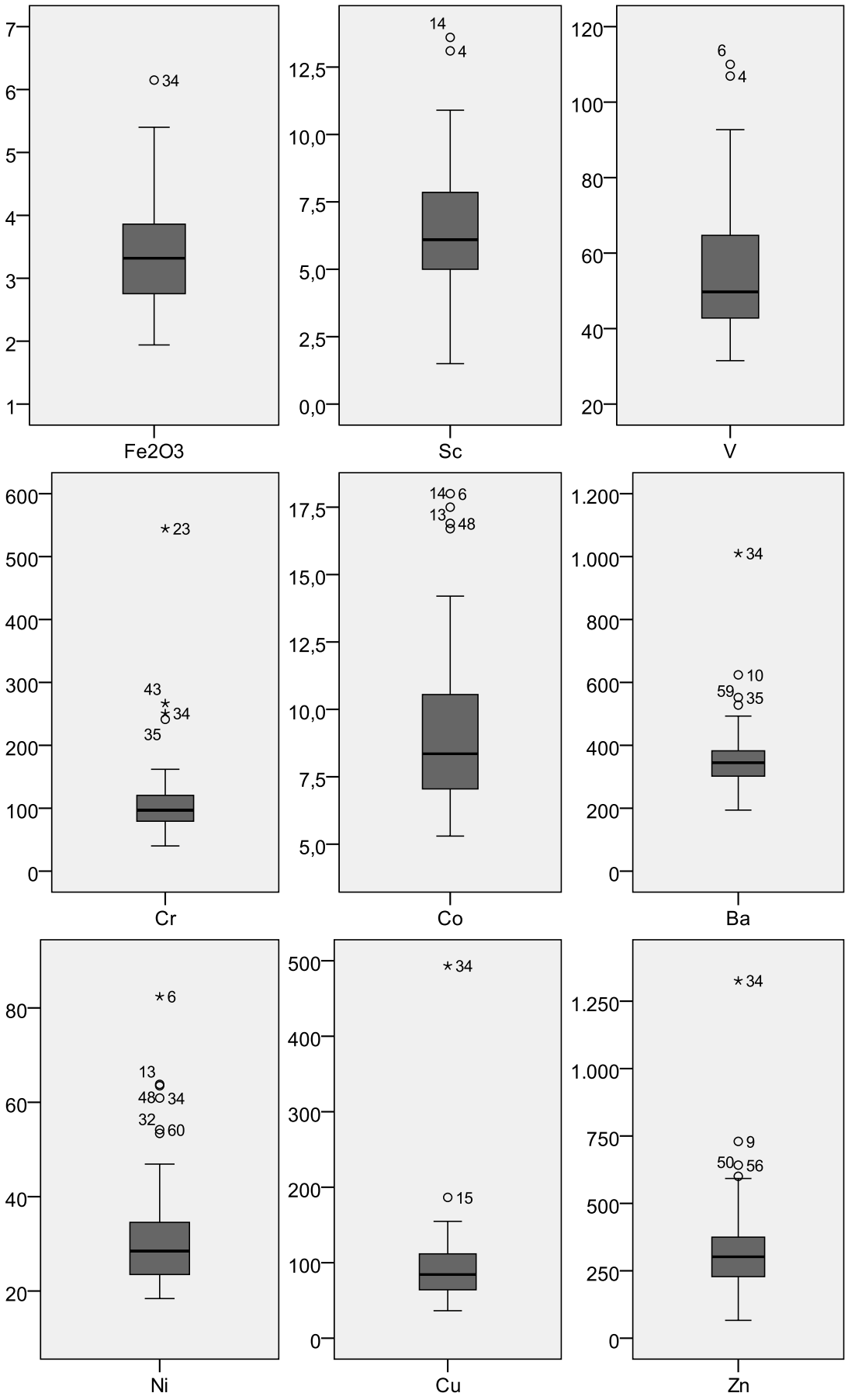
Fe2O3
Sc
V
Cr
Co
Ba
Ni
Cu
Zn

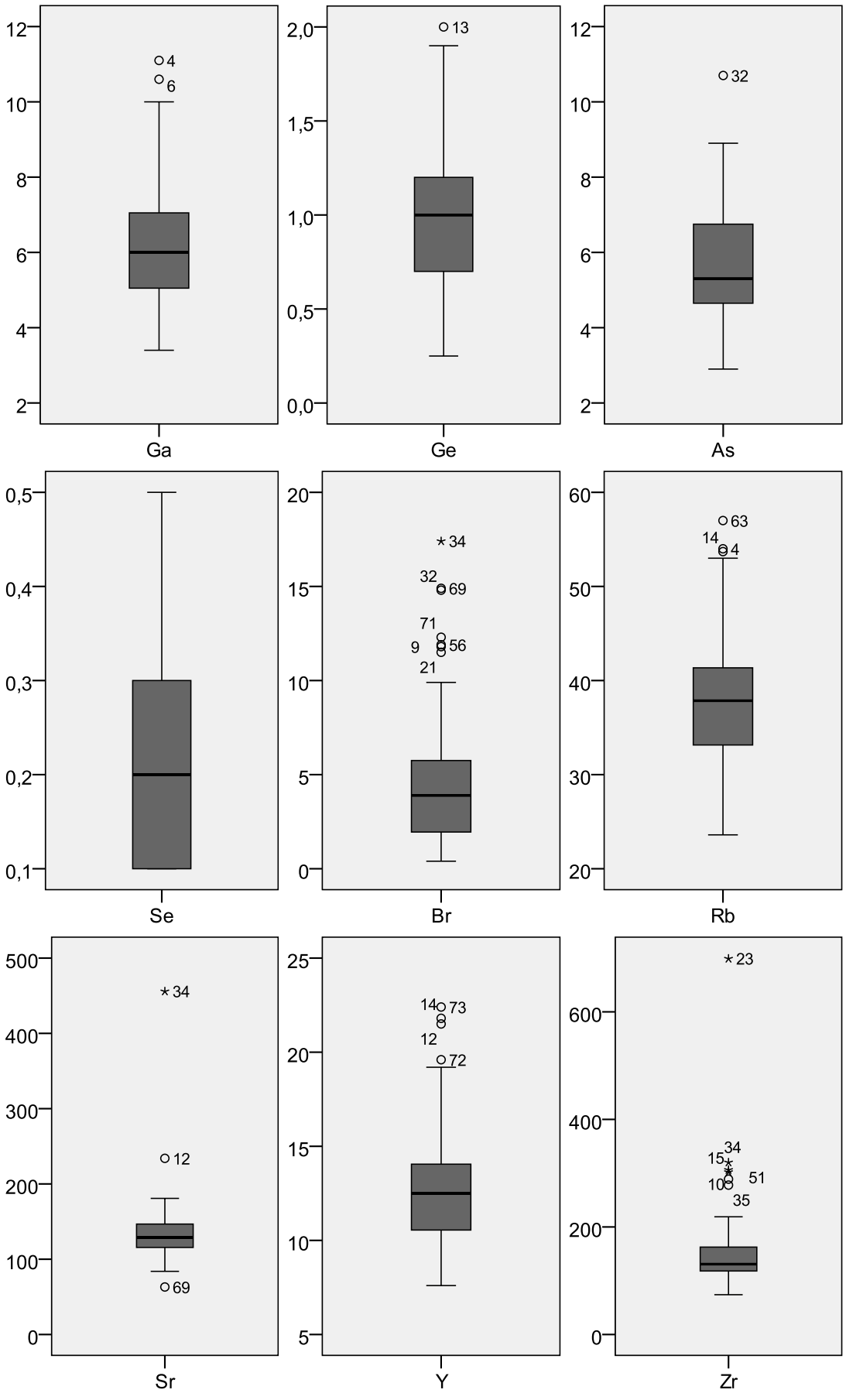
Ga
Ge
As
Se
Br
Rb
Sr
Y
Zr

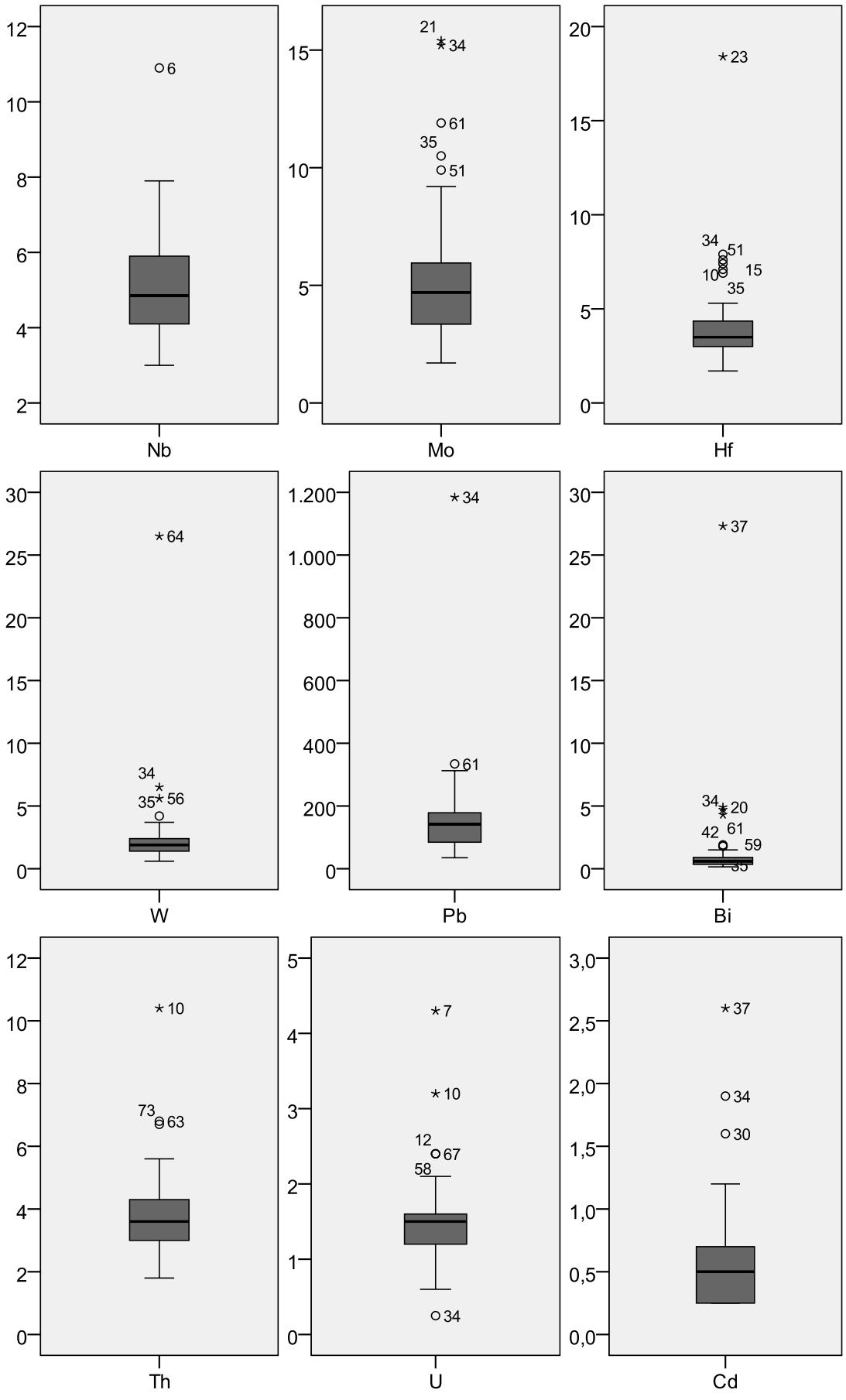
Nb
Mo
Hf
W
Pb
Bi
Th
U
Cd

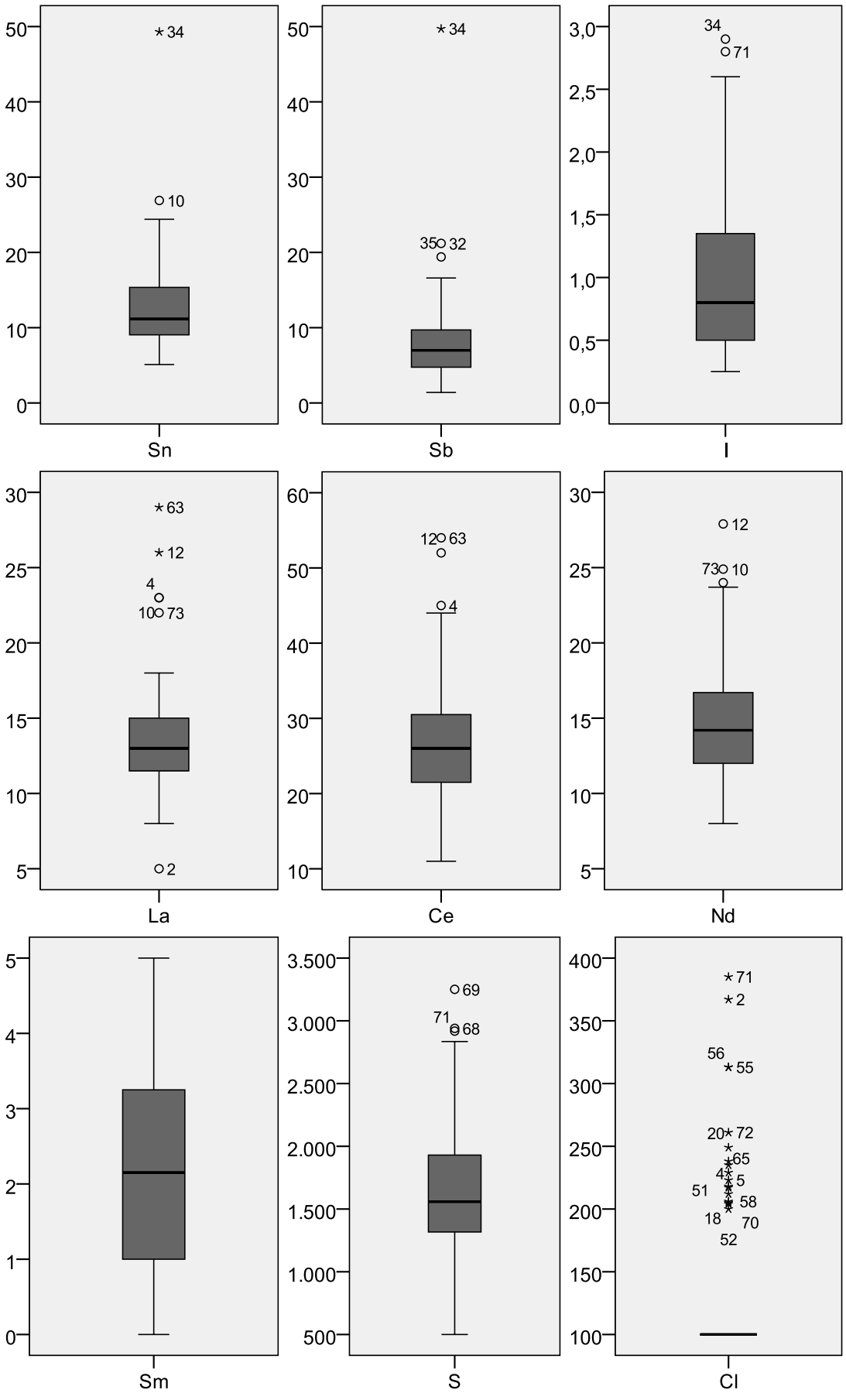
Sn
Sb
I
La
Ce
Nd
Sm
S
Cl

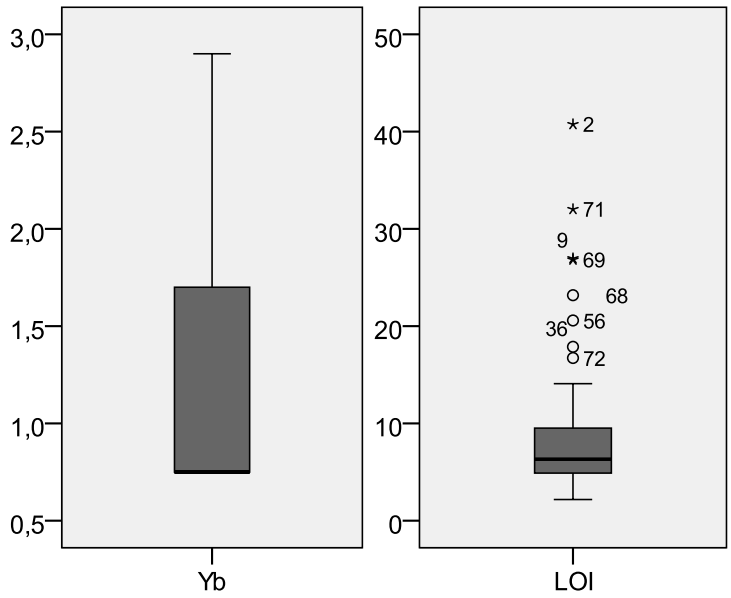


Figure 116: Box-and-whisker plots for RDS winter variables (oxides and LOI are expressed in wt. %; other chemical elements in mg/kg).

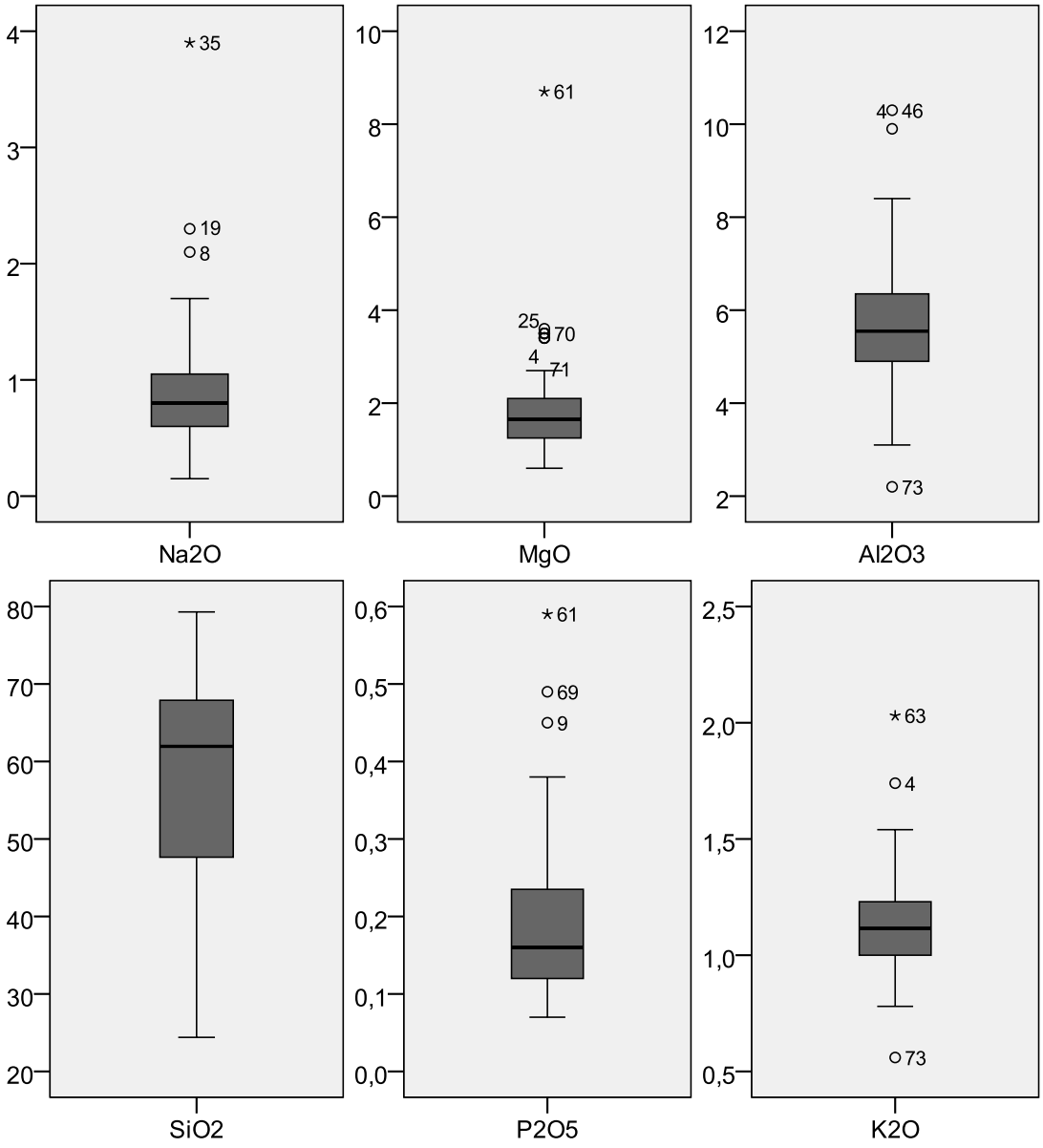

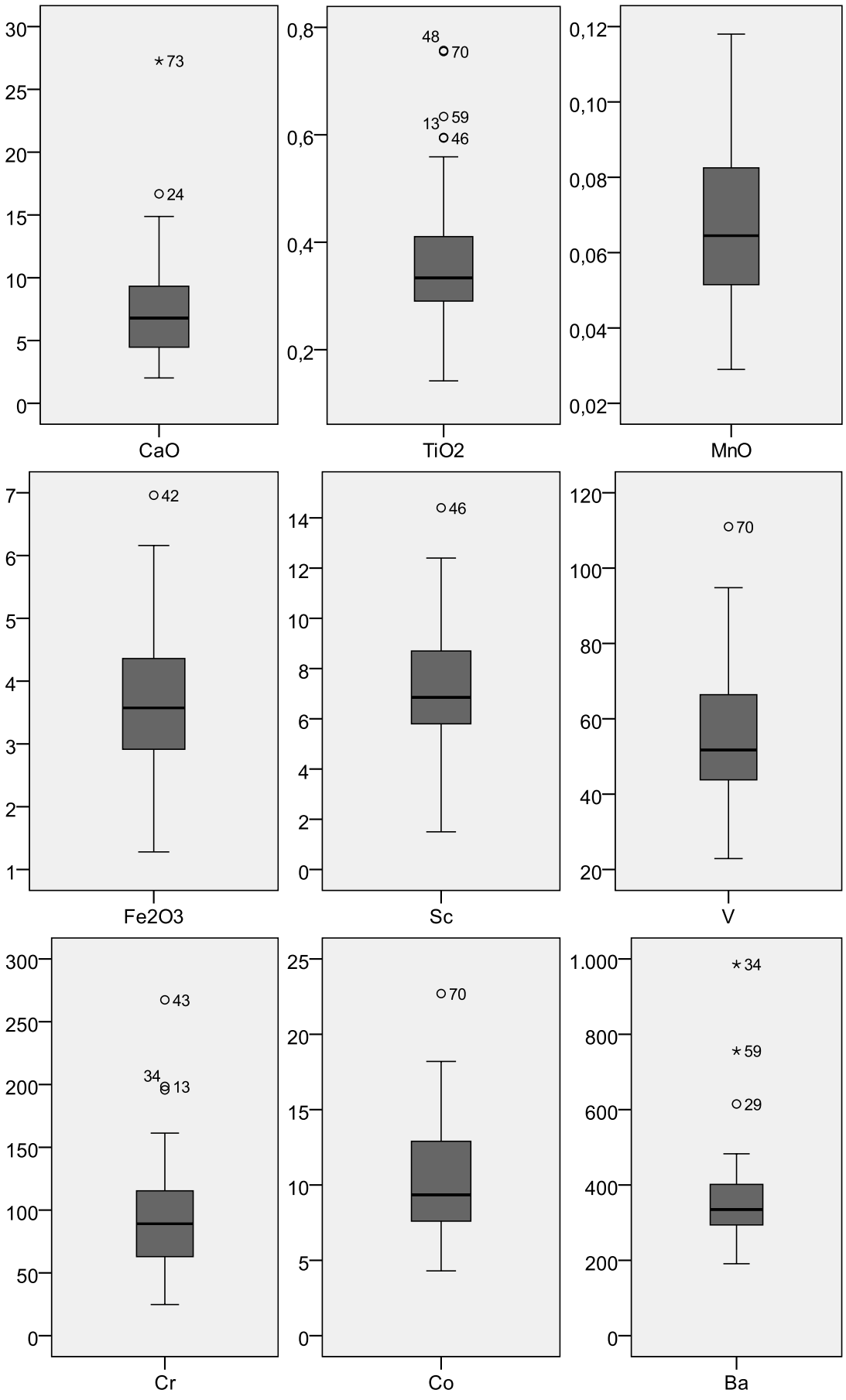
CaO
TiO2
MnO
Fe2O3
Sc
V
Cr
Co
Ba

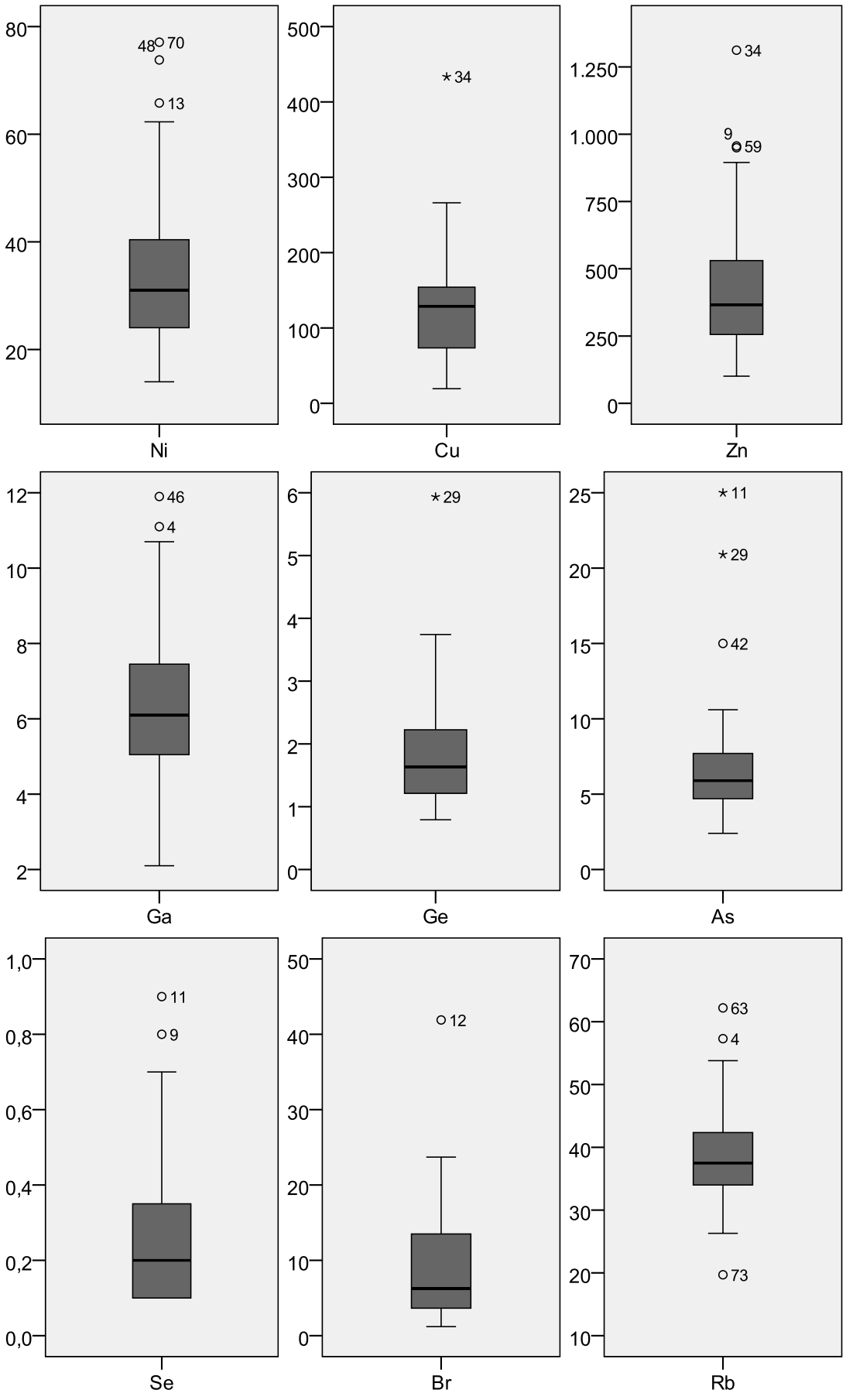
80
60
40
20
48
70
13
Ni
500
400
300
200
100
0
34
Cu
1.250
1.000
750
500
250
0
34
9
59
Zn
12
10
8
6
4
2
46
4
Ga
6
5
4
3
2
1
0
29
Ge
25
20
15
10
5
0
11
29
42
As
1,0
0,8
0,6
0,4
0,2
0,0
11
9
Se
50
40
30
20
10
0
12
Br
70
60
50
40
30
20
10
63
4
73
Rb

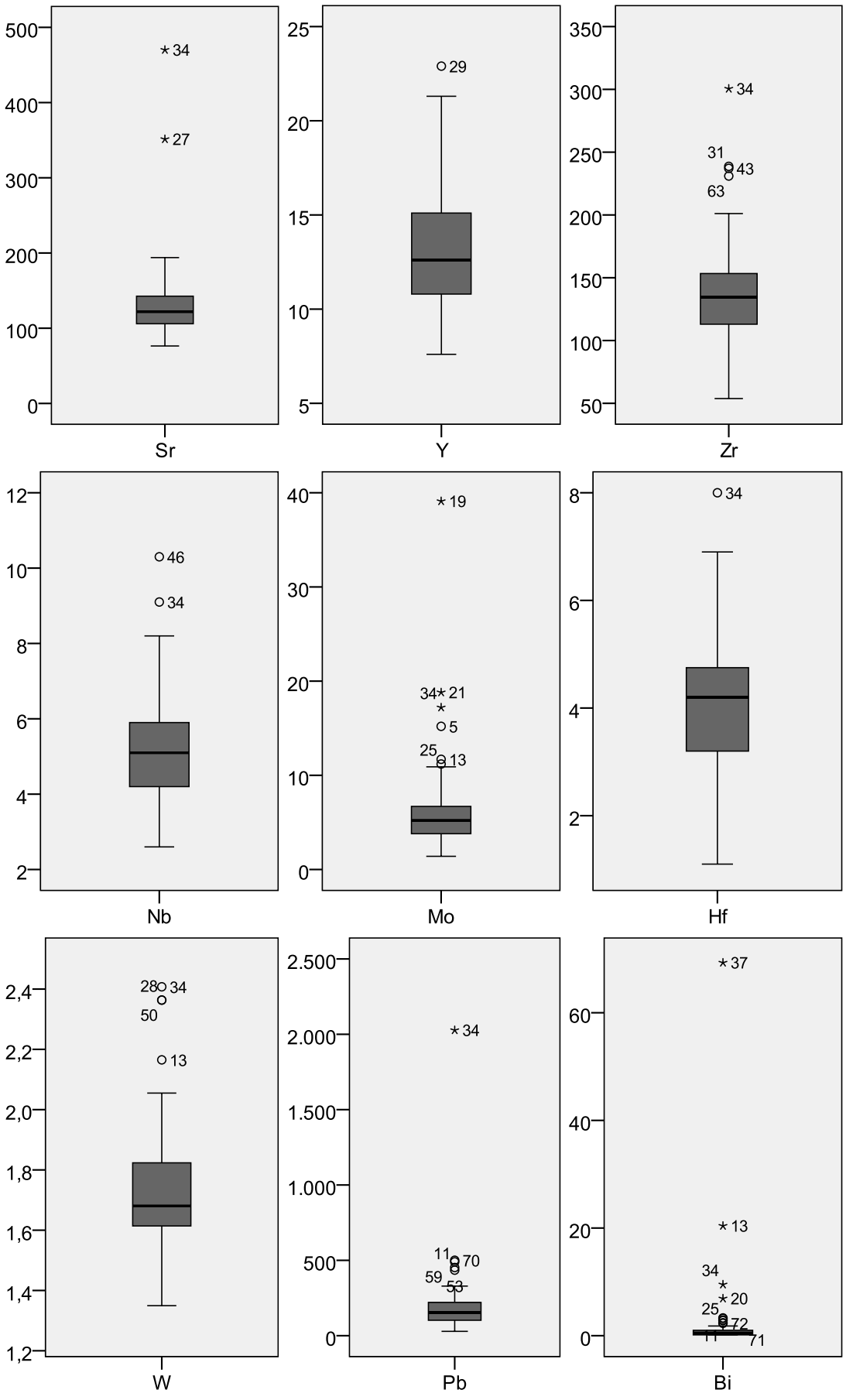
Sr
Y
Zr
Nb
Mo
Hf
W
Pb
Bi

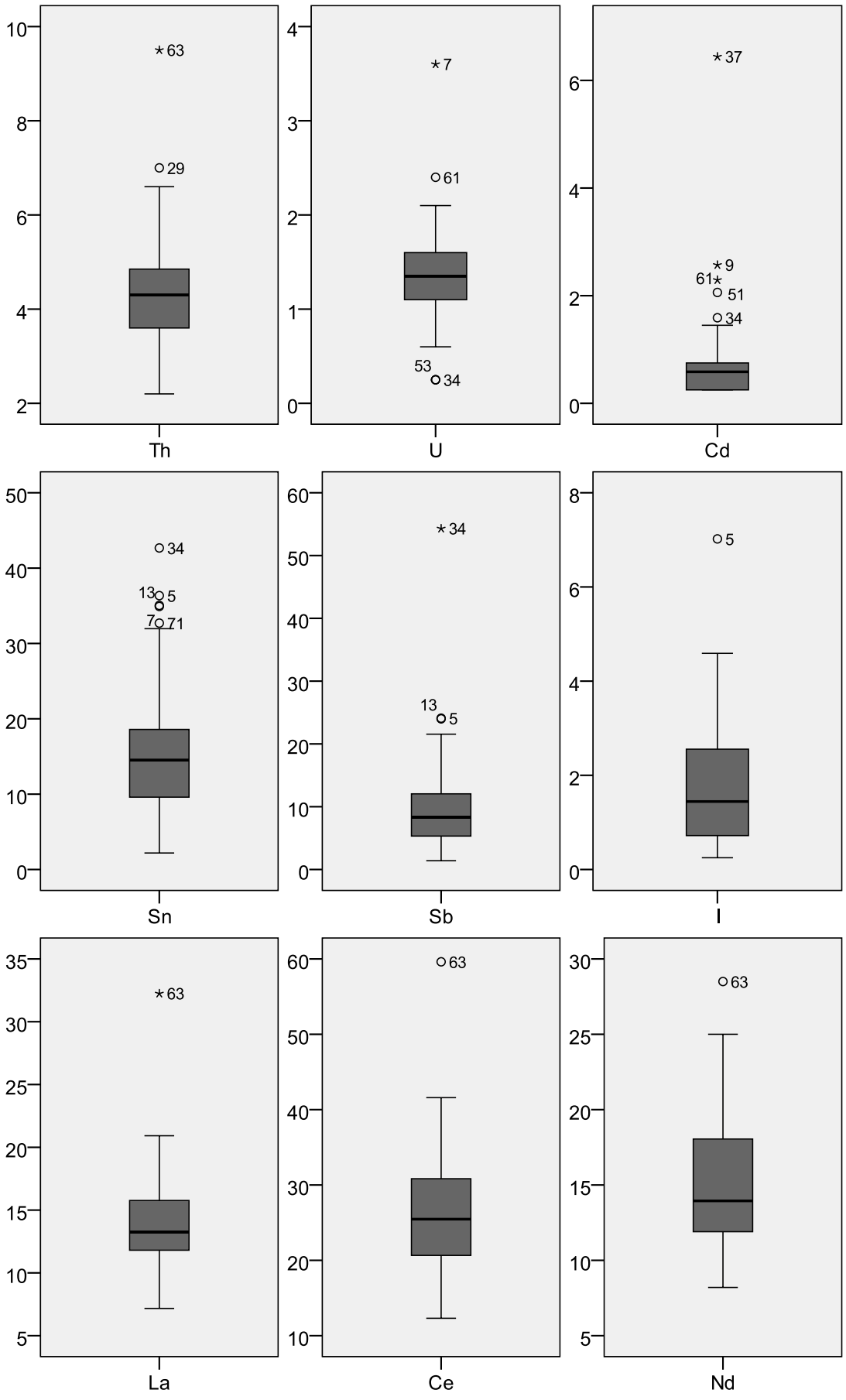
Th
U
Cd
Sn
Sb
I
La
Ce
Nd

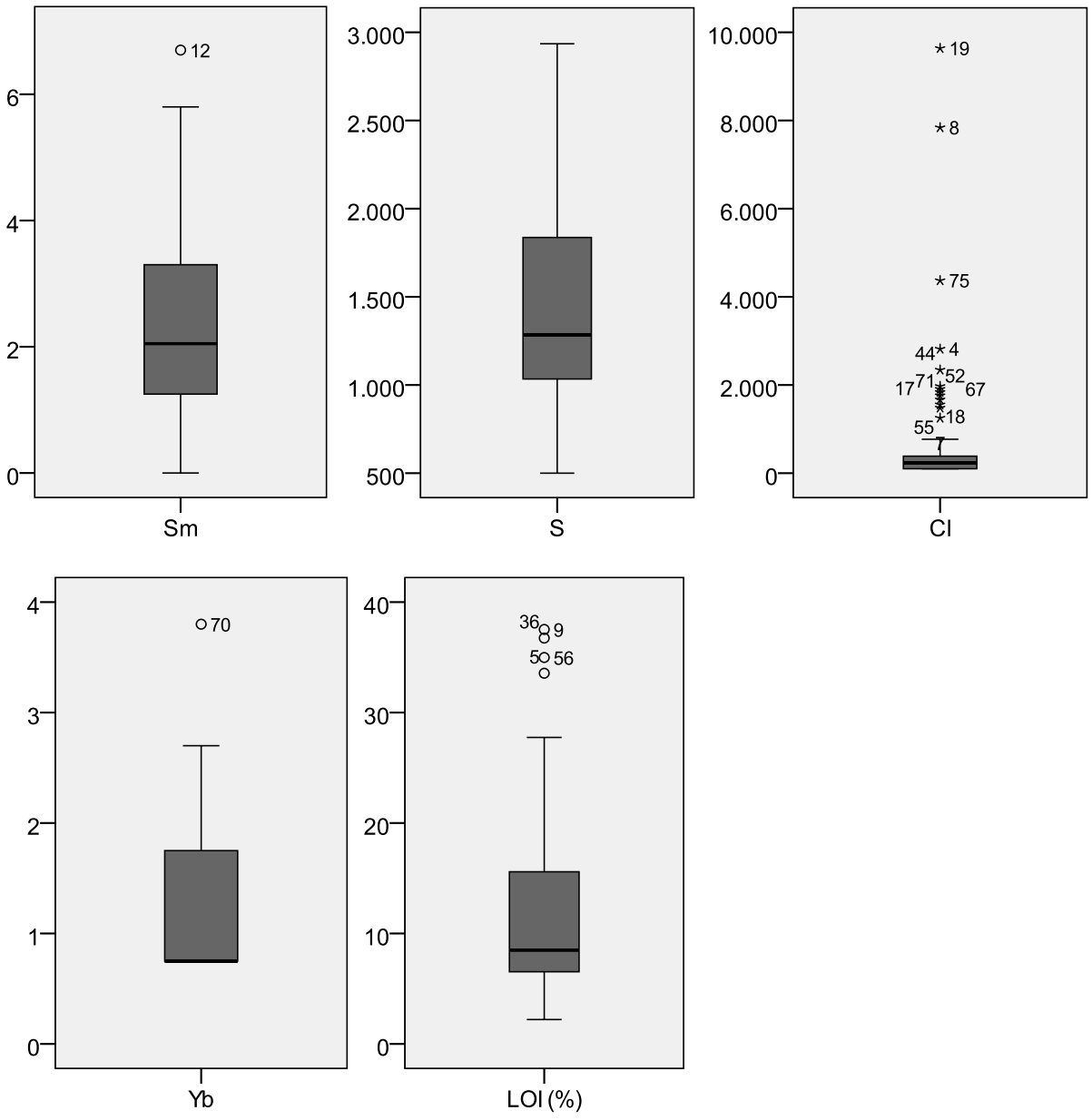
12
6
4
2
0
Sm
3.000
2.500
2.000
1.500
1.000
500
S
19
8
75
4
52
71
17
67
18
55
10.000
8.000
6.000
4.000
2.000
0
Cl
70
4
3
2
1
0
Yb
36
9
5
56
40
30
20
10
0
LOI (%)

Table 89: Kolmogorov-Smirnov test for RDS summer data distributions.

| Element | Kolmogorov-Smirnov | | | Element | Kolmogorov-Smirnov | | |
|---|---|---|---|---|---|---|---|
| | Statistic | df | Sig. | | Statistic | df | Sig. |
| Na2O | ,153 | 72 | ,000 | Sr | ,178 | 72 | ,000 |
| MgO | ,099 | 72 | ,080 | Y | ,132 | 72 | ,003 |
| Al2O3 | ,116 | 72 | ,017 | Zr | ,245 | 72 | ,000 |
| SiO2 | ,148 | 72 | ,000 | Nb | ,136 | 72 | ,002 |
| P2O5 | ,181 | 72 | ,000 | Mo | ,167 | 72 | ,000 |
| K2O | ,092 | 72 | ,200 | Hf | ,206 | 72 | ,000 |
| CaO | ,157 | 72 | ,000 | W | ,316 | 72 | ,000 |
| TiO2 | ,166 | 72 | ,000 | Pb | ,220 | 72 | ,000 |
| MnO | ,104 | 72 | ,052 | Bi | ,375 | 72 | ,000 |
| Fe2O3 | ,099 | 72 | ,077 | Th | ,128 | 72 | ,005 |
| Sc | ,120 | 72 | ,012 | U | ,219 | 72 | ,000 |
| V | ,165 | 72 | ,000 | Cd | ,234 | 72 | ,000 |
| Cr | ,228 | 72 | ,000 | Sn | ,174 | 72 | ,000 |
| Co | ,128 | 72 | ,005 | Sb | ,188 | 72 | ,000 |
| Ba | ,214 | 72 | ,000 | I | ,137 | 72 | ,002 |
| Ni | ,163 | 72 | ,000 | La | ,166 | 72 | ,000 |
| Cu | ,182 | 72 | ,000 | Ce | ,116 | 72 | ,018 |
| Zn | ,175 | 72 | ,000 | Nd | ,081 | 72 | ,200 |
| Ga | ,098 | 72 | ,087 | Sm | ,130 | 72 | ,004 |
| Ge | ,087 | 72 | ,200 | S | ,133 | 72 | ,003 |
| As | ,119 | 72 | ,014 | Cl | ,458 | 72 | ,000 |
| Se | ,180 | 72 | ,000 | Yb | ,403 | 72 | ,000 |
| Br | ,166 | 72 | ,000 | OM | ,217 | 72 | ,000 |
| Rb | ,098 | 72 | ,086 | - | - | - | - |

Table 90: Kolmogorov-Smirnov test for RDS winter data distributions.

| Element | Kolmogorov-Smirnov | | | Element | Kolmogorov-Smirnov | | |
|---|---|---|---|---|---|---|---|
| | Statistic | df | Sig. | | Statistic | df | Sig. |
| Na2O | ,195 | 72 | ,000 | Sr | ,198 | 72 | ,000 |
| MgO | ,205 | 72 | ,000 | Y | ,125 | 72 | ,008 |
| Al2O3 | ,113 | 72 | ,023 | Zr | ,130 | 72 | ,004 |
| SiO2 | ,130 | 72 | ,004 | Nb | ,110 | 72 | ,032 |
| P2O5 | ,168 | 72 | ,000 | Mo | ,230 | 72 | ,000 |
| K2O | ,115 | 72 | ,019 | Hf | ,072 | 72 | ,200 |
| CaO | ,117 | 72 | ,016 | W | ,122 | 72 | ,010 |
| TiO2 | ,138 | 72 | ,002 | Pb | ,266 | 72 | ,000 |
| MnO | ,099 | 72 | ,078 | Bi | ,407 | 72 | ,000 |
| Fe2O3 | ,088 | 72 | ,200 | Th | ,108 | 72 | ,036 |
| Sc | ,098 | 72 | ,081 | U | ,097 | 72 | ,090 |
| V | ,119 | 72 | ,013 | Cd | ,282 | 72 | ,000 |
| Cr | ,098 | 72 | ,084 | Sn | ,134 | 72 | ,003 |
| Co | ,131 | 72 | ,004 | Sb | ,199 | 72 | ,000 |
| Ba | ,162 | 72 | ,000 | I | ,124 | 72 | ,008 |
| Ni | ,112 | 72 | ,027 | La | ,123 | 72 | ,009 |
| Cu | ,110 | 72 | ,032 | Ce | ,098 | 72 | ,087 |
| Zn | ,165 | 72 | ,000 | Nd | ,125 | 72 | ,007 |
| Ga | ,120 | 72 | ,012 | Sm | ,114 | 72 | ,021 |
| Ge | ,138 | 72 | ,002 | S | ,131 | 72 | ,004 |
| As | ,170 | 72 | ,000 | Cl | ,351 | 72 | ,000 |
| Se | ,269 | 72 | ,000 | In | ,508 | 72 | ,000 |
| Br | ,174 | 72 | ,000 | OM | ,227 | 72 | ,000 |
| Rb | ,084 | 72 | ,200 | - | - | - | - |

Table 91: Kolmogorov-Smirnov test for log-transformed RDS summer data distributions.

| | Kolmogorov-Smirnov | | | | Kolmogorov-Smirnov | | |
|---|---|---|---|---|---|---|---|
| | Statistic | df | Sig. | | Statistic | df | Sig. |
| Na2O | ,129 | 72 | ,005 | Sr | ,107 | 72 | ,039 |
| MgO | ,056 | 72 | ,200 | Y | ,084 | 72 | ,200 |
| Al2O3 | ,068 | 72 | ,200 | Zr | ,136 | 72 | ,002 |
| SiO2 | ,178 | 72 | ,000 | Nb | ,082 | 72 | ,200 |
| P2O5 | ,116 | 72 | ,018 | Mo | ,081 | 72 | ,200 |
| K2O | ,068 | 72 | ,200 | Hf | ,112 | 72 | ,025 |
| CaO | ,081 | 72 | ,200 | W | ,140 | 72 | ,001 |
| TiO2 | ,103 | 72 | ,058 | Pb | ,068 | 72 | ,200 |
| MnO | ,062 | 72 | ,200 | Bi | ,101 | 72 | ,066 |
| Fe2O3 | ,075 | 72 | ,200 | Th | ,072 | 72 | ,200 |
| Sc | ,191 | 72 | ,000 | U | ,166 | 72 | ,000 |
| V | ,121 | 72 | ,011 | Cd | ,271 | 72 | ,000 |
| Cr | ,108 | 72 | ,037 | Sn | ,089 | 72 | ,200 |
| Co | ,078 | 72 | ,200 | Sb | ,061 | 72 | ,200 |
| Ba | ,140 | 72 | ,001 | I | ,135 | 72 | ,002 |
| Ni | ,089 | 72 | ,200 | La | ,150 | 72 | ,000 |
| Cu | ,081 | 72 | ,200 | Ce | ,104 | 72 | ,051 |
| Zn | ,083 | 72 | ,200 | Nd | ,082 | 72 | ,200 |
| Ga | ,051 | 72 | ,200 | Sm | ,181 | 62 | ,000 |
| Ge | ,148 | 72 | ,000 | S | ,091 | 72 | ,200 |
| As | ,077 | 72 | ,200 | Cl | ,056 | 72 | ,200 |
| Se | ,214 | 72 | ,000 | Yb | ,144 | 67 | ,001 |
| Br | ,086 | 72 | ,200 | OM | ,089 | 72 | ,200 |
| Rb | ,067 | 72 | ,200 | - | - | - | - |

Table 92: Kolmogorov-Smirnov test for log-transformed RDS winter data distributions.

| | Kolmogorov-Smirnov | | | | Kolmogorov-Smirnov | | |
|---|---|---|---|---|---|---|---|
| | Statistic | df | Sig. | | Statistic | df | Sig. |
| Na2O | ,104 | 72 | ,051 | Sr | ,102 | 72 | ,062 |
| MgO | ,092 | 72 | ,200 | Y | ,076 | 72 | ,200 |
| Al2O3 | ,090 | 72 | ,200 | Zr | ,085 | 72 | ,200 |
| SiO2 | ,168 | 72 | ,000 | Nb | ,070 | 72 | ,200 |
| P2O5 | ,081 | 72 | ,200 | Mo | ,092 | 72 | ,200 |
| K2O | ,087 | 72 | ,200 | Hf | ,118 | 72 | ,014 |
| CaO | ,065 | 72 | ,200 | W | ,099 | 72 | ,080 |
| TiO2 | ,075 | 72 | ,200 | Pb | ,082 | 72 | ,200 |
| MnO | ,110 | 72 | ,030 | Bi | ,192 | 72 | ,000 |
| Fe2O3 | ,103 | 72 | ,057 | Th | ,078 | 72 | ,200 |
| Sc | ,119 | 72 | ,013 | U | ,181 | 72 | ,000 |
| V | ,058 | 72 | ,200 | Cd | ,193 | 72 | ,000 |
| Cr | ,070 | 72 | ,200 | Sn | ,080 | 72 | ,200 |
| Co | ,065 | 72 | ,200 | Sb | ,080 | 72 | ,200 |
| Ba | ,092 | 72 | ,200 | I | ,115 | 72 | ,020 |
| Ni | ,069 | 72 | ,200 | La | ,076 | 72 | ,200 |
| Cu | ,126 | 72 | ,006 | Ce | ,055 | 72 | ,200 |
| Zn | ,071 | 72 | ,200 | Nd | ,068 | 72 | ,200 |
| Ga | ,086 | 72 | ,200 | Sm | ,096 | 63 | ,200 |
| Ge | ,120 | 72 | ,012 | S | ,110 | 72 | ,032 |
| As | ,087 | 72 | ,200 | Cl | ,166 | 72 | ,000 |
| Se | ,216 | 72 | ,000 | In | ,116 | 69 | ,022 |
| Br | ,082 | 72 | ,200 | OM | ,131 | 72 | ,004 |
| Rb | ,072 | 72 | ,200 | - | - | - | - |

Table 93: Kolmogorov-Smirnov test for Box-Cox-transformed RDS summer data distributions.

| | Kolmogorov-Smirnov | | | | Kolmogorov-Smirnov | | |
|---|---|---|---|---|---|---|---|
| | Statistic | df | Sig. | | Statistic | df | Sig. |
| Na2O | ,129 | 72 | ,005 | Rb | ,067 | 72 | ,200 |
| MgO | ,056 | 72 | ,200 | Sr | ,099 | 72 | ,076 |
| Al2O3 | ,068 | 72 | ,200 | Y | ,050 | 72 | ,200 |
| SiO2 | ,097 | 72 | ,090 | Zr | ,101 | 72 | ,067 |
| P2O5 | ,098 | 72 | ,085 | Nb | ,060 | 72 | ,200 |
| K2O | ,068 | 72 | ,200 | Mo | ,081 | 72 | ,200 |
| CaO | ,081 | 72 | ,200 | Hf | ,114 | 72 | ,022 |
| TiO2 | ,049 | 72 | ,200 | W | ,094 | 72 | ,194 |
| MnO | ,048 | 72 | ,200 | Pb | ,068 | 72 | ,200 |
| Fe2O3 | ,075 | 72 | ,200 | Bi | ,101 | 72 | ,066 |
| Sc | ,131 | 72 | ,004 | Th | ,076 | 72 | ,200 |
| V | ,072 | 72 | ,200 | U | ,174 | 72 | ,000 |
| Cr | ,122 | 72 | ,010 | Cd | ,288 | 72 | ,000 |
| Co | ,046 | 72 | ,200 | Sn | ,052 | 72 | ,200 |
| Ba | ,104 | 72 | ,051 | Sb | ,061 | 72 | ,200 |
| Ni | ,048 | 72 | ,200 | I | ,135 | 72 | ,002 |
| Cu | ,078 | 72 | ,200 | La | ,150 | 72 | ,000 |
| Zn | ,083 | 72 | ,200 | Ce | ,104 | 72 | ,051 |
| Ga | ,044 | 72 | ,200 | Nd | ,082 | 72 | ,200 |
| Ge | ,104 | 72 | ,051 | S | ,073 | 72 | ,200 |
| As | ,077 | 72 | ,200 | Cl | ,056 | 72 | ,200 |
| Se | ,214 | 72 | ,000 | OM | ,068 | 72 | ,200 |
| Br | ,086 | 72 | ,200 | - | - | - | - |

Table 94: Kolmogorov-Smirnov test for Box-Cox-transformed RDS winter data distributions.

| | Kolmogorov-Smirnov | | | | Kolmogorov-Smirnov | | |
|---|---|---|---|---|---|---|---|
| | Statistic | df | Sig. | | Statistic | df | Sig. |
| Na2O | ,104 | 72 | ,051 | Rb_w | ,066 | 72 | ,200 |
| MgO | ,073 | 72 | ,200 | Sr | ,064 | 72 | ,200 |
| Al2O3 | ,091 | 72 | ,200 | Y | ,064 | 72 | ,200 |
| SiO2 | ,089 | 72 | ,200 | Zr | ,085 | 72 | ,200 |
| P2O5 | ,072 | 72 | ,200 | Nb | ,070 | 72 | ,200 |
| K2O | ,087 | 72 | ,200 | Mo | ,092 | 72 | ,200 |
| CaO | ,065 | 72 | ,200 | Hf | ,067 | 72 | ,200 |
| TiO2 | ,075 | 72 | ,200 | W | ,101 | 72 | ,066 |
| MnO | ,107 | 72 | ,041 | Pb | ,082 | 72 | ,200 |
| Fe2O3 | ,070 | 72 | ,200 | Bi | ,236 | 72 | ,000 |
| Sc | ,087 | 72 | ,200 | Th | ,078 | 72 | ,200 |
| V | ,058 | 72 | ,200 | U | ,110 | 72 | ,030 |
| Cr | ,070 | 72 | ,200 | Cd | ,217 | 72 | ,000 |
| Co | ,065 | 72 | ,200 | Sn | ,075 | 72 | ,200 |
| Ba | ,080 | 72 | ,200 | Sb | ,080 | 72 | ,200 |
| Ni | ,069 | 72 | ,200 | I | ,089 | 72 | ,200 |
| Cu | ,093 | 72 | ,199 | La | ,076 | 72 | ,200 |
| Zn | ,071 | 72 | ,200 | Ce | ,055 | 72 | ,200 |
| Ga | ,085 | 72 | ,200 | Nd | ,068 | 72 | ,200 |
| Ge | ,120 | 72 | ,012 | S | ,089 | 72 | ,200 |
| As | ,095 | 72 | ,176 | Cl | ,085 | 72 | ,200 |
| Se | ,229 | 72 | ,000 | OM | ,131 | 72 | ,004 |
| Br_w | ,082 | 72 | ,200 | - | - | - | - |

Figure 117: Grain size relative frequency charts, classified according to Friedman and Sanders, 1978 (left) and relative vs. cumulative frequency distributions (right) for RDS summer and winter samples.

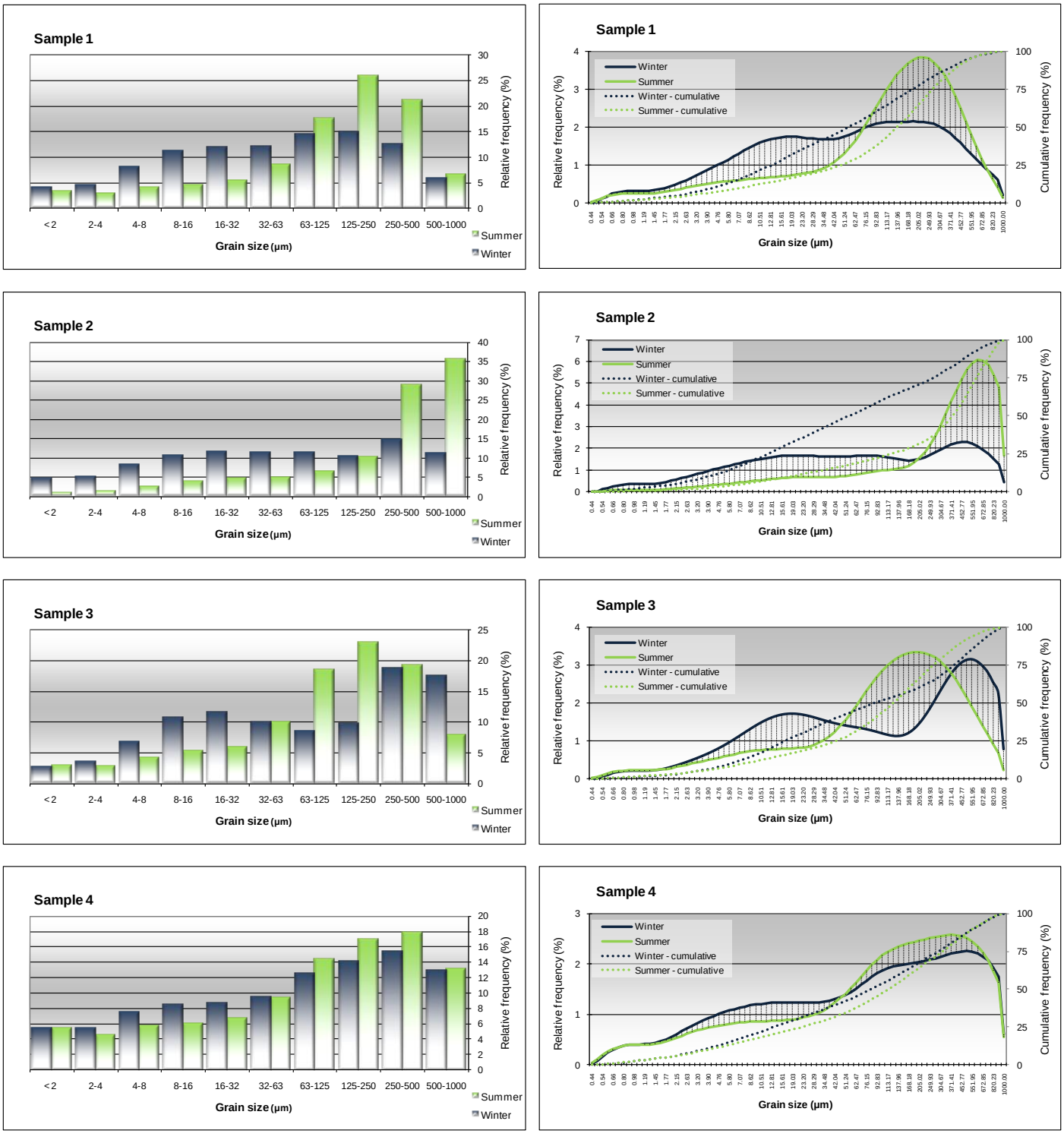

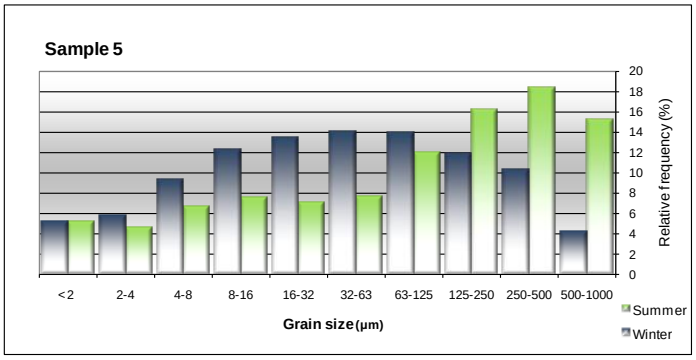
Sample 5
Relative frequency (%)
Grain size (µm)
<2
2-4
4-8
8-16
16-32
32-63
63-125
125-250
250-500
500-1000
Summer
Winter

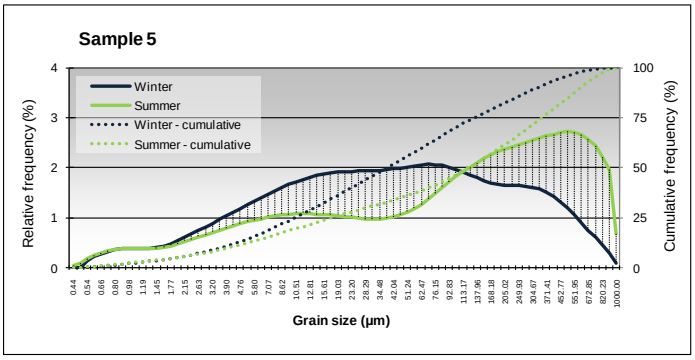
Sample 5
Winter
Summer
Winter - cumulative
Summer - cumulative
Relative frequency (%)
Cumulative frequency (%)
Grain size (µm)

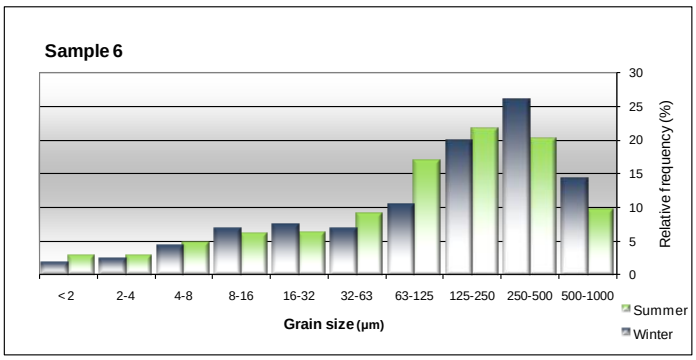
Sample 6
Relative frequency (%)
Grain size (µm)
<2
2-4
4-8
8-16
16-32
32-63
63-125
125-250
250-500
500-1000
Summer
Winter

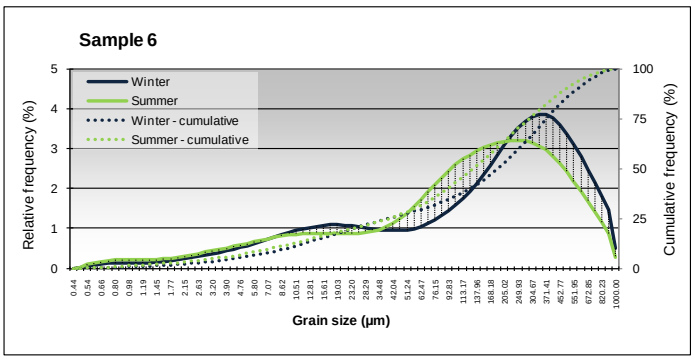
Sample 6
Winter
Summer
Winter - cumulative
Summer - cumulative
Relative frequency (%)
Cumulative frequency (%)
Grain size (µm)

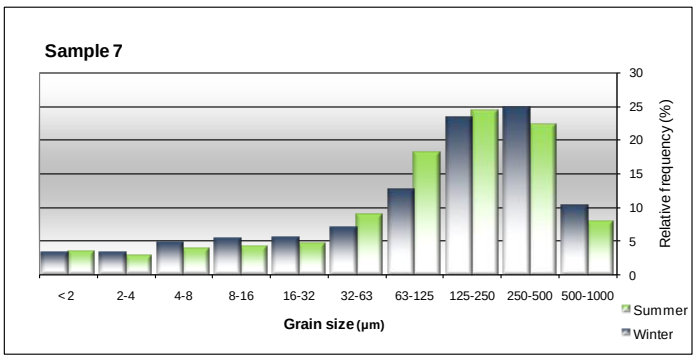
Sample 7
Relative frequency (%)
Grain size (µm)
<2
2-4
4-8
8-16
16-32
32-63
63-125
125-250
250-500
500-1000
Summer
Winter

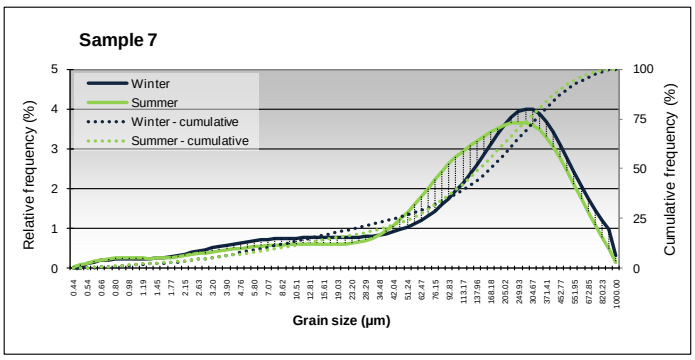
Sample 7
Winter
Summer
Winter - cumulative
Summer - cumulative
Relative frequency (%)
Cumulative frequency (%)
Grain size (µm)

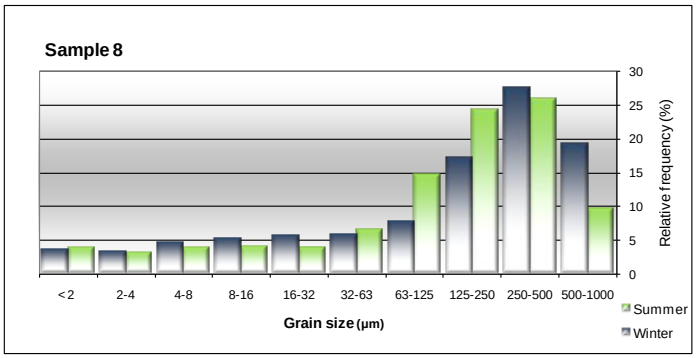
Sample 8
Relative frequency (%)
Grain size (µm)
<2
2-4
4-8
8-16
16-32
32-63
63-125
125-250
250-500
500-1000
Summer
Winter

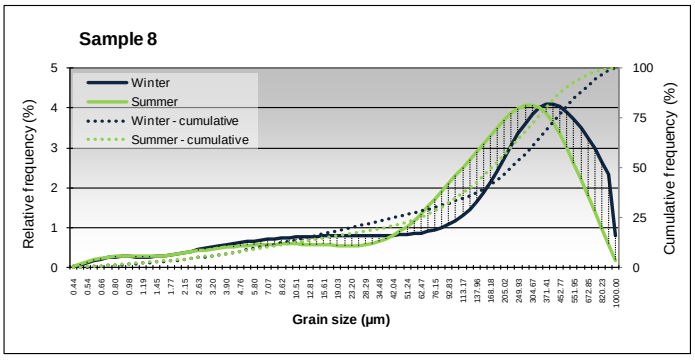
Sample 8
Winter
Summer
Winter - cumulative
Summer - cumulative
Relative frequency (%)
Cumulative frequency (%)
Grain size (µm)

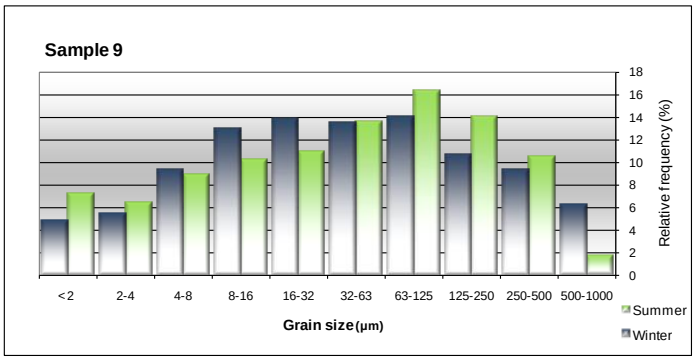
Sample 9
Relative frequency (%)
Grain size (µm)
<2
2-4
4-8
8-16
16-32
32-63
63-125
125-250
250-500
500-1000
Summer
Winter

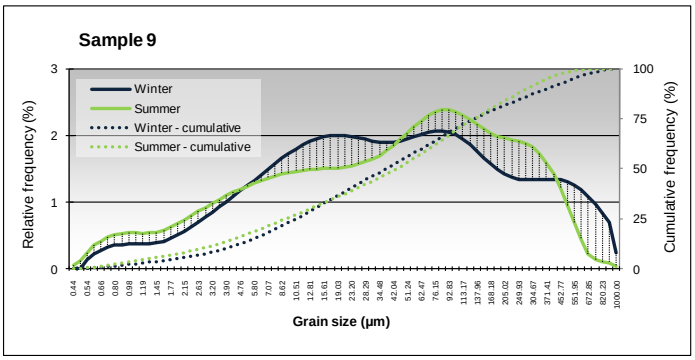
Sample 9
Winter
Summer
Winter - cumulative
Summer - cumulative
Relative frequency (%)
Cumulative frequency (%)
Grain size (µm)

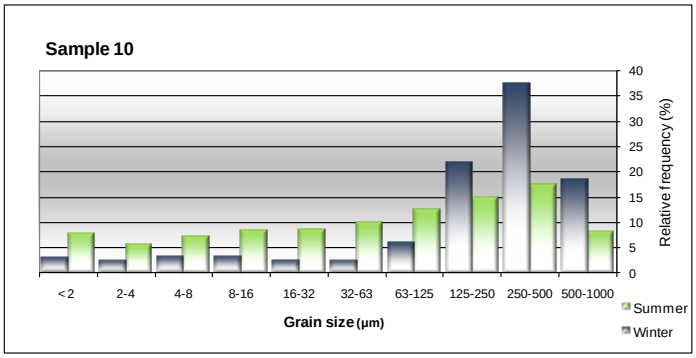
Sample 10
Relative frequency (%)
0
5
10
15
20
25
30
35
40
< 2
2-4
4-8
8-16
16-32
32-63
63-125
125-250
250-500
500-1000
Grain size (µm)
Summer
Winter

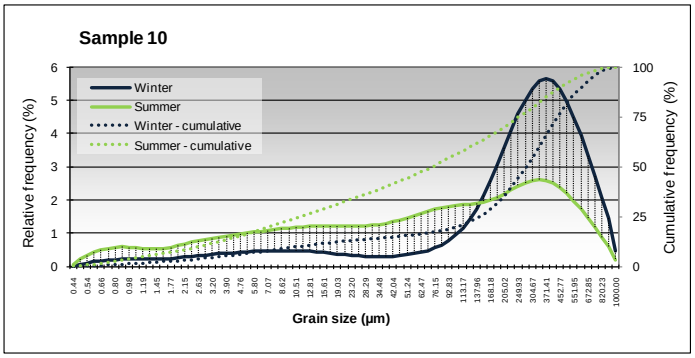
Sample 10
Relative frequency (%)
Cumulative frequency (%)
Winter
Summer
Winter - cumulative
Summer - cumulative
Grain size (µm)

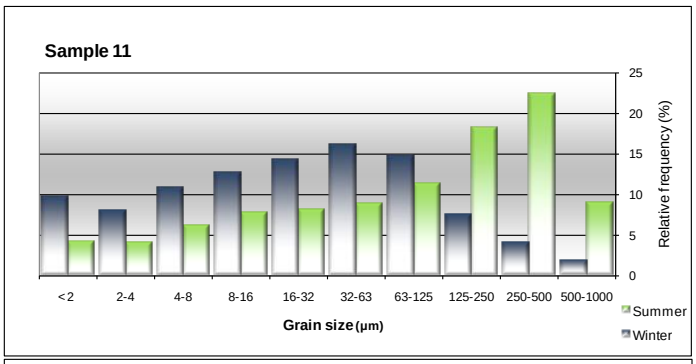
Sample 11
Relative frequency (%)
0
5
10
15
20
25
< 2
2-4
4-8
8-16
16-32
32-63
63-125
125-250
250-500
500-1000
Grain size (µm)
Summer
Winter

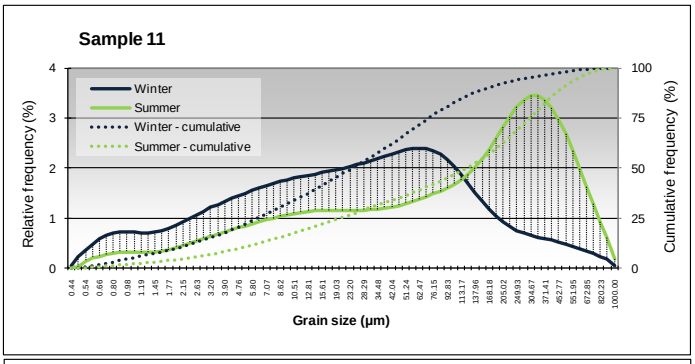
Sample 11
Relative frequency (%)
Cumulative frequency (%)
Winter
Summer
Winter - cumulative
Summer - cumulative
Grain size (µm)

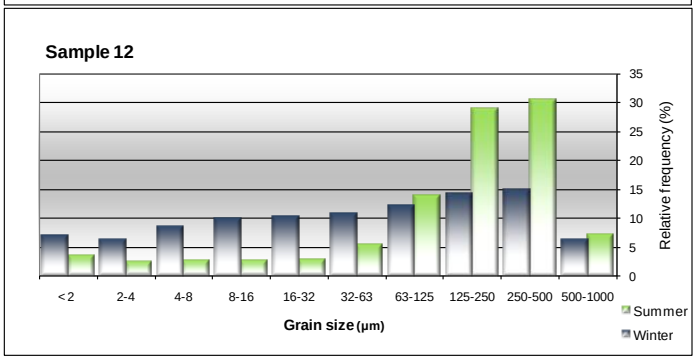
Sample 12
Relative frequency (%)
0
5
10
15
20
25
30
35
< 2
2-4
4-8
8-16
16-32
32-63
63-125
125-250
250-500
500-1000
Grain size (µm)
Summer
Winter

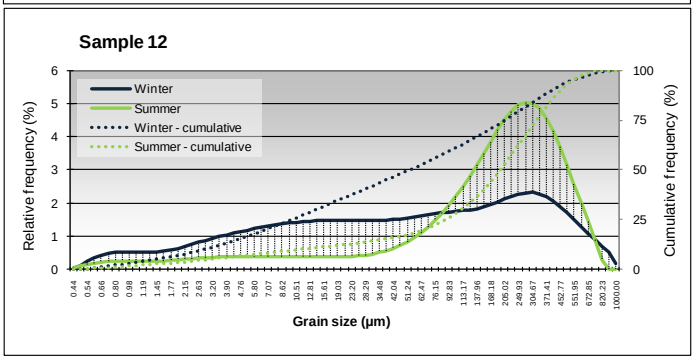
Sample 12
Relative frequency (%)
Cumulative frequency (%)
Winter
Summer
Winter - cumulative
Summer - cumulative
Grain size (µm)

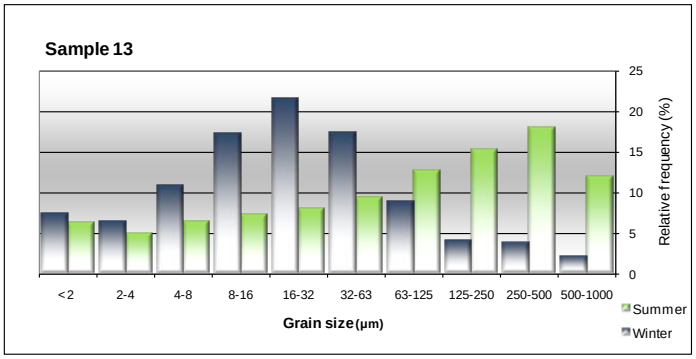
Sample 13
Relative frequency (%)
0
5
10
15
20
25
< 2
2-4
4-8
8-16
16-32
32-63
63-125
125-250
250-500
500-1000
Grain size (µm)
Summer
Winter

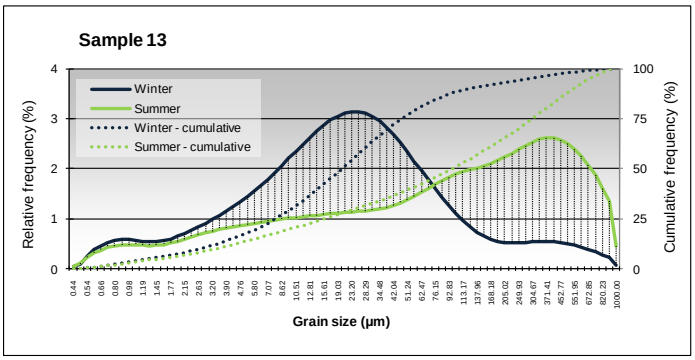
Sample 13
Relative frequency (%)
Cumulative frequency (%)
Winter
Summer
Winter - cumulative
Summer - cumulative
Grain size (µm)

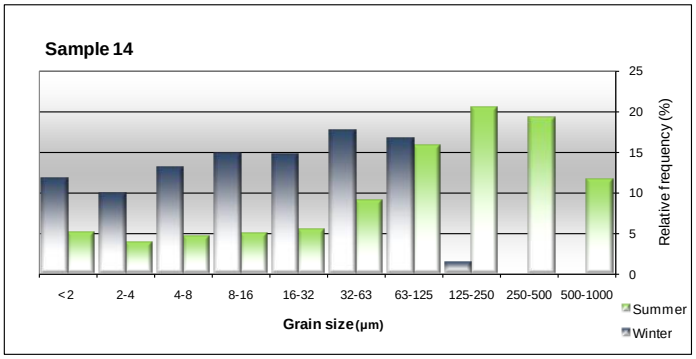
Sample 14
Relative frequency (%)
0
5
10
15
20
25
< 2
2-4
4-8
8-16
16-32
32-63
63-125
125-250
250-500
500-1000
Grain size (µm)
Summer
Winter

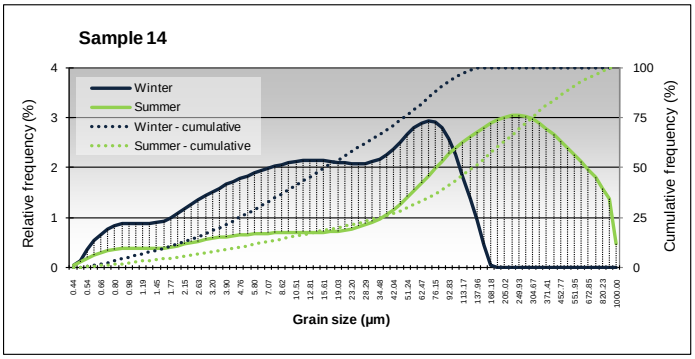
Sample 14
Relative frequency (%)
Cumulative frequency (%)
Winter
Summer
Winter - cumulative
Summer - cumulative
Grain size (µm)

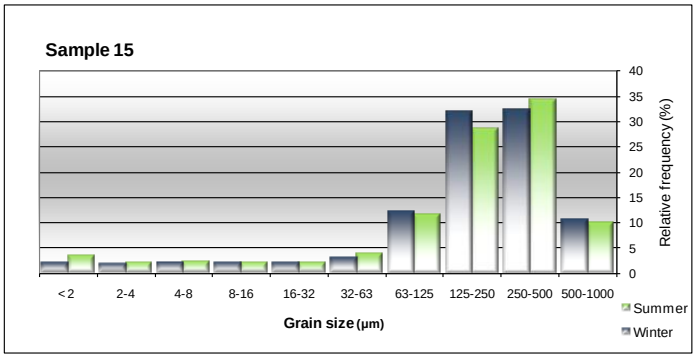
Sample 15
Relative frequency (%)
< 2
2-4
4-8
8-16
16-32
32-63
63-125
125-250
250-500
500-1000
Grain size (µm)
Summer
Winter

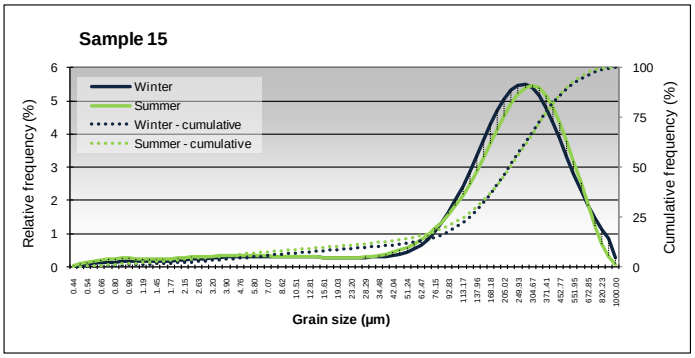
Sample 15
Winter
Summer
Winter - cumulative
Summer - cumulative
Relative frequency (%)
Cumulative frequency (%)
Grain size (µm)

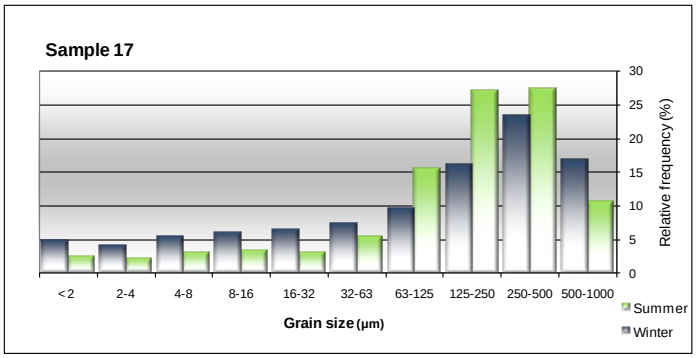
Sample 17
Relative frequency (%)
< 2
2-4
4-8
8-16
16-32
32-63
63-125
125-250
250-500
500-1000
Grain size (µm)
Summer
Winter

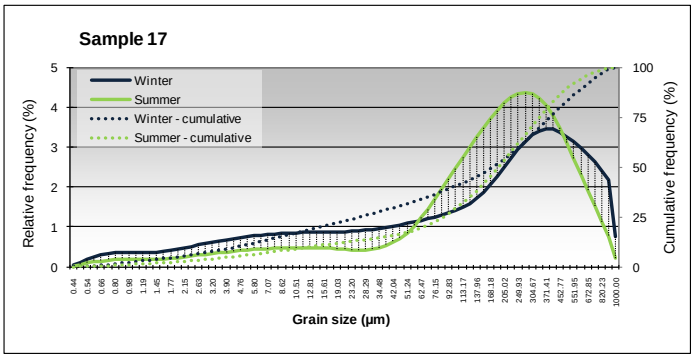
Sample 17
Winter
Summer
Winter - cumulative
Summer - cumulative
Relative frequency (%)
Cumulative frequency (%)
Grain size (µm)

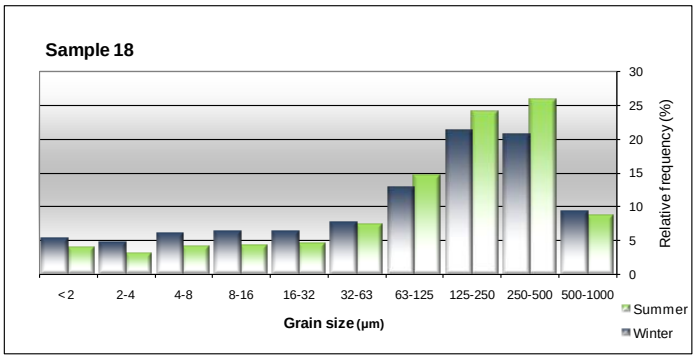
Sample 18
Relative frequency (%)
< 2
2-4
4-8
8-16
16-32
32-63
63-125
125-250
250-500
500-1000
Grain size (µm)
Summer
Winter

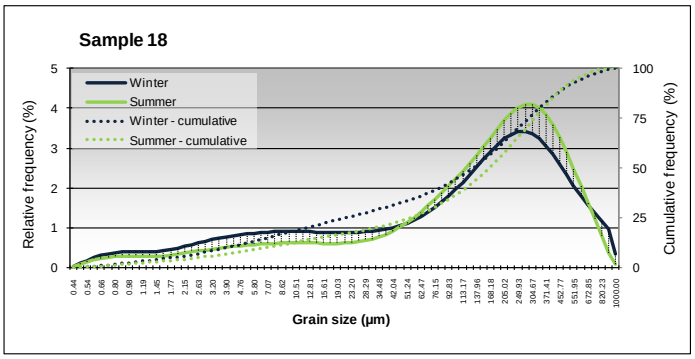
Sample 18
Winter
Summer
Winter - cumulative
Summer - cumulative
Relative frequency (%)
Cumulative frequency (%)
Grain size (µm)

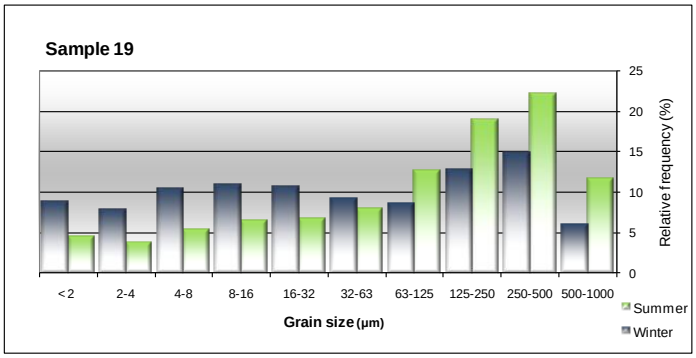
Sample 19
Relative frequency (%)
< 2
2-4
4-8
8-16
16-32
32-63
63-125
125-250
250-500
500-1000
Grain size (µm)
Summer
Winter

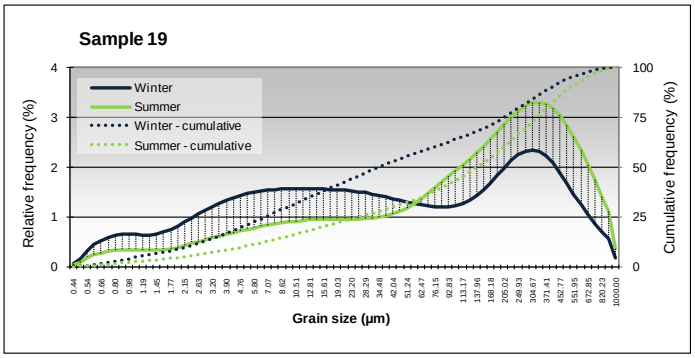
Sample 19
Winter
Summer
Winter - cumulative
Summer - cumulative
Relative frequency (%)
Cumulative frequency (%)
Grain size (µm)

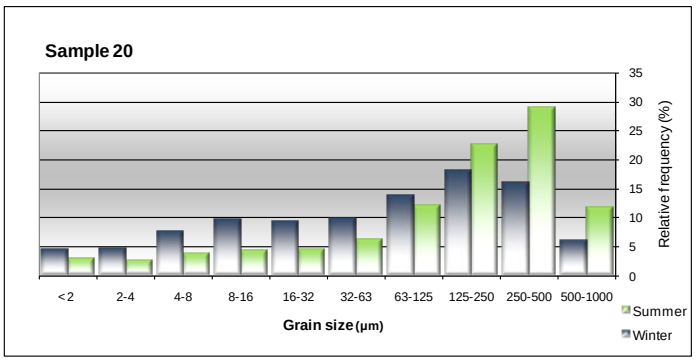
Sample 20
Relative frequency (%)
< 2
2-4
4-8
8-16
16-32
32-63
63-125
125-250
250-500
500-1000
Grain size (µm)
Summer
Winter

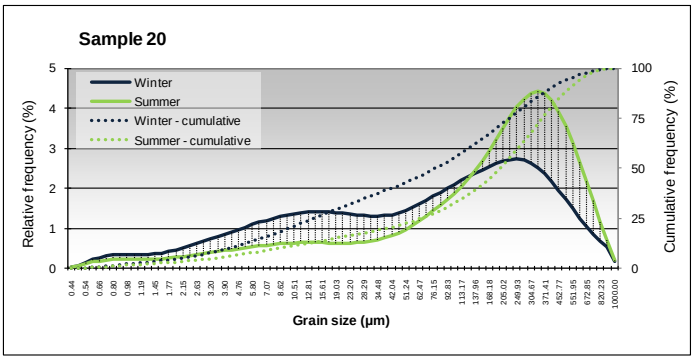
Sample 20
Winter
Summer
Winter - cumulative
Summer - cumulative
Relative frequency (%)
Cumulative frequency (%)
Grain size (µm)

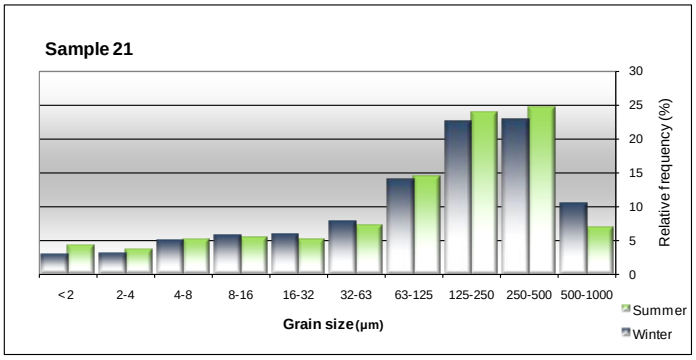
Sample 21
Relative frequency (%)
<2
2-4
4-8
8-16
16-32
32-63
63-125
125-250
250-500
500-1000
Grain size (µm)
Summer
Winter

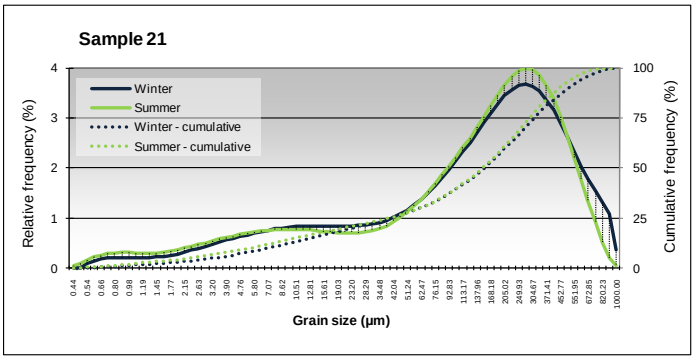
Sample 21
Winter
Summer
Winter - cumulative
Summer - cumulative
Relative frequency (%)
Cumulative frequency (%)
Grain size (µm)

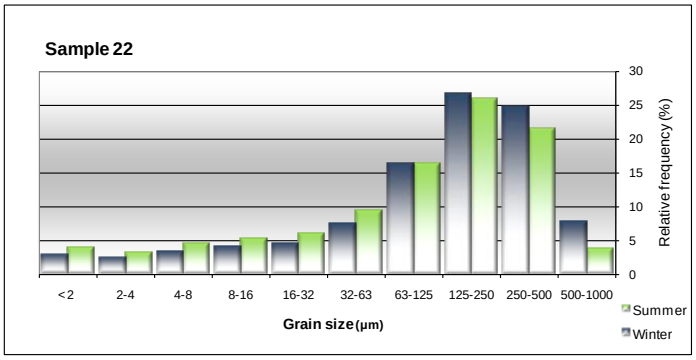
Sample 22
Relative frequency (%)
<2
2-4
4-8
8-16
16-32
32-63
63-125
125-250
250-500
500-1000
Grain size (µm)
Summer
Winter

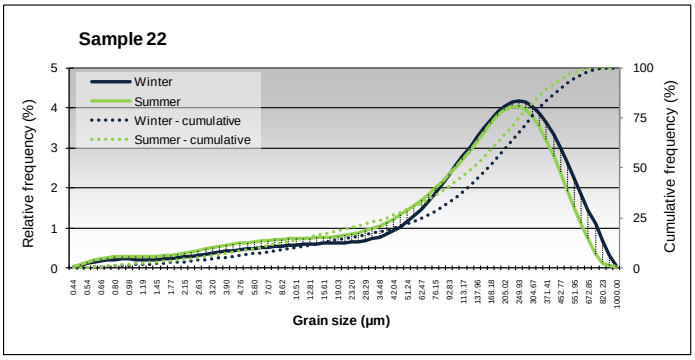
Sample 22
Winter
Summer
Winter - cumulative
Summer - cumulative
Relative frequency (%)
Cumulative frequency (%)
Grain size (µm)

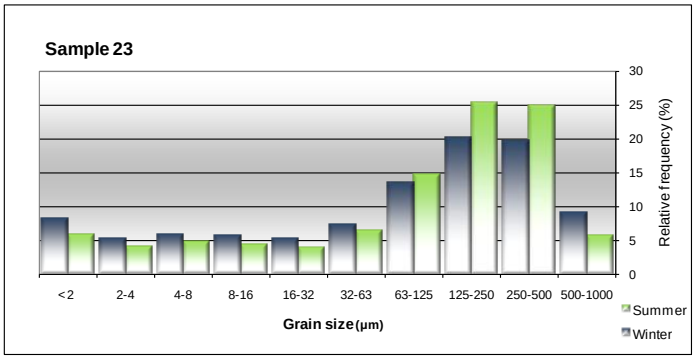
Sample 23
Relative frequency (%)
<2
2-4
4-8
8-16
16-32
32-63
63-125
125-250
250-500
500-1000
Grain size (µm)
Summer
Winter

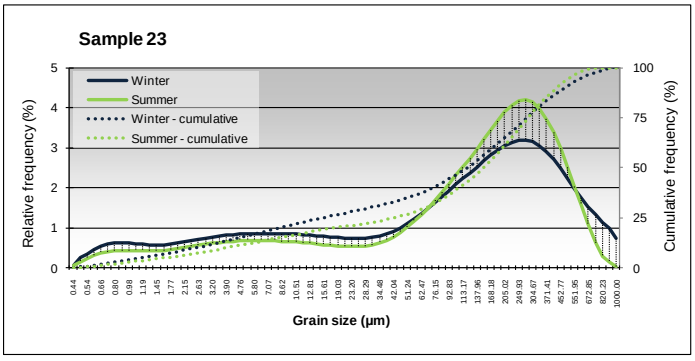
Sample 23
Winter
Summer
Winter - cumulative
Summer - cumulative
Relative frequency (%)
Cumulative frequency (%)
Grain size (µm)

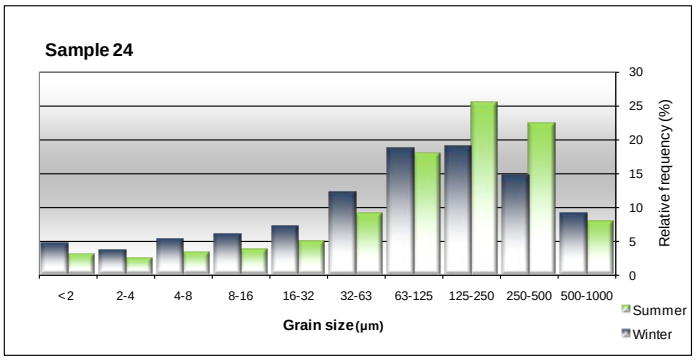
Sample 24
Relative frequency (%)
<2
2-4
4-8
8-16
16-32
32-63
63-125
125-250
250-500
500-1000
Grain size (µm)
Summer
Winter

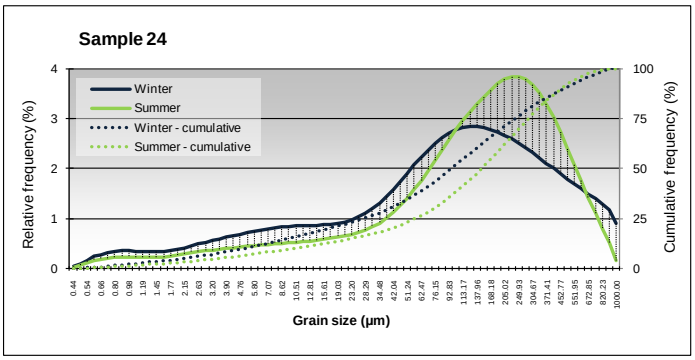
Sample 24
Winter
Summer
Winter - cumulative
Summer - cumulative
Relative frequency (%)
Cumulative frequency (%)
Grain size (µm)

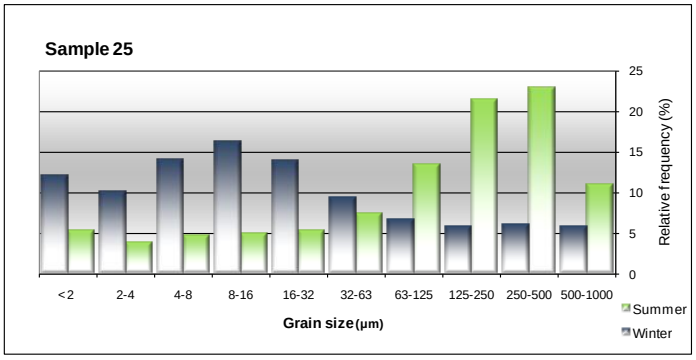
Sample 25
Relative frequency (%)
<2
2-4
4-8
8-16
16-32
32-63
63-125
125-250
250-500
500-1000
Grain size (µm)
Summer
Winter

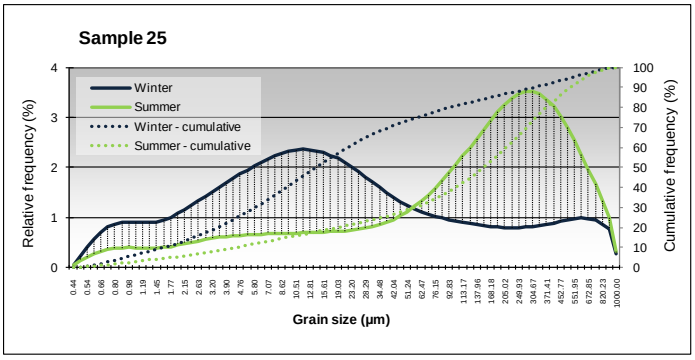
Sample 25
Winter
Summer
Winter - cumulative
Summer - cumulative
Relative frequency (%)
Cumulative frequency (%)
Grain size (µm)

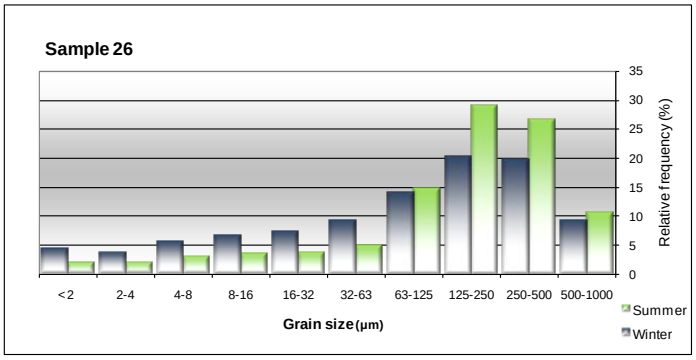
Sample 26
Relative frequency (%)
Grain size (µm)
<2
2-4
4-8
8-16
16-32
32-63
63-125
125-250
250-500
500-1000
Summer
Winter

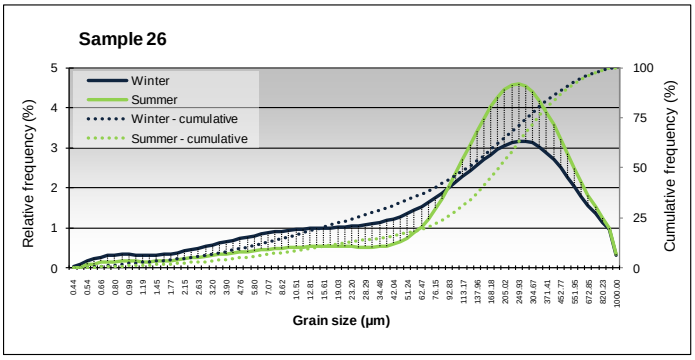
Sample 26
Winter
Summer
Winter - cumulative
Summer - cumulative
Relative frequency (%)
Cumulative frequency (%)
Grain size (µm)

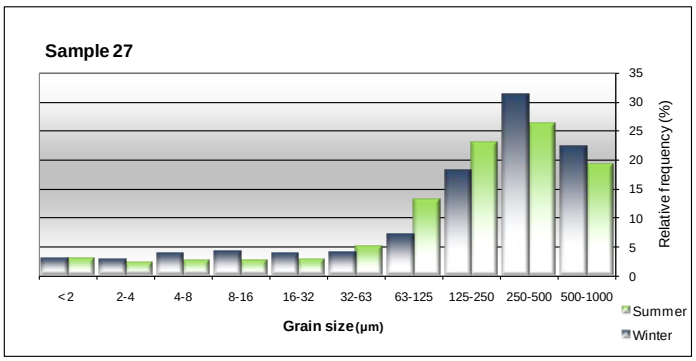
Sample 27
Relative frequency (%)
Grain size (µm)
<2
2-4
4-8
8-16
16-32
32-63
63-125
125-250
250-500
500-1000
Summer
Winter

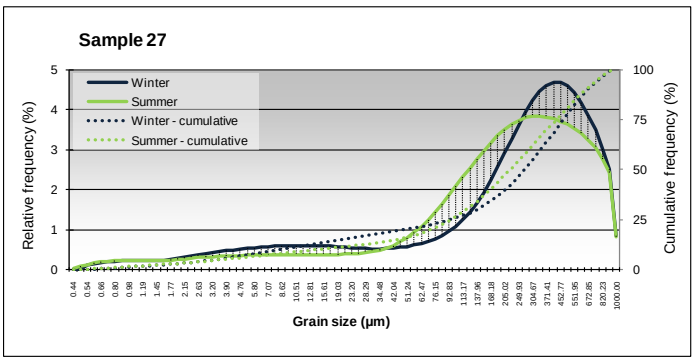
Sample 27
Winter
Summer
Winter - cumulative
Summer - cumulative
Relative frequency (%)
Cumulative frequency (%)
Grain size (µm)

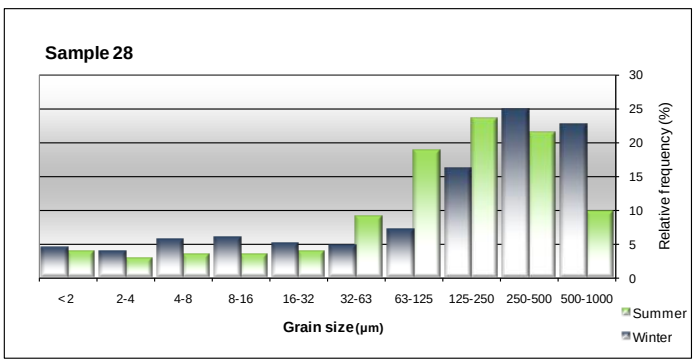
Sample 28
Relative frequency (%)
Grain size (µm)
<2
2-4
4-8
8-16
16-32
32-63
63-125
125-250
250-500
500-1000
Summer
Winter

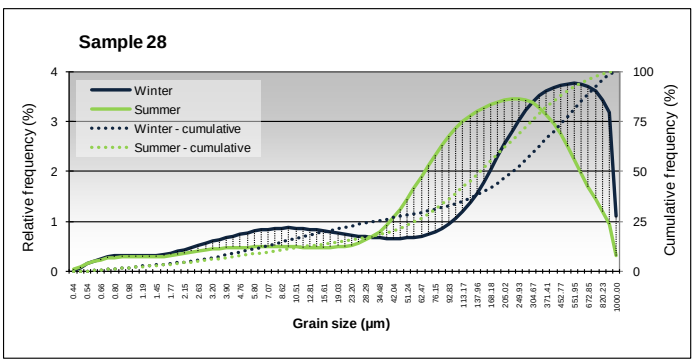
Sample 28
Winter
Summer
Winter - cumulative
Summer - cumulative
Relative frequency (%)
Cumulative frequency (%)
Grain size (µm)

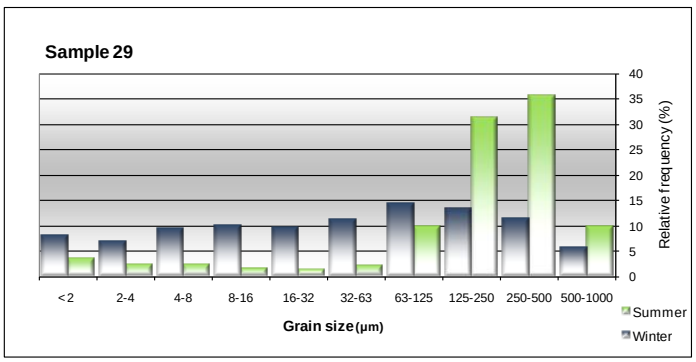
Sample 29
Relative frequency (%)
Grain size (µm)
<2
2-4
4-8
8-16
16-32
32-63
63-125
125-250
250-500
500-1000
Summer
Winter

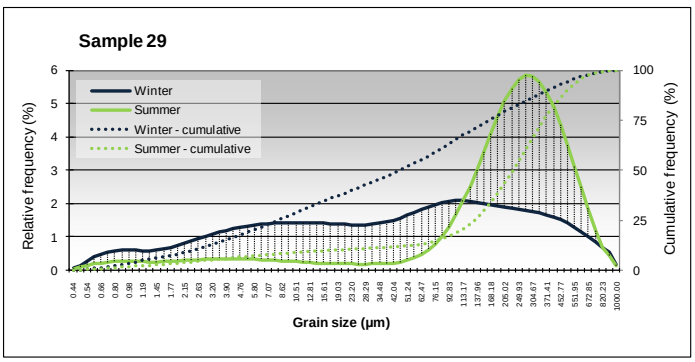
Sample 29
Winter
Summer
Winter - cumulative
Summer - cumulative
Relative frequency (%)
Cumulative frequency (%)
Grain size (µm)

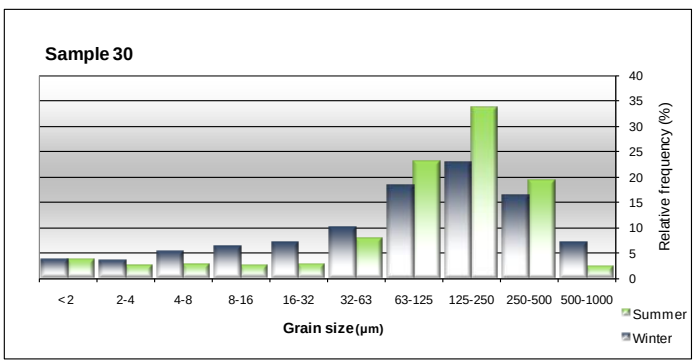
Sample 30
Relative frequency (%)
Grain size (µm)
<2
2-4
4-8
8-16
16-32
32-63
63-125
125-250
250-500
500-1000
Summer
Winter

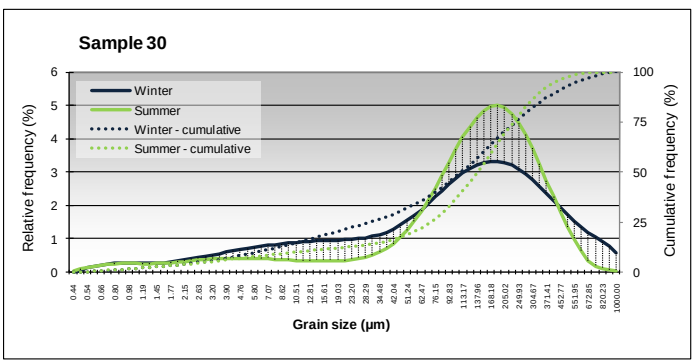
Sample 30
Winter
Summer
Winter - cumulative
Summer - cumulative
Relative frequency (%)
Cumulative frequency (%)
Grain size (µm)

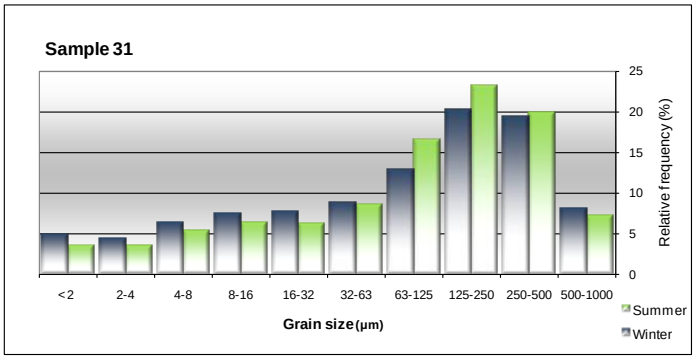
Sample 31
Relative frequency (%)
<2
2-4
4-8
8-16
16-32
32-63
63-125
125-250
250-500
500-1000
Grain size (µm)
Summer
Winter

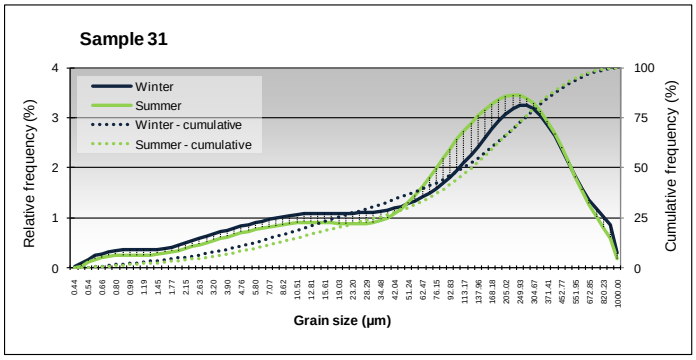
Sample 31
Winter
Summer
Winter - cumulative
Summer - cumulative
Relative frequency (%)
Cumulative frequency (%)
Grain size (µm)

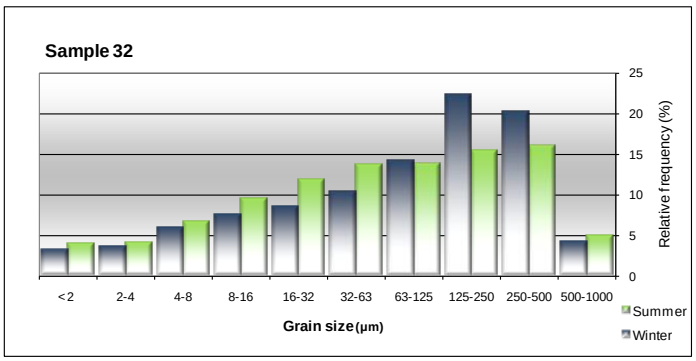
Sample 32
Relative frequency (%)
<2
2-4
4-8
8-16
16-32
32-63
63-125
125-250
250-500
500-1000
Grain size (µm)
Summer
Winter

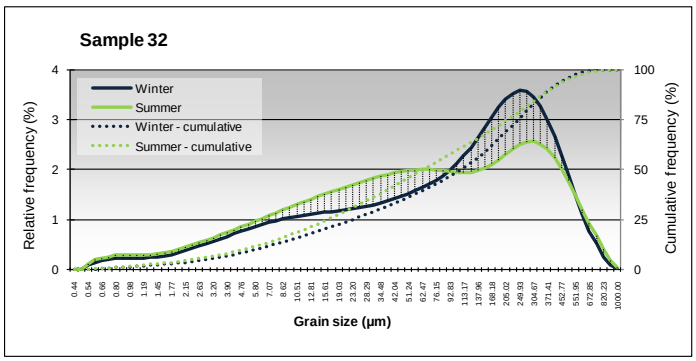
Sample 32
Winter
Summer
Winter - cumulative
Summer - cumulative
Relative frequency (%)
Cumulative frequency (%)
Grain size (µm)

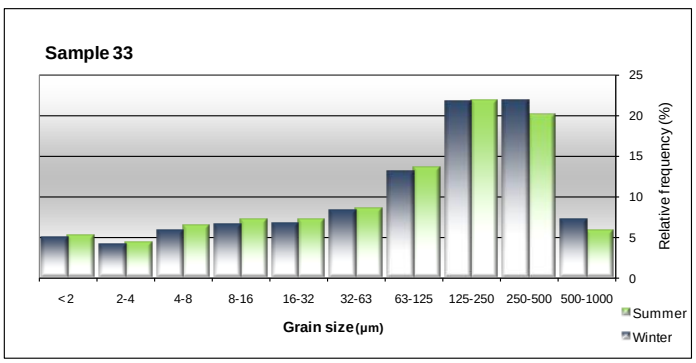
Sample 33
Relative frequency (%)
<2
2-4
4-8
8-16
16-32
32-63
63-125
125-250
250-500
500-1000
Grain size (µm)
Summer
Winter

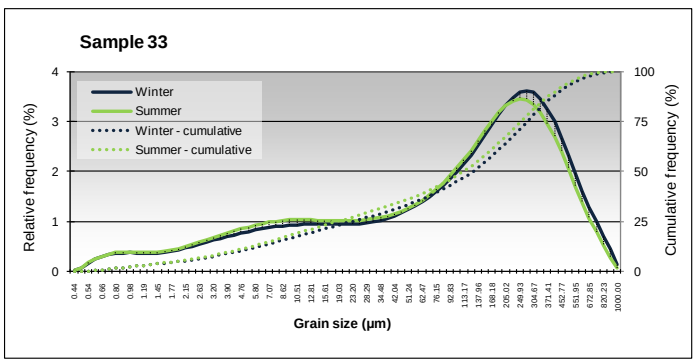
Sample 33
Winter
Summer
Winter - cumulative
Summer - cumulative
Relative frequency (%)
Cumulative frequency (%)
Grain size (µm)

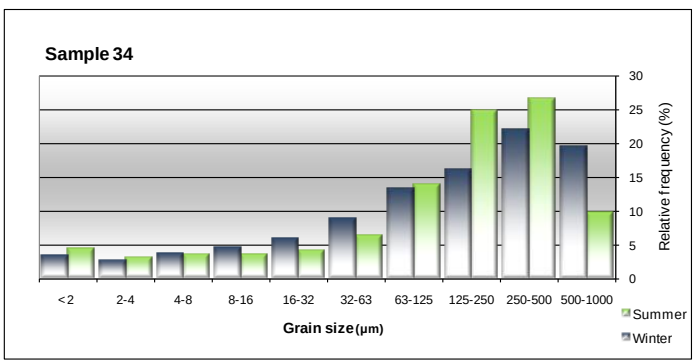
Sample 34
Relative frequency (%)
<2
2-4
4-8
8-16
16-32
32-63
63-125
125-250
250-500
500-1000
Grain size (µm)
Summer
Winter

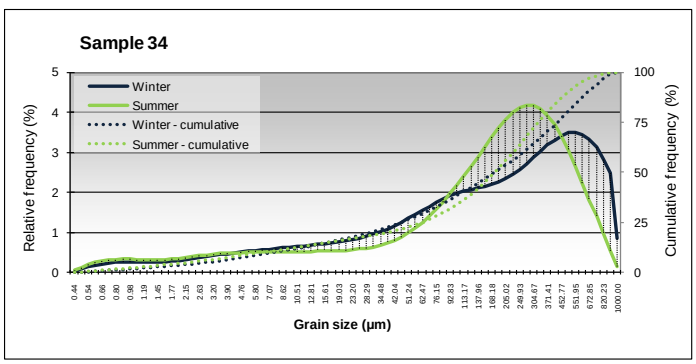
Sample 34
Winter
Summer
Winter - cumulative
Summer - cumulative
Relative frequency (%)
Cumulative frequency (%)
Grain size (µm)

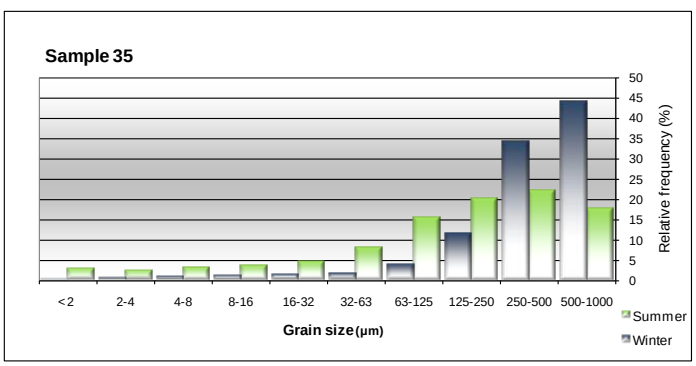
Sample 35
Relative frequency (%)
<2
2-4
4-8
8-16
16-32
32-63
63-125
125-250
250-500
500-1000
Grain size (µm)
Summer
Winter

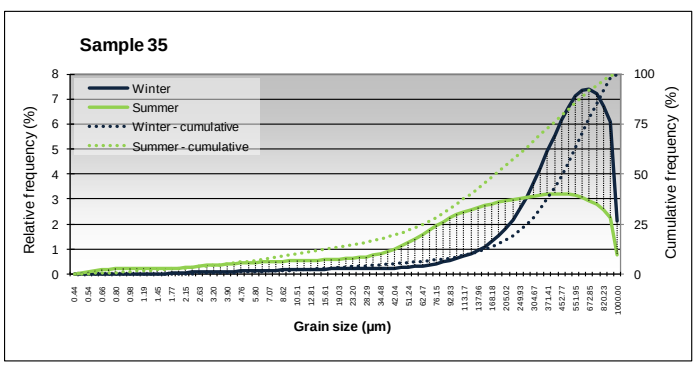
Sample 35
Winter
Summer
Winter - cumulative
Summer - cumulative
Relative frequency (%)
Cumulative frequency (%)
Grain size (µm)

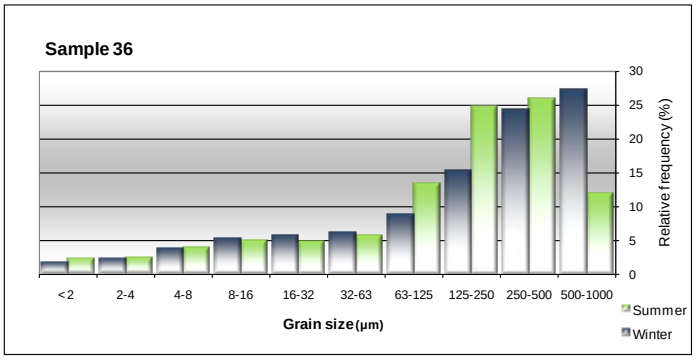
Sample 36
Relative frequency (%)
<2
2-4
4-8
8-16
16-32
32-63
63-125
125-250
250-500
500-1000
Grain size (µm)
Summer
Winter

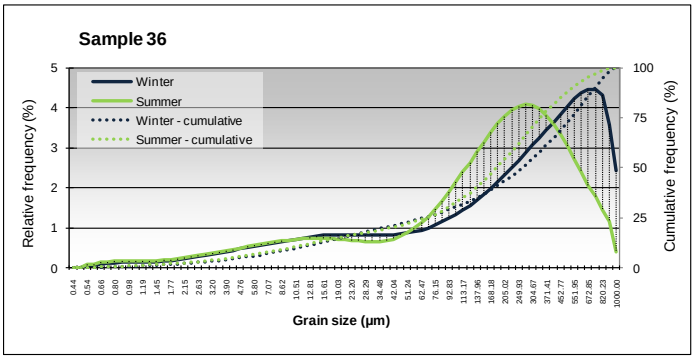
Sample 36
Winter
Summer
Winter - cumulative
Summer - cumulative
Relative frequency (%)
Cumulative frequency (%)
Grain size (µm)

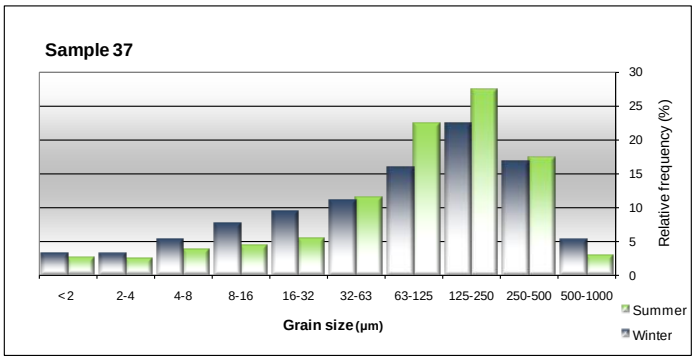
Sample 37
Relative frequency (%)
<2
2-4
4-8
8-16
16-32
32-63
63-125
125-250
250-500
500-1000
Grain size (µm)
Summer
Winter

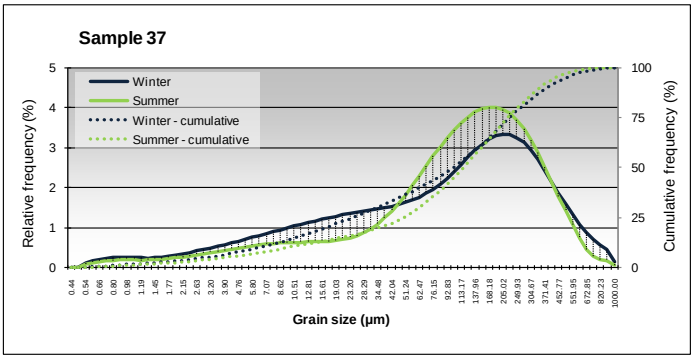
Sample 37
Winter
Summer
Winter - cumulative
Summer - cumulative
Relative frequency (%)
Cumulative frequency (%)
Grain size (µm)

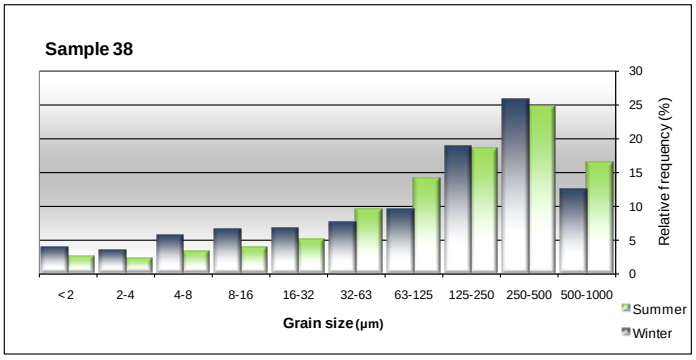
Sample 38
Relative frequency (%)
<2
2-4
4-8
8-16
16-32
32-63
63-125
125-250
250-500
500-1000
Grain size (µm)
Summer
Winter

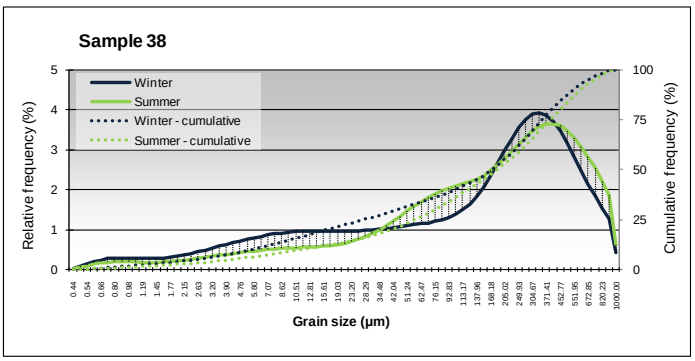
Sample 38
Winter
Summer
Winter - cumulative
Summer - cumulative
Relative frequency (%)
Cumulative frequency (%)
Grain size (µm)

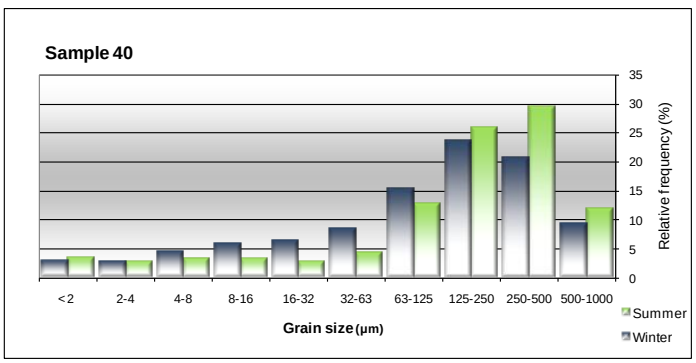
Sample 40
Relative frequency (%)
<2
2-4
4-8
8-16
16-32
32-63
63-125
125-250
250-500
500-1000
Grain size (µm)
Summer
Winter

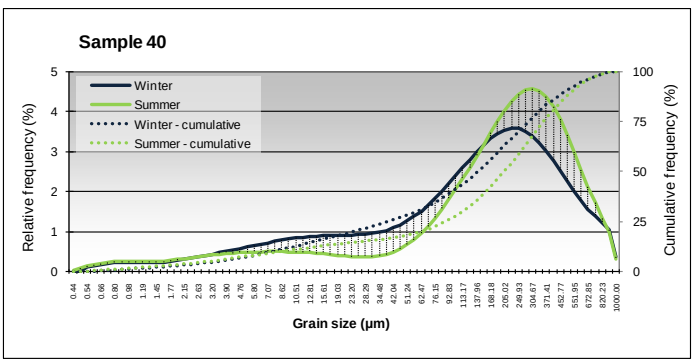
Sample 40
Winter
Summer
Winter - cumulative
Summer - cumulative
Relative frequency (%)
Cumulative frequency (%)
Grain size (µm)

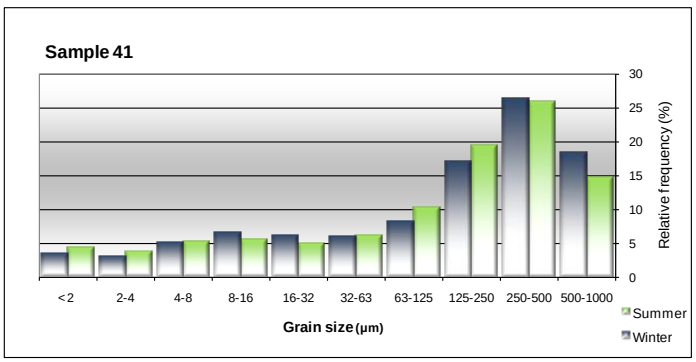
Sample 41
Relative frequency (%)
<2
2-4
4-8
8-16
16-32
32-63
63-125
125-250
250-500
500-1000
Grain size (µm)
Summer
Winter

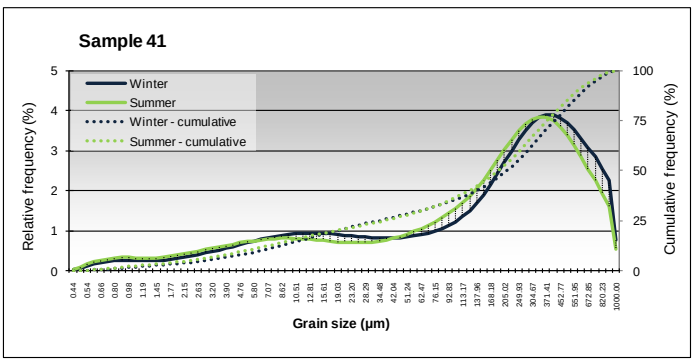
Sample 41
Winter
Summer
Winter - cumulative
Summer - cumulative
Relative frequency (%)
Cumulative frequency (%)
Grain size (µm)

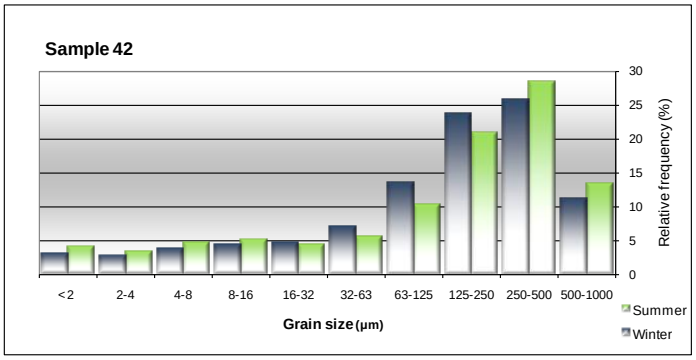
Sample 42
Relative frequency (%)
<2
2-4
4-8
8-16
16-32
32-63
63-125
125-250
250-500
500-1000
Grain size (µm)
Summer
Winter

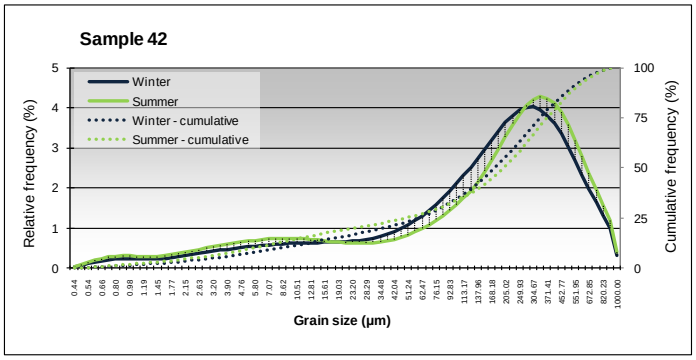
Sample 42
Winter
Summer
Winter - cumulative
Summer - cumulative
Relative frequency (%)
Cumulative frequency (%)
Grain size (µm)

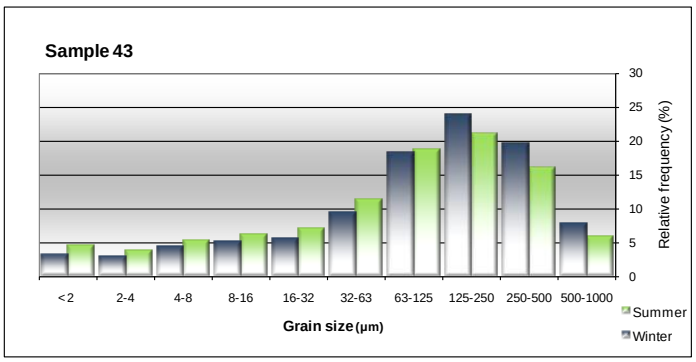
Sample 43
Relative frequency (%)
<2
2-4
4-8
8-16
16-32
32-63
63-125
125-250
250-500
500-1000
Grain size (µm)
Summer
Winter

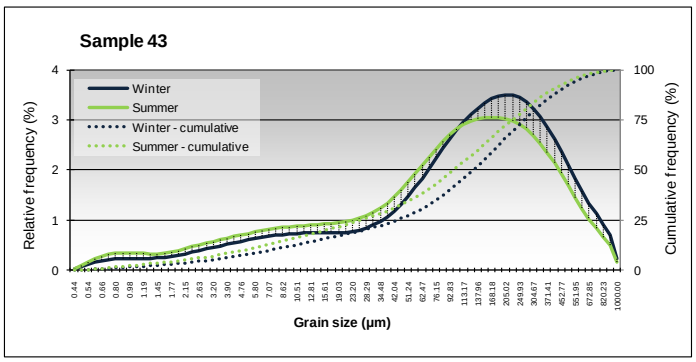
Sample 43
Winter
Summer
Winter - cumulative
Summer - cumulative
Relative frequency (%)
Cumulative frequency (%)
Grain size (µm)

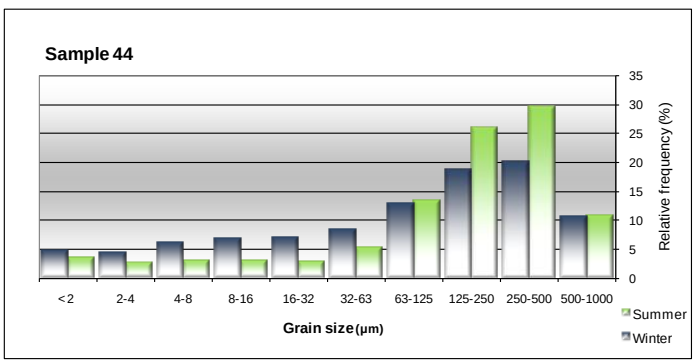
Sample 44
Relative frequency (%)
<2
2-4
4-8
8-16
16-32
32-63
63-125
125-250
250-500
500-1000
Grain size (µm)
Summer
Winter

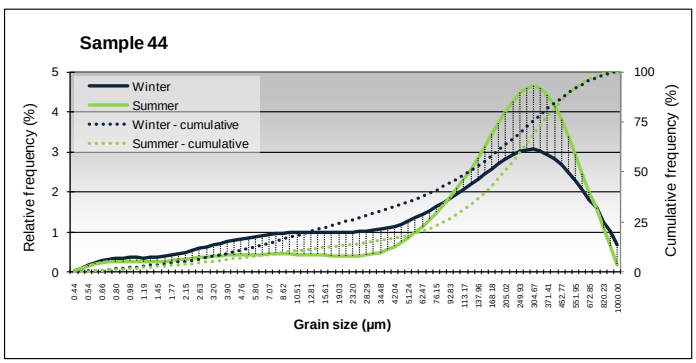
Sample 44
Winter
Summer
Winter - cumulative
Summer - cumulative
Relative frequency (%)
Cumulative frequency (%)
Grain size (µm)

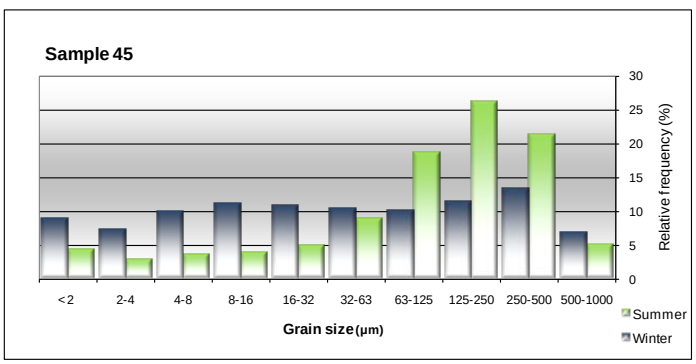
Sample 45
Relative frequency (%)
<2
2-4
4-8
8-16
16-32
32-63
63-125
125-250
250-500
500-1000
Grain size (µm)
Summer
Winter

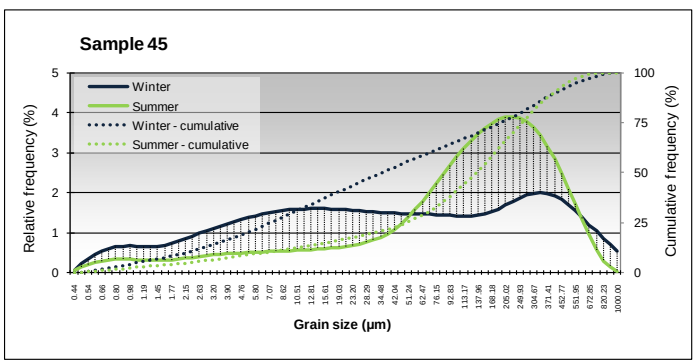
Sample 45
Winter
Summer
Winter - cumulative
Summer - cumulative
Relative frequency (%)
Cumulative frequency (%)
Grain size (µm)

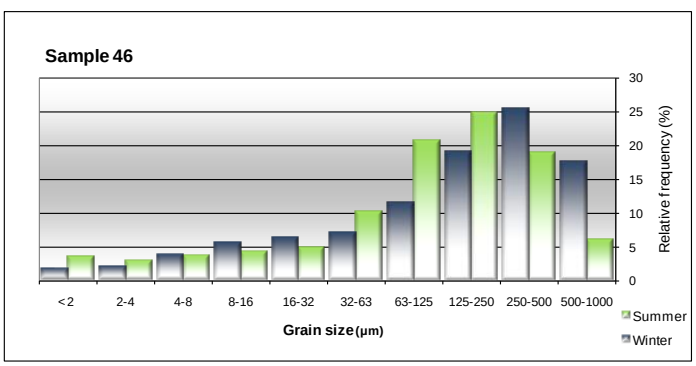
Sample 46
Relative frequency (%)
<2
2-4
4-8
8-16
16-32
32-63
63-125
125-250
250-500
500-1000
Grain size (µm)
Summer
Winter

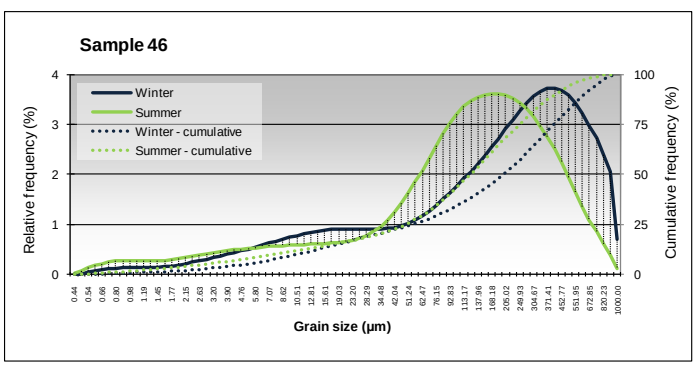
Sample 46
Winter
Summer
Winter - cumulative
Summer - cumulative
Relative frequency (%)
Cumulative frequency (%)
Grain size (µm)

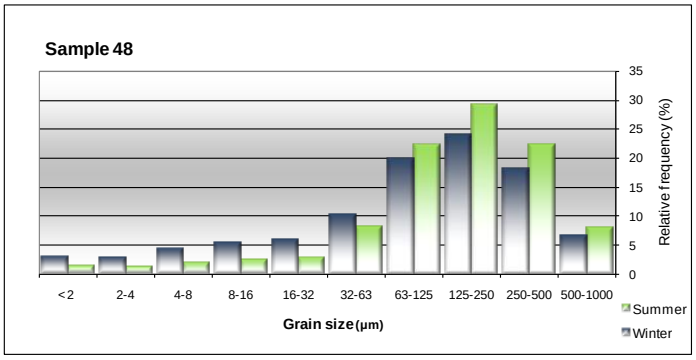
Sample 48
Relative frequency (%)
Grain size (µm)
<2
2-4
4-8
8-16
16-32
32-63
63-125
125-250
250-500
500-1000
Summer
Winter

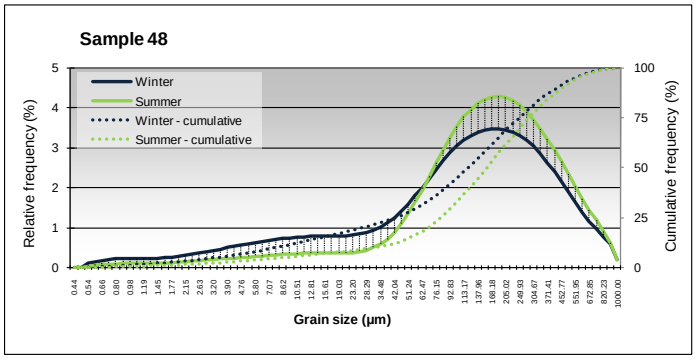
Sample 48
Winter
Summer
Winter - cumulative
Summer - cumulative
Relative frequency (%)
Cumulative frequency (%)
Grain size (µm)

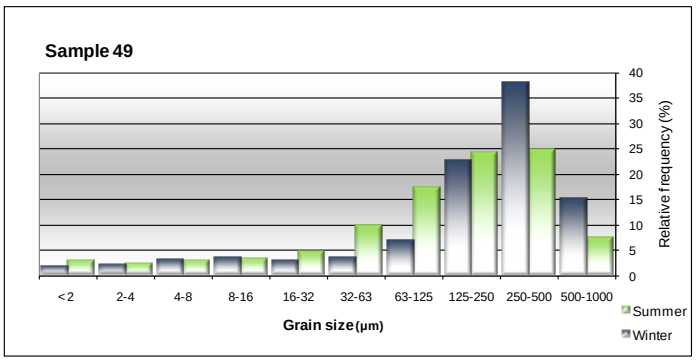
Sample 49
Relative frequency (%)
Grain size (µm)
<2
2-4
4-8
8-16
16-32
32-63
63-125
125-250
250-500
500-1000
Summer
Winter

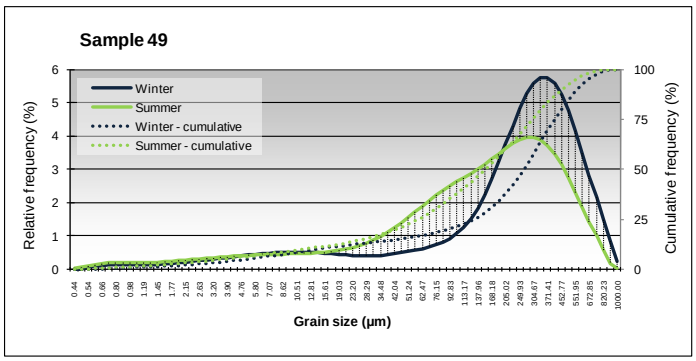
Sample 49
Winter
Summer
Winter - cumulative
Summer - cumulative
Relative frequency (%)
Cumulative frequency (%)
Grain size (µm)

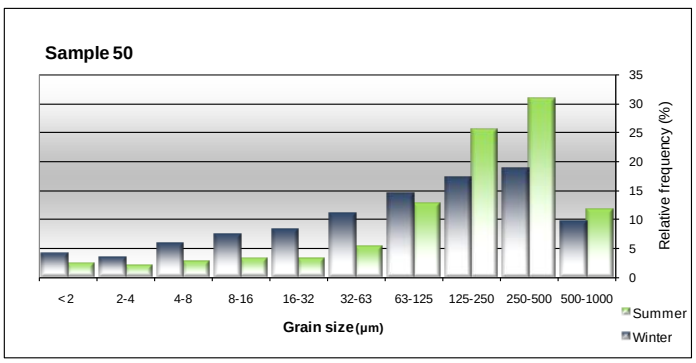
Sample 50
Relative frequency (%)
Grain size (µm)
<2
2-4
4-8
8-16
16-32
32-63
63-125
125-250
250-500
500-1000
Summer
Winter

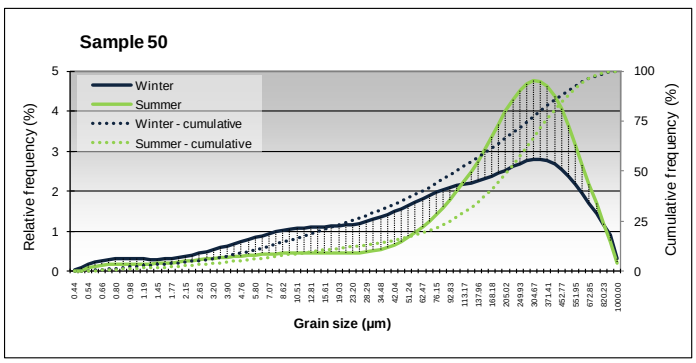
Sample 50
Winter
Summer
Winter - cumulative
Summer - cumulative
Relative frequency (%)
Cumulative frequency (%)
Grain size (µm)

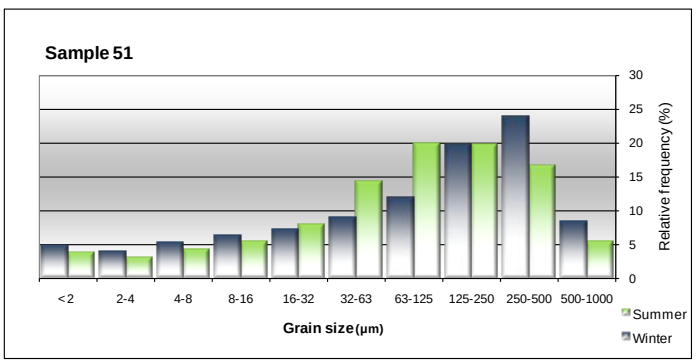
Sample 51
Relative frequency (%)
Grain size (µm)
<2
2-4
4-8
8-16
16-32
32-63
63-125
125-250
250-500
500-1000
Summer
Winter

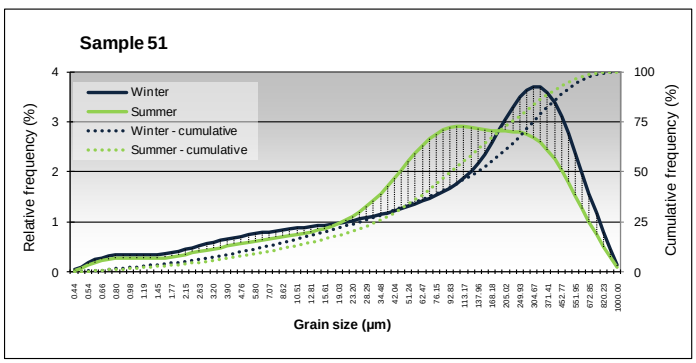
Sample 51
Winter
Summer
Winter - cumulative
Summer - cumulative
Relative frequency (%)
Cumulative frequency (%)
Grain size (µm)

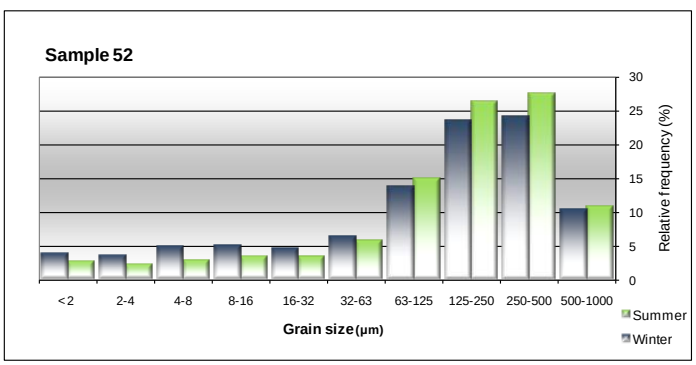
Sample 52
Relative frequency (%)
Grain size (µm)
<2
2-4
4-8
8-16
16-32
32-63
63-125
125-250
250-500
500-1000
Summer
Winter

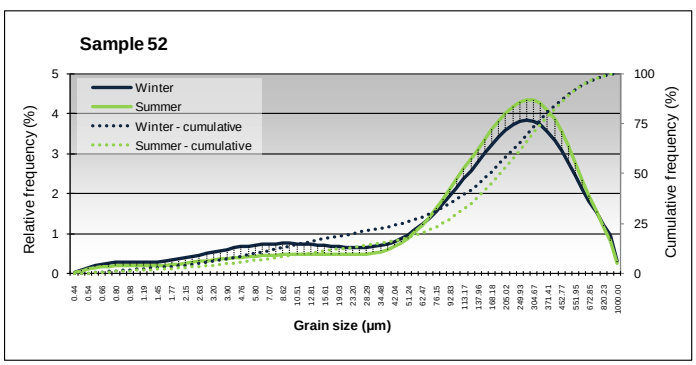
Sample 52
Winter
Summer
Winter - cumulative
Summer - cumulative
Relative frequency (%)
Cumulative frequency (%)
Grain size (µm)

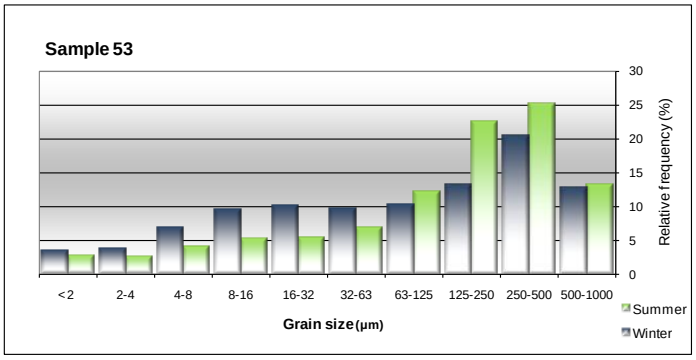
Sample 53
Relative frequency (%)
<2
2-4
4-8
8-16
16-32
32-63
63-125
125-250
250-500
500-1000
Grain size (µm)
Summer
Winter

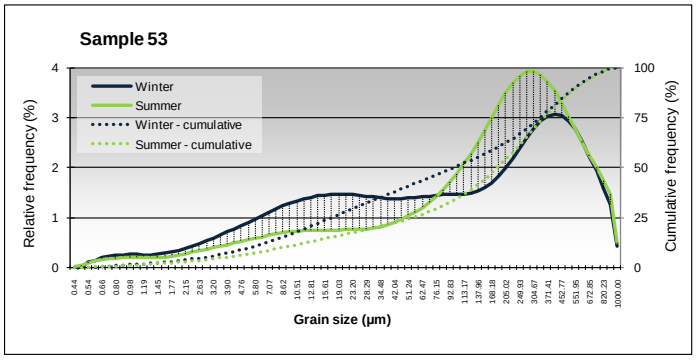
Sample 53
Winter
Summer
Winter - cumulative
Summer - cumulative
Relative frequency (%)
Cumulative frequency (%)
Grain size (µm)

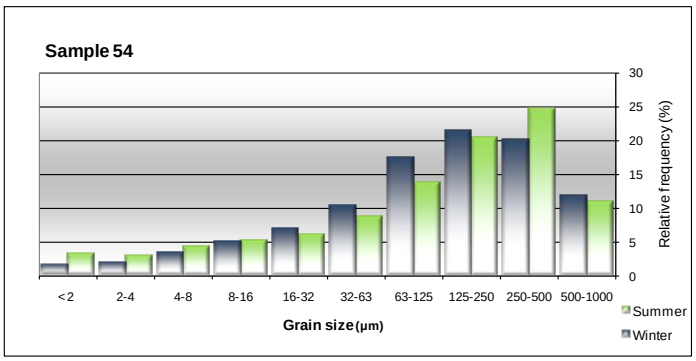
Sample 54
Relative frequency (%)
<2
2-4
4-8
8-16
16-32
32-63
63-125
125-250
250-500
500-1000
Grain size (µm)
Summer
Winter

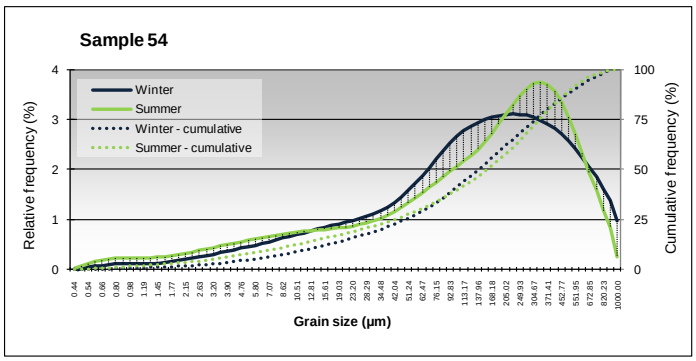
Sample 54
Winter
Summer
Winter - cumulative
Summer - cumulative
Relative frequency (%)
Cumulative frequency (%)
Grain size (µm)

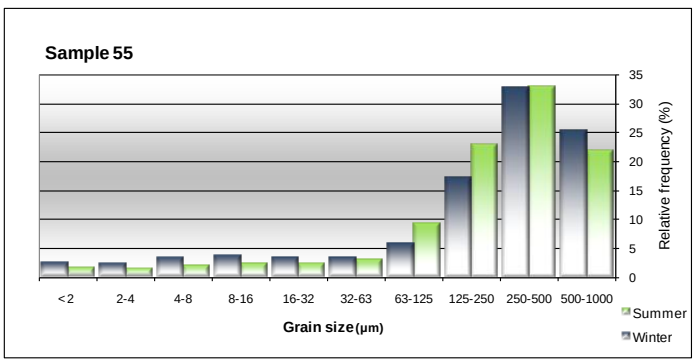
Sample 55
Relative frequency (%)
<2
2-4
4-8
8-16
16-32
32-63
63-125
125-250
250-500
500-1000
Grain size (µm)
Summer
Winter

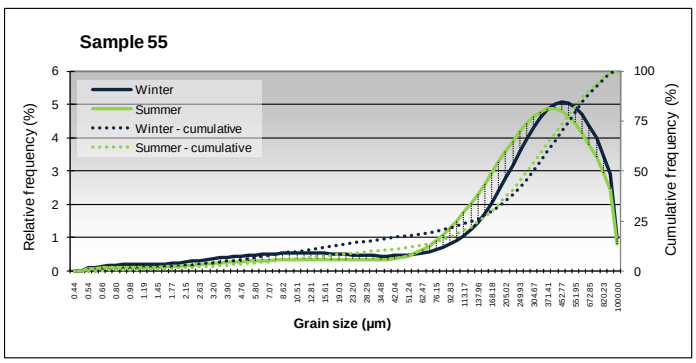
Sample 55
Winter
Summer
Winter - cumulative
Summer - cumulative
Relative frequency (%)
Cumulative frequency (%)
Grain size (µm)

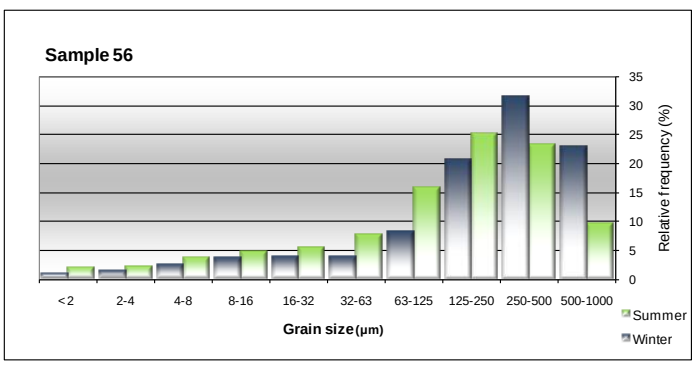
Sample 56
Relative frequency (%)
<2
2-4
4-8
8-16
16-32
32-63
63-125
125-250
250-500
500-1000
Grain size (µm)
Summer
Winter

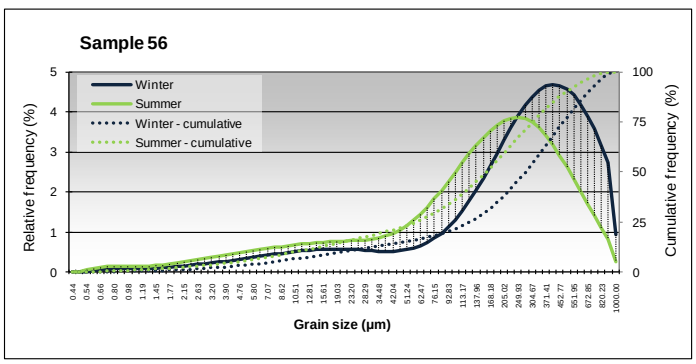
Sample 56
Winter
Summer
Winter - cumulative
Summer - cumulative
Relative frequency (%)
Cumulative frequency (%)
Grain size (µm)

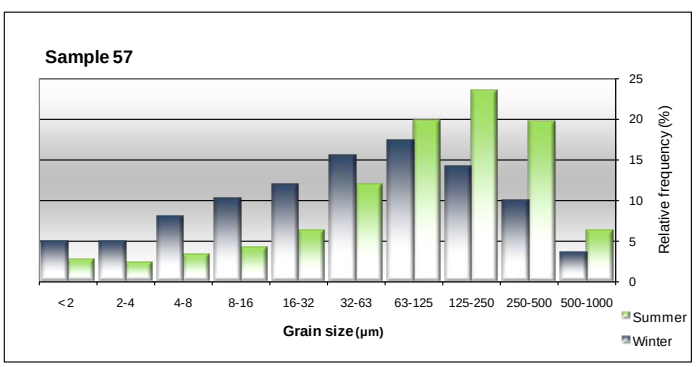
Sample 57
Relative frequency (%)
<2
2-4
4-8
8-16
16-32
32-63
63-125
125-250
250-500
500-1000
Grain size (µm)
Summer
Winter

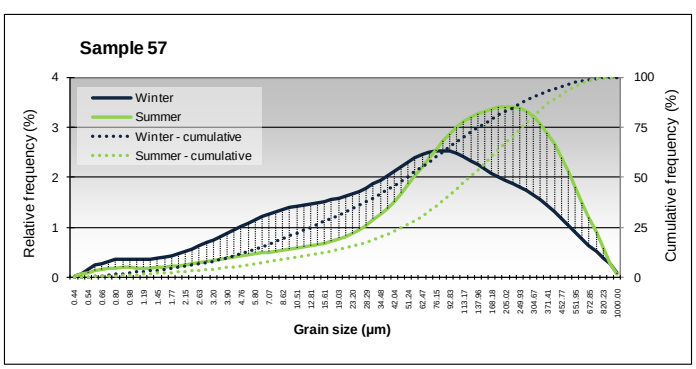
Sample 57
Winter
Summer
Winter - cumulative
Summer - cumulative
Relative frequency (%)
Cumulative frequency (%)
Grain size (µm)

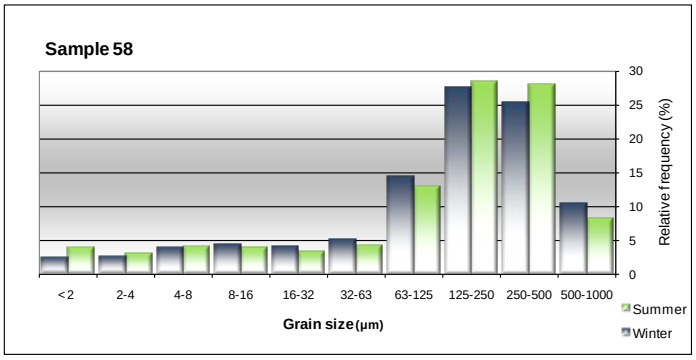
Sample 58
Relative frequency (%)
<2
2-4
4-8
8-16
16-32
32-63
63-125
125-250
250-500
500-1000
Grain size (µm)
Summer
Winter

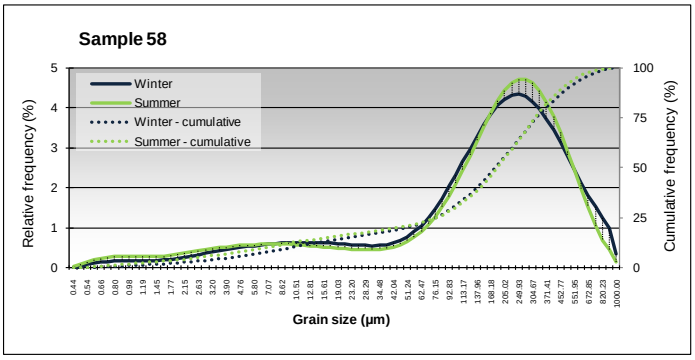
Sample 58
Winter
Summer
Winter - cumulative
Summer - cumulative
Relative frequency (%)
Cumulative frequency (%)
Grain size (µm)

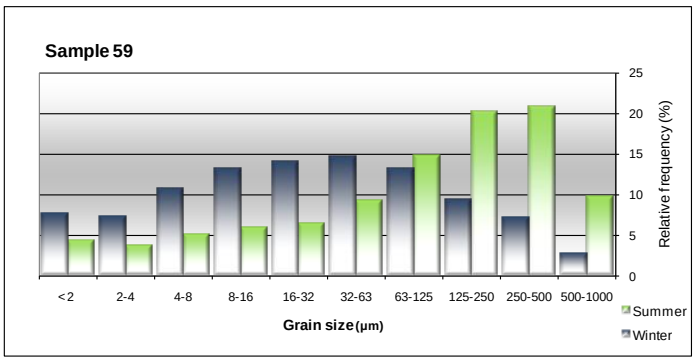
Sample 59
Relative frequency (%)
<2
2-4
4-8
8-16
16-32
32-63
63-125
125-250
250-500
500-1000
Grain size (µm)
Summer
Winter

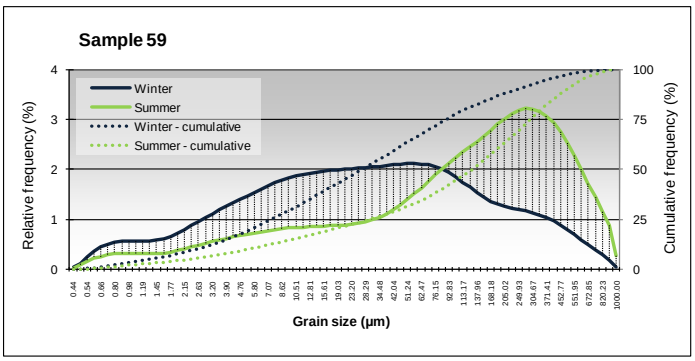
Sample 59
Winter
Summer
Winter - cumulative
Summer - cumulative
Relative frequency (%)
Cumulative frequency (%)
Grain size (µm)

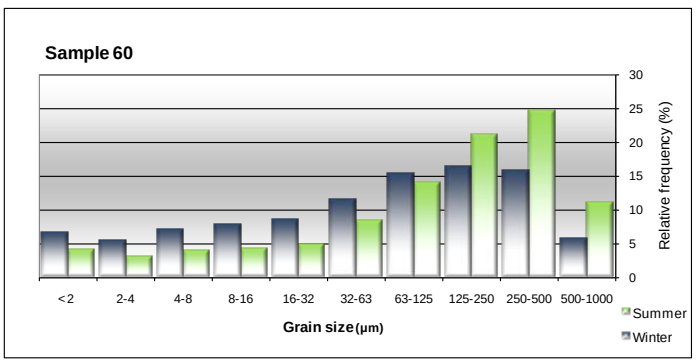
Sample 60
Relative frequency (%)
<2
2-4
4-8
8-16
16-32
32-63
63-125
125-250
250-500
500-1000
Grain size (µm)
Summer
Winter

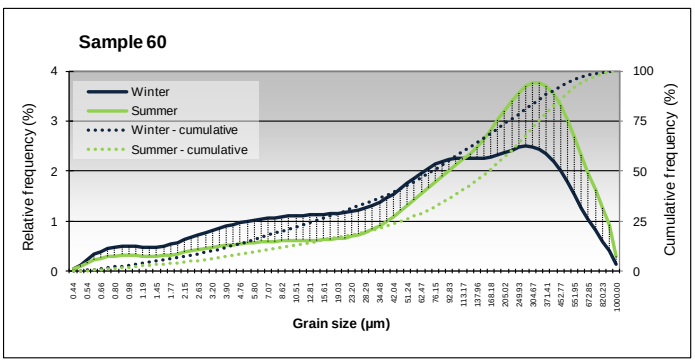
Sample 60
Winter
Summer
Winter - cumulative
Summer - cumulative
Relative frequency (%)
Cumulative frequency (%)
Grain size (µm)

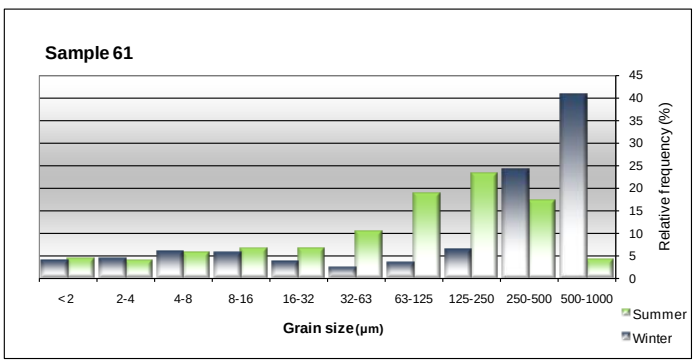
Sample 61
Relative frequency (%)
<2
2-4
4-8
8-16
16-32
32-63
63-125
125-250
250-500
500-1000
Grain size (µm)
Summer
Winter

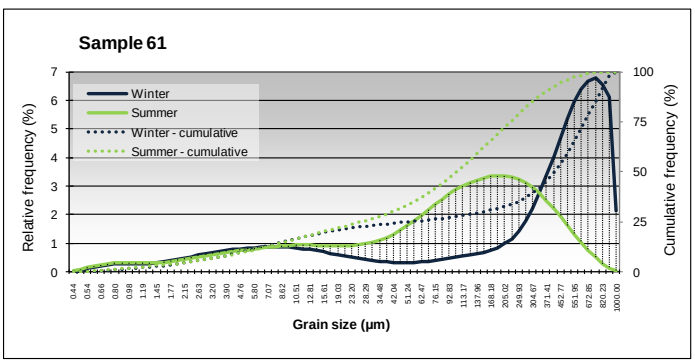
Sample 61
Winter
Summer
Winter - cumulative
Summer - cumulative
Relative frequency (%)
Cumulative frequency (%)
Grain size (µm)

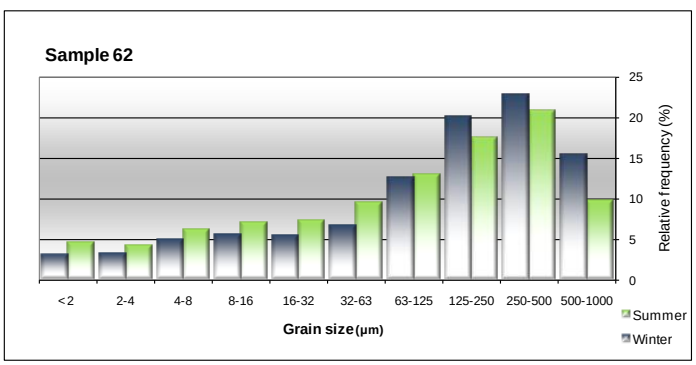
Sample 62
Relative frequency (%)
<2
2-4
4-8
8-16
16-32
32-63
63-125
125-250
250-500
500-1000
Grain size (µm)
Summer
Winter

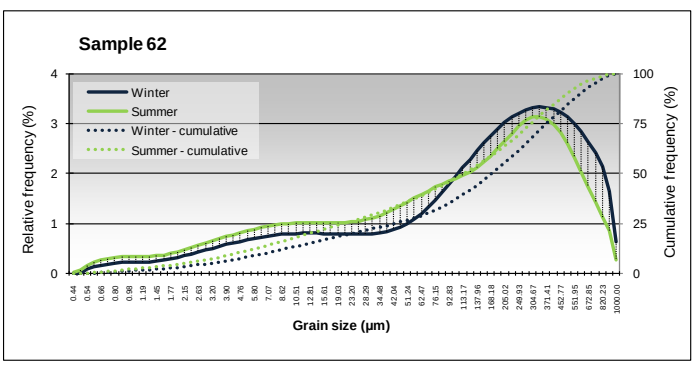
Sample 62
Winter
Summer
Winter - cumulative
Summer - cumulative
Relative frequency (%)
Cumulative frequency (%)
Grain size (µm)

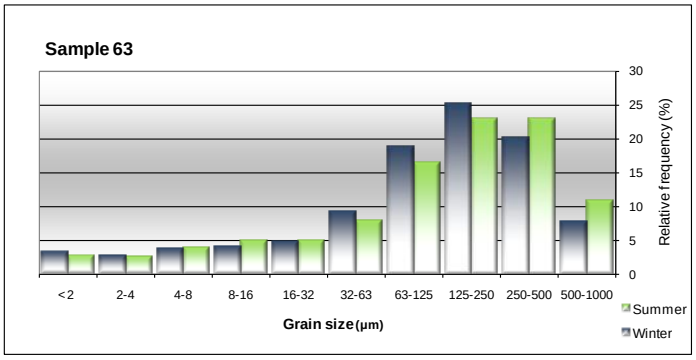
Sample 63
Relative frequency (%)
<2
2-4
4-8
8-16
16-32
32-63
63-125
125-250
250-500
500-1000
Grain size (µm)
Summer
Winter

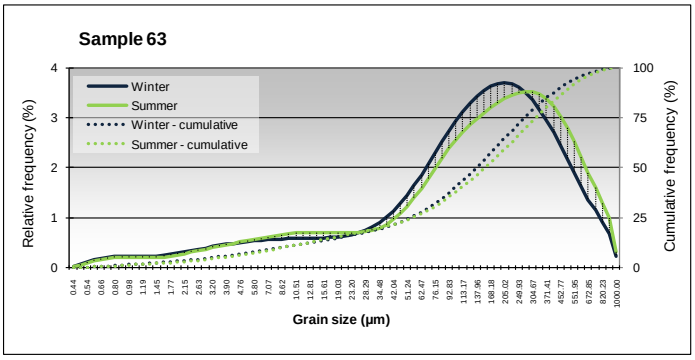
Sample 63
Winter
Summer
Winter - cumulative
Summer - cumulative
Relative frequency (%)
Cumulative frequency (%)
Grain size (µm)

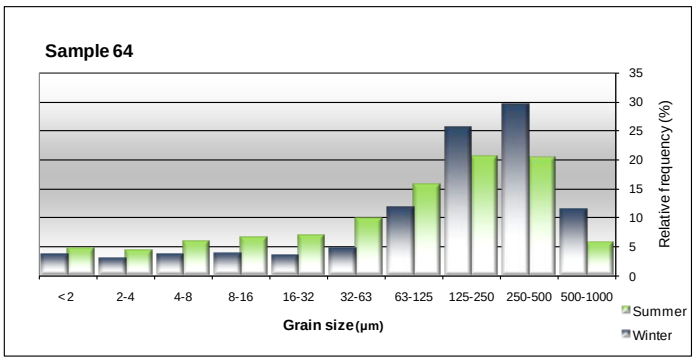
Sample 64
Relative frequency (%)
<2
2-4
4-8
8-16
16-32
32-63
63-125
125-250
250-500
500-1000
Grain size (µm)
Summer
Winter

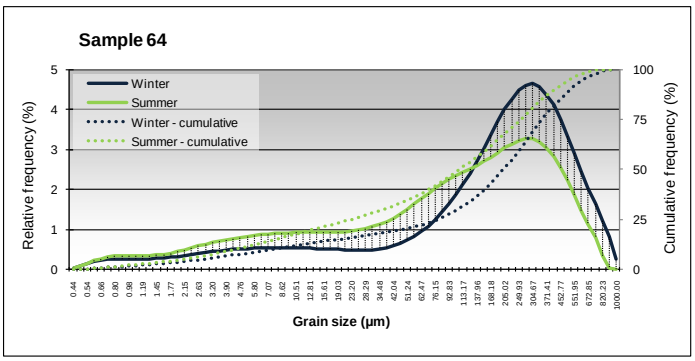
Sample 64
Winter
Summer
Winter - cumulative
Summer - cumulative
Relative frequency (%)
Cumulative frequency (%)
Grain size (µm)

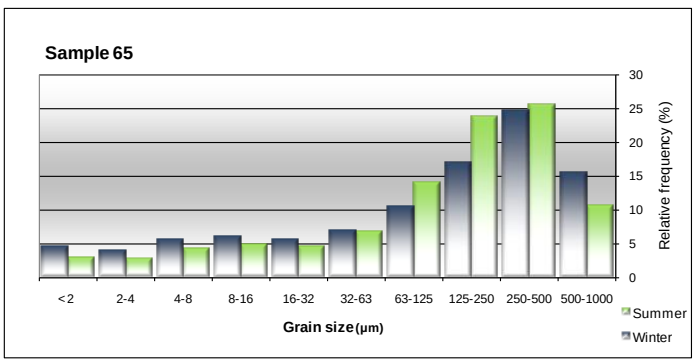
Sample 65
Relative frequency (%)
<2
2-4
4-8
8-16
16-32
32-63
63-125
125-250
250-500
500-1000
Grain size (µm)
Summer
Winter

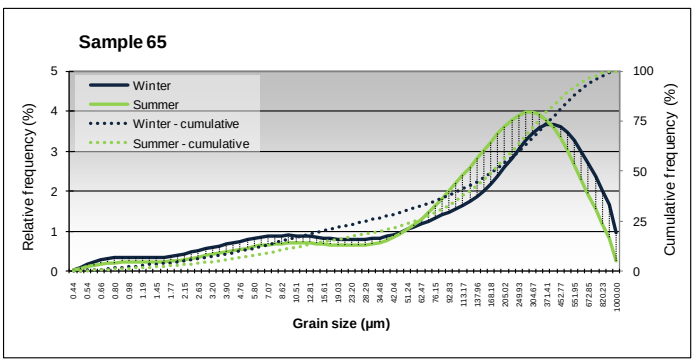
Sample 65
Winter
Summer
Winter - cumulative
Summer - cumulative
Relative frequency (%)
Cumulative frequency (%)
Grain size (µm)

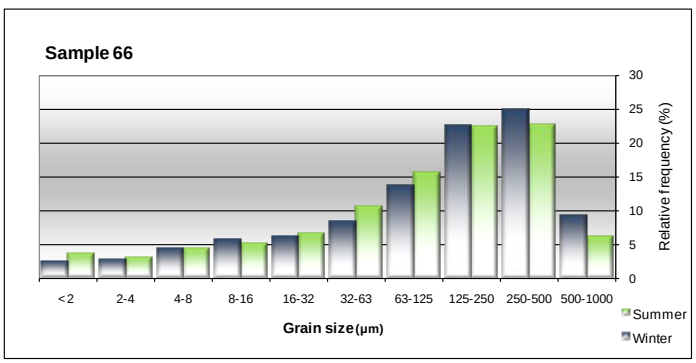
Sample 66
Relative frequency (%)
<2
2-4
4-8
8-16
16-32
32-63
63-125
125-250
250-500
500-1000
Grain size (µm)
Summer
Winter

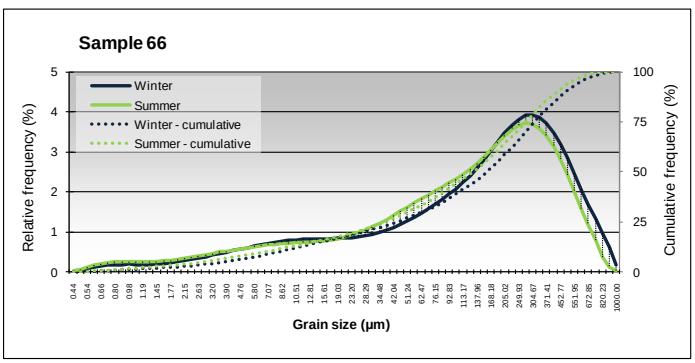
Sample 66
Winter
Summer
Winter - cumulative
Summer - cumulative
Relative frequency (%)
Cumulative frequency (%)
Grain size (µm)

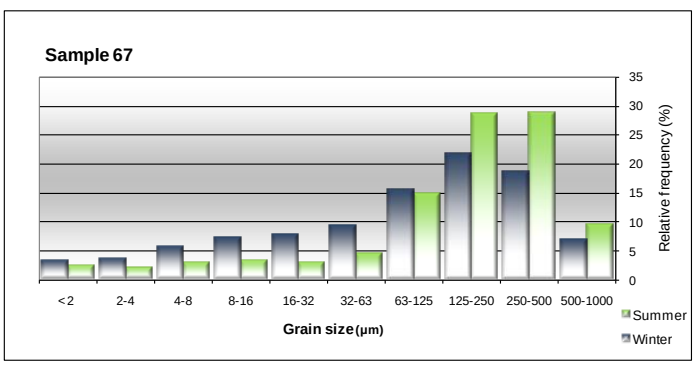
Sample 67
Relative frequency (%)
<2
2-4
4-8
8-16
16-32
32-63
63-125
125-250
250-500
500-1000
Grain size (µm)
Summer
Winter

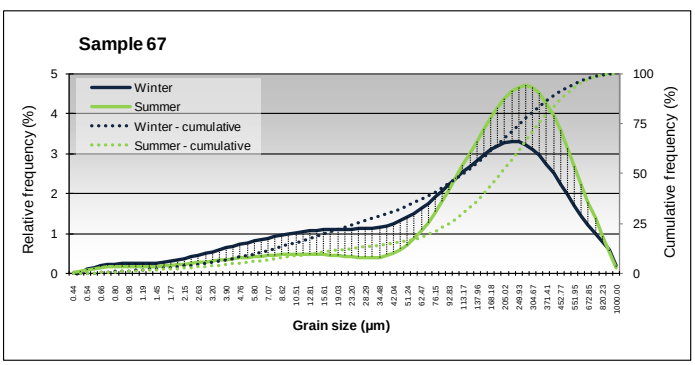
Sample 67
Winter
Summer
Winter - cumulative
Summer - cumulative
Relative frequency (%)
Cumulative frequency (%)
Grain size (µm)

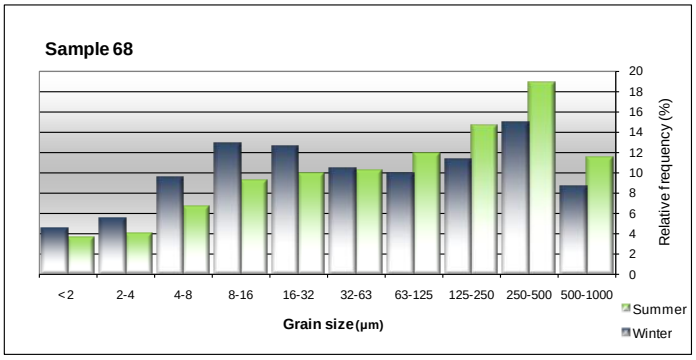
Sample 68
Relative frequency (%)
<2
2-4
4-8
8-16
16-32
32-63
63-125
125-250
250-500
500-1000
Grain size (µm)
Summer
Winter

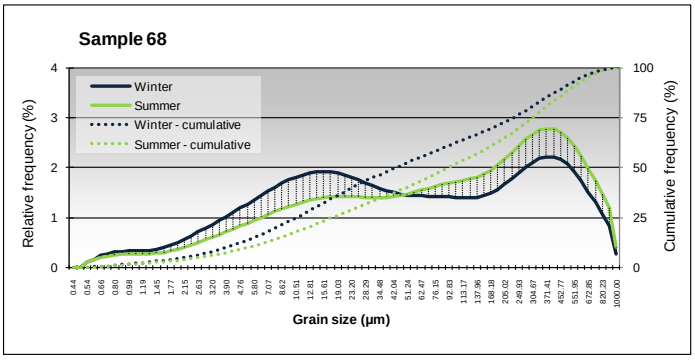
Sample 68
Winter
Summer
Winter - cumulative
Summer - cumulative
Relative frequency (%)
Cumulative frequency (%)
Grain size (µm)

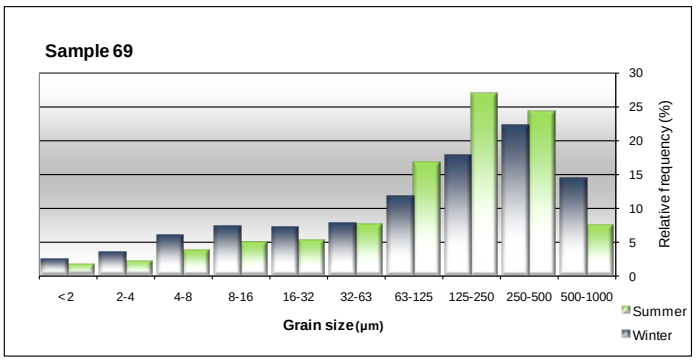
Sample 69
Relative frequency (%)
<2
2-4
4-8
8-16
16-32
32-63
63-125
125-250
250-500
500-1000
Grain size (µm)
Summer
Winter

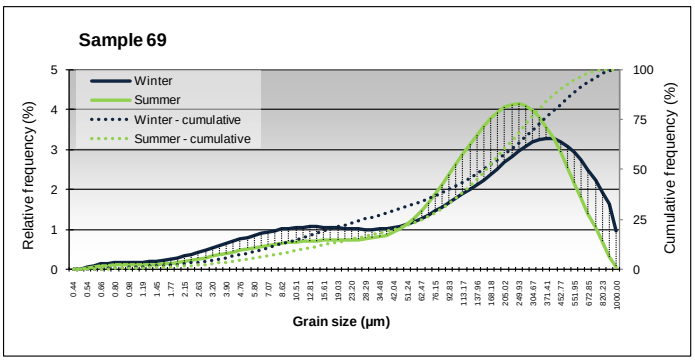
Sample 69
Winter
Summer
Winter - cumulative
Summer - cumulative
Relative frequency (%)
Cumulative frequency (%)
Grain size (µm)

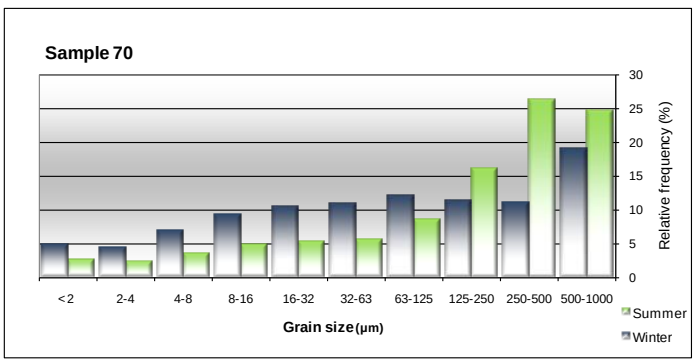
Sample 70
Relative frequency (%)
<2
2-4
4-8
8-16
16-32
32-63
63-125
125-250
250-500
500-1000
Grain size (µm)
Summer
Winter

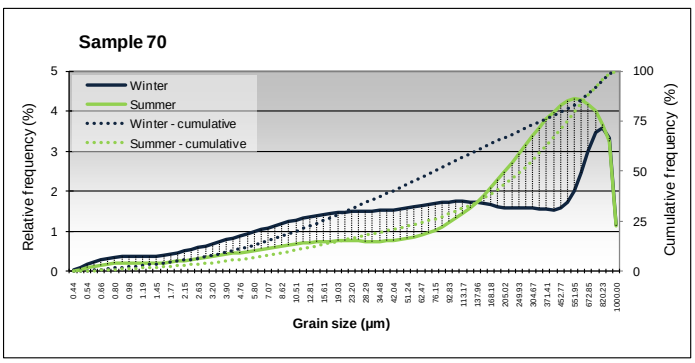
Sample 70
Winter
Summer
Winter - cumulative
Summer - cumulative
Relative frequency (%)
Cumulative frequency (%)
Grain size (µm)

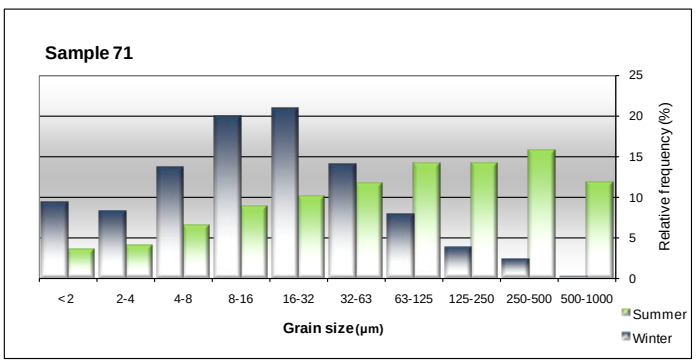
Sample 71
Relative frequency (%)
<2
2-4
4-8
8-16
16-32
32-63
63-125
125-250
250-500
500-1000
Grain size (µm)
Summer
Winter

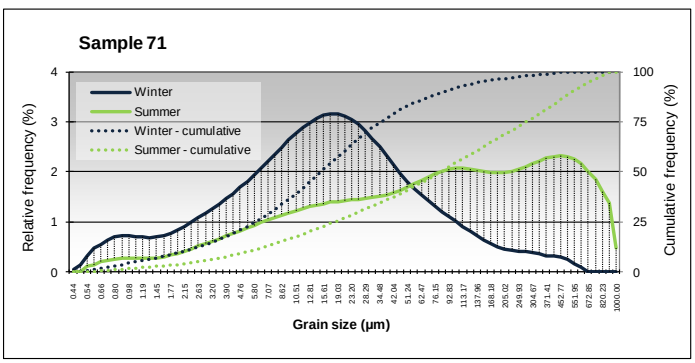
Sample 71
Winter
Summer
Winter - cumulative
Summer - cumulative
Relative frequency (%)
Cumulative frequency (%)
Grain size (µm)

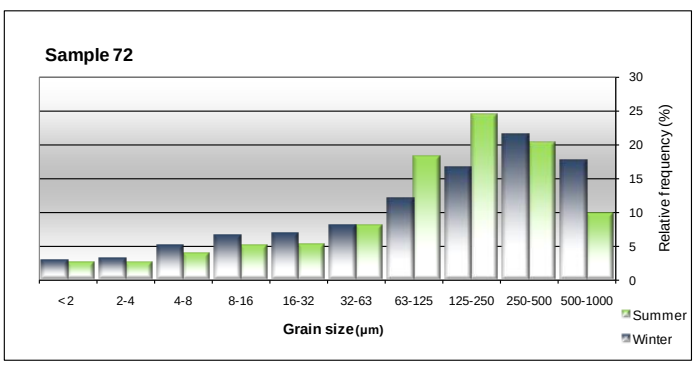
Sample 72
Relative frequency (%)
<2
2-4
4-8
8-16
16-32
32-63
63-125
125-250
250-500
500-1000
Grain size (µm)
Summer
Winter

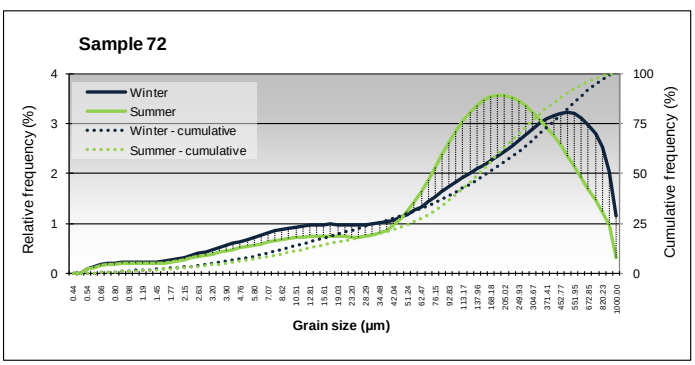
Sample 72
Winter
Summer
Winter - cumulative
Summer - cumulative
Relative frequency (%)
Cumulative frequency (%)
Grain size (µm)

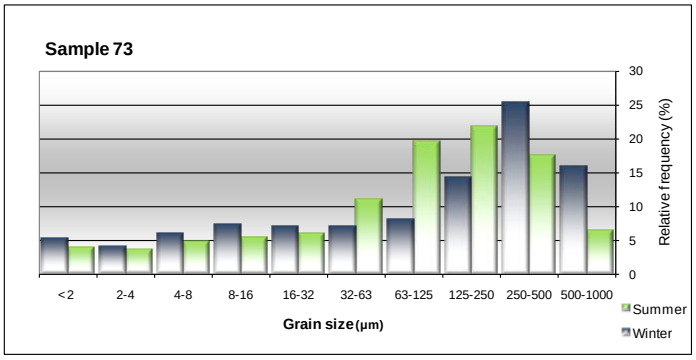
Sample 73
Relative frequency (%)
Grain size (µm)
<2
2-4
4-8
8-16
16-32
32-63
63-125
125-250
250-500
500-1000
Summer
Winter

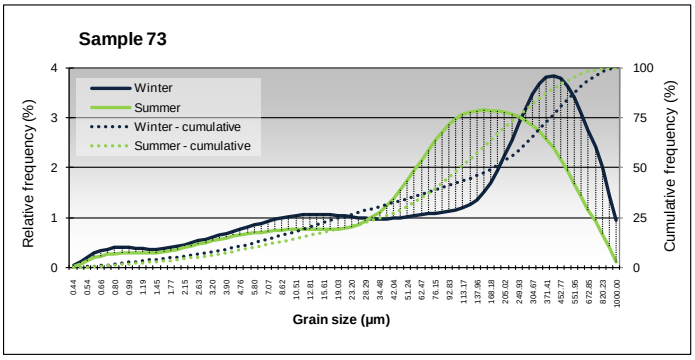
Sample 73
Winter
Summer
Winter - cumulative
Summer - cumulative
Relative frequency (%)
Cumulative frequency (%)
Grain size (µm)

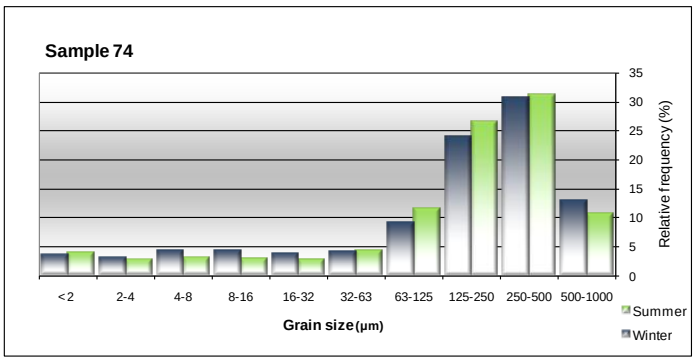
Sample 74
Relative frequency (%)
Grain size (µm)
<2
2-4
4-8
8-16
16-32
32-63
63-125
125-250
250-500
500-1000
Summer
Winter

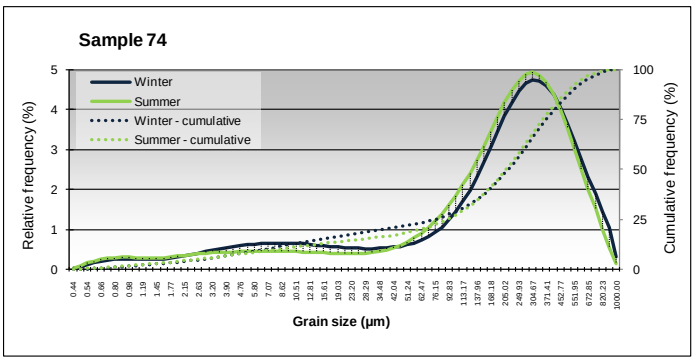
Sample 74
Winter
Summer
Winter - cumulative
Summer - cumulative
Relative frequency (%)
Cumulative frequency (%)
Grain size (µm)

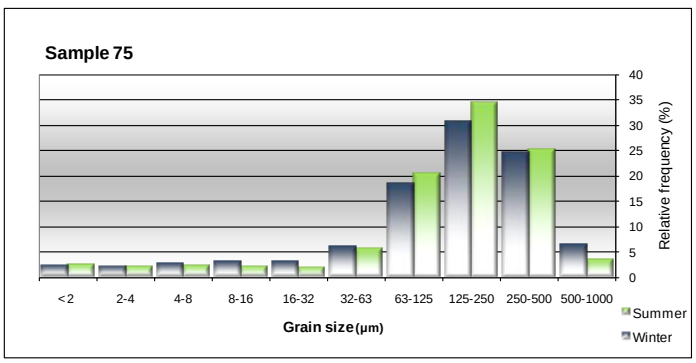
Sample 75
Relative frequency (%)
Grain size (µm)
<2
2-4
4-8
8-16
16-32
32-63
63-125
125-250
250-500
500-1000
Summer
Winter

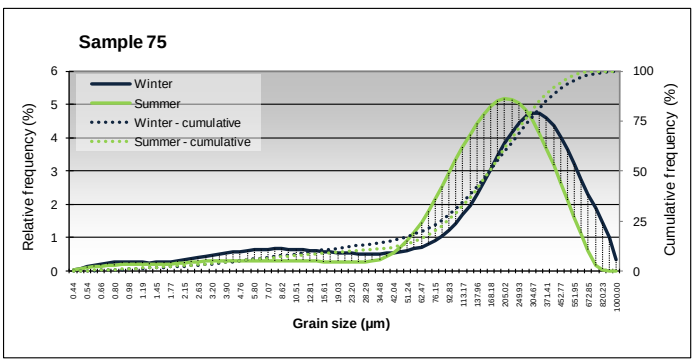
Sample 75
Winter
Summer
Winter - cumulative
Summer - cumulative
Relative frequency (%)
Cumulative frequency (%)
Grain size (µm)

Table 95: RDS-summer grain size analysis (72 samples).

| | Relative Frequencies | | | | | | | | | | | | | | | | |
|---|---|---|---|---|---|---|---|---|---|---|---|---|---|---|---|---|---|
| | 1S | 2S | 3S | 4S | 5S | 6S | 7S | 8S | 9S | 10S | 11S | 12S | 13S | 14S | 15S | 17S | 18S |
| 500-1000 µm | 6.55 | 35.71 | 7.90 | 13.13 | 15.23 | 9.53 | 7.75 | 9.65 | 1.70 | 7.99 | 8.94 | 7.16 | 12.00 | 11.54 | 9.85 | 10.54 | 8.60 |
| 250-500 µm | 21.21 | 28.92 | 19.24 | 17.88 | 18.36 | 20.25 | 22.26 | 26.04 | 10.58 | 17.37 | 22.47 | 30.47 | 17.90 | 19.22 | 34.33 | 27.44 | 25.80 |
| 125-250 µm | 25.87 | 10.20 | 23.08 | 17.02 | 16.13 | 21.76 | 24.35 | 24.35 | 14.08 | 14.81 | 18.19 | 28.90 | 15.26 | 20.44 | 28.64 | 27.10 | 24.14 |
| 63-125 µm | 17.65 | 6.54 | 18.60 | 14.37 | 11.90 | 16.92 | 18.11 | 14.70 | 16.31 | 12.50 | 11.36 | 13.89 | 12.69 | 15.74 | 11.52 | 15.52 | 14.46 |
| 32-63 µm | 8.51 | 4.98 | 9.92 | 9.34 | 7.57 | 9.04 | 8.85 | 6.59 | 13.64 | 9.87 | 8.83 | 5.35 | 9.35 | 9.08 | 3.77 | 5.41 | 7.34 |
| 16-32 µm | 5.40 | 4.70 | 5.91 | 6.63 | 7.04 | 6.16 | 4.55 | 3.90 | 10.89 | 8.56 | 8.09 | 2.84 | 7.92 | 5.50 | 1.99 | 3.04 | 4.49 |
| 8-16 µm | 4.59 | 3.85 | 5.32 | 6.06 | 7.47 | 5.98 | 4.18 | 4.04 | 10.25 | 8.30 | 7.71 | 2.70 | 7.27 | 4.89 | 2.10 | 3.35 | 4.30 |
| 4-8 µm | 3.95 | 2.61 | 4.28 | 5.65 | 6.60 | 4.65 | 3.73 | 3.85 | 8.91 | 7.21 | 6.19 | 2.74 | 6.37 | 4.65 | 2.29 | 3.00 | 4.00 |
| 2-4 µm | 2.93 | 1.47 | 2.81 | 4.50 | 4.60 | 2.86 | 2.72 | 3.03 | 6.41 | 5.64 | 4.08 | 2.41 | 4.97 | 3.85 | 2.14 | 2.16 | 3.05 |
| < 2 µm | 3.35 | 1.02 | 2.96 | 5.42 | 5.12 | 2.85 | 3.50 | 3.86 | 7.23 | 7.75 | 4.15 | 3.54 | 6.28 | 5.11 | 3.37 | 2.46 | 3.82 |
| Sum | 100.00 | 100.00 | 100.00 | 100.00 | 100.00 | 100.00 | 100.00 | 100.00 | 100.00 | 100.00 | 100.00 | 100.00 | 100.00 | 100.00 | 100.00 | 100.00 | 100.00 |

| | Relative Frequencies | | | | | | | | | | | | | | | | |
|---|---|---|---|---|---|---|---|---|---|---|---|---|---|---|---|---|---|
| | 19S | 20S | 21S | 22S | 23S | 24S | 25S | 26S | 27S | 28S | 29S | 30S | 31S | 32S | 33S | 34S | 35S |
| 500-1000 µm | 11.61 | 11.69 | 6.91 | 3.80 | 5.79 | 7.81 | 11.07 | 10.51 | 19.21 | 9.79 | 9.87 | 2.31 | 7.16 | 4.92 | 5.75 | 9.75 | 17.57 |
| 250-500 µm | 22.14 | 29.05 | 24.51 | 21.50 | 24.93 | 22.43 | 22.91 | 26.62 | 26.36 | 21.42 | 35.62 | 19.20 | 19.93 | 16.04 | 20.04 | 26.49 | 22.13 |
| 125-250 µm | 18.92 | 22.56 | 23.96 | 25.93 | 25.38 | 25.42 | 21.47 | 29.01 | 23.09 | 23.53 | 31.45 | 33.61 | 23.17 | 15.51 | 21.79 | 24.90 | 20.06 |
| 63-125 µm | 12.66 | 12.14 | 14.34 | 16.46 | 14.71 | 17.94 | 13.32 | 14.58 | 13.11 | 18.67 | 9.92 | 22.95 | 16.54 | 13.75 | 13.56 | 13.92 | 15.44 |
| 32-63 µm | 7.94 | 6.35 | 7.29 | 9.40 | 6.42 | 9.04 | 7.38 | 4.93 | 5.13 | 9.04 | 1.99 | 7.82 | 8.55 | 13.62 | 8.58 | 6.41 | 8.05 |
| 16-32 µm | 6.70 | 4.47 | 5.00 | 5.99 | 3.83 | 4.90 | 5.28 | 3.68 | 2.80 | 3.89 | 1.33 | 2.76 | 6.17 | 11.88 | 7.17 | 3.99 | 4.53 |
| 8-16 µm | 6.44 | 4.40 | 5.32 | 5.18 | 4.36 | 3.78 | 4.84 | 3.62 | 2.62 | 3.39 | 1.71 | 2.43 | 6.26 | 9.48 | 7.18 | 3.63 | 3.81 |
| 4-8 µm | 5.38 | 3.70 | 4.99 | 4.54 | 4.69 | 3.17 | 4.58 | 2.97 | 2.50 | 3.39 | 2.26 | 2.81 | 5.28 | 6.74 | 6.40 | 3.51 | 3.26 |
| 2-4 µm | 3.74 | 2.57 | 3.53 | 3.26 | 4.08 | 2.45 | 3.85 | 2.00 | 2.15 | 2.95 | 2.28 | 2.59 | 3.49 | 4.13 | 4.41 | 3.02 | 2.37 |
| < 2 µm | 4.48 | 3.06 | 4.15 | 3.93 | 5.81 | 3.05 | 5.31 | 2.09 | 3.05 | 3.93 | 3.56 | 3.52 | 3.45 | 3.95 | 5.13 | 4.38 | 2.79 |
| Sum | 100.00 | 100.00 | 100.00 | 100.00 | 100.00 | 100.00 | 100.00 | 100.00 | 100.00 | 100.00 | 100.00 | 100.00 | 100.00 | 100.00 | 100.00 | 100.00 | 100.00 |

| | Relative Frequencies | | | | | | | | | | | | | | | | |
|---|---|---|---|---|---|---|---|---|---|---|---|---|---|---|---|---|---|
| | 36S | 37S | 38S | 40S | 41S | 42S | 43S | 44S | 45S | 46S | 48S | 49S | 50S | 51S | 52S | 53S | 54S |
| 500-1000 µm | 11.92 | 2.97 | 16.42 | 12.00 | 14.80 | 13.43 | 5.85 | 10.85 | 4.98 | 6.06 | 8.09 | 7.38 | 11.81 | 5.39 | 10.87 | 13.22 | 10.82 |
| 250-500 µm | 25.85 | 17.38 | 24.71 | 29.34 | 25.85 | 28.33 | 16.12 | 29.60 | 21.45 | 18.82 | 22.20 | 24.84 | 30.88 | 16.56 | 27.60 | 25.30 | 24.69 |
| 125-250 µm | 24.78 | 27.35 | 18.55 | 25.94 | 19.33 | 20.86 | 21.06 | 25.89 | 26.26 | 24.89 | 29.32 | 24.23 | 25.60 | 19.74 | 26.37 | 22.53 | 20.42 |
| 63-125 µm | 13.47 | 22.39 | 14.08 | 12.75 | 10.23 | 10.25 | 18.66 | 13.29 | 18.68 | 20.75 | 22.32 | 17.42 | 12.71 | 19.84 | 14.85 | 12.22 | 13.67 |
| 32-63 µm | 5.79 | 11.47 | 9.36 | 4.33 | 6.12 | 5.50 | 11.40 | 5.34 | 8.89 | 10.21 | 8.21 | 9.89 | 5.37 | 14.23 | 5.69 | 6.88 | 8.75 |
| 16-32 µm | 4.77 | 5.35 | 5.07 | 2.73 | 4.95 | 4.39 | 7.13 | 2.86 | 4.86 | 4.94 | 2.79 | 4.70 | 3.20 | 7.92 | 3.38 | 5.36 | 6.13 |
| 8-16 µm | 4.97 | 4.41 | 3.89 | 3.30 | 5.50 | 4.99 | 6.20 | 3.00 | 3.97 | 4.17 | 2.45 | 3.34 | 3.14 | 5.43 | 3.35 | 5.14 | 5.28 |
| 4-8 µm | 3.87 | 3.74 | 3.23 | 3.38 | 5.17 | 4.78 | 5.30 | 3.02 | 3.55 | 3.70 | 1.93 | 2.96 | 2.81 | 4.24 | 2.97 | 4.10 | 4.23 |
| 2-4 µm | 2.35 | 2.45 | 2.15 | 2.73 | 3.67 | 3.46 | 3.75 | 2.59 | 2.92 | 2.87 | 1.32 | 2.33 | 2.09 | 2.99 | 2.22 | 2.56 | 2.85 |
| < 2 µm | 2.23 | 2.48 | 2.54 | 3.49 | 4.37 | 4.00 | 4.53 | 3.56 | 4.43 | 3.60 | 1.37 | 2.92 | 2.40 | 3.65 | 2.70 | 2.69 | 3.17 |
| Sum | 100.00 | 100.00 | 100.00 | 100.00 | 100.00 | 100.00 | 100.00 | 100.00 | 100.00 | 100.00 | 100.00 | 100.00 | 100.00 | 100.00 | 100.00 | 100.00 | 100.00 |

| | Relative Frequencies | | | | | | | | | | | | | | | | |
|---|---|---|---|---|---|---|---|---|---|---|---|---|---|---|---|---|---|
| | 55S | 56S | 57S | 58S | 59S | 60S | 61S | 62S | 63S | 64S | 65S | 66S | 67S | 68S | 69S | 70S | 71S |
| 500-1000 µm | 21.94 | 9.63 | 6.30 | 8.24 | 9.71 | 11.08 | 3.97 | 9.79 | 10.82 | 5.63 | 10.61 | 6.05 | 9.65 | 11.45 | 7.41 | 24.78 | 11.71 |
| 250-500 µm | 33.02 | 23.29 | 19.67 | 28.00 | 20.85 | 24.76 | 17.10 | 20.82 | 22.93 | 20.36 | 25.54 | 22.75 | 28.75 | 18.84 | 24.16 | 26.27 | 15.69 |
| 125-250 µm | 22.81 | 25.22 | 23.55 | 28.46 | 20.19 | 21.13 | 23.12 | 17.58 | 22.85 | 20.41 | 23.77 | 22.42 | 28.57 | 14.58 | 26.95 | 16.08 | 14.07 |
| 63-125 µm | 9.28 | 15.90 | 19.82 | 12.95 | 14.80 | 14.09 | 18.76 | 12.92 | 16.47 | 15.59 | 14.12 | 15.59 | 14.78 | 11.80 | 16.65 | 8.64 | 14.13 |
| 32-63 µm | 3.04 | 7.65 | 11.89 | 4.29 | 9.18 | 8.46 | 10.40 | 9.50 | 7.91 | 9.87 | 6.76 | 10.58 | 4.58 | 10.17 | 7.48 | 5.58 | 11.56 |
| 16-32 µm | 2.36 | 5.46 | 6.33 | 3.22 | 6.40 | 4.96 | 6.61 | 7.29 | 4.95 | 6.82 | 4.56 | 6.58 | 2.94 | 9.90 | 5.21 | 5.24 | 10.06 |
| 8-16 µm | 2.43 | 4.82 | 4.23 | 3.88 | 5.89 | 4.30 | 6.46 | 7.04 | 4.85 | 6.42 | 4.83 | 5.14 | 3.36 | 9.13 | 4.83 | 4.82 | 8.82 |
| 4-8 µm | 2.10 | 3.69 | 3.29 | 3.99 | 5.07 | 3.96 | 5.58 | 6.16 | 3.94 | 5.87 | 4.21 | 4.34 | 2.90 | 6.61 | 3.76 | 3.62 | 6.49 |
| 2-4 µm | 1.48 | 2.30 | 2.28 | 3.13 | 3.62 | 3.13 | 3.78 | 4.27 | 2.57 | 4.35 | 2.69 | 3.05 | 2.06 | 3.93 | 2.05 | 2.39 | 3.93 |
| < 2 µm | 1.54 | 2.04 | 2.63 | 3.84 | 4.29 | 4.12 | 4.21 | 4.63 | 2.71 | 4.66 | 2.91 | 3.49 | 2.41 | 3.60 | 1.50 | 2.58 | 3.55 |
| Sum | 100.00 | 100.00 | 100.00 | 100.00 | 100.00 | 100.00 | 100.00 | 100.00 | 100.00 | 100.00 | 100.00 | 100.00 | 100.00 | 100.00 | 100.00 | 100.00 | 100.00 |

| | Relative Frequencies | | | |
|---|---|---|---|---|
| | 72S | 73S | 74S | 75S |
| 500-1000 µm | 9.73 | 6.38 | 10.69 | 3.51 |
| 250-500 µm | 20.27 | 17.57 | 31.19 | 25.09 |
| 125-250 µm | 24.45 | 21.74 | 26.44 | 34.53 |
| 63-125 µm | 18.14 | 19.60 | 11.59 | 20.59 |
| 32-63 µm | 8.03 | 11.11 | 4.40 | 5.54 |
| 16-32 µm | 5.17 | 5.96 | 2.81 | 1.89 |
| 8-16 µm | 5.07 | 5.34 | 3.03 | 2.10 |
| 4-8 µm | 3.97 | 4.80 | 3.10 | 2.19 |
| 2-4 µm | 2.56 | 3.53 | 2.77 | 1.98 |
| < 2 µm | 2.61 | 3.97 | 3.99 | 2.58 |
| Sum | 100.00 | 100.00 | 100.00 | 100.00 |

Table 96: RDS-winter grain size analysis (72 samples).

| | Relative Frequencies | | | | | | | | | | | | | | | | |
|---|---|---|---|---|---|---|---|---|---|---|---|---|---|---|---|---|---|
| | 1W | 2W | 3W | 4W | 5W | 6W | 7W | 8W | 9W | 10W | 11W | 12W | 13W | 14W | 15W | 17W | 18W |
| 500-1000 µm | 5.87 | 11.19 | 17.59 | 12.94 | 4.15 | 14.31 | 10.21 | 19.21 | 6.23 | 18.45 | 1.89 | 6.15 | 2.20 | 0.00 | 10.59 | 16.89 | 9.23 |
| 250-500 µm | 12.58 | 14.81 | 18.80 | 15.38 | 10.25 | 25.97 | 24.87 | 27.58 | 9.32 | 37.54 | 4.12 | 14.78 | 3.73 | 0.00 | 32.33 | 23.44 | 20.79 |
| 125-250 µm | 14.97 | 10.58 | 9.70 | 14.14 | 11.85 | 19.80 | 23.29 | 17.20 | 10.60 | 21.75 | 7.56 | 14.27 | 4.06 | 1.45 | 32.01 | 16.09 | 21.20 |
| 63-125 µm | 14.43 | 11.37 | 8.60 | 12.55 | 13.93 | 10.35 | 12.52 | 7.85 | 14.05 | 5.97 | 14.75 | 12.09 | 8.97 | 16.65 | 12.12 | 9.56 | 12.81 |
| 32-63 µm | 12.14 | 11.35 | 10.05 | 9.48 | 13.98 | 6.82 | 6.94 | 5.74 | 13.51 | 2.37 | 16.21 | 10.75 | 17.42 | 17.66 | 2.95 | 7.38 | 7.56 |
| 16-32 µm | 12.03 | 11.57 | 11.66 | 8.68 | 13.44 | 7.38 | 5.48 | 5.55 | 13.79 | 2.40 | 14.25 | 10.27 | 21.54 | 14.67 | 1.98 | 6.30 | 6.25 |
| 8-16 µm | 11.28 | 10.83 | 10.67 | 8.50 | 12.29 | 6.82 | 5.32 | 5.33 | 12.89 | 3.18 | 12.75 | 9.99 | 17.33 | 14.82 | 2.08 | 5.98 | 6.28 |
| 4-8 µm | 7.99 | 8.40 | 6.74 | 7.49 | 9.29 | 4.38 | 4.80 | 4.62 | 9.30 | 3.11 | 10.81 | 8.52 | 10.92 | 13.15 | 2.16 | 5.40 | 5.97 |
| 2-4 µm | 4.60 | 5.27 | 3.47 | 5.39 | 5.71 | 2.30 | 3.30 | 3.30 | 5.44 | 2.38 | 7.93 | 6.11 | 6.41 | 9.97 | 1.75 | 4.07 | 4.61 |
| < 2 µm | 4.11 | 4.63 | 2.72 | 5.47 | 5.11 | 1.87 | 3.26 | 3.63 | 4.86 | 2.84 | 9.73 | 7.07 | 7.42 | 11.65 | 2.03 | 4.90 | 5.31 |
| Sum | 100.00 | 100.00 | 100.00 | 100.00 | 100.00 | 100.00 | 100.00 | 100.00 | 100.00 | 100.00 | 100.00 | 100.00 | 100.00 | 100.00 | 100.00 | 100.00 | 100.00 |

| | Relative Frequencies | | | | | | | | | | | | | | | | |
|---|---|---|---|---|---|---|---|---|---|---|---|---|---|---|---|---|---|
| | 19W | 20W | 21W | 22W | 23W | 24W | 25W | 26W | 27W | 28W | 29W | 30W | 31W | 32W | 33W | 34W | 35W |
| 500-1000 µm | 5.98 | 6.00 | 10.43 | 7.65 | 9.04 | 9.03 | 5.77 | 9.14 | 22.29 | 20.02 | 5.68 | 7.07 | 8.11 | 4.23 | 7.13 | 19.55 | 43.99 |
| 250-500 µm | 14.82 | 16.07 | 22.87 | 24.65 | 19.69 | 14.73 | 6.04 | 19.66 | 31.11 | 27.13 | 11.42 | 16.39 | 19.41 | 20.13 | 21.89 | 21.98 | 34.30 |
| 125-250 µm | 12.79 | 18.08 | 22.64 | 26.67 | 20.31 | 18.89 | 5.69 | 20.38 | 18.13 | 18.56 | 13.45 | 22.73 | 20.22 | 22.25 | 21.69 | 16.08 | 11.45 |
| 63-125 µm | 8.59 | 13.95 | 13.89 | 16.31 | 13.50 | 18.65 | 6.71 | 14.05 | 7.04 | 7.08 | 14.27 | 18.30 | 12.88 | 14.20 | 13.12 | 13.17 | 3.96 |
| 32-63 µm | 9.31 | 9.87 | 7.74 | 7.47 | 7.21 | 12.28 | 9.33 | 9.12 | 3.97 | 4.59 | 11.12 | 10.14 | 8.73 | 10.33 | 8.30 | 8.82 | 1.87 |
| 16-32 µm | 10.58 | 9.47 | 5.93 | 4.58 | 5.26 | 7.03 | 13.96 | 7.29 | 3.83 | 4.72 | 9.63 | 6.96 | 7.68 | 8.52 | 6.68 | 5.82 | 1.54 |
| 8-16 µm | 10.90 | 9.61 | 5.79 | 4.06 | 5.76 | 5.97 | 16.30 | 6.72 | 4.19 | 5.42 | 9.97 | 6.33 | 7.46 | 7.59 | 6.52 | 4.62 | 1.26 |
| 4-8 µm | 10.36 | 7.58 | 4.84 | 3.40 | 5.90 | 5.16 | 14.13 | 5.57 | 3.78 | 5.01 | 9.34 | 5.11 | 6.29 | 5.94 | 5.74 | 3.78 | 0.94 |
| 2-4 µm | 7.86 | 4.72 | 3.03 | 2.39 | 5.17 | 3.64 | 10.01 | 3.72 | 2.74 | 3.51 | 7.07 | 3.37 | 4.37 | 3.63 | 4.06 | 2.73 | 0.58 |
| < 2 µm | 8.80 | 4.63 | 2.84 | 2.83 | 8.17 | 4.61 | 12.06 | 4.34 | 2.91 | 3.95 | 8.07 | 3.61 | 4.86 | 3.17 | 4.87 | 3.44 | 0.12 |
| Sum | 100.00 | 100.00 | 100.00 | 100.00 | 100.00 | 100.00 | 100.00 | 100.00 | 100.00 | 100.00 | 100.00 | 100.00 | 100.00 | 100.00 | 100.00 | 100.00 | 100.00 |

| | Relative Frequencies | | | | | | | | | | | | | | | | |
|---|---|---|---|---|---|---|---|---|---|---|---|---|---|---|---|---|---|
| | 36W | 37W | 38W | 40W | 41W | 42W | 43W | 44W | 45W | 46W | 48W | 49W | 50W | 51W | 52W | 53W | 54W |
| 500-1000 µm | 27.29 | 5.14 | 12.47 | 9.32 | 18.31 | 11.23 | 7.70 | 10.57 | 6.92 | 17.49 | 6.69 | 15.17 | 9.57 | 8.42 | 10.37 | 12.74 | 11.97 |
| 250-500 µm | 24.15 | 16.76 | 25.73 | 20.63 | 26.31 | 25.79 | 19.61 | 20.04 | 13.33 | 25.32 | 18.10 | 37.97 | 18.67 | 23.88 | 24.09 | 20.37 | 20.10 |
| 125-250 µm | 15.16 | 22.43 | 18.67 | 23.60 | 17.11 | 23.65 | 23.92 | 18.77 | 11.31 | 19.07 | 23.93 | 22.84 | 17.17 | 19.71 | 23.55 | 13.21 | 21.35 |
| 63-125 µm | 8.75 | 15.86 | 9.44 | 15.47 | 8.14 | 13.60 | 18.17 | 12.92 | 9.99 | 11.51 | 19.81 | 6.98 | 14.48 | 11.88 | 13.69 | 10.23 | 17.44 |
| 32-63 µm | 6.02 | 11.13 | 7.49 | 8.39 | 5.88 | 7.05 | 9.45 | 8.51 | 10.35 | 7.00 | 10.19 | 3.54 | 10.98 | 8.91 | 6.38 | 9.75 | 10.34 |
| 16-32 µm | 5.77 | 9.40 | 6.75 | 6.41 | 6.06 | 4.74 | 5.54 | 7.00 | 10.89 | 6.33 | 5.86 | 2.95 | 8.27 | 7.21 | 4.59 | 10.14 | 6.84 |
| 8-16 µm | 5.17 | 7.56 | 6.62 | 5.93 | 6.48 | 4.36 | 5.11 | 6.87 | 11.08 | 5.59 | 5.35 | 3.54 | 7.47 | 6.19 | 5.09 | 9.51 | 5.11 |
| 4-8 µm | 3.72 | 5.27 | 5.50 | 4.52 | 5.13 | 3.79 | 4.37 | 6.12 | 9.88 | 3.82 | 4.29 | 3.12 | 5.83 | 5.29 | 4.91 | 6.83 | 3.39 |
| 2-4 µm | 2.19 | 3.16 | 3.45 | 2.82 | 3.13 | 2.72 | 2.94 | 4.36 | 7.29 | 2.12 | 2.82 | 1.97 | 3.44 | 3.87 | 3.50 | 3.79 | 1.94 |
| < 2 µm | 1.79 | 3.29 | 3.88 | 2.91 | 3.44 | 3.07 | 3.20 | 4.83 | 8.96 | 1.76 | 2.96 | 1.93 | 4.12 | 4.64 | 3.82 | 3.43 | 1.52 |
| Sum | 100.00 | 100.00 | 100.00 | 100.00 | 100.00 | 100.00 | 100.00 | 100.00 | 100.00 | 100.00 | 100.00 | 100.00 | 100.00 | 100.00 | 100.00 | 100.00 | 100.00 |

| | Relative Frequencies | | | | | | | | | | | | | | | | |
|---|---|---|---|---|---|---|---|---|---|---|---|---|---|---|---|---|---|
| | 55W | 56W | 57W | 58W | 59W | 60W | 61W | 62W | 63W | 64W | 65W | 66W | 67W | 68W | 69W | 70W | 71W |
| 500-1000 µm | 25.33 | 22.87 | 3.54 | 10.45 | 2.68 | 5.78 | 40.61 | 15.52 | 7.80 | 11.27 | 15.57 | 9.26 | 6.89 | 8.63 | 14.46 | 19.01 | 0.24 |
| 250-500 µm | 32.79 | 31.65 | 9.88 | 25.45 | 7.07 | 15.73 | 24.17 | 22.89 | 20.25 | 29.38 | 24.65 | 24.89 | 18.73 | 14.95 | 22.29 | 11.06 | 2.32 |
| 125-250 µm | 17.14 | 20.77 | 14.09 | 27.55 | 9.31 | 16.36 | 6.41 | 20.07 | 25.23 | 25.48 | 16.85 | 22.57 | 21.92 | 11.21 | 17.67 | 11.38 | 3.73 |
| 63-125 µm | 5.98 | 8.23 | 17.29 | 14.39 | 13.30 | 15.39 | 3.30 | 12.53 | 18.96 | 11.74 | 10.37 | 13.67 | 15.53 | 9.88 | 11.66 | 12.00 | 7.77 |
| 32-63 µm | 3.38 | 3.87 | 15.48 | 5.13 | 14.64 | 11.58 | 2.29 | 6.71 | 9.28 | 4.79 | 6.88 | 8.35 | 9.45 | 10.42 | 7.72 | 10.89 | 13.95 |
| 16-32 µm | 3.40 | 3.90 | 11.79 | 4.03 | 14.10 | 8.48 | 3.64 | 5.51 | 4.79 | 3.41 | 5.55 | 6.06 | 7.80 | 12.55 | 7.14 | 10.33 | 20.90 |
| 8-16 µm | 3.72 | 3.66 | 10.12 | 4.39 | 13.20 | 7.77 | 5.54 | 5.58 | 4.10 | 3.70 | 6.08 | 5.64 | 7.23 | 12.83 | 7.29 | 9.17 | 19.95 |
| 4-8 µm | 3.33 | 2.53 | 8.00 | 3.82 | 10.77 | 7.03 | 5.86 | 4.85 | 3.70 | 3.64 | 5.63 | 4.46 | 5.63 | 9.50 | 5.91 | 6.86 | 13.59 |
| 2-4 µm | 2.40 | 1.44 | 4.87 | 2.48 | 7.23 | 5.36 | 4.32 | 3.27 | 2.74 | 2.94 | 3.87 | 2.64 | 3.53 | 5.53 | 3.39 | 4.44 | 8.21 |
| < 2 µm | 2.52 | 1.07 | 4.96 | 2.32 | 7.69 | 6.51 | 3.85 | 3.07 | 3.16 | 3.64 | 4.56 | 2.46 | 3.31 | 4.49 | 2.47 | 4.87 | 9.35 |
| Sum | 100.00 | 100.00 | 100.00 | 100.00 | 100.00 | 100.00 | 100.00 | 100.00 | 100.00 | 100.00 | 100.00 | 100.00 | 100.00 | 100.00 | 100.00 | 100.00 | 100.00 |

| | Relative Frequencies | | | |
|---|---|---|---|---|
| | 72W | 73W | 74W | 75W |
| 500-1000 µm | 17.55 | 15.86 | 12.94 | 6.58 |
| 250-500 µm | 21.32 | 25.38 | 30.73 | 24.55 |
| 125-250 µm | 16.49 | 14.15 | 23.89 | 30.73 |
| 63-125 µm | 12.10 | 7.99 | 9.11 | 18.42 |
| 32-63 µm | 7.99 | 7.03 | 4.18 | 6.02 |
| 16-32 µm | 6.86 | 7.09 | 3.77 | 3.25 |
| 8-16 µm | 6.59 | 7.31 | 4.42 | 3.23 |
| 4-8 µm | 5.08 | 5.92 | 4.36 | 2.85 |
| 2-4 µm | 3.07 | 3.99 | 3.09 | 2.11 |
| < 2 µm | 2.95 | 5.26 | 3.52 | 2.25 |
| Sum | 100.00 | 100.00 | 100.00 | 100.00 |

Table 97: Spearman's rank correlation coefficients for RDS summer data (n=72).

| | | Na2O | MgO | Al2O3 | SiO2 | P2O5 | K2O | CaO | TiO2 | MnO | Fe2O3 | Sc | V | Cr | Co | Ba | Ni | Cu | Zn | Ga | Ge | As | Se | Br | Rb | Sr | Y | Zr | Nb | Mo | Hf | W |
|---|---|---|---|---|---|---|---|---|---|---|---|---|---|---|---|---|---|---|---|---|---|---|---|---|---|---|---|---|---|---|---|---|
| Na2O | CC (ρ) | | ,663 | **,777** | ,345 | -,036 | ,459 | -,200 | **,736** | ,687 | **,785** | ,610 | ,604 | ,397 | ,587 | ,462 | ,547 | ,128 | ,070 | **,701** | ,197 | ,010 | -,041 | -,262 | ,403 | ,393 | ,682 | ,332 | **,742** | ,157 | ,186 | -,029 |
| | Sig. (2-tailed) | | ,000 | ,000 | ,003 | ,761 | ,000 | ,093 | ,000 | ,000 | ,000 | ,000 | ,000 | ,001 | ,000 | ,000 | ,000 | ,285 | ,558 | ,000 | ,097 | ,936 | ,735 | ,026 | ,000 | ,001 | ,000 | ,004 | ,000 | ,188 | ,117 | ,808 |
| MgO | CC (ρ) | | | **,738** | -,019 | ,261 | ,429 | -,124 | **,854** | ,686 | **,721** | ,644 | **,841** | ,435 | ,694 | ,275 | **,705** | ,113 | ,210 | **,727** | ,171 | -,027 | ,089 | -,056 | ,414 | ,347 | ,574 | ,060 | ,614 | ,165 | -,022 | -,110 |
| | Sig. (2-tailed) | | | ,000 | ,876 | ,027 | ,000 | ,299 | ,000 | ,000 | ,000 | ,000 | ,000 | ,000 | ,000 | ,019 | ,000 | ,343 | ,077 | ,000 | ,151 | ,823 | ,458 | ,642 | ,000 | ,003 | ,000 | ,618 | ,000 | ,165 | ,853 | ,356 |
| Al2O3 | CC (ρ) | | | | ,255 | ,212 | **,719** | -,340 | **,889** | ,679 | **,758** | **,706** | **,785** | ,280 | **,731** | ,544 | ,575 | ,098 | ,063 | **,905** | ,310 | ,181 | ,002 | -,140 | ,690 | ,223 | **,801** | ,341 | **,834** | ,021 | ,195 | -,026 |
| | Sig. (2-tailed) | | | | ,030 | ,074 | ,000 | ,004 | ,000 | ,000 | ,000 | ,000 | ,000 | ,017 | ,000 | ,000 | ,000 | ,413 | ,600 | ,000 | ,008 | ,128 | ,988 | ,240 | ,000 | ,059 | ,000 | ,003 | ,000 | ,862 | ,100 | ,827 |
| SiO2 | CC (ρ) | | | | | -,560 | ,216 | -,261 | ,088 | ,021 | ,118 | ,042 | -,126 | ,050 | ,028 | ,243 | -,104 | -,023 | -,318 | ,075 | ,024 | ,070 | -,359 | -,546 | ,165 | -,099 | ,119 | ,351 | ,169 | -,040 | ,208 | -,068 |
| | Sig. (2-tailed) | | | | | ,000 | ,069 | ,027 | ,464 | ,858 | ,325 | ,725 | ,293 | ,679 | ,815 | ,040 | ,386 | ,848 | ,006 | ,529 | ,841 | ,560 | ,002 | ,000 | ,167 | ,406 | ,318 | ,003 | ,156 | ,740 | ,080 | ,568 |
| P2O5 | CC (ρ) | | | | | | ,307 | -,390 | ,316 | ,200 | ,205 | ,328 | ,459 | ,074 | ,350 | ,083 | ,370 | ,123 | ,446 | ,336 | ,225 | ,290 | ,467 | **,750** | ,282 | -,179 | ,199 | -,131 | ,198 | -,002 | -,071 | ,055 |
| | Sig. (2-tailed) | | | | | | ,009 | ,001 | ,007 | ,093 | ,084 | ,005 | ,000 | ,539 | ,003 | ,490 | ,001 | ,301 | ,000 | ,004 | ,057 | ,014 | ,000 | ,000 | ,016 | ,133 | ,093 | ,272 | ,095 | ,985 | ,555 | ,649 |
| K2O | CC (ρ) | | | | | | | -,497 | ,563 | ,441 | ,503 | ,520 | ,536 | ,204 | ,511 | ,587 | ,341 | ,123 | ,095 | ,656 | ,332 | ,386 | ,068 | ,073 | **,980** | -,131 | ,638 | ,400 | ,601 | -,020 | ,229 | ,145 |
| | Sig. (2-tailed) | | | | | | | ,000 | ,000 | ,000 | ,000 | ,000 | ,000 | ,086 | ,000 | ,000 | ,003 | ,303 | ,429 | ,000 | ,004 | ,001 | ,568 | ,545 | ,000 | ,273 | ,000 | ,000 | ,000 | ,867 | ,053 | ,224 |
| CaO | CC (ρ) | | | | | | | | -,200 | -,035 | -,145 | -,151 | -,200 | ,039 | -,186 | -,040 | -,069 | ,041 | -,002 | -,301 | -,087 | -,149 | -,087 | -,205 | -,404 | ,596 | -,100 | -,042 | -,177 | ,114 | ,095 | ,107 |
| | Sig. (2-tailed) | | | | | | | | ,092 | ,771 | ,226 | ,207 | ,092 | ,743 | ,117 | ,738 | ,565 | ,732 | ,989 | ,010 | ,465 | ,210 | ,466 | ,084 | ,000 | ,000 | ,404 | ,726 | ,138 | ,342 | ,430 | ,371 |
| TiO2 | CC (ρ) | | | | | | | | | **,759** | **,839** | **,740** | **,892** | ,415 | **,821** | ,493 | **,783** | ,236 | ,238 | **,884** | ,309 | ,165 | ,108 | -,024 | ,535 | ,349 | **,744** | ,282 | **,819** | ,162 | ,181 | -,003 |
| | Sig. (2-tailed) | | | | | | | | | ,000 | ,000 | ,000 | ,000 | ,000 | ,000 | ,000 | ,000 | ,046 | ,044 | ,000 | ,008 | ,166 | ,366 | ,842 | ,000 | ,003 | ,000 | ,016 | ,000 | ,174 | ,128 | ,981 |
| MnO | CC (ρ) | | | | | | | | | | **,778** | **,705** | **,717** | ,385 | **,717** | ,451 | ,688 | ,199 | ,250 | ,625 | ,156 | ,174 | ,168 | ,003 | ,435 | ,418 | **,833** | ,197 | ,674 | ,091 | ,089 | ,151 |
| | Sig. (2-tailed) | | | | | | | | | | ,000 | ,000 | ,000 | ,001 | ,000 | ,000 | ,000 | ,093 | ,034 | ,000 | ,191 | ,145 | ,158 | ,983 | ,000 | ,000 | ,000 | ,098 | ,000 | ,448 | ,457 | ,206 |
| Fe2O3 | CC (ρ) | | | | | | | | | | | ,630 | **,750** | ,578 | **,783** | ,588 | **,753** | ,446 | ,337 | **,784** | ,378 | ,266 | ,221 | -,039 | ,485 | ,348 | **,745** | ,380 | **,833** | ,343 | ,235 | ,080 |
| | Sig. (2-tailed) | | | | | | | | | | | ,000 | ,000 | ,000 | ,000 | ,000 | ,000 | ,000 | ,004 | ,000 | ,001 | ,024 | ,063 | ,744 | ,000 | ,003 | ,000 | ,001 | ,000 | ,003 | ,047 | ,504 |
| Sc | CC (ρ) | | | | | | | | | | | | ,677 | ,426 | ,592 | ,367 | ,530 | ,174 | ,205 | **,729** | ,216 | ,037 | ,049 | ,026 | ,486 | ,228 | ,661 | ,175 | ,632 | ,101 | ,077 | ,165 |
| | Sig. (2-tailed) | | | | | | | | | | | | ,000 | ,000 | ,000 | ,002 | ,000 | ,144 | ,084 | ,000 | ,069 | ,755 | ,681 | ,831 | ,000 | ,055 | ,000 | ,142 | ,000 | ,401 | ,522 | ,166 |
| V | CC (ρ) | | | | | | | | | | | | | ,294 | **,769** | ,376 | **,789** | ,132 | ,258 | **,801** | ,302 | ,128 | ,179 | ,113 | ,520 | ,288 | ,673 | ,072 | ,645 | ,051 | ,031 | -,036 |
| | Sig. (2-tailed) | | | | | | | | | | | | | ,012 | ,000 | ,001 | ,000 | ,269 | ,029 | ,000 | ,010 | ,284 | ,132 | ,343 | ,000 | ,014 | ,000 | ,551 | ,000 | ,674 | ,794 | ,762 |
| Cr | CC (ρ) | | | | | | | | | | | | | | ,390 | ,449 | ,505 | ,492 | ,316 | ,352 | ,167 | ,174 | ,220 | -,011 | ,191 | ,202 | ,357 | ,385 | ,514 | ,550 | ,255 | ,139 |
| | Sig. (2-tailed) | | | | | | | | | | | | | | ,001 | ,000 | ,000 | ,000 | ,007 | ,002 | ,162 | ,143 | ,064 | ,925 | ,109 | ,088 | ,002 | ,001 | ,000 | ,000 | ,031 | ,246 |
| Co | CC (ρ) | | | | | | | | | | | | | | | ,527 | **,750** | ,289 | ,302 | **,775** | ,277 | ,223 | ,243 | ,118 | ,498 | ,276 | ,662 | ,276 | **,705** | ,111 | ,204 | ,055 |
| | Sig. (2-tailed) | | | | | | | | | | | | | | | ,000 | ,000 | ,014 | ,010 | ,000 | ,018 | ,059 | ,040 | ,322 | ,000 | ,019 | ,000 | ,019 | ,000 | ,353 | ,085 | ,644 |
| Ba | CC (ρ) | | | | | | | | | | | | | | | | ,417 | ,439 | ,424 | ,461 | ,446 | ,519 | ,203 | ,014 | ,587 | ,232 | ,644 | ,600 | ,640 | ,339 | ,472 | ,333 |
| | Sig. (2-tailed) | | | | | | | | | | | | | | | | ,000 | ,000 | ,000 | ,000 | ,000 | ,000 | ,087 | ,905 | ,000 | ,050 | ,000 | ,000 | ,000 | ,004 | ,000 | ,004 |
| Ni | CC (ρ) | | | | | | | | | | | | | | | | | ,325 | ,427 | ,609 | ,284 | ,214 | ,219 | ,161 | ,352 | ,349 | ,595 | ,185 | ,604 | ,250 | ,097 | ,086 |
| | Sig. (2-tailed) | | | | | | | | | | | | | | | | | ,005 | ,000 | ,000 | ,016 | ,072 | ,065 | ,177 | ,002 | ,003 | ,000 | ,120 | ,000 | ,034 | ,418 | ,472 |
| Cu | CC (ρ) | | | | | | | | | | | | | | | | | | ,622 | ,186 | ,205 | ,321 | ,227 | ,182 | ,159 | ,007 | ,162 | ,405 | ,331 | **,716** | ,319 | ,307 |
| | Sig. (2-tailed) | | | | | | | | | | | | | | | | | | ,000 | ,117 | ,084 | ,006 | ,056 | ,126 | ,182 | ,956 | ,174 | ,000 | ,005 | ,000 | ,006 | ,009 |
| Zn | CC (ρ) | | | | | | | | | | | | | | | | | | | ,140 | ,265 | ,309 | ,358 | ,530 | ,103 | -,015 | ,180 | ,058 | ,229 | ,631 | ,104 | ,510 |
| | Sig. (2-tailed) | | | | | | | | | | | | | | | | | | | ,240 | ,025 | ,008 | ,002 | ,000 | ,388 | ,897 | ,131 | ,626 | ,053 | ,000 | ,384 | ,000 |
| Ga | CC (ρ) | | | | | | | | | | | | | | | | | | | | ,288 | ,149 | ,074 | ,013 | ,621 | ,208 | **,709** | ,285 | **,815** | ,114 | ,142 | ,014 |
| | Sig. (2-tailed) | | | | | | | | | | | | | | | | | | | | ,014 | ,213 | ,534 | ,915 | ,000 | ,079 | ,000 | ,015 | ,000 | ,339 | ,233 | ,909 |
| Ge | CC (ρ) | | | | | | | | | | | | | | | | | | | | | ,411 | ,184 | ,110 | ,350 | ,094 | ,311 | ,180 | ,339 | ,193 | ,239 | ,173 |
| | Sig. (2-tailed) | | | | | | | | | | | | | | | | | | | | | ,000 | ,121 | ,357 | ,003 | ,433 | ,008 | ,131 | ,004 | ,105 | ,043 | ,145 |
| As | CC (ρ) | | | | | | | | | | | | | | | | | | | | | | ,393 | ,338 | ,435 | -,050 | ,345 | ,464 | ,341 | ,100 | ,394 | ,190 |
| | Sig. (2-tailed) | | | | | | | | | | | | | | | | | | | | | | ,001 | ,004 | ,000 | ,679 | ,003 | ,000 | ,003 | ,404 | ,001 | ,110 |
| Se | CC (ρ) | | | | | | | | | | | | | | | | | | | | | | | ,515 | ,064 | ,031 | ,182 | ,091 | ,184 | ,179 | ,066 | ,100 |
| | Sig. (2-tailed) | | | | | | | | | | | | | | | | | | | | | | | ,000 | ,595 | ,798 | ,127 | ,446 | ,121 | ,133 | ,581 | ,403 |
| Br | CC (ρ) | | | | | | | | | | | | | | | | | | | | | | | | ,064 | -,208 | ,015 | -,050 | -,028 | ,115 | ,040 | ,268 |
| | Sig. (2-tailed) | | | | | | | | | | | | | | | | | | | | | | | | ,595 | ,079 | ,901 | ,677 | ,817 | ,338 | ,740 | ,023 |
| Rb | CC (ρ) | | | | | | | | | | | | | | | | | | | | | | | | | -,098 | ,638 | ,414 | ,580 | -,016 | ,245 | ,147 |
| | Sig. (2-tailed) | | | | | | | | | | | | | | | | | | | | | | | | | ,413 | ,000 | ,000 | ,000 | ,897 | ,038 | ,217 |
| Sr | CC (ρ) | | | | | | | | | | | | | | | | | | | | | | | | | | ,355 | ,201 | ,280 | -,001 | ,192 | -,064 |
| | Sig. (2-tailed) | | | | | | | | | | | | | | | | | | | | | | | | | | ,002 | ,091 | ,017 | ,994 | ,106 | ,590 |
| Y | CC (ρ) | | | | | | | | | | | | | | | | | | | | | | | | | | | ,428 | **,808** | ,027 | ,292 | ,221 |
| | Sig. (2-tailed) | | | | | | | | | | | | | | | | | | | | | | | | | | | ,000 | ,000 | ,819 | ,013 | ,063 |
| Zr | CC (ρ) | | | | | | | | | | | | | | | | | | | | | | | | | | | | ,511 | ,221 | **,816** | ,116 |
| | Sig. (2-tailed) | | | | | | | | | | | | | | | | | | | | | | | | | | | | ,000 | ,062 | ,000 | ,333 |
| Nb | CC (ρ) | | | | | | | | | | | | | | | | | | | | | | | | | | | | | ,231 | ,352 | ,107 |
| | Sig. (2-tailed) | | | | | | | | | | | | | | | | | | | | | | | | | | | | | ,051 | ,002 | ,371 |
| Mo | CC (ρ) | | | | | | | | | | | | | | | | | | | | | | | | | | | | | | ,203 | ,327 |
| | Sig. (2-tailed) | | | | | | | | | | | | | | | | | | | | | | | | | | | | | | ,088 | ,005 |
| Hf | CC (ρ) | | | | | | | | | | | | | | | | | | | | | | | | | | | | | | | ,087 |
| | Sig. (2-tailed) | | | | | | | | | | | | | | | | | | | | | | | | | | | | | | | ,467 |
| W | CC (ρ) | | | | | | | | | | | | | | | | | | | | | | | | | | | | | | | |
| | Sig. (2-tailed) | | | | | | | | | | | | | | | | | | | | | | | | | | | | | | | |

| | | Pb | Bi | Th | U | Cd | Sn | Sb | I | La | Ce | Nd | Sm | S | Cl | Yb | LOI | 500-1000 µm | 250-500 µm | 125-250 µm | 63-125 µm | 32-63 µm | 16-32 µm | 8-16 µm | 4-8 µm | 2-4 µm | below 2 µm | 1000-63 µm | 63-2 µm |
|---|---|---|---|---|---|---|---|---|---|---|---|---|---|---|---|---|---|---|---|---|---|---|---|---|---|---|---|---|---|
| Na2O | CC (ρ) | -,068 | ,290 | ,399 | ,056 | -,072 | ,079 | ,072 | -,212 | ,548 | ,619 | ,518 | ,151 | -,123 | ,074 | ,279 | -,148 | ,112 | -,107 | ,012 | ,127 | ,031 | -,089 | -,100 | -,071 | ,018 | ,045 | ,019 | -,041 |
| | Sig. (2-tailed) | ,573 | ,013 | ,001 | ,639 | ,549 | ,507 | ,550 | ,074 | ,000 | ,000 | ,000 | ,205 | ,302 | ,538 | ,017 | ,215 | ,351 | ,373 | ,921 | ,289 | ,797 | ,457 | ,403 | ,551 | ,882 | ,710 | ,875 | ,730 |
| MgO | CC (ρ) | ,071 | ,304 | ,323 | -,064 | -,191 | ,049 | ,192 | -,085 | ,466 | ,414 | ,470 | ,260 | ,214 | ,123 | ,215 | ,179 | ,139 | -,245 | -,210 | ,094 | ,224 | ,191 | ,147 | ,131 | ,127 | ,043 | -,187 | ,185 |
| | Sig. (2-tailed) | ,555 | ,009 | ,006 | ,590 | ,108 | ,682 | ,107 | ,479 | ,000 | ,000 | ,000 | ,027 | ,071 | ,302 | ,069 | ,132 | ,244 | ,038 | ,077 | ,435 | ,059 | ,108 | ,217 | ,274 | ,289 | ,719 | ,117 | ,119 |
| Al2O3 | CC (ρ) | -,005 | ,134 | ,653 | ,197 | -,106 | ,077 | ,044 | -,094 | **,770** | ,693 | **,708** | ,316 | ,057 | ,019 | ,381 | ,048 | -,117 | -,372 | -,132 | ,177 | ,261 | ,237 | ,243 | ,282 | ,340 | ,295 | -,323 | ,293 |
| | Sig. (2-tailed) | ,966 | ,260 | ,000 | ,096 | ,376 | ,518 | ,711 | ,432 | ,000 | ,000 | ,000 | ,007 | ,637 | ,871 | ,001 | ,686 | ,330 | ,001 | ,268 | ,137 | ,027 | ,045 | ,040 | ,017 | ,003 | ,012 | ,006 | ,013 |
| SiO2 | CC (ρ) | -,213 | -,102 | ,082 | -,012 | -,030 | -,052 | -,223 | -,514 | ,123 | ,115 | -,024 | ,060 | -,732 | -,298 | -,168 | -,671 | -,133 | ,297 | ,367 | -,069 | -,291 | -,406 | -,391 | -,276 | -,064 | ,125 | ,279 | -,338 |
| | Sig. (2-tailed) | ,073 | ,393 | ,492 | ,921 | ,800 | ,662 | ,060 | ,000 | ,303 | ,338 | ,840 | ,615 | ,000 | ,011 | ,159 | ,000 | ,266 | ,011 | ,002 | ,562 | ,013 | ,000 | ,001 | ,019 | ,595 | ,295 | ,017 | ,004 |
| P2O5 | CC (ρ) | ,255 | ,058 | ,121 | -,059 | ,033 | ,084 | ,202 | ,644 | ,062 | ,037 | ,163 | ,014 | **,800** | ,438 | ,183 | **,904** | ,033 | -,445 | -,454 | ,088 | ,388 | ,572 | ,597 | ,471 | ,219 | -,088 | -,443 | ,503 |
| | Sig. (2-tailed) | ,031 | ,629 | ,310 | ,620 | ,782 | ,481 | ,088 | ,000 | ,605 | ,761 | ,171 | ,907 | ,000 | ,000 | ,124 | ,000 | ,784 | ,000 | ,000 | ,460 | ,001 | ,000 | ,000 | ,000 | ,064 | ,464 | ,000 | ,000 |
| K2O | CC (ρ) | ,192 | ,058 | ,623 | ,063 | -,039 | ,169 | ,060 | ,062 | ,657 | ,549 | ,528 | ,280 | ,222 | ,004 | ,334 | ,155 | -,192 | -,393 | -,123 | ,219 | ,300 | ,303 | ,301 | ,311 | ,308 | ,260 | -,360 | ,349 |
| | Sig. (2-tailed) | ,107 | ,626 | ,000 | ,598 | ,746 | ,155 | ,614 | ,607 | ,000 | ,000 | ,000 | ,017 | ,061 | ,974 | ,004 | ,193 | ,107 | ,001 | ,303 | ,065 | ,010 | ,010 | ,010 | ,008 | ,009 | ,028 | ,002 | ,003 |
| CaO | CC (ρ) | ,169 | ,195 | -,124 | ,033 | ,059 | ,168 | ,140 | -,087 | -,081 | -,003 | -,031 | ,071 | -,237 | -,236 | -,158 | -,262 | ,053 | ,120 | ,050 | -,009 | -,025 | -,153 | -,178 | -,112 | ,004 | ,158 | ,074 | -,113 |
| | Sig. (2-tailed) | ,155 | ,101 | ,300 | ,784 | ,624 | ,159 | ,242 | ,467 | ,501 | ,982 | ,793 | ,555 | ,045 | ,046 | ,185 | ,026 | ,656 | ,315 | ,674 | ,938 | ,836 | ,200 | ,134 | ,350 | ,974 | ,186 | ,537 | ,344 |
| TiO2 | CC (ρ) | ,113 | ,300 | ,522 | ,091 | -,041 | ,187 | ,201 | ,011 | ,634 | ,583 | ,622 | ,240 | ,174 | ,146 | ,399 | ,176 | -,074 | -,371 | -,174 | ,194 | ,270 | ,247 | ,250 | ,261 | ,289 | ,228 | -,299 | ,279 |
| | Sig. (2-tailed) | ,346 | ,011 | ,000 | ,447 | ,730 | ,115 | ,091 | ,925 | ,000 | ,000 | ,000 | ,042 | ,143 | ,220 | ,001 | ,139 | ,536 | ,001 | ,143 | ,102 | ,022 | ,036 | ,034 | ,027 | ,014 | ,054 | ,011 | ,018 |
| MnO | CC (ρ) | ,178 | ,276 | ,497 | ,044 | -,091 | ,209 | ,154 | ,059 | ,588 | ,594 | ,647 | ,397 | ,177 | ,105 | ,293 | ,109 | ,148 | -,208 | -,188 | ,031 | ,100 | ,109 | ,137 | ,154 | ,217 | ,204 | -,158 | ,130 |
| | Sig. (2-tailed) | ,136 | ,019 | ,000 | ,714 | ,446 | ,078 | ,196 | ,623 | ,000 | ,000 | ,000 | ,001 | ,138 | ,378 | ,013 | ,363 | ,214 | ,079 | ,113 | ,796 | ,404 | ,362 | ,251 | ,197 | ,068 | ,086 | ,185 | ,277 |
| Fe2O3 | CC (ρ) | ,207 | ,410 | ,439 | -,046 | ,068 | ,393 | ,333 | ,032 | ,584 | ,593 | ,562 | ,235 | ,085 | ,147 | ,393 | ,092 | ,015 | -,298 | -,124 | ,167 | ,159 | ,103 | ,118 | ,137 | ,206 | ,218 | -,178 | ,150 |
| | Sig. (2-tailed) | ,081 | ,000 | ,000 | ,702 | ,569 | ,001 | ,004 | ,787 | ,000 | ,000 | ,000 | ,047 | ,478 | ,217 | ,001 | ,444 | ,898 | ,011 | ,300 | ,161 | ,181 | ,388 | ,323 | ,252 | ,083 | ,066 | ,135 | ,208 |
| Sc | CC (ρ) | ,231 | ,058 | ,523 | ,074 | -,067 | ,090 | ,155 | ,041 | ,528 | ,487 | ,478 | ,287 | ,154 | ,043 | ,268 | ,198 | -,008 | -,267 | -,048 | ,176 | ,154 | ,142 | ,145 | ,138 | ,129 | ,075 | -,155 | ,155 |
| | Sig. (2-tailed) | ,051 | ,629 | ,000 | ,537 | ,577 | ,450 | ,194 | ,730 | ,000 | ,000 | ,000 | ,015 | ,197 | ,723 | ,023 | ,096 | ,950 | ,023 | ,686 | ,139 | ,198 | ,234 | ,225 | ,248 | ,279 | ,529 | ,194 | ,193 |
| V | CC (ρ) | ,121 | ,273 | ,399 | -,001 | -,028 | ,125 | ,123 | ,141 | ,482 | ,414 | ,586 | ,310 | ,406 | ,139 | ,368 | ,340 | -,064 | -,431 | -,228 | ,198 | ,372 | ,332 | ,315 | ,318 | ,294 | ,175 | -,356 | ,345 |
| | Sig. (2-tailed) | ,311 | ,020 | ,001 | ,992 | ,814 | ,295 | ,302 | ,238 | ,000 | ,000 | ,000 | ,008 | ,000 | ,243 | ,001 | ,004 | ,593 | ,000 | ,054 | ,095 | ,001 | ,004 | ,007 | ,007 | ,012 | ,141 | ,002 | ,003 |
| Cr | CC (ρ) | ,354 | ,382 | ,213 | -,138 | ,059 | ,398 | ,544 | ,009 | ,303 | ,378 | ,177 | ,021 | -,058 | ,183 | ,148 | ,055 | ,130 | -,078 | -,054 | ,111 | -,035 | -,042 | -,009 | -,032 | -,051 | -,060 | ,042 | -,038 |
| | Sig. (2-tailed) | ,002 | ,001 | ,072 | ,248 | ,625 | ,001 | ,000 | ,942 | ,010 | ,001 | ,138 | ,858 | ,631 | ,124 | ,215 | ,646 | ,278 | ,514 | ,655 | ,352 | ,770 | ,728 | ,943 | ,790 | ,668 | ,616 | ,725 | ,753 |
| Co | CC (ρ) | ,192 | ,340 | ,410 | -,051 | ,101 | ,197 | ,202 | ,098 | ,504 | ,462 | ,547 | ,271 | ,201 | ,112 | ,398 | ,218 | -,101 | -,413 | -,166 | ,277 | ,298 | ,217 | ,230 | ,231 | ,254 | ,193 | -,270 | ,256 |
| | Sig. (2-tailed) | ,106 | ,003 | ,000 | ,668 | ,398 | ,097 | ,088 | ,411 | ,000 | ,000 | ,000 | ,021 | ,091 | ,351 | ,001 | ,066 | ,397 | ,000 | ,163 | ,019 | ,011 | ,067 | ,052 | ,051 | ,032 | ,104 | ,022 | ,030 |
| Ba | CC (ρ) | ,427 | ,397 | ,503 | -,047 | ,114 | ,546 | ,457 | ,106 | ,609 | ,653 | ,477 | ,273 | -,032 | ,096 | ,203 | ,003 | -,174 | -,290 | -,052 | ,244 | ,200 | ,142 | ,146 | ,182 | ,239 | ,278 | -,241 | ,199 |
| | Sig. (2-tailed) | ,000 | ,001 | ,000 | ,696 | ,339 | ,000 | ,000 | ,376 | ,000 | ,000 | ,000 | ,020 | ,788 | ,421 | ,088 | ,979 | ,144 | ,013 | ,665 | ,039 | ,093 | ,233 | ,222 | ,125 | ,043 | ,018 | ,041 | ,094 |
| Ni | CC (ρ) | ,209 | ,351 | ,238 | -,059 | ,124 | ,323 | ,293 | ,187 | ,327 | ,345 | ,459 | ,239 | ,273 | ,128 | ,274 | ,271 | -,023 | -,429 | -,317 | ,231 | ,388 | ,324 | ,296 | ,294 | ,306 | ,218 | -,355 | ,345 |
| | Sig. (2-tailed) | ,078 | ,002 | ,044 | ,625 | ,301 | ,006 | ,012 | ,115 | ,005 | ,003 | ,000 | ,044 | ,020 | ,285 | ,020 | ,021 | ,851 | ,000 | ,007 | ,051 | ,001 | ,005 | ,012 | ,012 | ,009 | ,066 | ,002 | ,003 |
| Cu | CC (ρ) | ,404 | ,402 | ,197 | -,057 | ,315 | **,724** | ,674 | ,217 | ,136 | ,206 | ,031 | ,082 | ,048 | ,382 | ,071 | ,165 | -,037 | -,136 | -,045 | ,087 | -,006 | ,073 | ,117 | ,115 | ,076 | ,048 | -,079 | ,081 |
| | Sig. (2-tailed) | ,000 | ,000 | ,097 | ,636 | ,007 | ,000 | ,000 | ,067 | ,256 | ,082 | ,795 | ,494 | ,689 | ,001 | ,551 | ,165 | ,759 | ,253 | ,704 | ,469 | ,958 | ,541 | ,330 | ,337 | ,527 | ,686 | ,509 | ,500 |
| Zn | CC (ρ) | ,541 | ,415 | ,107 | -,204 | ,229 | ,608 | **,758** | ,521 | ,041 | ,119 | ,103 | ,105 | ,448 | ,453 | ,016 | ,549 | -,057 | -,268 | -,210 | ,187 | ,261 | ,303 | ,285 | ,186 | ,056 | -,093 | -,216 | ,252 |
| | Sig. (2-tailed) | ,000 | ,000 | ,372 | ,086 | ,053 | ,000 | ,000 | ,000 | ,735 | ,320 | ,391 | ,380 | ,000 | ,000 | ,897 | ,000 | ,636 | ,023 | ,077 | ,116 | ,027 | ,010 | ,015 | ,118 | ,642 | ,436 | ,069 | ,033 |
| Ga | CC (ρ) | ,079 | ,150 | ,584 | ,135 | -,022 | ,100 | ,118 | ,028 | ,664 | ,594 | ,635 | ,230 | ,146 | ,118 | ,467 | ,186 | -,128 | -,400 | -,111 | ,244 | ,293 | ,245 | ,246 | ,265 | ,291 | ,223 | -,310 | ,299 |
| | Sig. (2-tailed) | ,511 | ,207 | ,000 | ,258 | ,851 | ,403 | ,322 | ,816 | ,000 | ,000 | ,000 | ,051 | ,221 | ,323 | ,000 | ,118 | ,285 | ,000 | ,353 | ,039 | ,012 | ,038 | ,037 | ,025 | ,013 | ,059 | ,008 | ,011 |
| Ge | CC (ρ) | ,371 | ,261 | ,184 | -,036 | ,115 | ,386 | ,315 | ,186 | ,269 | ,269 | ,152 | ,073 | ,067 | ,165 | ,156 | ,154 | -,162 | -,310 | -,126 | ,143 | ,204 | ,223 | ,212 | ,221 | ,241 | ,247 | -,247 | ,229 |
| | Sig. (2-tailed) | ,001 | ,027 | ,122 | ,764 | ,336 | ,001 | ,007 | ,119 | ,022 | ,022 | ,203 | ,540 | ,578 | ,166 | ,189 | ,198 | ,173 | ,008 | ,293 | ,231 | ,086 | ,059 | ,074 | ,063 | ,041 | ,036 | ,036 | ,053 |
| As | CC (ρ) | ,333 | ,166 | ,259 | -,082 | ,145 | ,384 | ,203 | ,345 | ,227 | ,233 | ,154 | ,155 | ,164 | ,143 | ,077 | ,204 | -,257 | -,338 | -,342 | ,029 | ,299 | ,390 | ,444 | ,456 | ,464 | ,426 | -,452 | ,427 |
| | Sig. (2-tailed) | ,004 | ,164 | ,028 | ,495 | ,224 | ,001 | ,088 | ,003 | ,056 | ,049 | ,195 | ,193 | ,168 | ,231 | ,523 | ,085 | ,030 | ,004 | ,003 | ,807 | ,011 | ,001 | ,000 | ,000 | ,000 | ,000 | ,000 | ,000 |
| Se | CC (ρ) | ,419 | ,384 | -,033 | -,169 | ,119 | ,266 | ,276 | ,508 | ,028 | ,101 | ,135 | ,046 | ,430 | ,217 | ,104 | ,462 | -,016 | -,271 | -,369 | -,020 | ,289 | ,370 | ,375 | ,293 | ,158 | ,028 | -,301 | ,333 |
| | Sig. (2-tailed) | ,000 | ,001 | ,781 | ,155 | ,319 | ,024 | ,019 | ,000 | ,816 | ,399 | ,260 | ,700 | ,000 | ,068 | ,385 | ,000 | ,896 | ,021 | ,001 | ,868 | ,014 | ,001 | ,001 | ,012 | ,186 | ,818 | ,010 | ,004 |
| Br | CC (ρ) | ,410 | ,052 | -,035 | -,235 | ,136 | ,156 | ,301 | **,806** | -,147 | -,080 | -,009 | -,161 | ,626 | ,366 | ,039 | **,776** | -,036 | -,396 | -,411 | ,087 | ,385 | ,554 | ,582 | ,472 | ,230 | -,039 | -,427 | ,486 |
| | Sig. (2-tailed) | ,000 | ,667 | ,769 | ,047 | ,255 | ,192 | ,010 | ,000 | ,219 | ,504 | ,938 | ,176 | ,000 | ,002 | ,748 | ,000 | ,763 | ,001 | ,000 | ,466 | ,001 | ,000 | ,000 | ,000 | ,052 | ,744 | ,000 | ,000 |
| Rb | CC (ρ) | ,204 | ,070 | ,637 | ,097 | -,029 | ,212 | ,069 | ,069 | ,663 | ,548 | ,530 | ,292 | ,226 | -,037 | ,317 | ,137 | -,215 | -,436 | -,165 | ,233 | ,343 | ,341 | ,341 | ,365 | ,378 | ,336 | -,418 | ,399 |
| | Sig. (2-tailed) | ,086 | ,561 | ,000 | ,416 | ,807 | ,074 | ,567 | ,567 | ,000 | ,000 | ,000 | ,013 | ,056 | ,757 | ,007 | ,250 | ,069 | ,000 | ,167 | ,049 | ,003 | ,003 | ,003 | ,002 | ,001 | ,004 | ,000 | ,001 |
| Sr | CC (ρ) | ,013 | ,215 | ,122 | ,131 | -,040 | ,108 | ,050 | -,046 | ,277 | ,406 | ,330 | ,199 | -,118 | -,175 | ,098 | -,162 | ,107 | -,041 | -,043 | ,048 | ,085 | -,053 | -,092 | -,041 | ,077 | ,163 | -,026 | -,013 |
| | Sig. (2-tailed) | ,912 | ,070 | ,309 | ,271 | ,737 | ,368 | ,679 | ,698 | ,019 | ,000 | ,005 | ,094 | ,324 | ,141 | ,415 | ,173 | ,372 | ,730 | ,718 | ,689 | ,478 | ,657 | ,441 | ,735 | ,523 | ,172 | ,826 | ,911 |
| Y | CC (ρ) | ,222 | ,190 | **,719** | ,130 | -,099 | ,246 | ,156 | ,127 | **,807** | **,810** | **,778** | ,365 | ,126 | -,007 | ,399 | ,086 | -,063 | -,421 | -,241 | ,148 | ,292 | ,267 | ,270 | ,311 | ,392 | ,390 | -,358 | ,319 |
| | Sig. (2-tailed) | ,061 | ,110 | ,000 | ,276 | ,407 | ,038 | ,189 | ,288 | ,000 | ,000 | ,000 | ,002 | ,292 | ,954 | ,001 | ,472 | ,598 | ,000 | ,042 | ,214 | ,013 | ,023 | ,022 | ,008 | ,001 | ,001 | ,002 | ,006 |
| Zr | CC (ρ) | ,079 | ,161 | ,453 | ,242 | ,117 | ,291 | ,193 | -,021 | ,492 | ,576 | ,299 | ,012 | -,230 | -,059 | ,219 | -,191 | -,285 | -,347 | -,034 | ,234 | ,208 | ,152 | ,154 | ,211 | ,305 | ,348 | -,273 | ,242 |
| | Sig. (2-tailed) | ,511 | ,178 | ,000 | ,040 | ,326 | ,013 | ,103 | ,858 | ,000 | ,000 | ,011 | ,918 | ,052 | ,622 | ,065 | ,108 | ,015 | ,003 | ,775 | ,048 | ,080 | ,202 | ,197 | ,075 | ,009 | ,003 | ,020 | ,040 |
| Nb | CC (ρ) | ,170 | ,274 | ,697 | ,152 | -,003 | ,284 | ,293 | ,046 | **,796** | **,786** | ,673 | ,232 | ,040 | ,163 | ,394 | ,091 | -,092 | -,368 | -,172 | ,191 | ,226 | ,233 | ,256 | ,269 | ,301 | ,290 | -,290 | ,277 |
| | Sig. (2-tailed) | ,152 | ,020 | ,000 | ,201 | ,983 | ,015 | ,013 | ,703 | ,000 | ,000 | ,000 | ,050 | ,736 | ,171 | ,001 | ,448 | ,441 | ,001 | ,148 | ,108 | ,056 | ,049 | ,030 | ,023 | ,010 | ,013 | ,014 | ,018 |
| Mo | CC (ρ) | ,449 | ,501 | ,024 | -,171 | ,271 | ,626 | **,790** | ,145 | ,074 | ,155 | -,056 | -,025 | -,038 | ,376 | -,010 | ,083 | ,054 | -,048 | -,012 | ,080 | ,001 | ,022 | ,017 | -,011 | -,044 | -,075 | ,003 | ,009 |
| | Sig. (2-tailed) | ,000 | ,000 | ,843 | ,150 | ,021 | ,000 | ,000 | ,224 | ,536 | ,193 | ,638 | ,835 | ,754 | ,001 | ,935 | ,489 | ,655 | ,689 | ,919 | ,502 | ,990 | ,857 | ,886 | ,925 | ,714 | ,532 | ,980 | ,942 |
| Hf | CC (ρ) | ,084 | ,226 | ,354 | ,296 | ,144 | ,336 | ,248 | ,104 | ,347 | ,442 | ,251 | -,068 | -,153 | ,021 | ,091 | -,086 | -,285 | -,297 | -,048 | ,167 | ,181 | ,183 | ,146 | ,174 | ,245 | ,262 | -,247 | ,219 |
| | Sig. (2-tailed) | ,481 | ,057 | ,002 | ,011 | ,229 | ,004 | ,035 | ,384 | ,003 | ,000 | ,034 | ,572 | ,200 | ,861 | ,446 | ,472 | ,015 | ,011 | ,691 | ,160 | ,128 | ,124 | ,222 | ,145 | ,038 | ,026 | ,036 | ,065 |
| W | CC (ρ) | ,605 | ,158 | ,283 | -,127 | ,333 | ,444 | ,494 | ,286 | ,210 | ,245 | ,201 | -,010 | ,089 | ,052 | ,117 | ,147 | -,010 | -,148 | -,130 | ,092 | ,140 | ,111 | ,102 | ,090 | ,085 | ,096 | -,096 | ,104 |
| | Sig. (2-tailed) | ,000 | ,184 | ,016 | ,287 | ,004 | ,000 | ,000 | ,015 | ,077 | ,038 | ,090 | ,932 | ,457 | ,666 | ,326 | ,219 | ,932 | ,216 | ,276 | ,444 | ,242 | ,355 | ,392 | ,452 | ,477 | ,421 | ,421 | ,382 |

| | | Pb | Bi | Th | U | Cd | Sn | Sb | I | La | Ce | Nd | Sm | S | Cl | Yb | LOI | 500-1000 µm | 250-500 µm | 125-250 µm | 63-125 µm | 32-63 µm | 16-32 µm | 8-16 µm | 4-8 µm | 2-4 µm | below 2 µm | 1000-63 µm | 63-2 µm |
|---|---|---|---|---|---|---|---|---|---|---|---|---|---|---|---|---|---|---|---|---|---|---|---|---|---|---|---|---|---|
| Pb | CC (ρ) | | ,354 | ,166 | -,463 | ,313 | ,607 | ,694 | ,402 | ,155 | ,197 | ,126 | ,086 | ,245 | ,122 | ,061 | ,305 | -,025 | -,272 | -,218 | ,108 | ,252 | ,273 | ,265 | ,220 | ,119 | ,094 | -,235 | ,249 |
| | Sig. (2-tailed) | | ,002 | ,164 | ,000 | ,007 | ,000 | ,000 | ,000 | ,195 | ,097 | ,291 | ,473 | ,038 | ,309 | ,612 | ,009 | ,832 | ,021 | ,066 | ,367 | ,033 | ,020 | ,025 | ,063 | ,320 | ,433 | ,047 | ,035 |
| Bi | CC (ρ) | | | ,021 | -,208 | ,215 | ,501 | ,515 | ,062 | ,120 | ,229 | ,203 | -,038 | ,083 | ,324 | ,090 | ,094 | -,032 | -,101 | -,089 | ,139 | ,130 | ,058 | ,054 | ,033 | ,035 | ,011 | -,072 | ,059 |
| | Sig. (2-tailed) | | | ,863 | ,079 | ,070 | ,000 | ,000 | ,606 | ,316 | ,053 | ,088 | ,753 | ,487 | ,006 | ,450 | ,433 | ,792 | ,400 | ,455 | ,246 | ,278 | ,631 | ,655 | ,781 | ,768 | ,926 | ,547 | ,624 |
| Th | CC (ρ) | | | | ,383 | -,021 | ,240 | ,187 | ,058 | **,870** | **,807** | ,681 | ,260 | ,089 | ,102 | ,403 | ,070 | -,196 | -,365 | -,131 | ,176 | ,204 | ,272 | ,299 | ,322 | ,333 | ,297 | -,317 | ,300 |
| | Sig. (2-tailed) | | | | ,001 | ,858 | ,042 | ,116 | ,628 | ,000 | ,000 | ,000 | ,028 | ,458 | ,392 | ,000 | ,562 | ,099 | ,002 | ,273 | ,139 | ,086 | ,021 | ,011 | ,006 | ,004 | ,011 | ,007 | ,011 |
| U | CC (ρ) | | | | | -,136 | -,127 | -,225 | -,090 | ,298 | ,288 | ,227 | ,068 | -,064 | ,017 | ,191 | -,080 | -,101 | -,017 | ,043 | ,022 | -,034 | ,008 | ,025 | ,060 | ,116 | ,106 | -,060 | ,045 |
| | Sig. (2-tailed) | | | | | ,255 | ,289 | ,057 | ,451 | ,011 | ,014 | ,055 | ,568 | ,593 | ,884 | ,108 | ,502 | ,400 | ,889 | ,718 | ,852 | ,779 | ,947 | ,837 | ,617 | ,334 | ,377 | ,615 | ,709 |
| Cd | CC (ρ) | | | | | | ,301 | ,279 | ,090 | -,100 | -,081 | -,082 | -,021 | -,004 | ,041 | ,211 | ,014 | -,114 | -,174 | -,111 | ,077 | ,151 | ,136 | ,141 | ,128 | ,094 | ,083 | -,140 | ,150 |
| | Sig. (2-tailed) | | | | | | ,010 | ,018 | ,452 | ,403 | ,500 | ,496 | ,864 | ,971 | ,735 | ,075 | ,907 | ,341 | ,144 | ,355 | ,519 | ,205 | ,255 | ,238 | ,283 | ,433 | ,487 | ,242 | ,208 |
| Sn | CC (ρ) | | | | | | | **,709** | ,331 | ,234 | ,278 | ,228 | ,047 | ,075 | ,262 | -,034 | ,094 | -,049 | -,126 | -,102 | ,044 | ,035 | ,120 | ,142 | ,154 | ,144 | ,165 | -,134 | ,114 |
| | Sig. (2-tailed) | | | | | | | ,000 | ,005 | ,048 | ,018 | ,054 | ,693 | ,531 | ,026 | ,777 | ,430 | ,685 | ,292 | ,392 | ,713 | ,769 | ,317 | ,233 | ,198 | ,229 | ,166 | ,263 | ,340 |
| Sb | CC (ρ) | | | | | | | | ,315 | ,192 | ,283 | ,115 | ,067 | ,190 | ,408 | ,039 | ,322 | ,069 | -,166 | -,172 | ,044 | ,093 | ,194 | ,179 | ,096 | -,014 | -,100 | -,104 | ,130 |
| | Sig. (2-tailed) | | | | | | | | ,007 | ,106 | ,016 | ,337 | ,574 | ,109 | ,000 | ,745 | ,006 | ,565 | ,163 | ,148 | ,713 | ,436 | ,103 | ,133 | ,422 | ,906 | ,401 | ,386 | ,276 |
| I | CC (ρ) | | | | | | | | | -,037 | ,019 | ,125 | -,180 | ,595 | ,307 | ,052 | **,701** | -,057 | -,378 | -,340 | ,104 | ,369 | ,477 | ,488 | ,394 | ,194 | -,014 | -,377 | ,424 |
| | Sig. (2-tailed) | | | | | | | | | ,760 | ,876 | ,294 | ,131 | ,000 | ,009 | ,664 | ,000 | ,632 | ,001 | ,003 | ,385 | ,001 | ,000 | ,000 | ,001 | ,103 | ,907 | ,001 | ,000 |
| La | CC (ρ) | | | | | | | | | | **,914** | **,764** | ,294 | ,028 | ,018 | ,419 | -,033 | -,045 | -,325 | -,186 | ,072 | ,162 | ,235 | ,270 | ,312 | ,371 | ,379 | -,311 | ,278 |
| | Sig. (2-tailed) | | | | | | | | | | ,000 | ,000 | ,012 | ,816 | ,881 | ,000 | ,782 | ,707 | ,005 | ,118 | ,548 | ,175 | ,046 | ,022 | ,008 | ,001 | ,001 | ,008 | ,018 |
| Ce | CC (ρ) | | | | | | | | | | | **,754** | ,276 | ,012 | ,091 | ,444 | -,018 | -,014 | -,290 | -,167 | ,092 | ,140 | ,192 | ,209 | ,246 | ,311 | ,322 | -,262 | ,228 |
| | Sig. (2-tailed) | | | | | | | | | | | ,000 | ,019 | ,922 | ,446 | ,000 | ,881 | ,908 | ,014 | ,162 | ,443 | ,240 | ,106 | ,077 | ,037 | ,008 | ,006 | ,026 | ,054 |
| Nd | CC (ρ) | | | | | | | | | | | | ,299 | ,177 | -,003 | ,313 | ,088 | -,109 | -,354 | -,203 | ,161 | ,281 | ,267 | ,288 | ,338 | ,402 | ,343 | -,352 | ,320 |
| | Sig. (2-tailed) | | | | | | | | | | | | ,011 | ,136 | ,982 | ,007 | ,461 | ,360 | ,002 | ,088 | ,177 | ,017 | ,024 | ,014 | ,004 | ,000 | ,003 | ,002 | ,006 |
| Sm | CC (ρ) | | | | | | | | | | | | | ,042 | -,158 | ,036 | -,023 | -,018 | -,095 | -,126 | -,157 | ,128 | ,196 | ,178 | ,203 | ,263 | ,282 | -,233 | ,201 |
| | Sig. (2-tailed) | | | | | | | | | | | | | ,729 | ,186 | ,766 | ,846 | ,878 | ,428 | ,293 | ,188 | ,282 | ,098 | ,135 | ,088 | ,026 | ,016 | ,049 | ,091 |
| S | CC (ρ) | | | | | | | | | | | | | | ,347 | ,250 | **,861** | ,035 | -,422 | -,453 | ,093 | ,414 | ,551 | ,538 | ,407 | ,168 | -,090 | -,422 | ,481 |
| | Sig. (2-tailed) | | | | | | | | | | | | | | ,003 | ,035 | ,000 | ,767 | ,000 | ,000 | ,436 | ,000 | ,000 | ,000 | ,000 | ,158 | ,451 | ,000 | ,000 |
| Cl | CC (ρ) | | | | | | | | | | | | | | | ,124 | ,412 | ,235 | ,028 | -,180 | -,087 | -,131 | ,116 | ,164 | ,091 | -,070 | -,251 | ,023 | ,013 |
| | Sig. (2-tailed) | | | | | | | | | | | | | | | ,301 | ,000 | ,047 | ,817 | ,130 | ,470 | ,272 | ,331 | ,168 | ,448 | ,559 | ,034 | ,848 | ,913 |
| Yb | CC (ρ) | | | | | | | | | | | | | | | | ,116 | -,159 | -,330 | -,018 | ,245 | ,131 | ,108 | ,145 | ,158 | ,205 | ,234 | -,177 | ,170 |
| | Sig. (2-tailed) | | | | | | | | | | | | | | | | ,332 | ,183 | ,005 | ,880 | ,038 | ,272 | ,366 | ,224 | ,186 | ,085 | ,047 | ,138 | ,153 |
| LOI | CC (ρ) | | | | | | | | | | | | | | | | | ,040 | -,423 | -,437 | ,093 | ,412 | ,580 | ,561 | ,399 | ,125 | -,186 | -,404 | ,483 |
| | Sig. (2-tailed) | | | | | | | | | | | | | | | | | ,736 | ,000 | ,000 | ,439 | ,000 | ,000 | ,000 | ,001 | ,295 | ,119 | ,000 | ,000 |
| 500-1000 µm | CC (ρ) | | | | | | | | | | | | | | | | | | ,447 | -,326 | -,695 | -,478 | -,201 | -,127 | -,151 | -,192 | -,188 | ,296 | -,294 |
| | Sig. (2-tailed) | | | | | | | | | | | | | | | | | | ,000 | ,005 | ,000 | ,000 | ,091 | ,289 | ,204 | ,106 | ,114 | ,012 | ,012 |
| 250-500 µm | CC (ρ) | | | | | | | | | | | | | | | | | | | ,473 | -,518 | -,895 | -,794 | -,707 | -,670 | -,603 | -,409 | **,830** | -,856 |
| | Sig. (2-tailed) | | | | | | | | | | | | | | | | | | | ,000 | ,000 | ,000 | ,000 | ,000 | ,000 | ,000 | ,000 | ,000 | ,000 |
| 125-250 µm | CC (ρ) | | | | | | | | | | | | | | | | | | | | ,331 | -,485 | -,742 | -,741 | -,689 | -,597 | -,416 | ,694 | -,698 |
| | Sig. (2-tailed) | | | | | | | | | | | | | | | | | | | | ,005 | ,000 | ,000 | ,000 | ,000 | ,000 | ,000 | ,000 | ,000 |
| 63-125 µm | CC (ρ) | | | | | | | | | | | | | | | | | | | | | ,531 | ,077 | -,047 | -,080 | -,095 | -,136 | -,129 | ,165 |
| | Sig. (2-tailed) | | | | | | | | | | | | | | | | | | | | | ,000 | ,518 | ,698 | ,507 | ,426 | ,254 | ,280 | ,165 |
| 32-63 µm | CC (ρ) | | | | | | | | | | | | | | | | | | | | | | **,794** | ,643 | ,588 | ,519 | ,330 | -,813 | **,841** |
| | Sig. (2-tailed) | | | | | | | | | | | | | | | | | | | | | | ,000 | ,000 | ,000 | ,000 | ,005 | ,000 | ,000 |
| 16-32 µm | CC (ρ) | | | | | | | | | | | | | | | | | | | | | | | **,934** | **,859** | **,706** | ,446 | -,936 | **,968** |
| | Sig. (2-tailed) | | | | | | | | | | | | | | | | | | | | | | | ,000 | ,000 | ,000 | ,000 | ,000 | ,000 |
| 8-16 µm | CC (ρ) | | | | | | | | | | | | | | | | | | | | | | | | **,961** | **,794** | ,522 | -,921 | **,933** |
| | Sig. (2-tailed) | | | | | | | | | | | | | | | | | | | | | | | | ,000 | ,000 | ,000 | ,000 | ,000 |
| 4-8 µm | CC (ρ) | | | | | | | | | | | | | | | | | | | | | | | | | **,913** | ,689 | -,927 | **,903** |
| | Sig. (2-tailed) | | | | | | | | | | | | | | | | | | | | | | | | | ,000 | ,000 | ,000 | ,000 |
| 2-4 µm | CC (ρ) | | | | | | | | | | | | | | | | | | | | | | | | | | **,901** | -,868 | **,799** |
| | Sig. (2-tailed) | | | | | | | | | | | | | | | | | | | | | | | | | | ,000 | ,000 | ,000 |
| below 2 µm | CC (ρ) | | | | | | | | | | | | | | | | | | | | | | | | | | | -,663 | ,565 |
| | Sig. (2-tailed) | | | | | | | | | | | | | | | | | | | | | | | | | | | ,000 | ,000 |
| 1000-63 µm | CC (ρ) | | | | | | | | | | | | | | | | | | | | | | | | | | | | -,988 |
| | Sig. (2-tailed) | | | | | | | | | | | | | | | | | | | | | | | | | | | | ,000 |
| 63-2 µm | CC (ρ) | | | | | | | | | | | | | | | | | | | | | | | | | | | | |
| | Sig. (2-tailed) | | | | | | | | | | | | | | | | | | | | | | | | | | | | |

Table 98: Spearman's rank correlation coefficients for RDS winter data (n=72).

| | | Na2O | MgO | Al2O3 | SiO2 | P2O5 | K2O | CaO | TiO2 | MnO | Fe2O3 | Sc | V | Cr | Co | Ba | Ni | Cu | Zn | Ga | Ge | As | Se | Br | Rb | Sr | Y | Zr | Nb | Mo | Hf | W |
|---|---|---|---|---|---|---|---|---|---|---|---|---|---|---|---|---|---|---|---|---|---|---|---|---|---|---|---|---|---|---|---|---|
| Na2O | CC (ρ) | | ,540 | ,553 | ,333 | -,234 | ,361 | -,138 | ,466 | ,396 | ,492 | ,366 | ,326 | ,419 | ,364 | ,269 | ,298 | ,215 | ,122 | ,430 | -,073 | -,040 | -,464 | -,163 | ,229 | ,375 | ,372 | ,319 | ,449 | ,260 | ,236 | -,009 |
| | Sig. (2-tailed) | | ,000 | ,000 | ,004 | ,048 | ,002 | ,249 | ,000 | ,001 | ,000 | ,002 | ,005 | ,000 | ,002 | ,022 | ,011 | ,070 | ,309 | ,000 | ,545 | ,741 | ,000 | ,172 | ,053 | ,001 | ,001 | ,006 | ,000 | ,028 | ,046 | ,937 |
| MgO | CC (ρ) | | | **,735** | -,189 | ,240 | ,371 | ,037 | **,894** | **,760** | **,760** | ,590 | **,842** | ,632 | **,711** | ,403 | ,695 | ,392 | ,484 | ,671 | ,200 | ,134 | -,100 | ,117 | ,407 | ,445 | **,703** | ,196 | ,667 | ,305 | ,140 | ,056 |
| | Sig. (2-tailed) | | | ,000 | ,112 | ,042 | ,001 | ,760 | ,000 | ,000 | ,000 | ,000 | ,000 | ,000 | ,000 | ,000 | ,000 | ,001 | ,000 | ,000 | ,092 | ,261 | ,401 | ,327 | ,000 | ,000 | ,000 | ,099 | ,000 | ,009 | ,240 | ,640 |
| Al2O3 | CC (ρ) | | | | -,048 | ,242 | **,707** | -,104 | **,838** | **,718** | **,733** | **,736** | **,806** | ,383 | ,646 | ,511 | ,580 | ,280 | ,207 | **,872** | ,416 | ,309 | -,091 | ,060 | **,755** | ,355 | **,849** | ,463 | **,841** | ,178 | ,439 | ,111 |
| | Sig. (2-tailed) | | | | ,686 | ,040 | ,000 | ,385 | ,000 | ,000 | ,000 | ,000 | ,000 | ,001 | ,000 | ,000 | ,000 | ,017 | ,081 | ,000 | ,000 | ,008 | ,445 | ,618 | ,000 | ,002 | ,000 | ,000 | ,000 | ,135 | ,000 | ,354 |
| SiO2 | CC (ρ) | | | | | -,581 | ,115 | -,275 | -,285 | -,262 | -,220 | -,283 | -,375 | -,112 | -,319 | -,084 | -,319 | -,238 | -,413 | -,289 | -,222 | -,258 | -,591 | -,525 | -,046 | -,255 | -,331 | ,138 | -,229 | -,156 | ,110 | -,223 |
| | Sig. (2-tailed) | | | | | ,000 | ,334 | ,020 | ,015 | ,026 | ,064 | ,016 | ,001 | ,351 | ,006 | ,482 | ,006 | ,044 | ,000 | ,014 | ,061 | ,029 | ,000 | ,000 | ,702 | ,031 | ,004 | ,247 | ,053 | ,190 | ,356 | ,060 |
| P2O5 | CC (ρ) | | | | | | ,134 | -,430 | ,347 | ,210 | ,233 | ,328 | ,510 | ,067 | ,269 | ,059 | ,395 | ,159 | ,355 | ,408 | ,398 | ,383 | ,642 | **,752** | ,291 | -,275 | ,340 | -,043 | ,262 | ,005 | ,018 | ,214 |
| | Sig. (2-tailed) | | | | | | ,260 | ,000 | ,003 | ,076 | ,049 | ,005 | ,000 | ,573 | ,022 | ,620 | ,001 | ,181 | ,002 | ,000 | ,001 | ,001 | ,000 | ,000 | ,013 | ,019 | ,004 | ,721 | ,026 | ,968 | ,884 | ,071 |
| K2O | CC (ρ) | | | | | | | -,235 | ,516 | ,405 | ,491 | ,415 | ,476 | ,125 | ,387 | ,664 | ,345 | ,229 | ,171 | ,535 | ,417 | ,450 | -,013 | ,156 | **,916** | ,174 | ,622 | ,568 | ,643 | ,187 | ,608 | ,187 |
| | Sig. (2-tailed) | | | | | | | ,047 | ,000 | ,000 | ,000 | ,000 | ,000 | ,295 | ,001 | ,000 | ,003 | ,052 | ,152 | ,000 | ,000 | ,000 | ,912 | ,191 | ,000 | ,144 | ,000 | ,000 | ,000 | ,115 | ,000 | ,115 |
| CaO | CC (ρ) | | | | | | | | -,001 | ,173 | ,038 | -,019 | -,039 | ,141 | ,077 | ,138 | -,024 | ,031 | -,057 | -,079 | -,235 | -,086 | -,104 | -,403 | -,178 | ,870 | ,069 | -,049 | ,042 | ,029 | -,100 | ,011 |
| | Sig. (2-tailed) | | | | | | | | ,995 | ,147 | ,752 | ,875 | ,742 | ,237 | ,522 | ,247 | ,838 | ,794 | ,636 | ,512 | ,047 | ,474 | ,383 | ,000 | ,135 | ,000 | ,563 | ,681 | ,726 | ,810 | ,404 | ,927 |
| TiO2 | CC (ρ) | | | | | | | | | **,825** | **,846** | **,739** | **,900** | ,580 | **,831** | ,529 | **,787** | ,459 | ,495 | **,814** | ,383 | ,236 | ,076 | ,216 | ,522 | ,419 | **,827** | ,350 | **,814** | ,327 | ,332 | ,208 |
| | Sig. (2-tailed) | | | | | | | | | ,000 | ,000 | ,000 | ,000 | ,000 | ,000 | ,000 | ,000 | ,000 | ,000 | ,000 | ,001 | ,046 | ,524 | ,069 | ,000 | ,000 | ,000 | ,003 | ,000 | ,005 | ,004 | ,080 |
| MnO | CC (ρ) | | | | | | | | | | **,853** | ,661 | **,807** | ,592 | **,777** | ,525 | **,732** | ,444 | ,427 | **,716** | ,373 | ,258 | ,080 | ,078 | ,429 | ,540 | **,829** | ,377 | **,773** | ,338 | ,366 | ,244 |
| | Sig. (2-tailed) | | | | | | | | | | ,000 | ,000 | ,000 | ,000 | ,000 | ,000 | ,000 | ,000 | ,000 | ,000 | ,001 | ,029 | ,506 | ,513 | ,000 | ,000 | ,000 | ,001 | ,000 | ,004 | ,002 | ,039 |
| Fe2O3 | CC (ρ) | | | | | | | | | | | ,617 | **,800** | **,704** | **,867** | ,643 | **,867** | ,633 | ,563 | **,748** | ,390 | ,379 | ,097 | ,175 | ,444 | ,479 | **,797** | ,443 | **,817** | ,515 | ,401 | ,312 |
| | Sig. (2-tailed) | | | | | | | | | | | ,000 | ,000 | ,000 | ,000 | ,000 | ,000 | ,000 | ,000 | ,000 | ,001 | ,001 | ,417 | ,143 | ,000 | ,000 | ,000 | ,000 | ,000 | ,000 | ,000 | ,008 |
| Sc | CC (ρ) | | | | | | | | | | | | **,725** | ,308 | ,662 | ,373 | ,553 | ,274 | ,217 | **,794** | ,410 | ,369 | ,175 | ,211 | ,445 | ,333 | **,707** | ,366 | ,639 | ,119 | ,388 | ,213 |
| | Sig. (2-tailed) | | | | | | | | | | | | ,000 | ,008 | ,000 | ,001 | ,000 | ,020 | ,068 | ,000 | ,000 | ,001 | ,141 | ,075 | ,000 | ,004 | ,000 | ,002 | ,000 | ,321 | ,001 | ,073 |
| V | CC (ρ) | | | | | | | | | | | | | ,461 | **,815** | ,471 | **,819** | ,347 | ,418 | **,815** | ,487 | ,361 | ,219 | ,306 | ,556 | ,371 | **,838** | ,208 | **,749** | ,178 | ,205 | ,189 |
| | Sig. (2-tailed) | | | | | | | | | | | | | ,000 | ,000 | ,000 | ,000 | ,003 | ,000 | ,000 | ,000 | ,002 | ,065 | ,009 | ,000 | ,001 | ,000 | ,080 | ,000 | ,134 | ,084 | ,113 |
| Cr | CC (ρ) | | | | | | | | | | | | | | ,602 | ,454 | ,649 | ,664 | ,617 | ,428 | ,020 | ,177 | ,058 | ,085 | ,102 | ,402 | ,447 | ,370 | ,504 | ,641 | ,291 | ,322 |
| | Sig. (2-tailed) | | | | | | | | | | | | | | ,000 | ,000 | ,000 | ,000 | ,000 | ,000 | ,869 | ,138 | ,629 | ,478 | ,396 | ,000 | ,000 | ,001 | ,000 | ,000 | ,013 | ,006 |
| Co | CC (ρ) | | | | | | | | | | | | | | | ,574 | **,875** | ,467 | ,464 | ,685 | ,442 | ,374 | ,233 | ,228 | ,347 | ,434 | **,739** | ,334 | **,707** | ,342 | ,286 | ,291 |
| | Sig. (2-tailed) | | | | | | | | | | | | | | | ,000 | ,000 | ,000 | ,000 | ,000 | ,000 | ,001 | ,049 | ,055 | ,003 | ,000 | ,000 | ,004 | ,000 | ,003 | ,015 | ,013 |
| Ba | CC (ρ) | | | | | | | | | | | | | | | | ,483 | ,489 | ,376 | ,517 | ,370 | ,513 | ,146 | ,114 | ,579 | ,453 | ,616 | ,445 | ,626 | ,332 | ,496 | ,349 |
| | Sig. (2-tailed) | | | | | | | | | | | | | | | | ,000 | ,000 | ,001 | ,000 | ,001 | ,000 | ,222 | ,339 | ,000 | ,000 | ,000 | ,000 | ,000 | ,004 | ,000 | ,003 |
| Ni | CC (ρ) | | | | | | | | | | | | | | | | | ,573 | ,563 | ,632 | ,433 | ,405 | ,340 | ,344 | ,324 | ,355 | ,681 | ,275 | ,662 | ,399 | ,228 | ,351 |
| | Sig. (2-tailed) | | | | | | | | | | | | | | | | | ,000 | ,000 | ,000 | ,000 | ,000 | ,003 | ,003 | ,005 | ,002 | ,000 | ,019 | ,000 | ,001 | ,054 | ,003 |
| Cu | CC (ρ) | | | | | | | | | | | | | | | | | | **,769** | ,343 | ,193 | ,309 | ,207 | ,285 | ,166 | ,266 | ,375 | ,387 | ,417 | ,684 | ,353 | ,364 |
| | Sig. (2-tailed) | | | | | | | | | | | | | | | | | | ,000 | ,003 | ,104 | ,008 | ,081 | ,015 | ,164 | ,024 | ,001 | ,001 | ,000 | ,000 | ,002 | ,002 |
| Zn | CC (ρ) | | | | | | | | | | | | | | | | | | | ,266 | ,197 | ,235 | ,352 | ,548 | ,125 | ,118 | ,344 | ,227 | ,406 | **,749** | ,244 | ,391 |
| | Sig. (2-tailed) | | | | | | | | | | | | | | | | | | | ,024 | ,096 | ,047 | ,002 | ,000 | ,295 | ,323 | ,003 | ,055 | ,000 | ,000 | ,039 | ,001 |
| Ga | CC (ρ) | | | | | | | | | | | | | | | | | | | | ,379 | ,338 | ,095 | ,214 | ,631 | ,349 | **,849** | ,373 | **,820** | ,203 | ,373 | ,241 |
| | Sig. (2-tailed) | | | | | | | | | | | | | | | | | | | | ,001 | ,004 | ,426 | ,072 | ,000 | ,003 | ,000 | ,001 | ,000 | ,088 | ,001 | ,042 |
| Ge | CC (ρ) | | | | | | | | | | | | | | | | | | | | | ,579 | ,419 | ,345 | ,451 | -,062 | ,488 | ,165 | ,377 | ,062 | ,185 | ,234 |
| | Sig. (2-tailed) | | | | | | | | | | | | | | | | | | | | | ,000 | ,000 | ,003 | ,000 | ,605 | ,000 | ,165 | ,001 | ,602 | ,119 | ,048 |
| As | CC (ρ) | | | | | | | | | | | | | | | | | | | | | | ,514 | ,371 | ,503 | ,170 | ,419 | ,271 | ,385 | ,157 | ,306 | ,376 |
| | Sig. (2-tailed) | | | | | | | | | | | | | | | | | | | | | | ,000 | ,001 | ,000 | ,154 | ,000 | ,021 | ,001 | ,189 | ,009 | ,001 |
| Se | CC (ρ) | | | | | | | | | | | | | | | | | | | | | | | ,656 | ,051 | -,124 | ,156 | ,014 | ,091 | ,050 | ,092 | ,423 |
| | Sig. (2-tailed) | | | | | | | | | | | | | | | | | | | | | | | ,000 | ,672 | ,299 | ,190 | ,904 | ,446 | ,675 | ,442 | ,000 |
| Br | CC (ρ) | | | | | | | | | | | | | | | | | | | | | | | | ,198 | -,248 | ,210 | ,040 | ,169 | ,210 | ,113 | ,288 |
| | Sig. (2-tailed) | | | | | | | | | | | | | | | | | | | | | | | | ,095 | ,036 | ,077 | ,741 | ,156 | ,076 | ,344 | ,014 |
| Rb | CC (ρ) | | | | | | | | | | | | | | | | | | | | | | | | | ,147 | **,710** | ,484 | ,685 | ,098 | ,497 | ,159 |
| | Sig. (2-tailed) | | | | | | | | | | | | | | | | | | | | | | | | | ,217 | ,000 | ,000 | ,000 | ,414 | ,000 | ,183 |
| Sr | CC (ρ) | | | | | | | | | | | | | | | | | | | | | | | | | | ,474 | ,116 | ,416 | ,126 | ,099 | ,091 |
| | Sig. (2-tailed) | | | | | | | | | | | | | | | | | | | | | | | | | | ,000 | ,331 | ,000 | ,291 | ,407 | ,450 |
| Y | CC (ρ) | | | | | | | | | | | | | | | | | | | | | | | | | | | ,454 | **,868** | ,219 | ,421 | ,225 |
| | Sig. (2-tailed) | | | | | | | | | | | | | | | | | | | | | | | | | | | ,000 | ,000 | ,065 | ,000 | ,058 |
| Zr | CC (ρ) | | | | | | | | | | | | | | | | | | | | | | | | | | | | ,530 | ,414 | **,867** | ,191 |
| | Sig. (2-tailed) | | | | | | | | | | | | | | | | | | | | | | | | | | | | ,000 | ,000 | ,000 | ,109 |
| Nb | CC (ρ) | | | | | | | | | | | | | | | | | | | | | | | | | | | | | ,366 | ,522 | ,300 |
| | Sig. (2-tailed) | | | | | | | | | | | | | | | | | | | | | | | | | | | | | ,002 | ,000 | ,011 |
| Mo | CC (ρ) | | | | | | | | | | | | | | | | | | | | | | | | | | | | | | ,360 | ,428 |
| | Sig. (2-tailed) | | | | | | | | | | | | | | | | | | | | | | | | | | | | | | ,002 | ,000 |
| Hf | CC (ρ) | | | | | | | | | | | | | | | | | | | | | | | | | | | | | | | ,255 |
| | Sig. (2-tailed) | | | | | | | | | | | | | | | | | | | | | | | | | | | | | | | ,031 |
| W | CC (ρ) | | | | | | | | | | | | | | | | | | | | | | | | | | | | | | | |
| | Sig. (2-tailed) | | | | | | | | | | | | | | | | | | | | | | | | | | | | | | | |

| | | Pb | Bi | Th | U | Cd | Sn | Sb | I | La | Ce | Nd | Sm | S | Cl | Yb | LOI (%) | 500-1000 µm | 250-500 µm | 125-250 µm | 63-125 µm | 32-63 µm | 16-32 µm | 8-16 µm | 4-8 µm | 2-4 µm | below 2 µm | 1000-63 µm | 63-2 µm |
|---|---|---|---|---|---|---|---|---|---|---|---|---|---|---|---|---|---|---|---|---|---|---|---|---|---|---|---|---|---|
| Na2O | CC (ρ) | -,072 | -,062 | ,280 | -,017 | -,290 | -,033 | ,203 | -,321 | ,352 | ,508 | ,335 | ,046 | -,071 | ,382 | ,007 | -,204 | ,126 | ,063 | ,053 | -,062 | -,137 | -,137 | -,161 | -,153 | -,108 | -,035 | ,157 | -,157 |
| | Sig. (2-tailed) | ,547 | ,602 | ,017 | ,888 | ,013 | ,783 | ,088 | ,006 | ,002 | ,000 | ,004 | ,700 | ,554 | ,001 | ,954 | ,088 | ,292 | ,597 | ,659 | ,606 | ,251 | ,252 | ,176 | ,199 | ,365 | ,769 | ,187 | ,189 |
| MgO | CC (ρ) | ,200 | ,189 | ,359 | ,008 | ,119 | ,257 | ,419 | ,122 | ,499 | ,481 | ,506 | ,046 | ,439 | ,254 | ,240 | ,218 | -,191 | -,407 | -,391 | -,021 | ,300 | ,343 | ,355 | ,374 | ,370 | ,368 | -,345 | ,344 |
| | Sig. (2-tailed) | ,092 | ,111 | ,002 | ,946 | ,319 | ,029 | ,000 | ,306 | ,000 | ,000 | ,000 | ,699 | ,000 | ,032 | ,042 | ,068 | ,108 | ,000 | ,001 | ,860 | ,010 | ,003 | ,002 | ,001 | ,001 | ,001 | ,003 | ,003 |
| Al2O3 | CC (ρ) | ,161 | -,055 | **,736** | ,337 | -,042 | ,108 | ,205 | ,091 | **,791** | **,732** | **,754** | ,315 | ,320 | ,102 | ,245 | ,153 | -,253 | -,384 | -,308 | -,015 | ,241 | ,305 | ,331 | ,385 | ,401 | ,393 | -,321 | ,315 |
| | Sig. (2-tailed) | ,176 | ,648 | ,000 | ,004 | ,727 | ,368 | ,083 | ,447 | ,000 | ,000 | ,000 | ,007 | ,006 | ,393 | ,038 | ,204 | ,032 | ,001 | ,008 | ,898 | ,042 | ,009 | ,004 | ,001 | ,000 | ,001 | ,006 | ,007 |
| SiO2 | CC (ρ) | -,450 | -,431 | -,101 | -,186 | -,475 | -,374 | -,296 | -,583 | -,187 | -,056 | -,294 | -,052 | -,793 | -,218 | -,125 | -,705 | ,119 | ,514 | ,636 | ,090 | -,444 | -,544 | -,546 | -,528 | -,474 | -,381 | ,520 | -,531 |
| | Sig. (2-tailed) | ,000 | ,000 | ,400 | ,118 | ,000 | ,001 | ,012 | ,000 | ,116 | ,643 | ,012 | ,667 | ,000 | ,066 | ,295 | ,000 | ,320 | ,000 | ,000 | ,450 | ,000 | ,000 | ,000 | ,000 | ,000 | ,001 | ,000 | ,000 |
| P2O5 | CC (ρ) | ,401 | ,187 | ,207 | ,070 | ,269 | ,229 | ,182 | **,829** | ,114 | ,007 | ,222 | ,023 | ,680 | ,101 | ,242 | **,842** | -,165 | -,486 | -,466 | ,105 | ,452 | ,536 | ,525 | ,459 | ,328 | ,107 | -,433 | ,478 |
| | Sig. (2-tailed) | ,000 | ,115 | ,081 | ,561 | ,022 | ,053 | ,125 | ,000 | ,340 | ,956 | ,060 | ,846 | ,000 | ,396 | ,041 | ,000 | ,167 | ,000 | ,000 | ,382 | ,000 | ,000 | ,000 | ,000 | ,005 | ,370 | ,000 | ,000 |
| K2O | CC (ρ) | ,229 | -,124 | ,675 | ,319 | -,167 | ,143 | ,218 | ,134 | ,688 | ,634 | ,582 | ,251 | ,268 | ,075 | ,196 | ,100 | -,311 | -,332 | -,233 | ,044 | ,287 | ,338 | ,323 | ,330 | ,313 | ,315 | -,343 | ,330 |
| | Sig. (2-tailed) | ,053 | ,298 | ,000 | ,006 | ,161 | ,231 | ,065 | ,262 | ,000 | ,000 | ,000 | ,033 | ,023 | ,529 | ,099 | ,405 | ,008 | ,004 | ,049 | ,715 | ,015 | ,004 | ,006 | ,005 | ,007 | ,007 | ,003 | ,005 |
| CaO | CC (ρ) | -,017 | ,210 | -,106 | ,111 | ,317 | ,116 | ,059 | -,307 | ,155 | ,147 | ,128 | -,035 | -,072 | -,061 | -,060 | -,370 | -,024 | -,007 | -,154 | -,168 | -,019 | -,064 | -,011 | ,083 | ,187 | ,332 | -,064 | ,012 |
| | Sig. (2-tailed) | ,888 | ,076 | ,378 | ,355 | ,007 | ,333 | ,623 | ,009 | ,194 | ,218 | ,283 | ,770 | ,549 | ,613 | ,618 | ,001 | ,842 | ,953 | ,198 | ,158 | ,875 | ,594 | ,928 | ,490 | ,116 | ,004 | ,592 | ,919 |
| TiO2 | CC (ρ) | ,337 | ,174 | ,549 | ,154 | ,207 | ,330 | ,410 | ,252 | ,649 | ,572 | ,641 | ,185 | ,511 | ,194 | ,358 | ,329 | -,334 | -,567 | -,398 | ,120 | ,458 | ,485 | ,479 | ,488 | ,474 | ,447 | -,488 | ,491 |
| | Sig. (2-tailed) | ,004 | ,145 | ,000 | ,196 | ,082 | ,005 | ,000 | ,033 | ,000 | ,000 | ,000 | ,120 | ,000 | ,103 | ,002 | ,005 | ,004 | ,000 | ,001 | ,314 | ,000 | ,000 | ,000 | ,000 | ,000 | ,000 | ,000 | ,000 |
| MnO | CC (ρ) | ,282 | ,249 | ,499 | ,231 | ,290 | ,304 | ,385 | ,168 | ,635 | ,614 | ,671 | ,189 | ,403 | ,116 | ,252 | ,130 | -,244 | -,497 | -,402 | ,085 | ,407 | ,391 | ,398 | ,434 | ,436 | ,452 | -,425 | ,410 |
| | Sig. (2-tailed) | ,017 | ,035 | ,000 | ,051 | ,014 | ,010 | ,001 | ,157 | ,000 | ,000 | ,000 | ,111 | ,000 | ,331 | ,033 | ,279 | ,039 | ,000 | ,000 | ,478 | ,000 | ,001 | ,001 | ,000 | ,000 | ,000 | ,000 | ,000 |
| Fe2O3 | CC (ρ) | ,464 | ,309 | ,502 | ,078 | ,174 | ,481 | ,571 | ,179 | ,611 | ,613 | **,701** | ,148 | ,453 | ,236 | ,319 | ,214 | -,312 | -,508 | -,326 | ,121 | ,446 | ,441 | ,409 | ,408 | ,403 | ,423 | -,443 | ,439 |
| | Sig. (2-tailed) | ,000 | ,008 | ,000 | ,513 | ,144 | ,000 | ,000 | ,132 | ,000 | ,000 | ,000 | ,213 | ,000 | ,046 | ,006 | ,074 | ,008 | ,000 | ,005 | ,313 | ,000 | ,000 | ,000 | ,000 | ,000 | ,000 | ,000 | ,000 |
| Sc | CC (ρ) | ,201 | -,016 | ,582 | ,358 | ,076 | ,172 | ,164 | ,224 | ,575 | ,500 | ,571 | ,296 | ,381 | ,193 | ,360 | ,247 | -,269 | -,466 | -,353 | ,020 | ,330 | ,384 | ,397 | ,442 | ,447 | ,389 | -,398 | ,405 |
| | Sig. (2-tailed) | ,091 | ,893 | ,000 | ,002 | ,528 | ,148 | ,168 | ,059 | ,000 | ,000 | ,000 | ,012 | ,001 | ,104 | ,002 | ,038 | ,022 | ,000 | ,002 | ,865 | ,005 | ,001 | ,001 | ,000 | ,000 | ,001 | ,001 | ,000 |
| V | CC (ρ) | ,318 | ,195 | ,501 | ,197 | ,231 | ,277 | ,307 | ,380 | ,587 | ,497 | ,674 | ,151 | ,596 | ,119 | ,317 | ,425 | -,283 | -,543 | -,472 | ,042 | ,438 | ,488 | ,510 | ,521 | ,478 | ,401 | -,484 | ,491 |
| | Sig. (2-tailed) | ,007 | ,101 | ,000 | ,097 | ,051 | ,018 | ,009 | ,001 | ,000 | ,000 | ,000 | ,206 | ,000 | ,318 | ,007 | ,000 | ,016 | ,000 | ,000 | ,727 | ,000 | ,000 | ,000 | ,000 | ,000 | ,000 | ,000 | ,000 |
| Cr | CC (ρ) | ,462 | ,461 | ,215 | -,172 | ,272 | ,535 | **,745** | ,072 | ,327 | ,476 | ,359 | -,019 | ,282 | ,293 | ,140 | ,108 | -,242 | -,436 | -,277 | ,155 | ,367 | ,291 | ,258 | ,264 | ,268 | ,301 | -,319 | ,315 |
| | Sig. (2-tailed) | ,000 | ,000 | ,070 | ,149 | ,021 | ,000 | ,000 | ,548 | ,005 | ,000 | ,002 | ,872 | ,016 | ,012 | ,241 | ,368 | ,040 | ,000 | ,019 | ,195 | ,001 | ,013 | ,029 | ,025 | ,023 | ,010 | ,006 | ,007 |
| Co | CC (ρ) | ,432 | ,246 | ,440 | ,075 | ,251 | ,377 | ,443 | ,256 | ,515 | ,520 | ,631 | ,121 | ,457 | ,159 | ,282 | ,266 | -,298 | -,540 | -,423 | ,078 | ,464 | ,472 | ,455 | ,462 | ,455 | ,447 | -,488 | ,491 |
| | Sig. (2-tailed) | ,000 | ,037 | ,000 | ,531 | ,033 | ,001 | ,000 | ,030 | ,000 | ,000 | ,000 | ,312 | ,000 | ,182 | ,016 | ,025 | ,011 | ,000 | ,000 | ,514 | ,000 | ,000 | ,000 | ,000 | ,000 | ,000 | ,000 | ,000 |
| Ba | CC (ρ) | ,537 | ,218 | ,553 | ,137 | ,103 | ,457 | ,545 | ,207 | ,635 | ,649 | ,612 | ,144 | ,318 | ,061 | ,247 | ,031 | -,231 | -,338 | -,342 | ,008 | ,306 | ,320 | ,309 | ,329 | ,321 | ,361 | -,354 | ,329 |
| | Sig. (2-tailed) | ,000 | ,066 | ,000 | ,250 | ,390 | ,000 | ,000 | ,081 | ,000 | ,000 | ,000 | ,229 | ,007 | ,608 | ,037 | ,799 | ,051 | ,004 | ,003 | ,946 | ,009 | ,006 | ,008 | ,005 | ,006 | ,002 | ,002 | ,005 |
| Ni | CC (ρ) | ,521 | ,353 | ,338 | -,038 | ,302 | ,488 | ,517 | ,354 | ,419 | ,411 | ,558 | ,008 | ,555 | ,170 | ,246 | ,368 | -,363 | -,603 | -,366 | ,184 | ,549 | ,514 | ,485 | ,484 | ,459 | ,420 | -,522 | ,530 |
| | Sig. (2-tailed) | ,000 | ,002 | ,004 | ,753 | ,010 | ,000 | ,000 | ,002 | ,000 | ,000 | ,000 | ,949 | ,000 | ,154 | ,038 | ,002 | ,002 | ,000 | ,002 | ,122 | ,000 | ,000 | ,000 | ,000 | ,000 | ,000 | ,000 | ,000 |
| Cu | CC (ρ) | ,647 | ,485 | ,280 | -,030 | ,316 | **,767** | **,794** | ,298 | ,336 | ,382 | ,358 | ,023 | ,396 | ,450 | ,166 | ,287 | -,308 | -,436 | -,235 | ,168 | ,402 | ,400 | ,355 | ,345 | ,335 | ,345 | -,389 | ,390 |
| | Sig. (2-tailed) | ,000 | ,000 | ,017 | ,803 | ,007 | ,000 | ,000 | ,011 | ,004 | ,001 | ,002 | ,850 | ,001 | ,000 | ,164 | ,015 | ,008 | ,000 | ,047 | ,157 | ,000 | ,001 | ,002 | ,003 | ,004 | ,003 | ,001 | ,001 |
| Zn | CC (ρ) | ,676 | ,585 | ,169 | -,171 | ,369 | **,734** | **,869** | ,490 | ,249 | ,258 | ,259 | -,081 | ,613 | ,436 | ,139 | ,533 | -,345 | -,567 | -,407 | ,172 | ,551 | ,587 | ,533 | ,468 | ,400 | ,363 | -,537 | ,547 |
| | Sig. (2-tailed) | ,000 | ,000 | ,155 | ,151 | ,001 | ,000 | ,000 | ,000 | ,035 | ,029 | ,028 | ,499 | ,000 | ,000 | ,245 | ,000 | ,003 | ,000 | ,000 | ,148 | ,000 | ,000 | ,000 | ,000 | ,000 | ,002 | ,000 | ,000 |
| Ga | CC (ρ) | ,288 | ,048 | **,711** | ,343 | ,060 | ,178 | ,259 | ,211 | **,733** | ,642 | **,741** | ,390 | ,493 | ,121 | ,337 | ,330 | -,265 | -,488 | -,380 | ,037 | ,341 | ,384 | ,404 | ,444 | ,445 | ,395 | -,397 | ,398 |
| | Sig. (2-tailed) | ,014 | ,688 | ,000 | ,003 | ,619 | ,136 | ,028 | ,075 | ,000 | ,000 | ,000 | ,001 | ,000 | ,312 | ,004 | ,005 | ,024 | ,000 | ,001 | ,756 | ,003 | ,001 | ,000 | ,000 | ,000 | ,001 | ,001 | ,001 |
| Ge | CC (ρ) | ,392 | ,034 | ,488 | ,193 | ,049 | ,241 | ,143 | ,449 | ,365 | ,300 | ,493 | ,102 | ,352 | -,034 | ,159 | ,300 | -,279 | -,400 | -,258 | ,111 | ,386 | ,415 | ,422 | ,459 | ,428 | ,311 | -,426 | ,427 |
| | Sig. (2-tailed) | ,001 | ,775 | ,000 | ,104 | ,681 | ,041 | ,232 | ,000 | ,002 | ,011 | ,000 | ,395 | ,002 | ,778 | ,183 | ,011 | ,018 | ,000 | ,028 | ,354 | ,001 | ,000 | ,000 | ,000 | ,000 | ,008 | ,000 | ,000 |
| As | CC (ρ) | ,517 | ,194 | ,402 | ,210 | -,027 | ,406 | ,359 | ,394 | ,368 | ,431 | ,421 | ,060 | ,443 | ,227 | ,098 | ,295 | -,253 | -,400 | -,399 | -,029 | ,344 | ,390 | ,405 | ,452 | ,442 | ,369 | -,430 | ,419 |
| | Sig. (2-tailed) | ,000 | ,103 | ,000 | ,077 | ,822 | ,000 | ,002 | ,001 | ,001 | ,000 | ,000 | ,617 | ,000 | ,055 | ,415 | ,013 | ,032 | ,001 | ,001 | ,808 | ,003 | ,001 | ,000 | ,000 | ,000 | ,001 | ,000 | ,000 |
| Se | CC (ρ) | ,569 | ,327 | ,074 | ,011 | ,425 | ,351 | ,267 | **,738** | -,011 | -,035 | ,102 | -,045 | ,576 | ,054 | ,173 | ,594 | -,324 | -,557 | -,414 | ,217 | ,574 | ,542 | ,512 | ,473 | ,380 | ,222 | -,523 | ,544 |
| | Sig. (2-tailed) | ,000 | ,005 | ,539 | ,927 | ,000 | ,003 | ,023 | ,000 | ,925 | ,768 | ,395 | ,709 | ,000 | ,653 | ,146 | ,000 | ,006 | ,000 | ,000 | ,067 | ,000 | ,000 | ,000 | ,000 | ,001 | ,061 | ,000 | ,000 |
| Br | CC (ρ) | ,564 | ,274 | ,120 | -,034 | ,230 | ,361 | ,404 | **,802** | ,049 | ,040 | ,132 | -,029 | **,700** | ,276 | ,150 | **,808** | -,243 | -,499 | -,432 | ,127 | ,507 | ,591 | ,541 | ,449 | ,313 | ,108 | -,483 | ,524 |
| | Sig. (2-tailed) | ,000 | ,020 | ,315 | ,778 | ,052 | ,002 | ,000 | ,000 | ,681 | ,740 | ,268 | ,810 | ,000 | ,019 | ,208 | ,000 | ,040 | ,000 | ,000 | ,288 | ,000 | ,000 | ,000 | ,000 | ,007 | ,368 | ,000 | ,000 |
| Rb | CC (ρ) | ,223 | -,139 | **,759** | ,428 | -,102 | ,093 | ,153 | ,216 | **,746** | ,682 | ,649 | ,244 | ,371 | ,058 | ,183 | ,205 | -,291 | -,372 | -,356 | -,025 | ,271 | ,349 | ,378 | ,426 | ,416 | ,369 | -,373 | ,357 |
| | Sig. (2-tailed) | ,059 | ,244 | ,000 | ,000 | ,394 | ,438 | ,200 | ,069 | ,000 | ,000 | ,000 | ,039 | ,001 | ,629 | ,123 | ,087 | ,013 | ,001 | ,002 | ,832 | ,021 | ,003 | ,001 | ,000 | ,000 | ,001 | ,001 | ,002 |
| Sr | CC (ρ) | ,141 | ,255 | ,125 | ,164 | ,181 | ,212 | ,279 | -,197 | ,439 | ,450 | ,477 | ,104 | ,203 | ,164 | ,014 | -,206 | ,012 | -,137 | -,341 | -,255 | ,058 | ,065 | ,095 | ,170 | ,253 | ,385 | -,150 | ,109 |
| | Sig. (2-tailed) | ,238 | ,031 | ,295 | ,170 | ,129 | ,074 | ,018 | ,098 | ,000 | ,000 | ,000 | ,387 | ,087 | ,169 | ,910 | ,085 | ,922 | ,252 | ,003 | ,031 | ,628 | ,590 | ,430 | ,154 | ,032 | ,001 | ,210 | ,361 |
| Y | CC (ρ) | ,397 | ,113 | ,694 | ,339 | ,167 | ,285 | ,338 | ,286 | **,796** | **,744** | **,842** | ,223 | ,530 | ,130 | ,312 | ,261 | -,231 | -,503 | -,527 | -,037 | ,383 | ,445 | ,467 | ,514 | ,508 | ,472 | -,466 | ,455 |
| | Sig. (2-tailed) | ,001 | ,346 | ,000 | ,004 | ,160 | ,015 | ,004 | ,015 | ,000 | ,000 | ,000 | ,060 | ,000 | ,278 | ,008 | ,028 | ,051 | ,000 | ,000 | ,757 | ,001 | ,000 | ,000 | ,000 | ,000 | ,000 | ,000 | ,000 |
| Zr | CC (ρ) | ,200 | -,041 | ,527 | ,352 | ,009 | ,295 | ,310 | ,034 | ,555 | ,646 | ,398 | ,274 | ,044 | ,221 | ,180 | -,091 | -,350 | -,353 | -,076 | ,195 | ,270 | ,257 | ,230 | ,259 | ,296 | ,346 | -,301 | ,287 |
| | Sig. (2-tailed) | ,092 | ,733 | ,000 | ,002 | ,941 | ,012 | ,008 | ,778 | ,000 | ,000 | ,001 | ,020 | ,714 | ,062 | ,130 | ,452 | ,003 | ,002 | ,527 | ,100 | ,022 | ,030 | ,052 | ,028 | ,012 | ,003 | ,010 | ,015 |
| Nb | CC (ρ) | ,359 | ,098 | **,730** | ,368 | ,116 | ,308 | ,414 | ,175 | **,820** | **,799** | **,776** | ,250 | ,454 | ,181 | ,285 | ,199 | -,269 | -,498 | -,396 | ,041 | ,383 | ,405 | ,410 | ,455 | ,457 | ,454 | -,432 | ,421 |
| | Sig. (2-tailed) | ,002 | ,414 | ,000 | ,001 | ,332 | ,009 | ,000 | ,142 | ,000 | ,000 | ,000 | ,034 | ,000 | ,129 | ,015 | ,096 | ,022 | ,000 | ,001 | ,729 | ,001 | ,000 | ,000 | ,000 | ,000 | ,000 | ,000 | ,000 |
| Mo | CC (ρ) | ,496 | ,472 | ,193 | -,027 | ,143 | ,577 | **,764** | ,086 | ,262 | ,342 | ,202 | ,053 | ,332 | ,400 | -,047 | ,196 | -,285 | -,371 | -,169 | ,131 | ,321 | ,332 | ,296 | ,268 | ,271 | ,318 | -,335 | ,326 |
| | Sig. (2-tailed) | ,000 | ,000 | ,104 | ,824 | ,229 | ,000 | ,000 | ,474 | ,026 | ,003 | ,089 | ,658 | ,004 | ,000 | ,698 | ,101 | ,015 | ,001 | ,157 | ,272 | ,006 | ,004 | ,012 | ,023 | ,022 | ,007 | ,004 | ,005 |
| Hf | CC (ρ) | ,223 | -,025 | ,491 | ,375 | -,030 | ,273 | ,330 | ,096 | ,547 | ,611 | ,363 | ,328 | ,080 | ,140 | ,126 | ,005 | -,335 | -,334 | -,074 | ,218 | ,278 | ,273 | ,220 | ,214 | ,213 | ,246 | -,281 | ,272 |
| | Sig. (2-tailed) | ,060 | ,832 | ,000 | ,001 | ,803 | ,020 | ,005 | ,423 | ,000 | ,000 | ,002 | ,005 | ,506 | ,241 | ,293 | ,969 | ,004 | ,004 | ,536 | ,066 | ,018 | ,020 | ,064 | ,071 | ,072 | ,037 | ,017 | ,021 |
| W | CC (ρ) | ,574 | ,348 | ,194 | ,019 | ,328 | ,338 | ,416 | ,287 | ,153 | ,201 | ,203 | ,173 | ,293 | ,113 | ,039 | ,183 | -,196 | -,346 | -,259 | ,090 | ,335 | ,255 | ,248 | ,292 | ,294 | ,264 | -,315 | ,301 |
| | Sig. (2-tailed) | ,000 | ,003 | ,102 | ,873 | ,005 | ,004 | ,000 | ,015 | ,200 | ,091 | ,087 | ,147 | ,013 | ,343 | ,744 | ,126 | ,099 | ,003 | ,028 | ,452 | ,004 | ,031 | ,036 | ,013 | ,012 | ,025 | ,007 | ,010 |
| Pb | CC (ρ) | | ,510 | ,288 | -,136 | ,373 | **,721** | **,711** | ,594 | ,246 | ,284 | ,367 | -,041 | ,614 | ,248 | ,154 | ,463 | -,283 | -,524 | -,488 | ,063 | ,523 | ,546 | ,508 | ,489 | ,433 | ,348 | -,533 | ,539 |
| | Sig. (2-tailed) | | ,000 | ,014 | ,255 | ,001 | ,000 | ,000 | ,000 | ,037 | ,016 | ,002 | ,733 | ,000 | ,036 | ,197 | ,000 | ,016 | ,000 | ,000 | ,599 | ,000 | ,000 | ,000 | ,000 | ,000 | ,003 | ,000 | ,000 |

| | | Pb | Bi | Th | U | Cd | Sn | Sb | I | La | Ce | Nd | Sm | S | Cl | Yb | LOI (%) | 500-1000 µm | 250-500 µm | 125-250 µm | 63-125 µm | 32-63 µm | 16-32 µm | 8-16 µm | 4-8 µm | 2-4 µm | below 2 µm | 1000-63 µm | 63-2 µm |
|---|---|---|---|---|---|---|---|---|---|---|---|---|---|---|---|---|---|---|---|---|---|---|---|---|---|---|---|---|---|
| Pb | CC (ρ) | | ,510 | ,288 | -,136 | ,373 | **,721** | **,711** | ,594 | ,246 | ,284 | ,367 | -,041 | ,614 | ,248 | ,154 | ,463 | -,283 | -,524 | -,488 | ,063 | ,523 | ,546 | ,508 | ,489 | ,433 | ,348 | -,533 | ,539 |
| | Sig. (2-tailed) | | ,000 | ,014 | ,255 | ,001 | ,000 | ,000 | ,000 | ,037 | ,016 | ,002 | ,733 | ,000 | ,036 | ,197 | ,000 | ,016 | ,000 | ,000 | ,599 | ,000 | ,000 | ,000 | ,000 | ,000 | ,003 | ,000 | ,000 |
| Bi | CC (ρ) | | | -,157 | -,274 | ,459 | ,527 | ,600 | ,285 | ,058 | ,037 | ,118 | -,132 | ,430 | ,250 | -,018 | ,334 | -,173 | -,346 | -,341 | ,015 | ,360 | ,357 | ,343 | ,288 | ,250 | ,268 | -,347 | ,341 |
| | Sig. (2-tailed) | | | ,187 | ,020 | ,000 | ,000 | ,000 | ,015 | ,629 | ,756 | ,324 | ,269 | ,000 | ,034 | ,878 | ,004 | ,145 | ,003 | ,003 | ,899 | ,002 | ,002 | ,003 | ,014 | ,034 | ,023 | ,003 | ,003 |
| Th | CC (ρ) | | | | ,545 | -,028 | ,133 | ,191 | ,155 | **,792** | **,773** | ,673 | ,353 | ,305 | ,167 | ,243 | ,177 | -,328 | -,414 | -,308 | ,006 | ,287 | ,379 | ,410 | ,482 | ,482 | ,412 | -,415 | ,405 |
| | Sig. (2-tailed) | | | | ,000 | ,814 | ,264 | ,108 | ,193 | ,000 | ,000 | ,000 | ,002 | ,009 | ,160 | ,039 | ,141 | ,005 | ,000 | ,008 | ,960 | ,014 | ,001 | ,000 | ,000 | ,000 | ,000 | ,000 | ,000 |
| U | CC (ρ) | | | | | -,072 | -,022 | -,162 | ,019 | ,451 | ,429 | ,347 | ,486 | ,101 | ,120 | ,077 | ,055 | -,044 | -,044 | -,107 | -,194 | -,106 | ,024 | ,099 | ,182 | ,205 | ,147 | -,067 | ,059 |
| | Sig. (2-tailed) | | | | | ,548 | ,856 | ,174 | ,876 | ,000 | ,000 | ,003 | ,000 | ,397 | ,316 | ,522 | ,651 | ,714 | ,713 | ,370 | ,103 | ,377 | ,839 | ,410 | ,126 | ,083 | ,217 | ,575 | ,621 |
| Cd | CC (ρ) | | | | | | ,325 | ,225 | ,404 | ,081 | -,007 | ,168 | -,052 | ,344 | -,013 | ,092 | ,218 | -,165 | -,364 | -,335 | ,144 | ,400 | ,309 | ,288 | ,266 | ,233 | ,209 | -,322 | ,325 |
| | Sig. (2-tailed) | | | | | | ,005 | ,057 | ,000 | ,498 | ,956 | ,158 | ,665 | ,003 | ,916 | ,441 | ,067 | ,166 | ,002 | ,004 | ,228 | ,000 | ,008 | ,014 | ,024 | ,049 | ,078 | ,006 | ,005 |
| Sn | CC (ρ) | | | | | | | **,765** | ,450 | ,194 | ,230 | ,294 | -,096 | ,456 | ,397 | ,251 | ,337 | -,278 | -,431 | -,300 | ,085 | ,422 | ,465 | ,438 | ,405 | ,357 | ,326 | -,448 | ,456 |
| | Sig. (2-tailed) | | | | | | | ,000 | ,000 | ,102 | ,052 | ,012 | ,424 | ,000 | ,001 | ,034 | ,004 | ,018 | ,000 | ,011 | ,478 | ,000 | ,000 | ,000 | ,000 | ,002 | ,005 | ,000 | ,000 |
| Sb | CC (ρ) | | | | | | | | ,337 | ,292 | ,400 | ,313 | -,039 | ,494 | ,430 | ,065 | ,359 | -,299 | -,488 | -,420 | ,058 | ,464 | ,495 | ,451 | ,411 | ,381 | ,380 | -,473 | ,475 |
| | Sig. (2-tailed) | | | | | | | | ,004 | ,013 | ,001 | ,008 | ,744 | ,000 | ,000 | ,589 | ,002 | ,011 | ,000 | ,000 | ,628 | ,000 | ,000 | ,000 | ,000 | ,001 | ,001 | ,000 | ,000 |
| I | CC (ρ) | | | | | | | | | ,061 | ,037 | ,201 | -,100 | ,662 | ,100 | ,196 | **,756** | -,176 | -,477 | -,556 | ,022 | ,491 | ,589 | ,565 | ,489 | ,353 | ,149 | -,491 | ,528 |
| | Sig. (2-tailed) | | | | | | | | | ,611 | ,761 | ,091 | ,405 | ,000 | ,405 | ,099 | ,000 | ,139 | ,000 | ,000 | ,852 | ,000 | ,000 | ,000 | ,000 | ,002 | ,212 | ,000 | ,000 |
| La | CC (ρ) | | | | | | | | | | **,871** | **,824** | ,329 | ,385 | ,163 | ,184 | ,099 | -,244 | -,382 | -,394 | -,050 | ,268 | ,347 | ,374 | ,460 | ,501 | ,550 | -,397 | ,367 |
| | Sig. (2-tailed) | | | | | | | | | | ,000 | ,000 | ,005 | ,001 | ,172 | ,122 | ,412 | ,039 | ,001 | ,001 | ,674 | ,023 | ,003 | ,001 | ,000 | ,000 | ,000 | ,001 | ,001 |
| Ce | CC (ρ) | | | | | | | | | | | **,751** | ,221 | ,267 | ,277 | ,078 | -,006 | -,194 | -,324 | -,385 | -,083 | ,201 | ,240 | ,255 | ,343 | ,395 | ,427 | -,293 | ,267 |
| | Sig. (2-tailed) | | | | | | | | | | | ,000 | ,062 | ,023 | ,019 | ,515 | ,959 | ,103 | ,006 | ,001 | ,491 | ,090 | ,042 | ,031 | ,003 | ,001 | ,000 | ,012 | ,023 |
| Nd | CC (ρ) | | | | | | | | | | | | ,253 | ,448 | ,099 | ,284 | ,167 | -,203 | -,394 | -,466 | -,121 | ,317 | ,366 | ,380 | ,450 | ,473 | ,484 | -,392 | ,376 |
| | Sig. (2-tailed) | | | | | | | | | | | | ,032 | ,000 | ,409 | ,016 | ,165 | ,087 | ,001 | ,000 | ,312 | ,007 | ,002 | ,001 | ,000 | ,000 | ,000 | ,001 | ,001 |
| Sm | CC (ρ) | | | | | | | | | | | | | ,037 | -,076 | ,063 | ,071 | -,143 | -,130 | -,032 | ,056 | ,035 | ,073 | ,086 | ,108 | ,118 | ,126 | -,094 | ,091 |
| | Sig. (2-tailed) | | | | | | | | | | | | | ,754 | ,525 | ,601 | ,556 | ,229 | ,275 | ,787 | ,641 | ,773 | ,544 | ,474 | ,365 | ,323 | ,291 | ,434 | ,445 |
| S | CC (ρ) | | | | | | | | | | | | | | ,299 | ,166 | **,804** | -,296 | -,682 | -,670 | ,030 | ,623 | **,705** | ,675 | ,637 | ,561 | ,451 | -,659 | ,678 |
| | Sig. (2-tailed) | | | | | | | | | | | | | | ,011 | ,163 | ,000 | ,012 | ,000 | ,000 | ,804 | ,000 | ,000 | ,000 | ,000 | ,000 | ,000 | ,000 | ,000 |
| Cl | CC (ρ) | | | | | | | | | | | | | | | ,097 | ,251 | ,010 | -,154 | -,196 | -,110 | ,033 | ,146 | ,147 | ,186 | ,223 | ,192 | -,146 | ,142 |
| | Sig. (2-tailed) | | | | | | | | | | | | | | | ,419 | ,035 | ,935 | ,195 | ,098 | ,357 | ,786 | ,220 | ,219 | ,117 | ,060 | ,106 | ,220 | ,234 |
| Yb | CC (ρ) | | | | | | | | | | | | | | | | ,158 | -,230 | -,226 | -,054 | ,161 | ,230 | ,226 | ,228 | ,223 | ,186 | ,154 | -,237 | ,236 |
| | Sig. (2-tailed) | | | | | | | | | | | | | | | | ,188 | ,052 | ,056 | ,649 | ,176 | ,052 | ,056 | ,054 | ,059 | ,118 | ,197 | ,045 | ,046 |
| LOI (%) | CC (ρ) | | | | | | | | | | | | | | | | | -,230 | -,559 | -,487 | ,105 | ,526 | ,659 | ,617 | ,500 | ,347 | ,148 | -,531 | ,579 |
| | Sig. (2-tailed) | | | | | | | | | | | | | | | | | ,053 | ,000 | ,000 | ,381 | ,000 | ,000 | ,000 | ,000 | ,003 | ,217 | ,000 | ,000 |
| 500-1000 µm | CC (ρ) | | | | | | | | | | | | | | | | | | **,759** | ,109 | -,583 | -,767 | -,647 | -,616 | -,609 | -,605 | -,571 | **,713** | -,709 |
| | Sig. (2-tailed) | | | | | | | | | | | | | | | | | | ,000 | ,361 | ,000 | ,000 | ,000 | ,000 | ,000 | ,000 | ,000 | ,000 | ,000 |
| 250-500 µm | CC (ρ) | | | | | | | | | | | | | | | | | | | ,548 | -,436 | -,937 | -,879 | -,845 | -,830 | -,790 | -,697 | **,921** | -,924 |
| | Sig. (2-tailed) | | | | | | | | | | | | | | | | | | | ,000 | ,000 | ,000 | ,000 | ,000 | ,000 | ,000 | ,000 | ,000 | ,000 |
| 125-250 µm | CC (ρ) | | | | | | | | | | | | | | | | | | | | ,373 | -,469 | -,674 | -,721 | -,729 | -,681 | -,578 | ,664 | -,661 |
| | Sig. (2-tailed) | | | | | | | | | | | | | | | | | | | | ,001 | ,000 | ,000 | ,000 | ,000 | ,000 | ,000 | ,000 | ,000 |
| 63-125 µm | CC (ρ) | | | | | | | | | | | | | | | | | | | | | ,520 | ,194 | ,088 | ,041 | ,029 | ,041 | -,220 | ,230 |
| | Sig. (2-tailed) | | | | | | | | | | | | | | | | | | | | | ,000 | ,102 | ,460 | ,733 | ,806 | ,735 | ,063 | ,052 |
| 32-63 µm | CC (ρ) | | | | | | | | | | | | | | | | | | | | | | **,889** | **,812** | **,744** | ,675 | ,591 | -,890 | **,904** |
| | Sig. (2-tailed) | | | | | | | | | | | | | | | | | | | | | | ,000 | ,000 | ,000 | ,000 | ,000 | ,000 | ,000 |
| 16-32 µm | CC (ρ) | | | | | | | | | | | | | | | | | | | | | | | **,971** | **,889** | **,782** | ,649 | -,957 | **,978** |
| | Sig. (2-tailed) | | | | | | | | | | | | | | | | | | | | | | | ,000 | ,000 | ,000 | ,000 | ,000 | ,000 |
| 8-16 µm | CC (ρ) | | | | | | | | | | | | | | | | | | | | | | | | **,956** | **,861** | **,721** | -,965 | **,973** |
| | Sig. (2-tailed) | | | | | | | | | | | | | | | | | | | | | | | | ,000 | ,000 | ,000 | ,000 | ,000 |
| 4-8 µm | CC (ρ) | | | | | | | | | | | | | | | | | | | | | | | | | **,962** | **,847** | -,952 | **,938** |
| | Sig. (2-tailed) | | | | | | | | | | | | | | | | | | | | | | | | | ,000 | ,000 | ,000 | ,000 |
| 2-4 µm | CC (ρ) | | | | | | | | | | | | | | | | | | | | | | | | | | **,942** | -,898 | **,866** |
| | Sig. (2-tailed) | | | | | | | | | | | | | | | | | | | | | | | | | | ,000 | ,000 | ,000 |
| below 2 µm | CC (ρ) | | | | | | | | | | | | | | | | | | | | | | | | | | | -,802 | **,751** |
| | Sig. (2-tailed) | | | | | | | | | | | | | | | | | | | | | | | | | | | ,000 | ,000 |
| 1000-63 µm | CC (ρ) | | | | | | | | | | | | | | | | | | | | | | | | | | | | -,994 |
| | Sig. (2-tailed) | | | | | | | | | | | | | | | | | | | | | | | | | | | | ,000 |
| 63-2 µm | CC (ρ) | | | | | | | | | | | | | | | | | | | | | | | | | | | | |
| | Sig. (2-tailed) | | | | | | | | | | | | | | | | | | | | | | | | | | | | |

Figure 118: Cr concentrations in RDS according to land use, black line: residential SGV; red line: Allotment SGV (EA, 2002).

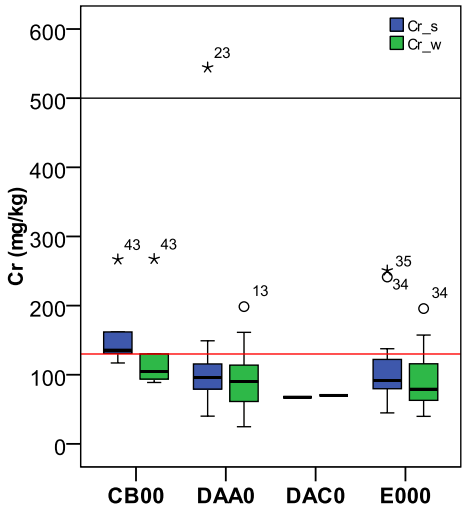


Figure 119: Ni concentrations in RDS according to land use.

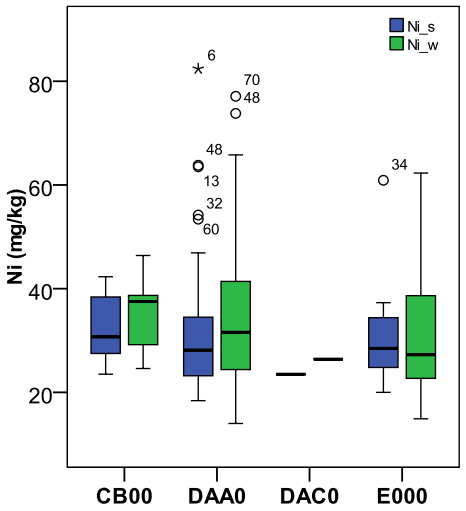


Figure 120: Cu concentrations in RDS according to land use, green line: proposed UK ecological guideline (EA, 2008).

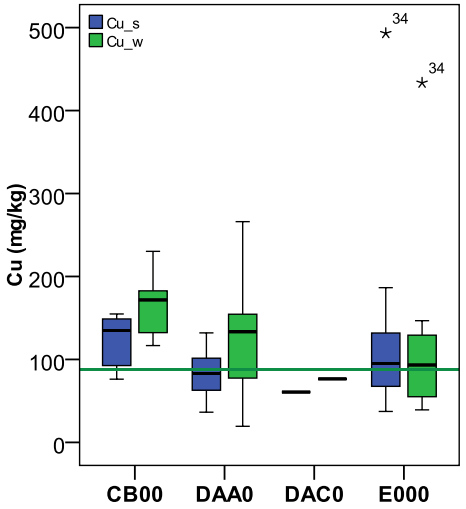


Figure 121: Zn concentrations in RDS according to land use, green line: proposed UK ecological guideline (EA, 2008); purple line: former UK ICRCL SGV (ICRCL, 1987).

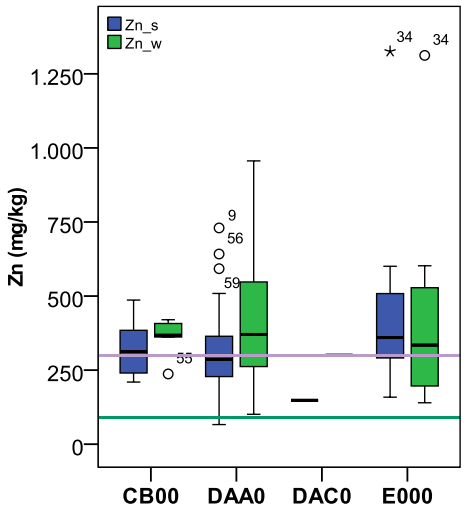


Figure 122: As concentrations in RDS according to land use.

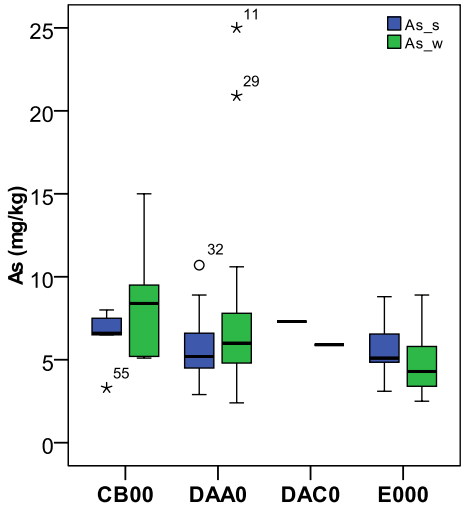

Figure 123: Pb concentrations in RDS according to land use, black line: residential and allotment SGV; brown line: commercial/industrial SGV (EA, 2002).

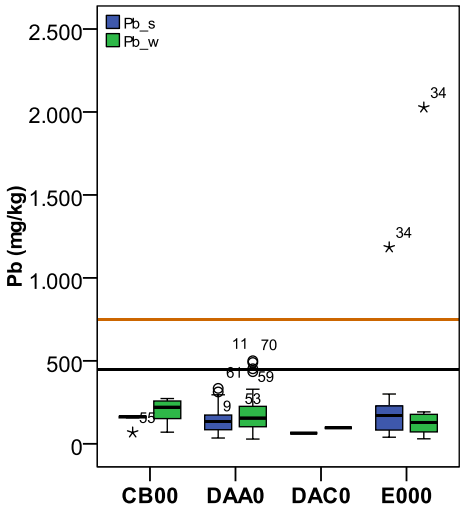

Figure 124: Cd concentrations in RDS according to land use, black line: residential SGV;
red: allotment SGV (EA, 2009b). (Note: logarithmic scale).

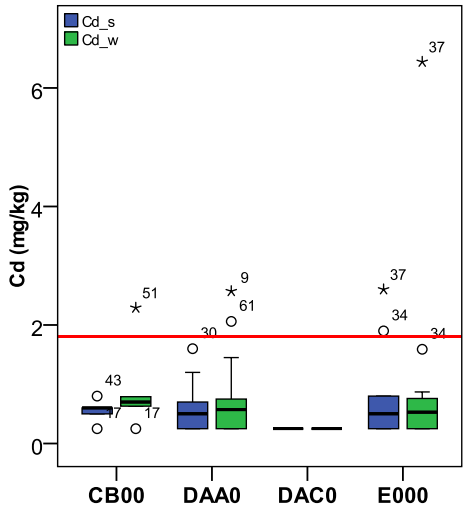


Figure 125: Box-and-whisker plots for Cr, Ni, Cu, Zn, As, Pb and Cd concentrations in RDS, grouped by bedrock geology type.

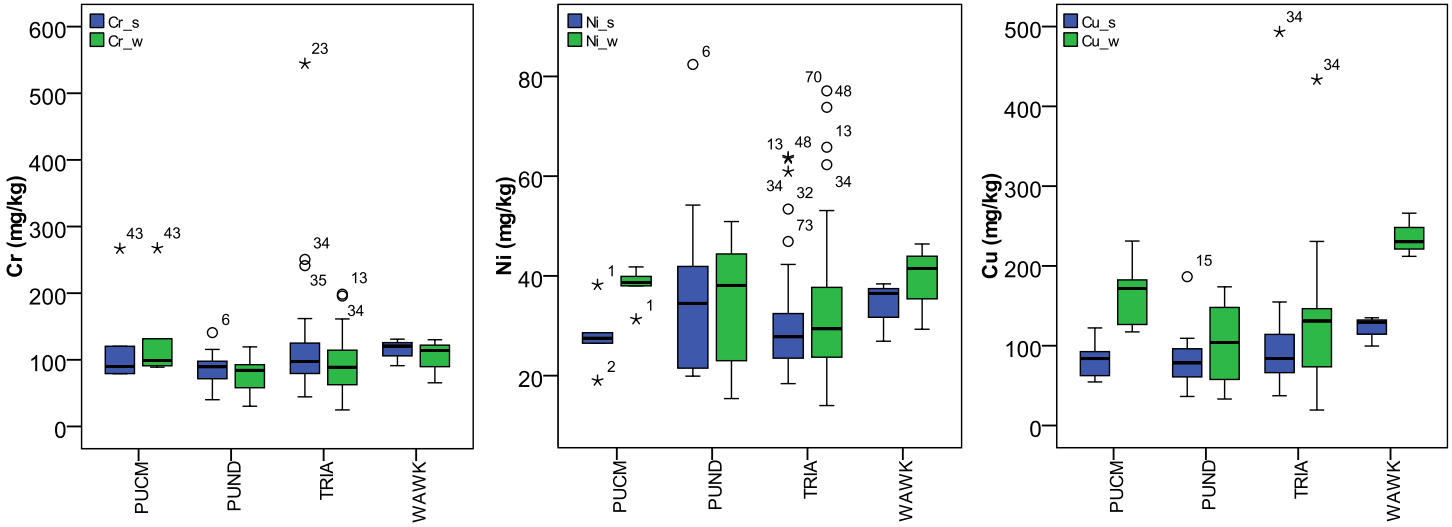

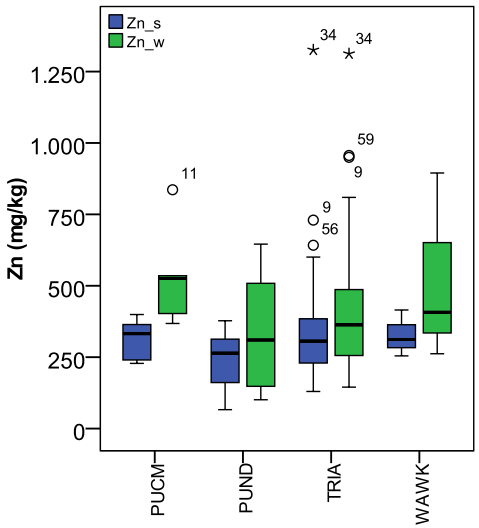
Zn_s
Zn_w
Zn (mg/kg)
0
250
500
750
1.000
1.250
PUCM
PUND
TRIA
WAWK

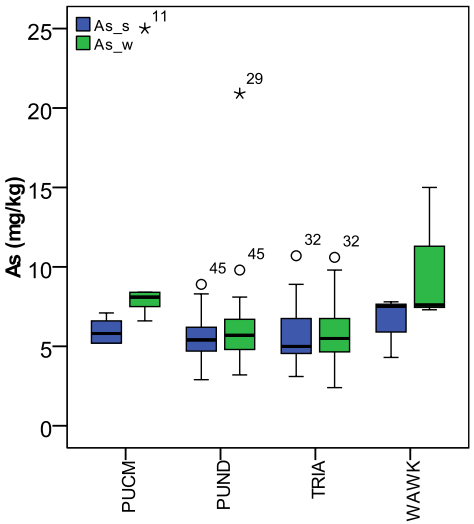
As_s
As_w
As (mg/kg)
0
5
10
15
20
25
PUCM
PUND
TRIA
WAWK

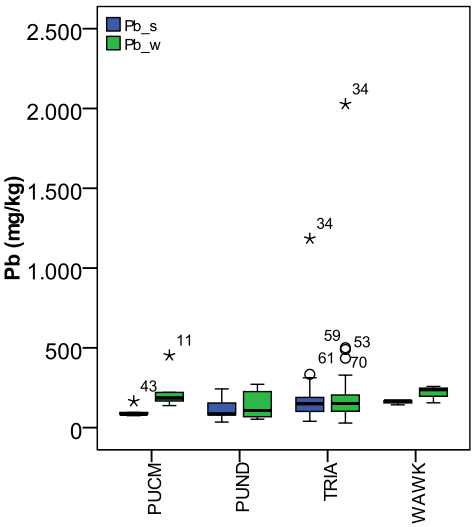
Pb_s
Pb_w
Pb (mg/kg)
0
500
1.000
1.500
2.000
2.500
PUCM
PUND
TRIA
WAWK

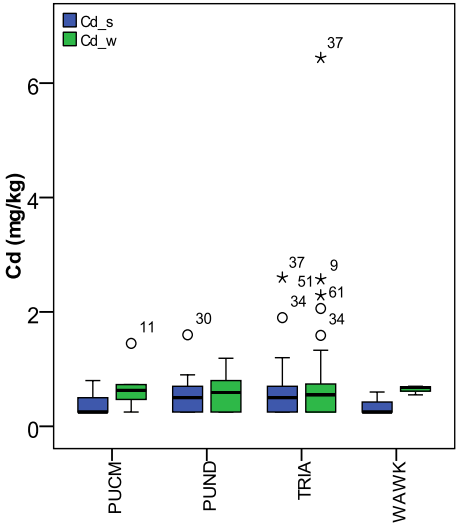
Cd_s
Cd_w
Cd (mg/kg)
0
2
4
6
PUCM
PUND
TRIA
WAWK

Figure 126: Box-and-whisker plots for Cr, Ni, Cu, Zn, As, Pb and Cd concentrations in RDS, grouped by superficial geology type.

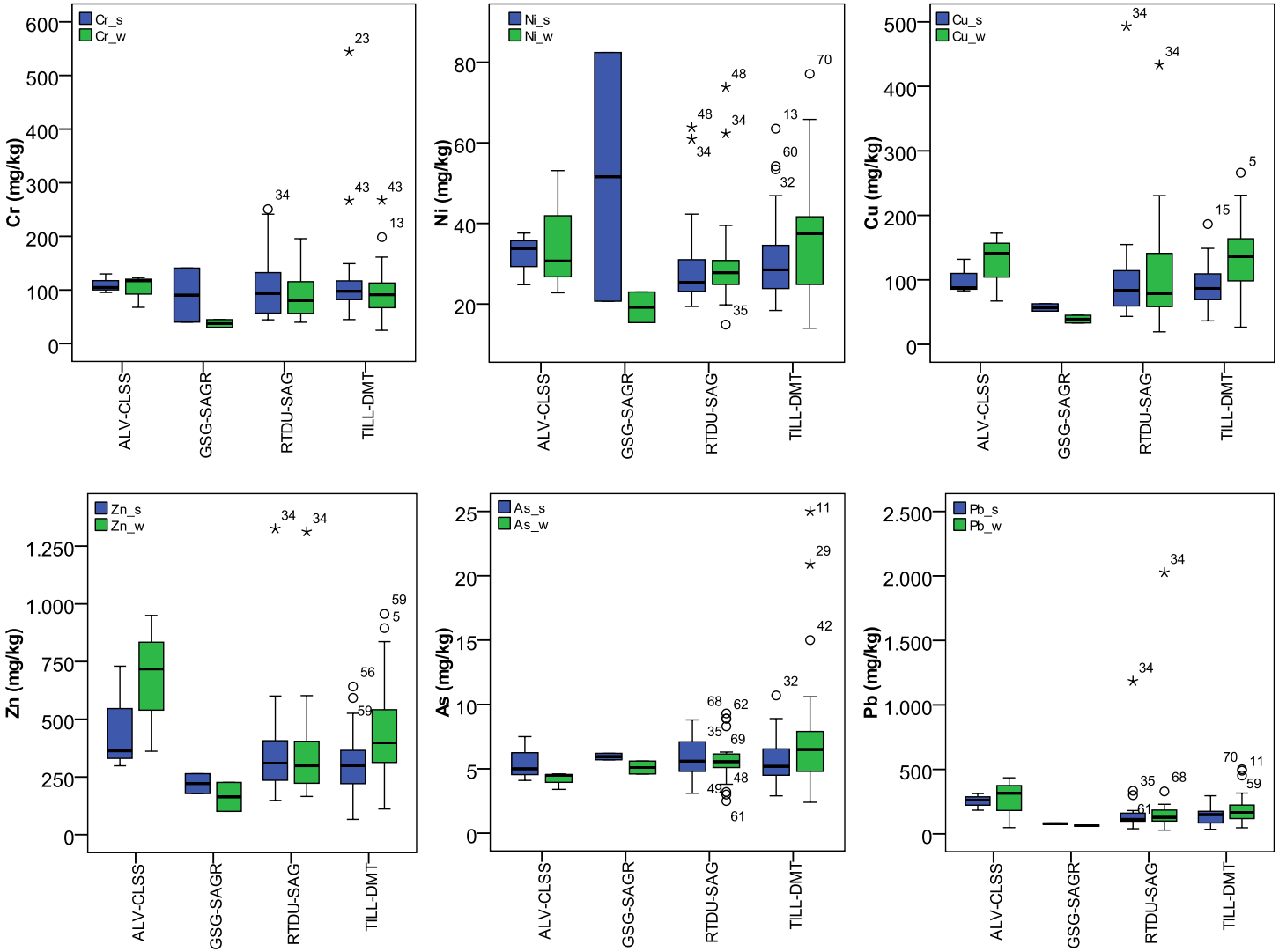

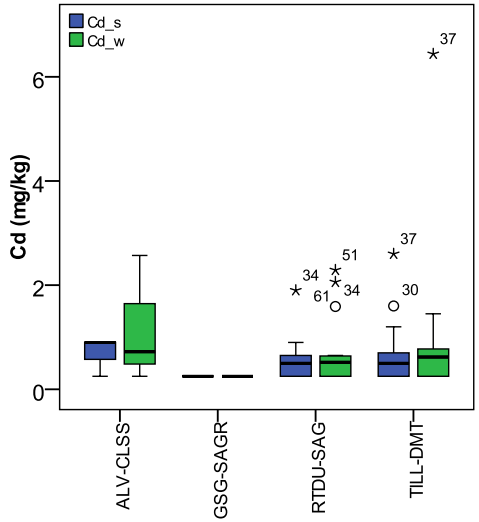


Figure 127: Box-and-whisker plots for RDS concentrations in $Al_2O_3$, $SiO_2$, $TiO_2$, $Fe_2O_3$, Sc, V, Rb, Zr, Co, Ga, Mo and REEs, grouped by bedrock geology type.

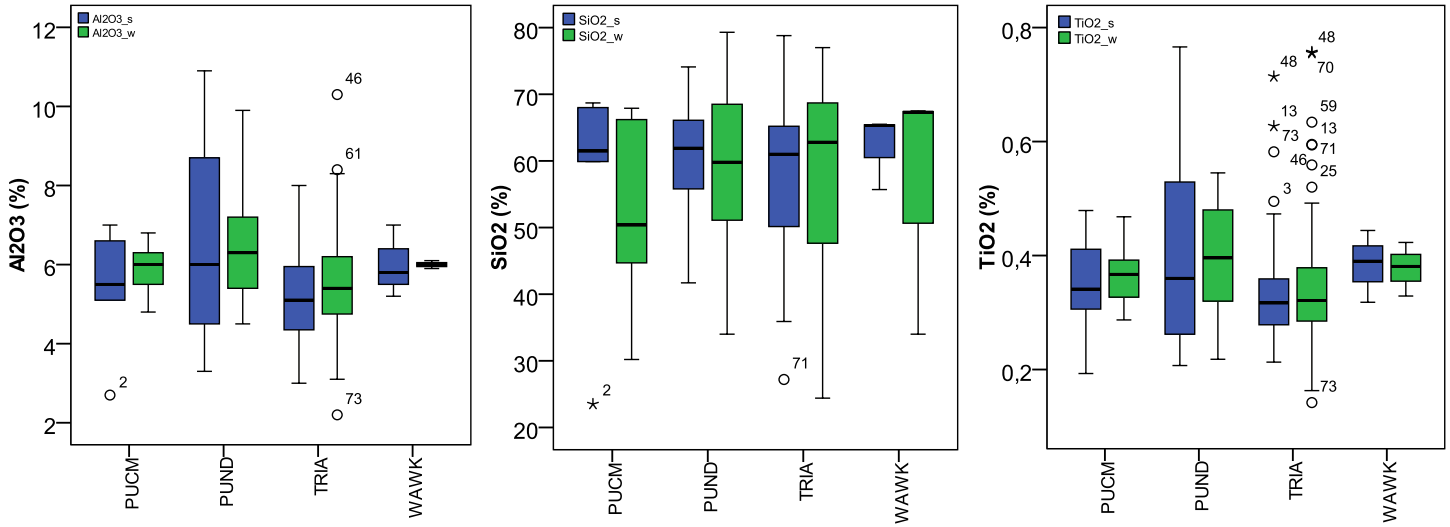

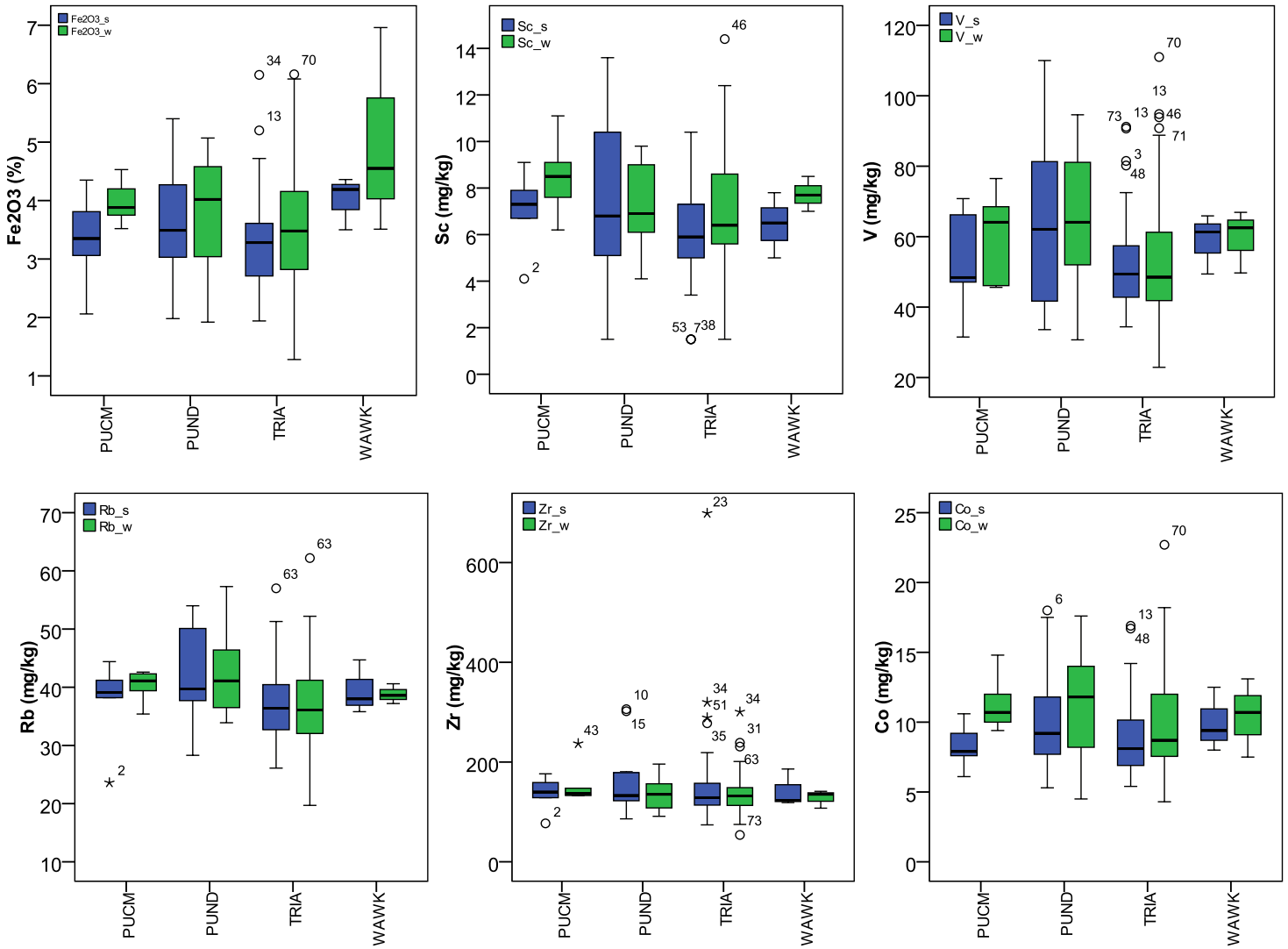
Fe2O3_s
Fe2O3_w
Fe2O3 (%)
Sc_s
Sc_w
Sc (mg/kg)
V_s
V_w
V (mg/kg)
Rb_s
Rb_w
Rb (mg/kg)
Zr_s
Zr_w
Zr (mg/kg)
Co_s
Co_w
Co (mg/kg)
PUCM
PUND
TRIA
WAWK

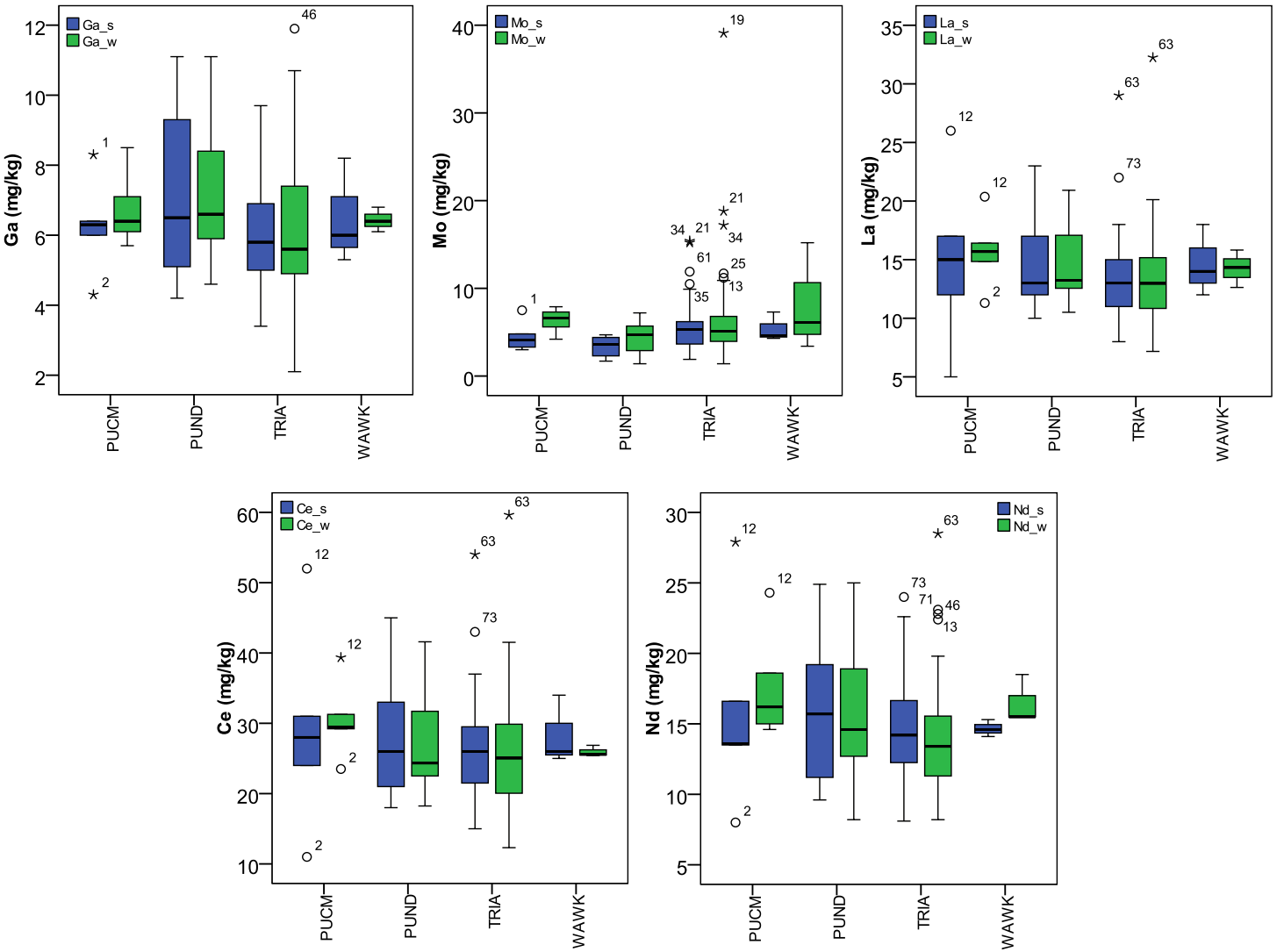
Ga_s
Ga_w
Ga (mg/kg)
Mo_s
Mo_w
Mo (mg/kg)
La_s
La_w
La (mg/kg)
Ce_s
Ce_w
Ce (mg/kg)
Nd_s
Nd_w
Nd (mg/kg)
PUCM
PUND
TRIA
WAWK

Figure 128: Box-and-whisker plots for RDS concentrations in $Al_2O_3$, $SiO_2$, $TiO_2$, $Fe_2O_3$, Sc, V, Rb, Zr, Co, Ga, Mo and REEs, grouped by superficial deposit type.

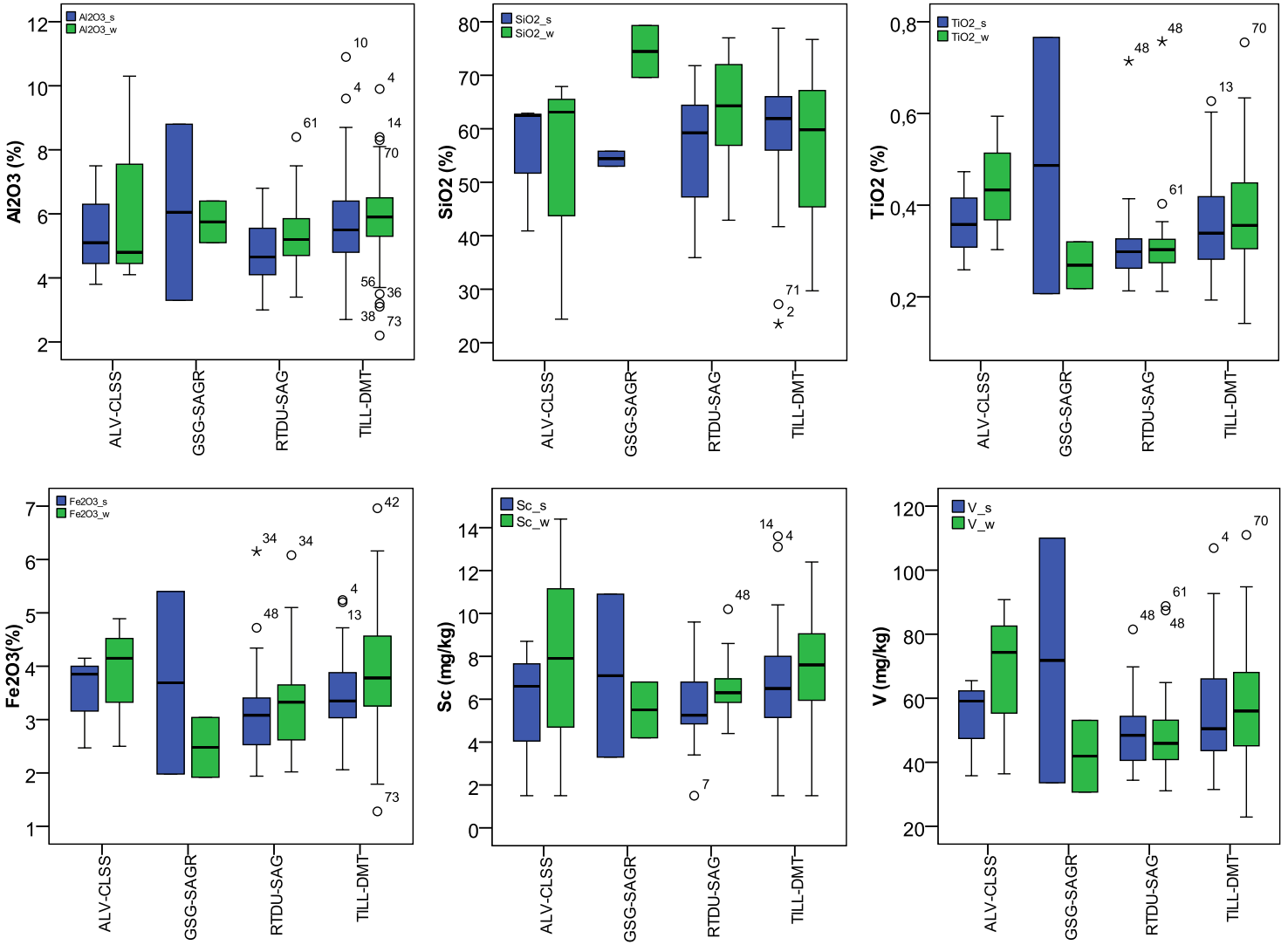

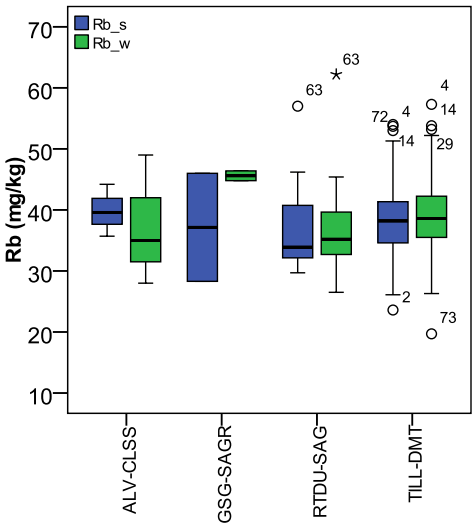
Rb_s
Rb_w
Rb (mg/kg)
70
60
50
40
30
20
10
63
63
72
4
14
14
29
4
2
73
ALV-CLSS
GSG-SAGR
RTDU-SAG
TILL-DMT

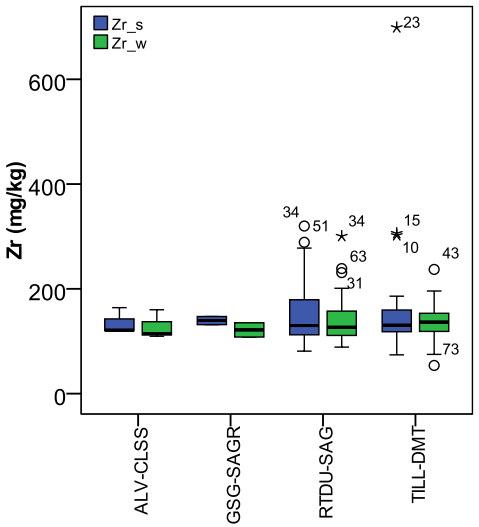
Zr_s
Zr_w
Zr (mg/kg)
600
400
200
0
23
34
51
34
63
31
15
10
43
73
ALV-CLSS
GSG-SAGR
RTDU-SAG
TILL-DMT

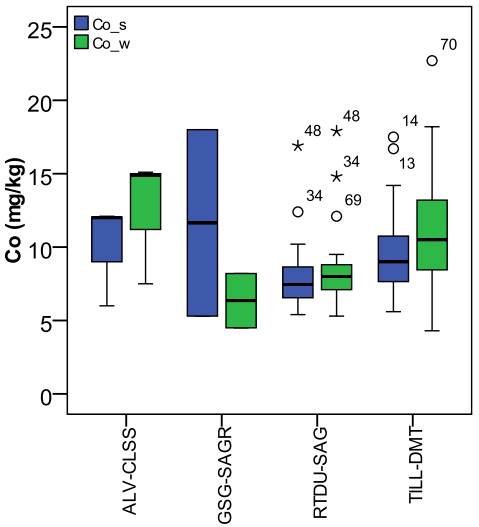
Co_s
Co_w
Co (mg/kg)
25
20
15
10
5
0
70
48
48
34
34
69
14
13
ALV-CLSS
GSG-SAGR
RTDU-SAG
TILL-DMT

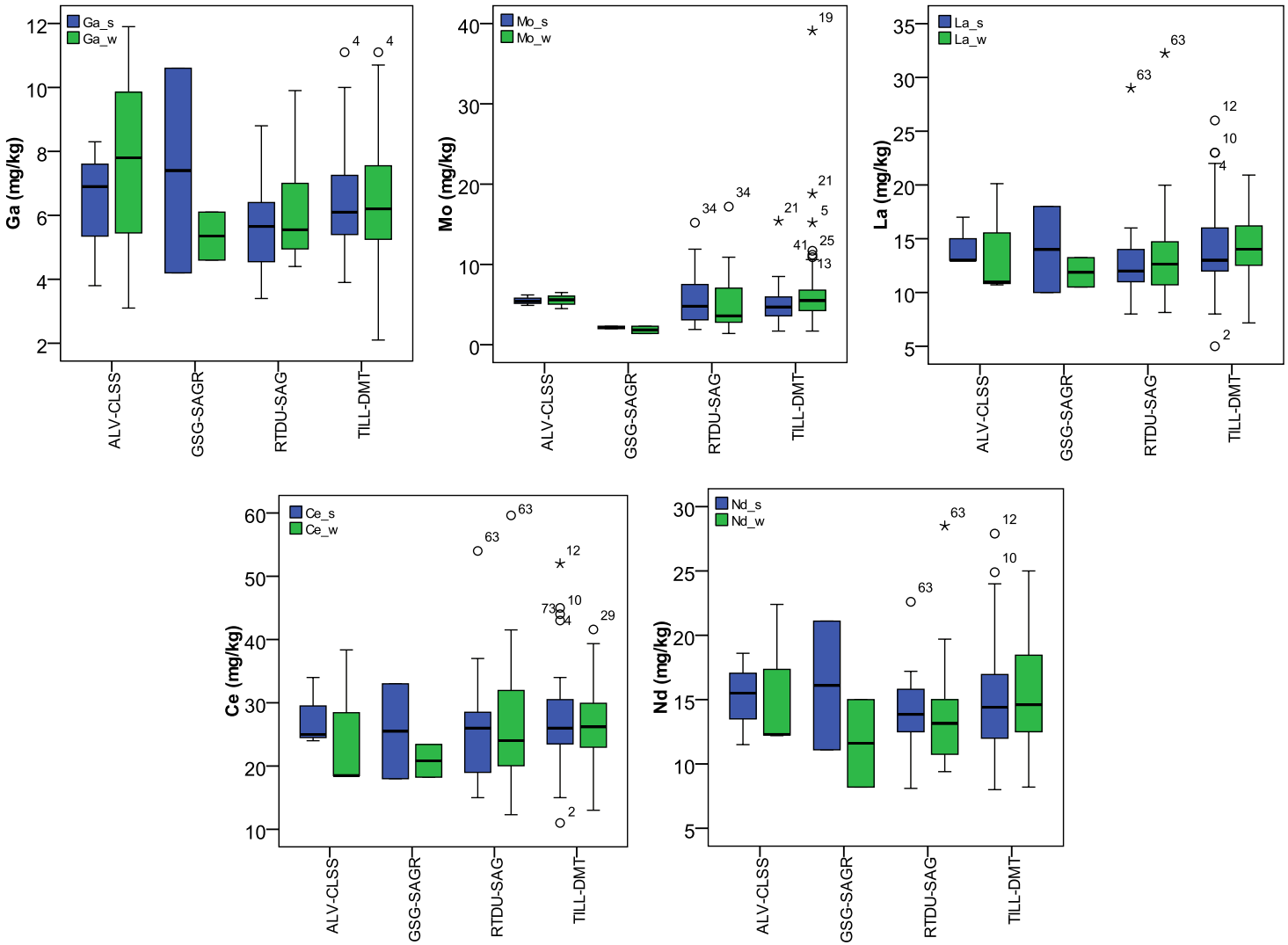
Ga_s
Ga_w
Ga (mg/kg)
Mo_s
Mo_w
Mo (mg/kg)
La_s
La_w
La (mg/kg)
Ce_s
Ce_w
Ce (mg/kg)
Nd_s
Nd_w
Nd (mg/kg)
ALV-CLSS
GSG-SAGR
RTDU-SAG
TILL-DMT

Figure 129: RDS extractable metal concentrations (% of total) in summer, plotted by extracted phase (N=17).

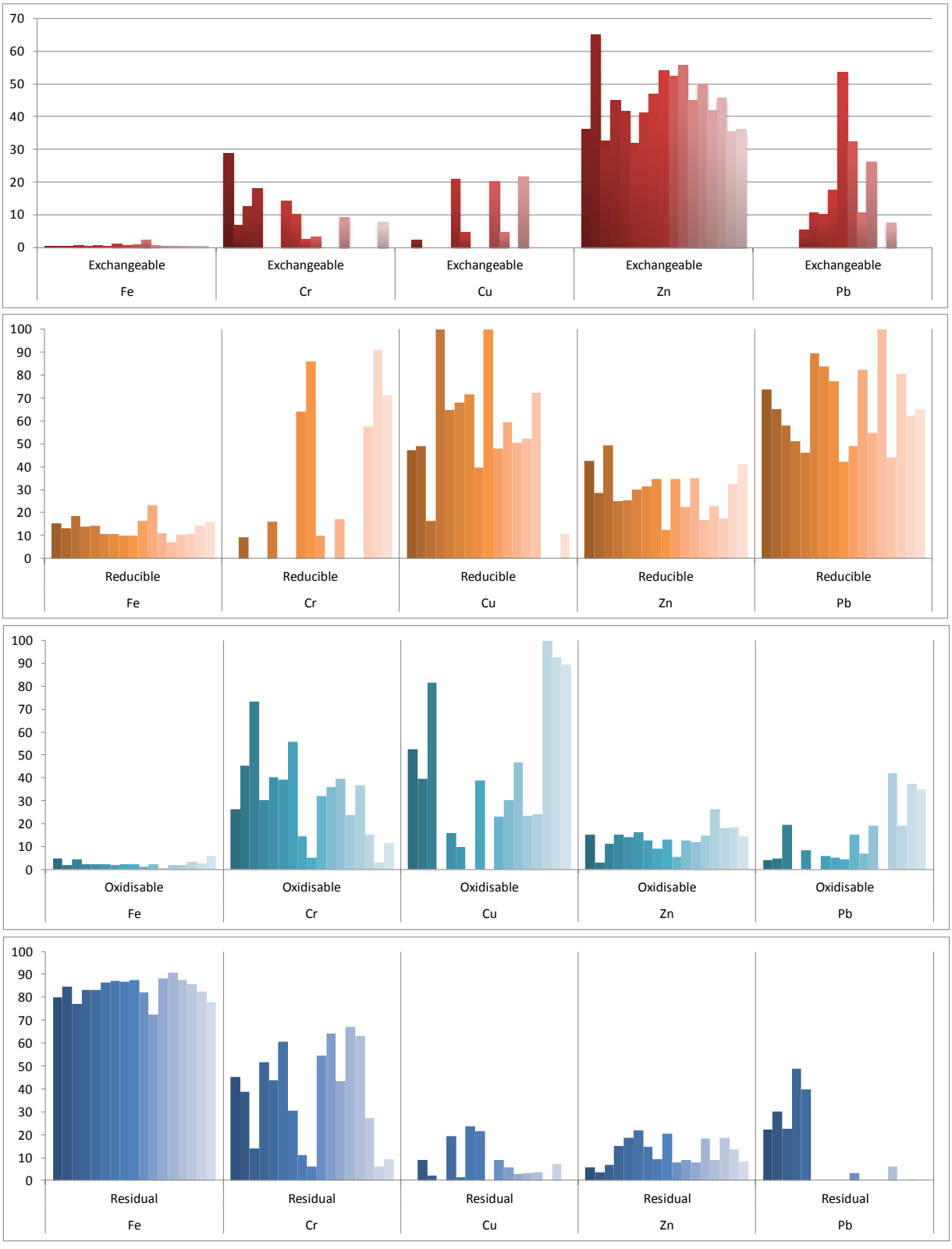

Figure 130: RDS extractable metal concentrations (% of total) in winter, plotted by extracted phase (N=17).

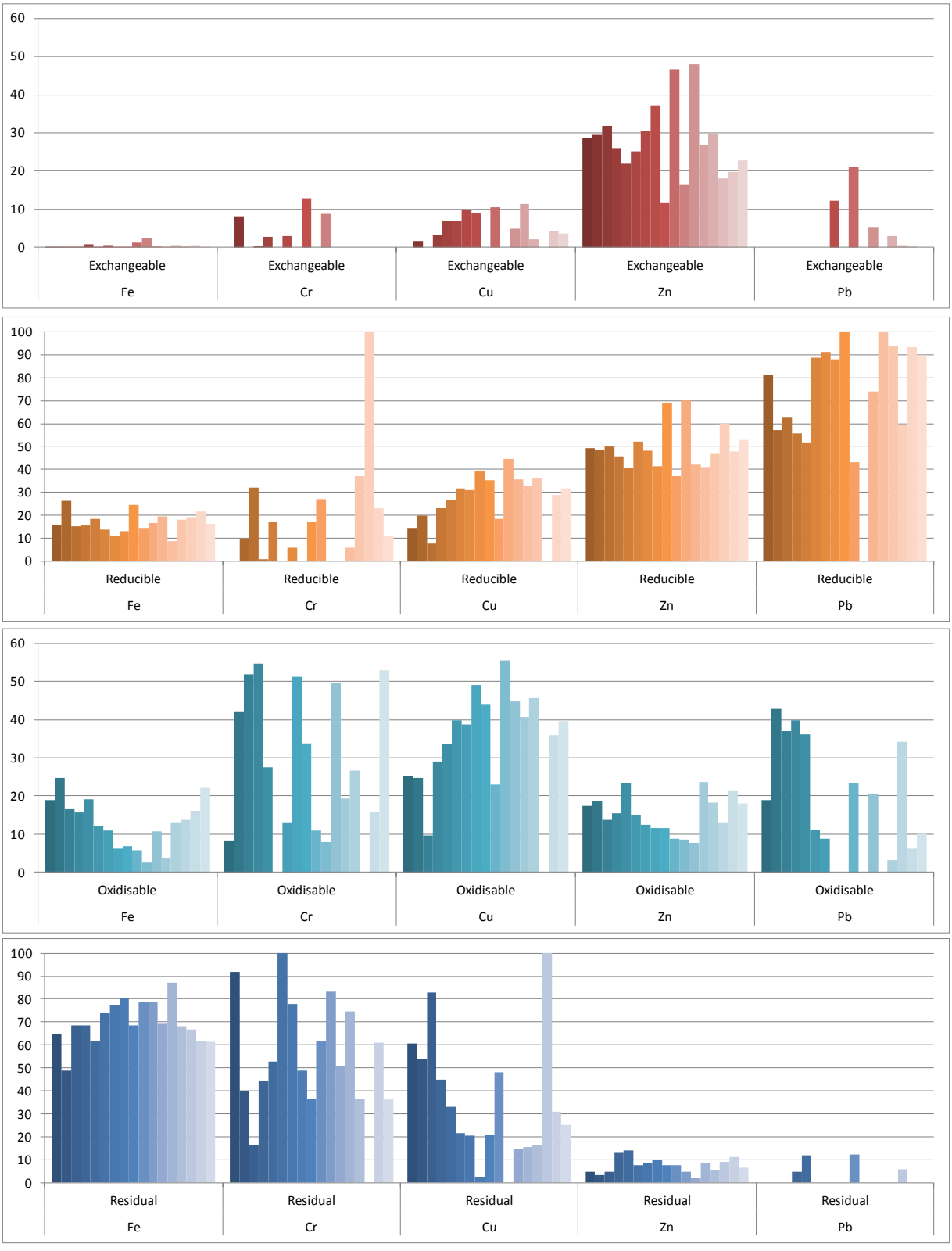

Figure 131: Box-and-whisker plots for RDS SEM data, grouped by grain type (all concentrations in wt%).

NOTE: Only 1 sample analysed for Fe-S and Ni-rich grain types.

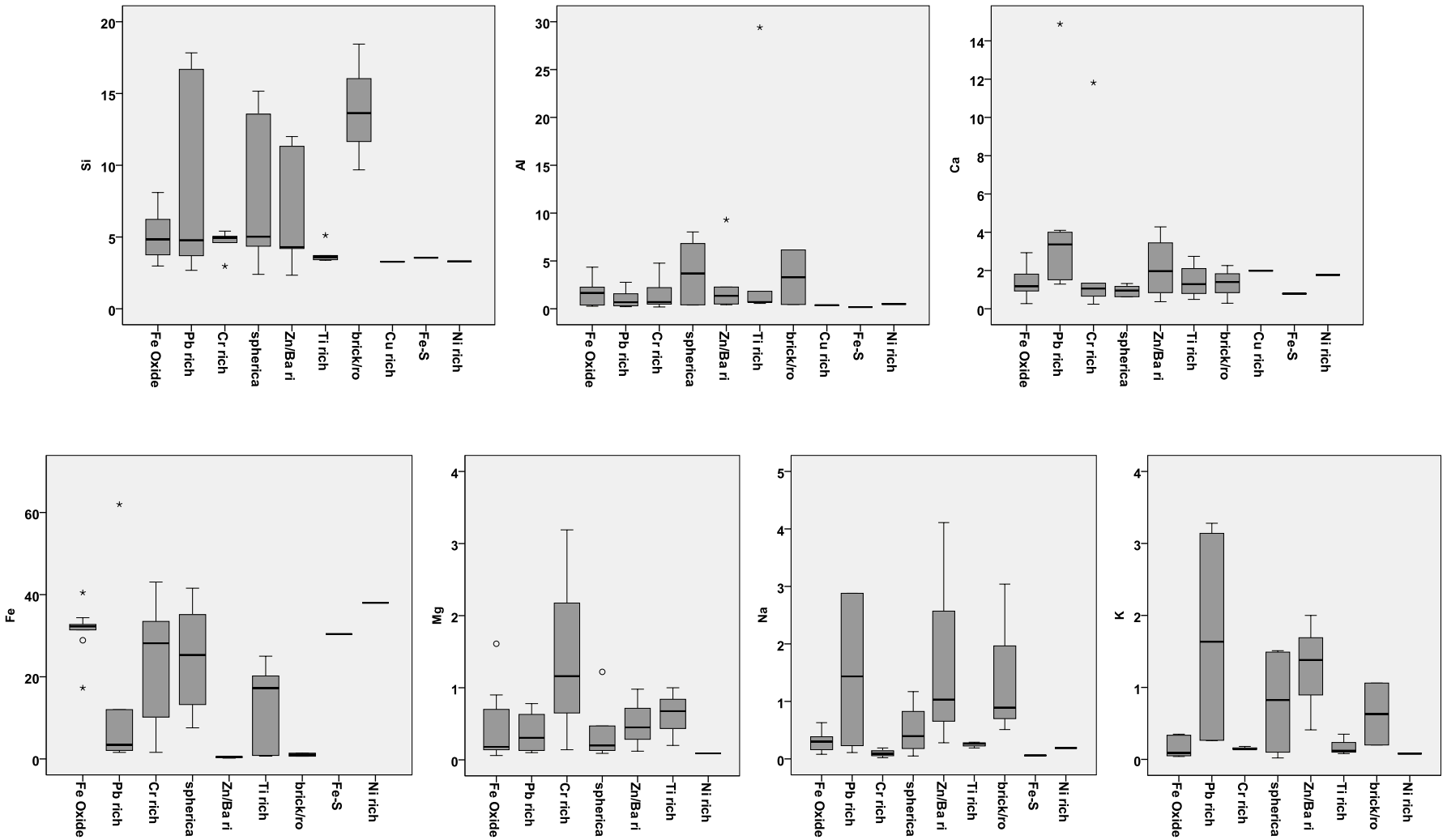

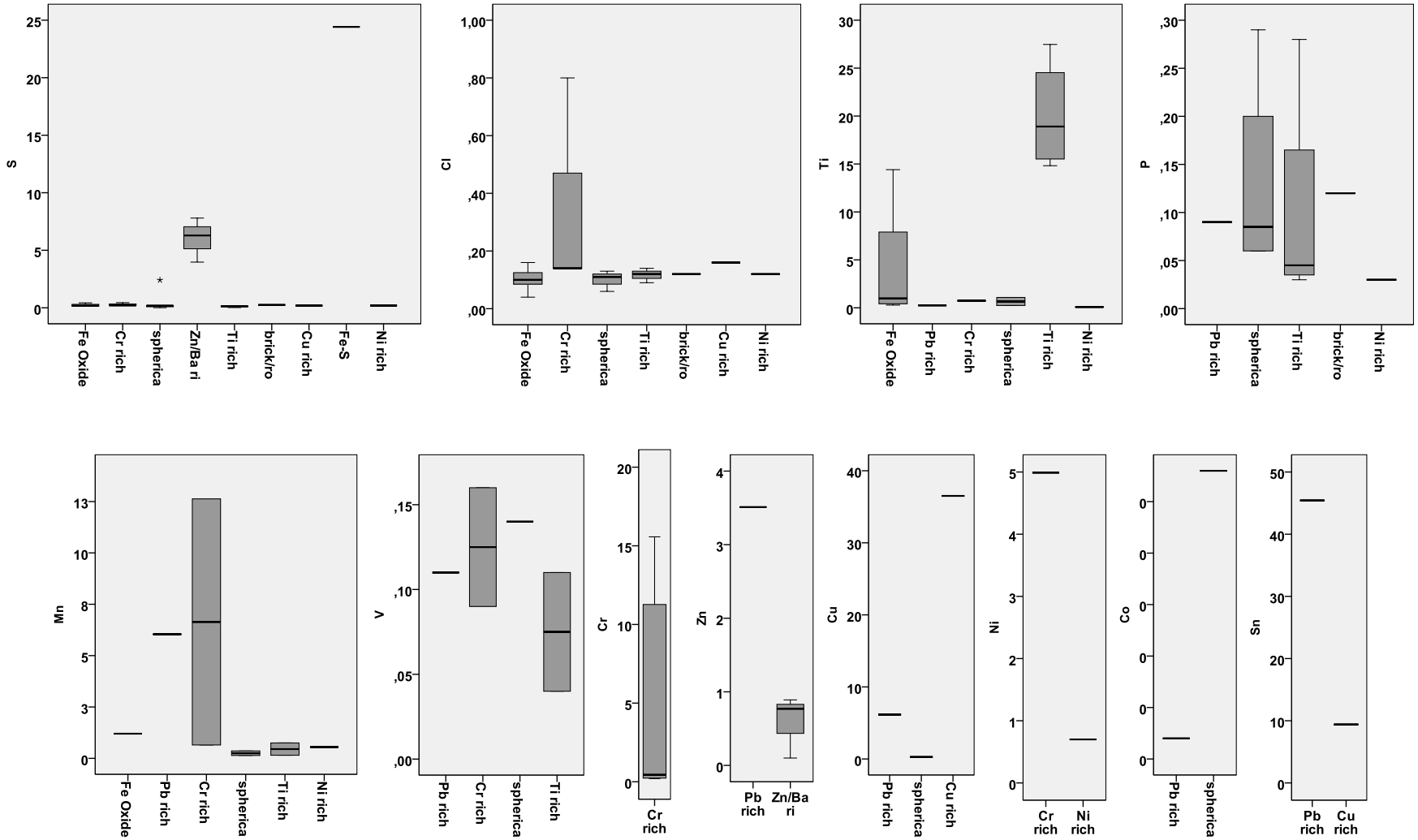
S
Fe Oxide
Cr rich
spherica
Zn/Ba ri
Ti rich
brick/ro
Cu rich
Fe-S
Ni rich
Cl
Fe Oxide
Cr rich
spherica
Ti rich
brick/ro
Cu rich
Ni rich
Ti
Fe Oxide
Pb rich
Cr rich
spherica
Ti rich
Ni rich
P
Pb rich
spherica
Ti rich
brick/ro
Ni rich
Mn
Fe Oxide
Pb rich
Cr rich
spherica
Ti rich
Ni rich
V
Pb rich
Cr rich
spherica
Ti rich
Cr
Cr rich
Zn
Pb rich
Zn/Ba ri
Cu
Pb rich
spherica
Cu rich
Ni
Cr rich
Ni rich
Co
Pb rich
spherica
Sn
Pb rich
Cu rich

Table 99: Communalities for RDS geochemical data: a) summer and b) winter (Extraction method: Principal component. PCA #A, n=72, 49 variables).

a)

**Communalities**

| | Initial | Extraction | | Initial | Extraction |
|---|---|---|---|---|---|
| Na2O_s | 1,000 | ,522 | Y_s | 1,000 | ,879 |
| MgO_s | 1,000 | ,874 | Zr_s | 1,000 | ,958 |
| Al2O3_s | 1,000 | ,931 | Nb_s | 1,000 | ,839 |
| SiO2_s | 1,000 | ,898 | Mo_s | 1,000 | ,616 |
| P2O5_s | 1,000 | ,892 | Hf_s | 1,000 | ,943 |
| K2O_s | 1,000 | ,907 | W_s | 1,000 | ,864 |
| CaO_s | 1,000 | ,827 | Pb_s | 1,000 | ,897 |
| TiO2_s | 1,000 | ,947 | Bi_s | 1,000 | ,889 |
| MnO_s | 1,000 | ,823 | Th_s | 1,000 | ,817 |
| Fe2O3_s | 1,000 | ,922 | U_s | 1,000 | ,769 |
| Sc_s | 1,000 | ,740 | Cd_s | 1,000 | ,835 |
| V_s | 1,000 | ,949 | Sn_s | 1,000 | ,867 |
| Cr_s | 1,000 | ,835 | Sb_s | 1,000 | ,912 |
| Co_s | 1,000 | ,876 | I_s | 1,000 | ,825 |
| Ba_s | 1,000 | ,891 | La_s | 1,000 | ,899 |
| Ni_s | 1,000 | ,821 | Ce_s | 1,000 | ,909 |
| Cu_s | 1,000 | ,865 | Nd_s | 1,000 | ,881 |
| Zn_s | 1,000 | ,858 | Sm_s | 1,000 | ,552 |
| Ga_s | 1,000 | ,916 | S_s | 1,000 | ,866 |
| Ge_s | 1,000 | ,699 | Cl_s | 1,000 | ,736 |
| As_s | 1,000 | ,690 | Yb_s | 1,000 | ,722 |
| Se_s | 1,000 | ,584 | LOI_s | 1,000 | ,883 |
| Br_s | 1,000 | ,836 | D_s | 1,000 | ,848 |
| Rb_s | 1,000 | ,875 | 63-inf2_s | 1,000 | ,809 |
| Sr_s | 1,000 | ,854 | | | |

b)

**Communalities**

| | Initial | Extraction | | Initial | Extraction |
|---|---|---|---|---|---|
| Na2O_w | 1,000 | ,747 | Y_w | 1,000 | ,904 |
| MgO_w | 1,000 | ,791 | Zr_w | 1,000 | ,845 |
| Al2O3_w | 1,000 | ,963 | Nb_w | 1,000 | ,876 |
| SiO2_w | 1,000 | ,928 | Mo_w | 1,000 | ,720 |
| P2O5_w | 1,000 | ,872 | Hf_w | 1,000 | ,876 |
| K2O_w | 1,000 | ,900 | W_w | 1,000 | ,444 |
| CaO_w | 1,000 | ,916 | Pb_w | 1,000 | ,872 |
| TiO2_w | 1,000 | ,906 | Bi_w | 1,000 | ,846 |
| MnO_w | 1,000 | ,791 | Th_w | 1,000 | ,864 |
| Fe2O3_w | 1,000 | ,881 | U_w | 1,000 | ,837 |
| Sc_w | 1,000 | ,764 | Cd_w | 1,000 | ,869 |
| V_w | 1,000 | ,960 | Sn_w | 1,000 | ,769 |
| Cr_w | 1,000 | ,652 | Sb_w | 1,000 | ,951 |
| Co_w | 1,000 | ,902 | I_w | 1,000 | ,878 |
| Ba_w | 1,000 | ,826 | La_w | 1,000 | ,891 |
| Ni_w | 1,000 | ,864 | Ce_w | 1,000 | ,891 |
| Cu_w | 1,000 | ,812 | Nd_w | 1,000 | ,859 |
| Zn_w | 1,000 | ,896 | Sm_w | 1,000 | ,523 |
| Ga_w | 1,000 | ,929 | S_w | 1,000 | ,902 |
| Ge_w | 1,000 | ,798 | Cl_w | 1,000 | ,840 |
| As_w | 1,000 | ,791 | Yb_w | 1,000 | ,573 |
| Se_w | 1,000 | ,832 | LOI_w | 1,000 | ,868 |
| Br_w | 1,000 | ,688 | D_w | 1,000 | ,918 |
| Rb_w | 1,000 | ,911 | 63-inf2_w | 1,000 | ,873 |
| Sr_w | 1,000 | ,799 | | | |

Table 100: Eigenvalues associated to each calculated component for RDS geochemical data: a) summer and b) winter (Extraction method: Principal component. PCA #A, n=72, 49 variables).

a)

| Total Variance Explained | | | | | | | | | |
|---|---|---|---|---|---|---|---|---|---|
| | Initial Eigenvalues | | | Extraction Sums of Squared Loadings | | | Rotation Sums of Squared Loadings | | |
| Component | Total | % of Variance | Cumulative % | Total | % of Variance | Cumulative % | Total | % of Variance | Cumulative % |
| 1 | 13,557 | 27,668 | 27,668 | 13,557 | 27,668 | 27,668 | 9,615 | 19,622 | 19,622 |
| 2 | 7,544 | 15,395 | 43,063 | 7,544 | 15,395 | 43,063 | 7,250 | 14,796 | 34,418 |
| 3 | 5,665 | 11,562 | 54,625 | 5,665 | 11,562 | 54,625 | 5,560 | 11,347 | 45,765 |
| 4 | 3,388 | 6,914 | 61,539 | 3,388 | 6,914 | 61,539 | 5,251 | 10,715 | 56,480 |
| 5 | 2,225 | 4,540 | 66,080 | 2,225 | 4,540 | 66,080 | 2,973 | 6,067 | 62,547 |
| 6 | 2,150 | 4,389 | 70,468 | 2,150 | 4,389 | 70,468 | 2,398 | 4,895 | 67,442 |
| 7 | 1,770 | 3,613 | 74,081 | 1,770 | 3,613 | 74,081 | 2,281 | 4,656 | 72,098 |
| 8 | 1,380 | 2,816 | 76,897 | 1,380 | 2,816 | 76,897 | 1,596 | 3,257 | 75,355 |
| 9 | 1,083 | 2,211 | 79,108 | 1,083 | 2,211 | 79,108 | 1,525 | 3,112 | 78,467 |
| 10 | 1,046 | 2,135 | 81,243 | 1,046 | 2,135 | 81,243 | 1,224 | 2,498 | 80,965 |
| 11 | 1,036 | 2,115 | 83,358 | 1,036 | 2,115 | 83,358 | 1,173 | 2,393 | 83,358 |
| 12 | ,902 | 1,840 | 85,199 | | | | | | |
| 13 | ,814 | 1,662 | 86,860 | | | | | | |
| 14 | ,739 | 1,507 | 88,367 | | | | | | |
| 15 | ,665 | 1,357 | 89,724 | | | | | | |
| 16 | ,550 | 1,122 | 90,846 | | | | | | |
| 17 | ,485 | ,990 | 91,835 | | | | | | |
| 18 | ,431 | ,879 | 92,714 | | | | | | |
| 19 | ,383 | ,782 | 93,495 | | | | | | |
| 20 | ,345 | ,704 | 94,199 | | | | | | |
| 21 | ,330 | ,673 | 94,872 | | | | | | |
| 22 | ,297 | ,606 | 95,478 | | | | | | |
| 23 | ,265 | ,541 | 96,019 | | | | | | |
| 24 | ,239 | ,488 | 96,507 | | | | | | |
| 25 | ,200 | ,408 | 96,915 | | | | | | |
| 26 | ,182 | ,372 | 97,287 | | | | | | |
| 27 | ,155 | ,315 | 97,602 | | | | | | |
| 28 | ,144 | ,295 | 97,897 | | | | | | |
| 29 | ,137 | ,280 | 98,177 | | | | | | |
| 30 | ,119 | ,244 | 98,421 | | | | | | |
| 31 | ,109 | ,222 | 98,643 | | | | | | |
| 32 | ,104 | ,213 | 98,856 | | | | | | |
| 33 | ,092 | ,187 | 99,043 | | | | | | |
| 34 | ,077 | ,157 | 99,201 | | | | | | |
| 35 | ,073 | ,148 | 99,349 | | | | | | |
| 36 | ,056 | ,114 | 99,463 | | | | | | |
| 37 | ,047 | ,096 | 99,559 | | | | | | |
| 38 | ,043 | ,087 | 99,646 | | | | | | |
| 39 | ,036 | ,073 | 99,719 | | | | | | |
| 40 | ,028 | ,057 | 99,776 | | | | | | |
| 41 | ,024 | ,049 | 99,825 | | | | | | |
| 42 | ,019 | ,039 | 99,864 | | | | | | |
| 43 | ,018 | ,036 | 99,900 | | | | | | |
| 44 | ,014 | ,029 | 99,930 | | | | | | |
| 45 | ,010 | ,021 | 99,950 | | | | | | |
| 46 | ,009 | ,019 | 99,969 | | | | | | |
| 47 | ,008 | ,016 | 99,985 | | | | | | |
| 48 | ,005 | ,010 | 99,995 | | | | | | |
| 49 | ,002 | ,005 | 100,000 | | | | | | |

b)

| Total Variance Explained | | | | | | | | | |
|---|---|---|---|---|---|---|---|---|---|
| | Initial Eigenvalues | | | Extraction Sums of Squared Loadings | | | Rotation Sums of Squared Loadings | | |
| Component | Total | % of Variance | Cumulative % | Total | % of Variance | Cumulative % | Total | % of Variance | Cumulative % |
| 1 | 16,111 | 32,880 | 32,880 | 16,111 | 32,880 | 32,880 | 8,794 | 17,948 | 17,948 |
| 2 | 6,568 | 13,403 | 46,283 | 6,568 | 13,403 | 46,283 | 7,250 | 14,796 | 32,743 |
| 3 | 5,151 | 10,512 | 56,795 | 5,151 | 10,512 | 56,795 | 7,091 | 14,471 | 47,215 |
| 4 | 2,963 | 6,047 | 62,842 | 2,963 | 6,047 | 62,842 | 5,624 | 11,477 | 58,692 |
| 5 | 2,163 | 4,414 | 67,256 | 2,163 | 4,414 | 67,256 | 2,177 | 4,443 | 63,135 |
| 6 | 1,997 | 4,075 | 71,330 | 1,997 | 4,075 | 71,330 | 2,134 | 4,356 | 67,491 |
| 7 | 1,875 | 3,827 | 75,157 | 1,875 | 3,827 | 75,157 | 2,075 | 4,236 | 71,727 |
| 8 | 1,576 | 3,217 | 78,375 | 1,576 | 3,217 | 78,375 | 2,028 | 4,140 | 75,866 |
| 9 | 1,233 | 2,517 | 80,891 | 1,233 | 2,517 | 80,891 | 2,013 | 4,109 | 79,975 |
| 10 | 1,170 | 2,387 | 83,278 | 1,170 | 2,387 | 83,278 | 1,619 | 3,303 | 83,278 |
| 11 | ,960 | 1,959 | 85,238 | | | | | | |
| 12 | ,889 | 1,815 | 87,052 | | | | | | |
| 13 | ,729 | 1,488 | 88,540 | | | | | | |
| 14 | ,650 | 1,327 | 89,866 | | | | | | |
| 15 | ,602 | 1,228 | 91,094 | | | | | | |
| 16 | ,570 | 1,164 | 92,258 | | | | | | |
| 17 | ,501 | 1,023 | 93,281 | | | | | | |
| 18 | ,361 | ,737 | 94,018 | | | | | | |
| 19 | ,343 | ,700 | 94,718 | | | | | | |
| 20 | ,310 | ,633 | 95,351 | | | | | | |
| 21 | ,259 | ,529 | 95,880 | | | | | | |
| 22 | ,240 | ,490 | 96,370 | | | | | | |
| 23 | ,218 | ,444 | 96,814 | | | | | | |
| 24 | ,181 | ,369 | 97,183 | | | | | | |
| 25 | ,158 | ,323 | 97,506 | | | | | | |
| 26 | ,143 | ,291 | 97,797 | | | | | | |
| 27 | ,128 | ,261 | 98,059 | | | | | | |
| 28 | ,118 | ,240 | 98,299 | | | | | | |
| 29 | ,102 | ,208 | 98,507 | | | | | | |
| 30 | ,090 | ,185 | 98,692 | | | | | | |
| 31 | ,087 | ,178 | 98,869 | | | | | | |
| 32 | ,077 | ,158 | 99,027 | | | | | | |
| 33 | ,069 | ,142 | 99,169 | | | | | | |
| 34 | ,063 | ,129 | 99,299 | | | | | | |
| 35 | ,051 | ,104 | 99,403 | | | | | | |
| 36 | ,048 | ,097 | 99,500 | | | | | | |
| 37 | ,043 | ,087 | 99,587 | | | | | | |
| 38 | ,037 | ,076 | 99,663 | | | | | | |
| 39 | ,033 | ,068 | 99,732 | | | | | | |
| 40 | ,029 | ,059 | 99,790 | | | | | | |
| 41 | ,020 | ,042 | 99,832 | | | | | | |
| 42 | ,017 | ,035 | 99,867 | | | | | | |
| 43 | ,016 | ,033 | 99,900 | | | | | | |
| 44 | ,015 | ,030 | 99,930 | | | | | | |
| 45 | ,013 | ,026 | 99,956 | | | | | | |
| 46 | ,008 | ,017 | 99,973 | | | | | | |
| 47 | ,006 | ,012 | 99,985 | | | | | | |
| 48 | ,004 | ,008 | 99,993 | | | | | | |
| 49 | ,003 | ,007 | 100,000 | | | | | | |

Table 101: Rotated component matrix (Varimax rotation with Kaiser normalisation) for RDS geochemical data: a) summer and b) winter (PCA #A, n=72, 49 variables).

a)

| Rotated Component Matrix | | | | | | | | | | | |
|---|---|---|---|---|---|---|---|---|---|---|---|
| | Component | | | | | | | | | | |
| | 1 | 2 | 3 | 4 | 5 | 6 | 7 | 8 | 9 | 10 | 11 |
| Na2O_s | ,491 | ,188 | ,237 | -,196 | ,119 | -,183 | ,138 | -,011 | -,077 | -,277 | ,040 |
| MgO_s | ,916 | -,071 | ,041 | ,004 | -,098 | -,009 | ,006 | -,074 | ,014 | -,023 | -,113 |
| Al2O3_s | ,750 | -,064 | ,520 | -,108 | ,016 | ,208 | ,172 | -,017 | -,066 | ,052 | -,049 |
| SiO2_s | ,085 | ,073 | ,084 | -,813 | ,122 | ,109 | ,402 | ,033 | ,114 | -,116 | ,044 |
| P2O5_s | ,125 | -,088 | -,047 | ,898 | -,099 | ,098 | ,173 | -,033 | -,086 | ,003 | -,049 |
| K2O_s | ,400 | -,039 | ,571 | ,047 | ,126 | ,089 | ,582 | ,037 | ,178 | ,132 | -,067 |
| CaO_s | -,224 | -,007 | -,020 | -,100 | ,035 | -,074 | -,851 | ,033 | ,176 | ,052 | -,038 |
| TiO2_s | ,944 | -,043 | ,193 | -,006 | ,016 | ,108 | ,030 | -,006 | -,048 | ,028 | -,017 |
| MnO_s | ,700 | ,157 | ,443 | ,066 | -,087 | -,218 | -,091 | -,065 | ,185 | -,067 | ,028 |
| Fe2O3_s | ,823 | ,438 | ,165 | -,074 | ,038 | ,057 | ,102 | ,003 | ,001 | ,044 | -,051 |
| Sc_s | ,738 | -,013 | ,308 | ,042 | -,003 | -,061 | ,271 | -,042 | -,055 | ,127 | -,030 |
| V_s | ,909 | -,069 | ,196 | ,230 | -,033 | ,080 | ,040 | ,017 | ,030 | ,112 | -,061 |
| Cr_s | ,156 | ,279 | -,039 | -,067 | ,845 | -,053 | ,018 | -,078 | ,016 | -,047 | -,033 |
| Co_s | ,908 | ,096 | ,049 | ,113 | ,022 | ,060 | ,057 | ,060 | ,089 | ,091 | ,013 |
| Ba_s | ,184 | ,787 | ,311 | -,103 | ,286 | ,099 | ,039 | ,086 | ,151 | -,081 | -,027 |
| Ni_s | ,819 | ,241 | -,138 | ,114 | ,051 | ,153 | -,122 | ,002 | ,125 | -,028 | ,062 |
| Cu_s | ,062 | ,903 | -,048 | -,003 | ,157 | -,026 | ,027 | ,067 | -,026 | ,085 | ,074 |
| Zn_s | ,089 | ,856 | -,023 | ,289 | -,018 | ,074 | ,027 | ,103 | ,000 | -,001 | ,128 |
| Ga_s | ,848 | -,047 | ,316 | ,051 | ,003 | ,084 | ,155 | -,012 | -,088 | ,210 | -,096 |
| Ge_s | ,160 | ,239 | ,196 | ,025 | -,065 | ,628 | ,150 | -,052 | -,153 | -,049 | -,357 |
| As_s | ,004 | ,272 | ,222 | ,164 | ,234 | ,579 | ,213 | -,077 | ,124 | -,277 | ,080 |
| Se_s | ,152 | ,331 | -,011 | ,557 | ,093 | ,251 | -,018 | -,024 | ,162 | -,204 | -,036 |
| Br_s | -,017 | ,437 | -,142 | ,739 | -,018 | ,189 | ,092 | ,024 | ,008 | ,093 | ,156 |
| Rb_s | ,373 | -,073 | ,582 | ,060 | ,153 | ,153 | ,501 | ,040 | ,220 | ,193 | -,057 |
| Sr_s | ,230 | ,706 | ,133 | -,100 | ,057 | -,161 | -,452 | ,114 | ,166 | -,023 | -,037 |
| Y_s | ,660 | ,075 | ,622 | ,055 | ,099 | ,005 | ,030 | -,064 | ,173 | -,020 | ,050 |
| Zr_s | -,013 | ,211 | ,203 | -,148 | ,916 | ,103 | ,010 | ,020 | ,009 | -,011 | ,013 |
| Nb_s | ,768 | ,125 | ,413 | -,045 | ,094 | ,164 | ,122 | -,051 | -,077 | -,010 | ,019 |
| Mo_s | ,009 | ,733 | -,104 | -,062 | ,078 | ,013 | ,087 | ,047 | -,198 | ,075 | ,049 |
| Hf_s | -,070 | ,192 | ,194 | -,103 | ,911 | ,126 | -,047 | ,028 | -,056 | ,001 | -,021 |
| W_s | -,112 | ,203 | ,038 | ,018 | -,031 | ,079 | ,024 | -,042 | -,018 | -,053 | ,892 |
| Pb_s | ,021 | ,906 | ,012 | ,156 | ,087 | ,000 | -,015 | ,029 | ,193 | ,076 | ,015 |
| Bi_s | -,017 | ,178 | -,020 | -,017 | -,011 | -,009 | -,046 | ,919 | -,006 | -,090 | -,044 |
| Th_s | ,213 | ,046 | ,825 | -,025 | ,106 | ,237 | ,096 | -,036 | -,066 | ,067 | ,043 |
| U_s | -,124 | -,338 | ,490 | -,056 | ,166 | ,137 | -,460 | -,083 | -,321 | ,164 | ,032 |
| Cd_s | -,127 | ,469 | -,068 | -,001 | -,010 | ,155 | ,051 | ,740 | ,022 | ,134 | ,018 |
| Sn_s | ,008 | ,868 | ,177 | ,023 | ,161 | ,153 | -,007 | ,112 | -,030 | -,133 | -,012 |
| Sb_s | ,027 | ,941 | ,030 | ,099 | ,083 | ,060 | -,012 | ,058 | -,022 | ,010 | ,017 |
| I_s | ,008 | ,369 | ,087 | ,767 | ,112 | ,205 | -,008 | ,089 | -,109 | ,027 | ,133 |
| La_s | ,364 | ,020 | ,857 | -,111 | ,048 | ,091 | ,032 | -,032 | ,069 | ,027 | -,018 |
| Ce_s | ,341 | ,186 | ,856 | -,113 | ,090 | ,032 | -,015 | -,015 | ,037 | -,023 | -,035 |
| Nd_s | ,475 | ,047 | ,777 | ,045 | ,024 | ,051 | -,150 | ,044 | ,115 | -,061 | ,052 |
| Sm_s | ,179 | ,106 | ,211 | -,098 | -,358 | ,102 | -,100 | -,104 | ,514 | -,067 | -,166 |
| S_s | ,104 | -,057 | ,080 | ,903 | -,110 | -,002 | ,086 | -,003 | ,040 | ,089 | -,037 |
| Cl_s | ,083 | ,033 | -,064 | ,365 | -,091 | -,187 | ,030 | -,065 | -,727 | -,081 | -,090 |
| Yb_s | ,271 | ,136 | ,106 | ,110 | -,033 | ,041 | -,006 | -,027 | ,017 | ,775 | -,050 |
| LOI_s | -,017 | -,034 | -,123 | ,890 | -,129 | -,011 | ,097 | -,025 | -,217 | -,013 | -,015 |
| D_s | -,172 | ,029 | -,138 | -,063 | -,103 | -,701 | -,009 | -,247 | -,257 | -,345 | -,214 |
| 63-inf2_s | ,190 | -,012 | ,170 | ,413 | ,049 | ,711 | -,063 | ,069 | ,174 | ,073 | ,145 |

b)

**Rotated Component Matrix**

| | Component | | | | | | | | | |
|---|---|---|---|---|---|---|---|---|---|---|
| | 1 | 2 | 3 | 4 | 5 | 6 | 7 | 8 | 9 | 10 |
| Na2O_w | ,192 | ,082 | ,213 | -,272 | -,059 | -,145 | -,130 | -,383 | ,603 | -,181 |
| MgO_w | ,722 | -,074 | ,247 | ,143 | -,346 | ,147 | ,068 | -,188 | ,038 | -,003 |
| Al2O3_w | ,736 | -,006 | ,628 | -,009 | -,002 | -,132 | -,077 | ,001 | ,050 | ,011 |
| SiO2_w | -,192 | -,077 | ,096 | -,781 | -,055 | -,472 | -,083 | -,130 | -,019 | -,128 |
| P2O5_w | ,260 | -,116 | ,031 | ,835 | -,039 | -,120 | ,043 | -,181 | -,204 | -,008 |
| K2O_w | ,186 | ,092 | ,855 | -,075 | ,064 | -,287 | -,088 | ,133 | ,093 | ,002 |
| CaO_w | -,046 | ,032 | -,141 | -,204 | ,007 | ,898 | ,130 | ,075 | -,021 | ,146 |
| TiO2_w | ,887 | ,145 | ,213 | ,096 | -,039 | -,086 | -,011 | ,168 | ,020 | -,080 |
| MnO_w | ,757 | ,288 | ,272 | ,070 | ,078 | ,171 | -,011 | ,055 | ,007 | ,134 |
| Fe2O3_w | ,749 | ,461 | ,208 | -,009 | ,180 | -,071 | -,023 | ,104 | ,123 | -,004 |
| Sc_w | ,756 | -,017 | ,289 | ,121 | ,154 | -,112 | ,002 | -,010 | ,121 | ,206 |
| V_w | ,874 | ,048 | ,309 | ,276 | ,078 | ,035 | -,002 | ,092 | -,049 | -,063 |
| Cr_w | ,453 | ,627 | -,006 | -,067 | -,119 | -,066 | ,012 | ,097 | ,141 | ,026 |
| Co_w | ,829 | ,303 | ,105 | ,118 | ,250 | ,042 | -,062 | ,145 | ,028 | -,087 |
| Ba_w | ,214 | ,733 | ,359 | -,068 | ,233 | ,108 | ,010 | -,117 | -,073 | -,159 |
| Ni_w | ,773 | ,422 | -,035 | ,131 | ,155 | -,025 | ,002 | ,174 | -,007 | -,122 |
| Cu_w | ,219 | ,829 | ,003 | ,107 | ,085 | -,052 | ,129 | ,130 | ,147 | ,019 |
| Zn_w | ,218 | ,744 | -,016 | ,430 | -,086 | ,002 | ,151 | ,228 | ,072 | -,148 |
| Ga_w | ,768 | -,018 | ,536 | ,153 | ,005 | -,073 | -,078 | ,033 | ,052 | ,110 |
| Ge_w | ,235 | ,001 | ,268 | ,223 | ,757 | -,018 | -,066 | ,072 | -,195 | -,020 |
| As_w | ,116 | ,184 | ,195 | ,202 | ,803 | ,050 | -,061 | ,097 | ,026 | ,052 |
| Se_w | ,077 | ,133 | -,089 | ,713 | ,483 | -,016 | ,039 | ,176 | -,160 | ,041 |
| Br_w | ,018 | ,127 | ,076 | ,790 | ,108 | -,104 | -,016 | ,115 | ,070 | -,035 |
| Rb_w | ,230 | ,021 | ,894 | ,070 | ,105 | -,162 | -,052 | ,080 | ,077 | ,034 |
| Sr_w | ,120 | ,672 | ,101 | -,172 | ,036 | ,459 | -,012 | -,275 | ,075 | -,024 |
| Y_w | ,679 | ,219 | ,565 | ,152 | ,142 | ,162 | -,003 | -,051 | -,001 | ,051 |
| Zr_w | ,101 | ,607 | ,410 | -,245 | -,035 | -,316 | ,111 | ,049 | -,013 | ,351 |
| Nb_w | ,619 | ,363 | ,586 | ,056 | -,024 | -,010 | ,032 | -,014 | ,073 | ,091 |
| Mo_w | ,077 | ,413 | ,126 | ,057 | -,114 | ,040 | -,004 | ,239 | ,669 | ,070 |
| Hf_w | ,086 | ,580 | ,464 | -,127 | ,016 | -,386 | ,017 | ,068 | -,031 | ,382 |
| W_w | ,011 | ,593 | ,105 | ,125 | ,074 | -,043 | -,128 | ,130 | -,156 | ,003 |
| Pb_w | ,034 | ,877 | ,043 | ,109 | ,077 | ,063 | ,074 | -,158 | -,051 | -,213 |
| Bi_w | -,077 | ,126 | -,014 | ,000 | -,060 | ,008 | ,896 | ,111 | ,008 | -,076 |
| Th_w | ,267 | -,050 | ,857 | ,008 | ,113 | -,087 | ,006 | ,074 | ,077 | ,157 |
| U_w | -,007 | -,247 | ,307 | ,086 | ,077 | ,108 | -,012 | -,113 | ,033 | ,802 |
| Cd_w | ,007 | ,122 | -,070 | ,137 | -,053 | ,130 | ,892 | ,024 | -,119 | -,032 |
| Sn_w | ,137 | ,705 | -,067 | ,230 | ,196 | ,008 | ,297 | ,163 | ,103 | ,179 |
| Sb_w | ,132 | ,918 | ,079 | ,196 | -,069 | ,091 | ,051 | ,076 | ,108 | -,114 |
| I_w | ,108 | ,217 | -,007 | ,832 | ,194 | -,174 | ,174 | ,037 | -,160 | -,036 |
| La_w | ,311 | ,094 | ,843 | -,049 | ,037 | ,188 | ,007 | ,077 | ,100 | ,139 |
| Ce_w | ,278 | ,323 | ,800 | -,102 | ,057 | ,074 | -,019 | -,062 | ,158 | ,149 |
| Nd_w | ,477 | ,225 | ,680 | ,068 | ,196 | ,255 | -,025 | ,051 | -,005 | ,085 |
| Sm_w | ,095 | ,001 | ,381 | -,016 | -,045 | ,128 | -,226 | ,209 | -,012 | ,505 |
| S_w | ,374 | ,196 | ,198 | ,736 | ,101 | ,167 | ,052 | ,262 | ,165 | -,083 |
| Cl_w | ,053 | -,087 | ,147 | -,050 | -,034 | ,019 | -,036 | -,023 | ,894 | ,044 |
| Yb_w | ,461 | -,017 | -,235 | ,117 | ,271 | -,276 | ,327 | ,080 | ,107 | ,131 |
| LOI (%)_w | ,043 | ,038 | -,136 | ,904 | -,028 | -,114 | -,059 | ,079 | ,033 | ,072 |
| D_w | -,231 | -,153 | -,205 | -,211 | -,171 | ,036 | -,131 | -,841 | ,010 | -,014 |
| 63-inf2_w | ,342 | ,197 | ,269 | ,416 | ,130 | ,137 | ,117 | ,648 | ,035 | -,030 |

Table 102: Eigenvalues associated to each calculated component for RDS geochemical data: a) summer and b) winter (Extraction method: Principal component. PCA #B, n=72, 49 variables).

a)

| Total Variance Explained | | | | | | | | | |
|---|---|---|---|---|---|---|---|---|---|
| | Initial Eigenvalues | | | Extraction Sums of Squared Loadings | | | Rotation Sums of Squared Loadings | | |
| Component | Total | % of Variance | Cumulative % | Total | % of Variance | Cumulative % | Total | % of Variance | Cumulative % |
| 1 | 13,557 | 27,668 | 27,668 | 13,557 | 27,668 | 27,668 | 11,596 | 23,665 | 23,665 |
| 2 | 7,544 | 15,395 | 43,063 | 7,544 | 15,395 | 43,063 | 7,686 | 15,685 | 39,350 |
| 3 | 5,665 | 11,562 | 54,625 | 5,665 | 11,562 | 54,625 | 5,741 | 11,716 | 51,066 |
| 4 | 3,388 | 6,914 | 61,539 | 3,388 | 6,914 | 61,539 | 5,132 | 10,474 | 61,539 |
| 5 | 2,225 | 4,540 | 66,080 | | | | | | |
| 6 | 2,150 | 4,389 | 70,468 | | | | | | |
| 7 | 1,770 | 3,613 | 74,081 | | | | | | |
| 8 | 1,380 | 2,816 | 76,897 | | | | | | |
| 9 | 1,083 | 2,211 | 79,108 | | | | | | |
| 10 | 1,046 | 2,135 | 81,243 | | | | | | |
| 11 | 1,036 | 2,115 | 83,358 | | | | | | |
| 12 | ,902 | 1,840 | 85,199 | | | | | | |
| 13 | ,814 | 1,662 | 86,860 | | | | | | |
| 14 | ,739 | 1,507 | 88,367 | | | | | | |
| 15 | ,665 | 1,357 | 89,724 | | | | | | |
| 16 | ,550 | 1,122 | 90,846 | | | | | | |
| 17 | ,485 | ,990 | 91,835 | | | | | | |
| 18 | ,431 | ,879 | 92,714 | | | | | | |
| 19 | ,383 | ,782 | 93,495 | | | | | | |
| 20 | ,345 | ,704 | 94,199 | | | | | | |
| 21 | ,330 | ,673 | 94,872 | | | | | | |
| 22 | ,297 | ,606 | 95,478 | | | | | | |
| 23 | ,265 | ,541 | 96,019 | | | | | | |
| 24 | ,239 | ,488 | 96,507 | | | | | | |
| 25 | ,200 | ,408 | 96,915 | | | | | | |
| 26 | ,182 | ,372 | 97,287 | | | | | | |
| 27 | ,155 | ,315 | 97,602 | | | | | | |
| 28 | ,144 | ,295 | 97,897 | | | | | | |
| 29 | ,137 | ,280 | 98,177 | | | | | | |
| 30 | ,119 | ,244 | 98,421 | | | | | | |
| 31 | ,109 | ,222 | 98,643 | | | | | | |
| 32 | ,104 | ,213 | 98,856 | | | | | | |
| 33 | ,092 | ,187 | 99,043 | | | | | | |
| 34 | ,077 | ,157 | 99,201 | | | | | | |
| 35 | ,073 | ,148 | 99,349 | | | | | | |
| 36 | ,056 | ,114 | 99,463 | | | | | | |
| 37 | ,047 | ,096 | 99,559 | | | | | | |
| 38 | ,043 | ,087 | 99,646 | | | | | | |
| 39 | ,036 | ,073 | 99,719 | | | | | | |
| 40 | ,028 | ,057 | 99,776 | | | | | | |
| 41 | ,024 | ,049 | 99,825 | | | | | | |
| 42 | ,019 | ,039 | 99,864 | | | | | | |
| 43 | ,018 | ,036 | 99,900 | | | | | | |
| 44 | ,014 | ,029 | 99,930 | | | | | | |
| 45 | ,010 | ,021 | 99,950 | | | | | | |
| 46 | ,009 | ,019 | 99,969 | | | | | | |
| 47 | ,008 | ,016 | 99,985 | | | | | | |
| 48 | ,005 | ,010 | 99,995 | | | | | | |
| 49 | ,002 | ,005 | 100,000 | | | | | | |

b)

**Total Variance Explained**

| Component | Initial Eigenvalues | | | Extraction Sums of Squared Loadings | | | Rotation Sums of Squared Loadings | | |
|---|---|---|---|---|---|---|---|---|---|
| | Total | % of Variance | Cumulative % | Total | % of Variance | Cumulative % | Total | % of Variance | Cumulative % |
| 1 | 16,111 | 32,880 | 32,880 | 16,111 | 32,880 | 32,880 | 9,150 | 18,673 | 18,673 |
| 2 | 6,568 | 13,403 | 46,283 | 6,568 | 13,403 | 46,283 | 7,749 | 15,813 | 34,486 |
| 3 | 5,151 | 10,512 | 56,795 | 5,151 | 10,512 | 56,795 | 7,313 | 14,924 | 49,410 |
| 4 | 2,963 | 6,047 | 62,842 | 2,963 | 6,047 | 62,842 | 6,582 | 13,432 | 62,842 |
| 5 | 2,163 | 4,414 | 67,256 | | | | | | |
| 6 | 1,997 | 4,075 | 71,330 | | | | | | |
| 7 | 1,875 | 3,827 | 75,157 | | | | | | |
| 8 | 1,576 | 3,217 | 78,375 | | | | | | |
| 9 | 1,233 | 2,517 | 80,891 | | | | | | |
| 10 | 1,170 | 2,387 | 83,278 | | | | | | |
| 11 | ,960 | 1,959 | 85,238 | | | | | | |
| 12 | ,889 | 1,815 | 87,052 | | | | | | |
| 13 | ,729 | 1,488 | 88,540 | | | | | | |
| 14 | ,650 | 1,327 | 89,866 | | | | | | |
| 15 | ,602 | 1,228 | 91,094 | | | | | | |
| 16 | ,570 | 1,164 | 92,258 | | | | | | |
| 17 | ,501 | 1,023 | 93,281 | | | | | | |
| 18 | ,361 | ,737 | 94,018 | | | | | | |
| 19 | ,343 | ,700 | 94,718 | | | | | | |
| 20 | ,310 | ,633 | 95,351 | | | | | | |
| 21 | ,259 | ,529 | 95,880 | | | | | | |
| 22 | ,240 | ,490 | 96,370 | | | | | | |
| 23 | ,218 | ,444 | 96,814 | | | | | | |
| 24 | ,181 | ,369 | 97,183 | | | | | | |
| 25 | ,158 | ,323 | 97,506 | | | | | | |
| 26 | ,143 | ,291 | 97,797 | | | | | | |
| 27 | ,128 | ,261 | 98,059 | | | | | | |
| 28 | ,118 | ,240 | 98,299 | | | | | | |
| 29 | ,102 | ,208 | 98,507 | | | | | | |
| 30 | ,090 | ,185 | 98,692 | | | | | | |
| 31 | ,087 | ,178 | 98,869 | | | | | | |
| 32 | ,077 | ,158 | 99,027 | | | | | | |
| 33 | ,069 | ,142 | 99,169 | | | | | | |
| 34 | ,063 | ,129 | 99,299 | | | | | | |
| 35 | ,051 | ,104 | 99,403 | | | | | | |
| 36 | ,048 | ,097 | 99,500 | | | | | | |
| 37 | ,043 | ,087 | 99,587 | | | | | | |
| 38 | ,037 | ,076 | 99,663 | | | | | | |
| 39 | ,033 | ,068 | 99,732 | | | | | | |
| 40 | ,029 | ,059 | 99,790 | | | | | | |
| 41 | ,020 | ,042 | 99,832 | | | | | | |
| 42 | ,017 | ,035 | 99,867 | | | | | | |
| 43 | ,016 | ,033 | 99,900 | | | | | | |
| 44 | ,015 | ,030 | 99,930 | | | | | | |
| 45 | ,013 | ,026 | 99,956 | | | | | | |
| 46 | ,008 | ,017 | 99,973 | | | | | | |
| 47 | ,006 | ,012 | 99,985 | | | | | | |
| 48 | ,004 | ,008 | 99,993 | | | | | | |
| 49 | ,003 | ,007 | 100,000 | | | | | | |

Table 103: Rotated component matrix (Varimax rotation with Kaiser normalisation) for RDS geochemical data: a) summer and b) winter (PCA #B, n=72, 49 variables).

a)

**Rotated Component Matrix**

| | Component | | | | | Component | | | |
|---|---|---|---|---|---|---|---|---|---|
| | 1 | 2 | 3 | 4 | | 1 | 2 | 3 | 4 |
| Na2O_s | ,533 | ,182 | -,249 | ,057 | Y_s | ,795 | ,035 | -,015 | ,416 |
| MgO_s | ,888 | -,093 | ,041 | -,158 | Zr_s | -,056 | ,362 | -,291 | ,622 |
| Al2O3_s | ,858 | -,120 | -,063 | ,379 | Nb_s | ,836 | ,090 | -,016 | ,311 |
| SiO2_s | ,143 | ,075 | -,751 | ,174 | Mo_s | ,011 | ,718 | -,010 | -,047 |
| P2O5_s | ,102 | -,108 | ,912 | ,009 | Hf_s | -,120 | ,343 | -,245 | ,621 |
| K2O_s | ,588 | -,095 | ,037 | ,544 | W_s | -,147 | ,228 | ,072 | ,130 |
| CaO_s | -,285 | ,055 | -,208 | -,107 | Pb_s | ,071 | ,894 | ,137 | ,051 |
| TiO2_s | ,933 | -,048 | ,039 | ,063 | Bi_s | -,052 | ,328 | -,023 | -,034 |
| MnO_s | ,808 | ,102 | -,016 | ,070 | Th_s | ,423 | -,033 | -,046 | ,725 |
| Fe2O3_s | ,854 | ,411 | -,031 | ,044 | U_s | -,072 | -,352 | -,110 | ,436 |
| Sc_s | ,814 | -,067 | ,060 | ,121 | Cd_s | -,137 | ,571 | ,061 | ,049 |
| V_s | ,911 | -,081 | ,261 | ,055 | Sn_s | ,071 | ,867 | ,017 | ,244 |
| Cr_s | ,059 | ,423 | -,209 | ,319 | Sb_s | ,069 | ,923 | ,111 | ,067 |
| Co_s | ,872 | ,116 | ,152 | -,031 | I_s | -,006 | ,393 | ,763 | ,244 |
| Ba_s | ,277 | ,798 | -,153 | ,364 | La_s | ,590 | -,064 | -,171 | ,622 |
| Ni_s | ,713 | ,291 | ,162 | -,119 | Ce_s | ,568 | ,106 | -,196 | ,600 |
| Cu_s | ,077 | ,906 | ,004 | ,011 | Nd_s | ,646 | ,003 | -,039 | ,507 |
| Zn_s | ,108 | ,844 | ,321 | ,006 | Sm_s | ,302 | ,019 | -,089 | -,001 |
| Ga_s | ,904 | -,093 | ,099 | ,165 | S_s | ,125 | -,084 | ,872 | ,052 |
| Ge_s | ,232 | ,165 | ,169 | ,352 | Cl_s | ,048 | -,027 | ,387 | -,231 |
| As_s | ,036 | ,292 | ,210 | ,571 | Yb_s | ,331 | ,074 | ,179 | ,076 |
| Se_s | ,122 | ,360 | ,542 | ,150 | LOI_s | -,057 | -,056 | ,895 | -,110 |
| Br_s | -,055 | ,443 | ,784 | ,039 | D_s | -,154 | -,043 | -,202 | -,510 |
| Rb_s | ,554 | -,118 | ,051 | ,596 | 63-inf2_s | ,168 | ,029 | ,516 | ,491 |
| Sr_s | ,259 | ,722 | -,187 | -,059 | | | | | |

b)

**Rotated Component Matrix**

| | Component | | | | | Component | | | |
|---|---|---|---|---|---|---|---|---|---|
| | 1 | 2 | 3 | 4 | | 1 | 2 | 3 | 4 |
| Na2O_w | ,292 | ,105 | ,139 | -,503 | Y_w | ,712 | ,243 | ,507 | ,142 |
| MgO_w | ,784 | -,072 | ,087 | -,031 | Zr_w | ,037 | ,610 | ,502 | -,193 |
| Al2O3_w | ,767 | ,015 | ,588 | -,045 | Nb_w | ,648 | ,386 | ,530 | ,014 |
| SiO2_w | -,233 | -,077 | ,128 | -,756 | Mo_w | ,154 | ,477 | ,136 | -,040 |
| P2O5_w | ,281 | -,185 | -,024 | ,724 | Hf_w | ,020 | ,562 | ,594 | -,076 |
| K2O_w | ,230 | ,128 | ,847 | -,079 | W_w | -,018 | ,553 | ,134 | ,185 |
| CaO_w | -,023 | ,093 | -,210 | -,146 | Pb_w | ,047 | ,861 | -,067 | ,091 |
| TiO2_w | ,885 | ,167 | ,173 | ,122 | Bi_w | -,079 | ,281 | -,176 | ,107 |
| MnO_w | ,747 | ,304 | ,270 | ,102 | Th_w | ,309 | -,001 | ,857 | ,008 |
| Fe2O3_w | ,728 | ,486 | ,233 | ,058 | U_w | -,056 | -,272 | ,522 | ,069 |
| Sc_w | ,736 | ,000 | ,360 | ,136 | Cd_w | -,003 | ,254 | -,243 | ,234 |
| V_w | ,886 | ,066 | ,256 | ,299 | Sn_w | ,090 | ,745 | -,010 | ,343 |
| Cr_w | ,436 | ,630 | -,014 | -,072 | Sb_w | ,161 | ,919 | -,011 | ,162 |
| Co_w | ,808 | ,324 | ,118 | ,216 | I_w | ,098 | ,191 | -,011 | ,860 |
| Ba_w | ,225 | ,743 | ,278 | -,029 | La_w | ,376 | ,154 | ,785 | -,071 |
| Ni_w | ,740 | ,436 | -,037 | ,231 | Ce_w | ,333 | ,361 | ,760 | -,157 |
| Cu_w | ,198 | ,849 | ,012 | ,159 | Nd_w | ,516 | ,266 | ,637 | ,099 |
| Zn_w | ,240 | ,758 | -,104 | ,430 | Sm_w | ,071 | -,024 | ,529 | ,005 |
| Ga_w | ,789 | -,008 | ,528 | ,118 | S_w | ,442 | ,228 | ,139 | ,720 |
| Ge_w | ,180 | ,017 | ,395 | ,455 | Cl_w | ,170 | -,006 | ,159 | -,237 |
| As_w | ,072 | ,216 | ,359 | ,423 | Yb_w | ,380 | ,036 | -,123 | ,257 |
| Se_w | ,032 | ,117 | ,018 | ,866 | LOI_w | ,064 | -,024 | -,101 | ,817 |
| Br_w | ,056 | ,103 | ,082 | ,746 | D_w | -,198 | -,247 | -,282 | -,483 |
| Rb_w | ,288 | ,059 | ,868 | ,050 | 63-inf2_w | ,357 | ,277 | ,267 | ,582 |
| Sr_w | ,158 | ,673 | -,004 | -,240 | | | | | |

Table 104: Communalities for RDS geochemical data: a) summer and b) winter (Extraction method: Principal component. PCA #C, n=72, 20 variables).

a)

**Communalities**

| | Initial | Extraction |
|---|---|---|
| Al2O3_s | 1,000 | ,855 |
| TiO2_s | 1,000 | ,945 |
| Fe2O3_s | 1,000 | ,900 |
| Cr_s | 1,000 | ,405 |
| Co_s | 1,000 | ,880 |
| Ba_s | 1,000 | ,876 |
| Ni_s | 1,000 | ,708 |
| Cu_s | 1,000 | ,858 |
| Zn_s | 1,000 | ,872 |
| Ga_s | 1,000 | ,875 |
| Ge_s | 1,000 | ,575 |
| As_s | 1,000 | ,727 |
| Sr_s | 1,000 | ,684 |
| Mo_s | 1,000 | ,537 |
| Pb_s | 1,000 | ,848 |
| Bi_s | 1,000 | ,830 |
| Cd_s | 1,000 | ,822 |
| Sn_s | 1,000 | ,850 |
| Sb_s | 1,000 | ,908 |
| LOI_s | 1,000 | ,845 |
| 63-inf2_s | 1,000 | ,691 |

b)

**Communalities**

| | Initial | Extraction |
|---|---|---|
| Al2O3_w | 1,000 | ,848 |
| TiO2_w | 1,000 | ,898 |
| Fe2O3_w | 1,000 | ,854 |
| Cr_w | 1,000 | ,597 |
| Co_w | 1,000 | ,853 |
| Ba_w | 1,000 | ,816 |
| Ni_w | 1,000 | ,770 |
| Cu_w | 1,000 | ,822 |
| Zn_w | 1,000 | ,871 |
| Ga_w | 1,000 | ,862 |
| Ge_w | 1,000 | ,845 |
| As_w | 1,000 | ,805 |
| Sr_w | 1,000 | ,738 |
| Mo_w | 1,000 | ,386 |
| Pb_w | 1,000 | ,811 |
| Bi_w | 1,000 | ,905 |
| Cd_w | 1,000 | ,903 |
| Sn_w | 1,000 | ,735 |
| Sb_w | 1,000 | ,932 |
| LOI_w | 1,000 | ,746 |
| 63-inf2_w | 1,000 | ,629 |

Table 105: Eigenvalues associated to each calculated component for RDS geochemical data: a) summer and b) winter (Extraction method: Principal component. PCA #C, n=72, 20 variables).

a)

**Total Variance Explained**

| | Initial Eigenvalues | | | Extraction Sums of Squared Loadings | | | Rotation Sums of Squared Loadings | | |
|---|---|---|---|---|---|---|---|---|---|
| Component | Total | % of Variance | Cumulative % | Total | % of Variance | Cumulative % | Total | % of Variance | Cumulative % |
| 1 | 7,520 | 35,808 | 35,808 | 7,520 | 35,808 | 35,808 | 6,405 | 30,498 | 30,498 |
| 2 | 4,525 | 21,548 | 57,356 | 4,525 | 21,548 | 57,356 | 4,949 | 23,567 | 54,065 |
| 3 | 1,800 | 8,569 | 65,925 | 1,800 | 8,569 | 65,925 | 2,036 | 9,695 | 63,759 |
| 4 | 1,400 | 6,668 | 72,593 | 1,400 | 6,668 | 72,593 | 1,644 | 7,830 | 71,590 |
| 5 | 1,245 | 5,928 | 78,521 | 1,245 | 5,928 | 78,521 | 1,456 | 6,931 | 78,521 |
| 6 | ,825 | 3,927 | 82,448 | | | | | | |
| 7 | ,731 | 3,480 | 85,928 | | | | | | |
| 8 | ,574 | 2,735 | 88,662 | | | | | | |
| 9 | ,459 | 2,184 | 90,847 | | | | | | |
| 10 | ,454 | 2,162 | 93,008 | | | | | | |
| 11 | ,336 | 1,599 | 94,607 | | | | | | |
| 12 | ,222 | 1,058 | 95,665 | | | | | | |
| 13 | ,194 | ,926 | 96,590 | | | | | | |
| 14 | ,170 | ,808 | 97,398 | | | | | | |
| 15 | ,128 | ,609 | 98,007 | | | | | | |
| 16 | ,113 | ,537 | 98,545 | | | | | | |
| 17 | ,103 | ,489 | 99,033 | | | | | | |
| 18 | ,067 | ,320 | 99,353 | | | | | | |
| 19 | ,053 | ,254 | 99,608 | | | | | | |
| 20 | ,052 | ,249 | 99,857 | | | | | | |
| 21 | ,030 | ,143 | 100,000 | | | | | | |

b)

| Total Variance Explained | | | | | | | | | |
|---|---|---|---|---|---|---|---|---|---|
| | Initial Eigenvalues | | | Extraction Sums of Squared Loadings | | | Rotation Sums of Squared Loadings | | |
| Component | Total | % of Variance | Cumulative % | Total | % of Variance | Cumulative % | Total | % of Variance | Cumulative % |
| 1 | 8,395 | 39,978 | 39,978 | 8,395 | 39,978 | 39,978 | 5,899 | 28,089 | 28,089 |
| 2 | 3,399 | 16,186 | 56,164 | 3,399 | 16,186 | 56,164 | 5,116 | 24,362 | 52,451 |
| 3 | 1,897 | 9,033 | 65,198 | 1,897 | 9,033 | 65,198 | 1,960 | 9,331 | 61,782 |
| 4 | 1,582 | 7,533 | 72,731 | 1,582 | 7,533 | 72,731 | 1,949 | 9,283 | 71,065 |
| 5 | 1,352 | 6,436 | 79,167 | 1,352 | 6,436 | 79,167 | 1,701 | 8,102 | 79,167 |
| 6 | ,855 | 4,070 | 83,236 | | | | | | |
| 7 | ,708 | 3,371 | 86,608 | | | | | | |
| 8 | ,523 | 2,492 | 89,099 | | | | | | |
| 9 | ,465 | 2,216 | 91,316 | | | | | | |
| 10 | ,411 | 1,955 | 93,271 | | | | | | |
| 11 | ,334 | 1,588 | 94,859 | | | | | | |
| 12 | ,228 | 1,088 | 95,947 | | | | | | |
| 13 | ,209 | ,997 | 96,944 | | | | | | |
| 14 | ,152 | ,726 | 97,670 | | | | | | |
| 15 | ,124 | ,588 | 98,258 | | | | | | |
| 16 | ,109 | ,520 | 98,779 | | | | | | |
| 17 | ,078 | ,371 | 99,150 | | | | | | |
| 18 | ,060 | ,288 | 99,438 | | | | | | |
| 19 | ,048 | ,228 | 99,666 | | | | | | |
| 20 | ,035 | ,169 | 99,835 | | | | | | |
| 21 | ,035 | ,165 | 100,000 | | | | | | |

Table 106: Rotated component matrix (Varimax rotation with Kaiser normalisation) for RDS geochemical data: a) summer and b) winter (PCA #C, n=72, 20 variables).

a)

| Rotated Component Matrix | | | | | |
|---|---|---|---|---|---|
| | Component | | | | |
| | 1 | 2 | 3 | 4 | 5 |
| Al2O3_s | -,104 | ,850 | ,289 | -,036 | -,190 |
| TiO2_s | -,041 | ,966 | ,077 | -,049 | -,047 |
| Fe2O3_s | ,421 | ,838 | ,100 | ,007 | -,103 |
| Cr_s | ,435 | ,087 | ,147 | -,260 | -,344 |
| Co_s | ,105 | ,925 | ,032 | ,030 | ,101 |
| Ba_s | ,786 | ,246 | ,284 | ,096 | -,329 |
| Ni_s | ,272 | ,788 | ,027 | -,011 | ,112 |
| Cu_s | ,917 | ,079 | -,007 | ,108 | -,007 |
| Zn_s | ,859 | ,080 | ,136 | ,143 | ,298 |
| Ga_s | -,055 | ,925 | ,114 | -,059 | ,005 |
| Ge_s | ,113 | ,206 | ,716 | ,056 | -,062 |
| As_s | ,244 | ,014 | ,815 | -,053 | -,017 |
| Sr_s | ,722 | ,250 | -,166 | ,161 | -,217 |
| Mo_s | ,728 | -,048 | ,011 | ,067 | ,001 |
| Pb_s | ,909 | ,042 | ,093 | ,082 | ,058 |
| Bi_s | ,145 | -,018 | -,007 | ,898 | -,050 |
| Cd_s | ,412 | -,082 | ,111 | ,795 | ,034 |
| Sn_s | ,853 | ,039 | ,287 | ,149 | -,125 |
| Sb_s | ,934 | ,031 | ,134 | ,112 | ,062 |
| LOI_s | ,008 | -,018 | ,098 | -,062 | ,912 |
| 63-inf2_s | -,017 | ,242 | ,683 | ,087 | ,398 |

b)

| Rotated Component Matrix | | | | | |
|---|---|---|---|---|---|
| | Component | | | | |
| | 1 | 2 | 3 | 4 | 5 |
| Al2O3_w | -,015 | ,903 | ,111 | -,104 | -,091 |
| TiO2_w | ,162 | ,930 | ,015 | ,025 | ,077 |
| Fe2O3_w | ,471 | ,774 | ,179 | -,025 | ,011 |
| Cr_w | ,602 | ,454 | -,150 | ,034 | ,060 |
| Co_w | ,317 | ,825 | ,255 | -,003 | ,074 |
| Ba_w | ,718 | ,289 | ,307 | ,001 | -,352 |
| Ni_w | ,427 | ,739 | ,148 | ,075 | ,121 |
| Cu_w | ,858 | ,210 | ,088 | ,103 | ,153 |
| Zn_w | ,793 | ,208 | ,026 | ,188 | ,405 |
| Ga_w | -,020 | ,917 | ,105 | -,080 | ,048 |
| Ge_w | -,030 | ,283 | ,872 | -,024 | ,057 |
| As_w | ,175 | ,148 | ,856 | -,047 | ,133 |
| Sr_w | ,723 | ,071 | ,039 | -,022 | -,456 |
| Mo_w | ,507 | ,190 | -,208 | -,059 | ,216 |
| Pb_w | ,876 | ,010 | ,138 | ,072 | -,139 |
| Bi_w | ,112 | -,053 | -,061 | ,941 | ,006 |
| Cd_w | ,121 | -,035 | ,001 | ,941 | ,045 |
| Sn_w | ,746 | ,091 | ,204 | ,251 | ,257 |
| Sb_w | ,944 | ,145 | ,012 | ,066 | ,122 |
| LOI_w | ,088 | ,019 | ,116 | -,005 | ,851 |
| 63-inf2_w | ,250 | ,462 | ,278 | ,169 | ,498 |

Table 107: Local settings of selected RDS samples.

| Sample | Location | Observations |
|---|---|---|
| 2 | Canal Bank | South of Worsley golf course, street intersection, residential area, residential and urban gardens |
| 5 | Cholmondeley Road | Street intersection, residential/commercial area, garage services/car selling businesses |
| 9 | Julia Street | Industrial street, near "Car Audio Centre Manchester" and "Salford Car Hire" |
| 11 | James street | Outside Victoria Mill (former textile mill), converted into apartments and office centre (next to former chemical works) |
| 13 | Bank Street | Street intersection, residential street, in front of community school, near "Mayne Coach Rental", gardens and green spaces |
| 14 | Assheton Road | Street intersection, residential street, near gardens and green spaces |
| 25 | Miller Street | Street intersection, high traffic, near Victoria train station |
| 27 | Cambrian Street | Commercial / industrial street, car repair services, scrapyards, and "Basic Welding Services Ltd." |
| 29 | Ashton New Road | Residential / commercial street, opposite M.O.T. center and garage services, tramline |
| 34 | Tenax Road | Industrial, double carriageway, entrance to "Trafford Distribution Centre", heavily industrialised area (Trafford Park) |
| 35 | Churchill Way | Entrance to Robert Wiseman & Sons (dairy) and MediaCo (large format graphic solutions), near Trafford Park Recycling Centre and Trafford Ecological Park |
| 53 | Wright Street | Street intersection, commercial / industrial street, near Ceramic Tile Centre and Quest Personal Care ltd. |
| 55 | Upper Brook Street | Street intersection, near the University of Manchester, green spaces, traffic island |
| 59 | Sunny Brow Road | Residential street off A57, nearby scrapyards/spare parts and other businesses ("Victoria Works") |
| 68 | Rufford Road | Residential street, residential gardens and green spaces, near St. Margaret church. |
| 70 | Parkfield Street | Residential street, off Moss Lane east |
| 71 | Oxford Place | Residential / commercial street, off Curry Mile |

Table 108: Summary statistics for RDS selected samples (RDS-summer n=17, RDS winter n=17).

| Variable | min | max | med | mean | std dev |
|---|---|---|---|---|---|
| Cr_s | 52,7 | 250,7 | 95,4 | 111,7 | 56,7 |
| Cr_w | 42,7 | 198,5 | 117,1 | 121,0 | 43,0 |
| Ni_s | 19,0 | 63,5 | 29,6 | 32,9 | 12,6 |
| Ni_w | 14,9 | 77,1 | 41,5 | 42,4 | 16,3 |
| Cu_s | 43,3 | 493,2 | 83,8 | 111,5 | 101,6 |
| Cu_w | 39,2 | 433,4 | 182,5 | 187,0 | 86,5 |
| Zn_s | 157,1 | 1325,6 | 304,4 | 398,1 | 282,9 |
| Zn_w | 165,6 | 1312,3 | 579,0 | 623,5 | 323,2 |
| As_s | 2,9 | 8,8 | 5,7 | 5,8 | 1,8 |
| As_w | 3,4 | 25,0 | 7,5 | 8,8 | 5,7 |
| Pb_s | 68,2 | 1184,0 | 160,9 | 229,6 | 260,2 |
| Pb_w | 70,2 | 2026,9 | 259,4 | 388,0 | 440,3 |
| Cd_s | 0,3 | 1,9 | 0,5 | 0,6 | 0,4 |
| Cd_w | 0,3 | 2,6 | 0,7 | 0,9 | 0,6 |
| OM_s | 2,6 | 40,7 | 6,9 | 12,4 | 11,2 |
| OM_w | 2,2 | 37,5 | 12,3 | 15,0 | 10,1 |
| 63-<2µm_s | 12,9 | 57,3 | 31,2 | 31,0 | 12,2 |
| 63-<2µm_w | 6,3 | 85,9 | 55,3 | 53,6 | 23,6 |
| d0.5_s | 44,3 | 381,8 | 152,9 | 169,8 | 84,4 |
| d0.5_w | 14,0 | 457,5 | 43,4 | 101,4 | 127,6 |
| D_s | 97,4 | 383,3 | 217,0 | 231,8 | 65,7 |
| D_w | 30,6 | 459,2 | 124,1 | 165,1 | 118,2 |

Table 109: Spearman's rank correlation coefficients for RDS summer data (n=17 samples).

| | | OM_s | 500-1000_s | 250-500_s | 125-250_s | 63-125_s | 32-63_s | 16-32_s | 8-16_s | 4-8_s | 2-4_s | inf2_s | 1000-63_s | 63-2_s | 63-inf2_s | d0.1_s | d0.5_s | d0.9_s | D_s |
|---|---|---|---|---|---|---|---|---|---|---|---|---|---|---|---|---|---|---|---|
| Al2O3_s | Correlation Coefficient | -,044 | -,379 | -,574 | -,049 | ,380 | ,522 | ,469 | ,429 | ,541 | ,651 | **,728** | -,529 | ,523 | ,529 | -,701 | -,610 | -,379 | -,588 |
| | Sig. (2-tailed) | ,866 | ,134 | ,016 | ,851 | ,132 | ,032 | ,058 | ,086 | ,025 | ,005 | ,001 | ,029 | ,031 | ,029 | ,002 | ,009 | ,134 | ,013 |
| Fe2O3_s | Correlation Coefficient | -,267 | -,390 | -,402 | ,199 | ,684 | ,370 | ,140 | ,091 | ,270 | ,456 | **,743** | -,306 | ,257 | ,306 | -,529 | -,434 | -,390 | -,382 |
| | Sig. (2-tailed) | ,300 | ,122 | ,110 | ,445 | ,002 | ,144 | ,593 | ,729 | ,295 | ,066 | ,001 | ,232 | ,319 | ,232 | ,029 | ,082 | ,122 | ,130 |
| Cr_s | Correlation Coefficient | -,390 | ,245 | ,059 | ,277 | ,201 | -,162 | -,297 | -,297 | -,201 | -,032 | ,147 | ,206 | -,196 | -,206 | -,069 | ,181 | ,245 | ,262 |
| | Sig. (2-tailed) | ,122 | ,343 | ,823 | ,282 | ,439 | ,535 | ,248 | ,248 | ,439 | ,903 | ,573 | ,428 | ,451 | ,428 | ,794 | ,486 | ,343 | ,309 |
| Ni_s | Correlation Coefficient | ,120 | -,277 | -,630 | -,169 | ,632 | ,566 | ,417 | ,363 | ,517 | ,652 | ,686 | -,532 | ,505 | ,532 | -,681 | -,564 | -,277 | -,500 |
| | Sig. (2-tailed) | ,646 | ,282 | ,007 | ,516 | ,006 | ,018 | ,096 | ,152 | ,034 | ,005 | ,002 | ,028 | ,039 | ,028 | ,003 | ,018 | ,282 | ,041 |
| Cu_s | Correlation Coefficient | ,059 | -,075 | -,237 | ,043 | ,671 | ,162 | ,004 | -,005 | ,085 | ,093 | ,261 | -,090 | ,060 | ,090 | -,162 | -,116 | -,075 | -,049 |
| | Sig. (2-tailed) | ,822 | ,775 | ,360 | ,870 | ,003 | ,535 | ,989 | ,985 | ,747 | ,722 | ,311 | ,733 | ,819 | ,733 | ,535 | ,656 | ,775 | ,852 |
| Zn_s | Correlation Coefficient | ,341 | -,152 | -,321 | -,203 | ,576 | ,314 | ,216 | ,221 | ,252 | ,179 | ,179 | -,275 | ,250 | ,275 | -,199 | -,223 | -,152 | -,184 |
| | Sig. (2-tailed) | ,181 | ,560 | ,209 | ,434 | ,016 | ,220 | ,406 | ,395 | ,328 | ,492 | ,492 | ,286 | ,333 | ,286 | ,445 | ,390 | ,560 | ,480 |
| Ga_s | Correlation Coefficient | ,215 | -,508 | -,651 | -,210 | ,405 | ,622 | ,585 | ,542 | ,668 | **,748** | **,765** | -,661 | ,619 | ,661 | -,722 | -,715 | -,508 | -,685 |
| | Sig. (2-tailed) | ,408 | ,037 | ,005 | ,419 | ,107 | ,008 | ,014 | ,025 | ,003 | ,001 | ,000 | ,004 | ,008 | ,004 | ,001 | ,001 | ,037 | ,002 |
| As_s | Correlation Coefficient | ,226 | -,357 | -,346 | -,309 | ,232 | ,357 | ,299 | ,324 | ,377 | ,361 | ,382 | -,366 | ,352 | ,366 | -,335 | -,372 | -,357 | -,312 |
| | Sig. (2-tailed) | ,384 | ,159 | ,174 | ,227 | ,370 | ,159 | ,243 | ,205 | ,136 | ,155 | ,131 | ,149 | ,166 | ,149 | ,189 | ,142 | ,159 | ,223 |
| Pb_s | Correlation Coefficient | -,044 | -,270 | -,255 | ,078 | ,544 | ,277 | ,100 | ,115 | ,194 | ,213 | ,306 | -,211 | ,184 | ,211 | -,245 | -,228 | -,270 | -,194 |
| | Sig. (2-tailed) | ,866 | ,295 | ,323 | ,765 | ,024 | ,282 | ,701 | ,660 | ,456 | ,411 | ,232 | ,417 | ,480 | ,417 | ,343 | ,379 | ,295 | ,456 |
| Cd_s | Correlation Coefficient | ,063 | -,422 | -,183 | ,109 | ,521 | ,312 | ,204 | ,178 | ,164 | ,225 | ,214 | -,271 | ,245 | ,271 | -,209 | -,256 | -,422 | -,349 |
| | Sig. (2-tailed) | ,809 | ,091 | ,481 | ,678 | ,032 | ,222 | ,433 | ,493 | ,528 | ,385 | ,410 | ,293 | ,342 | ,293 | ,421 | ,322 | ,091 | ,170 |
| Fe 1_s | Correlation Coefficient | -,757 | ,091 | ,512 | **,804** | ,108 | -,485 | -,662 | -,654 | -,605 | -,444 | -,189 | ,576 | -,598 | -,576 | ,375 | ,463 | ,091 | ,429 |
| | Sig. (2-tailed) | ,000 | ,729 | ,036 | ,000 | ,680 | ,048 | ,004 | ,004 | ,010 | ,074 | ,468 | ,016 | ,011 | ,016 | ,138 | ,061 | ,729 | ,086 |
| Fe 2_s | Correlation Coefficient | ,230 | -,221 | -,559 | -,311 | ,623 | ,525 | ,358 | ,314 | ,419 | ,502 | ,466 | -,468 | ,449 | ,468 | -,488 | -,485 | -,221 | -,417 |
| | Sig. (2-tailed) | ,374 | ,395 | ,020 | ,224 | ,008 | ,031 | ,158 | ,220 | ,094 | ,040 | ,060 | ,058 | ,071 | ,058 | ,047 | ,048 | ,395 | ,096 |
| Fe 3_s | Correlation Coefficient | ,571 | ,051 | -,645 | -,752 | ,333 | ,608 | ,544 | ,483 | ,500 | ,412 | ,221 | -,529 | ,547 | ,529 | -,370 | -,483 | ,051 | -,407 |
| | Sig. (2-tailed) | ,017 | ,844 | ,005 | ,000 | ,191 | ,010 | ,024 | ,050 | ,041 | ,101 | ,395 | ,029 | ,023 | ,029 | ,144 | ,050 | ,844 | ,105 |
| Fe 4_s | Correlation Coefficient | -,137 | -,301 | -,392 | ,130 | ,640 | ,368 | ,150 | ,088 | ,252 | ,392 | ,591 | -,289 | ,250 | ,289 | -,424 | -,390 | -,301 | -,350 |
| | Sig. (2-tailed) | ,599 | ,240 | ,119 | ,619 | ,006 | ,147 | ,567 | ,736 | ,328 | ,119 | ,013 | ,260 | ,333 | ,260 | ,090 | ,122 | ,240 | ,168 |
| Cr 1_s | Correlation Coefficient | ,107 | ,066 | ,254 | -,079 | -,290 | -,297 | -,102 | -,097 | -,170 | -,135 | -,109 | ,160 | -,165 | -,160 | ,150 | ,150 | ,066 | ,150 |
| | Sig. (2-tailed) | ,684 | ,801 | ,325 | ,764 | ,260 | ,247 | ,698 | ,713 | ,514 | ,607 | ,677 | ,540 | ,527 | ,540 | ,566 | ,566 | ,801 | ,566 |
| Cr 2_s | Correlation Coefficient | -,089 | ,190 | ,148 | ,137 | -,311 | -,207 | -,146 | -,135 | -,097 | -,115 | -,220 | ,133 | -,164 | -,133 | ,216 | ,098 | ,190 | ,148 |
| | Sig. (2-tailed) | ,733 | ,465 | ,572 | ,600 | ,225 | ,425 | ,576 | ,607 | ,711 | ,660 | ,396 | ,610 | ,529 | ,610 | ,405 | ,707 | ,465 | ,572 |
| Cr 3_s | Correlation Coefficient | -,034 | -,169 | -,328 | -,010 | ,373 | ,245 | ,213 | ,243 | ,282 | ,377 | ,451 | -,279 | ,275 | ,279 | -,444 | -,270 | -,169 | -,208 |
| | Sig. (2-tailed) | ,896 | ,516 | ,198 | ,970 | ,141 | ,343 | ,411 | ,348 | ,273 | ,135 | ,069 | ,277 | ,286 | ,277 | ,074 | ,295 | ,516 | ,422 |
| Cr 4_s | Correlation Coefficient | -,297 | ,110 | ,125 | ,265 | ,061 | -,123 | -,223 | -,194 | -,186 | -,105 | -,027 | ,169 | -,164 | -,169 | ,083 | ,162 | ,110 | ,199 |
| | Sig. (2-tailed) | ,248 | ,673 | ,633 | ,305 | ,815 | ,639 | ,390 | ,456 | ,474 | ,687 | ,918 | ,516 | ,529 | ,516 | ,751 | ,535 | ,673 | ,445 |
| Cu 1_s | Correlation Coefficient | -,416 | ,089 | ,175 | ,427 | ,235 | -,212 | -,381 | -,387 | -,270 | -,135 | ,109 | ,275 | -,287 | -,275 | ,043 | ,192 | ,089 | ,232 |
| | Sig. (2-tailed) | ,097 | ,734 | ,502 | ,087 | ,364 | ,414 | ,131 | ,125 | ,295 | ,606 | ,677 | ,285 | ,264 | ,285 | ,870 | ,460 | ,734 | ,370 |
| Cu 2_s | Correlation Coefficient | -,394 | ,018 | ,210 | ,422 | ,260 | -,250 | -,407 | -,401 | -,308 | -,196 | ,118 | ,304 | -,330 | -,304 | ,094 | ,255 | ,018 | ,281 |
| | Sig. (2-tailed) | ,118 | ,944 | ,419 | ,092 | ,314 | ,333 | ,105 | ,111 | ,229 | ,450 | ,653 | ,235 | ,196 | ,235 | ,719 | ,323 | ,944 | ,275 |
| Cu 3_s | Correlation Coefficient | ,499 | ,182 | -,179 | -,349 | ,174 | ,120 | ,135 | ,152 | ,155 | ,032 | -,138 | -,133 | ,123 | ,133 | ,042 | -,059 | ,182 | ,037 |
| | Sig. (2-tailed) | ,042 | ,485 | ,491 | ,170 | ,503 | ,645 | ,605 | ,559 | ,553 | ,903 | ,598 | ,612 | ,639 | ,612 | ,874 | ,822 | ,485 | ,888 |
| Cu 4_s | Correlation Coefficient | -,447 | ,144 | ,057 | ,377 | ,258 | -,176 | -,315 | -,305 | -,151 | -,017 | ,290 | ,199 | -,206 | -,199 | -,136 | ,127 | ,144 | ,226 |
| | Sig. (2-tailed) | ,072 | ,582 | ,828 | ,136 | ,317 | ,499 | ,218 | ,234 | ,562 | ,947 | ,258 | ,445 | ,428 | ,445 | ,601 | ,628 | ,582 | ,383 |
| Zn 1_s | Correlation Coefficient | ,064 | -,054 | -,189 | ,010 | ,426 | ,105 | ,039 | ,066 | ,110 | ,108 | ,172 | -,115 | ,088 | ,115 | -,123 | -,120 | -,054 | -,037 |
| | Sig. (2-tailed) | ,808 | ,837 | ,468 | ,970 | ,088 | ,687 | ,881 | ,801 | ,673 | ,680 | ,510 | ,660 | ,736 | ,660 | ,639 | ,646 | ,837 | ,889 |
| Zn 2_s | Correlation Coefficient | ,363 | -,037 | -,299 | -,172 | ,434 | ,203 | ,223 | ,240 | ,272 | ,211 | ,189 | -,260 | ,225 | ,260 | -,233 | -,203 | -,037 | -,132 |
| | Sig. (2-tailed) | ,152 | ,889 | ,244 | ,510 | ,082 | ,434 | ,390 | ,353 | ,291 | ,417 | ,468 | ,314 | ,384 | ,314 | ,368 | ,434 | ,889 | ,613 |
| Zn 3_s | Correlation Coefficient | ,424 | -,123 | -,434 | -,306 | ,615 | ,417 | ,319 | ,314 | ,321 | ,213 | ,140 | -,343 | ,338 | ,343 | -,208 | -,282 | -,123 | -,248 |
| | Sig. (2-tailed) | ,090 | ,639 | ,082 | ,232 | ,009 | ,096 | ,213 | ,220 | ,209 | ,411 | ,593 | ,178 | ,184 | ,178 | ,422 | ,273 | ,639 | ,338 |
| Zn 4_s | Correlation Coefficient | -,054 | -,326 | -,488 | ,093 | **,748** | ,414 | ,228 | ,203 | ,360 | ,475 | ,642 | -,365 | ,328 | ,365 | -,532 | -,429 | -,326 | -,365 |
| | Sig. (2-tailed) | ,837 | ,202 | ,047 | ,722 | ,001 | ,098 | ,379 | ,434 | ,155 | ,054 | ,005 | ,149 | ,198 | ,149 | ,028 | ,086 | ,202 | ,149 |
| Pb 1_s | Correlation Coefficient | -,640 | -,294 | ,349 | **,741** | ,277 | -,272 | -,454 | -,458 | -,365 | -,230 | ,182 | ,304 | -,387 | -,304 | ,124 | ,216 | -,294 | ,146 |
| | Sig. (2-tailed) | ,006 | ,253 | ,169 | ,001 | ,282 | ,291 | ,067 | ,064 | ,150 | ,374 | ,483 | ,235 | ,125 | ,235 | ,635 | ,405 | ,253 | ,576 |
| Pb 2_s | Correlation Coefficient | -,022 | -,441 | -,157 | ,235 | ,453 | ,206 | ,132 | ,130 | ,208 | ,252 | ,385 | -,230 | ,169 | ,230 | -,301 | -,225 | -,441 | -,277 |
| | Sig. (2-tailed) | ,933 | ,076 | ,548 | ,363 | ,068 | ,428 | ,613 | ,619 | ,422 | ,328 | ,127 | ,374 | ,516 | ,374 | ,240 | ,384 | ,076 | ,282 |
| Pb 3_s | Correlation Coefficient | ,209 | -,295 | -,189 | -,037 | ,248 | ,256 | ,209 | ,221 | ,270 | ,199 | ,192 | -,270 | ,226 | ,270 | -,177 | -,229 | -,295 | -,236 |
| | Sig. (2-tailed) | ,421 | ,251 | ,467 | ,888 | ,337 | ,322 | ,421 | ,394 | ,294 | ,444 | ,461 | ,294 | ,383 | ,294 | ,497 | ,378 | ,251 | ,362 |
| Pb 4_s | Correlation Coefficient | ,382 | -,316 | -,358 | -,393 | ,021 | ,326 | ,441 | ,433 | ,464 | ,547 | ,494 | -,443 | ,419 | ,443 | -,510 | -,387 | -,316 | -,358 |
| | Sig. (2-tailed) | ,130 | ,217 | ,158 | ,119 | ,936 | ,201 | ,077 | ,083 | ,060 | ,023 | ,044 | ,075 | ,094 | ,075 | ,037 | ,124 | ,217 | ,158 |

Table 110: Spearman's rank correlation coefficients for RDS winter data (n=17 samples).

| | | OM_w | 500-1000_w | 250-500_w | 125-250_w | 63-125_w | 32-63_w | 16-32_w | 8-16_w | 4-8_w | 2-4_w | inf2_w | 1000-63_w | 63-2_w | 63-inf2_w | d0.1 | d0.5 | d0.9 | D |
|---|---|---|---|---|---|---|---|---|---|---|---|---|---|---|---|---|---|---|---|
| Al2O3_w | Correlation Coefficient | ,155 | -,567 | -,667 | -,470 | ,205 | ,435 | ,510 | ,491 | ,635 | ,681 | **,754** | -,607 | ,560 | ,607 | -,661 | -,600 | -,532 | -,572 |
| | Sig. (2-tailed) | ,553 | ,018 | ,003 | ,057 | ,430 | ,081 | ,037 | ,045 | ,006 | ,003 | ,000 | ,010 | ,019 | ,010 | ,004 | ,011 | ,028 | ,016 |
| Fe2O3_w | Correlation Coefficient | ,346 | -,453 | -,596 | -,373 | ,306 | ,417 | ,475 | ,429 | ,488 | ,458 | ,618 | -,515 | ,502 | ,515 | -,490 | -,502 | -,417 | -,471 |
| | Sig. (2-tailed) | ,174 | ,068 | ,012 | ,141 | ,232 | ,096 | ,054 | ,086 | ,047 | ,064 | ,008 | ,035 | ,040 | ,035 | ,046 | ,040 | ,096 | ,057 |
| Cr_w | Correlation Coefficient | ,145 | ,020 | -,181 | -,260 | -,233 | -,027 | ,181 | ,123 | ,083 | -,032 | ,100 | -,118 | ,164 | ,118 | -,017 | -,152 | -,005 | -,059 |
| | Sig. (2-tailed) | ,580 | ,940 | ,486 | ,314 | ,368 | ,918 | ,486 | ,639 | ,751 | ,903 | ,701 | ,653 | ,529 | ,653 | ,948 | ,560 | ,985 | ,823 |
| Ni_w | Correlation Coefficient | ,510 | -,368 | -,520 | -,282 | ,385 | ,402 | ,419 | ,385 | ,400 | ,341 | ,505 | -,424 | ,441 | ,424 | -,402 | -,429 | -,314 | -,385 |
| | Sig. (2-tailed) | ,037 | ,147 | ,033 | ,273 | ,127 | ,110 | ,094 | ,127 | ,112 | ,181 | ,039 | ,090 | ,076 | ,090 | ,110 | ,086 | ,220 | ,127 |
| Cu_w | Correlation Coefficient | ,395 | -,304 | -,385 | -,140 | ,235 | ,284 | ,346 | ,250 | ,282 | ,292 | ,407 | -,353 | ,355 | ,353 | -,331 | -,360 | -,319 | -,319 |
| | Sig. (2-tailed) | ,117 | ,236 | ,127 | ,593 | ,363 | ,269 | ,174 | ,333 | ,273 | ,256 | ,105 | ,165 | ,162 | ,165 | ,195 | ,155 | ,213 | ,213 |
| Zn_w | Correlation Coefficient | ,436 | -,434 | -,473 | -,243 | ,510 | ,515 | ,490 | ,395 | ,297 | ,284 | ,363 | -,417 | ,434 | ,417 | -,326 | -,404 | -,417 | -,449 |
| | Sig. (2-tailed) | ,080 | ,082 | ,055 | ,348 | ,037 | ,035 | ,046 | ,117 | ,248 | ,269 | ,152 | ,096 | ,082 | ,096 | ,202 | ,107 | ,096 | ,071 |
| Ga_w | Correlation Coefficient | ,463 | -,642 | -,784 | -,618 | ,338 | ,559 | ,640 | ,650 | **,733** | **,745** | **,811** | -,713 | ,691 | **,713** | -,743 | -,728 | -,578 | -,667 |
| | Sig. (2-tailed) | ,061 | ,005 | ,000 | ,008 | ,184 | ,020 | ,006 | ,005 | ,001 | ,001 | ,000 | ,001 | ,002 | ,001 | ,001 | ,001 | ,015 | ,003 |
| As_w | Correlation Coefficient | ,093 | -,387 | -,218 | -,252 | ,115 | ,306 | ,248 | ,221 | ,341 | ,385 | ,338 | -,289 | ,267 | ,289 | -,360 | -,252 | -,336 | -,309 |
| | Sig. (2-tailed) | ,722 | ,125 | ,400 | ,328 | ,660 | ,232 | ,338 | ,395 | ,181 | ,127 | ,184 | ,260 | ,300 | ,260 | ,155 | ,328 | ,188 | ,228 |
| Pb_w | Correlation Coefficient | ,190 | -,216 | -,226 | -,086 | ,538 | ,326 | ,253 | ,157 | ,174 | ,134 | ,216 | -,167 | ,169 | ,167 | -,172 | -,159 | -,129 | -,199 |
| | Sig. (2-tailed) | ,465 | ,405 | ,384 | ,743 | ,026 | ,201 | ,328 | ,547 | ,504 | ,609 | ,405 | ,522 | ,516 | ,522 | ,510 | ,541 | ,622 | ,445 |
| Cd_w | Correlation Coefficient | ,261 | -,189 | -,183 | ,034 | ,528 | ,344 | ,163 | ,063 | ,021 | ,002 | ,119 | -,080 | ,113 | ,080 | -,080 | -,055 | -,145 | -,152 |
| | Sig. (2-tailed) | ,311 | ,468 | ,482 | ,896 | ,030 | ,177 | ,531 | ,811 | ,937 | ,993 | ,649 | ,761 | ,666 | ,761 | ,761 | ,833 | ,579 | ,560 |
| Fe 1_w | Correlation Coefficient | -,304 | ,221 | ,157 | -,005 | -,321 | -,221 | -,110 | -,044 | -,044 | -,135 | -,083 | ,120 | -,105 | -,120 | ,147 | ,098 | ,194 | ,179 |
| | Sig. (2-tailed) | ,236 | ,395 | ,548 | ,985 | ,209 | ,395 | ,673 | ,866 | ,866 | ,606 | ,751 | ,646 | ,687 | ,646 | ,573 | ,708 | ,456 | ,492 |
| Fe 2_w | Correlation Coefficient | ,240 | -,407 | -,419 | -,103 | ,613 | ,449 | ,292 | ,240 | ,321 | ,375 | ,529 | -,338 | ,297 | ,338 | -,431 | -,321 | -,321 | -,365 |
| | Sig. (2-tailed) | ,353 | ,105 | ,094 | ,694 | ,009 | ,071 | ,256 | ,353 | ,209 | ,138 | ,029 | ,184 | ,248 | ,184 | ,084 | ,209 | ,209 | ,149 |
| Fe 3_w | Correlation Coefficient | **,824** | -,598 | -,703 | -,564 | ,363 | **,721** | **,711** | ,613 | ,527 | ,483 | ,556 | -,650 | ,679 | ,650 | -,493 | -,610 | -,522 | -,618 |
| | Sig. (2-tailed) | ,000 | ,011 | ,002 | ,018 | ,152 | ,001 | ,001 | ,009 | ,030 | ,050 | ,020 | ,005 | ,003 | ,005 | ,045 | ,009 | ,032 | ,008 |
| Fe 4_w | Correlation Coefficient | -,221 | -,064 | -,172 | ,025 | ,221 | ,007 | ,020 | ,037 | ,172 | ,194 | ,346 | -,081 | ,066 | ,081 | -,257 | -,142 | -,108 | -,086 |
| | Sig. (2-tailed) | ,395 | ,808 | ,510 | ,926 | ,395 | ,978 | ,940 | ,889 | ,510 | ,456 | ,174 | ,758 | ,801 | ,758 | ,319 | ,586 | ,680 | ,743 |
| Cr 1_w | Correlation Coefficient | ,023 | -,149 | -,069 | -,014 | -,006 | ,057 | ,000 | ,006 | ,120 | ,184 | ,232 | -,098 | ,063 | ,098 | -,232 | -,109 | -,138 | -,106 |
| | Sig. (2-tailed) | ,930 | ,568 | ,793 | ,956 | ,983 | ,827 | 1,000 | ,983 | ,645 | ,481 | ,370 | ,710 | ,810 | ,710 | ,370 | ,677 | ,598 | ,685 |
| Cr 2_w | Correlation Coefficient | ,201 | -,186 | -,258 | -,057 | ,181 | ,226 | ,253 | ,266 | ,194 | ,117 | ,211 | -,226 | ,243 | ,226 | -,139 | -,218 | -,164 | -,201 |
| | Sig. (2-tailed) | ,439 | ,474 | ,317 | ,828 | ,487 | ,383 | ,327 | ,303 | ,457 | ,656 | ,416 | ,383 | ,347 | ,383 | ,595 | ,400 | ,530 | ,439 |
| Cr 3_w | Correlation Coefficient | ,323 | -,286 | -,232 | ,020 | ,128 | ,260 | ,253 | ,178 | ,108 | ,099 | ,115 | -,207 | ,221 | ,207 | -,132 | -,169 | -,269 | -,256 |
| | Sig. (2-tailed) | ,207 | ,266 | ,371 | ,940 | ,626 | ,314 | ,328 | ,495 | ,680 | ,704 | ,660 | ,425 | ,395 | ,425 | ,612 | ,516 | ,297 | ,321 |
| Cr 4_w | Correlation Coefficient | -,314 | ,223 | ,105 | ,047 | -,267 | -,238 | -,147 | -,194 | -,164 | -,223 | -,103 | ,172 | -,164 | -,172 | ,184 | ,164 | ,172 | ,179 |
| | Sig. (2-tailed) | ,220 | ,390 | ,687 | ,859 | ,300 | ,358 | ,573 | ,456 | ,529 | ,390 | ,694 | ,510 | ,529 | ,510 | ,480 | ,529 | ,510 | ,492 |
| Cu 1_w | Correlation Coefficient | -,144 | -,117 | -,251 | -,151 | -,194 | -,005 | ,221 | ,181 | ,213 | ,146 | ,221 | -,223 | ,218 | ,223 | -,154 | -,233 | -,208 | -,186 |
| | Sig. (2-tailed) | ,582 | ,656 | ,332 | ,562 | ,457 | ,985 | ,394 | ,487 | ,411 | ,575 | ,394 | ,389 | ,400 | ,389 | ,555 | ,368 | ,422 | ,474 |
| Cu 2_w | Correlation Coefficient | ,017 | -,404 | -,414 | -,196 | ,100 | ,228 | ,358 | ,377 | ,422 | ,426 | ,500 | -,417 | ,395 | ,417 | -,439 | -,422 | -,444 | -,412 |
| | Sig. (2-tailed) | ,948 | ,107 | ,098 | ,451 | ,701 | ,379 | ,158 | ,135 | ,092 | ,088 | ,041 | ,096 | ,117 | ,096 | ,078 | ,092 | ,074 | ,101 |
| Cu 3_w | Correlation Coefficient | ,044 | -,414 | -,424 | -,221 | ,113 | ,245 | ,370 | ,390 | ,431 | ,434 | ,510 | -,426 | ,407 | ,426 | -,449 | -,431 | -,451 | -,422 |
| | Sig. (2-tailed) | ,866 | ,098 | ,090 | ,395 | ,667 | ,343 | ,144 | ,122 | ,084 | ,082 | ,037 | ,088 | ,105 | ,088 | ,071 | ,084 | ,069 | ,092 |
| Cu 4_w | Correlation Coefficient | ,662 | -,424 | -,458 | -,279 | ,471 | ,498 | ,441 | ,333 | ,314 | ,297 | ,426 | -,417 | ,434 | ,417 | -,365 | -,392 | -,387 | -,412 |
| | Sig. (2-tailed) | ,004 | ,090 | ,064 | ,277 | ,057 | ,042 | ,076 | ,191 | ,220 | ,248 | ,088 | ,096 | ,082 | ,096 | ,149 | ,119 | ,125 | ,101 |
| Zn 1_w | Correlation Coefficient | ,208 | -,201 | -,203 | ,017 | ,414 | ,304 | ,240 | ,130 | ,027 | ,047 | ,091 | -,157 | ,169 | ,157 | -,091 | -,150 | -,230 | -,218 |
| | Sig. (2-tailed) | ,422 | ,439 | ,434 | ,948 | ,098 | ,236 | ,353 | ,619 | ,918 | ,859 | ,729 | ,548 | ,516 | ,548 | ,729 | ,567 | ,374 | ,400 |
| Zn 2_w | Correlation Coefficient | ,502 | -,466 | -,419 | -,184 | ,627 | ,522 | ,397 | ,297 | ,216 | ,252 | ,309 | -,370 | ,355 | ,370 | -,309 | -,324 | -,412 | -,436 |
| | Sig. (2-tailed) | ,040 | ,060 | ,094 | ,480 | ,007 | ,032 | ,115 | ,248 | ,406 | ,328 | ,228 | ,144 | ,162 | ,144 | ,228 | ,205 | ,101 | ,080 |
| Zn 3_w | Correlation Coefficient | ,667 | -,645 | -,706 | -,512 | ,478 | **,801** | **,721** | ,534 | ,453 | ,444 | ,522 | -,620 | ,637 | ,620 | -,461 | -,556 | -,574 | -,647 |
| | Sig. (2-tailed) | ,003 | ,005 | ,002 | ,036 | ,052 | ,000 | ,001 | ,027 | ,068 | ,074 | ,032 | ,008 | ,006 | ,008 | ,063 | ,020 | ,016 | ,005 |
| Zn 4_w | Correlation Coefficient | ,267 | -,446 | -,593 | -,385 | ,368 | ,458 | ,515 | ,373 | ,449 | ,422 | ,561 | -,478 | ,488 | ,478 | -,463 | -,478 | -,439 | -,475 |
| | Sig. (2-tailed) | ,300 | ,073 | ,012 | ,127 | ,147 | ,064 | ,035 | ,141 | ,071 | ,092 | ,019 | ,052 | ,047 | ,052 | ,061 | ,052 | ,078 | ,054 |
| Pb 1_w | Correlation Coefficient | -,453 | ,367 | ,393 | ,427 | -,026 | -,310 | -,313 | -,307 | -,344 | -,367 | -,390 | ,384 | -,384 | -,384 | ,404 | ,384 | ,364 | ,367 |
| | Sig. (2-tailed) | ,068 | ,147 | ,119 | ,087 | ,922 | ,226 | ,222 | ,231 | ,176 | ,147 | ,122 | ,128 | ,128 | ,128 | ,107 | ,128 | ,151 | ,147 |
| Pb 2_w | Correlation Coefficient | ,103 | -,238 | -,203 | -,123 | ,505 | ,238 | ,223 | ,218 | ,275 | ,238 | ,255 | -,196 | ,184 | ,196 | -,250 | -,201 | -,169 | -,216 |
| | Sig. (2-tailed) | ,694 | ,358 | ,434 | ,639 | ,039 | ,358 | ,390 | ,400 | ,286 | ,358 | ,323 | ,451 | ,480 | ,451 | ,333 | ,439 | ,516 | ,406 |
| Pb 3_w | Correlation Coefficient | ,561 | -,245 | -,232 | -,217 | ,417 | ,379 | ,374 | ,285 | ,200 | ,078 | ,075 | -,259 | ,295 | ,259 | -,115 | -,232 | -,215 | -,258 |
| | Sig. (2-tailed) | ,019 | ,342 | ,371 | ,403 | ,096 | ,134 | ,140 | ,268 | ,442 | ,767 | ,774 | ,316 | ,251 | ,316 | ,661 | ,371 | ,408 | ,318 |
| Pb 4_w | Correlation Coefficient | ,059 | -,076 | -,020 | -,053 | ,089 | ,099 | ,161 | ,102 | ,119 | -,030 | -,030 | -,086 | ,112 | ,086 | ,003 | -,059 | -,112 | -,079 |
| | Sig. (2-tailed) | ,821 | ,773 | ,940 | ,841 | ,734 | ,706 | ,536 | ,697 | ,650 | ,910 | ,910 | ,744 | ,669 | ,744 | ,990 | ,821 | ,669 | ,763 |

## *5. RDS Mapping*

### Part A: RDS summer

Chemical elements in alphabetical order followed by LOI, TC, TOC, TIC and pH.

# Aluminium

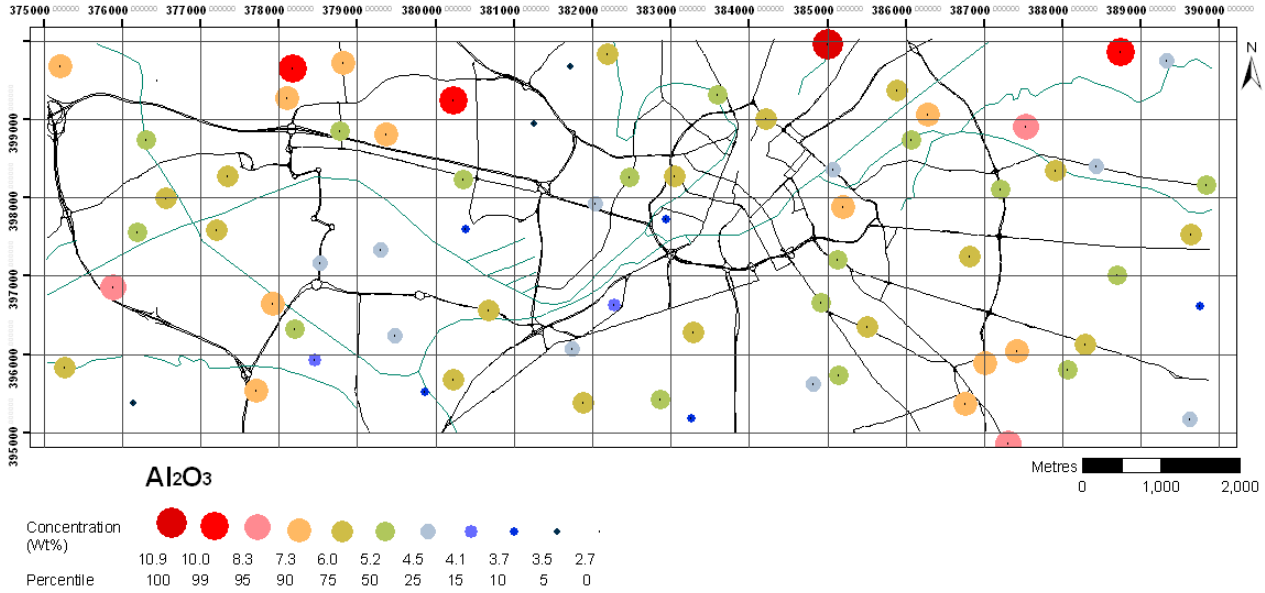


# Antimony

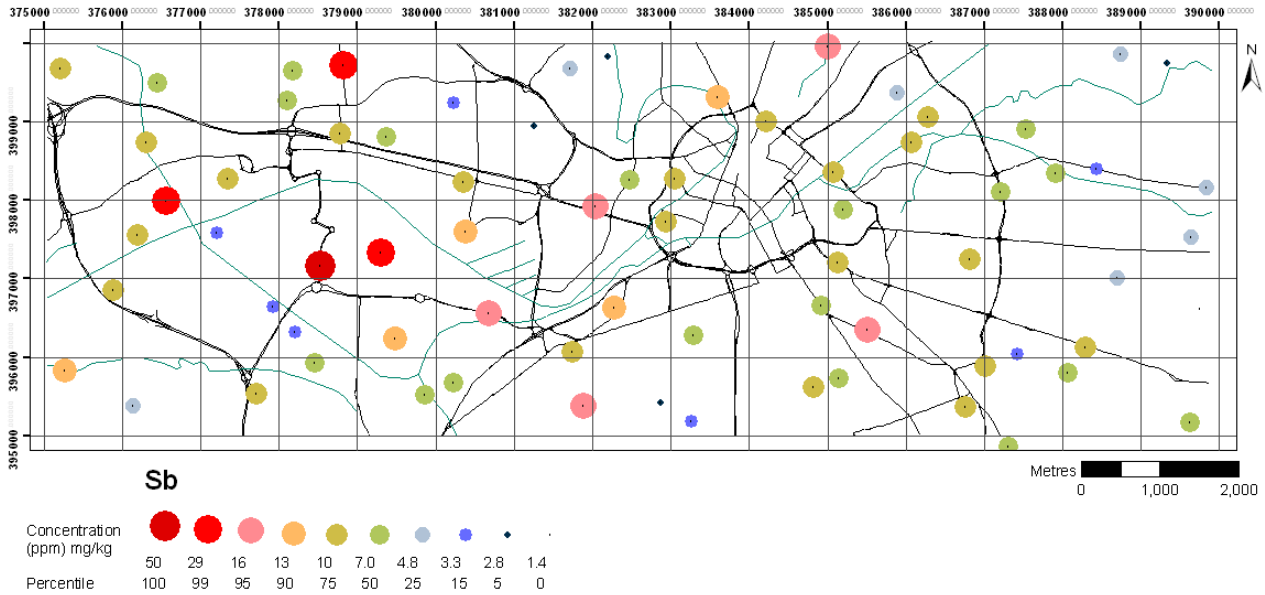

# Arsenic

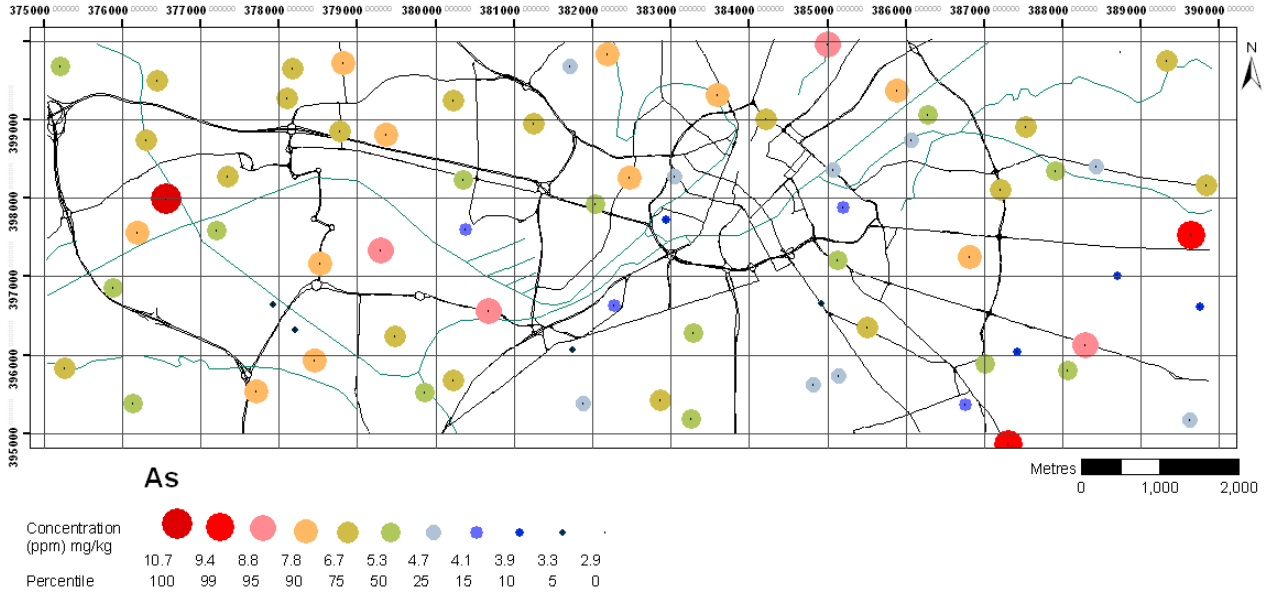


# Barium

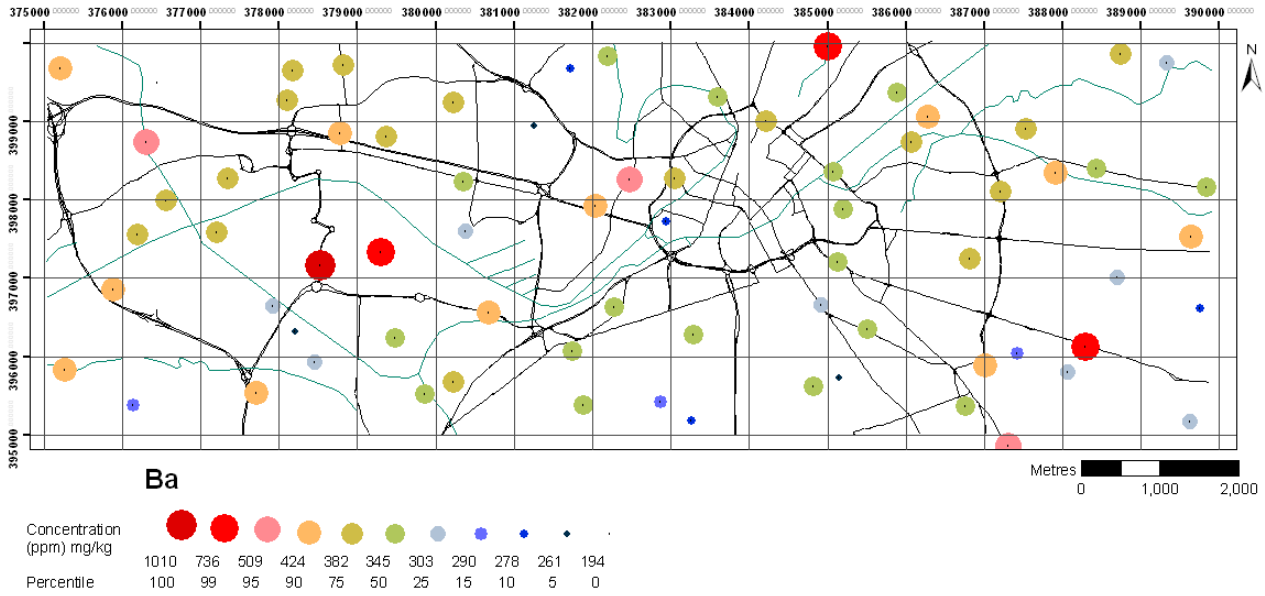

# Cadmium

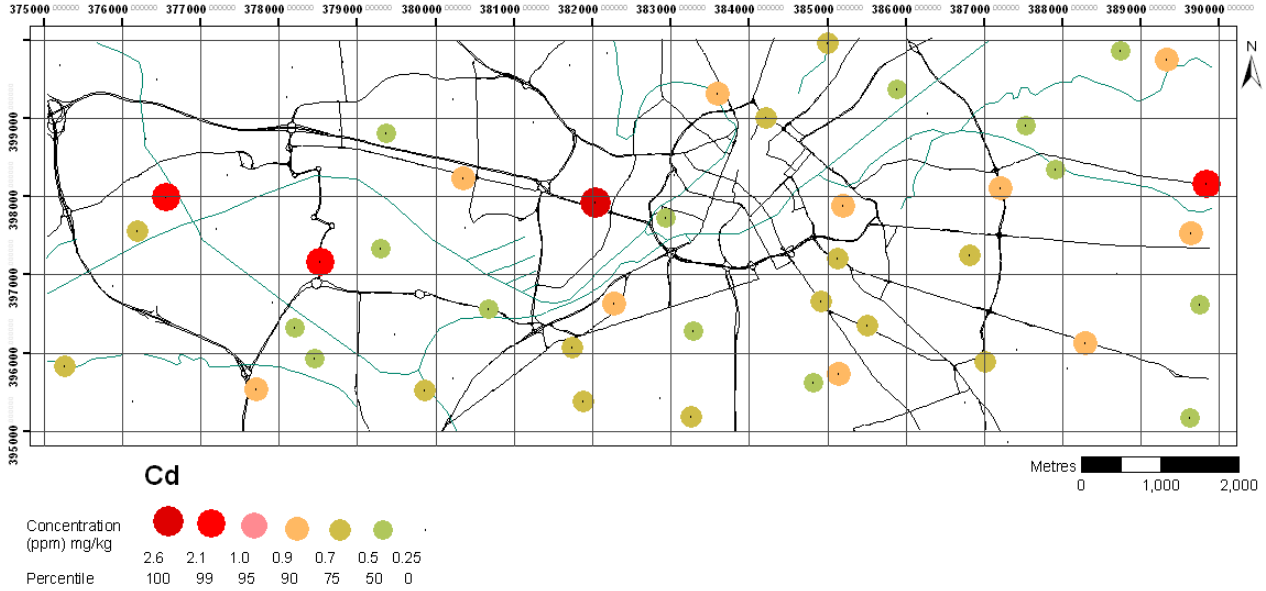


# Calcium

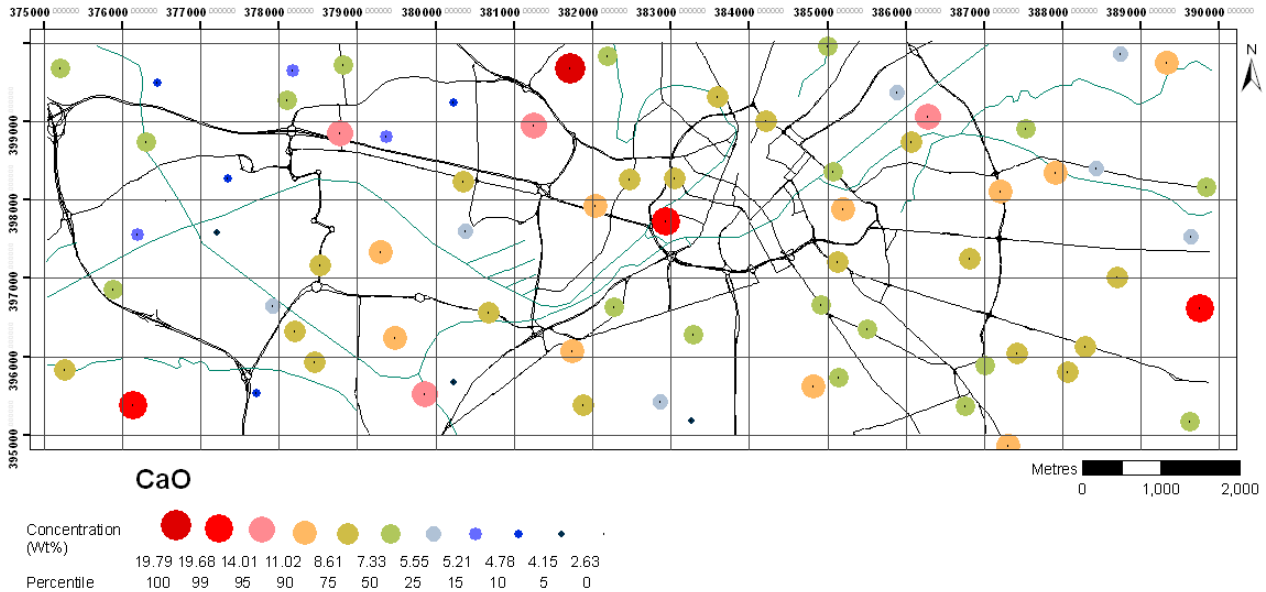

# Chromium

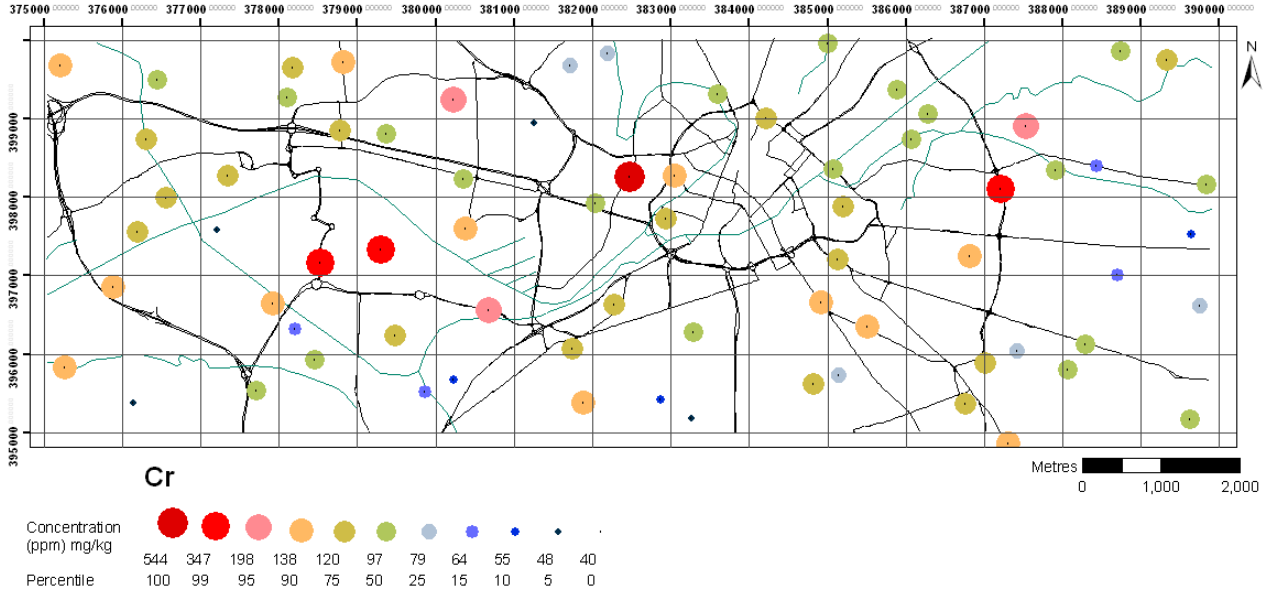


# Chlorine

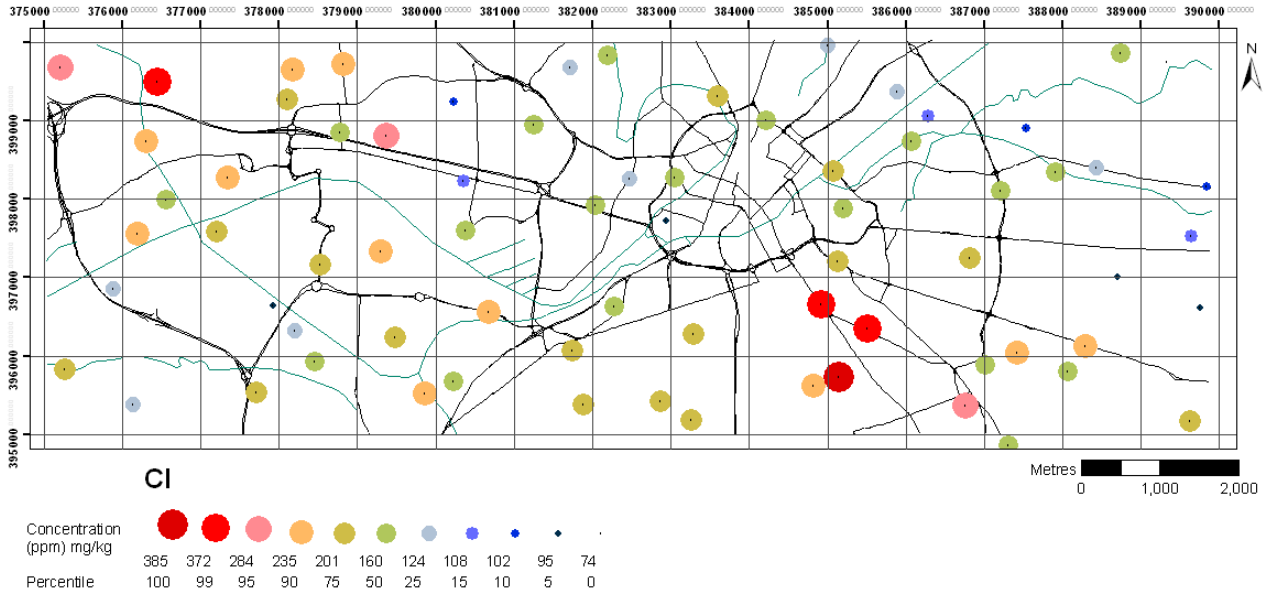

# Cobalt

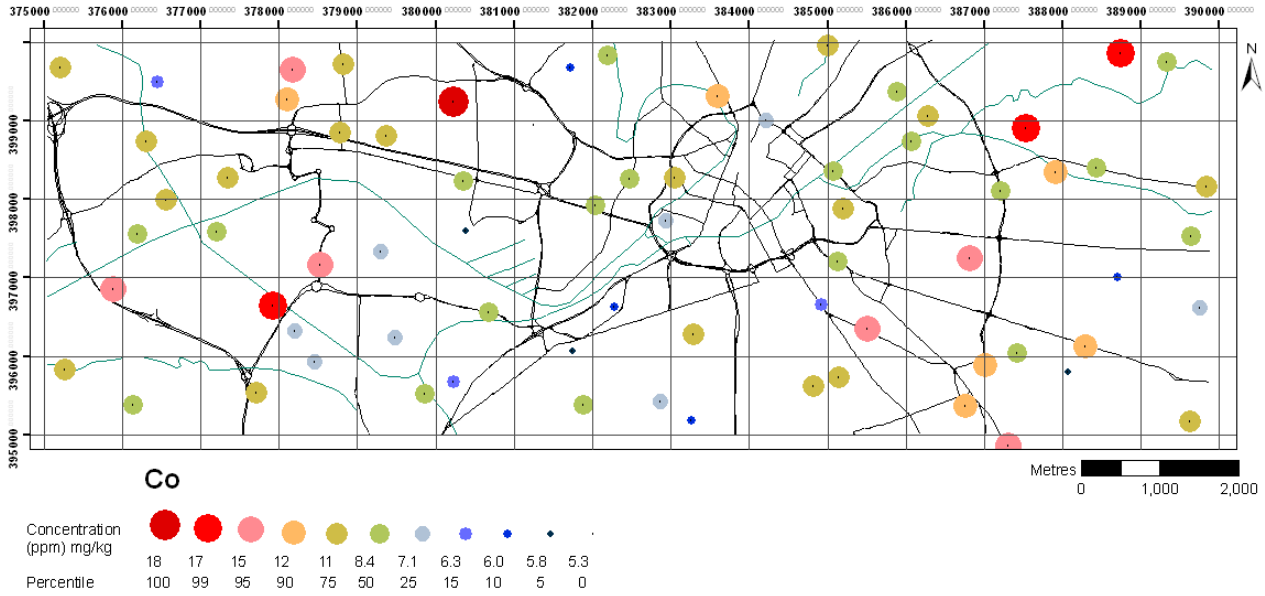


# Copper

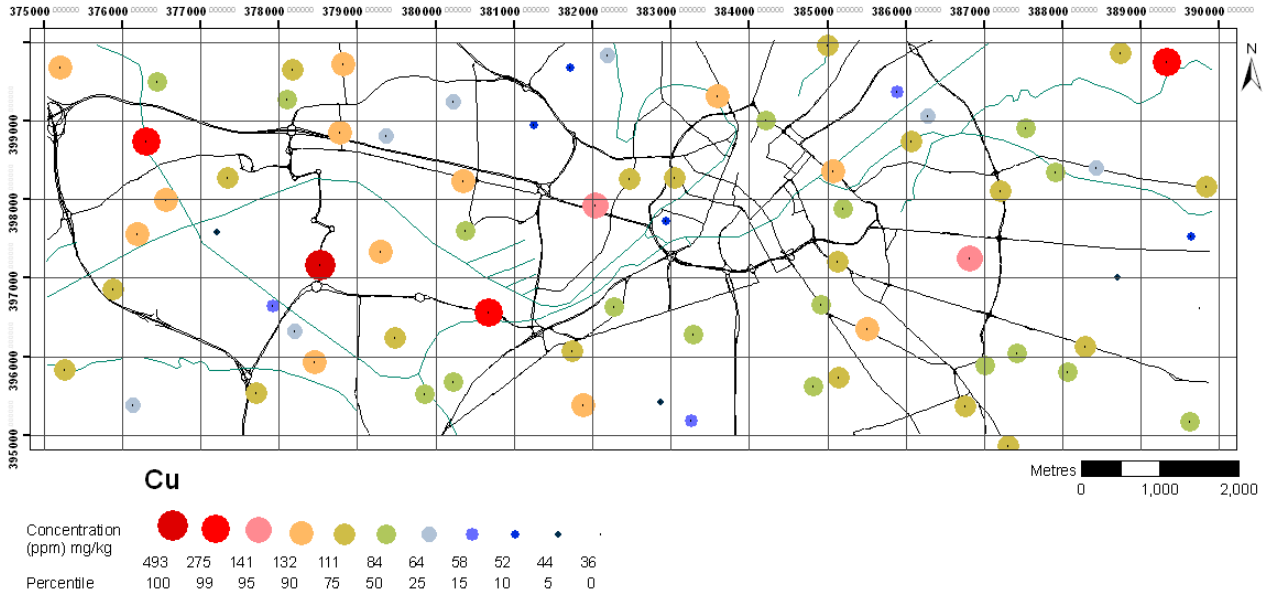

# Iron

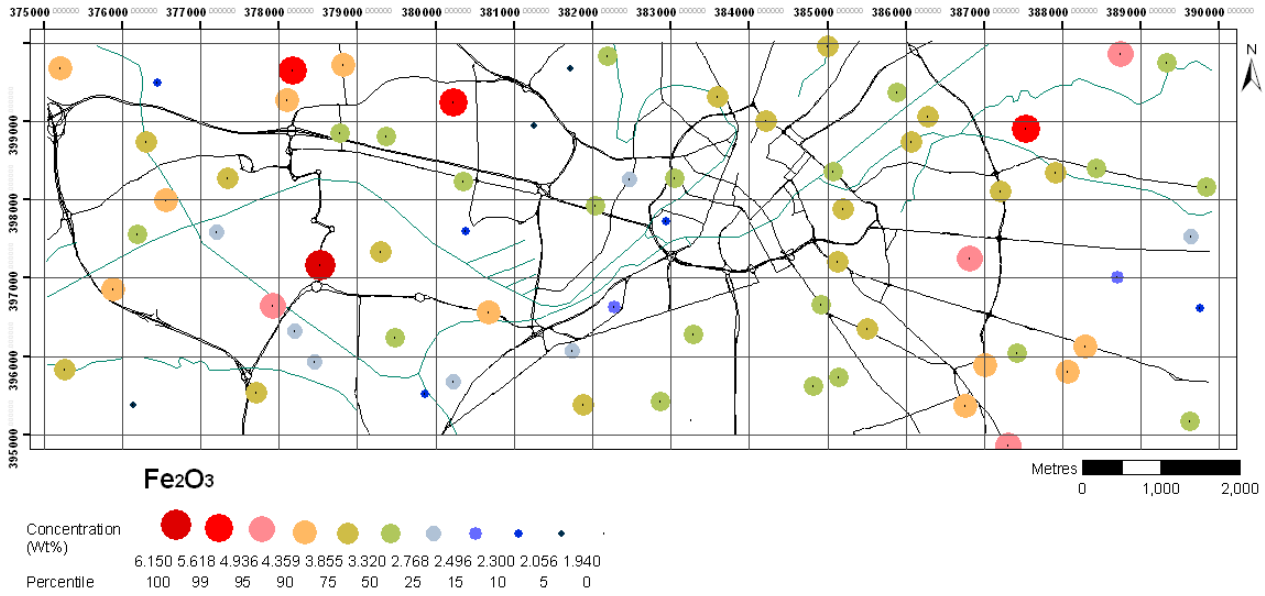
375000 376000 377000 378000 379000 380000 381000 382000 383000 384000 385000 386000 387000 388000 389000 390000
399000 398000 397000 396000 395000
N
Fe2O3
Metres
0 1,000 2,000
Concentration (Wt%)
6.150 5.618 4.936 4.359 3.855 3.320 2.768 2.496 2.300 2.056 1.940
Percentile
100 99 95 90 75 50 25 15 10 5 0

# Lead

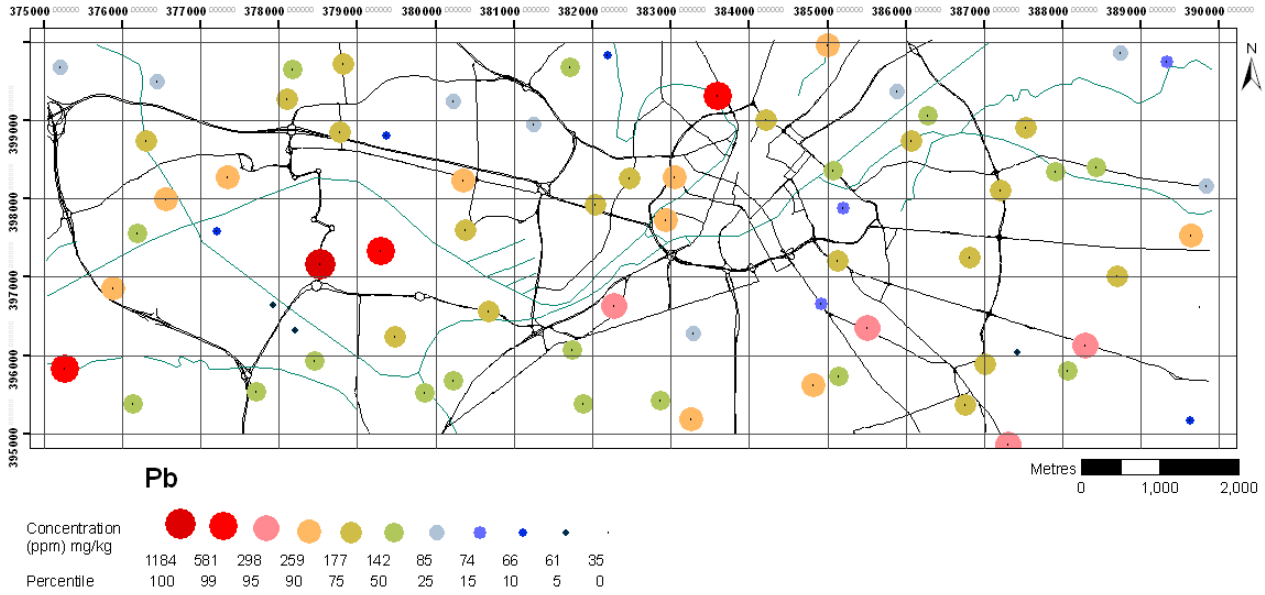
375000 376000 377000 378000 379000 380000 381000 382000 383000 384000 385000 386000 387000 388000 389000 390000
399000 398000 397000 396000 395000
N
Pb
Metres
0 1,000 2,000
Concentration (ppm) mg/kg
1184 581 298 259 177 142 85 74 66 61 35
Percentile
100 99 95 90 75 50 25 15 10 5 0

# Magnesium

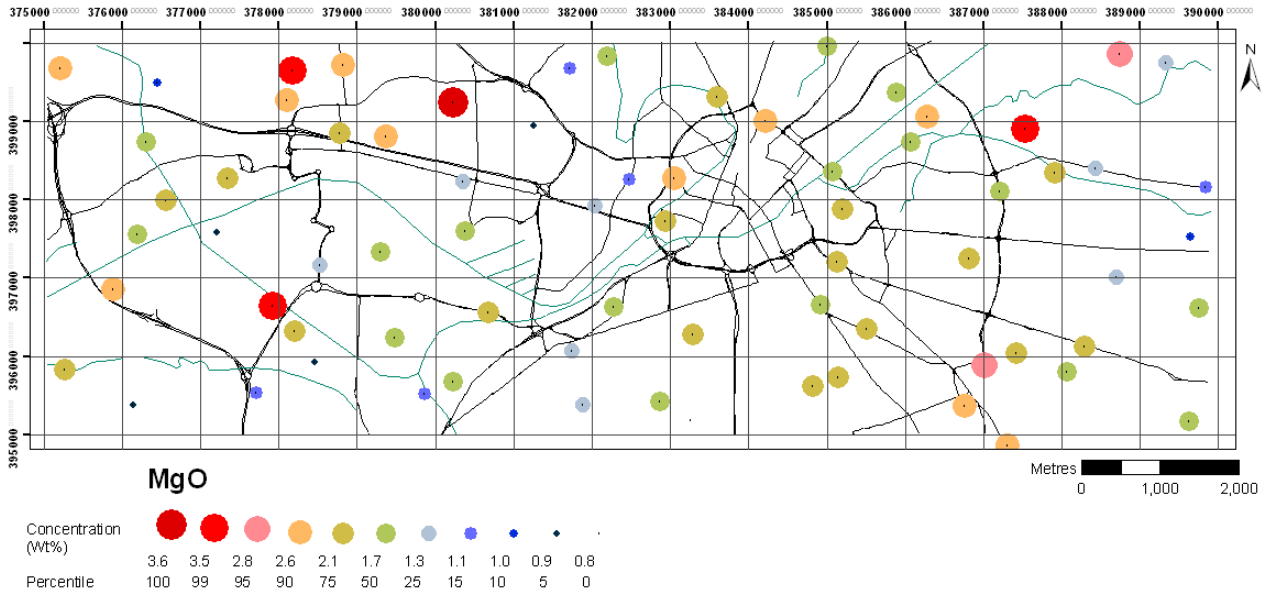


# Manganese

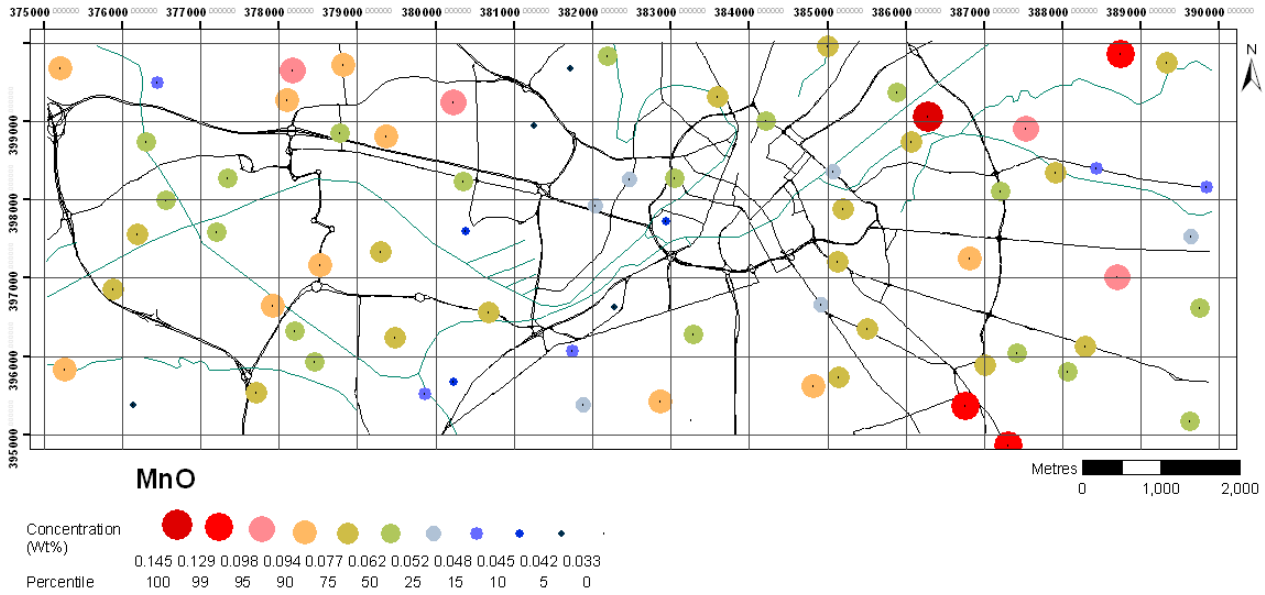

# Molybdenum

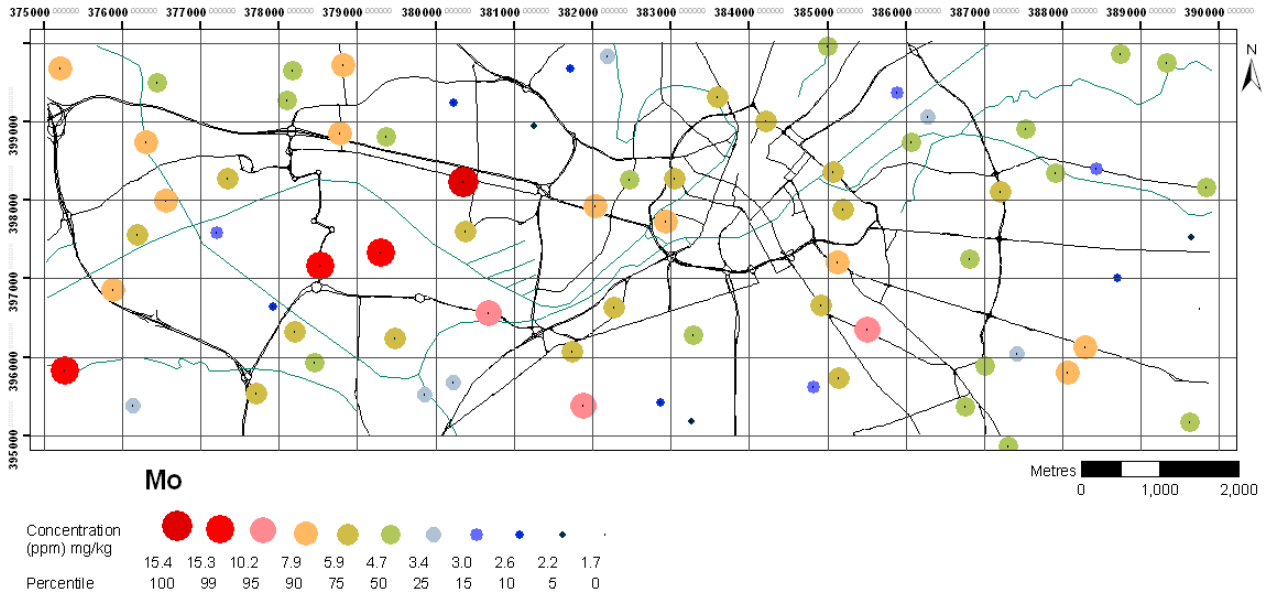


# Nickel

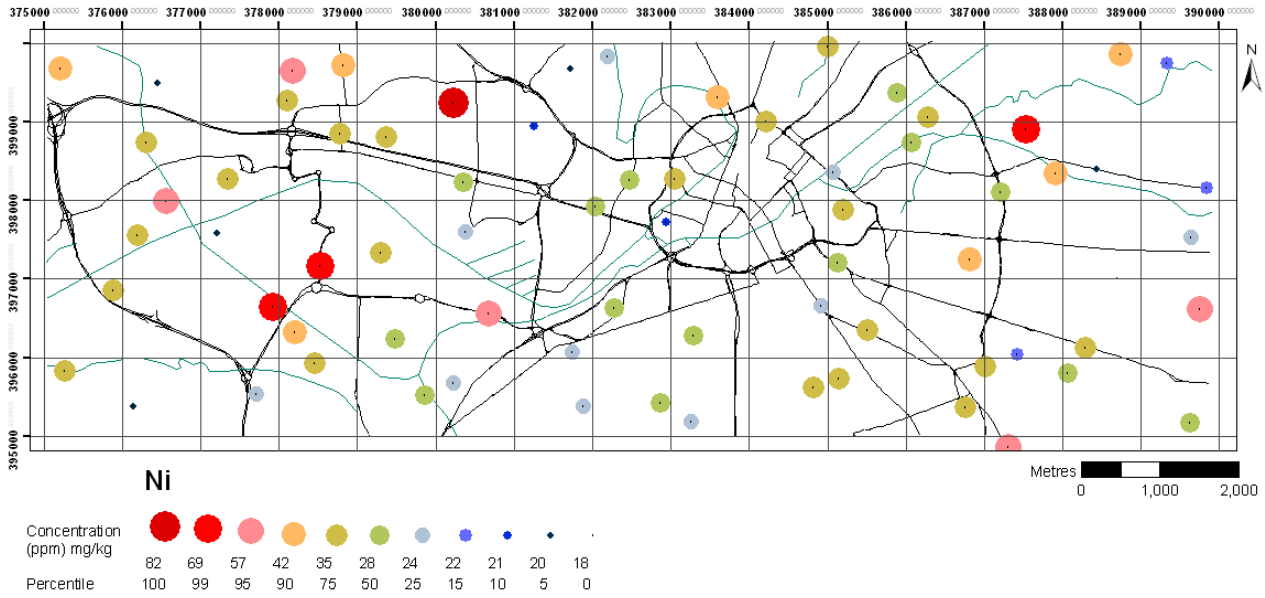

# Phosphorus

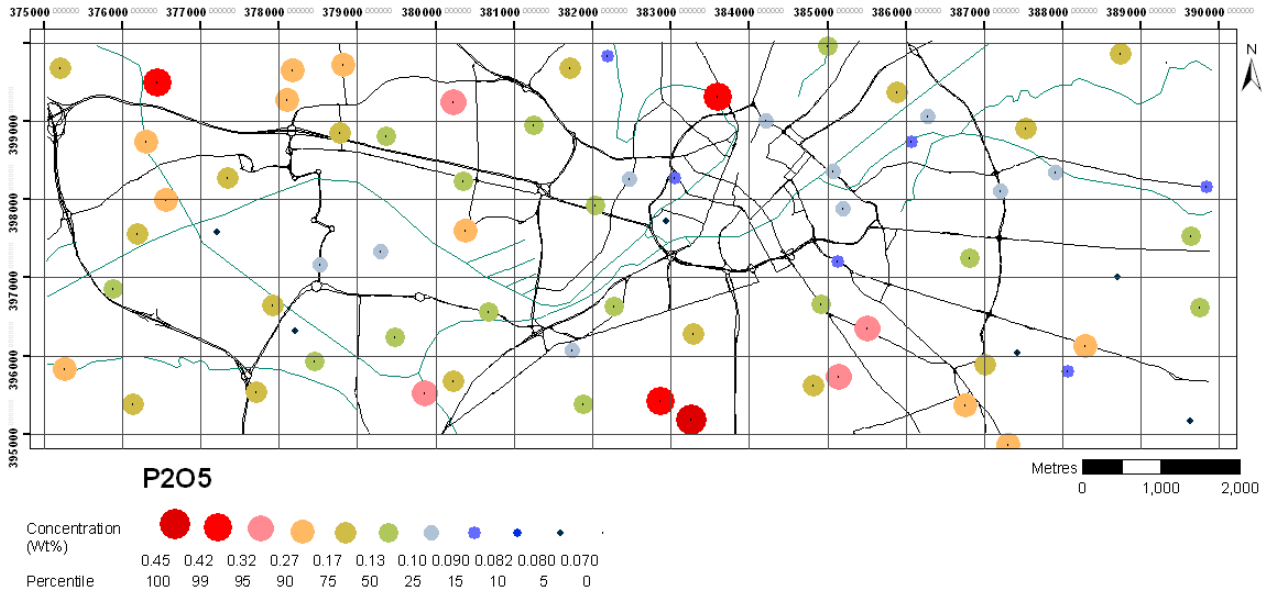


# Potassium

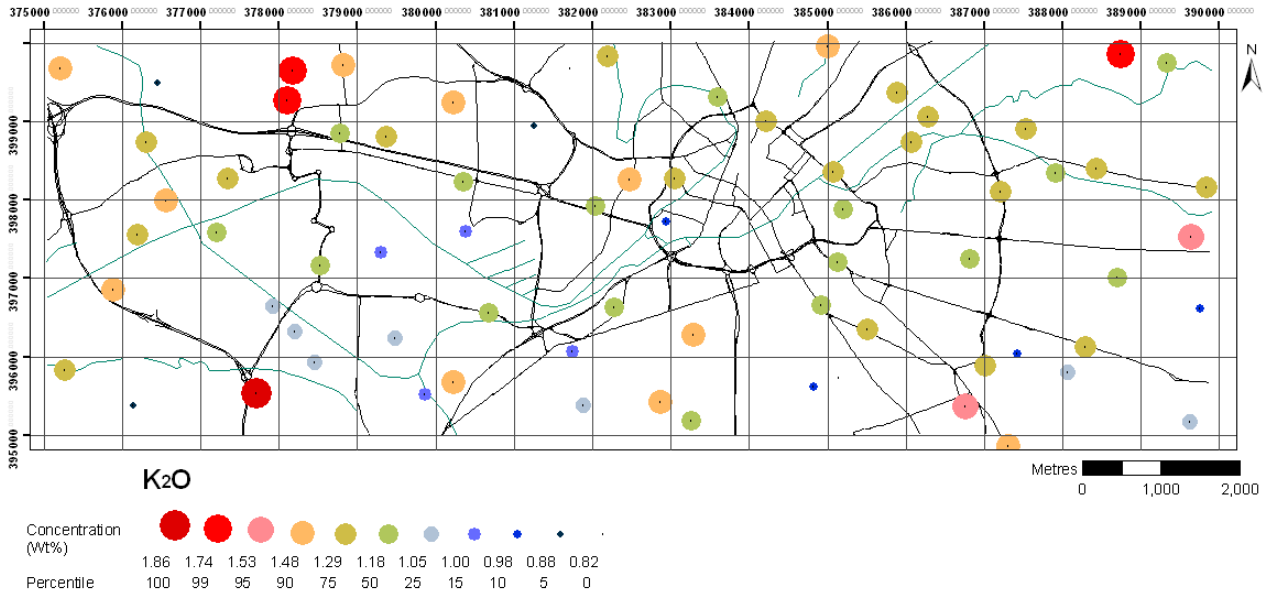

# Silicon

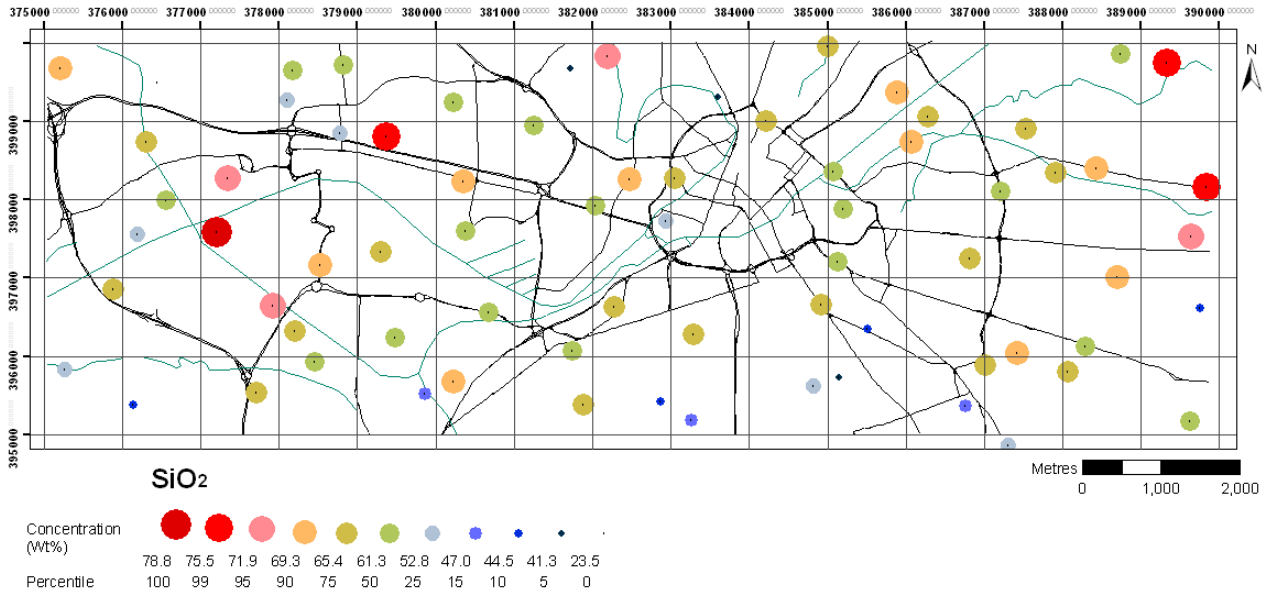


# Sulphur

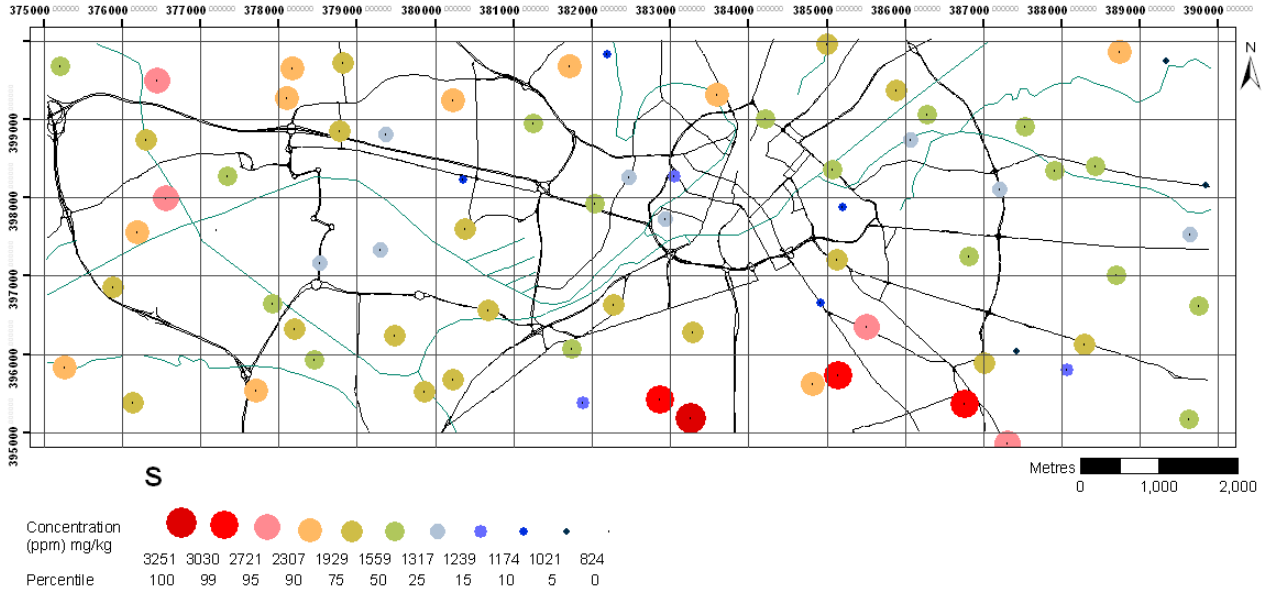

# Tin

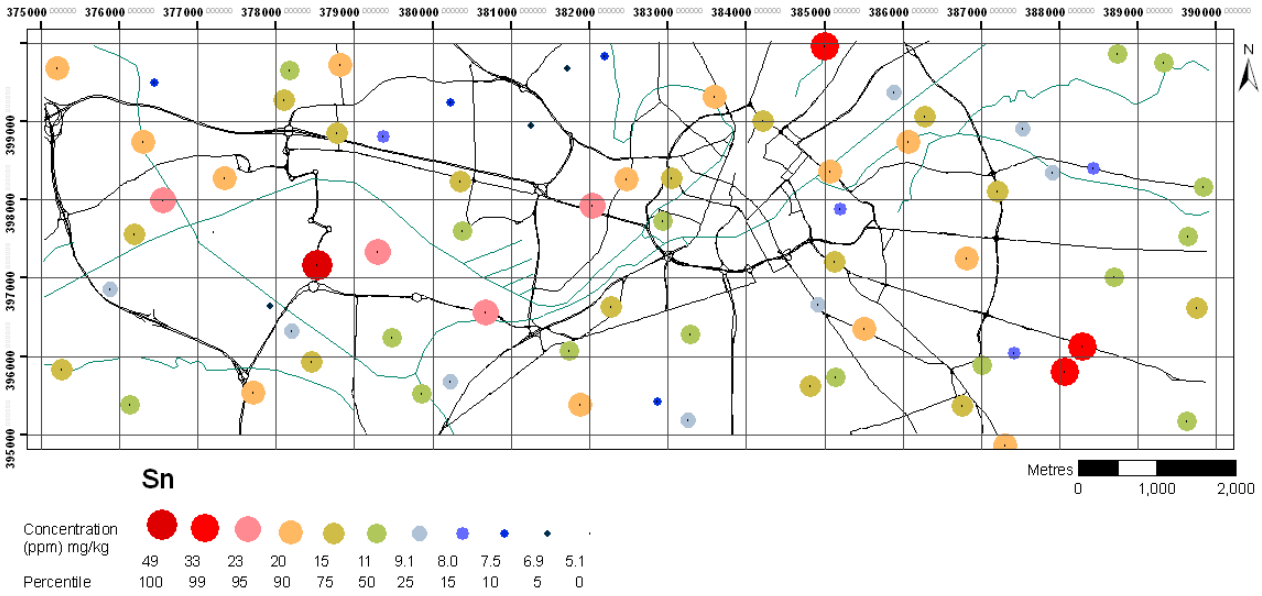


# Titanium

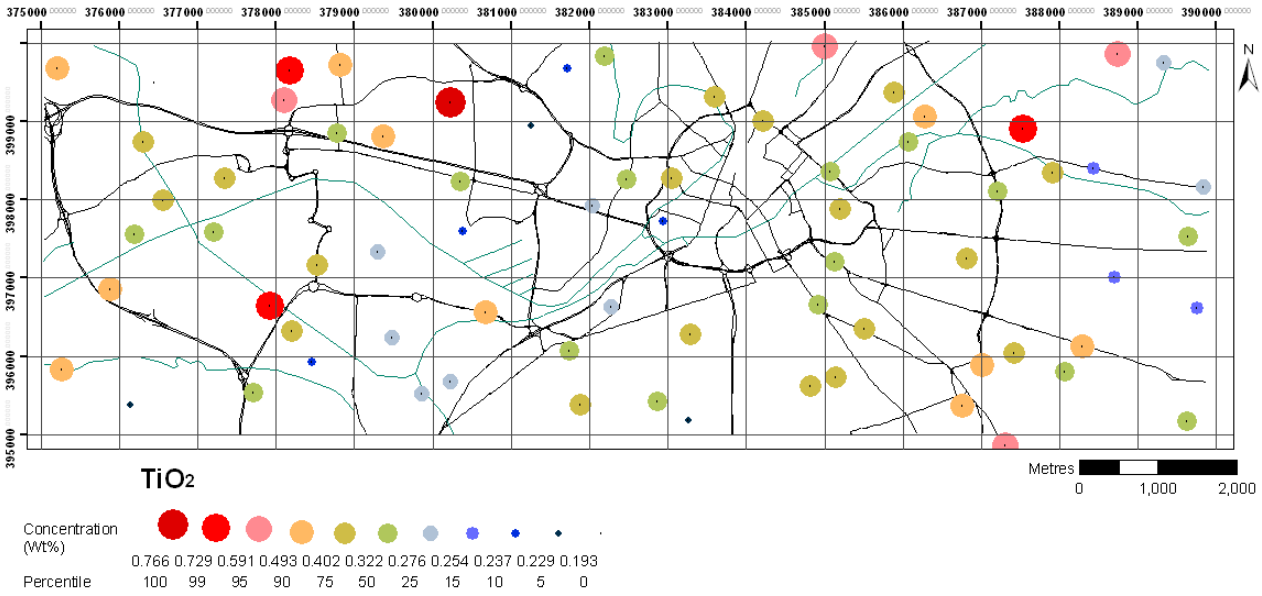

# Uranium

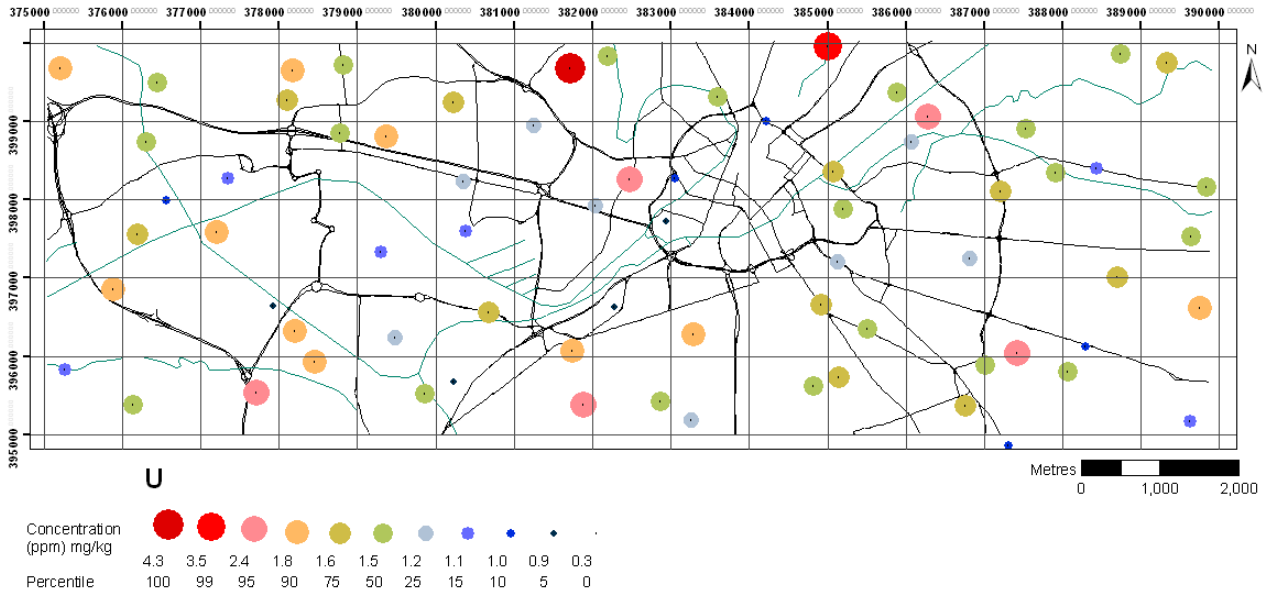


# Vanadium

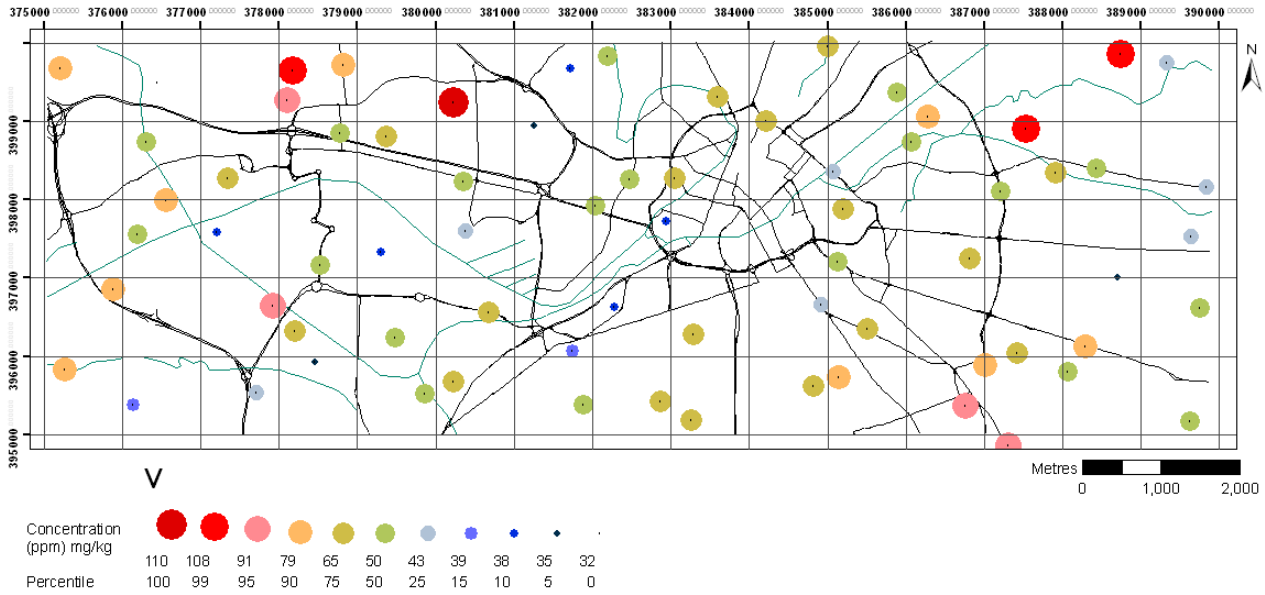

# Zinc

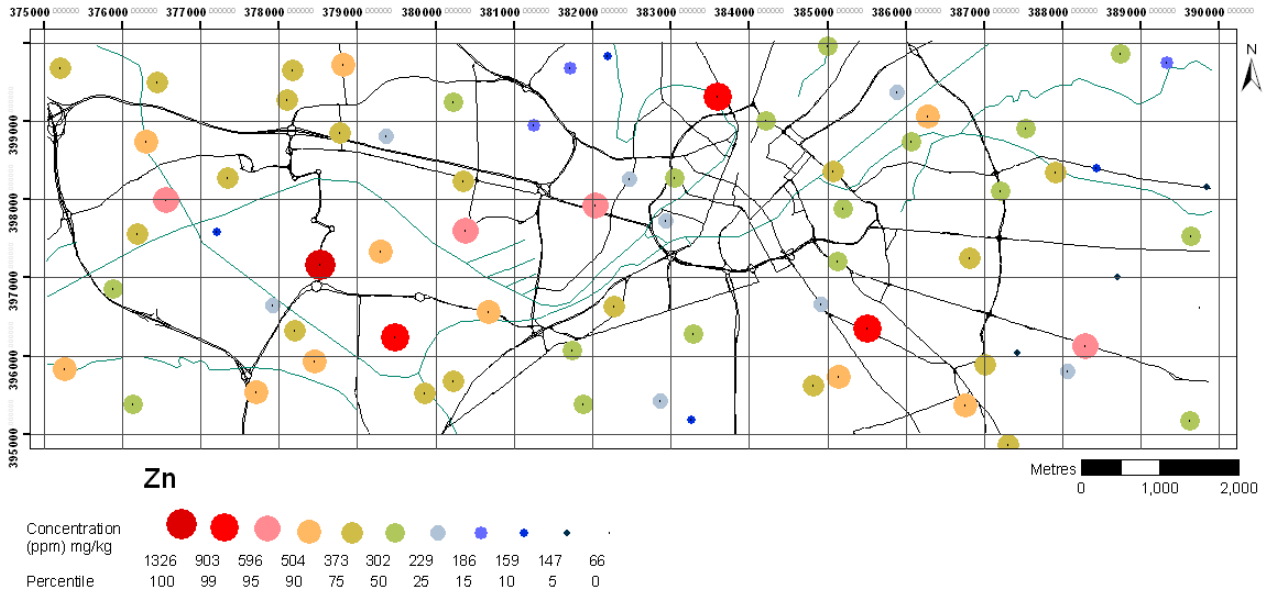


# Organic matter

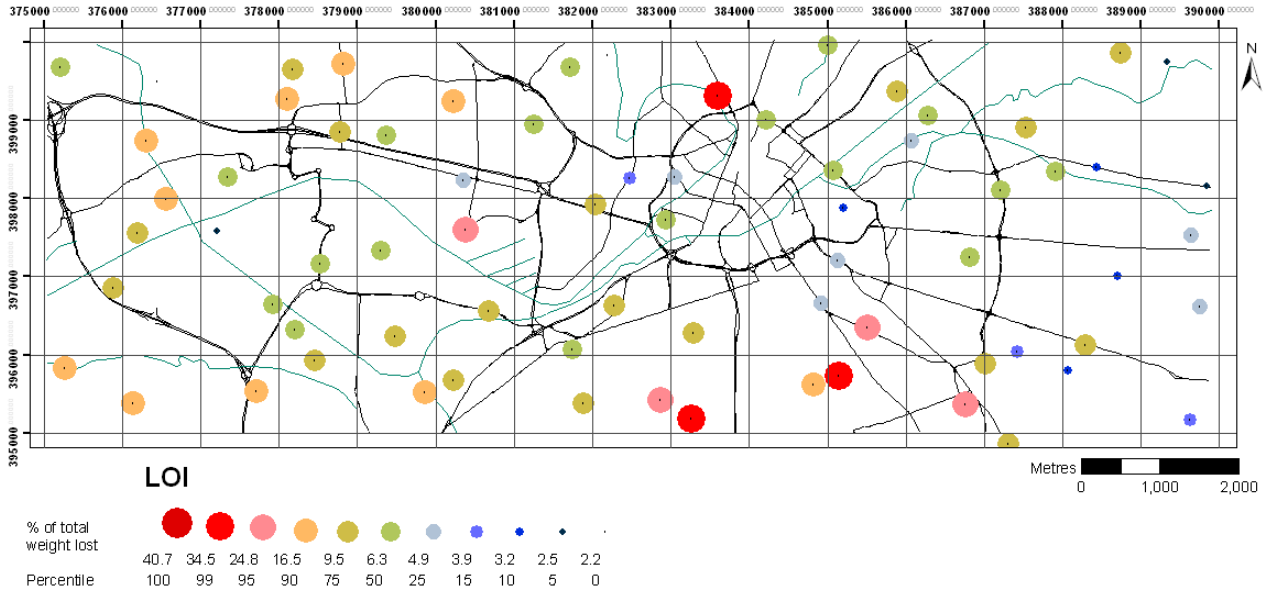

# Part B: RDS winter

Chemical elements in alphabetical order followed by LOI, TC, TOC, TIC and pH.

## Aluminium

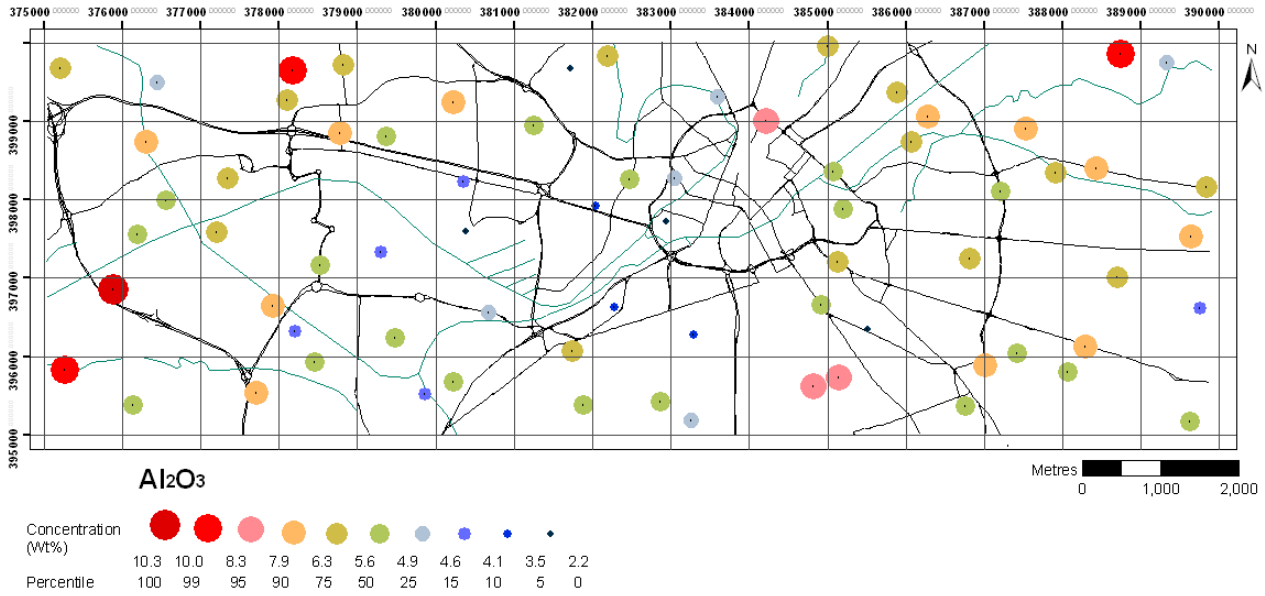


## Antimony

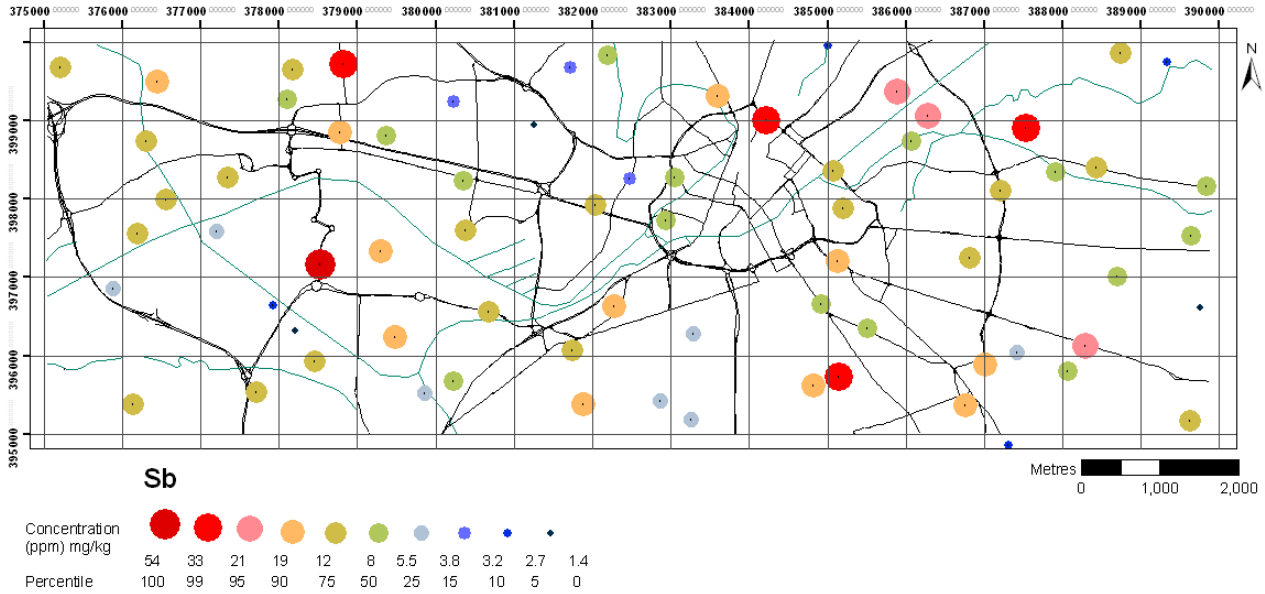

# Arsenic

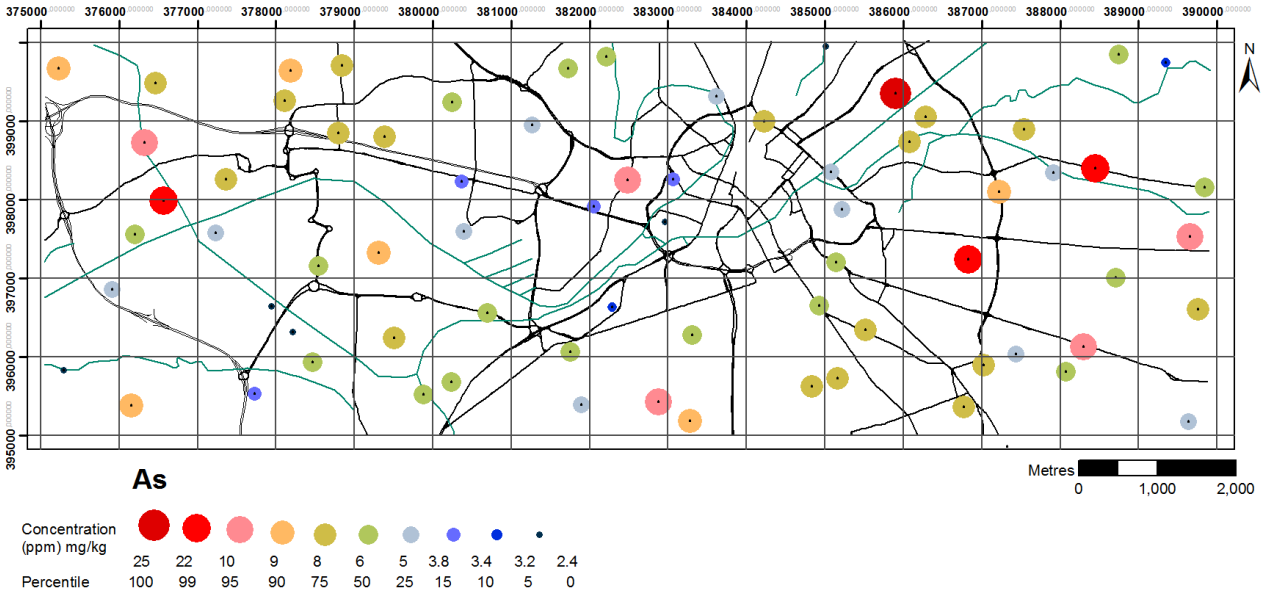


# Barium

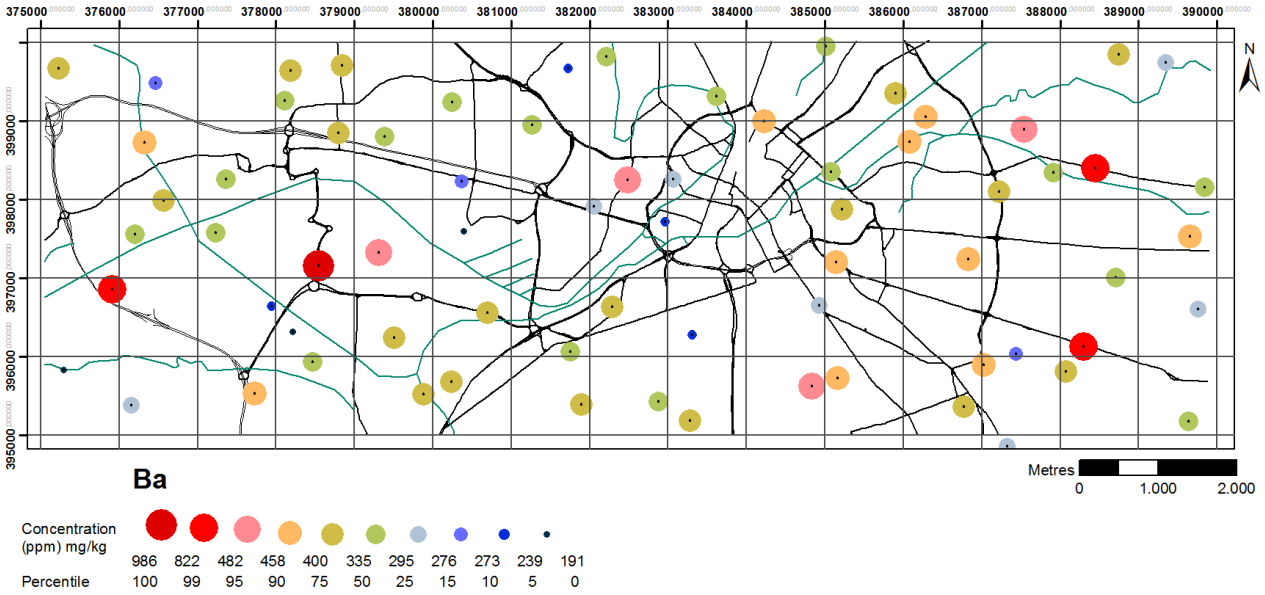

# Cadmium

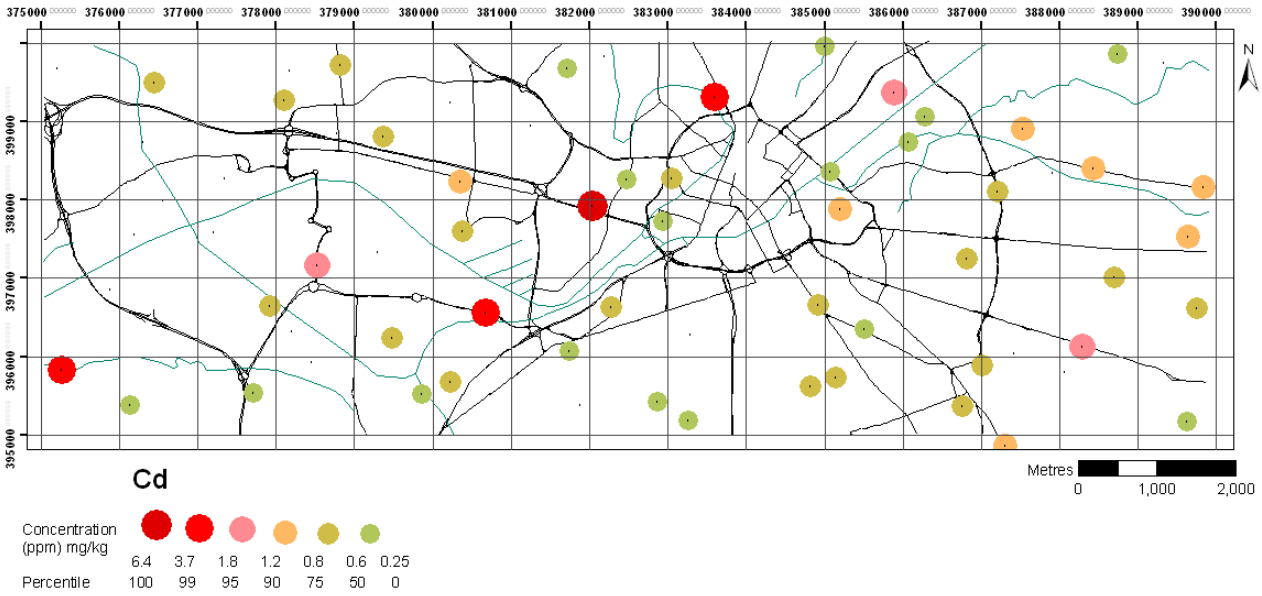


# Calcium

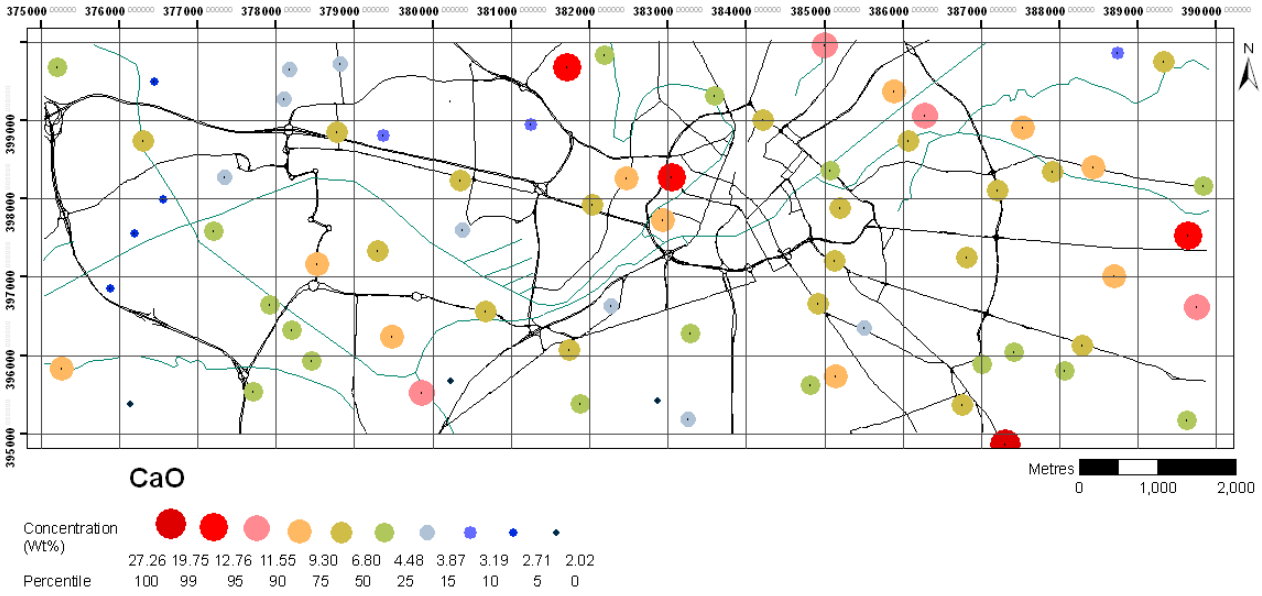

# Chromium

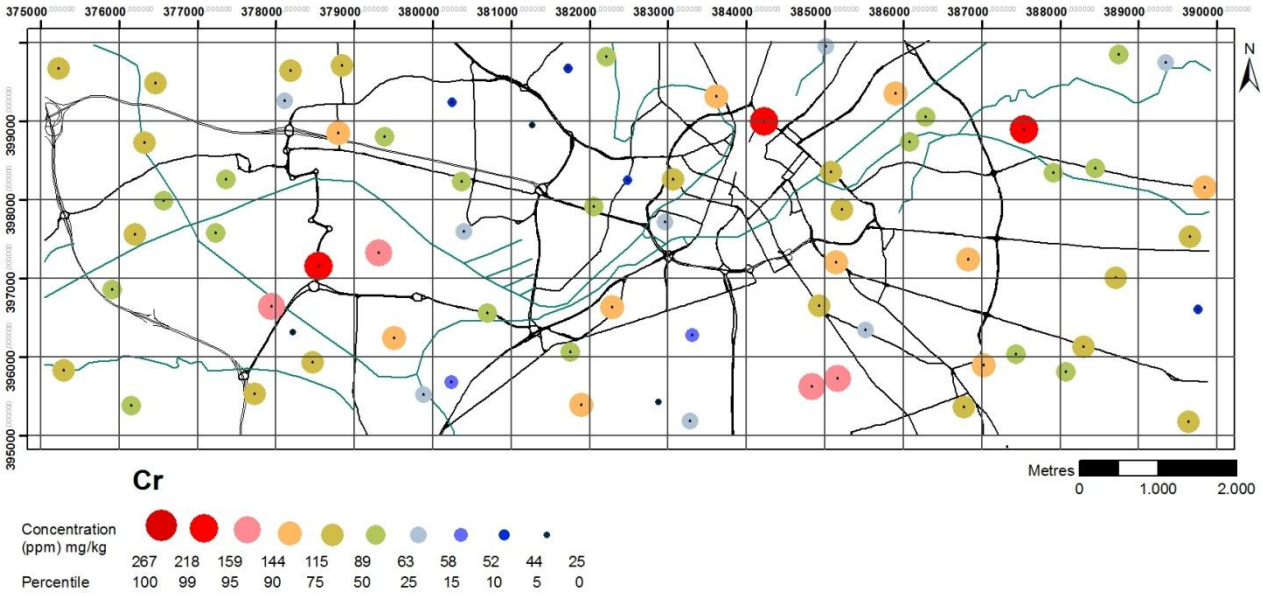


# Chlorine

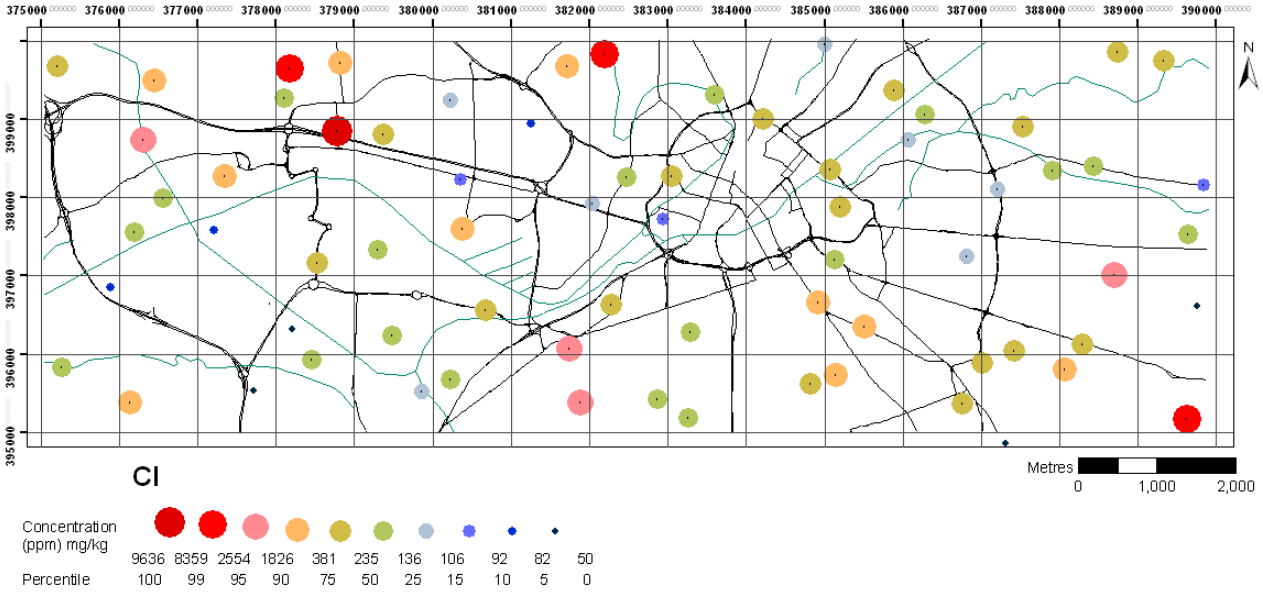

# Cobalt

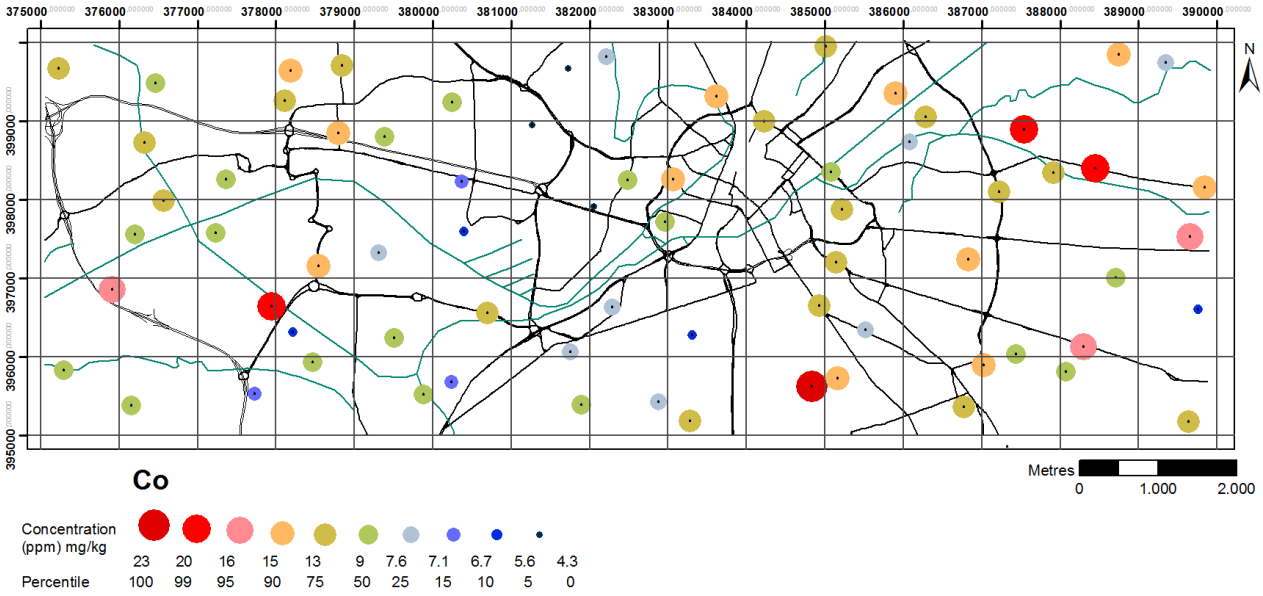


# Copper

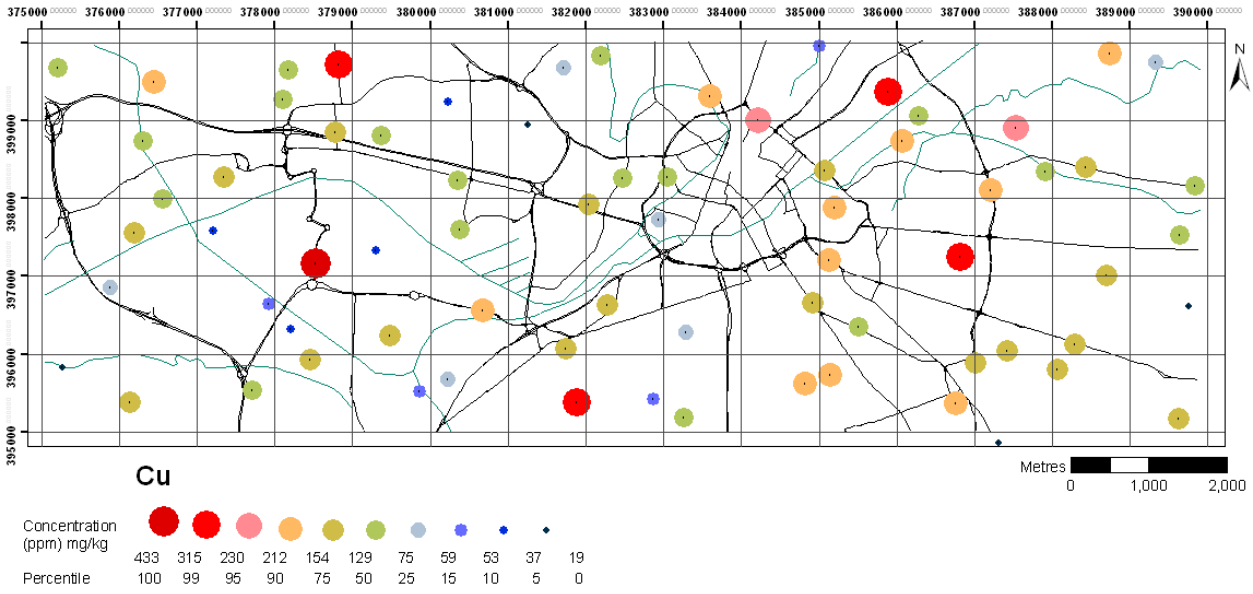

# Iron

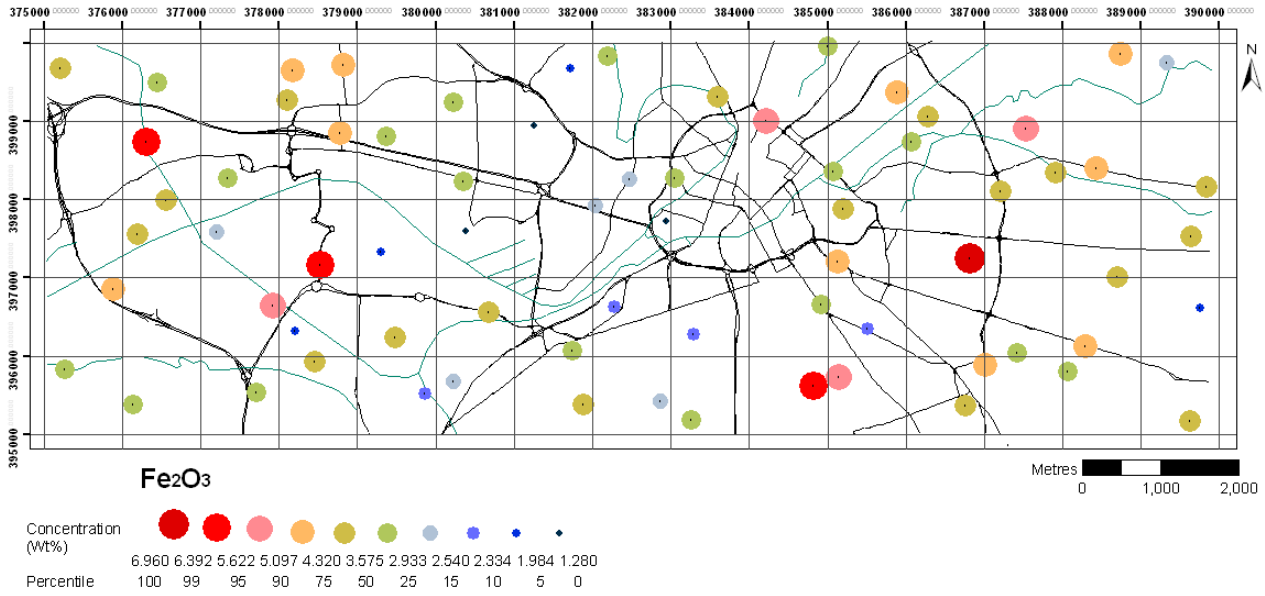
375000 376000 377000 378000 379000 380000 381000 382000 383000 384000 385000 386000 387000 388000 389000 390000
399000 398000 397000 396000 395000
N
Fe2O3
Metres
0 1,000 2,000
Concentration (Wt%)
6.960 6.392 5.622 5.097 4.320 3.575 2.933 2.540 2.334 1.984 1.280
Percentile
100 99 95 90 75 50 25 15 10 5 0

# Lead

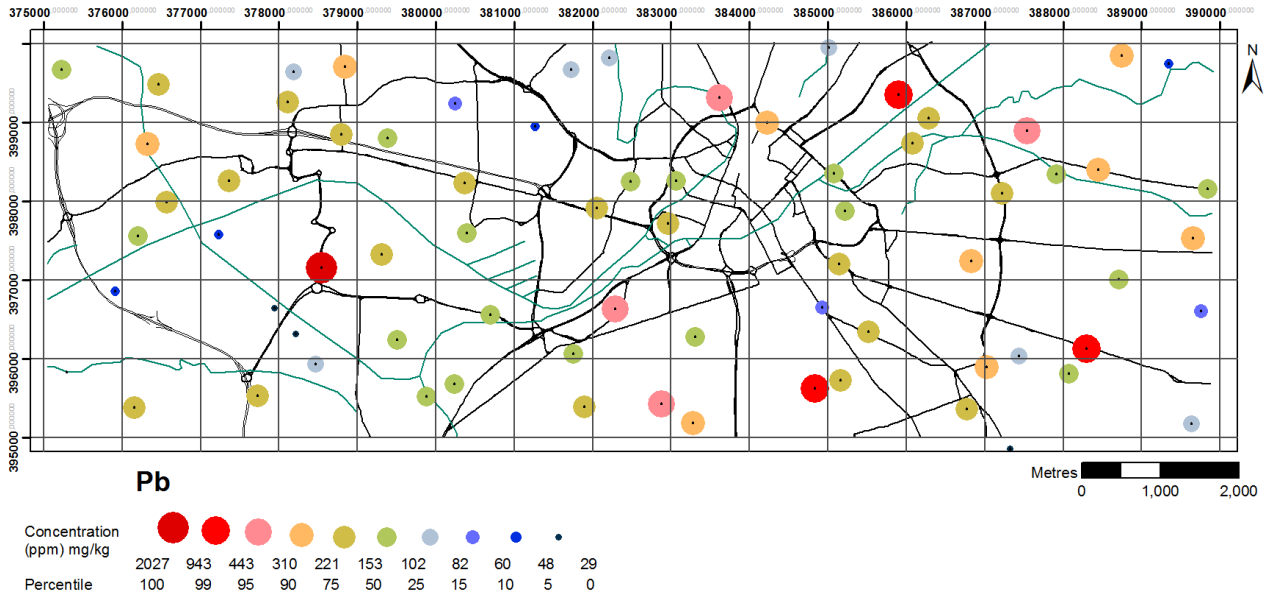
375000 376000 377000 378000 379000 380000 381000 382000 383000 384000 385000 386000 387000 388000 389000 390000
399000 398000 397000 396000 395000
N
Pb
Metres
0 1,000 2,000
Concentration (ppm) mg/kg
2027 943 443 310 221 153 102 82 60 48 29
Percentile
100 99 95 90 75 50 25 15 10 5 0

# Magnesium

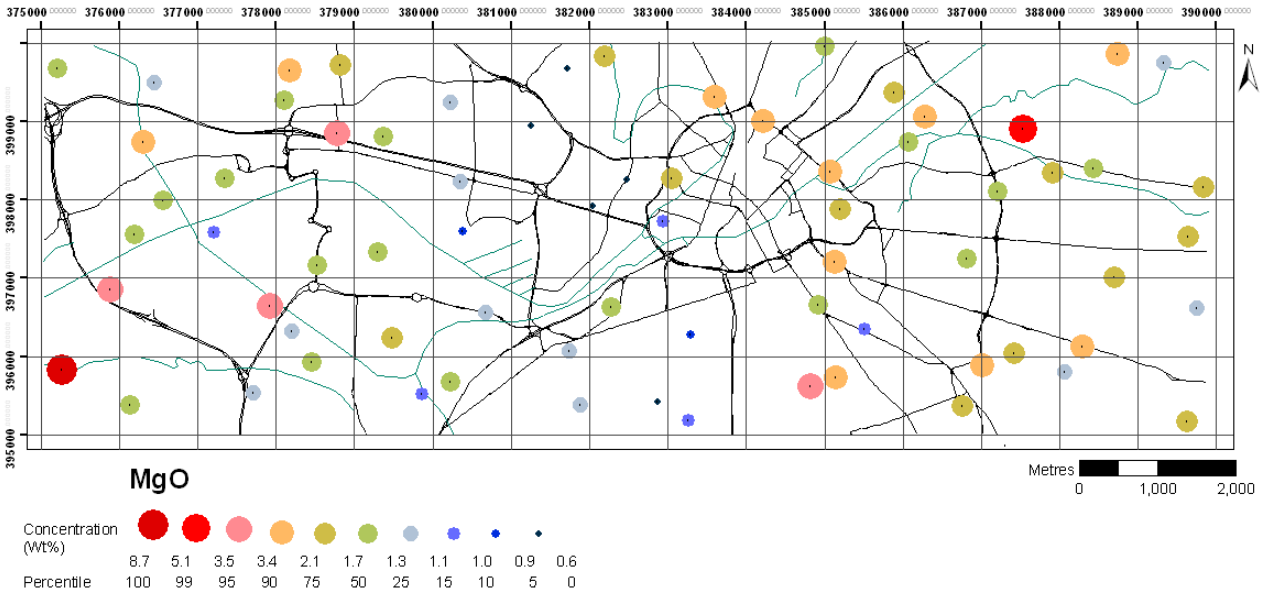


# Manganese

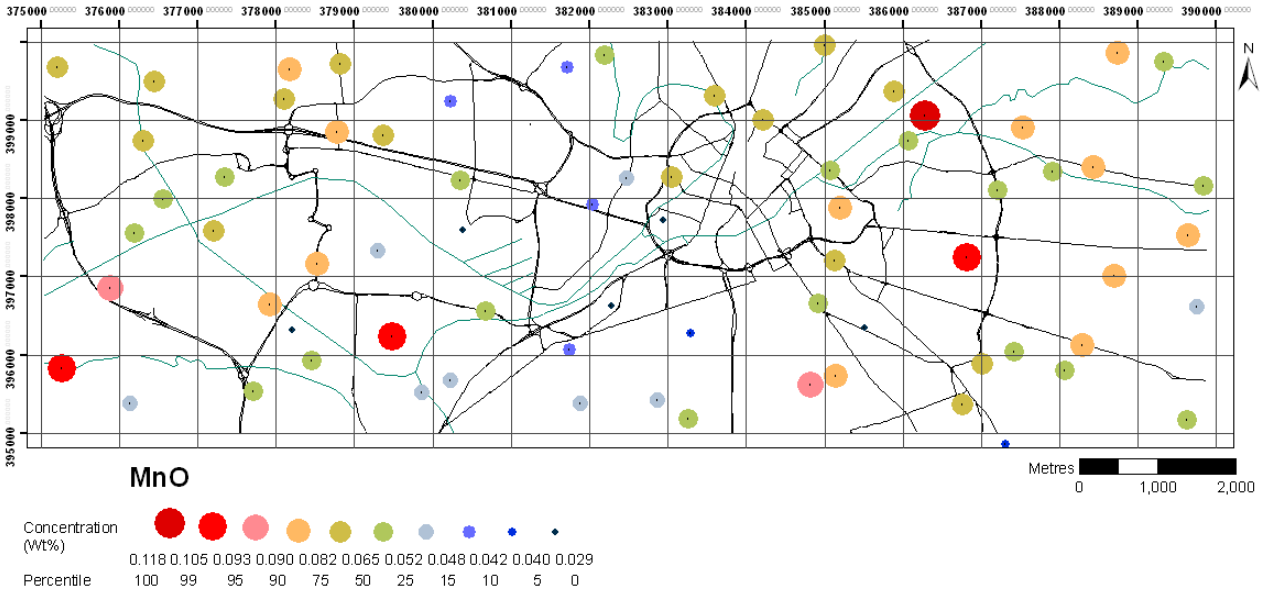

# Molybdenum

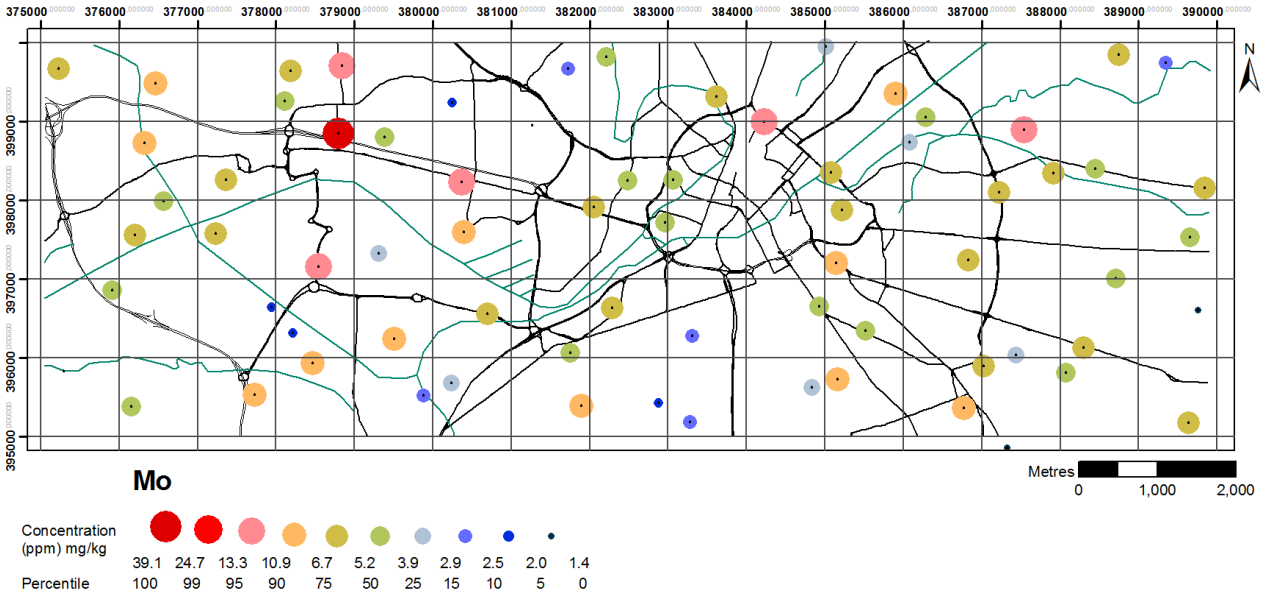


# Nickel

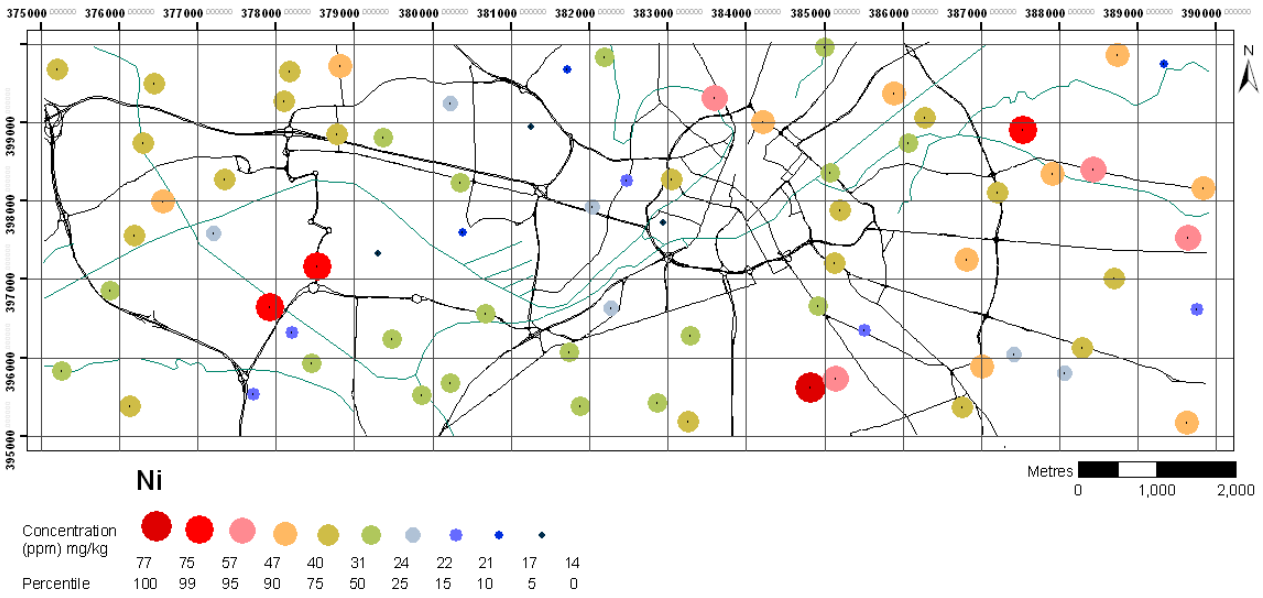

# Phosphorus

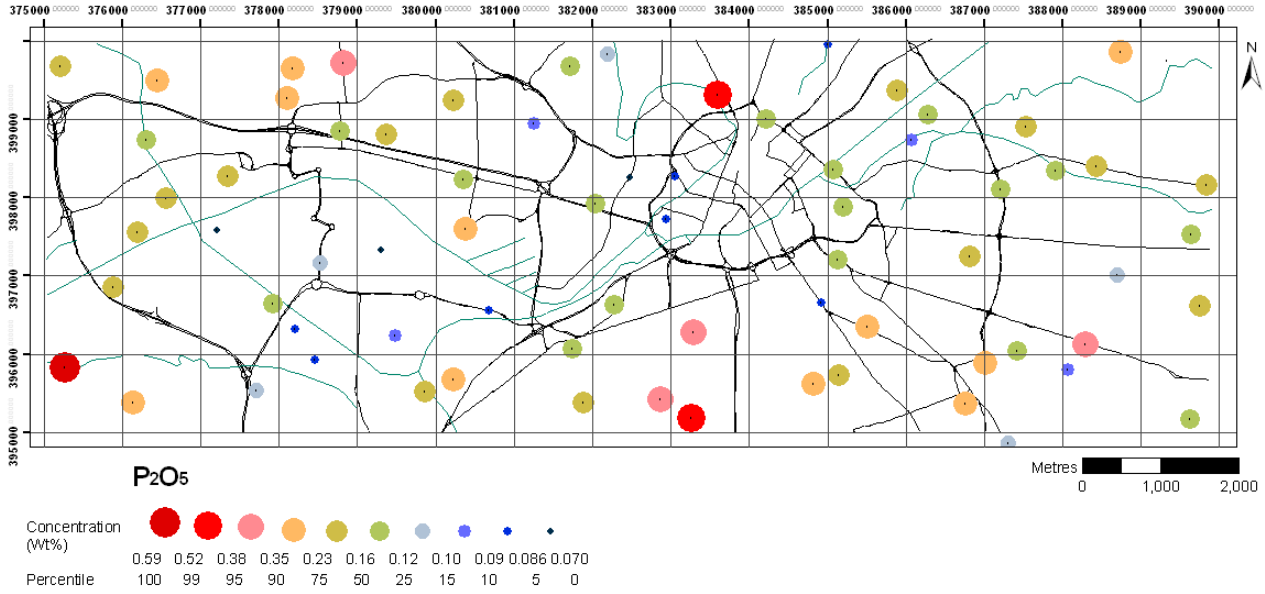


# Potassium

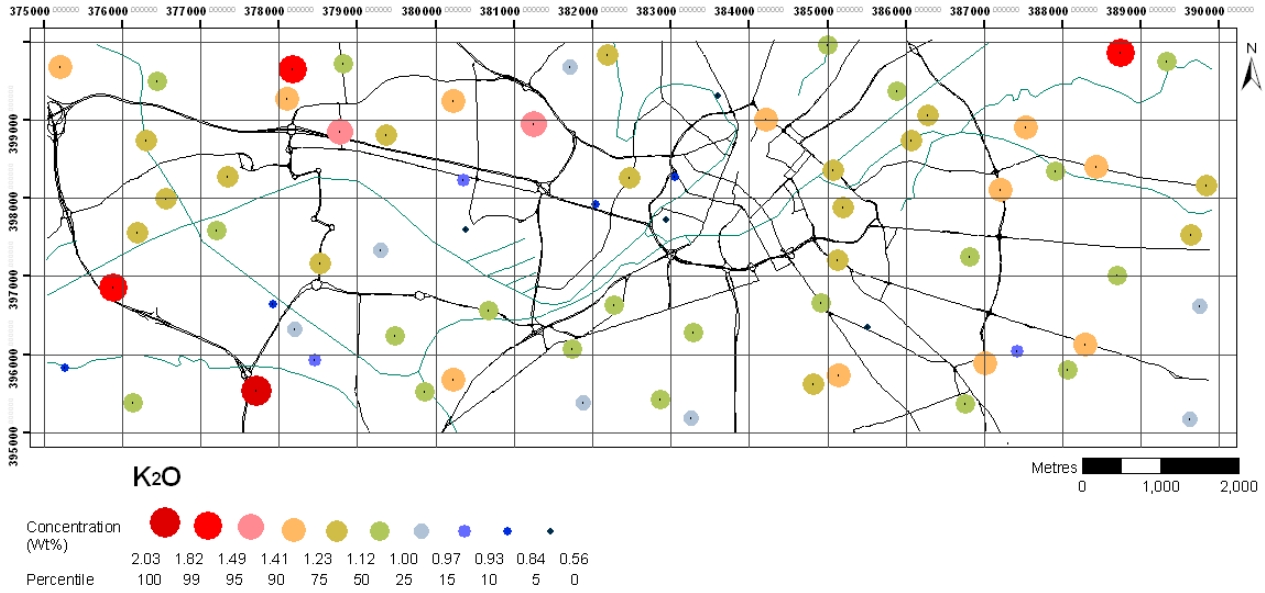

# Silicon

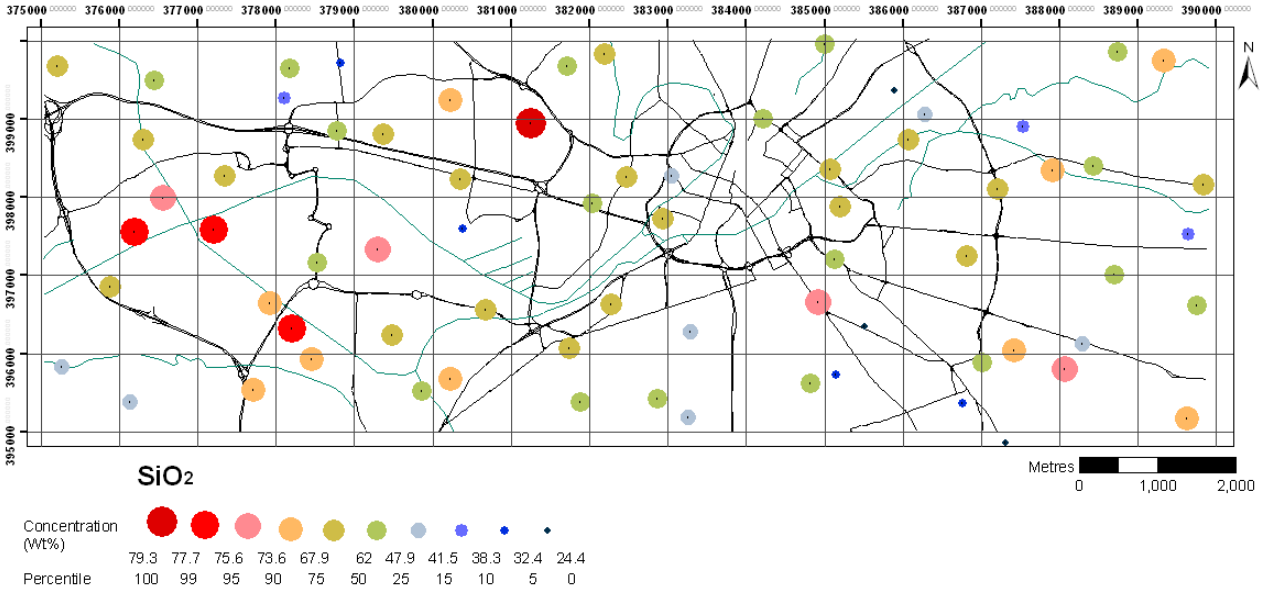


# Sulphur

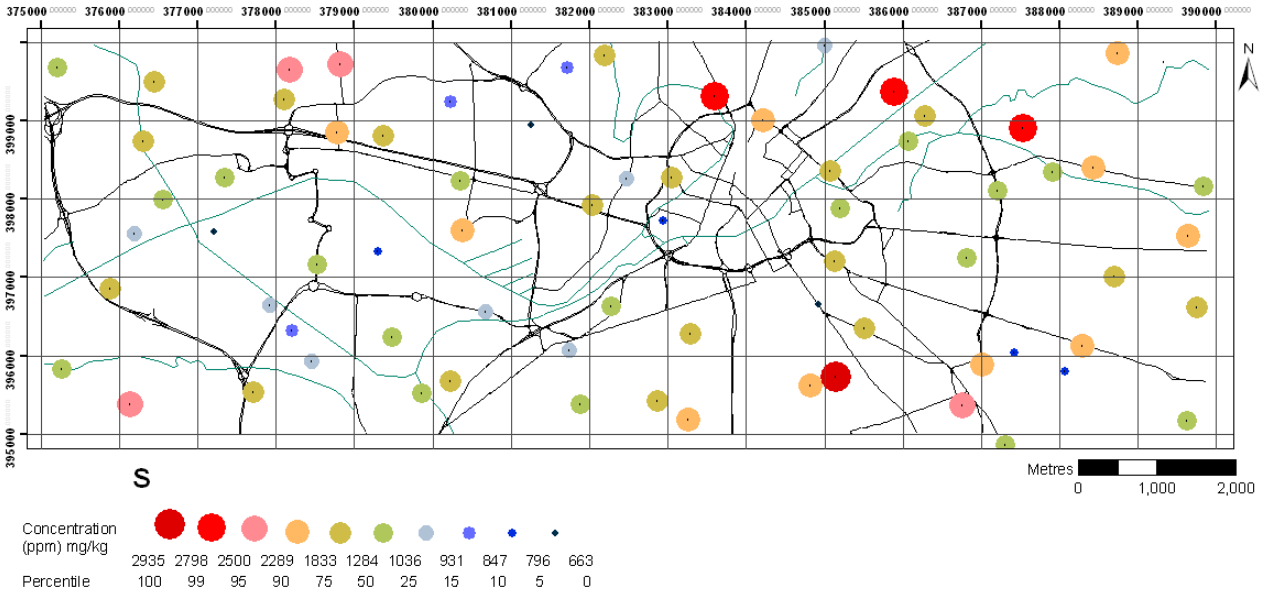

# Tin

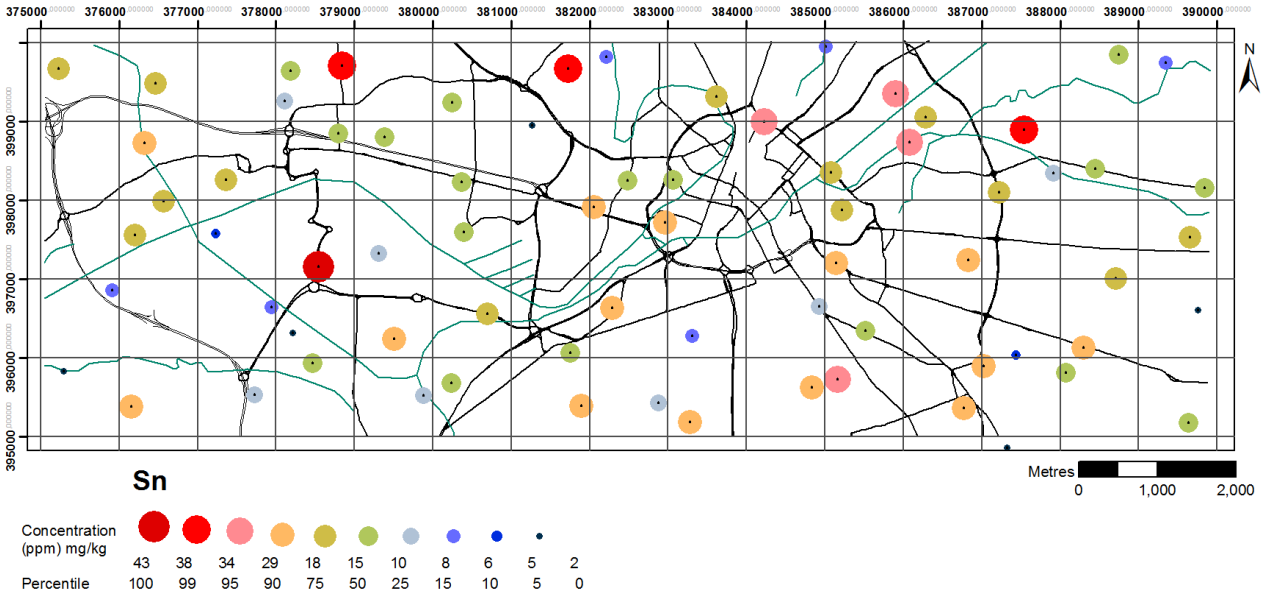


# Titanium

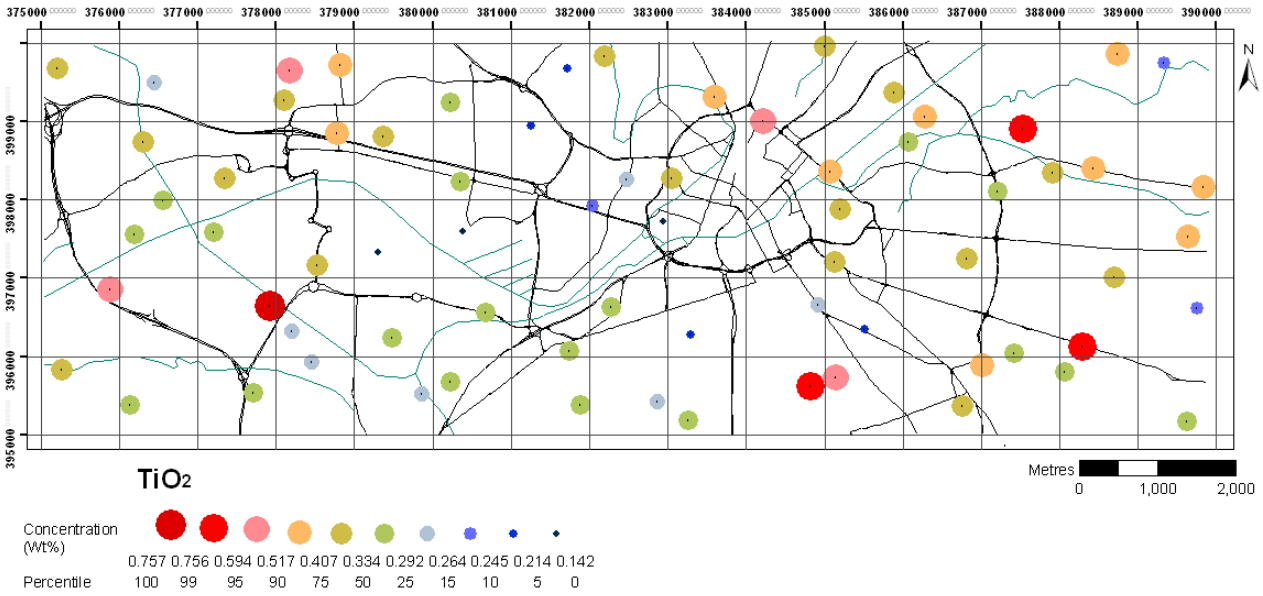

# Uranium

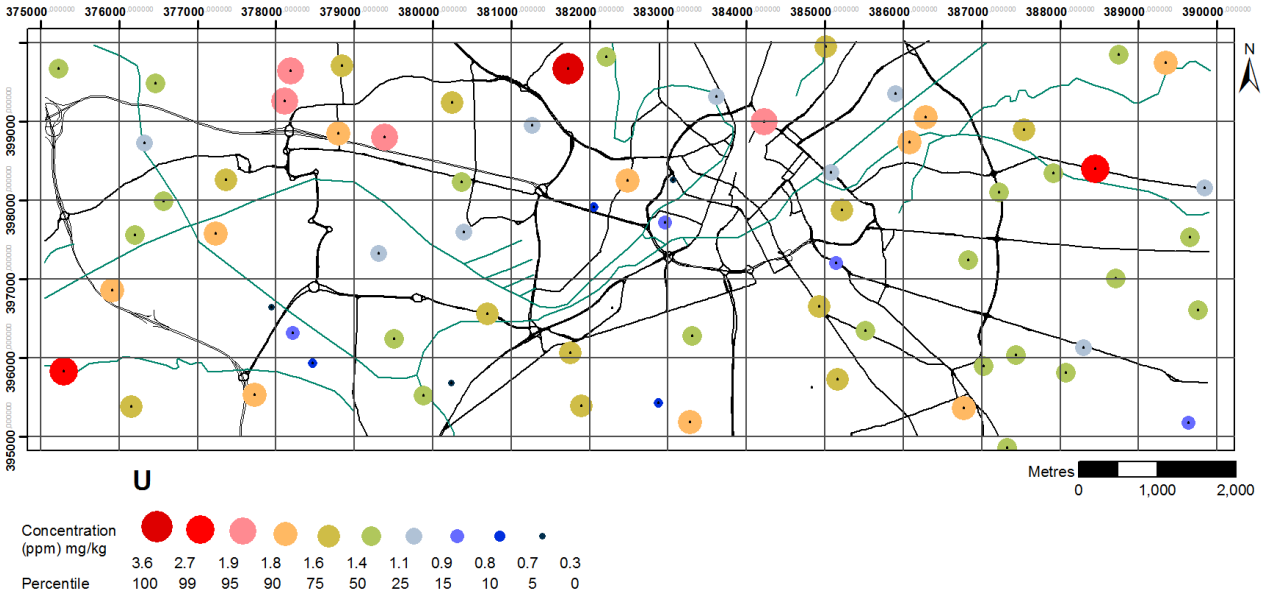


# Vanadium

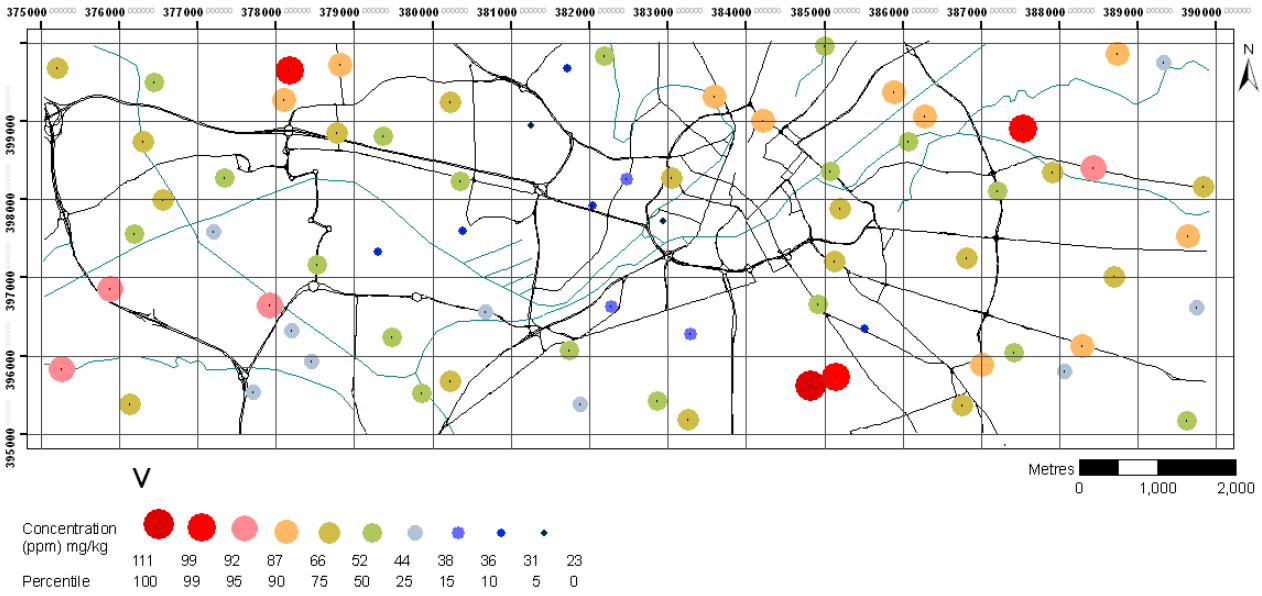

# Zinc

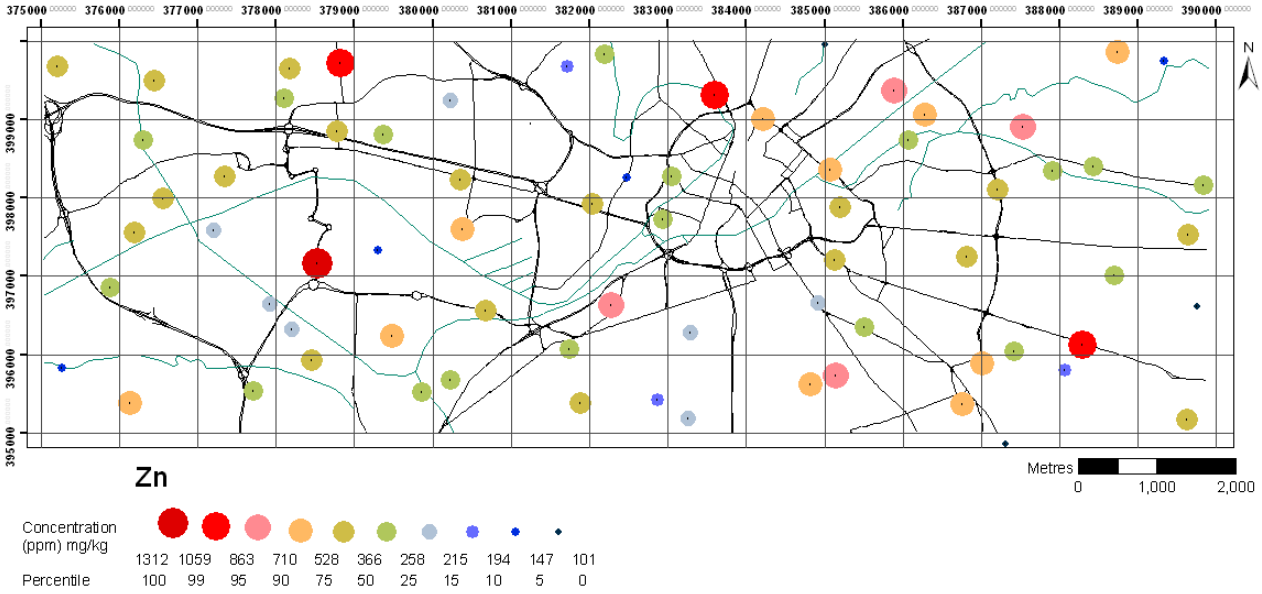


# Organic matter

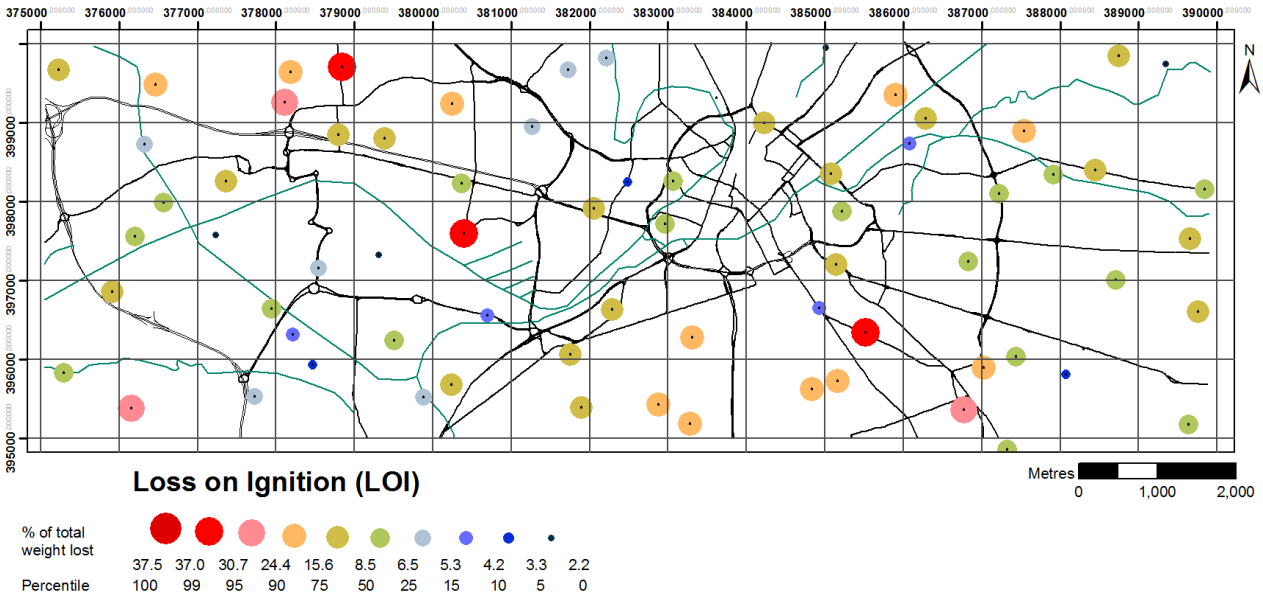

## 6. *Spatial statistical analysis*

**Part A: OLS models** (road data © OS MasterMap Integrated Transport Network™ layer)

*A.1. Residual maps - Soils - #B* (soil data ©BGS)

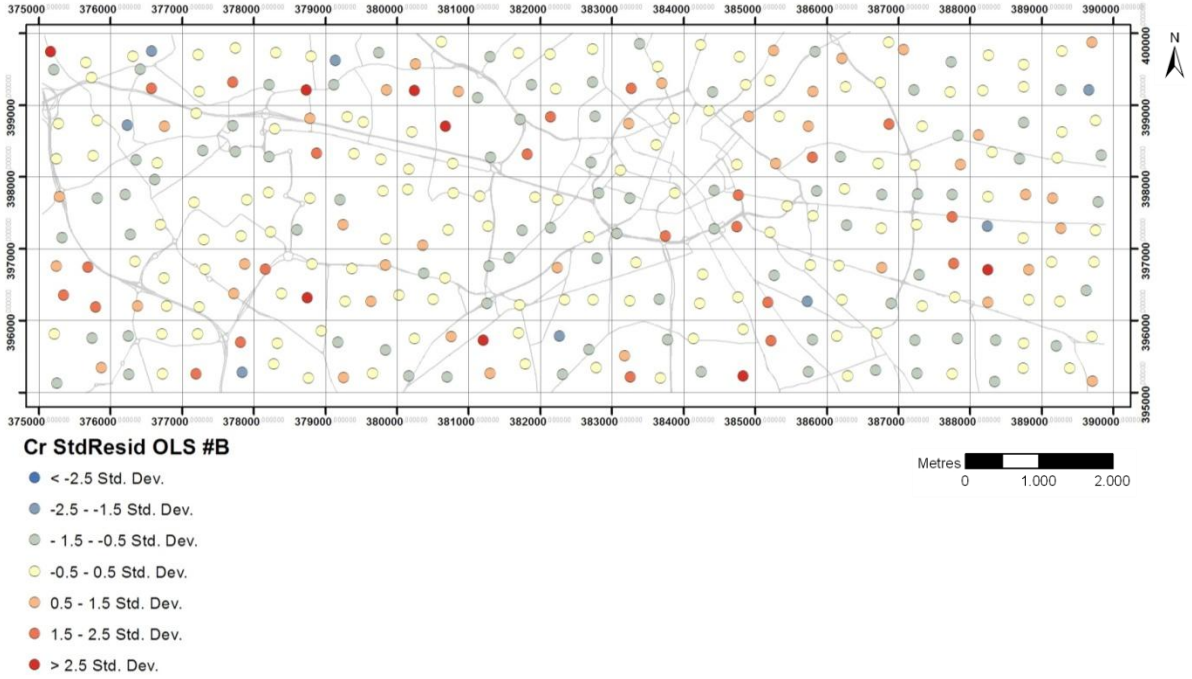


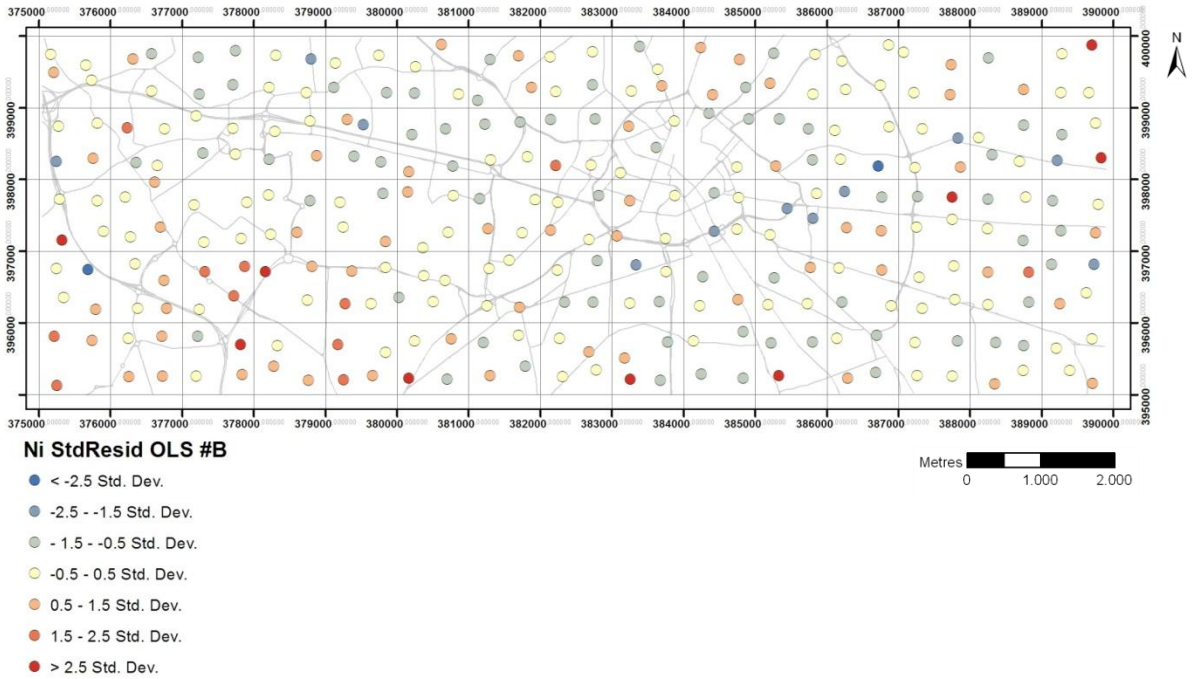

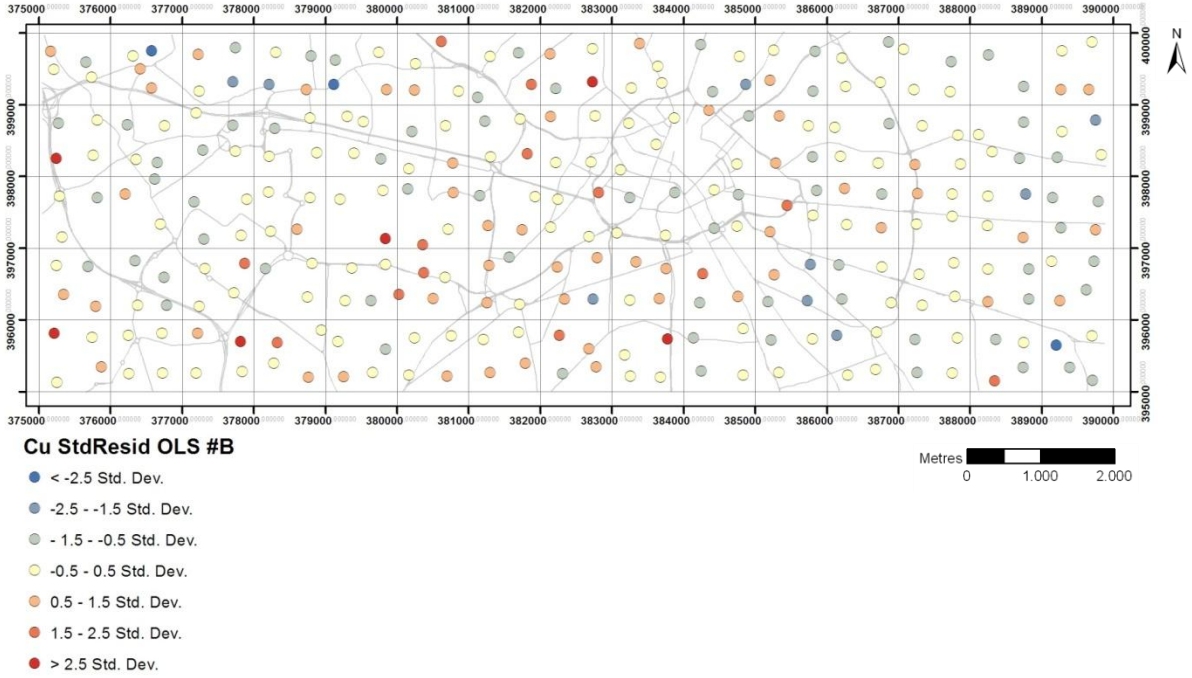
375000 376000 377000 378000 379000 380000 381000 382000 383000 384000 385000 386000 387000 388000 389000 390000
400000 399000 398000 397000 396000 395000
N
Cu StdResid OLS #B
< -2.5 Std. Dev.
-2.5 - -1.5 Std. Dev.
- 1.5 - -0.5 Std. Dev.
-0.5 - 0.5 Std. Dev.
0.5 - 1.5 Std. Dev.
1.5 - 2.5 Std. Dev.
> 2.5 Std. Dev.
Metres
0 1.000 2.000

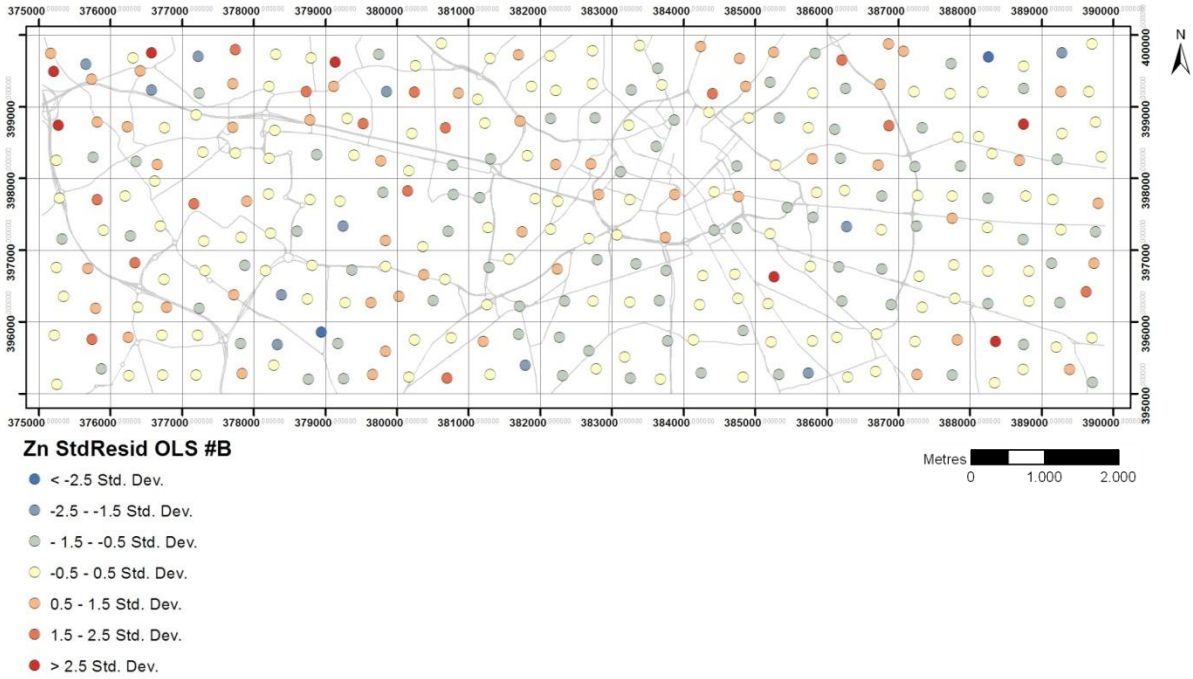
375000 376000 377000 378000 379000 380000 381000 382000 383000 384000 385000 386000 387000 388000 389000 390000
400000 399000 398000 397000 396000 395000
N
Zn StdResid OLS #B
< -2.5 Std. Dev.
-2.5 - -1.5 Std. Dev.
- 1.5 - -0.5 Std. Dev.
-0.5 - 0.5 Std. Dev.
0.5 - 1.5 Std. Dev.
1.5 - 2.5 Std. Dev.
> 2.5 Std. Dev.
Metres
0 1.000 2.000

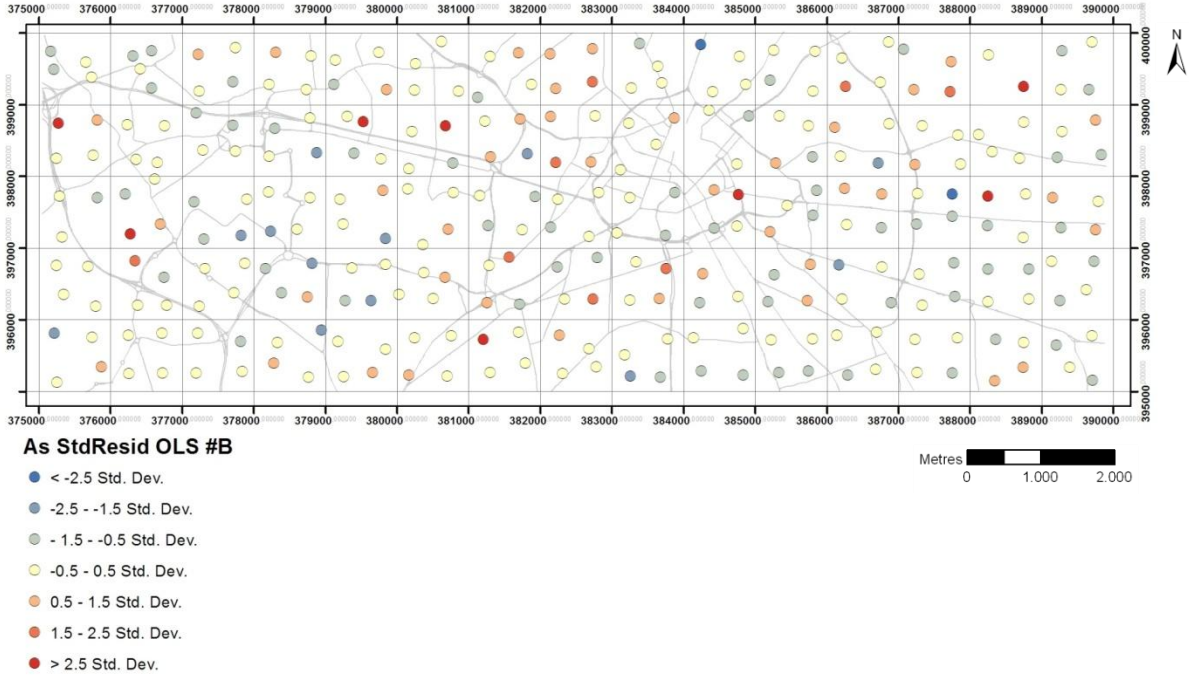
375000 376000 377000 378000 379000 380000 381000 382000 383000 384000 385000 386000 387000 388000 389000 390000
400000 399000 398000 397000 396000 395000
N
As StdResid OLS #B
< -2.5 Std. Dev.
-2.5 - -1.5 Std. Dev.
- 1.5 - -0.5 Std. Dev.
-0.5 - 0.5 Std. Dev.
0.5 - 1.5 Std. Dev.
1.5 - 2.5 Std. Dev.
> 2.5 Std. Dev.
Metres
0 1.000 2.000

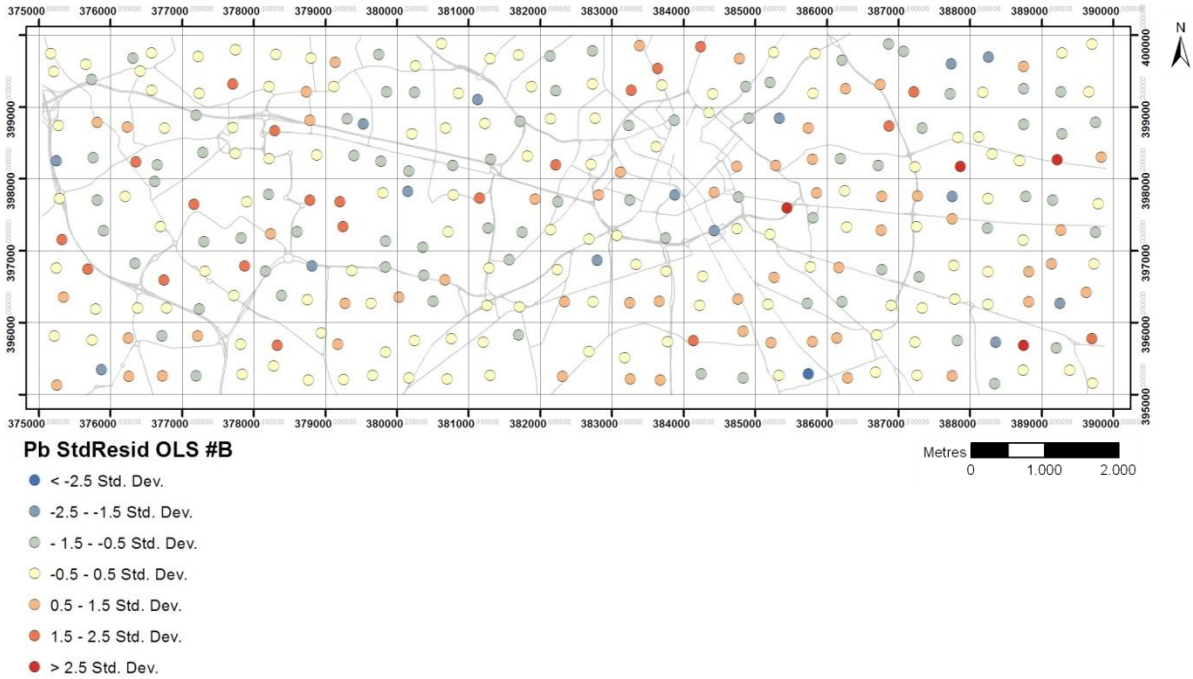
375000 376000 377000 378000 379000 380000 381000 382000 383000 384000 385000 386000 387000 388000 389000 390000
400000 399000 398000 397000 396000 395000
N
Pb StdResid OLS #B
< -2.5 Std. Dev.
-2.5 - -1.5 Std. Dev.
- 1.5 - -0.5 Std. Dev.
-0.5 - 0.5 Std. Dev.
0.5 - 1.5 Std. Dev.
1.5 - 2.5 Std. Dev.
> 2.5 Std. Dev.
Metres
0 1.000 2.000

## *A.2. Residual maps - RDS summer - #A*

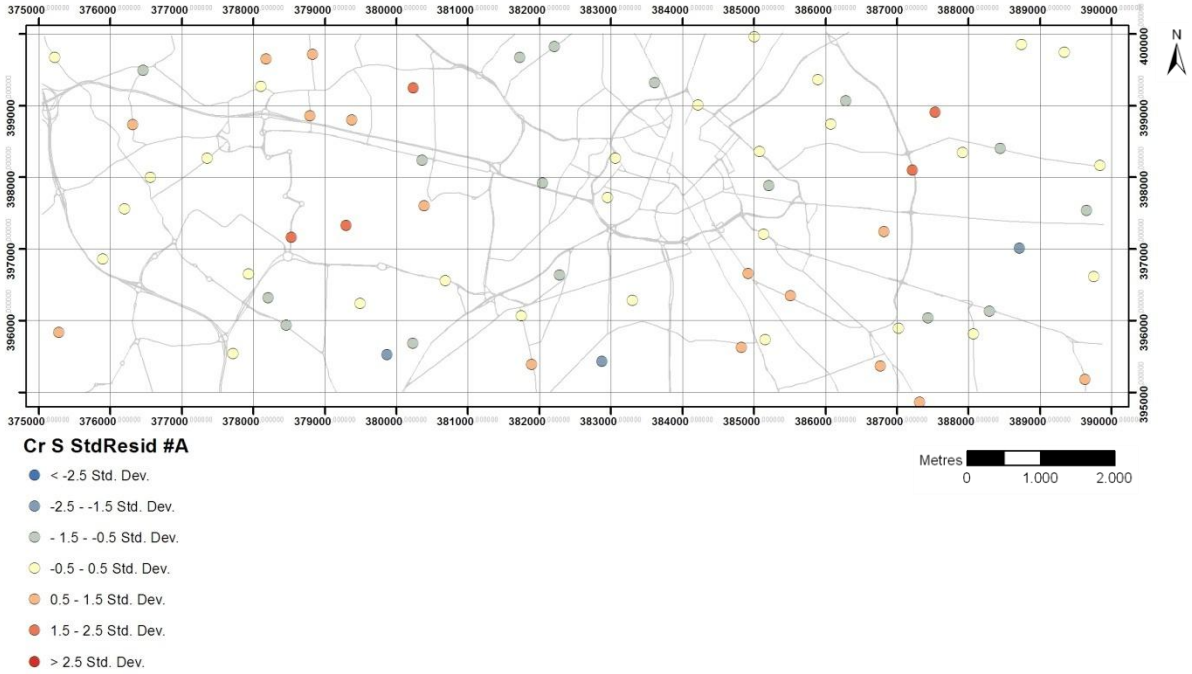


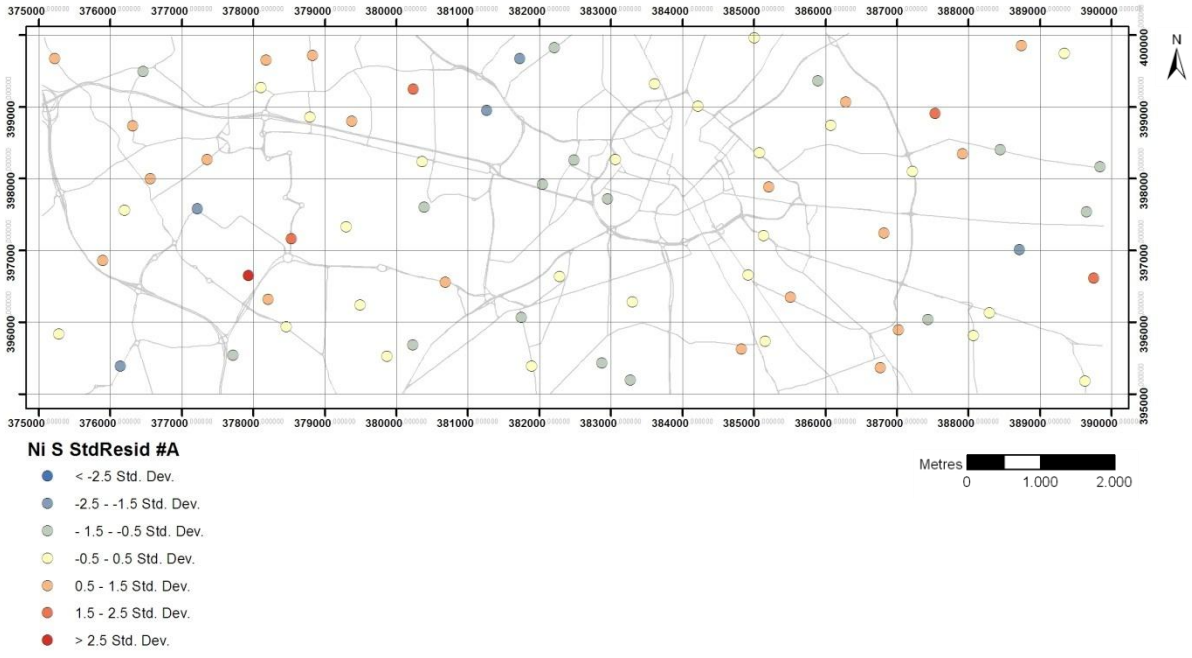

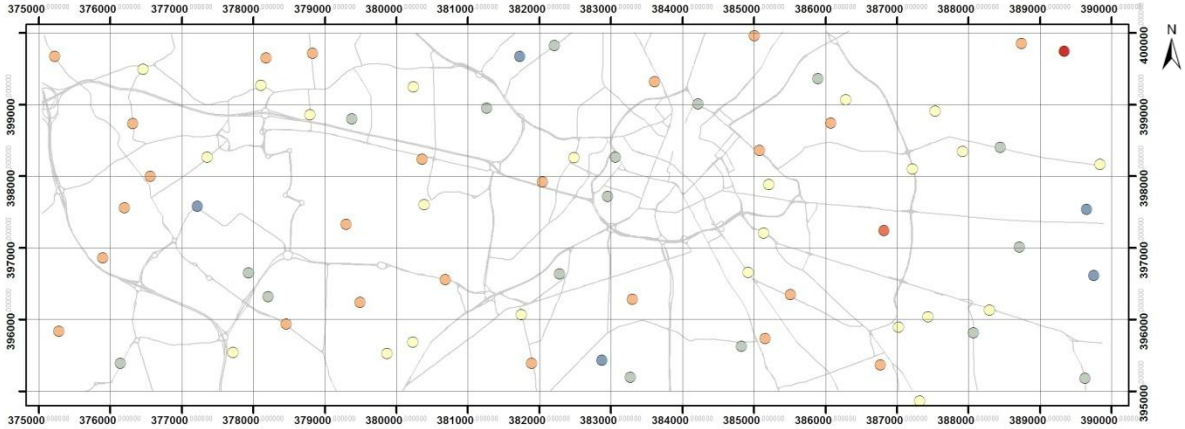
375000 376000 377000 378000 379000 380000 381000 382000 383000 384000 385000 386000 387000 388000 389000 390000
400000 399000 398000 397000 396000 395000
N
Cu S StdResid #A
< -2.5 Std. Dev.
-2.5 - -1.5 Std. Dev.
- 1.5 - -0.5 Std. Dev.
-0.5 - 0.5 Std. Dev.
0.5 - 1.5 Std. Dev.
1.5 - 2.5 Std. Dev.
> 2.5 Std. Dev.
Metres
0 1.000 2.000

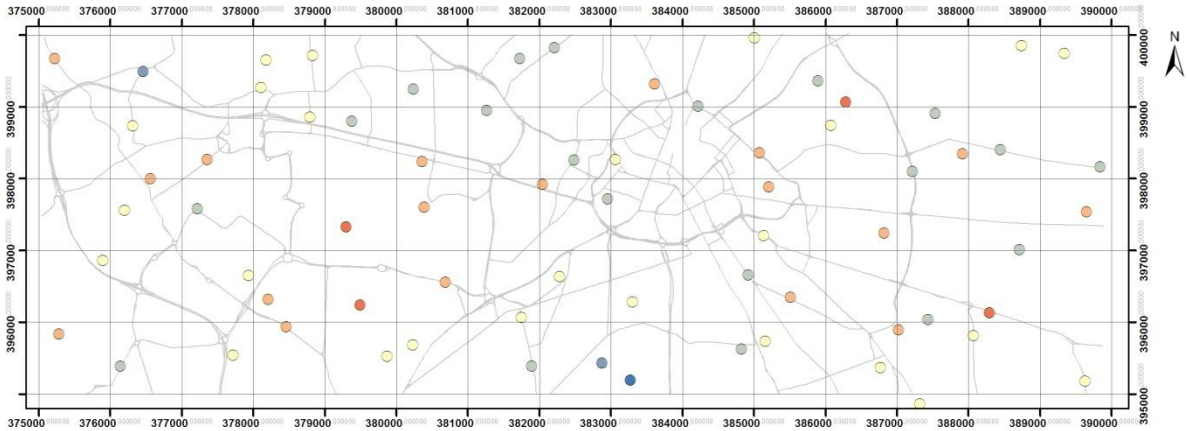
375000 376000 377000 378000 379000 380000 381000 382000 383000 384000 385000 386000 387000 388000 389000 390000
400000 399000 398000 397000 396000 395000
N
Zn S StdResid #A
< -2.5 Std. Dev.
-2.5 - -1.5 Std. Dev.
- 1.5 - -0.5 Std. Dev.
-0.5 - 0.5 Std. Dev.
0.5 - 1.5 Std. Dev.
1.5 - 2.5 Std. Dev.
> 2.5 Std. Dev.
Metres
0 1.000 2.000

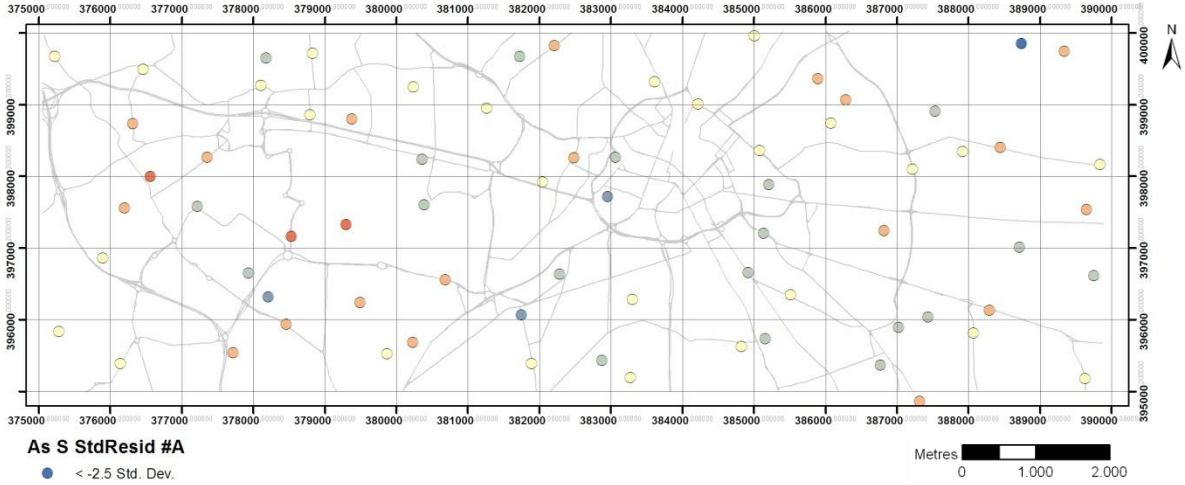
375000 376000 377000 378000 379000 380000 381000 382000 383000 384000 385000 386000 387000 388000 389000 390000
400000 399000 398000 397000 396000 395000
N
As S StdResid #A
< -2.5 Std. Dev.
-2.5 - -1.5 Std. Dev.
- 1.5 - -0.5 Std. Dev.
-0.5 - 0.5 Std. Dev.
0.5 - 1.5 Std. Dev.
1.5 - 2.5 Std. Dev.
> 2.5 Std. Dev.
Metres
0 1.000 2.000

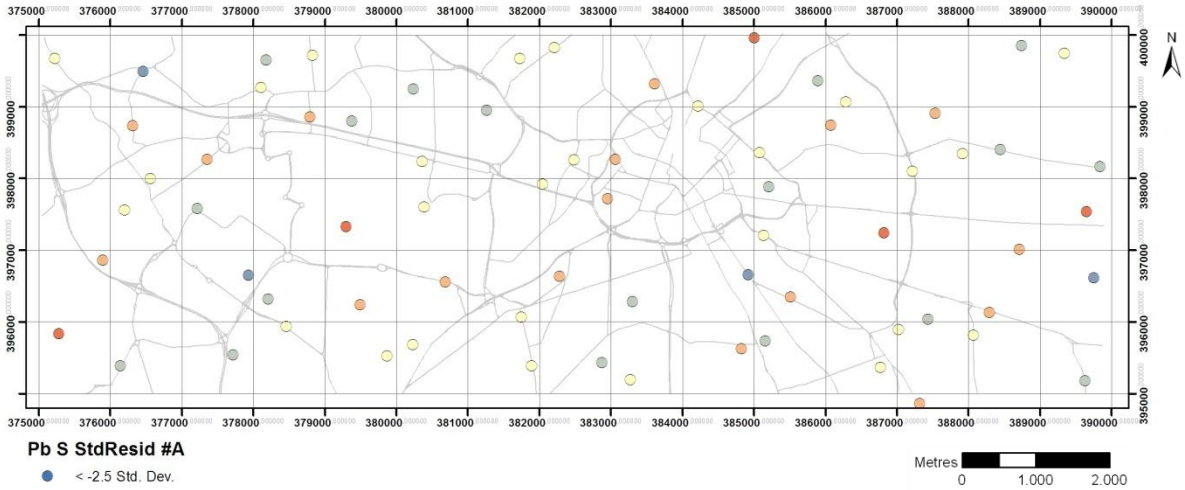
375000 376000 377000 378000 379000 380000 381000 382000 383000 384000 385000 386000 387000 388000 389000 390000
400000 399000 398000 397000 396000 395000
N
Pb S StdResid #A
< -2.5 Std. Dev.
-2.5 - -1.5 Std. Dev.
- 1.5 - -0.5 Std. Dev.
-0.5 - 0.5 Std. Dev.
0.5 - 1.5 Std. Dev.
1.5 - 2.5 Std. Dev.
> 2.5 Std. Dev.
Metres
0 1.000 2.000

## *A.3. Residual maps - RDS winter - #A*

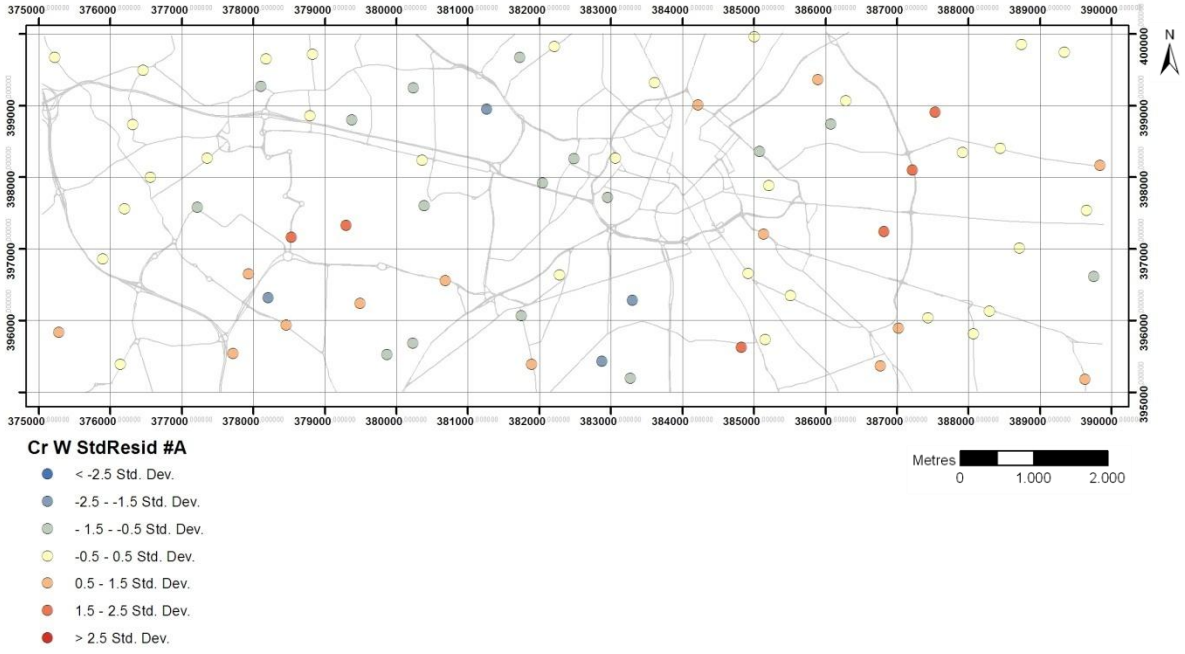


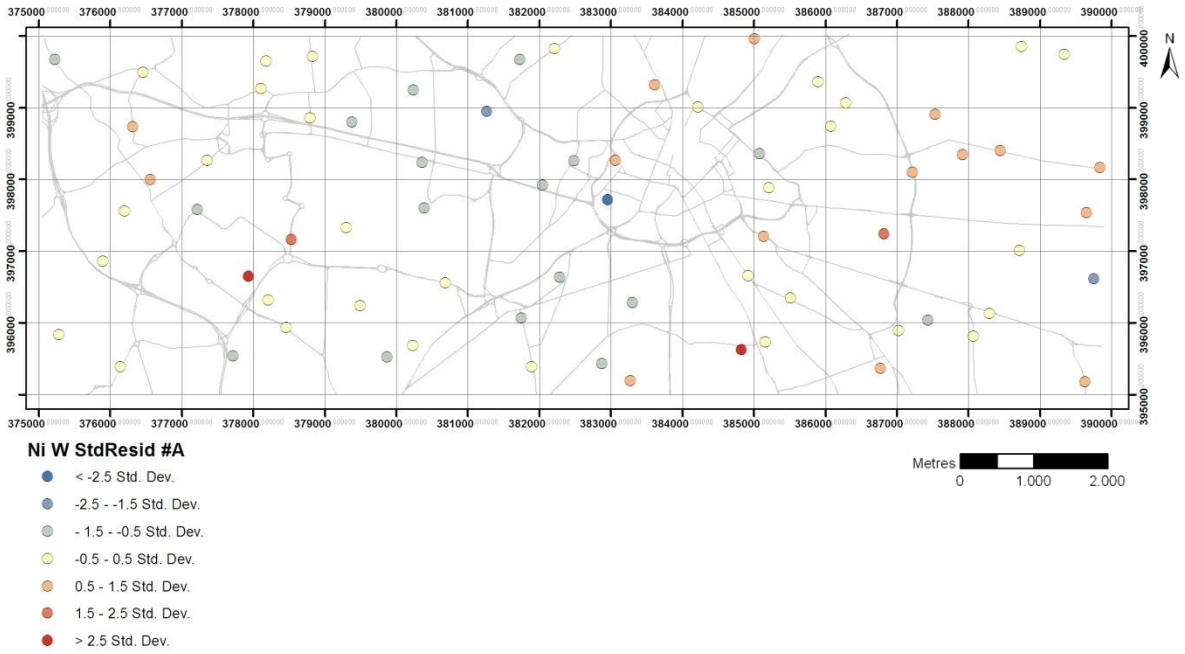

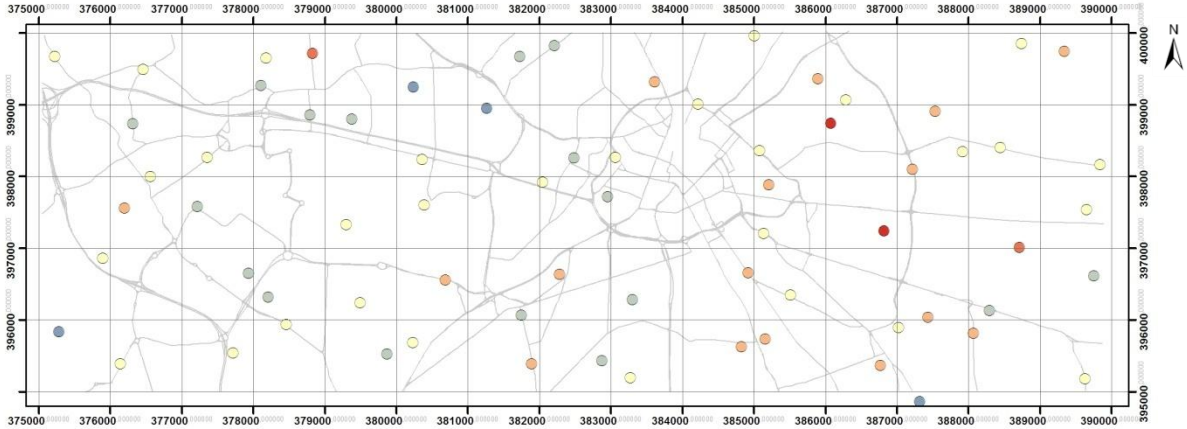
375000 376000 377000 378000 379000 380000 381000 382000 383000 384000 385000 386000 387000 388000 389000 390000
400000 399000 398000 397000 396000 395000
N
Cu W StdResid #A
< -2.5 Std. Dev.
-2.5 - -1.5 Std. Dev.
- 1.5 - -0.5 Std. Dev.
-0.5 - 0.5 Std. Dev.
0.5 - 1.5 Std. Dev.
1.5 - 2.5 Std. Dev.
> 2.5 Std. Dev.
Metres
0 1.000 2.000

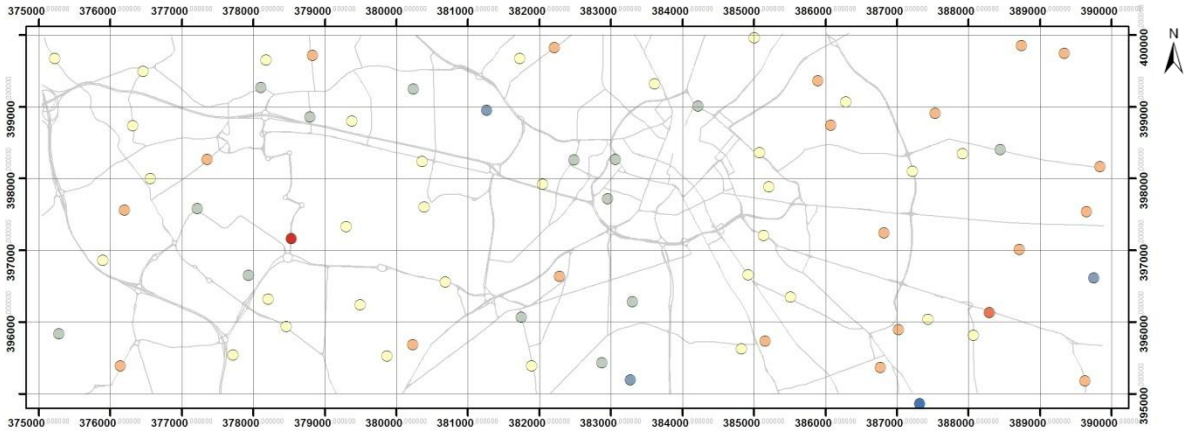
375000 376000 377000 378000 379000 380000 381000 382000 383000 384000 385000 386000 387000 388000 389000 390000
400000 399000 398000 397000 396000 395000
N
Zn W StdResid #A
< -2.5 Std. Dev.
-2.5 - -1.5 Std. Dev.
- 1.5 - -0.5 Std. Dev.
-0.5 - 0.5 Std. Dev.
0.5 - 1.5 Std. Dev.
1.5 - 2.5 Std. Dev.
> 2.5 Std. Dev.
Metres
0 1.000 2.000

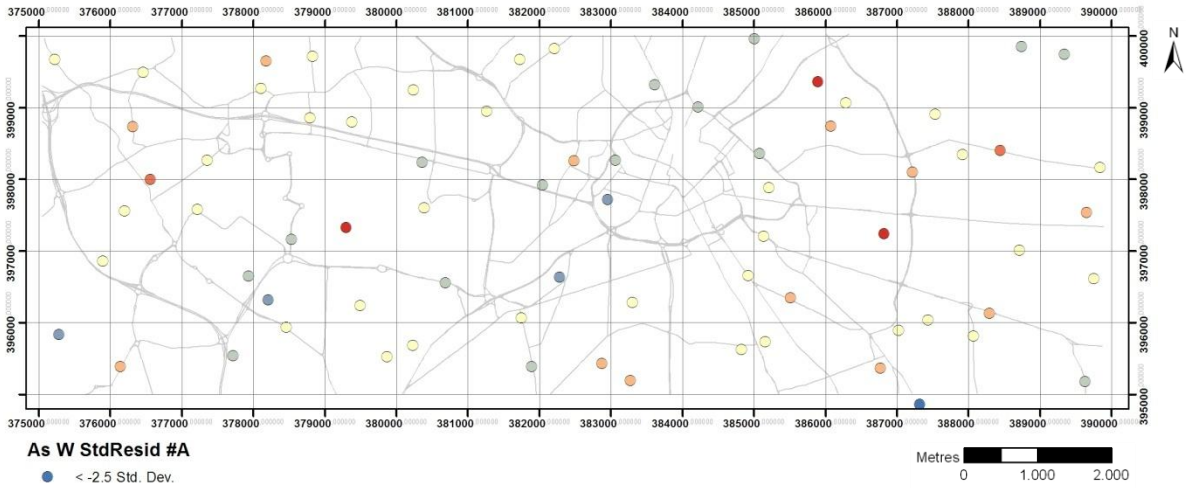
375000 376000 377000 378000 379000 380000 381000 382000 383000 384000 385000 386000 387000 388000 389000 390000
400000 399000 398000 397000 396000 395000
N
As W StdResid #A
< -2.5 Std. Dev.
-2.5 - -1.5 Std. Dev.
- 1.5 - -0.5 Std. Dev.
-0.5 - 0.5 Std. Dev.
0.5 - 1.5 Std. Dev.
1.5 - 2.5 Std. Dev.
> 2.5 Std. Dev.
Metres
0 1.000 2.000

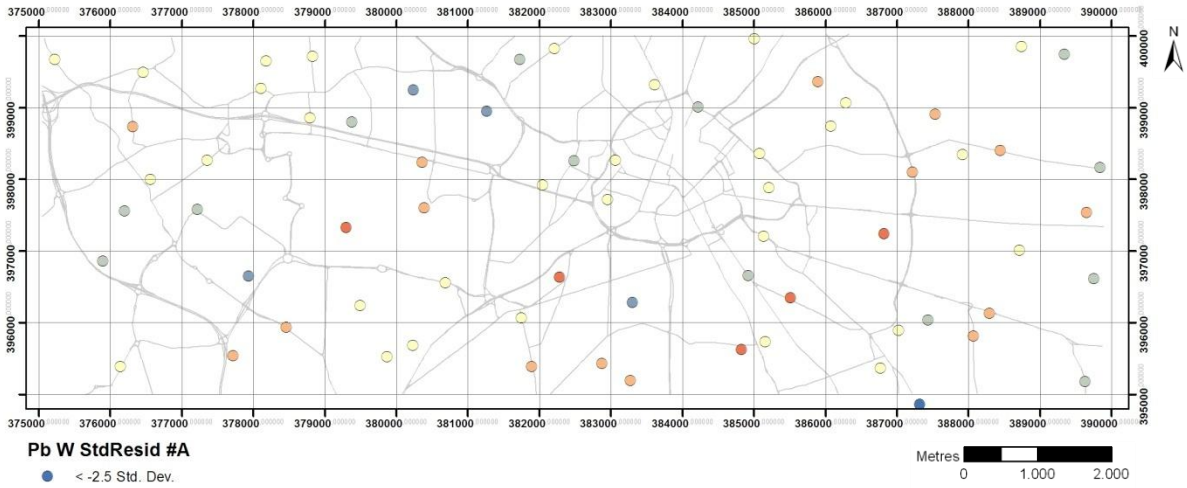
375000 376000 377000 378000 379000 380000 381000 382000 383000 384000 385000 386000 387000 388000 389000 390000
400000 399000 398000 397000 396000 395000
N
Pb W StdResid #A
< -2.5 Std. Dev.
-2.5 - -1.5 Std. Dev.
- 1.5 - -0.5 Std. Dev.
-0.5 - 0.5 Std. Dev.
0.5 - 1.5 Std. Dev.
1.5 - 2.5 Std. Dev.
> 2.5 Std. Dev.
Metres
0 1.000 2.000

## *A.4. Residual maps - RDS summer - #B*

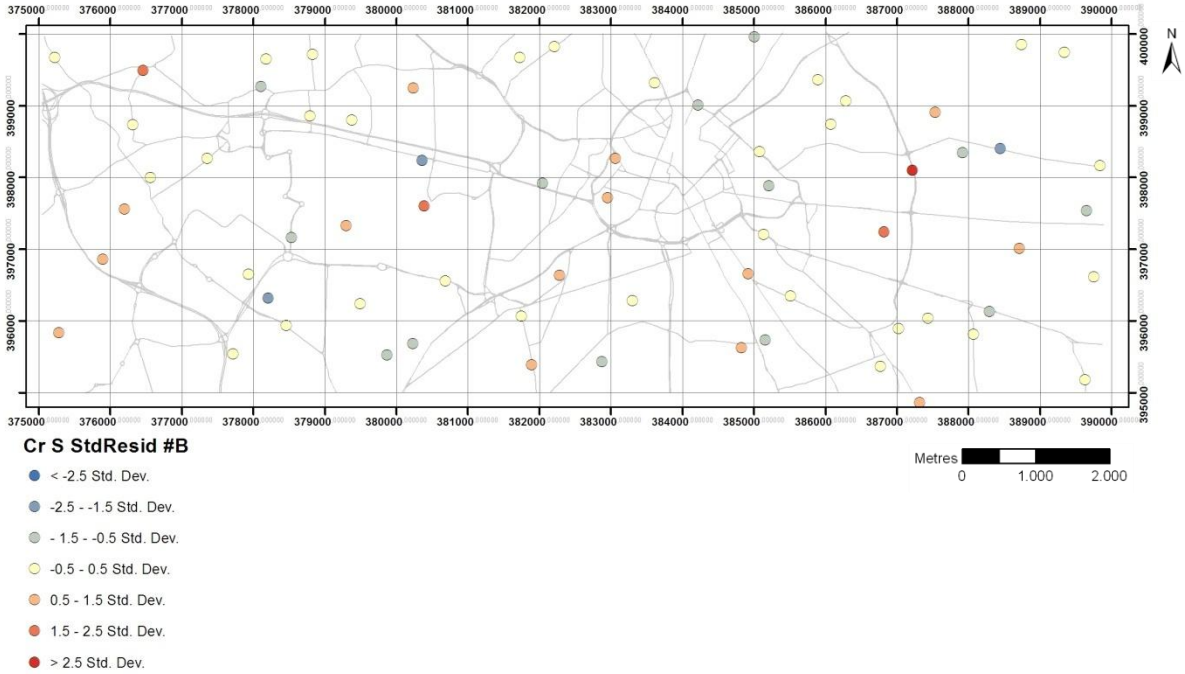


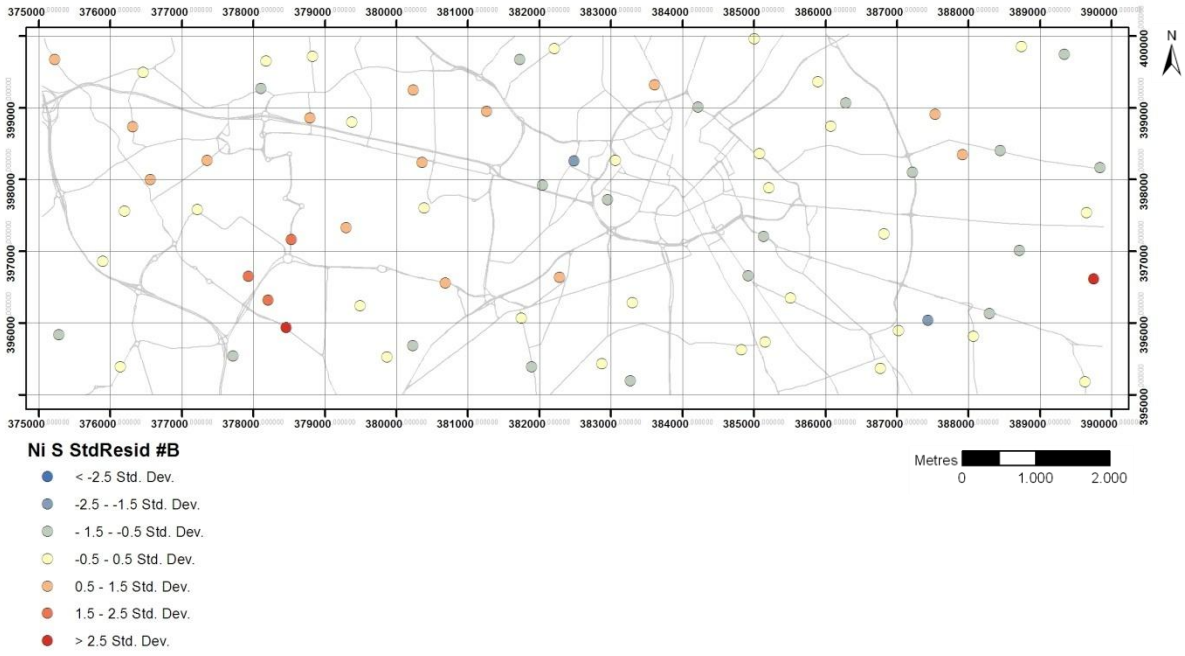

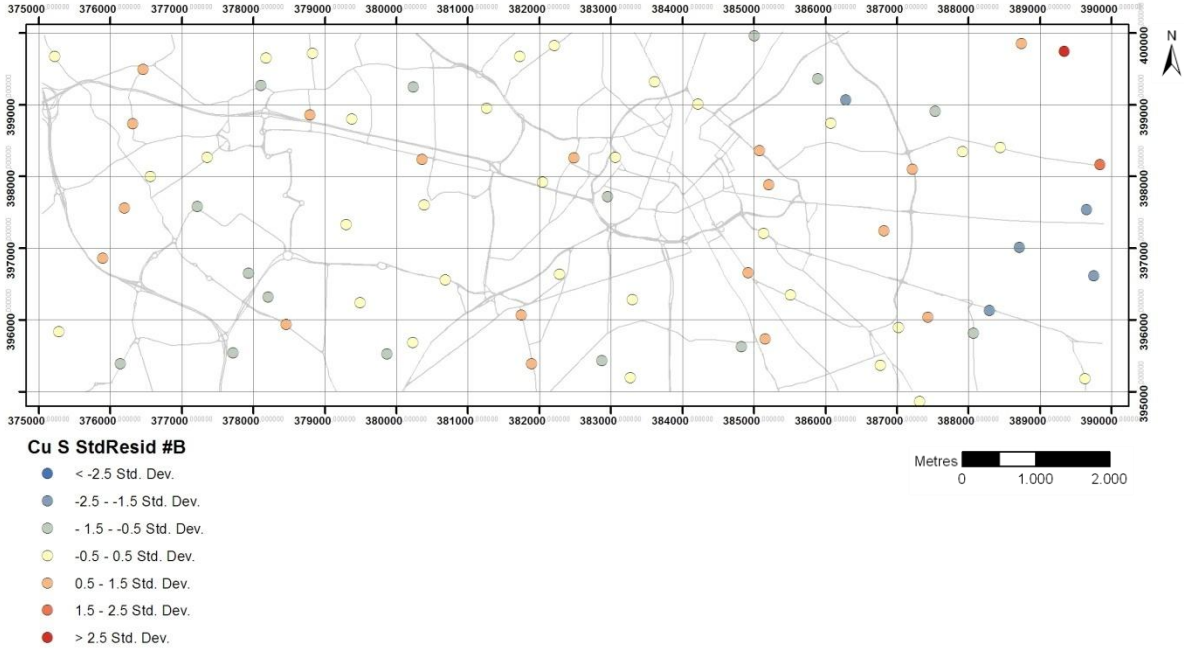
375000 376000 377000 378000 379000 380000 381000 382000 383000 384000 385000 386000 387000 388000 389000 390000
400000 399000 398000 397000 396000 395000
N
Cu S StdResid #B
< -2.5 Std. Dev.
-2.5 - -1.5 Std. Dev.
- 1.5 - -0.5 Std. Dev.
-0.5 - 0.5 Std. Dev.
0.5 - 1.5 Std. Dev.
1.5 - 2.5 Std. Dev.
> 2.5 Std. Dev.
Metres
0 1.000 2.000

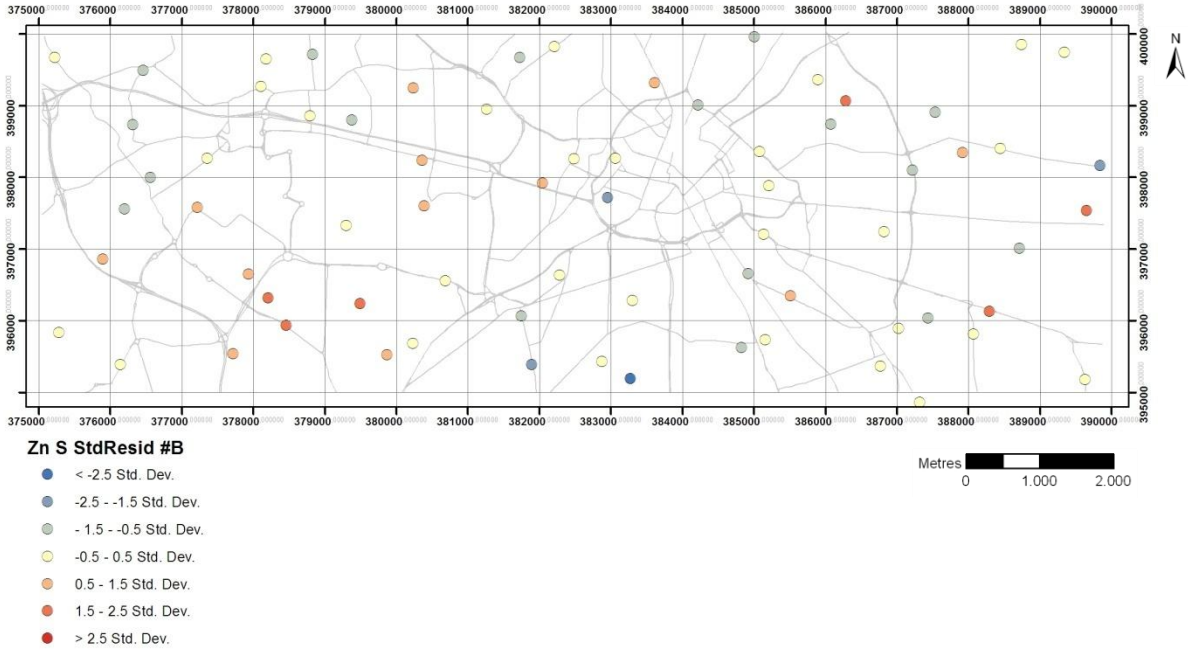
375000 376000 377000 378000 379000 380000 381000 382000 383000 384000 385000 386000 387000 388000 389000 390000
400000 399000 398000 397000 396000 395000
N
Zn S StdResid #B
< -2.5 Std. Dev.
-2.5 - -1.5 Std. Dev.
- 1.5 - -0.5 Std. Dev.
-0.5 - 0.5 Std. Dev.
0.5 - 1.5 Std. Dev.
1.5 - 2.5 Std. Dev.
> 2.5 Std. Dev.
Metres
0 1.000 2.000

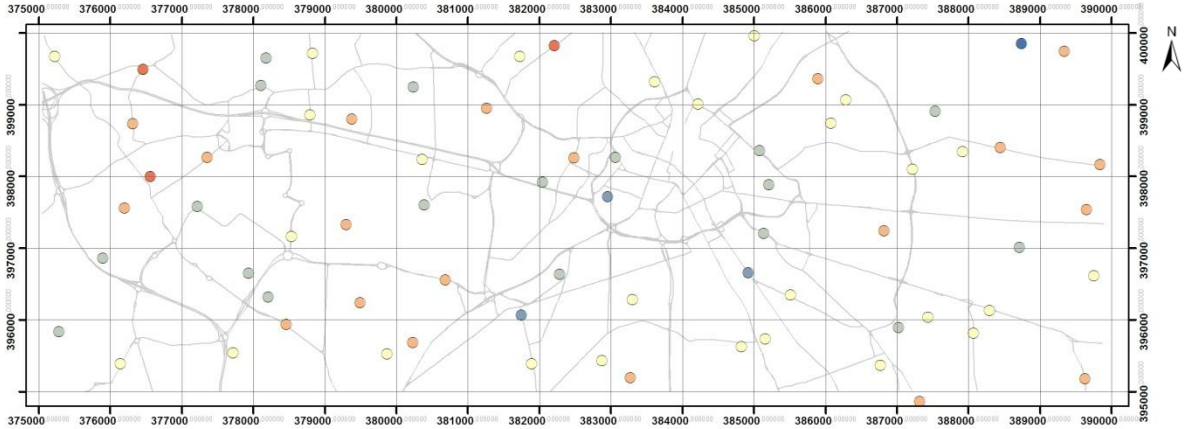
375000 376000 377000 378000 379000 380000 381000 382000 383000 384000 385000 386000 387000 388000 389000 390000
400000 399000 398000 397000 396000 395000
N
As S StdResid #B
< -2.5 Std. Dev.
-2.5 - -1.5 Std. Dev.
- 1.5 - -0.5 Std. Dev.
-0.5 - 0.5 Std. Dev.
0.5 - 1.5 Std. Dev.
1.5 - 2.5 Std. Dev.
> 2.5 Std. Dev.
Metres
0 1.000 2.000

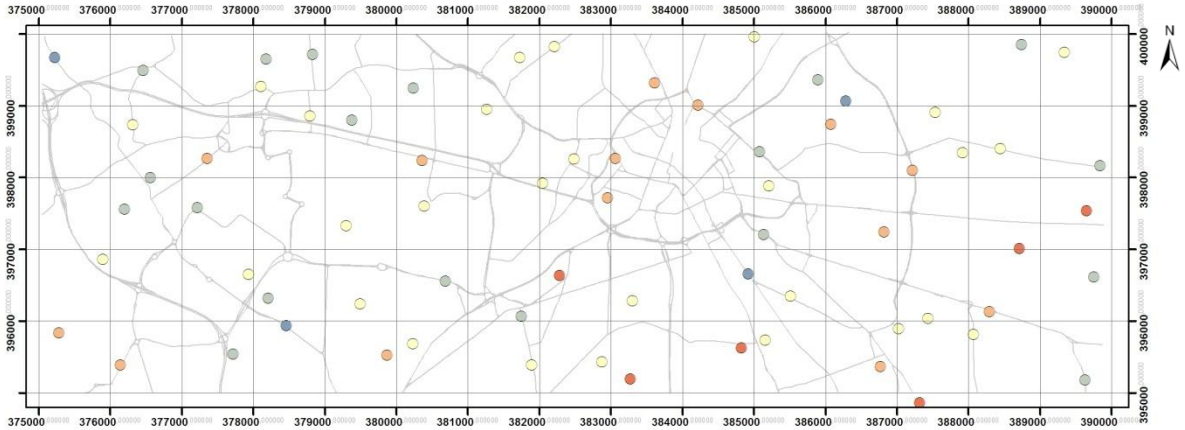
375000 376000 377000 378000 379000 380000 381000 382000 383000 384000 385000 386000 387000 388000 389000 390000
400000 399000 398000 397000 396000 395000
N
Pb S StdResid #B
< -2.5 Std. Dev.
-2.5 - -1.5 Std. Dev.
- 1.5 - -0.5 Std. Dev.
-0.5 - 0.5 Std. Dev.
0.5 - 1.5 Std. Dev.
1.5 - 2.5 Std. Dev.
> 2.5 Std. Dev.
Metres
0 1.000 2.000

## *A.5. Residual maps - RDS winter - #B*

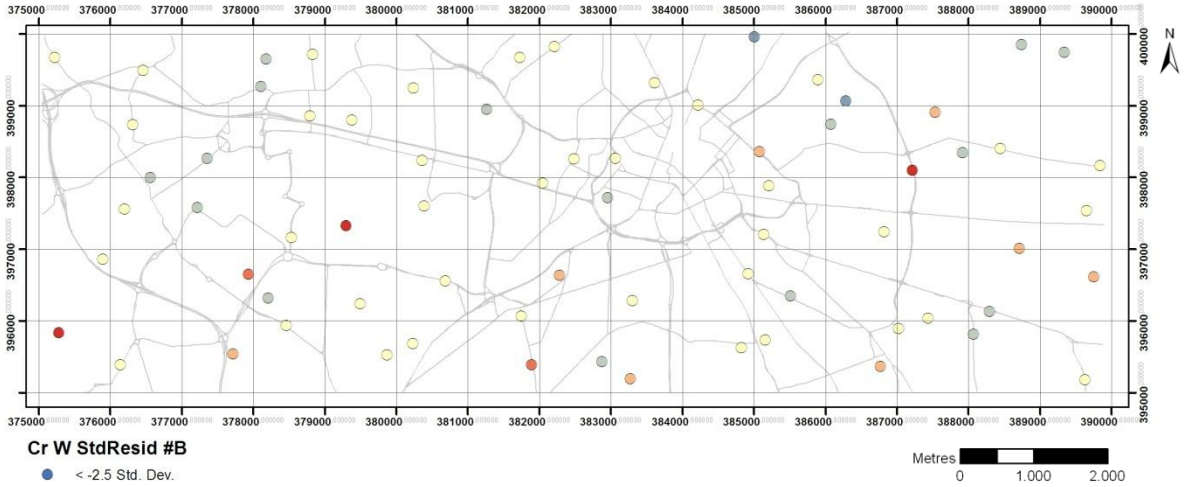


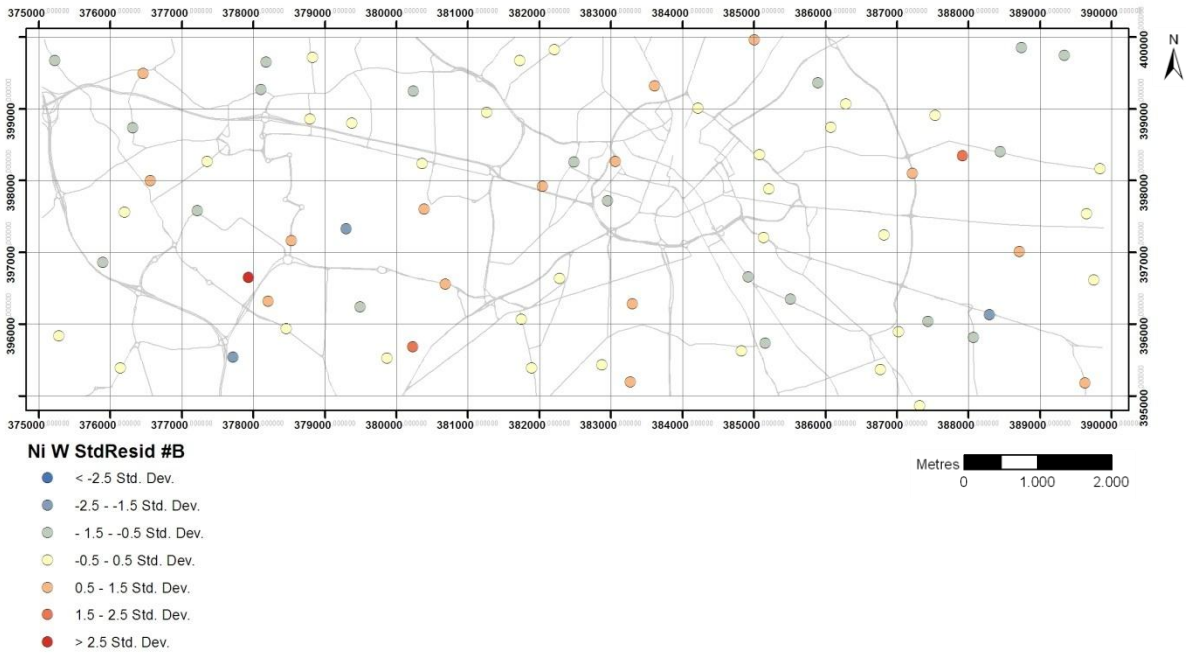

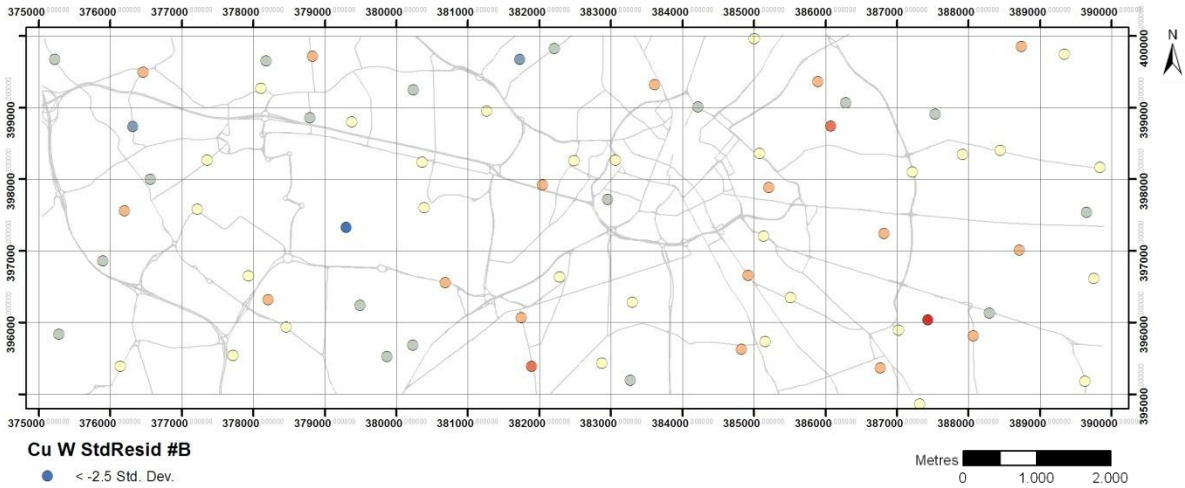
375000 376000 377000 378000 379000 380000 381000 382000 383000 384000 385000 386000 387000 388000 389000 390000
400000 399000 398000 397000 396000 395000
N
Cu W StdResid #B
< -2.5 Std. Dev.
-2.5 - -1.5 Std. Dev.
- 1.5 - -0.5 Std. Dev.
-0.5 - 0.5 Std. Dev.
0.5 - 1.5 Std. Dev.
1.5 - 2.5 Std. Dev.
> 2.5 Std. Dev.
Metres
0 1.000 2.000

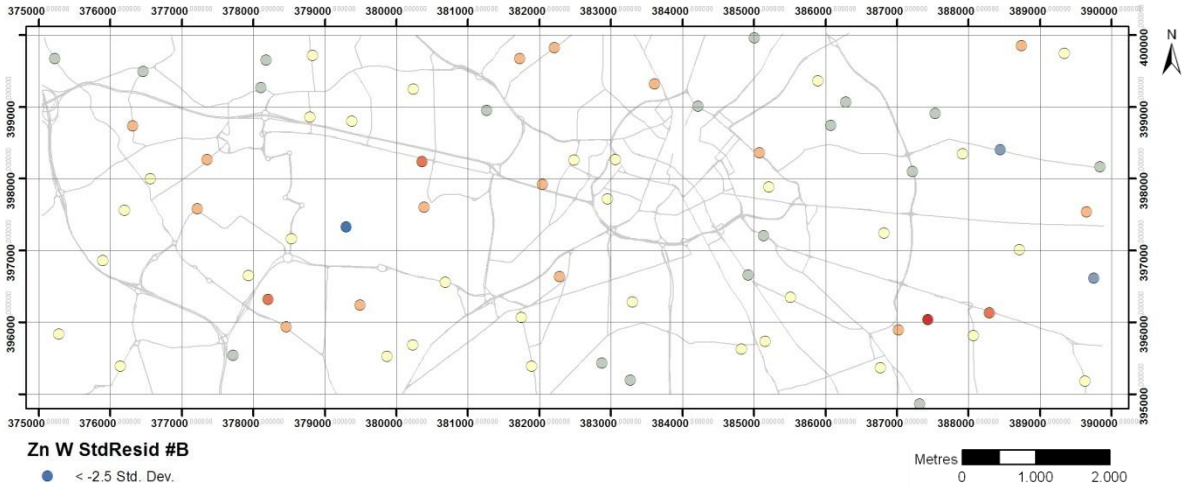
375000 376000 377000 378000 379000 380000 381000 382000 383000 384000 385000 386000 387000 388000 389000 390000
400000 399000 398000 397000 396000 395000
N
Zn W StdResid #B
< -2.5 Std. Dev.
-2.5 - -1.5 Std. Dev.
- 1.5 - -0.5 Std. Dev.
-0.5 - 0.5 Std. Dev.
0.5 - 1.5 Std. Dev.
1.5 - 2.5 Std. Dev.
> 2.5 Std. Dev.
Metres
0 1.000 2.000

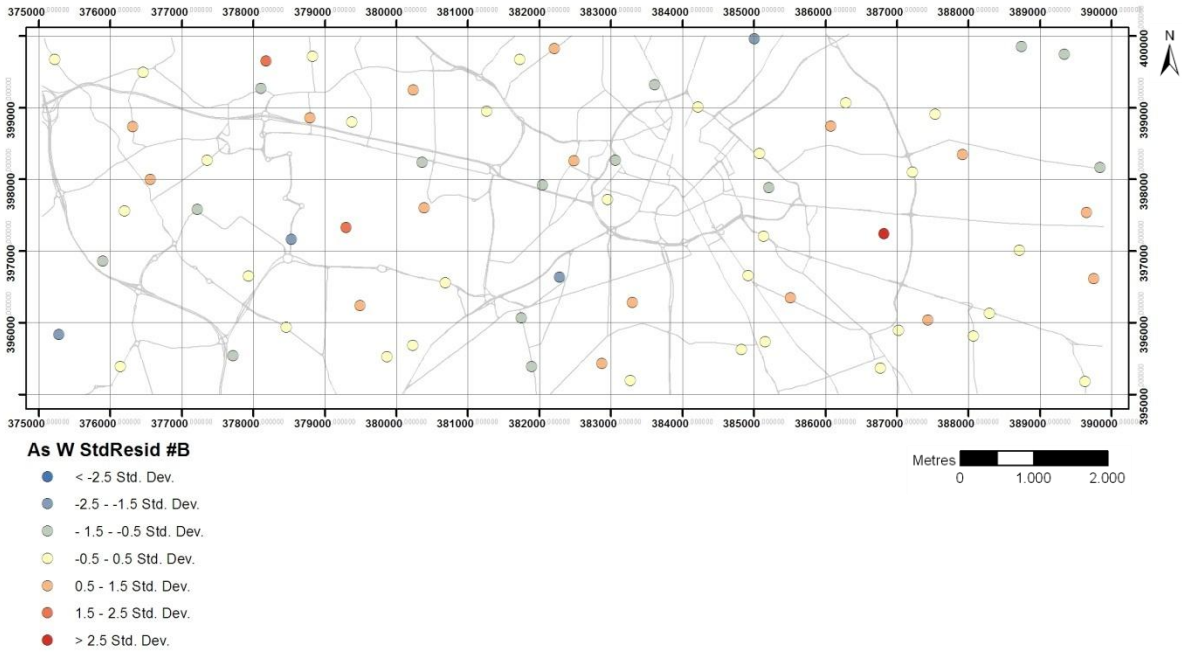
375000 376000 377000 378000 379000 380000 381000 382000 383000 384000 385000 386000 387000 388000 389000 390000
400000 399000 398000 397000 396000 395000
N
As W StdResid #B
< -2.5 Std. Dev.
-2.5 - -1.5 Std. Dev.
- 1.5 - -0.5 Std. Dev.
-0.5 - 0.5 Std. Dev.
0.5 - 1.5 Std. Dev.
1.5 - 2.5 Std. Dev.
> 2.5 Std. Dev.
Metres
0 1.000 2.000

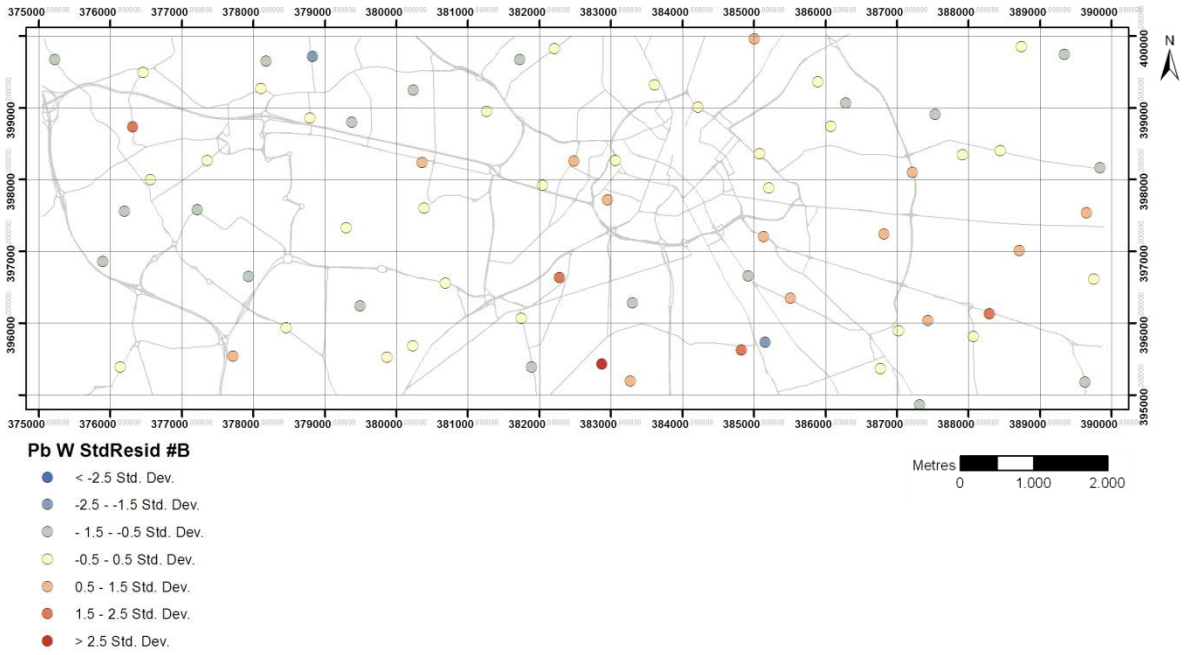
375000 376000 377000 378000 379000 380000 381000 382000 383000 384000 385000 386000 387000 388000 389000 390000
400000 399000 398000 397000 396000 395000
N
Pb W StdResid #B
< -2.5 Std. Dev.
-2.5 - -1.5 Std. Dev.
- 1.5 - -0.5 Std. Dev.
-0.5 - 0.5 Std. Dev.
0.5 - 1.5 Std. Dev.
1.5 - 2.5 Std. Dev.
> 2.5 Std. Dev.
Metres
0 1.000 2.000

## **Part B: GWR models** (road data © OS MasterMap Integrated Transport Network™ layer)

### *B.1. T-statistics and parameter estimates - Soils* (soil data ©BGS)

Figure 132: Chromium t-statistics and parameter estimates - soils - analysis set #A

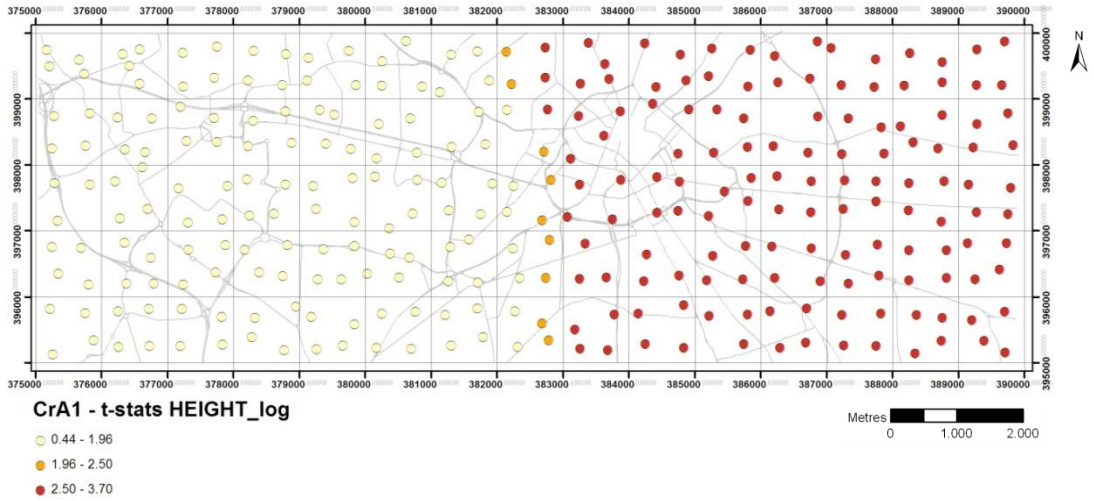


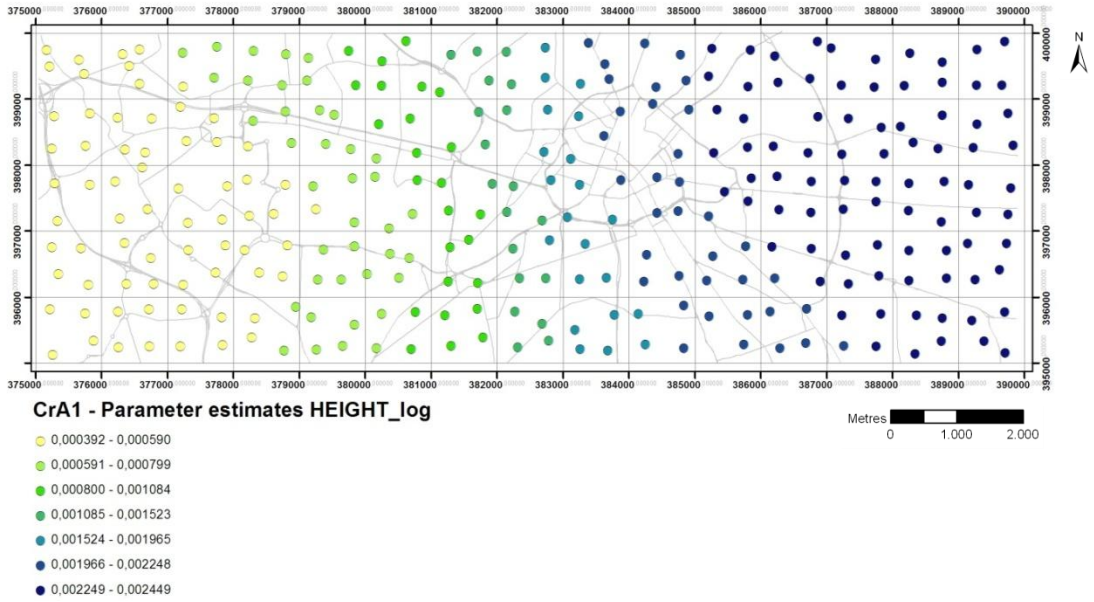


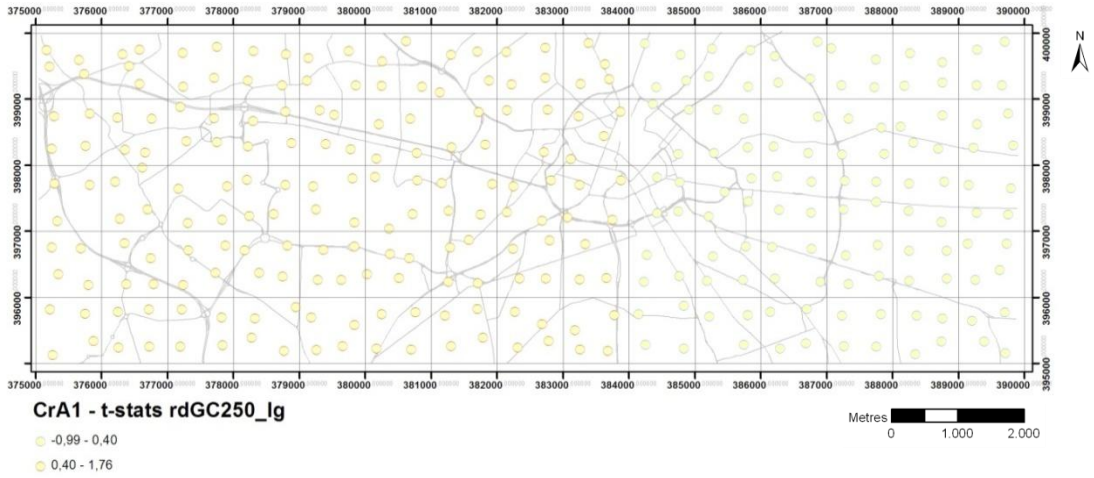

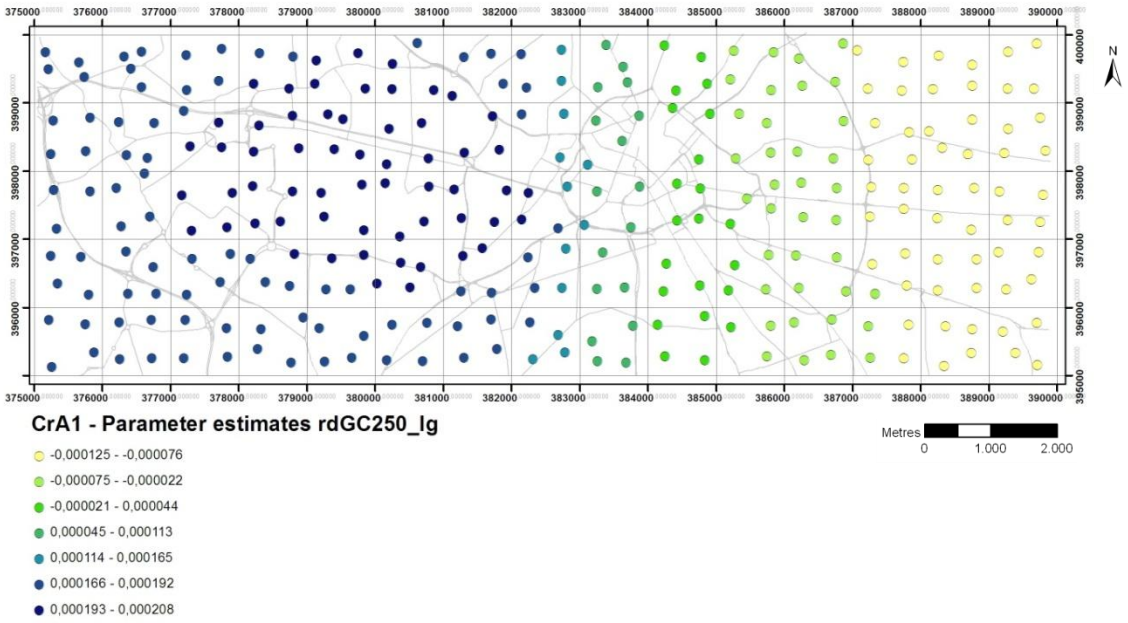


Figure 133: Copper t-statistics and parameter estimates - soils - analysis set #A

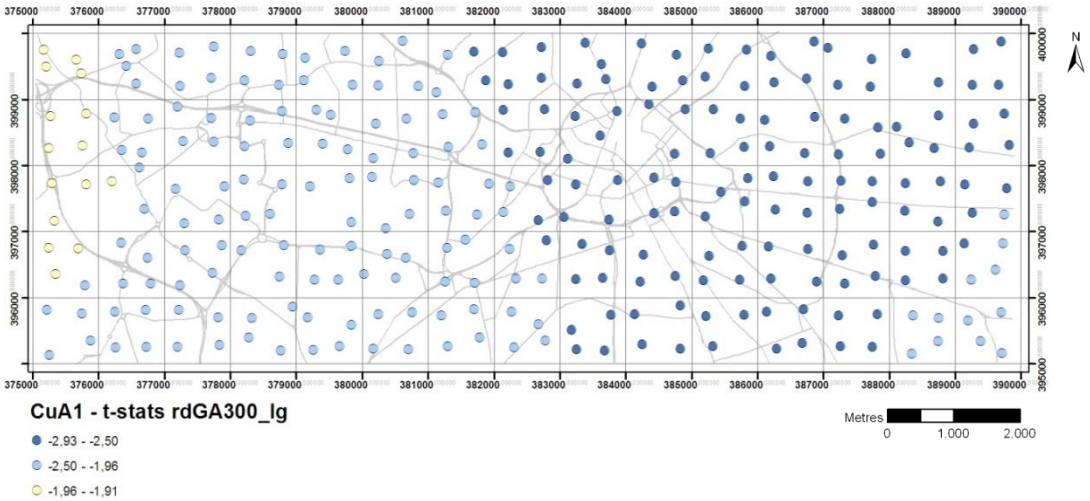


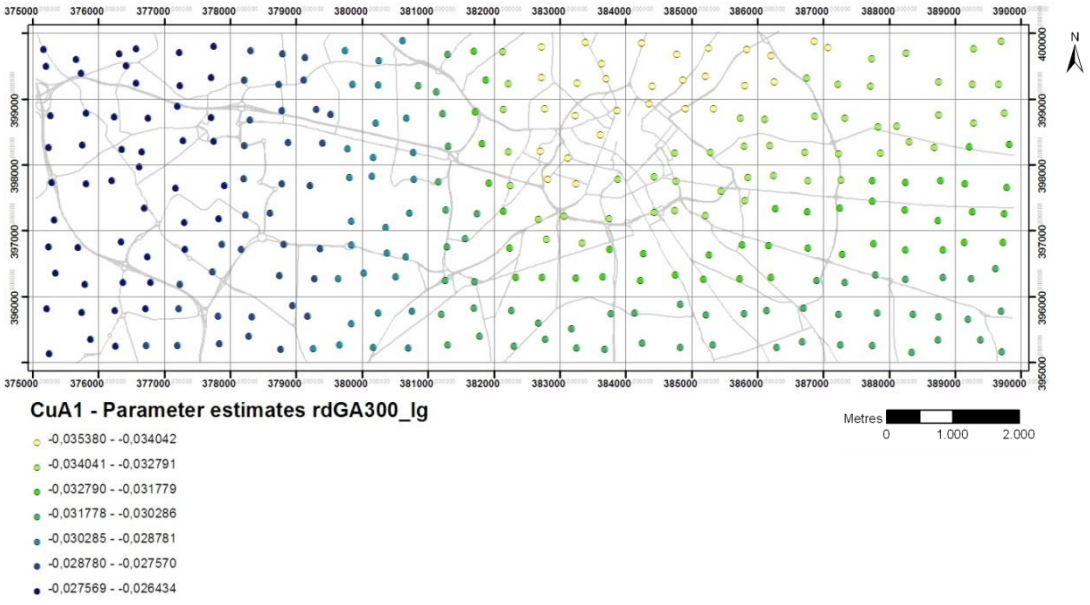

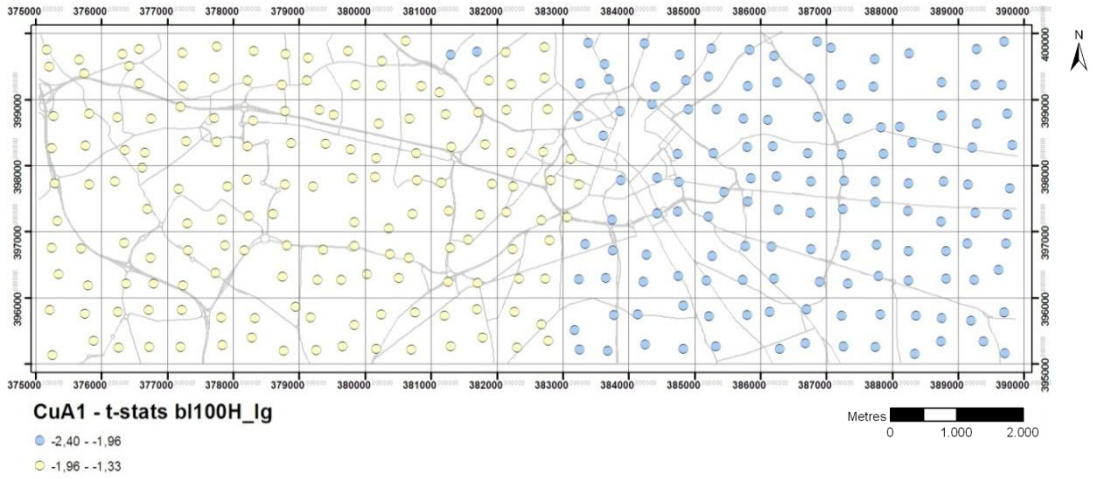
375000 376000 377000 378000 379000 380000 381000 382000 383000 384000 385000 386000 387000 388000 389000 390000
400000 399000 398000 397000 396000 395000
N
CuA1 - t-stats bl100H_lg
-2,40 - -1,96
-1,96 - -1,33
Metres
0 1.000 2.000

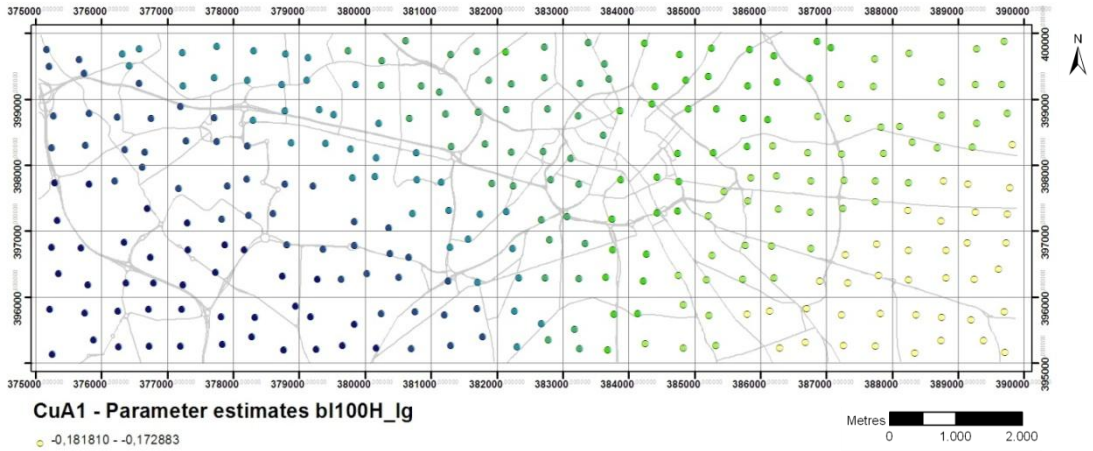
375000 376000 377000 378000 379000 380000 381000 382000 383000 384000 385000 386000 387000 388000 389000 390000
400000 399000 398000 397000 396000 395000
N
CuA1 - Parameter estimates bl100H_lg
-0,181810 - -0,172883
-0,172882 - -0,164613
-0,164612 - -0,153808
-0,153807 - -0,141347
-0,141346 - -0,130242
-0,130241 - -0,121661
-0,121660 - -0,113289
Metres
0 1.000 2.000

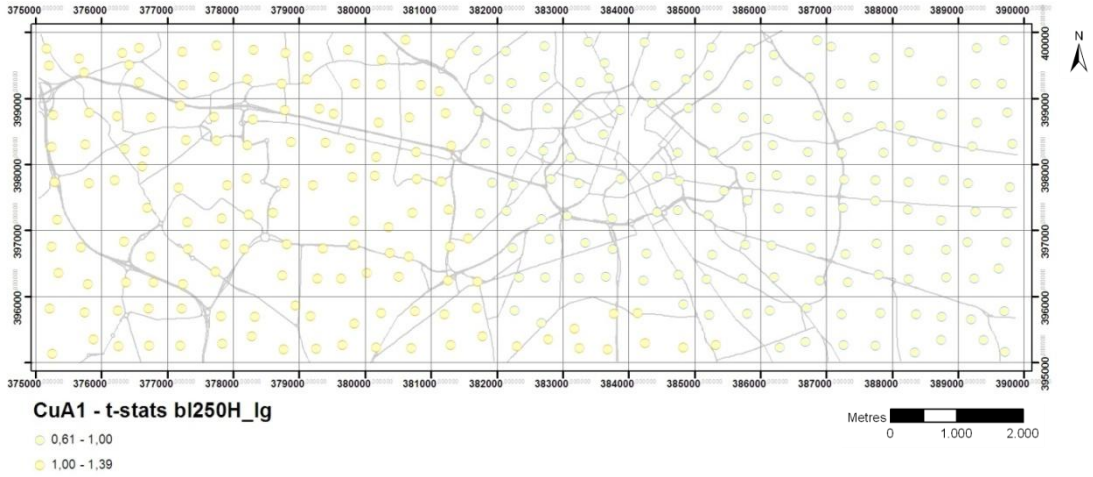
375000 376000 377000 378000 379000 380000 381000 382000 383000 384000 385000 386000 387000 388000 389000 390000
400000 399000 398000 397000 396000 395000
N
CuA1 - t-stats bl250H_lg
0,61 - 1,00
1,00 - 1,39
Metres
0 1.000 2.000

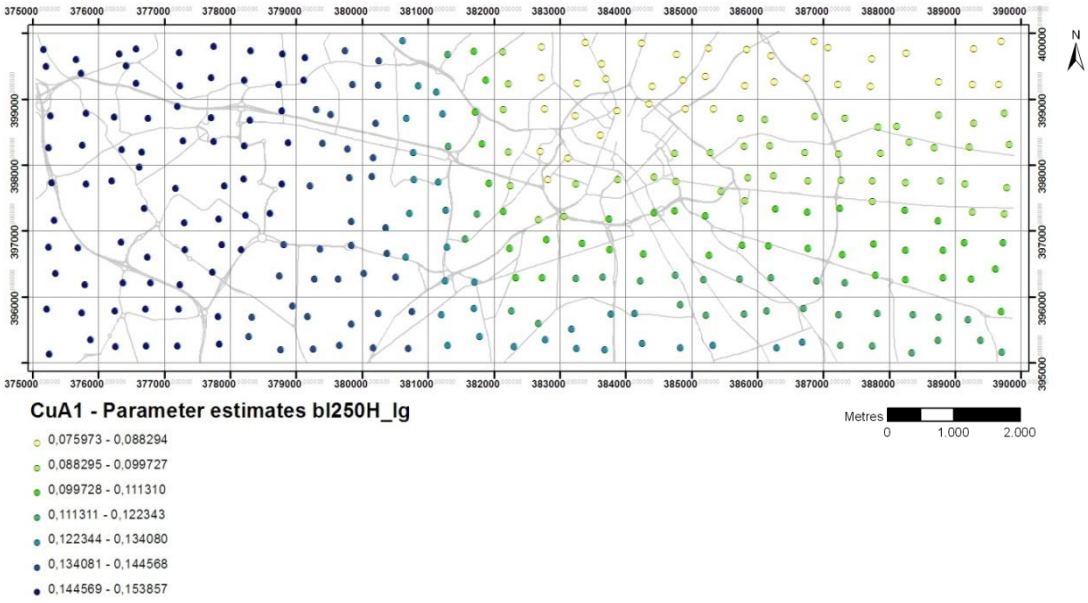


Figure 134: Zinc t-statistics and parameter estimates - soils - analysis set #A

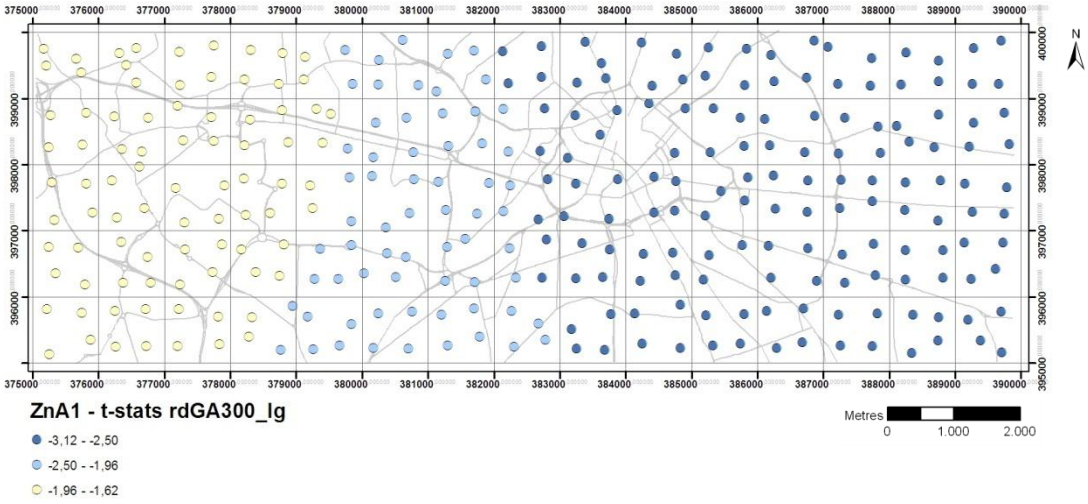

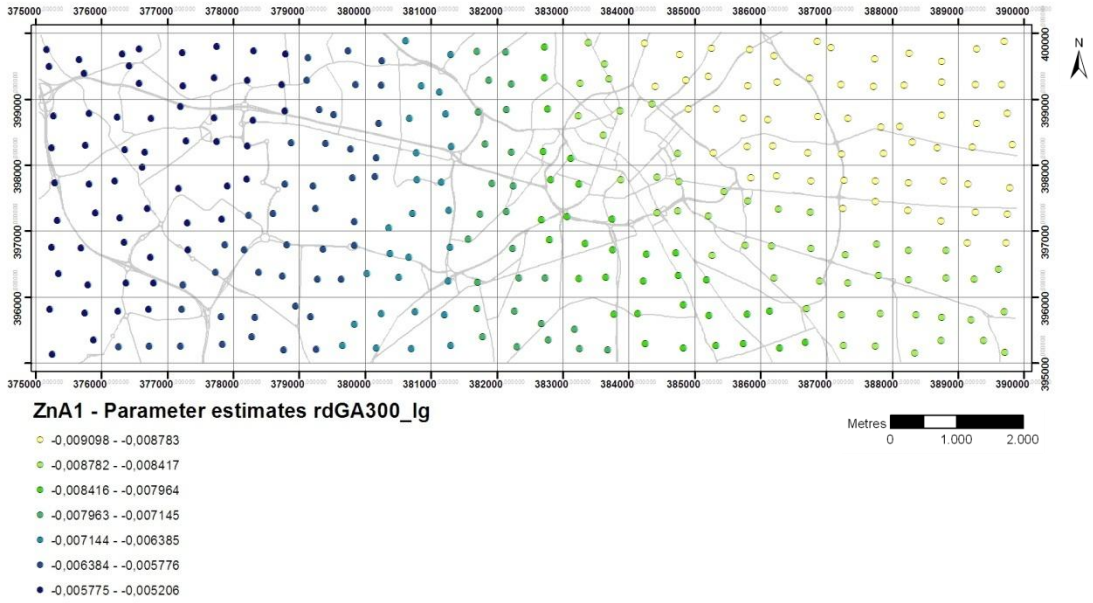


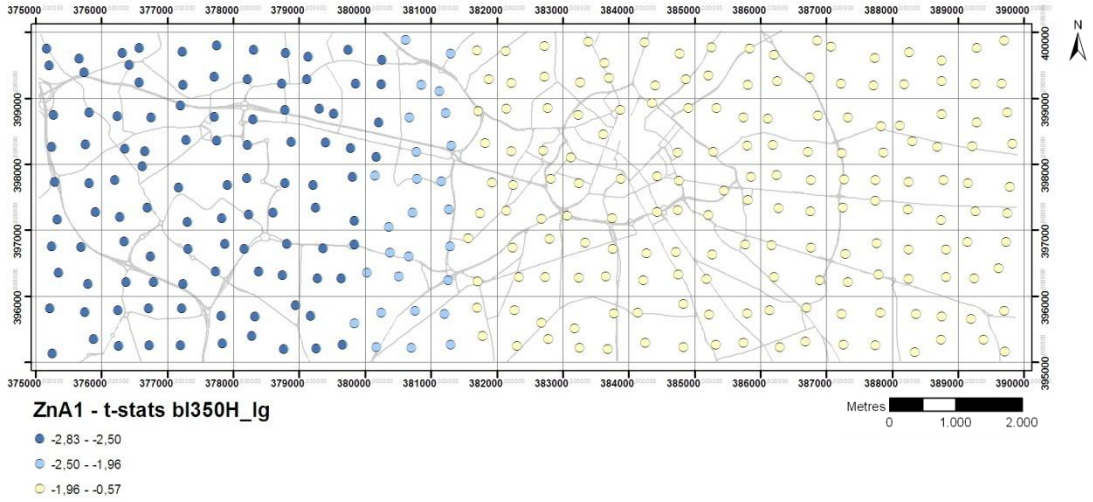


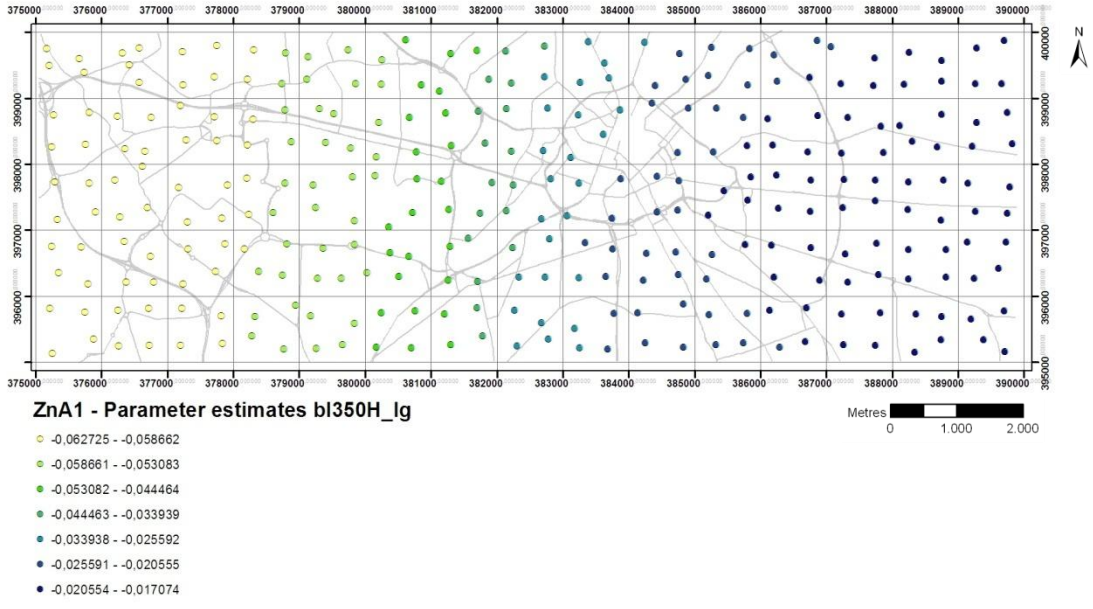


Figure 135: Arsenic t-statistics and parameter estimates - soils - analysis set #A

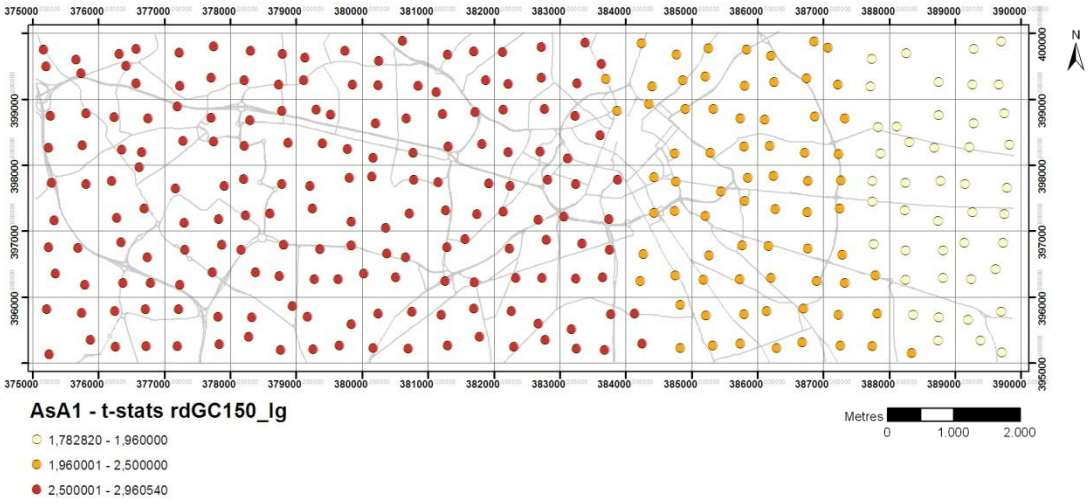
375000 376000 377000 378000 379000 380000 381000 382000 383000 384000 385000 386000 387000 388000 389000 390000
400000 399000 398000 397000 396000 395000
N
AsA1 - t-stats rdGC150_lg
1,782820 - 1,960000
1,960001 - 2,500000
2,500001 - 2,960540
Metres
0 1.000 2.000

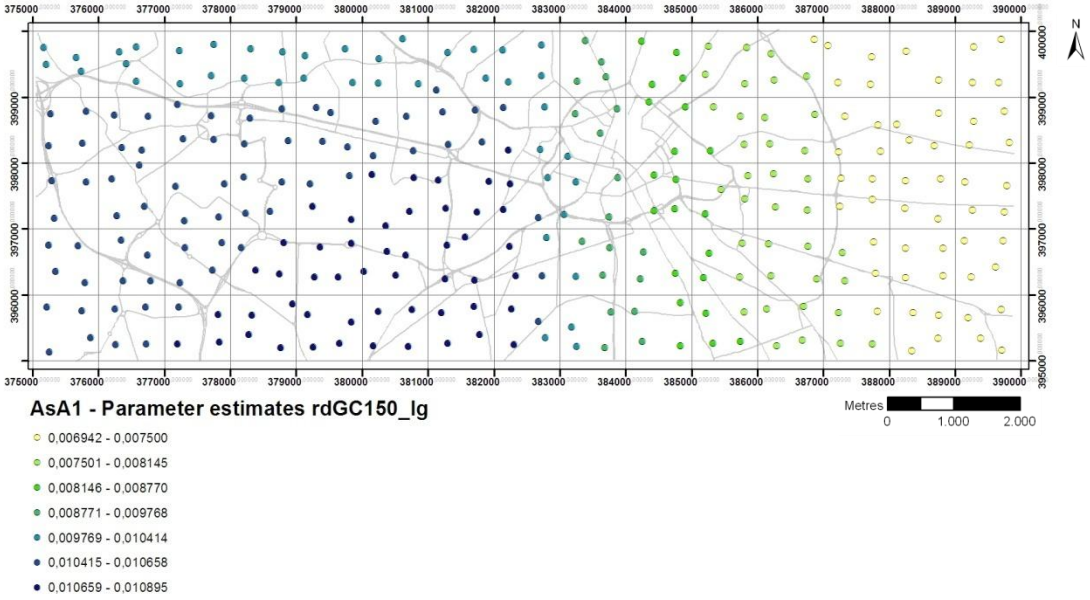
375000 376000 377000 378000 379000 380000 381000 382000 383000 384000 385000 386000 387000 388000 389000 390000
400000 399000 398000 397000 396000 395000
N
AsA1 - Parameter estimates rdGC150_lg
0,006942 - 0,007500
0,007501 - 0,008145
0,008146 - 0,008770
0,008771 - 0,009768
0,009769 - 0,010414
0,010415 - 0,010658
0,010659 - 0,010895
Metres
0 1.000 2.000

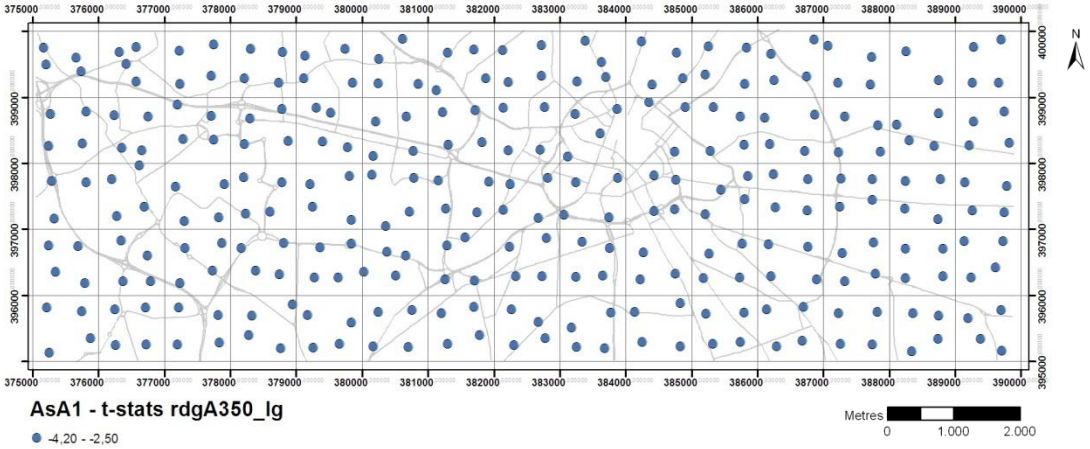
375000 376000 377000 378000 379000 380000 381000 382000 383000 384000 385000 386000 387000 388000 389000 390000
400000 399000 398000 397000 396000 395000
N
AsA1 - t-stats rdgA350_lg
-4,20 - -2,50
Metres
0 1.000 2.000

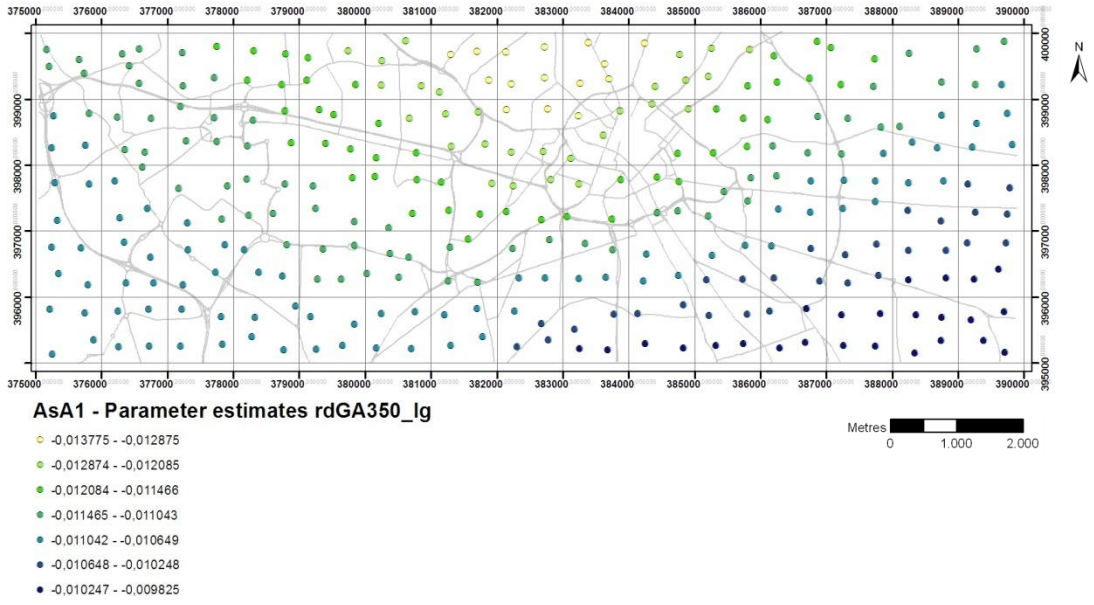


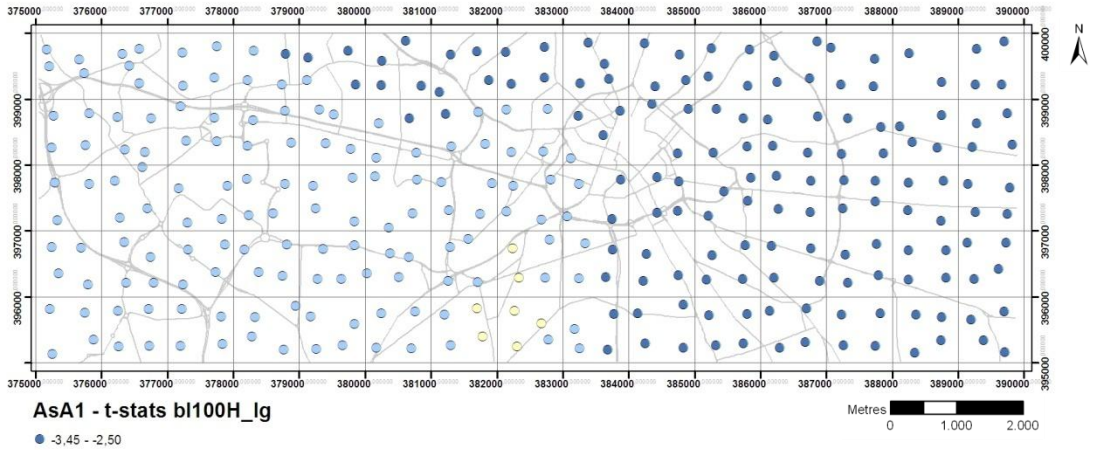


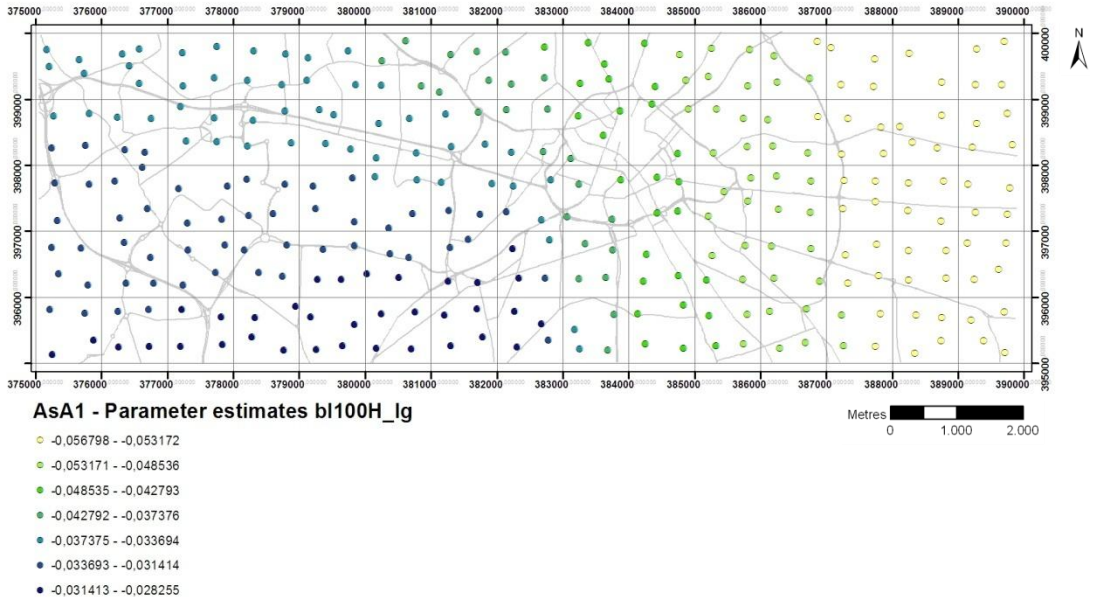


Figure 136: Lead t-statistics and parameter estimates - soils - analysis set #A

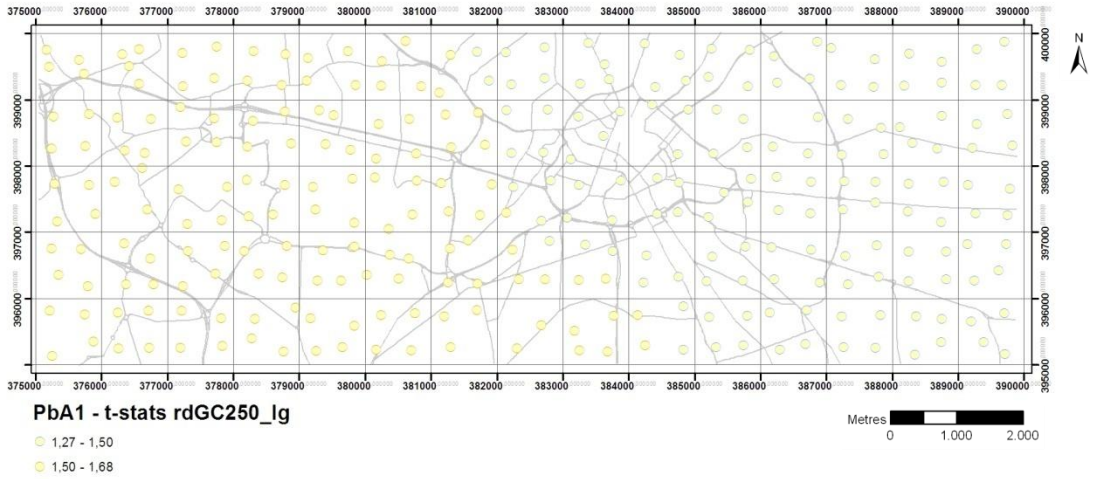
375000 376000 377000 378000 379000 380000 381000 382000 383000 384000 385000 386000 387000 388000 389000 390000
400000 399000 398000 397000 396000 395000
N
PbA1 - t-stats rdGC250_lg
1,27 - 1,50
1,50 - 1,68
Metres
0 1.000 2.000

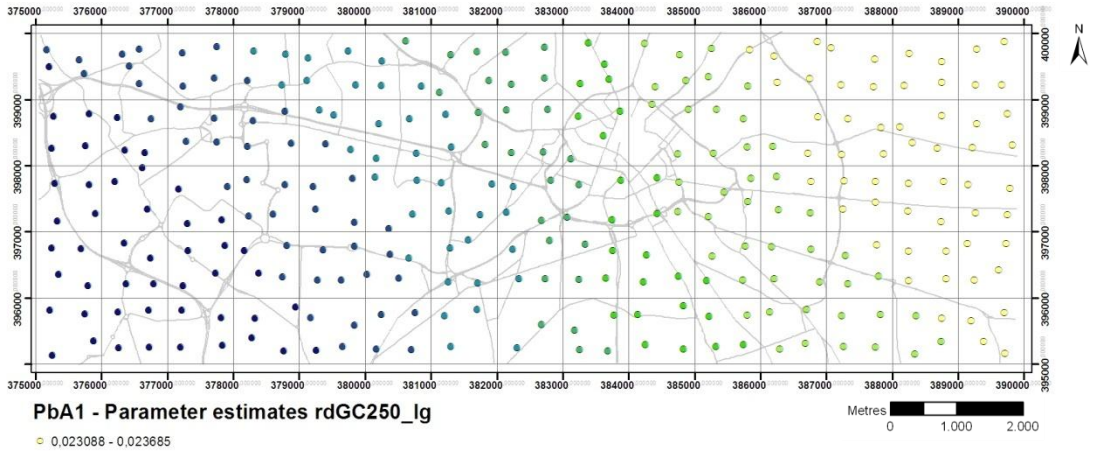
375000 376000 377000 378000 379000 380000 381000 382000 383000 384000 385000 386000 387000 388000 389000 390000
400000 399000 398000 397000 396000 395000
N
PbA1 - Parameter estimates rdGC250_lg
0,023088 - 0,023685
0,023686 - 0,024411
0,024412 - 0,025394
0,025395 - 0,026623
0,026624 - 0,027571
0,027572 - 0,028325
0,028326 - 0,029121
Metres
0 1.000 2.000

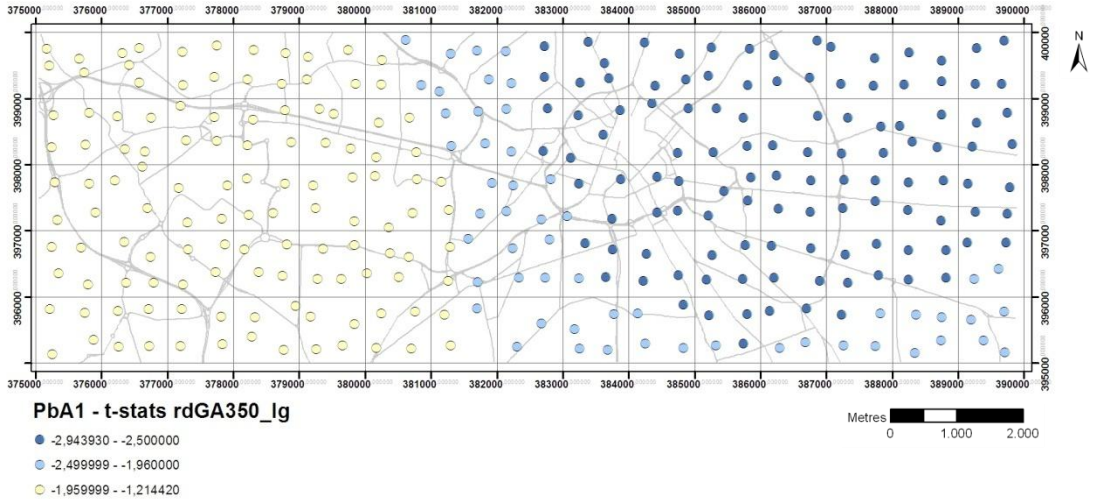
375000 376000 377000 378000 379000 380000 381000 382000 383000 384000 385000 386000 387000 388000 389000 390000
400000 399000 398000 397000 396000 395000
N
PbA1 - t-stats rdGA350_lg
-2,943930 - -2,500000
-2,499999 - -1,960000
-1,959999 - -1,214420
Metres
0 1.000 2.000

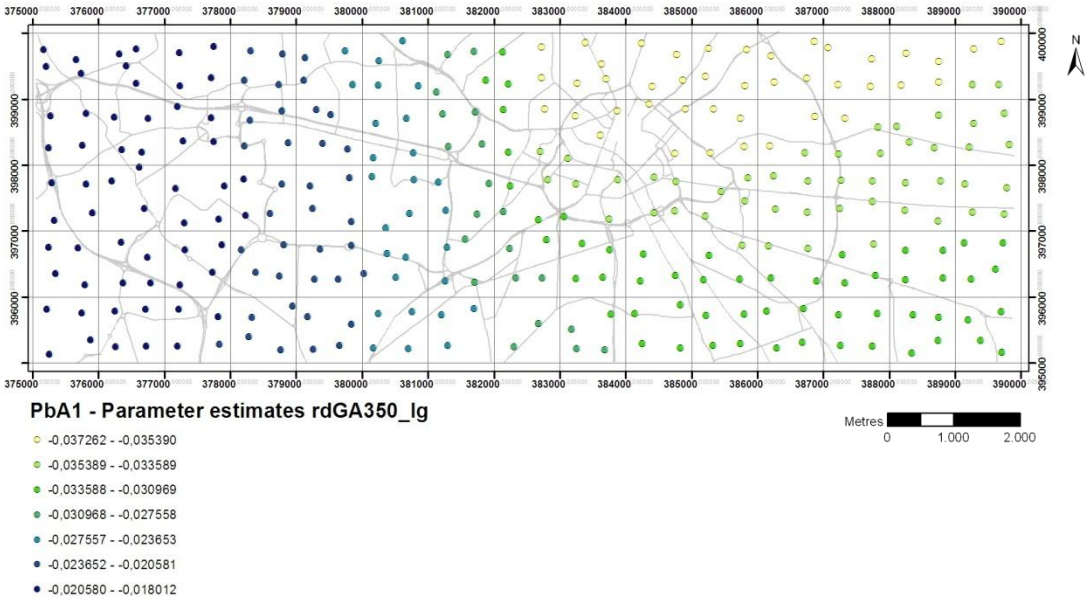


**PbA1 - Parameter estimates rdGA350_lg**

- -0,037262 - -0,035390
- -0,035389 - -0,033589
- -0,033588 - -0,030969
- -0,030968 - -0,027558
- -0,027557 - -0,023653
- -0,023652 - -0,020581
- -0,020580 - -0,018012

Metres
0 1.000 2.000

Figure 137: Lead t-statistics and parameter estimates - soils - analysis set #B

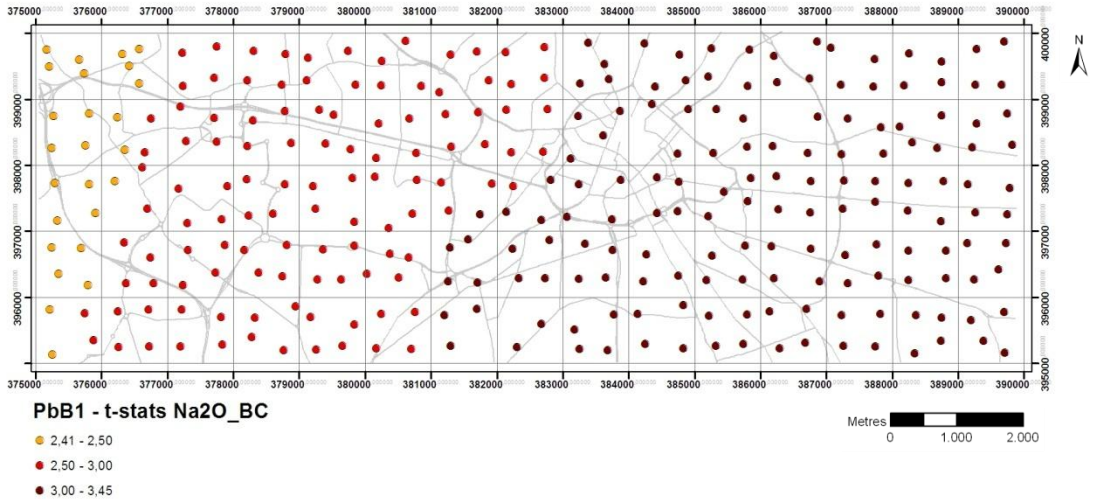


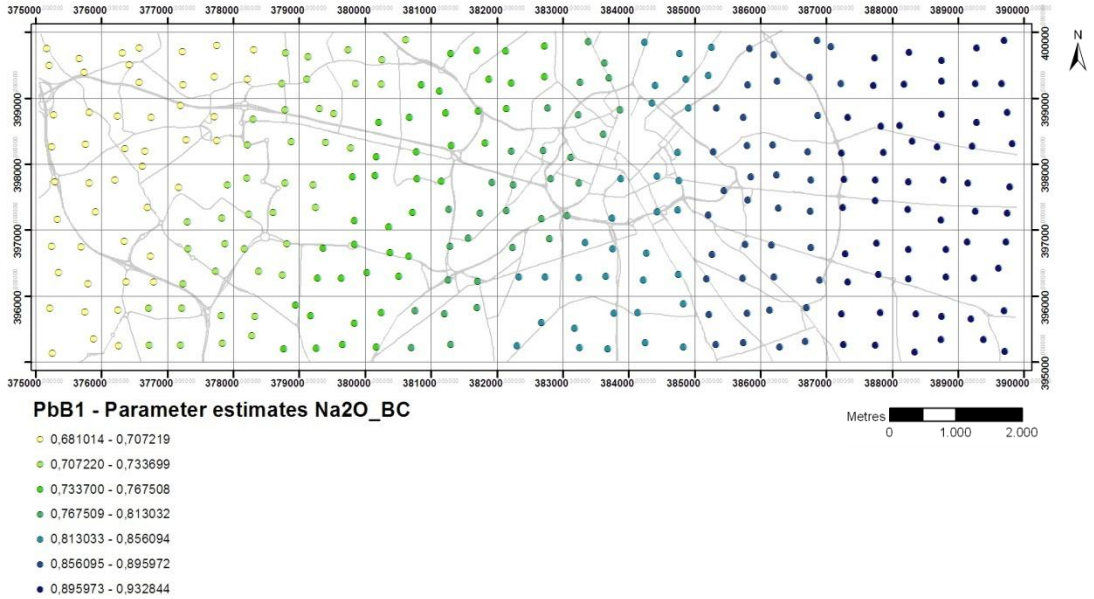


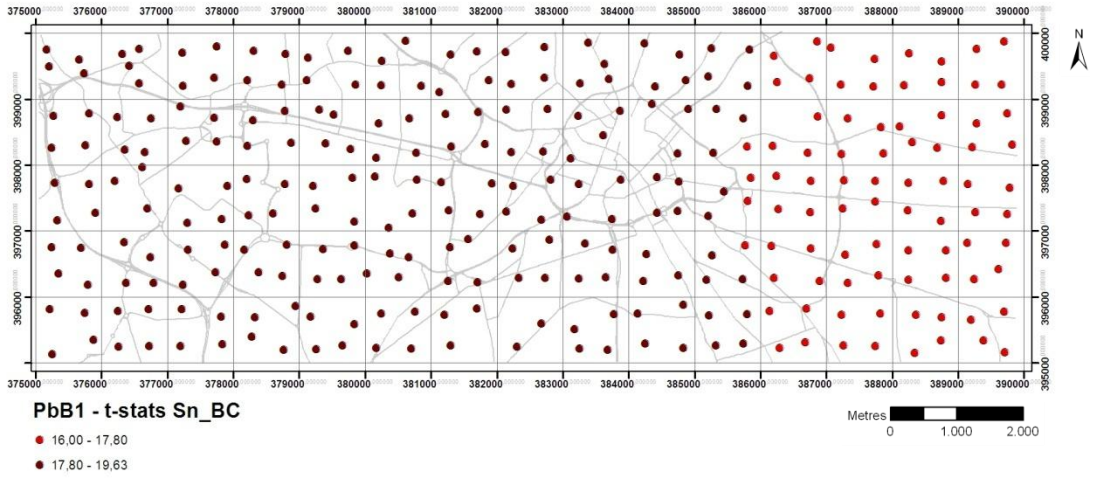

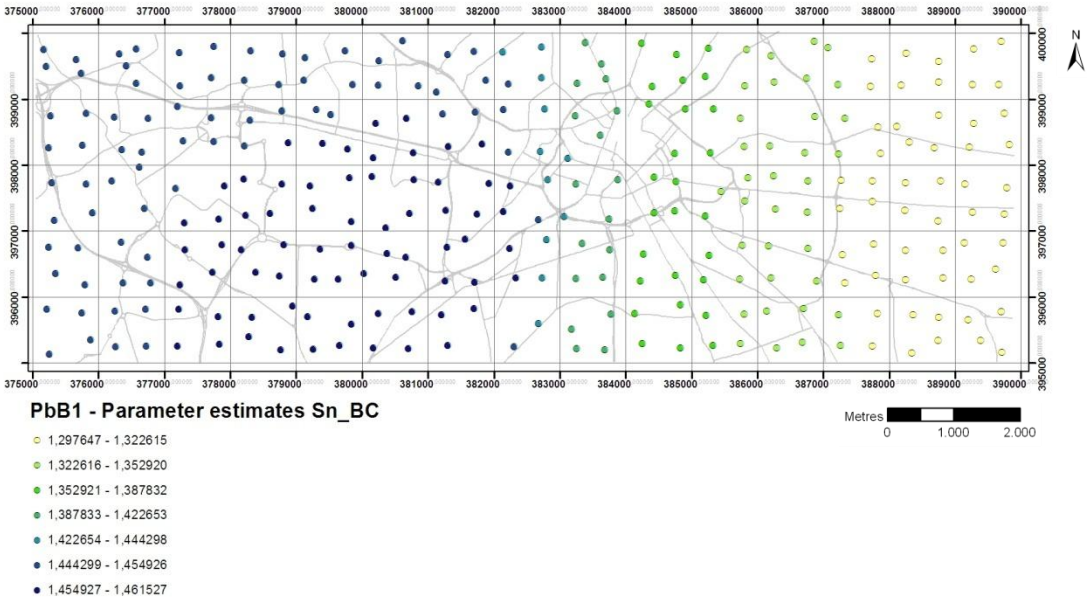
375000
376000
377000
378000
379000
380000
381000
382000
383000
384000
385000
386000
387000
388000
389000
390000
400000
399000
398000
397000
396000
395000
N
PbB1 - Parameter estimates Sn_BC
1,297647 - 1,322615
1,322616 - 1,352920
1,352921 - 1,387832
1,387833 - 1,422653
1,422654 - 1,444298
1,444299 - 1,454926
1,454927 - 1,461527
Metres
0
1.000
2.000

## *B.2. T-statistics and parameter estimates - RDS summer*

Figure 138: Copper t-statistics and parameter estimates - RDS summer - analysis set #A

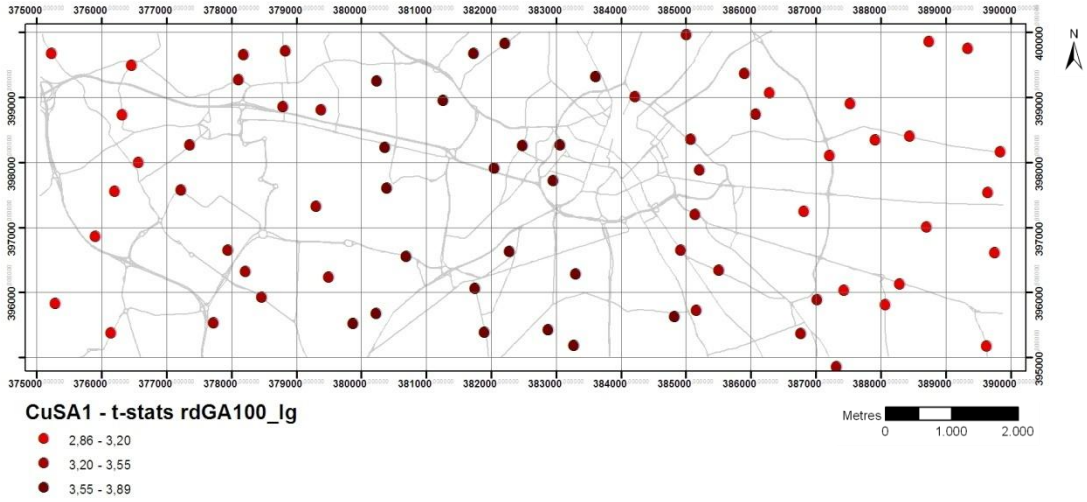


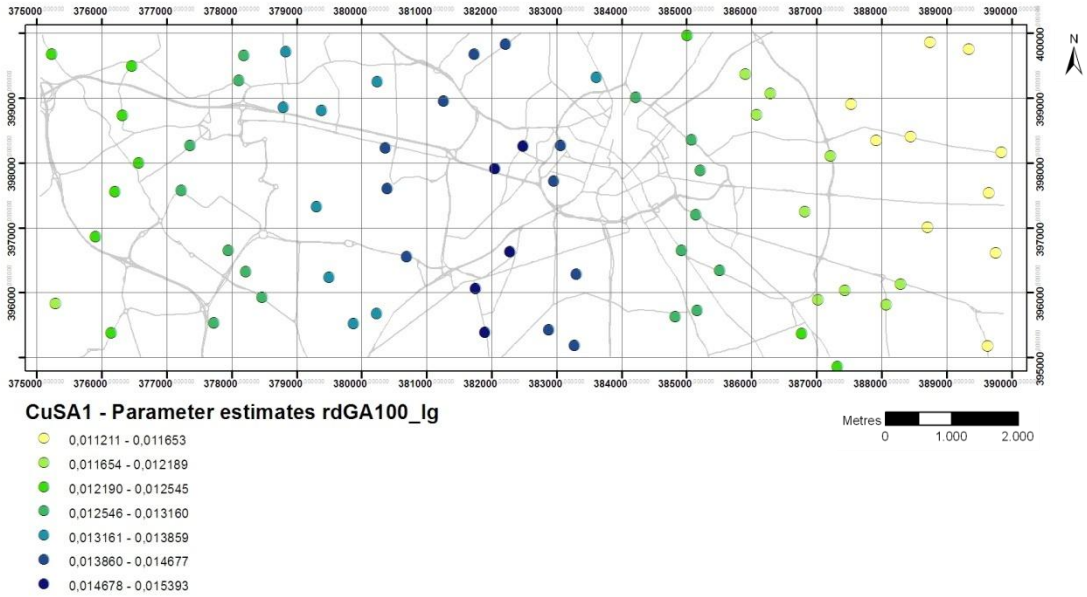


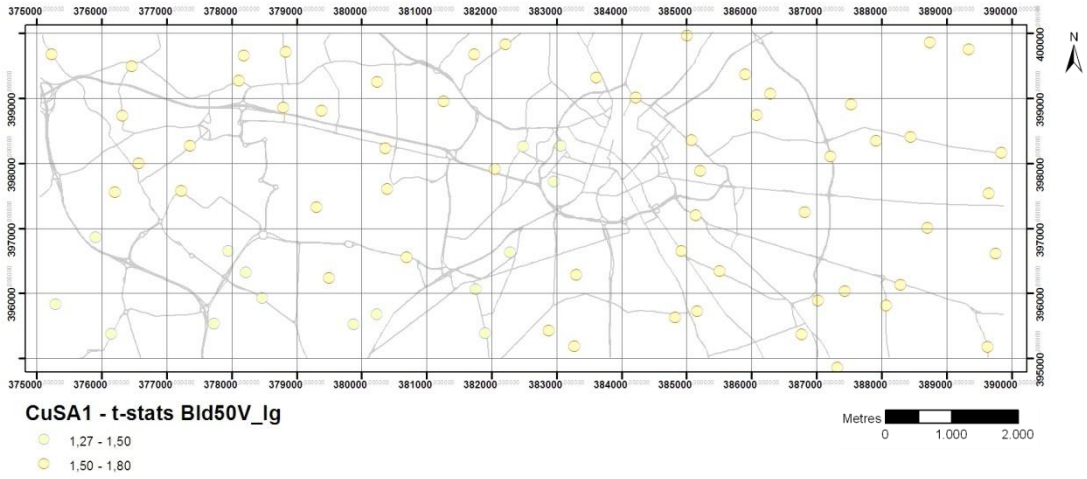

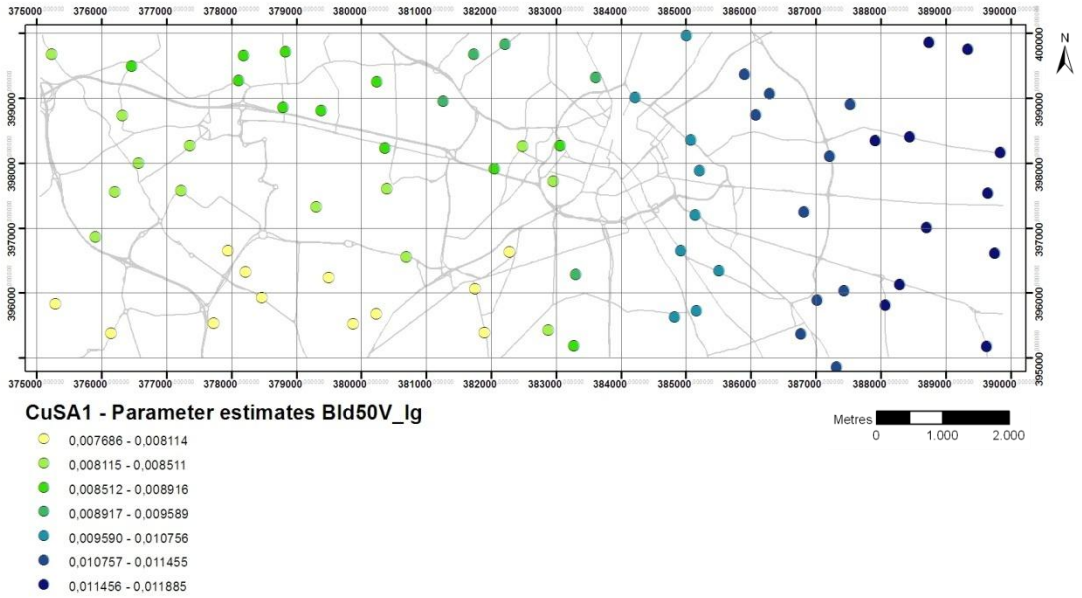


Figure 139: Zinc t-statistics and parameter estimates - RDS summer - analysis set #A

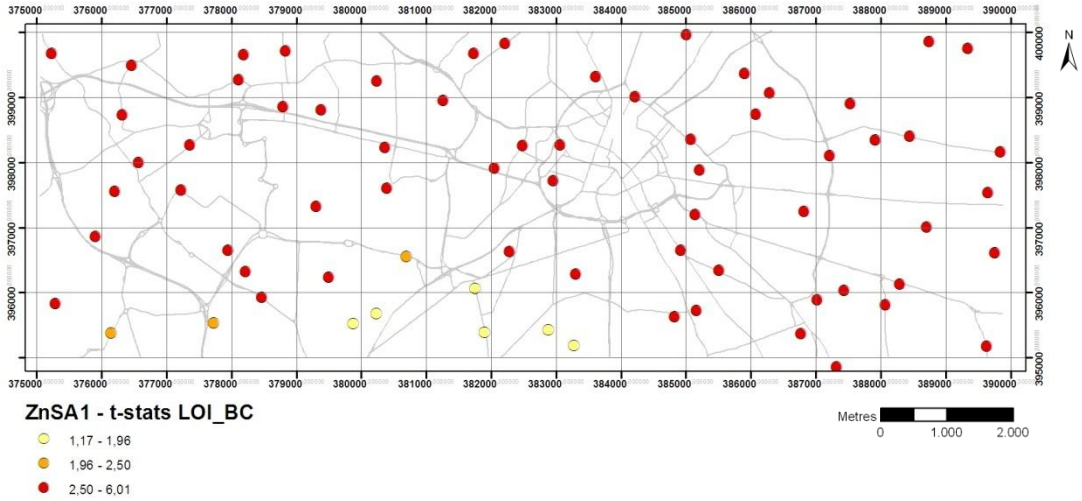


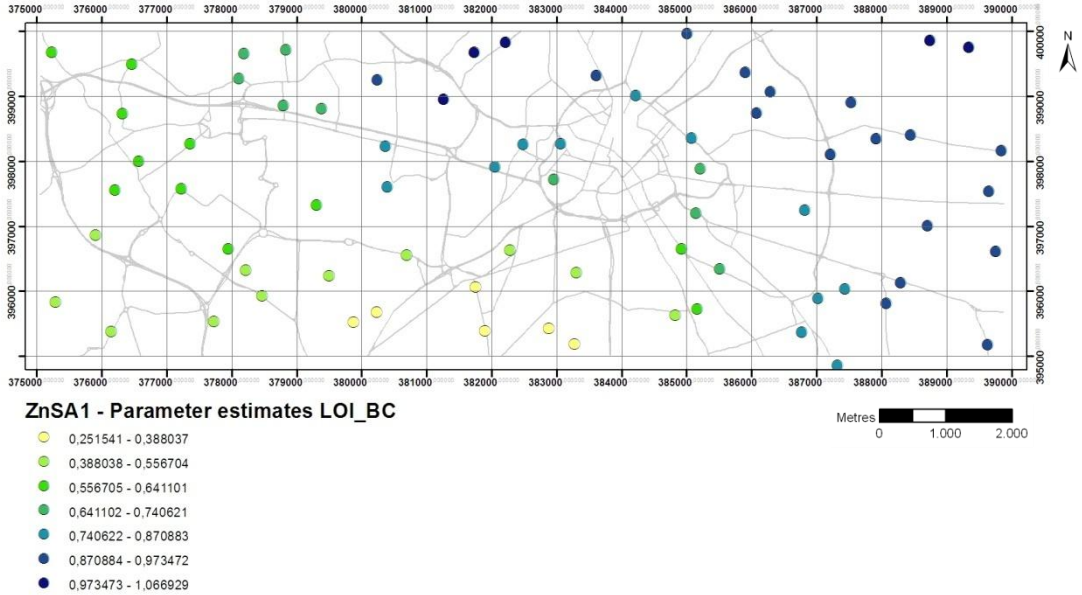

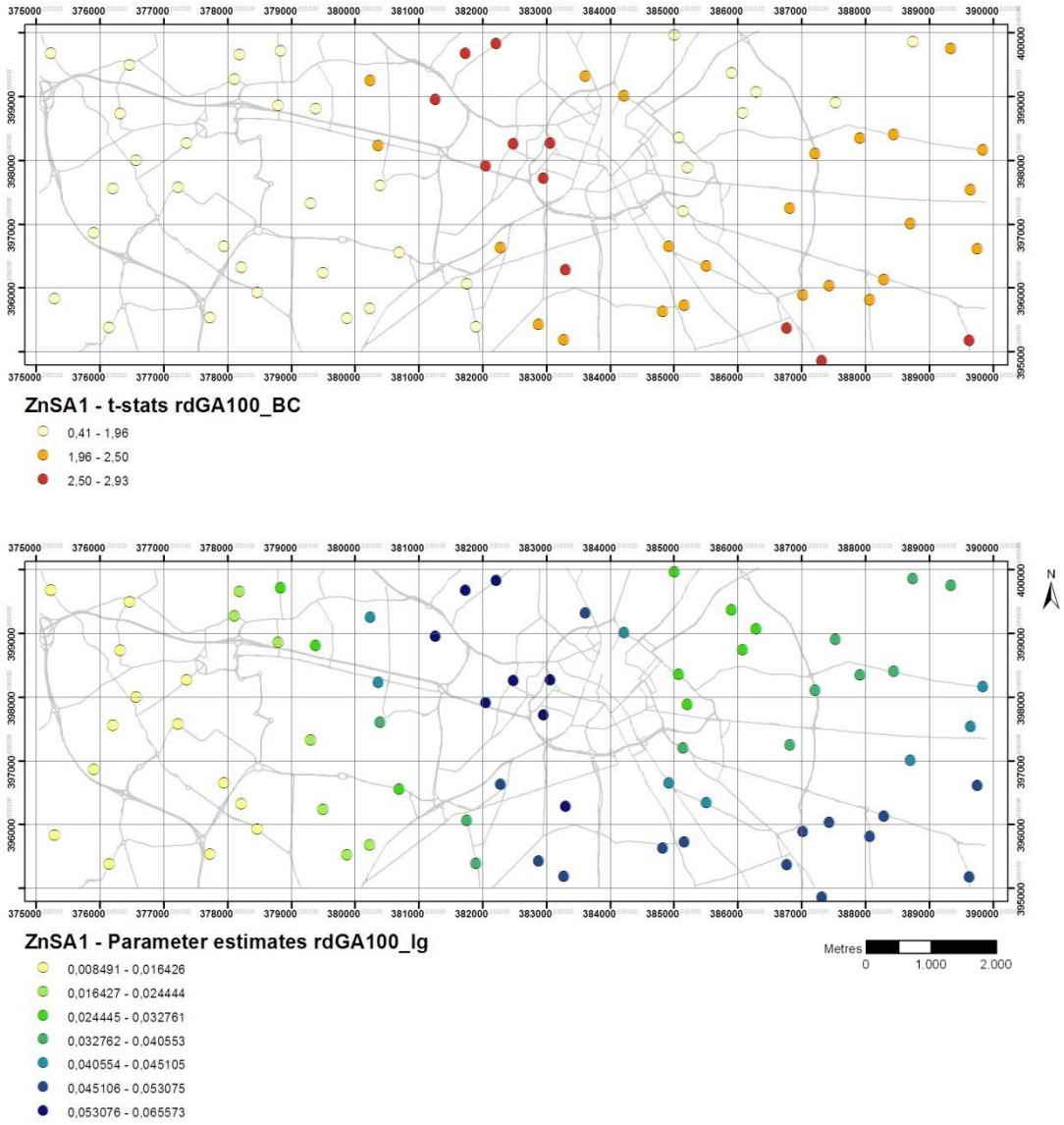


Figure 140: Lead t-statistics and parameter estimates - RDS summer - analysis set #A

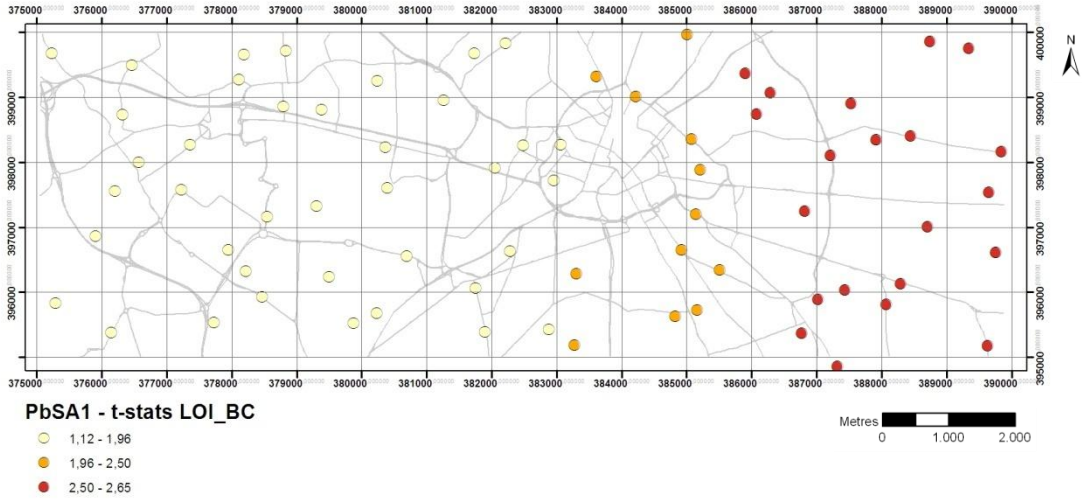

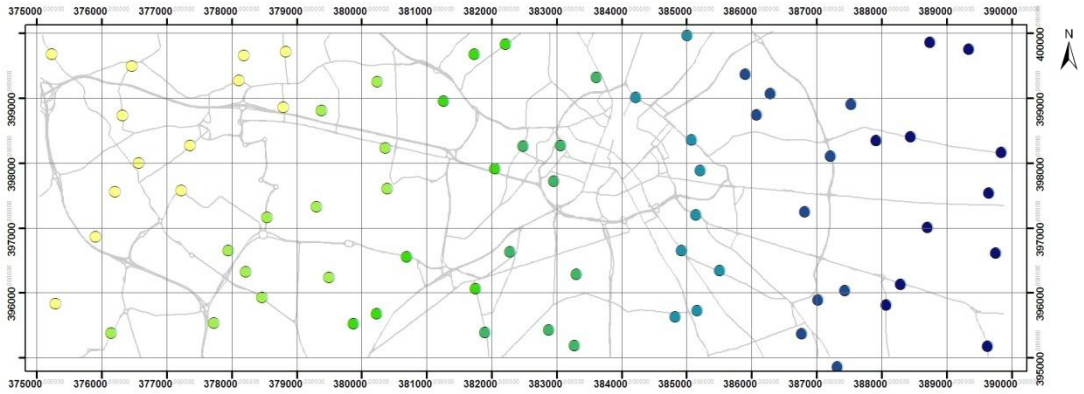


**PbSA1 - Parameter estimates LOI_BC**

- 0,287481 - 0,310488
- 0,310489 - 0,344055
- 0,344056 - 0,402108
- 0,402109 - 0,469878
- 0,469879 - 0,544336
- 0,544337 - 0,584423
- 0,584424 - 0,610912

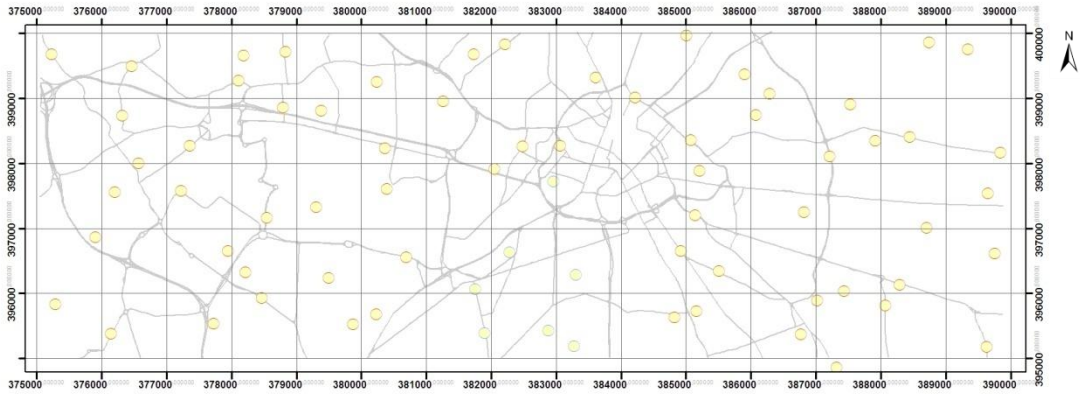


**PbSA1 - t-stats rdGB25_lg**

- 0,95 - 1,00
- 1,00 - 1,19

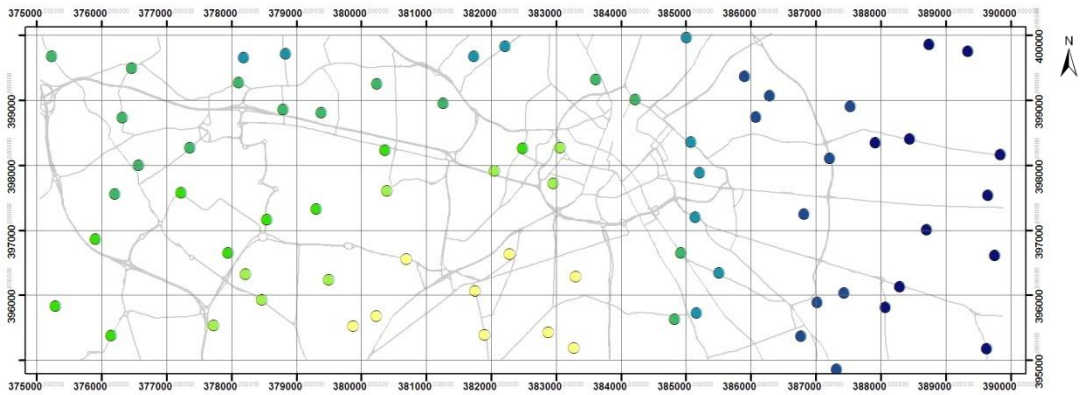


**PbSA1 - Parameter estimates rdGB25_lg**

- 0,045679 - 0,049257
- 0,049258 - 0,051508
- 0,051509 - 0,052911
- 0,052912 - 0,054542
- 0,054543 - 0,056218
- 0,056219 - 0,061383
- 0,061384 - 0,065774

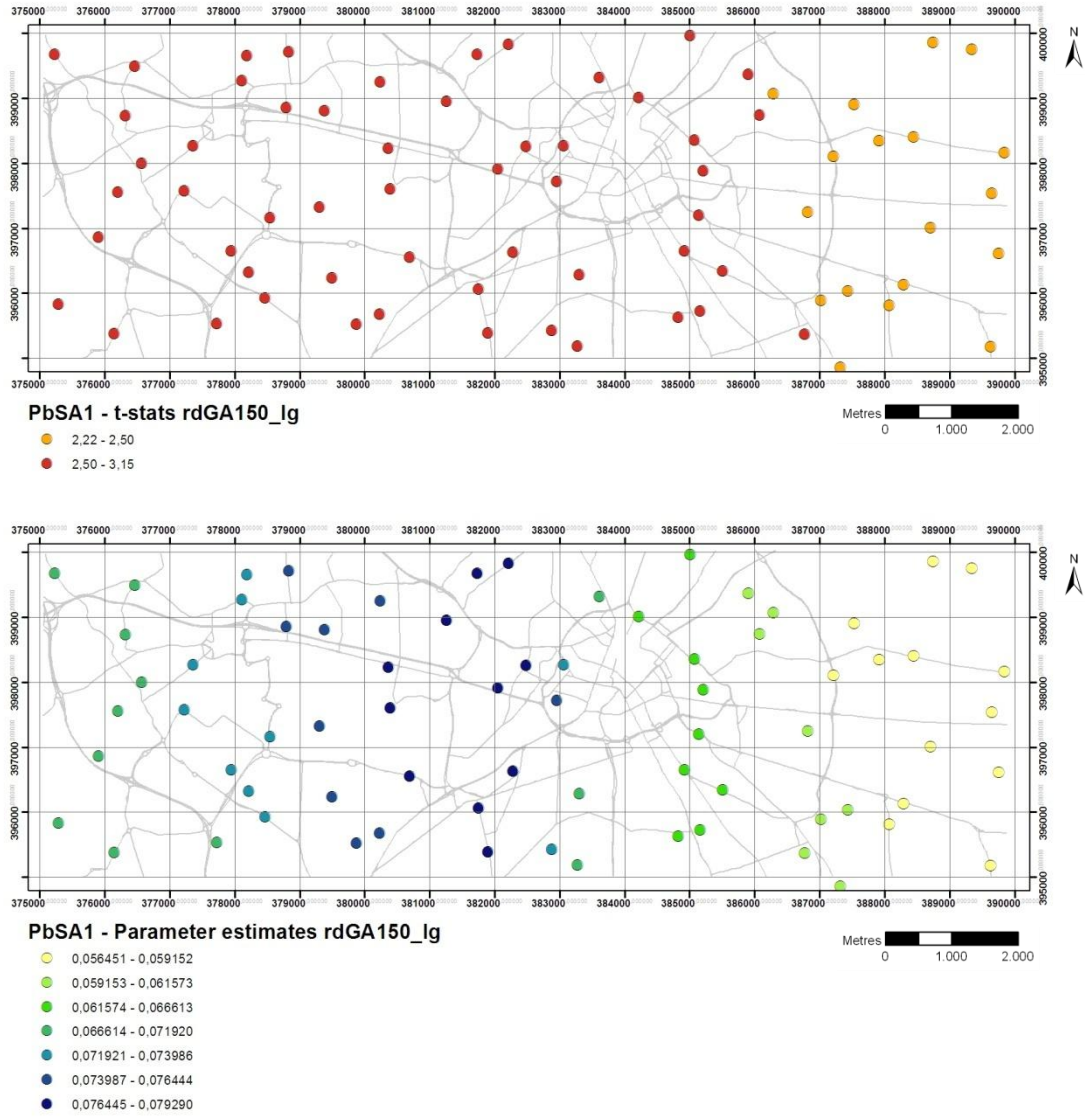


Figure 141: Lead t-statistics and parameter estimates - RDS summer - analysis set #B

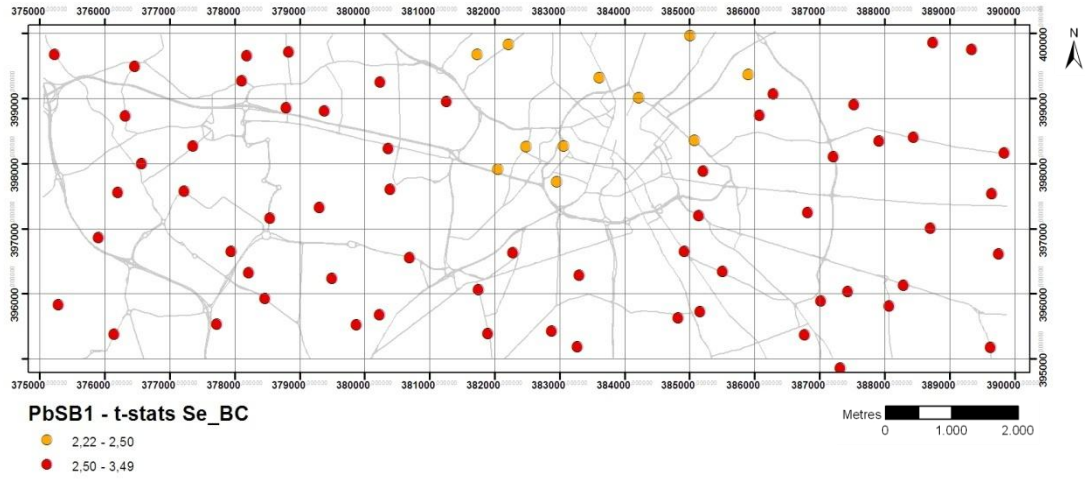

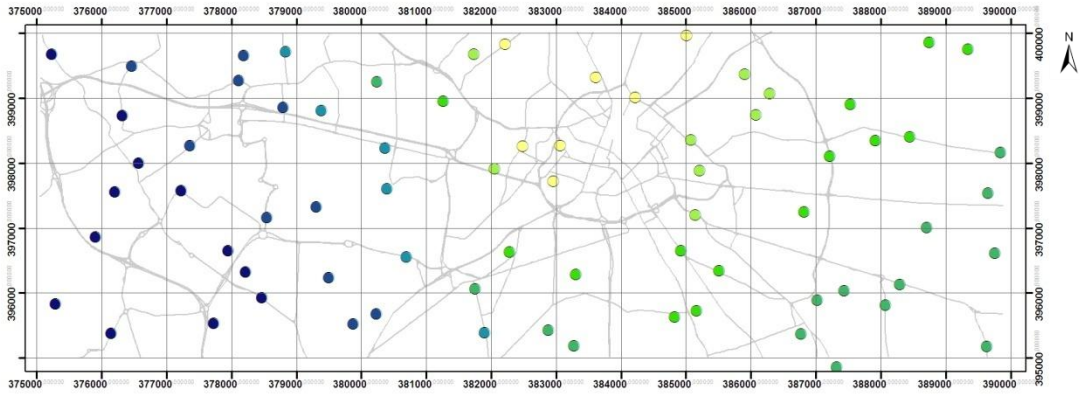


**PbSB1 - Parameter estimates Se_BC**

- 0,193507 - 0,207354
- 0,207355 - 0,225975
- 0,225976 - 0,241444
- 0,241445 - 0,257702
- 0,257703 - 0,273972
- 0,273973 - 0,298568
- 0,298569 - 0,321861

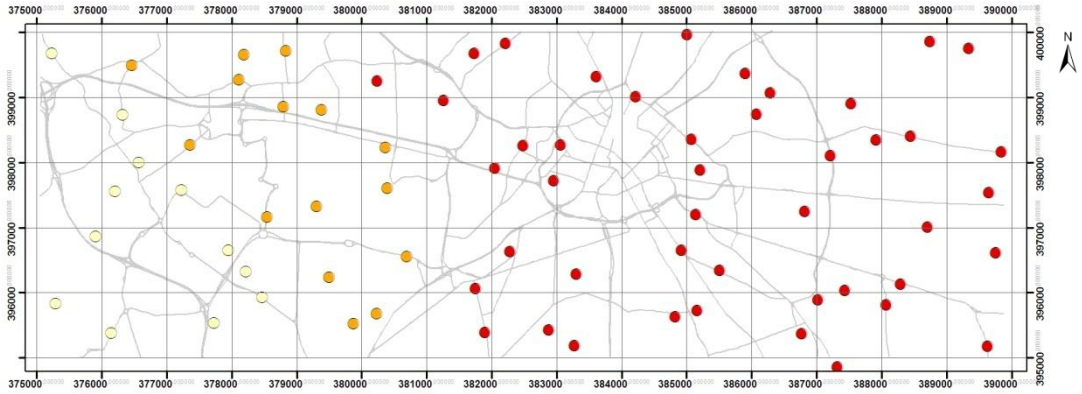


**PbSB1 - t-stats W_BC**

- 1,70 - 1,96
- 1,96 - 2,50
- 2,50 - 3,78

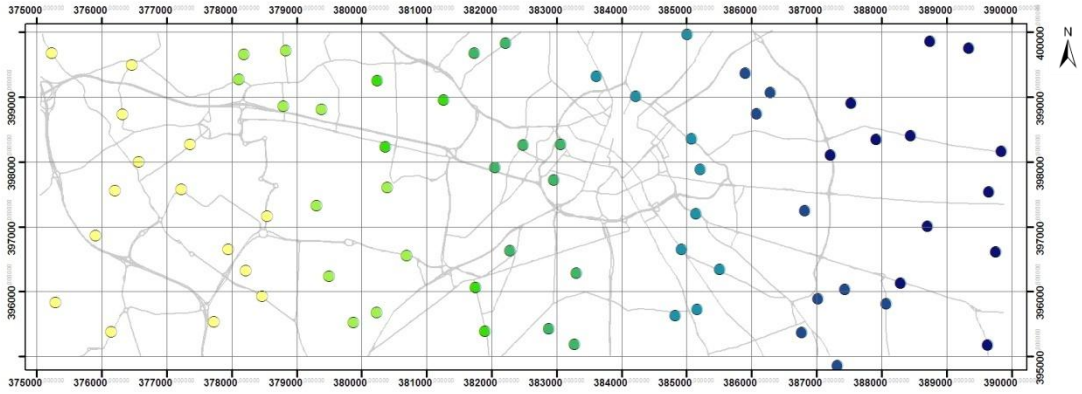


**PbSB1 - Parameter estimates W_BC**

- 0,243760 - 0,280735
- 0,280736 - 0,327416
- 0,327417 - 0,381480
- 0,381481 - 0,476265
- 0,476266 - 0,533763
- 0,533764 - 0,561364
- 0,561365 - 0,587180

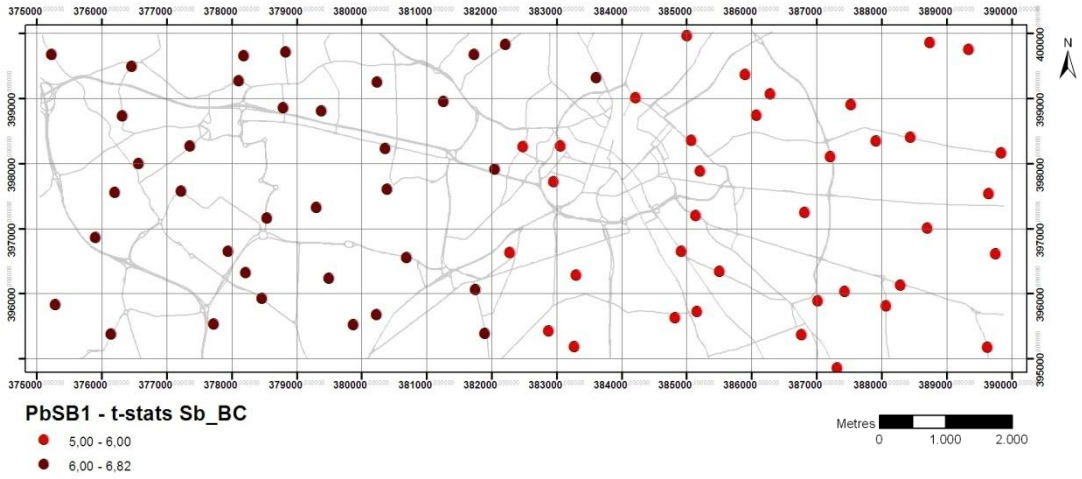
375000 376000 377000 378000 379000 380000 381000 382000 383000 384000 385000 386000 387000 388000 389000 390000
400000 399000 398000 397000 396000 395000
N
PbSB1 - t-stats Sb_BC
5,00 - 6,00
6,00 - 6,82
Metres
0 1.000 2.000

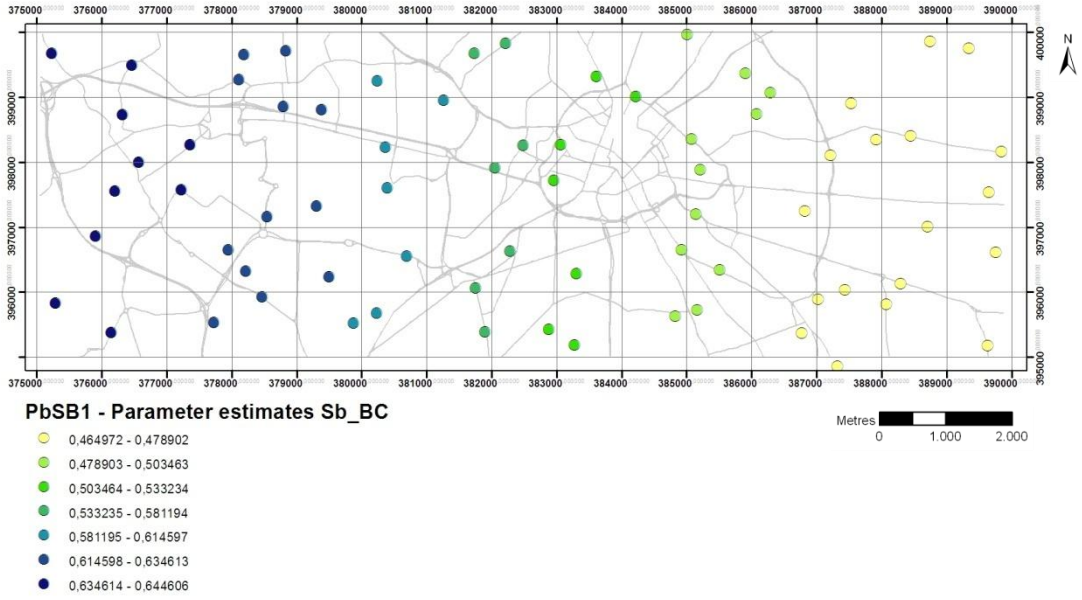
375000 376000 377000 378000 379000 380000 381000 382000 383000 384000 385000 386000 387000 388000 389000 390000
400000 399000 398000 397000 396000 395000
N
PbSB1 - Parameter estimates Sb_BC
0,464972 - 0,478902
0,478903 - 0,503463
0,503464 - 0,533234
0,533235 - 0,581194
0,581195 - 0,614597
0,614598 - 0,634613
0,634614 - 0,644606
Metres
0 1.000 2.000

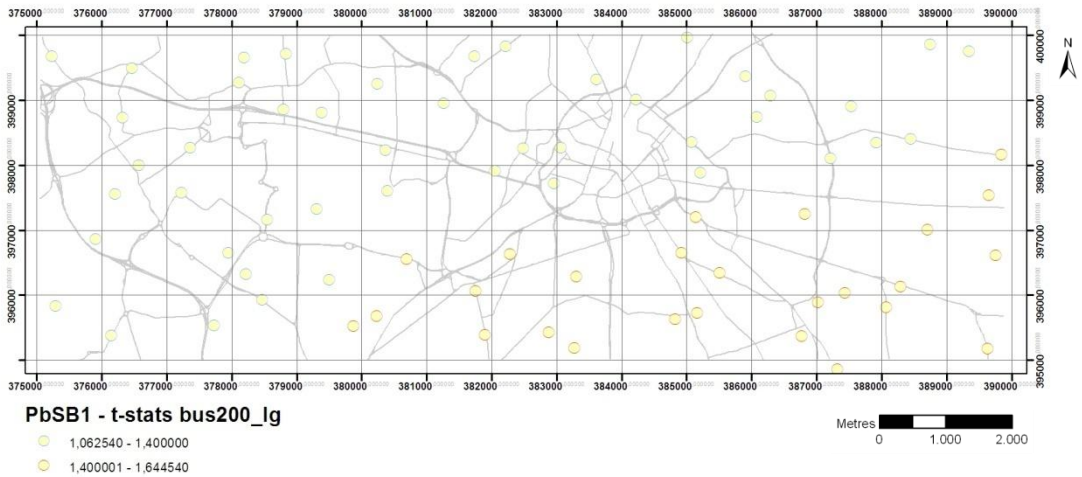
375000 376000 377000 378000 379000 380000 381000 382000 383000 384000 385000 386000 387000 388000 389000 390000
400000 399000 398000 397000 396000 395000
N
PbSB1 - t-stats bus200_lg
1,062540 - 1,400000
1,400001 - 1,644540
Metres
0 1.000 2.000

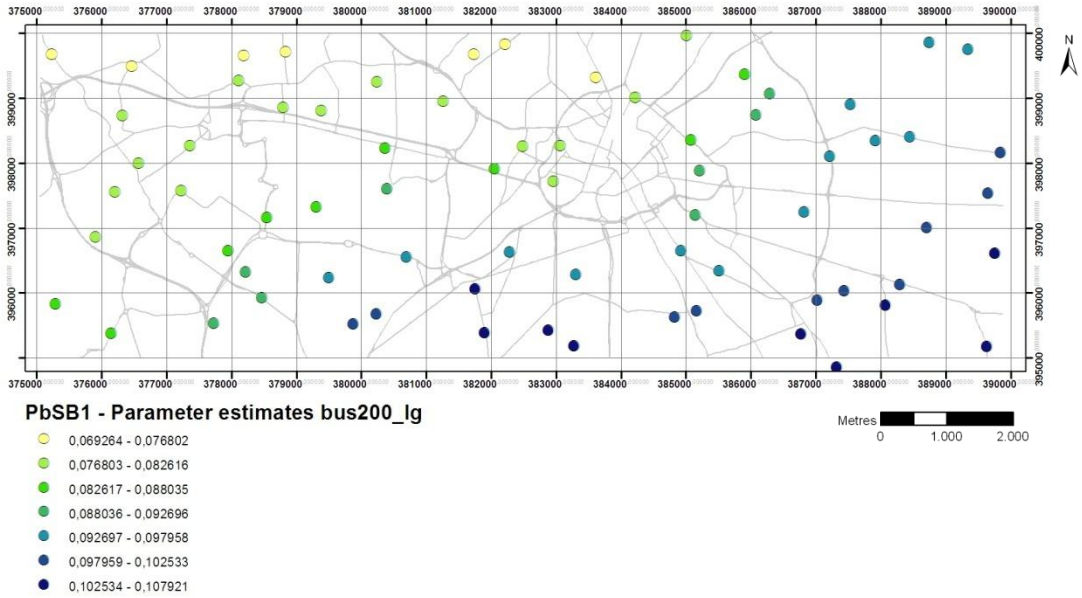


**PbSB1 - Parameter estimates bus200_lg**

- 0,069264 - 0,076802
- 0,076803 - 0,082616
- 0,082617 - 0,088035
- 0,088036 - 0,092696
- 0,092697 - 0,097958
- 0,097959 - 0,102533
- 0,102534 - 0,107921

Metres
0 1.000 2.000

## *B.3. T-statistics and parameter estimates - RDS winter*

Figure 142: Nickel t-statistics and parameter estimates - RDS winter - analysis set #A

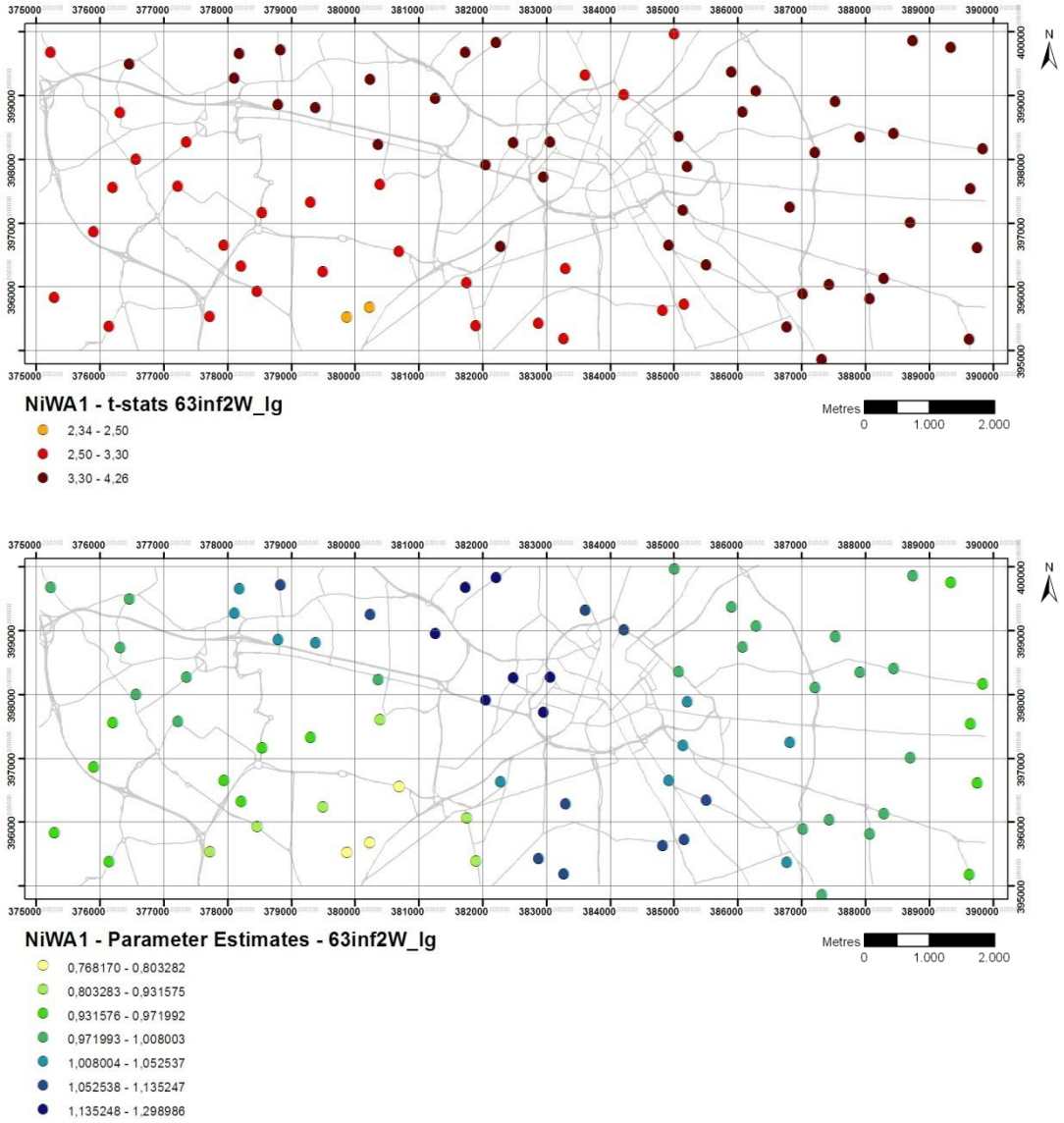


Figure 143: Copper t-statistics and parameter estimates - RDS winter - analysis set #A

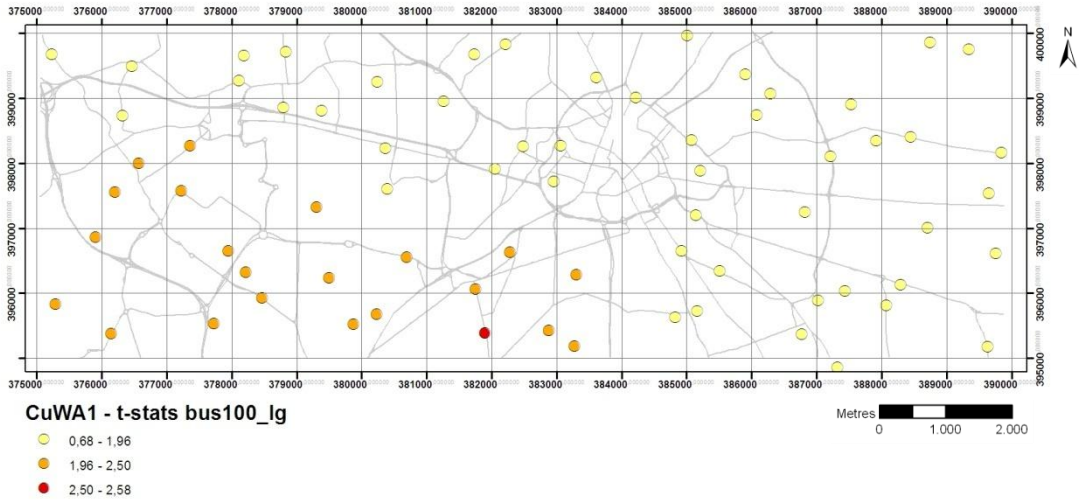

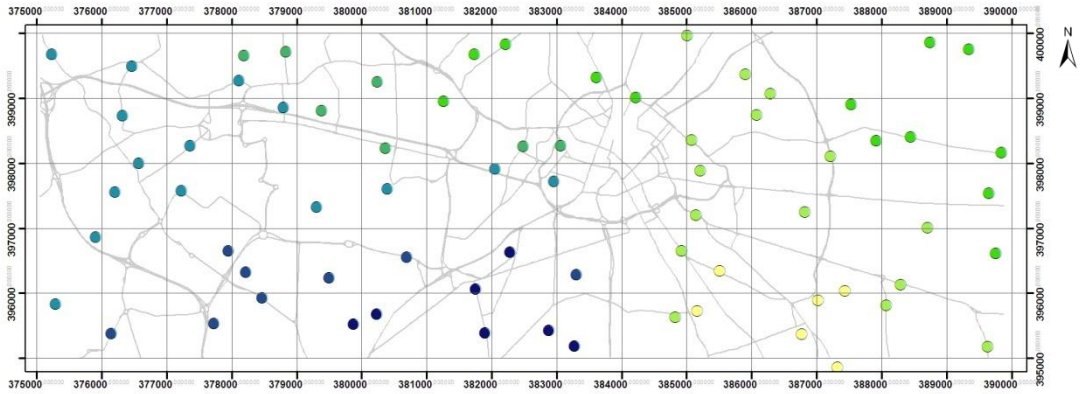


**CuWA1 - Parameter estimates bus100_lg**

- 0,533298 - 0,691311
- 0,691312 - 0,872363
- 0,872364 - 1,018932
- 1,018933 - 1,305361
- 1,305362 - 1,483334
- 1,483335 - 1,704598
- 1,704599 - 2,077096

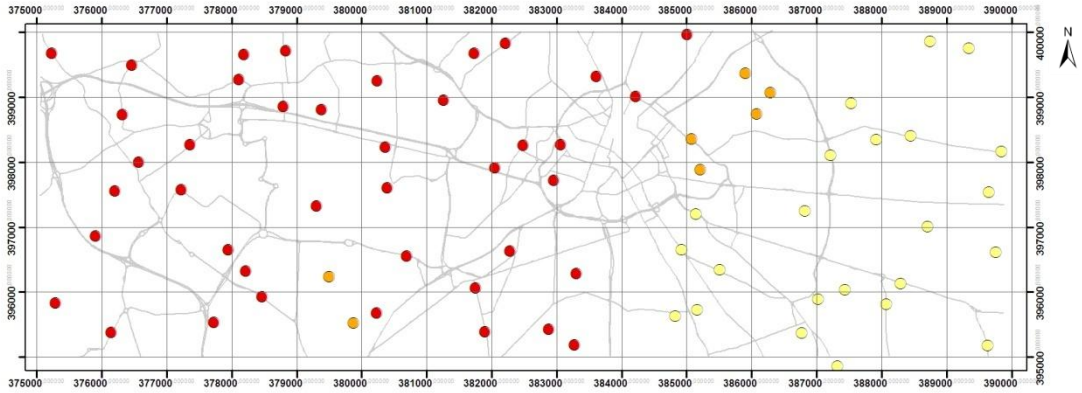


**CuWA1 - t-stats 63inf2W_lg**

- 1,16 - 1,96
- 1,96 - 2,50
- 2,50 - 4,08

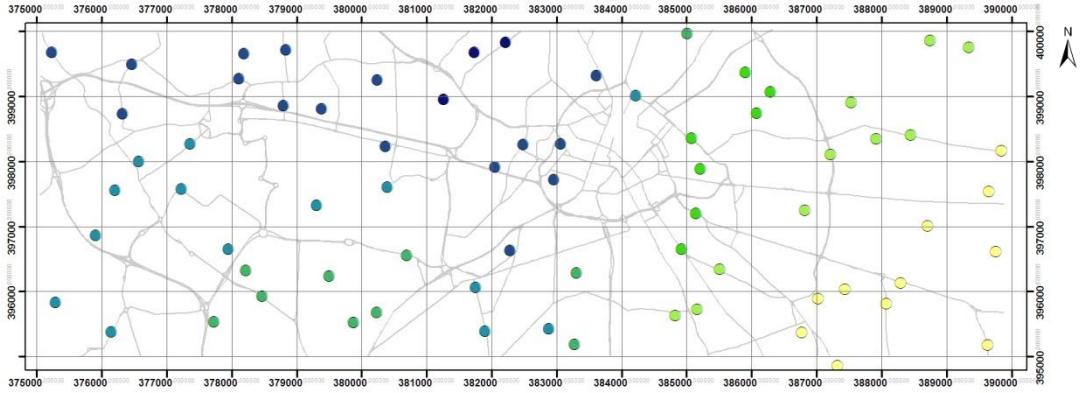


**CuWA1 - Parameter estimates 63inf2W_lg**

- 2,732943 - 3,328197
- 3,328198 - 4,252013
- 4,252014 - 5,492675
- 5,492676 - 7,036242
- 7,036243 - 7,748511
- 7,748512 - 8,763802
- 8,763803 - 9,871385

Figure 144: Arsenic t-statistics and parameter estimates - RDS winter - analysis set #A

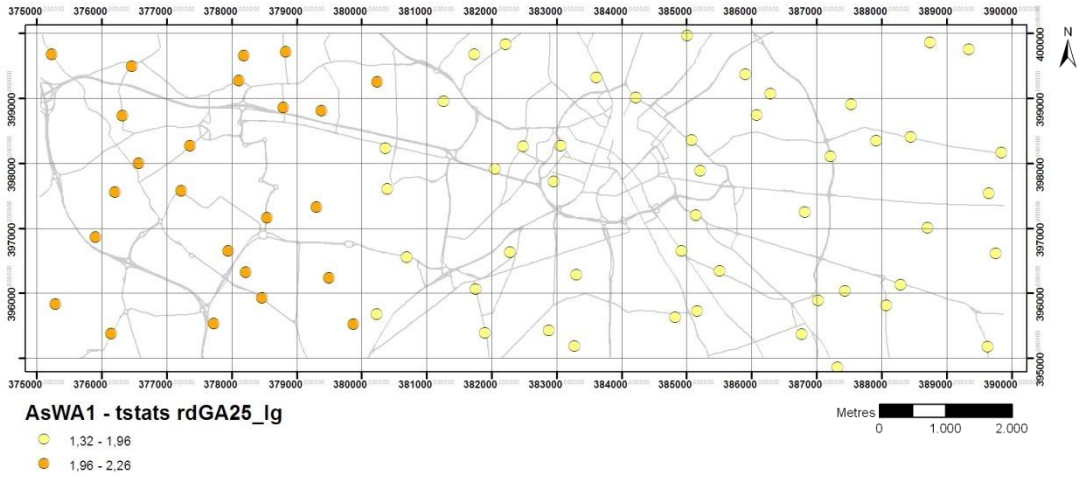


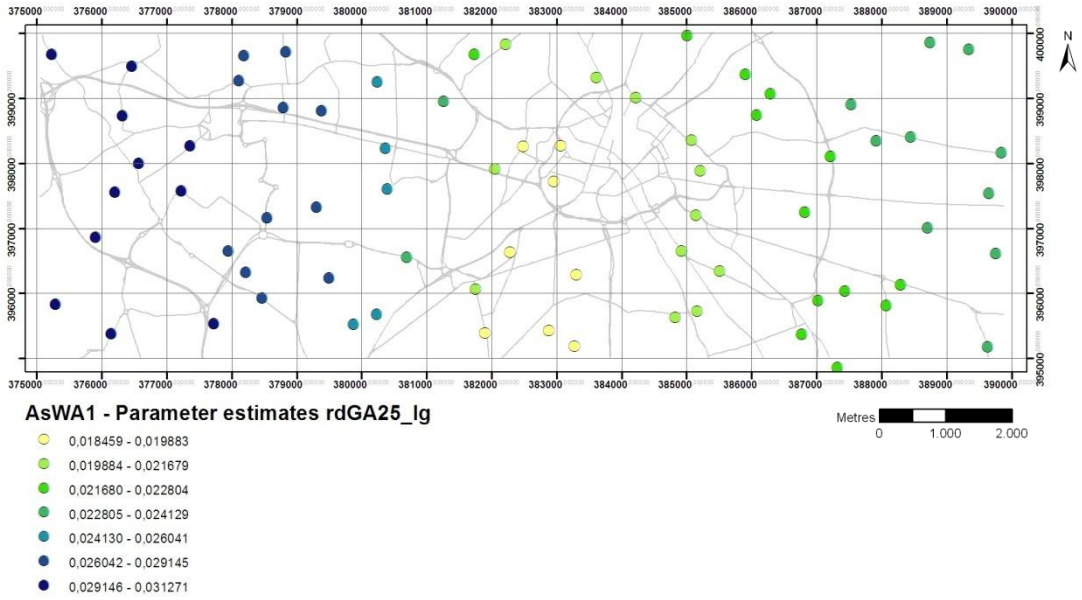


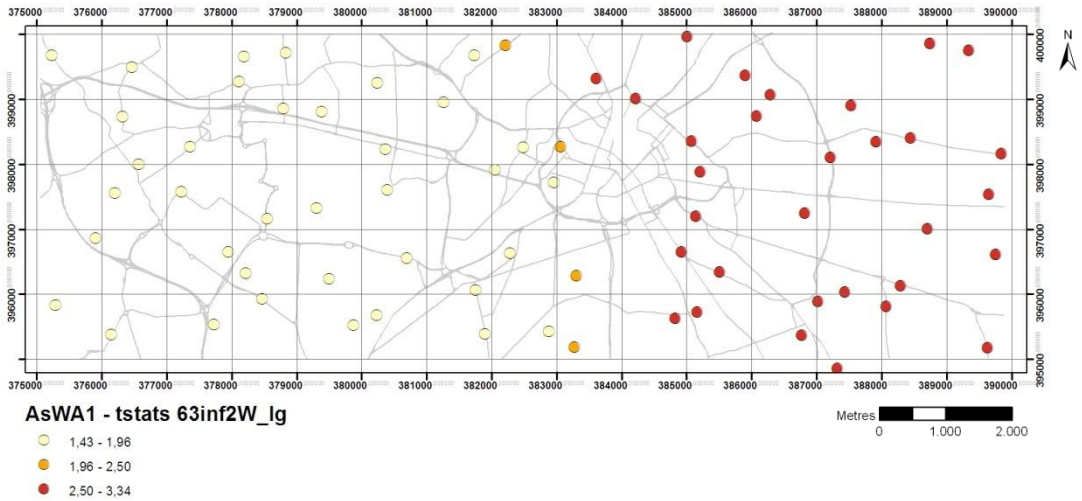

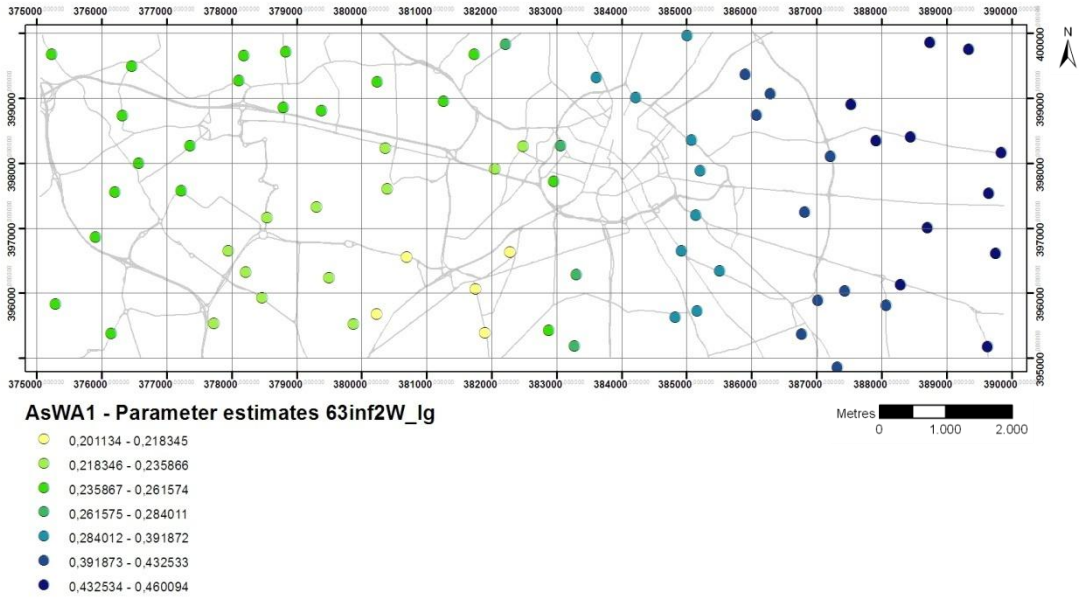


Figure 145: Copper t-statistics and parameter estimates - RDS winter - analysis set #B

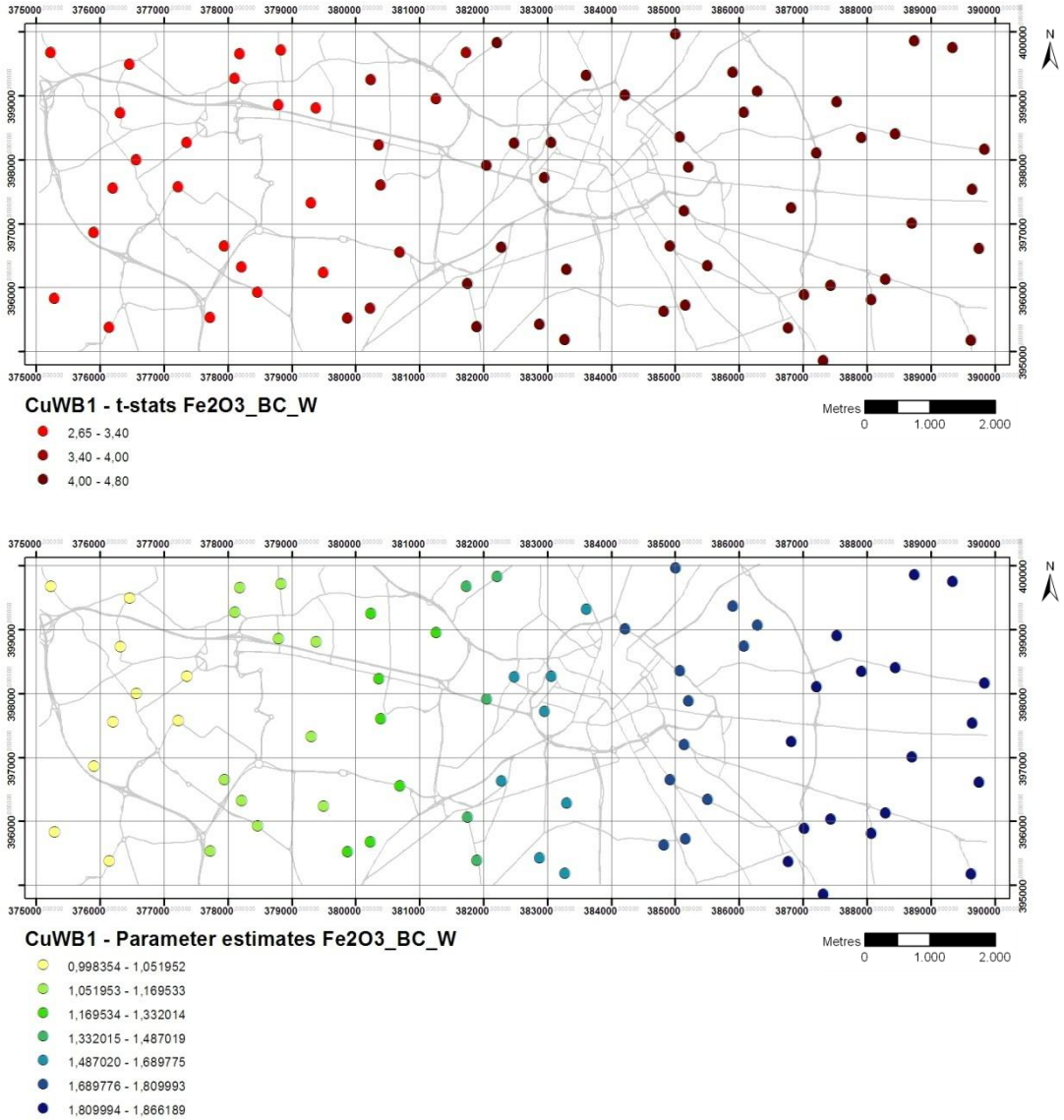

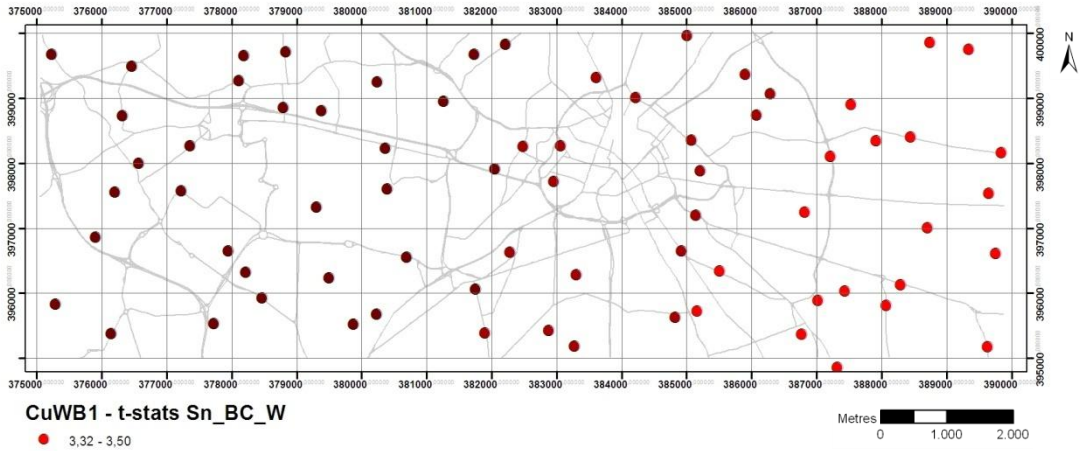


**CuWB1 - t-stats Sn_BC_W**

- 3,32 - 3,50
- 3,50 - 3,80
- 3,80 - 4,05

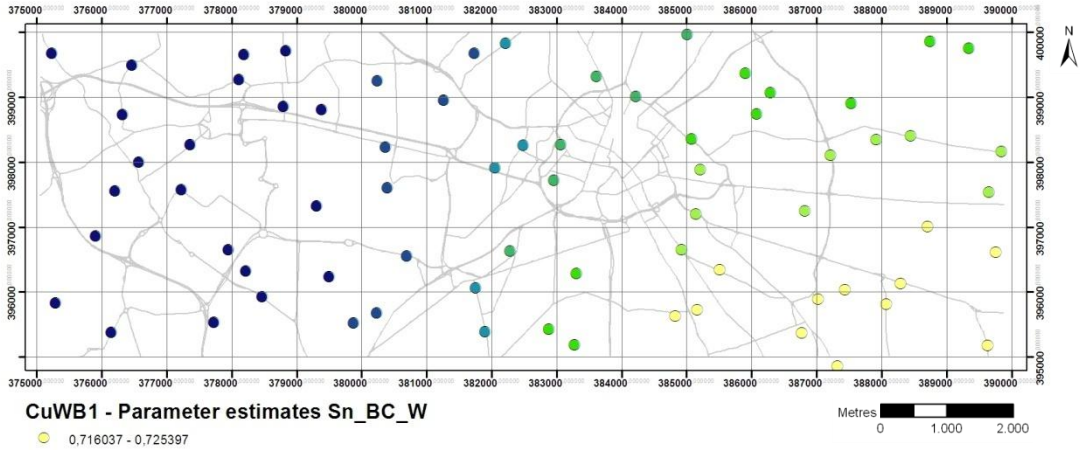


**CuWB1 - Parameter estimates Sn_BC_W**

- 0,716037 - 0,725397
- 0,725398 - 0,733505
- 0,733506 - 0,747288
- 0,747289 - 0,776769
- 0,776770 - 0,808751
- 0,808752 - 0,836471
- 0,836472 - 0,848273

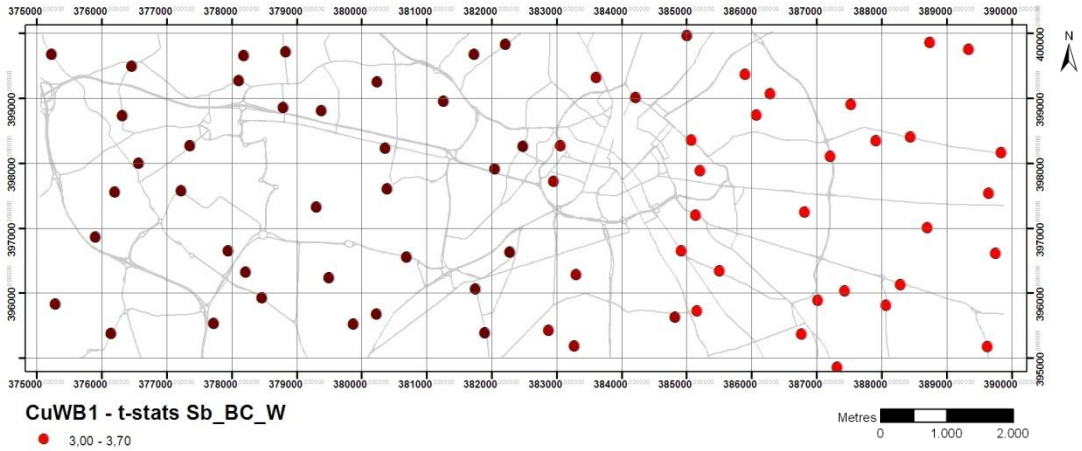


**CuWB1 - t-stats Sb_BC_W**

- 3,00 - 3,70
- 3,70 - 4,40
- 4,40 - 5,05

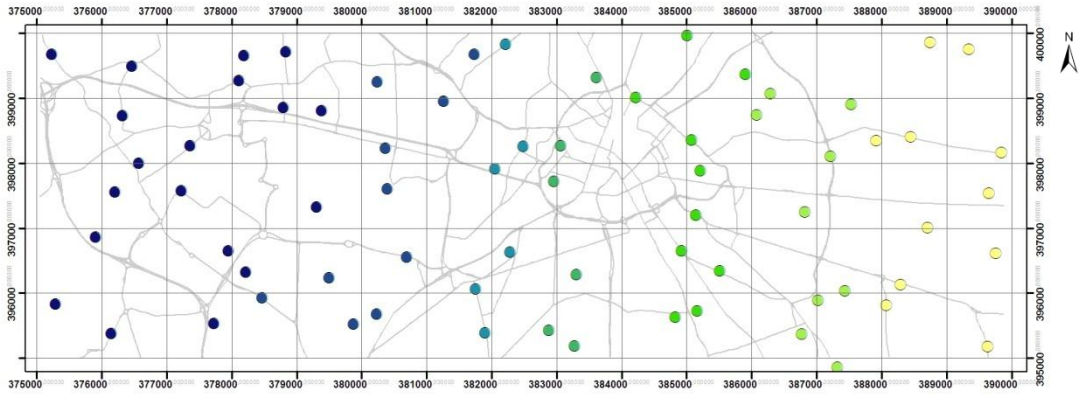


**CuWB1 - Parameter estimates Sb_BC_W**

- 1,445613 - 1,502484
- 1,502485 - 1,597928
- 1,597929 - 1,774908
- 1,774909 - 1,960498
- 1,960499 - 2,139440
- 2,139441 - 2,286630
- 2,286631 - 2,377848

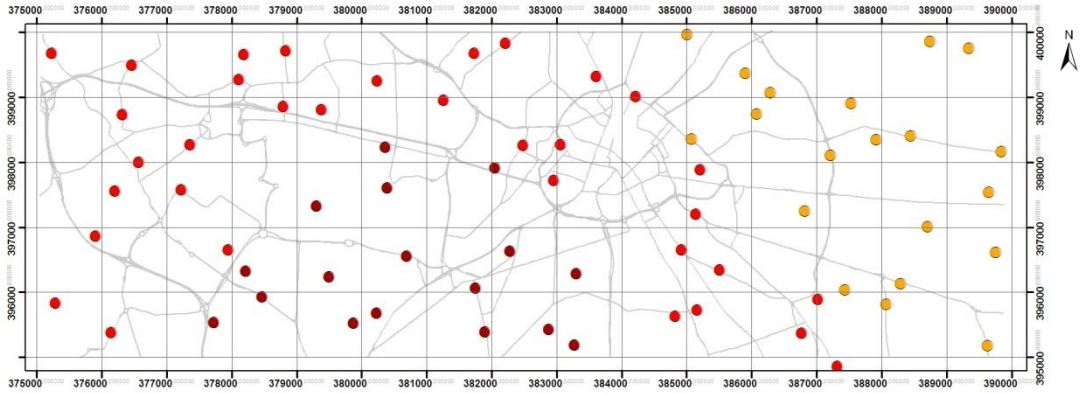


**CuWB1 - t-stats rdGA25**

- 2,15 - 2,50
- 2,50 - 3,00
- 3,00 - 3,43

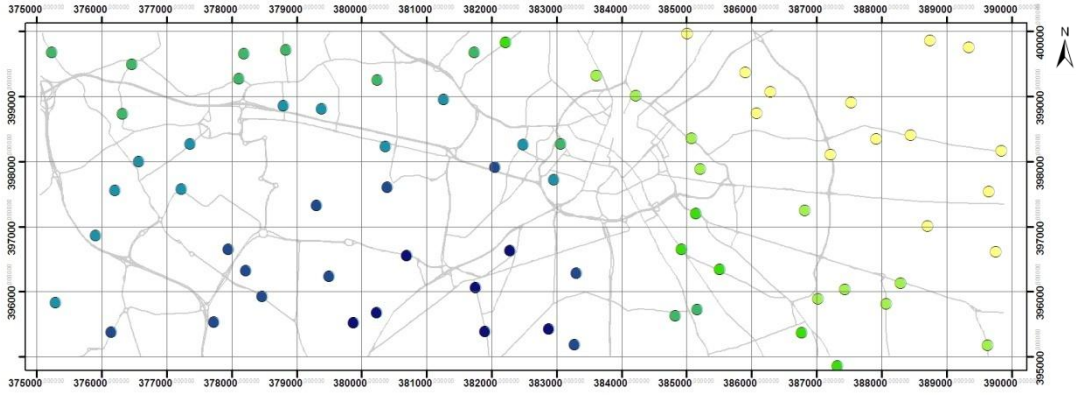


**CuWB1 - Parameter estimates rdGA25_lg**

- 0,219911 - 0,234783
- 0,234784 - 0,249921
- 0,249922 - 0,263470
- 0,263471 - 0,278276
- 0,278277 - 0,291912
- 0,291913 - 0,313230
- 0,313231 - 0,343231

Figure 146: Lead t-statistics and parameter estimates - RDS winter - analysis set #B

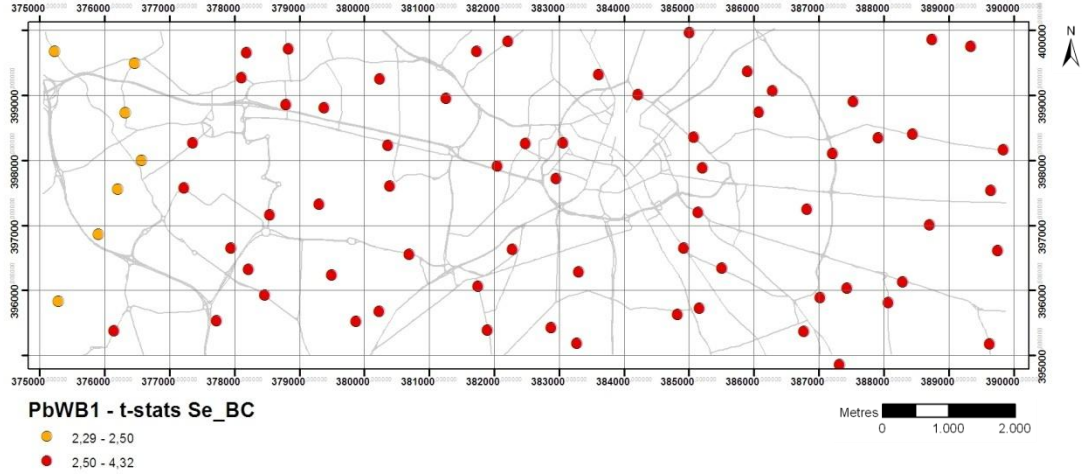


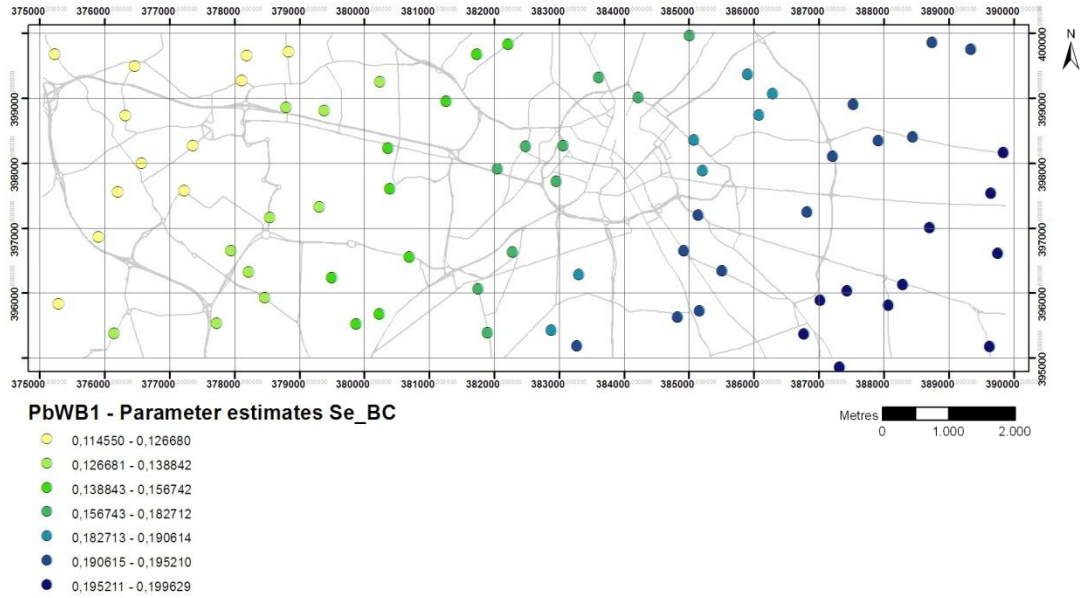


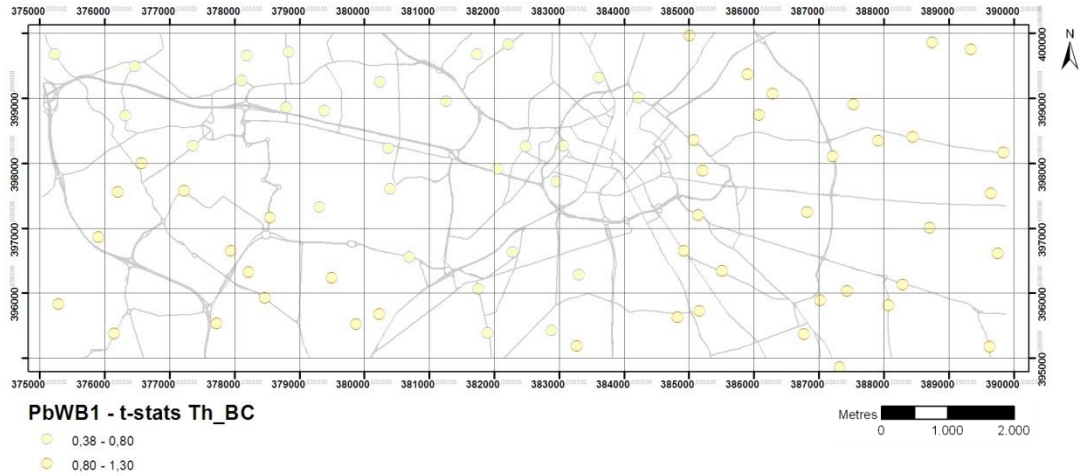

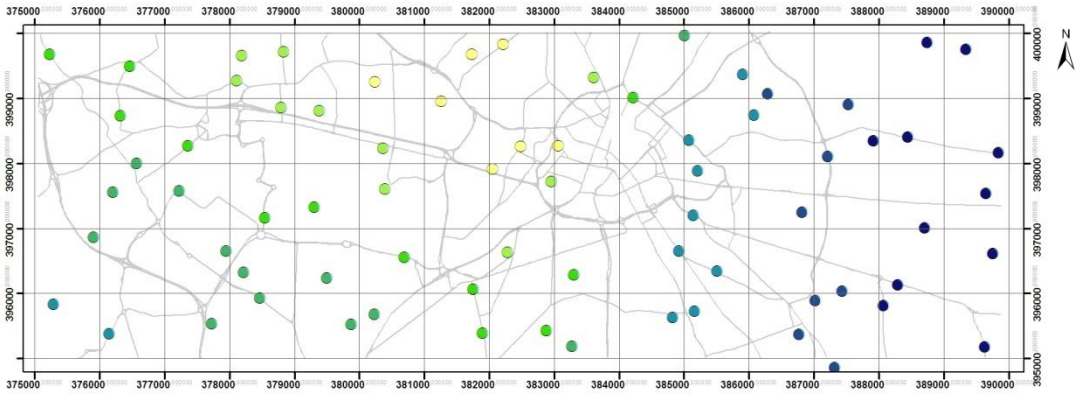


**PbWB1 - Parameter estimates Th_BC**

- 0,071819 - 0,103508
- 0,103509 - 0,128723
- 0,128724 - 0,151035
- 0,151036 - 0,176009
- 0,176010 - 0,211253
- 0,211254 - 0,240837
- 0,240838 - 0,274072

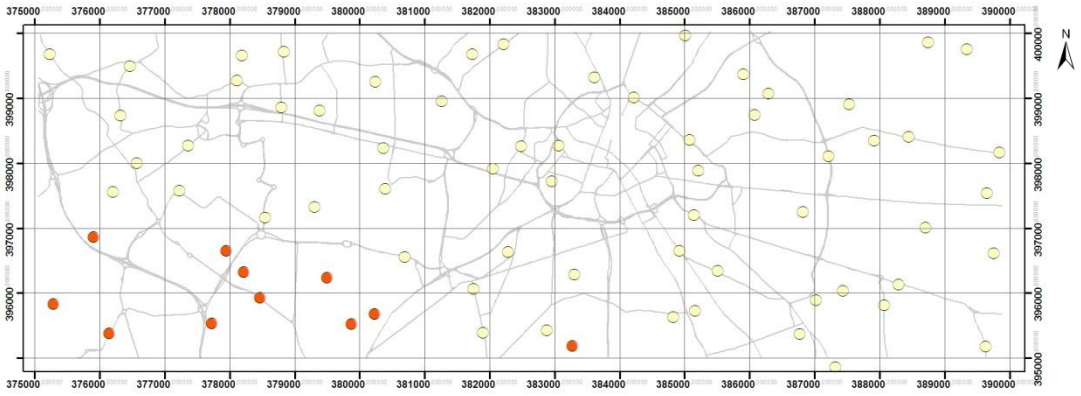


**PbWB1 - t-stats Sn_BC**

- 1,50 - 1,96
- 1,96 - 2,02

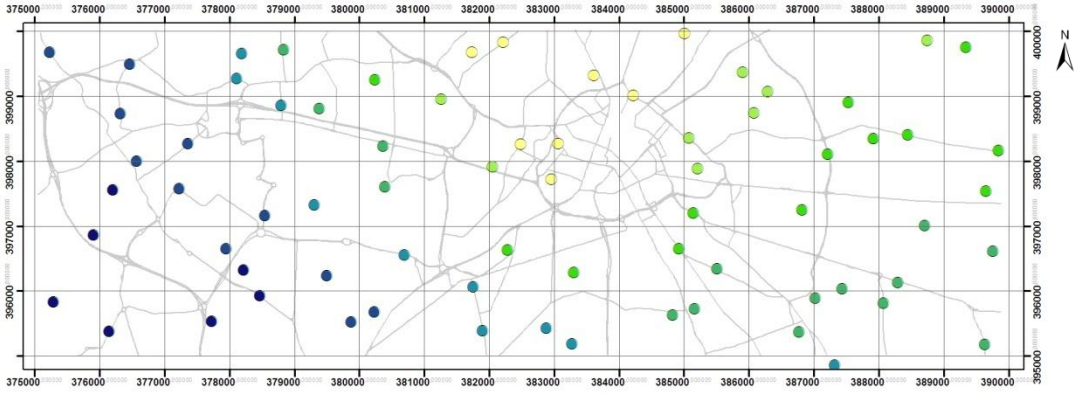


**PbWB1 - Parameter estimates Sn_BC**

- 0,082094 - 0,089590
- 0,089591 - 0,095201
- 0,095202 - 0,099343
- 0,099344 - 0,102677
- 0,102678 - 0,106905
- 0,106906 - 0,111489
- 0,111490 - 0,115826

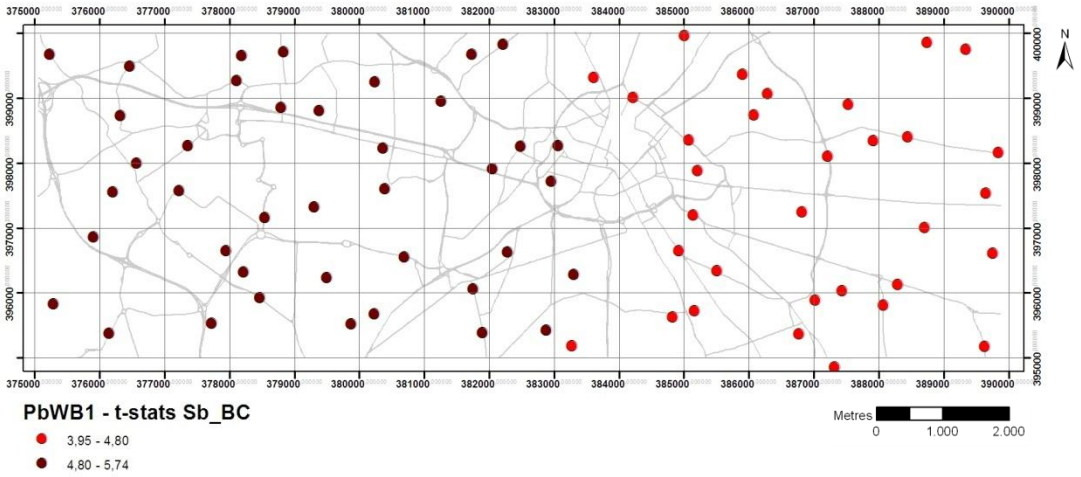
375000 376000 377000 378000 379000 380000 381000 382000 383000 384000 385000 386000 387000 388000 389000 390000
400000 399000 398000 397000 396000 395000
N
PbWB1 - t-stats Sb_BC
3,95 - 4,80
4,80 - 5,74
Metres
0 1.000 2.000

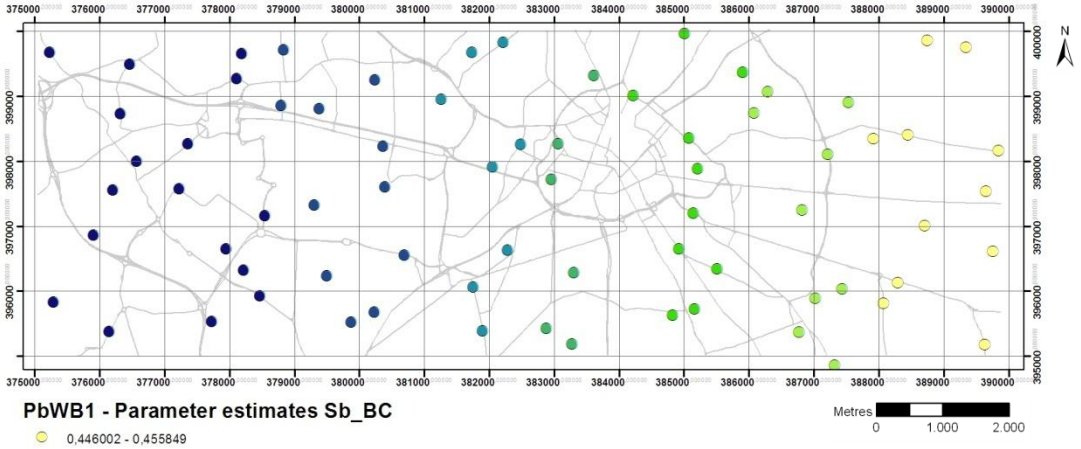
375000 376000 377000 378000 379000 380000 381000 382000 383000 384000 385000 386000 387000 388000 389000 390000
400000 399000 398000 397000 396000 395000
N
PbWB1 - Parameter estimates Sb_BC
0,446002 - 0,455849
0,455850 - 0,467945
0,467946 - 0,493976
0,493977 - 0,524894
0,524895 - 0,589117
0,589118 - 0,628510
0,628511 - 0,649068
Metres
0 1.000 2.000

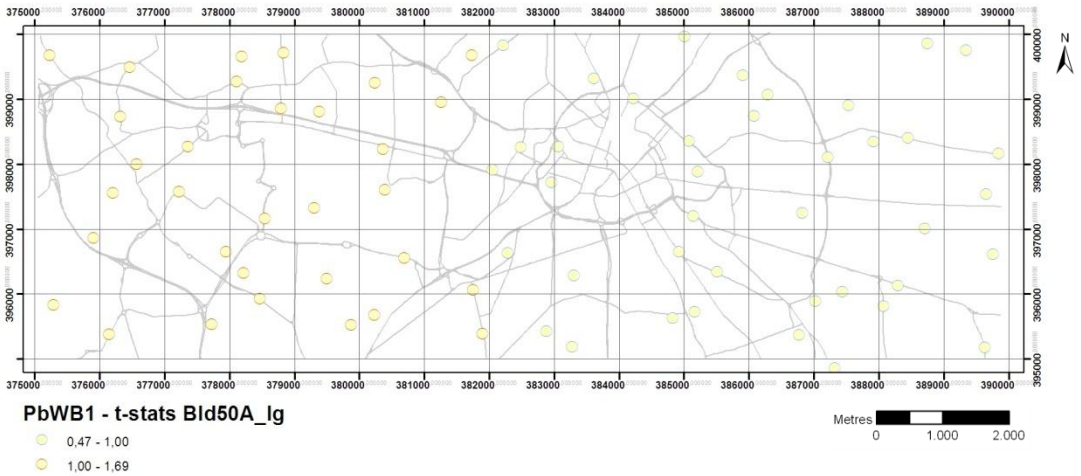
375000 376000 377000 378000 379000 380000 381000 382000 383000 384000 385000 386000 387000 388000 389000 390000
400000 399000 398000 397000 396000 395000
N
PbWB1 - t-stats BId50A_lg
0,47 - 1,00
1,00 - 1,69
Metres
0 1.000 2.000

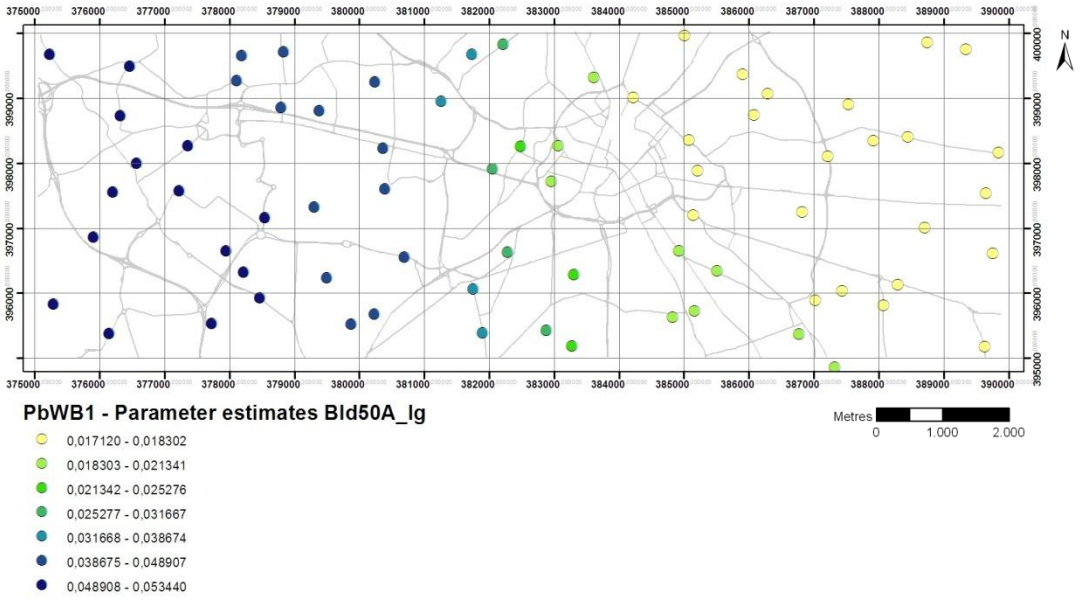
375000
376000
377000
378000
379000
380000
381000
382000
383000
384000
385000
386000
387000
388000
389000
390000
400000
399000
398000
397000
396000
395000
N
PbWB1 - Parameter estimates BId50A_lg
0,017120 - 0,018302
0,018303 - 0,021341
0,021342 - 0,025276
0,025277 - 0,031667
0,031668 - 0,038674
0,038675 - 0,048907
0,048908 - 0,053440
Metres
0
1.000
2.000

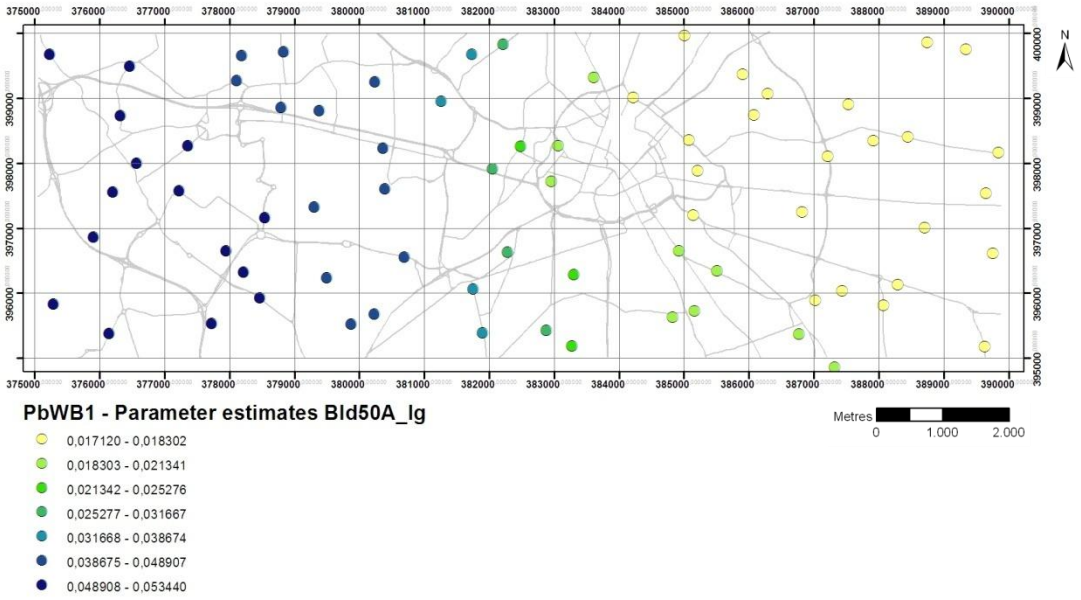
375000
376000
377000
378000
379000
380000
381000
382000
383000
384000
385000
386000
387000
388000
389000
390000
400000
399000
398000
397000
396000
395000
N
PbWB1 - Parameter estimates BId50A_lg
0,017120 - 0,018302
0,018303 - 0,021341
0,021342 - 0,025276
0,025277 - 0,031667
0,031668 - 0,038674
0,038675 - 0,048907
0,048908 - 0,053440
Metres
0
1.000
2.000